

COAL SCIENCE AND TECHNOLOGY 24

**J.A. PAJARES
J.M.D. TASCÓN
(EDITORS)**

COAL SCIENCE

VOLUME II



elsevier

COAL SCIENCE

COAL SCIENCE AND TECHNOLOGY

Series Editor:

Larry L. Anderson

Department of Fuels Engineering, University of Utah, Salt Lake City, UT 84112, U.S.A.

- Vol. 1: Geochemistry of Coal (Bouška)
- Vol. 2: Fundamentals of Coal Beneficiation and Utilization (Tsai)
- Vol. 3: Coal: Typology, Chemistry, Physics and Constitution (Van Krevelen)
- Vol. 4: Coal Pyrolysis (Gavalas)
- Vol. 5: Free Radicals in Coals and Synthetics Fuels (Petrakis and Grandy)
- Vol. 6: Coal Combustion Chemistry-Correlation Aspects (Badin)
- Vol. 7: The Chemistry of Coal (Berkowitz)
- Vol. 8: Natural Gas Substitutes from Coal and Oil (Qader)
- Vol. 9: Processing and Utilization of High-Sulfur Coals (Attia, Editor)
- Vol. 10: Coal Science and Chemistry (Volborth, Editor)
- Vol. 11: 1987 International Conference on Coal Science (Moulijn, Nater and Chermin, Editors)
- Vol. 12: Spectroscopic Analysis of Coal Liquids (Kershaw, Editor)
- Vol. 13: Energy Recovery from Lignin, Peat and Lower Rank Coals (Trantolo and Wise, Editors)
- Vol. 14: Chemistry of Coal Weathering (Nelson, Editor)
- Vol. 15: Advanced Methodologies in Coal Characterization (Charcosset, Editor – assisted by Nickel-Pepin-Donat)
- Vol. 16: Processing and Utilization of High-Sulfur Coals III (Markuszewski and Wheelock, Editors)
- Vol. 17: Chlorine in Coal (Stringer and Banerjee, Editors)
- Vol. 18: Processing and Utilization of High-Sulfur Coals IV (Dugan, Quigley and Attia, Editors)
- Vol. 19: Coal Quality and Combustion Performance: An International Perspective (Unsworth, Barratt and Roberts)
- Vol. 20: Fundamentals of Coal Combustion for Clean and Efficient Use (Smoot, Editor)
- Vol. 21: Processing and Utilization of High-Sulfur Coals V (Parekh and Groppo, Editors)
- Vol. 22: Atmospheric Fluidized Bed Coal Combustion. Research, Development and Application (Valk, Editor)
- Vol. 23: Lignites of North America (Schobert)
- Vol. 24: Coal Science (Pajares and Tascón, Editors)

COAL SCIENCE AND TECHNOLOGY 24

COAL SCIENCE

Proceedings of the Eighth International Conference on Coal Science

VOLUME II

edited by

J.A. PAJARES and J.M.D. TASCÓN

Instituto Nacional del Carbón, CSIC, Oviedo, Spain



1995

ELSEVIER

Amsterdam – Lausanne – New York – Oxford – Shannon – Tokyo

ELSEVIER SCIENCE B.V.
Sara Burgerhartstraat 25
P.O. Box 211, 1000 AE Amsterdam, The Netherlands

ISBN: 0-444-82227-5

© 1995 Elsevier Science B.V. All rights reserved.

No part of this publication may be reproduced, stored in a retrieval system or transmitted in any form or by any means, electronic, mechanical, photocopying, recording or otherwise, without the prior written permission of the publisher, Elsevier Science B.V., Copyright & Permissions Department, P.O. Box 521, 1000 AM Amsterdam, The Netherlands.

Special regulations for readers in the USA. This publication has been registered with the Copyright Clearance Center Inc. (CCC), 222 Rosewood Drive Danvers, MA 01923. Information can be obtained from the CCC about conditions under which photocopies of parts of this publication may be made in the USA. All other copyright questions, including photocopying outside of the USA, should be referred to the copyright owner, Elsevier Science B.V., unless otherwise specified.

No responsibility is assumed by the publisher for any injury and/or damage to persons or property as a matter of products liability, negligence or otherwise, or from any use or operation of any methods, products, instructions or ideas contained in the material herein.

This book is printed on acid-free paper.

Printed in The Netherlands

FOREWORD

Coal was, without any doubt, the fuel of the XIX century, making possible the Industrial Revolution. If asked about the use of coal in those days, the average newspaper reader would be able to give quite an accurate reply.

But if asked about the state of coal today, the average newspaper reader, or even a scientist or engineer, would probably be unaware that the worldwide production of coal is about 5,000 Mt, with 4,000 Mt being used for electricity production. Is it a miracle that this poor brother amongst the fuels of today holds about 30% of the energy market, with a growing share, as we enter into the third millennium?

Recent times have been difficult for Coal Science. Coal is much more than a dirty black solid. Our knowledge of coal composition and coal structure, taking advantage of modern physicochemical characterization techniques, has advanced enormously in the last twenty years. The contribution of this series of International Conferences on Coal Science, under the sponsorship of the International Energy Agency, should not be considered to be insignificant.

In this publication of the collected papers of the 8th International Conference on Coal Science, presented in Oviedo, Spain, September 10-15, 1995, there are 493 papers selected from 708 submissions from many countries. Volume I of this publication contains papers dealing with *Fundamentals and General Aspects*, *Combustion and Gasification* and *Pyrolysis and Carbonization*. Volume II contains papers discussing *Liquefaction and Hydrolysis* and *Coal and The Environment*.

There is no doubt that the width of topics covered will give to an interested reader a state-of-the-art impression with regard to coal characterization and depolymerization, coal-derived carbons, coal carbonization and liquefaction, and the progress in making coal an environmentally acceptable fuel during its combustion in electricity production. Coal will enter into the next millennium as a clean and efficient fuel.

THE EDITORS

This Page Intentionally Left Blank

ACKNOWLEDGEMENTS

The 8th International Conference on Coal Science was held under the auspices of the International Energy Agency (IEA). The support provided by IEA encouraged the submission of high-quality papers and the attendance of most renowned scientists from many countries.

The generous support from Spanish organizations ENDESA and OCICARBÓN is acknowledged with appreciation.

This Page Intentionally Left Blank

CONTENTS

VOLUME I

A. FUNDAMENTALS AND GENERAL ASPECTS	1
<i>A.1 PHYSICAL, CHEMICAL AND PETROGRAPHIC CHARACTERIZATION</i>	<i>1</i>
STUDY OF THE THERMODYNAMICS OF GAS ADSORPTION ON COAL BY A GC METHOD H. Huang, D.M. Bodily and V.J. Hucka	3
MEASUREMENT OF SURFACE ENERGY OF COALS BY INVERSE GAS CHROMATOGRAPHY M.C. Baquero, P. Granados, P. Rodríguez and J.M. Rincón	7
DETERMINATION OF THE CO ₂ SURFACE AREA OF COAL BY CONTINUOUS GAS DESORPTION AT 298 K H. Huang, D.M. Bodily and V.J. Hucka	11
THE INFLUENCE OF CARBON DIOXIDE TO CHANGING OF COAL STRUCTURE AND DURABILITY N.Tkachenko and A. Jigrin	15
FRACTAL APPROACH TO COAL PARTICLE SURFACE X. Zhang, C. Chen, X. Sun and C. Zheng	19
EFFECT OF GRAIN SIZE ON DIFFUSION OF GASES IN COAL A. Marecka	23
SORPTION INVESTIGATION OF COAL ON METHANE G. Ceglarska-Stefańska	27
GEOLOGICAL SURVEY OF CANADA COALBED METHANE RESEARCH W. Kalkreuth, M. Dawson and D. Hughes	31
CHANGE IN THE CONFORMATION OF LIGNITE MOLECULE DURING MOISTURE RELEASE PROCESS K. Norinaga, H. Kumagai, Y. Sanada, M. Sasaki and T. Kotanigawa	35

MICROPORES DIMENSION AND TURBOSTRATIC STRUCTURE STUDY OF AN STEAM ACTIVATED SEMIANTHRACITE J.C. Sousa, I.L. Torriani, J.B. Parra, J.J. Pis and J.A. Pajares	39
THE MICROTEXTURE OF ANTHRACITES: A KEY TO UNDERSTAND THEIR GRAPHITIZABILITY C. Blanche, D. Dumas and J.-N. Rouzaud	43
USE OF CARBON SCIENCE CONCEPTS TO UNDERSTAND COAL STRUCTURE AND REACTIVITY A. Cuesta, M.R. Fernández, J.M. Pastor, A. Martínez-Alonso and J.M.D. Tascón	47
X-RAY SCATTERING ANALYSIS OF UPPER FREEPORT COAL, APC 101 D.L. Wertz	51
A MODEL STRUCTURE OF ZAO ZHUANG BITUMINOUS COAL T. Takanohashi, M. Iino, H. Kumagai, Y. Sanada and K. Nakamura	55
VISCOELASTIC PROPERTY AND MACROMOLECULAR STRUCTURE OF COAL M. Iino, H. Watanabe and T. Takanohashi	59
CHARACTERIZATION OF INTERACTIONS OF COAL SURFACE WITH SOLVENT BY FLOW MICRO CALORIMETRIC MEASUREMENT N. Wang, M. Sasaki, T. Yoshida and T. Kotanigawa	63
THE CHEMICAL CONSTITUTION OF POCAHONTAS NO. 3 COAL L.M. Stock and M. Obeng	67
NEUTRON-GENERATOR BASED ON-LINE COAL ANALYSIS: A PROGRESS REPORT G. Vourvopoulos, L. Dep, S. Sudar, P.C. Womble and F.J. Schultz	71
THE NEED FOR ENHANCED COAL QUALITY DATABASES R.B. Finkelman	75
THE COMBUSTIBLE SULPHUR CONTENT OF TURKISH COALS D. Uzun, S. Özdoğan and M. Arikol	79
HYDROTHERMAL DECOMPOSITION CHEMISTRY OF SAPROPELITIC (ALGAL) COALS: A CONCEPT OF CARBON-TO-CARBON CROSSLINKED STRUCTURES IN ALGAENAN Yu.V. Rokosov, N.V. Bodoev and V.N. Sidel'nikov	83

STRUCTURAL ELUCIDATION OF ARGONNE PREMIUM COALS: MOLECULAR WEIGHTS, HETEROATOM DISTRIBUTIONS AND LINKAGES BETWEEN CLUSTERS R.E. Winans, Y. Kim, J.E. Hunt and R.L. McBeth	87
CO ₂ - A KEY FACTOR IN GAS CHARACTERIZATION J.W. Smith and R.J. Pallaser	91
COMPOSITION OF WAX FRACTION OF BROWN COAL BITUMEN V.V. Rodae, G.S. Golovin and E.A. Papirova	95
CHEMICAL COMPOSITION OF XYLITIC AND A HUMIC BROWN COALS AS SEEN BY PYROLYSIS-GAS CHROMATOGRAPHY-MASS SPECTROMETRY J.C. del Río, F. Czechowski, F.J. González-Vila and F. Martin	99
CHEMICAL AND MINERALOGICAL CHARACTERISTICS OF THE SUBBETUMINOUS COAL OF THE OLIGO-MIOCENE OF SOUTHERN- CENTER CHILE (X REGION) G. Alfaro and M.E. Cisternas	103
ORIGIN AND DISTRIBUTION OF THE HYDROPYROLYSATE COMPOUNDS IN UTRILLAS COAL F.X.C. de las Heras, M.A. Olivella, J.O. Grimalt and J. Albaigés	107
QUANTITATIVE SOLID STATE NMR AND FTIR SPECTROSCOPY OF LOW RANK COAL AND RELIABILITY OF STRUCTURAL PARAMETERS J. Černý and H. Pavlíková	111
CURVE-FITTING ANALYSIS OF FTIR SPECTRA OF COAL VARYING IN RANK E. Muñoz, R. Moliner and J.V. Ibarra	115
ASSESSMENT OF COAL DEPOSITIONAL ENVIRONMENT AND MATURITY BY REFLECTION FT-IR MICRO-SPECTROSCOPY O. Ruau, P. Landais, B. Pradier and J.L. Gardette	119
MINERALS IN COALS FROM THE YORKSHIRE-NOTTINGHAMSHIRE COALFIELDS: IDENTIFICATION AND QUANTIFICATION D.A. Spears	123
QUANTITATIVE X-RAY DIFFRACTION DETERMINATION OF MINERAL PHASES IN COAL AND ITS APPLICATION TO THE STUDY OF MINERAL TRANSFORMATIONS IN UTILISATION PROCESSES L.S. Dale, H.J. Hurst, C.E. Matulis, J.H. Patterson and J.C. Taylor	127

THE APPLICATION OF LOW-TEMPERATURE OXIDATION FOR INVESTIGATION AND RATIONAL UTILIZATION OF COALS A.N. Zaostrovsky, N. I. Fjodorova and V.A. Zubakina	131
PETROGRAPHIC AND MINERAL CHARACTERIZATION OF BALKAN COALS AND THEIR SOLID WASTE PRODUCTS FROM COAL PREPARATION M. Yossifova	135
MINERAL MATTER AND TRACE ELEMENTS DISTRIBUTION IN LATE PERMIAN COAL, COLLIE BASIN, WESTERN AUSTRALIA K.K. Sappal	139
MINERALOGY AND GEOCHEMISTRY OF THE BEYPAZARI LIGNITE, CENTRAL ANATOLIA, TURKEY X. Querol, M.K.G. Whateley, J.L. Fernández-Turiel and E. Tuncali	143
RAPID ANALYSIS OF COAL ASH COMPOSITION BY RADIOISOTOPE X-RAY FLUORESCENCE SPECTROMETRY G.P. Suarez-Fernandez, J. M.G. Vega, A.B. Fuertes, A.B. Garcia and M.R. Martínez-Tarazona	147
THE ANALYSIS OF TRACE ELEMENTS IN COAL L. Buggéy, B.P. Atkin, M. Cloke and N.J. Miles	151
MINERALOGY AND GEOCHEMISTRY OF COALS FROM THE GEVRA MINE, KORBA MADHYA PRADESH, INDIA B.R. Hart, M.A. Powell, K.C. Sahu, S. Tripathy and W.S. Fyfe	155
TRACE ELEMENTS IN SPANISH SUBBITUMINOUS COALS AND THEIR BEHAVIOUR DURING COAL COMBUSTION X. Querol, J.L. Fernández-Turiel and A. López-Soler	159
TRACE ELEMENT CONTENTS OF THE LAVA XYLITE/LIGNITE AND PTOLEMAIS LIGNITE DEPOSITS, MACEDONIA COUNTY, GREECE A. Georgakopoulos, J.L. Fernandez-Turiel, A. Filippidis, J.F. Llorens, A. Kassoli-Fournaraki, X. Querol and A. Lopez-Soler	163
TRACE ELEMENT DISTRIBUTIONS AND ASSOCIATIONS IN UK COALS A.J. Bushell and J. Williamson	167
GEOCHEMISTRY OF COALS FROM THE RED DEER RIVER VALLEY, ALBERTA, CANADA F. Goodarzi and T. Gentzis	171

MODES OF OCCURRENCE OF TRACE ELEMENTS IN COAL: GEOCHEMICAL CONSTRAINTS FROM XAFS AND PIXE SPECTROSCOPIC ANALYSIS OF ADVANCED COAL CLEANING TESTS	175
F.E. Huggins, B.K. Parekh, J.D. Robertson and G.P. Huffman	
SORPTION OF RARE EARTH ELEMENTS ON XYLAIN	179
G.M. Eskenazy and L.S. Chakarova	
THE EXAMINATION OF MINERAL/ORGANIC MATTER ASSOCIATIONS IN COAL	183
B.P. Atkin and D. Clift	
A METHOD FOR THE ASSESSMENT OF THE MINERAL/ORGANIC MATTER ASSOCIATION OF TRACE ELEMENTS IN COAL	187
B.P. Atkin, C. Somerfield and K.L. Laban	
ASSESSMENT OF THE VARIATION IN MINERAL MATTER-MACERAL ASSOCIATION CHARACTERISTICS OF A SUITE OF UK COALS	191
D.J.A. McCaffrey, D.G. Richards, D.A. Spears and M. Widdowson	
MINERAL MATTER IN UK POWER STATION COALS - DISTRIBUTIONS AND ASSOCIATIONS	195
F. Wigley and J. Williamson	
THE INTERACTION OF ORGANIC MATTER AND MINERAL SUBSTANCES IN THERMAL PROCESSING OF COAL ROCKS IN DIFFERENT GASEOUS MEDIA	199
L.A. Kost, L.N. Lebedeva, N.N. Novikova and M.Ya. Shpirt	
OBSERVATIONS OF MACERAL AND MINERAL HETEROGENEITY IN PULVERISED COALS	203
T.J. Beeley, J.C. Crelling, J.R. Gibbins, A.C. Scott and J. Williamson	
CHARACTERISTIC PROPERTIES OF SAPROPELITIC COAL COALIFICATION	207
N.V. Bodoev, O.A. Aref'ev, N.N. Rokosova and M.N. Zabrodina	
PETROGRAPHIC AND GEOCHEMICAL STUDY OF THE "PRINCIPAL" COAL SEAM, YANACANCHA BASIN (TERTIARY) OF PERU	211
E.R. Carrascal Miranda and I. Suárez-Ruiz	
STRUCTURAL EVOLUTION OF PURE VITRINITE DURING ARTIFICIAL COALIFICATION	215
F. Laggoun-Défarge, J.-N. Rouzaud, N. Cohaut, P. Landais, E. Lallier-Vergès and I. Suárez-Ruiz	

GEOCHEMICAL STUDY OF THE ARTIFICIAL THERMAL EVOLUTION OF PURE VITRINITE M.J. Iglesias, A. Jiménez, F. Laggoun-Défarge and I. Suárez-Ruiz	219
STRUCTURAL AND MICROTTEXTURAL CHARACTERISTICS OF NATURAL "COKES" J. Jehlička and J.-N. Rouzaud	223
SYSTEMATIC TRENDS IN PYROLYSIS PRODUCT EVOLUTION WITH COAL MATURITY S. Charpenay, M.A. Serio, R. Bassilakis and P.R. Solomon	227
CHARACTERIZATION OF HYDROGENATED PRODUCTS OF HYDROUS PYROLYSIS RESIDUES OBTAINED FROM CELLULOSE AND WOOD Y. Sugimoto and Y. Miki	231
RECENT ADVANCES IN SEPARATING AND CHARACTERIZING SINGLE COAL MACERALS J.C. Crelling and D.F. Bensley	235
AUTOMATIC MACERAL AND REFLECTANCE ANALYSIS IN SINGLE SEAM BITUMINOUS COALS J.C. Catalina, D. Alarcón and J.G. Prado	239
STRUCTURAL STUDIES OF COAL MACERALS F. Li, Y.-F. Zhang and K.-C. Xie	243
PETROGRAPHIC FABRIC ANALYSES OF SPORINITES: A NEW TECHNIQUE IN COAL CHARACTERIZATION L.L. Tsai	247
ADVANCES IN THE FLUORESCENCE MICROSCOPY OF LOW RANK COALS S.L. Bend and D.M. Kosloski	251
FT-IR SPECTROSCOPY OF WESTERN CANADIAN COALS AND MACERALS K.H. Michaelian, W.I. Friesen, S.L. Zhang, T. Gentzis, J.C. Crelling and S.G. Gagarin	255
THE RELATIONSHIP BETWEEN THE PETROGRAPHIC COMPOSITION AND SOME CHEMICAL PROPERTIES FOR THE PTOLEMAIS BASIN LIGNITES, GREECE S. Valceva, A. Georgakopoulos and K. Markova	259

PETROGRAPHIC CONSTITUTION, PHYSICAL, CHEMICAL AND TECHNOLOGICAL PROPERTIES OF THE FRACTIONS ISOLATED FROM METACOKING COAL AND SEMICOKING COAL BY THE METHOD OF SEPARATION IN HEAVY LIQUIDS S. Jasieńko and L. Róg	263
A CHEMICAL CHARACTERISATION OF MACERAL FRACTIONS FROM AN AUSTRALIAN COKING COAL J.D. Giuliani, A.M. Vasallo, J.V. Hanna, G.R. Dyrkacz and R.B. Johns	267
THE PROPERTIES OF JAPANESE COALS AND ITS RELATION WITH DEGRADINITE Y. Suzuki and K. Fujii	271
PETROLOGY AND ORGANIC GEOCHEMISTRY OF SELECTED SAMPLES OF THE LIGNITES FROM RIO MAIOR (PORTUGAL) D. Flores and W. Pickel	275
IMPLICATIONS OF VARIATIONS IN PETROGRAPHY ON THE ALIPHATIC HYDROCARBON COMPOSITION WITHIN THE BARRETT COAL MEMBER, UPPER PERMIAN WITTINGHAM COAL MEASURES, NORTHERN SYDNEY BASIN, NEW SOUTH WALES (NSW), AUSTRALIA F.E. Casareo, B.D. Batts, P.J. Conaghan, S.C. George and D.R. Jardine	279
RELATIONSHIPS BETWEEN PETROGRAPHIC COMPOSITION AND THERMAL BEHAVIOUR OF SOME SPANISH OIL SHALES A.G. Borrego, J.G. Prado, E. Fuente, M.D. Guillén and C.G. Blanco	283
THE INFLUENCE OF DEPOSITIONAL ENVIRONMENT ON THE METHYLPHENANTHRENE INDEX S.C. George and J.W. Smith	287
BIOMARKERS ASSEMBLAGE IN RELATION TO COAL RANK F. Czechowski	291
PETROGRAPHIC EFFECTS ON BITUMINOUS COALS AFTER TREATMENT WITH SUB- AND SUPERCRITICAL FLUID PHASES G. Götz, W. Pickel and M. Wolf	295
THERMAL BEHAVIOR OF MACERALS IN LOW-RANK COALS S.G. Gagarin and N.N. Ulanov	299
THE EFFECT OF INERTINITE CONTENT ON COAL COMBUSTION REACTIVITY R. Menéndez, A. Gómez Borrego, J. Bailey, E. Fuente and D. Álvarez	303

MACERAL AND RANK INFLUENCES ON THE MORPHOLOGY AND REACTIVITY OF COAL CHAR X. Zhang, C. Chen, X. Sun and Y. Zheng	307
THE EFFECT OF BROWN COAL PETROGRAPHIC COMPOSITION ON THE PROPERTIES OF HOT BRIQUETTS A.P. Fomin, S.G. Gagarin, G.I. Enik and N.V. Ruban	311
LARGE MOLECULES IN COAL - WHERE DO THEY HIDE? A.A. Herod, B.R. Johnson, K.D. Bartle and R. Kandiyoti	315
LASER DESORPTION MASS SPECTROMETRY: TECHNICAL LIMITATIONS, FUNDAMENTALS, AND APPLICATION TO COAL J.E. Hunt and R.E. Winans	319
COKING COAL ASSESSMENT BY SCANNING LASER FLUORESCENCE MICROPROBE J.R. Wilmshurst, C.F.K. Diessel, R.W.T. Wilkins, C.P. Buckingham and L. Gammidge	323
QUANTITATIVE DETERMINATION OF TRACE ELEMENT AFFINITIES IN COAL AND COMBUSTION WASTES BY LASER ABLATION MICROPROBE-INDUCTIVELY COUPLED PLASMA-MASS SPECTROMETRY S. Chenery, X. Querol and J.L. Fernández-Turiel	327
PREDICTING ¹³ C NMR MEASUREMENTS BASED ON COAL ELEMENTAL COMPOSITION D.B. Genetti, T.H. Fletcher and R.J. Pugmire	331
APPLICATIONS OF THE ¹³ C NMR MAGIC ANGLE TURNING EXPERIMENT TO THE STUDY OF COALS R.J. Pugmire, M.S. Solum, W. Wang and D.M. Grant	335
¹⁹ F- ¹³ C CROSS POLARIZATION ¹³ C NMR: AN EXPLORATORY STUDY OF STRUCTURE AND REACTIVITY OF FLUORINATED COAL USING ELEMENTAL FLOURINE E.W. Hagaman and S.K. Lee	339
PMRTA INVESTIGATION INTO THE NON-ADDITIVE SWELLING BEHAVIOUR OF COAL BLENDS A.J. Lowe, D.J.A. McCaffrey and D.G. Richards	343
ANALYSIS OF COAL USING SCANNING TUNNELING MICROSCOPY E.J. Hippo, S.R. Palmer, D. Tandon and E. Sebok	347

PHENOLIC RESITES AS CALIBRANTS FOR TEMPERATURE PROGRAMMED REDUCTION AND PROBES FOR THE THERMAL BEHAVIOUR OF ORGANIC SULPHUR FORMS IN COALS K. Ismail, S.D. Brown, O. Sirkecioglu, C.E. Snape, D.V. Franco, I.I. Maes and J. Yperman	351
DXRF: A NON-DESTRUCTIVE METHOD FOR ANALYSIS OF THERMAL COAL P.F. Viar, D. Ponte and J. Xiberta	355
THE USE OF MICROWAVES IN THE RAPID DETERMINATION OF COAL MOISTURE D. Ponte, I. Prieto, P. F. Viar and J.C. Luengo	359
<i>A.2 STRUCTURE AND CHEMICAL REACTIVITY</i>	363
SOLUBILIZATION OF BROWN COALS IN POLAR SOLVENT THROUGH LIQUID PHASE OXIDATION AT ROOM TEMPERATURE K. Mae, T. Maki, S. Inoue and K. Miura	365
SOLUBILIZATION OF TAIHEIYO COAL AT MILD CONDITIONS BY THE AID OF HF/BF ₃ K. Shimizu, A. Inaba and I. Saito	369
STUDIES ON THE EXTRACTION OF ILLINOIS NO. 6 COAL AND THE DETAILED ANALYSIS OF THE EXTRACT S. Murata, E. Kawakami and M. Nomura	373
CHANGES OF MACROMOLECULAR STRUCTURE OF COALS IN THE PROCESSES OF REDUCTION AND REDUCTIVE ALKYLATION IN LIQUID AMMONIA H. Wachowska and M. Kozłowski	377
SOLVENT EFFECTS IN SYNCHRONOUS UV FLUORESCENCE TO CHARACTERIZE THE SOLID/LIQUID PHASE MODIFICATIONS IN COAL STRUCTURE DURING THE PREHEATING PROCESS J. Kister, N. Pieri, M.A. Diez, R. Alvarez and J.J. Pis	381
RELATIONS BETWEEN FUNCTIONALITY AND MACROMOLECULAR PROPERTIES OF ALTERATED COALS: THE BEHAVIOUR IN SOLUBILITY AND SWELLING P.N. Kuznetsov, R. Gruber, J. Bimer, P.D. Salbut, G. Djega-Mariadassou, A.V. Kruchinin and L.I. Kuznetsova	385

STUDIES ON THE SWELLING AND EXTRACTION OF HARD COALS AND THEIR LITHOTYPES S. Jasieńko, H. Machnikowska, U. Świetlik and H. Kaczmarska	389
SIMULATION OF COAL SWELLING BY SYNTHETIC POLYMER T. Aida, Y. Shiotani and G.-i. Senga	393
INTERACTION BETWEEN COAL AND MIXED SOLVENT SYSTEM BY MEANS OF L-BAND EPR K. Matsuoka, H. Kumagai and Y. Sanada	397
EPR CHARACTERIZATION OF COAL E. Šebestová and V. Machovič	401
VARIABLE TEMPERATURE EPR STUDIES OF ILLINOIS NO. 6 COAL TREATED WITH DONOR AND ACCEPTOR MOLECULES. R.L. Thompson, K.S. Rothenberger and H.L. Retcofsky	405
ESR STUDIES OF COAL FOLLOWING NOVEL MICROWAVE DRIVEN REACTIONS P. Monsef-Mirzai and W.R. McWhinnie	409
PYROLYSIS OF LOW-RANK COALS IN PRESENCE OF COMPLEX CATALYST: ESR STUDY Yu.N. Shvachko, L.M. Bubnovskaya, N.E. Maksimova and M.B. Shkoller	413
TREATMENT OF BROWN COAL BY METHANOL VAPOR EXPLOSION AND ITS EFFECT ON THERMAL DEGRADABILITY S. Amamoto, J.-i. Hayashi, K. Kusakabe and S. Morooka	417
LOW-TEMPERATURE DEPOLYMERIZATION OF COAL UNDER THE INFLUENCE OF ELECTRON - ACCEPTORS N.E. Maksimova, I.B. Trunova, I.A. Polyakova and N.D. Rusianova	421
THE EXTRAORDINARY FORM OF THE ORGANIC MATTER FROM COAL I. Korobetskii, E. Korobetskaya and I. Zorina	425
MOLECULAR CHARACTERISATION ON CHINESE COAL MACERALS S. Guo, L. Li, S. Li, R. Du, Q. Lu and K. Qin	429
THERMAL REACTION STUDIES OF ORGANIC MODEL COMPOUND-MINERAL MATTER INTERACTIONS IN SOLIDS A.C. Buchanan III, P.F. Britt and K.B. Thomas	433

- PYROLYSIS OF AROMATIC POLYMERS CONTAINING CARBOXYLIC ACIDS: DOES DECARBOXYLATION CORRELATE WITH CROSS-LINKING? 437
P.F. Britt, A.C. Buchanan III and R.L. Hoenigman
- COAL REACTIVITY DESCRIBED BY MODEL COMPOUNDS OXIDATION 441
M. Stefanova, I.E. Nosyrev, S.P. Marinov and N. Dimova
- ON THE POSSIBILITY OF COAL DEGRADATION BY IONIZING RADIATION: RADIATION-INDUCED C-C BOND CLEAVAGE IN 1,2-DIARYLETHANES AS MODEL COMPOUNDS OF COAL 445
M.W. Haenel, U.-B. Richter, S. Solar and N. Getoff
- EFFECT OF RANK ON THE OXIDATION RATE OF COAL 449
P. Landais, L. Gérard-Zaugg and J. Kister
- BEHAVIOR OF PREHEATED AND OXIDIZED COALS DURING PYROLYSIS 453
P. Landais, E. Langlois, J.J. Pis, M.A. Díez, R. Álvarez and J. Kister
- KINETIC STUDIES ON LOW TEMPERATURE OXIDATION OF LOW RANK COAL LITHOTYPES BY MOLECULAR OXYGEN 457
K.I. Markova, M.I. Boneva and N.S. Shopova
- MODIFICATION OF THE COMBUSTION BEHAVIOUR OF COALS OF DIFFERENT ORIGIN AND RANK BY EFFECT OF AIR PREOXIDATION 461
J.J. Pis, G. de la Puente, E. Fuente, A. Morán, J.M. Rivas and F. Rubiera
- NATURE OF HIGH OXYREACTIVITY OF OXIDATIVE ALTERED BITUMINOUS COALS 465
B. Taraba, P. Martinec, Z. Klika, E. Šebestová, H. Pavlíková and V. Machovič
- MOLECULAR HYDROGEN EMISSION DUE TO BITUMINOUS COAL WEATHERING AS A POSSIBLE SOURCE OF EXPLOSIONS IN UNDERGROUND COAL MINES 469
S.L. Grossman, S. Davidi and H. Cohen
- HAZARDOUS AND EXPLOSIVE GAS EMISSIONS ACCOMPANYING THE LOW TEMPERATURE OXIDATION OF BITUMINOUS COALS 473
S. Grossman, S. Davidi, K. Sokolov and H. Cohen
- CHEMICAL CHANGES OCCURRING DURING AERIAL OXIDATION OF A BITUMINOUS COAL 477
A.G. Pandolfo, A.S. Buchanan and R.B. Johns

SPONTANEOUS HEATING IN NEW ZEALAND COALS A.H. Clemens and T.W. Matheson	481
EVOLUTION OF TEMPERATURE AND GAS COMPOSITION IN COAL PILES J.L. Miranda, C. Romero, J.M. Andrés and D. Schmal	485
WEATHERING OF FLAME COAL - EFFECT OF TIME ON PROPERTIES AND STRUCTURE OF COAL, SEPARATED VITRITE AND COKES I. Gerus-Piasecka, K. Bratek and W. Bratek	489
LOW TEMPERATURE OXIDATION TENDING AND NON-TENDING TO SELF-IGNITION UKRAINE COALS REDUCED AND LOW- REDUCED TYPES WITH ATMOSPHERIC OXYGEN L.V. Pashchenko, V.I. Saranchuk, L.Ya. Galushko and V.A. Khazipov	493
CHARACTERIZATION OF COALS WITH RESPECT TO THEIR SELF- IGNITION TENDENCY E. Pilarczyk, P. Leonhardt and W. Wanzl	497
RETARDATION OF THE SPONTANEOUS IGNITION OF BITUMINOUS COAL X. Dong and D. Drysdale	501
B. COAL COMBUSTION AND CONVERSION SCIENCE	505
<i>B.1 COMBUSTION AND GASIFICATION</i>	<i>505</i>
SIGNIFICANT DIFFERENCE IN THE DESORPTION BEHAVIOR OF OXYGEN SURFACE COMPLEX ON CARBON IN He AND IN O ₂ Q. Zhuang, T. Kyotani and A. Tomita	507
KINETICS OF LOW TEMPERATURE COMBUSTION OF MICROPOROUS CARBON: A FRACTAL APPROACH L.G. Gordeeva, S.I. Prokopiev, V.I. Zaikovskii, L.G. Okkel and Yu.I. Aristov	511
CHANGES IN COAL CHAR REACTIVITY AND STRUCTURE WITH PYROLYSIS CONDITIONS: EFFECT OF TEMPERATURE, HEATING RATE AND PRESSURE H.-Y. Cai, A.J. Guell, I.N. Chatzakis, J.-Y. Lim, D.R. Dugwell and R. Kandiyoti	515

- THE REACTIVITY OF PULVERISED COAL AND CHAR IN SHOCK
TUBE EXPERIMENTS WITH O₂ AND CO₂ 519
F.A.C.M. Commissaris, V.E. Banin and A. Veeffkind
- INVESTIGATIONS ABOUT THE REACTION KINETICS OF BROWN
COAL COKE 523
J. Engelhard, M. Erken and U. Lenz
- STUDY OF COAL/PETROLEUM COKE COMBUSTION
CHARACTERISTIC IN PULVERISED COAL FIRED FURNACE 527
Z. Zhiguo, S. Xuexin, C. Gang, Q. Jihua and L. Fujin
- EXPERIMENTAL MEASURING OF COAL EXPLOSIBILITY FOR ITS
USE AT HYPERBARIC CONDITIONS 531
J. García Torrent, E. Conde Lázaro, E. Menéndez Pérez and J.C. Ballesteros
Aparicio
- MEASUREMENT OF COAL REACTIVITY IN THE IRONMAKING
BLASTFURNACE RACEWAY 535
C.G. Thomas, M.E. Gosnell, E. Gawronski and P.M. Nicholls
- CHARACTERIZATION OF COAL INJECTION CHARS BY
THERMOGRAVIMETRIC ANALYSIS, SCANNING ELECTRON AND
OPTICAL MICROSCOPIES AND SURFACE ANALYSIS 539
J.A. MacPhee, W.P. Hutny, L. Giroux, A.D. Palmer, J.T. Price and R.F.
Haythornthwaite
- EXPERIMENTAL STUDY ON THE COMBUSTION BEHAVIOUR OF
COAL UNDER SIMULATED BLAST FURNACE CONDITIONS 543
W.P. Hutny, J.A. MacPhee, L. Giroux and J.T. Price
- THE REACTIVITY OF COAL CHARS IN THE BLAST FURNACE 547
J.A. Turner, K.M. Thomas, D.S. Way and D.G. Richards
- COMBUSTION CHARACTERISTICS OF DIFFERENT TYPES OF COAL
UNDER BLAST FURNACE CONDITIONS 551
A. Isidro, A. Formoso, J.J. Pis, S. Ferreira, E. Fuente, J.M. Rivas, L.
García and A. Cores
- EVAPORATION OF COAL-WATER SLURRY DROPLETS 555
T. Elperin and B. Krasovitev
- AN AUTOMATIC CONTROL SYSTEM FOR CLEAN COAL
COMBUSTION ON A CHAIN-GRATE STOKER 559
D. Neuffer, P.F. MacConnell, D.H. Owens, M.A. Patrick, D. Biss and A.R.
Butt

A STUDY OF GASIFICATION REACTIVITY OF AIR-BLOWN ENTRAINED FLOW COAL GASIFIER M. Kurimura, S. Hara, J. Inumaru, M. Ashizawa, K. Ichikawa and S. Kajitani	563
STEAM GASIFICATION OF TARFAYA'S (MOROCCO) OIL SHALES K. Nabih and L. Belkbir	567
GASIFICATION REACTIVITIES OF CHARs FROM DIFFERENT LIGNITE VARIETIES A. Martínez-Alonso, V. Perrichon and J.M.D. Tascón	571
REACTIVITY OF FILTER DUSTS FROM PRESSURISED GASIFICATION J. Ranta and A. Moilanen	575
CALCULATION AND EXERGY ANALYSIS OF PROCESS SCHEMES FOR COAL GASIFICATION TO PRODUCE COKE, METHANOL, ENERGY AND HEAT ACCOMPANIED BY A CATALYTIC LIQUID PHASE PURIFICATION OF GASES AND TOXIC COMPOUNDS A.V. Gudkov, V.I. Anikeev, A. Yermakova, Z.P. Pay and V.N. Parmon	579
GASIFICATION OF COAL AS EFFICIENT MEANS OF ENVIRONMENT PROTECTION AND HYDROGENATION OF HEAVY OIL RESIDUES A.A. Krichko and A.S. Maloletnev	583
IGNITION OF COAL PARTICLES L. Manzanares-P., E.S. Garbett, D.A. Spears, M. Widdowson and G. Richards	587
SHOCK TUBE EXPERIMENTS ON IGNITION OF PULVERISED COAL PARTICLES V.E. Banin, F.A.C.M. Comissaris and A. Veefkind	591
THE EFFECT OF OXYGEN ON THE COMBUSTION AND THE IGNITION OF A CLOUD OF COAL PARTICLES Y. Rhandi, R. Gadiou, G. Prado, O. Charon and L. Philippe	595
THE EFFECTS OF PROPERTIES AND PYROLYSIS CONDITIONS ON COAL AND CHAR IGNITION AND OXIDATION REACTIVITY W. Rybak and R. Matuszkiewicz	599
IGNITION MECHANISMS OF DIFFERENT RANKS OF COALS Y. Chen, S. Mori and W.-P. Pan	603

EFFECT OF THE MINERAL MATTER CONTENT ON THE IGNITION TEMPERATURES OF SOME TURKISH LIGNITES Ç. Şentorun and S. Küçükbayrak	607
STATISTICAL KINETICS FOR CHAR COMBUSTION AND CARBON BURNOUT R.H. Hurt, E.G. Brehob and D.J. Maloney	611
COAL CHAR REACTIVITY CHARACTERISATION FOR BURN-OUT PREDICTION IN UTILITY BOILERS T.J. Beeley, J.C. Crelling, J.R. Gibbins, R. Hurt, C.K. Man and J. Williamson	615
RELATIVE IMPORTANCE OF CHEMICAL COMPOSITION AND PHYSICAL CONDITION OF THE FUEL BED FOR CARBON BURNOUT IN STOKER COMBUSTION S.V. Pisupati, D.A. Clark and A.W. Scaroni	619
TEXTURAL ASPECTS OF SELECTED HIGH VOLATILE BITUMINOUS COAL CHARs J.B. Parra, R. Menéndez, D. Álvarez, E. Lester and M. Cloke	623
COMPARISON OF CHARs PRODUCED IN A DROP-TUBE FURNACE AND COMBUSTION TEST FACILITY FROM COALS CHARACTERISED USING IMAGE ANALYSIS TECHNIQUES E. Lester, M. Cloke and W. Gibb	627
THE EFFECT OF COAL LITHOTYPE GRINDABILITY AND CHAR DEVELOPMENT ON PULVERISED FUEL COMBUSTION J.G. Bailey	631
EFFECT OF FUEL/AIR MIXING ON CHAR BURNOUT DURING PULVERIZED COAL COMBUSTION P.M. Walsh	635
MODELING THE EFFECTS OF BURNOUT ON HIGH-TEMPERATURE CHAR OXIDATION W.C. Reade, K.W. Morris and W.C. Hecker	639
SOURCE DETERMINATION AND REACTIVITY OF UNBURNT CARBON IN FLY ASH J.E. Varey, K.M. Thomas and S.H. Bottrell	643

EXPERIMENTAL INVESTIGATION OF BROWN COAL COMBUSTION WITH SIMULATED GAS TURBINE EXHAUST GAS IN A COMBINED CYCLE APPLICATION E. Kakaras and P. Vourliotis	647
STUDY OF THE FRAGMENTATION NATURE OF GRANULAR COAL PARTICLES IN A HIGH TEMPERATURE ENVIRONMENT P.J. Dacombe, S.R. Graville, M. Pourkashanian, A. Williams and L. Yap	651
EXPERIMENTAL INVESTIGATION OF ASH BEHAVIOR DURING STAGED-AIR COMBUSTION OF PULVERIZED COAL P.N. Slater, N.L. Adair, M.B. Abbott, R.L. Newsom, E. Hmouz and J.N. Harb	655
A PHASE DIAGRAM APPROACH FOR PREDICTING THE TEMPERATURE OF CRITICAL VISCOSITY FOR SLAGS H.J. Hurst	659
CONTROL OF COAL SLAGGING IN FURNACE -AERODYNAMIC INFLUENCE ON SLAGGING Z. Zhiguo, L. Fujin, Q. Jihua, S. Xuexin, L. Shilou and C. Gang	663
FBC FOULING DEPOSITS FROM ARAGON COALS R. Juan, C. Ruiz, J.M. Andrés, J. Querol and J.L. Fernández	667
DEVELOPMENT OF A DROP TUBE FURNACE BASED METHOD FOR ASSESSING THE ASH DEPOSITION CHARACTERISTICS OF SMALL SAMPLES OF PULVERISED FUELS D.I. Barnes, A. Bullock, M.W. Lewitt, D.J.A. McCaffrey, M. Smith and M. Whitehouse	671
REDUCING FLY ASH DEPOSITION FROM A BROWN COAL BY SOLID ADDITIVES H.B. Vuthaluru, J.M. Vleeskens and T.F. Wall	675
MICROSCOPIC INVESTIGATION OF Na, K AND Ca TRANSFORMATIONS DURING PULVERIZED COAL COMBUSTION N. Shah, A.D. Shah, F.E. Huggins and G.P. Huffman	679
FATE OF METAL IONS IN A BROWN COAL DURING PYROLYSIS AT LOW TEMPERATURES C.-Z. Li, K. W. Riley, M.D. Kelly and P.F. Nelson	683
ALKALI VOLATILIZATION DURING PYROLYSIS AND GASIFICATION OF COAL T. Takarada, H. Ishikawa, H. Abe and Y. Nakaike	687

- EFFECT OF HNO_3 AND NH_3 TREATMENT ON THE CATALYTIC OXIDATION OF CARBON CATALYSED BY Cu, Mo AND THEIR MIXTURE AT THE EUTECTIC COMPOSITION 691
M.C. Palma, I.F. Silva, P. Lodewyckx, J.J.M. Órfão and L.S. Lobo
- EXAFS CHARACTERIZATION OF IRON SPECIES LOADED ON COAL CHAR 695
Z. Zhu, Y. Gu, Y. Xie, X. Chen and T. Hu
- CATALYSIS IN THE CARBON-GAS REACTION 699
K.B. Bota, L.L. Sims and G.M.K. Abotsi
- MICROSCOPIC INVESTIGATION OF THE DIFFUSION OF CARBON DIOXIDE AND CATALYSTS DURING COAL GASIFICATION 703
M. Shibaoka, S.P. Chatfield, J.F. Corcoran, P. Marvig, J.D. Saxby and M.J. Wornat
- MAGNESIUM OXIDE CATALYZED STEAM GASIFICATION OF NAPHTHALENE 707
E. Betancur, A.L. Gordon and X. García
- EFFECT OF SULPHUR CONTAINING COMPOUNDS UPON THE CATALYZED STEAM GASIFICATION OF NAPHTHALENE 711
E. Betancur, X. García and A.L. Gordon
- STEAM GASIFICATION OF COAL CHARs 715
A.H. Clemens, L.F. Damiano and T.W. Matheson
- SOME FEATURES OF LIGNITE GASIFICATION IN FLUIDIZED BED OF DISPOSABLE CATALYSTS 719
B.N. Kuznetsov, M.L. Shchipko and Yu.G. Golovin
- IRON CATALYZED HYDROGASIFICATION OF BROWN COAL CHAR PROMOTED BY SPILL-OVER HYDROGEN 723
S. Matsumoto and M. Nakada
- CATALYTIC REACTION OF CO_2 WITH CH_4 FOR MAKING SYNGAS 727
W.-Y. Li, K.-C. Xie and S.-C. Guo
- SEPARATION OF FISCHER-TROPSCH CATALYST/WAX MIXTURES USING DENSE- GAS AND LIQUID EXTRACTION 731
C.M. White, K.L. Jensen, P.C. Rohar, J. Tamilia, L.J. Shaw and R.F. Hickey

CHARACTERISATION OF FLOW AND CHEMICAL PROCESSES IN AN UNDERGROUND GASIFIER AT GREAT DEPTH J.P. Pirard, A. Coëme, M. Mostade and P. Pirlot	735
UNDERGROUND COAL GASIFICATION IN ABANDONED MINES M.S. Blinderman	739
UNDERGROUND COAL GASIFICATION WITH HEAT RECUPERATION M.S. Blinderman	743
MOLECULAR ORBITAL STUDY ON INTERACTIONS BETWEEN NITROGEN FUNCTIONAL GROUPS AND O ₂ , NO MOLECULES Y. Ninomiya, H. Kato and J. Koketsu	747
THE IMPORTANCE OF FUEL-NITROGEN GROUPS IN COALS AND CHARs TO NO _x AND N ₂ O EMISSIONS DURING COMBUSTION IN A FLUIDISED BED D. Boavida, I. Gulyurtlu and L.S. Lobo	751
IMPLICATIONS OF NITROGEN RELEASE FROM COALS AT ELEVATED TEMPERATURES FOR NO _x FORMATION DURING PF COMBUSTION J.R. Gibbins, F.C. Lockwood, C.K. Man and J. Williamson	755
DROP TUBE INVESTIGATIONS INTO THE FATE OF FUEL NITROGEN DURING COAL COMBUSTION B. Bonn, H. Baumann, W. Pauly and H. Seewald	759
FUEL NITROGEN CONVERSION. COMPARISON OF A DETAILED CHEMICAL KINETIC MODEL AND GLOBAL REACTION MODELS L.S. Pedersen, P. Glarborg and K. Dam-Johansen	763
NITROGEN AND SULPHUR SPECIES RELATED TO NO _x AND SO _x EMISSIONS FROM CARBON GASIFICATION A.W. Harding and K.M. Thomas	767
MODELING OF HYDROGEN CYANIDE AND AMMONIA RELEASE DURING COAL PYROLYSIS M.A. Wójtowicz, Y. Zhao, M.A. Serio, R. Bassilakis, P.R. Solomon and P.F. Nelson	771
NITROGEN SPECIES FROM THE OXIDATIVE PYROLYSIS AND COMBUSTION OF VARIOUS COALS S. Niksa and S. Cho	775

INFLUENCE OF PRESSURE ON BLENDS ON THE COMBUSTION RATE AND POLLUTANT EMISSIONS OF BLENDS OF CHAR AND CHARCOAL	779
C. Mallet, J.P. Rouan, J.R. Richard	
KINETICS OF CATALYTIC FORMATION OF NO _x FROM NH ₃ OVER CaO BASED SORBENTS DURING FLUIDIZED BED COMBUSTION OF COAL	783
W. Lin, K. Dam-Johansen and C.M. van den Bleek	
ANALYSIS OF NO _x FORMATION IN FLUID BED COMBUSTION ON THE BASIS OF CATALYTIC ACTIVITY OF ASH ELEMENTS	787
R. Köpsel and S. Halang	
NITROUS OXIDE FORMATION UNDER FLUIDIZED BED CONDITIONS	791
B. Feng, X.S. Wang, J.W. Yuan, Z.J. Lin, D.C. Liu and B.M. Gibbs	
SULPHUR AND NITROGEN RETENTION IN CHARs AFTER PYROLYSIS AND PARTIAL GASIFICATION	795
S.P. Middleton, J.W. Patrick and A. Walker	
CHAR-N RELEASE AND REACTIVITY DURING COMBUSTION: THE EFFECT OF PYROLYSIS TEMPERATURE AND HEATING RATE	799
W.X. Wang, K.M. Thomas, H.Y. Cai, D.R. Dugwell and R. Kandiyoti	
INVOLVEMENT OF DIFFERENT SURFACE OXIDES OF CARBON IN THE REDUCTION OF NO	803
H. Baumann, Y. Tian and K.H. van Heek	
ACTIVE AREA AND SURFACE STRUCTURE IN CHAR-NO REDUCTION	807
M.A.A. Matos and F.J.M.A. Pereira	
ADVANCED BURNER DESIGN FOR PULVERISED COAL COMBUSTION IN UTILITY BOILERS	811
W.L. van de Kamp, D.J. Morgan and J.P. Smart	
THE FATE OF CHLORINE IN COAL COMBUSTION	815
W.-P. Pan, J. Keene, H.X. Li, P. Gill and M. Quattrochi	
DISTRIBUTION OF SODIUM, POTASSIUM AND CHLORINE BETWEEN SOLID AND VAPOR PHASES UNDER COAL GASIFICATION CONDITIONS	819
C.B. Muchmore, E.J. Hippo, H.L. Chen, J.L. Joslin, Jr., L. Wang, A. Hughes, S. Sivanandan, E. Daman and D.D. Banerjee	

CHLORINE BEHAVIOUR AT SALTY COALS (SC) THERMAL TREATMENT (TT) T.G. Shendrik, V.V. Simonova and L.Ya. Afanasenko	823
<i>B.2 PYROLYSIS AND CARBONIZATION</i>	827
STUDY OF THE PYROLYSIS OF BROWN COAL LUMP S. Li, S. Guo and J. Qian	829
MODELING THE DEVOLATILIZATION OF LARGE COAL PARTICLES Y. Zhao, M.A. Serio and P.R. Solomon	833
MODELING THE PYROLYSIS PRODUCT DISTRIBUTIONS FROM VARIOUS COALS WITH FLASHCHAIN S. Niksa	837
CORRELATIONS OF PYROLYSIS YIELDS WITH COAL PROPERTIES: CHARACTERISATION USING A WIRE-MESH REACTOR AND FT-IR SPECTROSCOPY H.-Y. Cai, I.N. Chatzakis, D.R. Dugwell and R. Kandiyoti	841
GAS EVOLUTION IN THE PROGRAMMED-TEMPERATURE PYROLYSIS OF COAL H. Huang, D.M. Bodily and V.J. Hucka	845
KINETICS OF COAL PYROLYSIS: A COMPARISON BETWEEN THE ISOTHERMAL AND THE NON-ISOTHERMAL METHODS M.J. Lázaro, R. Moliner and J.V. Ibarra	849
NATURE OF CHANGES IN OXYGEN-CONTAINING GROUPS DURING PYROLYSIS OF BROWN COAL L.F. Butuzova, A. Krztoń and G.I. Zheryakova	853
DETERMINATION OF SULPHUR RELEASE FROM THE RAPID PYROLYSIS OF COALS. KINETIC DETERMINATION AND ITS APPLICATION TO LARGE COAL PARTICLES F. García-Labiano, J. Adánez, E. Hampartsoumian and A. Williams	857
INTERACTIONS BETWEEN WATER, TARS AND COKE DURING COAL PYROLYSIS L. Mansuy, P. Landais and R. Michels	861

LOW TEMPERATURE CONVERSION OF COALS THROUGH INTERCALATION AND NUCLEOPHILIC REACTIONS V.A. Kucherenko, T.I. Zubova and T.V. Khabarova	865
EFFECT OF FLAME ENVIRONMENT ON SOOT FORMATION IN COAL COMBUSTION J. Ma, T.H. Fletcher and B.W. Webb	869
PYROLYSIS OF COAL AND WASTE OIL MIXTURES C. Braekman-Danheux, F. Bruart, A. Fontana and A. Labani	873
EVALUATION OF SYNERGISM IN COAL/HEAVY OIL COPYROLYSIS BY PYROLYSIS/GAS CHROMATOGRAPHY I. Suelves, R. Moliner, M.J. Lázaro and J.V. Ibarra	877
COMPARISON OF BIOMASS ROTARY KILN PYROLYSIS TO COAL PYROLYSIS W. Klose and W. Wiest	881
CHARACTERIZATION OF PYROLYSIS-OILS FROM BIOMASS: A COMPARISON WITH COAL DERIVED LIQUIDS R. Maggi and B. Delmon	885
THERMOGRAVIMETRIC AND MASS SPECTROSCOPIC ANALYSES OF SOLVENT-REFINED POWELLTON COAL, WEST VIRGINIA (U.S.A.) E.L. Fuller, O.C. Kopp and M.R. Rogers	889
TREATMENT MECHANISM AND PROPERTIES OF LOW-RANK COAL THERMOBRIQUETTED PRODUCTS A.P. Fomin and O.G. Potapenko	893
STEP-WISE PYROLYSIS OF BITUMINOUS COAL IN A STREAM OF WATER VAPOUR V. Minkova, M. Razvigorova, M. Goranova, N. Russianova	897
THE PROPERTIES OF THE COAL AND STEAM CONDENSATE FROM PRESSURISED STEAM DRYING G.D. Bongers, F. Woskoboenko, W.R. Jackson, A.F. Patti and P.J. Redlich	901
FLASH PYROLYSIS OF COAL. FORMATION OF VOLATILES AT DIFFERENT TEMPERATURES J.V. Christiansen, S. Gouin, C. Jespersen and L. Carlsen	905

THE FATE OF SULPHUR, CHLORINE AND TRACE ELEMENTS DURING THE FLASH PYROLYSIS OF COAL M. Ściążko, K. Kubica, M. Czaplicka, K.M.L. Holden, K.D. Bartle and S.C. Mitchell	909
THE INFLUENCE OF CARBONIZATION VARIABLES ON CHAR STRUCTURE M.J. Lázaro, R. Moliner and J.V. Ibarra	913
THE EFFECTS OF ION-EXCHANGED METALS ON THE COMPOSITION OF BROWN COAL TARS PRODUCED IN A FLUIDIZED BED REACTOR M.J. Wornat, B.A. Vernaglia, C.-Z. Li and P.F. Nelson	917
EFFECT OF MINERAL MATTER AND OXIDATION ON THE EVOLUTION OF LOW MOLECULAR WEIGHT COMPOUNDS DURING PYROLYSIS F. Mondragon, A. Jaramillo, G. Quintero, F. Saldarriaga, E. Bedoya, W. Ruiz, J. Fernandez and P. Hall	921
KINETICS OF POROSITY EVOLUTION DURING FAST HEATING OF COAL J. Tomeczek and S. Gil	925
SIZE DISTRIBUTION OF MICROPORES IN RAPID PYROLYSIS CHAR Y. Matsuo, J.-i. Hayashi, K. Kusakabe and S. Morooka	929
CONSERVATION OF MICROPOROUS STRUCTURE OF COAL IN THE COURSE OF CARBONIZATION AND ITS TRANSITION INTO PRODUCTS OF HEAT TREATMENT Z. Weishauptová, J. Medek, V. Balek and I. Sýkorová	933
RELATION BETWEEN COAL TARS AND FORMATION OF CARBON DEPOSITS IN COKE OVENS J. Pajak, V. Krebs, J.F. Marêché and G. Furdin	937
STUDY OF CARBON DEPOSITION IN COKE OVENS V. Krebs, J.F. Marêché, G. Furdin and D. Dumay	941
MONITORING OF STRUCTURAL CHANGES DURING PITCH PREPARATION BY LC AND ¹³ C NMR Y. Martín, J.M. Andresen, R. García, R.A. Solé, C.A. Luengo, C.E. Snape and S.R. Moineo	945

CHARACTERISATION OF LARGE MOLECULAR MASS MATERIALS IN COAL TAR PITCH FRACTIONS SEPARATED BY PLANAR CHROMATOGRAPHY A.A. Herod and R. Kandiyoti	949
THIN-LAYER CHROMATOGRAPHY WITH FLAME IONIZATION DETECTION IN THE CHARACTERIZATION OF PITCHES V.L. Cebolla, L. Membrado, J. Vela and J.M. Andrés	953
QUANTITATIVE GROUP-TYPE ANALYSIS OF COAL TAR PITCHES L. Membrado, V.L. Cebolla and J. Vela	957
STRUCTURAL COMPOSITION OF COAL TAR PITCHES BY ¹³ C-NMR C.G. Blanco, C. Díaz and M.D. Guillén	961
COMPARISON OF DISTRIBUTION AND STRUCTURE OF EXTROGRAPHY FRACTIONS OF PITCHES DERIVED FROM COAL PYROLYSIS AND LIQUEFACTION J. Machnikowski, M.A. Díez, R. Álvarez, J. Bermejo and H. Machnikowska	965
IMPLICATIONS OF REDUCTIVE HYDROGENATION AND ALKYLATION IN THE CHARACTERIZATION OF TI FRACTIONS OF COAL TAR PITCHES A.I. González de Andrés, Y. Martín, R. García, J.M. Andresen, C.E. Snape and S.R. Moineiro	969
EFFECT OF AIR-BLOWING AND CARBON BLACK ADDITION ON PITCH CARBONIZATION BEHAVIOUR J.J. Fernández, A. Figueiras, M. Granda, J. Bermejo, Y. Korai, I. Mochida and R. Menéndez	973
EMPLOYMENT OF HYDROGENATED ANTHRACENE OIL AS A PITCH-MAKING ADDITIVE J. Álvarez, F. Díez, R. Rosal and H. Sastre	977
THERMOGRAVIMETRIC STUDY ON PYROLYSIS FOR FLUIDIZED BED GASIFICATION OF BIOMASS/POOR COAL BLENDS Y.G. Pan, E. Velo and L. Puigjaner	981
EXPERIMENTAL ANALYSIS OF A FREE FALL REACTOR H. Takahashi, T. Kojima, Y. Yamashita, H. Kawashima and A. Inaba	985
THE IDENTIFICATION OF DANGEROUSLY COKING COALS C. Barriocanal, J.W. Patrick, A. Walker and A.R. Walker	989

STUDY ON PYROLYTIC BEHAVIOR OF COKING COAL M. Nomura, K. Kidena, A. Yamamoto and S. Murata	993
CHEMISTRY OF COAL THERMOPLASTICITY A. Marzec and S. Czajkowska	997
STUDIES ON PERMEABILITY OF COAL PLASTIC LAYER B. Bujnowska and A. Kozłowski	1001
CHARACTERISATION OF A SERIES OF PARTIALLY-CARBONISED COALS BY SOLID STATE ^1H AND ^{13}C NMR M.M. Maroto-Valer, C.E. Snape, R.R. Willmers, C.J. Atkinson and K.W.G. Loudon	1005
INTERACTIONS BETWEEN COALS AND AROMATIC HYDROCARBONS AT ELEVATED TEMPERATURES R. Sakurovs	1009
EFFECT OF INFUSIBLE CARBONACEOUS ADDITIVES ON COKING COAL FUSIBILITY R. Sakurovs, L. Burke and R.J. Tyler	1013
THE INFLUENCE OF ALKYLATION ON THERMOPLASTIC PORPRTIES OF COALS A. Koch, R. Gruber, D. Cagniant and I. Nosyrev	1017
CONSTRUCTION AND OPERATION OF A DEMONSTRATIVE PLANT OF BEEHIVE OVENS FOR PRODUCING COKE WITH THE UTILIZATION OF THE ENERGY OF GASES A. Díaz Chaves and A. White	1021
PYROLYSIS OF SLIGHTLY COKING COAL UNDER THE LOAD OF MECHANICAL PRESSURE FOR ENHANCING CAKING PROPERTIES K. Miura, K. Niwa, D. Tsutsumi and H. Nakagawa	1025
PYROLYSIS BEHAVIOUR OF MIXTURES FROM DIFFERENT COALS WITH RESPECT TO COKE FORMATION I. Wegener, W. Wanzl and K.H. van Heek	1029
CO-COKING OF COAL WITH REACTIVE PITCHES FROM WASTE PLASTICS G. Collin and J. Polaczek	1033

- INFLUENCE OF HIGH-TEMPERATURE TREATMENT UP TO 2400°C ON STRUCTURAL PARAMETERS OF COKES PRODUCED FROM COAL WITH SOME ADDITIVES 1037
M. Legin-Kolar and A. Radenović
- ON THE EVALUATION OF THE REACTIVITY OF COALS IN CO-CARBONIZATION WITH ORGANIC ADDITIVES 1041
S.A. Aipshtein and V.V. Malkova
- CATALYSIS OF THERMOCHEMICAL TRANSFORMATIONS IN POORLY CAKING GAS COALS DURING COKING PROCESS 1045
M.B. Shkoller, N.D. Rus'yanova, N.E. Maximova, L.V. Shishmina and Ja.A. Belikhmaer
- SEMI-COKE OF HIGH SPEED BROWN COAL PYROLYSIS AS COMPONENT OF COAL BLENDS FOR COKING PROCESS AND FUEL FOR INJECTION INTO BLAST FURNACES 1049
M.B. Shkoller, V.A. Karasev, G.E. Slepzov, A.K. Gusarov and V.G. Misin
- THE RELATION BETWEEN PHYSICOCHEMICAL PROPERTIES OF HIGH VOLATILE BITUMINOUS COALS AND STRUCTURE OF SEMICOKES AND COKES 1053
B. Bujnowska and M. Zielińska-Blajet
- SIMULATION AND OPTIMIZATION OF COLOMBIAN COAL MIXTURES IN COKEMAKING 1057
J.E. Pedraza, D. Laverde, C. Vásquez, A. Rincon and S. Niño
- QUALITY OF INTERFACES BETWEEN TEXTURAL COMPONENTS IN METALLURGICAL COKES 1061
C. Barriocanal, S. Hanson, J.W. Patrick and A. Walker
- MICROTEXTURAL AND REFLECTANCE STUDIES OF COKES DERIVED FROM INERTINITE RICH COALS 1065
A.K. Varma
- ANTHRACITE COAL AS A LEANING COMPONENT OF COAL BLENDS.- PROPERTIES AND STRUCTURE OF BLENDS AND COKES 1069
K. Bratek, W. Bratek and I. Gerus-Piasecka
- COKE REACTIVITY AND MECHANICAL STRENGTH AFTER SOLUTION LOSS WITH VIEW TO BLAST FURNACE OPERATION 1073
P. Arendt, H. Bellenberg, W. Rohde and W. Eisenhut

DEPENDENCE OF MICROHARDNESS OF COKE ON CARBON CONTENT AND FINAL COKING TEMPERATURE M. Kaloč and P. Dvořák	1077
INFLUENCE OF NATURAL WEATHERING OF TWO COKING COALS OF SIMILAR RANK ON COKE QUALITY R. Alvarez, M.D. Casal, C.S. Canga, M.A. Diez, A.I. González, M. Lázaro and J.J. Pis	1081
INFLUENCE OF PREHEATING DIFFERENT RANK COALS ON COKE STRUCTURE M.A. Diez, J.N. Rouzaud, R. Alvarez, J.A. Menéndez and J.J. Pis	1085
THE VALORIZATION OF CARBON CONTAINING WASTES IN CLASSICAL COKING PLANTS A. Fontana, C. Braekman-Danheux and Ph. Laurent	1089
CHARACTERIZATION AND COCARBONIZATION BEHAVIORS OF DELAYED COKES PREPARED FROM COAL TAR AND PETROLEUM RESIDUE I. Mochida, M. Ando, K. Sakanishi, Y. Korai, T. Aramaki and T. Okuhara	1093
DRIFT STUDY OF PITCHES AND SEPARATED MESOPHASE J. Machnikowski, A. Krztoń, J.V. Weber, T. Zimny, J. Petryniak and I. Więcek	1097
PRODUCTION OF ADSORBENT CARBON FROM ILLINOIS COAL FOR NATURAL GAS STORAGE J. Sun, M. Rostam-Abadi, A.A. Lizzio and M.J. Rood	1101
ACTIVE CARBON FROM COAL BY CHEMICAL TREATMENT F. Mondragon, J.J. Fernandez, A. Jaramillo, G. Quintero, J. Zapata, L.J. Hoyos and P. Hall	1105
PRODUCTION OF ACTIVATED CARBON FROM A PEATY (AĞLAÇLI) COAL E. Apak, M. Jagtoyen, A. Akar, E. Ekinçi and F. Derbyshire	1109
ACTIVATED CARBONS FROM BITUMINOUS COAL IN A FLUIDIZED BED PILOT PLANT. INFLUENCE OF THE OPERATING VARIABLES I. Martín-Gullón, M. Asensio, A. Marcilla and R. Font	1113
FORMED ACTIVATED CARBONS FROM LOW RANK COAL M. Jagtoyen and F. Derbyshire	1117

- PRODUCTION OF ACTIVATED CARBON FROM CANADIAN COAL BY CHEMICAL ACTIVATION 1121
J. Hayashi, A.P. Watkinson, K.C. Teo, S. Takemoto and K. Muroyama
- ACTIVATED CARBONS FROM A BITUMINOUS COAL: INFLUENCE OF THE DEMINERALIZATION PROCESS 1125
M.V. López-Ramón, F.J. Maldonado-Hódar, F. Carrasco-Marín, C. Moreno-Castilla and J. Rivera-Utrilla
- ON THE PREPARATION AND THE CHARACTERIZATION OF MICROPOROUS CARBONS DERIVED FROM ASTURIAN ANTHRACITE AND BITUMINOUS COAL 1129
T.A. Centeno and F. Stoeckli
- MECHANICAL PROPERTIES OF SORBENTS FROM BROWN COALS 1133
P. Straka and J. Buchtele
- POROUS STRUCTURE OF STEAM ACTIVATED CHARs FROM FLAME COAL, ORTHOCOKING COAL AND ANTHRACITE, PEOXIDIZED IN DIFFERENT PARTICLE SIZES 1137
A. Jankowska
- NITROGEN, BENZENE, AMMONIA AND CARBON DIOXIDE ADSORPTION ON STEAM ACTIVATED CHARs FROM MIXTURES OF COAL TAR PITCH WITH GRAPHITE-FeCl₃ INTERCALATION COMPOUNDS 1141
A. Albiniak, E. Broniek, J. Kaczmarczyk, A. Jankowska, T. Siemieniowska, B. McEnaney, X.S. Chen, G. Furdin, D. Bégin, E. Alain and J.F. Mareché
- MAIN CARBONIZATION RELATIONSHIPS OF CAKING COAL DERIVED GRANULES 1145
S.I. Surinova
- SYNTHESIS OF CARBON MOLECULAR SIEVES FROM CHARs PRODUCED IN A COAL RETORTING PROCESS 1149
J. Qiu and S. Guo
- A NEW METHOD FOR THE REGENERATION OF ACTIVATED CARBON 1153
F. Salvador, C. Sánchez-Jiménez and M^aD. Merchán
- COAL BASED ACTIVATED CARBON FIBER COMPOSITES FOR GAS SEPARATION 1157
G.M. Kimber, Y.Q. Fei, M. Jagtoyen and F.J. Derbyshire

PREPARATION AND PROPERTIES OF CARBON FIBERS DERIVED FROM A SPANISH COAL TAR PITCH J. Alcañiz-Monge, D. Cazorla-Amorós, A. Linares-Solano, A. Oya, A. Sakamoto and K. Hoshi	1161
PETROLEUM AND COAL DERIVED COKES IN THE SYNTHESIS OF SiC F.J. Narciso-Romero, F. Rodríguez-Reinoso and M.A. Díez	1165
RESINOUS BINDERS FOR COAL AND CHARs E.S. Olson, R.K. Sharma and B.C. Young	1169
ELECTRODE GRADE CARBONS PREPARED WITH DIFFERENT PITCH BINDERS C.A. Luengo, J.D. Rocha, J.T. Julian, Y. Martín, R. García, and S.R. Moineiro	1173
INDUSTRIAL PROCESS FOR PREPARING FULLERENES FROM COAL M.A. Wilson, L.S.K. Pang and Y. Inukai	1177
MECHANISM OF PLASMA-ARC FORMATION OF FULLERENES FROM COAL AND RELATED MATERIALS L.S.K. Pang, M.A. Wilson, R.A. Quezada and R.J. Pallasser	1181
<i>Author Index</i>	<i>1185</i>

VOLUME II

<i>B.3 LIQUEFACTION AND HYDROLYSIS</i>	<i>1201</i>
A NOVEL REACTOR SYSTEM FOR STUDYING THE KINETICS OF COAL LIQUEFACTION AND RELATED PROCESSES AT VERY SHORT REACTION TIMES H. Huang, D.M. Fake, M.T. Klein and W.H. Calkins	1203
KINETICS OF THERMAL AND CATALYZED COAL LIQUEFACTION AT VERY SHORT REACTION TIMES USING A NOVEL BATCH REACTOR AND THERMOGRAVIMETRIC ANALYSIS H. Huang, K. Wang, M.T. Klein and W.H. Calkins	1207

NOVEL ASPECTS ON COAL LIQUEFACTION MECHANISM BY THE USE OF TRITIUM AND ³⁵ S TRACER METHODS M. Godo and T. Kabe	1211
RETROGRESSIVE REACTIONS IN CATALYTIC COAL LIQUEFACTION USING DISPERSED MoS ₂ C. Song, A.K. Saini and H.H. Schobert	1215
SIMULATION OF NONISOTHERMAL PROCESSES OF COAL LIQUEFACTION USING A DISPERSED CATALYST PRECURSOR E.F. Stefoglo, A.B. Garcia and H.H. Schobert	1219
KINETIC STUDY OF PRIMARY HYDROGENATION REACTION IN BROWN COAL LIQUEFACTION (BCL) PROCESS S. Yanai, M. Makino, S. Ueda, T. Okui, O. Okuma, Y. Kageyama and T. Matsumura	1223
BEHAVIOR OF HYDROGEN AT COAL LIQUEFACTION OF NEDOL PROCESS M. Mochizuki, K. Endo and K. Inokuchi	1227
RELATIONSHIP BETWEEN HYDROGEN-DONATING ABILITIES AND STRUCTURAL PARAMETERS OF SOLVENT SYSTEMS IN COAL LIQUEFACTION S. Futamura	1231
HYDROGEN TRANSFER IN BROWN COAL LIQUEFACTION IN BCL PROCESS -- INFLUENCE OF CATALYST AND FEED SOLVENT PROPERTIES ON LIQUEFACTION PERFORMANCE AND HYDROGEN TRANSFER -- O. Okuma, M. Yasumuro, T. Matsumura and S. Yanai	1235
HEAT TREATMENT OF COALS IN HYDROGEN-DONATING SOLVENTS AT TEMPERATURES AS LOW AS 175-300°C M. Iino, J. Shen, S. Ashida and T. Takanohashi	1239
COMPARATIVE ROLES OF HYDROGEN GAS AND SOLVENT IN LIQUEFACTION OF LOW-RANK COALS L. Huang and H.H. Schobert	1243
POSSIBLE IMPACTS OF COAL PROPERTIES ON THE COAL CONVERSION TECHNOLOGY K. Okada	1247

INFLUENCE OF LOW TEMPERATURE TREATMENT ON LIGNITE STRUCTURE AND ITS LIQUEFACTION BEHAVIOUR V.I. Sharypov, B.N. Kuznetsov, S.V. Baryshnikov, V.G. Chumakov and N.G. Beregovtsova	1251
DETERMINATION OF TRANSFERABLE HYDROGEN IN COAL (1). REACTION BEHAVIOR OF COAL WITH IODOMETHANE T. Yoshida, M. Sasaki, M. Yamamoto and T. Kotanigawa	1255
EFFECT OF ENHANCED CONTACT BETWEEN FINELY PULVERIZED COAL AND CATALYST ON LIQUEFACTION Y. Sato, T. Kamo and M. Shiraishi	1259
LIQUEFACTION OF BLENDED COALS AND THEIR EFFECT ON PRODUCT YIELDS A. Pickering, J. Taylor, A. Belghazi, M. Cloke and J.W. Patrick	1263
CHARACTERISATION OF COALS FOR LIQUEFACTION USING IMAGE ANALYSIS A. Pickering, E. Lester and M. Cloke	1267
LIQUEFACTION OF COAL AND COAL FRACTIONS OF DIFFERENT RELATIVE DENSITIES FROM A HYDROCYCLONE SEPARATOR J. Barraza, M. Cloke, A. Belghazi and N. Miles	1271
UTILIZATION OF THERMODYNAMIC DATABASE IN THE SYSTEMS USING MOLYBDATE AND IRON BASED CATALYSTS Y. Yoshimura, H. Yasuda, T. Sato, H. Shimada, N. Matsubayashi, M. Imamura and A. Nishijima	1275
IN-SITU XAFS SPECTROSCOPIC STUDIES OF DCL CATALYSTS N. Shah, J. Zhao, K.R.P.M. Rao, F.E. Huggins and G.P. Huffman	1279
INFLUENCE OF OPERATING CONDITIONS ON THE EFFECT OF CATALYSTS IN COAL LIQUEFACTION I. de Marco, B. Caballero, M.J. Chomón and J.A. Legarreta	1283
ADVANCED CATALYSTS FOR COAL-DERIVED LIQUIDS HYDROTREATING VIA ACIDIC SUPPORTS J.F. Cambra, P.L. Arias, B. Güemez, J.A. Legarreta, B. Pawelec and J.L.G. Fierro	1287
EFFECT OF TYPE OF Mo CATALYST ON COAL LIQUEFACTION S. Ohshima, M. Yumura, Y. Kuriki, K. Uchida, K. Kamiya and F. Ikazaki	1291

- LIQUEFACTION ACTIVITY OF SUPPORTED NiMo CATALYSTS WITH
FUNCTIONS FOR RECOVERY 1295
H. Taniguchi, H. Hasuo, S.H. Yoon, K. Sakanishi and I. Mochida
- THE EFFECT OF PRESSURE ON FIRST STAGE COAL LIQUEFACTION
AND SOLVENT HYDROGENATION WITH SUPPORTED CATALYSTS 1299
A.V. Cugini, K.S. Rothenberger, G.A. Veloski, M.V. Ciocco and C.
McCreary
- CARBON CATALYSTS FOR REACTIONS RELEVANT TO COAL
LIQUEFACTION 1303
M. Farcasiu, P.B. Kaufman, E.P. Ladner, F. Derbyshire and M. Jagtoyen
- THE ROLE OF CATALYST IMPREGNATION AND SOLVENT TYPE IN
IMPROVING LIQUEFACTION EFFICIENCIES 1307
F. Pinto, I. Gulyurtlu, L.S. Lobo and I. Cabrita
- SCALE FORMATION MECHANISM ON COAL HYDROGENATION
WITH IRON CATALYST 1311
O. Togari, M. Kobayashi, K. Hirano, S. Suzuki, H. Yoshida and S. Ueda
- DEACTIVATION OF PYRITE FeS_2 CATALYST WITH OXIDATION AND
ITS REACTIVATION 1315
E. Ogata, T. Hojo, A. Nishijima, E. Niki, K. Mashimo and T. Wainai
- EFFECT OF SYNTHETIC PYRITE AND PULVERIZED NATURAL
PYRITE AS COAL LIQUEFACTION CATALYST 1319
K. Inokuchi, Y. Nogami, T. Okada, M. Kobayashi, M. Mochizuki and K.
Endou
- SEPARATION OF IRON CATALYST FROM COAL LIQUEFACTION
CRUDE OIL WITH HIGH GRADIENT MAGNETIC SEPARATOR 1323
H. Narita, R. Yoshida and Y. Maekawa
- ACTIVITY AND SELECTIVITY OF Fe CATALYSTS FROM
ORGANOMETALLIC AND INORGANIC PRECURSORS FOR
HYDROCRACKING OF 4-(1-NAPHTHYLMETHYL) BIBENZYL 1327
C. Song, E. Schmidt and H.H. Schobert
- ENHANCING THE DISPERSION OF CATALYSTS IN DIRECT COAL
LIQUEFACTION 1331
J. Zhao, Z. Feng, F.E. Huggins and G.P. Huffman
- IRON FROM TWO DIFFERENT CATALYTIC PRECURSORS IN COAL
HYDROGENATION 1335
A.M. Mastral, M.C. Mayoral, B. Rubio, M.T. Izquierdo and J.M. Palacios

- PRECONVERSION CHEMISTRY AND LIQUEFACTION OF COAL IN THE PRESENCE OF A MOLYBDENUM-CONTAINING CATALYST 1339
R.P. Warzinski, B.C. Bockrath, G.A. Irdi, H.B. Booher and A.W. Wells
- APPLICATION OF EXFOLIATION TECHNIQUES TO THE PREPARATION OF MoS_2 LIQUEFACTION CATALYSTS 1343
B.C. Bockrath and D.S. Parfitt
- SYNTHESIS AND CATALYTIC ACTIVITY OF ULTRA FINE METAL SULFIDE PARTICLES 1347
Y. Kuriki, M. Yumura, S. Ohshima, K. Uchida and F. Ikazaki
- BATCH VS. CONTINUOUS EXPERIMENTS IN COAL HYDROGENATION 1351
B.O. Strobel
- THREE STAGE CATALYTIC HYDROLIQUEFACTION OF COAL: HOW TO IMPROVE HYDROGEN TRANSFERS TO COAL 1355
M. Jamond, R. Bacaud, B. Pepin-Donat, H. Charcosset and G. Djega-Mariadassou
- SINGLE AND MULTISTAGE REACTIONS OF VARIOUS COALS TO PRODUCE HIGH YIELDS OF FLUID FUEL 1359
C.K.J. Hulston, P.J. Redlich, W.R. Jackson, F.P. Larkins and M. Marshall
- MULTI-STAGE COAL REACTIONS IN CARBON MONOXIDE-CONTAINING ATMOSPHERES USING ALKALINE AND HYDROGENATION CATALYSTS 1363
C.K.J. Hulston, W.R. Jackson, F.P. Larkins, M. Marshall and P.J. Redlich
- EFFECT OF HEATING RATE ON NORMAL AND CATALYTIC FIXED-BED HYDROLYSIS 1367
L. Baoqing, S.C. Mitchell and C.E. Snape
- EFFECT OF INCREASE IN GAS FLOW RATE ON COAL LIQUEFACTION WITH HIGHLY DISPERSED CATALYSTS 1371
M. Yasumuro, S. Katsushima, Y. Kageyama and T. Matsumura
- EFFECTS OF COAL PRETREATMENT AND CATALYST RECOVERY ON THE LIQUEFACTION 1375
K. Sakanishi, H. Hasuo, H. Taniguchi, I. Mochida and O. Okuma
- EFFECT OF GAMMA-RADIATION ON STRUCTURE, REACTIVITY AND THE PROCESS OF LIQUEFACTION OF BROWN COALS 1379
G.B. Skripchenko, G.S. Golovin and V.I. Sekriyeru

- EFFECTS OF CHLOROBENZENE TREATMENT ON COAL STRUCTURE AND LIQUEFACTION BEHAVIOUR 1383
I. Cepni, O. Sirkecioglu, C.A. McArthur, P.J. Hall and C.E. Snape
- CHARACTERIZATION OF LIQUEFACTION/SOLUBILIZATION MECHANISMS OF SPANISH COALS BY NEWLY ISOLATED MICROORGANISMS 1387
F. Laborda, M.F. Redondo, N. Luna and I.F. Monistrol
- STRONG PROMOTING EFFECT OF H₂O ON COAL LIQUEFACTION USING WATER-SOLUBLE AND OIL-SOLUBLE Mo CATALYST PRECURSORS 1391
C. Song, A.K. Saini and J. McConnie
- LOW TEMPERATURE LIQUEFACTION OF COAL WITH SIMULATED COKE OVEN GAS 1395
H. Yamaguchi, Y. Sato and K. Matsubara
- COAL PYROLYSIS WITH METHANE IN A REDUCING ENVIRONMENT 1399
M.F. Voigtmann, M. Chen and B.D. Batts
- SUPERCRITICAL FLUID EXTRACTION OF HIGH VOLATILE BITUMINOUS COALS FROM THE SAAR REGION, GERMANY. INFLUENCE OF EXTRACTION PARAMETERS ON EXTRACT YIELD AND COMPOSITION 1403
G. Götz, H. Hammer and M. Wolf
- SUPERCRITICAL WATER EXTRACTION OF COAL AND CATALYTIC REFORMING OF EXTRACTS IN SUPERCRITICAL FLUID 1407
T. Adschiri, S. Nagashima and K. Arai
- ROLE OF AROMATIC STRUCTURE IN PATHWAYS OF HYDROGEN TRANSFER AND BOND CLEAVAGE IN COAL LIQUEFACTION: THEORETICAL STUDIES 1411
J.A. Franz, T. Autrey, D.M. Camaioni, J. D. Watts and R.J. Bartlett
- ROLE OF ADDITIVES IN DIARYLALKANE DEGRADATION AS A MODEL REACTION OF COAL LIQUEFACTION 1415
X.-Y. Wei, E. Ogata and E. Niki
- THE USE OF POLYSTYRENE NETWORKS AND PHENOLIC RESITES TO MODEL THE EFFECTIVENESS OF Fe AND Mo CATALYSTS IN COAL HYDROLYSIS 1419
S.D. Brown, M.C. Mayoral, O. Sirkecioglu and C.E. Snape

HYDROGEN TRANSFER MECHANISM IN THE CRACKING OF C-C BOND IN COAL MODEL COMPOUNDS N. Ikenaga, T. Sakoda, T. Matsui, K. Ohno and T. Suzuki	1423
THERMAL CRAKING OF COAL STRONG BONDS ON DIARYL ETHERS' AND DIARYLMETHANES' MODELS E.N. Grigorieva, T.L. Fedorova, D.N. Kagan, V.Yu. Korobkov, S.S. Panchenko and I.V. Kalechitz	1427
HYDROGEN SHUTTLING PATHWAYS IN THERMAL HYDROLIQUEFACTION: SOLVENT-INDUCED SCISSION OF COAL MODEL COMPOUND STRUCTURES T. Autrey, T. Powers, E.A. Alborn, D.M. Camaioni and J.A. Franz	1431
MOLECULAR MASS DISTRIBUTIONS OF COAL PRODUCTS RELEVANT TO PYROLYSIS, LIQUEFACTION AND COMBUSTION K.D. Bartle, A.A. Herod, P. John, B.R. Johnson, C.A.F. Johnson, R. Kandiyoti, J.E. Parker and G.P. Smith	1435
TRUCTURAL COMPARISON OF COAL LIQUEFACTION EXTRACTS AND HYDROCRACKING PRODUCTS S.-F. Zhang, B. Xu, A.A. Herod and R. Kandiyoti	1439
CHARACTERIZATION OF HYDROPYROLYSIS PRODUCTS A.M. Mastral, M.J. Pérez-Surio, M.C. Mayoral, M.S.Callén and R. Murillo	1443
SEPARATION OF COAL TAR COMPONENTS BY THE SUPERCRITICAL CO ₂ SOLVENT THROUGH THE ADSORPTION AND STRUCTURAL MODIFICATION K. Sakanishi, H. Obata, I. Mochida and R. Sakaki	1447
VAPOR PRESSURE ESTIMATION FOR HYDROCARBONS IN A COAL DERIVED LIQUID S.-y. Harikae, M. Satou, T. Chiba, S. Yokoyama and Y. Sanada	1451
ASSESSMENT OF QUALITY OF COAL-HEAVY OIL INTERACTION PRODUCTS BY MEANS OF FLUORESCENCE SPECTROSCOPY L. Pacheco, L.E. Henao and J.M. Rincón	1455
OPTICAL PROPERTIES OF SCT EXTRACTION RESIDUES OBTAINED FROM TURKISH COALS E.S. Vayisoğlu, K.D. Bartle and N.G. Erbatur	1459
PERSPECTIVE IN RESEARCH OF COAL LIQUIDS BY USING SPIN PROBE TECHNIQUE T.P. Miloshenko, S.A. Alekseev and A.A. Shklyayev	1463

- HYDROPROCESSING OF AN ASPHALTENIC COAL RESIDUE 1467
A.M. Benito, M.T. Martínez and J.L. Miranda
- EFFECT OF LOW TEMPERATURE TAR UPGRADING CONDITIONS 1471
ON CHEMICAL COMPOSITION OF FUEL FRACTIONS
E. Śliwka and J. Surygala
- SOLVENT EFFECTS OF FRACTIONS FROM COAL LIQUID ON THE 1475
UPGRADING REACTION OF COAL LIQUEFACTION RESIDUE
K. Mashimo, M. Sugano and T. Wainai
- ZEOLITE CATALYST FOR HYDROCRACKING COAL-DERIVED 1479
DISTILLATES -CLEAVAGE OF NAPHTHENIC RINGS OVER ZEOLITE
CATALYSTS-
T. Kameoka, K. Masuda, A. Kinoshita, T. Sato, Y. Yoshimura, H. Shimada,
N. Matsubayashi and A. Nishijima
- REMARKABLE INCREASE OF BTX YIELD BY ZEOLITE CATALYST 1483
IN THE HYDROCRACKING OF COAL VOLATILE MATTER
M. Chareonpanich, Z.-G. Zhang, A. Nishijima and A. Tomita
- HYDROCRACKING REACTIVITIES OF POINT OF AYR COAL 1487
EXTRACTS FROM A FLOWING-SOLVENT REACTOR, A MINIBOMB
AND A PILOT PLANT
S.-F. Zhang, B. Xu, A.A. Herod, D.R. Dugwell and R. Kandiyoti
- INFLUENCE OF HYDROGEN DONOR SOLVENT ON KINETIC 1491
FEATURES OF HYDROGENATION OF SOME FLUID PRODUCTS OF
COAL LIQUEFACTION
I.G. Sudakova
- CHARACTERIZATION OF Ni-W/Al₂O₃ CATALYST USED IN COAL 1495
LIQUID UPGRADING
N. Matsubayashi, T. Sato, H. Shimada, M. Imamura, Y. Yoshimura, A.
Nishijima, T. Kameoka and K. Masuda
- RETROGRESSIVE REACTIONS IN COAL/OIL COPROCESSING IN 1499
VIEW OF SPECTROSCOPIC AND MICROSCOPIC EXAMINATION
J. Černý, I. Sýkorová, G. Šebor, D. Maxa and J. Blažek
- USE OF IRON-BASED DISPOSABLE CATALYSTS FOR 1503
COPROCESSING OF COAL AND HEAVY OIL RESIDUES IN SOLVENT
AUGMENTED COAL LIQUEFACTION
M.W. Badger and G. Harrison

COPROCESSING COAL AND NATURAL GAS FOR LIQUID FUEL WITH REDUCED GREENHOUSE GAS CO ₂ EMISSION M. Steinberg	1507
FLASH CO-PYROLYSIS OF COAL RETAINING DEPOLYMERIZED POLYETHYLENE AS RADICAL DONOR H. Tomita, J.-i. Hayashi, K. Kusakabe and S. Morooka	1511
COLIQUEFACTION OF COAL AND WASTE POLYMERS L.L. Anderson, W. Tuntawiroon and W.B. Ding	1515
DIRECT LIQUEFACTION OF WASTE PLASTICS AND COLIQUEFACTION OF WASTE PLASTICS WITH COAL G.P. Huffman, Z. Feng, F.E. Huggins and V. Mahajan	1519
LIQUEFACTION OF COAL/WASTE PLASTIC MIXTURES S.R. Palmer, E.J. Hippo, D. Tandon and M. Blankenship	1523
PYROLYSIS OF COAL IMPREGNATED WITH WASTE PLASTICS UTILIZING METHANOL AS A SWELLING REAGENT K. Miura, K. Mae, T. Maki and M. Takase	1527
EFFECT OF INTRODUCING TYRE PYROLYSIS OIL INTO TWO-STAGE COAL LIQUEFACTION G. Harrison and A.B. Ross	1531
COAL-TIRES HYDROPROCESSING A.M. Mastral, R. Murillo, M.S. Callén, M.J. Pérez-Surio and M.C. Clemente	1535
CATALYTIC EFFECT OF HIGHLY DISPERSED Zn/CARBON BLACK FROM AUTOMOBILE TIRE ON COAL LIQUEFACTION Y. Sato, T. Kamo, Y. Yamamoto, K. Miki and S. Kurahashi	1539
C. COAL AND THE ENVIRONMENT	1543
<i>C.1 PRE-UTILIZATION ASPECTS</i>	<i>1543</i>
COAL CHARACTERISATION STRATEGY FOR PHYSICAL DESULPHURISATION PROCESSES F. Rubiera, S. Ivatt and N.J. Miles	1545

PARTITIONING AND BEHAVIOR OF COAL MACERALS DURING DRY COAL CLEANING	1549
J.M. Stencel, H. Ban, J.L. Schaefer and J.C. Hower	
PRODUCTION OF COAL MACERAL CONCENTRATES BY FLOTATION	1553
S. Kizgut, N. Miles and M. Cloke	
A RANK INDEPENDENT FLOTATION PROCESS FOR COMBINED CYCLE GASIFIERS, INTRINSIC BUBBLE FLOTATION	1557
E.J. Hippo, M. Blankenship and D. Tandon	
MICROFLOTATION OF COAL PARTICLES SUSPENSIONS	1561
A.A. Baichenko and Al.A. Baichenko	
DIRECTIONS OF DEVELOPMENT IN COAL CLEANING	1565
A.A. Baichenko and G.I. Gritsko	
SELECTIVE AGGLOMERATION OF HIGH RANK COALS WITH VEGETABLE OILS	1569
J.M.G. Vega, M.R. Martínez-Tarazona and A.B. Garcia	
MINERAL MATTER REMOVAL BY ALKALI LEACHING AND THE CHARACTERIZATION OF REMAINED MINERAL MATTER	1573
J. Wang, Y. Kobayashi, A. Tomita and Z.-G. Zhang	
DEMINERALIZATION OF ANTHRACITE CHAR BY MOLTEN SALTS	1577
M. Alfaro-Domínguez, F.J. Higes-Rolando and V. Gómez-Serrano	
EFFECTS OF COAL CLEANING ON GASIFICATION AND COMBUSTION REACTIVITY OF COALS AND CHARS	1581
D.J. Harris, C.G. Thomas, P.J. Mullins, M.E. Gosnell, E. Gawronski, P.M. Nicholls and A.B. Waugh	
RHEOLOGY OF COLOMBIAN COAL-WATER SLURRY FUELS: EFFECT OF PARTICLE-SIZE DISTRIBUTION	1585
J.E. Pulido, C.P. Rojas, G. Acero, M. Durán and M. Orozco	
STRUCTURAL CHARACTERISTICS OF COAL SURFACE AND COAL SLURRYABILITY	1589
C.-G. Sun, B.-Q. Li, W. Yuchi and B. Cao	
EFFECT OF MINERAL MATTERS ON THE PROPERTIES OF COAL WATER SLURRY	1593
Y.-X. Xie, B.-Q. Li and C.-G. Sun	

REAL-TIME ON-LINE FUGITIVE DUST MEASUREMENT AND CONTROL A. Sutton, S. Sutton and D.G. Osborne	1597
CONTROL OF HAZARDOUS METAL EMISSIONS FROM POWER PLANTS VIA PRECOMBUSTION COAL CLEANING C.J. Lafferty, J.D. Robertson, B.K. Parekh and F.E. Huggins	1601
PRECOMBUSTION REMOVAL OF MERCURY FROM COAL BY MILD PYROLYSIS T.C. Keener, A.C. Gieske and S.J. Khang	1605
ION EXCHANGE PROPERTIES OF BROWN COALS G.S. Golovin, E.B. Lesnicova and N.I. Artymova	1609
A NOVEL COAL BASED PROCESS FOR GROUNDWATER TREATMENT C.J. Lafferty, E.A. McGonigle, S. Barry, J. Andresen and C.E. Snape	1613
EVALUATION OF WATER CONTAMINATION DEGREE IN AREAS AFFECTED BY COAL RELATED ACTIVITIES - RIO GRANDE DO SUL STATE, BRAZIL I.H. Lagreca, R.B. Binotto, E.C. Teixeira, J.C.D. Sanchez and A. Jablonski	1617
A CRITICAL COMPARISON OF SPECTROPHOTOMETRIC AND POTENTIOMETRIC METHODS FOR THE DETERMINATION OF FLUORIDE AND CHLORIDE IN COAL FLY ASH AND CLAY E. Andrés-García, E. Blanco-González and M.E. Díaz-García	1621
VOLATILE ELEMENTS AND RADIONUCLIDES IN HIGHVALE AND WHITEWOOD MINES, ALBERTA, CANADA F. Goodarzi and T. Gentzis	1625
LATEST DEVELOPMENTS IN THE UTILIZATION OF COAL MINING WASTES J. González Cañibano	1629
APPLICATION OF COALCONTAINING WASTE IN PRODUCTION OF BRICK AND EXPLANDED CLAY AGGREGATE E.J. Galpern	1633
PHASE COMPOSITION OF COAL MINING AND PREPARATION WASTES AND ITS ROLE IN DETERMINING THE TRENDS OF THEIR USAGE G.B. Skripchenko, R.Ya. Kleyman, M.Ya. Shpirt and I.M. Shchadov	1637

- BRIQUETTING OF BROWN COAL WITH HYDROLIZED LIGNIN 1641
V.I. Saranchuk, L.Ja. Galushko, L.V. Pashchenko and V.A. Khazipov
- EXPERIMENTAL STUDY ON THE CHARACTERISTICS OF GANGUE
BRIQUETTING COMBUSTION IN INDUSTRIAL BOILERS 1645
B. Zhang, Q. Zhang and S. Liu
- METALLIFEROUS COALS: A NEW POTENTIAL SOURCE OF
VALUABLE TRACE ELEMENTS AS BY-PRODUCTS 1649
V.V. Seredin and M.Y. Shpirt
- ANALYSIS OF FORMS OF SULPHUR WITHIN COAL, AND MINOR
AND TRACE ELEMENT ASSOCIATIONS WITH PYRITE BY ICP
ANALYSIS OF EXTRACTION SOLUTIONS 1653
P.F. Cavender and D.A. Spears
- ORIGIN AND FATE OF SULPHUR IN SPANISH COALS 1657
R. Gorchs, C. Catalan, J. Campà, P. Danishfar, L. Cabrera and F.X.C. de
las Heras
- THE SULFUR GEOCHEMISTRY OF SOME AUSTRALIAN BROWN
COALS 1661
Z. Song, B.D. Batts and J.W. Smith
- THERMAL BEHAVIOUR OF SULPHUR FORMS IN SPANISH LOW-
RANK COALS 1665
A.J. Bonet, J.V. Ibarra and R. Moliner
- INTERPRETATION OF AP-TPR PROFILES BY NON-ISOTHERMAL
KINETICS 1669
H. Van den Rul, I.I. Maes, J. Yperman, D. Franco, J. Mullens and L.C.
Van Poucke
- A STUDY OF THE ORGANIC SULPHUR DISTRIBUTION IN SOLID
FUELS BY MEANS OF ATMOSPHERIC PRESSURE TEMPERATURE
PROGRAMMED REDUCTION (AP-TPR) 1673
J. Yperman, D. Franco, J. Mullens, L.C. Van Poucke, C.E. Snape and S.C.
Mitchell
- STUDY OF THE SULPHUR FUNCTIONALITIES AND PHYSICAL
CHARACTERISTICS OF A BULGARIAN LIGNITE BY
DESULPHURIZATION TECHNIQUES 1677
I.I. Maes, D.V. Franco, J. Yperman, J. Mullens, L.C. Van Poucke, S.C.
Mitchell and S.P. Marinov

- A STUDY OF SULPHUR AND NITROGEN IN TWO HIGH SULPHUR COALS 1681
Z. Zhu, Y. Gu, S.C. George, M.A. Wilson, F.E. Huggins and G.P. Huffman
- CHANGES IN THE FORMS OF NITROGEN AND OXYGEN DURING RAPID COAL PYROLYSIS 1685
M. Watt, W. Allen and T. Fletcher
- CHANGE IN CHAR NITROGEN FUNCTIONALITY DURING IRON-CATALYZED NITROGEN REMOVAL 1689
Y. Ohtsuka, T. Watanabe, H. Mori and K. Asami
- XPS EVIDENCES FOR CHANGES IN THE NITROGEN FORMS IN RESULT OF HYDROPYROLYSIS OF MODEL CHARs 1693
Z. Piwowarska, K. Stańczyk and R. Dziembaj
- PROMOTION OF NITROGEN REMOVAL DURING COAL PYROLYSIS BY USING IRON CATALYST IMPREGNATED BY SOLVENT SWELLING METHOD 1697
J.-i. Hayashi, K. Kusakabe, S. Morooka and E. Furimsky
- FORMATION OF N₂ DURING THE FIXED-BED PYROLYSIS OF COALS 1701
Z. Wu, Y. Ohtsuka and E. Furimsky
- REGULARITIES OF CHLORINE CONCENTRATION AND FORM LOCATION IN RUSSION COALS 1705
Iu.N. Zharov
- ORGANIC SULFUR REMOVAL FROM COAL BY RAPID PYROLYSIS WITH ALKALI LEACHING AND DENSITY SEPARATION 1709
K. Sugawara, K. Abe and T. Sugawara
- OXIDATIVE PRETREATMENTS FOR THE ENHANCED REMOVAL OF ORGANIC SULFUR FROM COAL 1713
S.R. Palmer, E.J. Hippo and Y. Liu
- EFFECT OF NITRIC ACID ATTACK ON THE ORGANIC SULPHUR CONTENT OF COALS 1717
R. Álvarez Rodríguez and C. Clemente
- CHEMICAL DESULPHURIZATION METHODS OF ORGANIC SULPHUR OF EOCENE COAL, JAINTIA HILLS, MEGHALAYA 1721
M. Ahmed and A. Rahim

- NOVEL METHODS FOR THE ORGANIC DESULFURISATION OF COAL 1725
K. Singh and W.R. McWhinnie
- COAL DESULPHURIZATION WITH HYDROIODIC ACID AND MICROWAVES 1729
A.C. Ferrando, J.M. Andrés and L. Membrado
- OXYDESULPHURIZATION OF COAL USING TRONA MINERAL 1733
S. Yaman, S. Küçükbayrak
- SOLUBILIZATION AND DESULPHURIZATION OF HIGH SULPHUR COAL UNDER MILD CONDITION WITH TRIFLUOROMETHANE SULPHONIC ACID 1737
K. Shimizu, Y. Iwami, T. Hamada, A. Suganuma and I. Saito
- MICROBIAL DESULFURIZATION OF DIFFERENT COAL TYPES 1741
G. Olsson, O. Holst and H.T. Karlsson
- BIOLOGICAL SULPHUR REMOVAL BY THIOBACILLUS THIOOXIDANS IN FINE COAL COMING FROM A FLOTATION WASHING PLANT 1745
G. González Benito, G. Osorio and D. Bonilla
- BIODESULPHURIZATION OF COALS FROM THE NORTH OF LEÓN (SPAIN). OPTIMIZATION OF PROCESS VARIABLES 1749
O. Martínez, A. Aller, J. Alonso, E. Gómez and A. Morán
- MICROBIAL DEGRADATION OF ILLINOIS No. 6 COAL BY MEANS OF COMETABOLISM WITH PHENOLS 1753
Y. Kabe, T. Furuta, M. Takai, K. Higashi, S. Katoh and T. Kojima
- BIOLOGICAL TREATMENT OF COALS FOR THEIR CONVERSION TO METHAN 1757
S. Shumkov and S. Terehova
- SOME PROPERTIES OF LIGNITE BIOCONVERSION PRODUCTS 1761
Yu.G. Golovin, M.L. Shchipko, B.N. Kuznetsov, V.V. Golovina and A.O. Eremina

<i>C.2 UTILIZATION AND POST-UTILIZATION ASPECTS</i>	1765
A TWO MIXTURE FRACTION APPROACH FOR MODELING TURBULENT COMBUSTION OF COAL VOLATILES AND CHAR OXIDATION PRODUCTS D.V. Flores and T.H. Fletcher	1767
EXPERIMENTAL STUDY AND MODELING OF THE INFLUENCE OF THE INLET NO CONCENTRATION IN THE NATURAL GAS REBURNING PROCESS R. Bilbao, A. Millera and M.U. Alzueta	1771
NO _x REDUCTION USING COAL PYROLYSIS GAS AS REBURN FUEL: EFFECTS OF PYROLYSIS GAS COMPOSITION H. Spliethoff, U. Greul, H. Rüdiger, H.-C. Magel, U. Schnell, K.R.G. Hein, C.-Z. Li and P.F. Nelson	1775
THE EFFECT OF REBURNING COAL PROPERTIES ON THE REDUCTION OF NO IN A DROP-TUBE FURNACE E. Hampartsoumian, H. Liu, B.M. Gibbs and J.P. Smart	1779
PRIMARY MEASURES FOR REDUCTION OF NO _x IN LOW VOLATILE COALS COMBUSTION A. Plumed, L. Cañadas, P. Otero, M.I. Espada, M. Castro, J.F. González and F. Rodríguez	1783
NO _x REDUCTION BY COAL BRIQUETS A. García-García, M.J. Illán-Gómez, A. Linares Solano and C. Salinas-Martínez de Lecea	1787
COAL-BASED ACTIVATED CARBONS: NO _x AND SO ₂ POSTCOMBUSTION EMISSION CONTROL J.M. Stencel and A.M. Rubel	1791
REDUCTION OF NO WITH CARBONS USING COPPER BASED CATALYSTS C. Márquez-Álvarez, I. Rodríguez-Ramos and A. Guerrero-Ruiz	1795
NO REDUCTION BY ACTIVATED CARBONS. SOME MECHANISTIC ASPECTS OF UNCATALYZED AND CATALYZED REACTION M ^a J. Illán-Gómez, A. Linares-Solano, L.R. Radovic and C. Salinas-Martínez de Lecea	1799

ACTIVE CARBON MONOLITHS AS CATALYST SUPPORTS FOR SCR (SELECTIVE CATALYTIC REDUCTION) OF NO _x WITH AMMONIA J. Trawczyński and M. Kułazyński	1803
THE PERFORMANCE OF A NEW MONOLITHIC SCR CATALYST IN A LIFE TEST WITH REAL EXHAUST GASES. EFFECT ON THE TEXTURAL NATURE J. Blanco, P. Avila, M. Yates, A. Bahamonde, J. Belinchon, E. Medina and A. Cuevas	1807
ECOLOGICAL ASPECTS OF DIFFERENT TYPES COAL FUEL USE S.A. Kudashkina, E.P. Volynkina and M.B. Shkoller	1811
ROLE OF COAL MACERAL COMPOSITION IN REDUCING SULFUR DIOXIDE AND OXIDES OF NITROGEN EMISSIONS FROM PULVERIZED COAL FLAMES S. Rajan and J.K. Raghavan	1815
SORBENT CHARACTERIZATION FOR BOILER INJECTION PROCESS J. Adánez, J.A. de Diego, V. Fierro, L.F. de Diego and F. García-Labiano	1819
ABATEMENT OF SO _x ON MONOLITHIC CARBON CATALYST M. Kułazyński, J. Trawczyński and B. Radomyski	1823
EFFECT OF ALKALINE METAL OXIDES ON THE ADSORPTION OF SO ₂ BY ACTIVATED CARBONS M.A. Álvarez-Merino, F. Carrasco-Marín and C. Moreno-Castilla	1827
SULFUR DIOXIDE CAPTURE BY CALCIUM CONTAINING CARBON M.C. Macías-Pérez, A. Linares-Solano and C. Salinas-Martínez de Lecea	1831
SIMPLE DESULFURIZATION TECHNOLOGY USING LIMESTONE SUPPORTED IN COAL BRIQUETTE S. Uemiy, K. Itoh and T. Kojima	1835
SULPHUR RETENTION IN CIRCULATING FLUIDIZED BED COAL COMBUSTION. MODELLING AND SIMULATION J. Adánez, L.F. de Diego, F. García-Labiano and P. Gayán	1839
FLUE GAS DESULFURIZATION IN A CIRCULATING FLUIDIZED BED R. Ortiz de Salazar, P. Ollero, A. Cabanillas, J. Otero-Ruiz and L. Salvador	1843
REGENERATIVE DESULFURIZATION IN COAL CONVERSION PROCESSES APPLYING THE INTERCONNECTED FLUIDIZED BED SYSTEM O.C. Snip, R. Korbee, J.C. Schouten and C.M. van den Bleek	1847

LABORATORY TESTING OF DIFFERENT SO ₂ SORBENTS FOR DRY SORBENT INJECTION A.B. Fuertes and M.J. Fernández	1851
ADVANCED FLUE GAS TREATMENT SYSTEM USING LILAC ABSORBENT PREPARED FROM FLYASH T. Ishizuka, T. Ueno, A. Tatani and S. Kotake	1855
KINETIC STUDIES ON LOW TEMPERATURE, DRY FLUE GAS DESULPHURIZATION G. Aichinger, Ch. Brunner, J. Khinast, V. Seebauer, G. Staudinger, A. Garea, I. Fernandez, J.R. Viguri and A. Irabien	1859
DESULFURIZATION RATE AT LOW TEMPERATURES USING CALCIUM HYDROXIDE AND FLY ASH A. Garea, J.R. Viguri and J.A. Irabien	1863
A MATHEMATICAL MODEL OF A SPRAY-DRYER FLUE GAS DESULFURIZATION SYSTEM A. Abad, P. Ollero and L. Salvador	1867
RECOVERY OF LIME FROM COAL GASIFIER WASTE CONTAINING CALCIUM SULFIDE S.B. Jagtap and T.D. Wheelock	1871
²⁹ Si-NMR STUDY OF THE ABSORBENT FOR FLUE GAS DESULFURIZATION H. Hattori, N. Kanuka and R.-i. Kanai	1875
DESIGN OF A HOT GAS DESULPHURISATION PLANT V. Artos, Y. Benito, P. García and J. Otero-Ruiz	1879
HOT GAS DESULFURIZATION USING ZINC-FERRITE REGENERABLE SORBENTS C. Cilleruelo, E. García, R. Moliner, J.V. Ibarra, M. Pineda, J.L.G. Fierro and J.M. Palacios	1883
INFLUENCE OF PHYSICAL PROPERTIES OF IRON OXIDE SORBENTS ON THEIR REACTIVITY FOR HIGH TEMPERATURE REMOVAL OF HYDROGEN SULFIDE S. Kushiyama, R. Aizawa, S. Kobayashi, I. Uemasu, K. Mizuno, M. Kaiho and Y. Yamashita	1887
REACTION OF HYDROGEN SULFIDE WITH LIMESTONE PARTICLES S.Y. Lin, A. Al-Shawabkeh, M. Horio, H. Matsuda and M. Hasatani	1891

- STUDY OF NH₃ REMOVAL FROM COAL GASIFIED FUEL 1895
T. Hasegawa and M. Sato
- ACOUSTIC PRECONDITIONING OF COAL COMBUSTION FUMES FOR 1899
ENHANCEMENT OF ELECTROSTATIC PRECIPITATOR
PERFORMANCE: I. THE ACOUSTIC PRECONDITIONING SYSTEM
J.A. Gallego, E. Riera, L. Elvira, G. Rodríguez, F. Vázquez, T.L.
Hoffmann and F. Montoya
- ACOUSTIC PRECONDITIONING OF COAL COMBUSTION FUMES FOR 1903
ENHANCEMENT OF ELECTROSTATIC PRECIPITATOR
PERFORMANCE: II. PERFORMANCE EVALUTION
J.J. Rodríguez Maroto, F.J. Gómez Moreno, M. Martín Espigares, J.A.
Gallego, E. Riera, L. Elvira, G. Rodríguez, F. Vázquez, T.L. Hoffmann and
F. Montoya
- THE SIGNIFICANCE OF POROSITY OF GASIFICATION FILTER DUST 1907
J. Ranta, M. Nieminen and E. Kurkela
- CATALYTIC N₂O DECOMPOSITION IN FLUIDIZED BED 1911
COMBUSTION
J. Rodríguez-Mirasol, E. Ito, C.M.van den Bleek, L. Monceaux, P.
Courtine, F. Kapteijn and J.A. Moulijn
- GAS INJECTION AS A MEASURE TO REDUCE N₂O EMISSIONS FROM 1915
FLUIDIZED BED COMBUSTION OF COAL
G. Marbán, F. Kapteijn and J.A. Moulijn
- COAL UTILIZATION TECHNOLOGY FOR REDUCING CARBON 1919
DIOXIDE EMISSION
A. Inaba and K. Okada
- PRESSURISED FLUIDISED BED COMBUSTION OF COALS IN 1923
MIXTURES OF RECYCLED FLUE GAS AND OXYGEN
B. Bonn and H. Baumann
- POLYMER MEMBRANE CONDITIONING AND DESIGN FOR 1927
ENHANCED CO₂ - N₂ SEPARATION
S.P. Kaldis, G.C. Kapantaidakis and G.P. Sakellaropoulos
- OBSERVATIONS OF CO₂ CLATHRATE HYDRATE FORMATION AND 1931
DISSOLUTION UNDER DEEP-OCEAN DISPOSAL CONDITIONS
R.P. Warzinski, A.V. Cugini and G.D. Holder

- CHARACTERISATION OF POLYCYCLIC AROMATIC COMPOUNDS (PAC) IN COAL PRODUCTS AND RELATED MATERIALS BY GC AND COUPLED LC-GC TECHNIQUES 1935
K.M.L. Holden, A.C. Lewis, K.D. Bartle, and S.C. Mitchell
- POLARITIES AND RING SIZE DISTRIBUTIONS OF POLYCYCLIC AROMATIC COMPOUND EMISSIONS DURING SECONDARY PYROLYSIS WITH VARIOUS COALS 1939
L.E. Yu, J. DaDamio, L.M. Hildemann and S. Niksa
- EFFECT OF COAL PYROLYSIS CONDITIONS ON POLYCYCLIC AROMATIC HYDROCARBONS CONTENT IN LIQUID PRODUCTS 1943
K. Kubica, M. Czaplicka and T. Kordas
- DISTRIBUTION OF PAH GENERATED IN FLUIDIZED BED COMBUSTION AND PYROLYSIS EXPERIMENTS 1947
A.M. Tobías, R. García, K.M.L. Holden, S.C. Mitchell, J.J. Pis, C. McRae, C.E. Snape and S.R. Moinelo
- POLYCYCLIC AROMATIC HYDROCARBONS FROM COAL FLUIDISED BED COMBUSTION 1951
A.M. Mastral, M.S. Callén, M.C. Mayoral, R. Juan and J. Galbán
- STABILIZATION/SOLIDIFICATION OF INDUSTRIAL INORGANIC WASTES USING COAL FLYASHES FROM DESULPHURISATION PROCESSES 1955
J. Vale, C.F. Pereira, M. Rodríguez-Piñero, C. Ruiz de Elvira, J. Olivares and L. Salvador
- CHARACTERIZATION OF ACFBC AND PFBC RESIDUES 1959
L. Armesto, J.L. Merino and A. Cabanillas
- PILOT PLANT DEVELOPMENT OF A NEW CATALYTIC PROCESS FOR IMPROVED ELECTROSTATIC SEPARATION OF FLY ASH IN COAL-FIRED POWER PLANTS 1963
J. Olivares del Valle, L. Salvador Martinez, B. Muñiz Baum and V. Cortés Galeano
- THE FATE OF TRACE ELEMENTS IN COAL DURING GASIFICATION 1967
A.J. Bushell and J. Williamson
- EVALUATION OF THE DISTRIBUTION OF TRACE ELEMENTS IN COAL COMBUSTION PRODUCTS 1971
R. Álvarez Rodríguez, C. Clemente, C. Serrano, J. de Marcos and V. Velasco

- TRACE ELEMENT PARTITIONING IN STACK EMISSIONS FROM
COAL-FIRED POWER STATIONS 1975
L.S. Dale, J.F. Chapman and S.A. Lavrencic
- SYNTHESIS OF INDUSTRIAL MINERALS FROM FLY ASH 1979
X. Querol, F. Plana, A. Alastuey, J.L. Fernández-Turiel and A. López-Soler
- PRODUCTION OF POROUS MATERIAL FROM COAL ASH
DISCHARGED FROM FLUIDIZED BED COMBUSTOR 1983
T. Okajima, Y. Chen and S. Mori
- SYNTHETIC AGGREGATES FROM COAL-FIRED FLUIDIZED-BED
COMBUSTION RESIDUES 1987
R.A. Winschel, M.M. Wu and F.P. Burke
- THE RELATIONSHIP OF MINERALOGY AND STRENGTH
DEVELOPMENT IN DRY FGD DERIVED CEMENTS 1991
U. Graham, K.G. Sutterer and T.L. Robl
- REUTILISATION STUDIES FOR BROWN COAL FLY ASH 1995
U. Lenz, H. Meyrahn, N. Möhlenbruch, H.-P. Päßgen and M. Reich-
Walber
- SEPARATION OF FLY ASH USING DENSITY GRADIENT
CENTRIFUGATION 1999
S.R. Palmer, S. Sivanandan and W. Huggett

Author Index

2003

This Page Intentionally Left Blank

SECTION B

***COAL COMBUSTION AND
CONVERSION SCIENCE***

Sub-section B.3

Liquefaction and hydrolysis

This Page Intentionally Left Blank

A novel reactor system for studying the kinetics of coal liquefaction and related processes at very short reaction times

He Huang, D.M. Fake, M.T. Klein, and W.H. Calkins*

Department of Chemical Engineering
University of Delaware
Newark, DE 19716, USA

1. INTRODUCTION

In many high-pressure and high-temperature reactions, important information concerning the chemical and physical processes can be obtained through study of the reactions at the very early stages (the first few seconds to 2-3 minutes) before secondary reactions occur. However, this is not easy to do because the equipment required to carry out such reactions must be relatively massive to contain the sample at the high pressures and high temperatures. Direct coal liquefaction, for example, is generally run in the range of 350-450 °C at over 7 MPa (1000 psig). The heat capacity of experimental equipment is, therefore, often large compared to that of the sample being studied. This makes the heat up and cool down times of the reactor system large compared to the actual reaction times for many reactions. A number of workers have taken various approaches to solving this problem¹⁻³. However, most of these either were not able to follow the reactions at sufficiently short reaction times, or the equipment required was complicated and expensive so that it was not practical to run experiments to screen many important variables.

At the University of Delaware, we have devised a simple reactor system which can be conveniently operated in the laboratory on a small scale at elevated temperatures and pressures so that many experiments can be run quickly and at relatively low cost^{4,5}.

2. APPARATUS AND ITS OPERATION

2.1. Apparatus

A diagram of the apparatus is shown in Figure 1. It consists of a blowcase, a preheater and reactor, a cooling coil and a product receiver. Above the reactor a small condenser is mounted, followed by a disengaging space and then a let down valve. While various reactor sizes can be used, the reactor volume of our particular apparatus is about 70 cm³. The preheater coil is about 21 feet of 1/4 in. 316 stainless steel tubing (0.035 in. wall thickness) and the reactor is constructed of 3/4 in. 316 stainless steel tubing approximately 12 inches in length with a wall thickness of 0.433 in.

In operation, the preheater, a coil of high pressure tubing, and the reactor are mounted in an industrial size fluidized sand-bath and brought up to a predetermined reaction temperature. The reaction mixture is charged to the blowcase. At the appropriate time, the contents of the blowcase are driven through the preheater into the reactor with high pressure gas. When the reactants are in the reactor, gas is bubbled through the mixture from the bottom at a rate controlled by the let down valve. This rate must be sufficient to agitate the

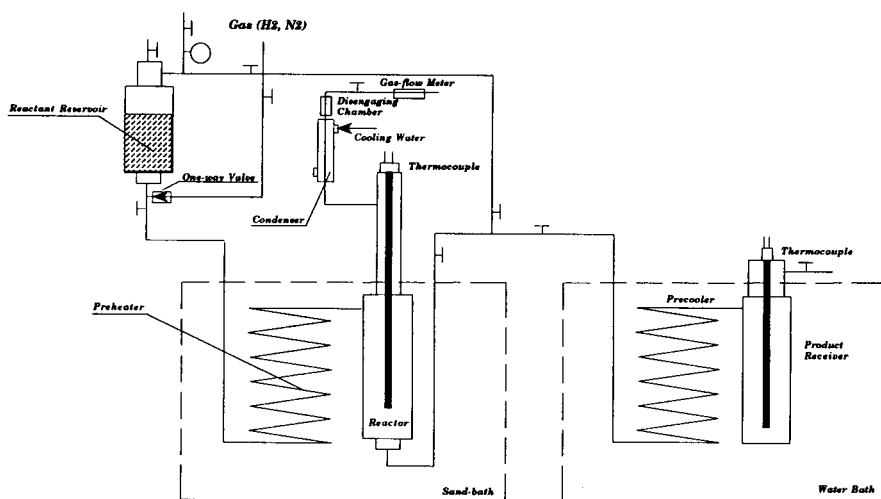


Figure 1 Apparatus for direct coal liquefaction from short contact times

reaction mixture as determined by separate experiments. If a reactant gas such as hydrogen is used, the gas is used as the propellant as well as the agitating gas and a reactant. In this way excellent contact is achieved between the reacting gas and the fluid medium. At a selected time, the reaction products are blown out of the reactor through the cooling coil and into the receiver.

Critical factors are the rate of heat up of the reactant mixture to the predetermined reaction temperature and the transfer time of the reaction mixture through the preheater. The results of extensive testing of our reactor system using high pressure gas (above 1000 psig) and detailed energy and momentum balance calculations reveal that the transfer of the reaction mixture from the blowcase through the preheater must be by plug and turbulent flow. These are primarily determined by the preheater design. The inside diameter of the preheater must be small enough to maintain plug and turbulent flow. With our current apparatus, the reaction mixture is transferred into the reactor in 0.3 sec and is heated to within 5-8 °C of the predetermined reaction temperature (e.g. 400 °C) during the transit. This 5-8 °C deviation is recovered within 20 s. A temperature profile is shown in Figure 2 for a liquefaction run of Illinois #6 in tetralin at 390°C. Temperature-time measurements across the system agree closely with the heat transfer calculations.

2.2. Sample Recovery

After the reactor charge is recovered, the system is thoroughly cleaned by a series of flushes with process solvent. Experience has shown that, in this way, the system can be adequately cleaned. The surfaces of the blowcase, preheater, reactor, and precooler do tend to hold up some of the material so that 100% recovery is not possible during the reactor evacuation. Therefore, kinetic measurements and other analyses must be made on aliquots. For most coal liquefactions, the recovery varies from 80 wt% to slightly over 90 wt%. Highly viscous materials tend to hold up more on the surfaces of the system and therefore give lower recoveries. If high recoveries are needed, the system can be washed out with

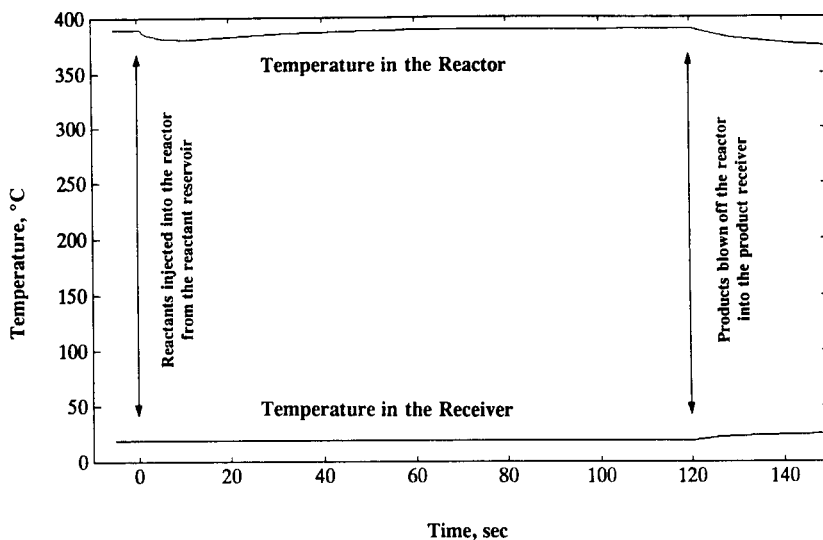


Figure 2 Representative temperature-time profile for a typical short-contact-time coal liquefaction run

a lower boiling and stronger solvent and the product collected followed by solvent removal in a rotovapor.

2.3. Applications of the Batch Reactor

This reactor system has been used to study the kinetics and mechanisms of coal liquefaction. The kinetics of the uncatalyzed Wyodak subbituminous coal liquefaction in both nitrogen and hydrogen at very short contact times from a few seconds to an hour is shown in Figure 3. The curve clearly shows an initial period of about one minute when tetralin soluble material in the coal is extracted. It is followed by a well defined induction period and then the slower breakdown of the coal structure itself. It has also been used to investigate the conversion of coal-derived vacuum residual oil to lighter products⁶. We have also run model compounds in the reactor to study the reaction mechanisms. These and many other high-pressure, high-temperature reactions appear to be suitable for this type of reactor system.

3. CONCLUSIONS

A novel laboratory scale short contact time batch reactor capable of operation up to 450°C and 17MPa (2500 psi) that provides samples at well defined contact times from a few seconds to an hour or longer is described. The rapid heat-up of the sample occurs because of the prior heating of the metal preheater tubing and batch reactor and because of the rapid and efficient transfer of the sensible heat from the preheater to the process stream. Agitation is maintained by bubbling gas through the reactor.

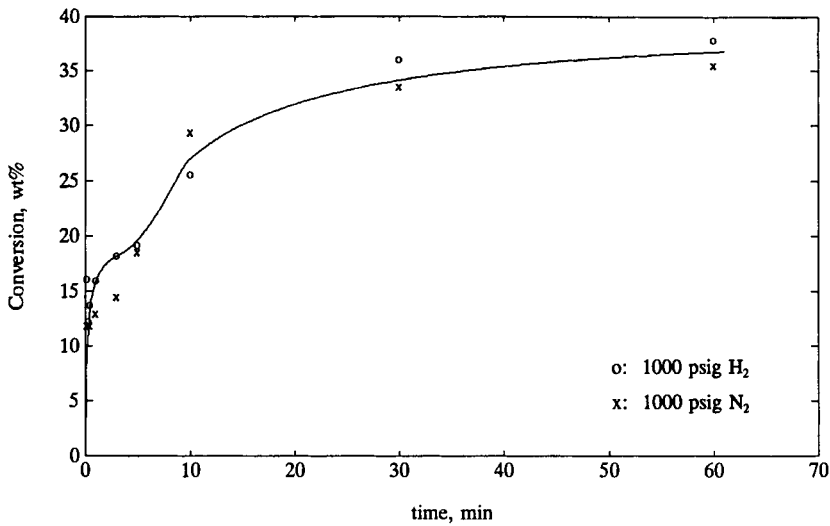


Figure 3 Kinetics of the Wyodak subbituminous coal liquefaction in tetralin (390 °C; T:C = 8:1)

4. REFERENCES

1. Whitehurst, D.D.; Mitchell, T.O.; Farcasiu, M. *Coal Liquefaction: The Chemistry and Technology of Thermal Processes*, 1980, Academic Press.
2. McPherson, W.P.; Foster, N.R.; Hastings, D.W.; Kalman, J.R.; Okada, K.; Heng, S. *Fuel* 1985, **64**, 454
3. Provine, W.D.; Jung, B.; Jacintha, M.A.; Rethwisch, D.G.; Huang, H.; Calkins, W.H.; Klein, M.T.; Scouten, C.G.; Dybowski, C.R. *Catalysis Today* 19 (1994) 409.
4. Huang, H., Calkins, W.H., and Klein, M.T. *Energy and Fuels* 1994, **8**, 1304-1309.
5. Huang, H., Fake, D.M., Calkins, W.H. and Klein, M.T. *Energy and Fuels* 1994, **8**, 1310 - 1315.
6. Huang, H., Calkins, W.H. and Klein, M.T. *I&EC Research* 1994, **33**, 2272.

Kinetics of thermal and catalyzed coal liquefaction at very short reaction times using a novel batch reactor and thermogravimetric analysis

He Huang, Keyu Wang, M.T. Klein, and W.H. Calkins*

Department of Chemical Engineering
University of Delaware
Newark, DE 19716, USA

1. INTRODUCTION

Direct coal liquefaction is run at high-temperature and high-pressure and is basically a series of complex free radical processes. These include the usual initiation, propagation and termination steps involving not only the coal and solvent reactants but also the products. For that reason, obtaining a basic understanding of liquefaction requires investigation of the process at very short reaction times, before secondary reactions become important. While this has been attempted by a number of researchers¹⁻³, an accurate picture of the kinetics at short reaction times in both thermal and catalyzed liquefactions is still not available. This is in part due to equipment limitations. Because high-temperature, high-pressure reactions require massive equipment, the heat capacity of the equipment far exceeds that of the reactants, resulting in heatup and cool down times usually very long compared to the actual reaction times. To this end, a special reactor system was devised in our laboratory which is capable of running liquefaction reactions as short as 10 seconds and as long as an hour or more.

2. EXPERIMENTAL

A brief description of the reactor system is being presented in another paper at this conference. In this equipment, the reactants can be introduced into the preheated reactor within 5 - 8°C of the reaction temperature in 0.3 seconds. Liquefaction experiments were run using Illinois #6 bituminous and Wyodak subbituminous coals in tetralin, with and without catalyst, at three temperatures. In the product work-up, the reaction mixture was separated by vacuum filtration. The solid was then washed with pure tetralin to remove soluble coal liquefaction products, and then with methylene chloride to remove residual tetralin. The solid residue was then dried in a vacuum oven at 105°C for 48 hours. The liquid and solid fractions were analyzed separately.

Since we have shown that no mineral matter goes into the tetralin or liquid portion⁴, the conversion was determined by measurement of the ash content of the liquefaction residue by thermogravimetric analysis (TGA). The conversion is determined by an ash balance equation:

$$Conversion = \left(1 - \frac{X_0}{X}\right) \times 100 \quad (wt\%) \quad (1)$$

where X_0 is the ash content of the coal processed at room temperature and X is that of the coal residue after the liquefaction reaction.

3. RESULTS AND DISCUSSION

The change in weight of unreacted Illinois #6 coal in nitrogen as the temperature increases at 10°C/min is shown in Figure 1. There is a small initial drop in weight due to

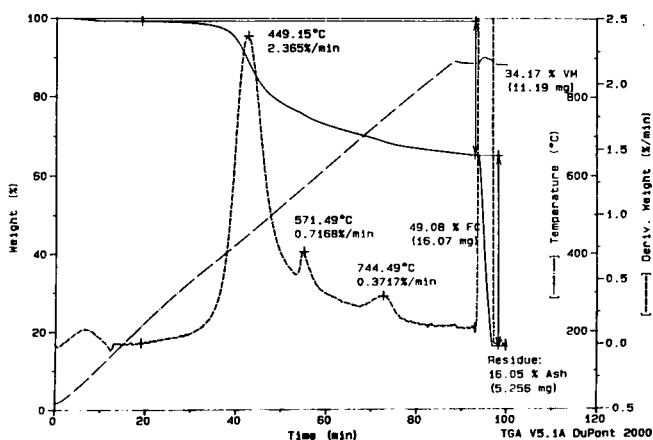


Figure 1 A TG scan on Illinois #6

loss of water, followed by a large drop around 450°C, which defines the loss of "Volatile Matter". When the weight has stabilized at 950°C, oxygen is introduced to burn off the combustible materials "Fixed Carbon", leaving the inorganic residue "Ash". The dotted line represents the DTG (differential of the weight loss curve) and shows the different weight loss processes occurring during the analysis.

The conversion vs time for the thermal liquefaction of the Illinois #6 coal in tetralin (8:1 of tetralin:coal) at three different temperatures (390°C, 408°C and 422°C) is shown in Figure 2. These curves clearly show an initial period of about one minute when tetralin-soluble material in the coal is extracted.

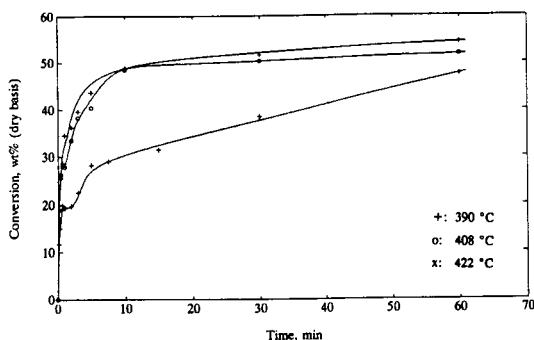


Figure 2 Kinetics of the Illinois #6 coal liquefaction in tetralin under 1000 psig N_2 (T:C = 8:1)

It is followed by a well defined induction period, and then the slower breakdown of the coal structure itself. This may be explained as the build up of free radicals during the liquefaction process. As the temperature increased, the amount and rate of tetralin-soluble material extracted increases, and the induction period becomes less pronounced.

The degree of un-catalyzed coal conversion clearly increases

substantially in going from 390°C to 408°C. However, the conversion increases little above 408°C, and may approach a constant value. The reason for this becomes clearer when the changes in Volatile Matter and Fixed Carbon are plotted against liquefaction time at the three temperatures in Figure 3. While the Volatile Matter is decreasing rapidly at all three temperatures thus increasing the conversion,

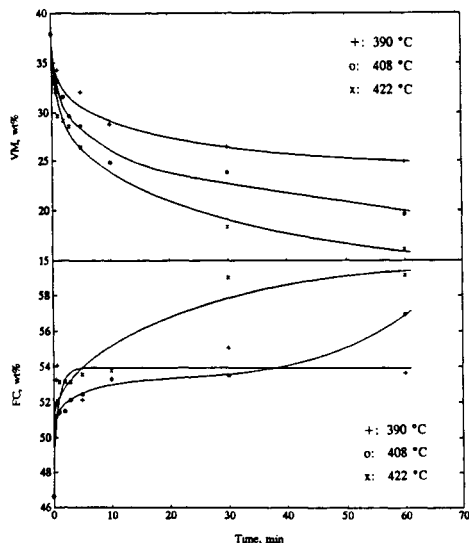


Figure 3 VM (Volatile Matter) and FC (Fixed Carbon) in liquefaction residues determined by TGA (Liquefaction: T:C = 8:1; 1000 psig N₂; TG scan: 100 cm³(STP)/min N₂; 100 °C/min)

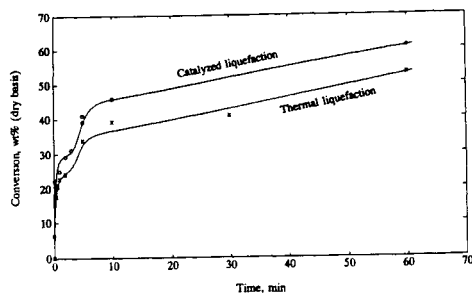


Figure 4 Conversion of the Illinois #6 coal in the thermal and catalyzed liquefaction under 1000 psig H₂ (390 °C; Catalyst: ca. 0.9 wt% sulfided molybdenum naphthenate; T:C = 8:1)

the Fixed Carbon is increasing rapidly as the temperature increases. These compensating effects slow or even halt the conversion to liquid product as the temperature increases. Increase in Fixed Carbon appears to indicate the build up of retrograde products.

Running the same liquefaction in the presence of a hydrogenation catalyst (sulfided molybdenum naphthenate) increases the conversion significantly⁴ (Figure 4). Table 1 shows that only the sulfided catalyst in the presence of hydrogen is active and the sulfiding agent (methyldisulfide) itself has no effect on conversion. In the presence of sulfided molybdenum naphthenate catalyst and hydrogen, the rate of decrease in Volatile Matter in the liquefaction residue is essentially the same in nitrogen or in hydrogen in the absence of a catalyst. However, the rate of formation of Fixed Carbon is considerably reduced, indicating the suppression of the retrograde reaction (Figure 5).

We have run the liquefaction of Wyodak subbituminous coal in both nitrogen and hydrogen at 390°C. Similarly, an extraction stage followed by an induction period was observed.

Liquefaction in a hydrogen atmosphere without added catalyst made only a very small difference in the liquefaction conversion of the Wyodak coal. On the other hand, experiments with Illinois #6 show an observable effect of hydrogen. It is possible that in the Illinois #6 coal, which contains 1.81 wt% pyritic sulfur, the liquefaction is being weakly catalyzed by pyrite (or pyrrhotite derived from it). In the Wyodak coal, which contains only 0.16 wt% pyritic sulfur, there is little if any catalysis

Table 1 Catalysis of coal liquefaction by molybdenum naphthenate (Illinois #6; 8 of T/C; 390 C; 5 min.)

molybdenum naphthenate g	methyl disulfide g	Mo wt%	Conversion wt%
under 1000 psig nitrogen gas			
0.00	0.00	0.00%	28.1%
0.00	1.03	0.00%	27.5%
0.59	0.00	0.85%	28.0%
0.62	1.07	0.86%	28.4%
under 1000 psig hydrogen gas			
0.00	0.00	0.00%	33.8%
0.00	1.03	0.00%	32.3%
0.61	0.00	0.87%	33.5%
0.61	1.15	0.87%	41.8%

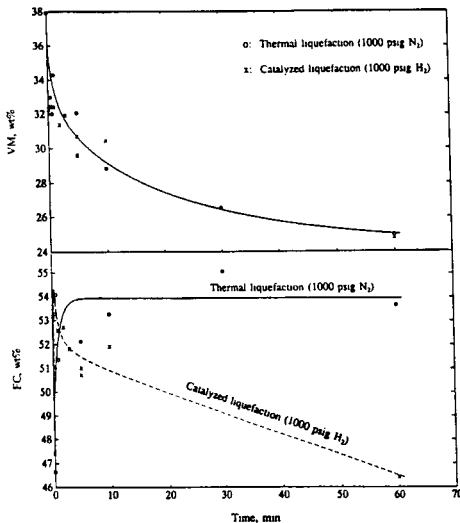


Figure 5 VM (Volatile Matter) and FC (Fixed Carbon) in liquefaction residues determined by TGA (Liquefaction: T:C = 8:1; 1000 psig N₂; TG sacn: 100 cm³(STP) /min N₂; 100 °C/min)

C.G.; Dybowski, C.R. *Catalysis Today* **19** (1994) 409.

4. Calkins, W.H.; Huang, He; Klein, M.T. *Proceedings of the 1994 Pittsburgh Coal Conference* 475-480.

by the mineral matter in the coal.

4. CONCLUSIONS

1. Coal liquefaction consists of an initial rapid extraction of material soluble in tetralin and an induction period, followed by the slow breakdown of the coal structure itself. As the temperature increases, the amount of extraction increases and the induction period becomes shorter.

2. In the liquefaction of the coal structure itself, several simultaneous processes are competitive. The Volatile Matter of the coal is removed. Some of the coal structure is converted to coal liquids. The formation of Fixed Carbon, which is a precursor to the retrograde (tar and coke) processes, becomes more important as the temperature increases.

3. The use of a known hydrogenation catalyst (sulfided molybdenum naphthenate) increases the coal liquefaction rate and yield and reduces the formation of the Fixed Carbon.

4. In the absence of an added catalyst, the mineral matter in the coal may catalyze coal liquefaction in the presence of hydrogen. The pyrite in the coal (or pyrrhotite derived from it) appears to be a weak catalyst for the reaction.

5. REFERENCES

1. Whitehurst, D.D.; Mitchell, T.O.; Farcasiu, M. *Coal Liquefaction: The Chemistry and Technology of Thermal Processes*, 1980, Academic Press.

2. McPherson, W. P.; Foster, N. R.; Hastings, D.W.; Kalman, J.R.; Okada, K.; Heng, S. *Fuel* 1985, **64**, 454

3. Provine, W. D.; Jung, B.; Jacintha, M. A.; Rethwisch, D. G.; Huang, H.; Calkins, W. H.; Klein, M. T.; Scouten,

Novel aspects on coal liquefaction mechanism by the use of tritium and ^{35}S tracer methods

Masazumi Godo and Toshiaki Kabe

Department of Chemical Engineering, Tokyo University of Agriculture and Technology, Nakamachi, Koganei, Tokyo 184, Japan

1. INTRODUCTION

In order to develop practical processes for coal liquefaction, it is important to elucidate the mechanisms of coal liquefaction. Although a number of attempts has been made to elucidate the reaction mechanism of coal liquefaction [1], there were few studies which enable the quantitative analysis of the hydrogen exchange in coal liquefaction. We have reported that the tritium tracer techniques were effective to trace the behavior of hydrogen atoms in coal liquefaction and gave the quantitative information related to hydrogen exchange [2-4]. In the course of our studies concerning coal liquefaction, we attempted to investigate the effects of the addition of pyrrhotite (Fe_{1-x}S) and sulfur on the behavior of hydrogen in coal. Further, in order to understand the behavior of sulfur, ^{35}S was also used in the systems.

2. EXPERIMENTAL

Materials: Taiheiyo coal (C 77.2, H 6.7, N 1.1, S 0.2, O 14.9daf%, ash 16.1d%) was used as a raw coal. Pyrrhotite was synthesized from Fe_2O_3 and sulfur under the hydrogen atmosphere.

Procedure: The coal liquefaction was performed in a 350ml autoclave with a glass inside batch. It was charged with 25g of coal, 75g of tetralin solvent, 0 or 5g of synthesized pyrrhotite catalyst and 0 or 1g of sulfur (or ^{35}S -labelled sulfur) and was pressurized with tritium-labelled hydrogen (about 500,000 dpm as total count) at an initial pressure of 5.9MPa. The autoclave was heated at a heating rate of $10^\circ\text{C}/\text{min}$, and maintained at 400°C for 30min. The products were separated as follows: Naphtha (distillate under 200°C), light oil (distillate between $204\text{-}350^\circ\text{C}$), SRC (THF extract from distillation residue over 350°C), oil (hexane soluble of SRC), asphaltenes (hexane insoluble and benzene soluble of SRC), preasphaltenes (benzene insoluble and THF soluble of SRC) and residue (THF extraction residue). Gaseous products, naphtha, solvent and light oil were analyzed by gas chromatography to get more precise separation data. The specific activities of tritium and ^{35}S in the reaction products were measured with a liquid scintillation counter. Colorless or light colored products were directly dissolved into the scintillator, while the colored liquid, solid and gaseous products were oxidized to H_2O and SO_x to avoid color quenching.

Calculation: Amounts of exchanged hydrogen and transferred hydrogen between the gas phase and coal/solvent, were calculated from the distribution of tritium and changes in the composition of products.

3.RESULTS AND DISCUSSION

3.1 Reaction of tetralin with tritiated hydrogen in the absence of coal

Before examining complicated reactions with coal, the reaction of tetralin with tritiated hydrogen in the absence of coal were performed. Figs.1 and 2 show the product and tritium distributions in the exchange reaction between tetralin and tritiated hydrogen, respectively. Table 1 shows the amount of hydrogen exchanged between gas phase and solvent. Although naphthalene, decalin, n-butylbenzene and 1-methylindane were produced in the absence of catalyst and sulfur (Run 1), the yield of each product was very low (below 0.6 wt%). In this case, the exchange reaction of hydrogen hardly occurred. With sulfur (Run 2), 2.3 wt% of naphthalene was produced, and exchanged hydrogen was 7.7%. Most of added sulfur changed into hydrogen sulfide under this condition. The amount of hydrogen transferred from solvent to hydrogen sulfide were about three times of that from gas phase to hydrogen sulfide. These results indicate that sulfur promotes dehydrogenation of tetralin to

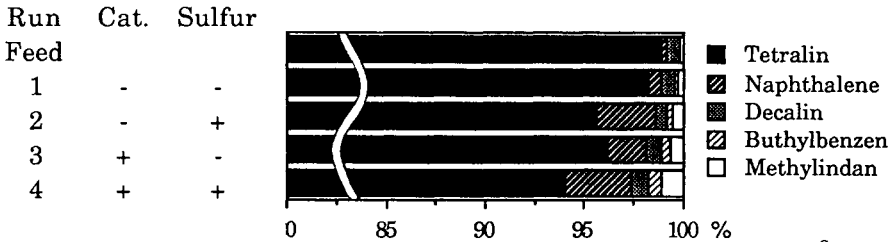


Fig.1 Products in Exchange Reaction between Tetralin and Gaseous ^3H

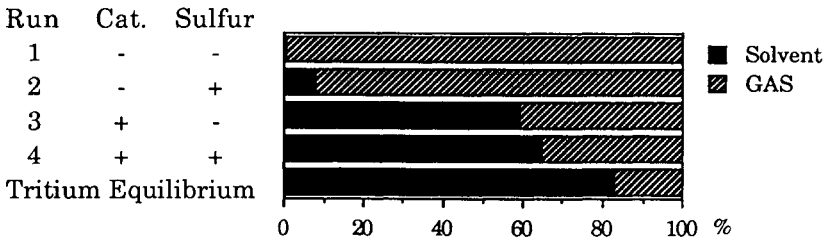


Fig.2 ^3H Distributions in Exchange Reaction between Tetralin and Gaseous ^3H

Table 1 Hydrogen Transfers between Gas Phase and Solvent (g)

Run	Cat.	Sulfur	Exchanged hydrogen	Generated H_2S	The amount of hydrogen transferred	
					from solvent to H_2S	from gas phase to H_2S
1	-	-	0.012	0.000	0.000	0.000
2	-	+	0.111	0.800	0.035	0.012
3	+	-	0.817	0.121	0.000	0.007
4	+	+	0.882	1.011	0.045	0.015

produce naphthalene. It was also suggested that sulfur would promote the formation of tetralyl radicals to increase the hydrogen exchange between gas phase and tetralin. [4]

With the catalyst (Run 3), exchanged hydrogen in solvent was 58.9%, and with the catalyst and sulfur (Run 4), it amounted to 63.8%. It was very close to the calculated equilibrium value 80% on the assumption of the complete scrambling of hydrogen atoms between gas phase and solvent.

3.2 Behavior of added sulfur

In order to trace the behavior of added sulfur, the same experiment as Run 4 was conducted using ^{35}S -labelled sulfur. After the reaction, 8.8% of added sulfur transferred to the catalyst. It was 4.5% of sulfur atoms in the pyrrhotite catalyst. Because the recovery of the catalyst was 98.2%, it was considered that the sulfur exchange reaction between added sulfur and the catalyst occurred.

3.3 Effects of the catalyst and sulfur on liquefaction of Taiheiyō coal

The reaction of Taiheiyō coal with tritiated gaseous hydrogen was performed. Figs.3 and 4 show the product and tritium distributions, respectively. Table 2 shows the hydrogen transfer (the sum of hydrogen addition and exchange) between the gas phase and solvent / coal.

Without solvent (Run 5), residue, naphtha and gas were main products, and SRC was hardly produced. With solvent (Run 6), products of liquefaction (= 100 - residue) increased to 62.4% and SRC was 58.5%. With sulfur (Run 7), residue and light fractions (such as gas, naphtha and light oil) increased slightly, while SRC decreased to 53.8%. It was suggested that sulfur promoted simultaneously both thermal decomposition and polycondensation of coal. In Run 7, the tritium distribution in solvent increased, and that in coal decreased in comparison with Run 6. It was considered that sulfur promoted the tritium transfer from gas phase to solvent, and hydrogen addition from solvent to coal.

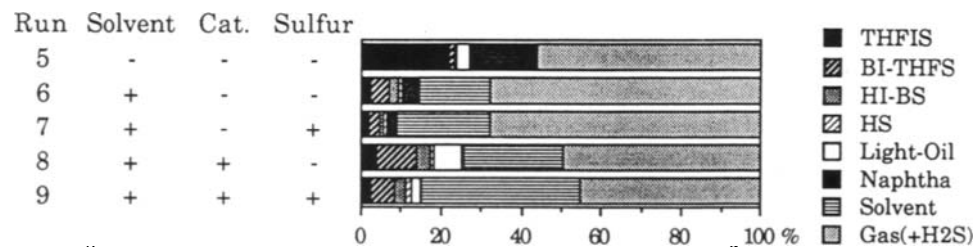
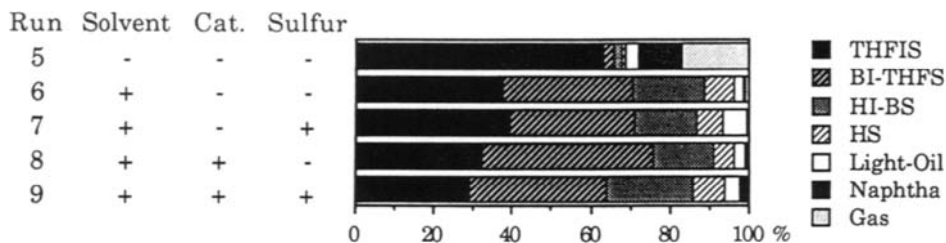


Table 2 Hydrogen Transfers between Gas Phase and Solvent / Coal (g)

Run	Cat.	Sulfur	The amount of hydrogen transferred		The amount of hydrogen added into Coal	The amount of hydrogen transferred	
			from gas to solvent	from gas to coal		from solvent to H ₂ S	from gas to H ₂ S
6	-	-	0.229	0.192	0.264	0.000	0.000
7	-	+	0.301	0.116	0.335	0.016	0.004
8	+	-	0.320	0.328	0.330	0.005	0.004
9	+	+	0.510	0.207	0.348	0.031	0.012

With the catalyst (Run 8), the amount of products in liquefaction was 67.9%, and with the catalyst and sulfur (Run 9), it was 71.2%. The amount of hydrogen added into coal was 0.330g in Run 8 and 0.348g in Run 9, respectively. The catalyst promoted the reaction of hydrogen exchange. In Runs 8 and 9, the amounts of tritium in solvent and coal were about 1.5 ~ 1.8 times of those in the absence of the catalyst. On the other hand, although the amount of hydrogen added into coal increased in Run 9, the tritium distribution in coal was less than in Run 8. It is likely that sulfur plays a role of promoter in the hydrogen exchange between gas and solvent, and between coal and solvent. The amount of hydrogen transferred from solvent to hydrogen sulfide were about 2.5 ~ 4 times of those from gas phase to hydrogen sulfide. This indicated that added sulfur produced hydrogen sulfide mainly with hydrogen in solvent. It was assumed that hydrogen sulfide dissociated into H and SH groups on the catalyst surface. H and SH groups may contribute to stabilize the free radicals formed by pyrolysis of coal. This mechanism was supported by the sulfur exchange reaction between sulfur and the pyrrhotite catalyst, because the sulfur exchange reaction suggested the existence of SH group on the catalyst surface in the presence of hydrogen sulfide.

4. CONCLUSIONS

The effects of addition of the catalyst (pyrrhotite) and sulfur on liquefaction of Taiheiyo coal were investigated using tritium and ³⁵S, and the following results are obtained.

- (1) The hydrogen exchange reaction between gas phase and solvent was promoted by added catalyst and sulfur.
- (2) With the pyrrhotite catalyst, the hydrogen addition to coal and liquefaction products increased with the addition of sulfur.
- (3) Added sulfur reacted mainly with the hydrogen of solvent to produce hydrogen sulfide.
- (4) A part of added sulfur participated in the sulfur exchange reaction with the pyrrhotite catalyst.

REFERENCES

1. For example, King, H. H. and Stock, L. M., *Fuel*, 61 (1982) 129
2. Kabe, T., Nitoh, O., Nagai, M. and Ito, T., *J. Japan Petrol. Inst.*, 26 (1983) 286
3. Ishihara, A., Takaoka, H., Nakajima, E. and Kabe, T., *Energy & Fuels*, 7 (1993) 363
4. Ishihara, A., Morita, S. and Kabe, T., *Fuel*, 74 (1994) 63

Retrogressive Reactions in Catalytic Coal Liquefaction Using Dispersed MoS₂

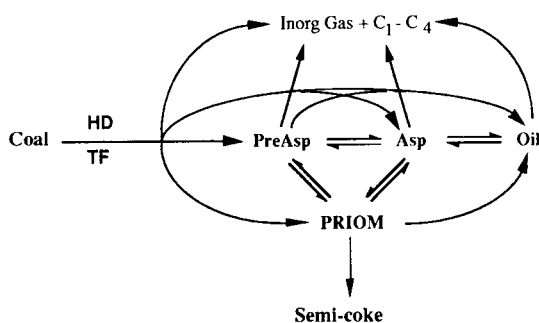
Chunshan Song*, Ajay K. Saini, and Harold H. Schobert

Fuel Science Program, The Pennsylvania State University, University Park, PA 16802, USA

INTRODUCTION

Coal liquefaction involves parallel and consecutive pathways, as illustrated in a lumped reaction model in Scheme 1 (Song et al., 1989). While details of coal structures remain to be clarified, it has been recognized that coals, especially low-rank coals, are more reactive than had been thought previously (DOE COLIRN, 1989). The initial thermal fragmentation (TF) of coal yields many reactive fragments (radicals) with different molecular sizes and functionality. When these reactive fragments are stabilized by hydrogen available (HD) in the reaction systems, they form preasphaltene, asphaltene, oil, and gases. Otherwise, they can undergo prompt radical coupling or cross-linking to form more refractory materials, called PRIOM in Scheme 1. The single most important factor affecting primary coal liquefaction is the balance between the rate of TF and the HD capacity of the system to stabilize the reactive fragments.

Retrogressive reactions occur when TF rate is faster than HD rate. In the recent past, retrogressive reactions occurring during coal liquefaction and pyrolysis have begun to receive attention (McMillen et al., 1985; Suuberg et al., 1985; DOE COLIRN, 1989; Solomon et al., 1990; Saini et al., 1993; Song et al., 1989, 1992; Huang et al., 1993; Shen and Iino, 1994; McMillen and Malhotra, 1995). The objective of this paper is to discuss whether and how retrogressive reactions occur in catalytic liquefaction using dispersed Mo sulfide catalyst.



Scheme 1 (left).

A general reaction model for coal liquefaction.

TF: thermal fragmentation of coal

HD: hydrogen donation by hydrogens in coal, vehicle, and gas-phase hydrogen

PRIOM: promptly repolymerized or re-crosslinked (fragments-derived) insoluble organic materials

PreAsp: preasphaltene (THF-soluble)

Asp: asphaltene (toluene-soluble)

Oil: oils (hexane-soluble)

EXPERIMENTAL

Wyodak subbituminous coal (≤ 60 mesh) from DOE/Penn State Coal Sample Bank (DECS-8) was used. This coal contains 28.4% moisture, 32.4% volatile matter, 29.3% fixed carbon, and 9.9% ash, on as-received basis; 75.8% C, 5.2% H, 1.0% N, 0.5% S, and 17.5% O, on dmmf basis. Ammonium tetrathiomolybdate (ATTM), which is known to decompose into Mo sulfide at $\geq 325^\circ\text{C}$ [Derbyshire et al., 1986b; Garcia and Schobert, 1989; Burgess et al., 1991; Artok et al., 1993], was dispersed onto the coal by incipient wetness impregnation from

* Corresponding author (Fax: 814-865-3075; Tel: 814-863-4466)

its aqueous solution (1 wt% Mo on dmmf basis). The impregnated coal samples and the raw coal were dried in a vacuum oven at 100 °C for 2 h before use. Liquefaction was carried out in 25 mL horizontal reactor with vertical shaking (200 cycles/min) at 325-450°C (25°C interval) for 30 min under an initial H₂ pressure of 6.9 MPa. The reactions were carried out either without or with an organic solvent (solvent/coal = 4 g/4 g). The products were separated into gases, oil, asphaltene, and preasphaltene, and the gases were analyzed by GC [Song et al., 1994].

RESULTS AND DISCUSSION

Importance of Early Stage of Catalytic Liquefaction

An intriguing question is, does a catalyst affect any reactions of a coal prior to its partial dissolution, or its primary liquefaction? We have tried to answer this question by monitoring the system pressure change, which showed that catalytic reactions can happen during and after heat-up. Figures 1 and 2 show the time-pressure profiles for reactions of Wyodak coal with and without dispersed ATTM at 350 and 400°C, respectively. The reactor heat up in the fluidized sandbath to the given temperature takes about 5 minutes. For the non-catalytic run at 350°C, the reactor pressure reached steady state in 5 min; the use of ATTM begin to cause pressure drop during heat-up period, indicating the uptake of H₂ from gas-phase. For runs at 400°C, the first 3 min of heat-up profiles for non-catalytic and catalytic runs are identical. In the subsequent 5 min, there was a very rapid pressure drop in the catalytic run (Figure 2), whereas the pressure for non-catalytic run continued to increase and reached steady state in about 8 min.

Figure 2 reveals that H₂ uptake in the catalytic runs at 400°C occurs most rapidly in the first 5 min after the initial 3-4 min heat-up period, and the subsequent H₂ uptake proceeds gradually and more slowly. These results suggest that the period of the first few minutes at high temperatures involves rapid radical generation and radical stabilization by catalytic hydrogen transfer; this period is most critical. Considering that the impregnated ATTM is only a precursor salt, the above results indicate that the precursor was at least partially transformed in-situ to catalytically active form for H₂ dissociation during the heat-up period. H₂ promotes ATTM transformation into a form close to MoS₂, even at 275°C (Artok et al., 1993).

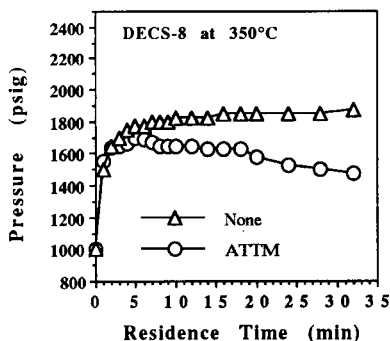


Figure 1. Reactor T-P for heat-up to and runs at 350°C.

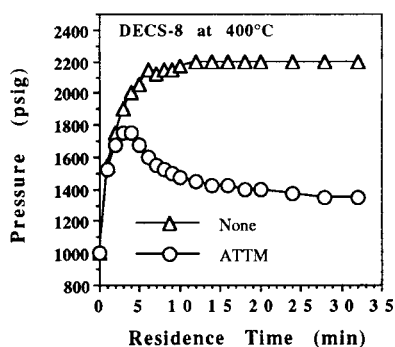


Figure 2. Reactor T-P for heat-up to and runs at 400°C.

Retrosession of Coal Conversion Using Dispersed Mo Sulfide Catalyst

Figure 3 shows the coal conversion versus temperature. Non-catalytic runs were conducted as baseline tests. In the absence of a catalyst and solvent, coal conversion into THF-solubles plus gases is very limited. Using high pressure of H₂ without catalyst did not improve coal conversion, since replacing H₂ with N₂ gave very similar conversions at 350 and 400°C. These runs provide a measure of capacity of transferable hydrogen present in the coal itself.

In the solvent-free catalytic runs, coal conversion (Figure 3) as well as H₂ consumption (Figure 4) increased with increasing temperature up to 400°C. Increasing reaction temperature to 425°C caused a decrease in coal conversion, indicating the occurrence of more retrogressive reactions at 425°C than those at 400°C. Such a decrease is indicative of the lack of available hydrogen within the system to cap the reactive radicals. This trend continued with further increasing temperature to 450°C, where coal conversion even dropped to below 65 wt%. We

have also observed the same trends in the catalytic runs of a Texas subbituminous coal (DECS-1) under comparable conditions (Huang et al., 1993).

Even though there are frequent references to "catalytic hydrogenation" of coal, it is now clear that coal hydroliquefaction is significantly different from catalytic hydrogenation of aromatic compounds. In the latter case, the reactants are thermally stable and most reactions occur only on catalyst surface. In the former case, coal is thermally reactive; retrogressive reactions can occur significantly at high temperatures and a catalyst is required both for suppressing retrogressive reactions and for promoting hydrogenation and hydrocracking reactions. Consequently, for the runs with rapid heat-up, the key to effective coal conversion in the early stage to THF-soluble products seems to be the effective stabilization of the radicals and other unstable species, rather than promoting the cleavage of strong bonds.

The lack of hydrogenating ability of the solvent-free catalytic system at higher temperatures (425-450°C), is due to two factors. The first is the rapid radical generation at higher temperatures. Recent high-temperature ESR (electron spin resonance) studies have demonstrated that the radical concentration in many low-rank coals (including Wyodak subbituminous coal) and some bituminous coals increase rapidly with increasing temperature in the range of about 325-480°C (Sanada and Lynch, 1993). The second is due to the nature of thermodynamics of catalytic hydrogenation, which is favored at lower temperatures. Figure 4 indicates that the H₂ consumption increased with increasing temperature up to 400°C, but level off with further increasing temperature up to 450°C. Even thermal dehydrogenation to form H₂ becomes measurable under N₂ at 450°C (Song et al., 1989).

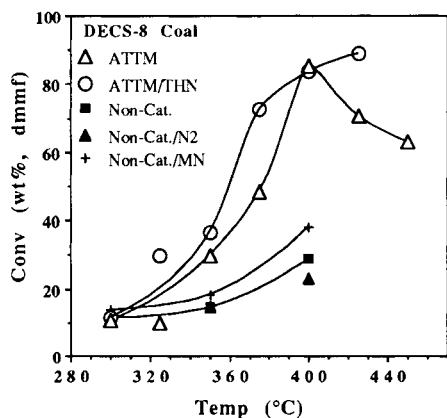


Figure 3. Catalytic and non-catalytic conversion of coal.

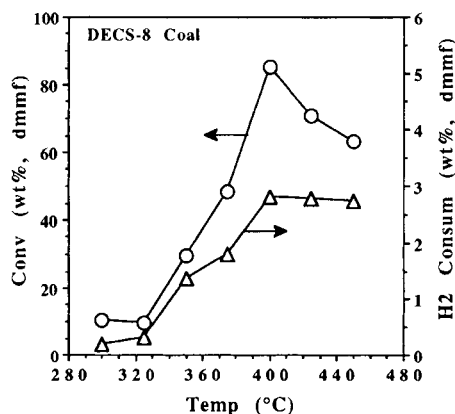


Figure 4. H₂ consumption and coal conversion at 300-450°C.

Relative Importance of Dispersed Catalyst and H-Donor Solvent

The conversions of Wyodak coal with ATTM alone and with tetralin alone at 400°C are 85.4 and 71.4 wt%, respectively, and the oil yields are 45.8 and 27.3 wt%, respectively. At moderate liquefaction temperatures such as 400°C, using dispersed Mo catalyst alone is better than H-donor solvent alone, in that the catalyst affords better product distribution, particularly, more oil products. The free hydrogen atom generated on the catalyst surface can not only cap the free radicals, but also induce C-C bond cleavage, as observed in model compound studies at 400°C (Schmidt et al., 1994). This kind of C-C bond hydrocracking reactions contributes to higher oil yields in catalytic runs. Spillover of the free hydrogen atom from catalyst surface to nearby coal surface is expected to occur under liquefaction conditions, which contributes to radical stabilization, C-C bond cleavage, and hydrogenation of aromatics. Adding tetralin to catalytic runs at 400°C did not lead to any improvements in conversion or product distribution.

However, the situation is different when the reaction temperature is increased to 425-450°C. Relative to the solid catalyst particles, H-donor solvent has the advantage of being able to diffuse into the pores to stabilize reactive fragments (radicals) through H-donation. Using H-

donor solvent in catalytic runs at $\geq 425^\circ\text{C}$ offer advantages in improving coal conversion and oil yields (Figure 3), as also observed for DECS-1 coal (Huang et al., 1993).

Type of Retrogressive Reactions

Probably there are three types of retrogressive reactions: 1) intramolecular rearrangement of some reactive structures/compounds to form more stable structures/compounds, 2) coupling of radicals and addition of reactive fragments (radicals, ions) to aromatics to form stronger C-C bond, and 3) bimolecular condensation of reactive compounds, such as the condensation and polymerization of phenolic and dihydroxy aromatic structures. Related to the type 1 and type 2 reactions are the rearrangement and coupling reactions of benzylphenyl ether- and dibenzylether-type compounds. When the thermally initiated benzyl radical and phenoxy radical are stabilized, they form toluene and phenol, respectively. However, the reaction does not always happen in the desirable direction. Benzylphenol, dibenzyl and dibenzylphenol can also be formed from benzylphenylether, and dibenzyl and methyl-diphenylmethane from dibenzylether (Song et al., 1991). Similar cross-linking reactions occur when coal is mixed with benzyl radical precursors (Saini et al., 1994). These products indicate the formation of a strong C-C bond from cleavage of relatively weak C-O bond. Type 3 reactions include condensation of phenolic and dihydroxy aromatics; the rate of such reactions decrease with dilution by solvents (McMillen et al., 1985, Wang et al., 1989). Some crosslinking associated with decarboxylation was also suggested in pyrolysis studies (Suuberg et al., 1985; Solomon et al., 1990) but model compound studies seem to suggest coupling associated with phenols may be more important in liquefaction (Manion et al., 1992). In liquefaction with the co-use of water and dispersed catalyst, enhanced coal conversion is accompanied by increased CO_2 formation (Song and Saini, 1995).

CONCLUDING REMARKS

Retrogressive reactions can occur seriously in coal liquefaction at $425\text{-}450^\circ\text{C}$ in 25 mL reactors, even in the presence of dispersed Mo sulfide catalyst. Using H-donor solvent in catalytic runs at higher temperatures ($425\text{-}450^\circ\text{C}$) help to mitigate the retrogressive reactions.

Two approaches can be considered for improving the balance between TF and HD: 1) modifying the rate of coal fragmentation at high temperatures by incorporating low-temperature coal pretreatment, temperature-staging, temperature-programming, and catalytic pretreatments; 2) increasing the hydrogen transfer capacity by using H-donor and hydrogen shuttler, in combination with hydrogenation catalyst under high pressure of hydrogen.

REFERENCES

- Artok, L., A. Davis, A., G.D. Mitchell., H.H. Schobert. *Energy & Fuels*, 1993, 7, 67.
 Burgess, C.B. and H.H. Schobert. *Fuel*, 1991, 70, 372.
 DOE COLIRN Panel, Coal Liquefaction. Final Report, DOE-ER-0400, Vol. I & II, 1989.
 Garcia, A.B. and H.H. Schobert. *Fuel*, 1989, 68, 1613.
 Huang, L., C. Song, and H. H. Schobert. *Am. Chem. Soc. Div. Fuel Chem. Prepr.*, 1993, 38 (3), 1093.
 Manion, J.A., D.F. McMillen, and R. Malhotra. *Am. Chem. Soc. Div. Fuel Chem. Prepr.*, 1992, 37 (4), 1720.
 McMillen, D.F., S. Chang, S.E. Nigenda, and R. Malhorta. *Am. Chem. Soc. Div. Fuel Chem. Prepr.*, 1985, 30, 414.
 McMillen, D.F. and R. Malhotra. *Am. Chem. Soc. Div. Fuel Chem. Prepr.*, 1995, 40 (2), 221.
 Saini, A.K., M. M. Coleman, C. Song, and H. H. Schobert. *Energy & Fuels*, 1993, 7 (2), 328.
 Sanada, Y. and L.J. Lynch. *High-Temperature Electron Spin Resonance and NMR Methods Applied to Coal*. *Adv. in Chem. Ser. No. 229*, Ed by R.E. Botto and Y. Sanada, ACS: Washington DC, 1993, pp. 139-172.
 Shen, J. and M. Iino, *Energy & Fuels*, 1994, 8, 978.
 Schmidt, E. and C. Song. *Am. Chem. Soc. Div. Fuel Chem. Prepr.*, 1994, 39 (3), 737.
 Solomon, P.R., M.A. Serio, G.V. Deshpande, and E. Kroo. *Energy & Fuels*, 1990, 4, 42.
 Song, C., K. Hanaoka, and M. Nomura. *Fuel*, 1989, 68, 287.
 Song, C., M. Nomura, and T. Ono. *Am. Chem. Soc. Div. Fuel Chem. Prepr.*, 1991, 36 (2), 586.
 Song, C., H.H. Schobert, and P.G. Hatcher. *Energy & Fuels*, 1992, 6 (2), 326.
 Song, C., A. K. Saini, and H.H. Schobert. *Energy & Fuels*, 1994, 8 (2), 301.
 Song, C. and A.K. Saini. *Energy & Fuels*, 1995, 9 (1), 188.
 Suuberg, P.E. Unger, and J.W. Larsen. *Fuel*, 1985, 64, 1668.
 Wang, F.M., V. P. Senthilnathan, and S.E. Stein. *Proc. 1989 Int. Conf. Coal Sci.*, Tokyo, Japan, pp. 165.

Simulation of nonisothermal processes of coal liquefaction using a dispersed catalyst precursor

Evgeni F. Stefoglo,^a Ana B. Garcia,^b and Harold H. Schobert^c

^aInstitute of Coal, Siberian Branch, Russian Academy of Sciences, Kemerovo 650610, Russia

^bInstituto Nacional del Carbón, Consejo Superior de Investigaciones Científicas, 33030 Oviedo, Spain

^cFuel Science Program, Department of Materials Science and Engineering, The Pennsylvania State University, University Park, PA 16802, USA

1. INTRODUCTION

This paper is a preliminary report on a collaborative effort to simulate the effect of a catalyst precursor on coal liquefaction and to develop a mathematical model describing coal dissolution by hydrogen diffusion from bulk solution into coal particles. The catalysis of the initial reactions in the dissolution or liquefaction of coal involves the interaction of a solid reactant, coal, with a solid catalyst. It is desirable to disperse the catalyst particles across the surface of the coal particles to achieve effective coal-catalyst contact. Unfortunately, many substances of good catalytic activity in liquefaction, such as MoS_2 , are insoluble. A strategy for achieving good catalyst dispersion is to use a soluble salt—the catalyst precursor—that should transform into the active catalyst at liquefaction temperatures. Thus $(\text{NH}_4)_2\text{MoS}_4$ is often used as a precursor for MoS_2 [e.g., 1]. Although it is often said in the literature that the coal has been "impregnated" with the catalyst (or catalyst precursor), in fact there is good evidence from microscopy that the catalyst particles are essentially confined to the surface of the coal, and do not extensively penetrate the pore system in the coal [2].

Some models for catalytic reactions are conceptually attractive and have been solved for other systems, but are of questionable validity when applied to coal particles having catalyst or precursor particles dispersed only on the surface. For example, a simple solid core model is based on a catalyst particle with a spherical shell of growing around it, which determines its average concentration in the coal grain. Hydrogen dissolved in the solvent or coal-derived liquids diffuses through the coal pores to the catalyst and reacts with the carbonaceous portion of the coal. The effective diffusion coefficient of hydrogen is varied between its limits in pure solvents and in coal liquids. The solid core model includes both non-steady state heat and mass transfer processes with chemical reactions producing preasphaltenes, asphaltenes, oils, and gases.

A more complex model is the multigrain model. It is based on the assumption that the catalyst precursor breaks up into many small fragments which are dispersed through the coal particle. An idealization of this physical picture is a large macroparticle comprised of many small coal microparticles including a nonuniform catalyst distribution. The small coal microparticles can be considered to be lined up, touching each other, along the radius of the macroparticle. This system is considered isothermal and the kinetics are known. There is both macrodiffusion in the interstices between microparticles and microdiffusion within microparticles. The effective diffusion coefficients for the two regimes are not necessarily equal. The catalyst has a nonuniform distribution along the radius of the macroparticle, diminishing toward the center of the coal particle. For the microparticles, the model is similar to

that used for the core model, except that each microparticle experiences a different bulk hydrogen concentration in each spherical shell, depending on microdiffusion.

In the present work, we have considered a preliminary treatment of the dissolution of Mequinenza (Spanish) lignite with NiSO_4 as catalyst precursor. The experimental details have been published elsewhere [3]. Briefly, the reactions were conducted in batch microautoclave reactors at various temperatures, using a H_2 overpressure of 7 MPa at ambient temperature. Donor solvents were not used.

2. THEORETICAL TREATMENT

We consider a process in which the concentration of organic materials to be hydrogenated, in kmol/m^3 , is assumed to be constant during the reaction. We assume that the process of coal hydrogenation is quasi-stationary, that is, that the hydrogen diffusion rate into the reacting coal particle is 10^2 – 10^3 times faster than the rate of change of the size of the yet-unconverted particles of coal. In this case, the reaction rate is equal to the hydrogen diffusion rate through a spherical shell of ash. For a given value of the radius of the unconverted coal particle the change (with respect to time) of the moles of hydrogen diffused into the coal particle is constant, but if the shell of ash is growing, the diffusion of hydrogen slows. A very simplified physical picture of this model is shown in Figure 1, where R is the initial radius of the coal particle, V the volume, and r the "current" radius of the coal particle. (i.e., the radius of the yet-unconverted portion of the coal). The model allows the determination of dependencies of the reaction on r and on the concentration of hydrogen in the coal liquids, C_H , for non-catalytic and catalytic coal dissolution processes, and, in the latter case, for different descriptions of catalyst distribution.

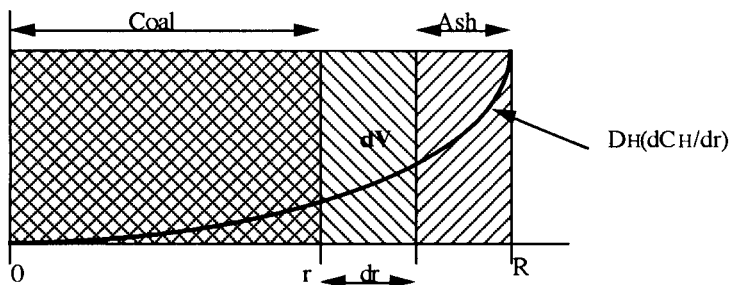


Figure 1. Simplified physical picture of coal particle of original radius R undergoing reaction, with external ash shell and yet-unreacted particle of radius r .

3. RESULTS

We have modeled two sets of reactions of Mequinenza lignite, one being reaction without catalyst at temperatures 250–325°C, and the other for the lignite treated with NiSO_4 with a loading of 1.5% Ni (as the element, not precursor). The relevant background is given in the monograph by Gianetto and Silveston [4], and the paper by Peter and Weiner [5]. In Figure 2 we show the fit of experimental data to three conditions: 1) the non-catalytic reaction, 2) catalytic reaction with the assumption of a parabolic distribution of catalyst along the radius of

the coal particle, and 3) agreement of the model with experimental results for the non-catalytic reactions. Case 2 is represented by an equation of the form

$$C_{\text{cat}} = C_{\text{cat}0} \{ 1 - [(R - r)/R]^2 \}$$

where $C_{\text{cat}0}$ is the catalyst originally applied to the coal (in our case, 1.5% Ni as NiSO_4) and r and R have been defined above. In the linear distribution, case 3, we have

$$C_{\text{cat}} = C_{\text{cat}0} \{ 1 - [(R - r)/R] \}$$

The data for catalytic reactions, particularly the two cases at longer reaction times and higher conversions, appear to be a better fit for case 2 (parabolic distribution of catalyst concentration). This is not unreasonable in light of the microscopic observations on other low-rank coals that indicated the catalyst being highly concentrated on or near the surface of the coal particles.

In addition, we estimated the concentration of hydrogen dissolved in the reacting mixture of coal-derived liquids (in mol/L or kmol/m³) as a function of time. The results are shown in Figure 3. The calculation used an effective hydrogen diffusion coefficient, D_{H} , of $3 \cdot 10^{-6}$ cm²/s. The equilibrium hydrogen concentration dissolved in the liquid would thus be $6 \cdot 10^{-2}$ kmol/m³.

4. CONCLUSIONS

We have achieved good agreement between the model and experimental data for non-catalytic liquefaction of Mequinenza lignite for reaction times up to 2 h. The comparison of experimental data with two models of catalytic reactions suggests that nickel-catalyzed liquefaction of Mequinenza lignite is better modeled by assuming a parabolic distribution of the impregnated catalyst through the coal particles, which is in reasonable agreement with direct observation of catalyst distribution in other low-rank coals.

This preliminary work has been limited to solvent-free reactions of only one coal, at relatively mild conditions (specifically, $T \leq 325^\circ\text{C}$) and, hence, at relatively low conversions. In our future work we will seek both to continue to refine the model and to extend it to other coals, more severe conditions, and much higher conversions.

REFERENCES

- 1 A.B. Garcia and H.H. Schobert, *Fuel*, 68 (1989) 1613.
- 2 L. Artok, A. Davis, G.D. Mitchell, and H.H. Schobert, *Fuel*, 71 (1992) 981.
- 3 A.B. Garcia and H.H. Schobert, *Coal Prep.* 9 (1991) 185.
- 4 A. Gianetto and P.L. Silveston (Eds.) *Multiphase Chemical Reactors: Theory, Design, Scale-up*, Hemisphere, Washington, 1986, pp. 564ff.
- 5 S. Peter and M. Weiner, *Z. Phys. Chem.* 115 (1955) 114.

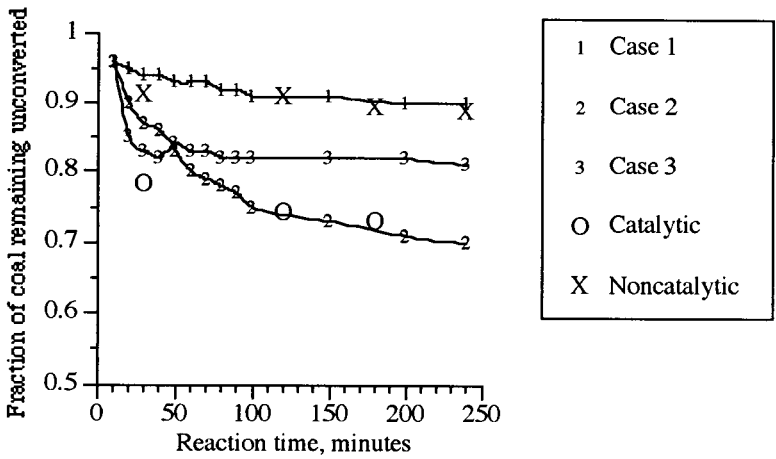


Figure 2. Comparison of experimental and predicted results for conversion of Mequenza lignite as a function of time. Models (cases 1–3) described in text.

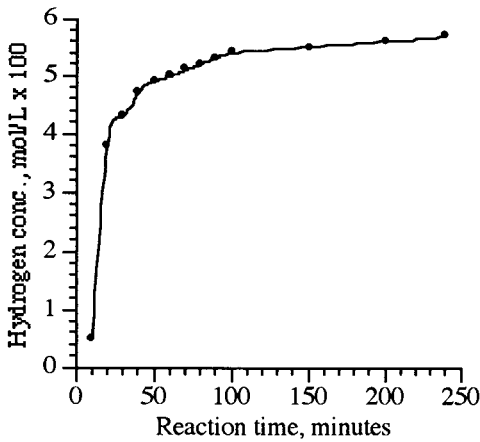


Figure 3. Predicted concentration of hydrogen (mol/L or kmol/m3) dissolved in coal liquids as a function of time.

Kinetic Study of Primary Hydrogenation Reaction in Brown Coal Liquefaction (BCL) Process

Shunichi Yanai^a, Mitsunori Makino^a, Shigeru Ueda^a, Toshiaki Okui^b, Osamu Okuma^b, Yoichi Kageyama^b, and Tetsuo Matsumura^b

^aNew Energy and Industrial Technology Development Organization (NEDO),
Sunshine 60, 1-1, 3-Chome Higashi-Ikebukuro Toshima-ku, Tokyo, 170 Japan

^bNippon Brown Coal Liquefaction Co., Ltd. (NBCL),
5-3, Yaesu 1-chome Chuo-ku, Tokyo 103, Japan

1. INTRODUCTION

NEDO and NBCL have developed a coal liquefaction process (BCL process) suitable for Australian brown coal. It is a two stage process which is composed of new slurry-dewatering, primary hydrogenation, deashing and secondary hydrogenation sections.

Regarding the primary hydrogenation section, it is generally understood that the thermal decomposition reaction occurs mainly in the preheater, and the hydrogenation and hydrocracking reactions occur mainly in the reactors. Many researchers have conducted quantitative analysis to describe these reactions, but most of the papers so far reported are concerned with reactions using bituminous or sub-bituminous coal. Kinetic study on brown coal liquefaction reactions has been rarely reported. The purpose of this paper is to present a brown coal liquefaction reaction model that was constructed using results from the 0.1t/d Process Development Unit (PDU) experiments, and to show the applicability of this model to the 50t/d Pilot Plant (PP) results.

2. MODEL FORMULATION

2.1. Flow Patterns in Primary Hydrogenation Preheater and Reactors

Two flow patterns can be found in the primary hydrogenation section of PDU and PP : the preheater region and the reactor region.

Each preheater of PDU and PP is a tubular type and its inner diameter is small compared with its length, so the flow pattern can be almost considered as plug flow.

PDU has three tank reactors in series and PP has four bubble column reactors in series. The reactors of PDU are equipped with magne-drive stirrers which run at 1000rpm to ensure minimum mass transfer effects. The mixing state of the reactor was investigated with a cold model apparatus which used the tracer injection method, and it was found that the reactor was in an ideally stirred state, approximately. The flow pattern of the PP reactors was investigated using the Neutron Absorbing Tracer (NAT) technique and it was confirmed that the reactor

was almost in an ideally stirred state also. With these results it can be concluded that the stirred-tank reactors in series model can be used in the kinetic analysis of the reactor region.

2.2. Estimation of Yields at Preheater Outlet (Reactor Entrance)

Because it is difficult to measure the yield at the preheater outlet in the PDU and PP due to instrumental limitations, and because the flow pattern of the preheater can be considered as plug flow, the yields in the preheater were empirically estimated using autoclave experiments that were simulated preheater conditions. This yield data was used as the reactor entrance composition in the next step.

2.3. Kinetic Model

The reaction model that was obtained by the PDU and autoclave data is shown in Figure 1. The dotted lines represent the pathways of the reaction in the preheater and the solid lines represent the pathways of the reaction in the reactor. In the preheater, the coal thermally decomposes and produces gases, pre-asphaltenes (BI fraction) and asphaltenes (BS fraction). The autoclave data suggests that in this step some decrease of recycle solvent occurs, and it is supposed that the recycle solvent makes an adduct with pre-asphaltenes and asphaltenes. The products are named as BI* and BS*, respectively, and are shown in Figure 1. Since BI* and BS* are very reactive, they promptly convert to more stable products (paths 1-4 and 13-18). They then change gradually to oils, hydrocarbon gases and water (paths 5-12) by the hydrogenation reaction and hydrocracking reaction in the reactor.

2.4. Kinetic Rate Constant (Reactor Region)

Besides the reaction temperature, reaction time, bottom recycle ratio and hydrogen partial pressure, it is generally known that many parameters affect the liquefaction reaction, e.g. the coal properties, bottom properties, and amount of catalyst [1-2]. These parameters should be added to the kinetic rate constant in order to improve the accuracy of estimation. The following modified Arrhenius equation containing these reaction parameters was used in the analysis.

$$k_i = \alpha \left(\frac{H / C_{coal}}{0.83} \right)^{a_i} \left(\frac{O / C_{coal}}{0.30} \right)^{b_i} \left(\frac{cat}{2.0} \right)^{c_i} \left(\frac{HDAO - B / BTM + 1}{1} \right)^{d_i} \times \left(\frac{H / C_{BTM}}{1} \right)^{e_i} \left(\frac{pH_2}{120} \right)^{f_i} \left(\frac{pH_2 / pH_{2O}}{10} \right)^{g_i} \exp \left[\frac{-E_i}{RT} \right] \quad (1)$$

where k_i : Kinetic Rate Constant , α : Frequency Factor , E_i : Activation Energy

H / C_{coal} : Atomic Ratio of Hydrogen to Carbon in Coal

O / C_{coal} : Atomic Ratio of Oxygen to Carbon in Coal , cat : Catalyst Concentration

$HDAO - B / BTM$: Ratio of Secondary Hydrogenation Recycle Bottom to Total Recycle Bottom

H / C_{BTM} : Atomic Ratio of Hydrogen to Carbon in Recycle Bottom

pH_2 : Hydrogen Partial Pressure

pH_2 / pH_{2O} : Ratio of Hydrogen Partial Pressure to Water Partial Pressure

$a_i - g_i$: Constants , i : No. of Reaction Pathway

The ratio of hydrogen partial pressure to water partial pressure was also added to the

pathways that produce water (paths 7,11,15 and 18), because it was found that water gas shift reaction affects the water yield.

3. RESULT AND DISCUSSION

The frequency factors, the activation energy, and the exponents of the reaction parameters in equation (1) were calculated by the non-linear optimization method using PDU data. Figure 2 shows the comparison between the experimental oil yield and the calculated oil yield that was obtained using equation (1). This data shows close agreement, indicating that the reaction model can accurately predict oil yield under various reaction conditions. Table I shows the correlation coefficients and standard errors of estimation regarding PDU experiments. The correlation coefficients of BI, BS and oil yields are very high (more than 0.8) and the standard errors of the estimation are negligibly small. The correlation coefficient of C1-C4 gas and H₂O yield are a little lower but the standard errors are small enough for estimation.

Table I Correlation coefficient and standard error

		BI	BS	Oil	C1-C4	H2O
PDU	Correlation Coefficient[-]	0.82	0.94	0.91	0.77	0.74
	Standard Error [%MAFC]	3.8	3.3	4.4	1.9	2.1
PP	Correlation Coefficient[-]	0.77	0.87	0.85	0.84	0.05
	Standard Error [%MAFC]	3.7	3.7	5.1	1.0	1.8

The close agreement between the experimental yields and the calculated yield confirms the validity of the assumptions of the reaction model, and it was been proved that the model is useful for estimating the liquefaction performance of the primary hydrogenation section.

This equation was directly applied to the PP operation results, but the precision was rather low. The parameters of equation (1) were then corrected by the PP data, and the precision of estimation improved (Table 1). It was found that the modified kinetic rate constants could predict the PP results accurately (Figure 3).

4. CONCLUSION

A reaction model for the brown coal liquefaction reaction has been presented. The calculated yields obtained from the reaction model showed good agreement with the actual experimental yields which proves the validity of the reaction model for the brown coal liquefaction reaction.

REFERENCES

1. S. Yanai, T. Okui, S. Oya and T. Ozawa, Proceedings of the 5th Australian Coal Science Conference, Melbourne, 1992
2. S. Yanai, T. Yoshida, S. Ueda, T. Okui, Y. Kageyama, and T. Matsumura, Proceedings of the 6th Australian Coal Science Conference, Newcastle, 1994

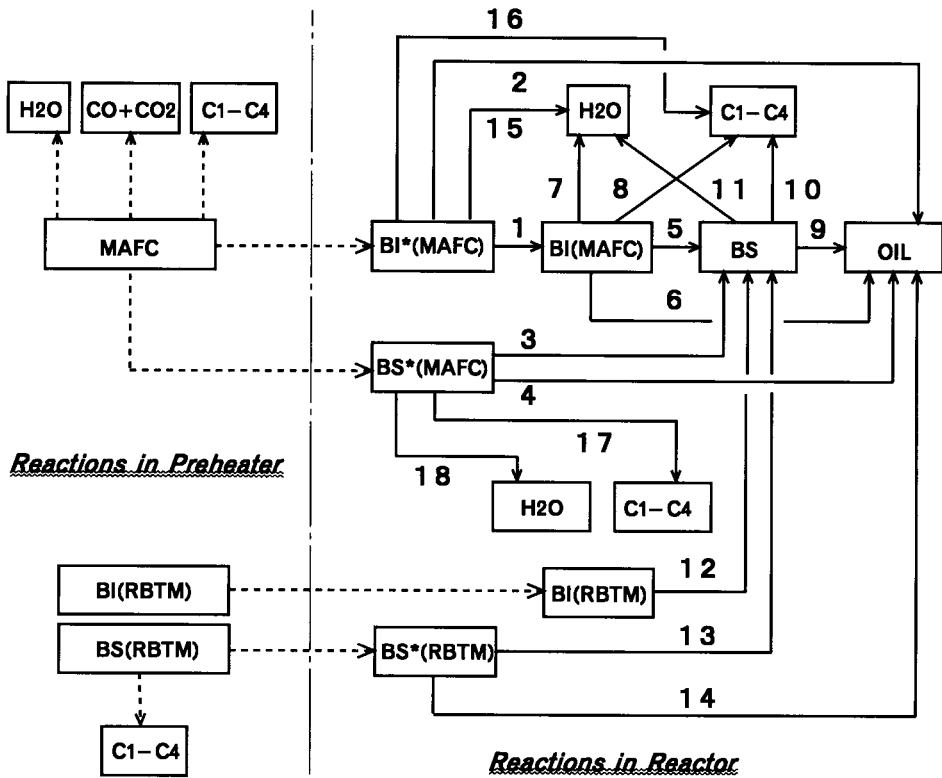


Fig. 1 Reaction Model

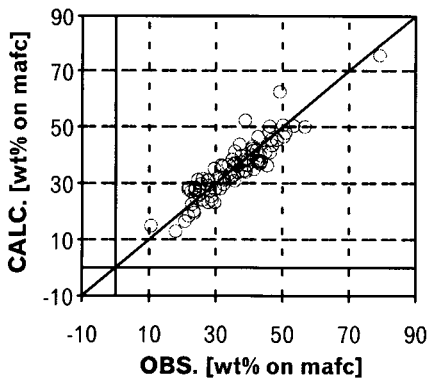


Fig. 2 Parity plot for oil yield(PDU)

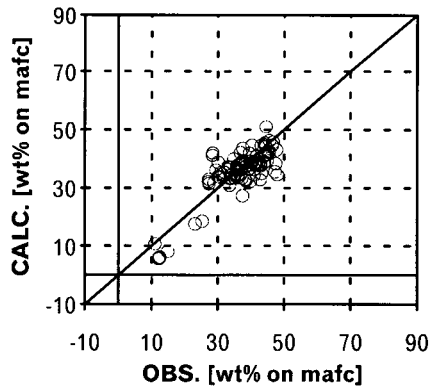


Fig. 3 Parity plot for oil yield(PP)

Behavior of hydrogen at coal liquefaction of NEDOL process

M. Mochizuki * , K. Endo * , K. Inokuchi

* Nippon Steel Corporation, 1, Kimitsu, Kimitsu-shi, Chiba-ken, Japan

Mitsui SRC Development Co., Ltd. 1-12-13 Nihonbashi Muromachi, Chuo-ku, Tokyo, Japan

1. INTRODUCTION

There are many reports^{1)~3)} concerning the behavior of hydrogen at coal liquefaction. However, all of them are the results by autoclave batch tests, and there are few reports discussing results of continuous coal liquefaction tests in long term operation.

Coal liquefaction tests were conducted on Wandoan, Illinois No.6, Wyoming and Tanito Harum coal at the NEDOL Process 1t/d Process Supporting Unit (PSU), and the behavior of hydrogen and deheterogeneity at coal liquefaction were investigated. Furthermore, the effect of *fa* (fraction of aromatic) of recycle solvent on the behavior of hydrogen was also studied.

2. EXPERIMENTAL

Wandoan coal from Australia, Illinois No.6 coal, Wyoming coal from U.S.A., and Tanito Harum coal from Indonesia were used as the raw coal, synthetic pyrite was the catalyst, and 50-50 mixture of creosote oil and anthracene oil was the initial solvent. Table 1 shows the properties of the coal used.

Table 2 shows the operating conditions. The basic condition of the PSU is a combination of reaction temperature 450°C, reaction pressure 170kg/cm²G, amount of catalyst addition 3wt%, gas/slurry ratio(G/L) 700Nℓ/kg, and difference of aromatic fraction (*fa*) of recycle solvent 0.06. Each experiment was conducted by changing only one factor of the basic condition.

3. RESULTS AND DISCUSSION

Table 3 shows the products yield of four coals under the basic liquefaction condition. The oil yield of Illinois No.6 coal is lower than the other coals and the residue yield is higher than the others. The gas yield and the water yield of Wyoming coal and Tanito Harum coal are higher than the others. Fig.1 shows the hydrogen balance supplied by coal, hydrogen gas and consumed to oil, gas, water and residue under the basic condition. The hydrogen consumption to H₂S and NH₃ gas in Illinois No.6 coal is much higher than the others because the total N and S content are much higher than the others. The hydrogen consumption to H₂O in Wyoming, Tanito Harum coals are much higher than the others because the O content of the two coals is much higher than the others.

Fig.2 shows the relation between the hydrogen consumption to liquefied oil and the oil yield in each Runs under the condition of various reaction temperature. In Illinois No.6 and Wyoming coal, the hydrogen consumption to the liquefied oil increases with increasing of liquefaction temperature, and the oil yield also increases. In Wandoan coal, hydrogen consumption to liquefied oil has its maximum point at the temperature of 450°C, and the oil yield also has its maximum point at the temperature, but above that temperature, hydrogen consumption to liquefied oil and oil yield decreases.

Fig.3 shows the relation between the amount of catalyst addition and the hydrogen consumption in Run3. The hydrogen gas consumption and the hydrogen consumption to the liquefied oil increase with addition of catalyst under the same reaction temperature. By autoclave test, T.Kabe⁴⁾ reported that the liquefaction catalyst promotes the hydrogen gas transfer to coal and solvent, and in our study, the behavior of hydrogen was recognized to be the same.

Fig.4 shows the relation between the Δf_a (f_a before hydrotreating - f_a after hydrotreating) of the recycle solvent and the hydrogen consumption. Δf_a of the recycle solvent increases and the proton donor capacity (PDQI⁵⁾) increases with the progressing of the solvent hydrotreating reaction. As the result, the hydrogen consumption to the liquefied oil increases and the oil yield also increases because the hydrogen would be used effectively to increase the proton donor capacity of the recycle solvent. And in our study, it is confirmed that Δf_a should be maintained above 0.04 to obtain over 50 wt% daf coal oil yield.

Table 4 shows the deheterogeneity in each coal. The degree of desulfurization in Illinois No.6 coal is the highest among the coals. And it is considered that this is caused by the high sulfur content in Illinois No.6 coal and the degree of desulfurization is mainly affected by the content of inorganic sulfur.

4. CONCLUSIONS

The hydrogen supplied for the coal liquefaction is easily consumed to the gas in high N, S, content coal such as Illinois No.6 coal and the degree of deheterogeneity is high. And the hydrogen is consumed to the water in high oxygen content coal such as Wyoming and Tanito Harum coal.

The hydrogen consumption at coal liquefaction depends on the properties of coal under the various liquefaction conditions.

5. ACKNOWLEDGMENT

This work is supported by the New Energy and Industrial Technology Development Organization (NEDO). The authors wish to express their sincere appreciation to that organization for having allowed them to make this study.

REFERENCES

1. T.Kabe et al, Fuel, Vol.66, No.10, 1326, 1987
2. M.Makabe et al, Fuel, Vol.65, No.2, 296, 1986
3. T.Kabe et al, Sekiyu Gakkaishi, Vol.28, No.2, 136, 1985
4. T.Kabe et al, Nenryo Kyokaishi, Vol.65, No.3, 180, 1986
5. Y.Sanada et al, Nenryo Kyokaishi, Vol.62, 106, 1983

Table 1 Properties of raw coals

Coal	C	H	N	S	O	Ash	(wt%)
Wandoan coal	78.1	5.9	0.9	0.1	15.0	9.9	
Illinois No.6 coal	78.8	5.4	1.3	3.6	10.9	12.2	
Wyoming coal	75.6	5.0	1.0	0.1	18.3	7.0	
Tanito Harum coal	76.6	5.6	1.4	0.2	16.2	4.8	

Table 2 Operating conditions at 1t/d PSU

Run	Coal	Temperature (°C)	Amount of catalyst (wt%)	Δ fa of recycle solvent (-)
1	4 coals	450	3.0	0.06
2	Wandoan	435 ~ 465	3.0	0.06
3	Wyoming	450	0~4.0	0.06
4	Wyoming	450	3.0	0.03~0.08

Table 3 Products Yield (wt% daf coal at basic condition)

Coal	Oil	Residue	Gas	Water	Consumed Hydrogen
Wandoan	50.87	25.20	19.25	10.02	-5.34
Illinois No.6	48.15	29.40	18.66	9.46	-5.67
Wyoming	49.80	22.63	21.39	11.89	-5.72
Tanito Harum	49.41	23.31	21.99	10.82	-5.54

Table 4 Deheterogeneity of coals (wt% at basic condition)

	Wandoan	Illinois No.6	Wyoming	Tanito Harum
Degree of denitrification	79.92	81.83	86.70	82.45
Degree of desulfuration	89.44	98.51	92.96	89.12
Degree of deoxidation	91.30	92.71	90.71	92.68

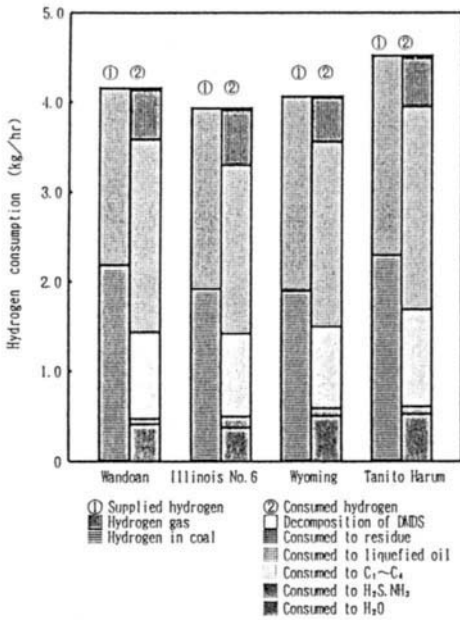


Fig. 1 Hydrogen balance between supplied hydrogen and consumed hydrogen

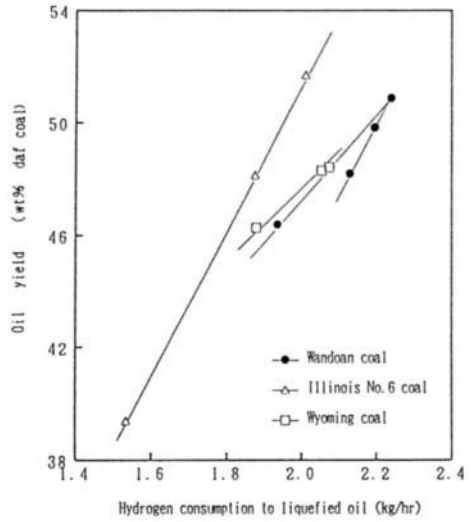


Fig. 2 Relation between hydrogen consumption to liquefied oil and oil yield

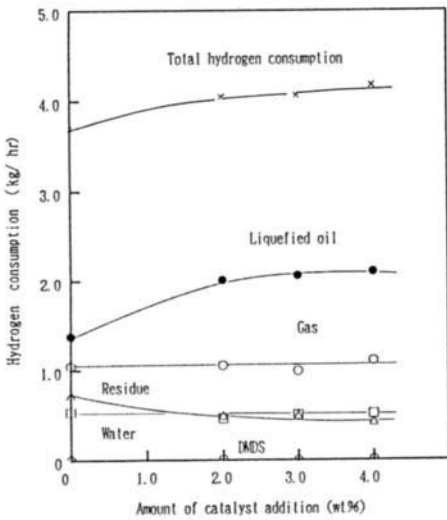


Fig. 3 Relation between amount of catalyst addition and hydrogen consumption

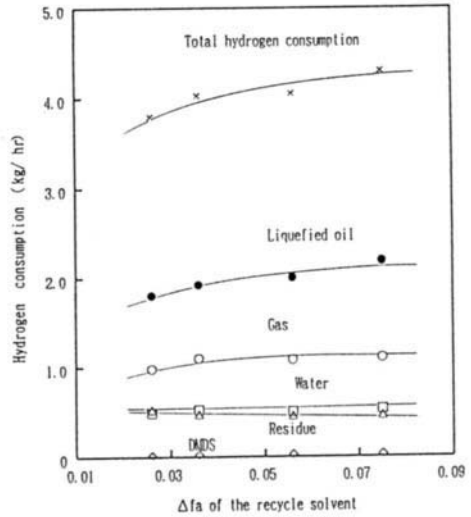


Fig. 4 Relation between Δf_a of recycle solvent and hydrogen consumption

Relationship between hydrogen-donating abilities and structural parameters of solvent systems in coal liquefaction

Shigeru Futamura

National Institute for Resources and Environment
16-3, Onogawa, Tsukuba, Ibaraki 305 JAPAN

It has been shown that the hydrogen-donating abilities of coal liquefaction residues (CLRs) are strongly affected by their molecular structures surrounding donatable hydrogens, based on the correlation analysis with the CLR structural parameters and the reaction variables of probe molecules. Candidate structures have also been proposed as key moieties of CLRs involved in hydrogen transfer processes under coal liquefaction conditions.

1. INTRODUCTION

In coal liquefaction processes, maintenance of solvent quality is vitally necessary in order to achieve high coal conversion and liquid yield. The author has already shown that CLRs are effective hydrogen donors to promote hydrogenation or hydrogenolysis of different types of hydrogen acceptors [1] and that deashed CLRs also act as hydrogen shuttler even with use of poor hydrogen-donating solvent [2]. This paper will present that the CLR abilities of radical capping, hydrogen shuttling and molecule-induced hydrogen transfer are strongly affected by their molecular structures rather than their α -hydrogen contents themselves, based on the correlation analysis with the reaction variables of probe molecules and the structural parameters of the solvent-fractionated CLRs and numerous model compounds of different structures.

2. EXPERIMENTAL

trans-Stilbene and the solvents were purchased and purified before use. The CLR samples were donated from Nippon Coal Oil Co., Ltd. Original coals are Wandoan (WA) and Wyoming (WY). CLR was fractionated by sonication in hexane (H), dichloromethane (D) and pyridine (P) successively. For example, WA₄₅₀DI-PS denotes dichloromethane insoluble-pyridine solubles of the residue obtained in the liquefaction of Wandoan coal at 450°C. Table 1 shows the chemical compositions and structural parameters of the CLR samples.

Batch reactions were carried out with a stainless steel, magnetically stirred

Table 1
Chemical compositions and structural parameters of solvent-fractionated CLRs

Residue	Chemical composition/wt%					Structural parameters			
	C	H	N	S+O	H/C	fa	Hau/Ca	σ	n
WA ₄₅₀ HS	86.30	6.65	0.54	6.51	0.92	0.73	0.73	0.39	2.42
WA ₄₅₀ HI-DS	87.44	5.92	0.79	5.85	0.81	0.79	0.69	0.36	1.82
WA ₄₅₀ DI-PS	85.78	5.20	1.67	7.35	0.73	0.84	0.67	0.34	1.51
WY ₄₅₀ HS	89.56	6.73	1.16	2.55	0.90	0.69	0.73	0.33	1.80
WY ₄₅₀ HI-DS	84.39	5.65	1.55	8.41	0.80	0.71	0.68	0.44	1.97
WY ₄₅₀ DI-PS	86.04	5.23	3.81	4.92	0.73	0.76	0.64	0.37	1.46

autoclave. Prescribed amounts of substrate and additive were put into the autoclave. Pressurized by nitrogen, the autoclave was heated up to a prescribed temperature and maintained for the prescribed period of time. After the reaction, the autoclave was cooled in ice water with an electric fan.

The products were collected with dichloromethane. Identification of the products derived from *trans*-stilbene has been described in the previous paper [1]. Quantitative analyses of the products were carried out with GC.

3. RESULTS AND DISCUSSION

3.1. Hydrogen Abstraction Selectivities of Intermediate Radicals

In the hydrogenation of *trans*-stilbene, bibenzyl was obtained along with 1,2-diphenyl-3-1-naphthylpropane (DPNP), 1,2-diphenylbenzo[a]indan (DPBI), 1-phenyl-2-1-naphthylethane (PEN) and toluene. During the course of the reaction, 1,2-diphenylethyl radical was formed via a hydrogen atom addition to *trans*-stilbene or secondary decomposition of DPNP. 1,2-Diphenyl-3-1-naphthyl-1-propyl radical was exclusively formed in addition of 1-naphthylmethyl radical to *trans*-stilbene. S(DPE) and S(DPNP) give the hydrogen abstraction selectivities of 1,2-diphenylethyl and 1,2-diphenyl-3-1-naphthyl-1-propyl radicals initially formed via the addition of a hydrogen atom or 1-naphthylmethyl radical to *trans*-stilbene, where C_{t-ST} , Y_{BB} , Y_{DPNP} , Y_{DPBI} and Y_{TOL} denote the *trans*-stilbene conversion and the yields of bibenzyl, DPNP, DPBI and toluene, respectively.

$$S(DPE) = 100 (Y_{BB} - 15Y_{TOL}/11) / (C_{t-ST} - Y_{DPNP} - 26Y_{TOL}/11 - Y_{DPBI}) \quad (1)$$

$$S(DPNP) = 100 (Y_{DPNP} + 26Y_{TOL}/11) / (Y_{DPNP} + 26Y_{TOL}/11 + Y_{DPBI}) \quad (2)$$

Figures 1 and 2 show the additive effect of CLRs on S(DPE) and S(DPNP). Although higher than 90%, S(DPE) doesn't correlate with $H\alpha$ ($2.0 \leq \delta \leq 4.5$ ppm) content of CLR. The DI-PS fractions seem to have unexpectedly lower hydrogen-donating abilities for their $H\alpha$ contents. In the capping of sterically more hindered 1,2-diphenyl-3-1-naphthyl-1-propyl radical, a similar trend has been observed for

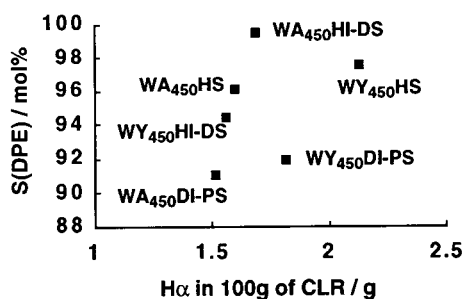


Figure 1. Relationship between H α content of CLR and S(DPE).

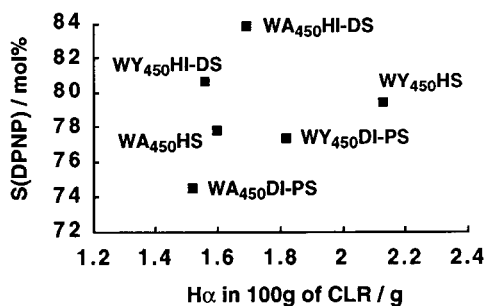


Figure 2. Relationship between H α content of CLR and S(DPNP).

the additive effect of CLR. All these data strongly suggest that the sterically congested molecular structures of the DI-PS fractions are responsible for the low mobilities of their donatable hydrogens.

3.2. Solvent Effect on Hydrogen Shuttling by CLR

The amounts of hydrogen atoms transferred from 1-methylnaphthalene (1-MN) and tetralin were determined by monitoring the yields of the products derived from the solvents. Figure 3 shows that in 1-MN, hydrogen shuttling effect of CLR increases with their degrees of aromatic ring condensation. These facts suggest that in poor hydrogen donor solvent like 1-MN, the step of the first hydrogen atom transfer from 1-MN to CLR is rate-limiting. The two straight lines separately obtained for the WA and WY residues indicate that they have different types of structures responsible for hydrogen shuttling.

On the other hand, a maximum value was obtained at around 0.68 of Hau/Ca in the plot of CLR Hau/Ca vs. the amount of hydrogens transferred from tetralin (Figure 4). These facts suggest that the first hydrogen atom transfer from tetralin to CLR is less endothermic and that the second hydrogen atom transfer from the

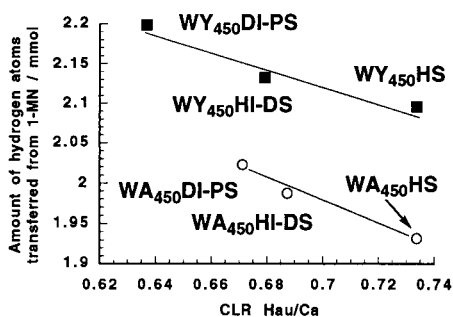


Figure 3. Relationship between CLR Hau/Ca and the amount of hydrogen atoms transferred from 1-MN at 380°C.

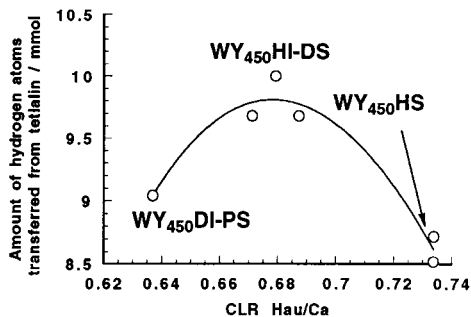


Figure 4. Relationship between CLR Hau/Ca and the amount of hydrogen atoms transferred from tetralin at 380°C.

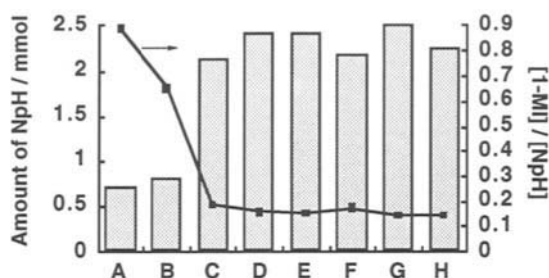


Figure 5. Additive effect on the chemical behavior of tetralin.

A: No additive; B: Anthracene; C: WA₄₅₀HS; D: WA₄₅₀HI-DS;
E: WA₄₅₀DI-PS; F: WY₄₅₀HS; G: WY₄₅₀HI-DS; H: WY₄₅₀DI-PS

hydrogenated CLR to *trans*-stilbene is also rate-limiting. Since recycle solvent abounds in tetralin-type hydroaromatic compounds, Hau/Ca can be a good measure to control hydrogen-shuttling ability of recycle solvent.

3.3. Additive Effect of CLR on Chemical Behavior of Tetralin

In the above reaction, addition of CLR increased naphthalene yields and decreased the molar ratios of 1-methylindan to naphthalene [1-MI]/[NpH] (Figure 5). All the CLR's increased naphthalene yields much more than anthracene, suggesting that the efficiency of hydrogen shuttling can be governed by the hydrogen-donating ability of the hydrogenated form of the shuttler rather than by the hydrogen-accepting ability of the shuttler at 380°C. The [1-MI]/[NpH] ratios sharply decreased on addition of the CLR's. Therefore, selective hydrogen transfer from tetralin can be promoted by CLR's with suppressed skeletal rearrangement of tetralin.

The ability to transfer hydrogen atoms from tetralin under the same conditions decreased in the order of Ni > active carbon > CLR >> Mo > Fe > graphite > Zn on the weight basis. Thus, CLR can be expected to act as efficient and selective hydrogen-transfer agent under coal liquefaction conditions.

3.4. Correlation Analysis of the Structural Parameters for CLR's

Correlation analyses with the structural parameters of the CLR's and 33 model hydrocarbons have shown that perhydro-derivatives of aromatic hydrocarbons with tertiary hydrogens such as tetrahydrofluoranthene, hexahydrochrysene and tetrahydrobenzophenylene are possible key structures acting as hydrogen donor and affording hydrogen-shuttling moieties after their dehydrogenation.

REFERENCES

1. S. Futamura and K. Ohkawa, J. Jpn. Inst. Energy, 72 (1993) 951.
2. S. Futamura, Preprints, Am. Chem. Soc., Div. Petroleum Chem., 39(3) (1994) 327.

Hydrogen transfer in brown coal liquefaction in BCL process -- Influence of catalyst and feed solvent properties on liquefaction performance and hydrogen transfer --

Osamu OKUMA^a, Motoharu YASUMURO^b, Tetsuo MATSUMURA^b and Shnichi YANAI^c

^aPolymer & Chemical Technology Laboratory, Kobe Steel, Ltd.
Takatsukadai 1-5-5, Nishi-ku, Kobe 651-22, Japan

^bNippon Brown Coal Liquefaction Co., Ltd. (c/o Kobe Steel, Ltd., Takasago Works)
Niihama 2-3-1, Arai-cho, Takasago, Hyogo 676, Japan

^cNew Energy and Industrial Technology Development Organization (NEDO)
Higashi-Ikebukuro 3-1-1, Toshima-ku, Tokyo 170, Japan

1. INTRODUCTION

A two-stage brown coal liquefaction (BCL) process has been developed for Victorian brown coal in Australia by Nippon Brown Coal Liquefaction Co.(NBCL). As shown in Fig.1, in this process, the coal is liquefied in the primary hydrogenation (PH) section using a disposable iron/sulfur catalyst and a mixture of the solvents from both the primary and secondary (SH) hydrogenations to obtain high distillate yield under mild liquefaction conditions[1]. The amount of hydrogen transferred among the coal, solvent and H₂ gas is a crucial factor to determine the liquefaction performance of the process.

This paper discusses the relationship between hydrogen transfer and liquefaction yields of the brown coal under the conditions varied in temperature and pressure and focuses on the role of the catalyst and solvent to estimate the efficiency of the transferred hydrogen.

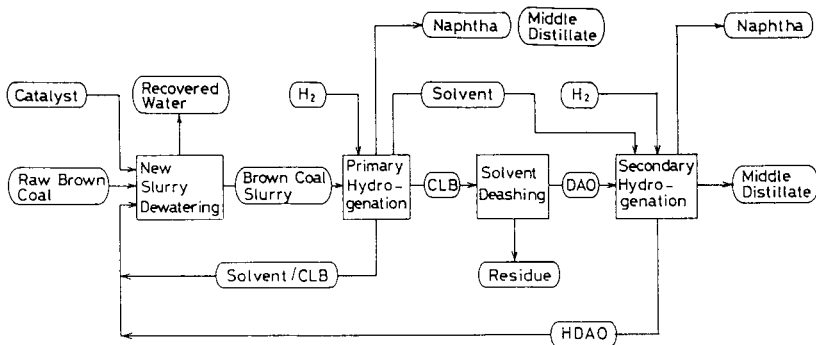


Figure 1 Block flow diagram of BCL process

2. EXPERIMENTAL

Morwell brown coal was used for liquefaction. It contained 10.7 wt.% moisture, 2.4 wt.% ash, and C 67.8, H 4.8, N 0.6, S 0.3 and O 26.3 (diff.) on moisture and ash free (maf-C) basis. The solvents (b.p. 180-420°C) used were the recycled solvent in the PH section and the recovered solvent from the SH section. These solvents were prepared using each process development unit. Table 1 shows the properties of these solvents. The catalyst used was Fe₂O₃ and sulfur (S/Fe atomic ratio 1.2). The liquefaction was carried out using a 5L magnet-driven autoclave under the conditions shown in Table 2. Product yields were calculated for naphtha (b.p.<180 °C), solvent (b.p.180-420°C), CLB (coal liquid bottom, b.p.>420°C), H₂O, C₁-C₄, CO and CO₂ [2]. Hydrogen transfer was evaluated by the following method.

ΔH_2 : H₂ gas consumption

H(t): Amount of transferred hydrogen from feed solvent and H₂ gas to total liquefaction products, $H(t) = \Delta H_2 - H(s)$.

H(s): Change in hydrogen content of feed solvent, $H(t) = W_s \cdot (C_p - C_f)$,

W_s: Weight of feed solvent, C_p: hydrogen content of feed and recovered solvent, C_f: hydrogen content of recovered solvent.

*Negative value of H(s) gives transferred hydrogen from feed solvent to products.

H(p): Amount of hydrogen contained in produced distillate (b.p.< 420°C).

DY/H(t): Distillate yield per unit H(t),

*Efficiency of hydrogen consumption on distillate production.

H(p)/H(t): Amount of hydrogen in produced distillate per unit H(t),

*Efficiency of transferred hydrogen to distillate.

Table 1 Properties of feed solvents

Solvent	Ultimate Analysis (wt%)						Structural Parameters				
	C	H	N	S	O(diff.)	H/C	fa	σ	Hau/Ca	Ln	
P-1 ^a	89.2	7.6	0.7	0.2	2.3	1.01	0.72	0.24	0.86	2.00	
P-2 ^a	88.3	7.7	0.6	0.2	3.2	1.04	0.72	0.27	0.90	1.90	
S-1 ^b	89.4	9.0	0.2	<0.1	1.4	1.19	0.57	0.35	0.90	2.63	
S-2 ^b	90.1	9.5	0.2	<0.1	0.2	1.25	0.53	0.35	0.90	2.83	

a: Recycle solvent in primary hydrogenation using iron/sulfurcatalyst with PDU.

b: Recovered solvent from secondary hydrogenation over Ca-Ni-Mo catalyst with PDU.

3. Results and discussion

3.1. Influence of catalyst and solvent property (Run A series)

As shown in Table 2 and Fig.2, the liquefaction reaction was accelerated and the distillate yield (DY) increased by addition of the catalyst in both feed solvents (P-1, S-1) although the effect of the catalyst on the DY was larger in P-1 than in S-1. The yields of H₂O, CO and CO₂ were little affected by the catalyst and feed solvent properties. The S-1, a hydrogen-donor solvent, provided higher DY than the P-1 at the lower catalytic condition and/or shorter reaction time. The P-1 provided higher DY than the S-1 at the higher catalytic condition and longer reaction time. This is because the hydrogen transfer from the donor solvent (expressed by negative value of H(s) in the S-1) is fast and plays an important role in non-catalytic liquefaction, and the catalyst is more effective in the non-donor and high aromatic solvent (P-1) and plays an important role in conversion of the CLB to the solvent fraction [2]. ΔH_2 and H(t) were markedly increased with addition of the catalyst although they were saturated above its concentration of 3 wt.% on maf-C as Fe. C₁-C₄ gas yield was suppressed

Table 2 Liquefaction conditions, yields and transferred hydrogen

Run A Series														
Conditions: Temp. 430 °C, H ₂ int. press. 6 MPa, Feed solv/maf-C (wt/wt) 2.5														
Run	Solv. ^a	Cat. ^b	Time	Yields(wt% on maf-C)					Transferred Hydrogen (wt% on maf-C)					
				CLB	Solv.	Naph.	C ₁ -C ₄	DY ^c	ΔH ₂	H(s)	H(t)	H(p)	H(p)/H(t)	
RA-01	P-1	1.5	0	74.5	-3.2	5.2	2.4	2.0	2.25	0.15	2.10	0.33	0.16	
RA-02		3.0		69.2	3.1	6.8	2.3	9.9	2.61	0.25	2.36	0.99	0.42	
RA-03		5.0		62.9	7.2	6.5	2.3	13.7	2.83	0.50	2.33	1.26	0.54	
RA-04		10.0		58.4	12.7	7.9	1.9	20.6	2.90	0.52	2.37	1.87	0.79	
RA-11	P-1	0	60	76.6	-13.1	6.6	6.5	-6.5	1.88	-0.03	1.91	-0.19	-	
RA-12		1.5		53.7	6.0	12.7	6.7	18.7	3.44	0.32	3.11	2.02	0.65	
RA-13		3.0		48.6	15.0	10.9	6.0	25.9	3.80	0.50	3.30	2.57	0.78	
RA-14		5.0		44.3	18.2	10.4	6.0	28.6	4.06	0.60	3.46	2.69	0.78	
RA-15		10.0		37.5	27.4	11.7	5.4	39.1	4.07	0.60	3.47	3.54	1.02	
RA-21	S-1	0	0	70.9	-2.3	9.7	2.2	7.4	0.46	-2.25	2.71	1.03	0.38	
RA-22		3.0		66.0	2.4	9.8	2.3	12.2	1.78	-1.68	3.46	1.38	0.39	
RA-23		10.0		59.3	9.6	9.8	2.1	19.4	2.18	-1.08	3.25	2.09	0.64	
RA-31	S-1	0	60	58.9	-3.3	11.2	6.6	7.9	0.93	-2.88	3.81	1.14	0.30	
RA-32		3.0		47.6	13.5	13.6	4.5	27.1	2.24	-1.98	4.21	3.52	0.84	
RA-33		10.0		45.5	6.5	22.9	4.5	29.4	2.69	-1.70	4.39	3.30	0.75	
a: See Table 1, b: Fe ₂ O ₃ , wt% on maf-C as Fe, S/Fe atomic ratio 1.2, c: Distillate yield (b.p. <420°C) = Naphtha (b.p.<180°C) yild+ Solvent (b.p.180-420 °C).														
Run B Series														
Conditions: Reaction (hold) time 60 min, Cat.(Fe ₂ O ₃) 3 wt% on maf-C as Fe, S/Fe 1.2														
Run	Solv.	Press ^d	Temp.	Yields(wt% on maf-C)					Transferred Hydrogen					
				CLB	Solv.	Naph.	C ₁ -C ₄	DY	ΔH ₂	H(s)	H(t)	H(p)	H(p)/H(t)	
RB-01	P-2	250	3	430	63.5	2.0	10.6	6.3	12.6	2.53	-0.24	2.77	1.04	0.37
RB-02	S-2				54.9	7.9	13.9	5.2	21.8	1.45	-1.45	2.90	1.95	0.67
RB-11	P-2	250	3	460	62.5	-12.6	15.4	16.6	2.8	3.44	-1.04	4.48	-	-
RB-12	S-2				46.9	-1.6	22.2	13.3	20.8	2.22	-2.41	4.63	2.37	0.51
RB-21	P-2	250	6	430	53.2	14.8	9.6	5.0	24.4	3.64	0.31	3.33	2.03	0.61
RB-22	P-2/S-2	150/100			52.4	15.2	10.3	5.1	25.5	2.85	-0.64	3.49	2.30	0.65
RB-23	S-2	250			47.4	18.7	11.3	4.0	30.0	2.49	-1.08	3.57	2.31	0.64
RB-31	P-2	250	6	460	40.3	11.6	16.0	14.1	27.6	5.13	0.07	5.06	2.68	0.52
RB-32	P-2/S-2	150/100			39.5	15.7	14.7	12.2	30.4	4.14	-0.96	5.10	2.99	0.57
RB-33	S-2	250			37.3	12.9	20.9	11.7	33.8	3.40	-1.38	4.78	3.32	0.69
RB-41	P-2	250	12	430	46.4	21.1	10.5	5.8	31.6	3.83	0.89	2.94	3.01	1.02
RB-42	P-2/S-2	200/50			45.7	20.5	11.3	5.1	31.8	3.70	0.38	3.32	3.08	0.93
RB-43	S-2	250			45.5	19.6	13.0	4.0	32.6	3.21	-0.12	3.33	2.66	0.79
RB-51	P-2	250	12	460	26.5	27.2	16.8	12.9	44.0	6.18	0.77	5.41	4.17	0.77
RB-52	P-2/S-2	200/50			27.4	21.8	20.4	12.4	42.2	6.11	0.43	5.67	4.42	0.77
RB-53	S-2	250			33.2	18.8	20.9	9.7	39.7	4.82	-0.43	5.25	3.88	0.74
d: H ₂ initial pressure at room temp., e: See Table 1, f: wt% on maf-C (Solv/maf-C 2.5, wt/wt)														

by the catalyst and hydrogen-donor solvent (S-1), and every ΔH₂ in the S-1 was smaller than that in the P-1. However, H(t) in the S-1 was larger than that in the P-1, and hydrogen efficiencies (DY/H(t), H(p)/H(t)) were smaller in the S-1 than in the P-1 as shown in Fig. 2 and Table 2. This is because the S-1 provided higher naphtha yield and the liquid products (CLB, solvent and naphtha) of higher hydrogen content compared with the P-1.

3.2 Influence of temperature and hydrogen pressure (Run B series)

Table 2 and Fig. 3 shows the results of the liquefaction under the conditions varied in

temperature and hydrogen pressure in the presence of the catalyst of 3 wt.% on maf-C as Fe. In both hydrogen-donor (S-2) and non-donor (P-2) solvents, the DY increased with an increase in the hydrogen pressure. However, the effect of the hydrogen pressure on the DY was larger in P-2 than in S-2. The S-2 provided higher DY than the P-1 at lower temperature and lower hydrogen pressure. The P-2 provided higher DY than the S-1 at higher temperature and higher hydrogen pressure. The effect of the solvent properties on the hydrogen transfer (ΔH_2 , H(t), H(s)) was similar to that mentioned above. The S-2 gave higher DY/H(t) and H(p)/H(t) at lower hydrogen pressure, and the P-2 gave them at higher hydrogen pressure. In both solvents, a lower temperature (430°C) gave higher hydrogen efficiency because C1-C4 gas yield increased markedly at a higher temperature (460°C). The mixture solvent of the P-2 and S-2 which are used in the PH section of BCL process gave the results between those of the P-1 and S-1 as shown in Table 2.

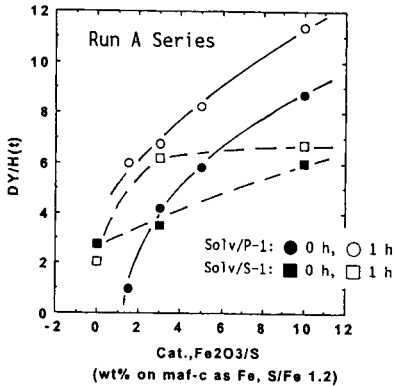


Figure 2 Effects of catalyst and feed solvent

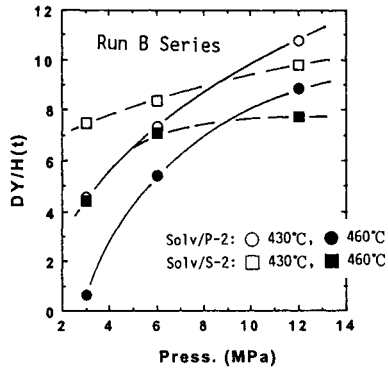


Figure 3 Effects of hydrogen pressure and temperature

4. CONCLUSION

This study made clear the influence of the important liquefaction factors such as the catalyst, hydrogen-donor ability of the solvent and conditions (temperature, hydrogen pressure and reaction time) on the performance and hydrogen transfer of the brown coal liquefaction in BCL process. The results obtained are as follows; (1) Hydrogen-donor solvent recovered from the SH section is effective in the initial stage of the liquefaction and suitable for the liquefaction under mild conditions. This is because the transferred hydrogen plays an important role in these conditions. However, it does not provide a higher distillate yield without the catalyst. (2) Non-donor solvent recycled in the PH section is suitable for the liquefaction under severe conditions. (3) Hydrogen transfer to the products increases with an increase in the severity of the liquefaction conditions. However, at higher temperatures, the hydrogen efficiency decreases due to an increase in C1-C4 gas yield. The hydrogen transfer and efficiency are quantitatively evaluated by calculation of the hydrogen balance before and after the liquefaction.

REFERENCES

1. O.Okuma, et al., Fuel Processing Technology, 14 (1986) 23-37
2. O.Okuma, et al., Nenryo-kyokai-shi (J. Fuel Society, Japan), 69 (1989), 46-55

Heat treatment of coals in hydrogen-donating solvents at temperatures as low as 175-300°C

M. Iino, J. Shen, S. Ashida and T. Takanohashi

Institute for Chemical Reaction Science, Tohoku University,
Katahira 2-1-1, Aoba-ku, Sendai 980 Japan

Heat treatment of 7 coals of different rank was carried out in various solvents at 175-300°C under N₂ atmosphere. Retrogressive reaction of the coal was observed in TET at 175 and 250°C, while, in DHA and HHA, which are much stronger hydrogen donors than TET, the coal underwent dissolution reactions at 175-300°C. Hydrogen donation to coal radicals from DHA or HHA is suggested for the dissolution reaction observed in this study.

1. INTRODUCTION

The mechanisms of retrogressive reactions in coal liquefaction and pyrolysis and how to prevent them efficiently have received increased attention. Although the details of retrogressive reactions are still obscure, hydrogen donation to coal fragments is known to be a key reaction for the suppression of the retrogressive reactions. Especially, the radicals formed during the initial stages of coal liquefaction must be stabilized efficiently to prevent retrogressive reactions which could lead to the formation of refractory, high-molecular-weight species.

Carbon disulfide-N-methyl-2-pyrrolidinone (CS₂-NMP) mixed solvent (1:1 by volume) has been reported to give high extraction yields (40-65%, daf) at room temperature for many bituminous coals [1, 2]. No significant occurrence of reactions of the solvents with the coals, which would result in an increase of the extraction yields, is indicated for this extraction, suggesting that the extracts obtained originally existed in the coals [1]. We also found that the extracts obtained with the CS₂-NMP mixed solvent include a considerable amount of the very heavy extract component which is not soluble in THF or pyridine, but soluble in the mixed solvent.

We have used the mixed solvent as an extraction solvent for the heat treatment products of the bituminous coals at 300-450°C in tetralin

(TET) or naphthalene(NAP) without a catalyst. The results obtained showed that retrogressive reactions occur more readily for the heaviest fraction, i. e., THF-insoluble, the CS_2 -NMP mixed solvent-soluble fraction(TIMs), than for other lighter fractions such as benzene-insoluble, THF-soluble (preasphaltene) and n-hexane-insoluble, benzene-soluble (asphaltene) fractions. The heat treatment of TIMs itself, which was obtained from the extraction of Zao Zhuang raw coal with the CS_2 -NMP mixed solvent at room temperature, in several solvents at 100-350°C, showed that the retrogressive reactions, i. e., the conversion of TIMs to the mixed solvent insoluble fraction(MI), was suppressed by adding a strong hydrogen-donating solvent such as 9, 10-dihydroanthracene(DHA) or 1, 4, 5, 8, 9, 10 hexahydroanthracene(HHA). It was also found that, as more hydrogen was transferred from the solvent to TIMs, the extent of the retrogressive reactions decreased[4].

In this study, heat treatments of several coals were carried out at 175-300°C in various solvents[5]. The coals were found to undergo either retrogressive reactions or dissolution reactions even at temperatures as low as 175°C, depending on the hydrogen donatability of the solvent used. The mechanisms for these reactions are discussed.

2. EXPERIMENTAL

Pocahontas No. 3(89.7% C, daf), Zao Zhuang(86.9% C, daf), Upper Freeport(86.2% C, daf), Pittsburgh No. 8(82.6 % C, daf), Illinois No. 6(80.0% C, daf), Wyoming(75.1% C, daf) and Beulah-Zap(71.6% C, daf) coals were used. The solvents used are TET, NAP, 1-methylnaphthalene (MNA), DHA, HHA, and liquefaction recycle solvent(LRS, 88.5% C, 9.7. % H). Heat treatment of 1g of a coal was carried out at 175, 250 and 300°C for 1h in 5g of a solvent under N_2 atmosphere (5MPa), by using a 50ml magnetically stirred autoclave. After the heat treatment, the coal was fractionated into MI and MS, and then into TIMs and TS(and the solvent), at room temperature, as shown in Figure 1.

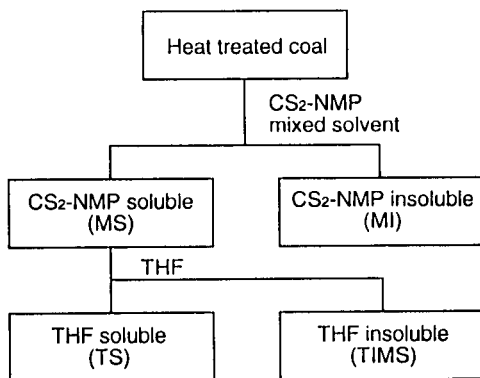


Figure 1. Fractionation procedure of heat treated coal

3. RESULTS AND DISCUSSION

Figure 2 shows fraction distribution after the heat treatment of Upper Freeport coal in MNA, TET, DHA, HHA, and LRS at 175°C, 250°C, and 300°C for 1 h, together with that for the raw Upper Freeport coal, which was obtained from the extraction of the raw coal with the CS₂-NMP mixed solvent at room temperature and the fractionation of the extract obtained. At 175 and 250°C in MNA and TET, MI increased and TMS decreased, compared with those for the raw coal, suggesting the

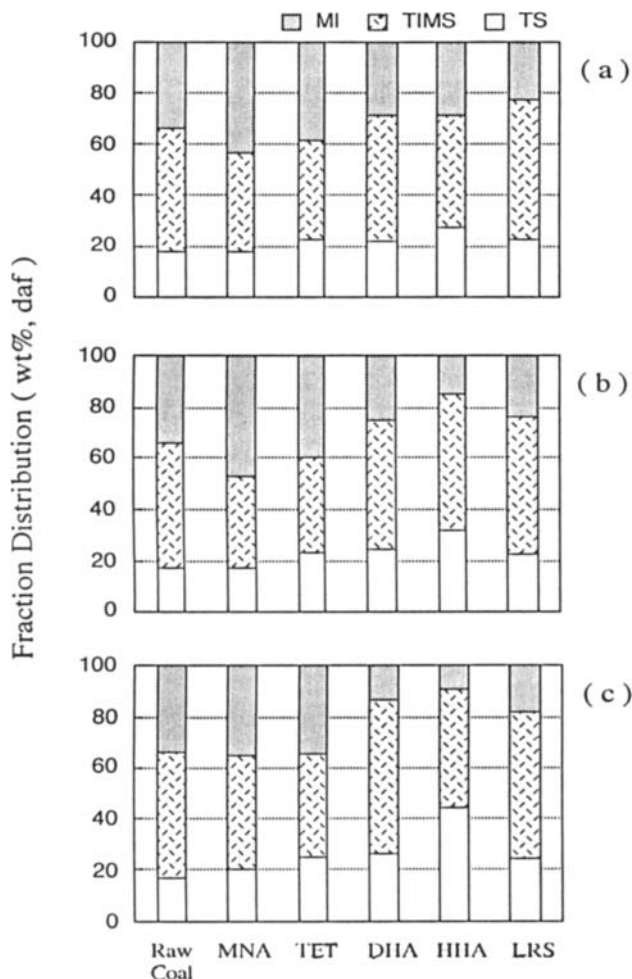


Figure 2 Fraction distribution after the dissolution reaction of Upper Freeport coal in 1-methylnaphthalene(MNA), tetralin (TET), DHA, HHA and LRS at 175 °C (a), 250 °C (b) and 300 °C (c) for 1 h, together with that for the raw coal.

occurrence of retrogressive reactions. While, in a strong hydrogen-donating solvent such as DHA, HHA, and LRS, MI decreased and TS increased by the treatment, i. e., dissolution reactions occurred. At 300°C in MNA and TET the quantity of MI is similar to that for the raw coal, and in DHA, HHA, and LRS the decrease of MI and the increase of TS were further enhanced. Especially, in HHA the dissolution yield of 90.6% was obtained at 300°C. Zao Zhang coal showed similar results as Upper Freeport coal. For other coals used here also gave similar, but smaller solvent and temperature dependencies as the two coals above described.

Figure 3 shows the plot of dissolution yield, which was expressed as the sum of the increase of TS (ΔTS) and the decrease of MI ($-\Delta MI$), versus hydrogen transferred from a solvent to coal during the dissolution of Zao Zhang and Upper Freeport coals in DHA and HHA at 175-300°C. Figure 3 shows that the dissolution yield is well correlated with the amount of hydrogen transferred during the reaction, suggesting that hydrogen donation to coal radicals from the solvent is a key step for the dissolution reaction. The nature of radicals responsible for this reaction will be discussed.

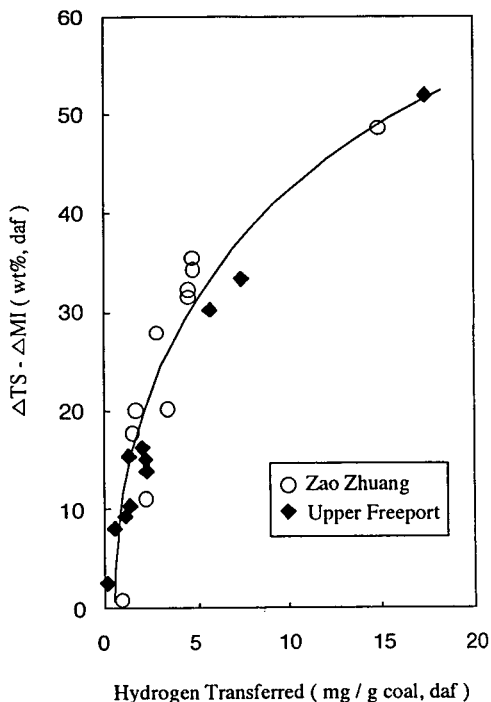


Figure 3 Plot of dissolution yields versus hydrogen transferred during the dissolution reaction of Zao Zhuang (○) and Upper Freeport (◆) coals in DHA and HHA at 175-300°C.

REFERENCES

1. M. Iino, T. Takanohashi, H. Ohsuga and K. Toda, *Fuel*, 67(1988) 1639.
2. M. Iino, T. Takanohashi, H. Ohsuga, H. Tsueta and Y. Sanokawa, *Fuel*, 68(1989) 1588.
3. X. Wei, J. Shen, T. Takanohashi and M. Iino, *Energy Fuels*, 3(1989) 575.
4. J. Shen, T. Takanohashi and M. Iino, *Energy Fuels*, 6(1992) 854.
5. J. Shen and M. Iino, *Energy Fuels*, 8(1994) 978.

Comparative roles of hydrogen gas and solvent in liquefaction of low-rank coals

Lili Huang and Harold H. Schobert

Fuel Science Program, Department of Materials Science and Engineering, The Pennsylvania State University, University Park, PA 16802, USA

Three U.S. low-rank coals were investigated at 250–450°C using tetralin and a molybdenum sulfide catalyst. Donor solvent provides high conversions and prevents retrogressive reactions throughout the temperature range investigated. Catalytic hydrogenation provides better product quality at low temperatures, but is not so effective at preventing retrogressive reactions at high temperatures. Up to 400°C donor solvent and catalyst are equally effective for providing high conversion. At 450° catalytic hydrogenation in the absence of donor solvent is not as effective as donor solvent reaction in the absence of catalyst. At this temperature gas-phase H₂ is not sufficient, even in the presence of catalyst, to prevent retrogressive reactions. The highest conversions at 450° were achieved only by combining catalytic hydrogenation with presence of a donor solvent.

1. INTRODUCTION

For the low-rank coals in this study we presume that initial bond breaking and radical formation results from thermolysis, based on earlier work by others [1–3]. Effective conversion can be achieved only with external hydrogen. The strategies for supplying external hydrogen are to use a donor solvent, gaseous H₂ (usually with a good catalyst), or both. When both are used, the presence and composition of the solvent may influence the effectiveness of the catalyst, or vice versa. We conducted studies to compare how solvent, catalyst, and the two together influence conversion and product distribution in low-rank coal liquefaction.

2. EXPERIMENTAL

The coals used in this work were Texas subbituminous C (DECS-1), Montana subbituminous B (DECS-9), and a North Dakota lignite (DECS-11), obtained from the Penn State Coal Sample Bank and Data Base. Characteristics of the coals are given in Table 1.

Liquefaction was done in microautoclaves of nominal 25 mL capacity. Gas pressure was 7 MPa at ambient temperature. Sample weights were 4 g of coal and 4 g of solvent (if a solvent were used). The reactor was immersed into a fluidized sandbath preheated to the desired temperature and was shaken during reaction. Reaction proceeded for 30 min after the reactor had reached temperature (usually in 3–5 min). Several solvents were used [4]; here we give results with tetralin and 1-methylnaphthalene. For catalytic experiments, coals were impregnated with ammonium tetrathiomolybdate (ATTM) applied from a slurry in 1:1 water:tetrahydrofuran (THF). After venting gases, the products were extracted sequentially with hexane (to recover oils), toluene (asphaltenes) and THF (preasphaltenes). Conversion is determined from the weight of the THF-insolubles. An extensive description of experimental and analytical techniques and parametric studies of the effects of impregnation methods, reaction time, moisture, and heating strategies has been published elsewhere [4].

Table 1.
Characteristics of coals used in this work.

	DECS-1	DECS-9	DECS-11
Proximate (wt % as received)			
Moisture	30.0	24.7	33.4
Ash	11.1	4.8	6.4
Volatile matter	33.2	33.5	37.4
Fixed carbon	25.8	37.1	22.9
Ultimate (wt% dmmf basis)			
Carbon	76.1	76.1	74.2
Hydrogen	5.5	5.1	4.4
Nitrogen	1.5	0.9	1.0
Sulfur (organic)	1.1	0.3	0.4
Oxygen (by difference)	15.8	17.5	20.0

3. RESULTS AND DISCUSSION

3.1 Behavior of solvents in the absence of catalyst

Results obtained from all coals and solvents and several heating strategies are documented and discussed elsewhere [4]. As an example, Figure 1 shows the effects of solvent for liquefaction of DECS-1 as a function of temperature. Several effects are evident. At 250° there is no distinction among results; the very low conversion indicates that little occurs at this temperature. At 300–350°, a solvent is better than reaction without solvent, but there is no distinction between a donor (tetralin) or non-donor (1-methylnaphthalene) solvent. We attribute the superior results (compared to reaction without solvent) to solvation of molecular fragments removed from the coal. Solvation and subsequent dispersion of these fragments throughout the reacting medium may reduce occurrence of retrogressive reactions. Above 350°, where thermal decomposition of the coal becomes significant, the distinction between the donor solvent and non-donor solvent becomes marked. In this regime, the donor solvent is crucial to attaining high conversions. The distinction between the non-donor solvent and reaction in absence of solvent is lessened at these higher temperatures, again suggesting the ability of the solvent to donate hydrogen is crucial. At high temperatures physical solvation effects may become less important if a significant portion of the solvent is in the vapor phase. Similar results to those of Figure 1 have been obtained for the other two coals [4].

3.2 Behavior of catalyst in the absence of solvent

Figure 2 shows results for the coals impregnated with ATTM. Because conversions are quite low <350°, experiments with DECS-9 and DECS-11 were not done at the lower temperatures. Below 350° and in the absence of solvent, this catalyst does not enhance conversion, consistent with work showing that ATTM transforms to an active catalyst at temperatures between 300 and 350° [5]. At 350–400°, conversions for reaction with ATTM and no solvent are similar to those for donor solvent without catalyst, illustrated in Table 2. For DECS-1, ATTM without solvent is superior to tetralin without catalyst. However, for the other two coals the similarity is remarkable, and suggests that, if conversion were the only criterion, the two conditions are essentially interchangeable. However, product quality is also an issue. No consistent trend was observed in comparing catalytic, solvent-free reactions with non-catalytic reactions in donor solvent for these coals. For DECS-1 and -9, reaction with catalyst resulted in substantially higher oil yield (e.g., for DECS-1, 59% from the catalytic reaction vs. 37% from donor solvent reaction) and corresponding reduction of preasphaltenes. This suggests that the catalyst also participates in hydrotreating of the heavy products. DECS-11

Table 2
Comparison of conversions (wt% dmmf) from non-catalytic donor-solvent reactions and catalytic solvent-free reactions at 400°

Coal sample	Non-catalytic, donor solvent	Catalytic, solvent-free
DECS-1	82.0	95.5
DECS-9	74.2	78.5
DECS-11	65.9	63.5

showed the opposite trend. Gas make is slightly lower in catalytic, solvent-free reactions. The third characteristic of catalytic, solvent-free reactions is evident from Figure 2—the onset of retrogressive reactions above 400°. Conversions are invariably lower at 450° than at 400°.

3.3 Reactions with both catalyst and donor solvent

An issue of concern is a possible synergistic effect of catalyst and solvent. For reactions at 400°, no effect was observed for DECS-1, but conversion in the presence of catalyst alone was already 96%, and it would be difficult to improve this. DECS-11 shows some enhancement, conversion being 77% with solvent and catalyst together vs. 64–66% shown in Table 2. Much of the increased conversion is due to higher yields of preasphaltenes. DECS-9 shows a remarkable effect, conversion increasing from 74–78% (Table 2) to 98%, with a 40% oil yield. The other important factor is the ability of the donor solvent to intercept retrogressive reactions at 450°. For catalytic reactions without solvent, conversions at 450° drop by 10–25 percentage units relative to those at 400°. When ATTM and tetralin are used together, decreased conversions obtained at 450° are only 0–5 percentage units relative to those at 400°. Reaction at 450° requires an "extra" 50° processing temperature and a good solvent to stave off retrogressive reactions, but provides the highest oil yields. There is a marked shift of the product slate to light materials at 450°, the best case being DECS-1, for which a 66% oil yield and only 5% preasphaltene yield were obtained (comparative results at 400° being 44% and 22%, respectively). Reaction at 450° also increases gas make, gas yields being 12–24% at 450° (depending on coal and solvent) vs. 4–12% at 400°.

4. CONCLUSIONS

Solvents have two major effects on non-catalytic liquefaction of low-rank coals: dissolution of coal-derived radicals to reduce their local concentration and prevent recombination; and participation in the chemical depolymerization of the coal. Below 350°, physical solvation appears to be more important than the chemical nature of the solvent. Both characteristics are important at 350–400°. At 450° the crucial role of the solvent is the prevention of retrogressive reactions. Catalysis by ATTM is clearly beneficial in enhancing conversion. At ≤400° nearly comparable conversions are obtained from either ATTM without a donor solvent or tetralin with no catalyst. There are, however, differences in the product slates obtained from a given coal in these two cases. At 450° the donor solvent is vital in preventing retrogressive reactions. The highest conversions and highest oil yields (accompanied by the highest gas makes) are obtained at 450° for reactions with both ATTM and tetralin.

5. ACKNOWLEDGMENTS

We thank the U. S. Department of Energy's Pittsburgh Energy Technology Center for support. We thank Dr. Michael Nowak of PETC for technical discussions. It is a pleasure to acknowledge our colleagues Chunshan Song, Wei-Chuan Lai, and Ronald Copenhagen.

REFERENCES

- 1 F.J. Derbyshire, A. Davis, M. Epstein, and P.G. Stansberry, *Fuel*, 65 (1986) 1233.
- 2 C. Song, M. Nomura, and M. Miyake, *Fuel*, 65 (1986) 933.
- 3 C.Song, M. Nomura, and T. Ono, *Prepr. Pap. Amer. Chem. Soc. Div. Fuel Chem.*, 36 (1991) 586.
- 4 L. Huang, Ph.D. Dissertation, The Pennsylvania State University, University Park, PA (1995).
- 5 A.B. Garcia, and H.H. Schobert, *Fuel* 68 (1989) 1613.

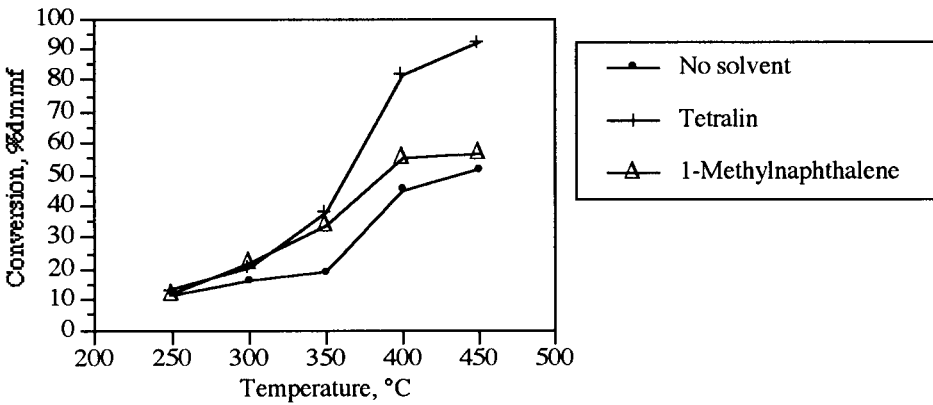


Figure 1. Solvent and temperature effects on non-catalytic liquefaction of DECS-1 coal.

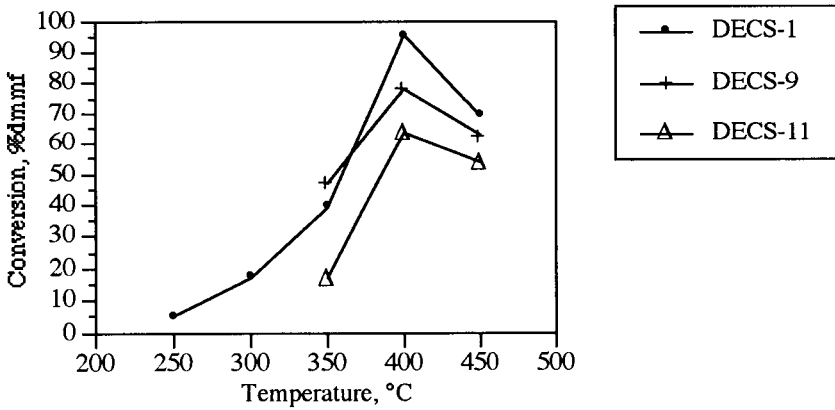


Figure 2. Effect of temperature in solvent-free catalytic reactions.

Possible impacts of coal properties on the coal conversion technology

K.Okada

Coal Mining Research Centre, Japan
 Minami-Sakaecho 14-1, Kasukabe, 344 Japan

1. INTRODUCTION

The Coal Selection for Conversion Program aims at clarifying the properties of coals usable for liquefaction and gasification with the ultimate purpose of establishing methods to evaluate converted energy potential for whole coal fields and mines. It is expected that the information collected by this program can be extensively used to promote the development of coal liquefaction and gasification technologies. This paper describes some possible impacts of coal properties on future coal utilization technologies, based on the current data obtained from analytical and experimental work.

2. COAL PROPERTIES AND THEIR LIQUEFACTION CHARACTERISTICS

Properties and liquefaction characteristics of eleven coals from Canada, the United States, Australia, Japan, and China have been examined (Table 1). Our previous work has demonstrated that a relationship between coal properties and their liquefaction characteristics can be developed, and that the degree of coalification and petrographic composition are important coal parameters. Figure 1 illustrates such a relationship between the petrographic parameter, given by the sum of exinite and vitrinite (E+V), and the coal rank, determined by the vitrinite reflectance (R_o), e.g., subbituminous coals with an R_o value of ~0.5% and an

Table 1. Properties and oil yield of coals

COAL	H/C ATOMIC RATIO (-)	INERTINITE (vol. %)	OIL (%)	VITRINITE REFLECTANCE (%)
BATTLE RIVER	0.768-0.781	3-9	57-68	0.47-0.49
WABAMUN	0.732	39	49	0.45
ILLINOIS #6	0.789-0.796	5- 9	64-65	0.52-0.57
WYOMING	0.780-0.854	9-27	58-66	0.37-0.41
LIDDELL	0.765	15	54	0.75
BAYSWATER	0.801	45	52	0.76
ROSEWOOD	0.888-0.912	1	58-66	0.51-0.57
BLAIR ATHOL	0.664	62	43	0.75
TAIHEIYO	0.942	1	69	0.48
WANDOAN	0.902	8	70	0.44
TIANZHU	0.912	2	66	0.58

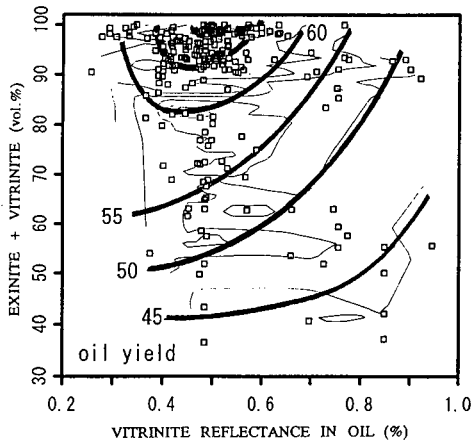


Figure 1. Relationship between petrographic parameters and oil yield (kg/100kg daf coal)

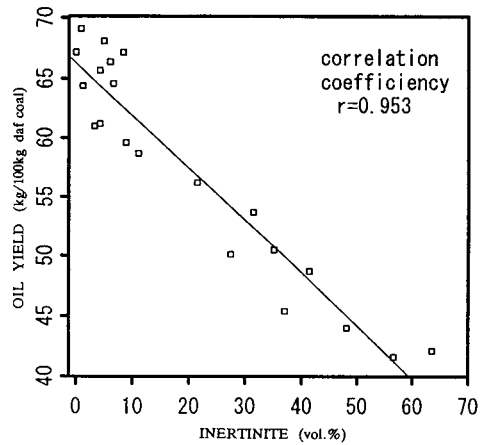


Figure 2. Relationship between inertinite content and oil yield in the similar rank with vitrinite reflectance around 0.48%

abundance of exinite and vitrinite will liquefy favorably. Oil yield in this case is defined as the n-hexane-soluble fraction obtained from autoclave experiments. By deduction, coals abundant in inertinite will have low oil yields, as in the cases of high inertinite content coals such as Wabamun and Bayswater. However, oil yields will vary depending on coal rank (R_o) as inertinite content decreases. For example, high R_o or high rank coals such as Liddell and Bayswater have low oil yields, while Illinois #6 and Rosewood coals, which bear some extent of swelling still give good oil yields.

Thus it is thought that coal rank is the first criterion for liquefaction suitability. The results suggest an optimal range with R_o values between 0.6 and 0.7%. But if coals of higher rank are used as liquefaction stock, oil conversions of up to 40-50% may be attainable. Second, inertinite content should be used as a second criterion. Oil yield has been found to vary drastically in accordance with inertinite content (Figure 2) and that part of the inertinite is discharged in the form of unreacted particulates during the liquefaction reaction. Hence, it is concluded that inertinite is not suitable for liquefaction. Similar to high rank coals, oil conversion yields as high as 40-50% can be expected when liquefying high inertinite content coals. However, inertinite can be removed to a certain extent by coal pretreatment, or the feed coal can be separated into inertinite-rich and inertinite-lean fractions.

In viewing these coals of varying properties from the standpoint of liquefaction and gasification, investigation is also still needed in determining the practicality of using single coals for simultaneous liquefaction and gasification, or whether a portion of a coal can be used for liquefaction with the remainder being used for gasification.

3. SUITABILITY FOR LIQUEFACTION AND GASIFICATION

Based on the above discussion, low inertinite content coals as well as subbituminous coals such as Battle River, Illinois #6, Wyoming, Wandoan, Rosewood, Tianzhu, Taiheiyu, etc. are suitable stocks for liquefaction. However, the wide variation in inertinite content of Wyoming coal should be noted. Liquefaction characteristics of coals particularly abundant in exinite macerals are excellent.

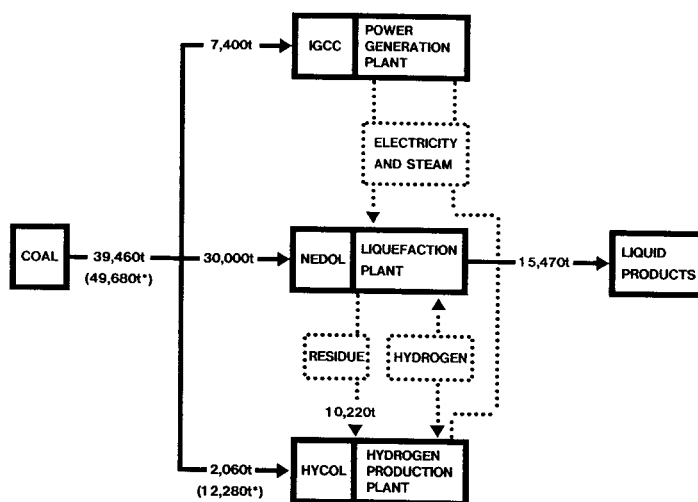


Figure 3. High efficiency integrated NEDOL system: in the case when the liquefaction residue is consumed outside the system

A coal liquefaction plant ordinarily necessitates a power plant and a hydrogen plant to furnish electricity, steam, and hydrogen. To meet these needs, NEDO has been studying ways to integrate an IGCC power plant and a hydrogen-producing HYCOL plant with the NEDOL plant (Figure 3). A demonstration-scale, high-efficiency NEDOL system is expected to have a liquefaction capacity of 30,000 tons of coal per day, integrating a 7,400 tons of coal per day IGCC plant and a HYCOL plant which would process daily 2060 tons of coal and 10,220 tons of liquefaction residue. However, some problems in processing liquefaction residues remain unsolved. If the residues cannot be consumed by the HYCOL plant, coal requirements for this plant will increase to 12,280 tons per day. Thus for this case, approximately 20000 tons coal/day (7400 + 12280) to produce gases necessary for the coal liquefaction plant (30000 tons coal/day). Hence, three cases for coal usage are imaginable:

- (1) using Coal A for both liquefaction and gasification.
- (2) using Coal A for liquefaction and Coal B for gasification
- (3) fractionating Coal A into two portions based on physical properties, where Fraction A1 is used for liquefaction and Fraction A2 is used for gasification.

Assuming that all coals cost the same regardless of their properties, case (1) can be utilized provided that the coal is suitable for both liquefaction and gasification. In general, a highly reactive, liquefactive coal is also suitable for gasification, but the converse is not always true. If Coal B is more suitable for gasification than Coal A, then case (2) is preferable. For a country like Japan where various coals are imported, this case will utilize coal more efficiently if the coal costs do not differ significantly. Moreover, if Coal A (liquefaction stock) and Coal B (gasification stock) differ in costs due to their usage, then case (2) will be more economical than case (1).

Table 2. Comparison of coal usages in NEDOL system (T/D)

CASE	NEDOL	IGCC	HYCOL	LIQUID	RESIDUE
NEDOL STANDARD (WANDOAN)	30,000	7,400	12,280	15,470	10,220
WABAMUN COAL	30,000	7,400	12,280	9,480	16,210
WABAMUN-1 (3 PARTS)	30,000			13,200	12,490
WABAMUN-2 (2 PARTS)		7,400	12,280		

In cases where oil yield is of primary importance, case (3) must be considered where the better liquefactive portion of the coal (Fraction A1) is processed. In this case however, the material balance as well as the overall efficiency must be considered after the residual Fraction A2 has been gasified. Case (3) becomes more worthy of consideration if environmentally and/or mechanically harmful impurities could be removed in the coal separation process, especially where only high inertinite content coals are available. Where Fraction A1 yield exceeds 60%, the gasification stock, Fraction A2, should be supplemented by the parent coal. Where Fraction A1 yield falls below 60%, gas production may exceed demand and other uses for Fraction A2 must be considered. Table 2 examines a case in which Wabamun coal is separated by specific gravity into three parts for liquefaction and two parts for gasification. It suggests that the yield of liquid products in this case is approximately 40% more than the case where non-treated coal was liquefied.

A general problem affecting case selection is whether or not coal prices in the future will vary based on their properties. It may not be unrealistic that the price of coals with less inertinite and good liquefaction properties will rise in the future.

4. CLASSIFICATION OF COALS FOR LIQUEFACTION

Suitability of coals for liquefaction has until now been discussed based on coal type, and there appears to be a need to develop general criteria for their classification. Perhaps coal can be reclassified as "light", "middle", and "heavy", following the light, middle, and heavy fractions obtained from the refining crude oil. Similar to how Ro and MF (maximum fluidity) are used to evaluate coking coals, H/C ratio and inertinite content could possibly be used to classify coals for liquefaction. Under the reclassification, coal which has a high H/C ratio and low inertinite content would be considered "light", the converse regarded as "heavy", with the intermediates called "middle". According to this new nomenclature, Taiheiyō, Wandoan, and Tianzhu coals are typical "light" coals, while Wabamun, Bayswater and Blair Athol coals belong in the "heavy" coal category.

5. ACKNOWLEDGEMENTS

Support was provided under the Coal Selection for Conversion Program administered by the New Energy and Industrial Technology Development Organization, Japan.

Influence of low temperature treatment on lignite structure and its liquefaction behavior

V.I.Sharypov, B.N.Kuznetsov, S.V.Baryshnikov, V.G.Chumakov, N.G.Beregovtsova

Institute of Chemistry of Natural Organic Materials Siberian Division of Russian Academy of Sciences, Akademgorodok, Krasnoyarsk, 660036, RUSSIA.

The elucidation of correlations between structural characteristics of coal and its reaction ability is very important problem in coal science. The structure of coal can be varied by its thermal treatment even at mild conditions. It is known the treatment of coal at 200 °C changes the total concentration of oxygen and its relative content in different types of functional groups of coal [1,2]. The most significant effects were observed for low-rank coals with high concentration of oxygen [2]. Since coal liquefaction processes are accompanied by the rupture of oxygen-containing bonds [3] the variation of these groups concentration should change the coal conversion degree.

The influence of low-temperature treatment of Kansk-Achinsk lignite on its composition, structure and reactivity for liquefaction was studied in this work.

1.EXPERIMENTAL

Lignite of Kansk-Achinsk coal pit with composition (in wt%): C_{daf} 70.1, H_{daf} 4.6, N_{daf} 0.8, S_{daf} 0.2, A_d 4.2 was used as initial material. Air-dry lignite was crushed up to particles with size less 0.5 mm and then treated by flowing air or helium at 100 °C and 200 °C in a steel autoclave. The process of lignite liquefaction was studied in a shaken steel autoclave with glass for reaction mixture. The composition of the latter - 5.0g of modified lignite, 0.13 mole of organic solvent - for thermal liquefaction by solvent, and 0.04 mole of organic solvent, 0.5g of iron- containing catalyst (FeS₂) - for catalytic hydrogenation process. Tetralin, toluol and ethanol were applied as solvents. Lignite liquefaction by solvents was carried out at initial pressure of inert gas (He) 1.0 MPa. Pressurized autoclave was heated up to 380 °C and kept 1 hour at this temperature. The degree of lignite conversion was calculated as difference in weights of initial lignite and solid rest after product extraction. The process of lignite catalytic hydrogenation was conducted at 380 °C, initial H₂ pressure 20.0 MPa, according to [4].

Gaseous products were analyzed by gas-liquid chromatograph using metallic columns with "Porapak-Q" and molecular sieve CaA. Modified lignites were studied by elemental analysis, chemical methods, IR spectroscopy and X-ray diffraction techniques using Specord-75IR and Dron-3 with CuK_α irradiation. The analysis of main parameters of X-ray diffraction spectra was carried out by procedure [5].

2. RESULTS AND DISCUSSION.

Results of chemical analysis of modified lignites are given in table. These data show the significant influence of lignite treatment parameters (temperature, reaction medium, time)

Table
Some characteristics of modified lignites

Sample No*	Functional groups content (mg/g)			Elemental composition (wt%)				X-ray structural parameters		
	>C=O	-COOH	-OH	O ^a	O ^b	C ^{daf}	H ^{daf}	d ₀₀₂	L _c	n
1	12.00	0.16	73.12	8.5	14.0	71.7	4.8	0.346	0.835	3.4
2	28.57	0.18	42.35	7.1	16.6	70.9	4.6	0.370	0.760	3.0
3	21.14	0.28	34.82	5.6	18.6	70.1	4.6	0.404	0.685	2.7
4	12.57	0.23	37.65	5.1	21.1	69.3	3.6	0.390	0.692	2.2
5	27.43	0.05	24.47	5.2	15.9	72.6	5.0	0.396	0.635	2.6

$$O^a = O(>C=O) + O(-OOH) + O(-OH), n=1+L_c/d_{002}$$

$$O^b = 100 - (C^{daf} + H^{daf} + N^{daf} + S^{daf} + O^a)$$

*sample 1- treated by He at 100 °C, 3 h; 2 - by He at 100 °C, 1,5h and than by air at the same conditions; 3 - by air at 100 °C, 3 h; 4 - by air at 100 °C, 6 h; 5 - lignite treated by air at 200 °C, 3 h

on the total oxygen content and its distribution in different functional groups. The main part of oxygen is presented as O^b and can be attributed to simple and complex ethers, to oxygen heterocycles, which could not identify by used chemical methods. Such type of oxygen is presented, mainly, by ether groups in Kansk-Achinsk lignite, according to data [6]. The concentration of oxygen-containing groups is decreased for this lignite in sequence: -OH > >C=O > -COOH >> -OCH₃. The content of -OCH₃ groups is very low.

The increasing a time of lignite treatment by air reduced hydrogen and carbonyl groups content parallel with rising a total oxygen concentration. These data and the observed decreasing of intensity of adsorption bands in IR spectra of air-treated lignite at 2960, 2920, 2860 cm⁻¹, which attributed to -CH and >CH groups, points on oxidation of lignite aliphatic groups. Hydrogen is removing apparently, in form of water, since only CO, CO and H₂O were presented in gaseous products of lignite oxidation by air.

Lignite, treated in helium at 100-200 °C, has higher content of hydrogen and OH-groups, but less total amount of oxygen and groups with O^b as compared to air-treated one. According to chemical analysis and IR study the concentration of OH-group was 2 times higher in sample, treated by helium during 3 hours, as compared to one, oxidized by air at the same conditions. Some indications suggest that the observed reduction of OH-group concentration is connected with their transformation to O^b containing groups, like ether ones. The formation of ether groups at the similar conditions was found in [7].

The increasing of temperature of lignite treatment both in air and helium flow resulted to reducing of adsorption bonds in the region at valence vibration of CH_2 and CH_3 groups ($2960, 2920, 2860 \text{ cm}^{-1}$), OH-groups in the regions about 3400 cm^{-1} and 1250 cm^{-1} . The latter adsorption bands can indicate, the presence of different oxygen-containing compounds (phenols, aromatic ethers, acids et al.). With temperature increasing the band at 1600 cm^{-1} was shifted to lower frequency region and the maximum at 870 cm^{-1} was appeared. These changes in IR spectra can indicate on the reinforcement of polyconjugating aromatic structures formation in treated lignite.

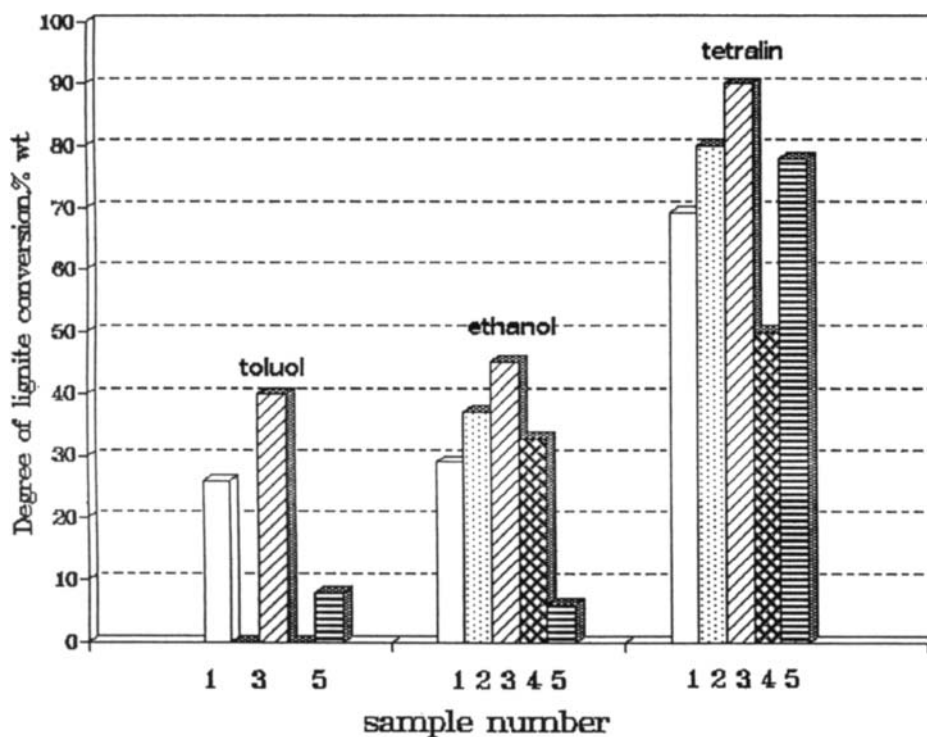


Figure. Influence of lignite modification parameters on its liquefaction degree at 380°C in different solvents. Numbers of samples are the same, as in Table.

Data of X-ray spectra analysis in the region of 002 band, presented in table, show that lignite oxidation by air increased the interlayer distances (d_{002}) and diminished the sizes of parallel stacking of the molecular layers (L_c) as result of decreasing the number of layers (n) in these stacks in comparison with lignite treated in helium. At the same time both intensity and symmetry of 002 peak were increased. Obtained data demonstrate the loosening of over-molecular structure of lignite after its oxidation by air. Modified lignite structure

become close to graphite-like structure with parallel aromatics layers. In the framework of the latter the X-ray data of coals are usually interpreted [3]. Taking into account the data on oxygen distribution in different functional groups of lignite one can suggest that the putting in order of lignite structure during its oxidation takes place as a result of some blocks sewing together via chemical bonds, containing oxygen. The increasing of lignite oxidation temperature up to 200 °C results to higher intensity of 002 peak and to higher ratio of this maximum height to its half-width, showing the increased regulation of lignite structure. According to IR data, the important role in this regulation can play the reactions of aromatic rings condensation.

Some correlations were found between structural characteristics of modified lignites and their reaction ability in liquefaction processes. Data on thermal liquefaction of modified lignites by organic solvents are presented in figure . The degree of conversion is increased for all samples in a sequence of solvents: toluol < ethanol < tetralin .

The conditions of lignite pre-treatment have the significant effect on its reactivity in thermal liquefaction by solvents. For air-treated lignites the degree of conversion on 15-20% higher as compared to samples treated in helium during 3 hour. Lignite, treated by helium at 100 °C during 1,5h and than by air at the same conditions, had the average reaction ability in thermal liquefaction processes regardless of used solvent nature. The increasing of temperature and time of lignite oxidation decreased the conversion degree but these changes were depended on solvent nature. So the growth of oxidation temperature from 100 °C up to 200 °C resulted to 5-fold reduction of lignite conversion in toluene and ethanol. But only a little changes were observed with tetralin. The increasing of oxidation time from 3 up to 6 hours resulted to less reduction of lignite conversion in ethanol than in experiments with tetralin. The comparison of data on lignite liquefaction and results of the study of modified lignite composition and its structure makes possible to draw the conclusion that highest degree of conversion was observed for samples with higher distances between aromatics layers, which have, according to IR data, relatively low degree of aromatic rinds condensation, i.e. with loosening over-molecular structure. For samples, oxidized at 100 °C, the correlation between degree of lignite liquefaction and content of phenolic groups in lignite organic mass was observed. This fact suggests the important role of phenolic groups in lignite transformation to liquid products. The analogous results were obtained for the process of modified lignites hydrogenation in the presence of iron catalysts.

REFERENCES.

1. V.I.Saranchuk, L.V.Paschenko, *Khim. tverd.topl.*, N 1(1989).43.
2. K.I.Markova, *Khim. tverd.topl.*, N 4 (1989),41.
3. M.W.Haenel, *Fuel*, N.11 (1992)1211.
4. V.I.Sharypov, P.N.Kuznetsov, E.D.Korniets et.al. *Khim. tverd.topl.* N3, (1990) 48.
5. V.I.Saranchuk et al, *Nadmolekulyarnaya organisaziya, struktura i svoistva uglya. K.: Naukova dumka*, (1988) 191.
6. E.A.Grigoryeva, M.N.Sharova, E.B.Lesnikova, *Khim. tverd.topl.* N 4 (1984) 16
7. T.A.Kucharenko, *Okisleniye. v plastakh burykh i kamenykh uglyei.M.: Nedra*,(1972) 215.

Determination of transferable hydrogen in coal (1) -- Reaction behavior of coal with iodomethane --

T. Yoshida, M. Sasaki, M. Yamamoto and T. Kotanigawa

Hokkaido National Industrial Research Institute
2-17 Tsukisamu-Higashi, Toyohira, Sapporo 062, Japan

1. INTRODUCTION

It is known that transferable hydrogen of coal plays important roles in the carbonization of coal¹⁾ and coprocessing of coal/bitumen.²⁾ Therefore, the determination of transferable hydrogen would be useful for the analysis of these reaction characteristics as well as coal structure. Some works on the determination of hydrogen evolved from coal in the presence of metal catalysts³⁾ or sulfur⁴⁾ have been reported. However, the measurements at higher temperatures might accompany side reactions other than selective dehydrogenation from hydroaromatic structure of coal. Yokono et al.⁵⁾ have measured the amount of transferable hydrogen of different ranks of coal with anthracene as a hydrogen acceptor and revealed that the amount of hydrogen measured was small for low-rank coals and was maximum at 87 wt%C. We have found that their values were only 5~10 % of our data which was determined by use of solid state NMR technique⁶⁾, suggesting that the procedure of Yokono et al. can not capture all of hydrogen transferred from coal.

In recent years, Vassallo et al.^{7,8)} have studied the liquefaction of coal with iodomethane and found that hydroaromatic rings in coal are converted into aromatic rings around 300 C at which the thermal decomposition of coal hardly occurs. Their results suggest that iodomethane would be one of the good reagents for the determination of transferable hydrogen in coal. The objective of the present work is to investigate the reaction characteristics of coal with iodomethane in order to determine the transferable hydrogen in coal. Model compounds and ¹³C isotope of iodomethane were used to elucidate the mechanism of reaction.

2. EXPERIMENTAL

Taiheiyo subbituminous coal (C, 74.9; H, 6.2; O, 16.6; wt%, daf coal basis), mined in Hokkaido, Japan, was used as coal sample. The coal was pulverized to pass through a 100 mesh screen and then dried in vacuum before use. Iodomethane (Kishida Chemical Co. Ltd., Japan) was used as received. A given amount of coal and iodomethane was charged into a quartz glass tube (a volume of 20 ml) and then sealed after the replacement of air by nitrogen gas. The reaction was done at temperatures of less than 280 C. After reaction, coal products were recovered with acetone and then dried sample was weighed, followed by ultimate analysis and solid state NMR analysis.

3. RESULTS AND DISCUSSION

3.1 Reaction characteristic of model compounds

The effect of reaction temperature on the dehydrogenation of tetralin is shown in Figure 1. The decomposition temperature of iodomethane is ca. 270 C and hence the conversion of tetralin into naphthalene was negligibly small at 260 C and almost 100% at 300 C. Most of the reactions was done at 280 C in benzene solvent to avoid side reactions and carbonization of sample.

Table 1 summarizes the conversion of various types of model compounds under the same reaction conditions. The distinct difference in reactivity was observed between cycloparaffins (decalin) and hydroaromatics (tetralin), indicating that the dehydrogenation from hydroaromatics readily takes place. Also, the reactivities of anthracene and phenanthrene derivatives greatly depended on their chemical structures and the reactivity of 9,10-dihydroanthracene was especially low. Aromatic compounds with alkyl side chains and phenolic OH group hardly reacted with iodomethane and the transfer of hydrogen from these substituents was found to be small.

3.2 Reaction characteristic of coal

Figure 2 shows the change in the spectral pattern of coals treated with iodomethane at various temperatures. With reaction temperatures, the carbon aromaticity f_a of coal increased evidently and the intensity of area from 25 to 50 ppm, which was assigned to aliphatic CH and CH₂ carbons, decreased drastically. The result shows that iodomethane reacts selectively with aliphatic parts of coal.

Figure 3 shows the change in the weight of aromatic, CH₂ and CH₃ carbons of coal with reaction time. The weight of each type of carbon in coal was calculated from the variations of weight, carbon content and carbon distribution of coal after reaction and was normalized to 100 g of coal sample before reaction. The result shows the significant increase in aromatic carbon with reaction time, drastic decrease in CH₂ carbon at the initial stage of the reaction and slight increase in CH₃ carbon. When assuming the transfer of hydrogen from hydroaromatic or naphthenic rings during the reaction, the gain in aromatic carbon and the loss in CH₂ carbon should be balanced each other. Actually, the increase rate of aromatic carbon did not correspond to the decrease rate of CH₂ carbon, indicating that the reaction is more complex. The decrease in CH₂ carbon might be mainly due to the decomposition of naphthenic ring, not to the transfer of hydrogen from it. On the other hand, the increase in the aromatic carbon of coal is considered to be a result of the propagation and aromatization of CH₃ carbon which was incorporated into coal from iodomethane.

Figure 4 shows the change in the weight of aromatic, CH₂ and CH₃ carbons of coal with reaction temperature. The aromatic carbon decreased at lower temperatures up to 240 C and then increased remarkably with temperature. The reduction of aromatic carbon observed at lower temperatures would be caused by the hydrogenation of aromatic ring. The increase in aromatic carbon due to the incorporation of CH₃ carbon from iodomethane was proved by the spectrum of coal reacted with ¹³CH₃I in Figure 5. This coal sample contains about 11% of ¹³C to the sum of ¹²C and ¹³C after the reaction with ¹³C isotope of iodomethane at 260 C. The spectrum of the treated coal shows the formation of aromatic ring during the reaction.

4. CONCLUSION

The reaction characteristic of coal with iodomethane has been investigated in order to determine the transferable hydrogen in coal. The reaction of model compounds with iodomethane showed that the dehydrogenation from hydroaromatic compounds strongly depended on the chemical structures of compounds, but side reactions such as dealkylation were not observed. The reaction of coal with iodomethane was found to be more complex. The CH₂ carbon of coal decreased readily and aromatic carbon increased significantly. The increased aromatic carbon was found to be a result of the propagation and aromatization of CH₃ carbon which was incorporated into coal from iodomethane.

REFERENCES

1. T. Obara, T. Yokono, K. Miyazawa and Y. Sanada, *Carbon*, 19 (1981) 263.
2. T. Yoshida, H. Nagaishi, M. Sasaki, M. Yamamoto, T. Kotanigawa, A. Sasaki, K. Idogawa, T. Fukuda, R. Yoshida and Y. Maekawa, submitted for publication in *Energy & Fuels*.
3. L. Reggel, I. Wender and R. Raymond, *Fuel*, 47 (1968) 373.
4. B.K. Mazumdar, S.K. Chakrabarty, N.G. De, S. Ganguly and A. Lahiri, *Fuel*, 41 (1962) 121.
5. T. Yokono, T. Obara, S. Iyama, J. Yamada and Y. Sanada, *J. Fuel Soc. Jpn.*, 63 (1984) 239.
6. T. Yoshida and Y. Maekawa, *Fuel Process. Tech.*, 14 (1986) 57.
7. A.M. Vassallo, M.A. Wilson and M.I. Attalla, *Energy & Fuels*, 2 (1988) 539.
8. M.I. Attalla, M.A. Wilson, R.A. Quezada and A.M. Vassallo, *Energy & Fuels*, 3 (1989) 59.

Table 1 Conversion of various types of hydrocarbon

Compound	Conversion (%)	Main products
Tetralin	88	Naphthalene
Decalin	19	Naphthalene, Tetralin
9,10-dihydroanthracene	25	Anthracene
Hexahydroanthracene	99	Dihydroanthracene
		Unknown
9,10-dihydrophenanthrene	99	Phenanthrene
Octahydrophenanthrene	66	9,10-dihydrophenanthrene
		Phenanthrene
Ethylbenzene	6	Ethyltoluene(?)
α -methyl-naphthalene	trace	---
Phenol	trace	---

*Conditions: temperature, 280°C; time, 30 min; solvent, benzene; sample/CH₃=1/4 mole ratio

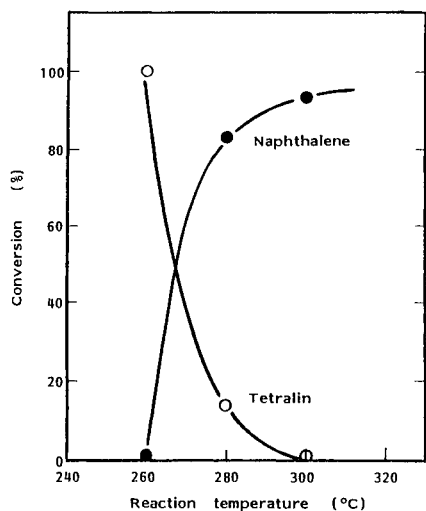


Fig. 1 Effect of reaction temperature on conversion of tetralin (Tetralin/CH₃=1/4 mole ratio; time, 30 min)

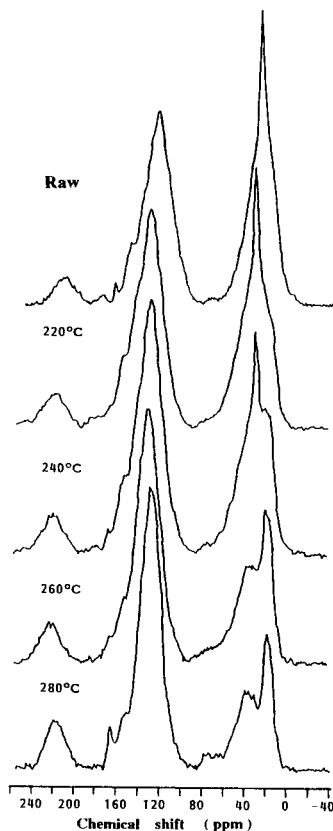


Fig. 2 Solid state ¹³C NMR spectra of raw and treated coals

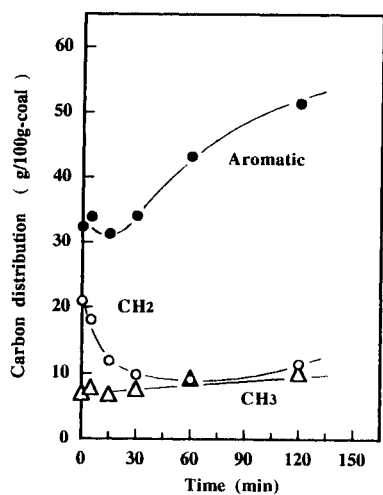


Figure 3 Change in weights of aromatic, CH₂ and CH₃ carbons with reaction time (Coal/CH₃I=1/7.2 (w/w), temp. 280 C)

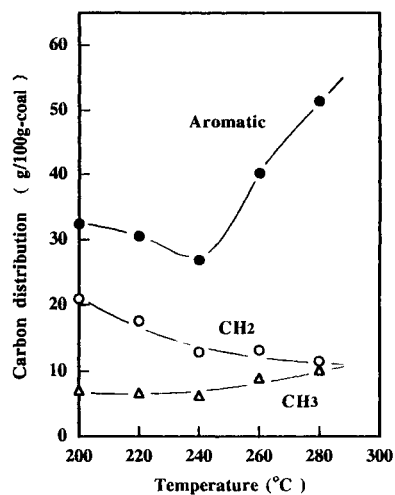


Figure 4 Change in weights of aromatic, CH₂ and CH₃ carbons with temperature (Coal/CH₃I=1/7.2 (w/w), time, 120min)

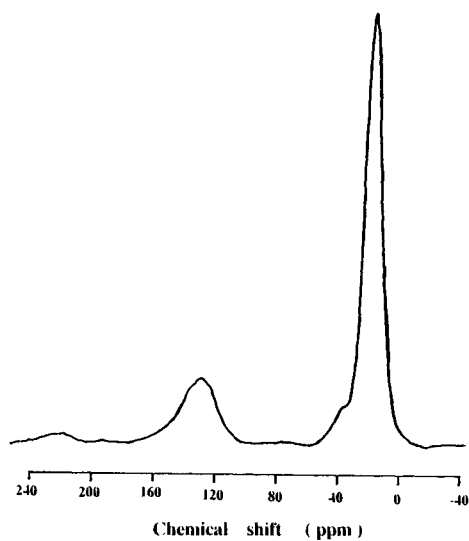


Fig. 5 Solid state ¹³C NMR spectrum of coal treated with ¹³CH₃I

EFFECT OF ENHANCED CONTACT BETWEEN FINELY PULVERIZED COAL AND CATALYST ON LIQUEFACTION

Yoshiki SATO, Tohru KAMO and Minoru SHIRAISHI

National Institute for Resources and Environment,
16-3 Onogawa, Tukuba-shi, Ibaraki 305 JAPAN

1. INTRODUCTION

To enhance economic feasibility and process operability by decreasing the amount of added catalyst, coal liquefaction using highly dispersed catalyst has actively been investigated. Attempts on the dispersion of nm particle size iron catalysts have recently been reported by Derbyshire et al [1,2]. Comparisons of various catalyst precursors impregnated by aqueous solutions of inorganic salts and of solvent-soluble organic complex catalysts have also been discussed in connection with coal swelling [3]. However the detailed mechanisms of hydrogen transfer by catalyst are not completely clarified. In these experimental studies, conventionally ground coals (-100 mesh) are used, which causes some limitation on the surface dispersion with fine catalyst particles and on contact between the coal and solvent, due to the relatively large coal particle size.

The use of finely pulverized coal for liquefaction experiments is expected to result in a very different behavior from that previously reported, due to high surface dispersion and intimate contact between the coal and slurry. In this study, the effect of the finely pulverized coal particle on the products distribution of Taiheiyo coal liquefaction was experimentally compared with that of conventional particle size coal. The effect of surfactant addition to the coal-catalyst slurry on the HS yield is also examined.

2. EXPERIMENTAL

The Japanese subbituminous Taiheiyo coal, used here, was first crushed using a conventional dry grinder and sized to pass 100 mesh, then was mixed with recycle solvent and fed to a recently developed slurry jet mill for pulverization to fine particle. Principle, operating procedures and pulverization results were described in our previous report [4]. Reagent grade iron oxide as a catalyst for the liquefaction was also pulverized in a same way as for the coal. The recycle solvent is a Taiheiyo coal-derived solvent (b.p. 350-538°C) produced a 1t/d NEDOL plant at kimitsu, Chiba. Particle size distribution of coal and catalyst was measured with a Microtrac-Particulatesize Analyzer and a Transition Electron Microscope.

The coal liquefaction experiments were carried out in 200 ml stainless steel magne-drive autoclave at 420, 440 and 450°C under 8.5 MPa of initial hydrogen

pressure with 60 min of reaction time. In all runs, solvent to coal weight ratio is about 2.5, catalyst to coal weight ratio is 0.043 and catalyst to sulfur weight ratio is 0.8. Conversion and yield were gravimetrically calculated from the amount of THFI and THFS, TS and HS on a daf coal basis respectively.

3. RESULTS AND DISCUSSION

3.1 Liquefaction behavior of finely pulverized coal and catalyst

Elemental analyses and average particle size of conventional -100 mesh coal and finely pulverized coal are shown in Table 1. No remarkable differences in elemental analyses and ash content were observed between -100 mesh coal and pulverized coal with water and tetralin. When the mill is operated at a pressure of 1300 kg/cm², the average feed coal particle size of 80 μm (-100 mesh) is reduced to 4 μm . No obvious differences were found in coal particle size distribution when water was substituted for tetralin or the coal-derived recycle solvent in the feed slurry to the jet mill.

Table 1 Analyses of Taiheiyo Coal Samples

	C	H (wt%, daf)	N (wt%, daf)	S	O(diff)	Ash (wt%, dry)	Particle Diameter (μm)
A	75.7	6.3	1.3	0.2	16.5	14.2	80
B	73.0	6.5	1.2	-	19.3	14.5	4
C	71.8	6.2	1.4	-	20.6	14.4	8

A : Original 100 mesh coal, B : Pulverized with water, C : with tetralin

For this series of experiments, slurries of coal and catalyst, which were pulverized separately with recycle solvent, were mixed together with sulfur and additional solvent to make the reactant slurry. The effect of reaction temperature on the liquefaction of finely pulverized coal and -100 mesh coal is illustrated in Fig.1.

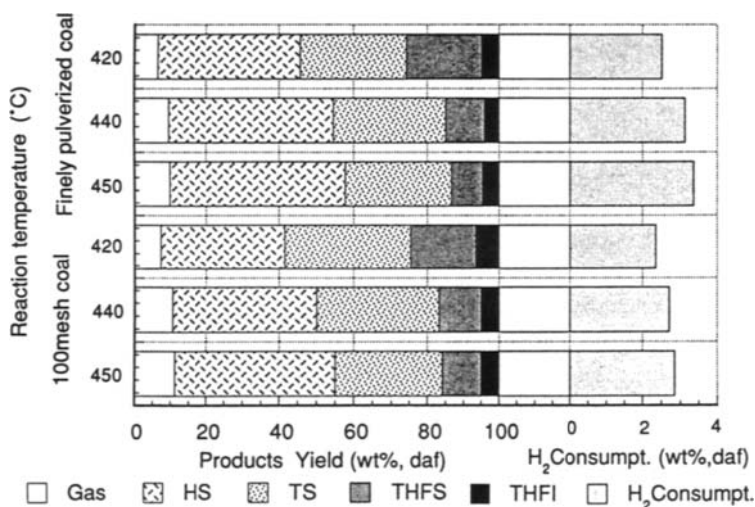


Fig. 1 Effect of Reaction Temperature on the Yield of Products, Conversion and Hydrogen Consumption.

Conversions of the two coals, on a daf basis, calculated from THF insoluble, were similar (95-96 wt% in either case). However, the finely pulverized coal showed much higher HS yield of 48 wt%, while -100 mesh coal had only 44 wt% HS yield at the same reaction conditions of 450°C and 60 min. Similar differences in HS yield were seen at 420 and 440°C. Conversely, the yields of THFS and gases were higher for -100 mesh coal. The higher hydrogen consumption and higher H/C atomic ratios of TS and THFS for the finely pulverized coal were obtained. These indicate that the much effective contact among coal-catalyst-solvent-hydrogen caused by the increased surface area plays an important role to enhance conversion and the yield of light oil with lower amounts of retrogressive products. To clarify the effect of pulverization of coal or catalyst, the experiments using reagent grade Fe_2O_3 , which particle size is 1 μm , were carried out. The results indicate that pulverization of catalyst to fine particle is much effective on the HS yield than that of -100 mesh coal.

3.2 Effect of surfactant addition on liquefaction

To examine the effective dispersion among the components in the slurry for liquefaction, the effect of surfactant addition, which was developed and used now for preparing stable COM slurry, on the yield of liquid product and the conversion from liquefaction was examined. Result of the product yield and the hydrogen consumption using some of the nonionic and the cationic surfactant is shown in Fig. 2. Surfactant A is a mixture of nonionic and cationic type with 1:1. B is a different type of nonionic surfactant and C is a mixture of B and cationic type with 1:1.

In the case of finely pulverized coal, the HS yield increased to 52.4 wt% by 0.5 wt%/slurry addition of surfactant A, while the HS yield, obtained without surfactant, was 45.1 wt%. The increased conversion of 98.1 wt% was also observed. However, the HS yield decreased by 0.25 wt%/ slurry addition of surfactant B and any positive effect was not observed in the case of surfactant C. In all cases, the gas yield decreased 2 wt% by the addition of surfactant. From our experimental result, the HS yield decreased and the THFS yield increased by the use of nonion type surfactant.

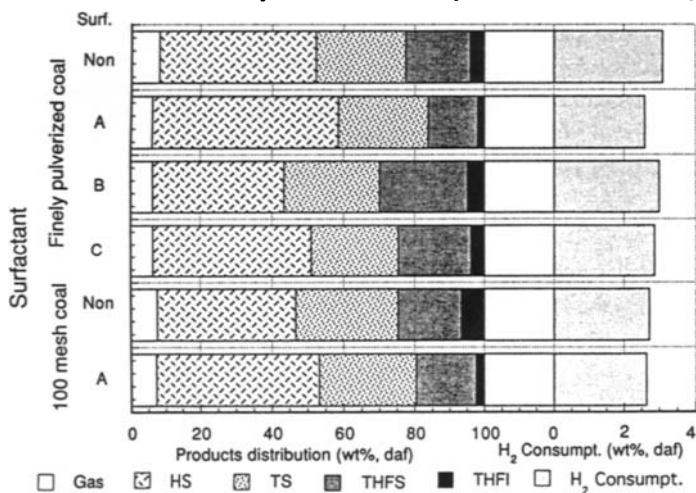


Fig.2 Effect of Surfactant Addition on the Liquefaction
(Catalyst : Fe_2O_3 4wt%, 440°C, 60min, Initial H_2 Press. : 8.5 MPa)

The correlation between the amount of surfactant and the dispersion effect has not yet been studied in detail and further investigation is needed. The increased HS yield of 45.9 wt% and the higher conversion of 97.7 wt% from the -100 mesh coal with surfactant A were also observed as similar as the finely pulverized coal. The hydrogen consumption and H/C atomic ratio of TS and THFS did not change by the addition of surfactant.

The effect of the added amount of surfactant A to the slurry for the -100 mesh coal on the product yield is shown in Fig. 3. The added amount of 0.25 wt%/slurry was however not so effective on the HS yield and the HS yield and the conversion increased with increasing the amount of surfactant. The increments on the HS yield are 6 wt% in the case of 0.5 wt% and 1.1 wt%/slurry addition of surfactant. These results indicate the addition of surfactant is effective to disperse coal and catalyst in the slurry with decreasing retrogressive coking and gas production.

ACKNOWLEDGMENT

The authors are grateful to Mr. Y. Wada of Japan COM Co., LTD for helpful suggestion and to Lion Corporation and KaO Corporation for providing the surfactant samples.

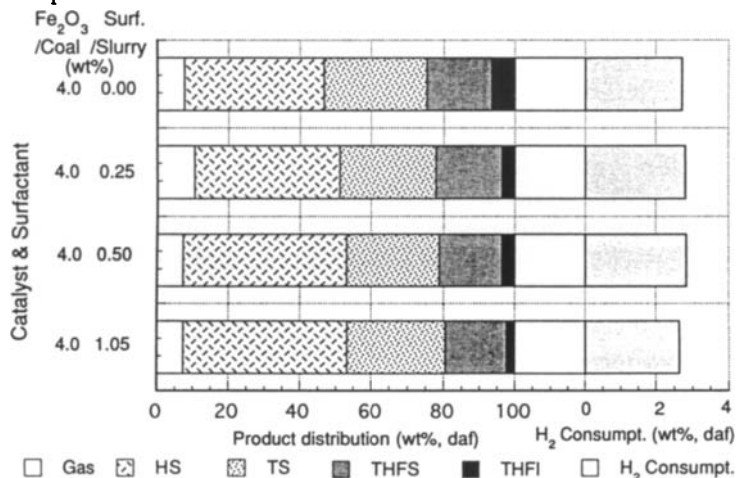


Fig.3 Effect of Surfactant Addition on the Liquefaction (-100 mesh, 440°C, 60min, Initial H₂ Press : 8.5MPa)

REFERENCES

- [1] G.T.Hager, X.X.Bi, P.C.Eklund and F.J.Derbyshire, *Am. Chem. Soc. Div. Fuel Chem. Preprints*, **38(1)** (1993) 34.
- [2] P.C.Eklund, J.M.Stencil and X.X.Bi, *Am. Chem. Soc. Div. Fuel Chem. Preprints*, **36(2)** (1991) 551.
- [3] K.L.Artok, A.Davis, G.D.Mitchell and H.H.Schobert, *Energy & Fuels*, **7** (1993) 67.
- [4] Y.Sato, T.Kamo and M. Shiraishi, *10th Japan-USA Joint Tech. Meeting*, Hokkaido, Japan, (Jan. 1994) 79.

Liquefaction of Blended Coals and their effect on Product Yields

Andrew Pickering^a, Jeremy Taylor^b, Ahmed Belghazi^a, Michael Cloke^a and John W Patrick^b.

^a Coal Technology Research Group, Department of Chemical Engineering, University of Nottingham, University Park, Nottingham. NG7 2RD. United Kingdom.

^b Carbon Research Group, Department of Chemical Engineering, Loughborough University of Technology, Loughborough, Leicestershire. LE11 3TU. United Kingdom.

1. Introduction

The direct liquefaction of coal may play a very important role in providing transport fuels and petrochemicals, as current crude oil supplies diminish and new reserves become less economic to exploit. Extensive research has been carried out examining the liquefaction of single coals and maceral concentrates, determining fundamental mechanisms and attempting to prove commercial viability. A commercial coal liquefaction plant would utilise a large amount of coal and it is unlikely that the coal requirements could be met from one source. Coals from different sources may liquefy differently, affecting the product distribution, which could have a serious effect on downstream processing units, such as hydrocrackers. It may be useful if coals could be blended during dissolution, to attempt to standardise the conditions downstream and reduce the more extreme variations in product yields.

Research in Japan during the 1980's was initially contradictory, with Ouchi *et al* countering claims, by previous workers, that Yallourn and Shin Yubari coals produced higher than expected yields when blended¹. Ouchi *et al* also found that the liquefaction of coal blends under a deficient hydrogen supply led to a lower than expected yield, proposing that this may be attributed to the more reactive coal in the blend consuming the available hydrogen preferentially. Further work found that, with creosote oil and tetralin as the donor solvents, liquefaction of blended coals followed additivity^{1,2}. More recently, work at the University of Nottingham has shown that 50/50 blends of British coals of similar rank follow additivity for overall conversion³. Further work at Nottingham, in larger scale apparatus, confirmed that blends of Point of Ayr and Crumlin coals follow additivity, not only for conversion but also for product yields⁴. However, work at Loughborough University demonstrated that blends containing Baddesley coal showed a marked improvement in oils yield when liquefied for 30 minutes⁵.

Work presented here demonstrates the effect of blending coals on the product yields from the first stage of direct coal liquefaction.

2. Experimental

The coals used in this work were Point of Ayr, Baddesley, Crumlin, Trentham and Littleton, all high volatile, bituminous coals, with the exception of Crumlin, which is a lignite from

Northern Ireland. All of the coals were either pulverised fuel or sieved to less than 100 μ m. Two experimental procedures were followed:

2.1. Method 1 (Loughborough University)

A 25ml tubing bomb micro-reactor was used to liquefy coals and their blends in a fluidised bed heater for 30 minute and 60 minute reaction periods. 3g of coal and 6g of hydrogenated anthracene oil (HAO) were charged to the reactor and the air was purged using nitrogen prior to sealing the reactor. The tubing bomb was then placed in the preheated fluidised bed at 425°C and subjected to continuous agitation throughout the reaction period. After the reaction time expired, the tubing bomb was removed from the heater and was rapidly cooled by quenching in cold water.

The gaseous products of the reaction were vented into an evacuated vessel for subsequent measurement and analysis by gas chromatography. The solid and liquid residues were carefully removed from the reactor and were then classified by sequential solvent extraction in tetrahydrofuran (THF), toluene and pentane, giving a THF insoluble fraction and preasphaltenes, asphaltenes and oils product classes.

2.2. Method 2 (University of Nottingham)

A 500 ml electrically heated, magnetically stirred batch autoclave was used to liquefy coals and their blends for 60 minute reaction periods. 87.5g of coal and 175g of HAO were charged to the autoclave and mixed well prior to reassembly. The temperature controller was set to 415°C and the stirrer speed set to 300rpm. Upon reaching 380°C, a 60 minute timer was started, as 380°C was considered as the temperature above which reaction is believed to be proceeding. During the reaction the autoclave was vented when the pressure reaches 3MPa and the pressure was maintained as close to 30MPa as possible throughout the reaction. At the end of the reaction period, the electrical heaters were removed from the autoclave and it was allowed to cool in the air.

Gaseous products were not collected and analysed, so an allowance was made for material lost as gas during the calculations. A representative solid/liquid sample was removed from the autoclave, carefully mixed with hexane and refluxed for three hours. The solid residue at the end of this time was the hexane insolubles. A sample of the hexane insolubles was taken and the same procedure carried out with toluene. Then the same procedure was used with THF on the toluene insolubles. An assessment of quinoline insolubles was also performed. Assumptions on which the calculations were based are as follows:

1. All moisture in the coal is evaporated and lost during venting,
2. 2 % of the dmmf coal is converted into gaseous product and escapes during venting,
3. 1% of the HAO is evaporated and is lost during venting, and
4. All the HAO is soluble in hexane, i.e., classed as oils.

3. Results and Discussion

Results from the micro-reactor experiments, given in Tables 1 and 2, clearly show that the product yields of blends of Baddesley with other single coals deviate from those predicted by additivity. For Baddesley and Trentham, the THF insolubles values demonstrate an improvement in the amount of material converted, both over 30 minutes and 60 minutes. This

improvement seems to come mainly from increases in the yields of oils and asphaltenes, but there is also a reduction in the preasphaltenes yield. In blends of Baddesley and Littleton, the THF insolubles shows a less significant improvement after 60 minutes than after 30 minutes. However, the increase in oils yield for the blend after 60 minutes is very large and could indicate that enhancement of product distribution will continue, even after overall conversion has ceased to increase.

Table 1
Product Yields for Baddesley and Trentham coals (% daf coal)

Amount of Baddesley in the blend	0 %		50 %		100 %	
	30 mins	60 mins	30 mins	60 mins	30 mins	60 mins
Gas	1.9	4.9	2.5	3.5	2.2	4.5
Oils	0.1	13.5	25.3	35.6	2.0	15.2
Asphaltenes	26.1	24.6	35.8	34.7	38.5	22.7
Preasphaltenes	24.0	29.5	11.6	5.0	23.1	26.8
THF insolubles	47.9	27.5	24.8	21.2	34.2	30.8

Table 2
Product Yields for Baddesley and Littleton coals (% daf coal)

Amount of Baddesley in the blend	0 %		50 %		100 %	
	30 mins	60 mins	30 mins	60 mins	30 mins	60 mins
Gas	2.1	4.8	2.4	3.7	2.2	4.5
Oils	0.4	16.6	26.6	50.1	2.0	15.2
Asphaltenes	36.4	22.1	24.1	16.1	38.5	22.7
Preasphaltenes	23.9	33.6	17.9	7.1	23.1	26.8
THF insolubles	37.2	22.9	29.0	23.0	34.2	30.8

Results from the autoclave experiments, given in Tables 3 and 4, exhibit a more synergistic effect when the blend contains 50 % Baddesley or higher. For blends of Baddesley and Point of Ayr, there appears to be a slight improvement in conversion, oils yield and heavy organics, and a corresponding reduction in the yields of asphaltenes and preasphaltenes. Blends of Baddesley and Crumlin, the lignite, again show an improvement in conversion, mainly when Baddesley accounts for 50 % or more of the blend. However, in this case the oils yield has decreased slightly from expected, with a corresponding increase in asphaltenes and preasphaltenes.

These results would appear to suggest that blends of Baddesley with similar ranked coals will give an enhancement of oils yield, and a reduction in the heavier liquids, that may be beneficial in further processing, especially hydrocracking. However, when blended with Crumlin, which gives the best single oils yield, Baddesley appears to induce an increase in the production of the heavier liquids that can be so damaging to catalysts in hydrocracking.

Table 3

Product Yields and Conversion for Baddesley and Point of Ayr coals (% dmmf coal)

Amount of Baddesley in the blend	0 %	25 %	50 %	75 %	100 %
Oils	15.1	19.0	21.2	21.7	19.5
Asphaltenes	40.0	37.2	35.4	35.4	36.9
Preasphaltenes	13.0	11.6	11.0	10.9	12.0
Heavy organics	19.9	19.2	20.2	19.6	15.1
Conversion	87.9	87.0	87.7	87.5	83.5

Table 4

Product Yields and Conversion for Baddesley and Crumlin coals (% dmmf coal)

Amount of Baddesley in the blend	0 %	25 %	50 %	75 %	100 %
Oils	56.7	41.9	32.3	20.8	19.5
Asphaltenes	24.4	35.8	35.3	41.0	36.9
Preasphaltenes	4.1	6.4	10.1	12.3	12.0
Heavy organics	7.6	7.0	11.4	14.5	15.1
Conversion	92.9	91.1	89.2	88.6	83.5

4. Conclusions

It is interesting to note that separate researchers, in different laboratories, using different techniques, have observed very similar results; but it is difficult to make any clear explanations as to why Baddesley should produce an effect like this without having a detailed knowledge of the structure of the coals used and the exact mechanism for the dissolution process. However, it would appear that Baddesley, in some way, shortens the time taken by the blends to convert to heavy liquid products, possibly through the donation of hydrogen from Baddesley to the other coal in the blend. After this initial conversion, it is possible that the coals will make use of the hydrogen from the donor solvent, to convert into lighter liquids, allowing the observed improvement in product distribution. When blended with Crumlin, Baddesley may in some way interfere with Crumlin's own auto-hydrogenation processes, thereby reducing the production of oils.

References

1. Ouchi, K., Ibaragi, S., Kobayashi, A., Tanimoto, K., Makabe, M., Itoh, H., Matsubaru, K. and Takekawa, T., FUEL, 63 (1984) 78
2. Sato, Y., FUEL, 61 (1982) 875
3. Pickering, A. and Cloke, M., The 1994 IChemE Research Event, 664
4. Pickering, A., Belghazi, A., Cloke, M. and Lester, E., The 1995 IChemE Research Event, 399
5. Taylor, J. and Patrick, J.W., The 1995 IChemE Research Event, 303

Characterisation of Coals for Liquefaction using Image Analysis

Andrew Pickering, Edward Lester and Michael Cloke.

Coal Technology Research Group, Department of Chemical Engineering, University of Nottingham, University Park, Nottingham. NG7 2RD. United Kingdom.

1. Introduction

Coal petrology can provide very important information about the sources of certain coals and the coalification processes which created them. However, for coal utilisation purposes it does not always give a complete assessment of a coal's behaviour. Rank, measured as mean random vitrinite reflectance, can also provide useful information for utilisation purposes, but its use is limited, especially where coals contain a large amount of macerals other than vitrinite. If petrographic composition or rank are used on their own as a means of predicting the behaviour of coals during coal liquefaction, then unsatisfactory results may be obtained, since coals with similar rank or petrographic composition may behave in different ways.

In 1978, Abdel-Baset *et al* found that simple correlations of rank, petrographic composition or total sulphur with conversion in liquefaction reactions gave very poor results¹. They also found that only when a multiple regression was performed were these parameters able to be related to conversion. Later work found that it was possible to split these and further coals into three populations². Work at Nottingham, for the combustion industry, has proposed that image analysis systems may be able to provide a better predictive information on a coal than either petrographic composition or rank³. Cloke and Lester, following a review of coal characterisation, concluded that any predictive system would need to assess both rank and composition⁴.

Work presented here will attempt to relate classification by both manual methods and image analysis, to overall conversion of coal during liquefaction.

2. Experimental

The coals in this study were classified in two ways: the first involved manual petrographic analysis and was used as Total reactive macerals %, which were derived from the formula:

$$\text{Total reactive macerals \%} = \text{vitrinite \%} + \text{ligninite \%} + (1/3 * \text{semifusinite \%}) \quad (1)$$

The second analysis was performed by an Image Analysis System. The image analyser that was used was an IBAS 2000 Image Processing System, connected to a Leitz Ortholux II POL-BK microscope via a Hamamatsu C2400-07 Newvicon video camera. The polished coal mounts were prepared to BS 6127: Part 2: 1981, details of this procedure are given in a previous publication⁵. The analysis method for the image analysis involved capturing a series of images under reflected light. The image analyser divided each image up into a square, 512

by 512 pixels, giving 262144 pixels in total. Each pixel was then assigned a grey scale value between 0 and 255. However, there is a drawback with this system, the liptinite and the mounting medium have very similar grey scale values, making it difficult to distinguish between the two. To rectify this a high pressure mercury light source was used to fluoresce the liptinite in the same series of images. When plotted on a grey scale histogram the combined liptinite/mounting medium area could be seen and removed, and replaced with a normalised liptinite block over an agreed grey scale range. A cumulative grey scale histogram could then be plotted to provide the data for the determination of the threshold between reactive and unreactive, which gave the values for Reactives content. The method is fully described in a previous publication⁶.

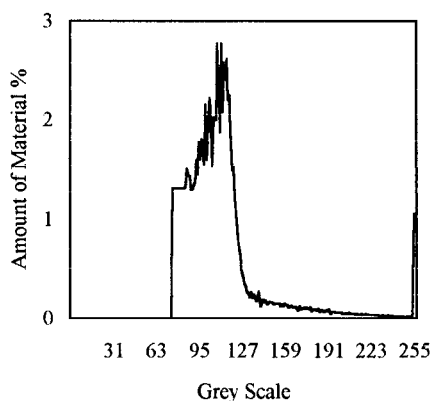


Figure 1. Grey Scale Histogram, corrected for mounting resin, for a typical bituminous coal.

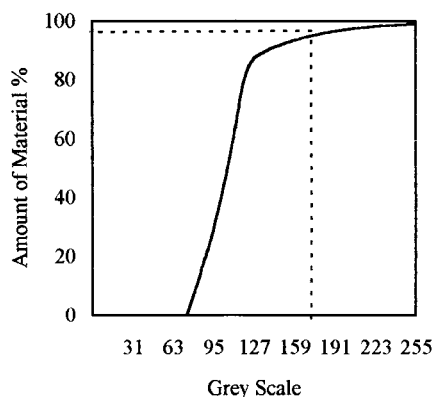


Figure 2. Cumulative Grey Scale Histogram for a typical bituminous coal, showing the threshold grey scale value.

Overall conversions for the coals were then determined by liquefying them in a 10ml tubing bomb micro-reactor. 1.1g of coal and 2.2g of hydrogenated anthracene oil were charged to the reactor, which was then placed in a fluidised bed sand bath heater at 425°C for 60 minutes, whilst undergoing constant agitation. After the reaction period expired, the micro-reactor was removed from the sand bath and allowed to cool in air. The reactor was then vented. The solid/liquid residue was extracted using hot quinoline and an ultrasonic bath. This left a residue of mineral matter and undissolved coal, or quinoline insolubles. The weight of the residue plus the weight of HAO added to the reactor was subtracted from the total weight of material added to the reactor, to give a weight of coal extract. This was divided by the weight of dry mineral matter free coal in the reactor to give a conversion on a dmmf basis.

3. Results and Discussion

The results, presented in Tables 1 and 2, show that for the complete set of coals the Reactives content % gives a much better correlation with conversion than the Total reactive macerals %. This is mainly due to the values obtained for Mager coal, which is a blend, predominantly a

German anthracite, with approximately 20% of another bituminous coal. While it has some liptinite and low reflectance vitrinite, it consists mainly of high reflectance vitrinite. From the results of a manual point count, and the formula for reactive macerals (equation 1), a Total reactive maceral result of 94.4% for Mager would suggest that this coal should give a liquefaction conversion in the mid eighties. However, using Image Analysis, the difference in the rank of the two coals in the blend is picked up, and the Reactives content value of 8.1%, gives a more accurate picture of its liquefaction potential. If Mager is removed from the set of coals, then it can be seen that there is only a small difference in the correlation statistics, with Total reactive macerals % giving a slightly better correlation than Reactives content %. However, when only the British coals from the set are considered, which was attempted in earlier work, Reactives content % again shows better correlation results.

Table 1
Coal conversions, total reactive macerals and Reactives content

	Conversion % dmmf coal	Total reactive macerals %	Reactives content %
Baddesley	86.9	85.7	94.6
Bentinck	86.9	91.9	95.1
Blair Atholl	63.4	64.5	84.8
Coccerr	87.4	85.1	96.3
Czezcot	83.6	88.0	95.6
Gdansk	84.0	87.2	89.3
Gedling	86.4	84.6	96.2
Hunter Valley	84.2	80.0	92.0
Kaltim Prima	97.1	97.8	100.0
Kromdraai	59.2	73.0	55.9
Littleton	81.1	84.3	88.8
Longannet	90.7	92.9	99.0
Mager	17.1	94.4	8.1
MCQuarie	82.0	91.7	95.3
Point of Ayr	90.1	92.0	94.7
SSM China	84.1	85.5	80.0
Trentham	82.9	87.1	87.3
Vartan	89.2	88.1	91.2

Table 2
Correlation results for predictive variable against conversion

	Correlation Coefficients	
	Total reactive macerals	Reactives content
All coals	0.1985	0.9573
All coals (excluding Mager)	0.8782	0.8165
British coals	0.7480	0.8762

4. Conclusions

These results appear to indicate that when unusual coals, or coals from a geologically different source, are to be used, then image analysis is a much more reliable predictive tool than manual petrography. Image analysis allows a non-subjective assessment of a coal's constituents in terms of what may react and what may not react, and it could prove useful as a means of assessing why coals are unsuitable for utilisation purposes.

Further Work

The results shown here are interesting, but require verification with further coals. It has already been proposed to add more South African coals to the study, in order to increase the amount of data points in the 40 to 70% conversion range. It may also be useful to add some coals similar to Mager, in terms of rank, in an attempt to provide a more even distribution of data points throughout the range of conversions considered.

References

1. Abdel-Baset, M.B., Yarzab, R.F. and Given, P.H., *FUEL*, 57 (1978) 89
2. Yarzab, R.F., Given, P.H., Spackman, W. and Davis, A., *FUEL*, 59 (1980) 81
3. Lester, E., PhD Thesis, University of Nottingham, (1994)
4. Cloke, M. and Lester, E., *FUEL*, 73 (1994) 315
5. Lester, E., Allen, M., Cloke, M. and Miles, N.J., *FUEL*, 73 (1994) 1729
6. Cloke, M., Lester, E., Allen, M. and Miles, N.J., *FUEL*, 74 (1995) 659

Liquefaction of coal and coal fractions of different relative densities from a hydrocyclone separator

J. Barraza, M. Cloke, A. Belghazi, N. Miles

Coal Technology Research Group, Department of Chemical Engineering,
University of Nottingham, Nottingham, NG7 2RD, UK

1. INTRODUCTION

Studies have shown that the coal characteristics, particularly petrographic and mineral compositions, are important parameters which affect overall conversion and product distribution in direct coal liquefaction [1,2]. Work has been carried out in a two-stage liquefaction unit in order to improve conversion and product distribution, mainly towards oils production, and to reduce the content of potential deactivating elements of the hydrocracking catalyst in filtered coal extracts [3, 4,]. Coal fractions concentrated in organic matter and reduced in mineral matter (beneficiated) may have an important contribution in the achievement of these aims.

The purpose of this study was to produce, in a hydrocyclone separator, coal fractions with varying petrographic and mineral compositions, and to liquefy each coal fraction in order to assess the roles of petrographic and mineral composition on conversion and product distribution.

2. EXPERIMENTAL

Two bituminous coals, Point of Ayr and Blidworth, UK, of particle size -250+63 and -500+63 μm respectively, were processed in a hydrocyclone separation unit (closed circuit sump-pump-cyclone), using an aqueous solution of Calcium Nitrate Tetrahydrate. Relative density of 1.26 was used for Point of Ayr, while densities of 1.25, 1.30 and 1.45 were used for Blidworth coal. Two coal fractions, overflow (OF) and underflow (UF), were obtained from each hydrocyclone run. Liquefaction runs were carried out in a 2 litre autoclave with Hydrogenated Anthracene Oil (HAO) as solvent in a ratio HAO/Coal: 2/1, w/w. 350 g. of coal was fed to the autoclave. The liquefaction was carried out for 45 minutes and a temperature of 420 °C. Digestion pressure of 40 barg was used for the fractions of Point of Ayr coal, while 30 barg was used for Blidworth coal. The product of the digestion was filtered to produce a filter cake and a coal extract solution.

3. RESULTS AND DISCUSSION

3.1 Hydrocyclone separations

Table 1 shows the results of yield (on a mass basis, with respect to the original coal fed to the hydrocyclone), ash and petrographic analysis for the original coal and the coal fractions obtained at different relative densities. Results show that at relatively the same density (1.25), the overflow yield

of Point of Ayr coal (43 %) is approximately double that of Blidworth coal (23%). Either, the difference of particle size used or the difference of intrinsic specific gravity of each original coal,

Table 1
Mass yield and analysis of original coal and coal fractions

	Relative density	Yield %,w/w	Ash %, db	Petrographic analysis, %, v/v, mmf		
				Vitrinite	Liptinite	Inertinite
Point of Ayr						
Original	-	100.0	14.5	80.9	10.1	9.0
Overflow	1.26	43.0	1.2	77.0	15.7	7.3
Underflow	1.26	57.0	16.0	78.3	8.0	13.7
Blidworth						
Original	-	100.0	14.4	80.6	5.1	14.3
Overflow	1.25	23.1	1.3	87.0	8.8	4.2
Overflow	1.30	49.6	1.4	91.4	3.8	4.8
Overflow	1.45	67.3	2.9	82.0	5.1	12.9
Underflow	1.25	76.9	18.5	78.9	3.7	17.3
Underflow	1.30	50.4	27.1	63.0	5.4	31.6
Underflow	1.45	32.7	37.5	63.6	3.1	33.2

may have produced these changes in yield [5]. Increasing the density of separation in Blidworth, increases the yield of overflow significantly from 23.1 to 67.3 % w/w. However, from the maceral analysis there is not a significant difference between the original coal and the 1.45 overflow. On the other hand, the 1.25 and 1.30 overflow products do show significant concentration of the non-inertinite macerals. These maceral compositions would have an effect on the coal reactivity, which will be analysed further on. The overflow fractions of the two coals and the underflow fraction from Point of Ayr were the selected samples for the liquefaction runs experiments.

3.2 Liquefaction of original coal and coal fractions

Results of conversion and product distribution in the coal extract liquids are shown in Figure 1.

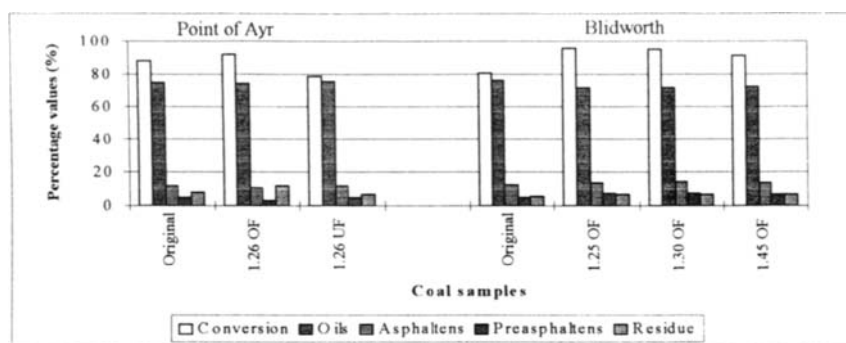


Figure 1. Conversion and product distribution in coal extracts

In this study, the percentages of products are defined as : oils, (100 - hexane insolubles); asphaltenes, (hexane insolubles - toluene solubles); preasphaltenes, (toluene insoluble - THF solubles) and residue, (THF insolubles). The coal conversion (on a dmmf basis) is determined from ash and quinoline solubility measurements. In general, the overflow fractions produced higher conversions than the original coal, while the underflow fraction from Point of Ayr produced the lowest conversion. In order to analyse the role of the maceral content on the conversion, a study [1] found a correlation between the most reactive macerals (liptinite+vitrinite) and the liquefaction yield. Figure 2 shows our results for the two coals. As can be seen in Figure 2 a fair correlation was also obtained; the overflow fractions, which are concentrated in reactive macerals, produced the highest liquefaction yields, while the underflow, of low reactive macerals content, gave the lowest conversion.

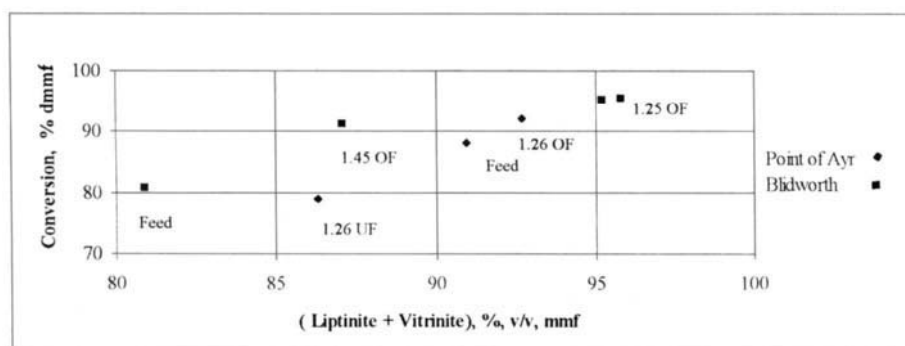


Figure 2. Dependence of liquefaction conversion with the reactive macerals

The product distributions shown in Figure 1 indicate that the oils fraction is lower in the overflow fractions compared with the original feed and underflow. However, these results do not take account of the higher proportion of converted coal in the product and that part of the HAO is recorded as oils. Therefore, a mass balance is needed to calculate the oils production from the coal alone. A basis of 100 kg of coal as received, processed in the hydrocyclone and then liquefied in the autoclave, was taken for the mass balance. Also, it was assumed that the amount of gas produced is 2% of the coal converted and the HAO ends up as oils and none of it as other product. Results of the net product distribution are shown in Figure 3. In general the overflow samples gave higher net proportion of oils in the product than the original coal, with small reductions in the asphaltenes. By contrast, the oils produced from the underflow of Point of Ayr was the lowest. These findings are in opposition with the product distribution which includes the solvent. Then, this appears to show that the maceral analysis also plays an important role in the net product distribution where coal fractions concentrated in reactive macerals benefit the net oils production. Also, the products distribution from the overflow samples of Blidworth at different densities is approximately similar. In mass term this means that for this coal the split using 1.45 relative density is very beneficial with a lower underflow proportion and good split, requiring a smaller liquefaction processing plant for the same total liquid product output.

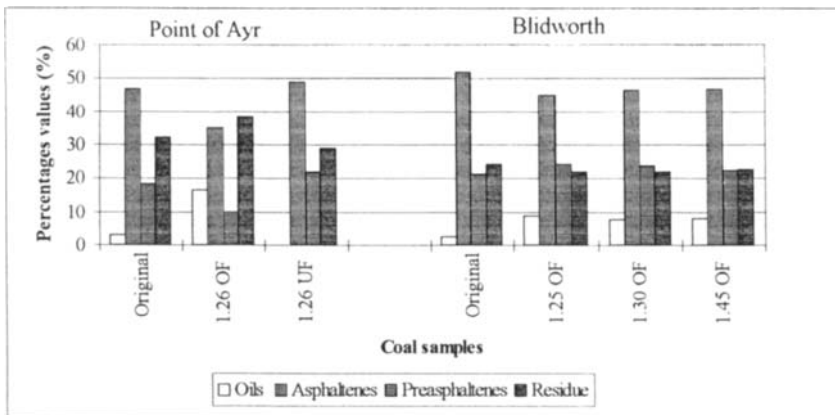


Figure 3. Liquefaction product distribution on a basis of 100 kg of as received

4. CONCLUSIONS

The overflow fractions obtained by hydrocyclone separation, concentrated in reactive macerals and reduced in mineral content, produced an improvement in liquefaction conversions over the original coal, together with a shift in the net product distribution towards higher oils and lower residue content in the liquid products. Also, the quantity of mineral matter removed at the stage of filtration decreased. Using these beneficiated coal fractions possible economic benefits may be obtained due to the reduced size of the liquefaction unit. More results are required to confirm these findings and work is being carried out using coal fractions obtained by froth flotation.

ACKNOWLEDGEMENTS

The financial support for this work by the Science and Engineering Research Council, UK, the Colombian Institute of Science and Technology (COLCIENCIAS) and the British Coal Utilisation Research Association is gratefully acknowledged. The views expressed are those of the authors and not necessarily those of the funding bodies.

REFERENCES

- [1] Given P.H., Cronauer D.C., et. al., *Fuel*, 54, (1975), 40
- [2] Moore, S.A., Jones, M.A., Hughes R.D., Kimber G.M., 1991. International Conference on Coal Science, University of Newcastle upon Tyne, UK,
- [3] Cloke M., 1986. *Fuel*, 65, 417
- [4] Cloke, M., Belghazi A., Martin S., Kelly B., Snape C.E., McQueen P., Steedman, W., 1993. International Conference on Coal Science, Banff, Canada
- [5] Sand, P., Sokaski M., Geer, R., 1968, BuMines, RI 7067

Utilization of thermodynamic database in the systems using molybdate and iron based catalysts

Yuji Yoshimura, Hiroyuki Yasuda, Toshio Sato, Hiromichi Shimada,
Nobuyuki Matsubayashi, Motoyasu Imamura and Akio Nishijima

National Institute of Materials and Chemical Research, AIST/MITI, Tsukuba 305, JAPAN

1. INTRODUCTION

Sulfide catalysts have been used for coal dissolution and upgrading coal-derived liquids in the coal liquefaction processes. Several species of the transition metals such as Fe, Mo, Ni, W, Sn and Zn, were used in various forms of the precursors, such as oxides, sulfates, chlorides and carbonyls in the dispersed or supported forms[1–5]. Catalytic activities of these starting materials were influenced by the sulfidation method, e.g., presulfidation or in situ sulfidation during hydrotreating reaction with H₂S or S. However, information on the effect of sulfidation conditions, such as P(H₂S)/P(H₂), P(H₂O), temperature etc, on the structural transformations of these starting materials was quite limited[6–8]. Such structural transformations of the catalyst precursors are quite important not only for determining the active species and their stability but also for optimizing the activation conditions as well as the preheating and hydrotreating reaction conditions. In this report the thermodynamic analyses using chemical potential diagrams were done to better understand the structural changes/stability of the molybdate and iron based catalysts during the sulfidation and hydrotreating reaction processes, though no kinetic informations were obtained from them.

2. EXPERIMENTAL SECTION

Catalysts. α -Fe₂O₃, Fe₃O₄ and FeSO₄·7H₂O(Wako pure chemical) were used as received for preparing the non-supported iron based catalysts. Mo catalysts(MoO₃=15.5 wt%) were prepared by the incipient wetness impregnation of γ -Al₂O₃ with aqueous Mo solutions containing citric acid as a complexing agent. These precursors(under 100 mesh) were sulfided with H₂S/H₂ (5%/95%) gas at 673 K(heating rate=10 K/min) for 1 h.

Characterization of Catalysts. The EXAFS experiments were done at the Photon Factory of the National Laboratory for High Energy Physics in Tsukuba, Japan. The Mo K-edge and Fe K-edge measurements were done at room temperature in transmission mode at beam lines of BL-10B and BL-7C. The radial distribution function around Mo or Fe was obtained by k³-weighted Fourier transforms of the EXAFS data ($\Delta k=10.0$ (2.8<k<12.8 Å⁻¹) for Fe, and $\Delta k=14.0$ (3.15<k<17.15 Å⁻¹) for Mo. Detailed procedures for the EXAFS analysis are described elsewhere[9].

Thermodynamics. Chemical potential diagrams[10–12] were used to evaluate the stability/reactivity of the metal sulfides, oxides and sulfates during sulfidation. A commercially accessible PC-based database of MALT2[13] and JANAF data base[14] were

used. For calculating an equilibrium composition of several gaseous and condensed species, and for predicting the paths of structural changes, we used the gradient projection method[15] which minimized the free energy of the system considered.

3. RESULTS AND DISCUSSION

3.1 EXAFS analysis of the sulfided iron precursors

Figure 1 shows the Fourier transforms of the EXAFS spectra (Fe K-edge) for the sulfided iron based catalysts. After sulfidation of α - Fe_2O_3 , four main peaks were observed at 0.19, 0.25, 0.30 and 0.35 nm. The peak at 0.25 nm corresponds to that of the Fe-S coordination in pyrrhotite(Fe_7S_8). The peaks at 0.19 and 0.31 nm correspond to Fe-O and Fe-Fe coordinations of Fe_2O_3 , but the peak at 0.34 nm likely corresponds to Fe-Fe coordination of Fe_3O_4 (cf, 0.37 nm for Fe_2O_3). These data suggested that Fe_2O_3 , Fe_3O_4 and pyrrhotite phases coexisted, which might be mainly due to the sulfiding gas diffusion and reaction rate limitations. After sulfidation of Fe_3O_4 , four main peaks were observed. The peak(0.25 nm) corresponds to Fe-S coordination of pyrrhotite, and other peaks correspond to Fe-O(0.20 nm) and Fe-Fe(0.30 and 0.35nm) coordinations of Fe_3O_4 . The intensity of Fe-S coordination was lower than that of the sulfided Fe_2O_3 catalyst, which indicated the difficulty in sulfiding of the precursor of Fe_3O_4 . The Gibbs free energies of sulfidation(673K) of iron oxides into $\text{Fe}_{0.877}\text{S}$ were -58.2 kJ/mol- H_2S and -48.6 kJ/mol- H_2S for Fe_2O_3 ad Fe_3O_4 , respectively. This supported the difficulty of Fe_3O_4 in sulfiding

compared with Fe_2O_3 , but difference in diffusibility of sulfiding gas into the bulk phases would be a dominant factor(much more packed inverse spinel structure for the former and corundum structure for the later). On the contrary, after sulfidation of $\text{FeSO}_4 \cdot 7\text{H}_2\text{O}$ two main peaks observed, which correspond to Fe-S(0.242 nm) and Fe-Fe(0.297 nm) coordinations in pyrrhotite. This indicated that iron sulfate was one of the suitable precursors to form the pyrrhotite phase selectively. Artok et al. indicated that ferrous sulfate salt was entirely converted into pyrrhotite at 698 K under $\text{H}_2\text{S}(5\%)/\text{H}_2(95\%)$ sulfiding gas[1].

The Fourier transform of the EXAFS spectra(Mo K-edge) for the sulfided $\text{MoO}_3/\gamma\text{-Al}_2\text{O}_3$ catalysts, indicated that almost of MoO_3 was converted into MoS_2 -like crystallites in the same sulfidation conditions($\text{Mo}^{4+}/(\text{Mo}^{4+}+\text{Mo}^{6+})>85\%$ by XPS).

3.2 Thermodynamic analysis of the sulfidation pathways

Figure 2 shows the chemical potential diagram of the Fe-O-S system at 673K. The vertical axis indicates the ratio of partial pressure of hydrogen sulfide to hydrogen and the horizontal axis indicates the partial pressure of oxygen. In the sulfidation condition($\text{H}_2\text{S}(5\%)/\text{H}_2(95\%)$), i.e. $\log(P(\text{H}_2\text{S})/P(\text{H}_2)) = -1.28$, each of Fe_2O_3 , Fe_3O_4 and $\text{FeSO}_4 \cdot 7\text{H}_2\text{O}$ could be converted

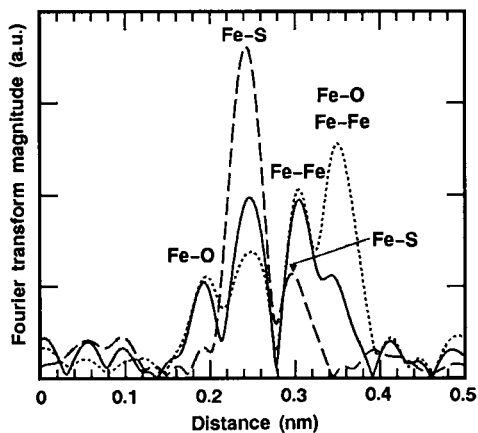


Figure 1. Fourier transforms of Fe EXAFS spectra: sulfided Fe_2O_3 (—), sulfided Fe_3O_4 (.....) and sulfided $\text{FeSO}_4 \cdot 7\text{H}_2\text{O}$ (---).

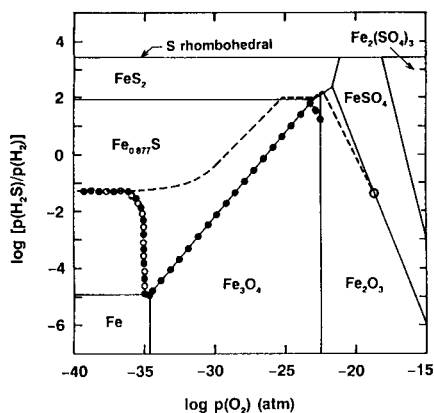


Figure 2. Chemical potential diagram for Fe–O–S–H system at 673 K: sulfidation pathways for Fe_2O_3 (●), Fe_3O_4 (○) and $\text{FeSO}_4 \cdot 7\text{H}_2\text{O}$ (■).

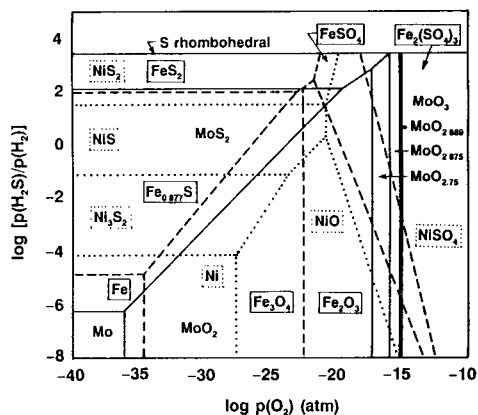


Figure 3. Chemical potential diagram for Fe(Mo,Ni)–O–S–H systems at 673 K: Fe–O–S–H (---), Mo–O–S–H (—) and Ni–O–S–H (.....).

into thermodynamically more stable pyrrhotite($\text{Fe}_{0.877}\text{S}$)(left hand side in Fig. 2). However, the sulfidation pathways(shown in points) differed from one another, where we assumed that sulfidation gas will slowly penetrate into the bulk oxides and sulfates, and that sulfidation proceeded quite rapidly so that the local equilibrium state would be attained within a relatively short time. In practice, there might be an sulfur potential gradient insides of the bulk oxides and sulfates, transient intermediates would coexisted after sulfidation as shown in Fig. 1. In sulfiding of $\text{FeSO}_4 \cdot 7\text{H}_2\text{O}$, formation of FeS_2 (pyrite) would be expected as transient intermediate under the relatively high $\text{H}_2\text{S}/\text{H}_2$ potential. FeS_2 as transient intermediate would be better to minimize the carbonaceous deposits on the acidic oxidic phases on the transient intermediates and minimize the solid phase and hydrothermal interactions between the oxidic phases and mineral matters.

3.3 Stability of Fe and Mo compounds

Figure 3 shows the chemical potential diagram of the Mo–O–S and Ni–O–S systems at 673 K. The chemical potential diagram of Ni–O–S system is included for comparison. In the presulfiding condition($\text{H}_2\text{S}(5\%)/\text{H}_2(95\%)$), i.e., $\log[\text{P}(\text{H}_2\text{S})/\text{P}(\text{H}_2)] = -1.28$, Fe_2O_3 , MoO_3 and NiO could be converted into thermodynamically more stable $\text{Fe}_{0.877}\text{S}$, MoS_2 and Ni_3S_2 , respectively. As mentioned before, assumption of local equilibrium made it possible to predict the coexistence of sulfides and oxides. Shifts of the equilibrium lines between oxides and sulfides to the more reducing conditions indicated that sulfidation of oxides become more difficult, i.e. $\text{MoO}_3 > \text{Fe}_2\text{O}_3$ in the order of ease of sulfidation, which were recognized in many experiments. On the contrary, the equilibrium lines between sulfides and metals indicate the reducibility of metal sulfides. Their reducibility, i.e., ease of S^{2-} vacancy sites formation, decreased in the order of $\text{Ni}_3\text{S}_2 > \text{Fe}_{0.877}\text{S} > \text{MoS}_2$. As excess reduction of the sulfidic phases might result in an increase in the amount of carbonaceous deposits, H_2S concentration needed to keep their proper sulfidic states decreased in the same order.

Figure 4 shows the potential of volatile species during the sulfidation/steaming conditions at 698 K under the gas phase conditions of $\log p(\text{H}_2\text{O}) = -1.0$ (atm) and $\log[\text{p}(\text{H}_2\text{S})/\text{P}(\text{H}_2)] = -1.28$. Vapor pressure of Fe and Mo hydrates was quite high compared with their oxides and sulfates under the reducing condition(left hand side in Figure 4), and vapor pressure of

$\text{Fe}(\text{OH})_2$ was higher than that of $\text{MoO}_3 \cdot \text{H}_2\text{O}$. This suggested that iron species were subject to vapor phase transport which might result in an agglomeration of $\text{Fe}_{0.877}\text{S}$ particles ($\Delta G = -153.4 \text{ kJ/mol-H}_2\text{S}$ for $\text{Fe}(\text{OH})_2 \rightarrow \text{Fe}_{0.877}\text{S}$, $\Delta G = -58.8 \text{ kJ/mol-H}_2\text{S}$ for $\text{Fe}_2\text{O}_3 \rightarrow \text{Fe}_{0.877}\text{S}$). Vapor pressure of volatile species over the condensed iron sulfate phases was lower than those of iron oxides and sulfides (no condensed phases of $\text{Fe}_2(\text{SO}_4)_3$ existed under $\log P(\text{O}_2) > -10.7$). This means that iron sulfates were relatively stable precursors for the pyrrhotite formation, though those will be dissolved into H_2O under the more oxidizing conditions. For minimizing the agglomeration induced by vapor transport of iron species and thermal sintering etc., dispersion of ferrous sulfate on supports, e.g. coal, would be effective.

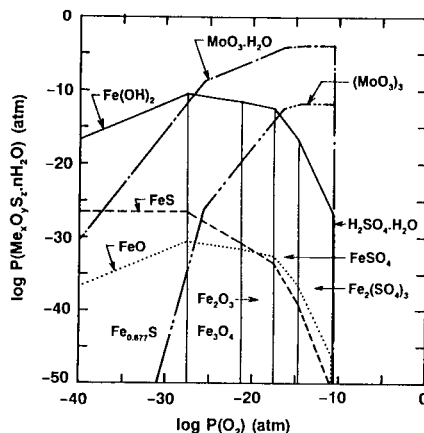


Figure 4. Potential of volatile species at 673 K under $\log P(\text{H}_2\text{O}) = -1$ (atm) and $\log [P(\text{H}_2\text{S})/P(\text{H}_2)] = -1.28$.

CONCLUSIONS

1. Iron sulfate ($\text{FeSO}_4 \cdot 7\text{H}_2\text{O}$) would be a favorable precursor for the formation of pyrrhotite (Fe_{1-x}S) phases during sulfidation, compared with oxidic precursors such as hematite (Fe_2O_3) and magnetite (Fe_3O_4). Oxidic precursors were more refractory in sulfiding than sulfates.
2. Water would contribute the formation of metal hydrate compounds, e.g. $\text{Fe}(\text{OH})_2$ and $\text{MoO}_3 \cdot \text{H}_2\text{O}$, which compounds are volatile and might cause the undesirable sintering and agglomeration of the catalytic active phases during sulfidation and hydrotreating reactions.
3. Thermodynamic analysis using database would be a very promising method to predict *a priori* the chemical/thermal/hydrothermal stabilities of Mo and Fe based catalysts.

REFERENCES

1. L. Artok, H.H. Schobert and A. Davis, *Fuel Proc. Technol.*, 32(1992)87.
2. S.W. Weller, *Energy & Fuel*, 8(1994)415.
3. T. Suzuki, *J. Jpn. Inst. Energy*, 73(1)(1994)3.
4. F.J. Derbyshire, *Catalysis in coal liquefaction*, IEA coal research, IEACR/08, 1988.
5. V.R. Pradham, J.W. Tierney, I. Wender and G.P. Huffman, *Energy & Fuels*, 5(1991)497.
6. T. Okutani, S. Yokoyama, Y. Maekawa, R. Furuichi and T. Ishii, *Ind. Eng. Chem. Process Des. Dev.* 22(1983)306.
7. H. Zimmer, M. Andres, H. Charcosset and G. Djega-Mariadassou, *Appl. Catal.*, 7(1983)295.
8. Y. Yoshimura, T. Sato, H. Shimada, N. Matsubayashi, M. Imamuar and A. Nishijima, *J. Jpn. Inst. Energy*, 74(3)(1995)178.
9. N. Matsubayashi, Ph.D. Thesis, Osaka Univ., 1986.
10. H. Yokokawa, T. Kawada and M. Dokiya, *Denki Kagaku*, 56(9)(1988)751.
11. H. Yokokawa, T. Kawada and M. Dokiya, *J. Am. Ceram. Soc.*, 72(11)(1989)2104.
12. H. Yokokawa, N. Sakai, T. Kawada and M. Dokiya, *J. Am. Ceram. Soc.*, 73(3)(1990)649.
13. *Soc. Calorim. Therm. Anal. Jpn.*, Thermodynamic Database MALT 2, Kagakujijutsusha, Tokyo, 1992.
14. M.W. Chase, Jr., C.A. Davis, J.R. Downey, Jr., D.J. Frurip, R.A. McDonald, and A.N. Syverud, *J. Phys. Chem. Ref. Data*, 14, Suppl., (1985).
15. T. Matsumoto and H. Yokokawa, *Netsu Sokutei*, 19(4)(1992)170.

In-situ XAFS Spectroscopic Studies of DCL Catalysts

Naresh Shah, J. Zhao, K.R.P.M. Rao, F.E. Huggins and G.P. Huffman

Consortium for Fossil Fuel Liquefaction Science, University of Kentucky,
341 Bowman Hall, Lexington, KY 40506-0059, USA

1. Introduction

Traditionally, the role of catalysts in coal liquefaction has been inferred by examining samples before and after reaction. To further enhance this knowledge, observation of the actual active catalytic species at liquefaction conditions is essential. However, few attempts have been made in this direction due to the experimental difficulties. The catalyst characterization capabilities of X-ray Absorption Fine Structure (XAFS) spectroscopy have been demonstrated in our previous investigations [1] of the nature of Fe-based catalysts before and after liquefaction experiments on coals and oils. We have now built an *in situ* XAFS cell capable of reproducing direct coal liquefaction conditions to examine several novel Fe based direct coal liquefaction (DCL) catalysts.

2. Design of *in situ* XAFS cell

As shown in figure 1, we have modified the Neils and Burlitch [2] design to construct our *in situ* cell for XAFS investigation of direct coal liquefaction (DCL) catalysts. Two layers of graphite cloth were glued to each other and were then sandwiched between two copper gaskets. The graphite cloth provides the necessary mechanical strength to the window without substantial attenuation of the X-ray beam.

The total hydrogen volume is kept low for safety considerations. A thin pellet of the sample (coal with the added catalyst) is placed in the sample cell and the window assemblies are attached to the sample cell with the outer two water cooled flanges. The sample cell is charged with about 1000 psig cold hydrogen and then is disconnected from the hydrogen supply. The sample within the cell is heated to reaction temperatures with four cartridge heaters embedded in the center flange. This design of the cell can reproduce the elevated temperature and hydrogen pressure (up to 1800 psig hydrostatic pressure) employed in autoclave or micro autoclave (tubing bomb) reactors while allowing a seven KeV synchrotron generated x-ray beam to pass through the cell windows and the sample.

3. Catalyst systems investigated

Three different catalyst systems were investigated *in situ*: (1) Black thunder coal, ion-exchanged using iron acetate solution to get 3.78 wt.% Fe loading by a procedure established by Taghiei et al. [3], (2) 5 wt.% of binary ferrihydrite catalyst (with 5 wt.% SiO₂) in Blind Canyon (DECS-17) coal and (3) 5 wt.% of citric acid treated ferrihydrite catalyst in Blind Canyon (DECS-17) coal. To maintain realistic catalyst loading, the total Fe contents of all samples were kept less than five weight percent. Enough elemental sulfur was added to achieve complete sulfidization of all the iron present in the samples.

4. XAFS results

In situ iron K edge XAFS spectra for all standards and samples were acquired at the X-19A beamline of the National Synchrotron Light Source. To conserve space only the X-ray Absorption Near Edge Structure (XANES) and Radial Structure Functions (RSF) of the Extended X-ray Absorption Fine Structure (EXAFS) data for the SiO₂ treated binary ferrihydrite catalyst are discussed in this paper (see figure 2). A more detailed paper is in preparation.

Before the cell is heated, but under pressurized hydrogen atmosphere, both the XANES and RSF are characteristics of very finely dispersed iron oxyhydroxide phase. As the temperature of the sample is raised, the finely dispersed iron starts reacting with sulfur, presumably as hydrogen sulfide (H₂S). The XAFS spectra do not indicate any significant sintering of catalyst particles [4] or reduction to the metallic state. The main peak of XANES spectra broadens and the inflection point moves toward zero suggesting reduction of the formal oxidation state of iron. The preedge feature also becomes weaker and appears more like a shoulder than a peak. This transition of the XANES from that characteristic of iron oxyhydroxide to that of pyrrhotite is gradual and occurs over a range of time and temperature conditions.

The EXAFS data also support this observation. The RSFs of the unreacted catalysts exhibit peaks at 1.5 and 2.8 Å for the oxygen and iron shells respectively. With increasing temperature, the peak due to iron shell (at 2.8 Å) diminishes rapidly, the peak due to oxygen (at 1.5 Å) decreases gradually, and a new peak due to the sulfur in pyrrhotite appears (at 2.0 Å). The magnitude of the sulfur peak continues to increase, while the peak for the oxygen shell decreases. Note that (for SiO₂ treated catalyst) even after prolonged exposure at 500 °C, the oxygen shell is not eliminated completely. Back transform analysis indicates that SiO₂ treated catalyst is quite resistant to sulfidization while the other two catalysts undergo complete transformation to pyrrhotite.

It is observed that the transition conditions are quite different for different catalysts. If we identify the condition of equal height of the oxygen and sulfur peaks in the RSF as a transition condition, the iron in the ion exchanged coal is highly reactive with a "transition temperature" of 325 °C, while the ferrihydrite catalysts have higher "transition temperatures" of 400 °C (citric acid treated catalyst) and 425 °C (SiO₂ treated catalyst). Though they are somewhat harder to quantify, the XANES spectra support this catalyst reactivity ordering.

5. Conclusions

A high pressure (up to 1000 psig cold hydrogen), high temperature (up to 500 °C), XAFS cell has been developed for the *in situ* investigations of the structure and reactions of direct coal liquefaction catalysts. Three different nanoscale iron based catalysts were examined and found to exhibit a transformation of the iron oxyhydroxide phase to the pyrrhotite phase. The transformation temperatures were significantly different for the three catalyst systems. For all of the catalysts, the transformation occurs over a range of temperature. The lack of a sharp transition is probably due to a range of particle sizes, with smaller catalyst particles transforming at a lower temperature and larger particles at higher temperatures. It is well known that pyrrhotite exhibits several phases depending on the vacancy in Fe_{1-x}S matrix. Vacancy rearrangement over a range of temperatures and can also lead to changes in the XAFS results.

References

1. G.P. Huffman, B. Ganguly, J. Zhao, K.R.P.M. Rao, N. Shah, F. Zhen, F.E. Huggins, M.M. Taghiei, F. Lu, I. Wender, V. R. Pradhan, J.W. Tierney, M.S. Seehra, M.M. Ibrahim, J.S. Shabtai, E.M. Eyring, **Energy & Fuels**, 7, (1993), 285-296.
2. T.L. Neils, J.M. Burlitch, **J.Catal.**, 118, (1989), 79-84.
3. M.M. Taghiei, F.E. Huggins, B. Ganguly, G.P. Huffman, **Energy & Fuels**, 7(3), (1993), 399-405.
4. J. Zhao, F.E. Huggins, Z. Feng, F. Lu, N. Shah, G.P. Huffman, **J. Catal.**, 143, (1993), 499-509.

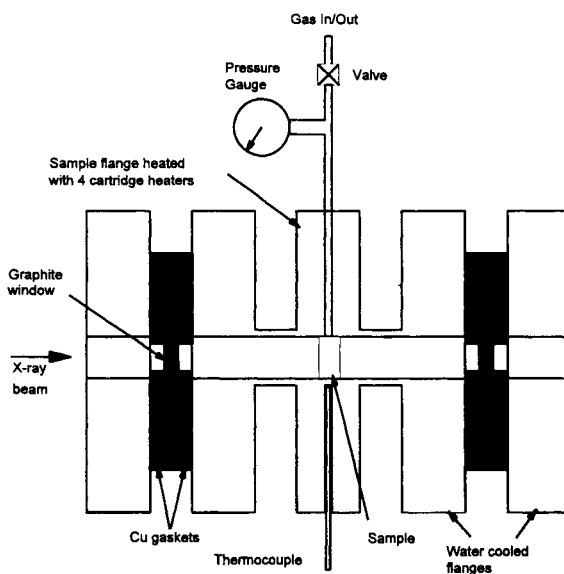


Figure 1. Schematic of modified high pressure high temperature XAFS cell for *in situ* characterization of DCL catalysts.

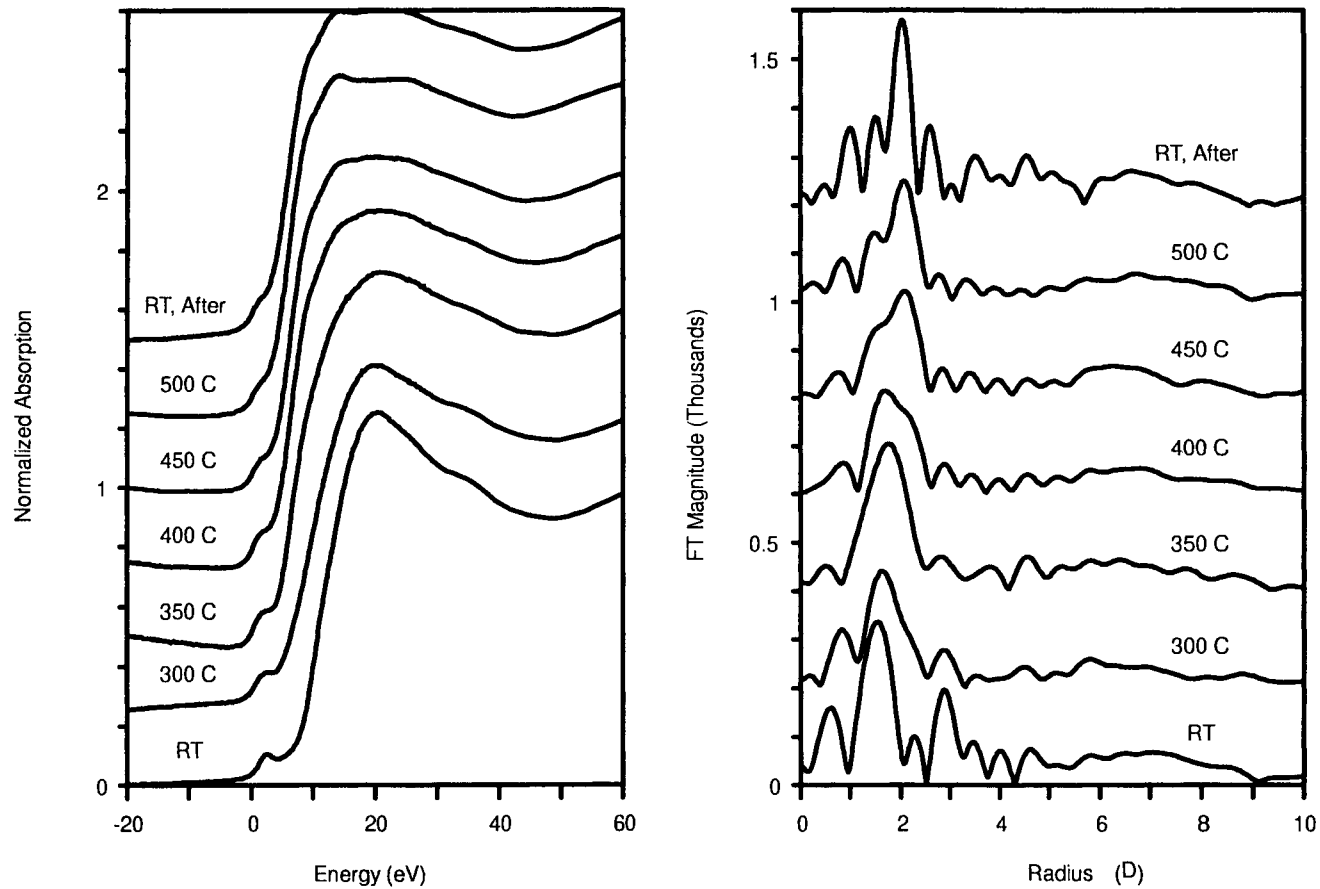


Figure 2. Fe K edge *in situ* XANES and RSF of 5 wt. % SiO₂ treated binary ferrihydrite catalyst in Blind Canyon (DECS-17) coal. 1000 psig (cold) hydrogen pressure.

Influence of operating conditions on the effect of catalysts in coal liquefaction

I. de Marco, B. Caballero, M.J. Chomón and J.A. Legarreta

Escuela Técnica Superior de Ingenieros Industriales y de Telecomunicación
Alda. Urquijo s/n, 48013 Bilbao, Spain

A Spanish subbituminous A coal has been liquefied in anthracene oil and in tetralin, without catalyst, with red mud and with a $\text{CoZnMo/Al}_2\text{O}_3$ catalyst, at 425, 450 and 475 °C, and using 3/1 and 2/1 solvent/coal ratios. The influence of operating conditions on the effect of catalysts has been analysed. It has been observed that there are significant influences of operating conditions on catalysts effects and that there are important relationships among such influences.

1. INTRODUCTION

The beneficial effect of catalysts in coal liquefaction is well known. The main functions fulfilled by catalysts are promoting coal structure cracking and helping to hydrogenate the free radicals formed, either by H-transfer via the solvent, or by promotion of direct reaction of H_2 gas with coal. Therefore the effect of catalysts may well be very much influenced by the operating conditions used, specially by those related to hydrogen supply, such as hydrogen pressure and amount and type of solvent, and by those related to cracking, such as temperature. In this paper the liquefaction yields obtained with several catalysts when different solvents, solvent/coal ratios and temperatures are used, are presented. The influence of the mentioned operating conditions on catalysts effects is analysed.

2. EXPERIMENTAL

The liquefaction experiments were carried out with a Spanish subbituminous A coal named Encasur. Its analysis, wt% on an air dried basis (as was used for the experiments) is the following: moisture = 4.5, ash = 22.3, volatile matter = 25.9, G.C.V. = 5540 kcal/kg, C = 61.5, H = 4.1, N = 1.2, S = 0.4, O (by difference) = 6.0. Total moisture, on an as received basis, is 11.1 wt%. Maceral analysis (% volume mineral free basis) of Encasur coal is: 73.5 % vitrinite, 8.9% exinite, 17.6 % inertinite.

Two solvents, tetralin and hydrogenated anthracene oil, were used in this study. Two catalysts were tested, red mud (R.M.), which is an inexpensive by-

product of the aluminium industry that contains about 36 wt % of Fe_2O_3 and has a particle size of 5-100 μm . and CZMFA.7 which is a fluorinated alumina (0.7 wt% F) supported catalyst that contains 2 wt % CoO, 2 wt % ZnO and 12 wt% MoO_3 and has a particle size < 50 μm .

The liquefaction experiments were conducted with 10 g of coal in a 250 ml autoclave. The catalyst was added in a proportion of 1.2 wt % as active metal oxides [Fe_2O_3 for red mud and (CoO + ZnO + MoO_3) for CZMFA.7] with respect to dry and ash free (daf) coal. Elemental sulphur was added to activate the catalyst, in a proportion of 157 wt % with respect to active metal oxides (equivalent to 50 wt % with respect to red mud). The operating conditions used were 1 hour reaction time, 17 MPa operating pressure and 400 rpm stirring speed. Three temperatures (425 , 450 and 475 °C) and two solvent coal ratios (3/1 and 2/1) were tested. Coal conversions were calculated from the residue remaining after exhaustive Soxhlet extraction of the reactor contents with THF.

3. RESULTS AND DISCUSSION

The results obtained in this study are presented in Figure 1. It can be seen that the variation of coal conversion with temperature is quite different depending on the amount and type of solvent used. In all cases a decrease in conversion with temperature is observed, which is attributed to the well-known retrogressive or repolymerization reactions, which convert the liquid products initially formed in solid unreactive residue (char or coke) which is hardly convertible to liquids. These retrogressive reactions are more pronounced as less hydrogenating are the operating conditions used, because if there is no hydrogen available for the free radicals thermally cracked from coal, they recombine one another leading to solid residue. In this way Figure 1 shows that retrogressive reactions when anthracene oil, (poor H-donor solvent) is used are more pronounced than when tetralin (typical H-donor compound) is used. In the same way repolymerization is stronger for 2/1 than for 3/1 solvent/coal ratio. Moreover with anthracene oil and 2/1 ratio, which are the less hydrogenating conditions tested in this study, coal conversions obtained at 475 °C were below zero, that is why they have not been included in Figure 1. This is attributed to the fact that with such conditions not only coal products but also the solvent itself repolymerizes to solid residue.

On the other hand concerning catalysts effects three aspects are obvious. (i) CZMFA.7, a Co-Zn-Mo alumina supported catalyst, gives better results than red mud, an inexpensive dispersion catalyst. (ii) The catalyst effect is in most cases much more pronounced with anthracene oil than with tetralin, which is logical since when a strong H-donor solvent is used, the functions fulfilled by the catalyst, either rehydrogenation of the solvent or promotion of direct reaction of hydrogen gas with coal, are reduced or masked. (iii) The greater catalyst effects are obtained with anthracene oil and 3/1 solvent/coal ratio; in this case it can be seen that with a very active catalyst, such as CZMFA.7, retrogressive reactions are drastically diminished, since it helps to hydrogenate (either via the solvent or via gas phase) coal free radicals avoiding consequently repolymerization.

In order to better analyse the influence of operating conditions on catalysts effects, the increase in % conversion caused by red mud and by CZMFA.7 has been plotted in Figure 2.

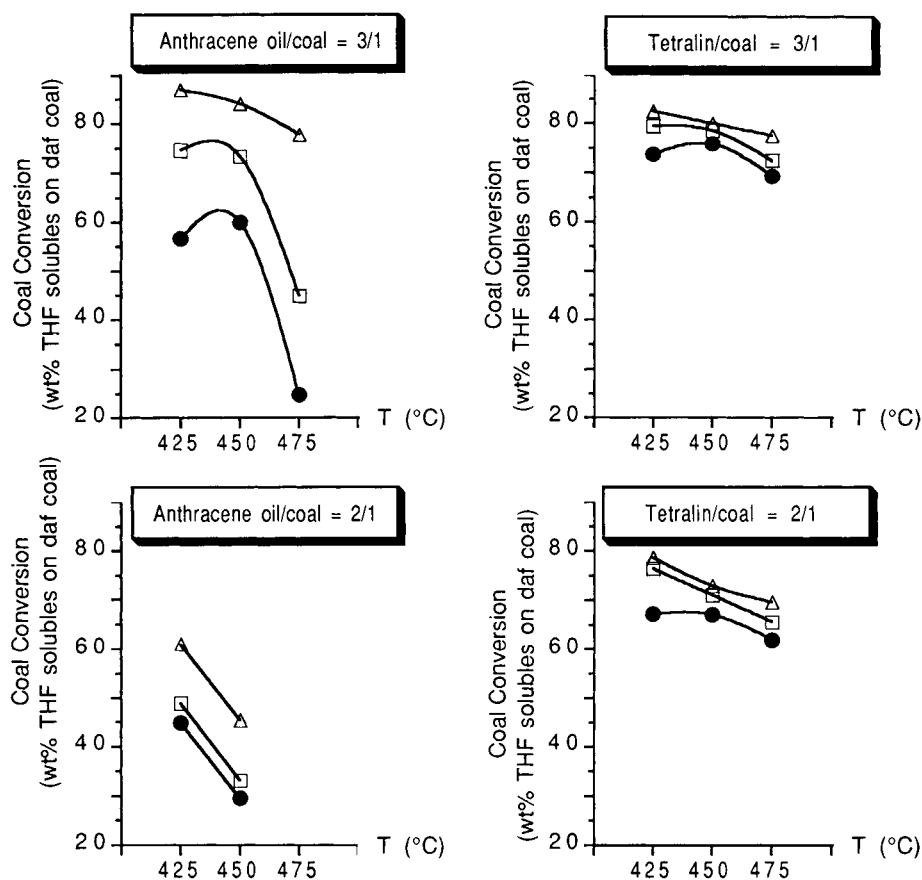


Figure 1. Coal conversions. (O) without catalyst ; (□) with red mud (Δ) with CZMFA.7

It can be seen that for 3/1 solvent/coal ratio, the influence of temperature on catalysts effects is quite similar with anthracene oil and with tetralin, despite the fact that with the latter catalysts effects are very low (less than 10 points in % conversion), due to the strong H-donor capacity of tetralin. The effect of the catalysts diminishes from 425 to 450 °C and then increases from 450 to 475 °C, specially with anthracene oil and CZMFA.7 catalyst, which causes an increase in % conversion of 53 points). This behaviour may be explained taking into account that the functions fulfilled by catalysts are of two types: help to crack or hydrocrack coal and coal derived products, and help to hydrogenate (via the solvent or via gas phase) coal free radicals. The first function is most likely reduced or masked as temperature is raised since more thermal cracking is produced. The second one is expected to increase with temperature since more free radicals are produced and therefore greater H-transfer is needed. The combination of both functions may consequently give the behaviour observed in Figure 2 for 3/1 solvent/coal ratio.

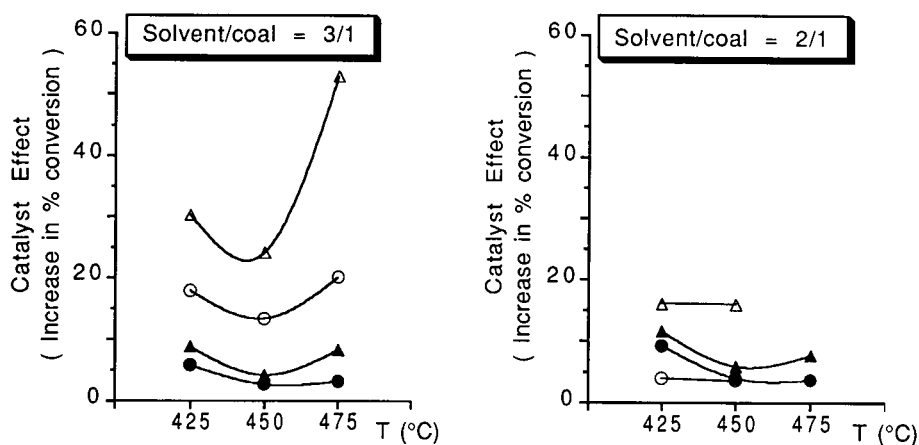


Figure 2. Effect of catalysts on coal conversion. (O) anthracene oil + red mud
 (Δ) anthracene oil + CZMFA.7 ; (O) tetralin + red mud ; (Δ) tetralin + CZMFA.7

On the other hand for 2/1 solvent/coal ratio, it might have been expected greater catalysts effects with both solvents than for 3/1 ratio. If now there is less solvent there are less H-donor compounds and therefore the action of the catalysts of promoting hydrogenation of coal free radicals might have been more pronounced. However it is so only with tetralin while with anthracene oil catalysts effects for 2/1 ratio are much lower than for 3/1 ratio. This may be explained as follows. Anthracene oil is a complex mixture of hydrocarbons which contains H-donors, H-shuttlers and inert compounds. It seems possible that for 2/1 anthracene oil/coal ratio the amount of compounds capable of transferring hydrogen, either intrinsically or by hydrogenating and dehydrogenating by means of the catalyst, is too low and therefore, in spite of the catalyst, hydrogen is not transferred to coal free radicals quickly enough, and consequently they recombine one another leading to low conversions and lower catalysts effects that might have been expected. To put it in another way, with anthracene oil in a 2/1 ratio the catalysts help to hydrogenate, but they can only act in a few solvent compounds which are not enough to yield high conversions and reveal great catalysts effects.

The conclusion is that the effect of catalysts in coal liquefaction depends very much on the temperature, solvent/coal ratio and type of solvent used. However no definite conclusion about the influence each of such variables on coal liquefaction catalysts effects, can be established, since there is an important relationship among such influences. Moreover such influences also depend on the type of catalyst that is being considered, and they may be probably also affected by the type of coal used and by other operating conditions not analysed in this study such as hydrogen pressure, reaction time, etc.

Acknowledgements. The authors would like to thank the Commission of the European Communities and the Basque Country University for financial assistance for this work.

Advanced catalysts for coal-derived liquids hydrotreating via acidic supports

J.F. Cambra^a, P.L. Arias^a, M.B. Güemez^a, J.A. Legarreta^a, B. Pawelec^b and J.L.G. Fierro^b

^aEscuela de Ingenieros, Alda. de Urquijo s/n, 48013 Bilbao, Spain

^bInstituto de Catálisis y Petroleoquímica (CSIC), Campus Universidad Autónoma, Cantoblanco, 28049 Madrid, Spain

Advanced hydrotreating catalysts combine metal and acid active sites. The acid function is usually provided by the carrier in which active metals are supported. This function must be tailored to avoid coking deactivation. In this work two types of CoMo and NiMo catalysts on two different acid carriers (fluorinated γ -alumina and ultrastable Y zeolite) will be compared in terms of acidity and catalytic activities correlations.

1. INTRODUCTION

Heavy oils, residues and coal-derived liquids contain relatively high concentrations of heteroatoms (S and N), metals (Ni and V) and polynuclear aromatics. As the necessity to exploit these fractions and environmental regulations to reduce pollution are growing, the development of new catalyst compositions and improved catalytic processes are of interest.

Previous work showed that fluorination of alumina increases its surface acidity, enhancing acid-catalyzed reactions (1). When zeolites are employed for hydrotreating catalysts more desired products (light hydrocarbons and gasolines) are obtained, being more resistant to poisoning by S and N-containing compounds present in the feed (2,3)

In this work the HDS and HDN activities of CoMo and NiMo hydrotreating catalysts are compared versus the acidity for two different types of supports, fluorinated alumina and ultra-stable zeolite (USHY).

2. EXPERIMENTAL

Alumina supported catalysts were prepared by multistep impregnation, the carrier was a γ -alumina (Girdler T-126, BET surface $188\text{m}^2\text{g}^{-1}$, pore volume $0.39\text{cm}^3\text{g}^{-1}$). The first step of preparation was the incorporation of the acidic function to the support by the incipient wetness procedure, with

aqueous solutions of NH_4HF_2 , nominal F contents are displayed in Table 1. Metal loads were the same for all the catalysts (12 wt% MoO_3 , 2 wt% CoO , 2 wt% ZnO), detailed preparation procedure is described in Cambra et al. (4).

An ultrastable HY zeolite (Conteka) was used in the preparation of these catalysts. The characteristics of this USY zeolite are as follows: $\text{SiO}_2/\text{Al}_2\text{O}_3$ mole ratio 5.6, Na_2O content 0.14 wt% and unit cell 2.454 nm. Compositions as determined by atomic absorption are shown in Table 1, Ni was incorporated first by ion exchange from aqueous solutions of $\text{Ni}(\text{NO}_3)_2$ and then Mo via solid-solid ion exchange with MoCl_5 precursor, more detailed description of the preparation method is available in Pawelec (5).

Activity tests were performed in a conventional high pressure bench-scale plant described elsewhere (5, 6). Reaction products were analyzed by gas chromatography. The activity was measured as the moles of model compound reacted relative to the moles of model compound fed. Operating conditions and activity results are summarized in Figures 1 and 2.

Surface exposure of fluorine in alumina supported catalysts was determined by XPS measurements (4). The acidity of zeolite catalysts was measured by FTIR spectra of adsorbed pyridine.

Table 1
Catalyst compositions

Alumina supported catalysts			Zeolite supported catalysts			
	F (wt%) ^a	$I_{\text{F}}/I_{\text{Al}}$ ^b		Mo (wt%) ^c	Ni (wt%) ^c	I_{1543} ^d
A	0.0	---	A1	5.2	0.8	2.72
B	0.4	0.395	B1	5.3	1.5	1.81
C	0.7	0.896	C1	5.6	2.3	2.79
D	1.0	0.835	D1	6.0	5.3	2.15
E	1.3	0.812	E1	6.3	10.2	2.23
F	2.0	1.147	F1	---	---	9.95

^aNominal composition.

^bXPS intensities ratio.

^cAs determined by atomic absorption.

^dAdsorbed pyridine: intensity of 1543 cm^{-1} band.

3. RESULTS AND DISCUSSION

From XPS analysis, the F/Al XPS intensities ratio has been calculated and summarized in Table 1. As can be observed there surface F increases in general with F loading.

The Brönsted and Lewis acid sites in zeolite supported catalysts were determined by the observation of the bands at ca. 1543 and 1452 cm^{-1} , respectively (5). From the data in Table 1, a decrease in the Brönsted acidity can be observed, relative to the bare zeolite (F1), when metal atoms are incorporated.

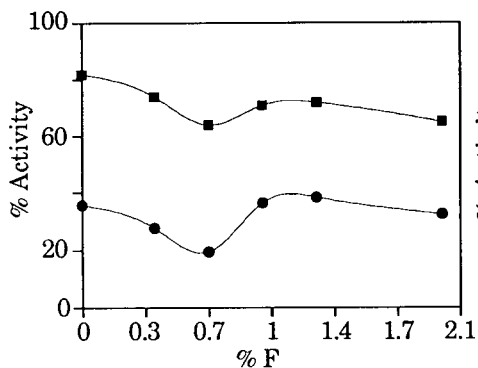


Figure 1. Alumina supported catalysts. Comparison HDS and HDN activities versus nominal F content: ● HDN (7 MPa, 648 K, 256 h $g_{\text{cat}}/\text{mol}$); ■ HDS (3 MPa, 648 K, 6 h $g_{\text{cat}}/\text{mol}$)

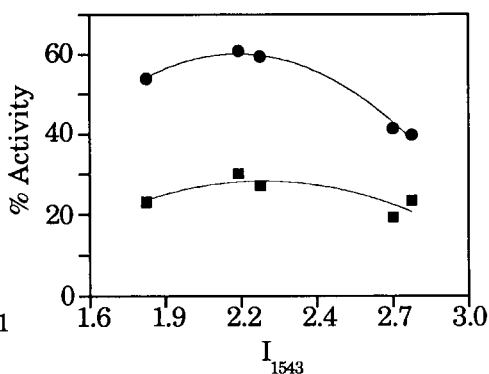


Figure 2. Zeolite supported catalysts. Comparison of HDS and HDN activities versus Brönsted acidity: ● HDN (5 MPa, 648 K, 132 h $g_{\text{cat}}/\text{mol}$); ■ HDS (3 MPa, 623 K, 20 h $g_{\text{cat}}/\text{mol}$)

As it is shown in Figures 1 and 2, acidity influences both HDS and HDN activities in alumina or zeolite supported catalysts. The activities for the alumina supported catalysts is not correlated to the fluorine content (nominal or XPS intensities) which is indirect measurement of the catalyst acidity (Figure 1). This behaviour is very similar to the one obtained correlating activities to active metal dispersion. The controlling phenomena could be the textural changes of the Al_2O_3 carrier occurring along the genesis of the catalysts (6). Nevertheless for the samples containing from 0.7 to 2.0 wt% of F Figure 1 shows that HDS and HDN activities reach a maximum for the intermediate contents. Assuming that textural changes of the support are not very different for these samples a very likely explanation could be that increasing acidity favours higher activities until some level is reached. Further increase of acidity provokes a decay in activity.

A similar effect appears for the zeolite supported catalysts where the acidity was measured through pyridine adsorption. For these zeolitic catalysts activities and Brönsted acidity are correlated (Figure 2) but the

number of acid sites and its strength must be carefully tailored because acidity increases the surface concentration of the N-containing reactant molecules and hence the probability of reaction, but conversely deactivation becomes more important.

In both supports the influence on HDN activity is more significant due to the probable importance of acid sites in both nitrogen containing compounds adsorption and hydrogenating activity (the controlling step for HDN mechanisms use to be an hydrogenation step when cyclic molecules are considered).

4. CONCLUSIONS

Initial activities for the zeolite supported catalysts are far higher than that corresponding to the alumina supported catalysts (7) but important deactivation occurs in a few hours on stream for zeolitic samples. The development of catalysts with intermediate acidities showing high hydrotreating activities and limited hydrocracking activity (to avoid coking) are of enormous interest.

ACKNOWLEDGEMENTS

We thank the Commission of the European Communities, Non Nuclear Energy and JOULE R&D Programmes and the Universidad del País Vasco for financial assistance for this work.

REFERENCES

1. P.M. Boorman, R.A. Kidd, Z. Sarbark and A. Somogybari. *J. Catal.*, 100 (1986) 287.
2. J.W. Ward, in "Preparation of Catalysts III" (G. Poncelet, P. Grange and P.A. Jacobs, Eds.) Elsevier, Amsterdam, (1983) 587.
3. C. Marcilly and J.P. Frank. *Std. Surf. Sci. Catal.* 5 (1980) 93.
4. J.F. Cambra. Ph. D. Thesis, Universidad del País Vasco at Bilbao, Spain, 1989.
5. B. Pawelec. Ph. D. Thesis, Universidad Complutense at Madrid, Spain, 1994.
6. J.F. Cambra, P.L. Arias, M.B. Güemez, J.A. Legarreta and J.L.G. Fierro. *Ind. Eng.Chem. Res.* 30 (1991) 2365.
7. P.L. Arias, J.F. Cambra. M.B. Güemez, J.A. Legarreta, B. Pawelec and J.L.G. Fierro. *Bull. Soc. Chim. Belg.* 104 (1995) 197.

Effect of Type of Mo Catalyst on Coal Liquefaction

Satoshi Ohshima, Motoo Yumura, Yasunori Kuriki, Kunio Uchida, Kunio Kamiya,
Fumikazu Ikazaki

National Institute of Materials and Chemical Research, Dept. of Chemical Systems
1-1 Higashi, Tsukuba, Ibaraki, 305 Japan

1. Introduction

For purpose of specify the effect of the Mo catalyst on the coal liquefaction, we experimented on the coal liquefaction using different types of Mo catalyst.

We used Co-Mo/Al₂O₃ catalyst in two different shapes, i.e., particle and powder from the same composition of the catalyst. Comparing the two shapes, we can say that the powder catalyst has larger contact area with solvent than that of the particle ones.

We used oil soluble Mo in two different types; in case of dissolving in the solvent and in case of impregnating in the coal in advance. In the former case, Mo dissolving in the solvent was decomposed in process of heating and dispersed in the solvent becoming the fine particle of the Mo under the condition of the liquefaction reaction, Therefore we can say that there is no limitation of the diffusion of the reactant when we stirred enough the reactant in the reactor. In the case when we impregnate Mo in the coal in advance, Mo contact directly with the coal and we can expect the increase of the activity when the catalyst act directly in the reaction of coal liquefaction.

According to the above experiment, we investigate the effect of type of Mo catalyst on coal liquefaction.

Table 1 Property of HDS1442A

Composition	[wt%]	
CoO		3.2
MoO ₃		15.2
SiO ₂		0.2
Surface area	[m ² /g]	330
Pore volume	[ml/g]	0.8
Av. pore diameter	[nm]	6
apparent density	[g/cm ³]	0.64

Table 2 Experimental conditions

Reactor	: Rocking autoclave
Temperature	: 673K and 723K
Initial H ₂	: 9.8 MPa
Reaction time	: 60 min
Coal/Solvent	: 3g/7g

2. Experimental

2.1. Catalyst

We used HDS1442A 1/16" as Co-Mo/Al₂O₃ made from Cyanamid Co.Ltd and properties of HDS1442A is shown in Table 1. We use two different shapes of these catalyst sulfurizing in advance in the experiment.

(a) : Original Co-Mo/Al₂O₃ catalyst (1.6mm ϕ x 10 mm).

(b): Powder of Co-Mo/Al₂O₃ catalyst comminuted by stamp mill (average diameter = 2.5 μ m).

Molybdenum dioxyacetylacetonate (MoO₂-AA) was used as oil soluble Mo catalyst. We used MoO₂-AA in two different types as indicated below.

(c): Oil soluble Mo catalyst dispersed in liquefaction solvent.

(d): Impregnation of coal with MoO₂-AA.

We impregnated dried Taiheiyo coal with methanol solution of MoO₂-AA . Amount of Mo in the coal were controlled by concentration of MoO₂-AA in methanol. The concentration of Mo in these coals were 0.277, 0.50 and 1.14 wt% of coal. In the case of (c) and (d) , we added sulphur equivalent to Mo.

2.2. Apparatus

For the liquefaction, we used the 50 ml autoclave. We reported already the characteristics of the apparatus and the method of the experiment [1]. We surely recognized that the reactants were stirred enough in the reactor. The conditions of the experiment is indicated in Table2. The yields of conversion from coal to benzene soluble were 98% - 100% at 723K and were 98% - 83% at

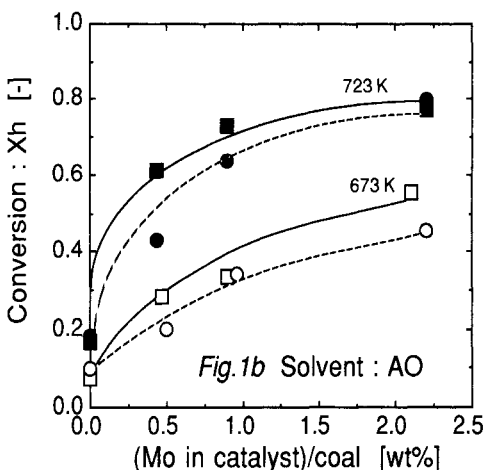
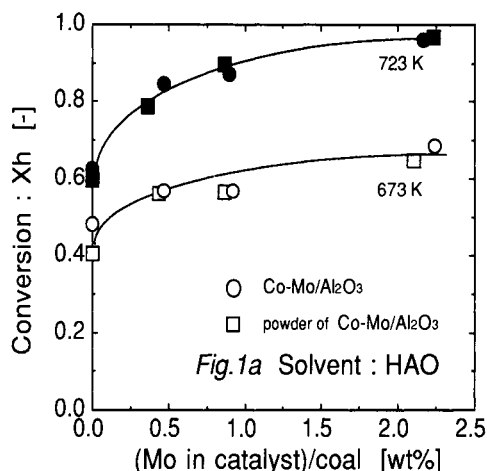


Figure 1 Liquefaction of Taiheiyo coal by using supported Mo Catalyst. (\square, \blacksquare): catalyst(a) (Original Co-Mo/Al₂O₃ catalyst). (\circ, \bullet): catalyst(b) (powder of Co-Mo/Al₂O₃ catalyst, average diameter=2.5 μ m)

673K, therefore we compared yields of hexane soluble to investigate an effect of type of Mo catalyst.

3. Results and Discussion

3.1. Co-Mo/Al₂O₃ supported catalyst

When we used the hydrogenated anthrathene oil (HAO) as a solvent, the conversion is increasing according to the increase of the amount of the catalyst metal added as indicated in Fig.1a and we can not find the effect of the type of the catalyst. When we used the anthrathene oil (AO) as a solvent, the conversion indicated in Fig.1b is higher in the case of the powder compared with the case of original Co-Mo/Al₂O₃ catalyst. The differences of the shape of the Co-Mo/Al₂O₃ catalyst is effected by the contact of catalyst and solvent in case of using the AO.

3.2. Oil soluble Mo

When we use HAO as a solvent, there is no difference in the conversion between the case of the oil soluble Mo catalyst dispersed in liquefaction solvent (catalyst(c)) and the case of impregnation of coal with MoO₂-AA (catalyst(d)). When we use AO as a solvent, there is no difference at 723K which is shown in Fig.2b. However, at 673K, the conversion is higher in catalyst(c) compared with catalyst(d). The higher conversion at 673K in case of using AO with catalyst(c) is caused by the good contacting of Mo metal and solvent. We expected the increase of the conversion in the case of catalyst(d) by the direct catalysis of hydrogenation of solid coal. However we cannot get higher conversion than the case of catalyst(c). The lower conversion at 673K in case of catalyst(d) is caused by the dissolving and dispersing process of MO metal to solvent. From these facts, we can see there is a little effect of the reaction when the Mo catalyst effects directly to the coal liquefaction in the case of using catalyst(d).

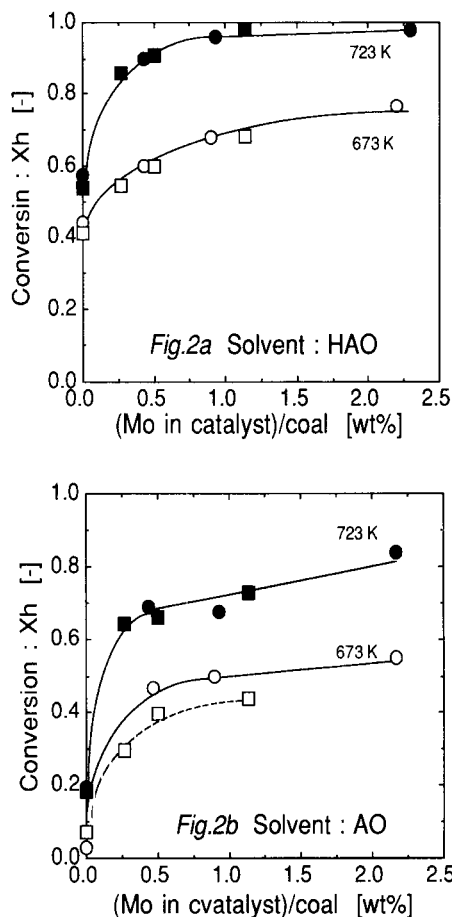


Figure 2 Liquefaction of Taiheiyo coal by using Oil soluble Mo. (○,●):catalyst (c) (dispersed in liquefaction solvent). (□,■): catalyst(d) (impregnation of coal with MoO₂-AA).

3.3. H₂ consumption

Fig. 3 shows the relationship between hydrogen consumption and yields Xh. The relationship between H₂ consumption and yields Xh is clearly divided in groups according to two kinds of solvent not concerning with the kinds and shapes of the catalyst. We can come to a conclusion from the relationship in this experiment as stated later. When we use AO as a solvent which is not containing the partially hydrogenated compound, the reaction consuming gas phase hydrogen and the reaction

producing oil from the coal are proceeding at the same time by appearance. On the other hand, when we use HAO, first of all the liquefaction proceeded as hydrogen atom derived from partially hydrogenated compound in HAO is consumed, then the reaction consuming hydrogen and the reaction producing oil are proceeding at the same time by appearance. In this system, the consumption of hydrogen is very small when hydrogen remains in the solvent. Therefore, we suppose by comparing the results of AO and HAO that gas phase hydrogen was transferred to the coal mainly through solvent.

4. Conclusion

We expected the increase of the conversion in the case of catalyst(d) by the direct catalysis of hydrogenation of solid coal. However, there is a little effect on the reaction.

Dispersion of Mo metal in the solvent was important to improve catalyst performance in case of using AO solvent. We suppose that contact of Mo metal and solvent is essential in the liquefaction reaction.

We suppose by comparing the results of AO and HAO that gas phase hydrogen was transferred to the coal mainly through solvent.

References

1. S. Ohshima et al, Journal of Japan Energy Soc.,71 (1992) 99

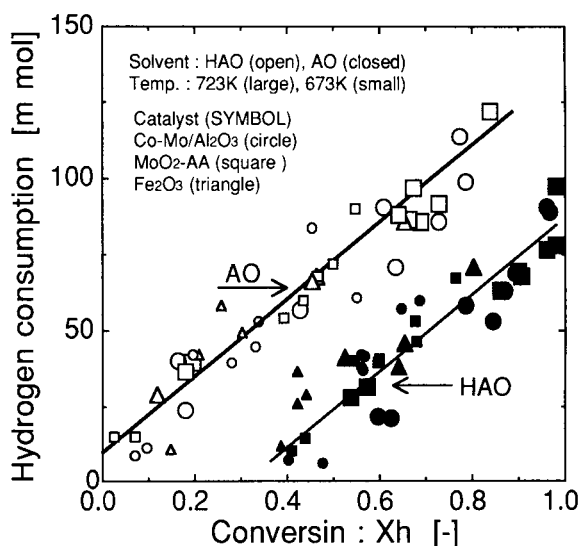


Figure 3 Relationship between hydrogen consumption and yields Xh of liquefaction of coal by using various type of catalyst.

Liquefaction activity of supported NiMo catalysts with functions for recovery

H. Taniguchi, H. Hasuo, S. H. Yoon, K. Sakanishi, and I. Mochida
Institute of Advanced Material Study, Kyushu University,
Kasuga, Fukuoka, 816, Japan

Two type of recoverable catalysts in coal liquefaction are designed with the functions of the gravity and magnetic gradient separation. One is a NiMo supported on carbon black of hollow spheres. The other is a NiMo supported on carbon coated ferrite. Their activity are investigated for the liquefaction of Tanitoharm coal and hydrogenation of naphthalene.

1. INTRODUCTION

Coal liquefaction has been investigated for longer than several decades to provide the liquid fuel from coal to substitute petroleum products by looking ahead the increasing demand in early next century. However, the cost of the coal liquid is, so far, high in comparison with the present price of crude oil.

Present authors have been studying recoverable catalysts for primary coal liquefaction stage in the multi-stage scheme which includes the coal pretreatment, coal dissolution, and catalytic up-grading.¹⁾ The recoverable catalysts can be designed using suitable supports for the magnetic gradient and gravity separation, while the hydrogenation activity can rely upon the supported NiMo sulfide.

In the present study, Ketjen Black(KB) and carbon coated ferrite are investigated as recoverable supports. KB is one of the unique carbon blacks which has extremely high surface area and low specific gravity of hollow spheres. It was selected as a catalyst support to prepare a highly dispersed NiMo catalyst with the function for gravity recovery and high activity for coal liquefaction. Carbon coated fine γ -ferrite powders were prepared as a support for the magnetic separation by wet coating method with pyridine soluble fraction of mesophase pitch.²⁾

2. EXPERIMENTAL

2.1. Catalysts preparation

Some properties of KB and γ -ferrite coated by polyethylene (FePE) supplied from Idemitsu Kosan Co. are showed in Table 1. Ni,Mo-supported KB catalyst(NiMo/KB) was prepared by impregnation method from Ni(OAc)₂ and Mo dioxycetylacetonate(MoO₂-AA) in their methanol solutions. The catalyst precursor was dried at 120°C for 12h in vacuo. The catalyst was presulfided in 5% H₂S/H₂ flow at 360°C for 2h prior to the reaction.

Table 1 The properties of Ketjen black and FePE

1. KB JD			2. FePE	
particle size (nm)	surface area (m^2/g)	density (g/l)	particle size (μm)	Ferrite:Polyethylene:carbon black (wt.%)
30	1270	115	ca. 40	95.6 : 4.0 : 0.4

Table 2 Elemental analyses of Tanitoharam coal

wt.%(d.a.f.)				Ash
C	H	N	(O+S)	(wt.%)
71.6	5.6	1.6	21.2	3.9

Coating material was pyridine soluble (PS) of methylnaphthalene pitch (mNP). MNP was prepared from methylnaphthalene using HF/BF₃ as catalyst by Mitsubishi Gas Chemical Co.³⁾ PS of mNP was dissolved into THF (20ml). The mixture of FePE and the pitch were stirred in THF at r.t. for 30min. After THF was removed in vacuo, it was heat-treated at 260°C at the heating rate 0.1°C/min in air. The produced carbon/ferrite particles were carbonized at 800°C for 10min at the heating rate of 5°C/min up to 200°C and then 1°C/min from 200°C to 800°C. The carbon yield in the spheres was estimated from the elemental analysis (EA). Shapes and diameters of carbonized spheres were observed with JEOL JSM 5400 scanning electron microscope(SEM). Ni and Mo were supported to the particle as described above. Synthesized pyrite powders provided by NEDO was used as a reference catalyst for comparison. This catalyst was also presulfided under the same condition as described above.

2.2. Liquefaction procedure

The elemental analyses of Tanitoharum coal are summarized in Table 2. Tetralin(TL) of commercial guaranteed grade was used as a liquefaction (hydrogen donating) solvent. The liquefaction was carried out using a magnetic-stirred autoclave of 50ml capacity at prescribed temperatures(380~450°C) and the stirring speeds were 500~1300r.p.m. The coal(3.0g), the solvent (4.5g) and catalyst (0.1g) were charged into the autoclave, which was then pressurized with hydrogen to 6~9.3MPa at room temperature after replacing the air with nitrogen gas. After the reaction, the product remaining in the autoclave was recovered with THF, and extracted in sequence with *n*-hexane, acetone and THF after evaporating THF. The *n*-hexane soluble(HS), *n*-hexane insoluble-acetone and soluble(HI-AcS), acetone insoluble-THF soluble(AcI-THFS), and THF insoluble(THFI) substances were defined as oil(O), asphaltene(A), preasphaltene(PA), and residue(R), respectively. The gas yield(G) was calculated by the difference between weights of the initial raw materials and recovered products.

2.3. Hydrogenation procedure

Hydrogenation of naphthalene(0.1g) in decane(10.0g) with catalyst (0.25g) was carried in an autoclave. Standard conditions for the hydrogenation were 320°C(reaction temperature), 30min (reaction time), and 8MPa(reaction hydrogen pressure). The conversion of hydrogenation was determined by GC-FID.

3. RESULTS

3.1. Liquefaction with NiMo/KB catalyst

Figure 1 illustrates the effect of reaction temperatures on the liquefaction of Tanitoharum coal with NiMo/KB catalyst under 10MPa at 380~450°C. The oil yield increased with reaction temperature in range of 380~430°C, reaching the maximum oil yield of 47% at 430°C, and then decreased at 450°C with a significant increase of gas yield. While the oil yield appeared to be saturated around 45% in the range of 415~450°C, the gas yield increased sharply.

Figure 2 illustrates the liquefaction conversion of Tanitoharum coal with 13MPa with NiMo/KB catalyst at 380~450°C. The oil yield increased very much with reaction temperature under the higher hydrogen pressure, reaching the maximum yield of 63% with least yields of preasphaltene(5%) and residue(1%). Figure 1 and 2 also show oil yields with synthesized pyrite. NiMo/KB catalyst exhibited higher activity than synthesized pyrite catalyst at all the temperatures, especially under 13MPa H₂ pressure.

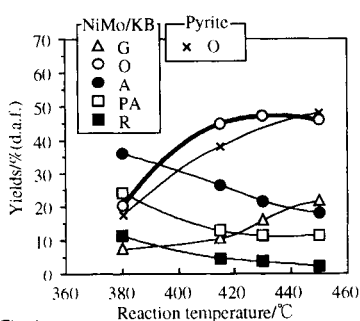


Fig. 1
Effect of reaction temperature on the liquefaction yields of Tanitoharum coal under lower H₂ pressure with Ni-Mo/KB JD and Synthesized pyrite as the catalyst.

Reaction conditions

solvent(tetrafin)/coal=1.5
 reaction temperature : 380 ~ 450°C
 reaction pressure : 10MPa
 reaction time : 60min
 heating rate : 20°C/min
 catalyst : 3.3wt.% addition to coal

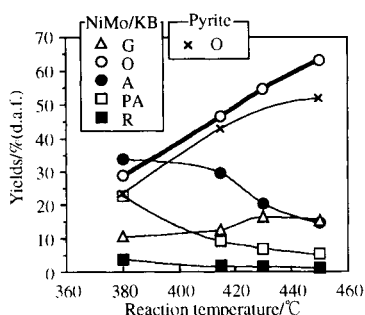


Fig. 2
Effect of reaction temperature on the liquefaction yields of Tanitoharum coal under higher H₂ pressure with Ni-Mo/KB JD and Synthesized pyrite as the catalyst

Reaction conditions

reaction pressure : 13MPa
 (Other conditions are same as Fig. 1)

Figure 3 illustrates the effects of reaction time on the liquefaction of Tanitoharum coal with NiMo/KB catalyst under 13MPa for 60~120min. Maximum oil yield was obtained when the reaction time was 90min. The oil yield decreased beyond 90min with increasing gas yield.

Figure 4 illustrates the effects of stirring speed on the liquefaction with NiMo/KB catalyst under 13MPa for 500~1300r.p.m. The oil yield increased up to 67%(+4%) by higher stirring speed(1300r.p.m.) with decreasing asphaltene(12%(-3%)).

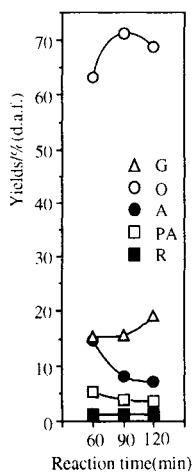


Fig. 3
Effect of reaction time on the liquefaction yields of Tanitoharum coal with Ni-Mo/KB JD as the catalyst .
 Reaction conditions
 reaction temperature : 450°C
 reaction pressure : 13MPa
 reaction time : 60 ~ 120min
 (Other condition are same as Fig. 1)

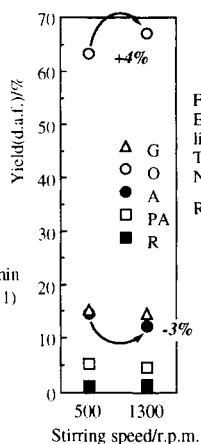


Fig. 4
Effect of stirring speed on the liquefaction yields of Tanitoharum coal with Ni-Mo/KB JD as the catalyst .
 Reaction conditions
 reaction temperature : 450°C
 reaction pressure : 13MPa
 stirring speed : 500~1300r.p.m.
 (Other condition are same as Fig. 1)

3.2. Hydrogenation of naphthalene

Figure 5 illustrates relationship between conversions of naphthalene and Mo(Ni) weight on carbon coated ferrite support. When Mo weight was 2wt% and 4wt% based on carbon coated

ferrite, the conversion of naphthalene were almost the same (ca.6%).

Figure 6 illustrates conversions of naphthalene over NiMo/carbon coated ferrite catalysts which was activated by CO₂ for 10 or 30 min. The longer activation time was superior to the shorter time in terms of the conversion of naphthalene. Addition of KB to carbon coated ferrite increased the conversion up to 20%.

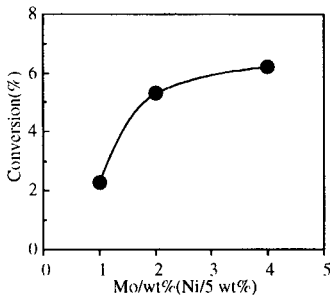


Fig. 5 Relationship between conversion of Naphthalene and Mo weight of catalyst

Reaction condition
 Naphthalene/Deane=0.1g/10g
 reaction time : 30min
 reaction temp. : 320°C
 reaction pressure : 8.0MPa
 heating rate : 20°C/min
 catalyst : 0.25g carbon coated FePE prepared
 by incipient wetness with MoO₂-AA.Ni(OAc)₂
 All catalysts were presulfidated at 360°C for 2h

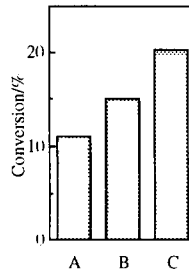


Fig. 6 Hydrogenation of naphthalene over NiMo/carbon coated FePE

(A) CO₂ activation at 800°C for 10min
 (B) CO₂ activation at 800°C for 30min
 (C) 5% KB JD addition to carbon coated FePE
 (Ni:0.4wt%,Mo:2wt% based on support)
 (Hydrogenation condition are same as Fig.5)

4. DISCUSSION

NiMo/KB with function for recovery had much higher activity for liquefaction than the synthesized pyrite which has been reputed to be highly active. It revealed the possibility of the catalyst amount reduction, because NiMo/KB catalyst gave the higher oil yield at the smaller catalyst amount. It can be recoverable and repeatedly used. Higher oil yield was obtained by increasing the stirring speed, suggesting that the higher dispersion of fine particle catalysts in the reactor should be important to achieve the high oil yield.

NiMo/carbon coated ferrite catalyst exhibited low activity for hydrogenation of naphthalene under the present condition. However, this catalyst maintained stable magnetism after hydrogenation and coal liquefaction reactions. Thus, this revealed the possibility of catalyst recycle which can be magnetically recovered from liquefaction products.

REFERENCES

- 1, Mochida, I., Sakanishi, K., Sakata, R., Honda, K., Umezawa, T., Energy & Fuels, 8,25(1994)
- 2, S.H.Yoon, F. Fortin, Y. Korai, K. Sakanishi, and I. Mochida, Carbon Conference, prep., p. 292(1993).
- 3, Y. Korai, M. Nakamura, I. Mochida, Y. Sakai, and S.Fujiyama, Carbon, 29,561(1991).

The Effect of Pressure on First Stage Coal Liquefaction and Solvent Hydrogenation with Supported Catalysts

A.V. Cugini^a, K.S. Rothenberger^a, G.A. Veloski^a, M.V. Ciocco^a, and C. McCreary^b

^aU.S. Department of Energy, Pittsburgh Energy Technology Center, P.O. Box 10940, Pittsburgh, PA, 15236-0940, USA

^bGilbert Commonwealth, Inc., Pittsburgh, PA 15236, USA

The hydrogenation activity of supported and unsupported catalysts in the presence and absence of coal was investigated. Coal inhibits hydrogenation of naphthalene solvent by both supported and unsupported[1,2] catalysts, the greater effect being observed for supported catalysts. Overall coal conversions are similar for the two types of catalysts.

1. EXPERIMENTAL

Materials. Purified grade 1-methylnaphthalene (1-MN) and tetralin from Fisher Scientific Company were used in these studies. Blind Canyon (DECS-6), a bituminous coal from the U.S. Department of Energy's Coal Sample Bank, was used. A high surface area MoS₂ catalyst, described in an earlier paper[1], was the unsupported catalyst in these studies. The supported molybdenum catalysts consisted of AKZO AO-60 obtained from HTI, Inc., and Shell-324 obtained from Shell (both were NiMo supported on alumina catalysts).

Reactions. Reactions were conducted in a stainless steel batch microautoclave reactor system (42 mL) constructed at PETC[1]. Sample work-up and coal conversions were calculated by a procedure described previously[1]. The tests were made at 425 °C for 0.5 h with 0.015 g Mo present (when used), corresponding to 5000 ppm Mo with respect to maf coal for a 3.3 g coal charge. H₂ pressure was 200 to 1000 psig (1.4 to 6.9 Mpa) cold.

Gas and Pressure Analyses. At the completion of each run, product gases were collected and analyzed by a previously published method[3]. Hydrogen consumption was determined by a method developed at PETC[4], based on initial and final pressures and temperatures, vapor phase compositions, and mass spectroscopy of the liquid products.

Low-Voltage, High-Resolution Mass Spectrometry (LVHRMS). Data were obtained with a Kratos MS-50 high-resolution mass spectrometer interfaced to a personal computer and evaluated using software developed at PETC[1].

2. RESULTS AND DISCUSSION

Tests were conducted to study the extent of hydrogenation of 1-MN and dehydrogenation of tetralin as a function of pressure with supported and unsupported catalysts. Table 1 shows the solvent hydrogenation and hydrogen consumption for these tests. Solvent hydrogenation calculations are based on LVHRMS measurement of the relative amounts of hydrogenated and dehydrogenated solvent. The use of supported catalysts consistently resulted in higher levels of hydrogenation than did unsupported catalysts.

Table 1.
Solvent Hydrogenation and H₂ Consumption

Catalyst:	Pressure H ₂ Cold (psig)	Solvent Hydr. (%)	H ₂ Consumed (mol)	Catalyst:	Pressure H ₂ Cold (psig)	Solvent Hydr. (%)	H ₂ Consumed (mol)
AO-60	400	20.50%	0.01575	MoS ₂	400	12.40% ^b	NA
	600	29.76%	0.02776		600	NA	0.02005
	800	37.42%	0.04079		800	20.44% ^b	0.02027
	1000	55.57%	0.0537		1000	28.32%	0.02751
	1000 ^a	-24.03% ^c	-0.03873		1200	36.16% ^b	0.03423
Shell-324	600	27.34%	0.0273	1000 ^a	-16.63% ^c	-0.0307	
	800	47.20%	0.04196	1000	-6.14% ^c	NA	
	1000	54.70%	0.05161				

a- N₂ used in place of H₂.

b- PANASOL[®] used in place of 1-MN.

c- Tetralin used in place of 1-MN.

The addition of coal to the feed results in the inhibition of 1-MN hydrogenation with supported and unsupported catalysts. Figure 1 shows the effect of pressure on solvent (6.6 g) hydrogenation with and without 3.3 g of added coal (DECS-6). While the supported catalyst results in higher levels of solvent hydrogenation than the unsupported catalyst without added coal, the solvent hydrogenation is virtually the same in the presence of coal. Figure 2 shows the effect of incrementally adding up to 3.3 g of coal to the system. It appears that the catalysts are approaching a similar level of solvent hydrogenation. Also shown in Figure 2 are the solvent hydrogenation data with no added catalyst.

An interesting feature of the hydrogen consumption in the presence of coal is that the unsupported catalyst results in higher levels of net hydrogen consumption with coal present than do the supported catalysts. Figure 3 shows the effect of H₂ pressure on hydrogen consumption with coal present. The hydrogen consumed was corrected by subtracting the amount of hydrogen consumed making C₁-C₄ and H₂S gases. The hydrogen consumption is higher for the unsupported catalyst than the supported catalyst, as opposed to the trend with no coal present.

The effect of catalyst type on coal conversion is shown in Figure 4. There is little difference in coal conversion for the supported and unsupported catalysts.

3. CONCLUSIONS

The supported catalysts appear to be much more effective than the unsupported catalyst employed for 1-MN hydrogenation and tetralin dehydrogenation. In the presence of coal, solvent hydrogenation is inhibited and both the supported and unsupported catalysts appear to approach a similar level of solvent hydrogenation.

Total hydrogen consumption in the presence of 3.3 g of coal is higher for unsupported than supported catalysts. Overall coal conversions are similar for the two types of catalysts.

An important role of the catalyst in the first-stage of coal liquefaction is to provide H_2 to cap thermally produced free-radicals, aid conversions and prevent retrogressive reactions. Unsupported catalysts, that provide higher H_2 consumptions than supported catalysts (in the presence of coal), may be better suited for first-stage coal liquefaction.

DISCLAIMER

Reference in this manuscript to any specific commercial product or service is to facilitate understanding and does not necessarily imply its endorsement or favoring by the United States Department of Energy.

REFERENCES

1. Rothenberger, K.S., Cugini, A.V., Schroeder, K.T., Veloski, G.A., and Ciocco, M.V., Proceedings: ACS, Div. of Fuel Chem., 39(1), 1994.
2. Suzuki, T., Energy & Fuels, 8, 1994, 341-347.
3. Hackett, J.P., and Gibbon, G.A., In Automated Stream Analysis for Process Control, Manka, D.P., Ed., Academic Press, 1982, 95-117 .
4. Ciocco, M.V., Cugini, A.V., Rothenberger, K.S., Veloski, G.A., and Schroeder, K.T., Proceedings: Eleventh Ann. Int. Pittsburgh Coal Conference, September 12-16, 1994, Pittsburgh, PA.

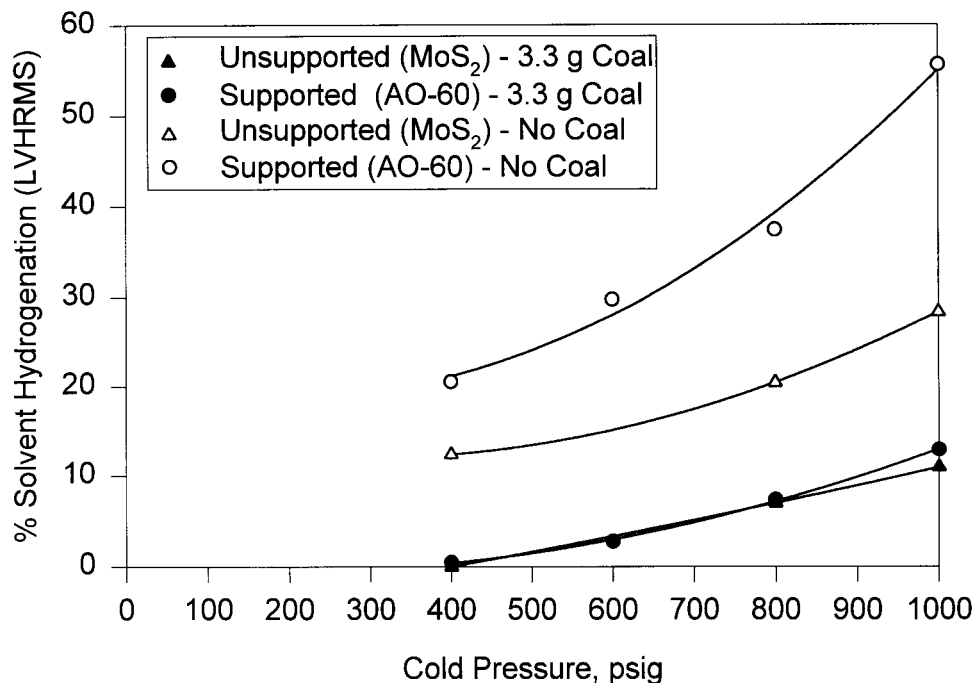


Figure 1. Effect of Pressure on Solvent Hydrogenation with and without Coal

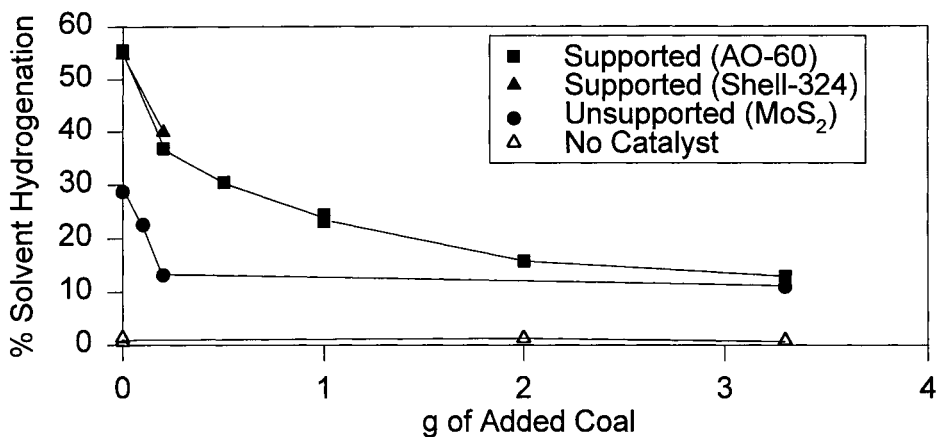


Figure 2. Effect of Added Coal on Solvent Hydrogenation

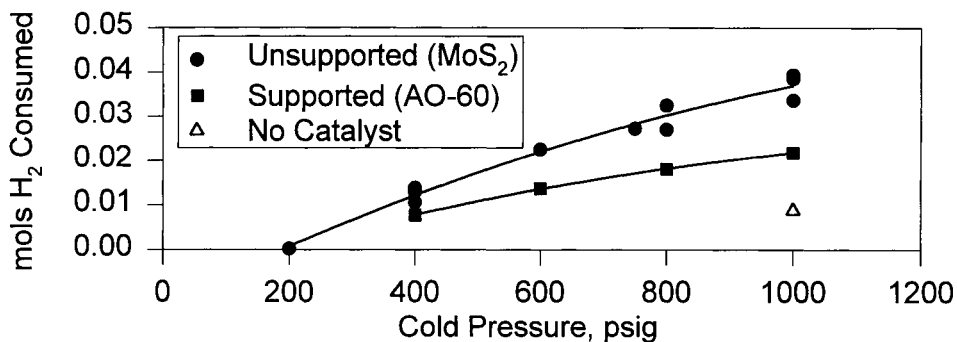


Figure 3. Effect of Pressure on mols H₂ Consumed

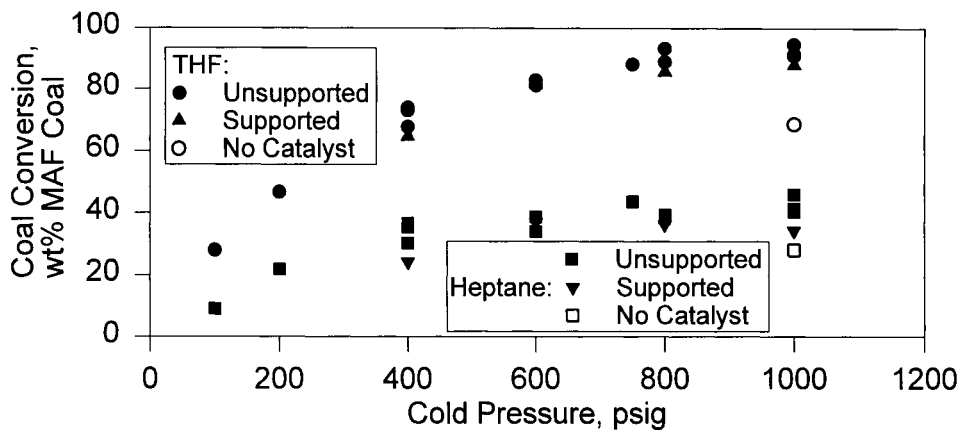


Figure 4. Effect of Pressure on Coal Conversion

CARBON CATALYSTS FOR REACTIONS RELEVANT TO COAL LIQUEFACTION

Malvina Farcasiu, Phillip B. Kaufman, Edward P. Ladner

U.S. DOE, Pittsburgh Energy Technology Center
P.O. Box 10940, Pittsburgh, PA 15236, U.S.A

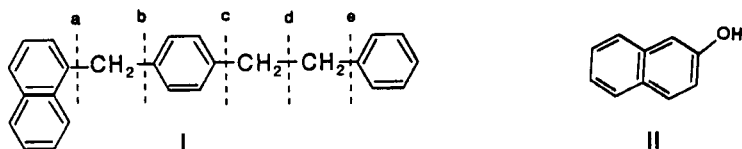
Frank Derbyshire and Marit Jagtoyen
University of Kentucky, Center for Applied Research,
3572 Iron Works Pike, Lexington KY 40511-8433, U.S.A.

KEY WORDS: Catalytic Coal Liquefaction, Carbon Catalysts

1. INTRODUCTION

In previous work, it was shown that carbon materials such as carbon blacks and the products of pyrolysis of resorcinol-formaldehyde resins and acrylonitrile polymers (1,2) are active and selective catalysts in reactions like hydrocracking (3,4) and hydrodehydroxylation (5,6). Both reactions are relevant to coal or coal liquids transformation into low-moleculcular weight hydrocarbons. Recently, we undertook some studies to develop catalysts from coal with activity similar to that of specialty high-surface-area carbon blacks or carbonized polymers, but with significantly lower cost.

We report here the preparation of catalysts based on chemically activated coals (7,8). We have found activation conditions which afford catalysts that perform as well as, or better than, the specialty carbon materials reported previously (1,2). The catalytic activity of the activated coals was measured in microtests, for carbon-carbon bond cleavage on 4-(1-naphthylmethyl)bibenzyl (I) and for dehydroxylation and hydrogenation on 2-hydroxynaphthalene (II).



2. EXPERIMENTAL

The carbon black used as material for comparison was BP2000, a high-

surface area (1475m²/g) material from Cabot. The graphite was obtained from Alpha Corp. Carbons of high surface area were produced by KOH activation of a bituminous coal at different heat treatment temperatures (7). The carbon catalysts were tested in the presence of a H-donor, 9,10-dihydrophenanthrene (9,10-DHP) and under conditions in which no thermal reaction takes place (Tables 2 and 4). When thermal reactions were present (Table 3), only the catalytic conversion is reported. The experimental conditions for hydrocracking and dehydroxylation reactions were described in references 3 and 5, respectively.

3. RESULTS AND DISCUSSION

The activation of coal or other materials with KOH to give high surface area active carbons has been developed on a limited industrial basis, but the materials usually obtained exhibit very low activity as catalysts in reactions of interest for coal liquefaction. We have found, however, a procedure for coal activation with KOH which increases the catalytic activity and gives materials with higher activity than the much more expensive carbonized polymers and carbon blacks. Table 1 presents the yield and pore structural characteristics of activated carbons as a function of the maximum temperature of preparation.

Table 1
Process Conditions and Pore Structural Characteristics of KOH Activated Coal

Highest Treatment Temp °C	Yield Char wt % dry coal	Surface Area, m ² /g		Pore Volumes, mL/g		
		B E T	Mesopores	micro	meso	macro
600	65	835	37	0.30	-	-
700	65	1081	42	0.46	0.08	0.82
800	58	1583	58	0.58	-	-
900	62	1605	62	0.58	0.12	1.29
Carbon Black BP2000	-	1475	-	-	-	-

The catalytic activity for selective cracking of compound I is shown in Table 2, again as a function of the maximum temperature used in the preparation of the activated carbons. A maximum is observed for a treatment temperature of 800°C. Table 3 compares the rates of conversion of compound I on the new coal-derived carbons and on the specialty carbon black BP2000; graphite is inactive for this reaction (9). An examination of the apparent activation energy as a function of the ratio catalyst/ substrate (Table 3) shows that there is less diffusion hindrance on the activated carbons than on BP2000. The presence of macropores in the former coals appears to improve the access of the rather large molecule I to the catalyst

Table 2 Hydrocracking Activity of KOH Activated Coals vs Highest Treatment Temperature of the Coal

Catalyst	Highest Activation Temp. °C	Conversion of Compound I ^a	
		%	μmoles/m ² catalyst x hour
A	600	12	4.45
B	700	33	9.47
C	800	56	10.99
D	900	42	8.12
BP2000		44	9.74

^a 1h, 400°C, catalyst:I:9,10DHP 1:10:40 (wt)

Table 3. Rate Constants, k, and Activation Energies E_a for Catalytic Cleavage of Bond a in Compound I. Carbon Black BP2000 and Catalyst C

Temperature °C	Rate Constant k x 10 ³ , min ⁻¹ , for:			
	BP2000 ^a		Catalyst C	
	wt% ^b		wt% ^b	
	<u>2</u>	<u>5</u>	<u>2</u>	<u>5</u>
360	0.8	2.7		
390			3.1	6.1
400	2.6	6.1	4.4	6.4
410			6.3	9.3
419	4.8	10.0		
E _a , kcal/mol	25	19	28	28

a data from reference 3

b weight % catalyst relative to I

The hydrodehydroxylation activity and the hydrogenation activity toward 2-naphthol are given in Table 4. The activated coal is superior to BP2000 with respect to both overall conversion and dehydroxylation activity, whereas graphite shows a low level of activity.

Table 4. Conversion and Dehydroxylation of 2-hydroxynaphthalene(II) in the Presence of BP2000, Graphite, and Catalyst C^a

Catalyst	Conversion %	Selectivity %	
		% dehydroxylation	% hydrogenation
BP2000	avg. 36	16	94
Graphite ^b	avg. 5	7	93
Catalyst C	avg. 48	22	94

^a catalyst:II:9,10-DHP 1:10:40 (wt); 400°C, 1 hr

^b approximate values

REFERENCES

1. Farcasiu, M.; Smith, C.M., Ladner, E.P., *ACS Preprints Fuel Chemistry Division*, **1991**, 36, 1869.
2. Farcasiu, M.; Petrosius, S.C.; Goellner, J.F.; Pekala, R.W., Sylwester, A.P.; Sault, A., submitted to I&EC Res.
3. Farcasiu, M.; Smith, C.M., *Energy & Fuels*, **1991**, 5, 83.
4. Farcasiu, M.; Smith, C.M.; Hunter, E.A., **1991** International Conference on Coal Science Proceeding, ed. by IEA Coal Research Ltd., Butterworth, Heineman Ltd., 1991, p. 166.
5. Farcasiu, M.; Petrosius, S.C., *J. Catal.* **1994**, 146, 313.
6. Farcasiu, M.; Petrosius, S.C., Eldredge, P.A., Anderson, R.R., Ladner, E.P., *Energy & Fuels*, **1994**, 8, 920.
7. Jagtoyen, M.; Toles, C.; Derbyshire, F. *ACS Preprints Fuel Chemistry Division*, **1993**, 38, 400.
8. Verheyen, V.; Jagtoyen, M.; Derbyshire, F. *ACS Preprints Fuel Chemistry Division*, **1993**, 38, 414.
9. Farcasiu, M.; Petrosius, S.C., *ACS Preprints Fuel Chemistry Division*, **1994**, 39, 723.

ACKNOWLEDGEMENTS

This research was supported in part by an appointment to the Postgraduate Research Training program under contract DE-AC05-76OR00033 between the U.S. DOE and Oak Ridge Associated Universities (PBK). Research at Center for Applied Research (CAER) was supported by the Commonwealth of Kentucky.

DISCLAIMER

Reference in the paper to any specific commercial product, process, or service is to facilitate understanding and does not necessarily imply its endorsement by the United States Department of Energy.

THE ROLE OF CATALYST IMPREGNATION AND SOLVENT TYPE IN IMPROVING LIQUEFACTION EFFICIENCIES

Filomena Pinto^a, I. Gulyurtlu^a, L. S. Lobo^b, I. Cabrita^a

^a INETI, Azinhaga Lameiros, Estrada Paço do Lumiar, 1699 Lisboa Codex, PORTUGAL

^b Universidade Nova de Lisboa, Quinta da Torre, 2825 Monte da Caparica, PORTUGAL

1. INTRODUCTION

In direct coal liquefaction processes chemical bonds in coal structure are broken down by the combined action of heat and pressure. A suitable catalyst and a hydrogen donor medium may also increase the cracking process and the stabilization of the intermediate species thus formed. These species go through several transformations resulting in the production of hydrocarbons of lower molecular weight.

Coal liquefaction produces gaseous hydrocarbons and a complex mixture, which can be separated into three fractions, according to their solubility in organic solvents, named as: oils, asphaltenes and preasphaltenes. Oils is the lighter fraction and the most economically valuable, because it contains products in the range similar to those of gasoline and gas oils. This fraction is soluble in *n*-hexane and insoluble in toluene. Asphaltenes is the intermediate fraction, which is soluble in toluene. Preasphaltenes is the heaviest fraction.

The porous nature of coal, most of it in the form of micropores, makes harder the access of reagents to coal reactive sites and is responsible for reactions being diffusion controlled. To increase coal liquefaction efficiency a better contact between reagents must be promoted, as this will improve mass transfer and reaction rates. This aim may be achieved by the action of a solvent or by impregnating the catalyst into coal structure. The solvent makes easier the access of reagents into coal structure, which decreases diffusional limitations. The solvent used may also have a second action, when it has hydrogen donor capacity. These solvents undergo some reactions that give to the reaction medium the hydrogen necessary to stabilize the intermediate species formed after the cracking process.

Catalyst impregnation into coal structure was done by dissolving the catalyst used in ethanol. Ethanol was chosen, because it dissolves the $ZnCl_2$ used as catalyst, is easier to remove by evaporation and also swells coal structure. Ethanol combines the effect of creating macropores in coal structure with the formation of active sites through breaking weaker bonds and at the same time impregnates the catalyst into coal structure. Previous work done with several swelling reagents showed that ethanol was the one that led to higher total conversions, though TBAH was more selective to the lighter fraction [1].

2. EXPERIMENTAL

Coal was pretreated with ethanol to impregnate $ZnCl_2$ in its structure and the following non hydrogen donor solvents were studied: hexane, benzene, ethanol, methanol and iso-propanol. The effect of some hydrogen donor solvents was also researched, such as: tetraline and

decaline. It was also studied the effect of using mixtures of solvents on products yields: tetraline mixed with ethanol and tetraline mixed with tetrahydroquinoline (THQ).

All experiments were carried out with a bituminous South African coal in a 1 liter autoclave, built in Hastelloy C276. The following experimental conditions were used: run temperature-400°C, run pressure-15.2 MPa, coal particle size-125 to 200 μm, coal/catalyst ratio-1.70 (w/w), coal/solvent ratio-1/3 (w/v) and reaction time-30 minute.

At the end of each run, the autoclave was cooled down to room temperature. Then gases were collected, measured and analyzed. The autoclave was opened and its contents were treated by solvent extraction to obtain three fractions, according to their solubility in organic solvents.

3. RESULTS AND DISCUSSION

As it is shown in Figure 1, coal impregnation with ZnCl₂, increased total conversion about 17%, and oils yield about 38%. This improvement was even higher when a larger amount of catalyst was used. When coal/catalyst ratio was changed from 1.7 to 0.75 (w), total conversion increased only 6%, as these values are near 100%, but oils yield rose to 42%.

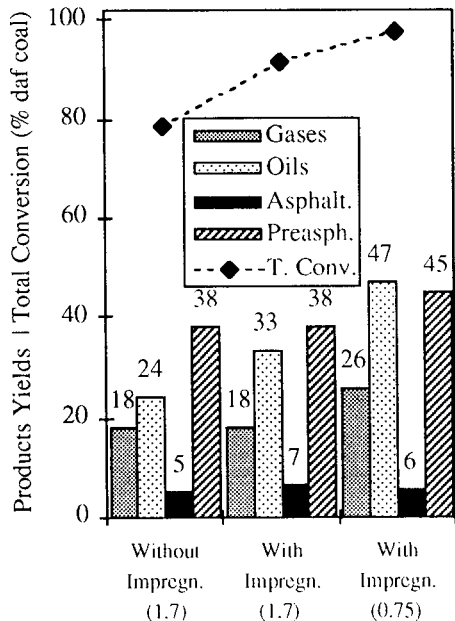


Figure 1. Effect of catalyst impregnation and of coal/catalyst ratio (w/w) on products yields and total conversion.

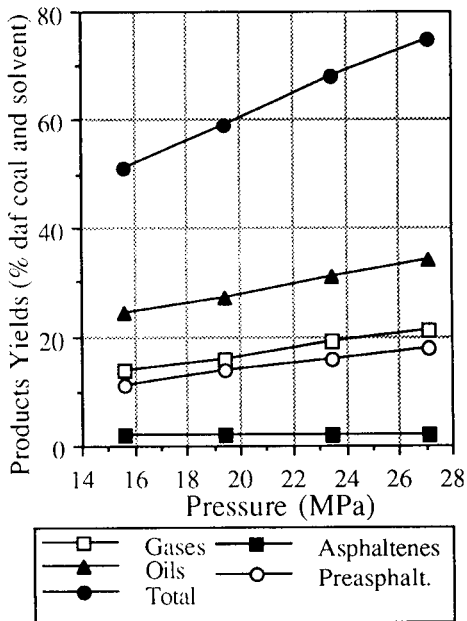


Figure 2. Effect of run pressure on products yields, when ethanol is used as solvent and coal/catalyst ratio is 1,7 (w/w).

In an attempt to understand the effect of catalyst impregnation on liquefaction process, coal structure before and after catalyst impregnation was studied by Scanning Electronic Microscopy (SEM), associated with X Ray Diffraction (XRD). Only when catalyst was

impregnated in coal structure, the formation of some needle like crystals was found, due to the deeper penetration of catalyst in coal structure. Due to this fact, a better contact between coal and catalyst was achieved, so higher mass transfer and higher efficiencies were obtained.

The effect of adding a solvent to the reactional medium was also studied. The first solvent used was ethanol, because alcohols may act in coal structure through two different ways: coal hydrogenation and coal alkylation [2]. For the same experimental conditions and for the coal/catalyst ratio of 1.7 the presence of ethanol led to an increase in oils yields of about 76%. This fraction yield is 58% of daf coal (dried and ash free), which was higher than the value obtained when the coal/catalyst ratio of 0.75 (w/w) was used.

In Figure 2 is shown the effect of run pressure on products yields, which are presented in terms of initial daf coal and solvent added, for this reason these values are lower than the ones obtained only in terms of daf coal. The pressure was found to increase the yields of all fraction, with the exception of asphaltenes, which yield was independent on run pressure. When this parameter varied from 15.6 to 27.1 MPa, gases yield rose 50%, while oils yield increased 42%, the highest increase was in preasphaltenes yield, being about 63%. The effect of pressure under these conditions was similar to the one obtained in previous studies with different experimental parameters [3]. Higher pressures enhance the cracking process, hydrogen dissociation and mass transfer, leading to higher products yields.

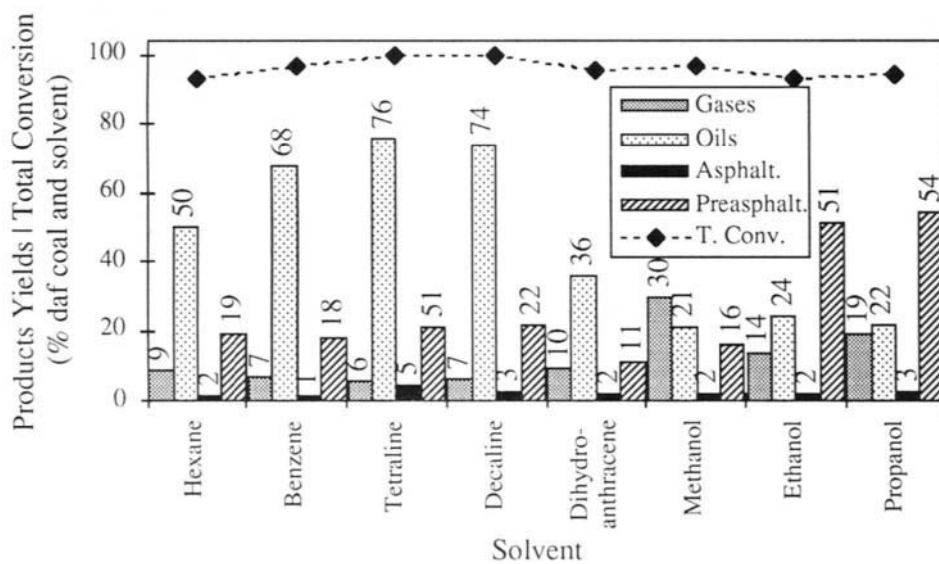


Figure 3. Effect of solvent on products yields.

The effect of using several solvents with different hydrogen donor capacities was studied as well and the results obtained are shown in Figure 3. Total conversion in the presence of a solvent was always higher than without solvent. SEM studies showed that whenever a solvent was used the residue structure had more pores and was not so compact, probably because with solvents a larger amount of organic matter was removed from coal structure. The residue structure obtained when tetraline and decaline were used showed even more pores and cavities. These solvents led to the highest total conversions and oils yields, due to their high hydrogen donor capacity. The results obtained with these two solvents were similar, which could mean that both solvents have similar behaviour in donating hydrogen to

this system. Alcohols produced total conversions similar to the one obtained with hexane, but higher gas yields and lower oils yields, probably because alcohols promote the conversion of oils into lighter molecules. All the alcohols led to similar oils yields, but with methanol the highest total conversion and the highest gas yield were obtained. For all situations, oils hydrogen/carbon ratio (H/C) was higher than the one of asphaltenes. Decaline produced oils with the highest H/C ratio, which could mean that these molecules were more hydrogenated. All alcohols produced oils with similar H/C values, which were higher than the ones obtained with tetraline.

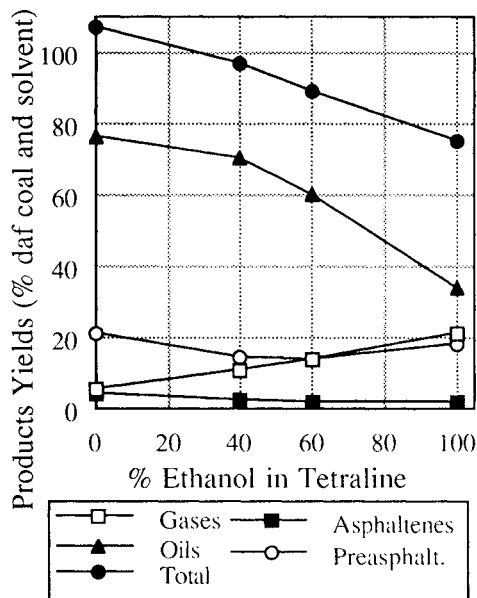


Figure 4. Effect of ethanol amount mixed with tetraline on products yields.

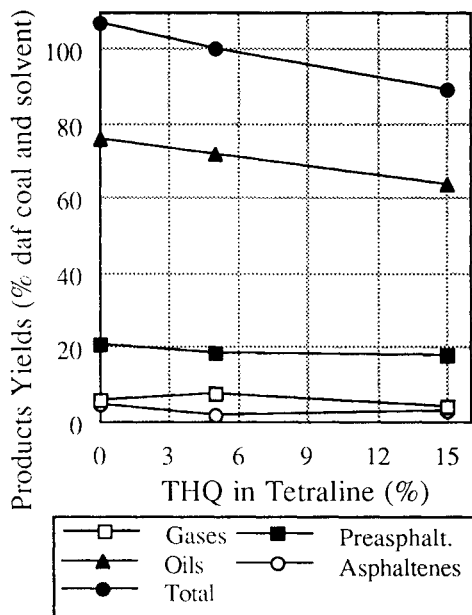


Figure 5. Effect of THQ amount mixed with tetraline on products yields.

It was also studied the effect of mixing ethanol with tetraline, to combine the high hydrogen donor capacity of tetraline with the alkylation properties of ethanol, but in opposition to the results obtained by Kuznetsov [2] only gas yields increased with ethanol concentration, whilst the yields of all the other fractions decreased.

The results obtained by Burgess [4] showed that THQ was not only a very good hydrogen donor solvent but also promoted the decomposition of coal macromolecular structure. As it is illustrated in Figure 4, there is no improvement by the addition of THQ to tetraline, as the yields of all fractions decreased with the reduction of tetraline concentration, which suggests that for the system studied THQ has a lower hydrogen donor capacity than tetraline.

REFERENCES

1. Filomena Pinto, I. Gulyurtlu, L. S. Lobo, I. Cabrita, Carbon '94, July, Spain, 1994.
2. Kuznetsov, Sukhova. Bimer, Salbut. Korniyets. Belskaya, Ivanchenko, Fuel, Vol 72, 1991, 1031.
3. Filomena Pinto, I. Gulyurtlu, L. S. Lobo, I. Cabrita, Eleven Annual International Pittsburgh Coal Conference. September, USA, 1994, 43.
4. J. T. Joseph. Fuel. Vol 70. 1991. 139 and 459.

SCALE FORMATION MECHANISM ON COAL HYDROGENATION WITH IRON CATALYST

O.Togari^{a*}, M.Kobayashi^a, K.Hirano^a, S.Suzuki^a, H.Yoshida^b and S.Ueda^b

^aNippon Coal Oil Co.,Ltd.(NCOL)

Sanbancho KS BLDG., 2, Sanbancho, Chiyoda-ku, Tokyo, 102 JAPAN

^bNew Energy and Industrial Technology Development Organization (NEDO)

3-1-1, Higashi-ikebukuro, Toshima-ku, Tokyo, 170 JAPAN

1. INTRODUCTION

Iron catalysts have been used as one way catalyst for coal liquefaction. However, in some cases, scale formation phenomena on to the inner wall of the preheater pipes have been reported. So, conditions of scale formation and it's mechanisms, and possibility of prevention methods were investigated.

2. SCALE FORMATION IN PREHEATER OF CONTINUOUS TYPE LIQUEFACTION PLANTS

In some continuous type liquefaction plants, increasing of the pressure difference in the preheater was observed under the presence of coal/solvent/iron oxide/sulfur/hydrogen. In this chapter, some data are reported.

2.1. Results of 0.1t/d BSU of HNIRI[1]

In the Hokkaido National Industrial Research Institute(HNIRI, former GIDLH), coal liquefaction tests(direct hydrogenation method)using 0.1t/d BSU were carried out under following conditions:

Coal:Wandoan(sub-bituminous coal)	Slurry feed rate:-7.7kg/hr
Solvent:Decrystallized anthracene oil	Pressure:19.2-28.8MPa
Catalyst:Red-mud(3%),S(0.3%)	Slurry temperature:-450°C
	(at the preheater outlet)

A cylindrical type preheater(4cm ϕ ,100cmL)heated by electric heater was used. In the run16, the tests were carried out at the inside temperature of 359°C(57hr),375°C(17hr) and 400°C(81hr) respectively. Test fluids and testing hours were(1)anthracene oil/red-mud(3wt%)/S(0.3%)for 103hr,(2)Taiheiyo coal(40%)/anthracene oil(60%)/red-mud(5.5wt%)/S(0.55%)for 32hr,(3)hydrogenated anthracene oil/red-mud(3%)/S(0.3%) for 20hr.

The scale was taken out at the wall of 30cm under from the top rim of the preheater, and it's thickness was 180 μ m. Main components were Fe(33.8%) and S(20.4%). The scale was composed of three layers reflecting the fluids tested. From the relations of scale thickness and testing hours, it was found that rapid scale formation occurred in the run containing coal. From X-ray analysis, monoclinical pyrrhotite crystal(Fe₇S₈), hexagonal pillar troilite(FeS), metallic

*Preset adress:CHIYODA Corporation

iron and magnetite(Fe_3O_4) were identified.

2.2. Results of 2.4t/d PDU of NKK[2]

In the Nippon Kokan K.K.(NKK), coal liquefaction tests(direct hydrogenation method)using 2.4t/d PDU were carried out under following conditions:

Coal:Taiheiyo(sub-bituminous coal)	Slurry feed rate:250kg/hr
Solvent:Decrystallized anthracene oil	Pressure:24.5MPa
Catalyst:Red-mud(3%),S(0.3%)	Slurry temperature:350-410°C (at the preheater outlet)

Film coefficient of heat transfer(inner side) of the preheater(which heated by hot gas blowing) was measured.

In a test of run600(average outlet temperature exceeded 400°C), the coefficient of heat transfer decreased from 950 to 450(53% decreasing)through 84 hr test.

On the contrary,at the tests of 370°C for 230hr and 350°C for 410hr, the reductions of the coefficient of heat transfer were limited to 25% and 1.4%, respectively. From these results,it was concluded that the operation under 350°C is recommendable.

By the analysis of scales,iron sulfide(troilitite) and coke were identified.

2.3 Results of 1t/d PDU of Sumitomo Metal[3]

In the Sumitomo Metal Industries,Ltd.,coal liquefaction tests(solvent extraction method) were carried out under following conditions:

Coal:Wandoan	Slurry feed rate:120l/hr
Solvent recycle ratio:Anthracene 1.5/coal	Pressure:14.7-15.7MPa
Catalyst:CGS dust(Fe 2.4wt% to maf coal)	Slurry temperature:-420°C (at the preheater outlet)
S(1.2%)	

Magnetic induction method was used for preheater. After operation of 625 hr,heating pipes were taken out from preheater,then the scale of inside wall of pipes were checked after cutting. The thickness of scale was in the range of 0.5 to 1.7mm. The scaling started at the zone of exceeded 400°C,and the thickness increased gradually with the temperature increasing. The analysed results of scale were as follows:

- Main components were fine crystalline pyrrhotite and heterogeneous carbon of low reflectance.
- The ratio of pyrrhotite content exceeded 50%(85% in weight) and pyrrhotite formed large particles having hundreds μm in diameter.
- Pyrrhotite particles contained small carbonaceous flakes which arranged in parallel to the pipe wall.

2.4 Results of NEDOL 1t/d PSU[4]

In the 1t/d PSU of the NEDOL process(which developed by NEDO) in Kimitsu, coal liquefaction tests were carried out under following conditions:

Coal:Wandoan, Wyoming,etc.	Slurry feed rate:-
Solvent:hydrogen donor solvent	Pressure:17MPa
Catalyst:Several kinds of pyrite	Temperature:450°C(in main reactor)

Magnetic induction method was used for the preheater. In the test runs,some

sediments were recognized in the reactors, however, no change of pressure difference in preheater has been recognized because of using pyrite.

2.5 Summary

No scaling was observed in the plant using iron sulfide such as pyrite. On the other hand, the scale formation was observed in the plants using iron oxide catalyst. In the latter case, scale formation has relation with the temperature of preheater. The results showed that the scaling does not occur under 350°C, and occurs without fail in the range over 400°C. The scales are consisted of pyrrhotite, troilite, carbonaceous and inorganic particles.

3. FUNDAMENTAL RESEARCHES ON THE CONDITIONS OF SCALE FORMATION

3.1 Autoclave tests in HNIRI[1].

Cylindrical test piece (5mm ϕ , 11mmL, SUS316) was set in a 100ml autoclave with red-mud/S/anthracene oil. Initial hydrogen pressure was 9.8MPa and reaction pressure was in the range of 13-13.6MPa. The autoclave was heated up from 200°C and kept at settled temperature for 2 hours. The scale formation started from 250°C. As to the relations of the amount of sulfur and the scaling, scale formation started at the sulfur content of 0.2-0.4g to 2g of red-mud.

3.2 Tests of hot model preheater in the NKK[2].

A coil type preheater having 1st and 2nd preheater (3mm inner dia, 1050mmL each) was made. Coal slurry (Wandoan coal/anthracene oil/catalysts) was sent under pressure of 24.5MPa. No change in pressure difference was found under 375°C operation.

After two level tests (preheater inlet temp. 370°C/outlet temp. 480°C for 30 hr and preheater inlet temp. 400°C/outlet temp. 480°C for 40hr), pipes were cut and checked at several points. The scale formation was found at the point exceed 415°C in each test level. Low flow rate test (inner dia. of 2nd preheater was changed to 4mm) was carried out from 40 to 80 hr. The scales of 0.5-1.0mm thickness were found in the cases using of red-mud/S and laterite/S catalyst. On the other hand, no scale was found in the synthesized or natural pyrite catalyst. Crystalline substances in the scale were analyzed with the X-ray diffraction method, and troilite (FeS) was identified.

3.3 Summary

- Scale formation temperature for iron oxide catalyst was confirmed as 250-300°C for autoclave tests and 350-400°C for continuous type preheater tests. Main components of scale were pyrrhotite and troilite.
- No scale was found in tests of pyrite catalyst.

4. BEHAVIOR OF IRON OXIDE/S AND PYRITE UNDER HIGH PRESSURE, HIGH TEMPERATURE

Analysis with DTA and DPA were carried out on coal slurry (Taiheiyo coal/red-mud/S) by Maekawa and others[5]. First exothermic peak appeared near 220°C, which peak corresponds to the change of S to H₂S, then iron oxide was sulfurized to pyrrhotite by H₂S. Peak of hydrogen absorption at 360°C and peak

of hydrogenation of coal at 380°C were observed. On the other hand, in the case of pyrite catalyst, broad peak result from change of pyrite to pyrrhotite at 240°C, and peak of hydrogenation of coal at 330°C were observed. It has been concluded that pyrite had high performance compared with iron oxide on the hydrogenation activity.

Sulfurization process of ultrafine Fe_2O_3 (10-30Å) by DMDS was observed using electron microscope by Srinivasan and others[6]. After 15min. sulfurization at 385°C, photograph of hexagonal plate crystal of pyrrhotite having 1000-5000Å of particle diameter was obtained.

Using iron oxides of 800 and 200Å, almost same results were obtained by Mariadassou and others[7]. And, they pointed out that sintering of pyrrhotite was restrained by the presence of coal molecules, and concluded that the presence of enough amount of coal molecules in the vicinity of fine pyrrhotite restrain the growth to coarse particles by the adsorption of coal molecules on to the fine and active pyrrhotite crystal surface.

5. CONCLUSION

Remarkable scale formation in the preheater was not found in the pyrite catalyst tests.

On the contrary, the iron oxide catalyst system caused scale formation under some conditions in the preheater. The scale formation mechanisms in the iron oxide catalyst system were summarized as follows:

- Fine iron oxides are sulfurized by hydrogen sulfide in the preheating process, then become fine and active crystalline pyrrhotite.
- Fine pyrrhotite crystal grows to coarse crystal on the hot pipe wall (over 400°C) of the preheater and forms the scale with inclusion of fine coal and inorganic particles.

To prevent the scale formation of the iron oxide catalyst system, following measures are considered:

- Maximum temperature of preheater has to keep under 400°C.
- By surrounding active pyrrhotite crystal with enough amount of coal molecules, coal molecules are adsorbed to the surface of activated pyrrhotite. Such condition arrests the growth to the coarse crystal of fine pyrrhotite crystal, and finally, the scale formation is restrained.

To make such condition, for example, the using of coal impregnated with iron oxide catalyst can be considered.

REFERENCES

1. T. Okutani, Y. Nakata and Y. Maekawa, Fuel Processing Tech., 17(1987)41
2. S. Moriguchi, NEDO, Entrust Report [Researches on 2.4T/d plant] (1985-87)
3. T. Kano, NEDO, Entrust Report [Researches on 1t/d plant] (1983-1986)
4. K. Hirano, Proc. of AIST/NEDO Joint Res. Meeting (Vol. 2) (1993)24
5. Y. Maekawa, S. Ueda, R. Yoshida, S. Yokoyama, T. Okutani, Y. Nakata, T. Yoshida, H. Narita, HNRI Report on coal liquefaction catalyst, (Oct. 1993)1
6. R. Srinivasan, R. A. Keogh and B. H. Davis, ACS Meeting Div. Fuel Chem., 37, No. 3 (1992)1265
7. G. D. Mariadassou, D. Krastman, D. V. Martello and G. D. Holder, Fuel Processing Tech., 12(1986)143

Deactivation of Pyrite FeS_2 Catalyst with Oxidation and Its Reactivation

Eisuke Ogata^{a@}, Tomo Hojo^b, Akio Nishijima^c, Etsuo Niki^a, Kiyoshi Mashimo^b
and Tohru Wainai^b

^a Department of Chemistry and Biotechnology, Faculty of Engineering, The University of Tokyo ; 7 - 3 - 1 Hongo, Bunkyo-ku, Tokyo 113, Japan.

^b Department of Industrial Chemistry, College of Science and Technology, Nihon University ; 1 - 8 Surugadai, Kanda, Chiyoda-ku, Tokyo 101, Japan.

^c Surface Characterization Laboratory, National Institute of Materials and Chemical Research ; 1 - 1 Higashi, Tsukuba-shi, Ibaraki, 305 Japan.

1. INTRODUCTION

A symposium on iron-based catalysts for coal liquefaction was held at the 205th ACS National Meeting [1], and some of the papers have been published in *Energy & Fuels* [2]. Reviews of the development of catalysts for coal liquefaction were also published in *Journal of the Japan Institute of Energy* [3]. The first-stage reactor in direct coal liquefaction requires a catalyst that is both inexpensive and disposable in order to develop an economically viable technology. We reported that catalysis of iron-sulfide catalyst was affected by the S/Fe ratio, the activity increased with pyrrhotite formation and was accelerated by the presence of excess sulfur [4-7]. Activity of pyrite for phenanthrene hydrogenation [8] and activity of natural ground pyrites for coal liquefaction [9] decreased with storage under air. The NEDOL process of a coal liquefaction pilot plant of 150 t/d, which is a national project in Japan, will use pyrites as one of the catalysts for the first-stage, because FeS_2 has high activity and is low in price. In this paper, the relationship between oxidation of pyrite and activity and selectivity for hydrogenation of 1-methylnaphthalene (1-MN) is discussed.

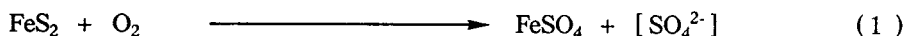
2. EXPERIMENTAL

Materials: The compounds used as substrates and solvents were commercial reagents and were purified by conventional methods if necessary. The catalyst pyrite FeS_2 used was synthesized by Asahi Chemical Industry Co. Ltd. **Procedure:** In a typical reaction, 1.0 g of 1-MN, 0.25 g of FeS_2 and 30 ml of decalin(DHN), and a prescribed amount of sulfur(S/Fe ratio = 2.0) if necessary, were placed in a 150 ml stainless steel, magnetically stirred autoclave. After pressurization with 10 MPa hydrogen or argon, the autoclave was heated to at 350°C and maintained for 1 hr. It was then immediately cooled in an ice-water bath. **Analysis:** The products were identified by GC-MS(Shimadzu GCMS QP-1000, equipped with a 0.24 mm (I.D.) x 50 m (L.) glass capillary column chemically bonded with OV-1) if necessary and quantified by GC (Shimadzu GC-15A, equipped with the same capillary column). **Oxidation of FeS_2 :** FeS_2 was oxidized at room temperature, 80°C, 150°C and 200°C for the desired time by atmospheric oxygen. FeS_2 oxidized was analyzed using XRD (Rigaku Denki Model RINT 2400) and XPS (Perkin-Elmer Model PHI 5500), and was tested for 1-MN hydrogenation.

3. RESULTS AND DISCUSSION

3-1. Oxidation of Synthetic Pyrite FeS₂ under Air

It is well known that large conglomerates of pyrite ore maintain a golden color for a long time on exposure to air. Before oxidation, synthetic pyrite used in this paper was a black powder with a specific surface area of 12 m²/g. Weight change profiles on oxidation of pyrites under air at 150°C and 200°C are shown in Fig. 1. Increases of about 30 wt% were observed at 150°C and 200°C. Oxidation of pyrites is considered to proceed as shown in eqs. (1) and (2). Increases of weight in eqs. (1) and (2) were calculated as 27 wt% and 67 wt%,



respectively, without excess sulfate anion. The results in Fig. 1 suggest that pyrite was oxidized to ferrous sulfate, not ferric sulfate, but the excess sulfur in ferrous sulfate formation from pyrites was missing.

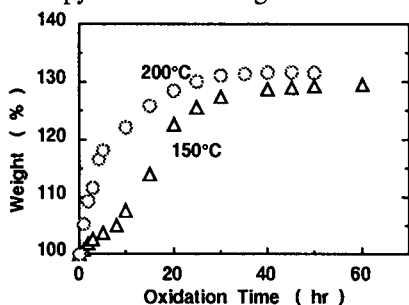


Fig. 1 Oxidation of FeS₂ Catalyst under Air at 150°C and 200°C.

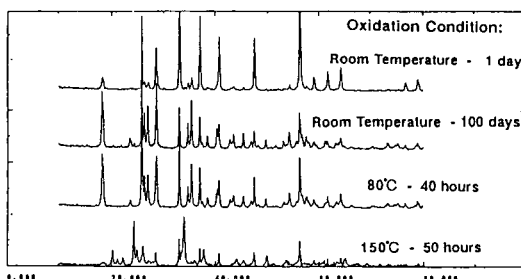


Fig. 2 XRD Patterns of Pyrite Oxidized under Air at Various Temperatures after Certain Period.

Typical XRD patterns of pyrite oxidized under some different conditions are shown in Fig. 2. FeS₂ was easily oxidized to ferrous sulfate with a Szomolnokite structure, FeSO₄·H₂O, under mild oxidation conditions such as exposure to air at room temperature. These results were obtained from measurements of XRD and showed that oxygen in air was diffused from the gas phase into the pyrite lattice, and the pyrite crystal lattice was destroyed and combined with oxygen to form ferrous sulfate, i.e., the crystal lattice of pyrite consisting of iron and sulfur atoms was transformed to a different crystal form as ferrous sulfate. This clearly shows that iron and sulfur atoms in the strict pyrite structure of a regular crystal lattice were moved and rearranged even at room temperature. One water molecule of crystallization in the Szomolnokite structure should be incorporated from moisture in the air, but pyrite oxidized at 150°C does not have the water of crystallization in ferrous sulfate.

3-2. Effect of Pyrite Oxidation under Air on 1-MN Hydrogenation

Hydrogenation of 1-MN is negligible in the absence of catalyst at 400°C. As shown in eq. (3), 1-MN was hydrogenated to 1-methyltetralin (1-MT) and 5-methyltetralin (5-MT) with selectivity of over 97% in the presence of FeS₂. Hydrogenation from methyltetralins to methyldecalin as shown in eqs. (4) and (5) was very difficult. Effects of pyrite oxidation on 1-MN hydrogenation are shown in Figs. 3 ~ 5. Catalytic activity decreased almost linearly in the initial one month of oxidation at room temperature, and then the activity was gradually reduced. The deactivation of pyrite was accelerated by raising the temperature of oxidation. Pyrites oxidized at room temperature for 500 days and at 150°C for 50 hrs had very low activities, and the color changed to dark gray and gray, respectively.

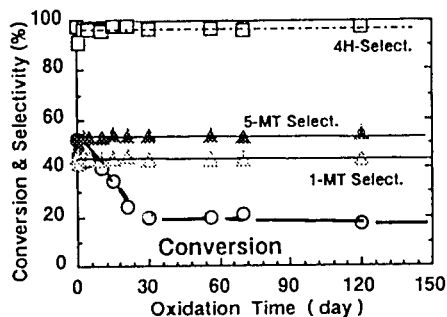
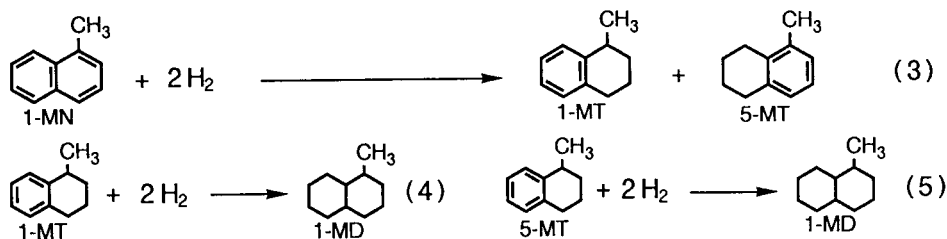


Fig. 3 Effect of FeS_2 Oxidation at Room Temperature on 1-MN Hydrogenation.

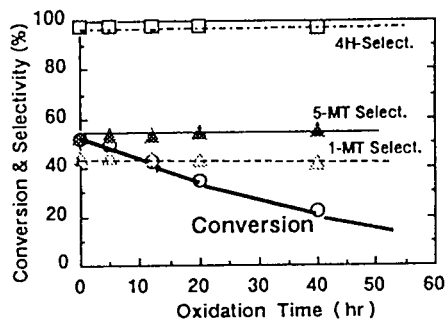


Fig. 4 Effect of FeS_2 Oxidation at 80°C on 1-MN Hydrogenation.

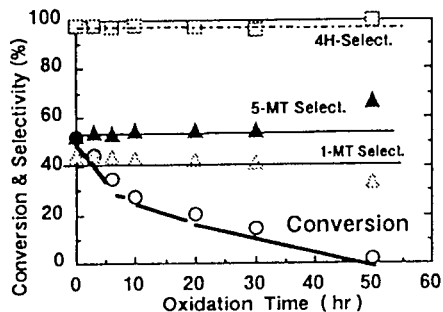


Fig. 5 Effect of FeS_2 Oxidation at 150°C on 1-MN Hydrogenation.

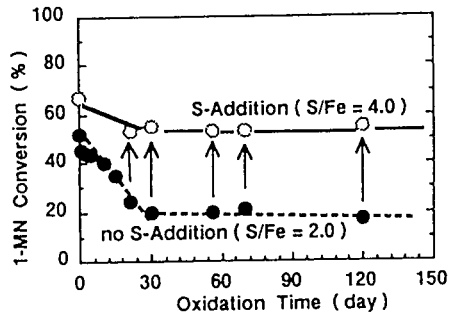


Fig. 6 Additive Effect of S on 1-MN Hydrogenation by Oxidized FeS_2 at Room Temperature.

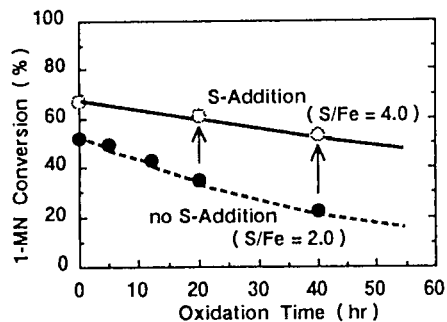


Fig. 7 Additive Effect of S on 1-MN Hydrogenation by Oxidized FeS_2 at 80°C .

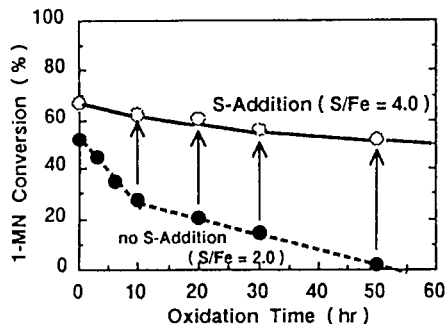
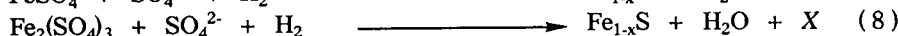
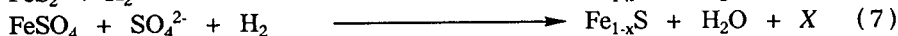
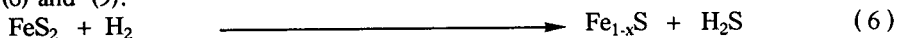


Fig. 8 Additive Effect of S on 1-MN Hydrogenation by Oxidized FeS_2 at 150°C .

All pyrites oxidized under any oxidation conditions below 150°C show about the same selectivity for 1-MN hydrogenation. This result suggests that the oxidation of pyrites decreases the number of active sites, and the nature of residual active sites is almost the same as that before oxidation. On the other hand, commercially available ferrous sulfate and ferric sulfate showed very low activity in the hydrogenation.

3-3. Reactivation of Oxidized Low Activity Pyrites.

Catalytic activity of pyrites greatly decrease with oxidation as shown in Figs. 3 ~ 5. It was found that the oxidized low activity pyrites were reactivated by addition of excess solid sulfur to the reaction system as shown in Figs. 6 ~ 8. The result is particularly exciting in view of the fact that pyrites deactivated by air oxidation were reactivated to almost the same or a higher level than before oxidation by fresh addition of sufficient sulfur at S/Fe ratio of 2 to the reaction system. As is evident from the pyrite FeS_2 formula, the S/Fe ratio of original pyrite crystal is 2.0. Under reaction conditions of 350°C for 1 hr and initial hydrogen pressure of 10 MPa and decalin, original pyrites and oxidized pyrites in the presence of excess sulfur were completely transformed to a pyrrhotite Fe_{1-x}S structure according to XRD analysis as shown in eqs. (6) and (9).



4. CONCLUDING REMARKS

Effects of oxidation of pyrite catalyst under air for the hydrogenation of 1-methylnaphthalene were investigated under coal hydroliquefaction conditions. Pyrite was oxidized to ferrous sulfates even at room temperature under atmospheric oxygen, and the catalytic activities of FeS_2 oxidized decreased by increasing the storage time. The deactivation of pyrites was enhanced by raising the atmospheric temperature. It was proved that pyrites deactivated by air oxidation were reactivated by addition of sufficient sulfur to the reaction system.

REFERENCES

1. Prepr. " Symposium on Iron-Based Catalysts for Coal Liquefaction" , Div. Fuel Chem., 205th ACS National Meeting(Denver), Vol. 38(No. 1), pp-1 - 238 (1993).
2. Energy & Fuels, 8,(1), (Special issue), p-2 - 123 (1994).
3. J. Jpn Instit. Energy, 73, (1), (Special issue), p-2 - 49 (1994).
4. E. Ogata, E. Niki, Proc. 27th Conf. Coal Sci. Jpn. Soc. Fuel(Tokyo), pp-115 (1990).
5. X.-Y. Wei, E. Ogata, E. Niki, Chem. Lett. 2199 (1991).
6. X.-Y. Wei, E. Ogata, Z.-M. Zong, E. Niki, Energy & Fuels, 6, 868 (1992).
7. E. Ogata, K. Ishiwata, X.-Y. Wei, E. Niki, Proc. 7th Inter. Conf. Coal Sci.(Banff), Vol. II, pp-349 (1993).
8. E. Ogata, T. Suzuki, K. Kawamura, Y. Kamiya, 26th Conf. Coal Sci. Jpn. Soc. Fuel (Sapporo), pp-121 (1989).
9. K. Hirano, T. Hayashi, K. Hayakawa, 30th Conf. Coal Sci. Jpn. Soc. Fuel(Tokyo), pp-161 (1993).

Effect of synthetic pyrite and pulverized natural pyrite as coal liquefaction catalyst

Inokuchi K, Nogami Y, Okada T *, Kobayashi M *, Mochizuki M **, Endou K **

MITSUI SRC DEVELOPMENT CO.,LTD., 1-12-3 Muromachi Nihonbashi Chuoku Tokyo Japan

* NIPPON COAL OIL CO.,LTD., 2 Sanbancho Chiyodaku Tokyo Japan

**NIPPON STEEL CORPORATION, 1 Kimitsu Kimitsushi Chiba Japan

1. INTRODUCTION

Coal liquefaction catalysts, which would greatly contribute to reduce the cost of liquefied oil, have been investigated as an elementary technology of coal liquefaction. As one of the catalysts, iron based catalyst has been widely used because of its cheaper cost, disposability and easy obtainability. At this point, a large number of studies on iron based catalyst have been done, especially highly dispersed catalysts.

In this paper, the effect of particle size of the catalyst on the liquefied oil yield using the synthetic pyrite and the pulverized natural pyrite as the catalyst in the test by use of an autoclave and the 1t/d process supporting unit(PSU) are reported.

2. EXPERIMENTAL

2.1 Autoclave test

Wandoan coal and Tanito Harumu coal as feed coal, synthetic pyrite (made by Asahi Chemical Industry, wet method) and natural pyrite (made from Hanaoka, and Finland) as liquefaction catalyst, hydrogenated anthracene oil and wash oil as solvent were used. The properties of these materials are shown in Table 1.

240g of the dried coal, 360g of the solvent and 7.2g of the catalyst were charged in a 5-L autoclave, pressurized to 75kg/cm²G by hydrogen gas, heated up to 450°C at the heating rate of 3°C/min, and then kept at this temperature for

Table 1 Properties of raw materials

Material	C	H	N	S	O	ASH	FeS _x	Na ₂ SO ₄	SiO ₂ +Al ₂ O ₃
Wandoan coal	78.1	5.9	0.9	0.1	15.0	9.9			
Tanito Harumu coal	76.6	5.6	1.4	0.2	16.2	4.8			
Synthetic pyrite							82.3	4.9	-
Natural pyrite									
Hanaoka							86.2	-	3.5
Finland							90.2	-	0.5
solvent	90.3	8.2	0.7	<0.1	0.8				

1 hour. Liquefied oil yield was obtained as the fraction of C5 to 538 °C by means of gas chromatograph and vacuum distillation.

2.2 Test at the 1t/d PSU

Tanito Harumu coal as feed coal, synthetic pyrite and pulverized natural pyrite(Finland) as catalyst and 50/50 mixture of creosote oil and anthracene oil as initial solvent were used. Operating conditions are shown in Table 2.

Table 2 Operating conditions at 1t/d PSU

Run	Catalyst (pyrite)	wt% vs dry coal	temperature °C	pressure kg/cm ² G	gas/slurry NL/kg
1	synthetic	3	450	170	700
2	synthetic	3	465	170	700
3	synthetic	4	465	190	900
4	natural	3	450	170	700
5	natural	3	465	170	700
6	natural	4	465	190	900

3. RESULTS AND DISCUSSION

The effect of the mean particle size of the pyrites on the liquefied oil yield at the autoclave test is shown in Fig.1. In the case both of the combination of Wandoan coal and pulverized natural pyrite made from Hanaoka, and Tanito Harumu coal and natural pyrite made from Finland, the liquefied oil yield increases with decreasing mean particle size of the pyrite. And as shown in Fig.1, liquefied oil yield data using the synthetic pyrite are plotted on the yield curve of the pulverized natural pyrite. From the results, it is considered that the liquefied oil yield is not affected by the kind of pyrite but mainly by those particle size.

Comparison of the oil yield between the synthetic pyrite(0.7 μ m) and natural pyrite(Finland, 0.55 μ m) was conducted by use of the

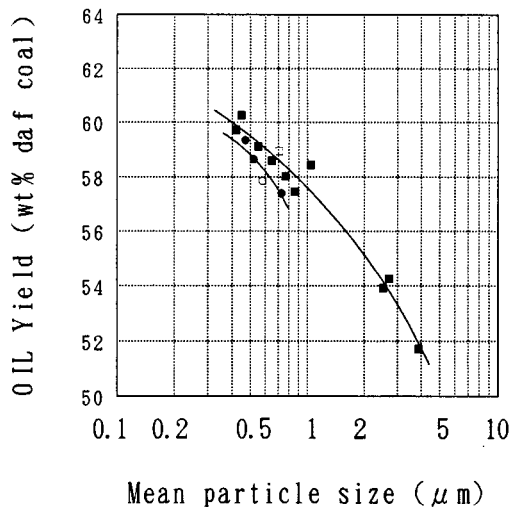


Fig.1 Relationship between mean particle size of pyrite and oil yield

Wandoan Tanito
Harumu
synthetic pyrite ○ □
natural pyrite ● ■

1t/d PSU. As the results of the above autoclave tests, the difference of oil yield of 1.5wt% daf between the two catalysts will be expected at the PSU test. But, as is shown in Fig.2, there is little difference between the two catalysts at the respective conditions (Run1 vs Run4, Run2 vs Run5, Run3 vs Run6).

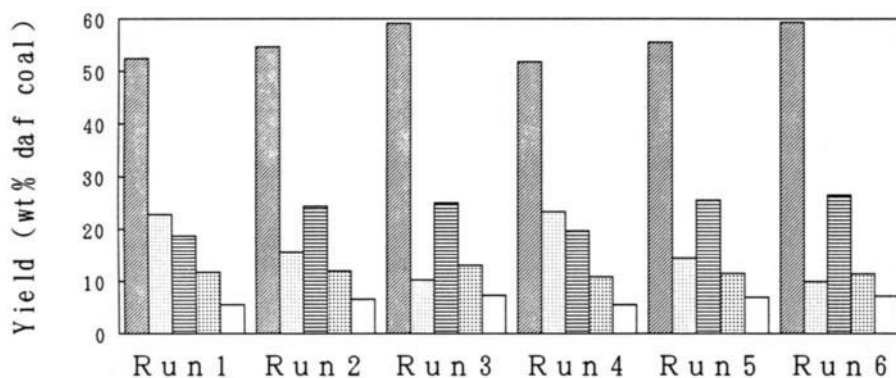


Fig.2 Comparison of product yield between synthetic pyrite and natural pyrite

■ Oil ▨ Residue ▩ Gas ▪ Water □ Consumed H₂

Nagaishi et al reported that a coal is assumed to consist of three different components: I₀, inherently inert for liquefaction; C₁, forming consecutively oil and gas via preasphaltenes and asphaltenes; C₂, forming oil and gas directly without consuming external hydrogen from the solvent and the gas phase¹⁾. Itou et al reported that a coal is rapidly converted to asphaltenes²⁾. And Moritomi et al also reported that the conversion of coal to benzene soluble varies depending upon the heating rate even if other operating variables are the same³⁾. And Suzuki et al reported that role of liquefaction catalyst is to stabilize free radicals formed from the thermal scission of covalent bonding in coal macromolecular structure⁴⁾.

From the above view points, the reason why there is little difference of liquefied oil yield between the two catalysts at the PSU test is mainly considered to be the influence of heating rate and agitating intensity. That is to say, at the autoclave test, thermal decomposition and hydrogenation will occur simultaneously at the heating up period because of low heating rate, and a catalyst is required at the time, so that the oil yield is largely affected by dispersion of the catalyst. Furthermore, pyrrhotite has been proposed to be the active species of pyrite^{5), 6)}, and pyrite changes to pyrrhotite at comparatively low temperature⁷⁾. The agglomeration of the pyrrhotite can occur even in the heating period. Therefore mixing is considered to be important to avoid the agglomeration. From this point of view, it is thought that the oil yield is affected by the mean particle size of the pyrite at the autoclave test which has large mixing intensity(500rpm). On the other hand, as mixing intensity is low

and heating rate is high at the PSU, the agglomeration of the pyrrhotite easily occur. Therefore, the initial particle size dose not affect the oil yield .

Fig.3 shows the comparison of the oil fraction between the two catalysts. There are some differences in the middle fraction at the temperature of 450 °C and 465°C. Yokoyama et al reported that the composition of the product is influenced by the impurities of natural pyrites⁸⁾. As the natural pyrite used contains some impurities and synthetic pyrite contains sodium sulfate, it is thought that the difference in the middle fraction is caused by these impurities in the pyrite.

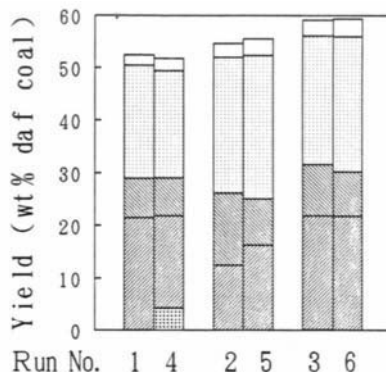


Fig. 3 Comparison of oil fraction between synthetic pyrite and natural pyrite

4. CONCLUSIONS

The effect of the synthetic pyrite and pulverized natural pyrite as a coal liquefaction catalyst on the oil yield by use of the 5-L autoclave and the 1t/d PSU was studied. As a result, it is found that the oil yield is only affected by the mean particle size of the pyrite at the autoclave test, but there is little difference of the oil yield between the synthetic pyrite(0.7 μm) and the pulverized natural pyrite(0.55 μm) because of higher heating rate and lower mixing intensity at the PSU test. And it is thought that product oil fraction is influenced by the impurities of the pyrite.

ACKNOWLEDGEMENT

This work is supported by the New Energy and Industrial Technology Development Organization(NEDO). The authors express their sincere appreciation to that organization for having allowed them to make this study.

REFERENCES

- 1) Nagaishi H, Moritomi H, Sanada Y, Chiba T, Energy & Fuels 1988, 2(4), 522-528
- 2) Itou H, Ouchi K, Shokubai 1980, 22(2), 78
- 3) Moritomi H, Kurouji A, Sanada Y, Chiba T, Liquid Fuels Technology 1984, 2(1), 1-17
- 4) Suzuki T, Energy & Fuels 1994, 8, 341
- 5) Montano P.A., Granoff B, Fuel 1980, 59, 214-216
- 6) Bommannarar A, Montano P.A., Fuel 1982, 61, 1288-1290
- 7) Yokoyama S, Yoshida R, Narita H, Kodaira K, Maekawa Y, Fuel 1986, 65, 164
- 8) Yokoyama S, Narita H, Itou S, Yoshida R, Maekawa Y, Nenryo Kyokaiishi 1989, 68(5), 415

Separation of iron catalyst from coal liquefaction crude oil with high gradient magnetic separator

Hideo Narita, Ryoichi Yoshida and Yosuke Maekawa

Hokkaido National Industrial Research Institute
2-17-2-1 Tsukisamuhigashi, Toyohiraku, Sapporo 062, Japan

1. INTRODUCTION

In a coal liquefaction process, a recovery and a reuse of catalyst can improve the economics as well as the environmental problem. In former work, Narita et. al. ¹ have investigated a magnetic separation of iron ore catalysts from a direct coal liquefaction crude oil. Maxwell et. al. ² studied the separation of sulphide solid from SRC by high gradient magnetic separator (HGMS) at 2T of magnetic field strength, and they found that a sulphidation treatment of SRC enhanced a magnetization.

In this study, effects of magnetic field and feed rates of coal liquefaction crude oil on a separation selectivity are investigated for a recovery of synthetic pyrite catalysts.

2. EXPERIMENTAL

2.1. Principal of HGMS

The forces which act to a magnetic particle in an uniform magnetic field are divided into three forces, a magnetic force (F_M), a gravity (F_G) and a fluid resistance (F_D).

$$F_M = (\pi/6)d^3 \rho \chi H(dH/dx) \quad (1)$$

$$F_G = (\pi/6)d^3 \rho g \quad (2)$$

$$F_D = 3\pi d \eta v \quad (\text{Stokes region}) \quad (3)$$

(d : diameter of particle, dH/dx : gradient of magnetic field, ρ : density of particle, χ : magnetic susceptibility, H : magnetic field strength, g : gravitational acceleration, η : viscosity of fluid, v : velocity of fluid)

From eq.(1) to eq.(3), the critical condition of magnetic separation is derived.

$$\chi H(dH/dx)/(g+18\pi\eta v/\rho/d^2) > 1 \quad (4)$$

Thus adequate conditions are high values of d , ρ , χ , H , dH/dx and low values of η , v for a magnetic separation procedure. The HGMS has a set of high magnetic metal

matrices in their canister, and it can produce a high gradient magnetic field, dH/dx . The magnetic force is attained several ten thousands times of a permanent magnet type separator and several ten times of a wet type magnetic separator.

2.2 HGMS SEPARATOR AND OPERATIONS

The separation part of the HGMS are constituted by a solenoid coil, a return frame and a canister, and high magnetic metal matrices are put into the canister. The dimension of the canister is 38mm ϕ \times 150mm and a set of expanded metal mesh with copper spacers was used to produce a high gradient magnetic field. The feed samples were the mixture of coal liquefaction crude oil produced by using the 0.1t/d Hokkouken Coal Liquefaction Bench Plant under 15MPa to 30MPa, 673K to 723K and 40 minutes of a mean residence time as reaction conditions. A feed coal was Taiheiyo coal and synthetic pyrite which had 2 μ m of mean particle size was used as catalyst. Some properties of the feed are shown in Table 1, and the viscosity of the feed were around 200 cP at 293 K as shown in Fig. 1.

When 1.0 litre of feed was supplied upward to the canister under magnetic field by a slurry pump at ambient temperature (293K to 295K), non-magnetic substance was passed through the canister and was ejected from the separator. After a rinsing of the canister with 2.0 litre of ash free creosote oil, a magnetic separated substance was withdrawn from the canister with compressed air. The feed rate of sample were about 0.4 litre/min. to 4.3 litre/min., and the magnetic field strength(H) were about 0.5kG to 20kG. This withdrawn sample was washed with benzene, and these insolubles(BI) were weighed. Quantitative analysis of Fe, S, Si, Al and Ca in the insolubles were also done by using a X-ray fluorescence analyzer.

3. RESULTS AND DISCUSSION

The selectivity of the separated elements were much affected by the magnetic field, shown in Figure 2(a) to Figure 2(e). In Figure 2, the iron content in BI of magnetic separated substances were increased as increase in the magnetic field strength and as decrease in the feed rate. Sulphur content was increased as increase in the iron content, and it suggested that iron and sulphur were separated as a chemical form of iron sulphides. On the other hand, the content of silicon, aluminum and calcium in BI of magnetic substance were decreased as increase in the magnetic field strength. From the X-ray diffraction patterns of BI of original crude oil, LTA (Low Temperature Ash) of Taiheiyo coal and magnetic separated substances separated at the condition of 21kG of magnetic field strength and 0.54 litre/min. of feed rate, it was found that quartz, kaolinite and calcite did not change their form during coal liquefaction process, and pyrite was changed to pyrrhotite ($Fe_{1-x}S$). After the magnetic separation of crude oil, the peak height of pyrrhotite in magnetic separated substances was increased comparing that of coal ash components. Ignition losses of magnetic separated substances separated under 0.54 kG, 6.2kG and 21.1kG are shown in Table 2. Ignition losses were increased as increase in the magnetic field strength. Also, this was increased as increase in the feed rate. At the condition of low feed rates, iron sulphide can easily reach to the

expanded metal matrix due to the long residence time in the canister. From this reason, it can be considered that the ignition loss at the condition of low feed rate was low. The ignition loss at the condition of high feed rates were higher than that of the original feed. This may concern a physical adhesion of heavy hydrocarbon fraction of crude oil to the expanded metal matrices. At this experiment, a series of operation was carried out at ambient temperature, and the viscosity of the feed was around 200 cP. It can be thought that the selectivity and the yields of the magnetic separation procedure are improved at higher temperature condition for decreasing of the viscosity of the feed.

4. CONCLUSION

A magnetic separation of iron catalyst was carried out for a coal liquefaction crude oil by using a HGMS separator. The iron catalyst (synthetic pyrite) was separated as a chemical form of pyrrhotite, and iron contents in BI of magnetic separated substance was concentrated 1.5 times, even though the mean particle size was small ($2 \mu\text{m}$). Concentrations of iron and sulphur in magnetic separated substances were increased as increase in the magnetic field, and decreased in the feed rate of coal liquefaction crude oil. On the other hand, mineral matter relating coal ash were decreased. Carbonaceous matter were also included in magnetic separated substances, and it may come from adherent heavy hydrocarbon fractions of crude oil. It suggests that the performance of a magnetic separation procedure can be improved at higher temperature condition.

REFERENCES

1. H.Narita, R.Yoshida, S.Yokoyama and Y.Maekawa, Proceedings of 1983 Summer Seminar of Japan Chemical Society Hokkaido, 50(1983)
2. E.Maxwell, D.R.Kelland, I.S.Jacobs and L.M.Levinson, Fuel, 4(1982)369

Table 1 Properties of crude coal derived oil

Specific weight	Benzene insolubles	Ignition loss of BI	Contents of each element in B.I.				
			Fe	S	CaO	Al ₂ O ₃	SiO ₂
(g/cm ³)	(wt%)	(wt%)	(wt%)				
1.15	13.4	46.0	10.16	4.36	4.31	8.89	27.10

Table 2 Loss of ignition of separated magnetic material

Mag. Field	Feed rate		
0.40	2.18	4.28	
(kG)	(l/min.)		
0.54	33.0 wt%	36.5 wt%	47.8 wt%
6.20	36.1	38.5	48.0
21.10	36.4	40.1	52.2

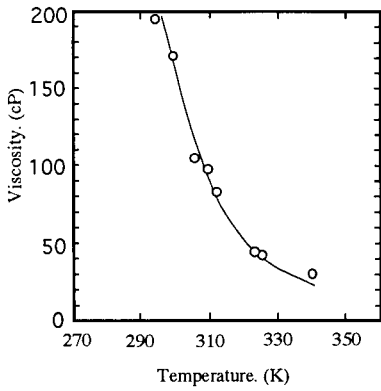


Fig. 1 Viscosity curve of crude coal-derived oil

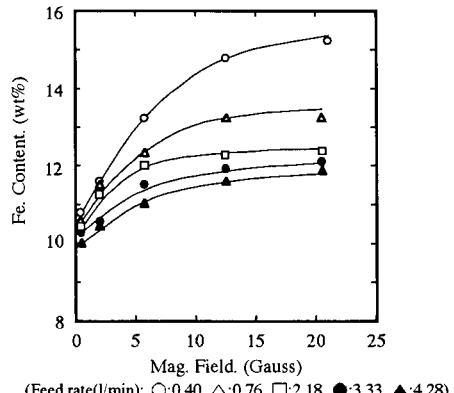


Fig. 2- (a) Relationships between mag. field and Fe content

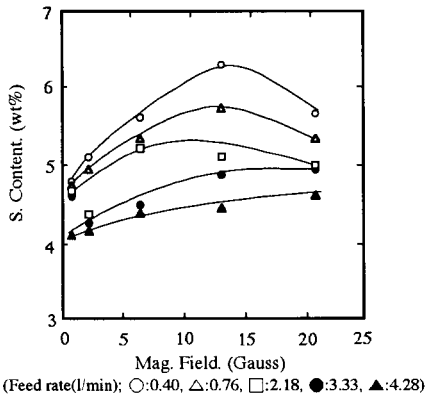


Fig. 2- (b) Relationships between mag. field and S content

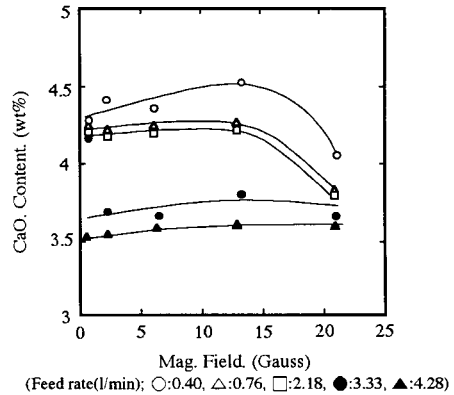


Fig. 2- (c) Relationships between mag. field and CaO content

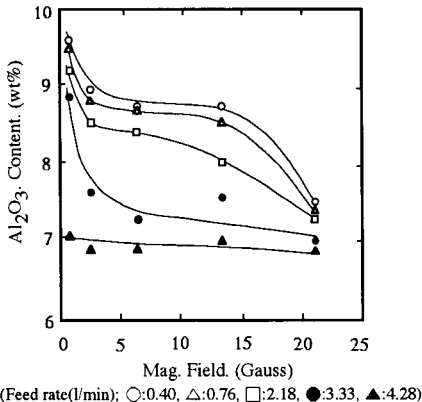


Fig. 2- (d) Relationships between mag. field and Al_2O_3 content

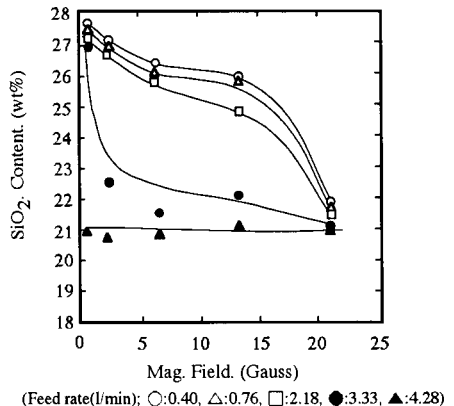


Fig. 2- (e) Relationships between mag. field and SiO_2 content

Activity and Selectivity of Fe Catalysts from Organometallic and Inorganic Precursors for Hydrocracking of 4-(1-Naphthylmethyl) Bibenzyl

Chunshan Song*, Eckhardt Schmidt, and Harold H. Schobert

Fuel Science Program, The Pennsylvania State University, University Park, PA 16802, USA

1. INTRODUCTION

Various iron containing catalysts have been investigated for their use in hydroliquefaction of coal ever since Bergius (1) demonstrated the feasibility of the process. Conventional iron (2,3) catalysts have been widely used either unsupported or as catalysts dispersed directly onto coal. Iron catalysts have generally a lower cost and lower environmental detriment than Mo, Ni and Co catalyst precursors. The search for active high surface area iron particles has become recently an important part in the development of a cost effective direct coal liquefaction process (4,5).

To examine what determines the activity and selectivity of Fe catalysts for hydrogenation and hydrocracking, various molecular precursors with Fe in different chemical environments have been tested in this work to help understand the influence of precursor structure and the effect of sulfur addition on the activity and selectivity of resulting Fe catalysts in model reactions of 4-(naphthylmethyl)bibenzyl (NMBB). We have examined various precursors, including a thiocubane type cluster $\text{Cp}_4\text{Fe}_4\text{S}_4$, a cyclopentadienyliron dicarbonyl dimer $\text{Cp}_2\text{Fe}_2(\text{CO})_4$, ferrocene Cp_2Fe , a series of carbonyl precursors including $\text{Fe}(\text{CO})_5$, $\text{Fe}_2(\text{CO})_9$, and $\text{Fe}_3(\text{CO})_{12}$, and superfine iron oxide with average particle size of 30 Å (SFIO).

2. EXPERIMENTAL SECTION

Runs with NMBB were carried out in 33 mL reactor using 0.78 mmol NMBB in n-tridecane solvent at 400°C for 30 min, in the presence of a Fe catalyst precursor (2.11 wt% Fe based on NMBB). Carbonyl precursors were purchased from Aldrich. Precursor synthesis and experimental details may be found elsewhere (6). SFIO sample was provided by Mach I Inc. in Pennsylvania. Catalyst samples for BET and XRD analysis were prepared in similar reactors from ca. 1 g precursor and 4 g tridecane at 400 °C under 6.9 MPa H_2 pressure for 30 min. XRD data were obtained from a Scintag I (Scientific Computer and Instruments, USA). Surface area measurements were conducted using a Quantachrome Autosorb I Gas Sorption system.

3. RESULTS AND DISCUSSION

3.1 Conversion of NMBB

The initial stage of a catalytic reaction involves catalyst activation at elevated temperatures, depending on the type of catalyst precursor. It is known (7,8,9) that some precursors like metal carbonyls require the addition of sulfur for sufficient activity. There seems (10) to be consensus that the sulfides of the transition metals are more active in catalytic hydroliquefaction than their oxides. The reason for this remains unclear. The activation reaction is difficult to perform and iron carbonyls tend to form less reactive iron carbides and oxides (11) during the activation process. The present results in Tables 1 and 2 revealed several interesting trends. Even the catalysts without sulfur can display certain activity. The particles from $\text{Cp}_2\text{Fe}_2(\text{CO})_4$ showed the highest activity among all the precursors examined in the absence of added sulfur. The activity of catalysts from Fe carbonyls decreased with increasing number of irons in the carbonyl compounds: $\text{Fe}(\text{CO})_5 > \text{Fe}_2(\text{CO})_9 > \text{Fe}_3(\text{CO})_{12}$; adding sulfur increased their activity but their activities rank the same both with and without sulfur addition.

Surprisingly, $\text{Cp}_4\text{Fe}_4\text{S}_4$ exhibited the lowest activity, although it has the S-to-Fe ratio closest to pyrrhotite (Fe_{1-x}S , where $X=0$ to 0.12) which is thought to be the active phase. The nano-scale SFIO particles performed at an activity level similar to that of $\text{Fe}_2(\text{CO})_9$ in the absence of

sulfur, but afforded the highest NMBB conversion when S was added. Ferrocene is more effective in hydrocracking reactions of NMBB than the inorganic iron complex $\text{FeSO}_4 \cdot 7\text{H}_2\text{O}$ (Table 2). Sulfur added to iron sulfate had the expected beneficial effect on NMBB conversion. But sulfur added to ferrocene decreased the activity of resulting catalyst. The other iron containing organometallic complex that showed a similar trend in conversion after sulfur addition was $\text{Cp}_2\text{Fe}_2(\text{CO})_4$. Both complexes have cyclopentadienyl ligands as common features. Another precursor with Cp-functionalities and sulfur in the precursor molecule ($\text{Cp}_4\text{Fe}_4\text{S}_4$) showed very low activity too. There is apparently a negative correlation between the conversion of iron containing complexes and the presence of cyclopentadienyl/sulfur units.

Table 1. Effect of Fe containing catalyst precursors on NMBB hydrocracking at 400 °C.

Catalyst Precursors	$\text{Cp}_2\text{Fe}_2(\text{CO})_4$	$\text{Fe}(\text{CO})_5$	$\text{Fe}_2(\text{CO})_9$	$\text{Fe}_3(\text{CO})_{12}$	$\text{Fe}(\text{CO})_5$ + S	$\text{Fe}_2(\text{CO})_9$ + S	$\text{Fe}_3(\text{CO})_{12}$ + S	$\text{Cp}_2\text{Fe}_2(\text{CO})_4$ +S
Conv, wt %	62.2	45.6	24.7	22.1	61.2	51.5	45.7	21.3
Prod, mol %								
Benzene	0.6				1.3		0.7	0.9
Toluene	1.6	1.3	0.8	1.5	2.3	2.3	1.9	
p-Xylene	0.5	0.2	0.2	0.3	0.8	0.4	0.7	0.2
Tetralin	8.5	4.2	2.2	2.0	2.6	1.5	2.0	0.3
Naphthalene	38.1	42.8	20.3	23.3	67.8	47.8	46.6	20.4
2-MTHN ^a								
1-MTHN	0.8	0.3	0.4					
2-MN ^b	0.2				1.3	1.1	0.8	0.1
1-MN	2.5	2.6	1.0	1.6	5.3	3.7	3.4	1.1
BB ^c	4.0	3.6	1.6	1.8	7.6	6.7	5.5	1.5
Benzyl-naphthlene	0.3	0.1						0.2
4-MBB ^d	40.1	35.7	20.3	16.2	52.7	41.1	33.6	18.5
TH-NMBB ^e	14.4	0.8	1.4					0.3

^aMethyltetrahydronaphthalene; ^bmethylnaphthalene; ^cbibenzyl; ^dmethylbibenzyl; ^etetrahydro-NMBB.

Table 2. Effect of Fe precursors with different ligands on NMBB hydrocracking at 400 °C.

Catalyst Precursors	Non-catalytic	Superfine Fe_2O_3	Superfine Fe_2O_3 + S	$\text{FeSO}_4 \times 7\text{H}_2\text{O}$	$\text{FeSO}_4 \times 7\text{H}_2\text{O}$ + S	Cp_2Fe	$\text{Cp}_2\text{Fe} + \text{S}$	$\text{Cp}_4\text{Fe}_4\text{S}_4$
Conv, wt %	3.9	27.1	78.2	3.7	23.9	15.8	9.6	11.7
Prod, mol %								
Benzene	0.6	0.2	0.5					2.5
Toluene	0.3	1.3	1.9		1.3	1.6	1.1	
p-Xylene		0.3	0.7					
Tetralin	0.2	3.0	4.0		0.6	0.4	0.3	
Naphthalene	0.6	16.4	64.1	4.5	24.0	13.8	10.3	10.9
2-MTHN ^a			0.2					
1-MTHN		0.5	0.4					
2-MN ^b			1.4					
1-MN			5.8		1.5	5.6	0.5	0.1
BB ^c		1.0	8.9	0.6	2.5	2.6	0.6	0.4
Benzyl-naphthlene	0.9							
4-MBB ^d	1.3	17.4	59.6	2.6	19.1	9.4	7.4	10.8
TH-NMBB ^e		7.3	5.5					

^aMethyltetrahydronaphthalene; ^bmethylnaphthalene; ^cbibenzyl; ^dmethylbibenzyl; ^etetrahydro-NMBB.

To better understand the relationship between catalyst composition and catalytic activity, surface area and XRD measurements were carried out. The surface area of freshly generated

catalyst particles was measured and the phase identified through X-ray diffraction. Our investigation of in situ generated iron catalyst from organometallic precursor revealed higher surface areas for pyrrhotite than magnetite particles. From XRD-measurement, it was found that iron carbonyl was transformed at 400 °C into magnetite Fe₃O₄. Sulfur added to Fe(CO)₅ yields pyrrhotite as black material. Generally iron sulfides have higher surface areas than magnetite. The effect of sulfur addition to iron carbonyls on the surface area is illustrated in Table 3.

Table 3. BET Surface area and phase of activated catalysts.

Precursor Molecule	BET m ² /g	Meso Pore m ² /g	Phase from XRD
Fe(CO) ₅	3.22	3.22	Fe ₃ O ₄
Fe ₂ (CO) ₉	7.73	7.73	Fe ₃ O ₄
Fe ₃ (CO) ₁₂	17.6	17.6	Fe ₃ O ₄
Fe(CO) ₅ + S	1.56	1.54	FeS
Fe ₂ (CO) ₉ + S	3.58	3.45	FeS
Fe ₃ (CO) ₁₂ + S	2.93	2.93	FeS
Ferrocene + S	21.7	20.5	FeS
Cp ₄ Fe ₄ S ₄	11.39	9.33	FeS
Fe ₂ O ₃	228	228	---

Surprisingly higher surface areas can be generated from higher iron carbonyl clusters. The BET surface area increases

dramatically with increasing number of inter iron bonds. A similar trend can be observed when sulfur is added to the corresponding iron carbonyls. However, pyrrhotite coming from Fe carbonyls has a substantially lower surface area than the analogue generated from ferrocene and sulfur. Even the sparingly soluble Cp₄Fe₄S₄ yields after thermal activation higher surface area material than most iron carbonyls which are more soluble in hydrocarbons and are expected to lead to higher dispersion. The XRD-pattern reveals pyrrhotite as main product. This excludes iron carbide as the activity inhibiting material. However, the microstructure can be influenced by minute traces of impurities. Further elemental analysis will help clarify this issue.

3.2. Distribution of products from NMBB

Hydrocracking of NMBB yields three product categories that can be explained by the cleavage of the bonds between the aromatic moieties. Those coming from hydrocracking reactions form the major pool of reaction products, followed by hydrogenation and isomerization products. As can be seen from Tables 1 and 2, all iron containing catalyst precursors give a similar ratio of main products. It is apparent that ferrous catalysts cleave NMBB preferably in position α . Increasing conversion leads in most experiments to a proportional increase in the ratio of major products. The following compounds can be found as main products: naphthalene, 4-MBB, bibenzyl and tetralin.

Farcasiu et al. (12,13,14) suggested a reaction mechanism in which the first stage consists of the formation of a radical cation. The loss of electron density leads to a weakened α -bond which can then be broken relatively easily. This is in contrast to model studies in which phenyl-containing compounds undergo preferably β -cleavage (15).

In the work of Penn and Wang (15) radical cations were generated in the mass spectrometer under a variety of conditions which had little impact on the bond cleavage pathway. Preference for β -cleavage was explained by resonance stabilization of the intermediates. Both intermediates are resonance stabilized. Thermochemical calculations (16) show that reaction pathway β is 30 kcal/mol lower for both neutral and radical cationic species than pathway α . In contrast, neither of the intermediates resulting from bond α cleavage is stabilized. However, in the presence of a catalyst, the major reaction pathway mainly involves the cleavage of bond α .

3.3. Possible reaction mechanism

The structure of NMBB influences the cleavage pathway. Catalyst particles act as hydrogen transfer agents and stabilize the intermediate radical. They prevent undesirable recombination of the free radicals to polymeric material. Naphthalene and 4-methylbibenzyl are formed predominantly in catalyzed reactions, indicating that bond α in NMBB is the most reactive unit in the Fe-catalyzed runs. However, different ligand environment and oxidation state of the precursor molecule can reverse the observed preference for bond α cleavage (e.g. MoCl₃). Related work (17) investigated the reaction mechanism of bond scission of naphthyl-derivatives

and proposed the addition of a hydrogen radical to the ipso position of the naphthyl-unit to generate a relatively stable benzylic radical. Our data, as shown in Tables 1 and 2 support the hypothesis that all iron containing catalyst precursors induce preferably the scission of bond α in NMBB. It is believed (18) that strong hydrogenation catalysts show higher selectivity towards α cleavage than less active iron catalysts. High catalytic activity is accompanied by rich hydrogen supply adsorbed on the catalyst surface. Model compounds with aromatic ipso positions are prone to subsequent reactions with hydrogen radicals, leading to hydrogenation products. The less active iron catalysts are not capable of multiple hydrogen transfer during the short contact time between NMBB and model compound. Thus cleavage of NMBB occurs with higher selectivity. The structure of the catalyst precursors and the sulfur addition affect the reactions on the surface of in situ generated catalysts.

4. CONCLUSIONS

Some iron containing catalysts have higher activity in the sulfur-free form, contrary to conventional wisdom. Adding sulfur to Fe precursors with Cp-ligands decreased the activity of the resulting catalyst. This is in distinct contrast to the cases with iron pentacarbonyl and superfine Fe₂O₃, where S addition increased their catalytic activity substantially. A positive correlation between sulfur addition and increased activity can be seen, but a reversed trend between Fe cluster size and hydrocracking conversion could be observed, for carbonyl-type Fe precursors. It is apparent that the activity and selectivity of Fe catalysts for NMBB conversion depends strongly on both the type of ligand environment, the oxidation state and the number of intermetal bonds in the molecular precursor.

ACKNOWLEDGMENTS

This project was supported by the U.S. Department of Energy, Pittsburgh Energy Technology Center under contract DE-AC22-92PC92122. We are grateful to Dr. U. Rao of PETC for his support. We also thank Mr. R. Copenhagen for the fabrication of reactors.

REFERENCES

1. F. Bergius and Billviller, German Patent No. 301, Coal Liquefaction Process, (1919), 231.
2. P.A. Montano, A.S. Bommanavar and V. Shah, *Fuel*, Vol. 60, (1981), 703.
3. T. Suzuki, H. Yamada, P.L. Sears, and Y. Watanabe, *Energy Fuels*, Vol. 3, (1989), 707.
4. A.V. Cugini, D. Krastman, R.G. Lett and V. Balsone, *Catalysis Today*, Vol. 19, (1994), 395-408.
5. F. Derbyshire, *Energy and Fuels*, Vol. 3 (1989), 273-77.
6. a) E. Schmidt and C. Song, *Prepr. Pap. - Am. Chem. Soc., Div. Fuel Chem.*, No. 35, (1990) 733-737.
b) C. Song, E. Schmidt and H.H. Schobert, DOE Coal Liquefaction and Gas Conversion, Contractors' Review Meeting in Pittsburgh, (September 7-8, 1994), 593-604.
7. O. Yamada, T. Suzuki, J. Then, T. Ando and Y. Watanabe, *Fuel Process. Technol.*, Vol. 11, (1985), 297-311.
8. T. Suzuki, T. Ando and Y. Watanabe, *Energy and Fuels*, Vol. 1, (1987), 299-300.
9. L. Artok, A. Davis, G.D. Mitchell and H.H. Schobert, *Energy Fuels*, Vol. 7, (1993), 67-77.
10. S. Weller, *Energy Fuels*, Vol. 8, (1994), 415-420.
11. D. Herrick, J. Tierny, I. Wender, G.P. Huffamn and F.E. Huggins, *Energy and Fuels*, Vol. 4, (1990), 231.
12. M. Farcasiu and C. Smith, *Prepr. Pap. - Am. Chem. Soc., Div. Fuel Chem.*, No. 35, (1990) 404-13.
13. M. Farcasiu and C. Smith, *Fuel Processing Technology*, No. 29, (1991), 199-208.
14. M. Farcasiu and C. Smith and E.P. Ladner, *Prepr. Pap. - Am. Chem. Soc., Div. Fuel Chem.*, No. 36, (1991), 1869-77.
15. J.H. Penn and J.H. Wang, *Energy Fuels*, Vol. 8, (1994), 421-425.
16. H.F. Ades, A.L. Companion, K.R. Subbaswamy, *Prepr. Pap. - Am. Chem. Soc., Div. Fuel Chem.*, Vol. 36, (1991) 420-430.
17. J.A. Franz, D.M. Camaioni, M.S. Alnajjar, T. Autrey and J.C. Linehan, *Prepr. Pap.-Am. Chem. Soc., Div. Fuel Chem.*, No. 40, (1995), 203-7.
18. M.T. Klein, C.F. Foley, D.T. Walter and S.M. Casey, Coal Liquefaction and Gas Conversion, Contractors' Review Meeting in Pittsburgh, (September 7-8, 1994), 565-78.

Enhancing the Dispersion of Catalysts in Direct Coal Liquefaction

Jianmin Zhao, Zhen Feng, Frank E. Huggins, and Gerald P. Huffman*

The Consortium for Fossil Fuel Liquefaction Science

341 Bowman Hall, University of Kentucky

Lexington, KY 40506

1. INTRODUCTION

Recently, considerable effort has been made to develop low cost, highly dispersed iron-based catalysts for direct coal liquefaction (DCL) [1]. Most iron-based catalysts studied are in fact the catalyst precursors as the catalysts convert to Fe_{1-x}S (pyrrhotite) under DCL reaction conditions. Therefore, a desirable catalyst must be able to maintain its dispersion and transform to an active pyrrhotite phase under DCL reaction conditions.

2. DISPERSION OF THE FERRIHYDRITE CATALYSTS

Ferrihydrite (FHYD) is a naturally occurring iron oxyhydroxide and is regarded as one of the eight major iron oxides by geologists [1]. The ferrihydrite we studied is also called "2-line" ferrihydrite, distinct from the more crystalline "6-line" ferrihydrite. The material has a large surface area of $> 200 \text{ m}^2/\text{g}$ and average particle size of 3-5 nm. Furthermore, the synthesis of the ferrihydrite requires a simple precipitation procedure and uses ferric nitrate as the starting chemical. Therefore, the catalyst is very economical. The major drawback of the material as a catalyst is that the nanoparticles quickly agglomerate and transform to larger, crystalline hematite ($\alpha\text{-Fe}_2\text{O}_3$) particles at $T \geq 250^\circ\text{C}$. Moreover, the presence of surface adsorbed water molecules accelerates the agglomeration and phase transformation.

Using X-ray absorption fine structure (XAFS) spectroscopy, we observed that although the iron atoms in the bulk are octahedrally coordinated, as in goethite, a significant number of surface iron atoms are coordinated by four O/OH, and they become coordination unsaturated (CUS) after dehydroxylation (Figure 1) [3, 4]. These CUS sites may adsorb water molecules to fill the coordination, which link the small particles to form particle aggregates. At elevated temperatures, the water molecules are evolved from the particle joints, leading to particle agglomeration and phase transition to hematite [5]. On the other hand, when impurity anions such as SiO_4 , PO_4 , MoO_4 and organics are present during precipitation, the CUS sites may preferentially adsorb the impurity anions to form a new surface layer. The impurity anions block the crystal growth sites and thereby effectively inhibit the phase transformation to hematite, allowing the catalyst to maintain its dispersion at higher temperatures (Fig. 1). For example, while the ferrihydrite-hematite transition occurs at 250°C for pure ferrihydrite, no hematite was formed at temperatures up to 425°C for a $\text{Si}_{0.05}/\text{FHYD}$ catalyst ($\text{Si}/\text{Fe} = 0.05$, atomic ratio) [4, 6]. Tubing bomb DCL tests using Si/FHYD and citric acid treated ferrihydrite (CA/FHYD) show significant increases of coal liquefaction conversion over that obtained from thermal reaction, or using pure ferrihydrite [6, 7].

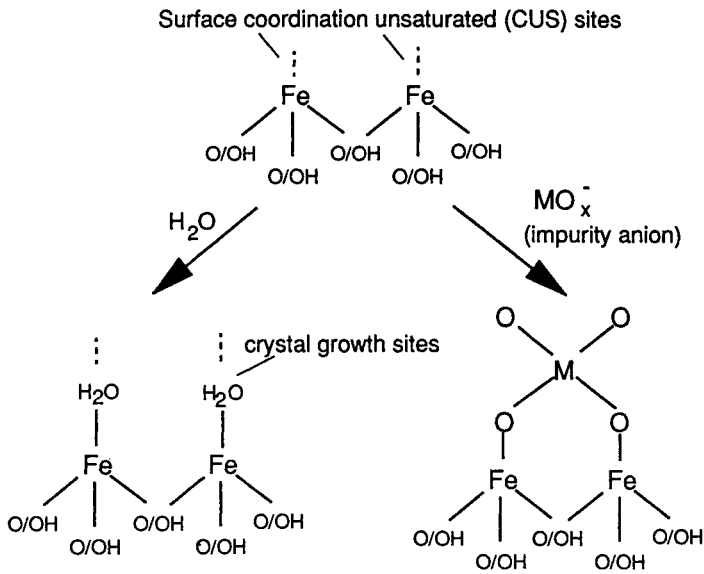


Figure 1. Scheme of the surface structure and adsorption.

3. DISPERSION OF THE PYRRHOTITE CATALYSTS

3.1 Sample preparation

Details for the preparation of the ferrihydrite catalysts can be found in Ref. 6 and 7. Sulfidation of the catalyst was performed in a tubing bomb under simulated DCL conditions without coal. The tubing bomb was loaded with 0.25 g of ferrihydrite catalyst mixed with tetralin along with dimethyl disulfide (DMDS) as a sulfur donor for the catalyst ($S/Fe = 2/1$, by weight). The reactor was then pressurized with H_2 to 1000 psi at room temperature and agitated vertically at 400 cycles/min in a fluidized sand bath at $415^\circ C$ for one hour.

3.2 Morphology of the pyrrhotite phases

For the sulfided pure ferrihydrite, transmission electron microscopy shows the formation of well crystallized, hexagonal-shaped $Fe_{1-x}S$ particles of $> 1000 \text{ \AA}$ (Fig. 2). Markedly improved dispersion of the $Fe_{1-x}S$ phase is obtained using Si/FHYD and CA/FHYD, as indicated in Fig 2, showing significantly smaller particles of less regular shapes.

3.3 Mossbauer spectra

$Fe_{1-x}S$ has the NiAs structure in which each Fe atom is surrounded by six sulfur atoms, and it has 1, 2, or 4 vacancies among its 12 nearest Fe neighbors. The monoclinic ($Fe_{0.875}S$) and hexagonal ($Fe_{0.909}S$) phases are the most common ones. The phase transition of monoclinic to hexagonal occurs at $T < 300^\circ C$. Quantitative analysis for the Fe vacancy distribution in

pyrrhotites can be obtained by Mössbauer spectroscopy analysis [8]. The Mössbauer spectrum for the hexagonal phase contains three sextets with magnetic hyperfine fields of $H_f = 302, 274,$ and 256 kOe, respectively [7]. These three components are assigned to three Fe positions with 0 (position A), 1(B), and 2(C) vacancies among their Fe neighbors. For the monoclinic pyrrhotite, the spectrum also consists of three sextets of $H_f = 300, 256,$ and 225 kOe, corresponding to the Fe atoms with 0 (A), 2(C), and 4(D) vacancies in their Fe neighbors. Figure 3 shows the Mössbauer spectra of the pyrrhotite catalysts. The spectrum for the sulfided ferrihydrite is very similar to that for hexagonal phase, which is dominated by A, B, and C positions. However, a fourth component (D) is discernible, therefore the spectrum is fitted with four sextets. The spectrum for the sulfided Si/FHYD is similar to that for the monoclinic phase, showing splitting of the magnetic hyperfine fields, due to decreased population of the B position and increased population of the C and D positions. The spectrum is fitted with four sextets representing A, B, C, and D positions, and a doublet at the center for the unsulfided ferrihydrite. The spectrum for the sulfided CA/FHYD also shows increased splitting of the magnetic components, indicating increased fractions of the C and D components and the spectrum is fitted with four sextets. According to the distribution of the four magnetic components estimated from the absorption areas, the compositions of the pyrrhotites are estimated to be $Fe_{0.90}S$ (FHYD), $Fe_{0.87}S$ (Si_{0.09}/FHYD), and $Fe_{0.89}S$ (CA/FHYD). Thus, all three pyrrhotites are mixed monoclinic-hexagonal phases. The pyrrhotites from Si/FHYD and CA/FHYD contain more Fe vacancies.

In conclusion, by chemisorption of impurity anions at the ferrihydrite surface, improved catalyst dispersion for both the precursor and the pyrrhotite phase have been obtained. In addition, the presence of surface impurity anions also increases the monoclinic-hexagonal phase transition temperature, thereby retaining more Fe vacancies in the pyrrhotite phase.

ACKNOWLEDGMENT

This research is supported by the U. S. Department of Energy, under contract No. DE-FC22-90PC90029, as part of the cooperative research program of the Consortium for Fossil Fuel Liquefaction Science.

REFERENCES

1. G. P. Huffman, et al. *Energy & Fuels* 7 (1993) 285.
2. U. Schwertmann and R. M. Cornell, *Iron Oxides in the Laboratory*, VCH, Weinheim (1991).
3. J. Zhao, F. E. Huggins, Z. Feng, F. Lu, N. Shah, and G. P. Huffman, *J. Catal.* 143 (1993) 499.
4. J. Zhao, F. E. Huggins, Z. Feng, and G. P. Huffman, *Clays & Clay Minerals* 42 (1994) 737.
5. Z. Feng, J. Zhao, F. E. Huggins, and G. P. Huffman, *J. Catal.* 143 (1993) 510.
6. J. Zhao, Z. Feng, F. E. Huggins, and G. P. Huffman, *Energy & Fuels* 8 (1994) 38.
7. J. Zhao, Z. Feng, F. E. Huggins, and G. P. Huffman, *Energy & Fuels* 8 (1994) 1152.
8. N. S. Ovanesyanyan, V. A. Trukhtanov, G. Yu. Ordinets, and G. V. Novikov, *Soviet Physics JEPT* 33 (1971) 1193.

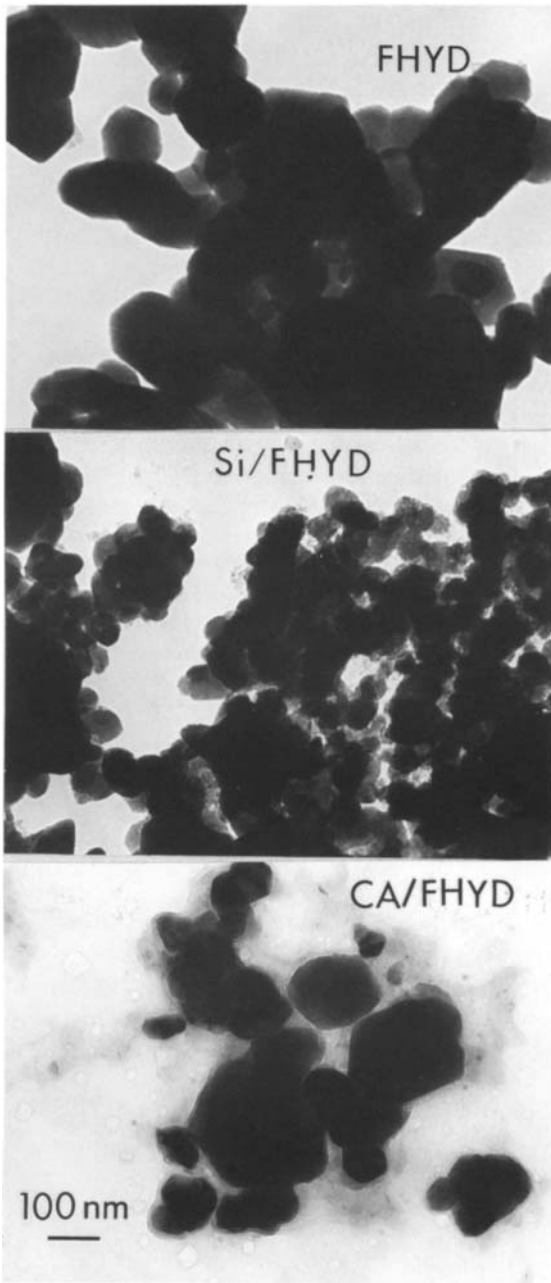


Figure 2. TEM micrographs of three ferrihydrates after sulfidation.

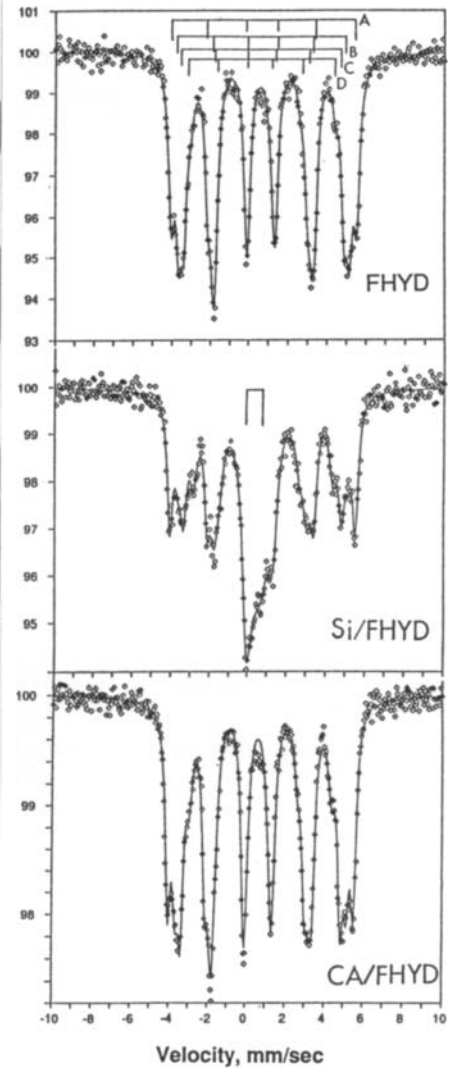


Figure 3. Mossbauer spectra of three sulfidated ferrihydrates.

Iron from two different catalytic precursors in coal hydrogenation

A. M. Mastral, M. C. Mayoral, B. Rubio, M. T. Izquierdo and M.J. Palacios

Instituto de Carboquímica, CSIC, Apdo. 589, 50080-Zaragoza, Spain.

1. INTRODUCTION

Catalyst activity is determined principally by the degree of dispersion and the composition of the catalyst under a given set of reaction conditions. These factors are related to each other and to the composition and mode of addition of the catalyst precursor. Although the catalyst dispersion and composition may be altered upon reaction, the nature and extent of these changes will be determined to some degree by the situation prevailing on the onset of reaction [1,2]. In fundamental research, a great deal of effort has been given to investigate the use of iron compounds, and in particular iron sulphides as liquefaction catalyst. There has been a continuing level of activity in this area, some of which has been concerned with trying to improve the performance of iron catalyst through modifying their chemical and physical properties [3]. The bulk of the available evidence indicates that pyrrhotite is the active form of the iron catalyst under liquefaction conditions [4]. The formation of species like $\text{Fe}_2\text{O}_3 \cdot \text{SO}_4$ is interesting since Hattori [5] reported that its presence increased the cracking activity of Fe_2O_3 .

The most modern techniques, such as Mössbauer spectroscopy, SEM-EDX and XRD have been used to the study and measurement of the size and distribution of these catalytic species, in the initial form as well as their evolution along reaction [6]. The coal hydrogenation catalysts performance is also observed throughout the characterization of the obtained solid and liquid products.

2. EXPERIMENTAL

2.1. Experimental procedure.

The hydrogenation experiments were carried out in a 160cc struck tubing bomb reactor in absence of solvent. The coals used are described in Table 1. The catalyst precursors used were Iron(II) sulphate dispersed on coal surface as a sulphide (IS), and Iron(III) oxide from Red Mud directly mixed as powder (RM), in a load of 5%wt in Fe.

The coal load was 10g daf in each run and an estequiometric ammount of CS_2 with the RM precursor to low sulphur content bituminous B25 coal. As settled conditions, the initial H_2 pressure was $100\text{kg}\cdot\text{cm}^{-2}$ and 30 minutes of immersion in a preheated sand bath at the fixed reaction temperature. As main variable, the coal was treated at a wide range of temeperatures: 300° , 350° and 400°C for blank tests, those and 425°C for catalyzed runs, and also 450° and 500°C for the bituminous coal. More details of the experimental procedure are described elsewhere [7].

Table 1. Coals used in this work.

COALS	Ultimate analysis (%wt, daf basis)					Proximate analysis (%wt, dry basis)		
	C	H	S _{tot(dry)}	S _{org}	S _{pir}	Ash	Vol. Mat.	Fixed C
S 13	67.4	7.6	7.2	5.9	1.43	13.6	35.4	50.8
B 25	79.4	5.3	1.2	0.7	0.51	8.8	39.5	51.7

2.2. Products characterization.

Residues of coal hydrogenation experimentes were analyzed using Mössbauer spectroscopy at room temperature (in a constant acceleration spectrometer of standard desing with radioactive source of 50-100mCi of ⁵⁷Co in a Pd matrix), scanning electron microscopy (SEM) with energy dispersive X-ray (EDX) in an electron microscope ISI DS-130 with a Si/Li detector and processor 8000-II KeveX, and X-ray photoelectronic spectroscopy (XPS) in a Perkin-Elmer PHI-5600 MultiTechnique system. X-ray diffractograms were obtained in a Rigaku Geiflex device.

3. RESULTS AND DISCUSSION

3.1. Application of Mössbauer spectroscopy to the study of hydrogenation residues.

Although pyrrhotite is the thermodynamically stable iron species at liquefaction conditions, the reduction of iron is not complete at 400°C, although its presence is high at 425°C as can be seen in Table 2.

Table 2. Mössbauer parameters of hydrogenation residues using RM and IS precursors.

Coal	Prec.	T(°C)	Iron Compound	Fe %	Fe _{1-x} S			Net Conversion ^d	% Oils ^c
					H _{av} ^a	X ^b	%Fe _{av} ^c		
S13	RM	400	Fe _{1-x} S	74	271	0.101	47.33	74	16
			spm Ox. ^f	26					
S13	IS	400	Fe _{1-x} S	72	268	0.108	47.13	72	19
			FeS ₂	28					
B25	RM	400	Fe _{1-x} S	78	270	0.102	47.29	70	14
			spm Ox.	23					
B25	IS	400	Fe _{1-x} S	87	278	0.083	47.82	70	13
			FeS ₂	13					
B25	RM	425	Fe _{1-x} S	80	269	0.106	47.18	75	23
			spm Ox.	20					
B25	IS	425	Fe _{1-x} S	93	280	0.079	47.93	79	20
			FeS ₂	7					

^a: Average magnetite hyperfine field (kOe).

^b: Number of vacancies of Fe in Fe_{1-x}S.

^c: Atomic percentage of Fe in Fe_{1-x}S.

^d: [(loaded coal wt)_{dry basis} - (solid residue wt)]/(loaded coal wt)_{daf basis}.

^e: n-hexane solubles.

^f: superparamagnetic oxohydroxides.

Table 2 shows that net conversion and oil production do not present a relationship with increasing Fe_{1-x}S formed nor with the number of vacancies (X) in Fe_{1-x}S . On the other hand, and as an evidence of hydrogenation activity, the percentage of obtained oils is not related with Fe_{1-x}S percentage nor with the number of vacancies. It is possible to find similar results in the literature [8].

The extent in which iron was reduced to pyrrhotite was similar at 400°C for both coals studied with RM as precursor, but not with IS. Apart from temperature, degree of dispersion and particle size, the extent in which an iron species onto coal surface reduces to pyrrhotite under hydrogenation conditions relies as well upon the coal rank [9]. The low-rank coal, with higher oxygen content, develops a surface oxydation of added iron which produced the troubles of detection for IS precursor in XPS measurement. Hence, the decomposition of iron sulphide will not be possible until sulphates decompose and expose the pyrite to the surrounding atmosphere. This effect seems to result in an additional difficulty in reaching pyrrhotite state in the low rank coal.

3.2. Red Mud.

Although RM is less likely to be transformed into pyrrhotite, the addition of this precursor to B25 coal implies the achievement of high conversions and oil percentages. Defect structures in the iron oxide/oxohydroxide network or a possible dispersion effect of the solid mass added as precursor have been desestimated by previous results [10]. The possible cracking performance by acid behaviour was preliminary evaluated by a model compound catalytic test [11] outlined for pure and heterogeneous iron-bearing powders as precursor for coal liquefaction catalyst. In this way it was possible to distinguish among the various mechanism routes, free radical and craking mechanisms. The results with washed RM (to avoid the presence of basic cations such Ca and Na) in the activity test confirm an acid behaviour of the precursor.

After a new series of hydrogenation experiments with coal, it was demonstrated that the effect of RM as received, in terms of net conversion and oil percentages, was the same than the washed RM at the load used in this work.

3.3. Sulfated oxides.

In a first approach, the reaction conditions performed in this work suggest that the formation of the superacid species $\text{Fe}_2\text{O}_3 \cdot \text{SO}_4^-$ could have happend in the system in which red mud is the catalytic precursor [5]. The instrumental techniques used to study the formation of the sulfate over the red mud used in this work were XPS and infrared spectroscopy, because an interaction between the sulphate ion and the iron oxide involves a shift in the characteristic bands [12].

The sample to test was the solid obtained in the red mud treatment with H_2O and elemental sulphur in a reactor with 100 kg.cm⁻² of initial hydrogen pressure, fast-heated to 400°C, temperature kept for 30 minutes. The S2p spectra in XPS confers to the sample a surface sulphur composition of both sulphide and sulphate, which indicates that sulphides can be easily oxidized. The technique is useful in this case because, apart from detecting the presence of sulphate, it also shows that the iron sulphide is more likely to be monosulphide than disulphide: the binding energy of the FeS_2 should be higher than 161.7 eV, obtained for this sample. This result confirms the iron asignation to pyrrhotite suggested by Mössbauer spectroscopy and EDX to the solid residues obtained in this work [9].

On the other hand, infrared spectroscopy has been unable to identify the sulfate oxide

formation: it could not be found any peak at the expected wavenumber because the complexity of the sample.

4. CONCLUSIONS

Iron dispersed onto coal surface as iron disulphide show different state and behaviour depending on the type of coal: over the subbituminous coal, the detection of added iron by XPS and XRD apperars to be screened by the rapid oxidation by the heteroatoms present in coal composition. On the other hand, apart from the better characterization, the iron dispersed on the high rank coal presents higher disposition to be reduced to pyrrhotite under hydrogenation conditions. The extent of reduction to pyrrhotite and the number of its vacancies do not present a direct relationship to the conversion degree achieved in dry hydrogenation nor to the selectivity to oil production for both catalytic precursors, iron sulphide and iron oxide from red mud. Although the results obtained with red mud characterization indicate an acid behaviour, which comprises free radical as well as craking mechanisms, the iron oxide does not seem to develop the sulphate ion chimisorption that would confer to the solid superacid characteristics.

ACKNOWLEDGEMENTS

Authors would like to thank Dr. M. Farcasiu and Dr. F. Huggins for their scientific contribution, and to the European Communnities (Proj. 7220/EC/755) and the Spanish CICYT (Proj. PB-413) for the financial support of this research.

REFERENCES

1. Derbyshire F.J., Stansberry P.G., Terrer M.T., Mastral A.M. *The mobile phase in coals: its nature and modes of release*. Proj. DoE-PC-60811-9,10, 1986.
2. Mastral A.M., Rubio B. *Liquefaction low-severity conditions. The catalyzed depolimerization as a pretreatment for coal licuefaction*. Contrato EN 3V-004E(A). CSIC-CE Comisión XII, New Energy Vectors. Final Report, April, 1990.
3. Bacaud R., Besson M., Djega-Mariadassou G. *Energy & Fuels*, 8, 3-9, 1994.
4. Montano P.A., Granoff F.B. *Fuel*, 59, 214-219, 1980.
5. Hattori H., Yamaguchi T., Tanabe K., Yokoyama S., Umematsu J., Sanada Y. *Fuel Proc. Tech.*, 8, 117.122, 1984.
6. Huffman G.P., Ganguly B., Zhao J., Rao K.R.P.M., Shah N., Feng Z., Huggins F.E., Mehdi M., Lu F., Wender I., Pradhan V.R., Tierney J.W., Seehra M.S., Ibrahim M.M., Shabtai J., Eyring E.M. *Energy & Fuels*, 7, 285-296, 1993.
7. Mastral A.M., Rivera J., Prado J.G., Rubio B., Ferro M.A., Izquierdo M.T., Mayoral M.C., Maldonado F.J., Pardos C. *Valorization of coal conversion by swelling measuring*. Contrat No. 7220/EC/755, ECSC, Final Report, June 1993.
8. Wang L., Cui Z., Liu S. (1992). *Fuel*, 71, 755-759, 1992.
9. Mastral A.M. Mayoral M.C., Palacios J.M. *Energy & Fuels*, 8, 94-98, 1994.
10. Mastral A.M. Mayoral M.C., Rubio B., Izquierdo M.T. *Energy & Fuels*, in press.
11. Farcasiu M., Smith C., Pradhan V., Wender I. *Fuel Proc. Tech.* 29, 199-208, 1991.
12. Kotanigawa T., Yokoyama S., Yamamoto M., Maekawa Y. *Fuel*, 68, 618-621, 1989.

Preconversion chemistry and liquefaction of coal in the presence of a molybdenum-containing catalyst

Robert P. Warzinski, Bradley C. Bockrath, Gino A. Irdi, Harold B. Booher, and Arthur W. Wells

United States Department of Energy, Pittsburgh Energy Technology Center, Pittsburgh, PA 15236, USA

1. INTRODUCTION

Catalysts and reactive solvents are used in modern direct coal liquefaction processes to facilitate breakdown and hydrogenation of the coal structure. Impressive process improvements have been made in the past decade; however, the roles and interactions of these components in the liquefaction process are still not well understood [1,2]. This paper reports the interactions of a catalyst and several different solvent media with a bituminous coal at various temperatures. Information on the influence of the catalyst during the early stages of conversion is also presented.

2. EXPERIMENTAL

All experiments were performed with DECS-17 (Blind Canyon) coal from the Penn State Coal Sample Bank. The elemental analysis (on a dry basis) provided with the coal was as follows: 76.3% carbon, 5.8% hydrogen, 1.3% nitrogen, 0.4% sulfur (0.02% pyritic sulfur), 6.6% ash, and 9.7% oxygen (by difference). The moisture content of the as-received coal was 3.7%.

The liquefaction and product recovery procedure has been reported [3,4]. In most cases, 3.3 g of coal was used along with a hydrogen/3% hydrogen sulfide gas mixture at 7.2 MPa cold pressure. Slow heat-up to reaction temperature and a rapid cool-down were employed. In catalytic tests, molybdenum hexacarbonyl ($\text{Mo}(\text{CO})_6$) was used as the catalyst precursor and was added directly to the microautoclave at a level of 1000 ppm Mo based on daf coal. When tetralin was added, its ratio to coal was 2:1. In other tests, a catalyst-containing coal-derived product was first generated at 425°C using the DECS-17 coal and $\text{Mo}(\text{CO})_6$. The microautoclave was then opened and 3.3 g of fresh coal was added to this product and liquefied at various temperatures. No additional $\text{Mo}(\text{CO})_6$ was added. To correct for additional conversion of the first charge of coal, especially to cyclohexane-soluble products, similar tests were conducted in which the same temperatures were used but fresh coal was not added in the second step.

Solid-state ^{13}C NMR spectra were obtained on some tetrahydrofuran (THF)-insoluble products according to published procedures [5]. The total hydroxyl content of the same samples was

also determined by potentiometric titration following reaction with tetrabutylammonium hydroxide [6]. Vitrinite reflectance measurements were made according to ASTM procedure D 2798-79.

3. RESULTS AND DISCUSSION

We have previously shown that $\text{Mo}(\text{CO})_6$ is an effective catalyst precursor for coal liquefaction even in the absence of added solvents and special impregnation procedures [3,4]. Table 1 contains the conversion results from the solvent-free liquefaction of the DECS-17 coal for one-hour reactions at temperatures from 325°C to 425°C, both with and without 1000 ppm Mo added as $\text{Mo}(\text{CO})_6$. All results are the average of at least two tests. The influence of native catalyst precursors is negligible, owing to the low levels of pyrite in this coal.

Table 1. Liquefaction of DECS-17 coal using $\text{Mo}(\text{CO})_6$ without added solvents

Reaction Temperature, °C	THF Conversion, %		Cyclohexane Conversion, %	
	Thermal	Catalytic	Thermal	Catalytic
325	14	19	7	9
350	29	46	12	15
375	46	83	23	25
400	48	94	31	52
425	45	93	38	65

Compared with uncatalyzed reaction, the conversion of coal to primary (THF-soluble) products was facilitated by the catalyst formed from $\text{Mo}(\text{CO})_6$ in a temperature-dependent manner [3,4]. A different role was observed regarding secondary (cyclohexane-soluble) products. In this case, the onset of catalyst activity occurred between 375°C and 400°C.

To compare the above solvent-free catalytic system to solvent-based media, tests were performed using tetralin with and without a catalyst and using a catalyst-containing coal-derived product produced from the DECS-17 coal and $\text{Mo}(\text{CO})_6$ at 425°C. All of the tests were performed in duplicate, except for the 325°C and 400°C tests with the catalyst-containing coal-derived product. These tests were done only once. All of the conversion results for these tests are summarized in Figure 1, which shows the changes in conversion for the respective solvent-based data relative to the results obtained using only $\text{Mo}(\text{CO})_6$ in the absence of added solvent (Table 1). The large error bars at zero represent the range of conversion values obtained using only $\text{Mo}(\text{CO})_6$. The small error bars associated with the symbols for the three solvent-based systems represent the range of values obtained for these tests. Error bars are not shown if they are smaller than the size of the symbol.

With respect to conversion to primary products, the data in Figure 1 show the importance of a solvent relative to catalyst at the lower reaction temperatures. At the lower temperatures, higher conversions are obtained if both the catalyst and solvent are present; the highest conversions were obtained in the presence of the catalyst-containing coal-derived material. At 425°C, all of the liquefaction schemes yielded nearly the same high levels of conversion.

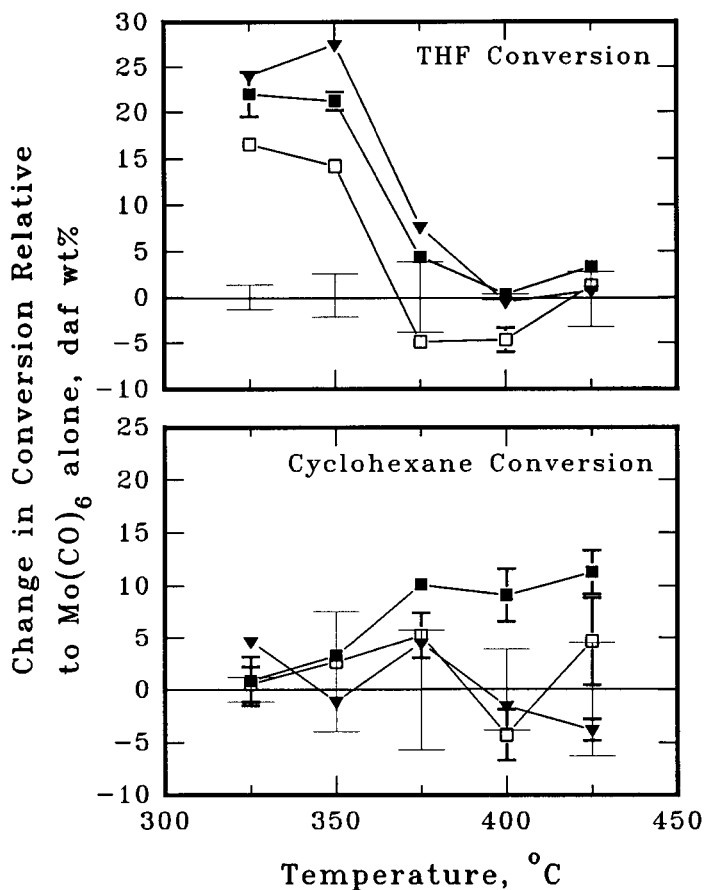


Figure 1. Effect of reaction medium on conversions of DECS-17 coal relative to results with $\text{Mo}(\text{CO})_6$ alone. (□ tetralin, no catalyst; ■ tetralin, $\text{Mo}(\text{CO})_6$; ▼ 425°C catalyst-containing coal-derived product.)

A different picture is observed in Figure 1 regarding secondary conversion. At the two lowest temperatures, the conversions were the same for all systems studied. At 375°C and above, the tetralin/catalyst system was clearly superior. The catalyst-containing coal-derived product did not show the same benefit.

Thermal and catalytic tests without solvent were also performed at 375°C using a zero-residence time (55-minute heat-up from room temperature) to determine the effect of the catalyst on the initial stages of primary dissolution. The starting quantities of coal and

Mo(CO)₆ were doubled and the liquefaction products from duplicate tests combined to prepare sufficient quantities of materials for subsequent characterization. No difference in the thermal and catalytic conversions to THF soluble products was observed (22% and 23%, respectively) at this short residence time. Based on ¹³C NMR analyses, using the catalyst resulted in lower aromaticities of the THF insols. Vitrinite reflectance measurements were in agreement with this observation. Other structural features of the insols did not appear to be affected by the catalyst. In particular, no difference in the hydroxyl content of the samples was indicated in either the ¹³C NMR data or in the results of direct hydroxyl group determinations by potentiometric titration.

4. CONCLUSIONS

The results presented above show the importance of a solvent medium in enhancing the primary dissolution of coal at lower reaction temperatures. With a catalyst, the presence of coal-derived products provided the best results under these conditions. Softening and solubilization of the coal are likely the important factors in this regime. Analysis of short-time products obtained at 375°C show that a major role of the catalyst in the beginning phases of coal dissolution was to facilitate transfer of hydrogen to aromatic species in the coal.

With respect to secondary conversion or upgrading of the primary dissolution products, none of the systems tested provided a benefit at the lower temperatures. Catalyst was effective above 375°C when used by itself. At 375°C and above, using tetralin and catalyst provided significantly higher secondary conversions than the catalyst alone. The capability of more effective hydrogen transfer by this combination may explain this observation. The onset of this activity, as in the previous work [3,4], appears linked to underlying thermally induced reactions.

ACKNOWLEDGMENTS AND DISCLAIMER

The authors would like to thank Richard Hlasnik and Jerry Foster for performing the microautoclave work. The NMR analyses were performed by Dr. Francis Miknis and Dr. Daniel Netzel of the Western Research Institute in Laramie, Wyoming. Reference in this report to any specific product, process, or service is to facilitate understanding and does not imply its endorsement or favoring by the United States Department of Energy.

REFERENCES

1. F.J. Derbyshire, *Catalysis in Coal Liquefaction: New Directions for Research*, IEA Coal Research, London (1988).
2. M.L. Gorbaty, *Fuel*, 73 (1994) 1819.
3. R.P. Warzinski, *Prep. Pap., Amer. Chem. Soc., Div. Fuel Chem.* 38 (1993) 503.
4. R.P. Warzinski, *Proc. Int. Conf. Coal Sci.*, Vol. 2 (1993) 337.
5. M.S. Solum, R.J. Pugmire and D.M. Grant, *Energy Fuels*, 3 (1989) 187.
6. A.W. Wells, manuscript to be submitted to *Fuel*.

Application of exfoliation techniques to the preparation of MoS₂ liquefaction catalysts

Bradley C. Bockrath and Derrick S. Parfitt

United States Department of Energy
Pittsburgh Energy Technology Center
Pittsburgh, PA 15236
USA

1. INTRODUCTION

Dispersed catalysts based on MoS₂ have often been used to promote the liquefaction of coal or to upgrade non-distillable liquids derived from coal or petroleum. The effectiveness of such catalysts should depend in part on the physical properties normally associated with catalytic activity: surface area, particle size, etc. One property whose role has been recently elucidated is particle morphology. The ratio of rim to edge sites has been reported to have an important effect on the selectivity of MoS₂ catalysts in the competitive reactions of hydrodesulfurization and hydrogenation [1]. Another recent publication describes a new method of disassembling the layer structure of MoS₂ then reassembling it in new forms [2]. The method has been used to create catalysts in a controlled way [3]. The technique of exfoliation was used in the work described below to generate a variety of MoS₂ catalysts for evaluation in both coal liquefaction and resid upgrading.

The initial phase of the experimental program sought to establish the range of effects that might be generated by use of exfoliation and restacking of MoS₂. An important concern was to determine appropriate methods of dispersing the catalysts and testing their performance. Once the effects of particle morphology are better known, the results may be applied to the generation of the preferred systems by more practical means.

2. EXPERIMENTAL

MoS₂ was exfoliated using the methods of Joensen, Frindt, and Morrison [2]. Application of exfoliation techniques to the dispersion of MoS₂ for use in coal liquefaction is described in greater detail in reference [4]. In brief, MoS₂ (Aldrich) was intercalated by mixing with n-butyllithium in hexane for 2-3 days after which it was filtered and dried. Exfoliation was achieved by adding the lithium intercalated material to water. Dispersion of the material was assisted by an ultrasonic bath. The suspension of exfoliated material was restacked by removal of the water. Once restacked, the material cannot be exfoliated again by re-addition of water. The amount of lithium hydroxide carried with the restacked material was shown by independent tests not to have a catalytic effect by itself. The stacking heights of the original and restacked MoS₂ samples were determined before mixing with the coal from the width of the 002 peak in their XRD patterns. This value decreased from 375 Å for the untreated sample to 185 Å for the restacked sample.

Methods for achieving satisfactory mixing of the catalyst on coal were surveyed. The preferred method was to conduct the exfoliation step by addition of intercalated MoS₂ to a slurry of coal in a 1:1 mixture of THF and water. This allows the deposition of exfoliated material directly on the coal, as was confirmed by examination by SEM. An alternate method was to recover the MoS₂ after restacking, then mix it with coal under the same conditions.

Liquefaction tests were conducted in 42-mL microautoclaves using 6 g of a 1:1 wt mixture of Blind Canyon bituminous coal and a coal-derived recycle solvent (Wilsonville V-178). This recycle solvent was determined to have 1.1% insolubles by tetrahydrofuran extraction. Catalyst was added at 2000 ppm Mo with 0.12 g elemental sulfur and 6.8 MPa (1000 psi) hydrogen. The reaction was held at 375° C for 1 hour. A rough estimation of the relative hydrogen consumption was made by taking the difference between the highest value of total pressure achieved after reaching reaction temperature and that before final cool-down.

Upgrading tests with the Hondo resid (C = 81.9%, H = 10.6%, S = 5.1%, N = 0.9%, 20% distilled below 934° F) were performed in the same way but without added solvent and at a higher temperature: 425° C. Catalyst was added in the amount of 10 wt% MoS₂ on resid, or the molar equivalent of total metals in the cases of NiMo and CoMo.

3. RESULTS AND DISCUSSION

The main effects on conversion due to the catalyst and the method of its addition to coal prior to liquefaction are illustrated in Table 1. The results show that the technique for dispersing the catalyst on coal is critical to its performance. Mixing the original MoS₂ with the coal prior to liquefaction leads to a small increase in THF conversion and hydrogen uptake over the result from the non-catalytic control experiment. Improved performance was obtained by exfoliating and restacking the MoS₂, then mixing the recovered product with the coal before the liquefaction test. Conducting the exfoliation in the presence of the coal gave still better liquefaction results. Of the variety of solvent systems surveyed so far, THF/water is the combination that provided the best performance in the latter procedure. This system both readily swells the coal and creates a favorable environment for exfoliation of MoS₂.

Table 1. Coal conversion after one hour at 375° C

Catalyst	Conversion, % daf Coal		H ₂ Uptake, psi	
	THF	Cyclohexane		
None	78	21	31	
MoS ₂	82	20	96	Mixed as recieved using sonication
MoS ₂	87	27	120	Exfoliated, recovered, and mixed using sonication
MoS ₂	88	32	160	Exfoliated in presence of coal

The case of upgrading petroleum resid provided different challenges. The reactions crucial to conversion of coal are different in kind from those for HDS or HDN of petroleum resid. The Hondo resid used as a test material was 82% soluble in heptane before treatment. In the case of resid upgrading, major interests lie in the extent of the HDS and HDN reactions in addition to conversion to heptane solubles. In the absence of coal, the solid particulate substrate used to carry the catalyst is missing. Accordingly, the exfoliated, restacked catalysts were mixed directly with the resid. The effect of catalyst promoters is conveniently studied in this way by conducting the exfoliation step in aqueous solutions of $\text{Ni}(\text{NO}_3)_2$ or $\text{Co}(\text{NO}_3)_2$. Elemental analyses of the finished catalysts were used to determine the atomic ratios of Co/Mo and Ni/Mo which were 0.61 and 0.66, respectively. The interlayer distance in the stacking dimension may be estimated from the position of the 002 line. Values for the original MoS_2 and restacked MoS_2 are 6.14 Å, as expected. The interlayer distance for the NiMo and CoMo catalysts were ~ 11.5 Å. A net expansion of the layered structure is evident from these data. Recovered catalysts were also examined by XRD after they were extracted with THF to remove the soluble organic material. In the case of exfoliated /restacked MoS_2 , the recovered catalyst exhibited properties similar to the fresh catalyst. The stacking dimension was unchanged, 185 Å. The diffraction spectrum still gave evidence of an extensive contribution by a turbostratic structure. The results from hydrotreatment tests are summarized in Table 2 along with some of the physical properties of these catalysts taken before mixing with the resid.

Table 2. Results of hydrotreatment of Hondo resid at 425° C for one hour, and some catalyst properties.

Catalyst	Heptane extract, wt%	S, wt%	N, wt%	Spins/g x 10 ⁻¹⁷	Stacking height, Å	Surface area, m ² /g
(Resid)	82	5.1	0.9	--	--	--
None	89	3.5	0.8	--	--	--
MoS_2 , as received	93	3.2	0.8	6.0	375	6.2
MoS_2 , exfoliated/ restacked	95	3.3	0.7	7.1	185	10
CoMoS_2	95	2.6	0.7	1.9	110	22
NiMoS_2	96	2.2	0.8	9.4	98	6.1

The main difference in performance between the catalysts is in the extent of HDS. Cobalt and especially nickel significantly promote desulfurization. Review of the catalyst properties in Table 2 does not produce a simple, consistent correlation of a property with HDS performance. For example, the surface area of the CoMo catalyst is 3.6 times that of the NiMo catalyst, but the latter exhibits a greater amount of HDS. A correlation between the EPR signal intensity assigned to Mo(IV) and the rate of catalytic conversion of dibenzothiophene for a

series of MoS₂ catalysts has been reported [5]. This correlation fails when promoted and unpromoted catalysts in Table 2 are compared. The CoMo catalyst has the lowest EPR signal intensity, but performed quite well in HDS. In contrast to the significant HDS activity, HDN activity is negligible for all catalysts tested here. These preliminary results are encouraging in that a variety of related dispersed catalysts can be prepared for comparative studies, although it is evident that no single physical parameter can be used to correlate with all of the differences in performance.

4. CONCLUSIONS

The preliminary results indicate that exfoliation/restacking is a promising methodology for exploratory studies into the relationship between the morphology and composition of layered catalysts and their performance. The starting point for this wide variety of catalysts was a single sample of MoS₂. Thus, comparisons may be drawn on the basis of alterations induced in the physical structure of or by the addition of a specific promoter to a sample of MoS₂, rather than on the broader range of variation that may be generated by uncontrolled in-situ syntheses starting with various precursors. Such information may then provide indications for the direction toward improvements in the preparation and use of specific practical catalysts.

REFERENCES

1. M. Daage and R. R. Chianelli, *J. Catal.*, 149 (1994) 414.
2. P. Joensen, R. F. Frindt, and S. R. Morrison, *Mater. Res. Bull.*, 21 (1986) 457.
3. B. K. Miremadi and S. R. Morrison, *J. Catal.*, 103 (1987) 334.
4. B. C. Bockrath and D. S. Parfitt, *Catalysis Letters*, in press.
5. B. G. Silbernagel, T. A. Pecoraro, and R. R. Chianelli, *J. Catal.*, 78 (1982) 380.

ACKNOWLEDGEMENTS

The performance of the X-ray diffraction studies and the interpretation of the data by Sidney Pollack and Elizabeth Frommell is gratefully acknowledged, as is the EPR study performed by Robert Thompson and SEM studies performed by Donald Martello. This publication is supported in part by an appointment of DSP to the U.S. Department of Energy Fossil Energy Technology Center administered by the Oak Ridge Institute for Science and Education.

DISCLAIMER

Reference in this work to any specific commercial product is to facilitate understanding and does not necessarily imply endorsement by the United States Department of Energy.

Synthesis and Catalytic Activity of Ultra Fine Metal Sulfide Particles

Yasunori Kuriki, Motoo Yumura, Satoshi Ohshima, Kunio Uchida, Fumikazu Ikazaki

National Institute of Materials and Chemical Research, Dept. of Chemical Systems
1-1 Higashi, Tsukuba, Ibaraki, 305 Japan

1. Introduction

For the purpose of developing new catalyst for coal liquefaction, many studies on the highly dispersed catalyst and ultra fine particles are going. Ultra fine metal sulfide particles were synthesized by two different methods and catalytic activity of these metal sulfide particles were investigated.

At first, we tried to develop novel catalyst based on mechano-chemical effects[1]. When mechanical energy such as vibration energy causes some chemical effects in solid state material, it is called mechano-chemical effects. We examined to apply this effects to coal liquefaction by using high speed shaking autoclaves.

Next, we used ultra fine metal particles produced by gas evaporation methods. The metals used were Co, Ni, Fe and alloy of Fe and Co and we studied physical properties and catalytic activities of hydrogenation.

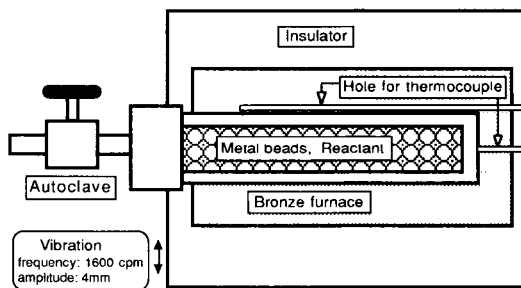


Figure 1 High speed shaking reactor

2. Experimental

2.1 In-situ preparation of fine metal sulfide particles using mechano-chemical effects.

Fig.1 shows schematic view of high speed shaking autoclave. Autoclave is made of SUS316, inner volume of reactor is 28 ml and maximum temperature is 450°C and maximum pressure is 20 MPa. Autoclave and furnace is put into high frequency vi-

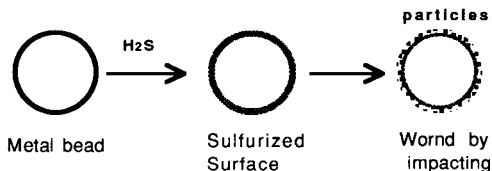


Figure 2 Mechanism of production of fine metal sulfide particles.

The 2g of phenanthrene(PHN) and 0.172g and 0.344g of sulfur were packed into autoclave at the case of hydrogenation of PHN. Reaction temperature was 400°C and H₂ pressure (initial) was 9.8 MPa.

2.2 Gas evaporation methods

The average diameter of these metal particles were 20nm and these fine metal particles were sulfided by H₂S. The catalytic activity of these fine metal sulfide particles were examined by using model compound. The experiments were carried out in 50ml stainless steel autoclave at 400-450°C under the initial hydrogen pressure of 7.9MPa.

3. Results and Discussion

3.1 In-situ preparation of fine metal sulfide particles using mechano-chemical effects.

We expected that mechano-chemical effects accelerate chemical reaction. However, the activation of metal surface (Mo, Co, Ni, Fe) by mechanical vibration was quite small, It was recognized that production of fine particle of metal sulfide. We suppose mechanism of production of fine metal sulfide particle is as follows. Surface of metal ball reacted with hydrogen sulfide, and metal sulfide crystal coated surface of metal ball. Those thin layers of metal sulfide were worn by impact, then produce quite fine particle of metal sulfide (Fig.2). Fig.3 shows particle size distribution of Mo sulfide. Fig.4 shows results of hydrogenation of phenanthrene by using Mo, Co, Ni, Iron ball. Hydrogenation activity of phenanthrene of each metal sulfide particles per weight were as follows, Mo = Co > Ni > Fe.

The activation of metal surface(Mo, Co, Ni, Fe) by mechanical vibration was quite small, it was usable that fine particles of metal sulfide (average diameter=0.5 micron) was produced by this method.

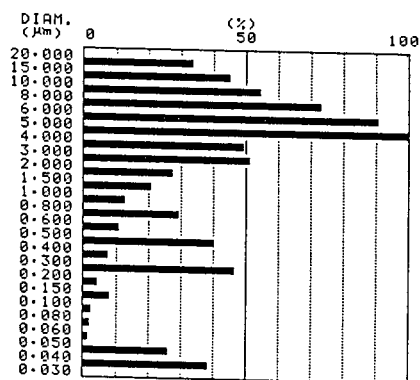


Figure 3 Particle size distribution of Mo

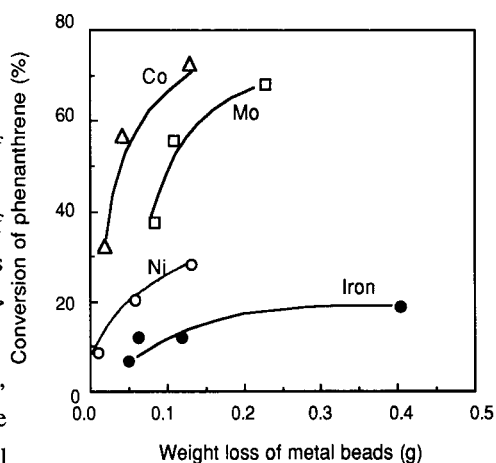


Figure 4 Correlation between hydrogenation activity and weight loss of metal ball. (Temp: 400°C, PH₂: 9.8 MPa)

3.2 Ultra fine metal sulfide particles produced by gas evaporation methods

We showed the conversion of 1-methylnaphthalene (MN) in Figure 5 when we use ultra fine particles of Fe,Co,Ni and Fe+Co. The reaction time and temperature were 60 minutes and 350-400°C. In ultra fine particles catalyst, Co showed the high hydrogenation activity. For the case of Ni, the yields shows maximum at 380°C. Only Ni showed this tendency and we guess that

the particles were agglutinated by sintering of ultra fine particles because of the high temperature and reaction with sulphur. We suppose the low activity according to the decreasing of active site and surface area. For the case of Fe the tendency was shown that the yields of conversion increased according to raising of the temperature because the catalyst activity is low. Fe+Co as composite ultra fine particle showed the increasing tendency according to the temperature, but we couldn't recognize the synergy effect by the composite of these only to find that the yields of conversion was same by guessing the rate of the each activity of Fe and Co.

To investigate the relationship between the sulfide and catalytic activity of the ultra fine particle, we experimented the changing of the sulfide adding and not adding the sulphur. The reaction temperature was 380°C. After the reaction we filtered the catalyst and washed and dried and analyzed by X ray diffraction and measured the surface area. We show the results of analysis of catalyst after the reaction in Table 2. For the case of Co, when we compared the hydrogen reduction not adding sulfide, the particles agglutinated by reduction at the high temperature and surface area decreased apparently and activity became low. It seem that the existence of the sulfide moderate the decrease of the surface area compared with not adding the sulfide and this caused the difference of the catalytic

Table 1 Properties of metal catalyst

Catalyst	Average diameter	surface area
Fe	20 nm	38 m ² /g
Co	20	32
Ni	20	35
Fe+Co	20	29

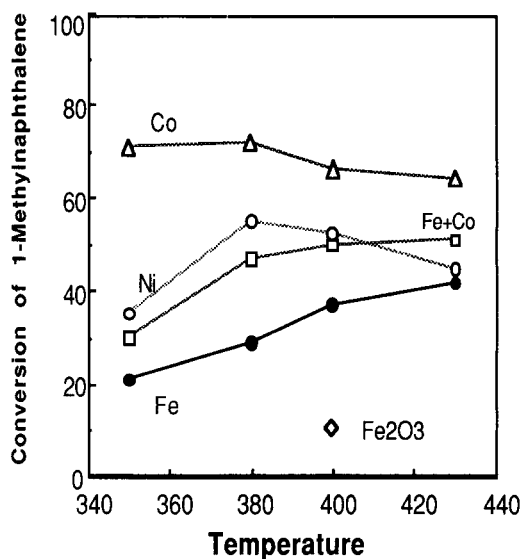


Figure 5 Relationship between temperature and conversion of 1-methylnaphthalene reaction time= 60min, PH₂=7.9 MPa, catalyst%= 5 wt%

Table 2 Influence of sulfur on hydrogenation reaction, structure and surface area of catalyst metal sulfide after the reaction.

Metal	Co					Ni				
	0*1	0	0.88	1.01	1.38	0*1	0	0.6	1.01	1.36
mol ratio of S and Metal	0*1	0	0.88	1.01	1.38	0*1	0	0.6	1.01	1.36
Conversion of 1-MN	14.5%	54.6%	77.9%	78.7%	76.3%	15.6%	72.8%	57.6%	72.6%	71.6%
Hydrogenation *2	11.2%	48.6%	62.7%	62.8%	61.4%	13.0%	67.6%	47.0%	64.4%	63.4%
Metal sulfide	-	-	Co ₉ S ₈	Co ₉ S ₈	Co ₉ S ₈	-	-	Ni ₃ S ₂	Ni _x S _y	Ni _x S _y
Surface area (m ² /g)	11	24	27	27	27	1.6	9.2	6.3	8.4	8.7

*1 ; reduced by hydrogen at 400°C for 3 hours before hydrogenation

*2 ; total yields of 1-methyltetralin and 5-methyltetralin

activity. We could recognize that the main ingredient of the cobalt sulfide was almost the structure of Co₉S₈ and could come into the same conclusion as the guessing from the diagram of Co-S-O by Yokokawa[2]. For the case of Ni, the pattern of the X ray diffraction was complicated and it's difficult to specify the structure. However we suppose the production of Ni₃S₂, NiS_{0.84} and NiS by examining the phase diagram[2]. According to the result of the measurement of the surface area, Co is keeping its surface area (15 to 30 m²/g) and Ni is lowering its surface area (6 to 9 m²/g). Therefore, we suppose that factor of low activity of Ni is small surface area.

4. Conclusion

The activation of metal surface(Mo, Co, Ni, Fe) by mechanical vibration was quite small, it was usable that fine particles of metal sulfide (average diameter=0.5 micron) was produced by this method.

Hydrogenation activity of these ultra fine metal particles per weight were as follows, Co > Ni > Fe. The structure of sulfided Co was Co₉S₈, but that of sulfided Ni was mixture of Ni_xS_y (x>y). We didn't find any synergy effect of Fe and Co in the case of alloy of Fe and Co. We are now applying these catalyst to the liquefaction of wandoan coal.

References

1. Y. Kuriki et al, J. Japan Energy Soc., 72 (1993) 892
2. H. Yokokawa et al, J. Am. Ceramic Soc., 72 (1989) 2104

Batch vs. Continuous Experiments in Coal Hydrogenation

Bernd O. Strobel

DMT-Gesellschaft für Forschung und Prüfung mbH, Dept. IKB 3

Franz-Fischer-Weg 61, D-45307 Essen, Germany

While any process for liquid fuels production from coal will be a continuously operated flow system, coal hydroliquefaction investigations are often carried out in batch (mini-)autoclaves. At first glance it does not seem too difficult to reproduce the respective operation parameters. But why then do so many results from batch type investigations correlate so poorly with those obtained from continuously operated units?

1. EXPERIENCES

In coal hydrogenation batch autoclave work, the conditions typically varied and hence controlled or adjusted in a given experiment are, initial (cold) hydrogen pressure, reactor temperature, hold time, and intensity of agitation. Other parameters routinely observed include the nature of the solvent, coal-to-solvent ratio, and catalyst type and concentration.

Of the above parameters, probably the only ones that play essentially identical roles in a continuously operated unit and in an autoclave are, reactor temperature and type of catalyst - but even this may be debated.

Hydrogen pressure

In an autoclave, the initial ("cold") pressure value is mostly chosen so as to attain a defined "hot" pressure under reaction temperature. There are a number of differences between the hot pressure in a flow system and in a batch vessel: Normally in the flow system, both a constant overall pressure and an essentially constant hydrogen partial pressure is effected for the entire residence time by means of a recycle gas loop, a gas scrubbing unit, and continuous hydrogen make-up. In contrast in the autoclave, the hydrogen pressure first increases with temperature, then drops as hydrogen is chemically consumed and as reaction gases form and low-boiling liquid products vaporize. With an unfavorably designed autoclave equipment, vapors can overlay the liquid phase so this may become deficient in hydrogen even if the autoclave is connected to a constant pressure hydrogen supply system. This is probably why in autoclave tests under seemingly identical overall conditions, hydrogen starvation hence coking reactions occur at much lower temperatures already than in flow reactors.

Recycle gas flow

With autoclave tests in coal hydrogenation, sometimes hydrogen consumption is made up for, but repeated or even continuous replacement of hot gas phase with fresh gas is rarely done. With flow reactor units, continuous hydrogen feed-in is indispensable and in most plants high-pressure gas recycling is applied, primarily in order to save hydrogen.

Throughout our coal hydrogenation PDU work we found that recycle gas flow rate is an undervalued, influential parameter. Beyond its main tasks (furnishing hydrogen for the chemical reactions and agitating the slurry phase in the reactor vessel), it can much improve conversion. Provided that reactor temperature is sufficiently high, an increased apparent gas flow rate gives a significantly enhanced oil yield (see Fig. 1 [1]) at the expense of residuum.

Both tracer residence time and dynamic vapor/liquid equilibrium measurements have confirmed that the high-pressure, high-temperature gas flow effects extensive stripping of even high-boiling oil fractions. The gas stream carries the vapors swiftly out of the reaction zone. Thus, the slurry phase is reduced in mass and volume and hence assumes a correspondingly longer residence time in the reactor space. Quantitatively speaking, residence time increases progressively with the amount of stripped off slurry phase components (and so does catalyst concentration in the slurry phase). In an autoclave as normally operated, all raw materials and products are confined in the reaction zone so that residence time is always just the hold time (even if extensive vaporization took place; only catalyst concentration in the slurry phase would become accordingly higher).

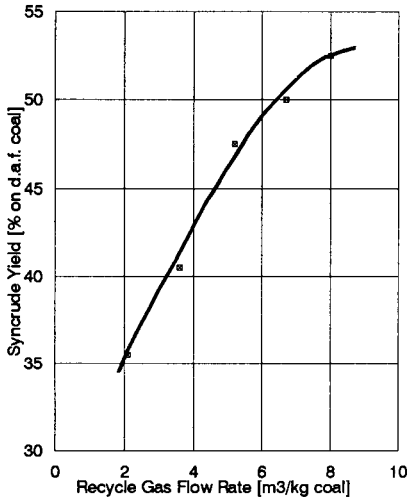


Fig. 1: Oil yield increased through stripping effect

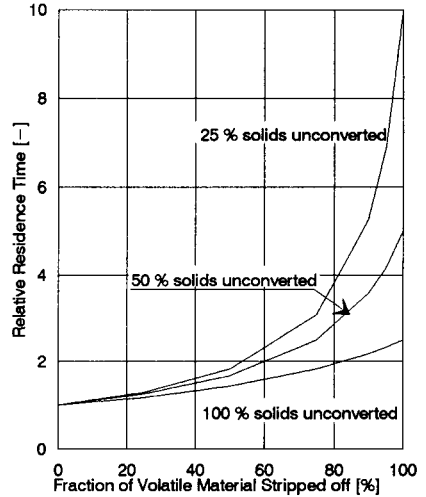


Fig. 2: Effect of oil stripping on residence time

Fig. 2 gives two computational examples for the effect of oil stripping on slurry phase residence time in a flow reactor at different levels of 'conversion'. In the illustration, 'unreacted material' includes the non-volatile slurry phase constituents as are asphaltenes, preasphaltenes, unconverted coal, coal minerals, and the dispersed catalyst. 'Volatile material' comprises the process solvent and the distillate-type oil products already formed as well as product water and product gases. The higher the conversion to volatile products from the beginning, the higher the increase in residence time and in catalyst concentration of the respectively remaining slurry phase. Thus, even more refractive coal components or primary products may now convert.

Naturally in the flow reactor with fresh coal slurry continuously fed in, residence time distribution will be observed, i. e., there will be a *mean* residence time value. The tracer tests in our PDU have revealed that under appropriate hot conditions the mean slurry phase residence can be nearly ten times the cold flow residence [2].

A further difference between coal hydrogenation experiments with and with no gas recycling used, respectively, relates to the activation of the dispersed catalyst by hydrogen sulfide. If the catalyst requires presulfiding, this is often left to the hydrogen sulfide formation that takes place during reaction anyway. Sometimes sulfidation is accomplished by elemental sulfur, carbon disulfide, or other sulfur compound addition when the autoclave is loaded. Then however hydrogen sulfide is formed only at elevated temperatures. This means that optimum catalyst activity is not available during heat-up hence during coal degradation which is but believed a determining step in coal hydroconversion. Hydrogen sulfide is to be added still before the coal slurry is heated. In a continuously operated unit, the recycle gas will always contain hydrogen sulfide so that this is present from early heat-up.

Solvent properties

In PDU coal hydrogenation, i. e. in strictly process related continuous operation, the solvent has to satisfy a number of requirements. Density and viscosity must be just right to give a manageable coal slurry i. e. to keep the solids from settling but at the same time permit a high coal-to-solvent ratio. The boiling point or range must be high enough to avoid dry-up and thus coke-up of the preheater. It should be low enough on the other hand to bring about the advantages of oil stripping as extensively as possible; even small differences in boiling range can make a difference in oil yield.

The solvent should be akin to coal, i. e., it should consist dominantly of aromatics and hydroaromatics. With paraffin containing solvents, precipitation of asphaltenes and preasphaltenes and thus plugging can occur at any place from the preheater to the vacuum distillation bottom. In the reactor, coking of the precipitated material may result in hot spots and even in severe temperature runaways. Whatever the source of the paraffins in the solvent (petroleum derived oils or polyolefin plastics in coprocessing; even low rank coals), adverse effects are experienced with bituminous coals anyway.

Phenols, which are usually appreciated as effective solvent components in coal dissolution, are able to create serious difficulties in continuous plant operation: Repeated rapid preheater fouling observed on a pilot plant scale was found to be caused by iron sulfide accumulation. Our investigations elucidated that traces of iron (both from the coal minerals and from the red mud catalyst) dissolved in the process recycle solvent as phenates. These decompose under preheater temperatures, and upon interaction with hydrogen sulfide the deposited material ends up as iron sulfide.

In autoclave work, the effects discussed above are hardly noticeable and hence do not seem to be of significance. Therefore in batch investigations on coal hydroconversion, solvents are sometimes chosen too freely and far from 'the real world'.

Process solvent balance

The term 'process recycle solvent' implies closed loop operation and complete recovery of the oil spent in slurry preparation. Under coal conversion conditions, as well the solvent is subjected to hydrocracking. In the liquefaction of a German bituminous coal at 474°C and 30 MPa, about 40 % of the solvent is cracked and thus becomes part of the syncrude product. In order to make up for this loss, a corresponding amount of oil boiling in the solvent range must be produced from the coal at the same time. Otherwise the process will not be in a solvent balance which means that neither conversion and yield nor product characterization data can be considered as reliable.

Similarly the product work-up procedure may have a significant influence on the recycle solvent composition i. e. on properties and thus on the coal hydroconversion results. The 'ballast effect' of otherwise practically inert solids became apparent in continuous PDU work [1]. This effect shows up in the solvent recovery (by vacuum distillation) from the hot separator letdown slurry. Within a given process configuration, the solids can inevitably limit oil yield but at the same time improve conversion. In autoclave tests with product work-up by solvent separation only ('oil', asphaltenes, preasphaltenes, solids), this would have hardly been realized and accounted for.

The use of 'optimal' solvents such as tetralin, methyl naphthalene, or other well-defined liquids is clearly limited to certain mechanistic studies and maybe to extracts (SRC) production. Even if these solvents survived coal conversion essentially unchanged, little chance is seen get them separated from the coal derived liquids and thus recover the 'process solvent'. For coal liquefaction process development, this kind of testing should only be used within a very specific scope and with limited and well-defined aims in mind.

2. CONCLUSION

From the above it is clear that any given coal as well as any given process will possess a specific equilibrium recycle solvent. Generally, any change in the operation conditions will inevitably change recycle solvent properties to a certain extent which in turn will have an effect in its own right on conversion, yields, etc. In the light of this, comparing various coals, catalysts or else with each other using a standard mini-autoclave procedure and a 'typical process solvent' seems of limited value.

Reservations apply also to autoclave tests that are used to investigate the influences of innocently looking parameters like temperature, (hydrogen) pressure, residence time, etc. General considerations plus experience from continuous work suggest that in the context of process development, autoclave experiments should more deliberately planned and conducted, and carefully be interpreted.

ACKNOWLEDGMENT

Continuous financial support from MWMT Nordrhein-Westfalen and from RAG is gratefully acknowledged. The work was performed for RAG.

REFERENCES

1. B.O. Strobel and F. Friedrich, Proceedings, 1981 Int. Conf. Coal Science, Düsseldorf, D, 556
2. B.O. Strobel, H. Schubert and K.N. Clark, Proceedings, 1991 Int. Conf. Coal Science, Newcastle-upon-Tyne, UK, 823
3. B.O. Strobel and F. Friedrich, Proceedings, 1987 Int. Conf. Coal Science, Maastricht, NL,

Three-stage catalytic hydroliquefaction of coal: how to improve hydrogen transfers to coal

M. Jamond, R. Bacaud, B. Pepin-Donat⁽¹⁾, H. Charcosset and G. Djega-Mariadassou⁽²⁾

Institut de Recherches sur la Catalyse, CNRS, 2, avenue Albert Einstein, 69626 Villeurbanne Cedex, France.

¹ DRFMC-SESAM-PMS CENG, BP 85X, 38041 Grenoble Cedex, France.

² Laboratoire de Réactivité de Surface, Université P. et M. Curie, CNRS URA 1106, 75232 Paris Cedex 05, France.

1. INTRODUCTION

The chemical structure of coal greatly determines its reactivity. The model of coal structure assuming a two-component system (a macromolecular three-dimensional network containing molecules of relatively low molecular weight) [1] allows interpreting the behaviour and transformation of coal during liquefaction [2]. Considering this model of coal structure we established a multi-stage experimental procedure of liquefaction (isotherms at 300°C, 400°C, 450°C), in order to enhance coal conversion by improving hydrogen transfers. The liquefactions were carried out in presence of iron oxide as non porous catalyst precursor. Therefore, the first stage was conducted under mild conditions (300°C) in order to produce the catalytic phase (pyrrhotite) in a highly dispersed state [3]. Results obtained will be rationalized considering the two-phase model of coal structure using the mechanism involving bond breakage of coal molecules and stabilization of the resulting radicals by hydrogen transfers [4].

2. EXPERIMENTAL

Liquefaction and product work-up procedure have been described elsewhere [5]. We used a high volatile bituminous coal from Freyming (France). Ultimate analysis (wt% d.a.f.) leads to: C = 85, H = 5.35, O = 7.7, N = 1.1, $S_{\text{total}} = 0.85$, $S_{\text{pyrritic}} = 0.3$. Iron aerosol oxides with different BET surface areas obtained by a flame method [5] were used as catalysts precursors (Fe(18), $S_{\text{BET}} = 18 \text{ m}^2\text{g}^{-1}$; Fe(71), $S_{\text{BET}} = 71 \text{ m}^2\text{g}^{-1}$). The liquefactions were performed in a non H-donor solvent, 1-methylnaphthalene (MeN). In order to assess the role of a H-donor solvent, some experiments were carried out in a mixture of tetraline (T) and MeN (15:85).

30 g of coal, 70 g of solvent, catalyst precursor (2 wt% with regard to coal), elemental S as sulfiding agent (1% of H₂S in the gas phase) were charged in a batch autoclave under hydrogen pressure (150 bar cold). The performances of this autoclave, heated by induction, were: heating rate up to 1,5 °C min⁻¹, isothermal stability better than ± 0.5 °C, cooling rate

0.5 °C min⁻¹[6]. Products work-up included: determination of coal conversion (hexane (HEX) and tetrahydrofuran (THF) solubles), gas recovery and analysis, solvent analysis (calculated parameters: %Hyd, wt% of MeN hydrogenated; %deMe, wt% of MeN demethylated). A mass balance for hydrogen utilization could be derived from the composition of the gaseous phase and from the amount of hydrogen involved in the evolution of the solvent (calculated parameter corresponding to the wt % of H₂ incorporated in coal and coal products (d.a.f.): %H₂coal). A multi-stage procedure was carried out: 10 min at 300 °C, 30 min at 400 °C, 60 min at 450 °C, with a high heating rate 70 °C min⁻¹. For comparison, some reactions were performed with only one step of temperature and a low heating rate (3 °C min⁻¹).

3. RESULTS

Comparison of run 2 (Table 1) and 3 (Table 2) shows the beneficial effect of the three-stage procedure in high heating rate autoclave versus the one-stage procedure at high temperature (450 °C, 3 °C min⁻¹). In run 3, the amount of hydrogen transferred to coal is higher than in run 2 and, so is consequently coal conversion. During liquefaction with low heating rate, regressive reactions of polymerisation occurred (as confirmed by the e.s.r. study of the THF insolubles) resulting in a lower conversion than in run 1 performed at 400 °C, 3 °C min⁻¹.

Table 1

Results of one-stage liquefaction (60 min) in MeN (low-heating rate)

Run	T (°C)	% soluble (d.a.f.)		%H ₂ coal
		THF	HEX	
1[7]	400	80	14	
2	450	43	23	2

3.1. Liquefaction without the 400°C stage

Even in presence of catalyst, during run 5 (without the 400°C stage)(Table 2), insoluble carbonaceous residues were formed, preventing any representative sampling for evaluation of coal conversion. Furthermore, less hydrogen was fixed by coal than in the case of the three-stage reaction (run 3). This proves that hydrogen transfers to coal were not high enough to avoid regressive reaction of polymerisation, even if sulfidation of the catalyst precursor was complete. Solvent demethylation is similar in these experiments, but the percentage of hydrogenated solvent is lower when the 400°C stage is suppressed.

3.2. Liquefaction without the 450°C stage

In Table 2, comparison between results of this two-stage liquefaction (run 6) and the three-stage one (run 4) shows great differences: (i) in the product distribution (larger amounts of light products in run 4) although very close values of total coal conversion are observed (ii) in the amounts of hydrogen fixed by coal (higher in run 4) (iii) in the % of gas produced by coal (run 4: 6 %, run 6: 2 % (wt % d.a.f.)). Furthermore, in run 6, the % of hydrogenated

solvent is higher than the % of demethylated solvent. Hence, for temperatures higher than 400°C, thermal cracking reactions are intensive, and the radicals thus formed seem to be well stabilized by hydrogen transfers in the three-stage procedure conditions.

Table 2
Results of multi-stage liquefactions (high-heating rate)

Run	Proced. ^a	Cata.	solvent	% soluble (d.a.f.)		% H ₂ coal	%Hyd	%deMe
				THF	HEX			
3	A	Fe(18)	MeN	85	49	2.7	14	33.3
4	A	Fe(71)	MeN	87	52	3.8	16.5	32.6
5	B	Fe(18)	MeN	-	-	1.9	6.8	35.8
6	C	Fe(71)	MeN	89	29	2.5	10.6	9.8
7	A	Fe(18)	MeN+T	88	52	3.2		
8	B	Fe(18)	MeN+T	85	52	3.1		

^a procedure: A: 300°C (10 min), 400°C (30 min), 450°C (60 min);
B: 300°C (10 min), 450°C (60 min); C: 300°C (10 min), 400°C (60 min)

3.3. Liquefaction in H-donor solvent

Three-stage liquefactions performed either in H-donor (run 7) or in a non donor solvent (run 3) led to very similar coal conversions and product distributions. Differences appear in liquefactions carried out without the 400 °C stage. In run 5 (MeN), formation of solid residues due to regressive reactions was observed, whereas in presence of T such coke formation did not occur. Furthermore, hydrogen transferred to coal was higher when tetralin was added.

It appears that in MeN, liquefactions resulting in high coal conversion degrees are characterized by high % of hydrogenated solvent. Hence, high % of hydrogenated solvent are consistent with efficient hydrogenations of solvent and hydrogen transfers from solvent to coal. Furthermore, results obtained in a H-donor solvent evidence the role of the 400°C stage for reactions carried out in MeN alone: this stage allows the solvent hydrogenation.

4. DISCUSSION

During pyrolysis many low and medium rank bituminous coals melt to form a transient plastic phase. In relation to the two-phase model of coal structure, Rouzaud et al. [8] have shown that during pyrolysis, cracking of the macromolecular component begins between 350 and 400°C yielding a "molecular mobile" phase which acts as a suspensive medium. The critical source of differences between pyrolysis and liquefaction is linked to the properties of the medium in which coal is heated. This phenomenon well established for the transformation of coal during pyrolysis, can be considered during the liquefaction: in this way, Grint et al. [9] have suggested that rapid catalyzed liquefaction at 425°C in tetralin of an iron/tin treated

Victorian brown coal, led to the formation of a plastic, viscous coal-derived product. The Freyming coal shows during its transformation with temperature the formation of a plastic phase between 360 and 410°C [10]. Furthermore, previous liquefaction studies of this coal [7] have established that at 350°C (before the plastic phase formation) hydrogen transfers occur between the gas phase and coal (via the catalyst), whereas at 400°C hydrogen transfers to coal mainly occur via the solvent. We can then consider that during the liquefaction of the Freyming coal, at about 400°C, it will form a plastic phase which acts as a suspensive medium allowing a better contact between reactive molecules and favouring hydrogen transfers.

At low temperature simultaneously occur the dissolution of the molecular phase and homolytic scissions of weak bonds such as benzylic ether linkage. In the case of low heating rate liquefaction in MeN, the slow increase in temperature seems to give time to more regressive reactions to occur (comparatively to liquefaction with high heating rate: run 1 and run 6). Thus, when the temperature reaches the level of plastic phase formation, some reticulation reactions have already been achieved and this phase will not be formed in optimum conditions. In consequence, the reactive medium thus formed will not favour the diffusion of reactants, and hydrogen transfers will be limited. Then when temperature is raised to 450°C, hydrogen availability is reduced, therefore free radicals created by thermal cracking reactions cannot be stabilized and regressive reactions of polymerisation occurred (compare run 1 and 2). For liquefactions conducted in the high heating rate autoclave, for $T > 300^\circ\text{C}$, scissions of weak bonds occur and as mentioned above, this high heating rate reduces the development of regressive reactions (comparatively to the low-heating rate). The consecutive plastic phase formed during the 400°C step acts as a better suspensive medium and favours a better contact between molecules and thus more efficient hydrogen transfers. Solvent is hydrogenated (via the catalyst) as well as the aromatic structures of macromolecular network (mainly via the solvent). A pool of H is thus created during this step. Therefore, when temperature is raised to 450°C and cracking reactions occur, hydrogen is available in the medium. Regressive reactions are limited and production of light products is enhanced. If the 400°C stage is suppressed (run 5), MeN will not be hydrogenated, the regressive reactions are enhanced and the development of the plastic phase is restricted. The reactive medium is not able to liberate sufficient hydrogen when the temperature reaches 450°C and cracking occurs. carbonaceous residues resulting from regressive reactions are thus formed.

REFERENCES

1. P.H. Given, A. Marzec, W.A Barton, L.J. Lynch and B.C. Gerstein, *Fuel*, 65 (1986) 155.
2. Y.F. Patrakov and S.V. Denisov, *Fuel*, 70 (1991) 267.
3. G. Djega-Mariadassou, M. Besson, D. Brodzki, H. Charcosset, H.V. Tran and J. Varloud, *Fuel Processing Technology*, 14 (1986) 247.
4. I. Mochida, A. Takayama, R. Sakata and K. Sakanishi, *Energy Fuels*, 4 (1990) 398.
5. a) R. Bacaud, H. Charcosset, M. Jamond, *Fuel Processing Technology*, 24 (1990) 163.
b) M. Jamond, PhD Thesis, Université Lyon I (France), 1991.
6. R. Bacaud, *Fuel Processing Technology*, 28 (1991) 203.
7. M. Oberson, PhD Thesis, Université Lyon I (France), 1987.
8. J.N. Rouzaud and A. Oberlin, H. Charcosset and B. Nickel-Pepin-Donat (eds.), *Advanced Methodologies in Coal Characterization*, Elsevier, (1990) 311.
9. A.Grint, W.R. Jackson, F.P. Larkins, M.B Louey, M. Marshall, M. Trehwella and I.D. Watkins, *Fuel*, 73 (1994), 381.
10. R. Loison, P. Foch and A. Boyer, *Coke Quality and Production*, Butterworths, (1989) 479.

Single and multistage reactions of various coals to produce high yields of fluid fuel

C.K.J. Hulston^a, P.J. Redlich^a, W.R. Jackson^a, F.P. Larkins^b and M. Marshall^a

^a Department of Chemistry, Monash University, Clayton, Victoria 3168, Australia*

^b School of Chemistry, University of Melbourne, Parkville, Victoria 3052, Australia

1. INTRODUCTION

Previous work has shown that residues from reaction of coals with CO/H₂O are not converted into CH₂Cl₂ soluble products in single stage reactions with hydrogen in the presence of hydrogenation catalysts [1]. Accordingly, two stage reactions have been carried out involving an initial CO/H₂O/NaAlO₂ stage followed by a hydrogenation of dry Ni/Mo treated residues. Recent work by Lim *et al* [2] has obtained higher conversions for subbituminous coals when a preliminary NaOH/CO/H₂O reaction was followed by a conventional catalysed dry hydrogenation. The starting point of this study was an adaptation of this procedure in which a preliminary NaAlO₂/CO/H₂O reaction was followed by dry hydrogenation using a well known catalyst, Ni/Mo. The Ni/Mo was not added as a conventional supported catalyst but was dispersed in the coal in water soluble form. It was found that the preliminary reaction with CO/H₂O was not beneficial but an alkaline treatment of the coal prior to addition of Ni/Mo and dry hydrogenation led to even higher yields of oil product.

2. EXPERIMENTAL

Four coals with C content 70-82 wt % daf ground to -250 μm were used in this work. Sodium aluminate (NaAlO₂, 1.2 wt % daf Na) Fe^{II}, Co^{II}, Ni^{II} acetates and ammonium molybdate ((NH₄)₆Mo₇O₂₄·4H₂O) were added to the coal or first-stage residue as aqueous solutions. Fe was added at a concentration of 1.7 wt % daf, Co/Mo and Ni/Mo at concentrations of 0.2 wt % daf for Co and Ni and 0.9 wt % daf for Mo unless otherwise stated.

The coal-water-catalyst slurry was stirred under vacuum for 1 h to remove trapped air and ensure good dispersion. NaAlO₂ was added before the metal catalysts in order to optimise conversion. The conversion for LY coal treated first with NaAlO₂ and secondly with Ni/Mo (87%) was 12% higher than for coal treated first with Ni/Mo and secondly with NaAlO₂. Indeed coal treated firstly with Ni/Mo and secondly with NaAlO₂ gave a conversion significantly lower than for coal treated with Ni/Mo alone (83%). After stirring, water was removed under vacuum at 30°C. Before use the treated coal was completely dried under vacuum at 30°C; drying at 105°C reduced subsequent conversion of the coal.

First stage CO/H₂O/NaAlO₂ reactions were performed in a 300 ml stirred autoclave with hot charge facility, the operation of which has been described in [3]. After the first stage the H₂O insolubles were treated with Ni/Mo.

For the second stage 1 g of vacuum-dried treated coal or first-stage residue was placed in a 35 ml horizontal tubular reactor. The same reactor and charge were used for single-stage coal reactions. Increasing the charge of coal to 3 g led to a significant reduction in conversion. Furthermore, vertical orientation of the reactor reduced conversions by one third, and even an orientation of 30° to the horizontal reduced the conversion from 92 to 82% in a typical case. These effects are larger but in the same direction as those observed in the presence of tetralin by Rhee *et al*. [4] and ourselves. The tubular reactor procedure and product work up are described in [5] and [6] respectively. The product was fractionated into CH₂Cl₂ insolubles and asphaltenes (CH₂Cl₂ soluble, hexane insoluble). Oil

* This research was supported by NEDO, Japan

(hexane soluble), gas and water (OGW) were determined by difference. Total conversion was defined as 100- wt % CH_2Cl_2 insolubles (daf coal charge).

3. RESULTS AND DISCUSSION

3.1 Two stage reactions of Loy Yang run-of-mine (LY ROM) coal

Figure 1 shows that a decrease in first stage ($\text{CO}/\text{H}_2\text{O}/\text{NaAlO}_2$) temperature resulted in an increase in overall conversion for 400°C , 60 min second stage reactions ($\text{H}_2/\text{Na}/\text{Ni}/\text{Mo}$). Coal treated with NaAlO_2 then Ni/Mo at room temperature as described above and reacted in a single stage at 400°C , 6MPa (cold) H_2 for 60 min gave the same conversion as a two stage reaction with 125°C first stage. Therefore a first stage $\text{CO}/\text{H}_2\text{O}/\text{NaAlO}_2$ reaction was ineffective when a 400°C second stage was employed. It should be noted that excellent conversions were obtained in all cases.

3.2 Single stage reactions at 400°C of LY ROM coal

These excellent results led us to make a detailed study of single stage dry, solventless hydrogenations with catalyst treated coal. A range of variables was studied as discussed below. The major results are summarised in Tables 1 and 2.

Table 1

The effect of reaction time on conversion of Ni/Mo and $\text{Na}/\text{Ni}/\text{Mo}$ treated LY ROM coal at 400°C

Catalyst	Time (min)	Conversion (wt % daf coal)		
		Total	Asph	OGW
Ni/Mo	30	83	25	58
	60	92	24	68
	90	94	14	80
Na/Ni/Mo	30	87	18	69
	60	96	20	76

Reaction conditions: 1 g db treated coal under 6MPa (cold) H_2 was heated at 400°C in a 35 ml reactor.

Reaction Time Increases in oil yield were observed with reaction time (up to 90 min), indicating that the catalyst was not being deactivated. The very high total conversions (> 90%) for reactions of 60 min or greater prompted us to reduce the reaction time to 30 min. The lower conversion (83%) allowed us to distinguish more clearly the effect of other variables.

Catalyst Loading Reduction of Ni/Mo loading to 0.1/0.45 wt % daf coal reduced conversion to 62% for 30 min reactions but increasing reaction time to 60 min raised conversion to 79%. It thus appears that catalyst loading can be traded off against time.

Preliminary Alkali Treatment A preliminary room temperature treatment with NaAlO_2 resulted in an increase in oil yield due to a slight increase in total conversion and a decrease in asphaltene yield. When the Na^+ ions were removed by acid-washing prior to Ni/Mo treatment, conversion was still high (87%) but the asphaltene yield increased to 26%, the same value as when Ni/Mo was used in the absence of NaAlO_2 . Substituting NaOH for NaAlO_2 gave similar results but Na_2CO_3 doubled the asphaltene yield to 33%, showing that it is the alkalinity and not the presence of sodium ions that is the major factor in improving the product quality.

Comparison of Ni/Mo and Co/Mo Co/Mo is a commonly used catalyst for coal liquefaction [7] and its effectiveness under these conditions was studied.

Table 2
Comparison between Ni/Mo and Co/Mo catalysed reactions of LY ROM coal with and without additives

Catalyst	Additive	Time (min)	Conversion (wt % daf)		
			Total	Asph	OGW
Ni/Mo	-	30	83	25	58
Co/Mo	-	30	39	2	37
Ni/Mo	-	60	92	24	68
Co/Mo	-	60	76	16	60
Ni/Mo	CS ₂	30	88	20	68
Co/Mo	CS ₂	30	89	20	69
Ni/Mo	Tetralin	30	73	16	57
Co/Mo	Tetralin	30	61	10	51

Reaction conditions as for Table 1. 0.03 g of CS₂ and 1 g of tetralin were added when included.

At the same concentration as for Ni/Mo reactions, using Co/Mo gave lower conversions, especially for 30 min reaction times (see Table 2). However, sulphiding (addition of 0.03 g CS₂ to the reactor) increased the conversion for Co/Mo promoted reactions to that for Ni/Mo/S (88%). Reaction of the coals with the single metal compounds showed that in the presence of sulphur Mo alone gave 88% conversion and thus Ni and Co were not required.

Addition of Tetralin Most coal hydrogenations involve the use of a good hydrogen donor solvent e.g. tetralin. The effect of adding tetralin to reactions of the Ni/Mo and Co/Mo treated coals under these conditions was briefly investigated (Table 2). Surprisingly, addition of tetralin to a Ni/Mo treated coal led to a decrease in conversion (to 73%). A significantly lower asphaltene yield was the reason for this decrease. In contrast, addition of tetralin to reaction of Co/Mo treated coal led to an increase in conversion (to 61%).

Use of Fe-based Catalysts LY ROM coal was treated with Fe (1.7 wt % daf coal) and reacted under identical conditions to those described above. Reaction for 60 min gave only 44% conversion but sulfiding led to an increase in conversion to 82%. The asphaltene yield in this reaction was 18%. Increasing the reaction temperature to 410°C led to a slight increase in total conversion (to 87%) and decrease in asphaltene yield (to 15%). The sulphided Fe-based catalyst, like Co/Mo, was slower in action than Ni/Mo; conversion after 30 min was only 53%. Thus sulfided iron-treated coals can give moderately high oil yields (> 40%) even in the absence of a hydrogen donor solvent for a 1 h reaction. In contrast it should be noted that ≥ 60% yields of oil can be obtained from LY ROM coal treated with unsulfided Ni/Mo.

3.3 Single and two-stage reactions of sub-bituminous and bituminous coals

Conversions of Ni/Mo treated higher rank coals at 400°C were significantly less than those from the typical brown coal, LY ROM, Figure 1. The difference in conversion between Ni/Mo and Co/Mo treated coals decreased with increasing carbon content (rank). Addition of NaAlO₂ to the coals decreased conversion by 8-26%, in contrast to the effect for LY ROM coal.

Two stage reactions using the higher rank coals were of marginal, if any, benefit as for LY ROM brown coal. This is in contrast to the findings of other workers [2]. It could be that our method of addition and catalyst loading in the second stage was so efficient as to mask any effect of the first stage. Another possibility is that our method of catalyst addition gave poorer dispersion for first-stage residues than for coal, on account of the change in oxygen functional groups in the first

stage. Methods of catalyst addition used by other workers could not have resulted in such a difference between coal and first-stage residues.

REFERENCES

1. C.K.J. Hulston, P.J. Redlich, W.R. Jackson, F.P. Larkins and M. Marshall, Proc. 8th International Conference on Coal Science, Oviedo. "Multi-stage coal reactions in carbon monoxide-containing atmospheres using alkaline and hydrogenation catalysts."
2. S.C. Lim, R.F. Rathbone, A.M. Rubel, E.N. Givens and F.J. Derbyshire, Energy and Fuels, 8 (1994) 294.
3. J.S.T. Chan, W.R. Jackson and M. Marshall, Fuel, 73 (1994) 1628.
4. Y-W. Rhee, J.A. Guin and C.W. Curtis, Fuel Proc. Tech., 22 (1989) 97.
5. C.P. Hughes, T. Sridhar, S.C. Lim, P.J. Redlich, W.R. Jackson and F.P. Larkins, Fuel 72 (1993) 205.
6. P.J. Cassidy, W.R. Jackson, F.P. Larkins, R.J. Sakurovs and J.F. Sutton, Fuel 65 (1986) 374.
7. M.R. Hatswell, W.R. Jackson, F.P. Larkins, M. Marshall, D. Rash and D.E. Rogers, Fuel 59 (1980) 442.

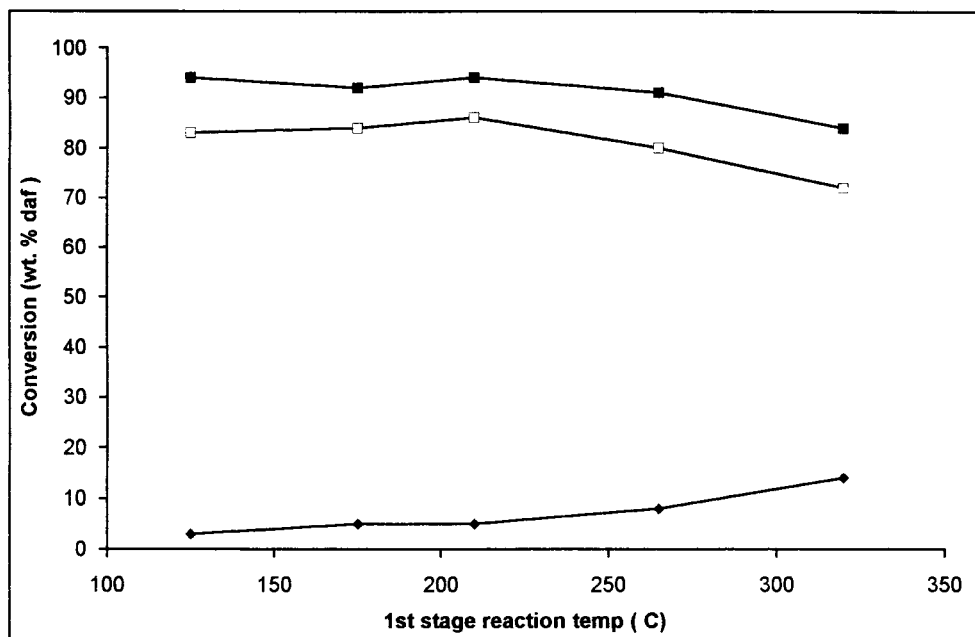


Figure 1 The effect of first-stage reaction temperature on conversions in two-stage reactions of Loy-Yang coal -◆- Total conversion, 1st stage ($\text{CO}/\text{H}_2\text{O}/\text{NaAlO}_2$), -□- overall conversion (both stages) 30 min 2nd stage ($\text{H}_2/\text{Na}/\text{Ni}/\text{Mo}$), -■- overall conversion (both stages) 60 min 2nd stage ($\text{H}_2/\text{Na}/\text{Ni}/\text{Mo}$)

Multi-stage coal reactions in carbon monoxide-containing atmospheres using alkaline and hydrogenation catalysts

C.K.J. Hulston^a, W.R. Jackson^a, F.P. Larkins^b, M. Marshall^a and P.J. Redlich^a

^a Department of Chemistry, Monash University, Clayton, Victoria 3168, Australia*

^b School of Chemistry, University of Melbourne, Parkville, Victoria 3052, Australia

1. INTRODUCTION

Alkali-catalysed CO/H₂O reactions for the fluidisation of coals were introduced in the 1920's [1]. This liquefaction method is particularly useful for low-rank coals, as the coal need not be pre-dried as is usually necessary for conventional liquefaction. Previous work in this laboratory has shown that good conversion to liquid products can be obtained under mild conditions, using CO/H₂O with alkaline catalysts particularly sodium aluminate (NaAlO₂) [2,3]. However, most of the CO introduced into the autoclave reacts with the H₂O, forming CO₂ and H₂ by the Water Gas Shift (WGS) reaction. It is therefore of interest to see if this generated hydrogen could be used to improve the quality of the product in the presence of suitable catalysts. In addition, it is much easier to prepare synthesis gas (CO + H₂) than either pure CO or H₂. Therefore, the use of CO/H₂ mixtures with a combination of alkali and hydrogenation catalysts was investigated.

2. EXPERIMENTAL

Three low-rank coals, Beulah, TH5 and Loy Yang run-of-mine (LY ROM) of oxygen content 23.2-23.7 wt % daf, three sub-bituminous coals, Wadge (16.0 wt % daf oxygen), Wyoming (19.1 wt % daf oxygen) and Taiheiyo (13.8 wt % daf oxygen) and one bituminous coal, Surat Basin (SSB, 8.8 wt % daf oxygen) with a range of atomic H/C ratios (Figure 1) were selected and characterized [4]. As received coals were ground to <250 μm and a representative sample washed with 0.1 M H₂SO₄ [5]. These acid-washed coals were used unless otherwise stated. Sodium aluminate (NaAlO₂), iron(II), copper(II) and nickel(II) acetate and ammonium molybdate ((NH₄)₆Mo₇O₂₄·4H₂O) were added to the coal as aqueous solutions and the coal-water-catalyst slurry stirred under vacuum for 1 h to aid dispersion. NaAlO₂ (1.2 wt % Na db coal), when added, was stirred in after the metal catalysts had been well dispersed, to avoid precipitation of oxymetal species and thus poor dispersion.

Liquid water was then removed under vacuum at 30°C. Treated coals were stored wet until just before reaction, when they were dried at 105°C in flowing nitrogen. The reactor was charged with 1 g of treated coal, 2.5 g H₂O and 3 MPa (cold) of gas and heated to temperature in 2 min in a heated sand-bath [4]. The reactor was then held at temperature for 30 min unless otherwise stated. For two-stage reactions the autoclave was cooled to room temperature after the first stage, repressurized with the required gas and heated to 365°C or 400°C. After completion of reaction the product was isolated [6] and fractionated into dichloromethane insolubles, asphaltene (soluble in dichloromethane, insoluble in hexane) with oil (soluble in hexane) and gas and water (OGW) determined by difference. Total conversion is 100- wt % dichloromethane insolubles (daf coal charge).

* This research was supported by NEDO, Japan.

3. RESULTS AND DISCUSSION

3.1 Reactions at 365°C with CO-containing atmospheres

Reactions of the coals with CO/H₂O gave small conversions but addition of NaAlO₂ led to significant increases in all cases (Figure 1). In contrast to conventional hydrogenation where CO₂-free conversion depends on the CO₂-free atomic H/C ratio and not on rank [7], conversion in CO/H₂O/NaAlO₂ depends on both coal atomic H/C ratio and oxygen content (rank), as can be seen by comparing Figure 1 results with coal oxygen contents given in the Experimental Section. Thus e.g. the conversion for the low rank LY ROM coal was significantly higher than that of the hv bituminous SSB coal even through its atomic H/C ratio was lower. A 1:1 mixture of CO and H₂ (referred to below as 'CO/H₂') gave similar conversions and trends with coal properties to pure CO, but OGW values were generally higher and asphaltene yields lower than in pure CO. However, for CO:H₂ ratios below 1:1 conversion fell except for the bituminous coal.

Conventional hydrogenation catalysts were added to the CO/H₂O/NaAlO₂ system in the hope that they would utilize the hydrogen produced via the WGS reaction or hydrogen initially present when CO/H₂ is used. For the three coals studied, LY ROM (brown), Taiheiyo (sub-bituminous) and SSB (hv bituminous) addition of Fe (1.7 wt % daf) and Ni (1.8 wt % daf) to NaAlO₂ treated coals increased conversion by 5-13 wt % daf coal for reactions with CO and CO/H₂. Addition of Cu (1.9 wt % daf) actually decreased conversion for LY ROM but conversion increased for the higher rank coals as with Fe and Ni. These results suggest that the hydrogen generated by the WGS reaction or present initially did not react beneficially with the coals or their derived materials even in the presence of good hydrogenation catalysts. Ni/Mo (0.2/0.9 wt % daf) did not affect conversion of LY ROM but increased conversion of SSB coal by 7%, similarly to Ni.

The non-effectiveness of added hydrogenation catalysts led us to investigate whether this was due to inherent lack of reactivity of the catalysts in aqueous media or due to the unreactivity of the initially formed materials from the CO/coal reactions.

3.2 Reactions at 365°C with H₂/H₂O

Accordingly reactions of all the coals with H₂/H₂O were investigated. Reactions in the absence of added catalyst gave conversions of only 25-30%. Sodium aluminate pretreatment of the coals increased conversions significantly for the higher rank but not the lower rank coals. Addition of Fe to NaAlO₂ treated coals had little effect on conversion. Cu increased conversion of the higher rank coals by up to 20% but did not affect conversion of LY ROM coal. Ni, on the other hand, increased conversion of coals of all ranks by up to 20% so that the conversions were similar to those in CO/H₂O/NaAlO₂.

3.3 Reactions at 400°C

Reactions were also carried out at 400°C because most hydrogenation catalysts are more active at this higher temperature. For Fe/NaAlO₂ promoted reactions with CO or CO/H₂ there was a significant increase in useful products for SSB but not for LY ROM. However, for all the coals Ni/NaAlO₂ and Ni/Mo/NaAlO₂ gave more useful products at 400°C in CO and CO/H₂ than at 365°C and (in the case of LY ROM) in H₂/H₂O also. For LY ROM the conversion at 400°C was ~ 70% for all reactions when Ni or Ni/Mo and NaAlO₂ were used as promoters.

These results show that the initial material from CO/NaAlO₂ reactions is not particularly susceptible to favourable reactions with H₂ in the presence of a good hydrogenation catalyst such as Ni. This is not due to lack of activity of such catalysts for addition of Ni/Mo to LY ROM led to an increase in conversion from 37 to 70% for reaction with H₂/H₂O at 400°C and, as noted in 3.2, Ni showed some activity even at 365°C.

3.4 Two-stage reactions

Two paths are therefore open to improve yields from CO/H₂O-type reactions, either removing the CO and water and carrying out a second dry catalysed hydrogenation stage or giving up the attempt to hydrogenate the initial CO/H₂O-reacted material and instead adding a second CO/H₂O stage

in the absence of hydrogenation catalyst. In this paper the second possibility is discussed. The first possibility has been the subject of another study [8].

Table 1 shows that cooling and recharging with CO increased the conversion over and above what would be expected for a total reaction time equal to that for the two stages combined. The low asphaltene and high OGW yields should be noted. The oil yield appears to be very similar to that obtained using a highly active Ni/Mo hydrogenation catalyst in reactions which gave conversions greater than 90% but with asphaltene yields of over 20% [8]. Furthermore, it appears that the low yields from single-stage CO/H₂O reactions are not due to irreversible polymerization but to low levels of the reaction intermediate which reacts with the coal (Ross *et al's* mechanism [9]).

Table 1
The effect of recharging with CO in a 2 stage reaction procedure

No. of Stages	Temperature (°C)	Conversion (wt % daf coal)		
		Total	Asph	OGW
1	365	57	8	49
1	400	68	8	60
2	365/365	66	9	57
2	330/400	77	11	66
2	365/400	81	12	69
2	400/400	82	10	72

Reaction conditions: 1st stage; 1 g db of coal treated with NaAlO₂ (1.2 wt % db Na), 2.5 g H₂O and 3MPa CO(cold) were heated for 30 min at temperature in a 35 ml tubular reactor.

2nd stage; after the 1st stage the reactor was cooled, vented, then charged with 3 MPa CO (cold) and heated for 30 min at temperature.

Single stage; as for 1st stage, except that reaction time was 60 min.

REFERENCES

1. F. Fischer and H. Schrader, *Brennstoff-Chemie* 2 (1921) 257.
2. C.P. Hughes, T. Sridhar, S.C. Lim, P.J. Redlich, W.R. Jackson and F.P. Larkins, *Fuel* 72 (1993) 205.
3. J.S.T. Chan, W.R. Jackson and M. Marshall, *Fuel* 73 (1994) 1628.
4. C.K.J. Hulston, P.J. Redlich, W.R. Jackson, F.P. Larkins and M. Marshall, accepted for publication by *Fuel*.
5. P.J. Redlich, W.R. Jackson, F.P. Larkins and D. Rash, *Fuel* 68 (1989) 222.
6. P.J. Cassidy, W.R. Jackson, F.P. Larkins, R.J. Sakurovs and J.F. Sutton, *Fuel* 65 (1986) 374.
7. P.J. Redlich, W.R. Jackson and F.P. Larkins, *Fuel* 68 (1989) 231.
8. C.K.J. Hulston, W.R. Jackson, F.P. Larkins, M. Marshall and P.J. Redlich, Proc. 8th International Conference on Coal Science, Oviedo, 'Single and multistage reactions of various coals to produce high yields of fluid fuels'.
9. D.S. Ross, G.P. Hum, T.-C. Miin, T.K. Green and R. Mansani, Prepr. Div. Fuel Chem. Am. Chem. Soc. 30(3) (1985) 94.

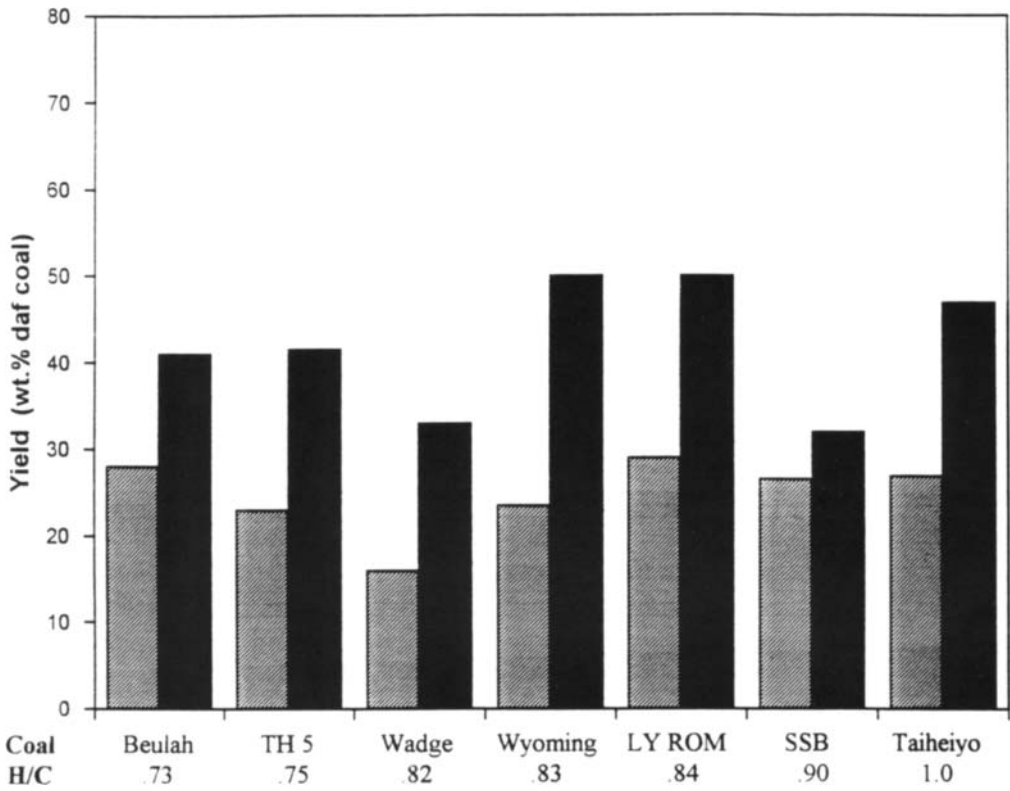


Figure 1 The total conversion of acid washed coals in CO/H₂O with and without NaAlO₂ at 365°C.

Effect of heating rate on normal and catalytic fixed-bed hydropyrolysis

L. Baoqing^a, S.C. Mitchell^b and C.E. Snape^b

^aThe State Key Laboratory of Coal Conversion, Institute of Coal Chemistry, Chinese Academy of Sciences, Taiyuan, Shanxi 030001, P.R. China

^bUniversity of Strathclyde, Dept of Pure & Applied Chemistry, Glasgow G1 1XL, Scotland, UK

Fixed-bed hydropyrolysis tests have been conducted on a UK bituminous coal (Gedling), the Wyodak Argonne Premium Coal Sample and the high-sulphur Mequinenza lignite at a pressure of 150 bar. The tar yields and overall conversions increased markedly by *ca* 5-20% daf coal as the heating rate was decreased from 300 to 5°C min⁻¹, both with and without a sulphided molybdenum catalyst, demonstrating the value of slow heating in analytical applications of hydropyrolysis which include the determination of organic sulphur forms in coals.

1. INTRODUCTION

Although pyrolysis processes have historically been associated with much lower yields of liquid products than vehicle solvent liquefaction processes, previous work has demonstrated that tar yields of *ca* 60% daf coal with relatively low gas yields can be achieved for bituminous coals in fixed-bed hydropyrolysis at 150 bar [1,2]. A sulphided Mo or other suitable dispersed catalyst is required as tar yields without catalyst are typically no more than 35%. For low-rank coals, catalysts are much less effective at high pressure, increasing tar yields typically by less than 10% daf coal but, without a catalyst, the tar yields of 40-50% are appreciably higher than for bituminous coals. Although rapid heating is used in process situations [3], slow heating is being applied in analytical applications of hydropyrolysis (temperature programmed reduction) to specify organic sulphur forms in coals [4] and to release covalently-bound biomarkers [5]. It is therefore important to ascertain how slow heating affects product yields, particularly in relation to pyrolysis in inert atmospheres where extremely rapid heating often gives rise to higher tar yields [6].

In this investigation, fixed-bed hydropyrolysis tests have been conducted on a UK bituminous coal (Gedling), the Wyodak Argonne Premium Coal Sample (APCS), and the high-sulphur Mequinenza lignite, both with and without a dispersed sulphided molybdenum (Mo) catalyst. This study extends recent work where it was shown that conversions approaching 100% could be obtained at 600°C for low-rank coals with slow heating [7].

2. EXPERIMENTAL

The analyses of the coals investigated are summarised in Table 1. The coals were dried *in vacuo* at 50°C prior to conducting the fixed-bed hydrolysis experiments in the resistively-heated reactor (0.8 cm i.d.) described previously [1,2,4]. The coals (4 g samples) were diluted in sand (2:1 mass ratio) to help overcome mass transfer restrictions to the release of volatiles. The tests were conducted using 150 bar hydrogen at temperatures of 520°C and 600°C with heating rates of 5, 50 and 300°C min⁻¹. For the catalytic tests, ammonium dioxodithiomolybdate was impregnated onto the coals to give a Mo loading of 1% (daf basis). For purposes of comparison, some tests were also conducted with nitrogen at 2 and 150 bar pressure. The total liquid yields were corrected for the amount of water present measured by the Dean-Stark method to give the tar yields.

Table 1
Elemental analyses of the coals

		Gedling	Wyodak	Mequinenza
(%dmmf)	C	83.0	76.0	66.4
	H	5.4	5.4	5.8
	N		1.1	1.6
(%db)	Total S		0.63	9.0

3. RESULTS AND DISCUSSION

The results obtained from the pyrolysis experiments in nitrogen on Gedling and Mequinenza lignite (Table 2) confirmed that heating rates in the range 5-300°C min⁻¹ had little effect on conversions [6,7]. The higher pressure of 150 bar gave rise to slightly lower tar yields and higher gas yields for both coals due to the longer

Table 2
Pyrolysis yields in nitrogen at 520°C

Heating rate	Pressure	Product distribution (%daf basis)		
		Char	Tar	C ₁ - C ₄ gases
<i>(a) Gedling</i>				
5	2	69	25	2
300	2	71	19	3
5	150	69	23	4
300	150	72	19	3
<i>(b) Mequinenza</i>				
5	2	51	35	2
300	2	51	33	2
5	150	51	29	6
300	150	56	29	5

residence times of the volatiles inside the reactor.

Tables 3-5 compare the hydropyrolysis product yields obtained at 5 and 300°C min⁻¹, with and without catalyst, for the three coals investigated. In contrast to pyrolysis in nitrogen, both tar yields and overall conversions increased markedly by 5-15% daf coal at 520°C as the heating rate was decreased from 300 to 5°C min⁻¹. For the bituminous coal, these increases occurred both with and without the catalyst. Further, the char yield with catalyst at 520°C was below 10% daf coal (Table 3), corresponding to a significant fraction of the inertinite being converted.

For both low-rank coals, the conversion was already close to 100% at 600°C with slow heating [7] and consequently the addition of catalyst gave no further increases in tar yield (Tables 4 and 5). With slow heating, overall conversions and tar yields increased by 10-20%. In contrast to the behaviour of the Wyodak APCS, catalyst addition to Mequinzenza did not increase the tar yield significantly at 520°C (Tables 4 and 5). This might imply that tar generation for Mequinzenza lignite commences at a lower temperature. Indeed, hydrocarbon gases have been observed to evolve at considerably lower temperatures from Mequinzenza lignite in TPR than from the Wyodak APCS, probably due to the cleavage of the weaker C-S bonds [4].

No significant variations in the composition of the hydropyrolysis tars obtained with slow and fast heating were identified by elemental and NMR analyses. The fact that conversions are nearly 100% at 600°C with catalyst (Tables 4 and 5) confirms that in high pressure TPR virtual complete desulphurisation must occur for organic forms [4]. The improved volatile yields are ascribed to the much longer times available with slow heating at temperatures below ca 450°C for the hydrogen and catalyst to mediate bond scission (hydrocracking and heteroatom removal) reactions. Although higher conversions have been reported for hydropyrolysis in heated-grid reactors as the heating rate falls [8], the effects appear less pronounced than in the fixed-bed reactor used here, probably due to a combination of the much lower gas velocities through the sample bed and that the slowest rate used was 60°C min⁻¹.

REFERENCES

1. C.E. Snape, C.J. Lafferty, H.P. Stephens, R.G. Dosch and E. Klavetter, *Fuel*, 70 (1991) 393.
2. C.E. Snape, C.J. Lafferty, G. Eglinton, N. Robinson and R. Collier, *Int. J. Energy Res.* 18 (1994) 233.
3. S. Furfari, IEA Report No. ICTIS/TR20 (1983).
4. S.C. Mitchell, C.E. Snape, K. Ismail, R. Garcia and K.D. Bartle, *Fuel*, 73 (1994) 1159.
5. G.D. Love, C.E. Snape and A.D. Carr, *Prepr. Am. Chem. Soc. Div. Fuel Chem.*, 38(4) (1993) 1281 and submitted to *Energy & Fuels*.
6. J.B. Howard in *Chemistry of Coal Utilisation* 2nd. Supp. Vol., Ed. M.A. Elliott, J. Wiley (1981) 655 and references therein.
7. E. Klavetter, S.C. Mitchell, R. Garcia and C.E. Snape, *Proc. 1993 Int. Conf. on Coal Science, Banff, Canada, Vol. I* (1993) 328.
8. C.Z. Li, S. Madrali, F. Wu, B. Xu, H-Y Cai, A.J. Guell and R. Kandiyoti, *Fuel*, 73 (1994) 851.

Table 3
Hydropyrolysis yields for Gedling coal at 520°C

Heating rate	Catalyst	Product distribution (% daf basis)		
		Char	Tar	C ₁ - C ₄ gases
5	No	42	39	11
300	No	57	34	7
5	Yes	8	76	9
300	Yes	22	62	7

Table 4
Hydropyrolysis yields for Wyodak APCS at 520 and 600°C

Heating rate	Catalyst	Product distribution (% daf basis)		
		Char	Tar	C ₁ - C ₄ gases
<i>(a) 520°C</i>				
5	No	21	57	9
300	No	30	52	8
5	Yes	8	73	9
300	Yes	22	62	7
<i>(b) 600°C</i>				
5	No	3	67	19
300	No	20	50	17
5	Yes	5	69	17
300	Yes	4	69	18

Table 5
Hydropyrolysis yields for Mequinenza lignite at 520 and 600°C

Heating rate	Catalyst	Product distribution (% daf basis)		
		Char	Tar	C ₁ - C ₄ gases
<i>(a) 520°C</i>				
5	No	24	58	10
300	No	42	44	9
5	Yes	16	59	14
300	Yes	19	61	9
<i>(b) 600°C</i>				
5	No	5	75	12
300	No	15	62	10
5	Yes	<1	76	13
300	Yes	3	74	10

EFFECT OF INCREASE IN GAS FLOW RATE ON COAL LIQUEFACTION WITH HIGHLY DISPERSED CATALYSTS

M. Yasumuro, S. Katsushima, Y. Kageyama and T. Matsumura

Nippon Brown Coal Liquefaction Co., Ltd.,
Niihama 2, Arai-cho, Takasago, Hyogo 676, Japan

1. INTRODUCTION

In a direct coal liquefaction process, pulverized coal is hydroliquefied in a solvent with catalyst under high temperature and high pressure. Hydrogen gas is blown into the coal slurry before the preheating stage and process gas is recycled into the reactors.

An increase in gas flow rate accelerates the liquefaction of the coal liquid bottom (CLB; b.p. >420 °C), then a higher yield of distillate is obtained.

In this paper, the effect of gas flow rate and effect of highly dispersed catalysts on liquefaction are investigated by analyzing the progress of hydrogenation of CLB in the continuous three reactors system. The hydrogenation of CLB under high gas flow rate is accelerated due to the increase of reaction time and concentration of CLB and catalyst by the vaporization of the lighter part of solvent fraction, where the catalyst is performed effectively.

2. EXPERIMENTAL

Yallourn coal from Victoria, Australia, was liquefied using the 0.1t/d continuous Bench Scale Unit, which has three stirred reactors in series. Table 1 shows the liquefaction conditions. Two types of iron based catalysts were used in these reactions (3 wt% on mafc as Fe). One is a finely divided pyrite ore (FeS₂), and the other is a γ -type iron hydroxide (FeOOH)

Table 1 Liquefaction Conditions

Run No.	Catalysts	Gas Flow (Nm ³ /kg mafc)
A11	FeS ₂ (2.0 μ m) ¹⁾	1.2
A12	FeS ₂ (2.0 μ m) ¹⁾	3.8
A13	FeS ₂ (0.5 μ m) ²⁾	3.8
B11	FeS ₂ (0.5 μ m) ¹⁾	2.6
B12	γ -FeOOH(0.5 μ m) ²⁾	2.6

1) pulverized in air stream

2) pulverized in solvent

Other Conditions : 450°C, 14.7 MPa,

H₂ Feed : 1.2Nm³/kg mafc

Table 2 Typical Properties of Catalysts

Catalysts	Particle Size (μ m)	Surface Area (m ² /g)	Crystallite Size (nm)	Composition	
				Fe (wt%)	S (wt%)
FeS ₂ ²⁾	2.0	4	—	41.89	47.47
FeS ₂ ²⁾	0.5	15	—	43.58	48.04
FeS ₂ ³⁾	0.5	16	300	44.38	52.86
γ -FeOOH ⁴⁾	0.5	63	40	59.28	0.73

1) Analyzed by laser diffraction

2) Pyrite ore pulverized in air stream

3) Pyrite ore pulverized in solvent

4) Synthetic iron hydroxide made by a precipitation method from iron sulfate.

Table 3 Product Yield Distribution (wt% on mafc)

Run No.	Catalysts	Gas Flow (Nm ³ /kg mafc)	Dist. ¹⁾	CLB	Solv.	Naph.	H ₂ O	C ₁ -C ₄	CO+CO ₂	ΔH ₂	θ rt ²⁾ (min)
A11	FeS ₂ (2.0 μm)	1.2	13.8	45.3	4.7	9.1	16.5	12.6	15.4	-3.5	22.3
A12	FeS ₂ (2.0 μm)	3.8	48.0	19.6	39.2	8.8	14.9	11.7	12.6	-6.9	79.4
A13	FeS ₂ (0.5 μm)	3.8	46.4	19.0	32.7	13.7	17.0	11.5	12.0	-5.9	88.7
B11	FeS ₂ (0.5 μm)	2.6	34.6	29.0	26.5	8.0	15.9	12.6	13.4	-5.4	27.2
B12	γ-FeOOH(0.5 μm)	2.6	40.2	27.2	30.6	9.6	16.0	10.6	12.4	-6.5	30.2

1) Distillate : Solv.(Solvent fraction)+Naph.(Naphtha fraction)

2) Actual residence time of RL in the 3rd reactor

added sulfur(S/Fe 1.2, atom/atom). Table 2 shows the properties of these catalysts used. The product liquid (PL) and the reactor liquid (RL), which was sampled directly from the reactors, were separated by distillation into CLB, solvent (SOL; b.p.180–420°C), naphtha (NAP; b.p.<180°C) fractions and H₂O. The actual residence time (θ_{RT}) of RL was estimated by comparing the distillation results of both RL and PL [1][2].

3.RESULT AND DISCUSSION

3.1.Effect of gas flow rate

Table 3 shows the effect of gas flow rate on the product yields.

Under high gas flow rate with pyrite catalyst (2.0 μm) (Run A12), CLB yield decreased to 19.6 wt% on mafc which was

45.3 wt% under normal condition(Run A11). In accordance with decrease in the CLB yield, the distillate yield significantly increased.

The hexane soluble fraction(HS) in the CLB increased up to 9.83 wt% on mafc which was about twice larger than that under normal condition as shown in Table 4.

Figure 1 shows the change in H/C atomic ratio of CLB collected from each reactor. The H/C value of CLB decreased with the actual residence time under normal condition. This indicates that the fraction of high H/C in the CLB converts into the distillate and the

Table 4 Solvent Extracts Yield (wt% on mafc)

Run No.	Catalysts	Gas Flow (Nm ³ /kg mafc)	HS ¹⁾	HI-TS ²⁾	TI-THFS ³⁾	THFlorg. ⁴⁾
A11	FeS ₂ (2.0 μm)	1.2	5.25	27.60	5.47	6.99
A12	FeS ₂ (2.0 μm)	3.8	9.83	7.42	1.08	1.30
A13	FeS ₂ (0.5 μm)	3.8	8.71	8.64	0.75	0.85
B11	FeS ₂ (0.5 μm)	2.6	4.58	17.73	2.96	3.68
B12	γ-FeOOH(0.5 μm)	2.6	10.98	12.97	1.08	2.22

1) Hexane solubles 2) Hexane insolubles-toluene solubles

3) Toluene insolubles-THF solubles 4) THF insolubles (ash free basis)

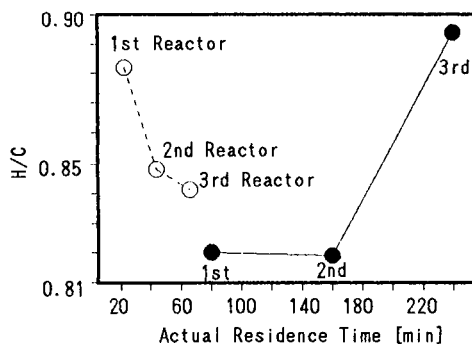


Fig.1 Change in H/C Ratio of CLB

○:Run-A11, Gas Flow 1.2Nm³/kg-mafc

●:Run-A12, Gas Flow 3.8Nm³/kg-mafc

remaining CLB has less hydrogen. On the contrary, the H/C value of CLB under the condition of high gas flow rate increased with the residence time. Especially, the H/C of final CLB product is very high in accordance with the high yield of HS fraction. It is clarified that increasing of gas flow rate promotes the hydrocracking and hydrogenation of CLB significantly.

The amount of solvent fraction vaporized in the reactor increased with gas flow rate. The vaporization of large amount of solvent caused high concentration and long residence time of CLB in the reactor [1][2]. In addition, the catalyst was concentrated in the reactor. These physical changes in the reactor promoted the hydrocracking and hydrogenation of CLB.

3.2. Effect of catalyst type under high gas flow rate

Figure 2 shows the change in H/C atomic ratio of each fraction of CLB with pyrite catalysts. The H/C value of HS increased with residence time, while that of TI-THFS slightly decreased. It was shown that the H/C value of CLB in the case of pyrite catalyst ($0.5 \mu\text{m}$) was higher than that of pyrite catalyst ($2.0 \mu\text{m}$). These results indicate that smaller particle size of catalyst enhances the hydrogenation activity for CLB, although not enough to obtain the higher distillate yield as shown in Table 3.

On the other hand, lower CLB yield, higher distillate yield and higher HS yield were obtained using $\gamma\text{-FeOOH}$ catalyst having smaller crystallite size under the same conditions with pyrite catalyst ($0.5 \mu\text{m}$). Figure 3 shows the change in values of H/C and Haru/Car of each fraction in CLB during liquefaction with $\gamma\text{-FeOOH}$ catalyst compared with pyrite catalyst. The value of H/C and Haru/Car of both HI-TS and TI-THFS decreased, while those of HS were nearly constant or slightly increased with residence time. It was found that the value of both H/C and Haru/Car of HS using

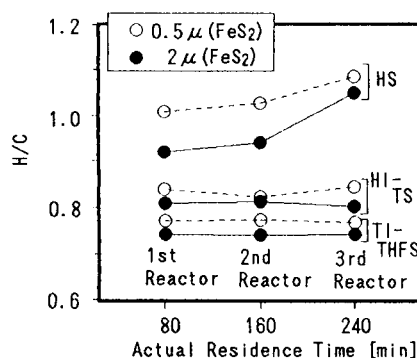


Fig. 2 Change in H/C Ratio of Solvent Extracts (Run-A12, A13)

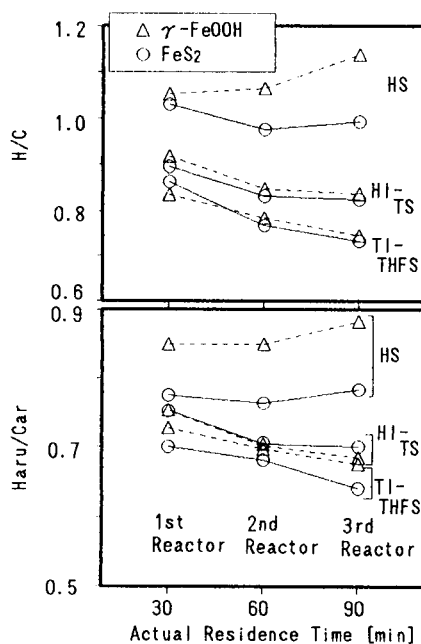


Fig. 3 Change in H/C Ratio & Haru/Car of Solvent Extracts (Run-B11, B12)

γ -FeOOH catalyst were higher than those in the case of pyrite catalyst. These results indicate that γ -FeOOH catalyst with a smaller crystallite size has a higher catalytic activity for the hydrogenation and hydrocracking of CLB to convert to lighter fractions. As shown in Table 2, γ -FeOOH was prepared by a precipitation method from iron sulfate followed by pulverizing in coal-derived solvent using a ultrafine mill to disperse the fine particles in the solvent. Therefore γ -FeOOH has a high surface area ($63 \text{ m}^2/\text{g}$), a small crystallite size (40 nm) and well dispersion in the solvent compared with a finely divided pyrite ore.

4. CONCLUSION

The gas flow rate was very effective to obtain the high distillate yield. The increase in the gas flow rate caused high concentration of both CLB and catalyst with a long residence time of CLB. This physical change brought the increase in the distillate yield and hydrocracking and hydrogenation of CLB.

On the other hand, it was clarified that the catalyst of small particle size is effective to hydrogenate light fraction in CLB and γ -FeOOH is an active catalyst to promote the hydrocracking and hydrogenation of CLB. Based on these results, it is suggested that the distillate yield could be further increased by increasing in gas flow rate with highly dispersed catalyst, such as γ -FeOOH.

5. ACKNOWLEDGEMENTS

This study was supported by the New Energy and Industrial Technology Development Organization (NEDO). The authors thank NEDO for permission to make this presentation.

REFERENCES

1. O. Okuma, et al, Proc. of 1987 Int. Conf. on Coal Sci., Maastricht, pp307.
2. O. Okuma, et al, Proc. of 1989 Int. Conf. on Coal Sci., Tokyo, pp701.

Effects of coal pretreatment and catalyst recovery on the liquefaction

K.Sakanishi^a, H.Hasuo^a, H.Taniguchi^a, I.Mochida^a, and O. Okuma^b

^aInstitute of Advanced Material Study, Kyushu University, Kasuga, Fukuoka 816, Japan

^bPolymer & Chemical Technology Lab., Kobe Steel, Ltd., Kobe, Hyogo 651-22, Japan

Liquefaction reactivities of Yallourn, Tanitoharum, and Wyoming coals are examined with or without coal pretreatment using sulfided Fe₃Al and NiMo supported on carbon blacks, which have functions for recovery. The combined effects of coal pretreatment and Mo salt impregnation are suggested to be marked probably due to the liberations of coal macromolecules through the pretreatment, improving the affinity to the catalyst species and the dispersion of Mo active species into the liberated coal macromolecules. The liquefaction behaviors of the coals are compared in terms of pretreatment effects, liquefaction conditions, and catalyst recovery.

1. INTRODUCTION

Coal liquefaction processes, which have been developing to substitute petroleum crude for next century, are required to break through the economical barrier for their commercialization. One of the economical breakthroughs is to develop a highly active catalyst with functions for recovery to increase distillate yield as well as to get rid of the waste derived from disposable catalysts.

The present authors proposed that design of recoverable catalysts for the primary liquefaction stage can improve the economy of coal liquefaction process^{1,2}. The basic idea is to recover the catalyst from the inorganic residues which are originated from the feed coal. According to the natures of inorganic residue, three approaches can be designed, 1) removal of inorganic residues such as carbonates and chlorides, 2) recovery of the ferromagnetic catalysts from the diamagnetic residue, and 3) gravimetric recovery of the catalysts supported on carbon black particles³. A multi-stage approach⁴, which consists of coal pretreatment, hydrogen-transfer dissolution, and catalytic steps, may facilitate the catalyst recovery by reducing both inorganic and organic residues. The organic residue has been recycled with the catalyst and minerals to the primary liquefaction stage as the bottom recycle⁵. Its favorable results have been reported, although the accumulation of inorganic solids requires a fixed rate of purging.

In the present study, combinations of coal pretreatment and catalyst dispersion or recovery procedures are examined to accelerate coal depolymerization as well as to increase oil yield with a smaller amount of catalyst. Such combinations have advantages for the catalyst recovery

through the complete conversion of coal with the least yield of inorganic and organic residues.

2. EXPERIMENTAL

Three coals of Yallourn (Australian brown), Tanitoharum (Indonesian subbituminous), and Wyoming (American subbituminous) were used for the liquefaction reactions. Their elemental analyses are summarized in Table 1. Tetralin of guaranteed grade was used as a hydrogen-

Table 1 Elemental analyses of coals

Coals	wt%, daf basis				H/C	Ash	Catalysts	Particle size (μm)	Surface area (m^2/g)	Specific gravity (-, $\text{H}_2\text{O}=1$)
	C	H	N	(O+S)diff.	(-)	(wt%)				
Wyoming	68.9	5.4	1.0	24.7	0.94	3.7	FeS ₂	1-16(78.4wt%)	< 20	-
Tanitoharum	76.3	5.6	1.4	16.7	0.87	4.8	Fe ₃ Al	7.2(<500 mesh)	0.5	6.5 - 7.9
Yallourn	66.9	4.7	0.5	27.7	0.84	1.6	KB-JD	30 x 10 ⁻³	1270	0.115

Table 2 Some properties of catalysts and supports

donor solvent. The coals were pretreated in 10% CH₃COOH aqueous solution or ammonium tetrathiomolybdate (ATTM) solution in 10% methanol/H₂O at room temperature for prescribed hours, followed by the filtration and drying at 60°C or the evaporation of solvent and drying at 60°C, respectively. Three types of the catalysts (see Table 2), sulfided Fe₃Al (ferromagnetic), NiMo / Ketjen Blacks, and a synthetic pyrite, were used for the liquefaction reactions.

The liquefaction was carried out in an autoclave (50ml volume) with . The ground coal (< 60 or < 200 mesh, 3.0g), the solvent (4.5g) and catalyst (0.09 - 0.10 g) were charged into the autoclave. After the liquefaction reactions, the product remaining in the autoclave was extracted with THF, acetone, and hexane. The hexane soluble, hexane insoluble-acetone soluble, acetone insoluble-THF soluble, and THF insoluble fractions were defined as oil(O), asphaltene(A), preasphaltene (P), and residue(R), respectively. The gas yield was calculated by the difference between the initial and recovered residual weights.

3. RESULTS AND DISCUSSIONS

3.1 Effects of Coal Pretreatment and Catalyst Dispersion on the Liquefaction

Figure 1 shows the liquefaction results of Wyoming and Morwell coals with sulfided Fe₃Al at 440°C, 60 min, and 13 MPa H₂, before and after the coal pretreatment. The pretreatment with 10% CH₃COOH at room temperature for 24 hr improved the products slates, increasing oil and asphaltene with decreased yields of gas and heavy products. The pretreatment was more effective for Morwell coal than for Wyoming coal, reflecting its higher content of bridging ion-exchangeable cations such as Ca²⁺ and Mg²⁺ through the oxygen functional groups⁶⁾.

Figure 2 illustrates the liquefaction results of Tanitoharum coal at 450°C, 60 min, and 10 MPa H₂ pressure before and after the coal pretreatment and/or ATTM impregnation. The combination of coal pretreatment and Mo impregnation increased the oil yield to 58% with decreasing asphaltene yield. It is noted that a smaller amount (0.5 wt% based on coal) of ATTM impregnation into coal exhibited the high activity, especially higher for the deashed coal.

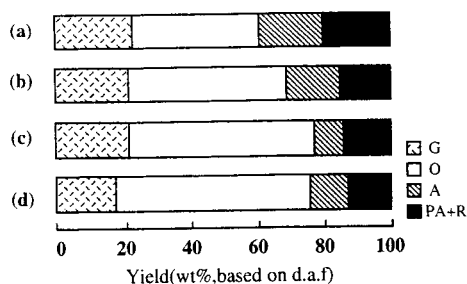


Figure 1 Effect of coal pretreatment on the liquefaction at 440°C, 60 min, and 13 MPa

- (a) Wyoming coal (b) Pretreated Wyoming coal
(c) Morwell coal (d) Pretreated Morwell coal

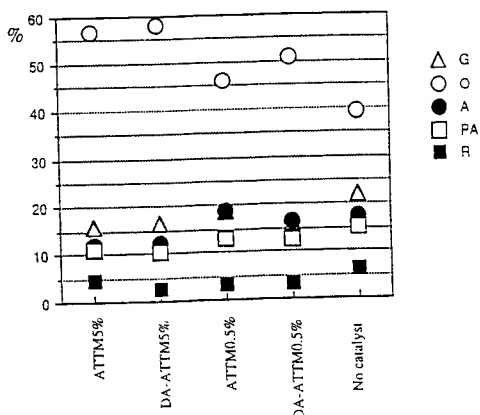


Figure 2 Effects of coal pretreatment and catalyst impregnation on the liquefaction at 450°C, 60 min, and 10 MPa H₂

3.2 Recovery and Repeated Use of NiMo/KB Catalyst

Figure 3 shows the activity of NiMo/Ketjen Black(KB) catalyst and its recovered one as THFI for the liquefaction of Wyoming coal at 440°C, 60 min, and 13 MPa H₂ pressure. The recovered catalyst as THFI residue, which contained the used catalyst at the concentration of 20 wt% with organic and inorganic insolubles, appeared to regenerate the activity to the similar level of the virgin catalyst by the resultfiding treatment with 5% H₂S/H₂ at 360°C for 2 h.

Figure 4 illustrates the activity of NiMo/KB catalyst and its recovered one as THFI for the liquefaction of Yallourn coal at 440°C, 60 min, and 13 MPa H₂ pressure. The virgin catalyst exhibited the high activity with 70% of oil and asphaltene yield, while the recovered one gave lower oil and asphaltene yield, although the yield was still much higher than that of non-catalytic liquefaction.

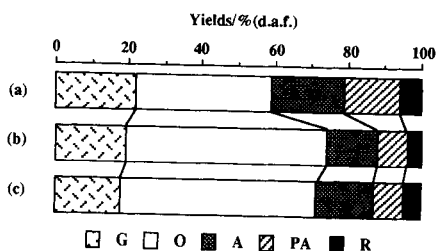


Fig.3 Activity of Ni-Mo/KB JD and its recovered one as THFI in the liquefaction of Wyoming coal.

- (a) no catalyst
(b) Ni-Mo/KB JD
(c) THF-I(catalyst 0.09g in THFI(0.4g))

Reaction conditions

reaction temperature : 440°C
reaction pressure : 13.0MPa
reaction time : 60min
heating rate : 22°C/min
catalyst : catalyst M
(3wt% addition to coal)
solvent(Tetralin)/coal = 1.5

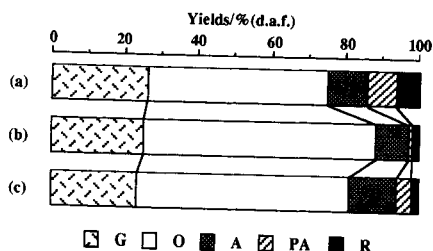


Fig.4 Activity of Ni-Mo/KB JD and its recovered one as THFI in the liquefaction of Yallourn coal.

- (a) no catalyst
(b) Ni-Mo/KB JD
(c) THF-I(catalyst 0.09g in THFI(0.2g))

Reaction conditions

reaction temperature : 440°C
reaction pressure : 13.0MPa
reaction time : 60min
heating rate : 22°C/min
catalyst : catalyst M
(3wt% addition to coal)
solvent(Tetralin)/coal = 1.5

KB-supported NiMo catalysts were found to be recovered from the whole product by gravity separation using methanol, hexane and water in this order as illustrated in Figure 5, although the weight of recovered catalyst was gained to some extent due to the inclusion of organic materials on the catalyst. The combination of deashing pretreatment and recoverable catalysts, such as NiMo supported on magnetic supports of Fe₃Al and ferrite / carbon or gravimetrically recoverable supports of carbon blacks, may facilitate the catalyst recovery as well as keep the initial catalytic activity in the repeated run.

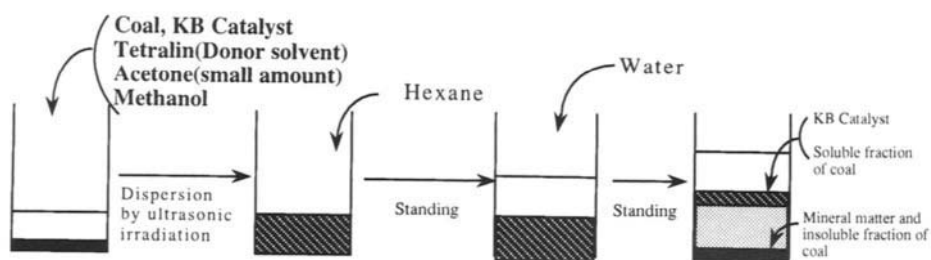


Figure 5 Recovery Scheme of the KB-supported Catalyst

4. CONCLUSIONS

The present study emphasized that the recovery and recycle of the catalyst are basically possible by using the catalyst supports with the functions for recovery, after the primary coal liquefaction, where the inorganic solid residues are present to contaminate the used catalyst. Although the catalytic activity so far is not super, more elaborate preparation of the catalyst can improve the activity without losing functions for recovery. Smaller particle size, better dispersion of active species, and strengthening favorable catalyst-support interactions are such ways to enhance the activity.

Recovered catalysts often lost their initial activity. The loss of sulfur and contamination with inorganic as well as organic poisons cause the deactivation. The multi-stage reaction schemes including coal pretreatment, solvent roles of hydrogen donation and dissolution, and the higher dispersion of active catalytic species should be further developed to achieve the maximum oil yield with the least amount of catalyst.

REFERENCES

1. I.Mochida, K.Sakanishi, M.Kishino, K.Honda, T.Umezawa, S.H.Yoon, ACS Div.Fuel Chem., **1993**, 38(1), 93.
2. I.Mochida, K.Sakanishi, R.Sakata, K.Honda, T.Umezawa, Energy & Fuels, **1994**, 8, 25.
3. I.Mochida, H.Hasuo, K.Sakanishi, H.Taniguchi, ACS Div.Fuel Chem., **1995**, 40,
4. I.Mochida, K.Sakanishi, Y.Korai, H.Fujitsu, Fuel Process.Technol., **1986**, 14, 113.
5. I.Mochida, K.Sakanishi, 'Advances in Catalysis(Academic Press)', vol.40, p.39-85 (1994).
6. I.Mochida, A.Yufu, K.Sakanishi, Y.Korai, Fuel, **1988**, 67, 114.

Effect of gamma-radiation on structure, reactivity and the process of liquefaction of brown coals

G. B. Skripchenko, G. S. Golovin, V. I. Sekriyeru

Fossil Fuel Institute, 29, Leninsky prospect, 117910 Moscow, Russia

Analysis of publication data allows to conclude, that ionising radiation might have a certain effect on the formation of the structure and properties of coals in the process of metamorphism. Additional effect of gamma radiation changes paramagnetic characteristic features of coals, the stability to thermal effect, the character of destruction. But concrete data on the character of changes of properties are quite contradictory.

In the present work the data are given, which resulted from complex investigation of the effect of radiation on structure, properties and the process of liquefaction of brown coals of Borodinsky and Berezovsky open pits of Kansk-Achinsk basin by IR, EMR spectroscopy, thermal and chemical analysis. These coals are proximate as for there petrographic and ultimate analysis ($C^{daf}=70.5 - 71.5 \%$, $H^{daf}=5.0 \%$), and volatile matter content. But they are somehow different by the distribution of elements over structural groups, organic-mineral structures and thermal destruction characteristics [1, 2].

Ground coal sized < 0.1 mm was previously dried by heating in vacuum up to $70 - 80^{\circ}\text{C}$. Then it was subjected to radiation at the ^{60}Co unit until 300 kGy adsorbed dose.

The data on ultimate composition and IR-spectra of coals before and after radiation were approximately the same. However, IR-spectra of radiated KBr pill exhibited considerable variation. With the dose absorbed a certain decrease of the intensity of CH_2 adsorption band occurs (frequency 2930 cm^{-1}), and more considerable effect take place for CH_3 band (2960 cm^{-1}). It indicates to deep chemical transformation in coal organic matter (COM), reactive structures formation and hydrogen redistribution as the result of dehydration, dealkylation and cyclization reactions [3]. These data are in good agreement with the results of investigations of the composition and the quantity of gases liberated during radiolysis of coals.

Within 100 - 200 kGy doses decrease of 1700 cm^{-1} and appearance of 2340 cm^{-1} adsorption bands intensities are observed (CO_2 is being accumulated in KBr matrix). These are consequences of carbon - oxygen bonds distraction and CO_2 removal from COM. Simultaneously 3400 cm^{-1} band intensity considerably decreases, which is associated with the destruction of hydrogen bonds. Decrease of intermolecular bonds in the course of brown coal radiation is supported by the data on their swelling [4].

The spin centres content (SCC) in coals is essentially varying under radiation. If an ampoules with samples of Beryozovsky coal were radiated at 293 K, the SCC increases with the increase of radiation dose up to 50 kGy, then it decreases dramatically with the increase of radiation dose up to 100 kGy, and then it decreases slowly with the increase of radiation dose up to 300 kGy. In the case of Borodinsky coal the SCC dependence from radiation dose the following: SCC sharply decreases approximately by two times within 5 - 7 kGy, then it returns to the initial value at 30 kGy dose. With further increase of a dose exceeding 50 - 70 kGy, SCC decreases the same way as it does in the case of Beryozovsky coal (figure 1).

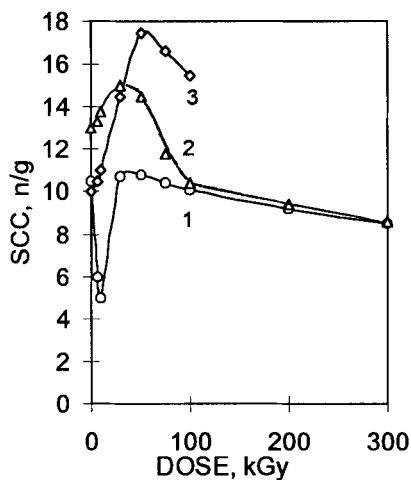


Figure 1. Effect of a dose of radiation on SCC ($\cdot 10^{-18}$) for Borodinsky (1,3) and Beryozovsky (2) coals. (1, 2 - at 293 K, 3 - at 77 K).

return to their initial values. The rate of interaction of coals and oxygen under heating increases with the increase of radiation dose up to 50 kGy, but afterwards, the rate of interaction drops to the initial value with the increase of dose.

Two methods have been used in studying the effect of radiation on hydrogenation ($P_{H_2} = 10$ MPa, $T = 425$ °C, $t = 1 - 2$ h) of brown coal pastes (1:1) with petroleum paste medium (fraction with $T_b > 260$ °C): preliminary radiation of coal pastes and immediate radiation during hydrogenation (radiated hydrogenation).

After radiation structural viscosity of pastes at 50 - 100 °C decreases by approximately 2 times, thermal stability of pastes also decreases [5,6]. Table 1 presents changes of group composition of paste and fractional composition of benzene extract yield under the effect of radiation.

Table 1

Effect of radiation on coal paste composition (%)

Sample	Group composition			Fraction composition of benzene extract		
	Oils	Asphalthenes	Residue	Yield of extract	$T_b < 300$ °C	$T_b > 300$ °C
Initial	46.2	3.8	50.0	51.4	8.9	91.4
Radiated	50.9	2.9	46.2	57.8	37.1	62.9

The yield of oils and the benzene extract percentage increase under radiation. But the main thing is that the percentage of fractions with the boiling point (T_b) less than

The observed decrease of SCC seems to be caused by the effect of sorbed O_2 or H_2O molecules, which were not removed in the process of coal surface purification. They became mobile under radiation and interact with spin centres.

If the samples of Borodinsky coal were radiated and stored before being investigated at 77 K, then SCC continuously increased with the increase of radiation dose. It indicates, that the reactions of formation and recombination of radicals goes during radiolysis of brown coal [3].

This conclusion is supported by the thermal destruction character and interaction with oxygen while heating data [3, 5]. With the increase of a radiation dose up to 50 kGy, the temperature of beginning of decomposition and the temperature of main decomposition maximum decreases by approximately 20 - 30 °C, then with the increasing of dose these characteristics

300°C considerably increases. It occurs at the expense of simultaneous radiolysis of coal and paste medium, and their interaction.

The extent of COM conversion and the yield of total liquid products (TLP) per paste organic matter (POM) slightly decreases under hydrogenation without a presence of a catalyst of radiated paste. But the percentage of light fractions in the liquid products increases and the percentage of unconverted coal (UnCoal) decreases (table 2).

Table 2

Result of hydrogenation of Beryozovsky coal (Al - Co - Mo Ct) (%)

Experimental conditions	Extent of conversion	Yield of products per POM				
		TLP	$T_b < 300^\circ\text{C}$	$T_b > 300^\circ\text{C}$	Gas	UnCoal
Without cat. without rad., 425 °C, 2h	58.5	60.8	14.7	46.1	13.8	25.0
Without cat. rad., 425 °C, 2h	57.4	52.0	23.6	24.3	25.3	22.1
Cat. without rad., 425 °C, 2h	85.5	76.7	26.4	50.3	15.4	6.7
Cat. rad., 425 °C, 2 h	91.6	78.0	64.1	13.9	17.0	3.9
Cat. rad., 425 °C, 1 h	69.7	66.0	27.8	38.2	18.7	14.5
Cat. rad., 390 °C, 2 h	71.0	68.2	42.1	26.0	19.7	9.2

Catalytic hydrogenation (Fe - Mo, Al - Co - Mo Ct) of radiated paste results in increasing of the extent of COM conversion and the yield of TLP per paste organic matter, and decreasing of percentage of unconverted coal. The percentage of light fractions sharply increases. Hydrogenation of radiated paste always results in the increased gas formation (table 2).

Extent of COM conversion goes through maximum value with the increase of the adsorbed dose of radiation. The yield of TLP decreases, the gas formation and hydrogen consumption increase at high radiation doses. Decrease of hydrogenation temperature and the time of endurance deteriorate characteristics of process.

Preliminary radiation of the paste leads to the change of hydrogenation liquid products. In the light fractions ($T_b < 300^\circ\text{C}$) of hydrogenate the phenol content decreases, but the content of paraffin-naftenic and olephinic structures increases. Heavy fractions ($T_b > 300^\circ\text{C}$) contain less aromatic structures and phenolic hydroxyls.

Proximate results were obtained in hydrogenation of radiated paste of Beryozovsky coal

Preliminary radiation of the paste leads to the change of hydrogenation liquid products. In the light fractions ($T_b < 300^\circ\text{C}$) of hydrogenate the phenol content decreases, but the content of paraffin-naphtenic and olephinic structures increases. Heavy fractions ($T_b > 300^\circ\text{C}$) contains less percentage of aromatic structures and phenolic hydroxyls, the content of methyl series is increased.

Hydrogenation of Beryozovsky coal was performed in the presence of catalyst (Fe-Mo) and in the absence of it in an autoclave ($P_{H_2} = 10\text{ MPa}$, $T = 425^\circ\text{C}$) immediately

under the action of radiation. The extent of COM conversion, yield of liquid products per POM, percentage of light fractions in TLP also increase (table 3).

Table 3

Result of radiated hydrogenation of Beryozovsky coal (Fe - Mo) (%)

Experimental conditions	Extent of conversion	Yield of products per POM				
		TLP	T _b <300°C	T _b >300°C	Gas	UnCoal
Without cat., without rad.	70.6	64.5	8.0	56.5	22.6	13.0
Without cat.,rad.	81.4	76.0	56.4	19.6	25.3	8.8
Cat.,without rad.	86.5	77.0	10.7	66.3	17.9	6.3
Cat., rad.	89.0	84.9	77.0	7.9	11.7	5.2

The yield of liquid products and the percentage of light fractions per TLP under radiated hydrogenation increases as compared to the hydrogenation of the radiated paste. The effect of radiation becomes apparent at essentially lower doses of radiation. Liquid products of radiated hydrogenation are characterised by lower content of phenol and nitride bases.

Thus, gamma-radiation considerably activates both coals and their mixtures with paste medium. Catalytic hydrogenation of the radiated pastes leads to the increased extent of COM conversion, yield of liquid products and percentage of light fractions in them. At radiated hydrogenation of coal pastes the same effects are observed at lower doses of absorption. Application of radiation leads to some changes of liquid products obtained.

REFERENCES

1. G.B. Skripchenko, N.K. Larina, A.F. Lucovnikov, *Solid Fuel Chemistry*, No. 5 (1984) 3.
2. G.B. Skripchenko, V.I. Sekriyeru, Z.S. Smutkina, *Kinetics and Catalysis in Coal Chemistry*, Naukova Dumka, Ukraine, Kiev, (1992) 159.
3. G.B. Skripchenko, V.I. Sekriyeru, V.V. Klinkova, Yu.N. Nedoshivin et al, *Solid Fuel Chemistry*, No. 4 (1988) 68.
4. G.B. Skripchenko, O.V. Khrennikova, S.N. Rybakov, *Solid Fuel Chemistry*, No. 5 (1987) 23.
5. Z.S. Smutkina, V.I. Sekriyeru, I.B. Krichko, G.B. Skripchenko, *Solid Fuel Chemistry*, No. 1 (1983) 37.
6. G.B. Skripchenko, V.I. Sekriyeru, N.K. Larina, Z.S. Smutkina et al, *Solid Fuel Chemistry*, No. 4 (1986) 55.

Effects of chlorobenzene treatment on coal structure and liquefaction behaviour

I. Cepni, O. Sirkecioglu, C.A. McArthur, P.J. Hall and C.E. Snape

University of Strathclyde, Dept of Pure & Applied Chemistry, Glasgow G1 1XL, Scotland, UK

The effects of chlorobenzene and other non-polar solvent treatments on liquefaction behaviour are extremely varied and depend both upon the coal and liquefaction regime used. The treatments give rise to significant, but non-uniform, conformational changes in the macromolecular structure of bituminous coals. Solvent swelling, NMR and vitrinite reflectance measurements have indicated that the increase in microporosity is accompanied by the formation of additional hydrogen-bonds, with aromatic moieties possibly being less ordered.

1. INTRODUCTION

Pre-treating coals with low-boiling solvents can give rise to significantly improved yields under relatively low-severity liquefaction conditions [1,2]. Interpretation of these phenomena is complicated by the fact some organic matter is being removed at the same time that conformational changes may be occurring. Chlorobenzene has the advantage of extracting virtually no organic matter from coals and a summary of our results on how the treatment affects liquefaction behaviour with hydrogen-donor solvents is presented here. Preliminary results for tetralin extraction and dry (solvent-free) hydrogenation of Pittsburgh No. 8 coal reported elsewhere [3] have demonstrated the ability of chlorobenzene treatment to markedly affect conversion, improved oil yields being achieved in both these regimes. SAXS and SANS have both indicated that chlorobenzene treatment gives rise to an increase in microporosity with a higher density of voids smaller than *ca* 30 Å [4,5] and the additional microporosity is accessible to small molecules, such as tetralin. Further information obtained from vitrinite reflectance, solvent swelling, NMR measurements has enabled a qualitative model to be proposed for the conformational changes in the macromolecular structure of coals induced by non-polar solvent treatments.

2. EXPERIMENTAL

The two bituminous coals (Point of Ayr, UK and the Pittsburgh No 8 Argonne Premium Coal Sample - APCS) were treated in chlorobenzene under nitrogen for 1 week in a Soxhlet apparatus using 10 g batches. The extracted coals were then dried *in vacuo* at 50°C for up to 24 hours to ensure that the residual chlorobenzene

content was well below 1% w/w. The initial coals were dried in the same way prior to the liquefaction experiments.

The hydrogen-donor solvent liquefaction experiments without a hydrogen overpressure have been conducted with tetralin and hydrogenated anthracene oil (380-420°C, 15-60 min.) using solvent to coal mass ratios of 2:1 and 4:1. Yields of DCM and pyridine-insolubles were determined and, for the tetralin extractions, the amounts of hydrogen donated to the coals during the were calculated from the mass ratios of tetralin to naphthalene in the recovered DCM solutions.

3. RESULTS AND DISCUSSION

3.1 Conversion trends

Table 1 and Figure 1 present the product yields from a series of experiments on Pittsburgh No.8 coal at temperatures of 385 and 400°C and extraction times between 15 and 60 min.(at 400°C). The results indicate that increased yields of DCM-solubles are obtained upon chlorobenzene treatment across a wide conversion range, but the increases are smaller at the higher conversions. The concentrations of hydrogen transferred to the coal during extraction (ca 0.6% daf coal) are similar for the initial and chlorobenzene treated coals at the short contact time of 15 min. This finding might suggest that the improved oil (DCM) yields arise primarily from the changes in the conformational structure of the coals limiting char-forming reactions rather than cleaving more bonds *per se*. However, for times over 30 min, the amounts of hydrogen transferred are somewhat higher (for example, 1.5 cf 1.9% at 60 min.).

Table 1 Effect of temperature on conversions in tetralin short contact time liquefaction for Pittsburgh No.8 coal samples

	% daf coal			
	% H transferred	% DCM conv.*	%Pyr-sols /DCM-insols	% Pyr-insols
<u>385°C</u>				
Initial coal	0.3	16	52	32
Chlorobenzene - treated	0.4	24	57	19
<u>400°C</u>				
Initial coal	0.6	30	60	10
Chlorobenzene - treated	0.6	49	57	9

* = 100 - % DCM-insols, includes DCM-soluble liquid product +gas+water.

Improvements in oil yields can often be accompanied by reductions in overall conversions to pyridine-solubles as found for Point of Ayr coal (DCM-solubles increasing from 26 to 30% daf coal, but pyridine-insolubles also increasing from 34 to 38%). This trend would appear to be consistent with the report by Larsen and co-workers [6] who found that the chlorobenzene treatment increased the yield of pyridine-insolubles from tetralin extraction of the Illinois No. 6 APCS.

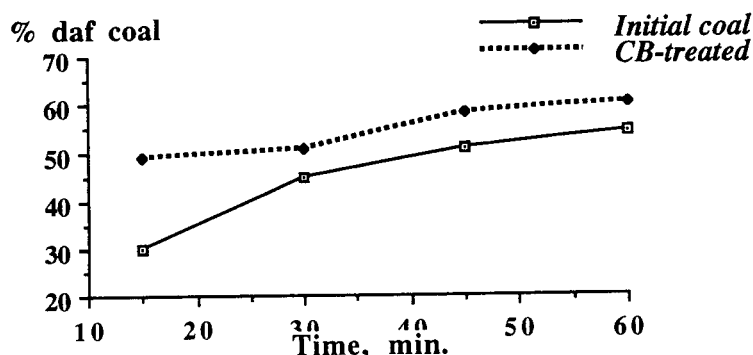


Figure 1 Effect of extraction time on yields of DCM-solubles for the Pittsburgh No.8 APCS in tetralin extraction

Similar yields of DCM-solubles and pyridine-insolubles were obtained for the untreated and chlorobenzene-treated bituminous coals with HAO at both short and long contact times ((Table 2 summarises the results at 15 min.). Further, the effects of presoaking the coals with HAO were minimal (Table 2), although a slight increase in conversion was evident for the Pittsburgh No. 8 APCS. The different behaviour compared to tetralin is attributed to the fact that HAO is largely in the liquid phase at reaction temperature and should be in better contact with the macromolecular structure of the reacting coal.

Table 2 Effects of pre-soaking and chlorobenzene treatment on HAO extraction yields for Point of Ayr and Pittsburgh No.8 coals (400°C, 15 min.)

	% daf coal		
	DCM-sols.*	DCM-insols. /Pyr.-sols.	Pyr.-insols
Point of Ayr			
Initial Coal			
Normal ext.	30	53	17
Pre-soaked	30	53	17
CB-treated coal			
Normal ext.	27	56	17
Pre-soaked	26	54	17
Pittsburgh No.8			
Initial Coal			
Normal ext.	35	51	14
Pre-soaked	38	52	10

*- includes DCM-solubles + water + gas. Slow heating follows pre-soak.

These results demonstrate that the effects of the chlorobenzene treatment are extremely varied and depend both upon the coal and liquefaction regime used. Pretreatments with toluene and chloroform gave rise to similar changes in conversion during short contact time tetralin liquefaction as chlorobenzene for the

Pittsburgh No.8 APCS, implying that the conformational changes are general for all non-polar solvents. In contrast to the liquefaction regimes investigated, chlorobenzene treatment has little effect on total volatile yields in pyrolysis and heat-treatment experiments which do not involve any prolonged contact with vehicle solvents or hydrogen gas.

3.2 Characterisation

Although little change was observed for the high volatile Pittsburgh No.8 bituminous coal, chlorobenzene treatment gave rise to decreases of between 0.1 and 0.2 in the random mean values for Point of Ayr coal and vitrinite concentrates from higher rank bituminous coals. These differences are significant in relation to the standard deviations of *ca* 0.05 to 0.1. Reflectance could decrease due to either the aromatic structures being less ordered or, merely, that less light is reflected as the microporosity of coal increases.

The pyridine swelling ratios for the Pittsburgh No. 8 and Point of Ayr coal increased by *ca* 5-10% upon chlorobenzene treatment. Similar increases were also observed for the chloroform and toluene-treated coals. As the volume increase upon contact with pyridine is higher for a hydrogen-bonded polar group in a macromolecule than it is for the corresponding free group, this result provides an indication that there are more hydrogen bonds in the treated coals. The swelling measurements are supported by previously reported ¹³C nOe measurements [7] which signified a less rotationally-mobile conformation containing more cross-links. Although little change was observed in the nitrogen BET surface areas (*ca* 2 m² g⁻¹), chlorobenzene treatment gave rise to significant increases in the amounts of CO₂ adsorbed, probably associated with the increases in microporosity [4,5].

To summarise, solvent treatment leads to a more energy-minimised conformation with more microporosity and hydrogen-bond cross-links. The driving force is sufficiently high to offset the possible loss of entropy from arising from the reduced mobility of segments of the macromolecular structure. Further, the ordering of aromatic moieties could be less pronounced in the more highly energy-minimised conformations obtained after solvent treatment.

4. ACKNOWLEDGEMENT

The authors thank the British Coal Utilisation Research Association, in conjunction with the Department of Trade and Industry for financial support.

REFERENCES

1. J.T. Joseph, *Fuel*, 70 (1991) 139 and 459.
2. C.E. Snape, F.J. Derbyshire, H.P. Stephens, R.J. Kottenstette and N.W. Smith, *Fuel Process. Technol.*, 24 (1990) 119 and references therein.
3. C.A. McArthur, P.J. Hall, A.J. Mackinnon and C.E. Snape, *Prepr. Am. Chem. Soc. Div. Fuel Chem.*, 38(2) and (4) (1993) 565 and 1290.
4. P.J. Hall and J.W. Larsen, *Energy and Fuels*, 5 (1991) 228.
5. P.J. Hall, M.M. Antxustegi, P. Burchill, R.E. Winans and P. Thiuyagarajan, *Energy & Fuels* 8 (1994) 1526.
6. J.W. Larsen, M. Azik and A. Korda, *Energy & Fuels*, 6 (1992) 109.
7. R.V. Law, G.D. Love and C.E. Snape, *Energy & Fuels*, 7 (1993) 1148.

Characterization of liquefaction/solubilization mechanisms of Spanish coals by newly isolated microorganisms

F. Laborda; M.F. Redondo; N. Luna and I.F. Monistrol

Departamento de Microbiología y Parasitología. Universidad de Alcalá de Henares. Ctra. Madrid-Barcelona, Km 33,6. E-28871 Alcalá de Henares (Madrid), Spain

1. INTRODUCTION

Since Fakoussa [1] first demonstrated in 1981 that microorganisms could metabolize coal, many authors have reported that mostly fungi, but some bacteria too, could solubilize and/or liquefy coal. Most of the successful results reported for coal solubilization were achieved using low rank coals [2]. Recently, several fungal and bacterial strains were isolated in our laboratory that could liquefy/solubilize Spanish coals (hard coal, sub-bituminous coal and lignite) [3]. Solubilization of high rank coals like hard coal was not described before. The mechanism of coal solubilization is not fully understood. However, it is known, that mainly three biological mechanisms are possible: enzymatic attack, basic metabolites and microbial chelators. In order to get some insight on the mechanism of the liquefaction/solubilization of the Spanish coals by new isolated microorganisms several studies were undertaken.

2. MATERIALS AND METHODS

2.1 Microorganisms and coals

The microorganisms used in this work were isolated from rotten wood chips, hard coal dumps and pieces of lignite and hard coal following Fakoussa's indications [1]. Most of them are moulds, but some bacteria active in the biotransformation of Spanish coals were isolated too.

Three different Spanish coals were used throughout this work: (i) lignite from Galicia; (ii) sub-bituminous coal from Teruel; (iii) hard coal from Minas Figaredo S.A. (Asturias). The different coals were cut in small pieces (2-4mm) and sterilized by dipping in 95% ethanol for 1h, rinsed in sterilized water and air dried. In some assays, to improve coal liquefaction, the lignite was pretreated with nitric acid 2M.

2.2 Lignite liquefaction on solid media

To study the influence of the culture medium in coal liquefaction, several isolated fungal strains were grown in solid media containing different carbon sources. When culture plates were covered by micelial mate, 0,5g of lignite pieces treated with NO_3H 2M were disposed over the plates. After incubation the formation of black drops from lignite particles indicated coal liquefaction.

2.3 Coal solubilization by cell-free culture filtrates

In previous work, the fungal strain M2 (belonging to the genera *Trichoderma*) showed a great activity in coal solubilization. This strain has been used to check the ability of the cell-free culture filtrate to solubilize different coals. M2 strain was grown in liquid media containing different carbon sources. After 10 days of incubation in a shaker rotator at 200 rpm and 28°C, cell-free culture filtrates were recovered by filtration through 0,45 and 0,22 μ millipore filters. Lignite, sub-bituminous coal and hard coal (0,5g) were added to the culture filtrates and incubated at 28°C under shaking. After incubation coal was separated by filtration. A₄₅₀ and pH values in the culture filtrates, before and after adding coals, were measured.

2.4 Scanning Electron Microscopy of microorganisms growing in the presence of coal

Several microbial strains (fungi and bacteria) were cultured in a minimal media with small coal pieces as the sole carbon source. When microbial growth was appreciated samples of coal were treated for Scanning Electronic Microscopy (SEM).

3. RESULTS AND DISCUSSION

3.1 Lignite liquefaction on solid media

When fungal strains were growing in a solid medium big drops of liquified lignite could be recovered in most of the cases. However, lignite liquified by the fungal strain S3A mostly diffused into the agar instead. Microorganisms growing in different culture media showed differential lignite liquefaction rates (Table 1). Fungal strains growing in different liquid culture media showed similar results.

Table 1
Rate of lignite liquefaction by fungal strains growing in different culture media

Fungal strain	Culture media						
	SG	SL	SM	YEMED	GL	LM	GM
S3A	D	D	+	D	+	D	D
S3X	++	+++	++	±	+++	++	D
S10H	+	+	++++	±	++	+	D
S12	±	D	+	±	+	+	D

SG (Sabouraud Glucose); SL (Sabouraud lactose); SM (Sabouraud maltose); YEMED (Yeast extract, malt extract and glucose); GL (Yeast extract and glucose); LM (Yeast extract and malt extract); GM (Malt extract and glucose); Coal diffusion into the agar (D); Very high liquefaction rate (++++); High liquefaction rate (+++); Moderate liquefaction rate (++); Low liquefaction rate (+); Lignite softening (±).

3.2 Coal solubilization by cell-free culture filtrates

Cell-free culture filtrates from M2 fungal strain were able to solubilize all Spanish coals studied (lignite, sub-bituminous and hard coal) in some degree (Table 2). When M2 strain was growing in the presence of maltose showed a greater solubilization activity than the cell-free culture filtrate containing glucose. In these conditions, lignite was solubilized in a greater degree than higher rank coals. Solubilization/liquefaction of low rank coals like leonardite has been reported by other authors [2] but solubilization of high rank coals, like Spanish sub-bituminous coal and hard coal, has not been described before. Nitric acid treatment of the coals did not change these results.

Table 2
Spanish coal solubilization by M2 cell-free culture filtrates (*)

Coal	Culture media			
	SG	MM	SM	SM + XY
Hard coal	0,170	1,557	0,911	0,375
Sub-bituminous coal	0,132	(**)	0,985	(**)
Lignite	0,254	2,240	1,853	1,068

(*) Measured as increase in A_{450} in the cell-free culture filtrates after coal incubation.

SG (Sabouraud glucose); MM (Minimal medium plus maltose); SM (Sabouraud maltose); SM + XY (Sabouraud maltose plus xyloidine); A_{450} lower than the control (**)

Table 3
pH values of the cell-free culture filtrates

Culture filtrate	Culture media			
	SG	MM	SM	SM + XY
CF without coal	4.4	7.0	7.0	7.1
CF + hard coal	4.1	6.9	7.0	7.2
CF + sub-bituminous coal	-	3.2	5.2	3.5
CF + lignite	3.8	5.4	6.1	4.7

SG (Sabouraud glucose); MM (Minimal medium plus maltose); SM (Sabouraud maltose); SM + XY (Sabouraud maltose plus xyloidine); CF (cell-free culture filtrate)

The pH values (Table 3) of the culture filtrates did not suggest that microbial alkaline substances might be responsible for the observed coal solubilization as has been reported in many cases. Generally, these initial pH values did not change in the presence of coal.

However, were greatly lowered in the presence of sub-bituminous coal. Xylidine has been described as an inducer compound of the enzyme laccase that has been claimed to be responsible of some coal solubilization [4]. However, the presence of xylidine in the culture medium had not a notable effect in coal solubilization. Production of other extracellular enzymes or chelator agents by M2 fungal strain to solubilize Spanish coals is currently studied.

3.3 Electron Microscopy observations of microorganisms growing in the presence of coal

By Scanning Electron Microscopy, bacteria (Figure 1A) and fungi (Figure 1B) were observed to grow on the coal surface and cover it. A fibrillar extracellular polymer was observed to be produced that could help not only the adhesion of the microorganisms to the coal particle, but the microbial attack too.

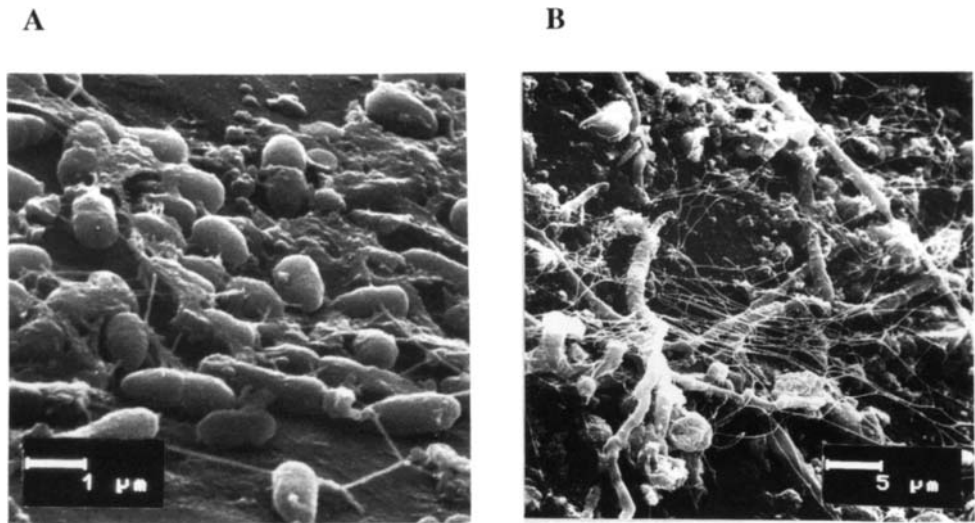


Figure 1. Scanning Electron Microscopy observations of bacteria (A) and Fungi (B) growing over coal particles

4. REFERENCES

1. R.M. Fakoussa, Coal as substrates for microorganisms: Investigation with microbial conversion of national coals. Ph.D. Thesis (1981), Friedrich-Wilhelms University, Bonn, Germany.
2. D.L. Crawford (Ed), Microbial Transformations of Low Rank Coals, CRC Press, Boca Raton, FL, 1993.
3. I.F. Monistrol and F. Laborda, Liquefaction and/or solubilization of Spanish coals by newly isolated microorganisms, Fuel Processing Technology, 40 (1994) 205-216.
4. J. Rogalski, A.L. Dawidowicz and A. Leonowicz, Purification and Immobilization of the Inducible Form of Extracellular Laccase of the Fungus *Trametes versicolor*, Acta Biotechnol., 10 (1990) 261-269.

Strong Promoting Effect of H₂O on Coal Liquefaction Using Water-Soluble and Oil-Soluble Mo Catalyst Precursors

Chunshan Song*, Ajay K. Saini, and Jessel McConnie

Fuel Science Program, The Pennsylvania State University, University Park, PA 16802, USA

INTRODUCTION

This paper reports on the unusual, and strong promoting effect of water on low-severity catalytic liquefaction of Wyodak subbituminous coal. For coal liquefaction using dispersed hydrogenation catalyst, removal of moisture or water by drying before reaction has been a common practice (Weller and Pelipetz, 1951; Derbyshire et al., 1986; Weller, 1994). In our recent work on drying effects, it was found that the primary drying effect on coal conversion at 350°C was due to water removal, rather than physicochemical changes within coal structure caused by drying (Song et al., 1993, 1994). Prompted by this observation, we examined the effect of water on catalytic runs and found that water can have very strong promoting effect on catalytic coal liquefaction with a dispersed Mo sulfide catalyst at 350°C (Song and Saini, 1994, 1995). In the present study, we examined the water effect using dispersed Mo catalysts generated in situ from both a water-soluble precursor, ammonium tetrathiomolybdate (ATTM), and an oil-soluble precursor, Molyvan L. The findings described in this paper may offer new opportunities for developing low-severity catalytic processes for coal liquefaction.

EXPERIMENTAL

Wyodak subbituminous coal (≤ 60 mesh) from DOE/Penn State Coal Sample Bank (DECS-8) was used. It contains 28.4% moisture, 32.4% volatile matter, 29.3% fixed carbon, and 9.9% ash, on as-received basis; 75.8% C, 5.2% H, 1.0% N, 0.5% S, and 17.5% O, on dmmf basis. We used both the fresh raw coal, and the coal predried either in a vacuum-oven (VD) or in an oven exposed to air (AD) at 100°C for 2 h. Ammonium tetrathiomolybdate (ATTM), which is a known water-soluble catalyst precursor [Derbyshire et al., 1986; Garcia and Schobert, 1989; Artok et al., 1993], was dispersed onto raw or dried coal by incipient wetness impregnation from its aqueous solution (1 wt% Mo on dmmf basis). The impregnated coal samples were dried in a vacuum oven at 100 °C for 2 h before use. Molyvan L is a commercially available, oil-soluble lubricant additive (Swanson, 1992) containing 8.1 wt% Mo, 6.4 wt% P, and 12.3 wt% S. Molyvan L was diluted in 1-MN solvent (1-methylnaphthalene) and added to raw or dried coal (0.5 wt% Mo on dmmf coal).

Liquefaction was carried out in 25 mL tubing bomb reactors at 350 or 400°C (unless otherwise mentioned) for 30 min under an initial H₂ pressure of 6.9 MPa. The reactions were carried out either without or with an organic solvent (solvent/coal = 4 g/4 g). For the experiments with added water, the weight ratio of water to dmmf coal was kept at 0.46 unless otherwise mentioned. The products were separated into gases, oil, asphaltene, and preasphaltene. The gases were analyzed by GC. More experimental details may be found elsewhere [Song et al., 1993, 1994].

RESULTS AND DISCUSSION

Effect of Water and Dispersed Mo Catalyst from Water-Soluble Precursor

Figure 1 summarizes the results of solvent-free runs of Wyodak coal at 350°C. Compared to the non-catalytic run of vacuum-dried coal, adding water increased coal conversion

* Corresponding author (Fax: 814-865-3075; Tel: 814-863-4466)

from 14.5 to 22.5 wt%. Using ATTM improved coal conversion to 29.8 wt%. Adding water to the catalytic run dramatically increased coal conversion to 66.5 wt%. Relative to the non-catalytic run of air-dried coal, adding water increased coal conversion from 14.8 to 26.1 wt%, and the use of ATTM improved conversion from 14.8 to 29.2 wt%. When ATTM was used in combination with H₂O, the coal conversion was again improved significantly, to 62.3 wt%. Loading ATTM on the fresh raw coal gave higher conversion compared to the runs when ATTM was impregnated on dried coals, 43.3 wt% vs. 29.2-29.8 wt%. The strong promoting effect of re-adding water was also observed in this case: adding water to the catalytic run led to a substantial increase in coal conversion, from 43.3 to 66.0 wt%.

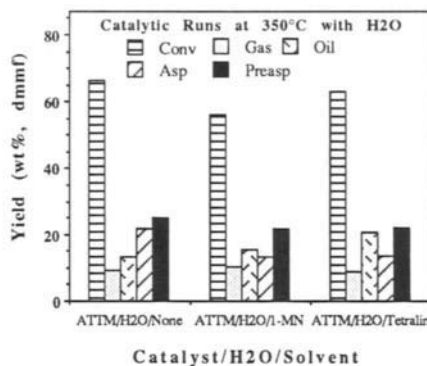
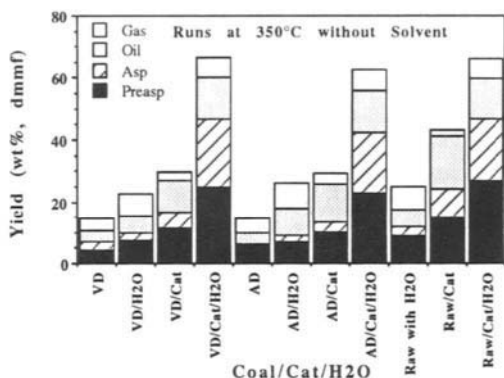


Figure 1. Effect of H₂O plus ATTM on coal conversion at 350°C.

Figure 2. Effect of solvent on conversion at 350°C.

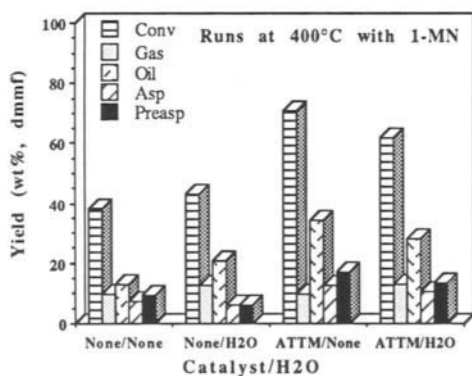


Figure 3. Effect of H₂O and ATTM on conversion at 400°C.

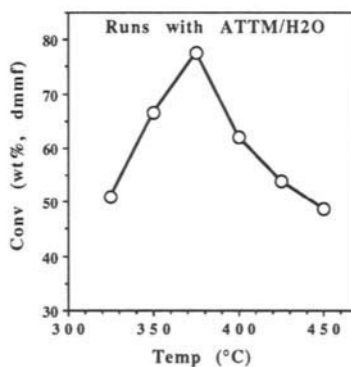


Figure 4. Effect of temp. on coal conversion.

From the above three sets of experimental results, it has now become unambiguous that water can have a dramatic promoting effect on catalytic coal conversion at a relatively low temperature, 350°C. Figure 2 shows that, in the presence of H₂O and Mo catalyst, the use of either a non-donor 1-MN or a H-donor tetralin solvent has no positive impact on coal conversion at 350°C. For runs at 400°C, however, using ATTM without H₂O addition always gives highest conversion, either with or without an organic solvent. An example is shown in Figure 3 for runs with 1-MN. It is interesting that adding water can dramatically increase coal conversion in catalytic runs at 350°C, but can decrease conversion in catalytic runs at 400°C.

Effect of Temperature on Coal Conversion with H₂O and ATTM

Figure 4 shows the effect of reaction temperature on coal conversion in the catalytic runs with added water (H₂O/dmmf coal = 0.46) but without any solvent. There appears to be a

temperature window, within which increasing temperature (325-375°C) significantly increases coal conversion, but beyond which the conversion decreases with increasing temperature (400-450°C). When compared to the catalytic runs without added water (Song et al., 1995), we can see the strong promoting effect of water on low-severity catalytic liquefaction of Wyodak coal in the temperature range of 325-375°C, but an inhibiting effect of water on catalytic runs at 400-450°C. One of the most interesting findings in this work is the strong synergistic effect between water and dispersed molybdenum sulfide catalyst at relatively low temperatures (325-375°C). It should be noted that, even in the low temperature regime, an excessive amount of water may have negative impacts on catalytic coal conversion (see below). Several prior papers reported on the negative effects or lack of any promotional effect of water on catalytic liquefaction (Bockrath et al., 1986; Kamiya et al., 1988; Ruether et al., 1987; Mikita et al., 1988).

Effect of Water and Dispersed Mo Catalyst from Oil-Soluble Precursor

Figure 5 presents the data for liquefaction of Wyodak coal using Molyvan L at 350°C. In these tests, Molyvan L and 1-MN solvent were added to either raw coal (containing 28.4 wt% moisture, $H_2O/dmmf \text{ coal} = 0.46$) or vacuum-dried coal (containing 2.5 wt% moisture, $H_2O/dmmf \text{ coal} = 0.03$). Figure 5 indicates that the coal conversion in catalytic runs is much higher when using raw coal (68.9 wt%, conv) than using dried coal (52.8 wt%) at 350°C. However, we also found that the catalytic runs using Molyvan L at 400°C afford substantially higher conversion with dried coal (91.2 wt%) than with the raw coal (58.3 wt%). These results are consistent with those observed for catalytic runs using ATTM at 350 and 400°C.

The effectiveness of oil-soluble Molyvan L as catalyst precursor becomes more apparent when compared to the well-known water-soluble ATTM. The 0.5 wt% Mo added as Molyvan L into 1-MN solvent is at least equally effective, or even better, than the 1.0 wt% Mo as ATTM impregnated onto coal, both for runs at 350 and 400°C with 1-MN solvent.

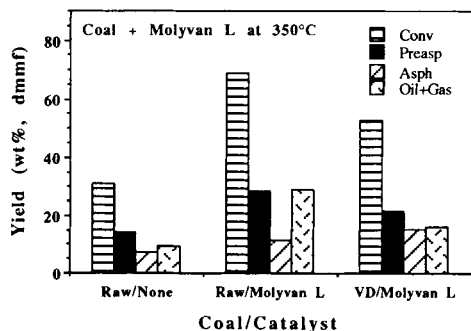


Figure 5. Effect of Molyvan L on conversion of at 350°C.

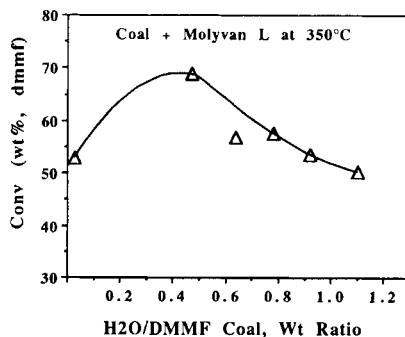


Figure 6. Effect of H_2O /coal ratio on conversion.

Effect of Water/Coal Ratio on Coal Conversion with Molyvan L

Figure 6 shows the effect of H_2O /coal ratio on conversion of Wyodak coal at 350°C using Molyvan L as catalyst precursor. It appears from the conversion data that there exist optimum H_2O /coal ratios for a given catalytic reaction system. With Molyvan L, the 0.3-0.6 range of the H_2O /coal ratio seems to be the best for achieving high conversion of Wyodak coal in the presence of 1-MN solvent. At too low a ratio, the amount of water is not enough for promoting catalytic conversion. When the amount of water is higher than certain value, catalytic coal conversion seems to be inhibited.

Mechanistic Considerations

The significant increase in coal conversion through co-use of water and dispersed catalyst at low-temperature is mainly manifested by a large increase in preasphaltene and asphaltene yields, indicating no extensive hydrocracking. The oils from runs with added water

contain more phenolic compounds, as shown by two-dimensional HPLC (Song and Saini, 1994). It is possible that water helps to break some covalent bonds, at least C-O bonds, in catalytic runs at low temperatures, which lead to increased coal conversion. At 350°C, there may be two types of reactions occurring in water-promoted reactions, radical and ionic. Water can promote cleavage of etheric C-O bonds, possibly via ionic pathways (Siskin and Katritzky, 1991). Rising temperature increases the portion of radical reactions, which are believed to be dominant at $\geq 400^\circ\text{C}$, where water addition showed negative impacts on catalytic runs. Adding water always causes substantial increase in CO₂ yields, regardless of the use of catalyst and temperature range. The CO₂ increase is far more than the decrease in CO yield, and this rules out water-gas-shift reaction as the major contributor (Song and Saini, 1995). It is possible that water enhances decarboxylation, and may oxidizes some O-containing compounds (Siskin and Katritzky, 1991, Lewan, 1992). It has also been reported that water can reduce retrogressive reactions (Tse et al., 1991; Serio et al., 1992). Beneficial effects of hydrothermal pretreatment on non-catalytic coal conversion in pyrolysis and liquefaction have been reported by several groups (Graff and Brandes, 1987; Pollock et al., 1991; Ross, 1992; Serio et al., 1992). However, using excessive amount of water, as used in previous hydrothermal pretreatments, has negative impacts on catalytic coal conversion. Fundamental questions concerning the nature of promotional effect of water on catalytic runs, its dependence on temperature, on water/coal ratio, and on coal rank, remain to be answered.

CONCLUSIONS

In summary, we have found that, for liquefaction using dispersed Mo sulfide catalysts from either water-soluble or oil-soluble precursor, adding a proper amount of water can dramatically improve coal conversion at temperatures (325-375°C) that are much lower than those used in conventional processes (400-470°C). The important factors affecting water-promoted catalytic conversion include, but are not limited to, H₂O/coal ratio and temperature.

ACKNOWLEDGMENTS

We are most grateful to Prof. Harold Schobert for his encouragement, support, and many helpful discussions. This work was supported partially by the U.S. Department of Energy, Pittsburgh Energy Technology Center, under contract No. DE-AC22-91PC91042.

REFERENCES

- Artok, L.; Davis, A.; Mitchell, G.D.; Schobert, H.H. *Energy & Fuels*, 1993, 7, 67.
 Bockrath, B.C.; Finseth, D.H.; Illig, E.G. *Fuel Process. Technol.*, 1986, 12, 175.
 Derbyshire, F.J.; Davis, A.; Lin, R.; Stansberry, P.G.; Terrer, M. *Fuel Process. Technol.*, 1986, 12, 127.
 Garcia, A.B.; Schobert, H.H. *Fuel*, 1989, 68, 1613.
 Graff, R.A.; Brandes, S.D. *Energy & Fuels*, 1987, 1, 84.
 Kamiya, Y.; Nobusawa, T.; Futamura, S. *Fuel Process. Technol.*, 1988, 18, 1.
 Lewan, M.D. *Am. Chem. Soc. Div. Fuel Chem. Prepr.*, 1992, 37 (4), 1643-1649.
 Mikita, M.A.; Bockrath, B.C.; Davis, H.M.; Friedman, S.; Illig, E.G. *Energy & Fuels*, 1988, 2, 534.
 Pollack, N.R.; Holder, G.D.; Warzinski, R.P. *Am. Chem. Soc. Div. Fuel Chem. Prepr.*, 1991, 36 (1), 15.
 Ross, D. *Am. Chem. Soc. Div. Fuel Chem. Prepr.*, 1992, 37 (4), 1555.
 Ruether, J.A.; Mima, J.A.; Kornosky, R.M.; Ha, B.C. *Energy & Fuels*, 1987, 1, 198.
 Serio, M.; Kroo, E.; Charpenay, S.; Solomon, P.R. *Am. Chem. Soc. Div. Fuel Chem. Prepr.* 1992, 37, 1681.
 Siskin, M.; Katritzky, A.R. *Science*, 1991, 254, 231.
 Song, C.; Saini, A.K.; Schobert, H. H. *Am. Chem. Soc. Div. Fuel Chem. Prepr.*, 1993, 38 (3), 1031.
 Song, C.; Saini, A.K.; Schobert, H. H. *Energy & Fuels*, 1994, 8, 301.
 Song, C.; Saini, A.K. *Am. Chem. Soc. Div. Fuel Chem. Prepr.*, 1994, 39 (4), 1103.
 Song, C.; Saini, A.K. *Energy & Fuels*, 1995, 9, 188.
 Song, C.; Saini, A.K.; Schobert, H. H. *Proc. 8th Int. Conf. Coal Sci.*, Oviedo, Spain, Sept. 1995.
 Swanson, A.; *Prepr. Pap. - Am. Chem. Soc. Div. Fuel Chem.*, 1992, 37 (1), 149.
 Tse, D.S.; Hirschon, A.S.; Malhotra, R.; McMillen, D.F.; Ross, D.S. *Am. Chem. Soc. Div. Fuel Chem. Prepr.*, 1991, 36 (1), 23.
 Weller, S.; Pelipetz, M.G. *Ind. Eng. Chem.* 1951, 43, 1243.
 Weller, S. *Energy & Fuels*, 1994, 8, 415.

LOW TEMPERATURE LIQUEFACTION OF COAL WITH SIMULATED COKE OVEN GAS

H. Yamaguchi¹, Y. Sato² and K. Matsubara³

¹ NKK Corp., 1-1 Minamiwatarida-cho, Kawasaki, 210 Japan

² National Institute for Resources and Environment, 16-3 Onogawa, Tsukuba,
305 Japan

³ NK Techno Service, 1-1 Minamiwatarida-cho, Kawasaki, 210 Japan

1. INTRODUCTION

Effective hydrogen supply to fragments generated from coal, due to thermal cracking, is of much importance in coal liquefaction. Hydrogen is supplied from coal itself, solvent and hydrogen gas, and large amount of molecular hydrogen is consumed during liquefaction as well as upgrading [1]. Therefore, total cost of produced coal liquids depends not only on severity of operating conditions, such as temperature and pressure, but also on the amount of hydrogen gas consumed. On the other hand, coke oven gas(COG) contains about 50-60 vol% molecular hydrogen and the cost is by far inexpensive than hydrogen gas. Possibility of hydrolysis using COG has been investigated [2]. Use of COG in coal liquefaction would substantially enhance economic feasibility, but few data have reported this matter. In this study, coal liquefaction using simulated COG or hydrogen gas was performed to produce solvent refined coal(SRC) as substitute of good caking coal for manufacturing metallurgical coke. Possibility of coal liquefaction using COG was discussed with the results of influences of temperature, time and gas atmosphere on coal liquefaction behavior.

2. EXPERIMENTAL

Catalytic and non-catalytic liquefaction of -100 mesh Taiheiyo coal(ash 15.29 wt%, ultimate analysis : C 76.57 %, H 6.03 %, N 1.35 %, S+O 16.05 %(dry ash free wt%)) were carried out in a 500 cm³ magnetically stirred autoclave. Three different solvents, NEDOL 1t/d PSU recycle solvent before hydrogenation, creosote oil and mixture of recycle solvent and the creosote oil(weight ratio 1:1) were used. Table 1 shows properties of solvents. Red mud/sulfur(weight ratio 1:1) was used as a catalyst. Hydrogen/ nitrogen gas mixture(volumetric ratio 1:1) was used as a simulated COG. Experimental conditions were as follows : (a) temperature 380-440 °C, (b) time 20-60 min, (c) coal/solvent 2/3(weight ratio), (d) catalyst addition 0-5 wt%(daf coal), (e) reactant gas of simulated COG or hydrogen gas, (f) total initial pressure 4, 8 MPa, (g) gas /slurry 40-110 NL/kg(hydrogen gas base). Coal conversion(to THF-solubles), hydrogen consumption, yields of oil(-538 °C) and SRC(+538 °C), and H/C atomic ratio and boiling point distribution of oil were measured by conventional methods.

Table 1 Properties of solvent

	Ultimate analysis (wt%)				boiling point distribution (wt%)					fa (-)
	C	H	N	S+O	IBP - 180°C	180 - 216°C	216 - 310°C	310 - 350°C	350 - 538°C	
1t/d PSU recycle solvent	88.31	9.57	0.25	1.86	0.0	3.6	56.5	16.9	23.0	0.45
creosote oil	89.81	6.83	0.47	2.89	5.5	17.2	72.9	2.6	1.8	0.89
mixed oil*	89.19	8.24	0.38	2.19	5.1	10.4	64.8	8.8	10.9	0.65

* recycle oil/creosote oil (weight ratio) = 1 / 1

3. RESULTS AND DISCUSSION

3.1 NON-CATALYTIC LIQUEFACTION

Results for 420-430 °C and 20 min with G/L of 40-100 NL/kg are listed in Table 2. SRC was sufficiently produced with maximum yield of 114 wt%(daf coal). Coal conversions were less than 77 %(daf coal), regardless of gas atmosphere. More than 10 wt% of solvent were not recovered, which gave no oil production. Higher fa of solvent accelerated semi-coke formation, retrogressive reaction in coal liquefaction, resulting in a decrease of coal conversion. Hydrogen consumption was less than 0.2 wt%(daf coal). This result indicated that hydrogen for coal liquefaction was mainly supplied from coal itself and solvent, and the contribution by hydrogen gas was small. Deposition of coke material to the inner surface of the autoclave was observed at more than 420 °C with solvent of creosote oil or the mixed oil.

Table 2 Results of non-catalytic Taiheiyo coal liquefaction

coal (g)/solvent* (g)	66.4	66.4	66.4
	/99.6	/100	/99.6
initial press. H ₂ (MPa)/N ₂ (MPa)	2/2	4/0	2/2
G/L (NL/kg)	49	99	50
temp. (°C)/time (min)	420	420	430
	/20	/20	/20
hydrogen consumption (wt%, daf coal)	0.08	0.14	0.07
coal conversion (%)	75.2	76.5	77.0
oil + water (wt%, daf coal)	-26.7	-26.4	-9.9
SRC (wt%, daf coal)	100	114	85.3

* 1t/d PSU recycle solvent

Table 3 Results of catalytic Taiheiyo coal liquefaction using COG

coal(g)/solvent* (g)	66.4/	66.4/
/catalyst** (g)	99.8/	99.4/
	3.4	3.4
initial press. H ₂ (MPa)/N ₂ (MPa)	2/2	2/2
G/L (NL/kg)	44	49
temp. (°C)/time (min)	420	430
	/20	/20
hydrogen consumption (wt%, daf coal)	0.44	0.74
coal conversion (%)	78.3	72.4
oil + water (wt%, daf coal)	-2.6	0.8
SRC (wt%, daf coal)	76	74

* mixed solvent

** red mud + sulfur (1 : 1)

3.2 CATALYTIC LIQUEFACTION

Table 3 shows results for simulated COG at 420-430 °C and 20 min with mixed oil and G/L of 40-50 NL/kg. Hydrogen consumption was 0.4, 0.7 wt%, much higher than without catalyst. Catalyst addition enhanced solvent recovery and retarded deposition

of coke material. This result indicated that catalyst addition would be indispensable in stable plant operation of coal liquefaction using COG.

Coal liquefaction using simulated COG and the recycle solvent was carried out to further enhance solvent recovery under the conditions of 380-440 °C, 20-60 min and G/L of 110 NL/kg with red mud addition of 5 wt%. The results are shown in Fig.1. Coal conversion and oil yield increased with temperature in the range of 380 to 420 °C, but then decreased with the higher temperature of 440 °C. Coal was also liquefied using hydrogen gas of 4 MPa initial pressure under the same condition as those in Fig.1. The differences in coal conversion, yields of oil and SRC between simulated COG and hydrogen gas are shown in Fig.2. No large difference of SRC yield was observed. Coal conversion and oil yield were clearly higher with hydrogen gas than with simulated COG. Solubility of hydrogen gas in coal slurry increases with molecular hydrogen partial pressure in gas phase. Thus, these results suggested that solubility of molecular hydrogen in coal slurry was smaller with simulated COG than with hydrogen gas, resulting in retard of solvent mediated donation of molecular hydrogen to the radical fragments from coal. Semi-coke formation would be more predominant with simulated COG than with hydrogen gas. In coal liquefaction using hydrogen gas, semi-coke formation occurs much more rapidly than coal depolymerization [3]. Efficient utilization of hydrogen donors in the initial stage of coal liquefaction would be more important to suppress semi-coke formation with COG than with hydrogen gas. Fig.3 shows differences in H/C atomic ratio and boiling point distribution of product oil between simulated COG and hydrogen gas. At less than 420 °C, no clear difference of properties was observed. At 440 °C, product oil contained a little lower boiling point species than original solvent, indicating that solvent partly decomposed into low molecular weight products at this temperature.

4. CONCLUSIONS

Coal liquefactions using simulated COG hydrogen gas as reactant gas were examined. Obtained results suggested that the use of inexpensive COG instead of hydrogen gas in coal liquefaction producing SRC would enhance economic feasibility. Semi-coke formation was more predominant with COG than with hydrogen gas. The desirable reaction temperature with COG was around 420 °C, lower than those for coal liquefaction using hydrogen gas to produce fuel oil.

ACKNOWLEDGMENTS

This study has been carried out, using samples obtained from NEDO. Authors would like to thank NEDO for their support.

REFERENCES

1. J.A. Gray and Y.T. Shah, "Reaction Engineering in Direct Coal Liquefaction" (Ed. Y.T. Shah), Addison-Wesley, 1981, Ch.2.
2. C. Braekman-Danheux, R. Cypres, A. Fontana and M.V. Hoegaerden, *Proc. of 1993 Int. Conf. on Coal Science*, Vol. II, p.271 (1993)
3. H. Moritomi, Y. Sanada, and T. Chiba, *Kagaku Kogaku Ronbunshu*, **14**, p.209 (1988).

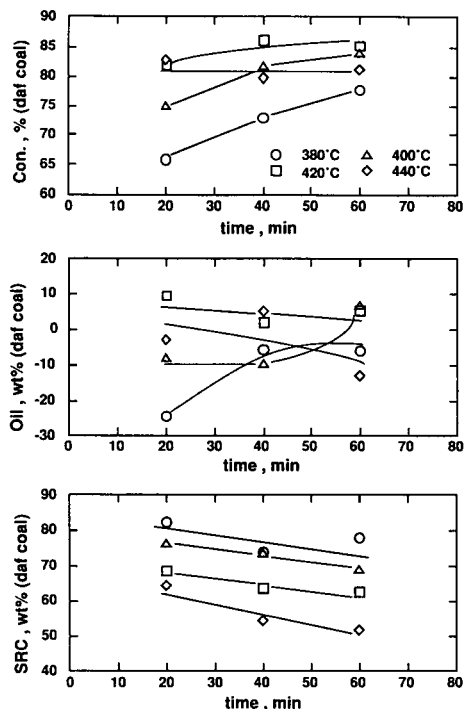


Fig.1 Change of coal conversion, oil yield and SRC yield with temperature and time for simulated coke oven gas
 Initial press. : hydrogen = 2MPa, nitrogen = 2MPa
 Catalyst : red mud 5wt%+ sulfur 5wt%(daf coal)
 G/L : 110NL/kg(hydrogen gas base)

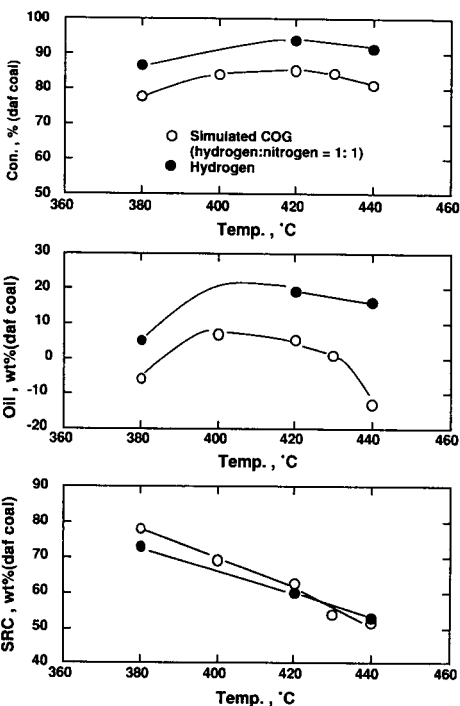


Fig.2 Influence of gas atmosphere on coal conversion, oil yield and SRC yield
 Initial press. : 4MPa
 Time : 60min
 Catalyst : red mud 5wt% + sulfur 5wt%(daf coal)
 G/L : 110NL/kg(hydrogen gas base)

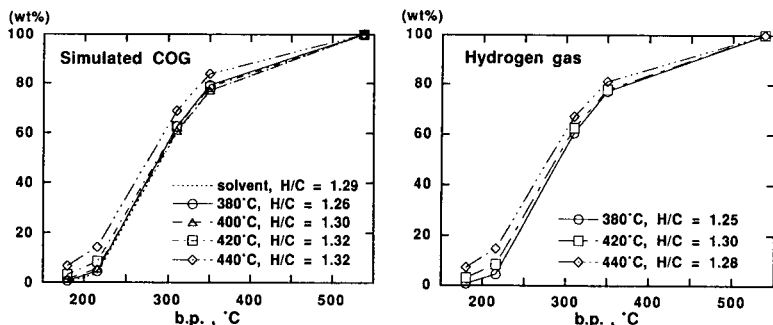


Fig.3 Difference of recovered oil properties between simulated coke oven gas and hydrogen
 Initial press. : 4MPa
 Time : 60min
 Catalyst : red mud 5wt% + sulfur 5wt%(daf coal)
 G/L : 110NL/kg(hydrogen gas base)

Coal pyrolysis with methane in a reducing environment

M. F. Voigtmann^a, M. Chen^a, B. D. Batts^a

^a School Of Chemistry, Macquarie University, N.S.W 2109, Australia

It is recognised that the largest contributor to the cost of coal liquefaction is the production of hydrogen gas¹. The potential of a cheaper substitute, methane, has been investigated.

1. METHODOLOGY

The Millmerran coal used for the liquefaction studies contained 4.2% w/w volatiles and 15.1% w/w ash. Elemental composition (%w/w daf) was determined to be 70.5% C, 6.2% H, 1.0% N, 0.5% S and 21.8% O, by difference. The commercially available Ni-Mo catalyst supported on Al₂O₃ (Cyanamid HDN-60) was sulfided at 380 °C for 20 hours in the presence of dimethyldisulfide had a surface area according to the BET method of 133 m²g⁻¹. Coal and 5% catalyst were heated under H₂, CH₄, N₂ and mixtures thereof at 400 °C for 64h. Gaseous products were analysed by gas chromatography using a Thermal Conductivity Detector (TCD). The CHCl₃/ MeOH soluble reaction products were analysed by GC and GC-MS.

2. RESULTS AND DISCUSSION

When Millmerran coal was heated in the presence of H₂ gas with no donor solvent, *n*-alkanes were released in the range of C₁₂ - C₂₈. On comparing the initial H₂ pressure with the relative abundance of these alkanes, it is found that higher pressure favours the release of higher molecular weight alkanes. It is well known that a homologous series of *n*-alkanes can be extracted from coals^{2,3} and low temperature hydrogenation studies without donor solvent suggest that the additional alkanes yielded by liquefaction can be attributed to physical trapping of additional material inside the coal macromolecule⁴. Products indicative of cracking, such as CH₄ and C₂H₆ were found to increase with decreasing H₂ pressure. Because the characteristic reaction of alkanes at temperatures at or greater than 400 °C is cracking to produce smaller olefins and alkanes via a radical chain mechanism⁵, radicals are more readily capped and cracking subsequently reduced as the H₂ availability increases. An indirect measure of H₂ availability can therefore be estimated from the *n*-alkane distribution of the oil products released.

When CH₄ and N₂ were reacted under conditions identical to those employed for hydrolysis, oil yields were higher under CH₄ and the alkane chain length distribution tended towards higher values as shown in Figure 1. Under these conditions therefore, CH₄ is less reactive than H₂ but more active than the blank run with N₂ in terms of hydrogenation or radical capping capability.

Similar observations have been made on coal / CH₄ reactions in the presence of tetralin donor solvent and Fe₂O₃ catalyst⁶.

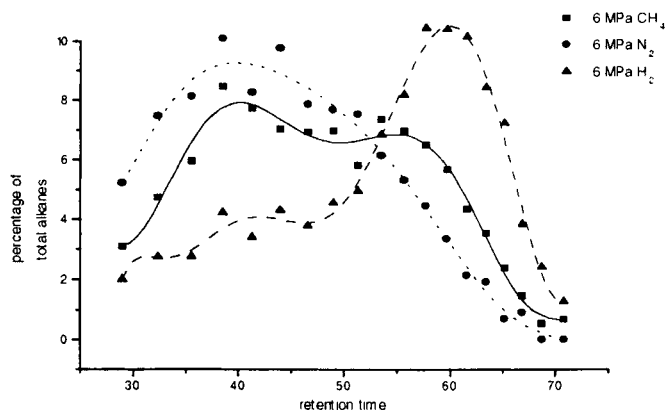


Figure 1 Comparison between initial gas charge and *n*-alkane distribution.

When H₂ was used as the reagent gas at 6 MPa, selectivity to C₂+ gaseous hydrocarbons relative to CO₂ was higher than for CH₄ which in turn was higher than that found for N₂. As the initial H₂ charge pressure was decreased, CO₂ and C₂+ hydrocarbon formation increased presumably due to cracking, however the selectivity was found to decrease, suggesting that CO₂ or its precursor is more readily converted to higher hydrocarbons when H₂ is present. At 6 MPa H₂, the amount of CO₂ detected was 7% that of the CH₄ + C₂H₆ total, whilst at 2 MPa the CO₂ contribution had risen to 25%.

This relationship can be rationalised in terms of general thermodynamic considerations taking C₂H₆ generation as the general case. The CO₂ consumed in equation 1 is formed via typical coal thermolysis reactions such as de-carboxylation and contributions from other oxygen containing groups⁷. The Gibbs free energy is calculated from standard thermodynamic data at 700K⁸.



The overall equation for C₂H₆ production is given by equation 3. Because of the decrease in total volume as reactions 2 and 3 proceed, higher pressures should enhance the degree of reaction. Furthermore, if CH₄ is initially present, reaction 2 will be suppressed and hence a reduced consumption of H₂ will occur. The consequence of adding CH₄ would therefore be to increase the amount of H₂ available for liquefaction. The reaction between CH₄ and CO₂ to form C₂H₆ has been documented⁹. Equation 3, which may proceed as shown, or possibly via a synthesis gas route, predicts that low temperature and high pressure will increase the equilibrium constant

for the formation of hydrocarbons, as expected from simple entropic arguments¹⁰.

The pyrolysate gas analysis differs significantly when varying $\text{CH}_4 : \text{H}_2$ ratios are used. The higher hydrocarbon yield over that obtained from 6 MPa H_2 is not solely due to cracking reactions, as this would require a maximum C_2+ formation to occur at 6 MPa of CH_4 . The addition of CH_4 increases the total C_2+ hydrocarbon formation maximising at a $\text{H}_2 : \text{CH}_4$ ratio of approximately 3:1 shown in Figure 2a and is considerably higher than the equivalent $\text{H}_2 : \text{N}_2$ experiment shown in Figure 2b. This ratio is similar to that predicted by the reaction stoichiometry of equation 3 for maximum conversion of CH_4 , H_2 and CO_2 to C_2H_6 . Corresponding oil yields are shown in Table 1.

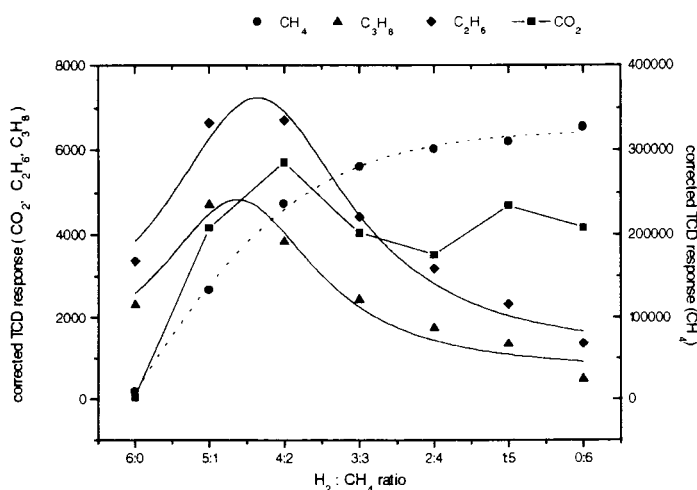


Figure 2a Gaseous product formation from $\text{H}_2 : \text{CH}_4$ pyrolysis.

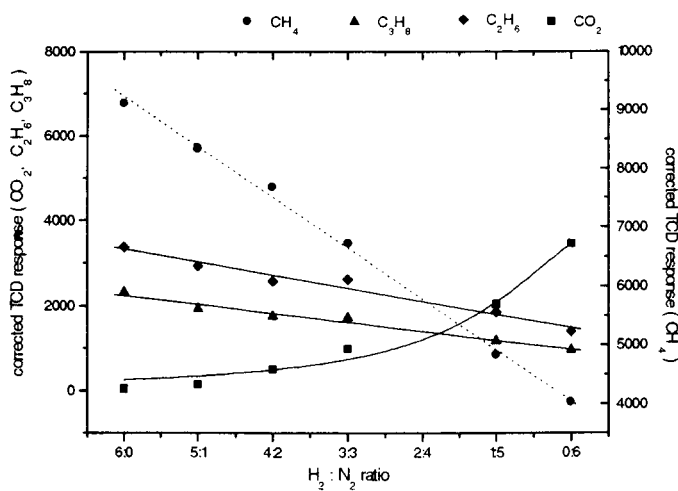


Figure 2b Gaseous product formation from $\text{H}_2 : \text{N}_2$ pyrolysis.

Table 1: The combined oil yield for chloroform and methyl alcohol soluble products from the liquefaction of Millmerran coal under different reactant gas compositions. Oil yield under 6 MPa N₂ was 4.53 %

H ₂ (MPa)	Oil %	CH ₄ (MPa)	Oil %	H ₂ +CH ₄	Oil %
1	21.25	5	10.00	1+5	23.90
2	26.86	4	8.00	2+4	29.09
3	50.19	3	7.20	3+3	49.52
4	52.68	2	5.60	4+2	54.72
5	60.90	1	3.25	5+1	55.44
6	58.80	6	13.55	6+0	58.80

3. CONCLUSIONS

When coal and methane were reacted at 400 °C for 64 h in the presence of catalyst, conversion to liquid products and gaseous hydrocarbons was higher than under nitrogen although significantly lower than when hydrogen was used. To achieve higher yields, methane and hydrogen mixtures were employed. Gaseous hydrocarbon yields were maximised at a H₂ : CH₄ ratio of 3:1 and some additive effects were seen for liquid hydrocarbon release, providing evidence for potential methane activity under hydrolysis conditions.

REFERENCES

1. F.J. Derbyshire, IEA Coal Research, Report No. IEACR/08, London (1988)
2. J.D.Brooks and J.W.Smith, *Geochim. Cosmochim. Acta* 31, (1968) 2389
3. D.Leythaeuser and D.H.Welte, *Advances in Organic Geochemistry*, 429, Pergamon Press (1968)
4. N. Robinson, G. Eglinton, C.J. Lafferty and C.E. Snape, *Fuel*, 70 (1991) 249
5. M.L.Poutsma, *Energy & Fuels* 4 (1990) 113
6. N.O Egiebor and M.R. Gray, *Fuel* 69 (1990) 1276
7. K.Chatterjee, B.Bal, L.M. Stock and R.F.Zabransky, *Energy & Fuels* 3 (1989) 427
8. D.R.Stull, E.F.Westrum and G.C.Sinke, *The Chemical Thermodynamics Of Organic Compounds*, John Wiley & Sons, 1969, New York.
9. A. Erdohelyi, J. Cserenyi and F. Solymosi, *J. Catal.*, 141 (1993) 287
10. W.F. Maier and R. Franke, *Fuel* 73 (1994) 5..

SUPERCritical FLUID EXTRACTION OF HIGH VOLATILE BITUMINOUS COALS FROM THE SAAR REGION, GERMANY. INFLUENCE OF EXTRACTION PARAMETERS ON EXTRACT YIELD AND COMPOSITION

G. Götz^a, H. Hammer^b and M. Wolf^a

^aLehrstuhl für Geologie, Geochemie und Lagerstätten des Erdöls und der Kohle; RWTH Aachen; Lochnerstr. 4-20; D-52056 Aachen; Germany (Telefax: +49-241-8888-152)

^bInstitut für Brennstoffchemie und physikalisch-chemische Verfahrenstechnik; RWTH Aachen; Worringerweg 1; D-52064 Aachen; Germany

1. Introduction

High volatile bituminous coals from the Saar region (Germany), often contain considerable amounts of free and trapped bitumen¹⁻³. This trapped bitumen is mainly located inside the vitrinite¹⁻⁴ causing a decrease of the vitrinite reflectance^{1,2,4,5}. Also it is responsible for the good coking quality of these coals^{6,7} even though they are relatively low in rank. Two high volatile (A and B) bituminous coals of Stephanian A (no. 1) and Westphalian C (no. 10) age from the Saar region, Germany, were extracted under supercritical conditions using methanol, ethanol, toluene, and an equimolar mixture of toluene and methanol at varying thermodynamic parameters to study the influence of pressure and temperature on the debituminization of hard coals. Especially the yield and the molecular composition of the extracts were points of interest.

2. Experimental

Experiments are performed using the method described by Pickel and Götz¹. Further informations are given in table 1. Basic data of the coals studied here are previously published^{1,2}.

3. Results and Discussion

Supercritical fluid extraction (SFE) of bituminous coals yield high amounts of extracts, especially if toluene^{1,3,8-11} or its mixture with methanol^{3,11,12} is used (table 1). In general increasing pressure vastly enhances the extract yield caused by an improved access of the supercritical fluid to the micropore system of the coal and the enhanced fluid density responsible for the increased solvent power. A higher temperature used in SFE increases the extract yields, because the fluid shows a decreased viscosity and an enhanced diffusivity, both improved properties make the transport of solvent loaded with solutes easier through the pore system of coal.

Table 1

Temperature (K) and pressure (MPa) used in the supercritical fluid extraction of two high volatile bituminous coals, and yields (mg/g C_{org}) and composition (%) of extracts

Sample no.	Solvent ¹	T _{Ex}	P _{Ex}	extract	alkanes	aromatics	NOS-compounds	(pre-)asphaltenes
1	M	527	10.0	25.0	3.9	18.9	22.6	54.7
1	M ₁	527	18.3	52.5	5.3	16.1	44.3	34.3
1	M ₂	608	32.0	116.0	1.0	13.3	37.6	48.1
1	E	530	17.8	64.9	2.5	15.7	61.1	20.7
1	TM	560	10.0	148.8	3.7	16.5	74.5	5.3
1	TM ₁	608	24.0	234.4	1.8	11.6	73.7	12.8
1	T	608	10.0	104.8	3.5	14.0	76.9	5.6
1	T ₁	608	12.5	165.3	4.2	29.5	34.6	31.7
10	M	527	10.0	26.6	11.3	39.6	31.6	17.4
10	M ₁	527	18.6	80.4	7.1	37.9	46.8	8.2
10	M ₂	608	31.8	89.5	4.4	27.9	47.4	20.3
10	E	530	16.8	87.1	4.6	25.1	48.2	22.1
10	TM	560	10.0	106.0	4.3	40.5	46.5	8.7
10	TM ₁	608	22.8	199.8	2.6	30.0	51.8	15.7
10	T	608	10.0	185.1	3.5	24.2	56.8	15.4
10	T ₁	608	16.0	214.6	1.9	18.9	53.0	26.1
10	T ₂	608	20.5	154.3	2.0	23.1	57.7	17.3

¹M=methanol, E=ethanol, T=toluene, TM=toluene-methanol

A supercritical toluene-methanol mixture releases considerable amounts of extractable coal compounds. Both components of the fluid have specific properties which are valuable for their use in coal extraction. Alcohols can interact with oxygen-containing functional groups of the coals's organic matter resulting in swelling of the cross-linked network of coal^{13,14}. Therefore ethanol compared with methanol yields more extract, because it swells the macromolecular phase of bituminous coal much more than its lower homologue^{13,14}. Methanol's low solvent power at reduced pressures can be enhanced by increasing the pressure. The interaction between toluene and the macromolecular phase of coal is relatively low, but increases with coal rank according to the more aromatic character of high rank coals^{1,3}. However supercritical toluene is a good solvent for the molecular phase (e. g. aliphatic and aromatic hydrocarbons, NOS-compounds, (pre-)asphaltenes) of coal. An equimolar toluene-methanol mixture show a synergistic swelling behaviour, it swells bituminous coals four times as strong as pure methanol¹³. The combination of the properties of both solvents explain the high solvent power of the mixture in coal extraction. The composition of the extracts show some significant differences (table 1). In general more aromatic hydrocarbons, NOS-compounds⁸ and (pre-)asphaltenes⁸ are released increasing extraction pressure, whereas the yields of aromatic hydrocarbons and NOS-compounds are enhanced by use of higher temperatures. Increasing temperature causes some pyrolytic reactions of coal components and the solvents. Minor amounts of olefins, which possible split off from coal's macromolecular phase, are detected in the extracts which are

produced at minimum temperatures of 560 K³. Further mesophases are generated inside the telo- and pseudovitrinite layers of the coal no. 10 during supercritical methanol or toluene extraction at 608 K and elevated pressures⁵. Toluene undergoes an autoreaction to 1,2-diphenylethane and methylated biphenyls^{3,9,15}. As a result of the reaction of supercritical alcohols with free and bound aliphatic and alicyclic acids high amounts of n-alkanoic and hopanoic acids and low amounts of isoprenoidal acids are liberated as esters from the coal matrix, respectively the pore system of coals³. The release of these esters is improved at high pressures or using the toluene-methanol mixture.

Organic geochemical parameters of each coal show considerable variations depending on the solvent and the extraction conditions used. CPI, pristane/phytane and pristane/n-C₁₇ ratios decreased with enhanced pressure, only the pristane/phytane ratio of the coal no. 10 increases slightly. The improved access of the solvent to the micropore system of the coal at high extraction pressures release more higher n-alkanes and sterically demanding molecules like isoprenoids, triterpenoids, polycyclic aromatic hydrocarbons and (pre-)asphaltenes. Further thermal labile compounds such as alkanes are better preserved at a higher extraction pressure which reduces the gas generation by decomposition of solvent, coal and its soluble products. Maturity (or rank) parameters are also affected by experimental conditions used in SFE. The moretane/hopane ratio (e. g. for the C₂₉- and C₃₀-homologues) gives unsatisfactory results for both coals. The more reliable methylphenanthrene indices (MPI) 1 and 2¹⁷ as well as methyl-naphthalene (MNR) and methylphenanthrene (MPR) ratios are clearly affected by the solvents and the thermodynamic parameters of the extraction process. In the most cases the values of these rank parameters rise with

Table 2
Organic geochemical parameters of supercritical fluid extracts of bituminous coals

Sample no. and solvent	CPI ₁₇₋₂₉	pristane phytane	pristane n-C ₁₇	$\frac{\beta\alpha(C_{29}+C_{30})}{\alpha\beta(C_{29}+C_{30})}$	MNR	MPR	MPI1	MPI2
1M	1.30	17.27	19.33	0.43	1.15	0.89	0.55	0.67
1M ₁	1.32	11.02	15.82	3.06	0.60	0.87	0.64	0.89
1M ₂	0.95	4.33	5.23	0.38	1.38	1.05	0.86	1.06
1E	1.27	15.21	15.25	0.37	1.07	0.85	0.64	0.79
1TM	1.35	17.76	15.98	1.53	1.35	1.21	0.54	0.74
1TM ₁	1.16	13.85	8.69	0.30	1.19	0.99	0.43	0.37
1T	1.15	11.45	8.62	0.63	0.75	0.42	0.46	0.47
1T ₁	0.96	5.30	2.19	n. d.	1.22	0.45	0.50	0.52
10M	1.04	2.30	0.62	n. d.	1.40	3.00	1.07	1.20
10M ₁	1.03	3.28	0.60	n. d.	1.19	1.30	1.16	1.01
10M ₂	1.00	4.57	0.57	n. d.	1.24	1.03	0.70	0.85
10E	1.01	3.64	0.73	0.25	1.44	1.12	0.80	0.88
10TM	1.05	4.75	0.75	1.31	1.36	0.32	0.41	0.22
10TM ₁	1.00	3.35	0.54	n. d.	1.19	1.17	0.89	1.06
10T	1.01	4.34	0.52	0.06	1.29	1.97	0.95	1.20
10T ₁	1.07	5.00	0.60	n. d.	1.46	1.18	0.75	1.06
10T ₂	1.02	2.42	0.54	n. d.	1.42	0.81	0.67	0.67

increasing pressure. The improved access of the supercritical fluid to "closed" micropores yield a biomarker distribution which is much different to those of "open" pores³.

4. Conclusions

Extract yield and composition varied strongly depending on process parameters like solvent, temperature, and pressure, each affected clearly fluid density and coal porosity. Organic geochemical parameters, based on biomarker yields, which are used in the evaluation of rank, facies or depositional conditions are significantly influenced by the extraction parameters. Supercritical fluid extraction using binary solvent mixtures and high pressures improve the release of coal molecular components and give more reliable information about free and trapped bitumen of bituminous coals.

References

1. W. Pickel and G. K. E. Götz, *Org. Geochem.* 17 (1991) 695-704.
2. C. M. Prange, Ph. D. thesis, RWTH Aachen, Aachen, 1989.
3. G. K. E. Götz and M. Wolf (Book of Abstracts, 17th Meeting on Organic Geochemistry 1995, Donostia-San Sebastian, Spain), 1995.
4. M. Wolf and E. Wolff-Fischer, *Glückauf Forschungsh.* 45 (1984) 234-246.
5. G. Götz, W. Pickel and M. Wolf, *Proc. 1995 International Conf. Coal Sci., Oviedo*, (Eds. J. A. Pajares and J. M. D. Tascon), Elsevier, Amsterdam, 1995.
6. H. W. Hagemann, K. Ottenjann, W. Püttmann, M. Wolf and E. Wolff-Fischer, *Erdöl & Kohle* 42 (1989) 99-110.
7. L. Wissing, Ph. D. thesis, RWTH Aachen, Aachen, 1989.
8. L. A. Amestica and E. E. Wolf, *Fuel* 63 (1984) 227-230.
9. W. Baumgartner and K. Hedden, *DGMK-Tagungsbericht 9206*, DGMK, Hamburg (1992) 245-254.
10. P. Cahill, G. Harrison and G. J. Lawson, *Fuel* 68 (1989) 1152-1157.
11. W. S. Fong, P. C. F. Chan, P. Pichaichanarong, W. H. Corcoran and D. D. Lawson, *Chemical Engineering at Supercritical Conditions* (Eds. M. E. Paulatis, J. M. L. Penninger, R. D. Gray and P. Davidson), Ann Arbor Science, Ann Arbor, MI (1988) 377-394.
12. N. Vasilakos, J. M. Dobbs and A. S. Parisi, *Ind. Eng. Chem. Process. Des. Dev.* 24 (1984) 121-128.
13. D. M. Bodily, J.-P. Wann and V. R. Kopp, *Proc. 1989 Intern. Conf. Coal Sci., Tokyo*, 201-204.
14. J. Goslar, L. S. Cooray and L. D. Kispert, *Fuel* 68 (1989) 1402-1407.
15. J. R. S. Kershaw, *S. Afr. J. Chem.* 31 (1978) 15-18.
16. R. Garcia, Ph. D. thesis, Univ. of Oviedo, Oviedo, 1990.
17. M. Radke, D. H. Welte and H. Willsch, *Geochim. Cosmochim. Acta* 46 (1982) 1-10.

Supercritical Water Extraction of Coal and Catalytic Reforming of Extracts in Supercritical Fluid

Tadafumi Adschiri, Susumu Nagashima, and Kunio Arai

Department of Chemical Engineering

Tohoku University

TEL/FAX 81-22-217-7246

1. INTRODUCTION

Supercritical fluid is a fluid above its critical temperature and pressure. Around the critical point, the fluid properties vary greatly with a little change of pressure and temperature. So far, quite a few research and development for the supercritical fluid extraction process have been reported by using fine control of solvent power and selectivity of extraction.

Also for a reaction media, supercritical fluid must be a promising solvent. The solvent effect on reaction equilibrium or reaction rate can be manipulated due to its controllable fluid properties.

We employ supercritical fluid as a reaction media of a new coal conversion process. First, this paper describes the specific features of supercritical water extraction of coal and elucidates the role of water on the reaction. Next, for catalytic reforming of coal tar pitch, supercritical toluene-tetralin mixture was used. This paper demonstrates enhancement of reaction rate and inhibition of coking on the catalyst by using supercritical fluid and elucidates the solvent effect on the reaction.

2. EXPERIMENTAL

2.1 Supercritical water extraction with semi-batch type reactor

Supercritical water(SCW) extraction of a Japanese sub-bituminous coal(Taiheiyo coal) was conducted in a semi-batch type reactor(653 K, 25-40MPa) and the results were compared with that for supercritical toluene extraction(653 K, 15-30MPa) of our previous study[1]. The procedure to the experiment was the same as in the previous study.

The conversion of coal was evaluated from the weight change of coal after the extraction. Since the considerable amount of ash(10-30 wt% of ash in coal) was extracted by SCW, the conversion was evaluated on the dry ash free basis as follows,

$$X=(W_s-W_r)/W_s \times 100$$

where W_s [g-daf] is weight of loaded coal, W_r [g-daf] is weight of residual coal. The amount of gas produced during the extraction was measured by a gas accumulator and was found to be negligibly small. The extract was collected with water in a sampling vessel. Water was distilled at 333 K under reduced pressure and the extract was dried at 383 K under vacuum. During this treatment, light components contained in the extracts were evaporated. Volatile matter was defined as the fraction volatiled during the drying under vacuum. The rest of the extract was defined as liquid products. Liquid product was further fractionated into acetone-soluble matter and insoluble matter. Liquid yield and the yield of acetone-soluble matter were also evaluated based on the initial weight of coal by dry ash free basis. Acetone-soluble matter was analyzed by GCMS and insoluble matter by TGA. Ultimate analysis was conducted for both fractions and the residual char.

2.2 Catalytic reforming of coal tar pitch in supercritical fluid

A flow type reactor was used in this experiment. Experimental procedure was the same as previous experiment[2]. A pitch(C 91.6 wt%, H 5.3 wt %, N 1.04 wt%, S 0.47 wt%) which was soluble in toluene was used as a sample. Catalyst used was NiMo/Al₂O₃ particle(0.11, 0.48 and 0.8 mm). The pitch was introduced to the catalyst bed with supercritical toluene-tetralin(30vol%) mixture by a high pressure pump. Reaction temperature was 703 K and pressure ranges from 4 MPa to 25 MPa. The product was collected in a sampling vessel. Ultimate and GCMS analyses were conducted for the recovered pitch.

In another series of experiment, 1-methyl naphthalene-tetralin mixture was used in stead of toluene-tetralin mixture. The effect of particle size(0.11-0.8 mm) on the reaction was also examined. For the detailed study of the reaction mechanism, benzocarbazole and benzoquinolin that were the main nitrogen compounds in the sample pitch were employed as a model compound.

3. RESULTS AND DISCUSSION

3.1 Supercritical water extraction of coal

The results obtained for SCW extraction and supercritical toluene extraction were compared in Fig.1. As shown in this figure, higher coal conversion(55 wt%) and liquid yield(45 wt%) were obtained for SCW extraction. Acetone-soluble matter was larger than for supercritical toluene extraction. On the basis of the ultimate analysis of the liquid product, O/C was larger for SCW extraction.

With increasing residence time of solution in the coal bed, liquid yield decreased while volatile matter yield increased for both cases. GC analysis of the acetone-soluble matter indicates the increase in the lighter component. Thus the increased volatile yield with increasing residence time is due to the decomposition of the liquid product.

In SCW extraction experiment, good carbon balance(>96%) was obtained, while hydrogen and oxygen balances were poor(around 80%). We think the deficient of hydrogen and oxygen balances is due to the dehydration from coal or the products. However, the hydrogen and

oxygen balances tended to become better with increasing residence time, while the amount of oxygen compounds in the acetone-soluble matter increased. According to the previous studies[3], hydrolysis is easy to take place at ether or ester bonds. Thus we think that 1)the higher yields of acetone-soluble matter, 2)more oxygen compound in the extract, and 3)deficient of hydrogen and oxygen balances for SCW extraction are all due to the hydrolysis.

The result of TGA analysis for acetone-insoluble matter indicates that with increasing residence time both heavier and lighter species were produced for supercritical toluene extraction. This suggests that both polymerization and decomposition take place for acetone insoluble matters. However, in SCW extraction, the shift of the product distribution toward the heavier side could not be observed. The result suggests that polymerization was suppressed in SCW.

From the above results, we may conclude that 1)elevated conversion, 2)elevated liquid yield, 3)lighter oil yield, and 4)more oxygen compounds yield in SCW extraction are because of 1)the hydrolysis of ether or ester bond in coal and 2)the inhibition of polymerization or recombination of the primary products of thermal decomposition of coal, perhaps due to the radical quenching with H or OH.

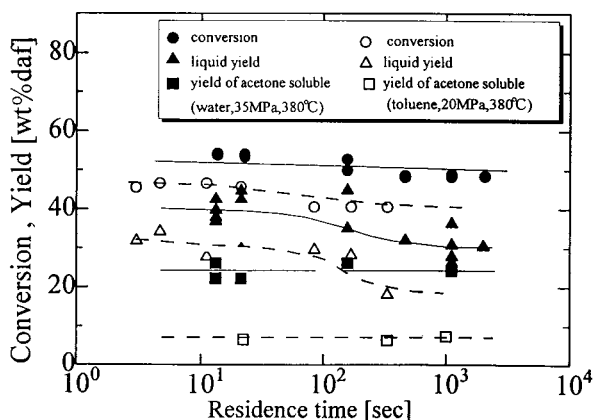


Fig.1 Comparison of SCW extraction with supercritical toluene extraction

3.2 Catalytic reforming of pitch in supercritical fluid

In a catalytic hydro-treatment of heavy oil, coking on the catalyst are significant problems. In this study supercritical toluene-tetralin mixture was employed as a solvent with expecting the in-situ removal of coke precursor from the catalyst surface.

Fig.2 shows that the variation of amount of coke formation on the catalyst(T:703 K, P:10-25 MPa, and contact time of solution:15 min.) in the supercritical fluid. The amount of coke formation increased with increasing reaction time at 10 MPa. However, the coke formation was suppressed above 10 MPa perhaps due to the higher solvent power.

Under this condition, the degree of nitrogen removal was around 0.4 even though the

contact time was as short as 15 min. In a conventional process of catalytic denitrogenation from liquid pitch by flowing hydrogen gas, around two hours are required for the same degree of denitrogenation(around 0.4). The higher rate of nitrogen removal was considered to be higher intraparticle mass transfer rate of hydrogen in supercritical fluid than in liquid pitch. Thus the effect of particle size on the reaction rate was examined. As a reference experiment, liquid phase experiment was also conducted by using 1-methyl naphthalene-tetralin mixture in stead of supercritical toluene-tetralin mixture. For both supercritical and liquid phase reactions, the effect of particle size(0.11-0.8 mm) on the reaction was negligible under this condition(703 K, 15 MPa).

Fig.3 shows the effect of pressure on the reaction rate for the catalyst particle size of 0.11 mm. As expected, pressure effect was not observed for the liquid phase reaction under this condition. However, for supercritical fluid phase reaction with elevating pressure, conversion was decreased.

These results suggest the importance of a solvent effect on the intrinsic reaction at active site of the catalyst.

For the elucidation of the solvent effect on the reaction, carbazole and benzoquinoline were employed as a model compound and detailed kinetic study was conducted. The result suggests that pressure affects the adsorption equilibrium of the reactant on the catalyst, equilibrium between tetralin and naphthalene, that between carbazole and tetrahydro-carbazole and the denitrogenation reaction rate. The details of the obtained results will be appeared elsewhere.

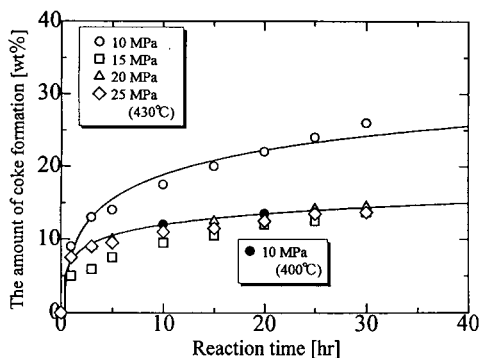


Fig.2 Effect of pressure on the amount of coke deposited on the catalyst

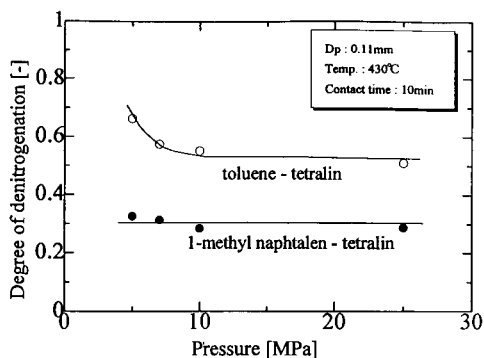


Fig.3 Effect of pressure on degree of denitrogenation

REFERENCES

1. T.Adschiri, S.Abe and K. Arai, J. Chem. Eng. Japan, 24(1991)715
2. T.Adschiri, T.Suzuki and K. Arai, Fuel, 70(1991)1483
3. T.Adschiri, S.Hirose, R.Malaluan and K.Arai, J. Chem. Eng. Japan, 26 (1993) 676.

Role of aromatic structure in pathways of hydrogen transfer and bond cleavage in coal liquefaction: Theoretical studies.

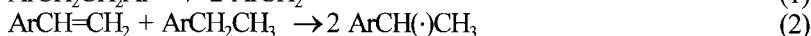
James A. Franz^a, Tom Autrey^a, Donald M. Camaioni^a, John D. Watts^b and Rodney J. Bartlett^b

^aPacific Northwest Laboratory, P.O. Box 999, Richland, Washington, 99337 USA

^bQuantum Theory Project, University of Florida, Gainesville, Florida 32611 USA.

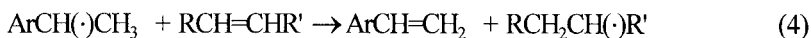
1. INTRODUCTION

The mechanisms by which strong carbon-carbon bonds between aromatic rings and side chains are cleaved under hydrolysis conditions remain a subject of wide interest to fuel science. It is now well understood that the primary modes of radical initiation during hydrolysis are unimolecular homolysis of weak carbon-carbon and carbon-heteroatom bonds (eq 1) and by reverse-radical disproportionation (RRD, eq 2) [1]. Once organic radicals are produced, the production of free hydrogen atoms by β -scission (eq 3)



from alkyl radicals and hydroaromatic radicals becomes an efficient pathway for free hydrogen atom production from cyclohexadienyl, hydronaphthyl, and phenanthrenyl radicals. Hydrogen atoms participate in strong bond cleavage, by means of direct *ipso*-displacement of alkyl groups attached to aromatic rings (HA pathway), or by the indirect pathway of hydrogen atom addition and abstraction of hydrogen by the adduct radical to form a dihydroaryl hydrocarbon, followed by unimolecular scission of the resulting weak C-C bond (RS, reduction/scission pathway). Even when hydrogen atom thermodynamic "sinks", such as anthracene, are present in liquefaction mixtures, it is now known that 1- and 2-hydroanthracenyl radicals are formed as well as 9-hydroanthracenyl radicals, thus the HA pathway is never completely suppressed [2]. Thus, when the outer ring of anthracene is partially reduced, it can serve as an efficient hydrogen atom source. In our modeling and model compound studies, the RRD, HA, and RS pathways appear to dominate bond scission reactions in non-catalytic hydrolysis reactions [3-8].

Recently, we have studied in detail an alternate pathway for hydrogen atom transfer to π -systems, radical hydrogen transfer (RHT). RHT is the direct, bimolecular transfer of hydrogen from the β -position of an organic radical to the target π -system (eq 4).



Scission of the group R then occurs rapidly (eq 5). The existence of the RHT pathway, proposed to account for strong bond cleavage rates and selectivities [9] has to date remained unproven because of the complexity of simultaneously competing RRD, HA, and RS pathways giving identical products in hydrocarbon decomposition reactions.

In our initial theoretical study we examined the reaction ethyl radical + ethylene \rightarrow ethylene + ethyl at the spin-projected UMP2/6-31G** level of theory [10]. Recently, we have used a calibrated ROHF-MNDO-PM3 method to predict thermoneutral RHT barriers for hydrogen transfer between hydroaryl radicals and the corresponding arene: the results were as follows: hydrogen transfer between cyclohexadienyl and benzene (17 kcal/mol), hydronaphthyl and naphthalene (22 kcal/mol), 9-hydrophenanthrenyl and phenanthrene (23.9 kcal/mol), and 9-hydroanthracenyl and anthracene (26 kcal/mol) and methallyl + butadiene (30 kcal/mol)[11]. The lower barriers in this family correspond to systems such as cyclohexadienyl radical that undergo facile scission of hydrogen atom with the result that systems with accessible RHT barriers ($< ca 20$ kcal/mol) will experience a substantial participation of the HA (free hydrogen atom) reaction pathway for strong bond scission.

Because of the inherent limitations of semiempirical methods such as ROHF-MNDO-PM3, we have extended our initial work with the ethyl + ethylene study to the examination of this reaction at the ROHF-MBPT[2]-6-31G** and ROHF-CCSD[T]-6-31G** levels of ab initio theory. The primary objective was to determine how intrinsic RHT barriers change with conjugative stabilization of the radicals. UHF wavefunctions for open shell systems suffer from varying degrees of spin contamination, which in the case of the RHT reaction, becomes severe for larger π -systems and is not removed using spin annihilation procedures. Hence, the spin-restricted ROHF approach has been applied to study several RHT reactions, and we present completed ROHF results for the ethyl + ethylene system and preliminary results for the methallyl + butadiene system. The methallyl + butadiene system serves as a model for highly stabilized hydroaryl radicals: the methallyl radical exhibits a C-H bond strength of 46.5 kcal/mol compared to 9-hydroanthracenyl, 43.1 kcal/mol [12].

2. COMPUTATIONAL PROCEDURES

The Gaussian-92 set of programs [13] was employed for open shell UHF calculations and the ACES-2 set of programs [14] was employed for advanced post-SCF restricted open shell Hartree-Fock (ROHF) calculations. Transition states were located using default ground state optimizers while imposing symmetry in the transferred hydrogen C-H-C bonds. Vibrational calculations were carried out in each case to verify ground or transition states, and to provide thermal corrections to room temperature.

3. RESULTS AND DISCUSSION

3.1 Ethyl Radical + Ethylene.

Table 1 presents results for the ethyl + ethylene RHT reaction. Spin annihilation of the UHF wavefunction was largely successful, resulting in a value of $\langle S^2 \rangle$ before projection of 1.224 and after projection of 0.807 (a pure doublet state has $\langle S^2 \rangle = 0.75$). In this case, the residual spin contamination has little effect on the energies of ground and transition state

Table 1. Activation Energies for RHT between Ethyl and Ethylene

Molecule	Energies, Level of Theory (hartree/particle) ^a		
	UHF- PMP2/6-31G**	ROHF- MBPT[2]-6-31G**	ROHF- CCSD[T]-6-31G**
Ethyl	-78.88791	-78.885998	-78.926824
Ethylene	-78.327231	-78.327231	-78.356658
TS, C ₂ H ₄ --H--C ₂ H ₄	-157.169781	-157.16622	-157.23657
ΔE(298 K) ^b	27.2 kcal/mol	28.23 kcal/mol	28.17 kcal/mol

^aAll geometries are fully optimized at the indicated level of theory

^bEnergy changes include thermal corrections based on analytical UHF MP2/6-31G** frequencies: Ethyl, 0.0656574; Ethylene, 0.0554475; TS, 0.1190859 hartree/particle.

structures (Table 1). A very useful result is the good agreement between the second-order ROHF treatment and the much more expensive CCSD[T] result. These results confirm the very much higher activation barrier of the RHT reaction compared to hydrogen abstraction barriers, and show that the RHT reaction is a highly unfavorable reaction, resembling a mostly dissociated hydrogen atom between two highly distorted olefinic structures.

3.2 Methallyl radical (Buten-3-yl Radical) + Butadiene

To estimate the intrinsic barrier of the methallyl + butadiene RHT reaction, UHF geometries optimized at MP2/6-31G** were used along with thermal corrections based on MP2/6-31G** vibrational calculations. ΔE(298 K) is estimated to be 25.8 kcal/mol for the RHT reaction from these numbers.

Table 2. Methallyl + Butadiene RHT Reaction (hartree/molecule)

	CH ₂ =CH-CH(·)CH ₃	+	Butadiene	→	C ₄ H ₆ --H--C ₄ H ₆ (TS)
Electronic:	-156.06657		-155.49100		-311.513466
Thermal:	0.10276		0.09147		0.1910344
Total:	-155.96395		-155.39953		-311.32243
ΔE(298 K) =	25.8 kcal/mol				

The activation energy predicted in Table 2 is based on single-point ROHF-MBPT[2] calculations. These in turn using UHF geometries which suffer from varying degrees of spin contamination, which are not removed by spin annihilation. Thus, the predicted activation barriers will undoubtedly change, probably to a higher value based on trends with smaller systems, by as much as 3-5 kcal/mol with full geometry optimization at higher levels of theory (ROHF-CCSD[T]).

4. CONCLUSIONS

The present results suggest that intrinsic barriers for the RHT pathway are quite high, in the range 25-30 kcal/mol for simple and conjugated olefins. The results lead to the prediction that the RHT pathway will not compete with HA, RRD, and RS mechanisms of strong bond scission. In particular, those olefinic and aromatic systems for which barriers may be relatively low, such as cyclohexadienyl radical, will be dominated by free hydrogen atom pathways, and systems such as anthracene will exchange hydrogen primarily by RRD pathways[3].

5. ACKNOWLEDGEMENT This work was supported by the U.S. Department of Energy, Office of Energy Research, Office of Basic Energy Sciences, at Pacific Northwest Laboratory, operated for the U.S. Department of Energy by Battelle Memorial Institute under contract DE-ACO6-76RLO 1830.

6. REFERENCES

1. S.E. Stein, *Acc. Chem. Res.* 24 (1991) 350.
2. T. Autrey, T.R. Powers, E.A. Alborn, J.A. Franz, and D.M. Camaioni, *Coal Science Proceedings, International Conference on Coal Science, 1995*, xxxx.
3. T. Autrey, E.A. Alborn, J.A. Franz, and D.M. Camaioni, *Energy Fuels* 9 (1995), in press.
4. S.T. Autrey, D.M. Camaioni, K.F. Ferris, J.A. Franz, *Coal Science Proceedings, International Conference on Coal Science, 1993*, 336.
5. T. Autrey, J.A. Franz, D.M. Camaioni, K. Ferris, G.J. Gleicher, *Coal Science Proceedings, International Conference on Coal Science, 1991*, 239.
6. D.M. Camaioni, S.T. Autrey, J.A. Franz, *J. Phys. Chem.*, 97 (1993) 5791.
7. T. Autrey, G.J. Gleicher, D.M. Camaioni, J.A. Franz. *Am Chem Soc, Div Fuel Chem. Preprints*, 36(2) (1991), 521.
8. T. Autrey, J.A. Franz. *Am Chem Soc, Div Fuel Chem. Preprints*, 35(2) (1990), 381.
9. See citations 1-8 in [2], accompanying paper in this volume.
10. J.A. Franz, K.F. Ferris, D.M. Camaioni, and S.T. Autrey, *Energy & Fuels*, 8 (1994) 1016.
11. D.M. Camaioni, S.T. Autrey, T.B. Salinas, and J.A. Franz, *J. Am. Chem. Soc.*, submitted for publication.
12. Methallyl: S.G. Lias, J.E. Bartmess, J.F. Liebman, J.L. Holmes, R.D. Levin, W.G. Mallard, *J. Phys. Chem. Ref. Data* 17 (1988), Sup.1. 9-Hydroanthracenyl: D. Griller, J.A. Martinho Simoes, B.A. Sim, D.D.M. Wayner, *J. Am. Chem. Soc.* 111 (1989), 7872.
13. Gaussian-92/DFT, Revision G.1, M.J. Frisch, G.W. Trucks, H.B. Schlegel, P.M.W. Gill, B.J. Johnson, M. W. Wong, J.B. Foresman, M.A. Robb, M. Head-Gordon, E.S. Replogle, R. Gomperts, J.L. Andres, K. Raghavachari, J.S. Binkley, C. Gonzales, R.L. Martin, D.J. Fox, D.J. DeFrees, J. Baker, J.J. P. Stewart, and J.A. Pople, Gaussian, Inc. Pittsburgh, PA, 1993.
14. ACE2 II (Advanced Concepts in Electronic Structure) Program: J.F. Stanton, J. Gauss, J.D. Watts, W.J. Lauderdale, and R.J. Bartlett, Quantum Theory Project, University of Florida, Gainesville, Florida 32611 USA.

Role of additives in diarylalkane degradation as a model reaction of coal liquefaction

Xian-Yong Wei*, Eisuke Ogata[®] and Etsuo Niki

Department of Chemistry & Biotechnology, Faculty of Engineering, The University of Tokyo; 7-3-1, Hongo, Bunkyo-ku, Tokyo 113, Japan

1. INTRODUCTION

As coal-related model compounds, α,ω -diarylalkanes (DAAs) have often been used to infer the mechanism of coal liquefaction [1-4]. Although several studies on model reactions have been undertaken, very limited answers in the published literature have been systematically given to the following questions: "What is the relationship between the structures and reactivities of DAAs? What roles do molecular hydrogen, hydrogen donors and catalysts play in the thermolysis, hydrocracking and hydrogenation of DAAs?" The answers to these questions are important not only to infer the mechanism of coal liquefaction but also to develop effective coal liquefaction processes.

To answer the above questions, we investigated the additive roles of molecular hydrogen, aromatic and hydroaromatic hydrocarbons (used as hydrogen donors), sulfur and catalysts in the reactions of DAAs and some other model compounds.

2. EXPERIMENTAL

1-Benzyl-naphthalene (1-BN) and di(1-naphthyl)methane (DNM) were synthesized by heating naphthalene with benzyl chloride and 1-chloromethylnaphthalene, respectively, in the presence of zinc powder [2]. 1,2-Di(1-naphthyl)ethane (DNE) and 1,3-di(1-naphthyl)propane (DNP) were synthesized according to the methods of Buu-Hoi [5] and Nishimura [6], respectively. The other compounds used as substrates or solvents, sulfur and metallic iron (Fe) catalyst, were commercial reagents purified by conventional methods if necessary. Synthetic pyrite (FeS_2) catalyst was provided by Asahi Chemical Industry Co., Ltd.

A substrate (7.5 mmol), prescribed amounts of sulfur, a catalyst and 30 ml of solvent (including aromatic or hydroaromatic additives) were placed in a 90 ml stainless steel, magnetically stirred autoclave. After pressurization with hydrogen and / or nitrogen to a desired level (total pressure 10 MPa) at 20°C, the autoclave was heated to the reaction temperature and kept at the temperature for 1 hr. It was then immediately cooled to room temperature in an ice-

* Present address: Department of Coal Preparation and Utilization, China University of Mining and Technology; Xuzhou (221008), Jiangsu, China

water bath. The reaction products were identified by GC-MS analysis if necessary and quantified by GC analysis.

3. RESULTS AND DISCUSSION

Table 1 summarizes the results of the reaction of diphenylmethane (DPM) under different reaction conditions. In the absence of gaseous hydrogen and catalyst, DPM was not converted at all, even at 400 °C, as shown in Run No. 1 - 3 & 15. It is especially noteworthy that addition of sulfur did not result in DPM degradation without catalyst (Run No. 2 & 3), but appreciably promoted DPM hydrocracking in the presence of FeS₂ (Run No. 18 - 20). Increase in H₂ pressure also increased DPM conversion (Run No. 15 - 17).

DPM is very stable thermally. Its degradation does not proceed even at 430 °C under H₂ in tetralin [2]. The low reactivity of DPM toward C_{ar}-C_{alk} single bond scission might be related to the large bond dissociation energy and the instability of phenyl radical resulting from cleavage of the C_{ar}-C_{alk} bond in DPM as shown in eq.(1).

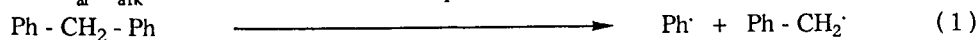
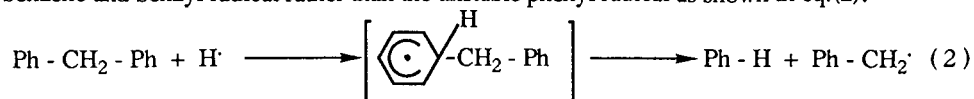


Table 1
Additive roles of molecular hydrogen, sulfur and catalysts in the hydrogenation and hydrocracking of DPM in decalin

Run No.	Reaction condition				Conv. (%)	Selectivity (mol%)	
	Catalyst	H ₂ IPP	S feed (g)	T (°C)		HG	HC
1	None	10	0	400	0		
2	None	10	0.05	400	0		
3	None	10	0.50	400	0		
4	Fe, 0.23 g	0	0	300	58.4	100	0
5	Fe, 0.23 g	10	0.066	300	0		
6	Fe, 0.23 g	10	0.132	300	0.8	0	100
7	Fe, 0.23 g	10	0.264	300	3.5	0	100
8	Fe, 0.23 g	10	0.528	300	6.4	0	100
9	Fe, 0.02 g	10	0	400	79.3	88.1	11.9
10	Fe, 0.02 g	10	0.006	400	1.0	0	100
11	Fe, 0.02 g	10	0.012	400	2.9	0	100
12	Fe, 0.02 g	10	0.023	400	4.9	0	100
13	Fe, 0.02 g	10	0.046	400	9.2	0	100
14	FeS ₂ , 0.5 g	10	0.050	300	3.1	0	100
15	FeS ₂ , 0.5 g	0	0.050	400	0		
16	FeS ₂ , 0.5 g	5	0.050	400	37.8	0.8	99.2
17	FeS ₂ , 0.5 g	10	0.050	400	59.1	2.4	97.6
18	FeS ₂ , 0.5 g	10	0	400	53.0	0.5	99.5
19	FeS ₂ , 0.5 g	10	0.200	400	71.1	0.9	99.1
20	FeS ₂ , 0.5 g	10	0.800	400	74.8	0.9	99.1

IPP, HG and HC denote initial partial pressure, hydrogenation and hydrocracking, respectively.

H-atom addition to the *ipso*-carbon of DPM is an essential step in the cleavage of the $C_{ar}-C_{alk}$ bond in DPM under mild reaction conditions, because H-atom induced DPM degradation yields benzene and benzyl radical rather than the unstable phenyl radical as shown in eq.(2).



Thomas et al. has reported FeS_2 facilitates the formation of free-radical intermediates such as $H\cdot$ and $HS\cdot$ during its decomposition to $Fe_{1-x}S$ [7]. Hence, It is difficult to rule out the possibility that the role of FeS_2 and H_2 in inducing DPM degradation is to produce H-atoms to attack the *ipso*-carbon of DPM. Since FeS_2 is rapidly decomposed to pyrrhotite above 300°C [7,8] and sulfur to H_2S at even lower temperatures [9], the promotional role of sulfur addition in the presence of FeS_2 may be attributed to the fact that increasing H_2S pressure favors the active site formation [10]. In the presence of some active catalysts, it is probably considered that the reactions do not proceed with such simple free radical chain mechanisms as initiating, propagating, and terminating. The reaction may be especially facilitated by the participation of the adsorbed species on the catalyst surface because free H-radical probably does not exist in high concentration and probably does not attack *ipso*-carbon of DPM selectively in the liquid-phase of reaction system since the free H-radical is a very unstable and a very active specie.

Quite different from FeS_2 , in the absence of sulfur, Fe mainly catalyzed DPM hydrogenation (Run No. 4 & 9). At 300°C , DPM degradation did not proceed at all. Even at 400°C , the main products were hydrogenation products rather than degradation ones. However, adding sulfur to the reaction system inhibited DPM hydrogenation (Run No. 5 - 8 & 10 - 13) and DPM conversion to benzene and toluene increased with increasing sulfur addition, similar to the reaction of DNМ [9]. These facts evidently indicate that, with H_2 and a iron catalyst (Fe or FeS_2), sulfur addition promotes the cleavage of the $C_{ar}-C_{alk}$ bond in diarylmethanes (DAMs). At 300°C , Fe also catalyzed the hydrogenation of other model compounds. Fe and FeS_2 were also observed to play very different roles in the reaction of DNМ [11].

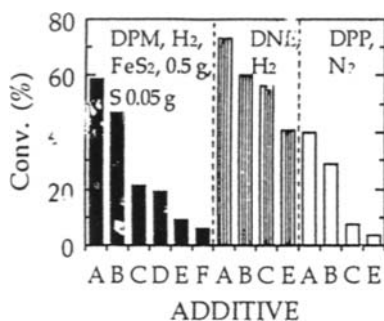
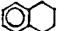
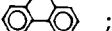

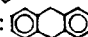
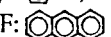


Figure 1 Additive roles of aromatic and hydroaromatic hydrocarbons in DAAs degradation at 400°C .

A: none; B:  ; C:  ;
 D:  ; E:  ; F:  .

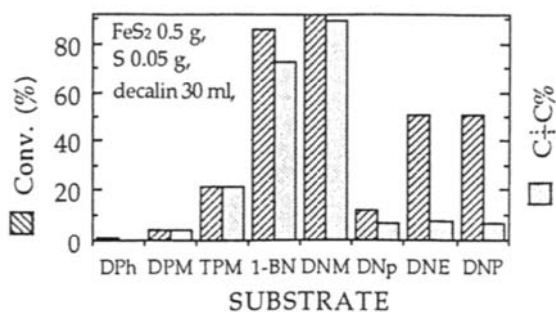


Figure 2 Comparison of the reactivities among DAAs, DPh (diphenyl), TPM (triphenylmethane) and DNp (1,1'-dinaphthyl) for hydrocracking at 300°C . C-C%: percentage of C-C bond cleavage.

Figure 1 shows the additive roles of aromatic and hydroaromatic hydrocarbons (molar ratio of additive to substrate = 1) in DAA degradation including hydrocracking, hydrogenolysis and thermolysis. Using the additives, the rate of DAA degradation decreased in the order: tetralin < 9,10-dihydrophenanthrene < 9,10-dihydroanthracene, which is consistent with the order for hydrogen abstraction of the hydrogen donors [12], e.g., a hydrogen donor with stronger "hydrogen donatability" has more inhibitory effects on DPM hydrocracking than the corresponding hydroaromatics. In the presence of catalyst, the results indicate that the adsorption of aromatics to the catalyst surface affected more than corresponding 9,10-dihydroaromatics.

Figure 2 compares the reactivities among DAAs, DPh, TPM and DNP to FeS₂-catalyzed hydrocracking. Without catalyst, all of the substrates was not converted at 300°C. Diarylmethanes (DAMs) and TPM were selectively hydrocracked to corresponding compounds by C_{ar}-C_{alk} bond cleavage, the conversions of which increased in the order: DPM < TPM < 1-BN < DNM. The selective hydrocracking of other compounds did not occur. These results can be interpreted by the hydrogen-acceptability of *ipso*-carbons in the substrates and the resonance stabilities of the resulting species after the C-C bond cleavage.

4. CONCLUDING REMARKS

The role of additives in α,ω -diaryllkane (DAA) degradation, as a model reaction of coal liquefaction, was investigated. Quite different roles between Fe and FeS₂, molecular hydrogen and hydrogen donors were observed, and the relationship between the structures of DAAs and their reactivities for hydrocracking was revealed.

ACKNOWLEDGMENT

The authors wish to thank to the New Sunshine Program Promotion Headquarters, Agency of Industrial Science and Technology, Ministry of International Trade and Industry of Japan for financial support.

REFERENCES

1. T. Ogawa, V.I. Stenberg and P.A. Montano, *Fuel*, 63 (1984) 1660.
2. S. Futamura, S. Koyanagi and Y. Kamiya, *Fuel*, 67 (1988) 1436.
3. L.W. Vernon, *Fuel*, 59 (1980) 102.
4. K. Ceylan and L.M. Stock, *Fuel*, 69 (1990) 1386.
5. N.P. Buu-Hoi and N. Hoan, *J. Org. Chem.*, 46 (1949) 1023.
6. J. Nishimura, N. Yanada, Y. Horiuchi, E. Ueda, A. Ohbayashi and A. Oku, *Bull. Chem. Soc. Jpn.*, 59 (1986) 2035.
7. M.G. Thomas, T.D. Padrick, F.V. Stohl and H.P. Stephens, *Fuel*, 61(1982) 761.
8. E. Ogata, T. Tamura and Y. Kamiya, *Proc. Inter. Conf. Coal Sci.(Maastricht)*, p-243 (1987).
9. B. Meyer, *Chem. Rev.*, 76 (1976) 367.
10. E. Ogata, K. Ishiwata, X.-Y. Wei and E. Niki, *Proc. Inter. Conf. Coal Sci.(Bannf)*, Vol. II, p-349 (1993).
11. X.-Y. Wei, E. Ogata and E. Niki, *Chem. Lett.*, (1991) 2199.
12. M.L. Poutsma, *Energy & Fuels*, 4 (1990) 113.

The use of polystyrene networks and phenolic resites to model the effectiveness of Fe and Mo catalysts in coal hydrolysis

S.D. Brown, M.C. Mayoral, O. Sirkecioglu and C.E. Snape

Dept. of Pure and Applied Chemistry, University of Strathclyde, Glasgow, G1 1XL, Scotland, U.K.

To model the effects of Fe and Mo catalysts in hydrolysis and temperature programmed reduction, a cured phenolic co-resin prepared from phenol and 4-hydroxy diphenylmethane and a polystyrene-divinylbenzene network have been used. The conversion characteristics of these models have been compared with those of a bituminous and a low-rank coal.

1. INTRODUCTION

Iron and molybdenum compounds have been the subject of much study with regard to their use as precursors for sulphided catalysts for both coal liquefaction and hydrolysis [1]. Previous work at Strathclyde has demonstrated that tar yields of ca 60% daf coal with relatively low gas yields can be achieved for bituminous coals in fixed-bed catalytic hydrolysis at 150 bar [2,3]. However, iron at relatively low concentrations, was much less effective than sulphided Mo. Further, for low-rank coals at high pressure, catalysts only increased tar yields typically by less than 10% daf coal but, without a catalyst, the tar yields of 40-50% are appreciably higher than for bituminous coals. Although rapid heating is used in process situations, slow heating is being applied in temperature programmed reduction (TPR) to specify organic sulphur forms in coals [4].

The use of model compounds is widely used to probe reaction pathways in coal liquefaction [5]. However, for hydrolysis in well-swept reactors, solid probes are required which do not melt before the onset of thermal decomposition [6]. In this study, the effects of Fe and Mo catalysts on bond scission and product distribution during hydrolysis has been investigated using two solid phase models, namely, a cross-linked polystyrene-divinylbenzene (PS-DVB) and a 4-hydroxydiphenylmethane-containing phenolic resin. The conversion characteristics of these models have been compared with those of a bituminous and a low-rank coal.

2. EXPERIMENTAL

The low-rank and bituminous coals used were SAMCA lignite (daf-C 67.4%, H 7.6 % and N 0.4 %, S(db) 6.0 %) and Gedling (daf-C 81.6%, H 5.2 % and N 1.7 %, S(db) 1.0 %). The diphenylmethane-containing resite was prepared as described previously [6] and the PS-DVB was commercially-available XAD-4.

Colloidal iron sulphide was prepared by bubbling H₂S through an aqueous solution of iron(II) sulphate at basic pH [7]. The finely divided precipitate, was filtered

and stirred with an aqueous suspension containing the correct amount of sample (coal, polystyrene or resite) to obtain a 5% weight loading of iron. Ammonium dioxidythiomolybdate was used as a precursor of sulphided molybdenum [2] and was impregnated onto the samples in water/methanol solution to give loadings of 1% Mo.

The hydropyrolysis apparatus [2] and the on-line mass spectrometry (MS) have been detailed elsewhere [4,6]. The hydropyrolysis experiments were conducted at a heating rate of $300^{\circ}\text{C min}^{-1}$ to a final temperature of 520°C , held for 10 minutes. Hydrogen pressures of 1 and 5 MPa were used with gas flow rates of 2 and $6 \text{ dm}^3 \text{ min}^{-1}$, respectively. Experiments were also conducted at 5°C/min to a final temperature of 450°C . The tars obtained were collected in a dry ice cooled trap. The runs with the on-line mass spectrometer were carried out under 5 MPa hydrogen at $5^{\circ}\text{C min}^{-1}$, to 600°C with a flow rate of $5 \text{ dm}^3 \text{ min}^{-1}$. The tars were characterised by $^1\text{H NMR}$ and GC-MS.

3. RESULTS AND DISCUSSION

3.1 Coals.

At the relatively low hydrogen pressure of 1 MPa, catalyst addition did not result in any increase in conversion for Gedling coal (Figure 1). However, for the more reactive lignite, both the Fe and Mo catalysts reduced char yields by *ca* 10% for coal, with iron being the more effective. At 5 MPa, Mo is more effective than Fe for Gedling, but for the lignite, Fe achieves similar yields as Mo, probably due to the decarboxylation ability of Fe sulphides. However, at the higher pressure, the increases in conversion for the lignite of *ca* 10% are no more than at 1 MPa (Figure 1), indicating that the catalysts are only effective for the more labile bonds. The higher activity of Fe found here compared to earlier studies [2,3] is ascribed to the much high loading (5% w/w) used. The ratios of aromatic to aliphatic hydrogen derived from $^1\text{H NMR}$ were lower for the tars from the Mo catalysed runs, indicating a higher hydrogenation efficiency for Mo compared to Fe.

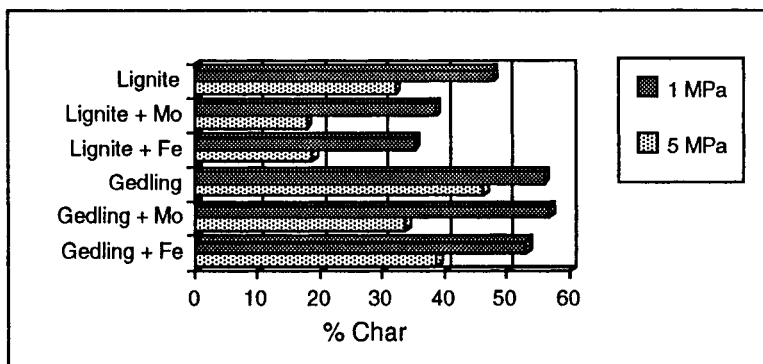


Figure 1. Char yields obtained in hydropyrolysis for the coals at the faster heating rate.

On-line MS showed that addition of Mo to Gedling (Figure 2) shifted the toluene evolution profile to much lower temperatures with a significant amount of toluene evolving in the temperature range $400\text{--}500^{\circ}\text{C}$. The maximum evolution temperature (T_{MAX}) obtained with Fe was intermediate between that for Mo and when no catalyst

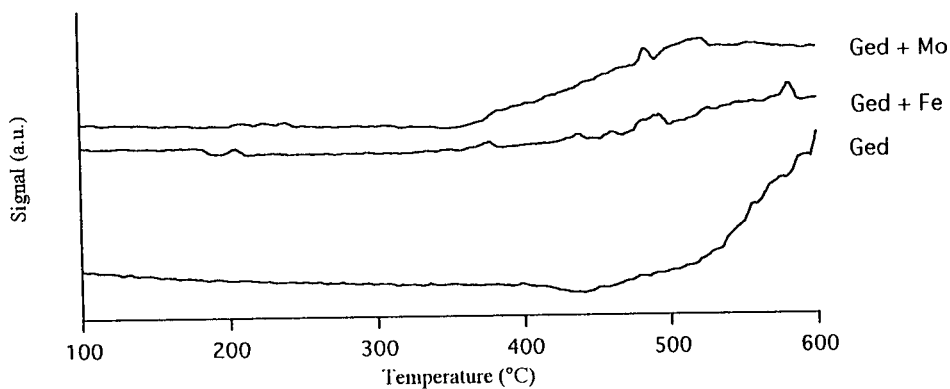


Figure 2. Hydropyrolysis-m.s. profile of toluene for Gedling with and without catalyst

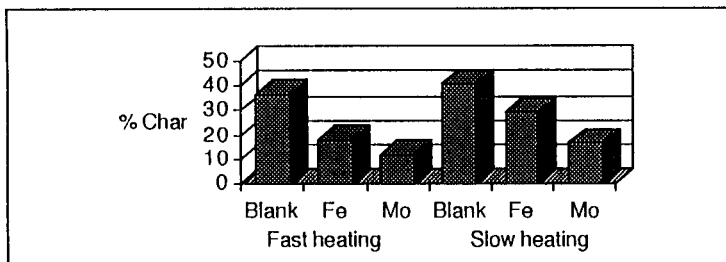


Figure 3. Hydropyrolysis of PS-DVB. Comparison of the char yields obtained at the faster and slower heating rates. Final temperature of 450°C for the slower rate.

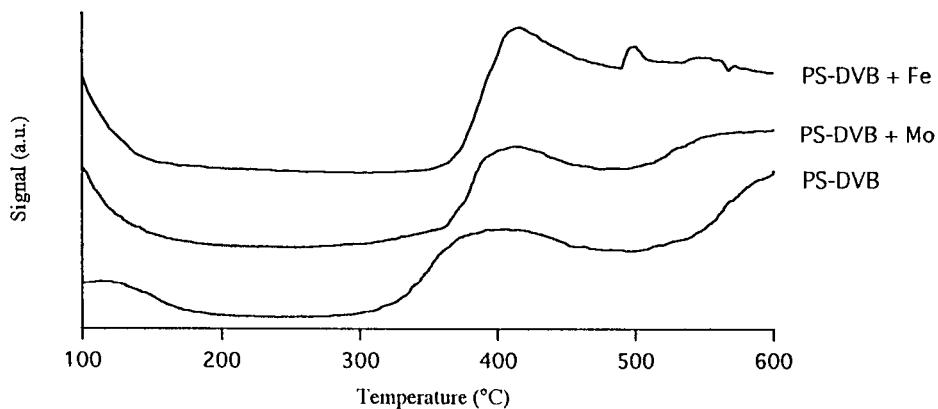


Figure 4. Hydropyrolysis-m.s. profile of toluene for PS-DVB with and without catalyst

was used (Figure 2). For the lignite, significant amounts of toluene evolved below 400°C but these were not significantly affected by catalyst addition.

3.2. Polystyrene and phenolic resites

The diphenylmethane-containing resite was chosen for investigation as benzene and toluene evolving below 500°C results exclusively from the cleavage of the methylene bridging the two phenyls [7]. Thus, the behaviour of a particular group can be studied within a macromolecular framework (in this case, the remaining phenolic resin). Catalyst addition had no significant effect on the overall conversion of the phenolic resite at the higher heating rate. Similar results were obtained from the on-line MS experiments at the slower heating rate where the benzene and toluene evolution profiles were unaffected by the catalysts. This effect is possibly attributable to (i) the stable methylene bridges in the phenolic matrix not being cleaved to temperatures well above 450°C and (ii) the catalysts not necessarily promoting keto-enol tautomerism which weakens the methylene bridges.

For PS-DVB, the catalysts gave rise to higher conversions, the highest being achieved with Mo (Figure 3, at both the faster and slower heating rates), as for the bituminous coal (Figure 1). Further, as found for coals, higher conversions were achieved with slow heating. Both GC and ¹H NMR indicated that the extent of hydrogenation, as gauged by the ratios of alkylbenzenes to the corresponding styrenes and the overall aromatic hydrogen contents, was higher for the Mo catalyst than for Fe which gave similar results to the uncatalysed test

The effect of the catalysts on the temperature of bond scission of the C₃ linkages in the PS-DVB was assessed using on-line MS. The results indicated that the addition of catalyst did not lead to the bonds between the bridging carbons breaking at lower temperatures, the primary thermal event occurring at approximately 400°C in all cases (Figure 4 shows the toluene profiles, m/z 79. Identical profiles were obtained for m/z 103 and 105). However the catalysts limited char formation by pushing the overall evolution profiles for the alkylbenzenes and styrenes to lower temperatures. In this respect, the high loading of Fe used seemed to be more effective than Mo (Figure 4).

REFERENCES

1. F. Derbyshire, *Energy & Fuels*, 3 (1989), 274.
2. C.E. Snape, C.J. Lafferty, H.P. Stephens, R.G. Dosch and E. Klavetter, *Fuel*, 70 (1991) 393.
3. C.E. Snape, C.J. Lafferty, G. Eglinton, N. Robinson and R. Collier, *Int. J. Energy Res.* 18 (1994) 233.
4. C.J. Lafferty, S.C. Mitchell, R. Garcia, C.E. Snape, *Fuel*, 72 (1993), 367.
5. M.L. Poutsma, *Energy & Fuels*, 4(2) (1990) 113 and references therein.
6. S.D. Brown, O. Sirkecioglu, K. Ismail, J. Andresen, C.E. Snape, A.C. Buchanan P.F. Britt, *Prepr. Am. Chem. Soc. Div. Fuel Chem.*, 39 (1994), 801.
7. A.M. Mastral, M.C. Mayoral, J.M. Palacios, *Energy & Fuels*, 8 (1994), 94.

Hydrogen Transfer Mechanism in the Cracking of C-C Bond in Coal Model Compounds

N. Ikenaga, T. Sakoda, T. Matsui, K. Ohno and T. Suzuki

Department of Chemical Engineering, Faculty of Engineering, Kansai University, Suita, Osaka, Japan 564

1. INTRODUCTION

In a previous paper [1], we have first elucidated quantitative hydrogen transfer processes in the cracking of benzyl phenyl ether and dibenzyl ether in tetralin with dispersed catalysts. In the reactions of above model compounds, all four hydrogen atoms in tetralin were quantitatively utilized to stabilize cracked radicals. However, in the presence of an active catalyst, hydrogen transfer from gas phase was promoted, and consequently that from tetralin decreased.

Reaction mechanisms [2, 3], the effect of a donor solvent [4, 5], and the effect of a catalyst [6, 7, 8] on the hydrocracking of diarylalkanes were discussed in detail. Yokokawa et al. reported that tetralin retarded the catalyzed hydrocracking of coal model compounds involving C-C bonds [9]. However, few studies dealt with quantitative hydrogen transfer reaction in the presence of a catalyst and a hydrogen donor solvent.

The purpose of this work is to establish quantitative hydrogen transfer processes of diarylalkane in thermolysis, hydrogenolysis and hydrogenation with a dispersed catalyst in the presence of a hydrogen donor solvent. Cracking of dinaphthylethane and diphenylethane was studied in 9,10-dihydrophenanthrene or tetralin in the presence of a highly dispersed catalyst such as $\text{Mo}(\text{CO})_6\text{-S}$, and $\text{Ru}(\text{acac})_3$.

2. EXPERIMENTAL

2.1. Materials

1,2-(1,1'-)dinaphthylethane (DNE) was synthesized according to the literature [10]. Other reagents were commercially obtained and were used without further purification.

2.2. Procedures

Cracking of DNE and DPE was carried out according to the preceding paper [1]. A stainless steel internal was used in order to reduce a dead volume of the autoclave when the cracking of DNE was carried out.

2.3. Product analysis

In order to measure the amount of hydrogen transferred, the amount of gas and the composition of the recovered gas and the liquid products were analyzed according to the methods previously reported [1].

Following definition and abbreviation are employed; $\text{H}_2\text{-G}$ (the amount of hydrogen transferred from gas phase), $\text{H}_2\text{-S}$ (the amount of hydrogen transferred from the donor solvent), $\text{H}_2\text{-R}$ (the amount of hydrogen required for stabilizing thermally decomposed radicals), $\text{H}_2\text{-A}$ (the amount of hydrogen consumed to hydrogenate aromatic rings), conversion (calculated from the difference between the amounts of model compound charged and recovered), and

decomposition (calculated from the amounts of decomposed products).

3. RESULTS AND DISCUSSION

3.1. Cracking of dinaphthylethane in dihydrophenanthrene

Effects of DHP concentration on the cracking of DNE are shown in Figures 1(a, b, c). In the absence of the catalyst, the conversion and the decomposition increased slightly with increases in the amounts of DHP and reached maxima at $\text{DHP/DNE} \approx 2$. $\text{Mo}(\text{CO})_6\text{-S}$ promoted the conversion and the decomposition of DNE to 94.4 and 41.2 %, respectively, and they decreased slightly with increasing the concentration of DHP. This indicates that Mo catalyst promoted hydrogenation of DNE, but the hydrogenation activity scarcely affected with DHP concentration. The conversion decreased from 93.8 to 38.4 % and the decomposition decreased from 58.0 to 33.0 % with increasing DHP concentration in the reaction with $\text{Ru}(\text{acac})_3$. These results indicate that an excess of DHP retarded the catalyzed hydrocracking and the hydrogenation of DNE. DNE and DHP would be competitively adsorbed on the Ru catalyst, consequently, interaction between the Ru catalyst and DNE decreased markedly due to the stronger interaction between the Ru catalyst and DHP at a higher concentration of DHP.

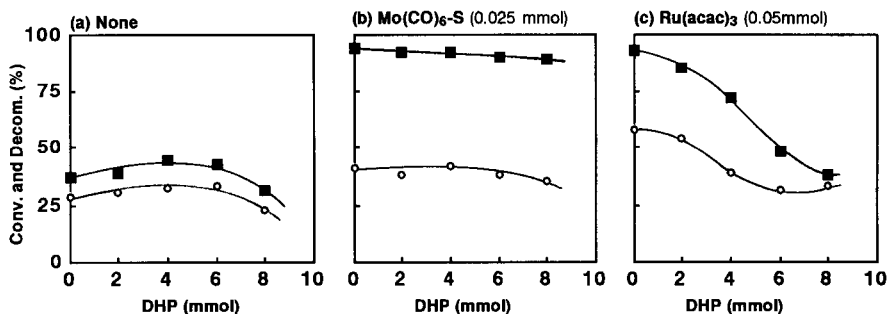


Figure 1 Effect of DHP concentration on the cracking of DNE

■ : Conversion (%) ○ : Decomposition (%)
DNE : 2.0 mmol, activated carbon : 0.5 g, $P(\text{H}_2)$ =8.0 MPa, 658 K, 60 min.

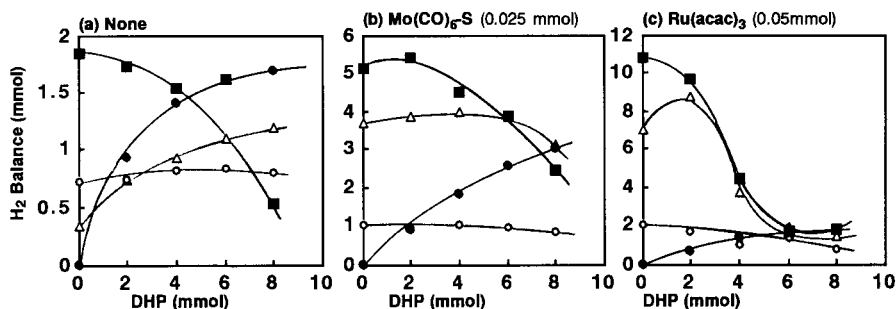


Figure 2 Effect of DHP concentration on the amount of hydrogen transferred in the cracking of DNE

■ : $\text{H}_2\text{-G}$ (mmol) ● : $\text{H}_2\text{-S}$ (mmol) ○ : $\text{H}_2\text{-R}$ (mmol) △ : $\text{H}_2\text{-A}$ (mmol)
DNE : 2.0 mmol, activated carbon : 0.5 g, $P(\text{H}_2)$ =8.0 MPa, 658 K, 60 min.

Figures 2(a, b, c) show effects of DHP concentration on the hydrogen balances (hydrogen transferred from gas phase and that from the donor solvent) in the reaction of DNE without catalyst, with $\text{Mo}(\text{CO})_6\text{-S}$, or $\text{Ru}(\text{acac})_3$. In the absence of the catalyst, $\text{H}_2\text{-S}$ and $\text{H}_2\text{-A}$ increased and $\text{H}_2\text{-G}$ decreased with increasing the concentration of DHP. $\text{H}_2\text{-R}$ remained almost constant in the entire range of the concentration of DHP. DHP contributed toward the hydrogenation of aromatic rings in the course of the cracking of DNE. In the reaction with $\text{Mo}(\text{CO})_6\text{-S}$, $\text{H}_2\text{-R}$ and $\text{H}_2\text{-A}$ remained almost constant, but $\text{H}_2\text{-G}$ decreased from 5.4 to 2.5 mmol and $\text{H}_2\text{-S}$ increased from 0 to 3.0 mmol respectively. These results indicate that the activities of the Mo catalyst for stabilizing the radicals and hydrogenating aromatic rings were not influenced by the addition of DHP. In the presence of $\text{Ru}(\text{acac})_3$, significant decreases in $\text{H}_2\text{-G}$ (from 10.9 to 1.8 mmol) and $\text{H}_2\text{-A}$ (from 7.1 to 1.5 mmol) were observed, indicating that Ru catalyst interacts with DHP more strongly than Mo catalyst.

3.2. Cracking of diphenylethane in tetralin

Effects of TL concentration on the cracking of DPE are shown in Figures 3(a, b, c). The conversion and the decomposition of DPE were almost constant even with increasing TL concentration in the reaction without catalyst, and the highest values were obtained in the

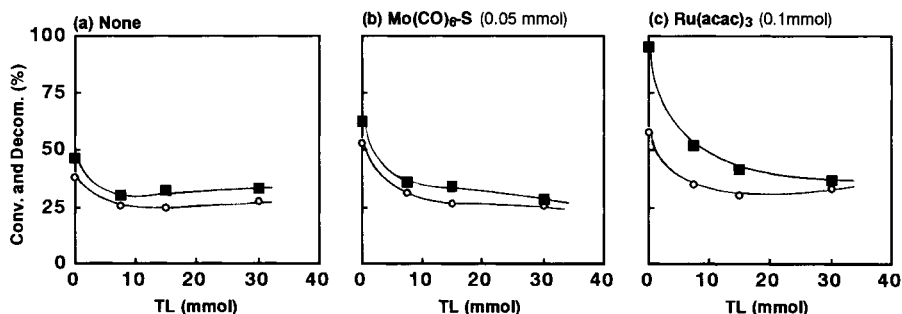


Figure 3 Effect of TL concentration on the cracking of DPE

■ : Conversion (%) ○ : Decomposition (%)
 DPE : 19.5 mmol, activated carbon : 0.5 g, $P(\text{H}_2)=8.0$ MPa, 698 K, 60 min.

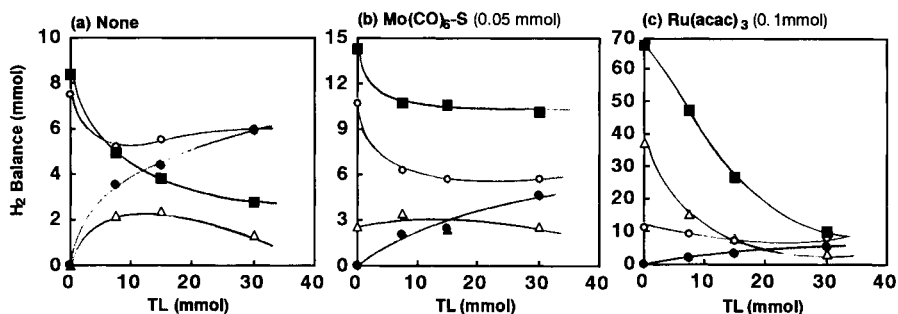


Figure 4 Effect of TL concentration on the amount of hydrogen transferred in the cracking of DPE

■ : $\text{H}_2\text{-G}$ (mmol) ● : $\text{H}_2\text{-S}$ (mmol) ○ : $\text{H}_2\text{-R}$ (mmol) △ : $\text{H}_2\text{-A}$ (mmol)
 DPE : 19.5 mmol, activated carbon : 0.5 g, $P(\text{H}_2)=8.0$ MPa, 698 K, 60 min.

reaction without TL (conversion : 46.6 %, decomposition : 37.5 %). In the reactions with $\text{Mo}(\text{CO})_6\text{-S}$, the conversion and the decomposition of DPE decreased from 57.2 to 36.3 %, from 47.0 to 30.3 %, respectively when 7.5 mmol of TL was added, and they decreased slightly with further increases in the amount of TL. In the presence of $\text{Ru}(\text{acac})_3$, similar tendencies as above were observed. These results clearly show that even a small amount of TL retarded the catalyzed cracking of DPE with Mo and Ru catalyst because of competitive adsorption of TL and DPE on the catalyst surface.

Figures 4(a, b, c) show effects of TL concentration on the hydrogen balances in the reaction of DPE without and with $\text{Mo}(\text{CO})_6\text{-S}$ or $\text{Ru}(\text{acac})_3$. In the reaction without catalyst, $\text{H}_2\text{-G}$ decreased from 8.4 to 2.7 mmol and $\text{H}_2\text{-S}$ increased from 0 to 5.91 mmol with increasing TL concentration. $\text{H}_2\text{-R}$ decreased from 7.5 to 5.5 mmol with the addition of 7.5 mmol of TL and it leveled off with further increase in the amount of TL. In $\text{Mo}(\text{CO})_6\text{-S}$ catalyzed runs, $\text{H}_2\text{-G}$ and $\text{H}_2\text{-R}$ decreased from 14.3 to 10.7 mmol, from 10.7 to 6.3 mmol respectively with the addition of 7.5 mmol of TL and no significant changes were observed with further increases in the TL. $\text{H}_2\text{-S}$ linearly increased from 0 to 4.5 mmol and $\text{H}_2\text{-A}$ remained almost constant with increasing the amount of TL. In the reactions with $\text{Ru}(\text{acac})_3$, considerable decreases in $\text{H}_2\text{-G}$ and $\text{H}_2\text{-A}$ were observed with increasing TL concentration. $\text{H}_2\text{-G}$ decreased from 67.4 to 1.5 mmol and $\text{H}_2\text{-A}$ decreased from 37.3 to 3.3 mmol. Therefore, TL mainly retarded the stabilization of thermally decomposed radicals in the presence of Mo catalyst and the hydrogenation of aromatic rings in the presence of Ru catalyst because DPE and TL competitively interact with the catalyst in the presence of TL.

4. CONCLUSION

In the cracking of dinaphthylethane and diphenylethane, the amount of hydrogen required for stabilizing free radicals and hydrogenating aromatic rings were predominantly supplied from gas phase in the absence of the hydrogen donor solvent. In the reactions with the hydrogen donor solvent, however, the amount of hydrogen transferred from gas phase considerably decreased and the conversion and the decomposition of DNE and DPE lowered even with the active catalyst such as dispersed Mo or Ru. The hydrogen donor solvent retarded the catalyzed cracking of DNE and DPE (specially with $\text{Ru}(\text{acac})_3$) because of competitive adsorption of the model compound and the hydrogen donor solvent on the catalyst surface. Such behaviours are much different from the results in the cracking of benzyl phenyl ether and dibenzyl ether with $\text{Mo}(\text{CO})_6\text{-S}$ and $\text{Ru}(\text{acac})_3$.

REFERENCES

1. Ikenaga, N., Kobayashi, Y., Saeki, S., Sakota, T., Watanabe, Y. and Suzuki, T., *Energy Fuels* **1994**, *8*, 947-952.
2. Penn, H. J. and Wang, J.-H., *Energy Fuels* **1994**, *8*, 421-425.
3. Shi, B., Ji, Y., Guthrie, R.D. and Davis, B.H. *Energy Fuels* **1994**, *8*, 1268-1275
4. McMillen, D.F., Malhotra, R., Chang, S.-J., Ogier, W.C., Nigenda, S.E. and Fleming, R.H. *Fuel* **1987**, *66*, 1611-1620
5. Futamura, S., Koyanagi, S. and Kamiya, Y., *Fuel* **1988**, *67*, 1436-1440.
6. Ouchi, K. and Makabe, M., *Fuel* **1988**, *67*, 1536-1541
7. Wei, X.-Y., Ogata, E., Zong, Z.-M. and Niki, E., *Fuel* **1993**, *72*, 1547-1552.
8. Farcasiu, M., Eldredge, A. P. and Petrosius, C. S., *Energy Fuels* **1994**, *8*, 53-55.
9. Yokokawa, C., Ikenaga, N., Fukumi, J. and Oda, H. *Proc. Int. Conf. Coal Sci.* **1989**, 911-914
10. Copeland, P. G, Dean, R. E. and McNeil, D., *Org. Chem.* **1961**, 1236.

THERMAL CRAKING OF COAL STRONG BONDS ON DIARYL ETHERS' AND DIARYLMETHANES' MODELS

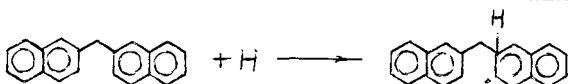
E.N. Grigorieva, T.L. Fedorova, D.N. Kagan, V.Yu. Korobkov, S.S. Panchenko, I.V. Kalechitz

Institute for High Temperatures, Russian Academy of Sciences, Izhorskaya St., 13/19, Moscow 127412, Russia (Coal organic matter, model substances)

INTRODUCTION

The monomethylene and oxygen links are widespread in coals but their cleavage is studied insufficiently because of high inertness. Rather numerous diarylmethanes were investigated by Futamura and coworkers [1].

All of diarylmethanes pyrolysed with energies activation less than energies of their bond dissociation formerly in [1 - 3] initiated by radicals which attack ipso-position and convert the bond $C_{ar}-C_{alk}$ into a weaker bond $C_{alk}-C_{alk'}$ for example



Recently in our group it has been shown [4], that the most of diarylmethanes submit dependence $\log k = f(\sum \Delta_t)$, but some of them strongly deviate from it.

In [5] a wide interval of diaryl ethers has been shown. They undergo the same destruction mechanism as diarylmethanes.

The purpose of this paper is to compare the conformities of diarylmethanes and diaryl ethers thermolysis.

EXPERIMENTAL

We have studied the thermolysis of 7 diarylmethanes namely diphenylmethane (DPM), 1,1'-, 1,2'- and 2,2'-dinaphthylmethanes (DNM) 1- and 2-benzyl-naphthalenes (BN) and 9-benzylanthracene (9-BA) and diphenyl ether (DPE). The data for other diaryl ethers namely phenyl 2-naphthyl ether (2-PNE), 2,2'-dinaphthyl ether (2,2'-DNE), phenyl 1-naphthyl ether (1-PNE), 1,2'-dinaphthyl ether (1,2'-DNE), 2-naphthyl 9-phenantryl ether (NPE) and phenyl 9-anthryl ether (9-BAE), were taken from paper Kamia et al. [5].

Thermolysis was carried out in a 20 cm³ steel rotary autoclave loaded with 1 g DAM or DPE, excess of tetralin (10 g). Hy-

drogen pressure was about 12 MPa. The temperature was used with in rather great interval 300-510°C. Products were analyzed by gas chromatography and gas chromatography-mass spectrometry.

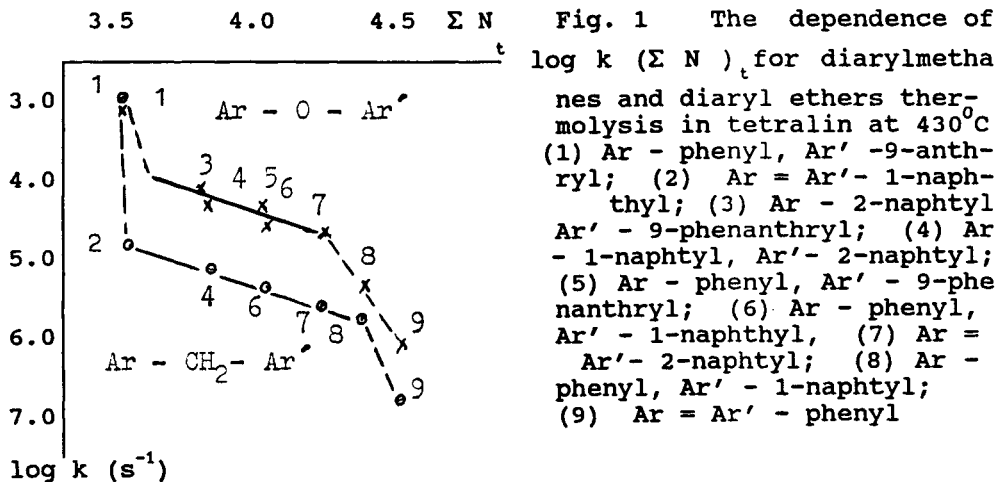
RESULTS AND DISCUSSION

The reactivity order of diarylmethanes has been as follows: DPM << 2-BN < 2,2'-DNM < 1-BN < 1,2'-DNM < 1,1'-DNM << 9-BA. The difference between the most reactive and the most inert compound is as much as 2000 times. The activation energies vary from 133 to 288.9 kJ/mol.

All diaryl ethers had more reactivity than analogous diarylmethanes. The order of reactivity has been analogous: DPE < PNE < 2,2'-DNE < 1-PNE < 1,2'-DNE < NPE << 9-BAE

In all experiments the relative concentrations of diarylmethanes satisfactorily fitted the straight line in semi-logarithmic coordinates. Rate constants were calculated assuming the reactions to be first order. Hence, their rate constants could be calculated from the dependence for pseudo-monomolecular reactions.

All data are summarized in Fig. 1. It has been established

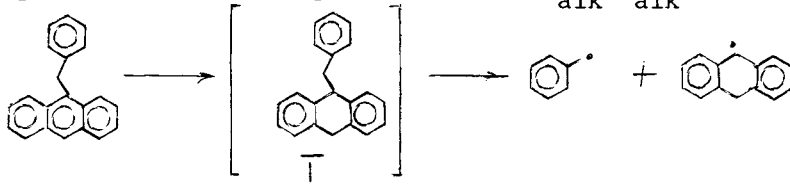


broken lines for correlations between the logarithms of the thermolysis rate constants diaryl ethers and diarylmethanes and parameters characterizing the chemical structure like reactivity indices of carbon atoms of aryl fragments with methylene or oxygen group (N_t). It shows three different mechanisms of diaryl ethers and diarylmethanes thermolysis.

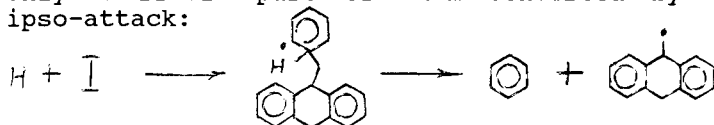
The most of them submit the linear correlation $\log k = f(\Sigma N_t)$ corresponding with mechanism of ipso-attack as limiting stage of all process. In fact this group of substances

gave arenas and according phenols as the main products of destruction (as it indicate in equation 1). It is necessary to notice that these lines are strongly parallel. Therefore, one can do three conclusions. The mechanism of ipso-attack is a limiting stage of the whole process in the large interval 3.5 - 4.5 units of N_t . Than, our and Kamiya data are correct because the line angle is a function of the reactivity of hydrogen-donor solvent, namely tetralin, and, at last, the correlations have common character.

9-BA and 9-BAE had nearly equal reactivity at 430°C ($k = 63.7 \times 10^{-5} \text{ s}^{-1}$ and $58 \times 10^{-5} \text{ s}^{-1}$ accordingly). The main products of 9-BA thermolysis are benzene, toluene, anthracene, 9,10-dihydroanthracene and 1,2,3,4-tetrahydroanthracene [4]. It should be notice that 9-BA thermolysis proceeded at low temperatures, when tetralin was itself stable: it stabilized .radicals converting into naphthalene only. According destructions of 9-BA and 9-BAE are similar and representative homolysis of bond $C_{\text{alk}}-C_{\text{alk}}$:



Only a little part of them converted by the scheme of ipso-attack:



DPM did not give the products of ipso-attack too. In tetralin it converted into fluoren only, giving H-atoms to tetralin. The latter underwent to ipso-attack and destructed more rapidly then pure tetralin itself. Pure DPM gave fluoren and destruction products benzene and toluene. Observed activation energy was equal to $289.1 \pm 34 \text{ kJ/mol}$, i.e. value vary close to $277.4 \pm 25.6 \text{ kJ/mol}$ observed during thermolysis of pure DPM. Hence limiting stage is cyclization and not ipso-attack.

DPE underwent ipso-attack partly and cyclization mainly.

CONCLUSIONS

Diarylmethanes and diaryl ethers have the same thermolysis dependencies.

The most of them undergo ipso-attack by H-atom of the solvent and destruct into smaller moleculaoos. Very little part of them have so strong reactivity that their hydrogenates destruct by homolysis. Both processes are useful for

liquefaction of coals.

The most inactive substances are H-donors to the solvent - tetralin. They undergo cyclization and destruct solvent. And this process is vary bad for liquefaction of coal.

These correlations can be employed to predict the reactivity of more complex systems encountered in coal.

REFERENCES

1. S. Futamura, S. Koyanagi and Y.Kamija. Proceedings of Intern. Conf. on Coal Science, October 23-27 (1989), Japan, Tokyo
2. D.F. McMillen, R. Malhotra, G.P.Hum and S.-J. Chang, Energy Fuels,1 (1987) 193
3. D.F. McMillen, R. Malhotra, S.-J. Chang, W.C. Ogier, S.E. Nigenda and R.H.Fleming, Fuel, 66 (1987) 1611
4. E.N. Grigorieva, S.S.Panchenko, V.Yu.Korobkov and I.V. Kalechitz, Fuel Process. Technol., 41 (1994) 39
5. Y.Kamija, E.Ogata, K.Goto and T.Nomi, Fuel, 65 (1986) 536

Hydrogen Shuttling Pathways in Thermal Hydroliquefaction: Solvent-Induced Scission of Coal Model Compound Structures.

T. Autrey, T. Powers, E.A. Alborn, D. M. Camaioni and J. A. Franz
Pacific Northwest Laboratory, P.O. Box 999, Richland, WA 99352 USA

1. INTRODUCTION. It has been demonstrated that donor solvents play a key role in the scission of "thermal stable" bonds in coal model compounds and therefore it has been speculated that they will improve liquefaction efficiencies.[1-8] We have been studying the transfer of hydrogen from dihydroarene donor solvents to arene model compounds to quantify the barriers of competing hydrogen transfer mechanisms.[9-16] Hydrogen can be transferred between arene rings by a variety of pathways. The specific hydrogen transfer pathway or pathways can be predicted given an understanding of the thermochemistry of the reactants intermediates and products. The individual pathways that contribute to strong bond scission have been shown to be dependent on the dihydroarene donor and the arene acceptor.

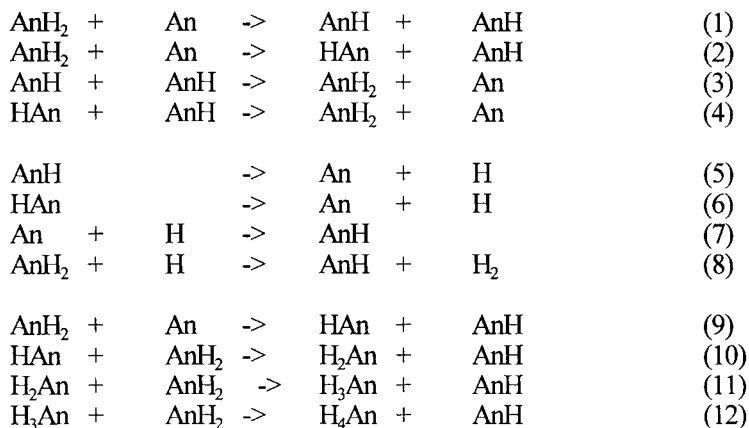
In this paper we quantify the hydrogen pathways between the solvent components anthracene and phenanthrene. In addition, we describe reaction conditions requiring consideration of an additional hydrogen transfer pathway: a multi-step nonipso hydrogen transfer to coal model compounds to evaluate the hydrogen transfer steps to cleave strong diarylmethane bonds in coal structures.

2. EXPERIMENTAL. Anthracene was sublimed, dihydroanthracene and phenanthrene recrystallized from ethanol, and dihydrophenanthrene recrystallized from methanol. Thermolysis experiments of mixtures containing arene and dihydroarene were prepared in Pyrex tubes degassed and sealed under vacuum. Stock mixtures of different ratios of arene/dihydroarene were prepared in bulk by grinding the pure compounds together with a roller ball mixer. A fluidized sand bath was used in the thermolysis studies. A Hewlett Packard 5890 GC equipped with an FID and/or a mass detector (HP 5971) and a J&W DB17, 15 or 30m capillary column was used for product analysis. An internal standard was added for quantitative analysis. 9,10-Dihydroanthracene- d_4 was prepared by the catalytic exchange with DMSO- d_6 and sodium hydride and the reaction mixture was heated to 70 °C for 3 h. After cooling to room temperature, the mixture was quenched with D₂O, then ammonium chloride, extracted with diethyl ether, and dried over sodium carbonate. The process was repeated three times, recrystallized from methanol to yield > 99 % (d4) isomer. ¹H-NMR and ²H-NMR were recorded on a Varian VXR 300 spectrometer. 9,10-dihydroanthracene- d_{12} was prepared by reduction of anthracene- d_{10} , sodium in EtOD. Acuchem [17] uses a variable step integrator to solve stiff integration problems. Temperature-dependent molar densities of anthracene were obtain from the American Petroleum Institute Reference Guide available through Chemical Abstracts online service in the file DIPPR.

3. RESULTS & DISCUSSION.

3.1 Hydrogen transfer between AnH₂ and An. Addition of arenes to hydrogen donor solvents may have beneficial effects: (1) lowers the barrier, required energy, for initiation events to generate hydrogen atom carriers and precursors, and (2) serves as a trap for hydrogen atoms, thus minimizing formation of hydrogen gas. We examined in detail the transfer of hydrogen from AnH₂ to An to quantify the barriers for hydrogen transfer with the solvent component, and then examined the hydrogen transfer to a coal model compound, 1,2'-dinaphthylmethane (1,2'-DNM). Utilizing mechanistic kinetic modeling and thermal product studies, we developed a scheme that quantitatively determines the important hydrogen transfer pathways between dihydroanthracene and anthracene. As shown in Scheme I, twelve reaction pathways are sufficient

Scheme I. Hydrogen Transfer Pathways in An/AnH₂



to describe the time-dependent, experimentally determined products in the thermolysis reaction between the temperatures of 350 to 425 °C. The transfer of a hydrogen atom to the 9- or 10- position of anthracene (eq 1) dominates the hydrogen transfer pathways. This thermoneutral hydrogen transfer pathway yields no new observable products unless a label is used. A competing hydrogen transfer pathway, hydrogen transfer to the 1-position of anthracene (eq 2), however, yields an adduct that will lead to reduced anthracene with an efficiency that strongly depends on the reaction conditions. At high donor concentrations, the adduct is reduced to yield 1,2-dihydroanthracene (eq 10) in competition with hydrogen atom scission (eq 6). Subsequent disproportionation (eq 11) and reduction (eq 12) leads to the formation of 1,2,3,4-tetrahydroanthracene. Little hydrogen gas is formed even at high donor concentrations (eq 8).

3.2. Hydrogen Transfer between Phenanthrene and dihydrophenanthrene. On the other hand, an examination of a solvent mixture composed of phenanthrene and 9,10-dihydrophenanthrene showed little transfer of hydrogen to the external rings (1,2,3 or 4-positions of phenanthrene). This is likely due to (1) the slower rate of formation and (2) the lower relative stability of the 1-hydrophenanthryl radical adduct, and (3) the slower rate of hydrogen donation by the 9,10-dihydrophenanthrene.

3.3 Hydrogen Transfer to 1,2'-Dinaphthylmethane (1,2'-DNM). A model compound 1,2-DNM was used to examine the hydrogen transfer pathways responsible for the solvent-engendered bond scission of diarylmethanes. Hydrogen transfer to the ipso position of the 1-substituted ring yields 2-methylnaphthalene and naphthalene, while hydrogen transfer to the ipso position of the 2-substituted ring yields 1-methylnaphthalene and naphthalene. Because the radical adduct formed by addition of a hydrogen atom to the 1-position of naphthalene is ca. 3 kcal/mol more stable than the adduct formed by addition to the 2-position, the ratio of 2-methylnaphthalene/1-methylnaphthalene has been used to probe the mechanism of hydrogen transfer. Two different competing hydrogen transfer pathways have been proposed to explain the selectivity differences in bond scission as a function of donor concentration. However, we believe a third pathway must be considered to explain the selectivity at high donor concentrations. Analogous to the above observations for the formation of tetrahydroanthracene, the adduct formed by hydrogen transfer to a nonipso position of 1,2'-DNM, specifically the 1-position of the 2-substituted ring, can be trapped at high donor concentrations to yield a thermally labile adduct that yields 1-methylnaphthalene. Further support for these suggestions comes from deuterium labeling studies. Thermolysis of 9,10-dihydroanthracene- d_4 in anthracene at 400 °C for 60 minutes yields extensive scrambling of the deuterium label into the anthracene 1,2, 9, and 10-positions. The amount of deuterium incorporated into the naphthalene formed in the thermolysis of 1,2'-DNM in a perdeuterated mixture of 9,10-dihydroanthracene- d_{12} and anthracene- d_{10} is dependent on the ratio of arene to dihydroarene. At high arene concentrations we detect ca. 1 deuterium per naphthalene, presumably through an ipso displacement. At high dihydroarene concentrations we detect ca. > 1.5 deuterium incorporated per naphthalene. This suggests that multiple hydrogen transfers occur between the substrate and the solvent and that at higher donor concentrations, nonipso reduction pathways may become important.

Hydrogen transfer from 9,10-dihydrophenanthrene to 1,2'-DNM results in both a lower observed selectivity and observed rate of bond scission. As discussed above, this the lower rate is due in part to the increase in the activation barrier for hydrogen transfer. However, this is partially compensated for by the operation of a free radical hydrogen atom chain pathway.

4. CONCLUSIONS. Hydrogen from donor solvent is transferred several times between other donor solvent components and coal model compounds before engendering bond scission by an ipso displacement mechanism. At sufficient donor concentrations, nonipso hydrogen addition yields bond scission. Addition of an anthracene to donor solvent mixtures will help minimize the formation of H_2 gas due to the competing addition reaction. The anthracene-solvent radical adduct becomes a less reactive hydrogenating agent than free hydrogen atoms. It can either (1) be reduced in a subsequent disproportionation step to regenerate a donor or (2) act as a shuttler of hydrogen atoms.

Although dihydrophenanthrene is less selective and slower to promote bond scission than dihydroanthracene in the model compound 1,2'-DNM, it is in general a better coal liquefaction solvent. This may be due in part to some physical solvency properties, but thermodynamic arguments suggest that a free radical chain pathway generating hydrogen atoms may compensate for the higher initial activation barrier initiating the hydrogen transfer pathways. In addition, while 9,10-dihydroanthracene, a good donor for capping thermally generated free radicals, yields anthracene as a product, and anthracene is a very good hydrogen atom acceptor and will compete with coal substrates for hydrogen in the liquefaction process.

5. ACKNOWLEDGMENT. This work was supported by the U.S. Department of Energy, Office of Basic Energy Research, Chemical Sciences Division, Process and Techniques Branch. The work was conducted at Pacific Northwest Laboratory, which is operated for the U. S. Department of Energy under Contract DE-ACO6-76RL0 1830. We thank the Chemical Kinetics Data Center at NIST for providing the modeling program, Acuchem. Support for EAA and TRP was provided through AWU-NW under grant DE-FG06-89ER-75522 with the U.S. Department of Energy.

6. GLOSSARY OF ACRONYMS.

Phen	phenanthrene
PhenH ₂	9,10-dihydrophenanthrene
An	anthracene
AnH ₂	9,10-dihydroanthracene
AnH	9-hydroanthryl
HAn	1-hydroanthryl
H ₂ An	1,2-dihydroanthracene
H ₃ An	1,2,3-trihydro-4-anthryl
H ₄ An	1,2,3,4-tetrahydroanthracene
1,2'-DNM	1,2'-dinaphthylmethane

7. REFERENCES AND NOTES.

1. McMillen, D. F.; Malhotra, R.; Chang, S.-J.; Fleming, R. H.; Ogier, W. C.; Nigenda, S. E. *Fuel* **1987**, *66*, 1611.
2. McMillen, D. F.; Malhotra, R. *Fuel Preprints*, **1985**, *30* (4), 297.
3. McMillen, D. F.; Malhotra, R.; Hum, G. P.; Chang, S.-J. *Energy Fuels* **1987**, *1*, 193.
4. Malhotra, R.; McMillen, D. F. *Energy Fuels* **1990**, *4*, 184.
5. McMillen, D. F.; Malhotra, R.; Tse, D. S. *Energy Fuels* **1991**, *5*, 179.
6. Malhotra, R.; McMillen, D. F. *Energy Fuels* **1993**, *7*, 227.
7. Stein, S. E. *Acc. Chem. Res.* **1991**, *24*, 350.
8. Smith, C. M. and Savage, P. E. *Energy Fuels* **1992**, *6*, 195.
9. Franz, J. A.; Ferris, K. F.; Camaioni, D. M.; Autrey, S. T. *Energy Fuels* **1994**, *8*, 1016.
10. Camaioni, D. M.; Autrey, S. T.; Franz, J. A., *J. Phys. Chem.*, **1993**, *97*, 5791.
11. Autrey, S. T.; Camaioni, D. M.; Ferris, K.; Franz, J. A. *Coal Science Proceedings, International Conference on Coal Science*, **1993**, 336.
12. Autrey, T.; Franz, J. A.; Camaioni, D. M.; Ferris, K.; Gleicher, G. J. *Coal Science Proceedings, International Conference on Coal Science*, **1991**, 239.
13. Autrey, T.; Gleicher, G. J.; Camaioni, D. M.; Franz, J. A. *Am Chem Soc, Div Fuel Chem. Preprints*, **1991**, (36) 2, 521.
14. Autrey, T.; Franz, J. A. *Am Chem Soc, Div Fuel Chem. Preprints*, **1990**, (35)2, 381.
15. Autrey, T.; Albom, E. A.; Franz, J. A. and Camaioni, D. M. *Energy Fuels* **1995**, *9*, xxxx.
16. Franz, J. A., Camaioni, D. M.; Alnajjar, M. S.; Autrey, T.; Linehan, J. C. *Am Chem Soc, Div Fuel Chem. Preprints*, **1995**, (40)2, 203.
17. Braun, B.; Herron, J. T.; Kahaner, D. K. *Int. J. Chem. Kin.* **1988**, *20*, 51.

Molecular Mass Distributions of Coal Products Relevant to Pyrolysis, Liquefaction and Combustion

K.D. Bartle^a, A.A. Herod^b, P. John^c, B.R. Johnson^a, C.A.F. Johnson^c,
R. Kandiyoti^b, J.E. Parker^c and G.P. Smith^c

^a School of Chemistry, University of Leeds, Leeds LS2 9JT, United Kingdom

^b Department of Chemical Engineering, Imperial College, University of London, London SW7 2BY, United Kingdom

^c Department of Chemistry, Heriot-Watt University, Edinburgh EH14 4AS, United Kingdom

1. INTRODUCTION

The two techniques most commonly employed to determine the molecular mass distributions (MMDs) of products derived from coal are mass spectroscopy (MS) and size exclusion chromatography (SEC). These procedures have traditionally yielded conflicting information, thought to be due not least to the unsuitability of the typically employed calibration of SEC with polystyrene standards. The recent advent of laser MS techniques has suggested the MMD of coal derivatives extends beyond 10,000 daltons. In this paper chromatograms and MMDs from SEC, using the traditionally employed tetrahydrofuran (THF) solvent, are compared to those obtained using a new mobile phase N-methyl-2-pyrrolidinone (NMP) and to mass spectra from laser induced mass analysis (LIMA).

2. EXPERIMENTAL

2.1 SAMPLES The principle coal product used in these investigations was a high temperature, soft coal tar pitch, with observations confirmed through similar experiments on a Point of Ayr Pilot Plant extract of Point of Ayr coal, and a synthetic naphthalene pitch. Solutions, of concentration 1-10 mg/ml, for SEC examination were prepared by sonication of the sample in the appropriate solvent.

2.2 SEC IN THF Two Jordi-Gel (styrene-divinylbenzene packing) SEC columns (10 μ m, 500 + 100A^o, Alltech Associates Inc.) with guard column, were operated at room temperature with a THF flow rate of 1.0 ml/min. Detection was through fixed wavelength uv absorption (254 or 280nm, ACS 750-11) and evaporative light scattering detection (Varex IIa, ELSD).

2.3 SEC IN NMP A single PL gel (divinylbenzene packing) SEC column (3 μ m, Mixed E Bed, Polymer Labs Ltd) with guard column was connected in series to a variable wavelength uv absorption detector (260-700nm, Jasco 875-UV) and a uv/vis fluorescence detector (300-750nm, Shimadzu RF-530). The columns were maintained at a temperature of 80^oC, with an NMP flow rate of 0.5 ml/min.

Both SEC apparatus were calibrated using narrow polystyrene standards, with sample volumes of 20 μ l injected on to the columns.

2.4 LIMA Mass spectra were collected using a LIMA 401L time-of-flight mass spectrometer (Cambridge Mass Spectrometry) with a Nd-YAG laser operating at 266nm and sample preparation as previously described¹.

3. RESULTS AND DISCUSSION

The THF-SEC chromatograms, from both uv absorption and ELSD, of the THF soluble portion of the soft pitch are shown in Figure 1. This also indicates the region over which the calibrants elute (410,000 - 92). The two uv wavelengths employed give very similar profiles, and the ELSD shows material eluting over the same time range, but gives a different profile, and therefore more information, at the shorter elution times. The most obvious feature of this figure is that the pitch sample elutes over a much greater time range than do the calibrants, and that the majority of the pitch sample elutes after the smallest calibrant.

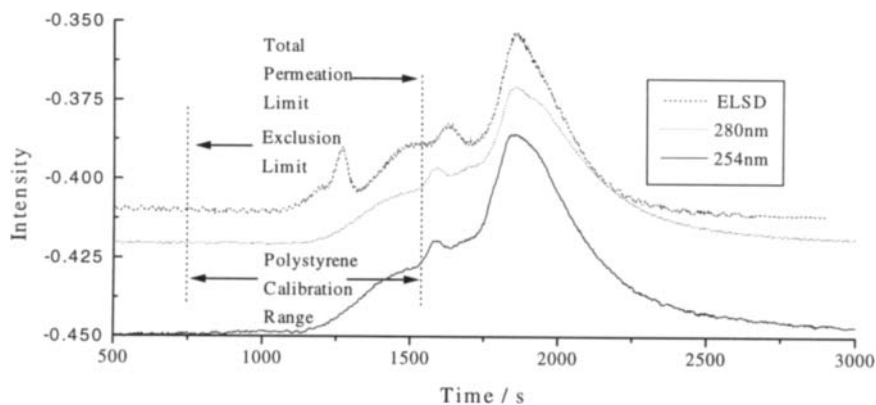


Figure 1 Chromatograms of soft pitch with THF mobile phase.

Obviously this 'late' material is not of very small mass, but is interacting with the column packing material, and so the separation occurring is through both adsorption and size exclusion mechanisms. This phenomena is well documented^{2,3} and means that a MMD cannot be assigned to the sample. Indeed one would not be confident in assigning an upper mass limit to the sample on the basis of this chromatogram.

A similar experiment has been performed on the NMP-SEC apparatus with detection at 280nm and Figure 2 shows the chromatogram for the NMP soluble portion of the soft pitch. The polystyrene calibration for this apparatus gave an exclusion limit at ~ 550s and a total permeation limit (peak of toluene elution) at ~ 1365s. The chromatogram shows two unresolved maxima. The first is at the exclusion limit indicating large molecular material, with the second within the columns resolving range. The important feature to note here is that there is no material eluting after the total permeation limit. This observation is repeated in the fluorescence detected chromatogram. Figure 2 also contains the chromatogram of the THF

soluble fraction of the soft pitch. Again there are two maxima, one at the exclusion limit and one within the columns resolving range but in this case these two peaks are baseline resolved.

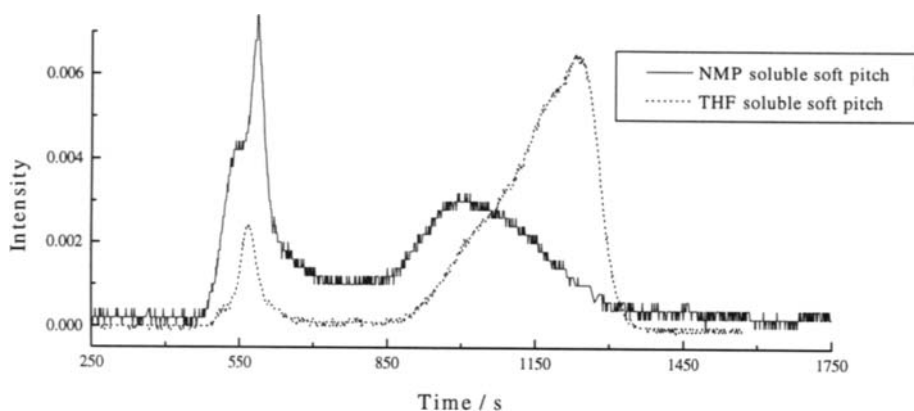


Figure 2 Chromatograms of soft pitch with NMP mobile phase.

Sample solubility tests reveal that NMP dissolves more of the coal derived material, and that all of the THF soluble material is also NMP soluble. Figure 3 shows the polystyrene equivalent MMDs derived from these two chromatograms, which indicate that NMP has solubilised material with masses greater than THF and up to the exclusion limit of the apparatus ($\sim 30,000$ polystyrene equivalent mass units, p.e.m.u.).

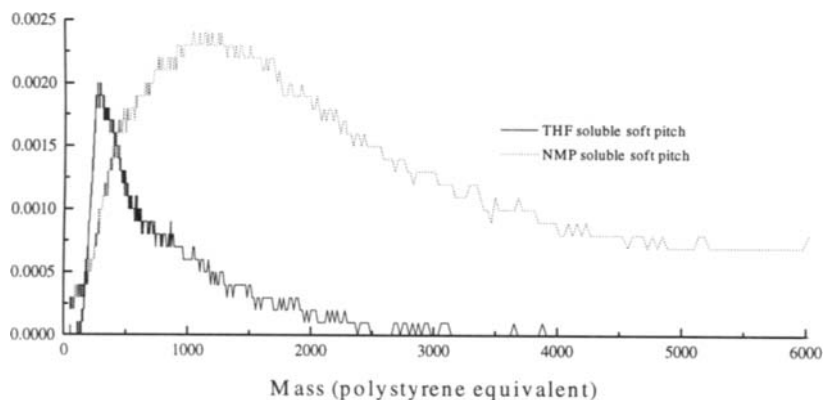


Figure 3 Molecular Mass Distributions of NMP and THF soluble fractions of soft pitch.

The mass spectrum produced from the LIMA instrument is presented in Figure 4. This indicates material up to the present high mass limit of the machine, 10,000amu. There are two main regions of intensity; 200 - 800amu and 1400 - 4500 amu., with the density and intensity of mass peaks decreasing thereafter on increases in mass. However, the weight of material of masses above 5000amu is still a significant part of the sample.

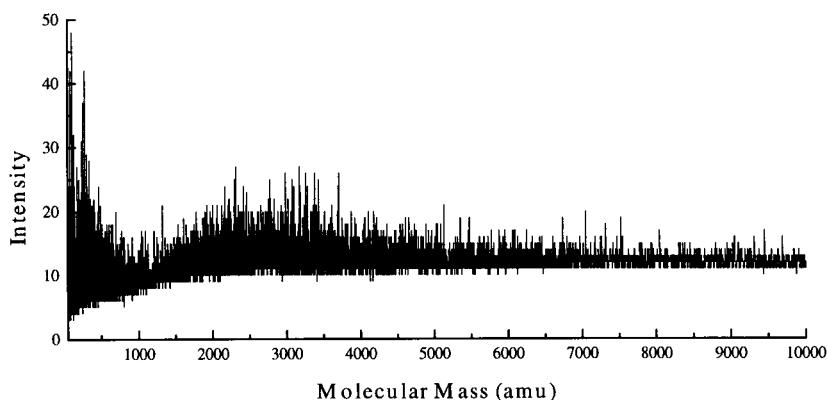


Figure 4 LIMA mass spectrum of whole soft pitch

When the NMP-SEC derived MMDs of Figure 2 and this mass spectrum are compared there are common features. The NMP soluble material MMD has greatest concentration up to ~ 4000 p.e.m.u., the LIMA spectrum up to 4500 amu. In addition, not shown here is the LIMA spectrum of the THF insoluble part of the soft pitch, in which there is an almost total absence of material in the 200 - 800 amu. This correlates well with the THF soluble MMD of Figure 2. Further experiments with narrow retention volume defined fractions produced by preparative scale THF-SEC have shown that the MMDs from their NMP-SEC agree well with their LIMA mass spectra for the latest eluting, lower mass, fractions, but less so for earlier eluting fraction.

4. CONCLUSIONS

From the results reported here it is clear that NMP surpasses THF as a mobile phase for coal derived materials. It offers the opportunity to analyse more of the sample, and has shown no adsorption effects⁴. Polystyrene calibration for these materials remains a source of error particularly for higher mass materials. The combination of NMP-SEC and mass analysis by LIMA, and other new MS techniques, provides a possible route to the manufacture of relevant coal calibrants and more accurate MMDs.

5. ACKNOWLEDGEMENTS

We would like to thank the EPSRC and ETSU for funding this work, and Dr Sam Moore of the Point of Ayr Liquefaction Plant, CTDD, for supplying the PoA coal extract.

REFERENCES

1. P. John, C. A. F. Johnson, J. E. Parker, G. P. Smith, A. A. Herod, A. F. Gaines, C.-Z. Li & R. Kandiyoti, *Rapid Communications in Mass Spectrometry*, 5 (1991) 364.
2. K. D. Bartle, M. J. Mulligan, N. Taylor, T. G. M. & C. E. Snape, *Fuel* 63 (1984) 1556.
3. A. L. Lafleur & M. J. Wornat, *Analytical Chemistry*, 60 (1988) 1096.
4. A. L. Lafleur & Y. Nakagawa, *Fuel* 68 (1989) 741.

Structural Comparison of Coal Liquefaction Extracts and Hydrocracking Products

S-F. Zhang, B. Xu, A.A. Herod and R. Kandiyoti
Department of Chemical Engineering, Imperial College, University of London,
London SW7 2BY, UK

1. INTRODUCTION

The accurate assessment of hydrocracking reactivities of coal liquefaction products requires a clean separation between the coal dissolution step and the subsequent reactions of solubilised extracts. When the liquefaction step is carried out in batch reactors (e.g. bomb reactors), it is not possible to remove solubilised products from the reaction zone until the end of the experiment; some degree of overlap between the liquefaction and hydrocracking steps then becomes inevitable. This paper describes the reactivities of coal extracts prepared in a flowing solvent reactor, where products released from coal are continuously removed from the reaction zone by a flow of solvent, allowing suppression of their extraparticle secondary reactions.

2. EXPERIMENTAL

Coal extracts were prepared from the set of Argonne PCS¹ and Point of Ayr (UK) coal (Table 1) in a flowing solvent-reactor (FSR)², by heating in a stream of tetralin at 5 K s⁻¹ to 450 °C and holding for 400 s. Product mixtures were vacuum distilled, to remove excess tetralin, and extracted in pentane (20:1 v/v pentane to conc. coal extract), removing residual tetralin and its thermal reaction products. Due to suppression of extraparticle reactions in the FSR, only insignificant amounts of the coal derived materials are normally found to be pentane soluble³. Pentane insoluble (PI) fractions were hydrocracked in a micro-bomb reactor (3 ml) at 440 °C and 190 bar H₂ (30 and 60 min). The charge consisted of approx. 75 mg PI coal extract, 25 mg presulphided NiMo/Al₂O₃ and 1,000 mg distilled tetralin. Conversions, defined as the change in the > 450 °C (b.p.) material content, were determined by a TGA based method: TGA evolution temperatures of pure standards were calibrated against true boiling points. Coal extracts were characterised by planar chromatography (PC) and matrix assisted laser desorption ionisation (MALDI) MS. Size exclusion chromatography (SEC) and UV-fluorescence spectroscopy (UV-F) were used to evaluate differences between the extracts and their hydrocracking products.

3. RESULTS and DISCUSSION

3.1 The coal extracts: Figure 1 compares (i) coal liquefaction conversion (sample weight loss) and (ii) yields of > 450 °C (b.p.) material in the coal extract PI-fraction, determined by TGA (% w/w initial daf coal) as a function of elemental-C content. Middle rank coals gave the highest yields of extract and of > 450 °C b.p. material. Whilst allowing for some tetralin adduction to coal extracts in evaluating > 450 °C (b.p.) material contents, Figure 1 suggests high rank coal extracts were mostly composed of > 450 °C (b.p.) material. Lower rank coal extracts contained more light material and may have produced more gas during liquefaction.

Previous MALDI-MS of coals and coal derived liquids^{4,5} indicated the presence of molecular ions over the 1,000 - 6,000 u mass range; the spectra extended to higher masses (> 200,000 u) at increased laser power. In the present study, molecular ion distributions have been monitored at low laser power; the spectra showed intense sample-dependent peaks in the 1,000 - 6,000 u mass range (Table 1), with ions extending up to 50,000 u. The

density of peaks at higher masses ($> 20,000$ u) increased with increasing coal rank (more components evident); this may reflect increased maturation of higher rank coals.

Planar chromatography has been used to compare pentane soluble (PS) fractions of the extracts, with successive development in tetrahydrofuran (THF) and toluene. The nine PS fractions showed similar traces under visible and UV light. Extracts from the FSR contain very little coal derived material (mostly alkanes) detectable by GC and GC-MS³ and the set of PS-fractions appear to contain mostly solvent - rather than coal - derived material. For the PI fractions developed in THF and toluene, however, shapes and intensities of spots changed systematically with coal rank under both visible and UV light. Relationships of these changes with extract structure are being investigated. At the origin, parts of the sample spots were not cleared away by THF: even the more powerful solvent, 1-methyl 2-pyrrolidinone (NMP) did not wholly mobilise the fractions remaining at the origin. Material from higher rank coal extracts were more difficult to move. As in the case of MALDI-MS, PC data showed more intractable material in higher rank coal extracts, possibly of high polarity and of high molecular masses (MM), compared to lower rank coals.

3.2 Hydrocracking products Table 1 presents hydrocracking conversions (30 and 60 min reaction times), defined as the proportion of > 450 °C (b.p.) material converted to lower boiling fractions; these have been found to correlate well with rank related parameters. The conversion decreased with increasing elemental carbon content (a linear trend, $R^2 = 0.93$) and with increasing mean random reflectance (a second-order trend, $R^2 = 0.96$; Figure 2). Observed lower reactivities of coal extracts from higher rank coals are in accordance with the expected greater stability of increasingly larger aromatic ring systems associated with structures of high rank coals.

SEC profiles of the nine coal PI-extracts showed major peaks at 16, 19 and 20 minutes (e.g. Figure 3). Long elution times would suggest the two prominent peaks (19 and 20 min) to correspond to low MM material. However, similar peaks were found in SEC chromatograms of residual spots during PC, *after* the removal of tetralin derived products by development in toluene/pentane, suggesting these peaks to represent large MM and possibly also highly polar material. The long retention times suggest a mode of sample-packing interaction other than size exclusion. The relative intensities of the peaks at 19 and 20 minutes compared to that at 16 min. decreased with increasing coal rank (not shown). The chemical nature of these materials and their changes with rank are being investigated.

The initial departures from baseline (allowing comparison of apparent large-MM limits) of the SEC-profiles lie between 10 and 12.5 min: Lewiston-Stockton and Blind Canyon at 10 min, Pittsburgh No.8, Point of Ayr and Wyodak Anderson at 11 min, Illinois No.6 at 11.5 min, Pocahontas at 12 min, Upper Freeport Port and Beulah-Zap at 12.5 min. A similar trend showing a maximum in MMs for middle rank coals has already been reported for a set of European coals⁶.

SEC plots comparing Pittsburgh No.8 and Point of Ayr coal extracts with their hydrocracking products are shown in Figure 3. A significant shift of the peak at 16 min to smaller MMs (18 min) may be observed after 30 min hydrocracking; a smaller increase in elution time occurred after 60 min hydrocracking. The peaks at 19 and 20 min in the coal extracts disappeared after hydrocracking, suggesting that these materials are easily hydrocracked. Similar observations were made in hydrocracking extracts from the other coals. The extent of the shift in MMs before and after hydrocracking, indicated by the initial departure of the profile from base line, was different across the set of coal extracts. Largest shifts were observed for Lewiston-Stockton, Blind Canyon, Pittsburgh No.8 and Point of Ayr coals; smaller shifts were observed for Pocahontas, Illinois No.6, Wyodak Anderson coals. The smallest reductions in upper molecular mass were observed for Upper Freeport and Beulah-Zap coals. These results suggest that the high MM material in the middle rank coal extracts may be easier to breakdown than those in extracts prepared from high and low rank coals; it is likely that the reasons for difficulty in hydrocracking extracts from coals at the two ends of the rank spectrum would be different.

Table 1. Summary of analytical data for coals, coal extracts and hydrocracking products

Name of coal	Coal		Coal extract			HC product	
	Ref.	Carbon	Conv. ⁽¹⁾	>450 °C(b.p.) ⁽²⁾	MALDI ⁽³⁾	Conv. (%wt) ⁽⁴⁾	
	%R _o	%daf	%daf	%daf	ku	60 min.	30 min.
Pocahontas	1.42	91.1	43.3	47.7	1~6	52.2	43.0
Upper Freeport	0.99	85.5	76.0	68.0	1~6	54.5	44.3
Point of Ayr (UK)	0.79	84.5	79.4	60.0	1~6	64.2	50.2
Pittsburgh No.8	0.72	83.2	84.6	83.1	1~6	67.5	58.6
Lewiston-Stockton	0.77	82.6	84.2	80.4	1~4	63.9	52.3
Blind Canyon	0.50	80.7	91.3	69.7	1~3	70.4	61.0
Illinois No.6	0.46	77.7	88.7	64.6	1~3	75.9	66.3
Wyodak Anderson	0.31	75.0	81.7	38.9	1~4	76.9	72.2
Beulah-Zap	0.28	72.9	62.8	36.7	2~4	84.4	80.4

(1) Conversion of coal determined by weight loss; (2) materials boiling above 450 °C determined by TGA; (3) mass ranges of the peak of ion intensity; (4) conversion of coal extract to distillate (b.p.<450 °C) determined by TGA.

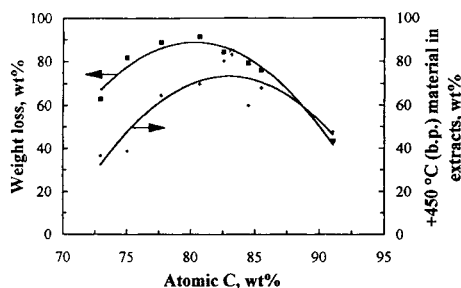


Figure 1. Comparison between liquefaction conversion determined by coal sample weight loss and the total yields of > 450 °C (b.p.) material in the coal liquefaction extract, as a function of coal rank.

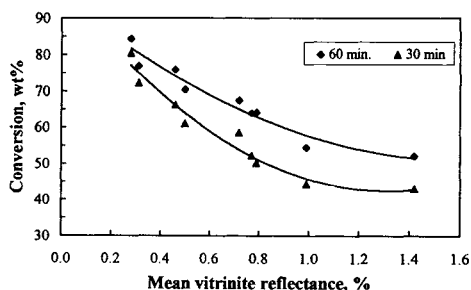


Figure 2. Conversion of > 450 °C (b.p.) material, determined by TGA, as a function of mean vitrinite reflectance of the original coals.

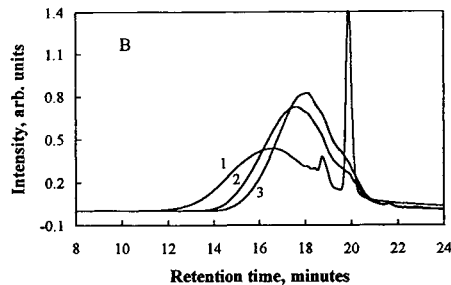
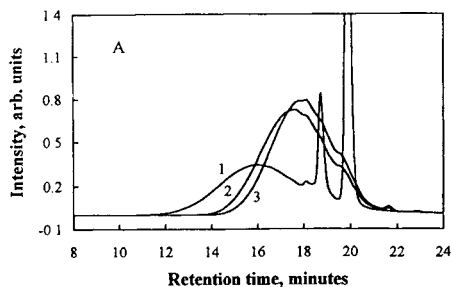


Figure 3. SEC chromatograms (normalised by area) of coal extracts (1) and their hydrocracking products after 30 (2) and 60 (3) minutes: (a) Pittsburgh No.8; (b) Point of Ayr coal.

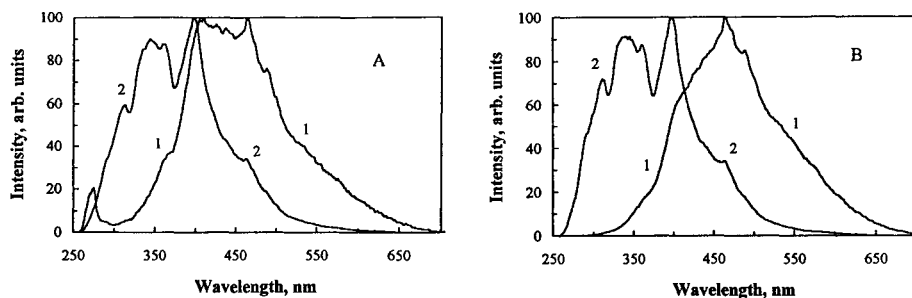


Figure 4. Comparison of UV-fluorescence spectra of (1) coal liquefaction extracts and (2) 60 min hydrocracking products: (a) Pittsburgh No.8; (b) Point of Ayr coal.

For the same two coals Figure 4 compares UV-F spectra of the liquefaction extracts and 60 min hydrocracking products, indicating very significant reductions in polynuclear aromatic ring system sizes during the hydrocracking process; little difference has been found between UV-F spectra of 30 and 60 min hydrocracking products suggesting that the breakdown of polynuclear aromatic ring systems takes place at short times: whether further reduction of ring system sizes is slowed down by catalyst deactivation or by the chemical stability of smaller ring systems is under investigation.

4. CONCLUSIONS

In hydrocracking coal extracts, the conversion of > 450 °C (b.p.) fractions to lower boiling material was found to decrease with rank and to correlate well with increasing elemental carbon contents and the vitrinite reflectances of the original coals. Results from SEC showed the largest shifts to smaller MMs to occur during the hydrocracking of extracts from middle rank coals. The observed *progressive* decrease of MMs and increase of hydrocracking conversion with increasing reaction time suggests that this method of hydrocracking removes smaller aromatic clusters from large molecules in a gradual step-wise progression rather than in the form of a catastrophic breakdown of large molecular structures. Our results clearly show, however, that the present hydrocracking process is instrumental in significantly reducing sizes of polynuclear aromatic ring systems within the extracts during early stages of the hydrocracking process.

5. ACKNOWLEDGEMENTS

We would like to thank the European Union for supporting the work under Research Contract No. ECSC 7220-EC/862. We would also like to thank G.M. Kimber and S.Moore for many helpful discussions.

6. REFERENCES

1. K.S. Vorres, Energy and Fuels 4, (1990), 420.
2. B. Xu and R. Kandiyoti, Rev. Sci. Instr. (1995), (in press).
3. D. Brodzki, A. Abou-Akar, G. Djèga-Mariadassou, C-Z. Li, B. Xu, and R. Kandiyoti, Fuel 73, (1994), 1331.
4. A.A. Herod, C-Z. Li, J.E. Parker, P.John, C.A.F. Johnson, G.P.Smith, P.Humphrey, J.R. Chapman, and R. Kandiyoti, Rapid Comm. Mass Spec. 8(1994), 808.
5. A.A. Herod, C-Z. Li, B. Xu, J. E. Parker, C.A.F. Johnson, P. John, G.P. Smith, P. Humphrey, J.R.Chapman and R.Kandiyoti, Rapid Comm. Mass Spec. 8(1994), 815.
6. J.R. Gibbins and R. Kandiyoti, Fuel 70, (1991), 909

Characterization of Coal Hydropyrolysis Products

Mastral, A.M.; Pérez-Surrio, M.J.; Mayoral, M.C.; Callén M.S. and Murillo R.

P.O. Box, 589, 50080- Zaragoza, España

I. INTRODUCTION

Hydropyrolysis is an alternative process to liquefaction for recovering oils from coal. By heating, the molecular component and part of the macromolecular component of coal, that what is joined to the three dimensional network by less strong bonds, are released as radicals. These radicals stabilize themselves in a different way wheater the hydrogenation is a liquefaction process or a hydropyrolysis (1) but in both processes the liquids can be the bulk of the conversion products from coal. Some work has been previously published (1-3) comparing both hydrogenation processes.

In the classic liquefaction process, using hydrogen donors as solvent, the nature of the conversion products are influenced by solvent incorporation and solvent side reactions (4). Trying to avoid these solvent troubles, hydropyrolysis shows to be an adequate route to liquids (1,5). In addition, residence time use to be shorter than in classic liquefaction diminishing secondary reactions conducting mainly to gas formation and repolymerization products (6) with higher H₂ consumption, which on the other hand increases the cost of the process. In this paper, liquids from coal hydropyrolysis in a swept fixed bed reactor as function of the process variables are analysed and commented.

II. EXPERIMENTAL

Experiments were conducted on a low-rank coal (SAMCA) from N-E of Spain . Its analyses are: C, 80.17% (daf); H, 7.69% (daf); N, 1.03% (daf); S, 5.68% (df); moisture, 22.05%; ash, 26.93% (df); volatile matter, 48.61% (daf).

The fixed bed reactor is presented schematically in Fig. 1 which shows the laboratory scale pilot plant where the sfb reactor is joined. A downward flow of hydrogen through the coal bed (5 g) was used to drive the conversion products into the cooled trap. The final temperature was held for 10 mm or 30 mm. The hydrogen was forced to pass at 40 kg/cm² pressure and the working flows were 0.5 l/min. or 2 l/min.

Gases were collected in a special sampling gas bag and C₁ - C₃, CO_x (CO + CO₂) and H₂S percentages were immediately determined, to eliminate gas diffusion through the sampling bag, by GC.

The liquids were recovered directly from the trap (tars) and by chars Soxhlet extraction (extracts) with THF. Results obtained are shown in Table 1.

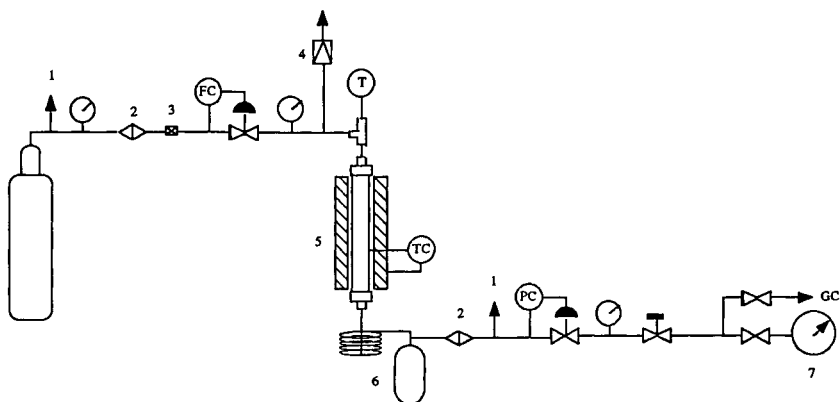


Fig. 1. Diagram of the hydropyrolysis plant (1, vent; 2, filter; 3, non-returning valve; 4, rupture disc; 5, furnace; 6, liquids traps; 7, gas counter)

The tars hydrocarbon types were analysed by TLC-FID in a Iatroscan and their hydrogen distribution by proton nmr in a Bruker CW-80SY. Data are compiled in Table 2.

The chars have been characterized by FTIR, elemental analysis and mineral matter content isolated by low temperature ashing LTA .

III. RESULTS AND DISCUSSION

Chars are composed by the inherent mineral matter of the coal, the unconverted material and the repolymerization and condensation products from retrogressive reactions. The char percentage diminishes from 59% to 47% with the severity of the process while their relative content in mineral matter increases from 44% to 64% The hydrogen content of the char organic fraction gradually decreases with temperature opposite to the trend followed by its total sulphur content which increases due to an intercorrelation between pyrite (the most abundant inorganic sulphur in this coal) and the organic sulphur (6,7) during the process.

Gas analyses show that the oxygenated groups are released at low severity hydropyrolysis while the H_2S lowering with increasing temperatures is due to the partial sulphur incorporation to the solid phase, according to the sulphur content increase in the corresponding chars.

Coal conversions in hydropyrolysis at 40 kg/cm², depending on the hydrogen flow rates and residence time, are compiled in Table 1. Working at the lower hydrogen flow (0.5 l/min.), an increase in the residence time does not mean an increase neither in

Table 1. Yields obtained from SAMCA coal (MS13) hydrolysis, (40Kg/cm2, 0.2-0.5mm).

	400°C				500°C	600°C			
	0.5l/min		2l/min		0.5l/min	0.5l/min		2l/min	
	10min	30min	10min	30min	30min	10min	30min	10min	30min
Conv.(%)	55	45	34	47	49	56	59	65	73
Tars (%)	9	11	13	17	13	15	15	26	29
Extrac(%)	9	14	11	17	1	4	traces	1	2
Char (%)	62	69	76	67	66	61	59	55	49

Table 2. TLC-FID and 1H nmr analyses of the tars from hydrolysis at 40Kg/cm2.

	400°C				500°C	600°C			
	0.5l/min		2l/min		0.5l/min	0.5l/min		2l/min	
	10min	30min	10min	30min	30min	10min	30min	10min	30min
Saturated(%)	3	5	2	2	4	--	2	2	1
Aromatic(%)	15	15	12	14	34	--	43	29	37
Polars(%)	82	79	86	84	63	--	55	69	62
H aliphatic(%)	--	73	--	--	66	--	60	--	--
H aromatic(%)	--	27	--	--	33	--	35	--	--

conversion nor in tars percentages which demonstrates that there is a lack in hydrogen. However, at the higher hydrogen flow (2 l/min), significative increases in both parameters are reached. About the temperature influence, the higher the hydrolysis temperature, the higher the conversions and the tars percentages.

The tars hydrocarbon type is predominantly polar, ranging from 55% to 86% depending on the process variables. The tars aromatic hydrocarbons range from 11% to 43% while the aliphatic hydrocarbons are the least abundant in all the runs carried out as it is show in Table 2.

The information provides by the nmr about the tars hydrogen type shows that the aliphatic hydrogen involved in methyl and ethyl groups decreases while the aromatic hydrogen increases with increasing hydrolysis temperatures, showing that tars aromatization is promoted with the severity of the process.

The amount of the products converted but not collected as tars, those which are THF-solubles, the extracts, diminishes with increasing temperatures. According to their chromatographic and spectroscopic analyses, their polar components are more abundant than in the corresponding tars obtained at the same conditions. This fact seems to show that the extracts are mainly composed by products wich have been selectively retained by the coal fixed bed due to their high polarity (8).

According to these results, it can be deduced that in spite of the tars nature is mainly aromatic, the substitution degree of their aromatic rings is high and mostly due to short alkyl chains. While the aromatic hydrogen ranges from 26% to 35%, the remaining aromatic carbons are mainly substituted by methyl and ethyl groups. Only the 6% of the aliphatic hydrogen is involved in positions gamma or further to the aromatic rings. This released tars have less polar nature than the conversion hydrolysis products, those solubles in THF, which seem to be selectbily retained on the coal bed probably due to their higher heteroatom contents.

ACKNOWLEDGEMENTS

Authors would like to thank the ECSC and Spanish CICYT the partial financial support of this work.

REFERENCES

1. AM Mastral, MT Izquierdo, P Burchill, S Harbottle, A Lowe, DJ MacCaffrey and D Way, *Fuel* 73 (1994) 449
2. JR Gibbins, R Kandiyoti, *Fuel* 70 (1991) 621
3. JR Gibbins, R Kandiyoti, *Fuel* 70 (1991) 909
4. AM Mastral, Final Report CSIC to ECSC, Ref 7220/EC/755, June 1993
5. E Klavetter, SC Mitchell, R Garcia, CE Snape, ICCS Proceedings, Vol 1 (1993) 328
6. AM Mastral, MC Mayoral, JM Palacios, *Energy & Fuels* 8 (1994) 94
7. AM Mastral, MC Mayoral, B Rubio, MT Izquierdo, *Energy & Fuels*, in press
8. AM Mastral, MJ Perez-Surrio, MS Callen and R Murillo, 22nd Conference on Carbon, San Diego, CA, USA, 1995

Separation of coal tar components by the supercritical CO₂ solvent through the adsorption and structural modification

K. Sakanishi^a, H. Obata^a, I. Mochida^a, and T. Sakaki^b

^aInstitute of Advanced Material Study, Kyushu University,
Kasuga, Fukuoka 816, Japan

^bKyushu National Industrial Research Institute, Tosu, Saga 841, Japan

Capture and recovery of nitrogen-containing compounds from coal tar fractions were examined using a continuous supercritical CO₂ extraction apparatus with the fixed bed of a solid acid adsorbent or an ion exchange resin. Quinoline bases and indole were separately adsorbed by Al₂(SO₄)₃ supported on silica gel and an anion exchange resin (Amberlite), and recovered by adding THF and methanol, respectively, as an entrainer solvent to supercritical CO₂ through the adsorption/desorption procedure. Nitrogen compounds and purified methyl-naphthalenes were alternatively recovered by the adsorption/desorption procedure.

1. INTRODUCTION

Coal tar components contain valuable nitrogen compounds for use in the preparation of pesticides, drugs, dyes, and pigments. The nitrogen compounds are undesirable impurities in hydrocarbon oils because they contribute to air pollution, have unpleasant odors, and deteriorate upgrading catalysts.

The present authors have proposed application of metal sulfates which is fairly acid when dehydrated, while neutral when hydrated.¹⁻²⁾ Thus, nitrogen compounds in crude methyl-naphthalene oil diluted in non-polar solvents are captured on the adsorbent and recovered with polar solvents such as methanol, regenerating the acidity of the adsorbent for its repeated use. Non-polar solvents appear to play a role of anti-solvent, accelerating the adsorption of bases on the adsorbent. Dispersion of the sulfate on silica gel of large surface area increases number and strength of acidity to capture more moles of nitrogen bases.

Supercritical fluids have been reputed to be a unique solvent for the selective and energy-saving extraction and separation procedures.^{3,4)} In addition to such advantages of supercritical extraction, the dissolving ability of supercritical CO₂ is easily controlled by changing its temperature and pressure, then the adsorption and desorption of the substrates being designed by the supercritical solvent.

In previous papers,^{5,6)} a batch-type extraction of methylnaphthalene oil using the supported sulfate adsorbent under the supercritical CO₂ flow was reported to be one of the promising way for the selective adsorption and desorption of quinolines in addition to the purification of methylnaphthalenes by controlling the dissolving ability of supercritical CO₂ through changing its temperature and pressure, and mixed with an entrainer solvent.

In the present study, the removal and recovery of nitrogen compounds in crude methylnaphthalene oil (CMNO) obtained from coal tar were investigated using aluminium sulfate supported on silica gel or an anion exchange resin to obtain highly denitrogenated CMNO as well as to recover basic quinoline bases or non-basic indole by adding an entrainer solvent to supercritical CO₂.

2. EXPERIMENTAL

Model methylnaphthalene oils containing quinoline and isonquinoline, and quinoline and indole in methylnaphthalenes were used for the present experiments, where aluminium sulfate supported on silica gel and an anion exchange resin were applied as an adsorbent, respectively. The former adsorbent was prepared by supporting 10 wt% Al₂(SO₄)₃ from its aqueous solution on the silica gel of MB-4B, of which surface area and mean pore diameter were 500 m²/g and 64 Å, respectively. The adsorbent was calcined at 350°C for 3 h in air before its use. Amberlite IRA-904, which has been reputed to have affinity to indole, was used as the anion exchange resin after drying at 50°C.

Figure 1 shows the continuous supercritical CO₂ extraction apparatus used in the present

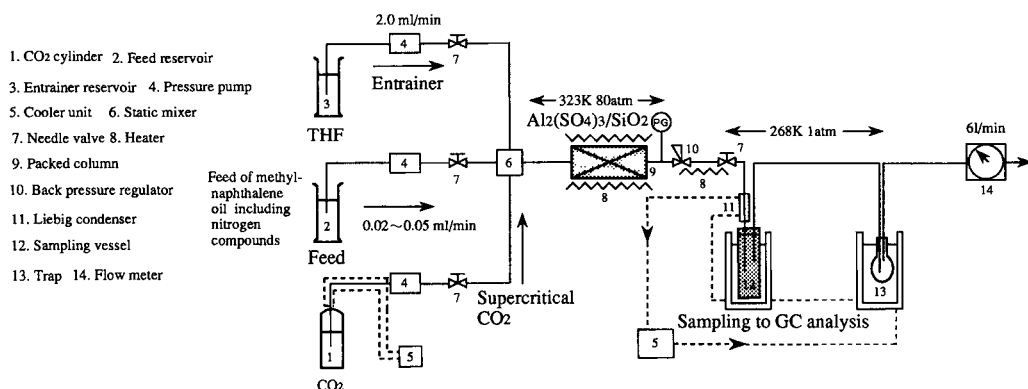


Figure 1 Continuous supercritical CO₂ separation apparatus

study. The model feed was fed at the flow rate of 0.02 - 0.05 ml/min to the fixed bed of the adsorbent with the supercritical CO₂ (50°C, 80 atm; flow rate: 6 l/min). After the adsorbent was saturated with nitrogen compounds when they started to elute from the adsorbent, THF or methanol was introduced at a level of ca. 4 vol% to the supercritical CO₂ flow, to recover the adsorbed species and to regenerate the adsorbent for its repeated use. The eluted and recovered

fractions which was sampled in 20 min intervals were analyzed and quantified by GC-FID (50 m capillary OV- 101 column, 110°C).

3.RESULTS AND DISCUSSIONS

3.1.Removal and Recovery of Quinolines

Figure 2 shows the elution profile of the model methylnaphthalene oil using 3.4 g $\text{Al}_2(\text{SO}_4)_3 / \text{SiO}_2$ as the adsorbent in the fixed bed under the supercritical CO_2 conditions. No nitrogen compounds were eluted until the extraction time of 120 min, denitrogenated methylnaphthalenes being recovered at the separation vessel. Quinoline first started to elute at 140 min, while isoquinoline appeared at 180 min, suggesting that quinoline and isoquinoline may be separated by optimizing the elution conditions. After 180 min, the base concentration of the eluate gradually increased to reach that of the feed.

Figure 3 illustrates the recovery profile of purified methylnaphthalenes in the repeated cycles of adsorption and desorption. The adsorbent was successfully regenerated under supercritical CO_2 flow mixed with ca. 4 vol% THF as an entrainer at 80°C before the next run. About 2 g of purified methylnaphthalenes was steadily recovered in every run, although slight deactivation of the adsorbent may take place during the adsorption / desorption repetition.

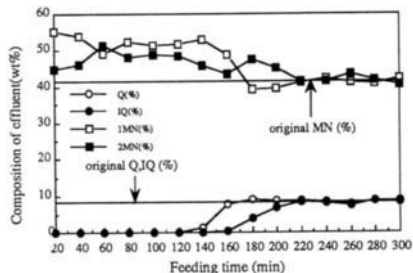


Figure 2 Extraction profile of model feed using continuous extraction apparatus under supercritical CO_2 conditions

Conditions : pressure 80atm, temperature 50°C, adsorbent $\text{Al}_2(\text{SO}_4)_3/\text{SiO}_2$ 3.4g
 CO_2 flow rate 6l/min, feed flow rate 0.035 ml/min
 feed composition : 1MN 42%, 2MN 42%, quinoline(Q) 8%
 isoquinoline(IQ) 8%

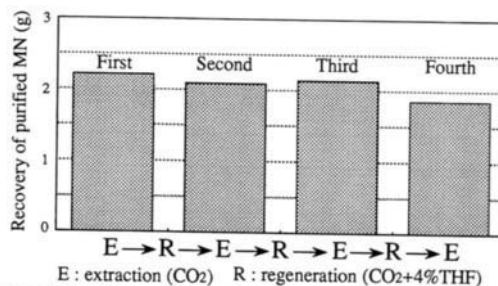


Figure 3 Repeated recovery profile of purified MN using continuous extraction apparatus under supercritical CO_2 conditions

Separation conditions : pressure 80atm, temperature 50°C, adsorbent $\text{Al}_2(\text{SO}_4)_3/\text{SiO}_2$ 3.4g,
 CO_2 flow rate 6ml/min, feed flow rate 0.03ml/min,
 feed composition : 1MN 42%, 2MN 42%, quinoline(Q) 8%
 isoquinoline(IQ) 8%
 Regeneration conditions : entrainer (THF, 50 ml) ca.4 vol% added to supercritical CO_2
 column temperature 80°C

3.2. Recovery and Concentration of Indole

Figure 4 shows the elution profile of the model methylnaphthalene oil. Indole was not eluted until the feeding time of 120 min, only methylnaphthalene and quinoline being recovered in the separation vessel and indole first started to elute at 140 min. After 140 min, indole concentration of the eluate gradually increased to reach that of the model feed. After the feed was stopped at 300 min and supercritical CO_2 was flowed later on for 60 min, 0.82 g of the concentrated indole was recovered by washing out with 4 vol% methanol-added supercritical CO_2 .

Table 1 shows the effects of CO_2 pre-extraction of saturated adsorbent on the concentration of recovered indole by methanol-added supercritical CO_2 . Supercritical CO_2 with 4% methanol

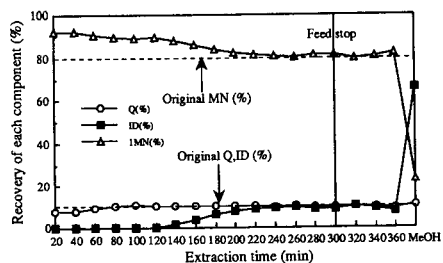


Figure 4 Elution profile of model feed using continuous supercritical CO₂ extraction apparatus
 Conditions : pressure 80atm, temperature 50°C, adsorbent IRA-904 2.0g, CO₂ flow rate 6l/min, feed flow rate 0.045ml/min (until 300min) feed composition 1MN 80wt%, Q 10wt%, ID 10wt%

Table 1
 Effects of CO₂ pre-extraction of saturated adsorbent on the concentration of indole.^{a)}

Run NO.	Pre-extraction conditions		Residual weight on the adsorbent (g)	Indole content (%) ^{b)}
	Pressure(atm)	Time(h)		
1	—	—	2.37	28.3
2	80	1	0.82	66.4
3	80	2	0.33	95.8
4 ^{c)}	80	2	0.28	98.0

a) Adsorption conditions : 50°C, 80atm, 300min, CO₂ flow rate 6l/min, Original Indole content 10%

b) Desorption conditions : Indole was recovered from ion-exchange resin with MeOH

c) Recycle use of adsorbent : Ion-exchange resin was washed with MeOH and dried at 50°C for 10h.

recovered the adsorbed compounds from adsorbent, although the concentration of indole in the adsorbate was only 28.3% when the pre-extraction was not performed, indicating that methylnaphthalene and quinoline remained in the dead space of the adsorbent column may elute with indole. Supercritical CO₂ at 50°C washed out such remaining methylnaphthalene and quinoline before the entrainer was flowed, leaving selectively indole on the adsorbent. Supercritical CO₂(50°C, 80atm; flow rate: 6l/min, pre-extraction time: 2h) concentrated indole of 96wt% on the adsorbate and they were effectively recovered by the following supercritical CO₂ with a small amount of methanol

Recycle use of adsorbent was achieved by washing the used resin with methanol and drying at 50°C for 10h before the next run. 0.28g of the concentrated indole was recovered at the concentration of 98wt% in the second run.

4. CONCLUSIONS

The present study revealed that a novel process for removal and recovery of quinolines and indole from methylnaphthalene oil can be designed by using supported aluminium sulfate and the anion exchange resin, respectively, in the continuous supercritical CO₂ extraction apparatus.

Supercritical fluid-mediated separation procedures can be applied not only to the capture of nitrogen compounds from coal-derived liquids, but also to the separation of sulfur compounds from crude naphthalene through the designs of selective dimerization of benzothiophene, followed by selective extraction of purified naphthalene under supercritical CO₂ conditions.

REFERENCES

1. I.Mochida, K.Sakanishi, H.Usaba, K.Miura, *Fuel*, **1991**, 70, 761.
2. K.Sakanishi, Y.N.Sun, I.Mochida, H.Usaba, *Fuel Process.Technol.*, **1992**, 32, 143.
3. D.R.Gere, R.Board, D.McManigill, *Anal.Chem.*, **1982**, 54, 736.
4. Campbell, R.M., Lee, M.L., *Anal.Chem.*, **1986**, 58, 2247.
5. K.Sakanishi, H.Obata, I.Mochida, T.Sakaki, *Prepr.Div.Fuel ACS*, **1994**, 39(3), 761.
6. K.Sakanishi, H.Obata, I.Mochida, T.Sakaki, *J.Energy Inst., Jpn.*, **1995**, 74(2), 109.

Vapor Pressure Estimation for Hydrocarbons in a Coal Derived Liquid

Shin-ya HARIKAE, Masaaki SATOU, Tadatoshi CHIBA,
Susumu YOKOYAMA and Yuzo SANADA

Center for Advanced Research of Energy Technology,
Hokkaido University, Sapporo 060, Japan

1. INTRODUCTION

The vapor pressure as well as the boiling point is one of the most fundamental properties for process design and control. In spite of numerous studies on vapor pressure estimation for pure organic compounds, their applicability to coal derived liquids has never been confirmed yet[1,2]. In our previous studies[3-5], simple equations for estimation of boiling point, molar volume and refractive index were derived on the basis of a new group contribution method, i.e., relationships between the chemical structure of hydrocarbons in coal derived liquid and their physical properties. This study aims at extension of our conception to vapor pressure estimation.

2. EXPERIMENT

Hydrocarbons in a recycle solvent derived from Wyoming coal liquefaction were characterized following a program of analytical methods using high performance liquid chromatography(HPLC) with an amine column and mass spectrometry(GC/MS)[6]. The recycle solvent was first separated by a spinning band distillation apparatus into 24 fractions having a boiling point temperature range from 464K to 630K, each fraction with a temperature interval of 2K to 28K. Some representative fractions were further separated into chemically homologous compounds called "compound classes" according to the number of aromatic rings by a HPLC. There were six hydrocarbon compound classes; alkanes(Fr-P), monoaromatics(Fr-M), naphthalene type diaromatics(Fr-D1), biphenyl type diaromatics(Fr-D2), tri- and tetra-aromatics (Fr-T1 and T2) and poly-, polar compounds (Fr-PP). GC/MS measurement was carried out to find the average numbers of total carbons, aromatic rings and naphthenic rings of each compound class.

The same narrow cut distillates were also separated into hydrocarbon portion(Fr-HC) and Fr-PP by the same HPLC. The vapor pressure of Fr-HC was determined from isothermal gas chromatographic measurement of relative retentions[7] on a non-polar OV-1 column. Measurements were made at every 10K from 373 to 573K. The experimental scheme is shown in Fig. 1.

3. RESULTS AND DISCUSSIONS

In our previous studies[3-5], the influences of component groups such as aromatic

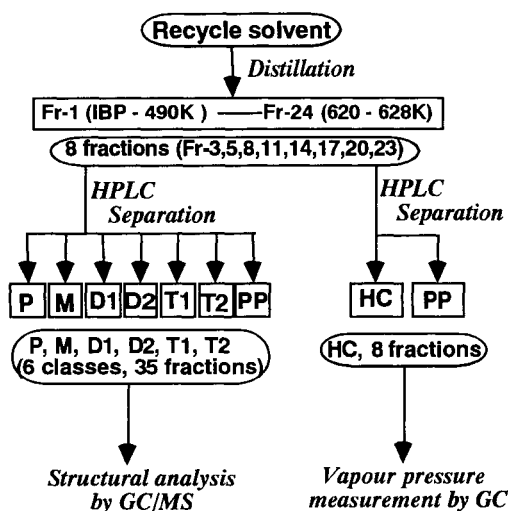


Fig.1 Experimental scheme

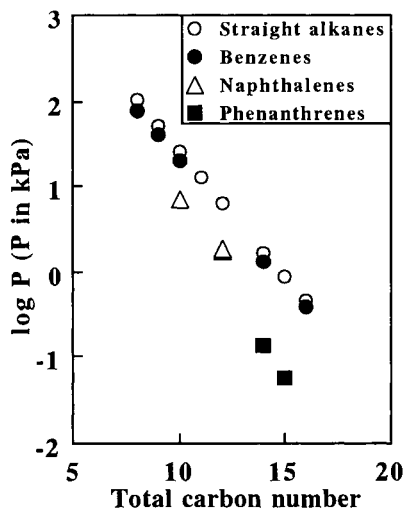


Fig.2 Change in vapour pressure of straight alkanes and aromatic hydrocarbons at 400K with total carbon number

ring and naphthenic ring to the values of boiling point, molar volume and refractive index have been systematically examined. In brief, the difference between the value of a property of a given compound and that of a reference is attributed to the contribution of a certain structural feature. For example, straight alkanes are selected for hydrocarbons as the reference and the structural contributions are evaluated on the basis of aromatic rings, naphthenic rings and so on. The property of a given non-paraffinic molecule is the sum of all the non-paraffinic structures being incremental to that of reference.

3.1. Vapor pressure of pure hydrocarbons

Figure 2 shows change of logarithmic values of the vapor pressure at 400K with the total carbon number for straight alkanes, benzenes, naphthalenes and phenanthrenes with one straight alkyl side chain, where values of vapor pressure are available as Antoine constants[8]. The relationships between the logarithmic values of the vapor pressure and total carbon number are linear for the homologous series, so far tested. Furthermore, each linear relationship is parallel with each other. In other words, the difference of logarithmic values of the vapor pressure of hydrocarbon homologue with those of straight alkanes ($\delta \log P$) having the same total carbons is invariable with the total carbon number. The difference gradually increases with the aromatic ring number.

In Figure 3, the values of $\delta \log P$ for these hydrocarbon homologous series are plotted against the reciprocal of temperature. The values are seen to be inversely proportional to the reciprocal of temperature with the slope becoming gradually steep with the number

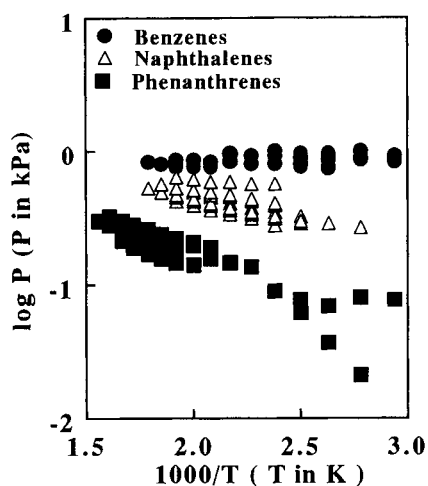


Fig. 3 Difference of logarithmic value of vapor pressure of aromatic hydrocarbons with those of straight alkanes

the particular component groups and the absolute temperature, respectively. Here, aromatic rings, naphthenic rings and aromatic conjunction carbons are considered as the component groups. The above equation means that the vapor pressure of hydrocarbons are calculated by adding the total increments of vapor pressure to those of the straight alkanes with the same total carbon number.

The $P_{\text{paraff.}}$ is expressed as a function of the total carbon number (N_t) of a given hydrocarbon as

$$\log P_{\text{paraff.}} = (2.439 - 347.9 / T - 7.105 \times 10^{-1} \times \log T) \times N_t + 4.153 \quad (2)$$

which was obtained by a regression analysis based on the vapor pressure of straight alkanes with total carbon numbers from 6 to 30 in the temperature range 300 to 720K in the literature [8]. The correlation coefficient and average absolute error between the literature values of temperature and values calculated using Equation (2) at a given vapor pressure are 0.998 and 1K, respectively. This equation is a generalized version of Antoine equation using the total carbon number as a parameter.

The values of group contributions (P_i) in Equation (1) were also determined by the regression analysis. The results are listed in Table 1. The values of 0.865 and 9K were obtained for the correlation coefficient and average absolute error, respectively. The influence of aromatic conjunction carbons to the value of vapor pressure can not be systematically considered because few data are available in literatures.

3.2. Vapor pressure of hydrocarbons in a recycle solvent

The major purpose of this study lies in the estimation of the vapor pressure for

of aromatic rings.

In the same manner, influence of naphthenic ring to the vapor pressure was examined. As a result, the values of $\delta \log P$ were found to be less than those of aromatic rings, and to be inversely proportional to the reciprocal of temperature with the slope gradually becoming steep with the numbers of naphthenic rings.

Based on the above findings, the following equation is derived for vapor pressure calculation.

$$\begin{aligned} \log P &= \log P_{\text{paraff.}} + \delta \log P \\ &= \log P_{\text{paraff.}} + \sum (P_i \times N_i) / T \quad (1) \end{aligned}$$

where, P , $P_{\text{paraff.}}$, P_i , N_i and T represent the vapor pressure of a given hydrocarbon, the vapor pressure of straight alkanes having the same total carbon number, the incremental vapor pressure contributed by i -th component groups, the number of

Table 1 Component contribution to vapor pressure

Component group	Contribution (Pi)
Aromatic ring	-91.63
Naphthenic ring	-42.56
Aromatic conjunction carbon	-29.57

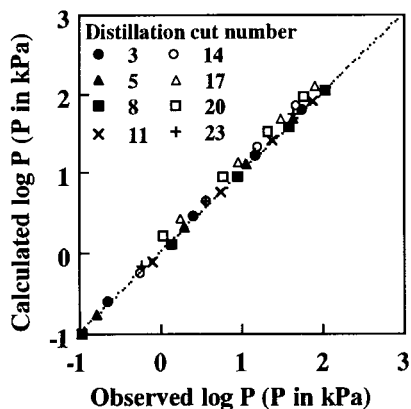


Fig.4 Comparison between observed and calculated log P

The value of $\delta \log P$ was found to be inversely proportional to the reciprocal of temperature with the slope gradually becoming steep with the numbers of aromatic and naphthenic rings. A simple equation is proposed based on these findings.

REFERENCES

1. H. Hartounian and D.T. Allen, *Fuel*, 68(1989) 480
2. L.E. Vajdi and D.T. Allen, *Fuel*, 68(1989) 1388
3. M. Satou, S. Yokoyama and Y. Sanada, *Fuel*, 71(1992) 565
4. M. Satou, H. Nemoto, S. Yokoyama and Y. Sanada, *Energy&Fuels*, 5(1991) 638
5. M. Satou, H. Yamaguchi, T. Murai, S. Yokoyama and Y. Sanada, *Sekiyu Gakkaishi*, 35(1992) 466
6. H. Uchino, S. Yokoyama, M. Satou and Y. Sanada, *Fuel*, 64(1985) 842
7. D.J. Hamilton, *J. Chromatogr.*, 195(1980) 75
8. R.M. Stephenson and S. Malanowski, *Handbook of the Thermodynamics of Organic Compounds*, Elsevier, New York, 1987

hydrocarbon mixture in a recycle solvent as well as of pure hydrocarbons. Application of the present method to a recycle solvent gives a good agreement between calculated and observed vapor pressures, as summarized in Figure 4. The average absolute error between the literature values of temperature and values calculated using Equation (2) at a given vapor pressure is as small as 8K.

Hence, it is now possible to estimate the vapor pressure of various hydrocarbons such as alkanes, aromatics, hydroaromatics and their alkyl derivatives in both forms of pure substance and mixture over a range of total carbon number from 6 to 20.

4. CONCLUSION

It was clarified that the difference ($\delta \log P$) of logarithmic values of the vapor pressure of hydrocarbon homologue with those of straight alkanes having the same total carbons is invariable at a given temperature with the total carbon number.

Assesment of quality of coal-heavy oil interaction products by means of fluorescence spectroscopy

L. Pacheco, L.E. Henao and J.M. Rincón.

Laboratorio de Combustible, Departamento de Química, Universidad Nacional de Colombia. Santafé de Bogotá, Colombia.

Interaction products of coal and mixtures with heavy oil, anthracene oil were supercritical extracted with water (HTT=380°C) and coal- heavy oil- o cresol (as model compound. HTT=350°C). Solubles products in THF, were fractionated by extrographic method and analyzed with a MPV-SP Leitz spectrophotometer fluorescence microscope. The spectra of fractions eluated with n-hexane (F1) and toluene-n hexane 85:15 (F2) exhibited máximo emision fluorescence wavelength at 463 nm. Normalized intensities increased depending upon type of additive. Being fractions (F3 to F6) insensitives toward ultraviolet excitation.

The greatest fluorescence intensity measured was achieved in F2 of the interaction coal-heavy oil-anthracene oil. Furthermore the extrographic amount of this fraction F2 was greater than coal alone and the other additives.

It is concluded that the quality of the interaction can be assesed meassurig fluorescence intensity and amount of fraction F2 wich maybe composed by stabilized molecules with the lowest molecular weight coming from coal. The extend of the interaction in terms of coal conversion can be evaluated from the quantity of extrografic fraction F6 and F7. (soluble in THF and retained products in the silica support respectively).

1. INTRODUCTION

Modern technology of coal utilization in liquefaction processes involves the use of H-donor compounds wich should be very cheap and available in industrial amount, Colombia has the largest known reserves of coal in Southamerica and is plenty of heavy crude oil, therefore it is a challenge research the development of processes using these raw materials in order to obtain valuable chemicals.

Moschophedis and coworkers (1) have shown the possibility of using heavy oil as H-donor solvent in direct coal liquefaction, Rincón et al (2) using anthracen oil as co-solvent in a mixture coal-heavy oil found a synergistic effect toward a greater conversion and better oil quality. Pacheco (3) using o-cresol as model compound proposed a mechanism of stabilization of thermal fragment of coal.

The study of chemical and structural characterization of coal derived liquids is very complex and many methods have been applied. Zander and coworkers (4) found a very good correlation between the molecular weight of coal tar pitch fractions as meassured by fluorescence spectra (meassured in Pyridine at room temperature) and preparative size-exclusion chromatography (s.e.c).

Rathbone and coworkers (5) using fluorescence intensities and spectral distribution analyzed non distillable coal liquids (Resid) from the Wilsonville CC-ITSL pilot plant and the HRI ebullated bed bench unit, found that fluorescence intensities and spectral distribution can potentially provide new insight into the structure, composition and reactivity of coal-derived resid.

2. EXPERIMENTAL

2.1. Materials

Fresh samples of La Jagua (bituminous coal) were provided by Ecocarbón, heavy oil (HO) was supplied by the Colombian petroleum company Ecopetrol. Solvents used for extrography and o-Cresol were of analytical grade. The heavy oil was fractionated into soluble (AS-HO) and insoluble (AI-HO) in acetone to assess its ability toward hydrogen donation. Analytical data are reported in reference (3).

2.2. Interaction procedure

The ground coal (100 mesh) was mixed with the solvent (3:9 g) placed with 10 ml of water in the reactor, HTT 390°C, 24.3 MPa, soak time 30 min. The reactor was vent-out and the extraction product under supercritical condition was condensed. One gram of products were analyzed for extrography method as described by Moimelo et al (6) using n-hexane, n-hexane-toluene (85:15), dichloromethane, dichloromethane-ether (90:10), dichloromethane-ethanol (97:3) and THF as eluents to give F1 to F6 fractions and the non recoverable products F7. This fraction is composed of: F1 saturate, F2 aromatics, F3 polar aromatics and heterocyclics non-basic, F4 monophenols, F5 and F6 basic heterocyclics, polyphenols and oxygenated compounds and F7 high molecular weight compounds of higher polarity.

2.3 Fluorescence Measurement

Energy-converted fluorescence excitation and emission spectra of the F1 to F6 extrography fractions of each interaction were recorded in n-pentane (quartz cell length 1 cm and 20x/0.45 NPL Fluotar air objective) at room temperature using a computer programmed Leitz MPV-SP microscope photometer equipped with a 100 W mercury arc lamp as a source of intense ultraviolet-violet and visible radiation. The excitation band 355-425 nm /RKP 455 /LP460 SB600 was isolated using a filter D in the epilluminateur housed. The reflected emission light from the cell was scanned from 400 to 800 nm using 6 nm SBW and corrected by microscope components using a stabilized halogen lamp to 2800°C and background. The spectra were recorded upon a weighted sample dissolved in 1 ml n-pentane and placed into the cell. The spectrometer was calibrated at 463 nm (maximum emission intensity of fluorescence) using an uranyl special glass standard with 0.624 relative fluorescence units. The signal of the sample was compared with the standard.

3. RESULTS AND DISCUSSION

As shown in Table 1 coal alone produces a condensable liquid with main characteristics are a low content of paraffin and monoaromatics (F1, F2), a rather high content of polar aromatics and heterocyclic non basic compounds (F3), and a remarkable amount of basic heterocyclic polyphenols and oxygenated compounds present in F6. Upon addition of heavy oil or its soluble and insoluble acetone fraction was observed a slight increase in F2 (The amount of F1 come from the heavy oil). However this increase in F2 is not relevant but upon addition of AO to the coal-HO mixture increase this fraction significantly demonstrating the synergistic effect proposed by Rincón and Angulo (2). Addition of *o*-cresol (as model compound) to the coal-HO mixture shows a similar effect, that means a better quality product indicated by the increase in F2 and a greater coal depolymerization as shown by the increase of F5 and F6.(3)

Tabla 1
Extrography distribution of coal liquids and interaction products

Sample	% F1	% F2	% F3	% F4	% F5	% F6	% F7
Coal	14.7	3.5	41.3	11.9	4.0	23.7	1.0
Coal + IA-HO	24.8	1.1	24.2	7.6	4.8	22.0	15.6
Coal + SA-HO	62.2	3.9	16.8	6.2	0.6	9.2	1.1
Coal + HO	49.7	4.7	7.4	4.5	1.0	11.0	21.6
Coal + HO + AO	47.6	10.6	8.7	4.9	2.7	6.6	18.8
Coal + IA-HO + <i>o</i> Cresol	13.5	6.7	24.5	20.4	11.4	22.0	3.5

SA is not too reactive to coal depolymerization because F6 decrease strongly while the reactive IA-HO and HO additive increases F6 and F7 but low increase in F2. Better reactivity is reached when AO is added to the coal-HO mixture such as viewed with the great value in F2. Although *o*-cresol has a significant effect on F2, the F6 value indicate greater condensation toward heavy weight macromolecular species so confirming the synergistic effect.

Figure 1 shows the fluorescence emission spectra of extrography fractions of coal derived products, only fractions F1 and F2 exhibited spectra with a maximum fluorescence emission wavelength at 463 nm, fraction F3 to F6 possessed a spectra similar to the spectra of *o* cresol (maximum wavelength 440nm) but with very low intensity. Therefore it was investigated fluorescence emission at 463 nm as shown in Table 2 the quality liquefaction products can be assessed by the intensity of fraction F2, the greatest value is presented when AO is added to the mixture coal+HO, this finding is in agreement with the extrography results and confirm the above mentioned synergistic effect.

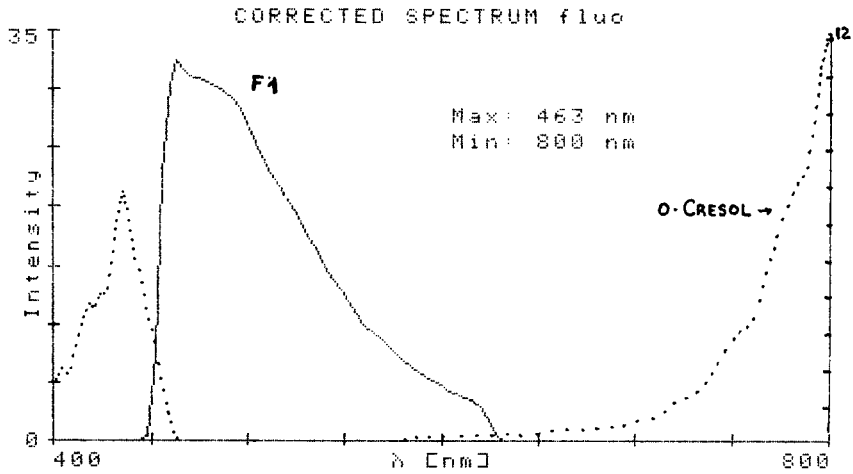


Figure 1. Fluorescent emission spectra of extrographic fraction F1 (coal + HO + AO) and o-Cresol dissolved in 1ml of n-pentane.

Tabla 2

Fluorescence emission intensity (I_f) of fractions

	I_f F1 g/ml	I_f F2 g/ml
Coal	2.47	2.71
Coal + IA-HO	0.86	13.85
Coal + SA-HO	0.07	Non fluoresc.
Coal + HO	0.08	0.77
Coal + HO + AO	0.07	1164
Coal + IA-HO + o Cresol	1.82	0.52

ACKNOWLEDGMENTS

Authors are very greatfull to Colciencias, Ecocarbón, Universidad Nacional de Colombia for encouragement and support to enable this investigation.

REFERENCES

1. S. E. Moschophedis. Fuel No 59 (1980) 67.
2. J. Rincón, R. Angulo. Fuel No 65 (1985) 889.
3. J. Rincón, L. Pacheco and R. Rodríguez. 7th International Conference on Coal Science, Banff (1993). Elsevier Science B.V. p 560.
4. M. Zander, M.W. Haenel. Fuel No 69 (1990) 1206.
5. R.F. Rathbone, J.C. Hower and F.J. Derbyshire. Fuel No 72 (1993) 1177.
6. S. Moinelo, S. Menendez and J. Bermejo. Fuel No 57 (1988) 683.

Optical properties of SCT extraction residues obtained from Turkish coals

E.Sultan Vayisoğlu^{1,2*}, Keith D.Bartle¹, N.Gaye Erbatur¹

¹Leeds University, School of Chemistry, Leeds LS7 2LR, UK

²Cukurova University, Chemistry Department, 01330 Adana, Turkiye

Abstract

Two Turkish coals of rank high volatile bituminous and sub-bituminous C were subjected to supercritical toluene (SCT) extraction at 400°C and 100 atm. The solid products of SCT extraction were examined with a Leitz MPV microscope since reflectance studies can provide some useful insights into the mechanisms involved through SCT extraction. The disappearance of liptinites is a feature of the optical texture of coals subjected to supercritical toluene. Both residues of coals produced a high reflecting vitroplast. Infinite macerals of these residues increased and showed an increasing reflectance. No other alterations were observed for the inertinite macerals in SCT extraction residues.

1. INTRODUCTION

Supercritical gas extraction is a technique that exploits the solvent power of supercritical fluids at temperatures and pressures near the critical point. Under such conditions, the condensed phase will begin to volatilize, which is interpreted as the dissolution of condensed phase in the supercritical gas phase. At supercritical densities which are much larger than typical gas densities, the gas acts as a strong solvent for the condensed phase (1). Because of these properties supercritical gas extraction is a promising route for the production of liquid fuels and chemical feed stocks from coal. The conversion and properties of the extraction products are known to depend on coal rank (2-4), the solvent used and the process conditions (5-8).

In previous work, SCT extraction of Turkish coals and their maceral concentrates was studied to determine the yield and chemical properties of whole coal and maceral extracts (9,10). Reflectance studies of the solid products of liquefaction have the potential to provide some useful insights into the mechanisms involved through the differing responses to liquefaction and carbonization which are likely to be competing processes (11-13). The purpose of the present study, therefore, is to examine the properties of the residues and discuss the reactions occurring in the extraction.

* Present Address
Mersin University
Chemistry Department
33000 Mersin- Turkiye

2. EXPERIMENTAL

The bituminous coal is from Western Black Sea Region and it is a high-volatile bituminous type of upper carboniferous origin. The sub-bituminous coal is low rank coal of tertiary age and from Western Anatolia. Proximate and ultimate analyses and optical results both of raw coals and SCT extraction residues are given in Table 1. In the table, C I, C II, R I and R II were used to describe raw bituminous coal, raw sub-bituminous coal, residue of bituminous coal and residue of sub-bituminous coal, respectively. Both of the coals were subjected to supercritical toluene extraction, as previously reported(10).

The residues were embedded in an epoxy resin and polished with aluminum oxide powders. Examination was undertaken with a Leitz MPV-II reflected light microscope under oil immersion. Mean reflectance determinations for residues were performed on high-reflecting vitroplast.

Table 1
Analytical and petrographic results of the coals studied^a

Sample	C I	C II	R I	R II
V.M%	30.7	40.1		
C%	88.4	71.6	80.5	70.6
H%	4.8	5.2	3.9	4.5
N%	1.5	1.8	1.1	3.4
S%	0.6	3.7	1.0	3.4
O% ^b	4.7	17.7	13.5	18.1
%R _v	0.7-1.1	0.3-0.5	1.9-2.7	0.9-2.6

^a : The values are on maf basis

^b : By difference

3. RESULTS AND DISCUSSION

In coal liquefaction the objective is to cleave large aromatic molecules into smaller units and forming products of lower molecular weight. The success or failure of these objectives is usually measured by the solubility of products but can also be assessed by the distribution and characteristics of microscopically definable components of the insoluble residue(11).

There were notable differences in the appearance of the residues from bituminous coal and sub bituminous coal. Figure 1a and 2a are photomicrograph illustrating the microscopic appearance of the untreated bituminous coal and sub-bituminous coal. The bituminous coal has 85% vitrinite, 5% liptinite and 10% inertinite and the major petrographic constituent of the bituminous coal used is pseudovitrinite. In contrast, the abundance of liptinite is greater in the studied sub-bituminous coal which has 80% vitrinite, 15% liptinite and 5% inertinite and vitrinites are mostly telocollinite. The most interesting microscopical result for raw sub-bituminous coal is that the vitrinite maceral has a coke-like appearance. This is unusual for sub-bituminous coal from West Anatolia and it may show a coal which has been thermally affected during coalification(14).

Following the SCT extraction on vitrinite produced anisotropic semi coke in higher concentration whereas only a minor amount was seen in the sub bituminous coal vitrinite. Figure 2b shows that the vitrinite have passed through a thermoplastic stage producing the isotropic residue component vitroplast. When heated; vitrinites decomposes and devolatilizes, leaving rounded vacuoles. However, pseudovitrinite behaves different than telocollinite, simply because of its different structure and chemical composition. It forms a more solid texture with low porosity. This gives an explanation why bituminous coal

produced mostly anisotropic texture without pores. Vitrinite maceral of bituminous coal developed mostly coarse-grained anisotropic and high reflecting optical texture, possibly because of the large size of the molecules produced during the SCT (figure 1b). The presence of anisotropic semicoke is usually indicative of retrogressive cooking reactions (11). The anisotropic texture of SCT residue provides a insight into the size and mobility of the molecules involved.

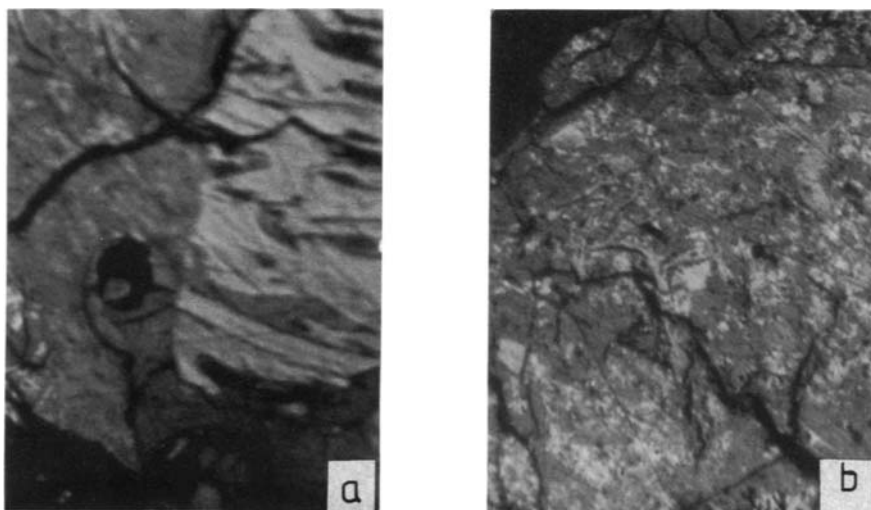


Figure 1. Photomicrographs of raw bituminous coal and SCT extraction residues a) raw bituminous coal b) anisotropic texture in residue of bituminous coal

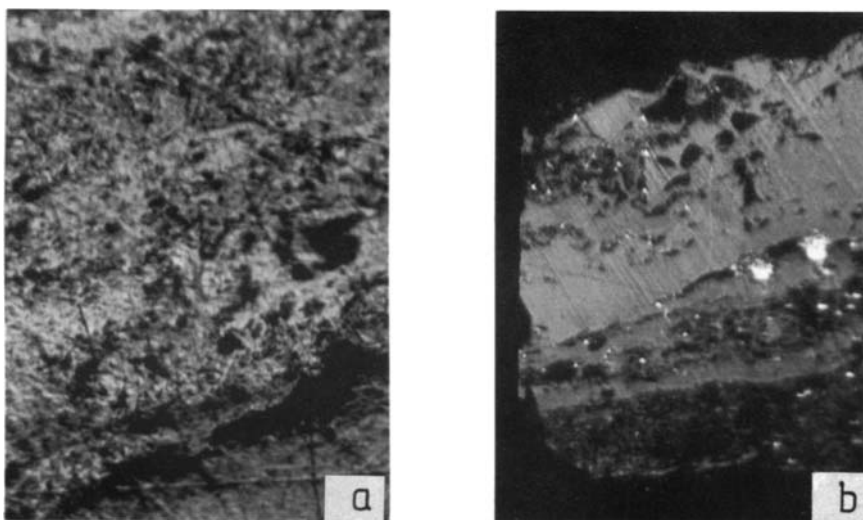


Figure 2. Photomicrographs of raw sub-bituminous coal and SCT extraction residues a) raw sub-bituminous coal b) isotropic texture in residue of sub-bituminous coal

The reflectance of anisotropic texture is differ between 2.36-5.00. Vitrinite maceral of bituminous coal developed mostly coarse grained anisotropic and high reflecting optical texture. Vitroplast which has been rendered both high reflecting and anisotropic is referred to as anisotropic semicoke. Some explanations may be offered to account for this occurrence in the vitrinite residue. The presence of anisotropic and high reflecting vitroplast suggests that, during extraction there was sufficient molecular mobility and planarity to form an ordered or stacked carbon structure. Because of this improved alignment of the aromatic structure, the residue should be extremely resistant to any further liquefaction. In addition, reflectance of residue is higher than raw coal which attests to the local dominance of condensation reactions following the production of these planar molecules. If the plastic mass is not effectively dispersed by vehicle solvent, the loss of porosity as the coal melts and tendency for the development of vitroplast could restrict the access of solvent to radicals as they form. When this situation arises polymerization of coal-derived materials can occur, leading to the development of a solvent-insoluble residue(11).

The reflectance differences of vitrinite maceral before and after SCT extraction are 0.80-2.73 and 0.65-2.60 for bituminous and sub-bituminous coals, respectively. The disappearance of liptinite maceral is a feature of the optical texture of coals induced by SCT extraction with toluene. However, literature data shows that inert material is not only inertinite but also liptinite is more stable especially in catalyzed liquefaction studies (11,15). Inertinite is the most stable maceral in both of the residues. We called them unreacted inertinites which is used to describe the macerals that no visible phase change was detected. However, inertinite maceral of SCT residues showed an increasing reflectance 2.00 to 3.80 and 1.20 to 2.40 for bituminous coal and sub-bituminous coal, respectively. The liptinite disappearance and increasing in inertinite shows the severity of reaction conditions. In sub-bituminous coal, the residue as well as the raw coal were found to be isotropic. The high reflectance of some vitroplast generated during SCT extraction of sub bituminous coal possibly a result of the smaller size and/or non-planar nature of the molecules involved. It is also the result of bond cleavage which suggests the dominance of thermal reactions(11). In addition, it shows that the vitrinite part of coal had depolymerized and condensed into an insoluble high molecular weight material. It is apparent that the optimum temperature for SCT extraction should be lower for the sub-bituminous coal used in this study than the bituminous coal.

REFERENCES

- 1) Deshpande, G.V., Holder, G.D., Bishop, A.A., Gopal, J. and Wender, I. *Fuel* 1984, 63,956
- 2) Kershaw, J.R., Overbeek, J.M. and Bagnell, L.J. *Fuel* 1985, 64, 1070
- 3) Stolarski, M. and Szezyguel J. *Fuel* 1991, 70, 1421
- 4) Cahill, P., Harrison, G. and Lawson G.J. *Fuel* 1989, 68, 1152
- 5) Ceylan, R. and Olcay, A. *Fuel* 1981, 60, 197
- 6) Kershaw, J.R. and Bagnell, L.J. *Fuel* 1987, 66, 1739
- 7) Amestica, L.A. and Wolf, E.E. *Fuel* 1984, 63, 227
- 8) Kershaw, J.R. J. *Supercrit. Fluids* 1989, 2, 35
- 9) Vayisoglu E.S., Erbatun, O., Bartle K.D., Erbatun N.G., Harput, B., Snape, C.E. and Garcia, R. *Fuel Proc. Tech.* 1993, 36, 25-32
- 10) Vayisoglu, E.S., Bartle, K.D., Erbatun, N.G., Frere, B and Snape, C.E., 1994 (Submitted to the *Fuel Process. Tech.*)
- 11) A.Davis., Mitchell, G.D., Deryshire, F.J., Rathbone, R.F. and Lin, R. *Fuel* 1991, 70, 352
- 12) Stolarski, M., Machnikowski, J. and Machnikowska, H. *Fuel* 1993, 72, 1497
- 13) Shibaoka, M. and Russell, N.J. in 'Proceedings of International Conference on Coal Science', Dusseldorf, 7-9, Verlag Gluckauf, Essen 1981, pp 453-458
- 14) Karayıgıt, A.I. Hacettepe University, Ankara (personal conversation)
- 15) Derbyshire, F., Davis, A., Epstein, M. and Stansberry, P. *Fuel* 1986, 65, 123

PERSPECTIVE IN RESEARCH OF COAL LIQUIDS BY USING SPIN PROBE TECHNIQUE

T.P.Miloshenko, S.A.Alekseev, A.A.Shklyaeu

Institute of Chemistry of Natural Organic Materials of Russian Academy of Science, Academgorodok, Krasnoyarsk, 660036, Russia

On example of some carbonaceous materials labeled with copper porphyrine complex, it was shown that the discrete stacks identical in their size and manner of packing effect a function of the carriers of the unpaired π -electrons as well as the primary building units. No doubt, the clarification of the paramagnetic centres, the application of high informative spin probe technique, especially, expands the possibilities of an ESR method in research and characterization on a molecular level of such extremely complicated and heteropolycondensed systems as coal liquids.

Various carbonaceous materials exhibit in ESR spectra the presence of high stable paramagnetic centres of organic nature. The exact nature of these centres has not so far remained unclear. As it has been pointed out earlier [1-3], the main contradictions concerning the origin of coal paramagnetism can avoid to assume that there exist distinct aromatic clusters or stacks which are capable to convert spontaneously to a stable paramagnetic state. This implies that ESR phenomenon is a co-operative effect attributed with the capability of a lot of the collectivized π -electrons within discrete stack to produce spin-unpaired paramagnetic states.

On the bases of this assumption, it is possible to interpret a non trivial, but unanswerable fact that the maximal content of spins which can be created in carbonaceous materials is limited. In fact, the same concentrations close to 10^{20} spin/g have been recorded for the pyrolyzed [1-5] or chemically oxidized [1,2] products. A cause of such limitation can be attributed to the conversion of all stacks to a paramagnetic state and the display of an effect of the saturation for a number of spins. One of the most reliable and convincing confirmation of the existence of the discrete stacks gives the results of ESR studies of coal structure with the aid of spin probe technique [3,6,7].

In this report, on two coals doped with copper porphyrine (CuP) complex, a high efficiency of spin probe technique in coal research was demonstrated. An original fashion of removal of the mineral inclusions through the initial inversion of the lowest rank coal in a water-soluble state was applied. It was emphasized that the so-called coal liquids contain large or even predominant amounts of high molecular immovable and rigid

blocks similar to the building elements of parent coals. As it may imanige, the further applications of stable paramagnetic complexes as spin probe allow better to characterize and investigate these systems.

CuP-LABELED COALS

Coals studied were the ordinary bituminous coal (C=85 %) and the demineralized water-soluble product derived from brown coal (C=69 %) after its special modification [8]. The mixture of coal, pyridine and CuP complex in the ratio approximately 1:1:0.1 was exposed at room temperature during two days.

Fig. 1 shows a plot upon a temperature of the intensities and linewidths of coal signals for the two parent and CuP-doped coals. Importantly, for both coals heated above 400°C, ESR parameters behave a similar way. The insertion of probes results in decreasing of the intensities with increasing of the linewidth of residual signals. Probably, the presence of mineral impurities gives rise to a drastic influence on ESR parameters of the heated above 550°C bituminous coal (Fig.1).

Fig.2 illustrates ESR spectra of the CuP-doped brown coal heated at 450 and 600°C. It is remarkable that for all centres at the high temperature range, single averaged by exchange broad and shifted lines are recorded. Hence, all areas of coal

matter convert ultimately to, a paramagnetic state. Spin exchange interactions are, sharply intensified with such conversion. The content of, spins after attainment of a maximum remains invariable in, the range from 550 to 700°C, (Fig.1).

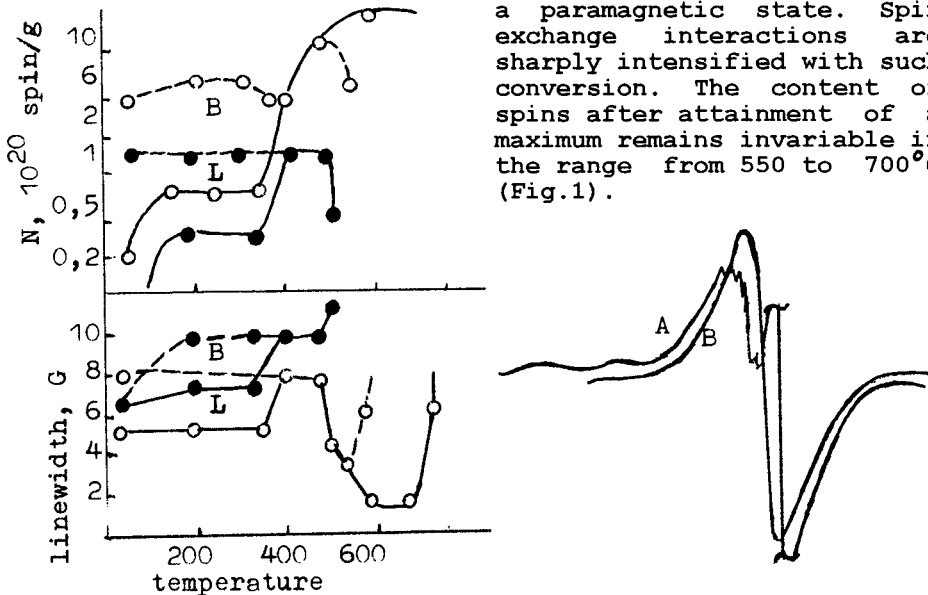


Fig.1 Effect of a pyrolysis temperature on the intensity and linewidth for (o) undoped and (●) CuP doped samples of (B) bituminous and (L) lowest rank coals.

Fig.2 ESR spectra of CuP-doped brown coal heated at A - 400 and B - 600°C.

The main statements, which can be made from ESR spectra of the CuP-doped coals, can be summary as following. First of all, in both coals, the same stacks effect a function of the trapps of the odd electrons. The stacks convert consecutively during pyrolysis to a stable paramagnetic state. An effect of the saturation for a number of spins occures when all the stacks become paramagnetic.

The size of the initialy paramagnetic stacks, which can be assessed from the magnititude of an additional linewidth increase caused by probes, is equal to 2.0 nm. [3,6,7]. It is remarkable that the same size of them follows also from concentration measurements. Indeed, the maximal number of spins ($\sim 10^{20}$ spin/g) are consistent again with the dimension 2.0 nm of the discrete paramagnetic units.

It needs to assume that the stacks differing in their accessibility and sensitivity to probes are compactly merged in the secondary more extended anisotropic blocks. These blocks carry out a function of the repeating elements on which are desintegrated solvent swollen coals. Clearly, these blocks are originally structurally anisotropic. In these blocks, every of the peripheral or surface stacks with the exception of the central are accessible to probes. This explains why the intensity of residual signals in the presence of probes is lowered on the same a factor of 15 (Fig.1) in comparision with its maximal value for the pyrolized undoped products. Hence, the seperate blocks involving about of 15 stacks and having a size of 6.0 nm function as the repeating units building the coal.

It is imazing that the anisotropic coal microdomain are created on a early stage of the coalification. The dictate of more compact packing requires the parallel packing of them. Hence, a close-range order must be present even in the lowest rank coal. The coal displaying the presence of structural anisotropy and periodicity in space should be classified as natural high molecular crystall.

COAL LIQUIDS

It is well known that soluble products extracted from a coal with good solvents repeat basically the parent material. This concern also of the water-soluble product studied. According to ^1H NMR data this product solvated in D_2O exhibits in NMR spectra the broad unstructural absorption belonging to the aliphatic protons. At the same time, the absorption corresponding to the aromatic protons is significantly smaller. This indicates strongly that a predominant part of coal substance remains in an unbroken solid state form. On the other hand, the profound structural rearrangments favouring to seperation of coal substance on the isolated microphases occures undobtedly during coal modification.

It is reasonable to assume that the so-named coal liquids, namely liquid phase products of coal liquefaction or hydrogenization, pitches, coal tars and another dirivatives of coal contain in their composition a large or even predominant

amount of high molecular components which are organized like to the parent coals. The preservation in ESR spectra of these materials of a large number of stable paramagnetic centres is consistent with this assumption.

Furthermore, in conformity with ESR data [1,3,7,9] the discrete paramagnetic stacks and anisotropic blocks analogous to the building units of the coal are present also in petroleum pitch, its isolated fractions. More probably, the identical stacks are responsible for paramagnetic properties of another carbonaceous materials independently upon their origin.

No doubt, the identification of the nature of paramagnetic centres gives us a powerful tool for structural research and characterisation on a molecular or submolecular level of such multicomponent and extremely complicated systems as coal liquids. The paramagnetic centres may consider natural spin probes ESR spectra of which are sensitive to their nearest environment, distribution, the impact of special solvents or impurities. The examples of such impurities of coal radicals are known [10,11].

The use of stable paramagnetic metal complexes as artificial spin probes with reference to carbonaceous materials enables to investigate and characterize of them in more detail. This concerns not only an of ESR, but NMR spectroscopy, too. Indeed, there is serious and entangled problem about the influence of paramagnetic species on the results of NMR measurements in both of liquid and solid phases. The use of spin probes makes possible to separate in common signals the contributions of the isolated microphases.

Finally, by using of the coal doped previously with some stable paramagnetic probes, the mechanism of the process occurring during coal liquefaction may be investigated in more detail. Thus, the application of spin probe technique opens wide perspectives in coal research.

REFERENCE

1. A.A.Shklyaev, T.P.Miloshenko and A.F.Lukovnikov, Chim. Tverd. Topl., No.2 (1988) 25,
2. A.A.Shklyaev, T.P.Miloshenko and A.F.Lukovnikov, Chim. Tverd. Topl., No.2 (1989) 26,
3. A.A.Shklyaev, Chim. Tverd. Topl., No.1 (1991) 37,
4. S.Mrozowski, Carbon, No.4 26 (1988) 521,
5. D.W.van Krevelan, in "Coal", Elsevier, Amsterdam, The Netherland (1969),
6. A.A.Shklyaev, T.P.Miloshenko and A.F.Lukovnikov, Chim. Tverd. Topl., No.6 (1988) 13,
7. T.P.Miloshenko, Ph.D. Thesis, Irkutsk University, USSR (1989),
8. T.P.Miloshenko, Yu.G.Golovin et al. Russian Patent No.93034073 (1993),
9. A.A.Shklyaev, T.P.Miloshenko and A.F.Lukovnikov, Chim. Tverd. Topl., No.1 (1988) 70,
10. A.A.Shklyaev, Chim. Tverd. Topl., No.3 (1992) 23,
11. A.A.Shklyaev, Chim. Tverd. Topl., No.4 (1992) 52,

HYDROPROCESSING OF AN ASPHALTENIC COAL RESIDUE

Benito, A.M., Martínez, M.T. and Miranda, J.L.

Instituto de Carboquímica. C.S.I.C. , P.O. Box 589. 50080-ZARAGOZA. SPAIN

A residue from deasphalting of coal liquids obtained by direct coal liquefaction of a subbituminous Spanish coal was processed by thermal and catalytic hydrotreatment under the conditions of hydrovisbreaking and hydrocracking respectively. The hydrotreatment reduced the viscosity of the starting material and the catalyst produced the inhibition of the coke formation.

1. INTRODUCTION

A residue from coal liquefaction or pyrolysis, a petroleum residue or a residual oil is characterised by a high viscosity, high heteroatoms and asphaltene contents, high molecular weight, high mean boiling point and low H/C ratio. Then, the objectives in the processes of hydrogen addition to residua or to heavy oils will be mainly to increase the H/C atomic ratio, to remove the metals and to reduce the heteroatom content (reaching a good desulfurization is specially important) to improve the product quality and to make easier the subsequent treatments [1].

The hydroconversion processes can be thermal or catalytic or consist of several thermal and/or catalytic stages. The hydroprocessing conditions currently used are high temperature and pressure, high hydrogen/feedstock ratios and high activity catalysts.

Among the processes of hydroconversion we focus our attention on hydrovisbreaking (thermal hydroprocessing) and hydrocracking (catalytic hydroprocessing). In the range of temperatures currently applied in hydroconversion processes, the driving force of the conversion reactions is essentially a thermal activation. The catalyst, the hydrogen pressure and the sophistication of the techniques basically limit and control the non-desirable side reactions of condensation [2]. These processes are very flexible and can be applied to a wide range of feedstocks from light naphthas to vacuum residues [3].

In this paper, a residue from deasphalting of coal liquids was processed by thermal and catalytic hydrotreatment under similar conditions to those used in hydrovisbreaking and hydrocracking processes respectively in petroleum industry. The aim of this work is to study the effect of the temperature and residence time during the hydroprocessing experiments by measuring the change produced in viscosity, coke content, elemental analysis and boiling point distribution.

2. EXPERIMENTAL

The material used in this work has been a residue from deasphalting of coal liquids obtained by direct liquefaction of a subbituminous Spanish coal. Operating conditions of the liquefaction and deasphalting processes have already been described in detail [4,5].

Experiments were conducted batchwise using 15 MPa of hydrogen pressure at the operating conditions. Temperature and residence time were the main variables modified during the processes. Experiments at 425, 450 and 475 °C of temperature and at 5, 10, 20, 30 y 40 minutes of residence time were carried out. A commercial catalyst, Harshaw HT-500E (Ni-Mo) was used in the hydrocracking process in a catalyst to sample ratio of 1/5.

The hydrovisbroken products obtained in each experiment were analysed for viscosity (measured at 65 °C with Canon-Fenske viscometers (ASTM D445, -86, ASTM D-446, -85)), coke content (determined by ultrasonic extraction as the material insoluble in toluene with a solvent to product ratio of 5), boiling point distribution (determined by gas chromatography in a Varian 3400 chromatographer with capillary SE 50 column and FID detector in the conditions: Injector temperature: 250 °C; detector temperature: 250 °C; initial temperature: 50 °C (5 minutes); final temperature: 300 °C and temperature gradient: 5 °C/ minute. Calibrating was carried out with several pure compounds (naphthalene, phenanthrene, fluoranthene and chrysene) and n-decane as internal standard was used for quantification), elemental analysis (C, H, N and S elemental analysis was carried out in an elemental analyser CARLO ERBA CHNS-O model EA1108)

3. RESULTS

The feedstock used in these experiments has a heavy nature (only 23.63 % boils under 350 °C and from the rest 14.95 % is coke) and it is characterised by a high viscosity (4608 cSt, 65 °C) and high heteroatom content (C:81.78%; H:6.38%; N:1.55%; S:4.65%;O:5.64%).

During the course of the reaction, the heavy fraction content (H) (b.p.< 350 °C) decreased with the time while the concentration of the light fraction (L) (b.p.>350 °C), gas (G) and coke (C) increased with the time (Figure 1).

The cracking reaction to produce light distillates followed a first order kinetic for all the temperatures essayed and a lineal correlation between coke and distillates has been observed in the hydrovisbreaking experiments. Taking into account that there is an hydrogen excess all the time and that the hydrogen pressure effect is the same in all the experiments, it can be considered that hydrogen concentration remains constant.

Kinetic study of both hydroprocessing treatments has been performed by proposing a first order mechanism. Two processes have been considered in this mechanism: 1)The cracking of the fraction with b.p.>350 °C to produce lighter structures (liquid fraction with b.p.<350 °C and Gases) and 2) the coke formation as a result of the condensation reactions produced in this

formation, has an activation energy much higher than the cracking reaction. Consequently, the coke formation was more important as the temperature increased. Thermodynamic control-like was observed in which as the temperature increased the tendency was to form the more stable product, in this case was the coke fraction that is a final product, because L and G fractions actually can condense to produce H.

At the lowest temperature essayed (425 ° C) the coke content hardly was modified with the time, but as the temperature went up an increase of C with the time was observed. The maximum coke percentage was reached at the more severe conditions used (475 ° C and 40 minutes) in which a light decrease in L was observed (Figure 1). Then at 425 ° C, a kinetic control seems to conduct the reaction. That is, the process with lower activation energy (cracking reaction) was more favourable and the reaction with higher activation energy (condensation reaction) remained almost completely inhibited.

In the catalytic hydroprocessing, the activation energy for the cracking reaction was found to be lower than on the hydrovisbreaking process and a total inhibition of the formation of coke was observed. Then, the effect of the utilised catalyst was reducing the activation energy for the cracking reaction making this process more favourable than the condensation reaction.

The maximum conversion to L obtained during the hydrovisbreaking experiments was 21 % and at these conditions (450 ° C, 40 minutes) the conversion to coke was 9 % and to gases 5%. During the catalytic process, the maximum conversion to L was 28 % and the conversion to gases was 7 %. Then, the catalyst has allowed a higher conversion to light products and the production of gases was lower.

The main effect observed in these experiments has been the inhibition of the condensation reaction to produce coke, as compared with previous studies of thermal treatment of the same residue done in our laboratory. A total inhibition of the coke formation has been observed when a catalyst was used.

In both processes, a sharp decrease of the viscosity with time and temperature was produced, going from 4600 cSt (at 65 ° C) in the starting residue to 147 cSt in the hydrovisbreaking process and to 79 cSt in the hydrocracking experiments.

Table 1.- Kinetic parameters obtained in the hydroprocessing experiments

Temperature (°C)	Hydrovisbreaking		Hydrocracking
	*k ₁ (s ⁻¹)	*k ₂ (s ⁻¹)	*k ₁ (s ⁻¹)
425	3.10 · 10 ⁻⁵	1.67 · 10 ⁻⁵	4.98 · 10 ⁻⁵
450	7.50 · 10 ⁻⁵	3.71 · 10 ⁻⁵	6.16 · 10 ⁻⁵
475	9.59 · 10 ⁻⁵	8.89 · 10 ⁻⁵	12.60 · 10 ⁻⁵
Ea(kJ/mol)	97	145	80

*k₁ kinetic constant for the cracking reaction

k₂ kinetic constant for the coke formation

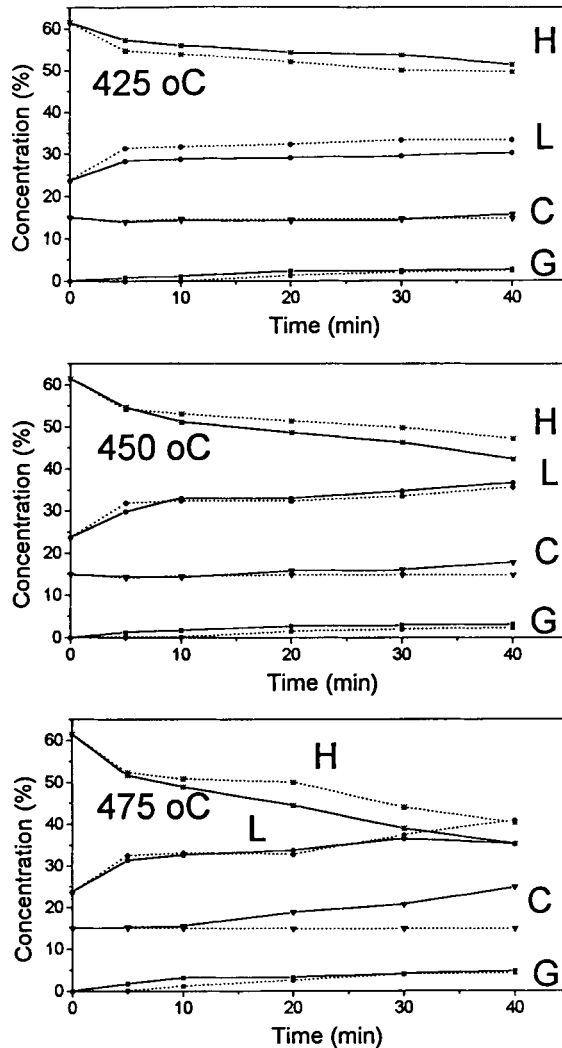


Figure 1.- Evolution of the heavy (H), light (L), gas (G) and coke (C) fractions during the hydroprocessing experiments (the solid lines represent the hydrovisbreaking experiments and the dot lines represent the hydrocracking experiments).

REFERENCES

1. Teichmann, D.P. Hydrocarbon Processing, 1982, 61(5), 105.
2. Sikoma, J.G., Hydrocarb. Proc., 1980, 59(6), 73.
3. Mavity, V.T., Ward, J.W. and Whitebread, K.E. Hydrocarbon processing, 1978, 57(11), 157.
4. Benito, A.M., Brower, L., Martínez, M.T., Severin, D. and Fernández, I. Accepted for publication in Fuel Science and Technology International (17-2-94).
5. Martínez, M.T., Fernández, I., Benito, A.M., Cebolla, V., Miranda, J.L. and Oelert, H.H., Fuel Processing Technology, 1993, 33, 159.

EFFECT OF LOW TEMPERATURE TAR UPGRADING CONDITIONS ON CHEMICAL COMPOSITION OF FUEL FRACTIONS

E.Śliwka and J.Surygała

Institute of Chemistry and Technology of Petroleum and Coal, Technical University of Wrocław, Poland

1. INTRODUCTION

Liquid products from processes of the low temperature pyrolysis of low rank coals can be used as raw materials for the production of fuel fractions [1]. The effectiveness of the upgrading process and the product composition depend both on the chemical structure of the raw material and the process conditions [2].

In this study, the oil components separated from tar obtained in the process of the low temperature pyrolysis of "Turów" brown coal were hydrogenated into fuel fractions. The effect of the process temperature, the hydrogen pressure, the liquid space velocity and the type of the catalyst used on the yields and the chemical composition of the fuel fractions has been investigated.

2. EXPERIMENTAL

The hydrogenation runs were carried out in a continuous flow laboratory unit with a "dropping bed" type reactor of 120 cc capacity.

The catalysts used were selected on the basis of their activity measured in the hydrogenation and the heteroatom removal from model compounds reactions [3]. The following catalysts were used: Am. Cyan. Co. HDS-1442B (CoMo/Al₂O₃) and Leuna-Werke No 8199/K (NiMoAl₂O₃). They were presulphided before the reaction. [4].

Distillate boiling in the range of 220-495 C separated from "Turów" brown coal tar was used as the raw material. Its chemical structure and composition had been investigated in our previous study [5]. Roughly, it contained about 14 wt % of the paraffin-naphthenes fraction, 20 wt % of aromatic hydrocarbons and more than 60 wt % of resins, including about 30 wt % of monocyclic phenols.

The tested range of parameters was as follows: temperature 340-400 C, hydrogen pressure 4-14 MPa, and liquid space velocity 0,5-2,0 h⁻¹.

The products were distilled into raw gasoline fractions boiling in the range of 20-200 C and raw fuel oil fractions boiling in the range of 200-350 C. The fuel oil fractions were subsequently separated into fractions and subfractions on alumina and silica gel, using an open-column separation technique described elsewhere [5]. The individual subfraction compositions were determined by the GC/MS method on a Hewlett Packard 5890 II chromatograph equipped with a 25 m HP-5 capillary column programmed for the temperature range of 50-290 C. The chromatograph was directly interfaced with a

Hewlett Packard mass detector. The samples dissolved in CHCl_3 , concentrations were determined on the basis of integrated peak areas.

3. RESULTS AND DISCUSSION

Almost all the classes of compounds present in the raw material were found in the hydrogenation products, which suggests incomplete conversion of even so reactive components as monocyclic phenols or methoxyphenols (table 1). Nevertheless, no oxygen compounds were found in the raw gasoline fraction (figure 1).

Table 1. Effect of reaction conditions on the products composition

Components	Raw material	Products from conditions					
		CoMo, 14 MPa		CoMo 380°C		400°C, 14 MPa	
		Temperature, °C		Pressure, MPa		Catalyst	
		340	400	14	4	CoMo	NiMo
Contents, wt %							
aromatics	26.3	43.8	32.4	31.8	66.4	32.4	28.0
resins	57.9	4.1	0.4	0.8	20.5	0.4	1.9
Yields, wt %							
raw gasoline fraction		13.8	37.3	28.1	8.7	37.3	33.2
raw fuel oil fraction		86.2	62.7	71.9	91.3	62.7	66.8
Selected compound classes, %							
Cycloalkanes	4.0	9.2	19.4	17.4	5.8	19.4	22.6
Alkylbenzenes	2.1	5.1	12.1	10.1	5.6	12.1	10.4
Dihydroindanes	0.5	4.1	4.9	4.8	2.7	4.9	4.7
Tetralins	0.5	6.8	9.5	11.3	4.6	9.5	9.4
Naphthalenes	6.9	1.7	1.8	1.3	8.1	1.8	1.9
Phenanthrenes + pyrenes	4.5	1.3	1.2	0.8	3.3	1.2	1.0
3-4 ring naphthene-aromatics	4.5	6.7	1.9	1.9	2.3	1.9	1.9
Monocyclic phenols	29.7	2.7	0.1	0.2	17.2	0.1	0.5
Dihydroxylic phenols	5.6	0	0	0	0	0	0
Naphthalenols and indanols	5.6	1	<0.1	<0.1	1.3	<0.1	0.3
Methoxyphenols +							
Methoxybenzenes	8.4	0.3	<0.1	<0.1	1.0	<0.1	0.1

3.1. Effect of temperature

In the tested range of temperatures (340-400°C), the resin content decreased from about 58 wt % in the raw material to about 4 wt % in the products at 340°C and to 0.4 wt % in the products at 400°C. At the same time, the aromatic content increased from 26 wt % in the raw material to 44 wt % in the products at 340°C but then decreased with an increasing temperature to 32 wt % at 400°C. The first effect is due to the conversion of phenols into appropriate aromatic compounds and the second one to the of saturation of some aromatic compounds to hydroaromatic derivatives.

The raw gasoline fraction yields increased from 14 % wt at 340°C to 37 wt % at 400°C, while the raw fuel oil fraction yields decreased from 86 wt % to 63 wt %.

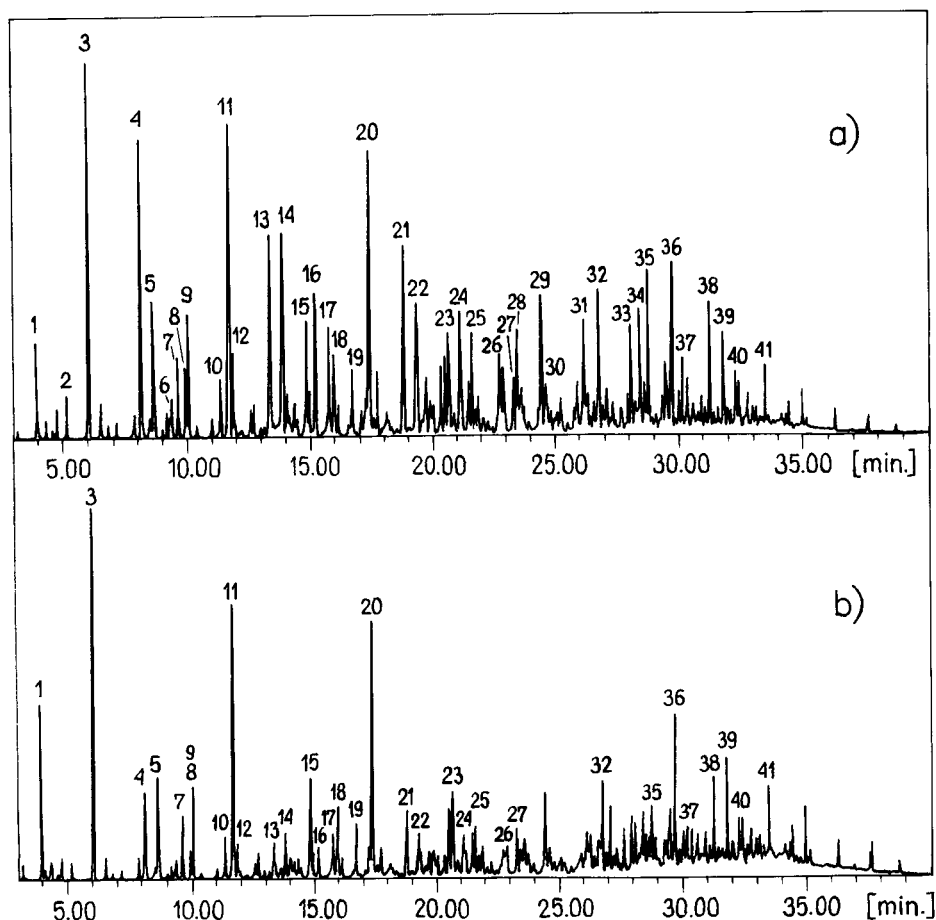


Figure 1. Gas chromatogram (total ion monitoring) of raw gasoline: a) CoMo catalyst, b) NiMo catalyst (400°C, 14 MPa, 0,5 h⁻¹) 1-cyclohexane, 2-heptane, 3-methylcyclohexane, 4-toluene, 5,6,7,9,10-dimethylcyclohexane, 8-octane, 11-ethylcyclohexane, 12-trimethylcyclohexane, 13-ethylbenzene, 14,16-xylenes, 15,18,19-ethylmethylcyclohexanes, 17-nonane, 20-propylcyclohexane, 21-propylbenzene, 22-ethylmethylbenzene, 23-octahydroindan, 24,26-trimethylbenzenes, 25-decane, 27-butylcyclohexane, 28-alkylbenzene, 29,31-propylmethylbenzenes, 30-butylbenzene, 32-undecane, 33,34-methylindanes, 35-tetralin, 36-dodecane, 37,38-methyltetralines, 39-tridecane, 40-dimethyltetralin, 41-tetradecane.

Under the reaction conditions used in this work, naphthalenes, phenathrenes, pyrenes, fluorenes, and 3-4 ring naphthene-aromatics were hydrogenated to quite a high degree. Monocyclic phenols, naphthalends, indanoles, methoxyphends, methoxybenzenes, dihydroxyphenols and phenanthrols were hydrodeoxygenated also

to a large degree. Similarly, the content of cycloalkanes, monocyclic aromatics, dihydroindenes, and tetra-lins increased markedly. The effect of temperature for all the reactions described below is advantageous (table 1).

3.2. Effect of hydrogen pressure

The effectiveness of aromatic hydrocarbons saturation is low at the hydrogen pressure 4 MPa. Similarly as that of the elimination of oxygen from phenolic compounds.

When the hydrogen pressure is increased to 14 MPa, this results in a significant increase in resin components conversion (over 20 times), a higher raw gasoline fraction yield (about 3 times) and a decrease in the aromatic hydrocarbon content (about double). The influence of hydrogen pressure on the hydrodeoxygenation of phenolic compounds is also noticeable, especially in the case of monocyclic phenols.

3.3. Effect of catalyst type

In the case of the NiMo catalyst at 400°C and 14 MPa, the raw gasoline fraction yield decreased from 32 to about 28 wt % and the degree of products refining decreased wt % slightly (1,9 wt % of resins) as compared to the CoMo catalyst in the same conditions. The NiMo catalyst affects mainly the higher aromatic hydrocarbons saturation degrees. There fore, the raw gasoline fraction obtained on the NiMo catalyst contained lighter and more saturated hydrocarbons than the ones obtained on the CoMo catalyst. (fig. 1).

4. CONCLUSIONS

In low temperature tar upgrading conditons, there are two key reactions: the hydrodeoxygenation of phenolic compounds and the saturation of aromatic rings. Both reactions are markedly temperature and hydrogen pressure dependent. The catalysts tested in this study work similarly, but in the same conditions, the CoMo one is better for hydrorefining reactions, whereas the NiMo one for ring saturatin reactions. The raw gasoline fraction yields 37 wt %, at 400°C, 14 MPa and 0,5 h⁻.

5. ACKNOWLEDGEMENTS

This work has been done within the framework of the Institute's (I-3) research program supported by the State Committee of Scientific Research. The authors acknowledge this financial support.

6. REFERENCES

1. J.H.Edwards, K.Schluter and R.J.Tyler, Fuel 65 (1986), 208.
2. J.H.Edwards, K.Schluter and R.J.Tyler, Fuel 64 (1985), 594.
3. J.Surygała, Ciecze węglowe. Budowa chemiczna i podatność na uwodornienie, Pr. Nauk. Inst. Technol. Nafty PWr., Monografia No 21, Wrocław, 1989. (in Polish).
4. J.Surygała, E.Śliwka and R.Wandas, 6th Int. Conf. on Coal Science Newcastle-upon-Tyne, UK, Sept. 16-20, 1991, Proceedings pp. 869-872.
5. E.Śliwka and J.Surygała, 7th Int. Conf. on Coal Science, Banff Canada, Sept. 12-17, 1993, Proceedings Vol.1 pp. 81-84.

Solvent effects of fractions from coal liquid on the upgrading reaction of coal liquefaction residue

Kiyoshi Mashimo, Motoyuki Sugano and Tohru Wainai

Department of Industrial Chemistry, College of Science and Technology,
Nihon University

1-8, Kanda Surugadai, Chiyoda-ku, Tokyo 101, Japan

Coal liquefaction residue (CLR) produced abundantly in the process of hydrogenolysis reaction of coal are constituted of the heavy materials of aromatic compounds with poor reactivities. Minerals in coal are also concentrated in CLR. However, it has been manifested that

dichloromethane soluble in CLR acts as a good hydrogen-donor¹⁾. Thus, the studies that utilize CLR as the useful carbon resources have been widely practiced. On the other hand, the primary hydrogenolysis products yielded simultaneously with CLR contain significant amounts of basic fraction²⁾, the secondary hydrogenolysis reactions for purposes of the effective denitrogenation of basic fraction are necessitated.

In this study, the co-upgrading reactions of mixture of CLR and coal liquid fraction were carried out, the synergistic effects for hydrogenolysis were investigated.

1. EXPERIMENTAL

1.1. Primary hydrogenolysis reaction of coal

Muswellbrook coal (30g) was hydrogenated with 40g of tetralin in a 200 cm³ autoclave at 400°C for 1 h under an initial pressure of 3.9 MPa. The hydrogenolysis products were separated into dichloromethane insoluble (coal liquefaction residue : CLR) and dichloromethane soluble (primary liquid oil : DS). Further, DS was separated into basic (B), neutral (N) and acidic (A) fractions by ion-exchange chromatography.

1.2. Secondary hydrogenolysis reactions

An amount (3.6g) of mixture of any one of A, N and B and CLR was further hydrogenated by adding 0.36g of red-mud and 0.036g of sulfur promotor as catalyst and 7.0g of decalin at 420°C for 1 h under an initial hydrogen

pressure of 5.9 MPa in a 200 cm³ autoclave, dichloromethane insoluble (DI) and dichloromethane soluble (secondary liquid oil) were obtained. Similarly, each hydrogenolysis reaction of B, N, A and CLR alone was also carried out. The secondary liquid oil was further extracted with hexane in a Soxhlet extractor. Hexane soluble (HS), and hexane insoluble and dichloromethane soluble (HIDS) materials were prepared.

2. RESULTS AND DISCUSSION

2.1 Properties of the primary hydrogenolysis products

The conversion of the coal was 50%. Because the proportion of yields of CLR and DS showed a ratio of 55 to 45, the proportion of CLR to each fraction in the secondary hydrogenolysis reactions was prepared at the same ratio. DS consists of 48% of basic, 39% of neutral and 13% of acidic fractions. B consists of nitrogen heterocyclic aromatic compounds having pyridine skeleton. N is mainly constituted of long straight-chain alkanes and aromatic compounds with long chain alkyl groups. A consists of polycyclic aromatic compounds containing oxygen functional groups such as phenolic hydroxyl group and carboxyl group.

2.2. Secondary hydrogenolysis reactions

The yields of constituents derived from the secondary hydrogenolysis reactions of single samples are shown in Figure 1. The yields in the secondary hydrogenolysis of mixture of CLR and any one of B, N and A are shown in Figure 2. Further, by using the results in Figures 1 and 2, and the equations (1) and (2), the increase and decrease in the yields of constituents was calculated from the yields in the reactions of each sample alone in addition to the yields in the reactions of mixture of CLR and any one of B, N and A. The variation in the yield of each constituent is shown in Figure 3.

$$\text{Yield (\%)} = F_{\text{mix}} - \left(F \times \frac{W}{W_{\text{mix}}} + F_{\text{CLR}} \times \frac{W_{\text{CLR}}}{W_{\text{mix}}} \right) \quad (1)$$

$$W_{\text{mix}} = W + W_{\text{CLR}} \quad (2)$$

where W and W_{CLR} are amounts (g) of liquid oil fraction and CLR, respectively. F_{mix} is yield (%) of each constituent from the secondary reaction of mixture, F and F_{CLR} are yields (%) of constituents from the secondary reactions of liquid oil fraction alone and CLR alone, respectively.

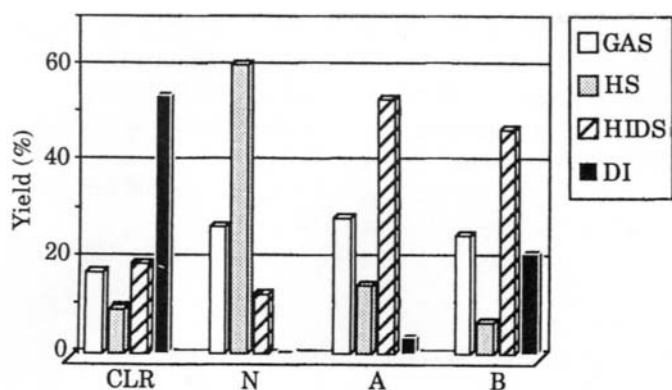


Figure 1. Secondary hydrogenolyses of single samples

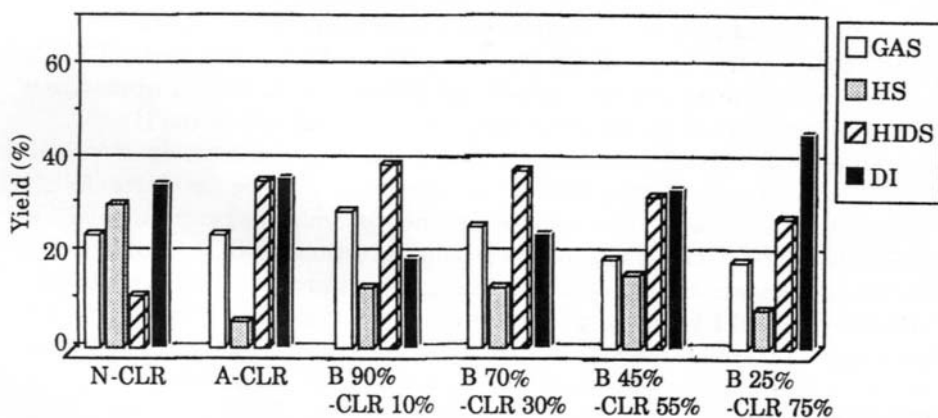


Figure 2. Secondary hydrogenolyses of mixture of CLR and any one of N, A and B

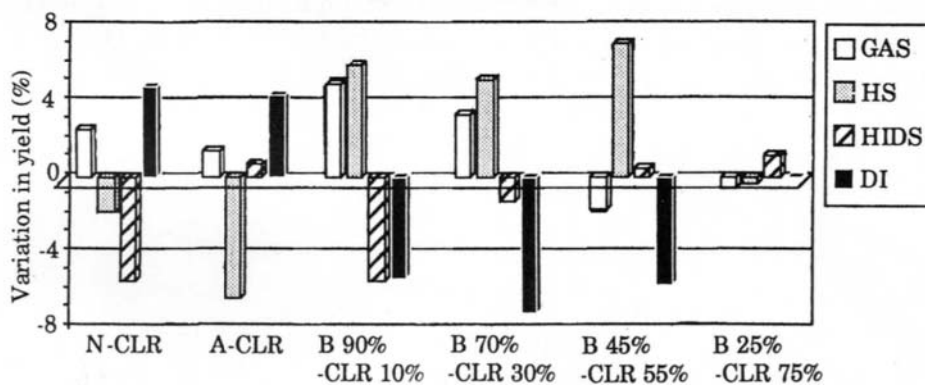


Figure 3. Variation in yields by the hydrogenolyses of mixture of CLR and any one of N, A and B

2.2.1. Reaction of CLR with neutral oil fraction (N) or acidic oil fraction (A)

In the reaction of mixture of CLR and N, the decreases of HS and HIDS and the increase of DI were observed. The catalyst deactivation occurred by the adsorption on the catalyst surface of highly condensed aromatic compounds in CLR. Therefore, the hydrogenolysis of aromatic compounds in N and the conversion of CLR to dichloromethane soluble were inhibited. In the reaction of mixture of CLR and A, since there were little interaction between CLR and phenols in A, the conversions of A to HS and CLR to dichloromethane soluble were inhibited by the catalyst deactivation described above.

2.2.2. Influence of composition changes in the reaction of CLR with basic oil fraction (B)

The reactions of various proportions of CLR and B were carried out. The degree in the increase and decrease of each constituent produced was calculated by the equations (1) and (2). The results are also shown in Figure 3. As shown in this figure, in the reaction of 10% of CLR, the yields of gas and HS increased, and those of HIDS and DI decreased. As the proportions of CLR were taken at higher concentration, the yields of gas and HIDS decreased and increased, respectively. Especially, in the reaction of 55% of CLR, the synergistic effects such as the increase of HS and the decrease of DI were observed. However, the effects were not found in the reaction of 75% of CLR. Therefore, in the reactions of the concentrations of CLR from 10% to 55%, B that penetrated into the structures of CLR promotes the dissolution and dispersion of CLR. The poisoning for catalyst is not easy to occur compared to the reaction of B or CLR alone, the synergistic effects appear.

REFERENCES

1. S. Futamura and K. Ohkawa, 1993 Proc. Int. Conf. on Coal Sci., II p.509
2. M. Sugano, K. Mashimo and T. Wainai, J. Japan Inst. Energy, 73, 203 (1994)

ZEOLITE CATALYST FOR HYDROCRACKING COAL-DERIVED DISTILLATES

–Cleavage of naphthenic rings over zeolite catalysts–

T. Kameoka^a, K. Masuda^a, A. Kinoshita^a, T. Sato^b, Y. Yoshimura^b, H. Shimada^b, N. Matsubayashi^b and A. Nishijima^b

^aCatalyst and Chemicals Industries Co.,Ltd,

13-2, Kitaminato-machi, Wakamatsu-ku, Kitakyushu-shi, 808, Japan

^bNational Institute of Materials and Chemical Research,

1-1, Higashi, Tsukuba, Ibaraki, 305, Japan

1. INTRODUCTION

Since unconventional feedstocks contain large amounts of aromatics and hetero-atoms, insufficient hydrocracking of aromatics occurs in a one-stage process. Therefore, conversion of polyaromatic hydrocarbons in middle and heavy distillates to lighter fractions using hydrocracking will best proceed via two fundamental steps. In the first step the aromatics are hydrogenated. In the second step these reduced aromatics are hydrocracked. Accordingly, two kinds of catalysts, each possessing higher hydrogenation or hydrocracking activity, are required for the two-stage upgrading [1,2]. In the course of research and development of the hydrogenation and hydrocracking catalysts, we had successfully developed a Ni-W/Al₂O₃ catalyst for the first-stage upgrading of coal-derived liquids [3,4].

In this work a new type of hydrocracking catalyst was designed for the second-stage upgrading. Optimizations of catalyst supports (a mixture Y-zeolite and alumina) and metal loadings (Ni-W, Ni-Mo and Co-Mo) of hydrocracking catalysts were performed in order to develop a new types of hydrocracking catalyst with high activity and long life.

2. EXPERIMENTAL

2.1. Catalyst

In the screening of hydrocracking catalysts, various kinds of catalysts were prepared by changing types of supports, active metal combinations and active metal loading. Mixtures of zeolite and alumina were prepared as supports of the hydrocracking catalysts. Y-type zeolite, mordenite and ZSM-5 type zeolite were selected among various zeolites because of higher hydrocracking activities. In some cases alumina and double oxides supports such as SiO₂-Al₂O₃ and B₂O₃-Al₂O₃ were used for preparing hydrocracking catalysts.

Table 1. Properties of distillates obtained from Brown-CDO

Feed	Brown-CDO
Specific gravity (15/4°C)	0.85
C (wt %)	87.4
H (wt %)	13.2
N (wt ppm)	125
S (wt ppm)	86
O(diff) (wt %)	5.1
H/C (-)	1.80

Boiling range (vol %)	
15~180°C	44.7
180~250°C	44.2
250~350°C	10.3
350°C*	0.8

¹ H-NMR	
H _a	5.3
H _α	12.1
H _β	57.3
H _γ	25.4

Active metal combinations selected were Mo, Ni-W, Ni-Mo and Co-Mo. Total active metal loadings on the catalysts were varied 10 to 35 wt% as WO_3 . Before reaction, each catalyst was subjected to pre-sulphurization (5 vol% $\text{H}_2\text{S}/\text{H}_2$, 400 °C, 2 h, 200 ml/min).

2.2. Model test Reactions

Model test reactions were carried out using batch type reactors in order to evaluate hydrocracking (HC) activities of the catalysts prepared. Reaction conditions of hydrocracking are as follows; initial H_2 pressure, 6.9 MPa; reaction temp., 400 °C; reaction time, 1 h; catalysts, 0.3 g; tetralin, 10 ml. The HC activities of naphthenic ring cleavage were calculated using yields of cyclohexane, benzene, alkylbenzenes and paraffins which were produced from tetralin.

2.3. Second-stage upgrading of a coal-derived liquid

The first-stage upgrading of a kerosene fraction obtained from Brown coal (Table 1) was carried out over the Ni-W/ Al_2O_3 catalyst using a continuous flow reactor. The second-stage upgrading was then carried out over newly prepared catalysts using a product of the first-stage upgrading. Reaction conditions of the second-stage upgrading are as follows; H_2 pressure: 6.9 MPa, reaction temp.: 370 °C, LHSV: 2.0 h^{-1} , H_2/Oil : 1000 NI/l, catalyst: 15 ml.

2.4. Analysis of feedstock and products

A gas chromatography with FID detector was used for the analysis of the feedstock and products.

3. RESULTS AND DISCUSSION

3.1. Catalyst support

Figure 1 shows typical results of model test reactions obtained over various sulfide catalysts. A mixture of Y-zeolite and alumina gave the highest HC activity among various supports prepared. Efficient HC activities were not obtained over sulfide catalysts based on double oxides and alumina support. The HC activity of the catalyst based on Y-zeolite was much higher than those based on other zeolite as shown in Figure 2. These results clearly show that the based on Y-zeolite is most effective for cleavage of naphthenic rings.

3.2. Active metal loading

Effect of active metal loading on HC activities of the sulfide catalysts is shown in Figure 3. When the mixture of Y-zeolite and alumina was used as the support of the sulfide catalysts, HC activities increased in the order of $\text{Mo} \ll \text{Co} < \text{Mo} < \text{Ni} < \text{Mo} < \text{Ni} < \text{W}$. From these results the active metal combination

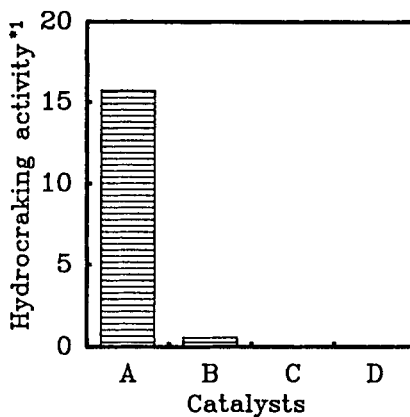


Figure 1. Hydrocracking activity of nickel-tungsten sulfide catalysts over various supports.

A, Y-zeolite- Al_2O_3 ; B, B_2O_3 - Al_2O_3 ; C, SiO_2 - Al_2O_3 ; D: Al_2O_3 . *1: Total yields of cyclohexane, benzene, alkylcyclohexane types, alkylbenzene types and paraffin types.

Tetralin was used as a model compound for evaluating hydrocracking activity.

Reaction conditions are as follows: H_2 initial pressure, 6.9 MPa; Reaction temperature, 400 °C; Reaction time, 1 h; Cat., 0.3 g; Tetralin, 10 ml.

of Ni and W was selected as active species of the zeolite catalyst for the second-stage upgrading.

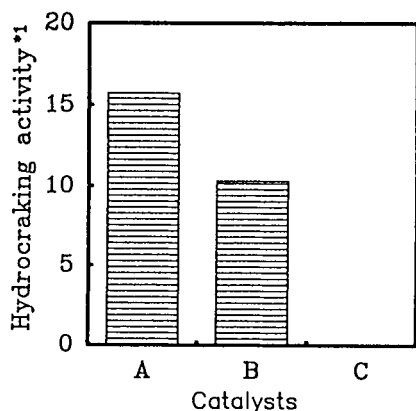


Figure 2. Hydrocracking activities of nickel-tungsten sulfide catalysts over various zeolite supports.

A, Y-zeolite; B, Mordenite; C: ZSM-5.

*1: Total yields of cyclohexane, benzene, alkylcyclohexane types, alkylbenzene types and paraffin types.

Reaction conditions are the same as described Figure 1.

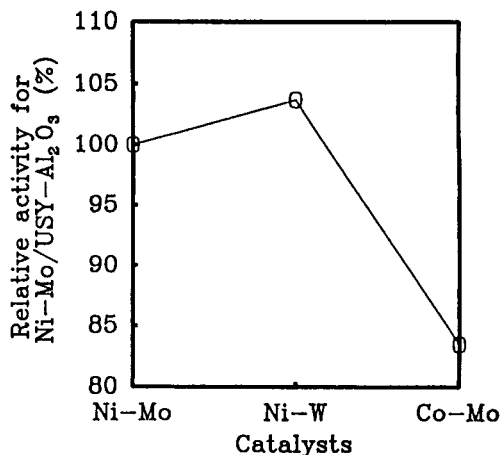


Figure 3. Hydrocracking activities of sulfide catalysts over various active metal species.

Reaction conditions are the same as described Figure 1.

3.3. Preparation of zeolite catalyst

Since research using model test reaction (hydrocracking of tetralin) showed that Ni-W catalyst based on Y-type zeolite gave the highest HC activity among various catalysts prepared, we decided to develop a Ni-W/Al₂O₃-Y-zeolite catalyst. In the course of research and development of the Ni-W/Al₂O₃-Y-zeolite catalyst, optimizations of support and active metal loading were carried out to enhance HC activity of the zeolite catalyst. Because the Y-zeolite must be thermally stable and nitrogen-tolerant, basic synthesized zeolite zeolites were highly modified. Dealuminated USY(Ultra Stable Y)-zeolite was applied to prepare a support of the hydrocracking catalyst. Then the ratio of USY-type zeolite and alumina was controlled to give the highest hydrocracking activity. The mixture of USY (60wt%) and Al₂O₃ (40wt%) was selected as the support. Physical and chemical properties of Al₂O₃ were also optimized. As active species, active metal loading of Ni and W was optimized for getting a superior hydrocracking activity and long life. Finally, 3.5wt%NiO-24.2wt%WO₃/USY-Al₂O₃ catalyst was designed and developed.

3.4. Hydrocracking of coal-derived liquids

After the first-stage upgrading of the coal-derived middle distillates, the zeolite catalyst developed was applied to the second-stage upgrading. Lighter fractions were successfully obtained in a great yield over newly prepared catalyst. This newly prepared catalyst showed superior hydrocracking activity as compared to a reference catalyst which was selected among commercially available ones because of the highest hydrocracking performance(Figure 4).

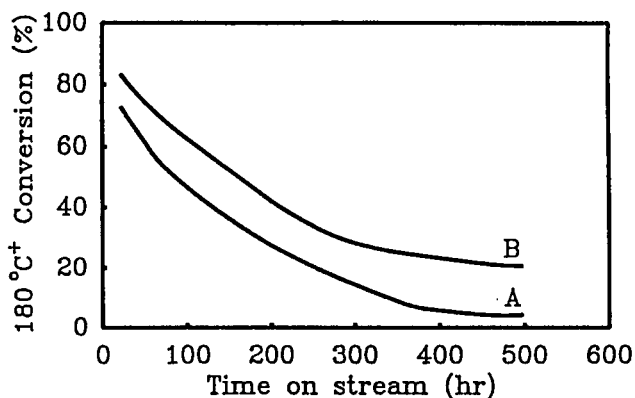


Figure 4. Deactivation of hydrocracking activity during accelerated aging tests.

A: Reference catalyst, B: 3.5wt%NiO-24.0wt%WO₃/US-Y-Al₂O₃ catalyst developed.

Reaction conditions are as follows: H₂ pressure, 6.9 MPa; Reaction temperature, 370 °C; LHSV, 2.0 h⁻¹; H₂/Oil, 1000 NI/l, Cat, 15 cm³.

ACKNOWLEDGMENT

The authors would like to thank New Energy and Industrial Technology Development Organization (NEDO) for permission to publish this paper.

REFERENCE

1. E.C.Maun, G.J.Thompson, J.K.Gorawara, D.K.Sullivan, Two-stage hydrodesulfurization and hydrogenation process for distillates hydrocarbons, U.S.Patent, 5, 114, 562 (to UOP).
2. J.W.Ward, Fuel Processing Technology, 35, 55 (1993).
3. A.Nishijima, S.Yoshitomi, T.Sato, Y.Yoshimura, H.Shimada, N.Matsubayashi, and E. Games, Poac. Intern. Conf. Coal Science, 763, (1987).
4. H.Shimada, T.Kameoka, H.Yanase, M.Watanabe, A.Kinoshita, T.Sato, Y.Yoshimura, N.Matsubayashi, and A.Nishijima, 10th International Congress on Catalysis, 288, (1992).

Remarkable Increase of BTX Yield by Zeolite Catalyst in the Hydrocracking of Coal Volatile Matter

M. Chareonpanich, Z.-G. Zhang, A. Nishijima* And A. Tomita

Institute for Chemical Reaction Science, Tohoku University,
Sendai 980-77, Japan

* National Institute of Materials and Chemical Research,
Tsukuba 305, Japan

1. INTRODUCTION

One possible way to economically utilize coal would be the production of as much as high value-added chemicals like BTX (benzene, toluene, xylenes) and PCX (phenol, cresols, xylenols), followed by using the residue as energy sources. The hydrolysis process is suitable for this purpose, but the yields of BTX and PCX are not satisfactorily high in most cases¹. We have proposed a post-cracking of nascent volatiles, and have achieved a high BTX yield, 14 wt%(daf), by using a two-stage reactor, where coal was pyrolyzed in the first stage and the volatile matter was hydrocracked over ultrastable Y-type zeolite (USY-zeolite) catalyst in the second stage under a high-pressure hydrogen². To our best knowledge, this is the first attempt to use a metal-free zeolite catalyst to upgrade heavy hydrocarbon feedstocks. In order to check the catalyst life, we carried out continuous pyrolysis experiments at a high hydrogen pressure. Preliminary data will be presented in this paper. The second object of this paper is to carry out model reactions over USY-zeolite under a high pressure hydrogen. Some two- or three-ring aromatic compounds which are found in coal volatile matter were similarly treated as above. The reactivities and the reaction pathways during the conversion of heavy hydrocarbons into lighter products were analyzed.

2. EXPERIMENTAL

Continuous catalytic reaction was carried out by pyrolyzing coal at 800°C in a free fall reactor and then the evolved volatile matter was hydrotreated at 600°C by using USY-zeolite. The coal feeding rate was 0.1 g/min and hydrogen pressure was 5 MPa. The coal used in this study was Taiheiyo coal, a Japanese subbituminous coal. USY-zeolite mixed with Al₂O₃ at a ratio of 6 : 4 by weight was used as a catalyst.

Commercial grade diphenyl methane, 1-methyl naphthalene, anthracene and phenanthrene were used as model compounds of coal volatile matter. The reactor used for model reactions was the same as used in the previous study³. H₂ pressure was 5 MPa unless otherwise stated. The H₂ flow rate was controlled at 200 ml (STP) min⁻¹. Model compounds in the first stage were vaporized at the temperature close to their boiling points, and then the vapor was introduced into the second stage packed with 800 mg of zeolite catalyst. The temperature of the second section was controlled at a constant temperature ranging from 300 to 600°C. The contact time of the model compound with catalyst was about 10 s at 600°C. The products were analyzed by gas chromatography.

3. RESULTS AND DISCUSSION

3.1. Effect of USY-zeolite catalyst on the hydrotreating of coal volatile matter

The high activity of USY-zeolite catalyst on the hydrocracking reaction of volatile matter from Millmerran coal has been reported elsewhere². Only a brief summary will be presented here. The BTX yield, under a hydrogen pressure of 5 MPa and at a secondary reaction temperature of 600°C, was 14.0 wt%(daf) with USY-zeolite whereas it was only 4.7 wt% without catalyst. Moreover, the presence of USY-zeolite significantly changed the product distribution pattern; the selectivity for lighter and less branched products was significantly increased. Tar and coke yields were quite small.

3.2. Continuous pyrolysis followed by a secondary catalytic reaction

It is very important for catalyst to have a long catalyst life. We have observed little change in the activity in the small-scale fixed-bed apparatus. Here, we set up a new pyrolyzer system to check the stability of catalyst by continuously feeding coal for a long time. A preliminary result in a continuous reactor showed a similar BTX yield, although the BTX yield in the uncatalyzed reaction was higher than that observed in the fixed bed reactor. The activity loss was not observed under the present conditions.

Wen and Cain⁴ have reported a high cracking activity of zeolite catalysts for the off-line cracking reaction of coal tar, but unfortunately the deactivation of catalyst took place quite rapidly due to coke formation. On the other hand, we did not observe such a severe deactivation in spite of a higher reaction temperature in our system. This is because we used hydrogen as a reaction medium instead of inert gas. Hydrogen is likely to remove most of precursors for coke formation.

3.3. Model reaction

The effectiveness of USY-zeolite catalyst in hydrocracking of diphenyl methane, 1-methyl naphthalene, anthracene, phenanthrene is shown in Table 1. The presence of catalyst considerably promoted the formation of BTX fractions in addition to light hydrocarbon gases. It is obvious that zeolite catalyst has not only a high hydrocracking activity but also a high hydrogenation activity, since it is generally said that the aromatic C-C bond is hardly cleaved without a prior hydrogenation. Figure 1 shows the effect of hydrogen pressure

Table 1 BTX yield without and with catalyst.

Compound	BTX yield (% , carbon)	
	No catalyst	USY-zeolite
Diphenyl methane	15	60
1-Methyl naphthalene	1	42
Anthracene	0.5	32
Phenanthrene	0.1	31

Hydrogen pressure: 5 MPa, Temperature: 600°C.

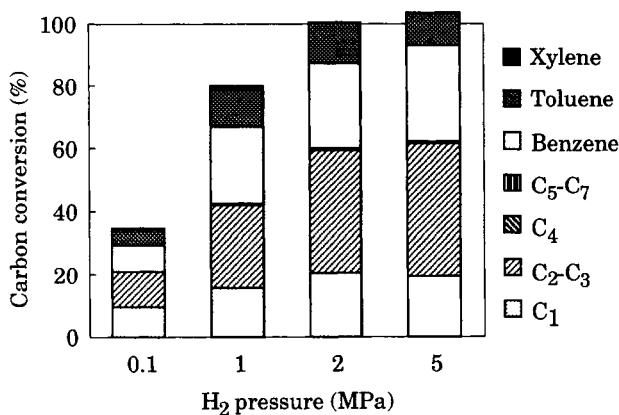


Figure 1 Effect of pressure on the product yield from 1-methyl naphthalene at 600°C.

on the reaction of 1-methyl naphthalene. The change in the product distribution pattern with pressure was small, but the total products yield increased with pressure until 2 MPa and beyond that the pressure effect became rather small.

Figure 2 shows the temperature effect on the reaction of phenanthrene. At 400°C, about 20 % of C₁-C₇ and about 20% of BTX were obtained. With an increase in temperature, the yield of lighter hydrocarbon gases increased. At 600°C, only C₁-C₃, benzene and toluene were main products, and the total carbon conversion was very close to 100%. This quantitative carbon conversion implies the almost negligible formation of other compounds including tarry materials and coke. Table 2 shows the product distribution at 600°C for other compounds. It is noteworthy that the results for 1-methyl naphthalene, anthracene and phenanthrene were similar to each other. The results at other temperatures were also similar to that shown in Figure 2 for the case of phenanthrene. The result for diphenyl methane was somewhat different from the others. It produced more BTX, 60% at 600°C. The BTX yield at 500°C, 77%, was even higher than at 600°C. The mass balance during the reaction of diphenyl methane was simply evaluated from the final yields. It is illustrated in Figure 3, where the following assumptions are made: (1) diphenyl methane was first hydrocracked to benzene and toluene and (2) the further cracking of toluene took place

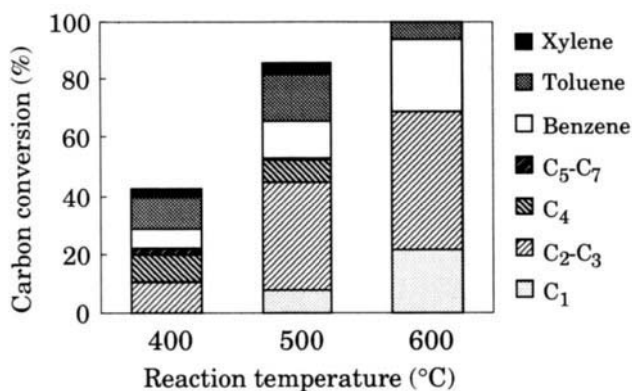


Figure 2 Effect of temperature on the product yield from phenanthrene at 5 MPa.

Table 2 Product yield with zeolite catalyst.

Compound	Product yield (% , carbon)			
	CH ₄	C ₂ -C ₄	Benzene	Toluene
Diphenyl methane	9	29	45	14
1-Methyl naphthalene	20	42	31	11
Anthracene	22	51	25	7
Phenanthrene	22	47	25	6

Hydrogen pressure: 5 MPa, Temperature: 600°C.

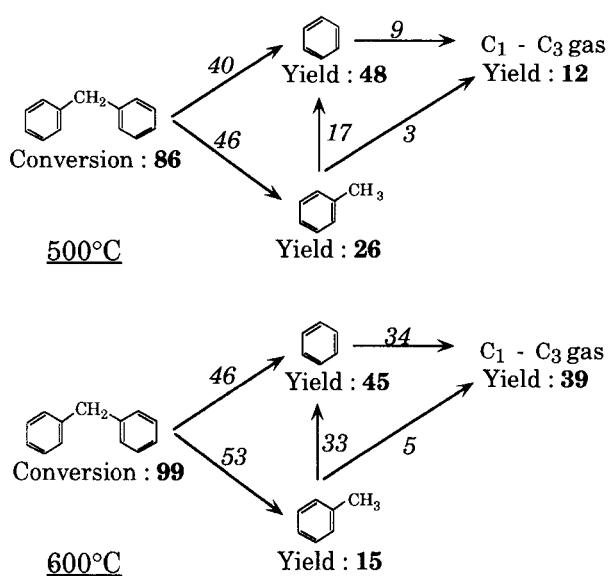


Figure 3 Mass balance in the reaction of diphenyl methane at 500 and 600°C.

only via benzene. Bold numbers indicate the conversion of starting material (100 parts in the beginning) and the final yields of the products, while italic numbers indicate the conversion rates. This Figure tells, for example, that 9 parts of benzene out of 57 parts were hydrocracked into light hydrocarbon gases at 500°C, and the extent of conversion increased to 43% (34 out of 79 parts) at 600°C.

Wiser *et al.* have reported the hydrogenation reaction of anthracene over Ni/W/S catalyst in autoclave⁵. The yield of BTX at 435°C after 200 min with a hydrogen pressure of about 10 MPa was less than 1%, whereas we obtained 20% of BTX at 400°C with a short contact time. The different reaction systems would be one of the reasons for this difference. Only a few studies have shown the activity of metal-free zeolite on the hydrogenation and hydrocracking reactions. Sano *et al.* showed for the first time a high activity of zeolite in the hydrogenation of ethylene and benzene^{6,7}. Hattori *et al.* have observed the formation of protonic acid sites on zeolite catalyst as a result of the interaction between Lewis acid sites and high-pressure hydrogen⁸. It is likely that the high cracking activity of zeolite in the present study is ascribed to the formation of protonic acid sites from molecular hydrogen. Of course the high-pressure hydrogen also accelerates the hydrogenation reaction, which lead to the increase of C₁-C₄ and BTX yields and the decrease of tar and coke yields. It seems that this reaction system would be promising for an effective conversion of heavy hydrocarbon resources into high-value added chemical feedstocks.

4. CONCLUSIONS

(1) Ultrastable Y-zeolite was active in the production of BTX from coal volatile matter. The deactivation of catalyst was not observed under the present conditions even in the continuous operation.

(2) The use of model compounds showed the high activity of zeolite catalyst in the hydrogenation and hydrocracking reactions.

ACKNOWLEDGMENTS

The authors wish to express their thanks to the Nippon Steel Corporation and Center of Coal Utilization, Japan for the financial supports.

REFERENCES

1. Nelson, P. F. and Tyler, R. J. *Energy Fuels* **1989**, *3*, 488.
2. Chareonpanich, Tomita, A. and Nishijima, A. *Energy Fuels*, **1994**, *8*, 1522.
3. Chareonpanich, M., Takeda, T., Yamashita, H. and Tomita, A. *Fuel* **1994**, *73*, 666.
4. Wen, W.-Y. and Cain, E. *Ind. Eng. Chem. Process Des. Dev.* **1984**, *23*, 627.
5. Wiser, W. H., Singh, S., Qader, S. A. and Hill, G. R. *Ind. Eng. Chem. Prod. Res. Develop.* **1970**, *9*, 350.
6. Sano, T., Hagiwara, H., Okabe, K., Takaya, H., Okado, H., Saito, K. *Sekiyu Gakkaishi* **1986**, *29*, 89.
7. Sano, T., Shoji, H., Okabe, K., Saito, K., Okado, H., Hagiwara, H., Hosoya, T. and Takaya, H. *Sekiyu Gakkaishi* **1986**, *29*, 257.
8. Tsuji, J., Ebitani, K., Hattori, H. and Kita, H. *React. Kinet. Catal. Lett.* **1992**, *48*, 17.

Hydrocracking Reactivities of Point of Ayr Coal Extracts from a Flowing-Solvent Reactor, a Mini-Bomb and a Pilot Plant

S-F. Zhang, B. Xu, A.A. Herod, D.R. Dugwell and R. Kandiyoti
Department of Chemical Engineering, Imperial College, University of London
London SW7 2BY, UK

1. INTRODUCTION

The structures of coal liquefaction extracts are known to change considerably with reaction conditions used during the extraction process. Clearly, the economics of coal liquefaction processes depend, among other factors, on the relative ease with which heavier coal extracts are converted to saleable products. In this paper, changes in the hydrocracking reactivity of coal extracts have been examined in terms of structural modifications induced by their previous process histories. The benchmark extract was prepared in a flowing-solvent reactor (FSR) where secondary reactions of extracts are suppressed by rapid removal from the reaction zone.

Point of Ayr coal liquefaction extracts from three sources have been included in the study: a bench scale flowing-solvent reactor using tetralin as vehicle (FSR: Sample S1), 10 and 60 min mini-bomb extractions in tetralin (MB: Samples S2 & S3, respectively) and a sample of extract from the digester of the British Coal Liquefaction Pilot Plant at Point of Ayr (Sample S4).

2. EXPERIMENTAL

Brief descriptions of the extracts have been presented in Table 1. The Pilot Plant sample was used 'whole', whereas the other three samples were extracted with pentane, to remove tetralin and its thermal reaction products, prior to hydrocracking. Details of the Pilot Plant¹, the mini-bomb² and the FSR have been reported elsewhere^{3,4}. The FSR is a fixed-bed reactor continuously swept by a solvent stream to remove solubilised products from the reaction zone in a matter of 6 - 10 s.

The hydrocracking step was carried out in a micro-bomb reactor⁵ (3 ml volume) in the presence of distilled tetralin, at 460 °C with 190 bar hydrogen; reaction times were between 30 and 150 min. Presulphided NiMo/Al₂O₃ (PBC-90D) was used as the catalyst (< 250 μm) with a feed ratio of 1: 0.5 : 5 (extract : catalyst : tetralin, by weight). Hydrocracked extracts have been assessed by TGA-distillation: boiling point distributions expressed as cumulative mass loss as a function of boiling point have been determined by a Perkin-Elmer TGA7 thermogravimetric balance. The method involves calibration of the TGA evaporation temperatures by true boiling points of pure standard compounds⁵. The calculation of mass loss was based on solvent free sample, i.e. amount of sample left after evaporation of tetralin and its light derivatives (b.p. < 210 °C - corresponding to 84 °C in TGA).

3. RESULTS AND DISCUSSION

Composition of untreated extracts: Figure 1 presents boiling point distributions of the set

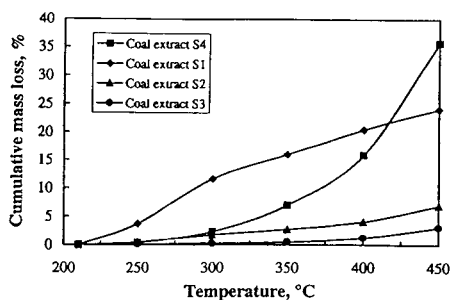


Figure 1 TGA-derived distillation curves: mass loss of coal extracts before hydrocracking; solvent free basis.

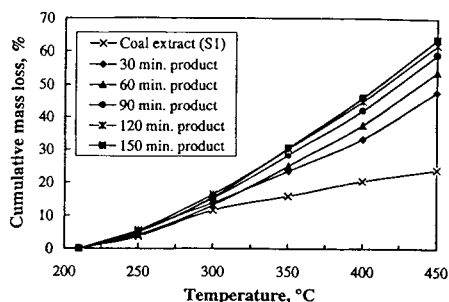


Figure 2 Effect of residence time on the TGA-derived distillation curves: mass loss of hydrocracking products prepared with the flowing-solvent extract (S1) at 460 °C and 190 bar hydrogen; solvent free basis.

of samples: the proportion of material boiling above 450 °C was lowest for the Pilot Plant extract, S4, and highest for the 60 min reaction time mini-bomb sample, S3. Our previous work has shown products from the FSR to contain more high molecular mass (MM) material compared to products prepared in closed (batch) reactors such as mini-bombs². This is explained by the shorter residence time of extracts released from coal in the heated zone of the FSR. Residence times in bomb reactors (normally minutes) allow the more reactive (labile) structures in extract molecules to break apart; this results in the formation of light products, which, in the context of the present experiments were removed by extraction with pentane. The mini-bomb derived samples thus represent material modified by secondary reactions during longer exposure to extraction conditions and subsequently stripped of lighter products. The Pilot Plant extract, S4, was used as received, and found by SEC to have by far the smallest molecular mass distribution (not shown). This appears due not just to the 60 min *mean* residence time in the digester, but also to the presence of recycle solvent, consisting of a heavy distillation cut of material that had already gone around the process loop at least once.

Hydrocracking of extracts: Samples of the FSR extract, S1, were hydrocracked in the micro-bomb for 30, 60, 90, 120 and 150 minutes. Boiling point distributions of the hydrocracked extracts are shown in Figure 2. The yield of distillate (defined as material with < 450 °C b.p.) was observed to increase with increasing residence time, indicating a progressive breakdown of larger molecules during the hydrocracking process. However the major increase in distillate yield was achieved in the first 30 minutes, with further exposure in the micro-bomb giving diminishing returns. Figure 3 compares the UV-fluorescence (UV-F) spectrum of the FRS-extract with spectra of a time-series of hydrocracked products, clearly showing most of the size reduction in polynuclear aromatic ring systems to take place during the first 30 min of hydrocracking.

Boiling point distributions of each of the four coal extracts, after hydrocracking in the

micro-bomb for 60 min, are shown in Figure 4. The Pilot Plant extract, S4, yielded more distillate on hydrocracking than the other three extracts; some of this distillate is thought to derive from the process recycle solvent in the product stream leaving the digester, where the presence of large saturated aromatic ring systems have been identified. The FSR and the 10 min mini-bomb extracts were found to have similar boiling point distributions after hydrocracking, suggesting that the latter liquefaction conditions are also comparatively mild. The lowest yield of distillate was obtained from hydrocracking the 60 min mini-bomb extract: this result must be seen in the context of removal of most light material formed during the 60 min liquefaction process, by extraction with pentane. It is tempting to suggest that the > 450 °C b.p. material increases in stability with increasing residence time during the 60 min extraction process. However, UV-F spectra in Figure 5 show the polynuclear aromatic ring systems in the FSR and 60 min mini-bomb extracts to be similar, showing no evidence of ring system size growth with extended times of extraction; the conversion of coal in the 10 min mini-bomb run was lower and the extraction not as complete as in the FSR and 60 min mini-bomb runs.

Hydrocracking effectiveness has also been assessed in terms of conversion of > 450 °C b.p. material in the original extract to lower boiling 'distillate' during hydrocracking (Figure 6): apparent reactivities followed the order $S1 > S2 > S4 > S3$. The conversion of PIs from the FSR were observed to increase by 13 % (wt % of > 450 °C b.p. material in extract) as hydrocracking residence time increased from 60 to 120 min but showed little change beyond 120 min (Figure 6), in line with observations on the boiling point distribution (Figure 2).

The greater conversion observed for the FSR derived product reflects the less thermally degraded nature of the extracts. It may be noted that whilst giving the largest amount of distillate, the Pilot Plant extract also contained a relatively unreactive > 450 b.p. fraction. It does not appear possible to conclude from this data, however, whether the relatively inert fraction (and that of hydrocracked Sample S3) originates from (i) molecular rearrangements leading to greater stability of > 450 °C material or (ii) the fact that the more reactive groups of the extracts have already split-off, during prolonged exposure to reaction (coal extraction) conditions. In the case of the Pilot Plant extract, components of the stream leaving the digester may have been around the recycle loop more than once.

4. ACKNOWLEDGEMENTS

We would like to thank the European Union for supporting the work under Research Contract No. ECSC 7220-EC/862. We would also like to thank the British Coal Liquefaction Project for the supply of the extracts, and G.M. Kimber and S.Moore for many helpful discussions.

5. REFERENCES

1. Harrison, J.S., Kimber, G.M. and Gray, M.D., *Proc. Int. Conf. on Coal Sci.*, Tokyo, (1989), 655.
2. Gibbins, J.R., Kimber, G., Gaines, A.F. and Kandiyoti, R., *Fuel*, **70**, (1991), 380.
3. Gibbins, J.R. and Kandiyoti, R., *Fuel*, **70**, (1991), 909.
4. Xu, B. and Kandiyoti, R., *Rev. Sci. Instrum.* 1995 (accepted for publication).
5. Xu, B., Zhang, S.-F., Wu, F., Herod, A.A., Madrali, E.S., Li, C.-Z., Dugwell, D.R. and Kandiyoti, R., ECSC Coal Research Project No.7220-EC/862, *Periodic Reports* No.1 (Sept. 1992) and No.4 (March 1994).

Table 1. Coal extracts used in the hydrocracking experiments (PI=pentane insolubles)

Extract label	Description of the coal extracts	>450 °C b.p. ⁽¹⁾
S1	5 K s ⁻¹ , 450 °C, 400 s, FSR extract, PI	72.7
S2	450 °C, 10 min mini-bomb extract (J457), PI	91.4
S3	450 °C, 60 min mini-bomb extract (J457), PI	95.5
S4	Coal extract solution from Point of Ayr Pilot Plant	63.9

(1) Proportion (wt. %) of b.p. >450 °C material in coal extract (PI) determined by the TGA.

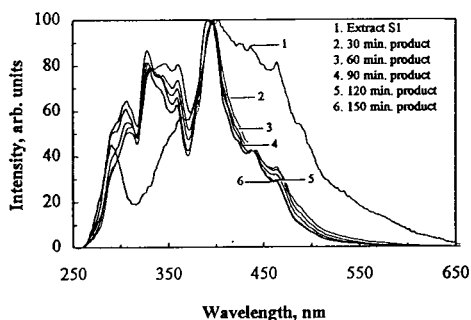


Figure 3 Comparison of synchronous UV-F spectra of the FSR extract (S1; curve 1) and its hydrocracking products. Reaction times are shown in the diagram. Hydrocracking at 460 °C, 190 bar hydrogen.

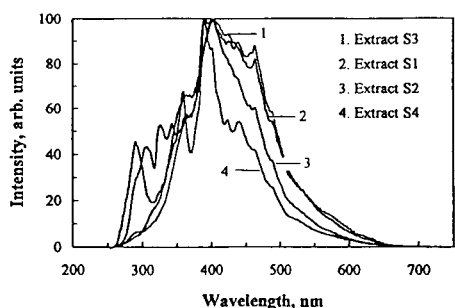


Figure 5 Synchronous UV-f spectra of the set of coal extracts before hydrocracking.

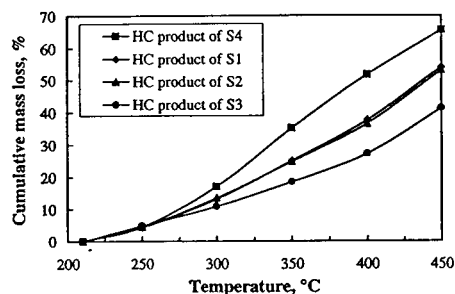


Figure 4 Comparison of the TGA-derived distillation curves: mass loss of hydrocracking products prepared with various coal extracts at 460 °C, 190 bar hydrogen and 60 minutes; solvent free basis.

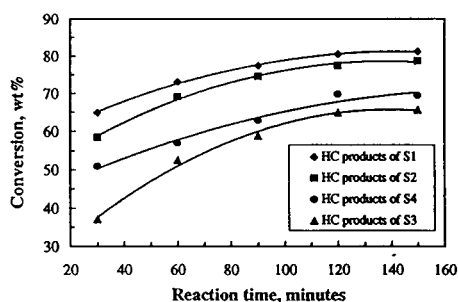


Figure 6 Effect of hydrocracking time on TGA-derived conversions of >450 °C (b.p.) material during hydrocracking at 460 °C under 190 bar hydrogen.

Influence of hydrogen donor solvent on kinetic features of hydrogenation of some fluid products of coal liquefaction

I.G.Sudakova

Russian Federation Ministry of Fuel and Energy, Research & Design Institute for Problems of Development of Kansk - Achinsk Coal Basin, 87 Kirensky-street, Krasnoyarsk 660041, Russia

The catalytic hydrogenation reprocessing of distillate products of coal liquefaction for production of standard motor fuels is hampered through the presence of unsaturated, aromatic and heteroatomic compounds, contained in such distillates. A significant enhancement of this process may be achieved by means of feeding of some hydroaromatic compounds, tetraline in particular, serving as hydrogen donors, into reaction admixture [1]. However, kinetics and mechanism peculiarities of the reactions occurring in this process are not practically investigated

1. EXPERIMENTAL

In this work some kinetic features of reactions of catalytic hydrogenation of heteroatomic, unsaturated and aromatic compounds contained in coal distillates having boiling points in range from 190 to 425°C, are considered at the presence of tetraline in reaction media. The coal distillates, obtained at liquefaction of coal of the Kansk - Achinsk coal basin, were investigated. The preliminary sulphidized wide-porous Al-Ni-Mo-catalyst, Type AS-24, was used. The catalyst had specific surface area of about 130 m²/g, mean diameter of pores exceeds 100 nm. This experiment was carried out with continuous-flow high-pressure laboratory-scale device. The influence of temperature, pressure and volume feeding rate of reaction media on the process of hydrogenation reactions with and without tetraline has been studied. Identification and determination of individual components of reaction admixture were accomplished by chromatography methods.

2. RESULTS AND DISCUSSION

Preliminary experiments with model substances and real coal distillates showed that hydrogenation reactions of the all studied compounds are governed by kinetic equation of the first order. This fact has allowed to compute rate constants of hydrogenation reactions and values of empirical coefficients of kinetic equation (Table 1).

The hydrogenation of unsaturated, aromatic and sulphurcontaining compounds proceeds in diffusion area, the dependence on temperature is quite slight. The hydrogenation of nitrogencontaining and oxygencontaining compounds takes place in

Table 1

The empirical coefficients and rate constants of hydrogenation reactions

Compounds	Temperature process, °C					
	380		400		420	
	$K_i \cdot 10^{-2}, s^{-1}$	B_i	$K_i \cdot 10^{-2}, s^{-1}$	B_i	$K_i \cdot 10^{-2}, s^{-1}$	B_i
Sulphurcontaining	1,88	1,10	2,30	0,98	2,44	1,57
Oxygencontaining	1,97	0,76	3,10	0,46	9,03	0,57
Nitrogencontaining	2,49	0,35	2,51	0,43	5,60	0,99
Aromatic	0,02	0,01	0,09	0,02	0,26	0,02
Unsaturated	0,81	1,54	0,67	1,90	1,10	1,98

kinetic area, moreover, these reactions are competitive. At diminished temperatures the hydrogenation of the oxygencontaining compounds is preferable; the increasing temperature promotes the hydrogenation of nitrogencontaining compounds.

The hydrogenation rate constant in the presence of tetraline as a function of temperature is shown in Figure 1 for various compounds contained in coal distillates.

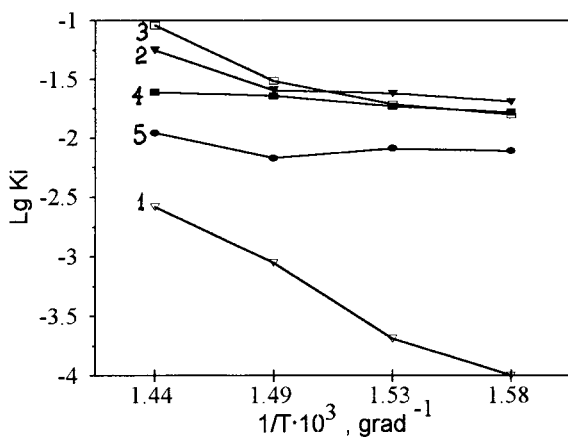


Figure 1. The hydrogenation rate constant at presence of tetraline as function of the temperature for various compounds contained in coal distillates.
4-sulphurcontaining; 2-nitrogencontaining; 3-oxygencontaining; 5-unsaturated; 1-aromatic.

At temperatures of about 340 - 360°C the catalytic hydrogenation of unsaturated compounds takes place. The subsequent temperature increase has no noticeable effect on conversion rate of these compounds. It can be assumed, that the temperature increase results in the absorption of tetraline molecules on active centers of catalyst. Due to this fact the access of molecules of the compounds to these centers will be difficult. The absorbed tetraline molecules dehydrogenate into naphthalene and release of active atomic hydrogen that reacts with heteroatomic and aromatic compounds occurs.

A comparison study of reaction admixtures of variable compositions has shown, that introduction of tetraline into reaction media allows to achieve the complete hydrogenation of such compounds as phenols and pyridine bases. The extent of conversion of unsaturated and aromatic compounds raises up to 3 - 5 times.

Even relatively small changes of process temperature results in considerable variations of the hydrogenation process of individual compounds. Thus, the average apparent activation energies of heteroatomic compounds, calculated for temperature about 400°C, may be arranged in the following consequence:

$$\text{O-cont. (46,5 kJ/mol)} < \text{S-cont. (77,3 kJ/mol)} < \text{N-cont. (144,0 kJ/mol)}.$$

For temperature of about 420°C the reverses consequence takes place:

$$\text{S-cont. (23,5 kJ/mol)} < \text{N-cont. (76,9 kJ/mol)} < \text{O-cont. (142,9 kJ/mol)}.$$

The difference in reactivity of individual compounds appears more distinctive if the comparison of rate constants of their total transformation with the rate constant of dehydrogenation of tetraline is carried out. (Fig. 2).

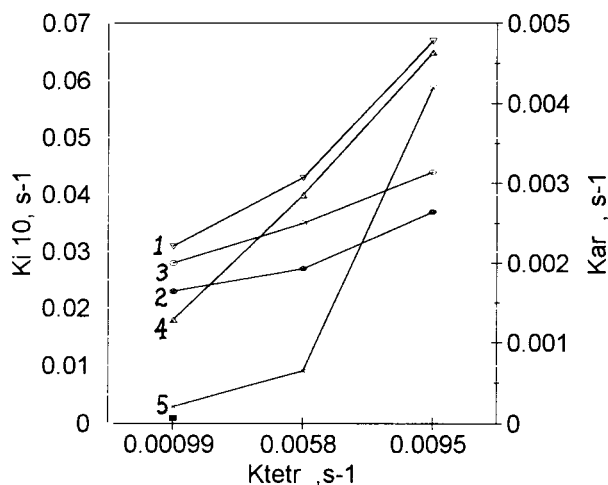


Figure 2. The rate constants of the transformation of the heteroatomic compounds, unsaturated and aromatic compounds as a function of the rate constant of tetraline dehydrogenation.

1-sulphurcontaining;2-nitrogencontaining 3-oxygencontaining;4- unsaturated;5-aromatic.

Variation of conditions of the catalytic processing (conditional time of contact, concentration of tetraline in reaction admixture, pressure of hydrogen, temperature) has shown, that tetraline participates directly in limiting stages of hydrogenation reactions.

Tetraline is supposed to play two roles simultaneously. Tetraline "brings together" splitting and hydrogenating centers. by sorption on active centers of catalyst. Thus it enables saturation of some unsaturated molecular fragments, obtained by withdrawing of heteroatoms from corresponding compounds. The other function of tetraline consists in transferring of hydrogen into reaction volume [2] resulting in significant decrease of diffusion restrictions of hydrogenation of coal distillates.

REFERENCES

1. J.Cusumano, R.Dalla Betta, R.Levy, Catalysis in coal conversion, Moscow, (1984).
2. E.J.Kuhlman, D.J.Jung, R.P.Guptill, et.al. Coal liquefaction using a hydrogenated creosote oil solvent. H-atom transfer from hydrogen donor components in the solvent, Fuel, V.64, No 11(1985)1552.

CHARACTERIZATION OF Ni-W/Al₂O₃ CATALYST USED IN COAL LIQUID UPGRADING

Nobuyuki MATSUBAYASHI^a, Toshio SATO^a, Hiromichi SHIMADA^a,
Motoyasu IMAMURA^a, Yuji YOSHIMURA^a, Akio NISHIJIMA^a, Takashi KAMEOKA^b and
Koji MASUDA^b

^aNational Institute of Materials and Chemical Research, Tsukuba, Ibaraki 305 Japan

^bCatalysts & Chemicals Industries Co., Ltd, Kitaminato, Wakamatsu, Kitakyushu, 808 Japan

A highly active Ni-W/Al₂O₃ catalyst developed to upgrade coal-derived liquids was characterized using x-ray absorption fine structure (XAFS) method. Local structures around Ni and W in the fresh catalyst were basically the same as those around Ni and Mo, respectively, in Ni-Mo catalysts. The changes in the local structures around W and Ni on the catalysts showed that most of W occurs as WS₂ crystal, and Ni as Ni₃S₂ crystal (heazlewoodite) like structure. These results suggest that the catalytically active phase of Ni-W-S structure decompose into bulk single sulfides after use in the upgrading reaction of coal-derived liquids.

1. Introduction

During the course of the study on the upgrading catalysts of coal liquid, we successfully designed and developed a Ni-W/Al₂O₃ catalyst which possessed high hydrogenation (HY) and hydrodenitrogenation (HDN) activities in model test reactions [1,2]. The catalyst developed showed higher HY and HDN activities, and slower catalyst deactivation in the upgrading of coal-derived middle distillates for *ca.* 1000 h, compared with other commercially available catalysts.

The fundamental activities of the catalyst were evaluated using model test reactions [3]. In spite of the small decline of the HDN activity during the upgrading reaction, considerable deterioration was observed in both HY and hydrocracking activity tests. X-ray photoelectron spectroscopic (XPS) analysis demonstrated the phase segregation of nickel and tungsten binary sulfide during the reaction. X-ray absorption fine structure (XAFS) analysis and transmission electron microscopic (TEM) observation indicated significant agglomeration of the tungsten disulfide species [4]. Thus, the catalyst deactivation was found to be related to the change in the structure of the Ni-W catalyst during the reaction. The above described structural change was dependent on feedstock properties, especially the concentration of polar compounds in the feedstock [5].

In the present report, analysis of XAFS has been performed using FEFF calculation[6], in which multiple scattering effect is well considered, to obtain more precise information on the local structure around Ni and W in the catalyst.

2. Experimental

The Ni-W/ γ -Al₂O₃ (NiO=4.2 wt%, WO₃=29.0 wt%, surface area=209 m²g⁻¹, pore volume=0.81 cm³g⁻¹) catalyst was prepared by the incipient wetness method using an aqueous solution of Ni(NO₃) and (NH₄)₆W₇O₂₄, followed by calcining for 1 h at 550 °C.

The catalyst was used for *ca.* 1000 h in the hydrotreating of a coal-derived liquid which was employed in a micro-scale catalyst screening unit. The feedstock used in the present study was Battelriver coal-derived kerosene (523-615 K, C; 89.2%, H; 9.8%, N; 0.57%, S; 0.018%, O; 0.4%).

The Ni K-edge and W L_{III}-edge XAFS measurements were performed in the transmission mode at the BL-10B of Photon Factory, National Laboratory for High Energy Physics with a Si(311) double crystal monochromator at room temperature. The samples were pressed into pellets under a dry nitrogen atmosphere.

All XAFS analyses were performed in *r*-space by Fourier transformation. Prior to Fourier transformation, each XAFS spectrum was transformed to normalized $\chi(k)$ by the method developed by one of the authors [7]. The spectra in *r*-space (Radial Distribution Functions, RDFs) were obtained by Fourier transformation of the $\chi(k)$ at a range of $k=2.8$ - 17.8 Å⁻¹ for W L_{III}-edge and at a range of $k=2.8$ - 16.8 Å⁻¹ for Ni K-edge with a hamming window width of 10 % of the range on both sides.

The phase shift correction during the Fourier transformation was done using the phase shift functions for W-S and Ni-S obtained by FEFF [6] calculation based on the known structures of WS₂ [8] and Ni₃S₂ [9], respectively.

3. Results and Discussion

Figure 1 shows Fourier transforms of experimental W L_{III}-edge XAFS for the catalyst before and after reaction and simulated data by FEFF calculation for crystalline WS₂. The simulated data was obtained using the Debye model for the crystalline WS₂ in which and Debye-temperature was varied as a parameter to fit the experimental data. However, the contribution of W-W scattering in the simulated RDF is much larger than that in the experimental RDF. This may be attributed to low crystallinity of the powdered WS₂. The RDFs of the catalyst before

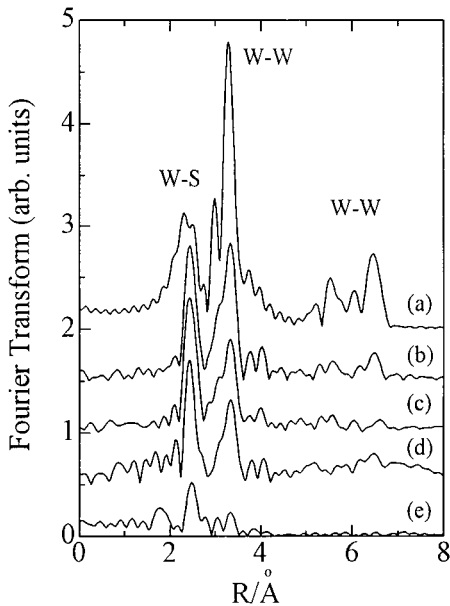


Fig1. Fourier transforms of W L III-edge XAFS for the catalysts and WS₂. (a) Simulated data for WS₂ by FEFF calculation, (b) Experimental data for WS₂, (c) Aged catalyst (Inlet), (d) Aged catalyst (outlet), and (e) Fresh catalyst.

and after reaction obviously exhibit the same features as WS_2 . This indicates that the catalyst has basically the same structure as WS_2 crystal. The peak intensities in the RDF of the fresh catalyst are significantly lower than those of WS_2 . The very low W-S peak at 2.41 Å of the fresh catalyst is mainly due to the co-existing oxide phase which remained unsulfided during presulfiding. In fact, the x-ray photoelectron spectroscopic analysis of the fresh catalyst showed that the ratio of $\text{W}^{4+}/(\text{W}^{4+}+\text{W}^{6+})$ was about 0.7.

The next nearest W-W peak at 3.15 Å is much weaker in the catalyst than in WS_2 , in contrast to the nearest W-S peak. This indicates that WS_2 crystallinity in the catalyst is low. To minimize the contribution of tungsten oxide phases to the estimation of WS_2 crystallinity, a new index of $\text{N(W)}/\text{N(S)}$ was introduced, where N(S) is the nearest coordination number of W with S and N(W) is the next nearest coordination number of W with W. For perfect WS_2 crystal the index is one, because $\text{N(S)}=\text{N(W)}=6$. The peak intensity is not directly proportional to the true coordination number, because the structural disorder of crystallites cannot be properly estimated in Debye-Waller terms. However, it is worthwhile to discuss qualitatively WS_2 crystallinity based on this index.

Two peaks corresponding to the W-W at 5.46 and 6.31 Å are observed in the spectra of the aged catalysts. The relative intensity of each peak to the next nearest W-W scattering was then calculated as another index. For WS_2 crystal, this index is 0.19 for W-W at 5.46 Å and 0.3 for W-W at 6.31 Å. The very close values obtained for the aged Ni-W/ Al_2O_3 catalyst to those for WS_2 suggests the presence of long range ordered structures. This is consistent with TEM photographs of the aged catalyst which showed crystals larger than one hundred Å [4].

Figure 2 shows Fourier transforms of experimental Ni K-edge XAFS of the catalyst and simulated data for crystalline Ni_3S_2 . The RDF of Ni_3S_2 is similar to that of the simulation. The peak at 2.48 Å is broad and intense perhaps because of the overlap of Ni-S scattering at 2.25 Å and Ni-Ni scattering at 2.50 Å. The peak at 4.00 Å of Ni_3S_2 is perhaps due to Ni-Ni scattering at 3.76 Å and 3.82 Å in the next shells. The RDF of the fresh catalyst exhibits a peak at 2.22 Å with a shoulder at 2.5 Å. This pattern is quite similar to those of fresh Ni-Mo/ Al_2O_3 catalyst [5]. The local structure around Ni in the fresh Ni-W catalyst is most likely similar to that in Ni-Mo/ Al_2O_3 catalysts. The peak observed at 2.48 Å

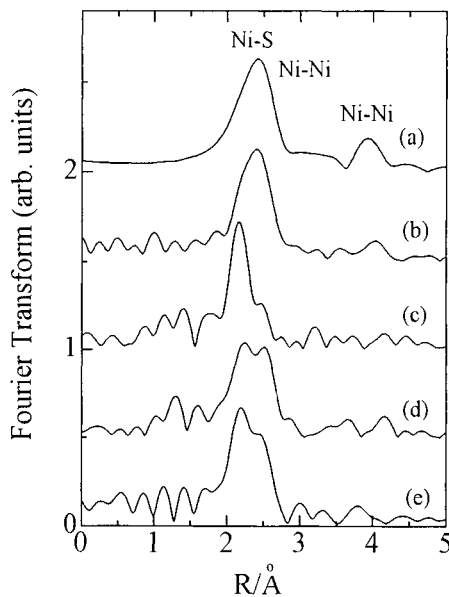


Fig.2 Fourier transforms of Ni K-edge XAFS for the catalysts and Ni_3S_2 . (a) Simulated data for Ni_3S_2 by FEFF calculation, (b) Experimental data for Ni_3S_2 , (c) Fresh catalyst, (d) Aged catalyst (Inlet), and (e) Aged catalyst (Outlet).

which corresponds to that of Ni_3S_2 is stronger in the aged catalyst at inlet of a reactor (Inlet) than in that at outlet (Outlet). Inversely the peak at 2.25 Å is weaker in Inlet than in Outlet. The peak at 2.25 Å is intermediate distance between of Ni-O or Ni-S. The peak can be assigned to Ni-S coordinated tetrahedrally, which may be related to active sites of Ni-W/ Al_2O_3 .

The local structures around Ni and W in the fresh catalyst are basically the same as those around Ni and Mo, respectively, in Ni-Mo catalysts. Fresh Ni-W catalysts are likely to have the "Ni-W-S" phase. During the reaction, however, WS_2 slabs grow in the lateral direction together with the change of the oxide phase in sulfides. At the same time, Ni atoms are released from the edge sites of WS_2 slabs and form crystalline Ni_3S_2 .

The sulfiding of tungsten oxides on $\gamma\text{-Al}_2\text{O}_3$ is slower than that of molybdenum oxides under presulfiding conditions. However, crystal growth of WS_2 is more rapid than that of MoS_2 , once tungsten sulfides formed with the breakage of W-O-Al bonds. The release of Ni from the "Ni-W-S" structure may trigger the crystal growth of the WS_2 slabs. On the contrary, the crystal growth of WS_2 may expel Ni atoms from the edge sites of WS_2 slabs. In this respect, the "Ni-W-S" phase is less stable than the "Ni-Mo-S" phase under the reaction conditions.

It is speculated that the decomposition of the "Ni-W(Mo)-S" structure is caused by catalyst poisoning materials such as oxygen- or nitrogen- containing molecules. Carbonaceous deposition on the aged catalyst was 5.65 wt% of carbon with a N/C atomic ratio of 0.046. There was no difference in the total amount of carbonaceous deposit in comparison with Ni-Mo/ Al_2O_3 catalysts (5.6 wt% of carbon with a N/C atomic ratio of 0.073), however, less nitrogen-containing materials were deposited on the Ni-W catalyst. This indicates that active sites on the Ni-W catalyst were less poisoned by basic compound deposited, resulting in the slower deactivation profile. Design and development of the active phase with high stability would improve the resistance to catalyst deactivation during hydroprocessing coal-derived liquids.

Acknowledgments

This work was partly supported by NEDO (New Energy and Industrial Technology Development Organization, Japan).

References

1. A. Nishijima, T. Kameoka, H. Yanase, T. Sato, Y. Yoshimura, H. Shimada, and N. Matsubayashi, Proc. 1991 Int. Conf. on Coal Science., p.759.
2. H. Shimada, T. Kameoka, H. Yanase, M. Watanabe, A. Kinoshita, T. Sato, Y. Yoshimura, N. Matsubayashi, and A. Nishijima, Proc. Int. Cong. on Catalysis (1993) 1915.
3. H. Shimada, T. Sato, Y. Yoshimura, J. Hiraishi, and A. Nishijima, *J. Catal.*, **110** (1988) 175.
4. T. Kameoka, H. Yanase, T. Sato, Y. Yoshimura, H. Shimada, M. Matsubayashi, and A. Nishijima, *Appl. Catal. A*, **123** (1995) 217.
5. N. Matsubayashi, H. Shimada, T. Sato, Y. Yoshimura, M. Imamura, and A. Nishijima, *Fuel Processing Technology*, **41** (1995) 261.
6. J. J. Rehr, S. I. Zabinsky, and R. C. Albers, *Phys. Rev. Lett.*, **69**, 3379 (1992).
7. N. Matsubayashi, The Ph. D. Thesis of Faculty of Science in Osaka Univ. (1986).
8. W. J. Schutte, J. L. deBoer, and F. Jellinek, *J. Solid State Chem.*, **70** (1987) 207.
9. J. B. Parise, *Acta Crystallographica B*, **36** (1980) 1179.

Retrogressive reactions in coal/oil coprocessing in view of spectroscopic and microscopic examination

J. Černý, I. Sýkorová^a, G. Šebor, D. Maxa and J. Blažek

Department of Petroleum Technology and Petrochemistry, Institute of Chemical Technology, Technická 5, 166 28 Prague, Czech Republic

^a Institute of Rock Structure and Mechanics, Czech Academy of Sciences, V Holešovičkách 41, 182 09 Prague, Czech Republic

1. INTRODUCTION

Some references on coal/oil coprocessing mentioned a possible synergistic interaction between coal and petroleum residue (or similar liquid) [1,2]. While an usual coal concentration in coal/oil mixture is about 25-30 wt %, results of recent research have limited the coal/oil synergy to a coal concentration as small as 5 wt % [3,4]. Additionally, severe reaction conditions can lead to extremely high yields of an insoluble fraction of reaction product, most likely as a consequence of different behavior of petroleum residue alone and in a coal/oil mixture. Production of insoluble organic matter (IOM) is accelerated in coprocessing under severe reaction conditions so that negative coal conversions can be obtained [5-8]. It means that amount of IOM in the coprocessing product can be higher than amount of coal entering the reactor. The intensive production of IOM can be explained either by a lack of hydrogen available at high reaction rate at elevated temperature [5] or by a suggestion that coal surface is occupied by active sites which can accelerate the reaction rate of retrogressive reactions producing IOM [6-8].

Generally, the yields of distillates and oils in coal/oil coprocessing seem to be governed, under mild reaction conditions, by the coal properties [9]. In turn, petroleum residue most likely plays a key role under severe condition, especially at temperatures near 450 °C. Residues from heavy crude oils, which contain an increased amount of asphaltenes, produce in coprocessing a much higher amount of IOM than residues from light crude oils [6-8].

This work is aimed at analysis of insoluble residue from coal/oil coprocessing experiments performed in the temperature range between 410 °C and 455 °C. An extent of retrogressive reactions was assessed by using quantitative FTIR spectroscopy and microscopic textural analysis of coprocessing residue, which is believed to reflect structural changes caused by retrogressive reactions.

2. EXPERIMENTAL

Coal/oil experiment were performed in a 0.5 dm³ rotating autoclave under the following conditions: coal/oil ratio was 1:2 (wt), reaction hydrogen pressure 20 MPa, temperature dependent experiments between 410 °C and 455 °C were done at reaction time of one hour, the reaction time dependent experiments between 30 and 90 min were done at temperature of 440 °C. Elemental analysis of coal and petroleum residue is presented in Table 1.

Table 1
Elemental analysis of feedstocks (wt %, daf)

Feedstock	Ash (d.b.)	H	C	S	N	O _{diff}	Asphaltenes
CSA coal	18.0	5.5	72.9	2.0	1.0	18.6	-
Petroleum residue	0.10	10.4	84.5	3.7	0.5	0.9	13.7

FTIR spectra were measured on a Bruker IFS 88 instrument. One hundred scans of a sample in a form of KBr pellet were accumulated at 2 cm^{-1} resolution. Spectra were adjusted to a concentration of 1 mg cm^{-2} , and aliphatic and aromatic CH stretching modes were quantitatively evaluated using the Painter's average integral absorptivities [10].

Textural analysis of IOM was performed in oil immersion by using an Opton UMSP 30 Petro optical microscope. Reflectance and optical texture were determined under monochromatic (546 nm) and polarized light, respectively.

3. RESULTS AND DISCUSSION

The IOM was obtained from the reaction products by an exhaustive Soxhlet extraction with toluene. Yields of the IOM for experiments performed at different temperature and/or reaction time are shown in Figures 1 and 2.

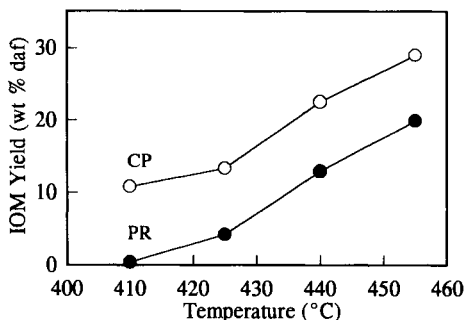


Figure 1. Yields of IOM in coal/oil coprocessing (CP) and petroleum residue reference (PR) at reaction time of 1 h.

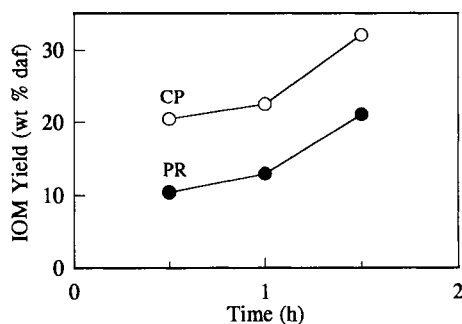


Figure 2. Yields of IOM in coal/oil coprocessing (CP) and petroleum residue reference (PR) at $440\text{ }^{\circ}\text{C}$.

Apparently, the amount of IOM in reaction product steadily increases over the temperature and reaction time ranges, being higher for the coprocessing than for the reference experiments. Interestingly, the difference in the IOM amount is almost constant independently on the reaction temperature or time. It could be deduced that the difference, creating about 10 wt % daf of the entire mixture, is for coprocessing formed by the IOM from coal. However, it is hard to believe that coal produced nearly the same amount of IOM over the whole temperature and/or time range, and some interaction between coal and residue can therefore be expected.

Table 2
Coal conversions to distillates and toluene solubles (wt % daf)

Temperature (°C)	Coal conversion	
	Distillates	Benzene solubles
410	32.5	57.6
425	38.7	58.9
440	50.9	45.8
455	60.8	32.6

Some indication for the coal/oil interaction is presented in Table 2, where coal conversions to benzene solubles are for severe reaction conditions shown to be smaller than coal conversions to distillates. Similar behavior of coal/oil mixtures, and even negative coal conversions, was also observed by others [5,6,8], and it can be attributed to accelerating the IOM production from petroleum residue in the presence of coal. That conclusion may be speculative without doing reference

experiments with coal. However, it cannot be found a petroleum residue-like and simultaneously 'inert' solvent for such reference experiment.

Quality of the IOM for different reaction conditions was examined by spectroscopic and microscopic analysis. Figures 3 and 4 display the hydrogen distribution for IOM from coprocessing and petroleum residue reference.

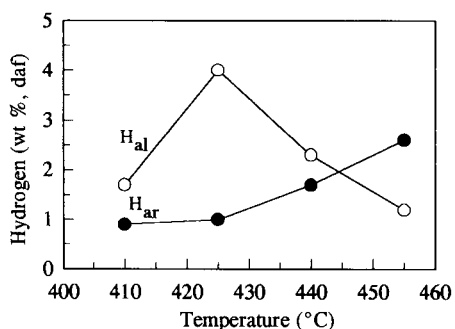


Figure 3. Hydrogen distribution in IOM from petroleum residue reference.

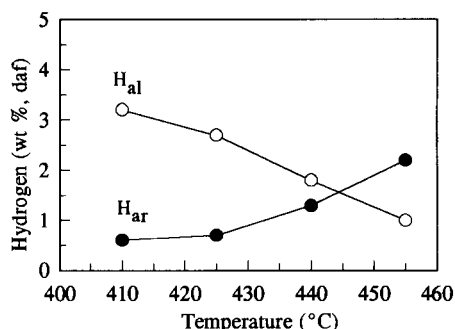


Figure 4. Hydrogen distribution in IOM from coprocessing.

Interestingly, the aliphatic hydrogen content for the petroleum residue reference passed a maximum at 425 °C, likely as a result of competitive reactions. Up to 425 °C, the main reactions occurred seem to be cracking and hydrogenation of the petroleum residue. Above 425 °C, cracking and dehydrogenation, i.e., aromatization, of the residue take place. For coprocessing, the tendency for the aromatic hydrogen concentration is similar as for the processing of the petroleum residue alone, i.e., it started to increase above 425 °C. However, the tendency for the aliphatic hydrogen concentration is quite different. It steadily decreased without passing any maximum in the temperature range examined. It seems that the presence of coal in the feed mixture promoted mainly the cracking reactions, and hydrogenation reactions are largely suppressed. The hydrogen distribution for the time dependent experiments is similar for both the petroleum residue reference and coprocessing experiments. The aromatic hydrogen concentration in IOM was similar for reaction time up to 1 h, after which the aromatic hydrogen concentration sharply increased. It can be concluded that retrogressive reactions were accelerated at temperatures above 425 °C and/or reaction time of 1 h.

Texture analysis of IOM was performed by microscopic analysis and results are presented in Table 3 for the temperature dependent experiments.

Table 3
Microscopic analysis of IOM texture (in %)

Sample	R_T	Isotropic material	Anisotropic material	
			Mosaic texture	Domain texture
CP410	1.20	97	3	0
CP425	1.31	92	8	0
CP440	2.35	17	76	7
CP455	3.01	11	75	14
PR410	1.73	12	42	46
PR425	1.23	69	14	17
PR440	2.34	50	0	50
PR455	2.68	29	0	71

Random reflectance (R_T) and amount of anisotropic material follow the same trend observed for hydrogen concentration. Severe reaction conditions led to an increase in mean reflectance of the IOM and in the amount of anisotropic material. Substantial difference in optical texture of IOM is apparent from Table 3. Whereas processing petroleum residue alone produced the IOM predominantly with domain texture, the IOM anisotropic material from coprocessing exhibited mainly mosaic texture. It is interesting, that IOM produced under more severe reaction conditions contained anisotropic material with a larger portion of domains. That was more apparent in the time dependent experiments, among which the IOM from coprocessing at 440 °C and 1.5 h reaction time contained even 44 % of domains.

REFERENCES

1. W. Dolkemeyer, U. Lenz and K.A. Theis, *Erdoel, Erdgas, Kohle* 105 (1989) 79.
2. B. Ignasiak, T. Ohuchi, P. Clark, D. Aitchison and T. Lee, *Prep. Pap., Am. Chem. Soc., Div. Fuel Chem.* 31 (1986) 200.
3. S.A. Fouda, J.F. Kelly and P.M. Rahimi, *Energy Fuels* 3 (1986) 154.
4. M. Miyake, K. Takahashi, J. Higashine and M. Nomura, *Fuel Process. Technol.* 30 (1992) 205.
5. J. Font, A. Fabregat, J. Salvado, A. Moros, C. Bengoa and F. Giralt, *Fuel* 71 (1992) 1169.
6. R. Rosal, L.F. Cabo, F.V. Díez and H. Sastre, *Fuel Process. Technol.* 31 (1992) 209.
7. J. Tomic and H.H. Schobert, *Prep. Pap., Am. Chem. Soc., Div. Fuel Chem.* 37 (1992) 770.
8. H.H. Schobert and J. Tomic, Report No. DOE/PC/88935, 1993.
9. C. W. Curtis and J.S. Hwang, *Fuel Process Technol.* 30 (1992) 47.
10. B. Riesser, M. Starsinic, E. Squires, A. Davis and P. C. Painter, *Fuel* 63 (1984) 1252.

Use of Iron-based Disposable Catalysts for Coprocessing of Coal and Heavy Oil Residues in Solvent Augmented Coal Liquefaction.

Mark W. Badger and Graham Harrison.

Staffordshire University, School of Sciences (Chemistry Division), College Road, Stoke-on-Trent, Staffordshire, ST4 2DE, England.

1. INTRODUCTION.

Two stage coal liquefaction processes, such as the British Coal Corporation's (BCC) Point of Ayr pilot plant, North Wales, UK, which use a process derived recycle solvent (PDRS) are intrinsically rigid in their operation. They rely heavily on the quality and quantity of the PDRS in the first stage digestion step. This reliance can be alleviated by the addition of heavy oil residues (HOR's) to the process via solvent augmentation.

The use of HOR's in coprocessing is well documented, and in a previous study [1] of four resids it was shown that Forties AR and Decant oil offered significant dissolution properties under the right conditions. However problems with coking hold this method back. Problems with coking of HOR's at elevated temperatures can be controlled by solvent augmentation with PDRS. Kubo and co-workers [2] and Del Bianco et al [3] have shown in thermal cracking processes that problematic coking has been dramatically reduced by the addition of compounds similar to those in PDRS. Thus coking may be expected to be reduced in mixed PDRS and HOR systems.

By nature HOR's have little H-donation capability, so in solvent augmentation the overall H-donor content of the solvent mixture will have been diluted, in comparison with the PDRS alone. To compensate for this shortfall, molecular hydrogen can be added together with a catalyst to the reaction mixture to promote H-transfer to stabilise the coal and HOR-derived radicals.

2. EXPERIMENTAL.

2.1. Materials

HOR samples (Forties AR and Decant oil) were supplied by BP, Sunbury-on-Thames, UK. Point of Ayr coal (CRC 702) was supplied by the BCC. All other chemicals were purchased from Aldrich Chemicals Co.

2.2. Catalysed Activated Coals.

A variety of sulphided iron catalysed activated coals (CAC's), with a range of percentage iron loadings on the coal surface, were produced by heterogeneous precipitation, by adding Na_2S solution to a slurry of coal and FeCl_3 . The activities of the CAC's were measured relative to the percentage dissolution at set conditions.

2.3. Dissolution Experiments.

Dissolution experiments were carried out in a 500ml spinning/falling basket autoclave manufactured by Baskerville & Lindsay Scientific and described elsewhere

[4]. Coal or CAC and solvent (1:2 ratio) were reacted at the desired temperature and time, at a stirrer speed of 500 rpm, under a H₂ overpressure, usually 20 bar. After cooling, the autoclave was emptied, the products were filtered under vacuum and washed thoroughly with dichloromethane (DCM). The solid residue was dried to a constant weight and ashed at 800 °C. The DCM was removed by rotary evaporation from the liquid products which were then analysed by GC, GC-MS .

3. RESULTS AND DISCUSSION.

Figure 1 shows the relative dissolutions (calculated by ash balance) of the range of different percentage iron loaded CAC's in experiments with Forties AR reacted at 380 °C for 60 minutes and Decant oil at 380 °C for 30 minutes. It can be seen that for both HOR's there was an increase in dissolution up to a maximum around 6% w/w iron CAC. The Decant oil showed higher dissolution values, due to the fact that it is mainly aromatic in composition and has the capability to transfer hydrogen from the gas phase to cap the coal and HOR derived radicals via H-shuttling reactions. The presence of mainly aromatic compounds in Decant oil may also explain the sudden drop in overall dissolution at loadings above 6%. The aromatic compounds are likely to undergo catalytic cracking to form carbonium ions, which then undergo retrograde reactions leading to coke formation and lower dissolution. The Forties AR is predominantly made up of saturated long chain aliphatic compounds which exhibit little H-donor or H-shuttling ability and hence it has a lower dissolution potential than the Decant oil (see relative dissolutions when no catalyst present), and is unlikely to undergo major catalytic cracking as saturated aliphatics do not readily form carbonium ions (shown by the smaller drop in dissolution at increased iron loadings).

The results shown in Table 1 are for a comparative study of coprocessing of PDRS in the presence of coal and CAC at 380 and 400 °C for 30 and 60 minutes. It can be seen that in the presence of catalyst there was an increase in dissolution indicating that the catalyst was active in H-transfer from molecular H₂. In addition dissolution increased with both increasing temperature and time.

Tables 2 and 3 show solvent augmentation studies using various additions of Forties AR and Decant oil to PDRS at 380 and 400 °C for 30 and 60 minutes with CAC. For a 10% addition of both Forties AR and Decant oil to PDRS there was no significant difference in dissolution, compared with PDRS and CAC under the same conditions (Table 1). In fact, there may be signs of synergism, especially at 400 °C for 60 minutes. A 20% addition of Forties AR showed a drop in dissolution suggesting cracking and coking reactions of the HOR were taking place, reducing the observed dissolution of coal. The Decant oil however showed no detrimental changes and an increase in dissolution was indicated. This suggests that the aromatic constituents of the Decant oil may be contributing to radical stabilisation by H-transfer reactions, shuttling hydrogen from the gas and donor solvent to coal and HOR derived radicals. With a 30% addition of Decant oil again there is little change in dissolution. The value for 60 minutes at 380 °C has increased slightly but the value at 60 minutes and 400 °C has fallen slightly, indicating the onset of retrograde reactions.

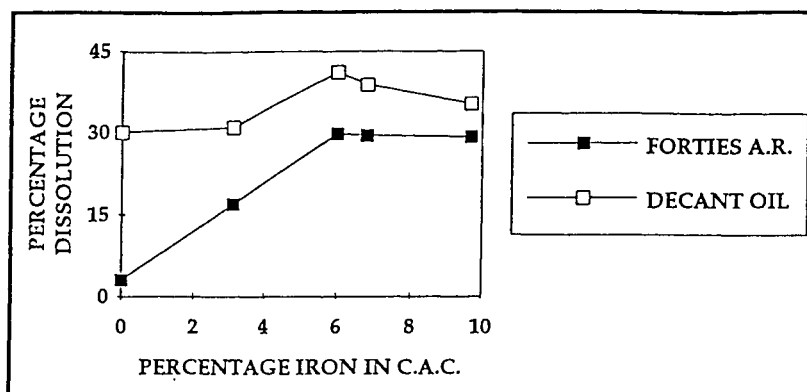


Figure 1. Effect of varying iron in CAC's on Forties AR and Decant oil coprocessing.

Table 1.

Dissolution comparison of coal and CAC in PDRS

PDRS + Coal			PDRS + CAC		
Temp. (°C)	Time (mins)	% dissolution	Temp. (°C)	Time (mins)	% dissolution
380	30	44.6	380	30	45.3
380	60	51.1	380	60	52.3
400	30	54.4	400	30	56.2
400	60	56.5	400	60	59.6

Table 2.

Solvent augmentation studies with Forties AR

Temp. (°C)	Time (mins)	Percentage dissolution with	
		10% added	20% added
380	30	45.5	40.3
380	60	50.2	42.7
400	30	56.7	52.1
400	60	59.8	50.9

Table 3.

Solvent augmentation studies with Decant oil

Temp. (°C)	Time (mins)	Percentage dissolution with		
		10% added	20% added	30% added
380	30	47.3	47.5	46.4
380	60	51.9	52.7	54.5
400	30	55.3	55.2	55.7
400	60	61.0	61.2	56.7

The chromatograms shown in Figure 2 are of the oils used, before and after coprocessing reactions. It can be seen that Forties AR during coprocessing was dramatically converted to lower boiling compounds. There was a slight increase in lower boiling point compounds in Decant oil after dissolution. For PDRS with 20% addition of Decant oil before and after coprocessing, it can be seen that there was a reduced peak density and an increase in the size of peaks corresponding to compounds such as pyrene, phenanthrene and tetralin, indicating loss of hydroaromatics as a result of H-donation. There also seems to be a reduction in the content of low boiling point compounds in the products compared with Decant oil and Forties AR, suggesting PDRS was effecting some control of HOR cracking.

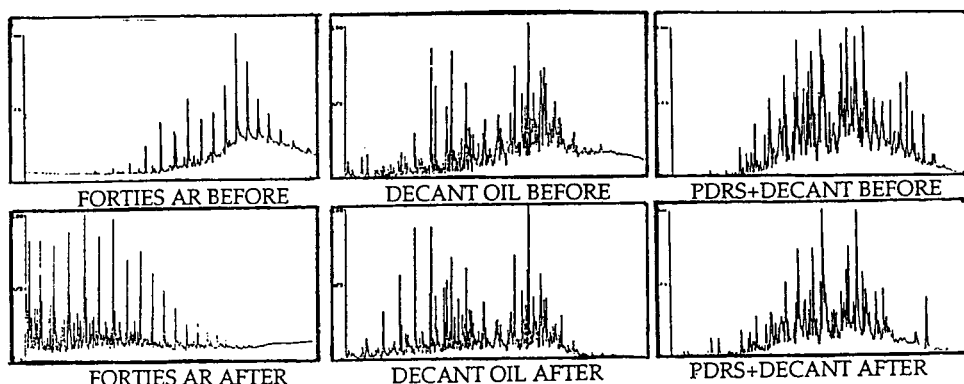


Figure 2. Chromatograms of the oils used, before and after coprocessing.

4. CONCLUSIONS.

An introduction of iron-based disposable catalyst in the form of a CAC improves the dissolution of coal. Solvent augmentation with HOR's, especially Decant oil, given the correct additions, will not detrimentally affect the dissolution of coal in PDRS. The problems associated with HOR coprocessing (*i.e.* coking and poor dissolution) can be significantly reduced and in some cases eliminated by their augmentation with a hydrogen donor solvent.

ACKNOWLEDGEMENTS.

The authors are grateful for the financial support from the European Coal and Steel Community (Project No. 7220-EC 866).

REFERENCES.

1. M.W. Badger, G. Harrison, A.B. Ross, ACS Div. of Pet. Chem. Preprints, 39, 4, (1994), 438.
2. J. Kubo, H. Higashi, Y. Ohmoto, H. Arao, ACS Div. of Pet. Chem. Preprints, 39, 4, (1994), 416.
3. A. Del Bianco, G. Garuti, C. Pirovano, R. Russo, ACS Div. of Pet. Chem. Preprints 39, 4, (1994), 408.
4. P.W. Doughty, Ph.D. Thesis, Staffordshire University, April (1988).

Coprocessing Coal and Natural Gas for Liquid Fuel with Reduced Greenhouse Gas CO₂ Emission

Meyer Steinberg

Brookhaven National Laboratory, Upton, N.Y. 11973

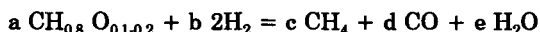
Introduction

Coal and Natural gas are abundant fossil fuels. Because of their physical and chemical properties, coal and natural gas are difficult to handle and utilize in mobile as well as stationary engines. The infrastructure is mainly geared to handle liquid fuels. In order to liquify coal it is generally necessary to increase its H/C ratio either by increasing its hydrogen content or decreasing its carbon content. In order to liquify natural gas it becomes necessary to decrease its hydrogen content. Thus, by coprocessing the hydrogen-rich natural gas with hydrogen deficient coal it should be possible to produce liquid fuels in an economically acceptable manner. For purposes of decreasing CO₂ greenhouse gas emissions, extracting carbon from coal and natural gas and utilizing the hydrogen-rich fraction of both fossil fuels, constitutes a CO₂ greenhouse gas mitigation procedure. In this paper we review several processes which coprocess coal with natural gas using known chemical reaction steps to produce liquid fuels with reduced CO₂ emissions. The particular liquid fuel of choice is methanol, a well-known automotive and stationary power fuel.

The Hydrocarb Process (1,2,3)

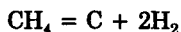
The Hydrocarb Process is based on the following three integrated chemical reaction steps:

1) Hydrogasification of Coal



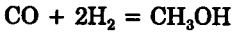
This reaction is exothermic and can take place efficiently at temperatures of 800 to 900°C and at pressures of 30 to 50 atm. A fluidized bed reactor is indicated for hydrogasification of solid carbonaceous feedstocks including coal and biomass. Limestone can be added to remove the sulfur.

2) Methane Decomposition

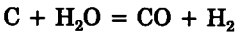


This reaction is endothermic, takes place efficiently at temperatures above 900°C and is favored by lower pressure. The methane produced by hydrogasification and additional feedstock methane provides the methane to be decomposed. This reaction produces the hydrogen for methanol synthesis in step 3 and the excess is recycled to the hydrogasification reactor in step 1.

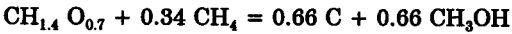
3) Methanol Synthesis



The syntheses of methanol from CO and H₂ is a well-known catalytic process which is usually practiced industrially at 260°C and 50 atm pressure. The CO is produced in the hydrogasification step from oxygen in the coal. The amount of CO formed depends on the water content of the coal according to the well-known gasification reaction:



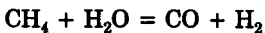
The Hydrocarb Process also works well with biomass as a cofeedstock because of its higher oxygen content. The overall reaction being:



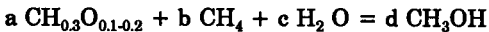
A generalized flow sheet of the Hydrocarb process is shown in Fig. 1. A computer simulation model has been developed for the process which can determine the mass and energy balances when supplying various types and amount of feedstocks. To reduce CO₂ greenhouse gas, the carbon produced in the Hydrocarb process can be sequestered or used as a materials commodity. Table 1 shows the methanol thermal efficiency and the degree of CO₂ emissions reduction compared to the production of methanol by conventional coal gasification and natural gas reforming processes. The addition of biomass can essentially reduce the net CO₂ emissions to zero because biomass removes CO₂ from the atmosphere. All the products of Hydrocarb can be converted to a liquid fuel by slurring the carbon in methanol to improve the energy utilization efficiency⁽⁴⁾, however, the degree of CO₂ reduction is decreased. The use of methanol as liquid fuel in automotive engines improves the thermal efficiency by 30% compared to gasoline fuels. Thus, an additional 40% reduction in CO₂ emission can be realized using methanol instead of gasoline in automotive engines.⁽⁶⁾

The Hynol Process⁽⁶⁾

For purposes of maximizing the methanol yield and simplifying the Hydrocarb process, the second step is changed from methane decomposition to the well-known reforming of methane with steam:



This is an endothermic process and can take place efficiently at temperatures above 900°C in the presence of nichel catalyst. Additional methane feedstock produced in the hydrogasification step significantly improves the methanol yield. In this process only liquid methanol is produced and there is no need to sequester carbon. The overall reaction involves the co-feedstocks coal and natural gas:

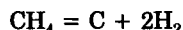


Biomass and municipal solid waste can also be used as co-feedstocks in addition to coal. Figure 2 shows a generalized flow sheet of this process. Hynol cannot reduce CO₂ emissions to zero, however, the yield of methanol by Hynol is greater than producing methanol by two separate conventional plants i.e., (1) coal gasifications and (2) methane reforming and thus, the Hynol plant becomes economically attractive.

The Carnol Process

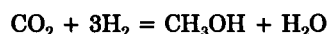
An interesting process has been investigated which can be applied to coal burning power plants to reduce CO₂ emissions. The Carnol process is based on two chemical reaction steps.

1) Methane decomposition:



In this case, natural gas feedstock is initially decomposed to form carbon and hydrogen at temperatures above 800°C and 1 atm pressure. The decomposition of methane is an endothermic reaction requiring only 18 Kcal/mol CH₄ compared to 212 Kcal/mol for the combustion of methane and thus, the Carnol process becomes a low cost source of hydrogen.

2) Methanol Synthesis from CO₂:



In this case, the CO₂ is obtained from the stack gases of a coal burning power plant. A solvent absorption-stripping system is used to remove and recover the CO₂ from power plant flue gases. The hydrogen is obtained from the methane decompositions reaction in step No 1. Figure 3 shows a schematic of the Carnol system. A conventional gas phase catalytic reactor can be used to convert the CO₂ with H₂ to form methanol. Liquid phase methanol synthesis can improve the process. A net zero CO₂ emission can be achieved with Carnol since one mole of CO₂ produced by combustion of methanol balances the one mole recovered from the emissions of a coal burning power plant. The advantage of the process is that it can be applied to any CO₂ waste stream.

The Carnol process also produces carbon which must be either sequestered or used as a materials commodity to achieve zero CO₂ emission.

Table 1 compares the methanol thermal efficiencies and the degree of CO₂ emissions reduction for the three processes discussed.

REFERENCES

1. M. Steinberg and E.W. Grohse "Production of a Clean Carbon Fuel and Coproduct Gaseous and Liquid Fuels from Coal by the Hydrocarb Process System" BNL 46490, Brookhaven National Laboratory, Upton, N.Y. (November 1990)
2. M. Steinberg "Technologies for Reducing Carbon Dioxide Emissions from Fossil Fuel Fired Installations, "J. Energy Exploration and Exploitation 9, No. 4, 186-204 (1991)
3. M. Steinberg, Y. Dong, and R.H. Borgewardt "The Coprocessing of Fossil Fuels and Biomass for CO₂ Emission Reduction in the Transportation Sector", BNL 49732, Brookhaven National Laboratory, Upton, N.Y., (October 1993)
4. G. Wei and M. Steinberg "Carbon Black Slurries, Preparation and Characteristics, BNL 43732, Brookhaven National Laboratory, Upton, N.Y. (December 1989)
5. "An analysis of the Economic and Environmental Effects of Methanol as an Automotive Fuel" EPA Report No.10730, Motor Vehicle Emissions Laboratory Ann Arbor, Michigan (September 1989)
6. M. Steinberg and Y. Dong "Hynol - An Economic Process for Methanol Production from Biomass and Natural Gas with Reduced CO₂ Emission" BNL 49733, Brookhaven National Laboratory, Upton, N.Y. (October 1993)
7. M. Steinberg and Y. Dong, "The Carnol Process for Methanol Production and Utilization with Reduced CO₂ Emissions" BNL 60575, Brookhaven National laboratory, Upton, N.Y. (June 1994)

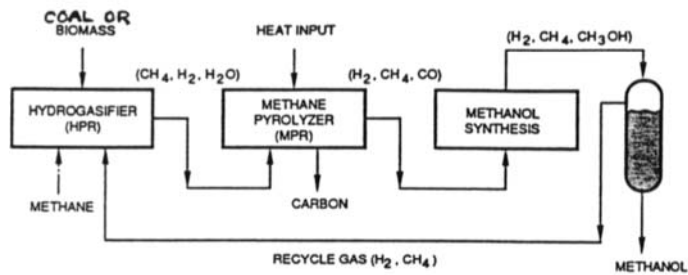


Figure 1 Hydrocarb process block diagram

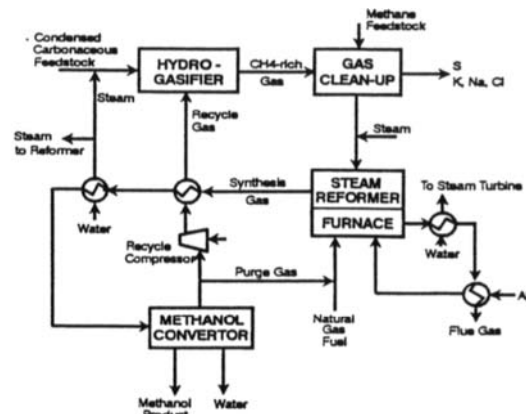


Figure 2 A block diagram of the Hynol process.

Table 1 METHANOL PRODUCTION WITH REDUCED CO₂ EMISSIONS

Process and Reactors	Feedstock	Products	MeOH Thermal Efficiency Based on Coal and Natural Gas - %	CO ₂ Emission from MeOH Combustion Lbs/MMBtu	CO ₂ - % Reduction from Convention ^a Processes
Hydrocarb HPR MPR MSR	Coal	MeOH+C	35%	130	60%
	Coal + Natural Gas	MeOH+C	40%	130	60%
	Coal + Natural gas	MeOH+C	45%	~0	~100%
	Coal + Natural gas + Biomass	MeOH+C			
Hynol HPR SPR MSR	Coal + Natural gas	MeOH	65%	260	30%
Carnol MDR MSR	CO ₂ from Coal Fired Power Plant + Natural Gas	MeOH+C	50%	~0	~100%

^aCO₂ emission from combustion of methanol produced by natural gas reforming = 170 lbs CO₂/M/MBtu produced by coal gasification = 330 lbs CO₂/M/MBtu

HPR - Hydropropyls Reactor
MPR - Methane pyrolysis Reactor
MSR - Methanol Synthesis Reactor
MDR - Methane Decomposition Reactor

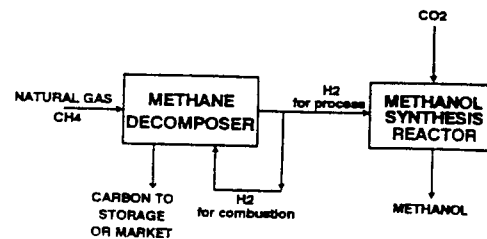


Figure 3 Carnol III process for producing methanol from natural gas and CO₂ for zero CO₂ emission.

Flash co-pyrolysis of coal retaining depolymerized polyethylene as radical donor

H. Tomita, J.-i. Hayashi, K. Kusakabe and S. Morooka

Department of Chemical Science and Technology, Kyushu University,
6-10-1, Hakozaki, Higashi-ku, Fukuoka 812-81, Japan

1. Introduction

Flash Pyrolysis is an attractive coal conversion process for the production of useful chemicals such as benzene and naphthalene derivatives. These light aromatics are mainly generated by the vapor-phase secondary pyrolysis of tar that is produced in the primary pyrolysis stage. To increase the yield of the tar that is the precursor of light aromatics, decomposition of the macromolecular network of coal should be enhanced in the primary pyrolysis. Rapid donation of hydrogen and hydrocarbon radicals to fragment radicals of coal molecules is essential both to promote tar evolution and to suppress char formation.

Recently, we studied flash copyrolysis of coal with polyolefins [1]. Polypropylene and polyethylene that were coated on the surface of a brown coal increased the tar yield by 5-12 wt% on the daf-coal basis by donating hydrogen and hydrocarbon radicals under atmospheric pressure. However, the pyrolysis was not very effective for promoting the flash pyrolysis of bituminous coals. The promotion of tar formation were strongly dependent on the contact between coal and polyolefin. To maximize the functions of radical donors, polyolefins should be retained in the coal matrix at molecular level. From this viewpoint, Ofosu-Asante et al. [2] chemically introduced long paraffinic chains into a bituminous coal by using an O-alkylation technique, although the process was rather complicated. In the present study, brown and bituminous coals were swollen with THF. The swollen coals were then physically incorporated with depolymerized polyethylene (DPE) and were subjected to flash pyrolysis with a Curie-point pyrolyzer and an entrained-flow pyrolyzer. The roles of the impregnated DPE in formation of tar and light aromatics were investigated.

2. Experimental

2.1. Samples

Yallourn brown coal (C: 63.9, H: 4.7, ash: 1.1 wt%,db) and Illinois No.6 coal (C: 68.4, H: 5.1, ash: 9.4 wt%,db) were pulverized and sized to 0.037-0.074 mm and dried at 70°C under vacuum. High-density polyethylene (HDPE) pellets were heat-treated at 400-450°C for 60 min under a nitrogen atmosphere at an initial pressure of 1.0 MPa. The treated samples were separated into n-hexane soluble and insoluble portions by extraction under ultrasonic irradiation at room temperature. Heat treatment at 435°C and 445°C gave hexane soluble yellowish wax (PWX, H/C atomic ratio: 1.98) and brown-colored oil (POL, H/C: 1.94), respectively. The yield of PWX and POL was 65 and 71 wt% of the initial HDPE. The hydrogen distribution in PWX and POL was investigated by ¹H-NMR spectrometry. Based on relative abundance of methylene and olefin hydrogen to chain-end methyl hydrogen, the average carbon number was calculated to be 21 for PWX and 15 for POL. The fraction of aromatic hydrogen was less than 2% of total hydrogen for both samples.

PWX or POL was added to each coal swollen in THF at 55°C and the mixture was gently stirred for 24 h. The solvent was evaporated at 55°C under atmospheric nitrogen flow and further by vacuum drying at 70°C. The weight ratio of DPE to dry coal was 0.22-0.25. On the other hand, HDPE was lightly heat-treated at 300°C and was pulverized and sized to 0.074-0.210 mm. The powder was mixed with pulverized coal in a HDPE/coal weight ratio of about

0.25. The mixture was heat-treated at 200°C in a tubing bomb in nitrogen with an initial nitrogen pressure of 1.0 MPa. Coal particles were thus coated with molten HDPE.

2.2. Flash pyrolysis

Raw coals, polyethylene and coal-polyethylene composites were subjected to flash pyrolysis at 764 and 920°C with a Curie-point pyrolyzer (CPP), in which the vapor-phase secondary reaction of volatiles was suppressed. To check the pyrolysis behavior of HDPE and DPE, each substance was supported on char particles that was prepared by carbonizing YL coal at 1000°C and was pyrolyzed in CPP. The char was considered to be inert because the pyrolysis of HDPE coated on this char gave the same result as that of unsupported HDPE. These samples were also pyrolyzed at 800-900°C in an entrained-flow pyrolyzer (EFP), where the secondary pyrolysis of volatiles proceeded. Yields of mono-, di- and tri-aromatics and gaseous products were determined. The details of pyrolysis experiment were reported elsewhere [1]. In both pyrolyses, the yield of tar was defined as the sum yield of volatile product heavier than C₆.

3. Results and Discussion

3.1. Contact of depolymerized polyethylene with coal matrix

When YL coal was mixed with pulverized HDPE and heat-treated at 200°C for 1 h, the color changed to black. This indicates that the HDPE melted and covered the coal particle surfaces without being absorbed into the coal matrix. On the other hand, the color of YL coal remained brown after the impregnation with PWX and POL. Fluidizability of the coal particles was maintained even after the swelling impregnation. These results suggest that PWX and POL were absorbed into the coal matrix that was swollen with THF and did not remain on the particle surface. THF-swelling was also effective for preparing composite particles of IL coal and polyolefin. When coals were impregnated with n-hexane instead of THF, PWX or POL remained on the outer surface of the coal particles and many agglomerates were formed. This reflects the difference in swelling ability between THF and n-hexane. The swelling ratios of YL and IL coals in THF were 2.0 and 1.7, respectively, while that in n-hexane was negligible.

Recently, we developed a method of inverse-liquid chromatography using coals as the stationary phase. The elution curve of n-paraffinic compounds was explained by size-exclusion mechanism [3]. By this method, we found that a lot of meso- and micropores into which n-paraffins could permeate were much developed after the THF swelling. For instance, pores into which n-decane could permeate accounted for only 2% of the total volume of YL coal immersed in n-hexane at 30°C. This volume was increased to about 25% when the coal was swollen in THF. The above results indicate that reduction in the molecular size of polyethylene and swelling of the coal are both indispensable for better contact between these two substances.

3.2. Curie-point pyrolysis

Figure 1 shows the product distributions resulting from copyrolysis of the YL-HDPE, YL-PWX and YL-POL composites at 764°C. IOG indicates CO, CO₂ and H₂O, and HCG means C₁-C₅ hydrocarbon gases. The yield of each product is expressed in units of kilograms per 100 kilograms of raw coal on a dry basis. In the evaluation of copyrolysis, raw coals should not be used as reference materials. The effect of copyrolysis should be calculated based on the coal treated without addition of polyethylene, but prepared in the same manner as the respective coal-polyethylene composite. The YL coal preheat-treated at 200°C for 1 h and that preswollen in THF at 55°C for 24 h were used as the reference samples for YL-HDPE and YL-DPE, respectively. Heat-treatment at 200°C increased the total volatile and tar yields from the YL coal by 1.0 and 2.0 g/100g of the initial YL coal, respectively. Preswelling with THF, however, hardly changed these yields.

If there is no interaction between coal and polyethylene in the primary pyrolysis, the yield of each pyrolysate from the copyrolysis is equal to the sum of the yields obtained by separate pyrolysis of the individual components. Copyrolysis of the YL-PWX and the YL-POL samples, however, increased the tar yield by 12 and 10 g per 100g of raw coal, while that of the YL-HDPE sample increased only by 4.5 g. More than 80 wt% of PWX and POL were converted

to tar at 764°C in the absence of coal. Thus, the increase in tar yield by the copyrolysis cannot be explained only by the promotion of tar evolution from polyethylene.

The reduction in hydrogen and hydrocarbon gases by the copyrolysis indicates the transfer of hydrogen and hydrocarbon radicals from polyethylene to YL coal. Hydrogen yield of the copyrolysis was equivalent to that of the pyrolysis of the YL coal alone. This suggests virtually all hydrogen radicals formed from polyethylene were transferred to the coal. On the other hand, the transfer of hydrocarbon radicals was less efficient. Thus, contact between coal and polyethylene is not a factor affecting the amount of hydrogen and hydrocarbon radicals. It is clear, however, that DPE impregnated into the coal matrix promoted tar formation much more significantly than HDPE coated on the coal surface.

The swelling impregnation of depolymerized polyethylene was also more effective for reduction of inorganic gas yield than simple coating of HDPE. CO, CO₂ and H₂O were generated by decomposition of acidic -OH groups and this was accompanied by formation of cross-links [4,5]. Such cross-linking reactions can be suppressed by breakage of hydrogen bonds by solvent swelling with a hydrogen donor solvent such as tetralin [6]. The present result suggests that PWX and POL which permeated into the swollen coal remained in the coal matrix after the removal of THF, and that a portion of hydrogen bonds were irreversibly broken.

Copyrolysis of the IL-PWX or IL-POL composite at 764°C increased the tar yield by 6-7 kg, while copyrolysis of the IL-HDPE sample hardly changed the tar yield. The yields of hydrogen and hydrocarbon gases from IL-PWX and IL-POL sample were nearly equal to the yields from the IL coal alone. Hydrogen and hydrocarbon radicals from PWX and POL were transferred quite efficiently to coal radicals and consumed without forming H₂ and HCG gases. The copyrolysis at 920°C enhanced the tar formation more significantly than that at 764°C for all combinations of coal and polyethylene derivatives.

3.3. Entrained-flow pyrolysis

Figure 2 shows the yields of pyrolysates by copyrolysis of YL-POL and IL-POL samples in EFP, expressed in the same manner as in Fig.1. The increase in tar yield by copyrolysis was thus evident under environment where the vapor-phase secondary reaction proceeded. Pyrolysis of the YL-PWX and IL-PWX samples gave quite similar product distributions as shown in Fig.2. The decrease in HCG yield by copyrolysis in EFP was lower than in CPP. This suggests that hydrocarbon fragments from POL, used to stabilize coal fragments in the primary pyrolysis, were partially decomposed to HCG in the vapor phase, and that transfer of hydrocarbon radicals seldom occurred there.

The reduction of H₂ by copyrolysis of the IL-POL composite was larger in EFP than in CPP. Hydrogen transfer reactions occurred among tar molecules in the secondary reaction as

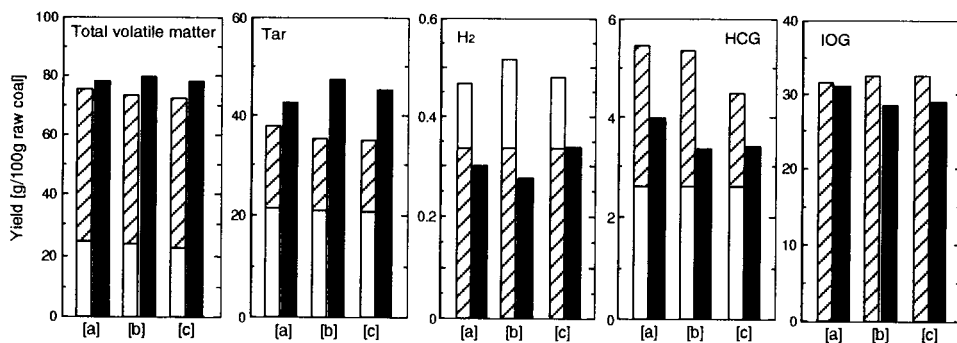


Figure 1. Comparison of product yield by copyrolysis of YL and polyethylene in CPP with sum yield by their separate pyrolysis. [a]: copyrolysis of YL - HDPE, [b]: YL - PWX, [c]: YL - POL. ■ : copyrolysis, ▨ : coal, □ : polyethylene

observed in the primary reaction. Contrary to this, copyrolysis of the YL-POL sample in EFP promoted H₂ generation due to dehydrogenation. Vapor-phase secondary reactions between coal and polyethylene-derived products thus vary significantly with coal rank. Copyrolysis of the YL-POL sample in EFP increased CO yield by 2-4 kg, while copyrolysis in CPP decreased the yield by 2-3 kg. In the primary pyrolysis, decomposition of phenolic -OH groups was suppressed and evolution of tar molecules carrying -OH groups was enhanced. In the secondary pyrolysis, these tar molecules were converted into CO [7].

The yields of BTX and naphthalenes (naphthalene, 1-methylnaphthalene and 2-methylnaphthalene) were increased by copyrolysis with any coal-DPE combination. Other aromatics such as indene, biphenyl, acenaphthylene and phenanthrene increased at the same time. The yield of di-aromatics by copyrolysis was equivalent to that obtained by pyrolysis of the reference coals.

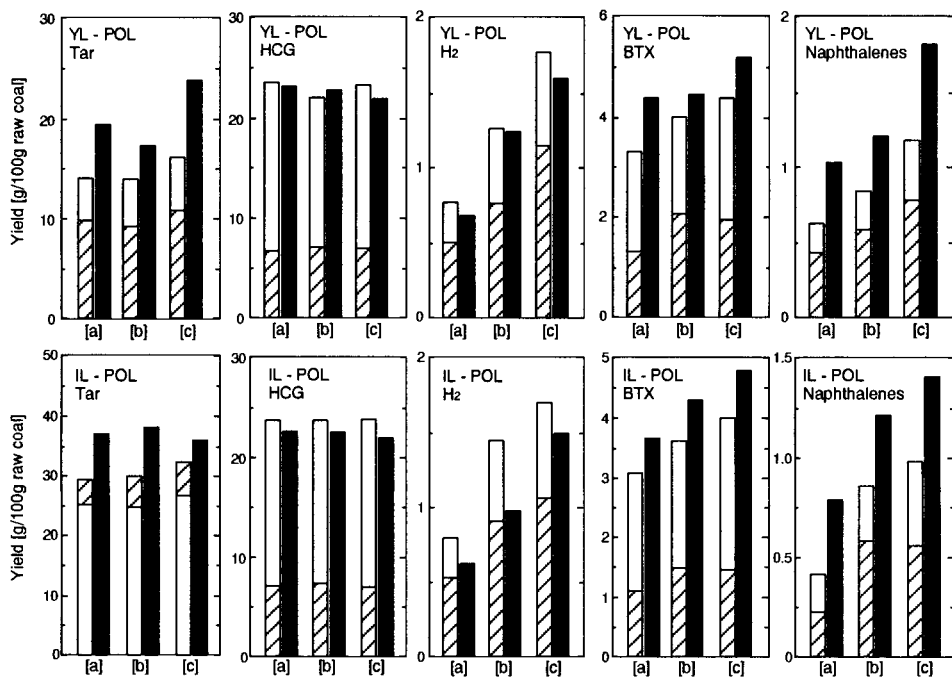


Figure 2. Comparison of product yield by copyrolysis of YL and POL in EFP with sum yield by their separate pyrolysis. [a]: 800°C, [b]: 850°C, [c]: 900°C
 ■ : copyrolysis, ▨ : coal, □ : polyethylene

References

- [1] J.-i. Hayashi, H. Mizuta, K. Kusakabe and S. Morooka, *Energy and Fuels*, 8 (1994) 1353.
- [2] K. Ofosu-Asante, L.M. Stock and R.F. Zabranski, *Fuel*, 68 (1989) 567.
- [3] J.-i. Hayashi, S. Amamoto, K. Kusakabe and S. Morooka, *Energy and Fuels*, 7 (1993) 1213.
- [4] E.M. Suuberg, P.E. Unger, J.W. Larsen, *Energy and Fuels*, 1 (1987) 305.
- [5] P.R. Solomon, M.A. Serio, G.V. Deshpande and E. Kroo, *Energy and Fuels*, 4 (1992) 42.
- [6] K. Miura, K. Mae, T. Yoshimura, K. Masuda and K. Hashimoto, *Energy and Fuels*, 5 (1991) 803.
- [7] J.-i. Hayashi, Y. Matsuo, K. Kusakabe and S. Morooka, *Energy and Fuels*, 9 (1995) *in press*.

COLIQUEFACTION OF COAL AND WASTE POLYMERS

L.L. Anderson, W. Tuntawiroon, and W. B. Ding
Chemical & Fuels Eng. Department - University of Utah
Salt Lake City, UT 84112 USA

INTRODUCTION

Coal can be converted into distillable liquid fuels with the addition of hydrogen. Waste polymers such as polyethylene (PE), polypropylene (PP), polystyrene (PS), polyethylene terephthalate (PET) contain hydrogen at levels of approximately fourteen per cent. Since such a small fraction of the plastic and other polymer materials are currently recycled these materials could, in principle, provide the hydrogen to aid in the liquefaction of coal. Coal alone and pure waste polymers, as well as a commingled waste polymer mixture, have been liquefied separately and mixtures of coal and various polymers have been coprocessed. Thermal and catalytic processing shows that such coprocessing can be a viable method to produce high quality liquid fuels and to mitigate the disposal problem of waste polymers.

MATERIALS AND EXPERIMENTAL

Blind Canyon coal (DECS 6, Penn State coal bank), a high volatile bituminous coal was ground to -60 mesh and stored under nitrogen. Pure plastic materials (PE, PP, PS, and PET) were obtained from manufacturers. A commingled waste plastic was obtained from a recycling center in Oregon (USA). This sample was composed of mostly soft drink containers and other plastic bottles. The major constituent of the commingled plastic mixture was HDPE. Ultimate and proximate analyses of DECS coal and the commingled plastic have been given previously.^{1,2}

Thermal and catalytic runs were done in stainless steel tubing reactors [reactor volume of 27 ml], which were heated by a fluidized sand bath. For further information on the nature of the products and to evaluate the most effective catalysts, runs were also done in stirred autoclaves. When catalysts were used they were added to the mixture and the concentration given as a weight per cent of the solid feed material. Before reaction the feed solids were vacuum dried at 100°C for one hour. Samples were placed in glass tubes which were stoppered and placed in the tubing reactors. The reactors were purged with nitrogen and pressurized to 6.89 MPa (1000 psi) with hydrogen. The tubing reactor was shaken vertically at 160 rpm for the reaction time, removed from the sand bath and immediately quenched in a water bath to room temperature. Products were removed from the reactor and extracted with pentane. The pentane was removed with a rotary evaporator and the pentane-insolubles were extracted with tetrahydrofuran [THF]. The fraction of the feed solids soluble in THF gave the conversion to liquids. The fraction soluble in pentane was referred to as "oil". Pentane/THF insolubles were considered as char or unreacted solids.

It should be emphasized that tubing reactor experiments are useful to study the various conditions and process variables for conversion of materials to liquids and gases. However, because tubing reactors cannot be optimized and cannot simulate continuous reactor systems, results from

such experiments should not be assumed to give the same results as those in larger and continuous processing systems. In fact, because tubing reactors give less than optimum results is why tubing reactors were used in these studies. Only in rare instances were very high conversions obtained. In the tubing reactor experiments described here no solvents were present.

RESULTS AND DISCUSSION

Blind Canyon coal (DECS 6, Penn State coal bank), a high volatile bituminous coal in earlier studies was catalytically converted in high yield to liquid products.³ In this research pure polymers PE, PP, PS and PET have been thermally and catalytically depolymerized. PS and PP were relatively easy to convert at low temperatures (less than 400°C) even without a catalyst. PE as low density PE (LDPE) was also found to be relatively easier than high density PE (HDPE) or commingled plastic [which was composed of mostly PE] to convert to volatile liquids. As shown in Figure 1 at temperatures higher than 420°C the conversion of HDPE and commingled plastic (both thermal and catalytic) increased dramatically relative to conversion at lower temperatures. The conversion yields rose in parallel with the pentane-solubles, (oil) also shown in Figure 1.

A variety of catalysts were tested for their ability to catalyze both the depolymerization of plastic material and coal. At the conditions found to be optimum for conversion of HDPE to liquid products (using 5% TiCl_3 at 430°C for one hour, under hydrogen [6.89 MPa, cold]) essentially all of the plastic material, as HDPE or commingled plastic waste, was converted to soluble products. Conversions of near 50 per cent of coal were obtained under the same conditions. However, when coal and HDPE were combined the coprocessing resulted in conversions of less than 50 per cent.

Differences in the type of bonds to be broken, steric factors, and aromaticity seem to make the catalytic processing of mixtures of coal and polymers more difficult than processing either material alone. This is in contrast to some earlier work by us and others which showed some synergism for the reaction of combinations of coal and waste materials.

Some catalysts such as HZSM-5 were too active in converting plastic wastes; that is, the conversion was high but the products were mostly gas. Other catalysts gave good conversion of coal. To determine if suitable catalysts could be used for coal/plastic mixtures some bifunctional, hydrogenation and hydrocracking catalysts such as Pt on $\text{SiO}_2/\text{Al}_2\text{O}_3$, Ni on $\text{SiO}_2/\text{Al}_2\text{O}_3$, and Pt on HZSM-5/ Al_2O_3 were also tested. As shown in Figure 2 these combinations gave moderate conversions, with the best combination being 2% Pt on Silica/Alumina, which gave higher conversions and higher oil yields.

Since the reaction of coal with polymers is difficult to catalyze an alternative method for converting coal and waste polymers was also tested for comparison. HDPE and commingled plastic samples were processed alone. The products were separated into gas, liquids, and solids. In a second step coal and the depolymerized liquid product from the plastic processing were coprocessed to liquids. Higher yields resulted from the two step processing and the quality of liquid products was also improved relative to the coliquefaction of coal and waste plastics together.

SUMMARY

It has been shown that processing of coal to liquids can be done with high yields of liquids. Plastic materials, either pure or as a commingled plastic waste containing different colors and impurities, can be processed with nearly 100% conversion to liquids and gases. Combinations of coal with plastic material can be processed to final products but with less conversion than expected from interpolation of the data from processing coal alone and plastic alone. Polymerization catalysts such as Titanium compounds can be utilized to depolymerize plastic materials containing HDPE at temperatures above 420°C. Bifunctional hydrogenation/hydrocracking catalysts can improve the conversion of coal/plastic mixtures but the highest conversions and oil yields were obtained when a two step procedure was used with liquefaction of plastic done in one step and coprocessing of plastic-derived liquids and coal in a second step.

ACKNOWLEDGMENT

The authors gratefully acknowledge the financial support of the US Department of Energy through the Consortium for Fossil Fuel Liquefaction Science, the University of Utah, and the State of Utah. Analytical support and assistance by Dr. Ronald J. Pugmire and Jing Liang is also gratefully acknowledged.

REFERENCES

1. Huffman, G.P., Z. Feng, V. Mahajan, P. Sivakumar, H. Jung, J.W. Tierney, and I. Wender, *Amer. Chem. Soc. Fuel Chem. Div. Preprints*, vol. 40, No. 1, pp 34-37, 1995.
2. Orr, E.C., W. Tuntawiroon, W.B. Ding, E. Bolat, S. Rumpel, E.M. Eyring, and L.L. Anderson, *Amer. Chem. Soc. Fuel Chem. Div. Preprints*, vol. 40, No. 1, pp.44-50, 1995.
3. Anderson, L.L., W.H. Yuen, and J. Jaturapitpornsakul, *Proc. ICCS*, vol.II pp. 263-266, 1993.

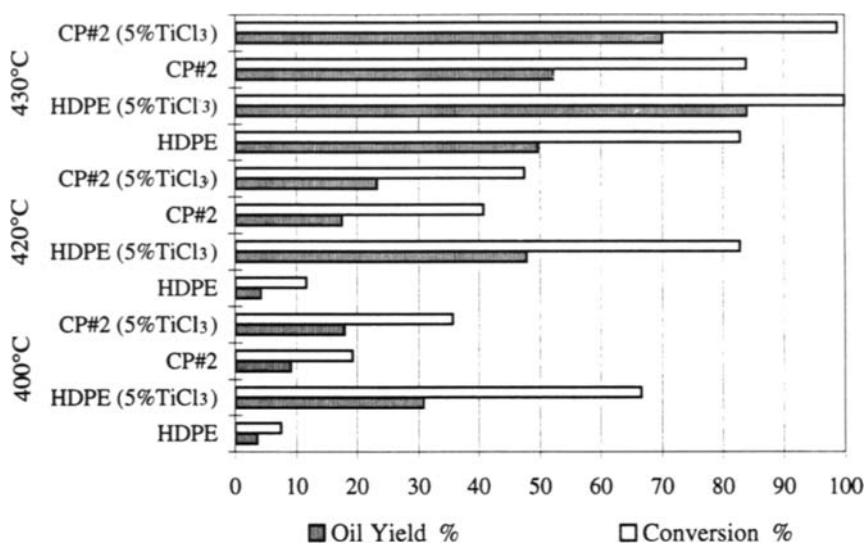


Figure 1. Effect of Temperature on Liquefaction Results for HDPE or CP#2 at 1000 psig H₂ (cold) for 1 Hour

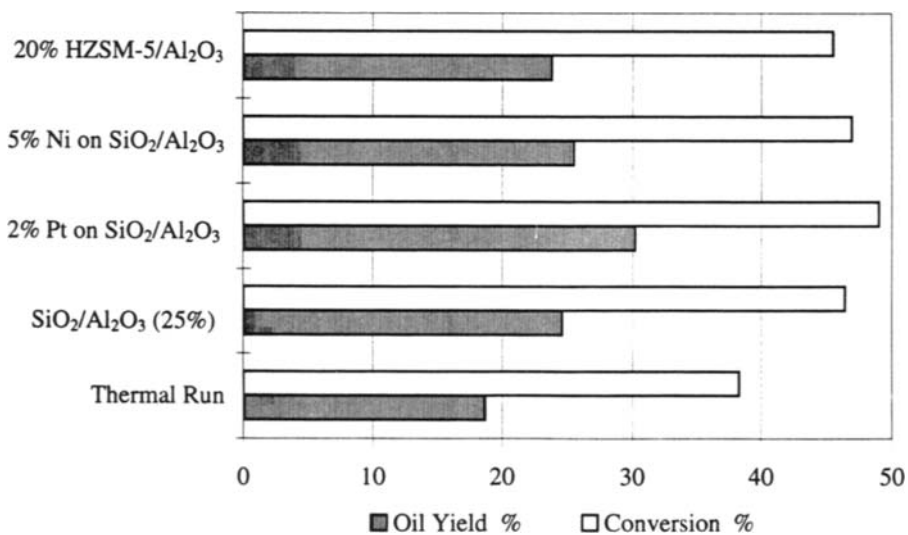


Figure 2. Results for Thermal and Catalytic Coliquefaction of DECS 6 Coal and HDPE (1:1) at 430 C, 1000 psig H₂ (cold), for 1 Hour (Catalyst:Coal+HDPE=1:10)

Direct Liquefaction of Waste Plastics and Coliquefaction of Waste Plastics With Coal

G.P. Huffman, Zhen Feng, F.E. Huggins, and Vikram Mahajan

Consortium for Fossil Fuel Liquefaction Science

341 Bowman Hall, University of Kentucky, Lexington, KY 40506, U.S.A.

1. INTRODUCTION

In previous work,⁽¹⁾ we have investigated the direct liquefaction of medium and high density polyethylene(PE), polypropylene(PPE), poly(ethylene terephthalate)(PET), and a mixed plastic waste, and the coliquefaction of these plastics with coals of three different ranks. The results established that a solid acid catalyst(HZSM-5 zeolite) was highly active for the liquefaction of the plastics alone, typically giving oil yields of 80-95% and total conversions of 90-100% at temperatures of 430-450 °C. In the coliquefaction experiments, 50:50 mixtures of plastic and coal were used with a tetralin solvent(tetralin:solid = 3:2). Using ~1% of the HZSM-5 catalyst and a nanoscale iron catalyst, oil yields of 50-70% and total conversions of 80-90% were typical.

In the current work, we have conducted further investigations of the liquefaction reactions of PE and a commingled waste plastic, and the coliquefaction reactions of PE, PPE and Black Thunder subbituminous coal. Several different catalysts have been used in these studies.

2. EXPERIMENTAL PROCEDURE

The feedstock materials used in the work reported in this paper included medium density polyethylene (PE), polypropylene (PPE), a commingled waste plastic obtained from the American Plastics Council(APC), and a subbituminous coal (Black Thunder). Proximate and ultimate analyses for the coal and APC waste plastic are shown in Table 1. The experiments used several types of catalysts: a commercial HZSM-5 zeolite catalyst⁽²⁾, an ultrafine ferrihydrite treated with citric acid(FHYD/CA), a ternary Al/Si/ferrihydrite with Al:Si:Fe=1:1:18 (FHYD_{0.90}/Al_{0.05}Si_{0.05}), a coprecipitated SiO₂-Al₂O₃, and a coprecipitated SiO₂-Al₂O₃ containing 5% ferrihydrite. All catalysts except the zeolite catalyst were synthesized in our laboratory. For all runs, 1 wt.% of catalyst was added. The preparation, structure, and liquefaction activity of the ferrihydrite catalysts has been discussed in detail elsewhere^(3,4).

The liquefaction experiments were conducted in tubing bomb reactors with a volume of 50ml which were shaken at 400 rpm in a fluidized sand bath at the desired temperature. The reaction time was 60 min. for most experiments and the atmosphere in the bomb was either hydrogen or nitrogen (cold pressure 100-800 psi). Usually 5 g of plastic or plastic + coal with 7.5 g of solvent(tetralin and/or waste oil) were charged in the tubing bombs. However, a number

of experiments were conducted with plastics alone. The reactor was cooled in a second sand bath, and gas products were collected and analyzed by gas chromatography. The other products were removed from the reactor with tetrahydrofuran (THF) and extracted in a Soxhlet apparatus. The THF solubles were subsequently separated into pentane soluble (oils) and pentane insoluble (PA + AS) fractions. Total THF conversion was determined from the amount of insoluble material that remained (residue). Any added catalyst was subtracted from the residue sample weight.

3. RESULTS AND DISCUSSION

Previously, we have shown that a solid acid catalyst(HZSM-5 zeolite) is highly active for the liquefaction of PE, PPE, and mixed waste plastic.⁽¹⁾ Some interesting new results for PE are shown in Figure 1, where it is shown that oil yields are not strongly dependent on hydrogen pressure. Moreover, the oil yield as determined by pentane solubility is as high under nitrogen as it is under hydrogen. The total conversion(THF soluble) was nearly 100% in all cases.

Our previous paper⁽¹⁾ examined the coliquefaction of a mixed waste plastic with both a bituminous and a subbituminous coal. Oil yields of 60-70% and total conversions of over 90% were observed in the presence of both the HZSM-5 catalyst and an iron catalyst(430 °C, 800 psi H₂-cold, 60 min., tetralin solvent). We are currently studying the response of individual plastic resins to various catalysts and conditions in more detail. Some typical results are shown in Figure 2, where the coliquefaction results for a 1:1 mixture of polyethylene(PE) and Black Thunder subbituminous coal are compared to those for a 1:1 mixture of polypropylene(PPE) with the same coal. It is evident that PPE undergoes considerably more synergistic reactions with coal than PE. Several solvents for plastics liquefaction are being explored. An example of this work is shown in Figure 3. The APC commingled plastic was liquefied in mixtures of tetralin and waste automotive oil; the percentage of waste oil in the mixture is indicated. At 445 °C, the effect of using waste oil rather than tetralin is obviously much greater than the effects of the added catalysts.

Currently, an experimental matrix of temperature, catalysts, pressure, solvent, and time is being explored for the APC commingled plastic. This work will be extended to include additional mixed waste plastics as well as individual resins. Some typical results are shown in Figure 4, where the use of a tetralin solvent is compared to liquefaction with no solvent for both

Table 1.

Proximate ^a	Coal	Plastic
% Ash	6.3	0.5
% Volatile	45.4	98.8
% Fixed Carbon	48.3	0.7
Ultimate ^b		
% Carbon	71.6	84.7
% Hydrogen	4.8	13.7
% Nitrogen	1.5	0.7
% Sulfur	0.5	0.01
% Oxygen	15.2	1.0

a = Dry basis, b = Dry ash free basis.

thermal and catalytic reactions. It is evident from both Figure 4 and Figure 3 that the aromatic structure of tetralin, which makes it a good solvent for coal liquefaction, is not the best choice for liquefaction of predominantly aliphatic plastics. It is also seen that the coprecipitated silica-alumina catalysts prepared in our laboratory give somewhat better yields than the commercial HZSM-5 zeolite.

ACKNOWLEDGEMENT

This research was supported by the U.S. Department of Energy through DOE contract No. DE-FC22-93-PC93053 as part of the research program of the Consortium for Fossil Fuel Liquefaction Science. We are grateful to Richard Anderson of the University of Kentucky Center for Applied Energy Research for his assistance with the liquefaction experiments.

REFERENCES

1. M.M. Taghiei, Z. Feng, F.E. Huggins, and G.P. Huffman, *Energy & Fuels*, **1994**, 8, 1228-1332.
2. United Catalysts Inc., P.O. Box 32370, Louisville, KY 40232.
3. J. Zhao, Z. Feng, F.E. Huggins, and G.P. Huffman, *Energy & Fuels*, **1994**, 8, 38-43.
4. J. Zhao, Z. Feng, F.E. Huggins, and G.P. Huffman, *Energy & Fuels*, **1994**, 8, 1152-1153.

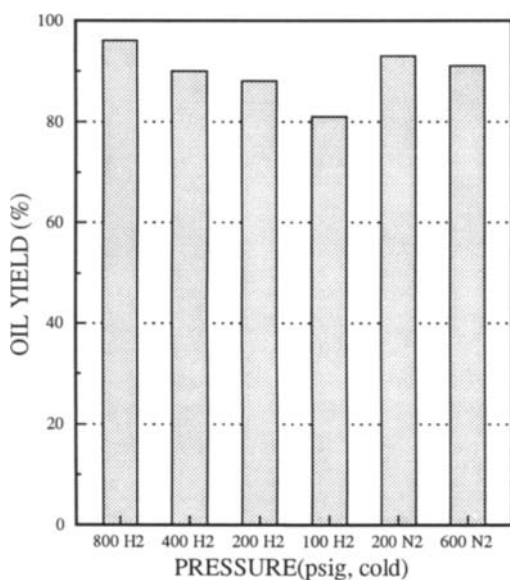


Figure 1. Liquefaction results for MDPE as vs. pressure: 430 C, 60 min, 800 psig H2(cold).

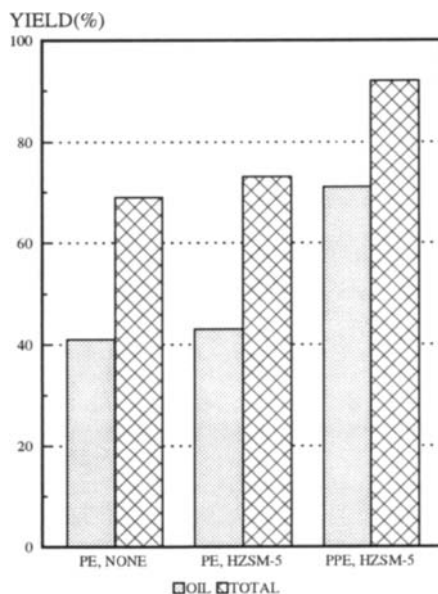


Fig. 2 Coliquefaction of coal with PE and PPE: 400 C, 60 min, 800 psig H2(cold).

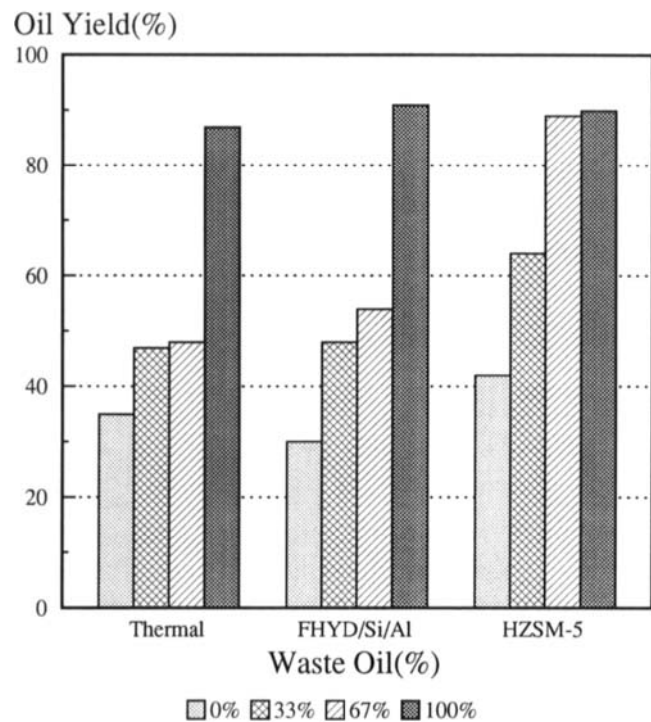


Figure 3. Effect of percentage of waste oil in solvent on oil yields for APC plastic: 445 C, 800 psig H₂(cold).

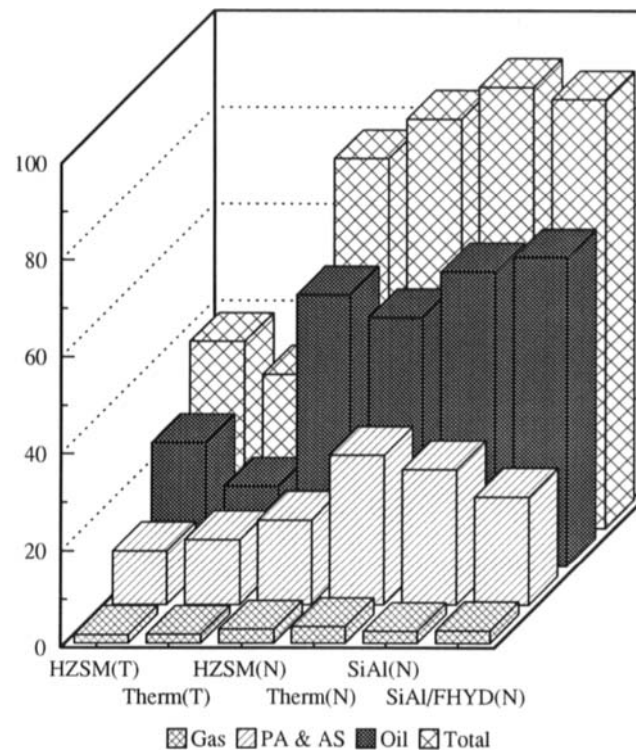


Figure 4. Liquefaction results for commingled plastic: 800 psig H₂(cold), 60 min, 430 C: solvent = tetralin(T) or none(N).

LIQUEFACTION OF COAL/WASTE PLASTIC MIXTURES

S.R. Palmer, E.J. Hippo, D. Tandon and M. Blankenship

Department of Mechanical Engineering and Energy Processes
Southern Illinois University at Carbondale,
Carbondale, Illinois 62901-6603, USA.

1. INTRODUCTION

The need for expensive hydrogen gas inflates the cost of current coal liquefaction processes (1). To potentially reduce these costs the co-liquefaction of coal mixed with waste plastics has been studied. This use for waste plastics could become possible because over 30 million tons of synthetic polymer material is produced in the United States every year (2). This is projected to double by the year 2000 (3). Most of this material ends up being landfilled and it is estimated that of the 160 millions tons of municipal solid waste produced every year in the United States, waste plastics contribute 7-9% by weight and over 20% by volume (4).

It is proposed that the hydrogen present in waste plastic can be recovered and used directly for coal hydrogenation during the co-liquefaction process. An added bonus of this concept is the fact that waste plastic is recycled instead of discarded. To explore these possibilities co-conversion experiments were performed on samples of polyethylene (PE), polypropylene (PP), coal/PE and coal/PP blends, as well as the raw coal. Nitrogen, hydrogen and steam pyrolysis conditions as well as the model liquefaction environment employing tetralin as a hydrogen donor solvent were used. The coal used was a sub-bituminous Illinois No.6. Various reaction times and temperatures were investigated.

This concept has been investigated by these authors as well as several other research groups (5-12). Many of these studies have concentrated on coprocessing in a hydrogen atmosphere with added catalysts with the emphasis placed on maximum plastic conversion (7-11). This paper differs in that no added catalysts are used and because maximum conversions of coal, not plastic, are emphasized. In many instances it has been determined that although conversions for individual materials are high, when they are mixed together liquid yields are somewhat diminished (8). Others report synergistic conversions when plastic and coal are processed together (5,12).

2. EXPERIMENTAL

2.1 Materials

Samples of PE and PP were obtained from Aldrich Chemical Company. The coal sample (Illinois No. 6) was obtained from the Illinois Coal Basin Sample Program. The coal was physically cleaned to remove mineral matter. Analysis of the cleaned coal gave: 76.2% C, 5.0% H, 1.1% N, 2.8% S, 3.9% ash and 7.3% moist. (Dry basis except moisture.)

2.2 Liquefaction experiments

The liquefaction experiments were conducted in 18 mL microreactors. Typical experiments used a 2g charge of coal, plastic or coal/plastic mixture. 2mL of tetralin were used for liquefaction while 2 mL of distilled water was used for steam pyrolysis. After the sample was loaded, air was purged by repeatedly pressurizing then depressurizing with the desired gas. Final cold pressures of 500psig were used throughout. The microreactor was immersed and continuously shaken in a fluidized sand bath maintained at the desired reaction temperature. After reaction the microreactor was cooled in a cold sand bath. Conversions were measured via extraction of the products with tetrahydrofuran (THF).

3. RESULTS AND DISCUSSION

Figure 1 shows the typical behavior for the coal/PE system for pyrolysis in a nitrogen atmosphere as a function of pyrolysis temperature. The coal/PP system behaved similarly. It can be seen that the conversion of coal to THF soluble material remains relatively constant throughout the temperature range. However, PE conversion does not increase significantly until a temperature approaching 425°C is reached. At temperatures above 475°C the conversion of PE to THF solubles is seen to decline with increasing temperature. This can be attributed to coke formation. From the conversion data for the individual materials (coal and PE alone) the conversion for a 1:1 mixture of coal and PE can be predicted if it is assumed that no interaction between the two components takes place. This predicted conversion together with the conversion obtained experimentally are also presented in Figure 1. It can be seen that throughout the temperature range 425°C to 550°C there is reasonably good agreement. This suggests a non-interacting system. However, the conversions for the 1:1 mixture obtained at the lower temperatures are significantly higher than those that would be predicted. Thus it would appear that at lower temperatures synergistic conversions of coal and PE are possible, but that these synergisms are lost if temperatures are increased.

Figure 2 reports the pyrolysis behavior of the coal/PE system, again in the nitrogen atmosphere, but this time as a function of reaction time at a constant temperature (425°C). Although the conversion of the coal remains relatively constant, the conversion of PE is seen to steadily increase with increasing reaction time. If we compare predicted and experimental conversions for the 1:1 mixture we can see that shorter reaction times result in synergistic conversion of the coal and PE. As was observed with increasing temperature, the apparent synergism is lost if longer reaction times are used.

Figure 3 compares the conversions of the coal/PE system in the four different conversion environments examined. All data shown was obtained at a temperature of 425°C for 1 hour. It can be seen that the conversions obtained in a steam or a hydrogen atmosphere are very similar to those obtained in a nitrogen atmosphere. The exception to this is the conversion of the coal/PE 1:1 mixture in a hydrogen environment which shows a significant decline when compared to the nitrogen experiment. Not surprisingly coal conversions are significantly higher in the liquefaction environment. However, the conversion of the individual plastics appears to be dramatically inhibited by these liquefaction conditions. Indeed, PP conversions as low as 14% were observed after 15 minutes at 425°C in the presence of tetralin and hydrogen gas. Under similar conditions in a nitrogen environment a PP conversion around 95-100% is observed. Due to the low conversions of the individual plastics, the conversions of the coal/plastic blends often indicate significant synergistic conversion.

Due to the apparent retardation of PE and PP decomposition in the liquefaction environment there was concern that the THF extraction of the liquefaction products derived from the coal/plastic mixtures might not truly represent the degree of coal conversion. To check this these extraction residues were pyrolyzed using a thermogravimetric analyzer. It was found that many of the extraction residues from the liquefaction experiments had very high volatile yields. As we can see from Figure 4. if we assume all the material soluble in THF is volatile, then distillation of the whole products would give distillate yields up to 96%. The volatile matter contents were highest for the lower temperature and shorter time reactions, indicating that the extraction residues become more intractable as time and temperature increase. The pyrolysis profile of the extraction residues with that of the virgin plastic demonstrates a high degree of similarity. This suggests that the THF insoluble material from the tetralin/hydrogen atmospheres is mostly unconverted plastic. If this is true then the conversions of the coal in these mixtures approach completion.

4. SUMMARY AND CONCLUSIONS

Although the results gathered so far are preliminary in nature, it can be appreciated that the use of waste plastics in coal liquefaction processes has great potential. Synergistic conversions of coal/plastic mixtures have been observed under many pyrolysis and liquefaction conditions. This suggests that strong interactions between the components of the system occur during co-processing. It is proposed that a free radical hydrogen abstraction mechanism is responsible for much of the observed behavior and that tetralin retards PE and PP decomposition via a radical capping or adduction mechanism. It is believed that the liquefaction conversions reported here are important because they were obtained using no added liquefaction catalyst, relatively low temperatures, low hydrogen pressures and using a relative poor H-donor solvent (tetralin).

ACKNOWLEDGEMENTS

We thank the following for support: Illinois Clean Coal Institute, United States Department of Energy, Office of Solid Waste Research at the Univ. of Illinois, and the Materials Technology Center at SIUC. We are grateful to Dr. D. Banerjee, our project manager at the ICCI.

REFERENCES

1. Farcasiu, M. PETC Review, 1991, p4-15.
2. Ainsworth, S.J. Chemical and Engineering News, August 31 1992, p34.
3. Reisch, M.S. Chemical and Engineering News, May 4 1992, p29-42.
4. Erwin, L. and L.H. Jr. Healy. Packaging and Solid Waste. Management Strategies. 1990, American Management Association, New York.
5. Palmer, S.R., Hippo, E.J., Tandon, D. and Blankenship, M. Am. Chem. Soc. Div. Fuel Chem. Prepr., 1995, 40(1), pp 29-33.
6. Taghiei, M.M., Huggins, F.E. and Huffman, G.P. Am. Chem. Soc. Div. Fuel Chem. Prepr., 1993, 38(3), pp 810-815.
7. Liu, K., Jakab, E., McClennen, W.H. and Meuzelaar, H.L.C. Am. Chem. Soc. Div. Fuel Chem. Prepr., 1993, 38(3), pp 823-830.

8. Anderson, L.L and Tuntawiroon, W. Am. Chem. Soc. Div. Fuel Chem. Prepr., 1993, 38(3), pp 816-822.
9. Orr, E.C., Tuntawiroon, W., Anderson, L.L. and Eyring, E.M. Am. Chem. Soc. Div. Fuel Chem. Prepr., 1994, 39(4), pp 1065-1072.
10. Liu, K., McClennen, W.H. and Meuzelaar, H.L.C. Am. Chem. Soc. Div. Fuel Chem. Prepr., 1995, 40(1), pp 9-14.
11. Orr, E.C., Tuntawiroon, W., Ding, W.B., Bolat, E., Rumpel, S. Eyring, E.M. and Anderson, L.L. Am. Chem. Soc. Div. Fuel Chem. Prepr., 1995, 40(1), pp 44-50.
12. Taghiei, M.M., Feng, Z., Huggins, F.E. and Huffman, G.P. Energy & Fuels, 1994, 8, p1228-1232.

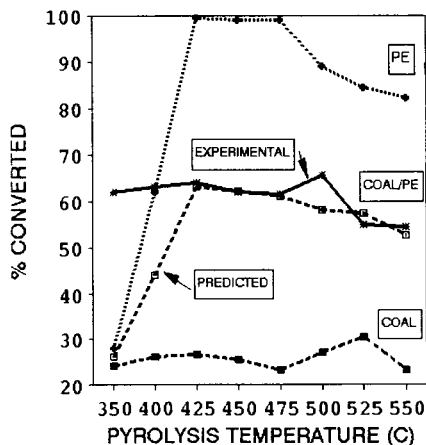


Figure 1. Conversions for Coal/PE in a nitrogen atmosphere as a function of reaction temperature. (Constant reaction time/ 60 mins)

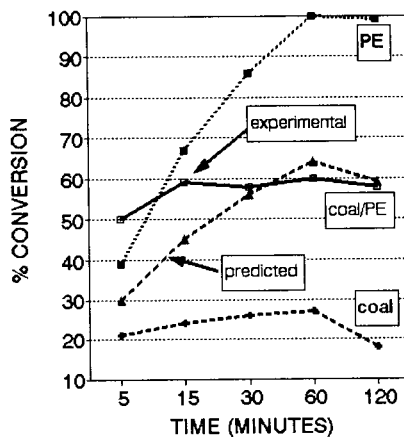


Figure 2. Conversions for Coal/PE in a nitrogen atmosphere as a function of reaction time. (Constant temp./ 425°C)

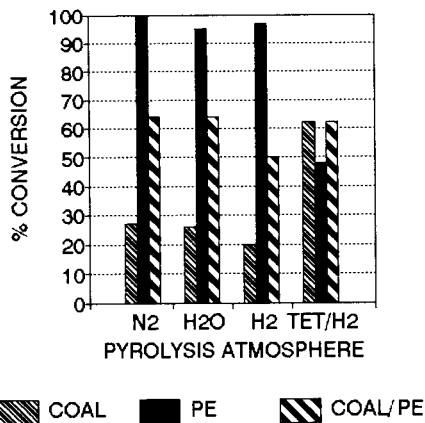


Figure 3. Conversions of coal/PE in various pyrolysis/liquefaction environments. (425°C for 15 minutes)

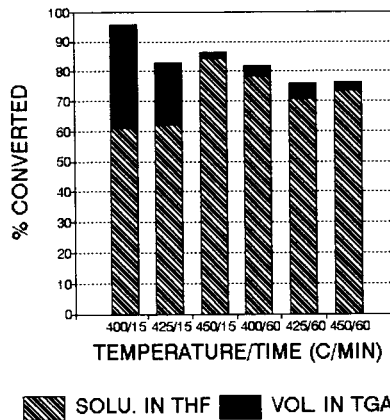


Figure 4. Total liquefaction conversions of coal/PE measured by THF extraction and TGA volatility.

Pyrolysis of coal impregnated with waste plastics utilizing methanol as a swelling reagent

Kouichi Miura, Kazuhiro Mae, Taisuke Maki and Masanori Takase
Department of Chemical Engineering and Research Lab. of Carbonaceous
Resources Conversion Technology, Kyoto University, Kyoto 606-01, JAPAN

1. INTRODUCTION

We have recently proposed that flash pyrolysis of coal-solvent slurry will be a promising process for recovering valuable chemicals in high yields from coal under mild conditions¹. The solvent molecules incorporated in micro space in the solvent-swollen coal contribute to suppress crosslinking reactions physically as well as to act as a hydrogen donor during the primary devolatilization², which significantly increases the yield of liquid products. The solvent in the vapor phase contribute to control the secondary gas phase reactions, which surprisingly increased the yield of BTX (benzene, toluene, and xylene) up to 0.1 kg/kg-coal when methanol was used as a solvent.

In this paper we propose to extend the above method to the treatment of waste plastics. Since plastics such as polyethylene, polypropylene, etc. are rich in hydrogen, they are expected to act as effective hydrogen donors when they were co-pyrolyzed with coal. One of the drawbacks of such a process is poor contact between coal and plastics when they are simply mixed. To overcome the drawback, pre-modification of plastics and/or coal was proposed. A polyethylene was partly degraded to a wax. A coal was pre-oxidized by H₂O₂ at room temperature. This treatment introduces -COOH groups into the coal, and the oxidized coal can be swollen to a larger extent in methanol³. The wax was impregnated into the coal and the oxidized coal utilizing the swelling phenomenon of the both coals.

First, the coal and the oxidized coal swollen by the wax were pyrolyzed using a Curie-point pyrolyzer to examine the validity of the proposed method. Then the pyrolysis of a coal-wax-methanol slurry was performed in a free fall pyrolyzer to realize the proposed concept in a practical process.

2. EXPERIMENTAL

2.1. Sample preparation

An Australian brown coal (Morwell, MW; C:64%, H:4.7%, N:0.7%, S:0.3%, O:30.3%) was used as a raw coal. The coal was ground into fine particles of less than 74 μ m, and dried in vacuo at 110 °C for 24 h before use. The oxidation of the coal was performed as follows: 2 g of coal were mixed with 3 ml of methanol, then 20 ml of 30% aqueous hydrogen peroxide were added to the mixture. After treating the mixture for 4 h in an water bath kept at a constant temperature of 25 °C, the oxidized coal was filtrated and evacuated for 24h at

60°C . Since the solid yield through oxidation was 0.96 kg/kg, the amount of carbon lost through the treatment was small. The oxidized coal was abbreviated to PO25.4, where PO means the oxidation by H₂O₂, and the figures 25 and 4, respectively, represent the treatment temperature (°C) and the treatment time (h).

A wax obtained by pyrolyzing a waste cross-linked polyethylene at 400°C was used as a model substance of plastics. The wax and the coal, or the oxidized coal, were mixed at the ratio of 0.28 to 0.50 kg/kg-coal, and heated up to 150°C under the 1 MPa of nitrogen. By this treatment coal particles were swollen, and all the wax was retained in the coal matrix. The swelling ratio of the solvent treated coal was measured by the volumetric technique⁴. The PO25.4 sample swollen by the wax was mixed with methanol at the ratio of 1 to 4 by weight to prepare an oxidized coal-wax-methanol slurry. Through this treatment the oxidized coal was swollen further.

2.2. Flash pyrolysis

The raw coal and the PO25.4 sample swollen by wax were pyrolyzed in an inert atmosphere using a Curie-point pyrolyzer (Japan Analytical Ind., JHP-2S). About 2 mg of sample wrapped up tightly by a ferromagnetic foil were placed in a small quartz reactor (4.0 mm I.D.), and heated up to a temperature between 590 and 920°C at the rate of 3000°C/s by an induction heating coil to be pyrolyzed rapidly. The experimental apparatus and the procedure were described in detail in the previous paper².

The PO25.4-wax-methanol slurry was pyrolyzed using a free fall pyrolyzer. The slurry was fed *via* a micro feeder made of plastic syringe to the reactor at the rate of around 12 g/h. Nitrogen was also fed to the reactor at the flow rate of 1 L/min. The reactor was made of quartz tube of 0.023m in inner diameter and 0.45 m in length. The solid product, char, was separated from tar and gases at the bottom of the reactor. The nitrogen stream containing tar and the gases passed an ice-cooled trap and two dry ice methanol-cooled traps placed in series to collect liquids completely. A part of the gases exiting the traps were collected in a gas bag, and it was analyzed by a gas chromatograph. The yields of char, gas, and tar were determined based on these analyses and measurements. The material balance of all the experiments were obtained within 95 to 105 %.

3. RESULTS AND DISCUSSION

3.1. Pyrolysis of coal and oxidized coal swollen by wax

Figure 1 compares the pyrolysis yields of the wax-swollen raw coal and the wax-swollen PO25.4 sample. Each yield is represented on the basis of 100 kg of raw coal (d.a.f. basis). The black bars represent the yields obtained by pyrolyzing the samples swollen by the wax. The white bars are the yields for either the raw coal or the oxidized coal, and the dotted bars are those for the wax. Comparison between the black bar and the sum of the white and dotted bars gives the effect of swelling by the wax.

For both the raw coal and the oxidized coal (PO25.4) swollen by the wax, the yields of total volatiles and tar significantly increased at the temperature between 400 and 600°C. Corresponding to these changes, the yields of H₂O and H₂ decreased at the same temperature region. This indicates that the wax

retained in the sample particles suppressed the crosslinking reaction forming H_2O and enhanced the hydrogen transfer from wax to coal during the pyrolysis¹⁻³.

Although the wax-swelling treatment is effective to both the raw coal and the oxidized coal, it is more effective to the oxidized coal as indicated by a large increase in the tar yield (19.9 kg/100kg-coal) for PO25.4. The large increase was judged to be brought about by the introduction of hydrogen bonding sites (-COOH groups) by the oxidation. This contributes to increase the swelling ratio of the coal by the wax, which would suppress the crosslinking reaction to a larger extent during the pyrolysis. This reasoning is well supported by large decreases in the yields of H_2O and CO_2 for the wax-swollen PO25.4.

3.2. Pyrolysis of coal-wax-methanol slurry

Pyrolysis of the wax-swollen coal was found to be very effective as stated above, but the method may not be practical because of the difficulty in handling the swollen coal. We have clarified that the pyrolysis of coal-methanol slurry is an effective and practical method¹. It increases the total volatiles and the BTX yield significantly. As an additional merit coal-methanol slurry facilitates the handling of coal significantly. Then this method was extended to the pyrolysis of wax-swollen coal.

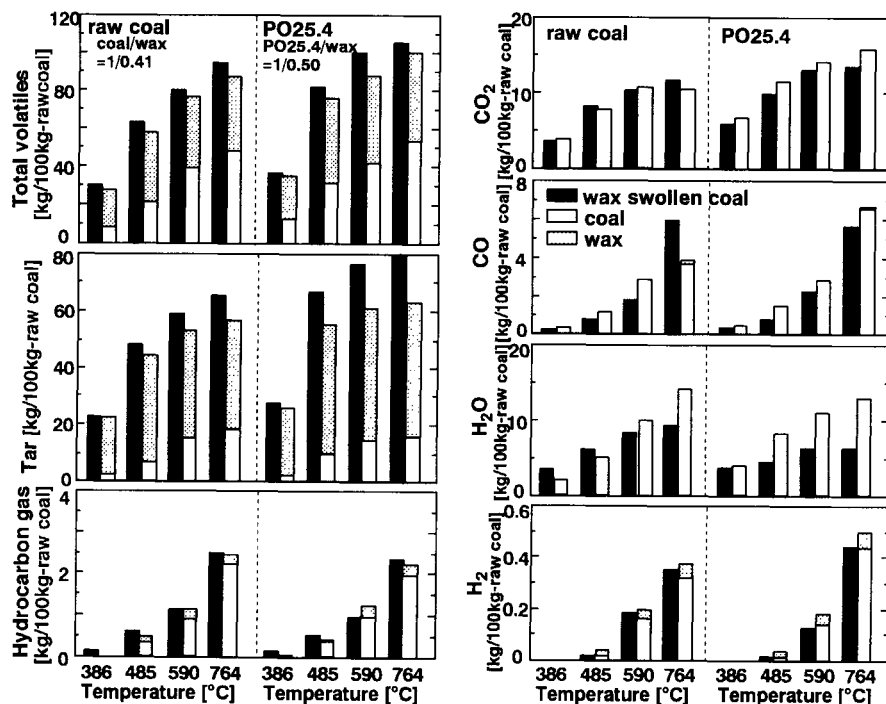


Figure 1 Pyrolysis yields for the raw coal and the PO25.4 sample swollen by wax.

A methanol slurry of the wax-swollen PO25.4 sample was prepared as stated above, and was served to the pyrolysis in a free-fall pyrolyzer. Figure 2 compares the yields obtained by pyrolyzing the slurry with the sum of the yields obtained by pyrolyzing PO25.4, the wax and methanol independently at 750 °C. The black bars are the product yields for the flash pyrolysis of the oxidized coal-wax-methanol slurry. The white bars are the product yields of the oxidized coal in the nitrogen atmosphere, the hatched bars are those obtained by pyrolyzing the wax, and the dotted bars are those obtained by pyrolyzing methanol. All yields are represented on the basis of 100 kg of raw coal (d.a.f. basis).

The char yield of the slurry was only 40.1 kg/100kg-coal, which was smaller than that of the oxidized coal by 9.7 kg/100kg-coal. This indicates that the wax and methanol in the coal, which are penetrating the coal matrix and are swelling the coal, affected the primary reaction as expected. The tar yield of the slurry increased by 6.0 kg/100kg-coal and reached 29.6 kg/100kg-coal. The yield of C₂-C₆ components interestingly increased by 12.9 kg/100kg-coal and reached 24.9 kg/100kg-coal. This amount was much larger than that attained by pyrolyzing the methanol slurry of the raw coal¹. The oxidation pre-treatment significantly increased the solvent-swelling ability of the coal, then larger amount of methanol was incorporated in the coal matrix. Methanol interacting intimately with the coal matrix is decomposed easily. This was supposed to be a main cause of the large increase in the yields of C₂-C₆ components during the pyrolysis of the PO25.4-wax-methanol slurry. Thus the validity of the pyrolysis of coal-wax-methanol slurry was clarified.

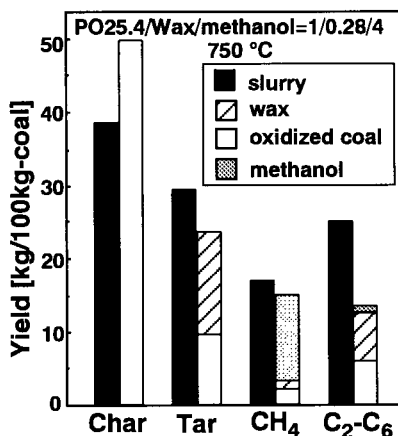


Figure 2 Pyrolysis yields for the PO25.4-wax-methanol slurry.

4. CONCLUSION

A concept was proposed for co-pyrolyzing coal and waste plastics. The intimate contact of coal and plastics is essential for the pyrolysis to be effective. To realize such intimate contact, impregnation of a wax, partly degraded polyethylene, to coal and/or oxidized coal through swelling was proposed. The coal oxidation pre-treatment by H₂O₂ was performed to introduce hydrogen bonding sites into the coal. Pyrolysis of the coal and the oxidized coal swollen by wax clarified the validity of the proposed method. To realize the method practically, pyrolysis of the methanol slurry of the wax-swollen coal was also proposed.

REFERENCES

1. K.Miura, K.Mae, H.Wakiyasu and K.Hashimoto, Proc. 7th ICCS, vol.I, (1993)250.
2. K.Miura, K.Mae, S, Asaoka, T. Yoshimura and K.Hashimoto, E&F, 5(1991)340.
3. K.Miura, K.Mae, S.Inoue, K.Hashimoto, Kagaku Kogaku Ronbun-shu, 20(1994)918.
4. T.K.Green, J.Kovac and J.W.Larsen, Fuel, 63(1984)935.

Effect of Introducing Tyre Pyrolysis Oil into Two-stage Coal Liquefaction

Graham Harrison and Andrew B. Ross .

School of Science (Chemistry Division), Staffordshire University, College Road, Stoke-on Trent, ST42DE, England.

1. INTRODUCTION

Work has been well documented on the use of heavy oil residues (HOR's) in coal liquefaction but low extraction yields often need to be increased by the use of catalysts (1). The HOR's have a high content of aliphatic compounds which readily coke; this problem would be less severe if there was a higher aromatic content such as that present in tyre pyrolysis oils (TPO's).

Environmental pressures are encouraging renewed attention into the recycling/disposal of tyres. One approach is pyrolysis whose oil product is highly aromatic. Many of the processes involving both pyrolysis and liquefaction of tyres have concentrated on the recovery of the carbon black, probably the most valuable product but the similarity of the oil product to coal liquids provides a potential for its incorporation into a coal liquefaction process. This introduction would introduce more flexibility into the process while making positive use of an eventually scrap material.

A high degree of success has already been achieved with coal / tyre co-processing (2) with possibilities of the carbon black playing a catalytic role and enhancing extraction (3). However, with direct introduction of scrap tyres, the presence of finely dispersed carbon black could cause problems with filtration after the first stage; such problems would be absent with the introduction of TPO.

TPO's contain significant amounts of phenanthrene and substituted phenanthrenes but contain very little hydrogen donor compounds. Coal extraction experiments with 100% TPO feeds have shown coking problems related to high viscosity and high concentrations of six ring and more compounds. Extraction yields can be increased using catalysed activated coals and by reducing the viscosity of the oil. Harrison and Ross (4) have shown that TPO's solvent ability can be enhanced by hydrogenation indicating introduction into the second stage of a two stage coal liquefaction process may be more beneficial.

2. EXPERIMENTAL

2.1 Materials.

A bulk TPO sample was provided by Bevan Recycling Ltd. The bpt distribution of the TPO sample was: 0-200°C = 27.4%, 200-250°C = 19.1%, 250-300°C = 19.1%, >300°C = 34.8%. Point of Ayr coal (CRC 702) was provided by British Coal Corporation (BCC) and had the following analysis: moisture 2.8, ash 9.8, volatile matter (dmmf) 38.0, C (dmmf) 87.2, H (dmmf) 5.8 wt%. A bulk coal liquid was provided by BCC. Hydrogenation of TPO and coal liquid used

either an unsulphided Co/Mo catalyst supplied by Akzo Chemie, Netherlands, or a used pre-sulphided Co/Mo catalyst provided by BCC.

2.2 Dissolution Experiments.

Coal (50g) and oil (100g) (1:2 ratio) were reacted in the spinning falling basket autoclave described elsewhere (5) at the required temperature and time at a stirrer speed of 500rpm. The product was removed and filtered under vacuum. The filter cake was washed with dichloromethane (DCM) and then Soxhlet extracted with tetrahydrofuran for ~ 6 hours. The THFI was ashed and the extent of dissolution was calculated by ash balance.

Solvent augmentation used a hydrogenated anthracene oil start up solvent (HAO) with incorporation of TPO in the range 10-50%. Three different variations of TPO feeds were used : (i) >275°C TPO cut (TPO+) (ii) whole bpt range TPO as received (TPO) (iii) hydrogenated TPO 275°C-450°C cut (HTPO).

2.3 Analysis of Liquid Products.

The hydrogen donor contents were derived from reaction with sulphur in a 10ml capacity autoclave, following a procedure described elsewhere (6). GC/MS characterisation used a Carlo Erba HRGC 5160 Chromatograph equipped with a DB5 capillary column linked to a VG Trio 1000 Mass Spectrometer.

3. RESULTS AND DISCUSSION

Table 1 summarises the results of the dissolution experiments with the different solvent feeds. Dissolutions calculated using DCMI were on average 10-20% lower than those calculated for THFI. The THF extracts contained additional polar compounds not removed by DCM. Extractions with TPO+ showed a decreasing trend in dissolution with increasing temperature. At temperatures above 400°C dissolution decreased due to retrograde coking reactions. However observable coking on the reactor walls, a problem using 100% TPO+, was completely eliminated at all temperatures even at 50% TPO+ incorporation. At 380°C, 20% introduction of TPO+ only caused a reduction in dissolution of about 5%. The asphaltene content decreased steadily from 12.3% at 100% HAO (380°C) to 7.7% at 50% TPO+ incorporation. This decrease suggested a reduction in ability for coal dissolution which related to the decrease in the values from the donor ability tests with sulphur, (shown relative to HAO in figure 1) as TPO+ incorporation increased. Figure 2 appears to show that the optimum reaction time at 380°C was between 0.5-1 hour; however at higher temperatures 400-420°C, reactions appeared to be complete after 0.5 hours. With increasing introduction of TPO+, the amount of high bpt material (>pyrene) in the extract increased which translated to a greater difficulty in filtration compared to filtration of 100% HAO and extracts with TPO and HTPO incorporation.

The extent of depletion in extraction yields is an important factor in the introduction of an alternative feed into a coal liquefaction scheme. However, TPO's unlike HOR's have a significant content of low bpt material containing mainly substituted benzenes and a small amount of naphthenic material. Consequently the yield of low boiling point material will effectively be increased. This increase may offset the slight reduction in extraction yields.

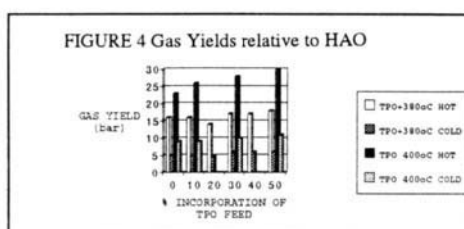
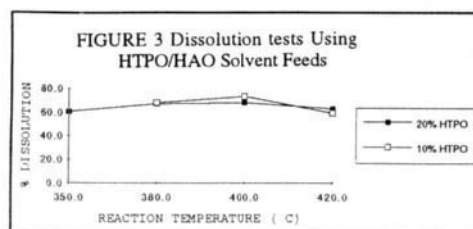
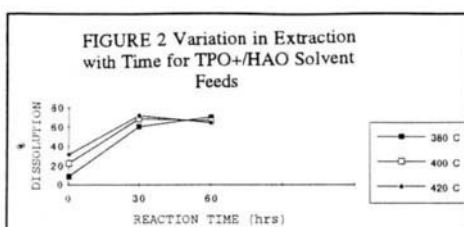
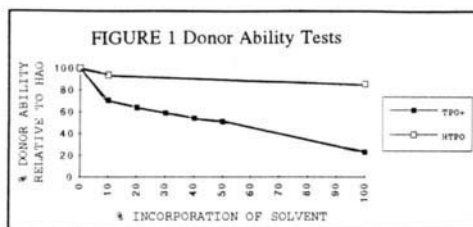
Table 1. Percentage dissolution as a function of temperature and percentage incorporation of TPO.

FEED	TEMP (°C)	% Dissolution at different % contents of TPO						
		0%	10%	20%	30%	40%	50%	100
TPO+	380	70.1	67.8	65.5	64.7	61.2	53.8	13.8
TPO+	400	66.1	62.1	-	73.1	-	58.2	7.0
TPO+	420	64.7	63.0	62.0	69.8	-	57.9	-7.3
TPO	400	66.1	63.7	62.8	57.1	-	41.0	39.0

The introduction of TPO+ would require a primary distillation step producing ~28% mainly monoaromatic hydrocarbons as the distillates. An alternative to pre-distillation would be the direct introduction of the whole bpt TPO into the first stage. The results in table 1 indicate that addition of upto 20% TPO would not affect the dissolution significantly compared to TPO+. Additions of greater than 20% gradually reduced yields, however, increased coking did not occur even at more severe temperatures. Increased pressures associated with the lower bpt material would be a major constraint. The pressure at temperature was higher than that encountered with HAO alone, due to an increase in material bpt <naphthalene. eg an increase from 4% at 100%HAO to 17% at 30% TPO incorporation. However even at 400°C-410°C the pressures, (figure 4), appeared not to be too excessive and restrictive. Gas production was evident with all TPO incorporation. The gas contained C1-C4 hydrocarbons and analysis has shown that as the incorporation of TPO increased there was an increase in the content of C1, for example 20% TPO+ (C1=7.2%, C2=0.2%, C3=0.01%, C4=0.02%) compared to 100% HAO (C1=6.8%, C2=0.26%, C3=0.01%, C4=0.02%).

Simulating introduction into the second stage has been assessed by introduction of HTPO/HAO mixtures into the first stage *ie.* a simulation of the recycle solvent produced if TPO was introduced into the hydrocracking second stage. Figure 3 indicated that a temperature of ~400°C was optimum and that the dissolution yields appeared to remain unchanged upto 20% incorporation. This would equate to the introduction of twice the amount of TPO+ to the second stage (*ie.* recycle cut of HTPO represents 44% of TPO+). The increased solvent ability of HTPO compared with TPO+ is clearly demonstrated in figure 1 in which the hydrogen donor content of the HTPO solvent was only 16% less than that of HAO. The percentage dissolution reduced from 71 (HAO) to 52% (HTPO).

Reaction with 20% HTPO at 400°C showed a dissolution value higher than 100% HAO, suggesting some synergism between the two solvents. Hydrogenation of TPO caused the yields of low bpt material to increase considerably. Reaction at 420°C for 2 hours using a pre-sulphided Co/Mo catalyst increased the yields of <275°C material from ~35% to over 50% with the H:C ratio increasing from ~1:1 to 2:1 (4). Sulphur contents were reduced from ~1.2% to ~0.3%. Approximately 28% of < 275°C material was produced from the hydrogenation of TPO+ to HTPO. This could however be increased significantly by direct introduction of the whole bpt range TPO into the second stage whilst still maintaining good coal dissolution. Work to this effect is currently underway and involves hydrogenation of mixtures of a bulk coal liquid with varying amounts of added TPO.



4. CONCLUSIONS

TPO can be co-processed in two stage coal liquefaction without any severe detriment in solvent ability measured by percentage dissolution of coal. The introduction of TPO did not appear to reduce solvent capability in comparison to TPO+ at upto 20% incorporation. However, introduction of TPO into the second stage at the right proportions eliminated any reduction in dissolution ability whilst also increasing light distillate yields and may provide the most beneficial option in solvent augmentation with TPO in two stage coal liquefaction.

ACKNOWLEDGEMENTS

The authors are grateful for the financial support from the European Coal and Steel Community (Project N0. 7220-EC 866) and for the supply of TPO by Beven Recycling and for the supply of coal and coal liquid by BCC.

REFERENCES

- (1) Badger, M.W.; Harrison, G.; Ross, A.B.; ACS Pet Div Preprints. 39, 4, (1994), 438.
- (2) Liu, Z.; Zondlo, J.W.; Dadyburjor, D.B. Energy and Fuels, 8, (1994), 607
- (3) Farcasiu, M; Smith, C.M.; ACS Fuel Div Preprints, 37, (1992), 472
- (4) Harrison, G.; Ross, A.B.; Int. proc. on Coal Science, Banff, Canada, (1993).
- (5) Doughty, P.W. PhD Thesis, (1988).
- (6) Bate, K.; Harrison, G. Int. Conf. Coal Science, Tokyo, (1989)

Coal-Tires Hydrocprocessing

Mastral AM, Murillo R, Callén MS, Pérez-Surio MJ, Clemente MC*

Instituto de Carboquímica, CSIC, Apdo. 589, 50015, Zaragoza, Spain

*CPS de Minas, Ríos Rosas 21, 2800 Madrid, Spain

It is calculated that the countries of the European Union will generate at the year 2000 about 2 million Tons/year of discarded tyres from which about 150 thousand Tons/year could correspond to Spain. This discarded tyres are a no biodegradable residue, so in spite of representing a small percentage of the total amount of residues, they should not be left at the open air dumped or landfilling. The alternative is incineration, but does not seem to be the most proper way to recover all their chemical and energetic potential.

Approximately 60-70 % of tire come from petroleum. Because of the vulcanisation process, the rubber components are not recyclable but part of tires could be reused with an important save of natural resources and avoiding environmental disturbances.

Tires composition depends on the brand and on their specific aim but about 50 % are synthetic elastomers and/or natural rubber which could be used to produce synthetic oils via pyrolysis (1), liquefaction (2,3) or, in general, through a thermal process which turn them into useful products for chemical industry like fuels (4), roads asphalt (5) or oils to produce new tires (6). In this way the European objective for the 2000 year of recovering 90 % of used tires could be reached.

In the other hand, there are coals no proper for combustion due to their content in Sulphur but they have shown to be appropriate for hydroconversion at low severity conditions (7).

Pyrolysis of mainly organic materials drives to gas, liquids and solids in a process involving radicals. If these radicals are generated under controlled conditions, the process variables can be focused to the selective obtention of products with commercial value.

Coal and rubber, raw material with similar organic structure, mainly aromatic, by pyrolysis in a inert atmosphere will drive mainly to gases + solid but under Hydrogen pressure, the liquids could be the major conversion products.

In this work both material coal and rubber, are coprocessed looking for high conversions into soluble products.

EXPERIMENTAL

The analysis of both materials is shown in Table 1. The experimental installation used for hydrocprocessing has been described elsewhere (7).

Minireactors are filled, purged, pressurized and once the absence of leaks is checked, they are plunged into the sand bath for 30 minutes with a frequency of vibration of 130 vpm and a piston displacement of 10 cm. Once the reaction time is over, minireactors are quenched. This way, heating and cooling times are minimized.

When minireactors reach ambient temperature, they are depressurized and gases are vented in a sample bag and they are analyzed in a GC (H_2S , CO_x and C_1-C_3) with Molecular Sieve and Poropak columns.

Table 1. Tire and coal immediate and ultimate analysis

	Tire	Coal
C (daf)	88.64	80.17
H (daf)	8.26	6.69
N (daf)	0.43	1.01
S (df)	1.43	5.68
moisture (af)	0.94	22.05
ash (df)	3.83	26.93
volatils	67.30	48.62
fix Carbon	31.14	28.45
calorific power (kcal/kg)	9.159	3.714

The reactor content is extracted with THF in Soxhlet and extract is fractionated into oils and asphaltenes. Solvents are removed in a rotatory evaporator and residue, asphaltenes and oils are dried in a vacuum oven till constant weight.

The percentages of residue, asphaltene and oils are calculated by direct weigh and the total conversion and oils selectivity are calculated using the following equations:

$$\% \text{ conv.} = \frac{\text{g sample (df)} - \text{g residue}}{\text{g sample (daf)}} \quad \% \text{ oils select.} = \frac{\text{g oils}}{\text{g solubles}}$$

RESULTS AND DISCUSSION

Low selective pyrolysis with a great generation of radicals is produced when coal, rubber and coal rubber mixtures are heated above 400 °C. These radicals can be stabilized:

- Capturing Hydrogen from bulk phase and in this way lighter products can be obtained.
- By reaction between themselves giving heavier products through repolymerization processes.

Table 2. Conversion percentages as a function of the reactor feed at 400 °C

Coal/rubber ratios	% conversion	% oils	% asphaltene	% residue	% oils select.
1/0	74.78	11.44	36.41	51.06	20.00
4/1	77.16	19.77	35.89	45.84	30.91
2/1	74.55	29.41	28.64	45.14	41.76
1/1	73.17	33.13	20.46	42.77	64.24
1/2	69.34	36.69	12.26	42.15	72.40
1/4	70.38	45.19	6.36	38.12	80.97
0/1	71.37	48.24	0.53	31.37	97.09

The existence of retrogressive reactions which drive to heavy products can not be avoid even under controlled hydrolysis. Anyway a good control of the process variables helps to minimize these kind of secondary undesirable reactions. This heavy products, the inorganic and the

unreacted organic compounds are a residue not THF soluble. Working at the variables process which show to be the best for this low-rank coal (7) and with different percentages of coal and rubber at the mixture feed, good conversions have been reached. The obtained percentages are shown in Table 2.

The reaction time has been 30 minutes in all experiments. This time is optimal in order to reach maximum conversions minimizing repolymerization and condensation reactions. Initial Hydrogen pressure is always 10 MPa, In this way availability of Hydrogen during reaction is sure. The composition of fed samples has been changed from 100% coal to 100% rubber with a gradual increase of rubber percentages.

Looking for better conditions to rubber processing, several experiments have been done at a lower temperature (350 °C) in order to determine the influence of this variable on the process

The results obtained at 350 °C are shown in Table 3. It can be seen that the lower the temperature, the lower the conversions, being lower by comparison with these obtained at 400 °C when the tire percentage increase en the feed. The minimum is reached when tire alone is fed. So, feeds rich in tire are less sensitive to temperature than feeds rich in coal.

Table 3. Conversion percentages as a function of the reactor feed at 350 °C

Coal/rubber ratios	% conversion	% oils	% asphaltene	% residue	% oils select.
1/0	42.92	6.83	25.67	71.91	17.94
4/1	47.65	15.52	22.29	66.55	41.46
2/1	47.41	20.22	16.88	65.10	52.75
1/1	49.92	24.44	14.67	60.85	62.34
1/2	54.13	35.09	6.92	54.86	80.64
1/4	58.57	42.23	3.91	48.56	91.59
0/1	66.50	50.81	1.69	36.05	96.45

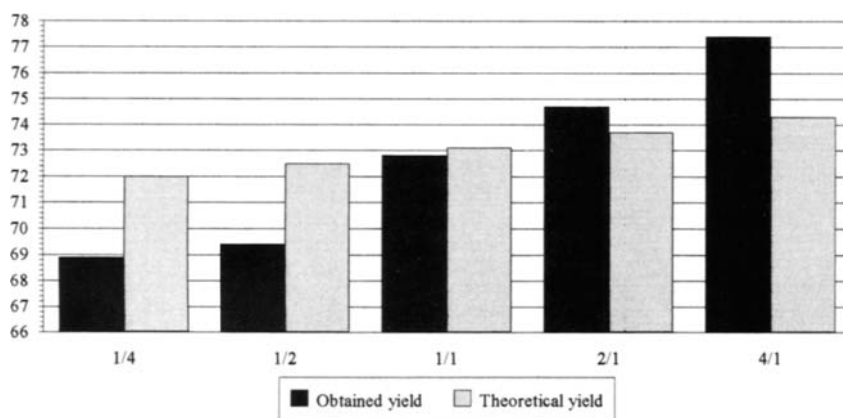


Figure 1. Obtained and theoretical conversion vs. coal/tire ratios

Gas formation have been analyzed by GC and it is shown that Carbon oxides (CO and CO₂) are the main products when composition of samples is rich on coal due to the high heteroatoms content of this low-rank coals, but this percentage decreases when percentage of rubber increases.

The same can be said in the case of H₂S. On the other hand, the percentage of hydrocarbons (C₁-C₃) is higher when samples are rich in rubber than when they are rich in coal. Quantitatively, there is no relation between gas formation and gas composition, possibly because of the way they are calculated: the errors in weight of residue, asphaltenes and oils appear in gas percentages because this last conversion is calculated by difference.

Feed mixture composition is very significative, while at 400 °C 71.2 % is the conversion obtained when rubber is processed separately, with a rich in rubber mixture feed, conversion is lower than the theoretically calculated. However higher conversions than the theoretical are reached with rich in coal feeds. A synergistic effect is observed when coal/rubber ratio is 4/1 and total conversion reach a value of 77.4 %. If we assume that conversion for coal and rubber are constant and equal to 75.1 % and 71.2 % respectively, the conversion obtained for coal would be 79.1 % and in the case of rubber 86.0 %. This synergistic effect is shown in Figure 1.

In spite of low total conversion (71.37 %) is obtained when tire is processed by isolate, the corresponding oils formation (48.24 %) and oils selectivity (97.09%) are maxima.

The same behavior is observed with the oils recovery. However, in this case the differences are not so notable than en the case of total conversion. Moreover when the feed is rich in rubber the amount of oil recovered practically the same that what is obtained at 400°C.

Concerning to asphaltenes, it could be seen that they show a similar behavior and the differences are not so great. The higher conversions at 400 °C are mostly due to a higher gas formation.

Sammarizing and according to the results above commented, an important synergistic effect is observed when coal and rubber are coprocessed and their ratio in the feed mixture is 4/1. However, the maximum oils recovery is reached when tire is hydrogenated by isolate.

Concerning to the coprocess temperature the lower the temperature, the lower the total conversion but mainly at the cost of the gas formation. While at 400 °C the THF-solubles are almost constant respecting to the composition of the fed mixture, at 350 °C there is a gradual increase with increasing percentages of tire in the feed composition. At both temperatures, the oils and asphaltenes evolution as a function of the feed composition follows different trends: while oils recovery increases the asphaltenes decreases with increasing tire percentages.

Acknowledgements

Authors would like to thank the Spanish Interministerial Commission for Science and Technology (CICYT) for their financial support (Project AMB94-0933-CO2-CI).

References

- (1) Williams PT, Besler S and Taylor DT, Fuel 1990, **69**, 1474
- (2) Farcasiu M, Smith CM, American Chemical Society div. Fuel Chemistry 1992, **37**, 472
- (3) Liu Z, Zondlo JW and Dadyburjor DB, Energy & Fuels 1994, **8**, 607
- (4) Oxford Energy Corporation, Modesto, USA
- (5) Rubber Asphalt Producers, Phoenix, USA
- (6) RN Technology, Cheshire, CT, USA
- (7) Mastral AM, Final Report CSIC to ECSC, Ref 7220/EC/755, June 1993

CATALYTIC EFFECT OF HIGHLY DISPERSED Zn/CARBON BLACK FROM AUTOMOBILE TIRE ON COAL LIQUEFACTION

Yoshiki SATO, Tohru KAMO, Yoshitaka YAMAMOTO, Keiji MIKI
and Suminobu KURAHASHI*

National Institute for Resources and Environment

16-3 Onogawa, Tukuba-shi, Ibaraki 305 Japan

*Bridgestone Corp.3-1-1 Ogawahigashi-cho, Kodaira-shi, Tokyo 187 Japan

1. INTRODUCTION

Chemical treatment of waste plastics has been an important and urgent subject being solved from the standpoints of environmental protection and of effective reuse of organic resources. Thermal cracking of plastic wastes was actively studied using bench scale unit to produce fuel oil, but the quality of fuel oil produced by cracking was not improved to the environmentally permitted level. Because of the lack of hydrogen in the cracking, the oil contains relatively higher boiling point fractions and higher concentration of environmentally hazard elements such as sulfur, chlorine, etc. When used tire is treated by cracking, the produced oil contains about two percentages of sulfur.

On the other hand, coprocessing of coal with waste material has actively been studied under the liquefaction conditions. Laboratory scale experiments on the liquefaction of coal with used tire conducted at University of Utah [1], Kentucky [2], West Virginia [3] and PETC [4] has pointed out that carbon black, an important constituent of tires, acts as a catalyst in the reaction. The liquefaction of coal with other waste plastics has also been conducted using PDU plant at DMT, Germany [5].

In this study, we studied liquid-phase cracking of used automobile tire using hydrogen donor and non-donor solvent under hydrogen or nitrogen pressure. In this reaction, there are no differences in the yield and the quality of oil with and without iron catalyst. This indicates that Zn/carbon black and sulfur, contained in tire, plays a catalytic role to crack organic components in tire to light oil.

Then, in the latter part of this study, catalytic effect of highly dispersed Zn/carbon black from automobile tire on the coal liquefaction has been examined experimentally. Liquefaction of coal mixed with and without tire was compared in terms of conversion and the yield of hexane-soluble fraction.

2. EXPERIMENTAL

The results of elemental analyses of Taiheiyo coal (Japanese subbituminous) and automobile tire is shown in Table 1. Liquid-phase cracking of coal mixed with

Table 1 Elemental Analyses of Reactant and residue

Solvent	C	H	N	S+O	Ash	H/C
	(wt%)				(wt%,daf)	Atomic Ratio
Coal	75.7	6.3	1.3	16.7	14.2	0.99
Used tire	86.9	8.1	0.7	4.3	5.03	1.1
Carbon black	97.7	0.7	0.4	1.2	0.0	0.08
Residue						
Coal liquid* ₁	89.9	1.2	0.4	8.6	27.3	0.15
Coal liquid* ₂	93.6	1.2	0.4	4.9	13.4	0.15
LCO* ₂	94.0	1.0	0.4	4.6	13.4	0.13
Tetralin* ₂	93.3	1.3	0.5	5.0	13.7	0.16
LCO* ₃	94.1	1.2	0.8	3.9	13.3	0.15
Tetralin* ₃	93.8	1.1	0.6	4.5	13.9	0.14

React. temp. : 440 °C, React. time. : 60min, Solv./Tire wt ratio : 2.5

*1 : Fe₂O₃ catalyst and H₂, *2 : H₂, *3 : N₂

automobile tire was carried out using a 200 ml autoclave with magnetic stirrer at 300-440°C, initial hydrogen or nitrogen pressure of 2.0-8.5 MPa and reaction time of 20-60 min. Taiheiyo coal-derived solvent, LCO from petroleum refinery, and tetralin were used with solvent to tire weight ratio of 2.5. Iron oxide-sulfur catalyst was used for comparison purpose. Liquid products, separated from the solid residue by filtration, were distilled under vacuum condition to measure the yield of oil and its property. The conversion was calculated from the THF insoluble fraction in the residue, on a daf tire basis. Liquefaction of coal with and without tire was conducted using the same autoclave at 440°C, initial hydrogen pressure of 8.5 MPa and reaction time of 60 min. Liquid products were separated into n-hexane soluble (HS), n-hexane insoluble-toluene soluble (TS) and toluene insoluble-THF soluble (THFS) fraction by an ultrasonic extraction method. The conversion was also gravimetrically calculated from the THF insoluble on a daf coal and tire base.

3. RESULTS AND DISCUSSION

3.1. Liquid-phase cracking of used automobile tire.

The experimental results at 440°C, 60 min using a variety of solvent under hydrogen or nitrogen pressure with or without iron-catalyst are shown in Fig. 1. The yields of gaseous products were very low of 2-5 wt% at any cases of experimental runs. This shows big difference from the gas yield of 20-30 wt% produced by the cracking without hydrogen sources. The conversion calculated from THF insoluble shows almost same level of 33 wt% in all cases. Elemental analyses of typical residue and carbon black used for the production of automobile tire are shown in Table 1. Ash contents in the residue were equal to the calculated value from the conversion and elemental analyses of the residue. According the elemental analyses, carbon contents of the residue were about 4 wt% lower than that of carbon black but hydrogen content and H/C atomic ratios showed somewhat higher value. The result from the thermobalance and differential thermal analysis indicates that the residue consists of 79 wt% of carbon black, 17.2 wt% of Ash and 3.8 wt% of organic matters. TEM picture of typical residue and carbon black, and the measurement of aggregate indicate that the carbon black is still dispersed to fine particle and the

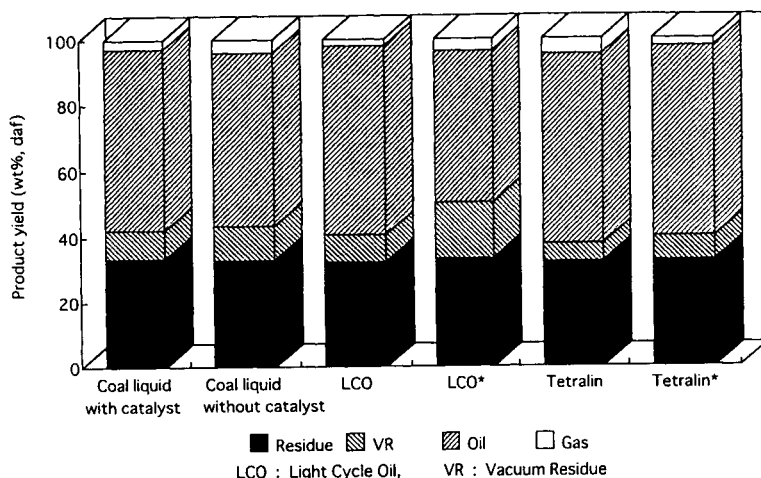


Fig.1 Liquid-Phase Cracking of Used Tires with Various Solvents
(Solvent/Tire wt ratio : 2.5, React. temp. ; 440°C, React. time : 60min)
(Initial H₂ Press : 8.5MPa, *Initial N₂ Press : 2.0MPa)

residue can be reuse for rubber manufacturing. X-ray analysis of the residue also showed the typical pattern of zinc sulfide. When hydrogen gas or hydrogen donor solvent such as coal-derived recycle solvent or tetralin was used for the cracking, almost all organic matter could be converted to the distillable oil (50-56 wt%) with very low sulfur content (less than 0.5 wt%) and the HS soluble fraction (5-10 wt%) with the exceptional case using LCO with nitrogen gas as shown in Fig.1. There is also no difference in the conversion and the yield of oil product with and without iron catalyst. This indicates Zn/carbon black and sulfur, contained in tire, plays a catalytic role to crack high molecular weight organic component to light oil when transferable hydrogen from gas-phase or from the solvent is exist in the reactor.

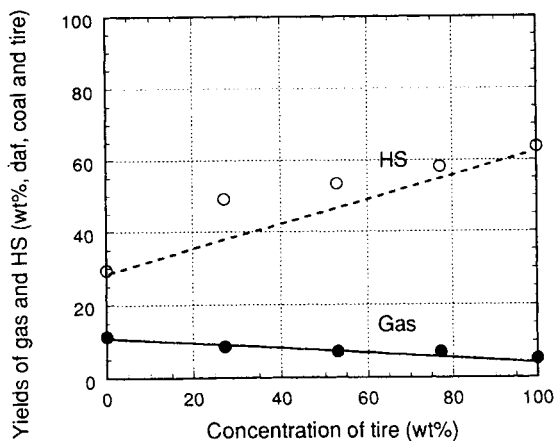


Fig.2 Liquefaction of Coal with Tire
(440°C, 60 min, Initial H₂ Press : 8.5MPa)

3.2. Liquefaction of coal with automobile tire.

The experimental results on the liquefaction of coal mixed with tire are plotted in Fig. 2. The conversion and the yields of gas and the HS fraction were calculated on daf basis of coal and tire. The HS yield observed at coal/tire weight ratio of 3.0 and 1.0 were 10 and 6 wt% higher respectively than that calculated from the linear correlation between the independent liquefaction of coal and tire. Using the conversion and the product yield of tire alone, we calculate the reactivity and the product distribution from coal when it is mixed with tire. The result, shown in Fig. 3 indicate the enhancement of the conversion and the HS yield but the yields of gaseous product do not change. The calculated HS yields from coal with coal/tire weight ratio of 3.0 and 1.0 were 43.1 and 41.2 wt% respectively. These are 12-14 wt% higher in comparison with the result obtained in the non-catalytic reaction (28.9 wt%) and show almost equivalent effect with iron oxide-sulfur catalyst (39.1 wt%). The liquefaction of coal with carbon black showed a little increase in the HS yield (34.8 wt%) with lower conversion of 88.0 wt% and higher gas yield of 12.2 wt%. This indicates that highly dispersed Zn/carbon black from automobile tire plays a positive catalytic effect on the coal liquefaction.

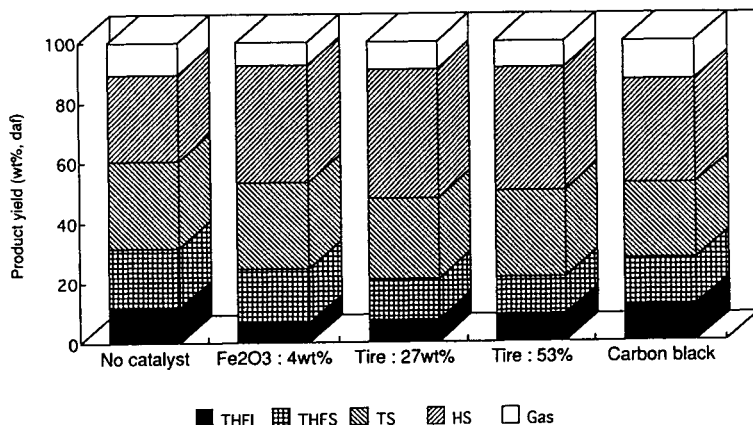


Fig.3 Effect of Tire Addition on the Liquefaction of Coal (440°C, 60min, Initial H₂ Press : 8.5MPa)

REFERENCES

- [1] X. Xiao, W. Zmierczak and J. Shabtai, *Am. Chem. Soc. Div. Fuel Chem. Preprints*, **40(1)** (1995) 4.
- [2] M. M. Taghiei, Z. Feng, F. E. Huggins and G. P. Huffman, *Energy & Fuels*, **8** (1994) 1228.
- [3] R. K. Sharma, D. B. Dadyburjor, J. W. Zondlo, Z. Liu and A. H. Stiller, *Am. Chem. Soc. Div. Fuel Chem. Preprints*, **40(1)** (1995) 56.
- [4] M. Farcasiu and C. M. Smith, *Am. Chem. Soc. Div. Fuel Chem. Preprints*, **37(1)** (1992) 472.
- [5] B. O. Strobel and K. D. Dohms, *Int. Conf. Coal Sci. Preprints*, **I** (1993) 536.

SECTION C

COAL AND THE

ENVIRONMENT

Sub-section C.1

Pre-utilization aspects

This Page Intentionally Left Blank

Coal Characterisation Strategy for Physical Desulphurisation Processes*

F. Rubiera^a, S. Ivatt^b and N. J. Miles^c

^aINCAR, Apartado 73, 33080 - Oviedo, Spain

^bETSU, AEA Technology, Harwell, Oxon, OX11 0RA, UK

^cDepartment of Mineral Resources Engineering, Nottingham University, NG7 2RD, UK

1. INTRODUCTION

Increasing concern about the environmental impact of sulphur emissions from coal combustion has led to the introduction of legislation with stricter controls being forecast for the future. One of the UK goals concerning its Coal R&D Programme is to try to maximise sulphur reduction before coal combustion[1]. Sulphur can be reduced before combustion by physical, chemical and biological coal cleaning, during combustion by sorbent addition or after combustion by flue gas desulphurisation. Present coal preparation methods alone are not capable of meeting the long term sulphur emission targets. However, they can make significant reductions in emission values and may play an important role in an integrated sulphur reduction strategy that considers all the options. Sulphur removal by physical techniques can be enhanced by grinding of coals to finer sizes to improve the liberation of pyrite. Laboratory float and sink separation can then be used to characterise the products and indicate the theoretical limits of physical coal desulphurisation. Unfortunately, traditional float and sink procedures become less selective when separating below 0.5 mm and are particularly difficult for the characterisation of ultrafine particles [2,3,4].

This paper outlines an improved fine coal float and sink procedure that involves the separation of particles in a centrifuge, using inorganic salt solutions of sodium polytungstate (SPT) as the dense liquid. With this method, it was possible to characterise coal fractions to below 0.020 mm [5]. Laboratory washability data, obtained for different coal samples, were then used in computer process simulation models to predict the sulphur reduction results that could be achieved in commercial operations. Finally, the initial results are presented from a test programme to investigate a number of intensive fine coal desulphurisation processes.

2. EXPERIMENTAL

The samples used in this study were four Electricity Supply Industry (ESI) blends, two middlings fractions (subsequently identified as SDM and HWM) and one raw coal (HWR). With the exception of the ESI blends, each sample was characterised in its uncrushed state

* This work was carried out with financial support from the ECSC, Proj. No. 7220-EA/003, and ETSU. Dr Rubiera also wishes to thank the European Union for the award of a research fellowship through the Human Capital and Mobility Programme.

and then crushed to different top nominal sizes for further characterisation. For the ESI blends, no characterisation was carried out on the uncrushed samples. A serial float and sink procedure was used for the sizes above 0.045 mm, where the sample was introduced into solutions of SPT at a range of densities starting with the lowest. The floats and the sinks were removed and both re-introduced into different separating funnels at the same density. The final floats fraction was analysed whilst the sinks fraction was subjected to separation at the next highest density. To prevent particle agglomeration a surfactant (Brij 35) was added to the SPT solutions. As a further precaution, size fractions below 0.25 mm were treated in an ultrasonic bath for 2 minutes before separation.

A parallel centrifugal float and sink procedure was used for the size fractions below 0.045 mm. The initial feed sample was divided into several representative sub-samples of approximately 15 g, and each sub-sample was separated at only one density within the range 1.3 to 2.4 relative density (RD). The separation was carried out using an MSE Centaur centrifuge with a 4-place swing-arm rotor at a centrifuge speed of 4000 rpm for 20 minutes. Polycarbonate transparent centrifuge tubes with a capacity of 50 ml were used. After the initial separation, the floats were removed and the sinks redispersed in the centrifuge tubes. The separation was repeated and the second floats added to the initial floats. These were mixed and separated again to produce a final floats product. In this work, all samples were analysed for ash and total sulphur content. Existing correlations between ash and calorific value (CV) were used to predict calorific values.

3. RESULTS AND DISCUSSION

The washability results were used to determine the theoretical reductions in sulphur emission that could be achieved by density separation. Table 1 shows the average float and sink results of the separation of the four ESI coal blends after crushing to 0.2 mm. The separation of these blends was accomplished by treating the whole of the minus 0.2 mm sample using the centrifugal float and sink procedure. Separation at 2.4 RD considerably reduced both the ash and sulphur content of the blends with only minimum calorific value losses. Separation at a lower cut-point of 1.5 RD reduced the sulphur emission value in grams of sulphur per gigajoule (SEV) by 40.1% on average, with a CV loss of 7.2%.

Table 1
Average density separation results for four typical ESI coal blends

Relative Density	Yield (%)	Ash (%)	Sulphur (%)	Sulphur Emission Value (gS/GJ)	Calorific Value Loss (%)	Sulphur Emission Value Reduction (%)
1.3	48.17	1.5	1.2	372	41.4	49.7
1.5	78.06	3.7	1.5	448	7.2	40.1
1.8	84.66	5.6	1.6	499	1.5	33.3
2.4	89.24	9.2	1.5	501	0.7	33.0
Blend	100.00	17.4	2.1	747	-	-

The above results shown that there is considerable potential for sulphur reduction in these coals, with only minimum CV losses. To further evaluate the effects of crushing on sulphur and ash liberation, a full washability analysis was carried out on the SDM (middlings) sample progressively crushed to finer sizes. Figure 1 shows the relationship between SEV and CV

loss. As the coal was crushed to finer sizes, SEV was reduced for any CV loss. At a nominal CV loss of 5% the reduction in SEV was 5% for the uncrushed sample, rising to 22%, 30% and 44% for the samples crushed to 2.8 mm, 0.5 mm and 0.2 mm respectively.

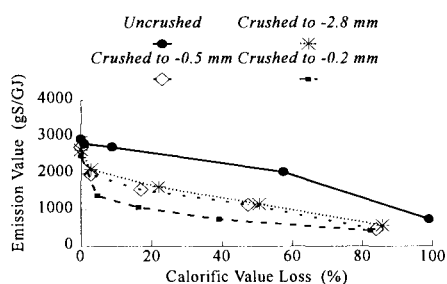


Figure 1. The effect of crushing on the SEV reduction for middlings coal sample (SDM).

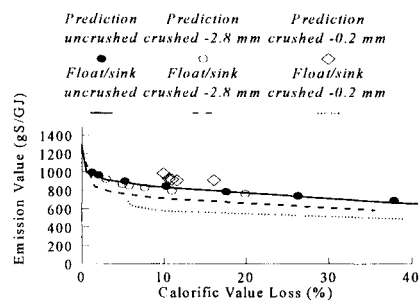


Figure 2. Comparison of the process simulation with the float/sink data for coal sample (HWR)

Washability studies were also carried out on the HWR raw coal in its uncrushed state and after crushing to different nominal top sizes, with the resulting data being introduced in computer prediction models. The aim of these process optimisation studies was to investigate the potential for sulphur reduction using commercial separators, considering a number of alternative plant designs and operating conditions. The performance prediction models used in this work are based in the application of partition coefficients and have been described elsewhere [6].

Of the prediction models considered, the plant configuration which produced the best relationship between SEV and CV recovery was a total washing system comprising the use of the LARCODEMS (Large Coal Dense Medium Separator) to clean the plus 2 mm fraction, a standard dense medium cyclone for the -2+0.063 mm fraction and froth flotation for the minus 0.063 mm fraction. Laboratory froth flotation tests were carried out to provide the performance data for the minus 0.063 mm fraction. The predicted results for the HWR coal are shown in Figure 2, which also includes the float and sink data for comparative purposes.

The predicted results for the uncrushed sample were very close to those produced from the float/sink analysis. Operating the LARCODEMS system at a cut-point of 1.8 RD reduced the SEV of the uncrushed coal by 28.6% for a CV loss of 3.2%. This result is fairly typical of conventional coal preparation operations within the UK. Reducing the density cut-point had a pronounced effect on both sulphur reduction and CV losses. At a cut-point of 1.35 RD, the SEV of the uncrushed coal was reduced by 42.6%, but this was only achieved at the expense of a CV loss of 26.3%. As the coal was progressively crushed to finer top sizes the difference between the float/sink and the predicted results widened. Figure 3 shows that there is a slight advantage to be gained by crushing the coal to 2.8 mm before separation. The predicted results for the -0.2 mm crushed sample indicate that, using existing techniques, there is no improvement in SEV to be gained by crushing the coal to this size.

The results of the computer predictions emphasise the need to improve fine coal cleaning methods in order to gain the full advantage of increased sulphur liberation by grinding to finer sizes. A number of enhanced density separators have recently been developed, primarily for

use in the minerals industry, a good example being the Knelson concentrator [7]. Figure 3 compares the float and sink results for the HWM coal middlings sample, after crushing to -0.2 mm, with those obtained by the Knelson concentrator and a water-only cyclone. For comparison, the float and sink results for the same sample after crushing to -2.8 mm are also shown. For a CV loss of 4% the SEV reduction was 16.1% for the -2.8 mm crushed sample and 39.5% for the -0.2 mm crushed sample. The results obtained when using the Knelson concentrator and the water-only cyclone seem slightly disappointing when compared against the float and sink data. However, the Knelson separator achieved a SEV reduction of 19.6% for a CV loss of only 1.5% whilst the water-only cyclone achieved a SEV reduction of 24.6% for a loss in CV of 8.3%. In both cases no further advantage was gained by operating under more exacting conditions; any small improvements in sulphur reduction were outweighed by the high CV losses incurred.

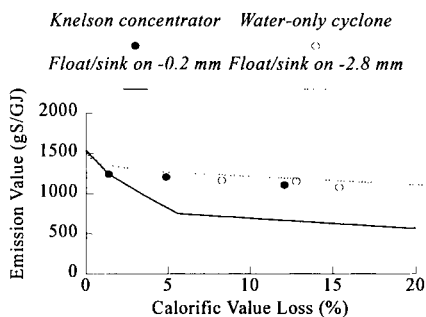


Figure 3. Comparison of float/sink data with fine coal separators for middlings coal sample (HWM).

4. CONCLUSIONS

4. CONCLUSIONS

Laboratory float and sink analyses were used to assess the degree of sulphur liberation after crushing selected UK coals. A modified washability technique, involving multiple-stage centrifugal separation and the use of solutions of an inorganic non-toxic salt (SPT) enabled the characterisation of coals down to extremely fine sizes. Subsequent process optimisation studies have highlighted the need to develop more advanced methods of fine coal cleaning. The poor selectivity of currently available fine coal cleaning techniques toward sulphur reduction largely offsets the benefits of increased pyrite liberation by crushing to finer sizes. A sulphur reduction test programme is currently being undertaken to investigate intensive fine coal cleaning techniques with the specific aim of developing a commercial desulphurisation system [8].

REFERENCES

1. Clean Coal Technologies - A Strategy for the Coal R&D Programme, Energy Paper 63, Report No: Coal R035, Department of Trade and Industry, HMSO, London (1994)
2. J-P. Franzidis and M.C. Harris, *J.S.Afr.Inst.Min.Metall.*, 86, 10, 409 (1986)
3. J.A. Cavallaro and R.P. Killmeyer, *J. Coal Quality*, 7, 2, 55 (1988)
4. T.F. Dumm and R. Hogg, *Miner. Metall. Proc.*, 5, 25 (1988)
5. F. Rubiera, S Ivatt and N.J. Miles, In Prep.
6. S. Ivatt, Coal Preparation Techniques for Sulphur Reduction, ECSC Proj. No 7220/EA/003, Final Report / ETSU Report No.COAL R022.
7. D.A. Butcher and N.A. Rowson, *Proc. 12th Int. Coal Prep. Cong.*, Vol. I, p.345 (1994)
8. The Development of a Commercial Scale Fine Coal Desulphurisation Process, ECSC Proj. No 7220/EA/010, Progress Report 1, March 1995.

Partitioning and behavior of coal macerals during dry coal cleaning

J.M. Stencel, H. Ban, J.L. Schaefer and J.C. Hower

Center for Applied Energy Research, University of Kentucky, Lexington, Kentucky 40511, USA

1. ABSTRACT

Fine coal cleaning has been studied using dry, triboelectrostatic experimentation. The 45-75 μm coals were pneumatically transported through a Cu-loop tribocharger, and then transported through a 100-200 kV/m electric field. Positively charged coal was deflected to the negative electrode and negatively charged minerals were deflected to the positive electrode. Samples were retrieved and subjected to petrographic analysis.

Petrographic analysis of these samples showed that, for high volatile A and B bituminous coals, vitrinite macerals were significantly enhanced in the clean-coal, whereas the fusinite + semifusinite + exinite maceral were enhanced in the tailings/minerals. For a high volatile C bituminous coal, this trend in enhancement was not observed. The vitrinite partitioning, greater for dry processing than for wet processing, may be related to differences in surface chemical and physical properties of the coals.

2. INTRODUCTION

Triboelectrostatic separation works because differential charge can be imparted on carbon and mineral constituents in coal, the primary reason for which is a difference in the surface work function of the carbon and mineral constituents. The fundamentals of triboelectrostatic separation are not fully understood, nor is dry electrostatic processing commercially practiced. There is renewed interest in the potential of such dry cleaning technology [1-5].

Wet processing of fine coal is commercially practiced and fundamentally understood [6,7]. This type of information is not readily available for dry coal cleaning. As a consequence, laboratory-scale experiments were performed to compare dry triboelectrostatic separation with oil agglomeration cleaning. Cleaned fractions were examined petrographically to determine whether differences exist between the effects of dry and wet beneficiation.

3. EXPERIMENTAL

Table 1 describes the coals that were used. Three eastern Kentucky samples (2180, 31011, 4977) provided a rank series of petrographically comparable coals. The Illinois Basin coals were lower rank and had high vitrinite and sulfur contents.

Table 1. Raw coal proximate and petrographic analyses.

Sample	Coal Bed	Location	mois.	ash	sulfur	Macerals (vol. %)								Rmax
						Vit	Fus	Sfs	Mic	Mac	Exn	Res		
2180	Peach Orchard	Magoffin Co., KY	4.77	8.94	0.76	49.0	10.1	24.8	4.4	0.0	11.6	0.1	0.73	
31011	Elswick	Pike Co., KY	0.71	5.90	2.21	58.1	10.8	15.4	5.2	0.0	10.3	0.2	0.95	
4977	Leatherwood	Harlan Co., KY	2.63	17.27	0.93	60.8	14.3	12.8	2.4	0.0	9.5	0.2	0.87	
71714	Springfield (W. Ky. 9)	Henderson Co., KY	10.97	10.68	5.09	79.1	11.6	4.8	0.6	0.2	3.7	0.0	0.45	
8377	Herrin (Illinois No. 6)	Saline Co., IL	5.68	21.55	6.44	88.0	6.0	2.4	0.1	0.1	2.8	0.6	0.69	

Figure 1 shows the triboelectrostatic experimental setup [1,2]. Coal samples were wet ground and sieved to a size fraction 45-75 μm , dried, and fed (rate: 0.1 - 1 g/s) into a carrier nitrogen gas (5-20 m/s) through a Cu tribocharger. Charged particles were deflected by an electric field. A 400 mesh screen was installed in the separator about 10 cm downstream of the electrodes to capture uncharged particles.

Clean coal reported to the negative electrode, whereas mineral matter reported to the positive electrode. Five fractions were collected from each separation test [3]. From the tube exit, deposits on the first 3 cm downstream were labelled as the first clean and tailing fractions, from 3 cm to 28 cm were labelled the second clean and tailing fractions, and the particles captured by the screen were labelled the center fraction.

Petrographic analysis was a combined maceral and microlithotype analysis (Table 2). The procedure used here differs slightly from the conventional microlithotype analysis.

Microlithotypes are defined on the basis on the maceral composition within the 50 μm diameter circle surrounding the center point in the field of view. Many of the particles examined in studies of fine coal cleaning, such as this investigation, are considerably smaller than 50 μm . The area counted as the microlithotype therefore is an entire particle if less than a 50 m diameter particle is exposed at the surface.

Table 2. Maceral group composition of microlithotypes

Monomaceral microlithotypes

Vitrite (Vt)	Vitrinite (V) > 95%
Liptite (Lp)	Liptinite (L) > 95%
Inertite (In)	Inertinite (I) > 95%

Bimaceral microlithotypes

Clarite (Cl)	V + L > 95%
Vitrinertite (Vi)	V + I > 95%
Durite (Du)	I + L > 95%

Trimaceral microlithotypes

Duroclarite (Dc)	V > L, I; each > 5%
Clarodurite (Cd)	I > V, L; each > 5%
Vitrinertoliptite (VI)	L > V, I; each > 5%

Carbominerite (Cm)

20% < silicates, carbonates < 60% (volume)
5% < sulfides < 20% (volume)

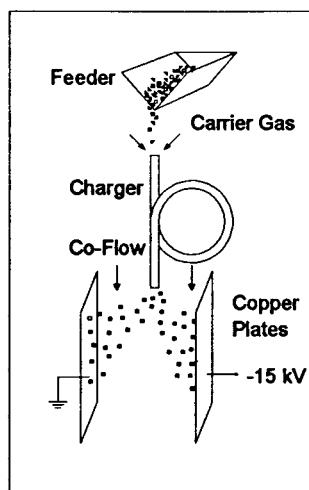


Figure 1 A schematic diagram of the triboelectrostatic separation system.

Extensive studies have been conducted to investigate particle charging and the effects of parameters such as velocity, temperature and relative humidity of the carrier nitrogen, as well as the coal type and particle size. Coal samples deposited on the two copper plates and those passing through the separator were collected, weighed and subjected to proximate, elemental and petrographic analyses.

4. RESULTS AND DISCUSSIONS

The petrographic analyses of two beneficiated coals (4977 and 8377) is given on Tables 3. In comparing the clean vs. tails (A vs. B, C vs. D) for the feed (F) from each sample, with the exception of sample 71714, there is a partitioning of the macerals between the clean and tails. Vitrinite was concentrated in the clean product whereas fusinite + semifusinite + macrinite and exinite were concentrated in the tailings. As expected, in the tailings there is also an increased concentration of mineral matter, including silicates, sulfides, and carbonates.

Table 3. Maceral and microlithotype analyses for coals 4977 and 8377.

			macerals and minerals (vol. %)													
Sample	Item	Type	mois.	ash	sulfur	Vit	Fus	Sfs	Mic	Mac	Exn	Res	Min*	Sil	Sul	Car
4977 200x32	A	1st clean	3.10	4.43	0.77	83.6	7.6	3.0	2.0	0.2	3.6	0.0	0.0	0.0	0.0	0.0
	B	1st tails	0.83	44.05	0.95	49.0	10.0	5.0	0.7	0.0	5.7	0.0	6.3	22.7	0.0	0.7
	C	2nd clea	2.95	5.22	0.78	78.8	7.6	3.2	3.2	0.0	7.0	0.0	0.2	0.0	0.0	0.0
	D	2nd tails	2.36	15.81	1.14	46.7	24.0	10.0	3.7	0.0	8.0	0.0	2.3	5.0	0.0	0.3
	E	center	1.20	11.37		52.7	23.3	6.3	6.3	0.0	8.0	0.0	0.7	1.0	1.0	0.0
	F	feed	2.14	10.87	0.87	65.8	14.2	5.4	1.6	0.2	7.8	0.0	1.6	3.4	0.0	0.0
8377 200x32	A	1st clean	3.67	4.27	2.20	95.8	1.6	0.6	0.2	0.0	1.6	0.2	0.0	0.0	0.0	0.0
	B	1st tails	1.73	39.66		58.2	4.4	5.6	0.0	0.0	4.0	0.0	17.6	8.0	1.2	0.8
	C	2nd clea	3.52	9.31	3.56	93.4	1.4	0.8	0.0	0.0	1.4	0.4	1.8	0.6	0.2	0.0
	D	2nd tails	2.07	26.54	11.40	73.1	8.0	3.4	0.0	0.0	1.7	0.0	4.9	1.1	7.4	0.3
	E	center	1.75	20.46	8.08	75.8	6.0	2.0	0.0	0.0	3.0	0.0	8.0	2.2	2.0	1.0
	F	feed	3.31	15.07	5.31	85.8	5.2	1.8	0.2	0.0	1.4	0.0	2.8	1.6	1.0	0.2
			microlithotypes (% mineral free)													
			monomacerites			bimacerites			trimacerites							
Sample	Item	Type	Vt	Lp	In	Cl	Du	Vi	Dc	Cd	VI	Cm				
4977 200x32	A	1st clean	49.6	0.0	5.6	4.0	4.6	6.8	25.0	1.8	0.6	2.0				
	B	1st tails	34.8	0.4	12.2	4.8	7.8	1.3	12.6	2.2	1.7	22.2				
	C	2nd clea	43.4	0.0	4.0	2.8	4.8	7.2	29.8	3.2	0.4	4.4				
	D	2nd tails	21.5	0.4	17.6	2.5	13.7	5.3	16.5	8.1	2.1	12.3				
	E	center	24.1	0.0	10.5	0.7	17.3	8.5	22.4	6.1	1.0	9.2				
	F	feed	36.2	0.4	10.1	3.7	7.5	6.0	21.1	4.1	0.8	9.9				
8377 200x32	A	1st clean	69.4	0.0	1.4	10.4	0.2	3.6	8.4	0.2	0.2	6.2				
	B	1st tails	37.3	0.4	4.4	5.3	0.9	1.3	4.0	0.0	0.4	45.8				
	C	2nd clea	55.6	0.0	1.0	15.5	0.0	3.6	7.7	0.2	0.0	16.3				
	D	2nd tails	46.4	0.3	8.8	9.7	0.3	3.4	5.3	0.3	0.0	25.4				
	E	center	43.2	0.4	5.9	8.6	0.2	3.8	8.6	0.2	0.2	28.7				
	F	feed	56.4	0.0	4.5	10.1	0.0	3.1	7.4	0.2	0.2	18.1				

Some of the partitioning is a consequence of mineral-maceral associations and not necessarily a consequence of maceral properties; similarly, not all of the partitioning can be ascribed to mineral association. For example, much of the inertinite in the tailings is present as a monomaceral with no apparent mineral matter. Some inertinite is associated with

increased proportions of durite and, in some cases, clarodurite and vitrineroliptite. The latter two associations are not as well established as the durite association.

Mineral matter reported rather efficiently to the tailings fractions. The high pyrite coals (31011, 8377, 71714), in particular, demonstrated a high partitioning of pyrite. Sample 71714, the high volatile C Springfield coal behaved differently than the higher rank coals in that its maceral partitioning was minimal and tailings ash content was considerably lower than from the higher rank coals. Rank, and moisture content, may govern the behavior of this coal.

Comparing the petrographic analysis of samples from the dry experiments to the petrographic analysis from the same coals beneficiated by oil agglomeration, we note that the triboelectric separation produced a consistently greater vitrinite enhancement in the clean fraction for all the coals except coal 4977. The fusinite + semifusinite + macrinite and exinite concentrations were decreased in the wet tailings, and were increased in the dry tailings.

5. CONCLUSIONS

When using dry triboelectrostatic separation and for high volatile A and B coals, vitrinite maceral concentrations were significantly enhanced in the cleaned fraction, whereas fusinite + semifusinite + exinite maceral concentrations were enhanced in the tailings. This partitioning is greater than that observed for the same coals subjected to wet processing. For a high volatile C coal, this enhancement was not observed in the dry separation results. Coal characteristics and process parameters leading to efficient dry coal cleaning techniques are continuing to be investigated.

6. ACKNOWLEDGEMENTS

Partial financial support of the U.S.D.O.E through Pittsburgh Energy Technology Center (DE-FG22-91PC290) and the Commonwealth of Kentucky is acknowledged.

REFERENCES

1. J. Schaefer, J. Stencel and H. Ban, *Proc. Ninth Annual International Pittsburgh Coal Conference*, Oct. 12-16, 1992, Pittsburgh, PA, USA, pp. 259-264.
2. H. Ban, J. Schaefer and J. Stencel, *Proc. of Tenth Annual International Pittsburgh Coal Conference*, Sept. 20-24, 1993, Pittsburgh, PA, USA, pp.138-143.
3. J.L. Schaefer, H. Ban and J.M. Stencel, *Proc. of 11th Annual Intn'l Pittsburgh Coal Conference*, Sept. 12-16, 1994, Pittsburgh, PA, USA, Vol. 1, pp. 624-629.
4. H. Ban, J. Yang, J. Schaefer, K. Saito and J. Stencel, *Proc. Seventh International Conference on Coal Science*, Sept. 12-17, 1993, Banf, Alberta, Canada, Vol. 1, pp.615-618.
5. H. Ban, J. Schaefer and J. D. Stencel, *Fuel*, 1994, Vol. 73, No. 7, pp.1108-1115
6. K.W. Kuehn, J.C. Hower, G.D., Wild, and B.K. Parekh, *Abstracts, 10th Ann. Meeting of The Society for Organic Petrology*, v, 10, pp. 65-66.
7. J.C. Hower, K.A. Frankie, G.D. Wild, and E.J. Trinkle, *Fuel Processing Technology*, v. 9, pp. 1-20.

Production of coal maceral concentrates by flotation

S. Kizgut, N. Miles, M. Cloke

Coal Technology Research Group, Department of Mineral Resources Engineering,
Nottingham University, NG7 2RD, UK.

1. INTRODUCTION

Coal utilisation processes can be significantly affected by the distribution of macerals within the feed coal. Some control over the maceral groupings in a feed coal would be advantageous. Most of the studies over the last 70 years have been directed towards generating coal blends with suitable proportions of reactive (vitrinites and liptinites) and inert (inertinites) constituents, primarily for the coke making process. Few, if any coals, have been deliberately processed with a view to producing concentrates of specific maceral composition on an industrial scale. In general, the separation of coal macerals has been confined to the laboratory where it is common practice to exploit the density differences between macerals in order to generate, albeit small, samples of relatively "pure" maceral concentrates for subsequent coal utilisation studies [1,2,3,4]. It is known that in coal preparation plants some degree of macerals concentration can be achieved by gravity separation processes [5]. It has been shown that differences in the physico-chemical properties of macerals can be used as a basis for separation, in particular the flotation process [6,7]. Early studies [8,9,10] reported that better quality coking coals could be produced by selective depression of the reactive or inert macerals. A number of workers [11,12] who have studied the differential flotability of coal macerals and microlithotypes implied that coal rank played a significant role in the process. Also, as noted in one study [6], the maceral recovery and "purity" was sensitive to the reagent chemistry and dosage.

Although it is evident from above that the concentration of coal macerals by flotation is feasible none of the studies have attempted to optimise the process in order to generate relatively "pure" maceral concentrates. In fact there is little evidence that any systematic studies have been conducted into beneficiation schemes specifically designed to separate and concentrate macerals.

A study is currently being conducted at the University of Nottingham to investigate how single coals can be beneficiated so as to concentrate desirable maceral groups. As a part of this study, and reported previously [13], the findings showed that the standard procedures for evaluating coal flotation (release and tree analysis) were not suitable for assessing the flotability of coal macerals. This was considered to be due to the relatively wide feed size range and excessive quantities of reagents used in such tests. These effects tended to mask any differential flotability between the macerals. Further tests, conducted using the timed batch approach on a relatively narrow feed size fraction, indicated that it was possible to produce an inertinite rich concentrate provided the only reagent added was a frother. Addition of collector to the system nullified this effect to the point where there was no differential flotability between the macerals. The work reported in this paper examines in more depth the selective flotation of macerals using laboratory batch flotation techniques.

2. FLOTATION TESTS

Three British coals were used in this study sourced from Point of Ayr, Bilsthorpe and Silverhill collieries. Coal from Point of Ayr was supplied as a run-of-mine sample and reduced to flotation size by jaw crushing and several stages of hammer milling. Silverhill and Bilsthorpe coals were supplied as flotation slurries which required no size reduction. All coals were classified by screening into various size fractions. The feed characteristics of some of these fractions are presented in Table 1. Maceral group analysis and vitrinite random mean reflectance, were carried out according to ISO 7404-2 [14] and ISO 7404-5 [15]. Conversion of the petrographic data from a volume to a mass basis (and vice versa) was also necessary for generating the reconstituted feed values. This was achieved by allocating the various constituents the following densities: vitrinite - 1.30 g cm^{-3} , liptinite 1.20 g cm^{-3} , inertinite 1.40 g cm^{-3} , mineral matter 2.60 g cm^{-3} and pyrite 5.0 g cm^{-3} . Although converting the data will have introduced errors it was considered acceptable since this work was directed towards assessing the trends in the flotability of macerals not determining absolute values.

All experiments were conducted using a Denver D12 laboratory flotation machine in conjunction with a 5 litre perspex cell at an air flow rate of 4 litres/minute and impeller speed of 1500 rpm

Table 1.
Feed coal characteristics

Coal Sample	Particle Size (μm)	Ash Content (%)	R_m (%)	Petrographic Analysis (% volume)				
				Vitrinite	Liptinite	Inertinite	Mineral	Pyrite
Point of Ayr	-250+75	11.1	0.79	76.3	7.8	11.4	4.3	0.4
	-100	15.6		81.6	7.0	8.4	2.4	0.6
Silverhill	-250+75	31.0	0.76	73.2	2.0	9.8	14.2	0.8
Bilsthorpe	-250+75	26.1	0.60	69.3	3.8	12.8	14.1	-

As mentioned above previous work had shown that by using only a frother an inertinite rich fraction could be floated. Some preliminary experiments were conducted in order to assess the effect of three different types of frother on the flotation of inertinite. Batch flotation tests were carried out on various size fractions of Point of Ayr coal using MIBC (an alcohol based frother) and two commercial polyglycol type frothers of different molecular weight. The results from this indicated that MIBC was more selective in floating inertinite than the two polyglycol frothers. MIBC was used in all the subsequent flotation test work.

The effect of adding a collector, in conjunction with a frother, on the flotation of inertinite was examined in a series of tests on -100 μm Point of Ayr coal. Details of the feed sample is shown in Table 1. The collector used in this case was paraffin and was added at dosage levels of 0 (control test), 50, 100 and 150 grams per tonne of dry feed. Frother addition was constant for all tests at a level of 250 grams per tonne of dry feed. Froth was collected over a 2 minute period after which the products were filtered and air dried for maceral analysis by point counting. The data is presented in Figure 1 as a graph of collector reagent addition versus enrichment ratio. The enrichment ratio is the ratio of the concentrate grade of a particular maceral (% volume) to its feed grade and is related to the efficiency of a flotation process [16]. This figure shows that by adding only a frother (zero collector addition) an enrichment ratio of nearly 2 was achieved which equated to an inertinite content in the froth concentrate of 16% by volume in comparison to a feed value of 8% by volume. However even with a small addition of collector this effect was diminished. At a collector addition rate of 100

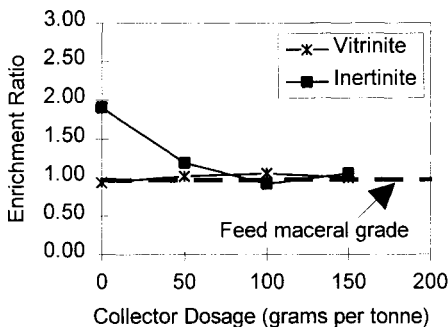


Figure 1. Effect of collector addition on enrichment ratio.

grams per tonne the inertinite enrichment ratio was reduced to approximately 1 which was indicative of no selective concentration of the inertinite macerals. With vitrinite there was little discernible difference in the enrichment ratio due to its relatively high content in the feed (approximately 82% by volume). In order to assess the flotability of inertinite of other British coals further tests were conducted. Discrete size fractions of -250 +75 μm coal were extracted from three coals (Bilsthorpe, Silverhill and Point of Ayr) the feed data for which are presented in Table 1. This particular size fraction was chosen since the inertinite feed values of the coals were fairly similar. Finer fractions of these coals gave widely varying inertinite values which it was felt would influence the flotation results. The flotation conditions were similar to those outlined above with the exception that only a frother (MIBC) was added and no collector. The results which are presented in Figure 2 clearly show the difference in the flotability of inertinite between the coals. The reason for this is not clear but it could be coal rank dependant. However a more likely explanation is that the liberation characteristics of the three coals are very different. The relatively high enrichment ratio for inertinite macerals of the Bilsthorpe coal would seem to indicate that these macerals have liberated to a much higher degree than

for which are presented in Table 1. This particular size fraction was chosen since the inertinite feed values of the coals were fairly similar. Finer fractions of these coals gave widely varying inertinite values which it was felt would influence the flotation results. The flotation conditions were similar to those outlined above with the exception that only a frother (MIBC) was added and no collector. The results which are presented in Figure 2 clearly show the difference in the flotability of inertinite between the coals. The reason for this is not clear but it could be coal rank dependant. However a more likely explanation is that the liberation characteristics of the three coals are very different. The relatively high enrichment ratio for inertinite macerals of the Bilsthorpe coal would seem to indicate that these macerals have liberated to a much higher degree than

In order to assess the flotability of inertinite of other British coals further tests were conducted. Discrete size fractions of -250 +75 μm coal were extracted from three coals (Bilsthorpe, Silverhill and Point of Ayr) the feed data

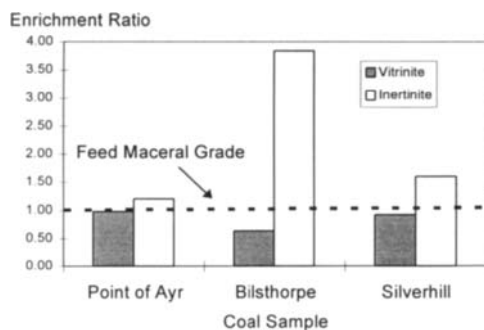


Figure 2. Variation of enrichment ratio for three British coals.

those of both the other coals. In general the results support the hypothesis that inertinite macerals are preferentially floated when only a frother is added.

3. CONCLUSIONS

It was possible with timed batch flotation tests to produce an inertinite rich concentrate provided the only reagent added was a frother. Of the three frothers tested MIBC was shown to be the most selective. Tests on Point of Ayr coal have shown that with the addition of even small quantities of collector (paraffin) this effect was nullified to the point where there was no differential flotability between the macerals. Results from flotation tests on discrete size fractions of three coals produced widely differing inertinite enrichment ratios. This differential flotability was considered to be due to variations in the liberation characteristics of inertinite macerals.

REFERENCES

1. G.R. Dyrkacz, C.A.A. Bloomquist and E.D. Horwitz, *Separation Sci. and Tech.*, 16 (1981).
2. G.R. Dyrkacz and E.D. Horwitz, *Fuel*, 61 (1982).
3. W.J.J. Fermont, J. Joziassé, K.A. Nater and A.M.H. van der Veen, *Fuel Processing Tech.*, 36 (1993).
4. G.R. Dyrkacz and C.A.A. Bloomquist, *Fuel*, 63 (1984).
5. J.C. Hower and B.K. Parekh, *Coal preparations*, eds. J.W. Leonard II and, B.C. Hardinge, 5th Ed., AIME, Colorado (1991).
6. B. Bujnowska, *Coal Preparation*, 1 (1985).
7. G.G. Sarkar, S. Ghose, S.G. Chaudhuri and S. Sakha, *Coal Preparation*, 1, (1984).
8. F.G. Price, *Improvement in or relating to the treatment of coal*, British Patent, no. 186143 (1922).
9. W. Schafer and W. Mertens, *Flotation process*, US Patent Office, no. 1944529 (1934)
10. E. Bierbrauer and J. Popperle, *A process for the preparation of coal by flotation*, British Patent, no. 4500044 (1936).
11. A.J.R. Bennet, H. Bustamante, A. Telfer and L.J. Warren, *Proc. of 2nd Aust. Coal Preparation Conf.*, Rockhamton, Aust (1983).
12. J.C. Hower, K.A. Frankie, G.D. Wild and E.J. Trinle, *Fuel Processing Tech.*, 9 (1984).
13. S. Kizgut, D. Rhodes, N. Miles and M. Cloke, *Progress in Mineral Processing Technology*, eds. H. Demirel, S. Ersayin, Balkema Pub., Rotterdam (1994).
14. ISO 7404/2, *Methods for the petrographic analysis of bituminous coal and anthracite*, document no. ISO/TC 27 N 1255 (1979).
15. ISO 7404/5, *Methods for the petrographic analysis bituminous coal and anthracite*, document no. ISO/TC 27 N 1236 (1979).
16. B.A. Wills, *Mineral Processing Technology*, Pergammon Press, 5th Ed., (1992).

A RANK INDEPENDENT FLOTATION PROCESS FOR COMBINED CYCLE GASIFIERS, INTRINSIC BUBBLE FLOTATION

E.J. Hippo, M. Blankenship, D. Tandon
Department of Mechanical Engineering & Energy Processes
Southern Illinois University at Carbondale
Carbondale, Illinois, USA

1. ABSTRACT

This paper reports work which is part of a joint international research project. The objective is to investigate methods of providing clean feedstocks for gasification. Precleaning the coal could minimize the problems associated with the mineral components such as clinkering, corrosion, erosion, catalyst poisoning, costly flue gas cleanup. In order to remove the inorganic portion of the coal, the mineral components must be liberated using ultrafine grinding. In order to overcome the problems associated with ultrafine particle flotation, a new approach to coal cleaning, known as Intrinsic Bubble Flotation (IBF), has been under development at Southern Illinois University at Carbondale (SIUC) over the past several years. This process utilizes the natural porosity of the organic coal particles and the lack of porosity of the inorganic mineral particles. Air trapped under pressure in the pores of the organic particles form bubbles on the surface of those particles upon depressurization. The information reported in this paper is a portion of the data generated to move the IBF process closer to commercialization.

2. INTRODUCTION

With the development of combined cycle gasification, removal of sulfur and trace elements prior to entering the turbine is paramount in minimizing erosion and deposition. Precleaning the coal could minimize the problems associated with the mineral components such as clinkering, corrosion, erosion, catalyst poisoning, costly flue gas cleanup. Ultrafine grinding (- 45 μ m) followed by deep cleaning is required to liberate and remove pyrite and other minerals from the organic components. Cleaning by conventional methods is ineffective at these particle sizes because particle/particle interactions dominate over process separation parameters. In order to overcome this problem, a new approach to coal cleaning, known as Intrinsic Bubble Flotation (IBF), has been under development at Southern Illinois University at Carbondale (SIUC) over the past several years. This process utilizes the natural porosity of the organic coal particles and the lack of porosity of the inorganic mineral particles. Air trapped under pressure in the pores of the organic particles form bubbles on the surface of those particles upon depressurization. Since the bubbles form from the pore openings, collision and attachment of bubbles is not required and free bubble formation is minimized.

In this process dried coal is fed into a lock hopper where it is pressurized using air. Water and additive (if required) are fed into the mixing chamber and are pressurized to the same pressure as the dried coal. Coal is then transferred into the mixing chamber where the flotation media is stirred until the coal is thoroughly wetted. Two 10,000 rpm motors are currently being used for mixing. A ball valve is used for slurry output and decompression control. The outlet pipe is immersed in a separation column that is half filled with water. Coal slurry is depressurized through a nozzle (maximum pressure drop) at the end of outlet pipe in the separation column. Clean coal float froth rises to the top and is collected in a trough attached to the top of the separation column. The slurry remaining in the column is termed the suspension and the solids (inorganic matter rich) that settle to the bottom are called sink. Air under pressure is trapped in the pores of the organic particles which forms bubbles on the surface of these particles upon depressurization due to capillary law effects. Inorganic particles are non-porous and do not form such bubbles, thus enabling a flotation separation process, Figure 1.

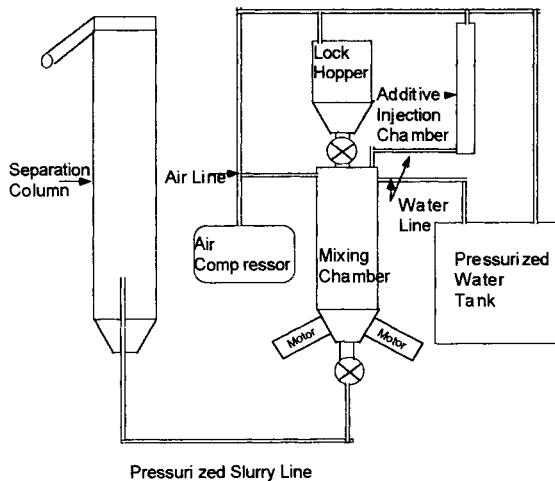


Figure 1. Intrinsic Bubble Flotation (IBF) circuit

3. RESULTS AND EXPERIMENTAL

To determine if this flotation was a result of capillary pore bubble formation or simply the flotation of coal by dissolved gases in water, several experiments were conducted under standard operating conditions (60 psig, 11 pH) except that the coal was mixed with the water before pressurization. No float was observed. The pressure was increased to 90 psig and rerun with the same results. This process is not a result of effervescence generated bubbles.

During previous work, we demonstrated that Illinois basin coals could be cleaned employing IBF [1-4]. This approach keeps flotation medium from penetrating pores and forms microbubble at all pore mouths upon depressurization of the slurry. Thus, the apparent

densities of the porous coal particles are decreased to less than 1.0 g/ml with non-porous mineral density remaining unchanged at about 2.7 g/ml. Since the pores contain compressed air, any moisture entering the outer region of the pore is displaced upon depressurization by the expansion of the trapped air. The moisture content of the floated coal is consistent with that required by combined cycle gasifiers, approximately 30%. This would allow floated coal to be injected into the gasifier directly without additional drying. Conventional flotation processes have float free moisture contents greater than 50%. Vacuum filtration of IBF float will reduce free moisture to approximately 15%. The remainder of the free moisture may be removed using free convective air drying at room temperature with air at 60 to 80% relative humidity. This produces moisture contents approaching inherent values in the Illinois coals.

This flotation process has been successfully used to float and clean North Dakota and Texas lignite, medium volatile Colorado coal, Pittsburgh #8, and several high volatile Illinois coals. Four coals from the Illinois Basin Coal Sample Program (IBC 101, 102, 104 and 106) and a run-of-mine Herrin #6 coal from Monterey #2 mine located near St. Louis, Missouri have been cleaned by this process. Washability curves were obtained for these coals. Washability curves are the graphs showing ash-density distribution and are indicative of the maximum cleaning potential of any physical coal cleaning process for a particular coal sample. SIUC has developed a method for rapidly and accurately evaluating fine and ultra fine coal liberation using Density Gradient Centrifugation (DGC), Micro Sulfur and Thermogravimetric Analysis (TGA) methods to establish these washability curves. Using a low pH flotation solution, 53% sodium removal and a 73% mineral rejection was obtained for North Dakota lignite.

Three particle sizes of -32 mesh, -100 mesh, and micronized (mean particle size of 8 micron) of IBC coals and micronized coal sample of Monterey #2 have been cleaned by this process. All the IBC coals at -32 mesh have been cleaned to their respective -100 mesh washability lines. Greater than 85 wt.% carbon recoveries and 90 wt.% ash rejections have been obtained. Except for octanol and corn oil, which are needed for high clay and ultra fine coals respectively, additives did not have positive effect on the process.

Pressure, in general, increased the hydrophobicity of the organic portion of the coal, and thus for micronized samples (more porosity) higher mixing rates were required to wet the coal. Sixty psig appears to be the optimum operating pressure. Higher mixing rates also increased the efficiency of the process. This high mixing rate not only helped in wetting the ultra fine coal and high pulp density slurries (>20%), but also helped in breaking some of the mixed phase mineral/coal interfaces which caused problems in the early phases of this project. Effect of pH appeared to be coal sample dependent. The process works effectively on weathered coals and pulp densities as high as 20%. Material balance for the process is >95%, and the small loss is due to the micron- and sub micron-sized particles, some of which is lost during filtration.

Presently, the work being performed with the IBF process is aimed at eliminating mineral entrainment and free bubble formation problems faced during previous experiments. Free bubble formation has been minimized by purging the system of any air that may be trapped in the piping and also slurring the coal with the mixer completely filled with water. Maceral content of the products and rejects have been studied to have a better understanding of the nature of the material that results from float froth. A typical flotation run was made on the

ROM (run of mine) Illinois #6 coal from Monterey II mine. The float was observed by point count to consist of almost 88% vitrinite, 0.5% inerts, and 6% pyrite. The pyrite and inerts are mostly mixed phase particles containing some vitrinite. However, about 10% of the inertinite and pyrite appear to be liberated. The point count of the sink showed the organic presence of 36% vitrinite and 64% fusinite. DGC analysis indicates that 93% of the sink material has a density close to that of clean coal. The suspension in the separation column is primarily liptinites and semi-fusinites.

4. CONCLUSIONS

The IBF flotation process can clean coals from lignite to medium volatile bituminous rank. This process has shown effective particle flotation at any size from 250 μm down to 8 μm . Since each coal particle generates its own bubble, contact angle is of little importance. Operating pressure is a significant operating parameter that must be adjusted to maximize bubble growth without detachment due to over development. Flotation performance consistently improves with decreasing particle size, but liberated mineral matter has been observed in the float. Current research is aimed at separating this liberated mineral by improved agitation of the mixing process and decreasing the amount of oil needed for agglomeration of ultra fine coal particles. The addition of surfactants has a detrimental effect on float recovery and mineral removal. Initial testing has shown that with adjusted pH levels in the flotation circuit pronounced reductions in sodium and potassium are possible with high levels of mineral rejection. Petrographic analysis of the flotation products have shown a means of initial maceral separation that could provide higher maceral concentrations after high energy DGC. Float moisture is at least 20% lower than that reported by conventional flotation methods.

5. ACKNOWLEDGMENTS

The authors would like to acknowledge the financial support of New Energy Development Organization (NEDO) of Japan.

REFERENCES

1. E.J. Hippo, D. Tandon, and D.P. Sarvela, Coal Flotation by Intrinsic Bubble Formation, Proceedings of the 1991 International Conference on Coal Science, 893-896.
2. E. J. Hippo, D. Tandon, M. Blankenship, and S. Kahn, Coal Flotation with IBF/Oil Froth, Fuel Div. Preprints, 204th Nation Meeting of the ACS, Washington, DC, 37(4) 1992, 1990-1995.
3. E. J. Hippo, D. Tandon, M. Blankenship, and S. Kahn, Cleaning of Micronized Coal Employing Insitu Bubble Formation and Oil Froths, Proceedings of the 9th Annual Pittsburgh Coal Conference, October 13-16, 1992, 18-23.
4. D. Tandon, Coal Cleaning by Intrinsic Bubble Formation, Master's Thesis, Southern Illinois University at Carbondale, September 1990.

Scientific Topic: C.1.1. Coal Cleaning Science

Key words: flotation, cleaning, coal

Microflotation of coal particles suspensions

A. A. Baichenko and Al. A. Baichenko

Institute of Coal, Russian Academy of Sciences,
21, Rukavichnikov st. 650610, Kemerovo, Russia

1. **ABSTRACT**

The factors affecting the efficiency of microflotation water purification are analyzed. Kinetic aspects of the flotation process taking account of the phenomena of absorption of macromolecules, aggregation of finely dispersed particles and microbubbles in the turbulent flow characterized by Reynolds number $Re = 5000-6500$ are considered.

2. **INTRODUCTION**

The beneficiation and clarification of coal-clay suspension involves a whole range of technological processes the efficiency of which depends significantly on the concentration of the finely dispersed coal and rock particles and activity of the reagents and polymer flocculants. One of the perspective directions of water purification containing finely dispersed particles and oil droplets is turbulent microflotation which makes possible to accelerate flotation purification in the conditions of intensified saturation of water with gas microbubbles and transportation of microparticles to the surface of microbubbles in the turbulent flow. The distinctive feature of microflotation compared to the conventional methods of purification (sedimentation, flocculation) is a possibility of extracting clay particles of colloidal degree of dispersivity as well as the rate and efficiency of the process.

3. RESULTS

While multiphase dispersed systems are flowing through the pipeline the conditions for their disintegration due to turbulent coagulation and heterocoagulation arise. The kinetics of variation of concentration of particles thanks to sedimentation on bubbles is described by the equation of the first order reaction [1,4]. It is shown experimentally that in a large scale fluid pulsation the sedimentation of particles on the surface of bubbles takes place as a result of gravity forces acting upon them according to just the same mechanism as in an ordinary flotation cell.

$$K_F = \frac{3E \varphi U(D)}{2D} \quad (1)$$

where K_F - the process intensivity according to the flotation mechanism, φ - volumetric concentration of bubbles, $U(D)$ - the rate of their sedimentation, E - the efficiency of capture of particles by gas bubbles coming to the surface in flotation.

The efficiency of capture of particles having the radius a by a bubble the surface of which is blocked by the layer of a surfactant is defined by the dependence

$$E \sim a^{3/2} / R^2 \quad (2)$$

where R - the bubble radius.

If $a \ll R$ it is very small and therefore it is advisable to enhance the size of the captured particles by flocculation. The process of aggregation of particles essentially affects the flotation if the concentration of particles exceeds some critical volume:

$$C \approx 0,1E/\alpha \quad (3)$$

where α - the efficiency of aggregation of particles in the field of a simple shift.

But the flocculation intensifies the extraction of micro-particles if the sizes of aggregates do not exceed some critical value determined by the adhesion force of single particles to a bubble, the size of particles and their compactness [3,4]. The tearing-off force F acting upon the aggregate in the field of a simple shift be estimated by the phormula

$$F = 6\pi a_A^2 \eta G \quad (4)$$

where a_A - the radius of an aggregate, η - viscosity of the medium and G - the shift gradient.

If this force turn out to be greater than the sum of single contacts in the median section of an aggregate

$$f_A = f_a n_a \quad (5)$$

where f_a - the adhesion force of two particles, n_a - the number of contacts in the median section then the aggregate can be teared off before it secures on the bubble. Obviously the value n_a depends only on the compactness of an aggregate. From this it is clear that floatability of aggregates can be limited not only by the force of adhesion to the bubble but by the force of coupling of separate particles into an aggregate. There is an optimum size of an aggregate providing the most intensive flotation in the conditions of turbulization. The strength and maximum size of flocs essentially depend on the size of initial particles, the shift gradient and the flocculant type [4]. The maximum aggregate size is

$$a_{Amax} \sim 1/a \sqrt{G} \quad (6)$$

By using the polymer flocculants the radius of stable flocs can constitute 50-100 μm even in comparatively hydrodynamic fields which are available in flotation cells [3].

4. DISCUSSION

In considering the kinetics of adsorption of polymer it is necessary to take count of the time of diffusion of macromolecules to the surface of particles as well as the kinetics itself that is the time required for the adsorped substance to be bakanced in the surface layer. In the initial stage of the process of adsorption when the coverage of the surface is low the kinetics of adsorption will be determined by diffusion of macromolecules to the surface. In filling it the adsorption will decrease because of the reduction of a number of places on the surface that is reflected in retarding of adsorption in terms of time.

The investigation of coagulation in the turbulent flow with high shift velocities showed the necessity of using flocculants providing high strength and compactness flocs. The study of the mechanism of turbulent microflotation technology will promote its improvement for solving ecological and resource-saving technologies.

REFERENCES

1. N.N.Rulyev and A.A.Baichenko. "Mechanism for catching particles by bubble in a turbulent stream", "Colloidal Journal" (in Russian), Vol. 48, No 1, p. 114-123 (1986)
2. Al.A.Baichenko and S.S.Dukhin "Intensification of water purification from finely dispersed particles by microflotation", "Chemistry and water technology" (in Russian), Vol. 11, No 6, p. 523-524 (1989)
3. Al.A.Baichenko and A.A.Baichenko "Adsorption of polyethyleneoxide and its influence on flocculation and flotation of coal suspensiones", "Chemistry of solid fuel" (in Russian), No 6, p. 129-135 (1990)
4. A.A.Baichenko, N.N.Rulyev, A.A.Baran "Flocromicroflotation", "Physical and technical problems of getting useful minerals" (in Russian), No 3, p. 103-108 (1992)

Directions of development in coal cleaning

A.A.Baichenko and G.I.Gritsko

Institute of Coal, Russian Academy of Sciences,
21, Rukavichnikov st. 650610, Kemerovo, Russia

1. **ABSTRACT**

The creation of technologies of rational use of mineral resources comprising complex extraction of wastes with an account of environmental impact of mining enterprises is possible only in wide application of the latest achievements of chemistry in mining industry. First of all it concerns the use of flotation reagents for selective separation of minerals, coagulants, polyelectrolytes and polymer flocculants to control the stability of disperse system in hydraulic mining, hydraulic transport, thickening, filtration, creaning of effluents.

2. **INTRODUCTION**

The necessity of taking nature protection measures created a complicated situation in the coal preparation plants: saving fresh water, cleaning of effluents and dewatering of fines (specially in winter) force to apply technological schemes with water operations playing the main part. And just water but not preparation operations consume the major capital investments, maintenance and labour expenditures. Every year this problem is becoming more acute. In the first instance it concerns the intensification of flotation, thickening filtration of coal slimes and clarification of effluents.

reagent consumption (2 kg/ton of aromatized apolar reagent AAR-2 and 0,3 kg/ton of vat residue of buthyl alcohol VRBA which is added to the slurry as emulsions in several steps at flotation front) [3].

The flotation concentrate goes to vacuum-filters where 10 g/ton of PEO is added. The filtrate is directed to the separate flotation machine for selective flotation of the fine particles. This process is carried out with diluted slurries containing 30-40 g/l solids. As flotation reagent VRBA is used only its emulsion is added fractionally - 40%, 30% and 30% into the 1st, 2nd, and 5th chamber at the total flow rate of 50 g/ton [4].

Table

Selective flotation of fine particles of the filtrate

Classes, μm	Supply			Concentrate			Tailings		
	Q	γ , %	A^d , %	Q	γ , %	A^d , %	Q	γ , %	A^d , %
+25	6.86	26.3	8.5	6.60	25.3	6.8	0.26	1.0	51.8
25 - 10	1.18	4.5	15.1	1.0	3.8	7.2	0.18	0.7	58.4
10 - 5	2.53	9.7	12.0	2.35	9.0	7.8	0.18	0.7	66.2
5 - 0.0	15.53	59.5	11.0	14.95	57.3	8.4	0.58	2.2	79.0
+0.0	26.10	100.0	10.6	24.90	95.4	7.9	1.20	4.6	68.0

Q - input, ton/hour; γ - yield, A^d - ash content.

The results of flotation of the filtrates are presented in the table. It is seen that the main part of particles has the diameter less than 25 μm . By the method described the high degree of separation of coal and rock particles is reached: the flotation of particles of the diameter less than 5 μm and ash of 11% yields coal concentrate with ash of 8.4% and the flotation tailings with ash of 79%.

So, the combine use of polymer flocculants and flotation reagents in the cycle of regeneration of the slime water enables not only to intensify the processes of sedimentation, filtration and flotation but to reach the selectivity of separation

3. RESULTS AND DISCUSSION

3.1. The intensive technology of slime water purification.

Therefore, the most rational way to realize the single-stage technological scheme is the intensification of flotation and filtration processes using more effective flotoreagents and flocculants [1,2], of Berezhovskaya Washery. Fig.1 gives the flow chart of selective purification of slime waters by complex use of apolar reagents and flocculant (PEO).

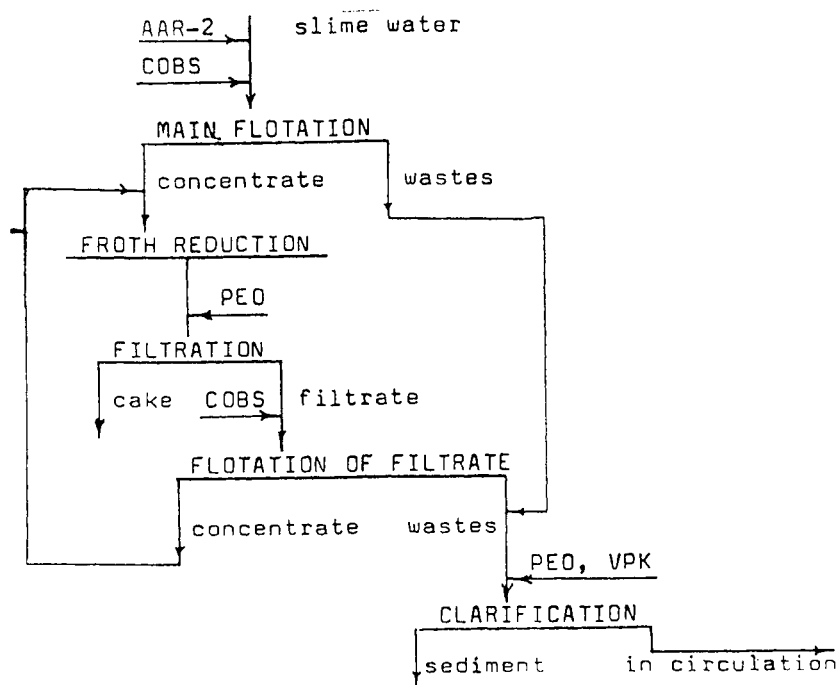


Figure 1. The points of introducing reagents into the flowsheet for slime water purification.

The slime waters after dredging sump go to the principal flotation, the task of which is maximal extraction of coal particles in flotation concentrate and obtaining the flotation tailings with high ash content. It is reached by some increase of

of coal particles as well.

4. CONCLUSIONS

Wide application of chemical reagents to control the stability of natural dispersions creates conditions for introducing radically new processes of regeneration of slime, mine and sewage waters, make the performance of the existing intensifies the technology of treatment of useful minerals and reduces the loss of concentrates improves their quality and environment in the region.

Introduction of technological processes of coagulation, flocculation, flotation and minimum use of reagents for them makes possible to lower sharply the consumption of reagents and automatize individual technological blocks (flotation and filtration of concentrates) without any danger of accumulating flotation reagents in the recycled water.

Selection of reagents, preparation of reagent solutions and choice of the points of their introduction into the technological process is to be made taking account of physical and chemical properties of water and raw material of the given enterprise.

REFERENCES

1. A.A.Baichenko, Al.A.Baichenko. The use of polymers in closed water cycle in coal preparation plants. News of high schools. Mining Journal. No 4, p. 81-85 (1981).
2. I.Roiter. The use of flocculants and polymers in coal preparation. Gluckauf. No 19, p. 19-23 (1970).
3. A.A.Baichenko, A.A.Baran, N.S.Mitina. Treatment of recycled water by flocculation in coal preparation. Chemistry and water technology. Vol. 7, No 4, p. 38-42 (1985).
4. V.T.Tyurnikova, M.E.Naumov. The increase of flotation effectiveness. Moscow: Nedra, 224 p. (1980).

Selective agglomeration of high rank coals with vegetable oils

J. M. G. Vega, M. R. Martínez-Tarazona and A.B. Garcia

Instituto Nacional del Carbón, C.S.I.C., Apdo. 73, 33080-Oviedo, Spain

1. INTRODUCTION

The problem of over-increasing production of coal fines together with the fact that in most coals significant amounts of minerals, specially pyrite, are very finely disseminated in the coal matrix, have lead to considerable research into physical methods to clean coal at finer sizes. Among them, oil agglomeration has been found to be one of the most effective [1,2]. Because of the relatively large amounts of oil used in this cleaning method, research and development work have been focused on finding a suitable low-cost and/or recoverable one. Although the effect of oil type on coal cleaning by agglomeration is considerable more complex, lighter oils (densities below about 0.9 g/cm³) with high paraffin content have been recognized to provide better ash rejection selectivities [3]. Recoverable light hydrocarbons such as pentane [4] and heptane [5,6] have been extensively tested. Although high-value ultraclean coal products and combustible recoveries over 90% were obtained in most cases by using these compounds, the price of the hydrocarbons themselves as well the necessary recovery step will inevitably make the process costs high. Consequently, the commercial viability of using light hydrocarbons as coal agglomerants is at moment uncertain. These results point to the necessity of testing the effectiveness of others light oils of lower cost as coal agglomerants.

The purpose of this paper is to study the feasibility of using vegetable oils for coal agglomeration. This objective complies with the European Union policy to use of vegetable oils for purposes others than food. In the work described below three high-ash Spanish anthracites were cleaned by agglomeration with refined sunflower and soyabean oils which may be considered as light compounds (density about 0.9 g/cm³); moreover they are less expensive than hydrocarbons. The response of these coals to agglomeration with these vegetable oils, over a wide oil concentration, was evaluated by measuring the percentages of organic matter recovery and ash rejection. These results were compared with those previously obtained in the agglomeration with n-heptane [7].

2. EXPERIMENTAL

2.1 Materials

Three anthracites AT, AG and AV, all of them run-of-mine from Narcea, Bierzo and Guardo basins (north-west Spain) were studied. The coal samples were sieved to 500 µm top size and kept under argon until the agglomeration experiments were carried out. The proximate and elemental analyses of the ≤500 µm fractions are given in Table 1. The sunflower GIR and soybean SOR refined oils used in this investigation were obtained from Instituto de la Grasa, CSIC in Sevilla (Spain). They are light oils (density 0.92 g/cm³) consisting mostly of glicerides (>98 wt%) with a very low concentration of free fatty acids (<0.1 wt%). The oils viscosities, as determined from ASTM procedure D445-86, were 7.5 cP for GIR and 8.8 cP for SOR.

2.2 Agglomeration procedure

Oil agglomeration experiments were conducted in a commercial seven speed Waring® blender equipped with a 1000 ml glass vessel. For each agglomeration test, 400 ml of distilled water and 16 g of coal were placed in the blender and mixed at 11000 rev min⁻¹ for 5 min to disperse the coal particles. A specific amount of oil, ranging from 5 to 40 wt% of coal, was then added and mixing was continued at the same speed for 60 s to produce agglomerates. The resultant agglomeration product was separated from the refuse using a No. 410 B.S. standard screen with openings of 500 µm. The agglomerates were then recovered from the screen using distilled water, filtered, water-washed, dried overnight at 50°C, weighed to calculate the percentage of recovery, and analyzed for moisture and ash.

The results of the agglomeration process were evaluated by (i) percentage of organic matter recovery OMR and (ii) percentage of ash rejection AR. These percentages were calculated as follows:

$$\% \text{ OMR} = 100(\text{wt agglomerate}/\text{wt feed})[(100-\text{ash}_{\text{agglomerate}})/(100-\text{ash}_{\text{feed}})]$$

$$\% \text{ AR} = 100[\text{ash}_{\text{feed}} - (\text{ash}_{\text{agglomerate}} \times \text{wt agglomerate}/\text{wt feed})]/\text{ash}_{\text{feed}}$$

Table 1
Proximate and elemental analyses and sulfur forms of ≤500 µm fraction of coals

	AT	AG	AV
Proximate analysis (wt%, dry basis)			
Moisture	1.2	1.2	3.3
Volatile matter	7.9	6.9	6.2
Ash	24.8	38.4	33.6
Elemental analysis (wt%, daf basis)			
Carbon	93.7	93.9	90.5
Hydrogen	3.2	2.0	1.3
Nitrogen	1.3	0.7	0.7
Sulfur ^a	0.92	2.25	0.97
Sulfur forms (wt%, dry basis)			
Pyritic	0.57	1.72	0.44
Sulfate	0.02	0.05	0.04
Organic	0.33	0.48	0.49

a dry basis

3. RESULTS AND DISCUSSION

Figures 1 and 2 illustrate the effect of refined soyabean SOR and sunflower GIR oils concentration on organic matter recovery and ash rejection. As can be seen, the agglomeration behavior of AT, AG and AV coals is similar. Thus, when SOR and GIR concentrations of 5 wt% were used, the organic matter recoveries were the smallest. By increasing the oil concentration up to 20 wt%, the percentage of combustible recovery was highly enhanced. For example, at SOR concentrations of 20 wt%, organic matter recoveries of AT and AV coals >90% have been achieved. However, any further increase in SOR or GIR concentrations up to 40 wt% had no significant effect on the combustible recovery of coal. In this way, the OMR of AG coal was decreased from 80 to 78% as the SOR concentration increases from 20 to 40 wt%; whereas the corresponding OMR values for AT coal were 93 and 94%. Unlike vegetable oils, concentrations of n-heptane over 20 wt% led to an important decrease in combustible recovery (Figure 1). According to the mathematical model developed by Petela [8] to calculate the final size of the agglomerate, the agglomerate diameter grows continuously as the amount of oil increases, the maximum size being achieved at the so-called critical oil concentration. After this

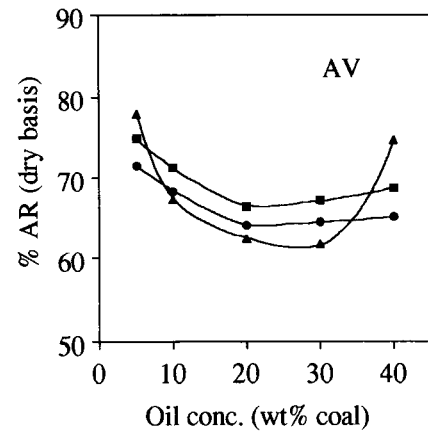
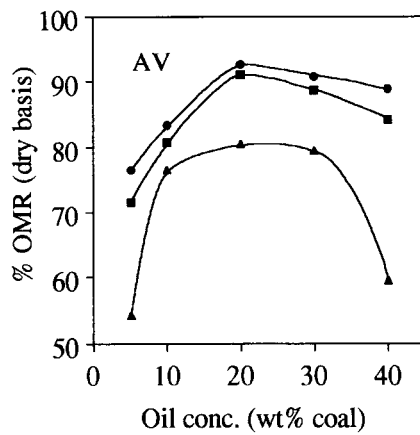
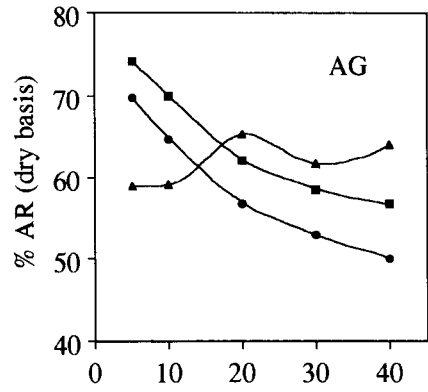
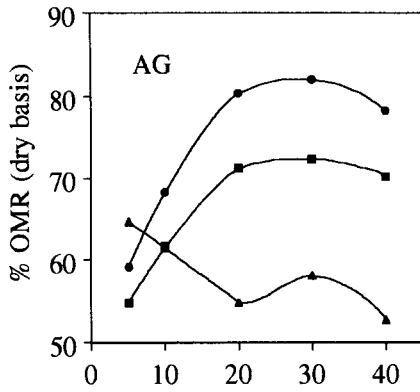
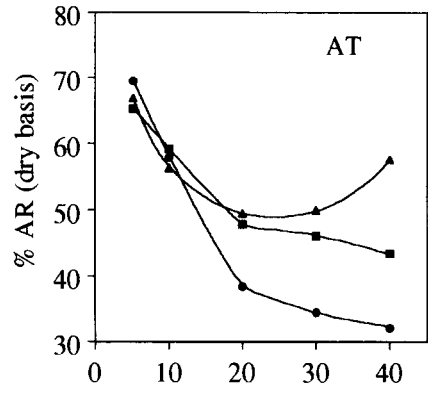
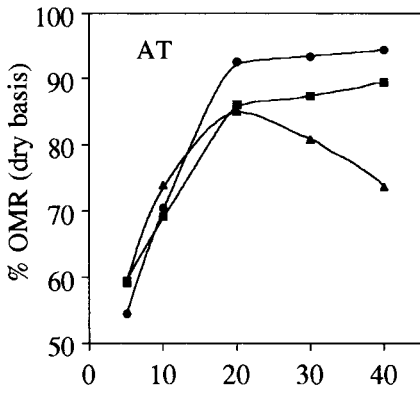


Figure 1. Effect of SOR (●), GIR (■) and HEP (▲) concentrations on organic matter recovery of coal

Figure 2. Effect of SOR (●), GIR (■) and HEP (▲) concentrations on ash rejection from coal

concentration has been reached, the agglomerate diameter and consequently, the recovery are expected to remain constant until the amount of oil in the aqueous suspension becomes excessive, the coal particles existing separately in an oil surrounding. These weak agglomerates go through the collecting screen, leading to a decline in coal recovery. Based on that model, under the experimental conditions employed in this work, the critical oil concentration for the agglomeration of AT and AV coals seems to be independent of the agglomerant. Thus, these coals exhibit critical oil concentration values of 20 wt% with both vegetable oils and heptane (Figure 1). However, the amount of oil necessary to become excessive relies on the characteristics of the oil, the difference between this and the critical one being greater when vegetable oils are used. Regardless of the type of oil, ash rejections from coals increased with decreasing coal recovery (Figure 2). As an example, ash rejection from AV coal was enhanced from 64 to 72% as the SOR oil concentration decreased from 20 to 5 wt%; the corresponding organic matter recoveries were 93 and 77%, respectively. At low oil-to-coal ratios, the amount of oil is insufficient to adsorb onto all of the coal particles present. As a result, only hydrophobic coal particles which contain low levels of mineral matter will be agglomerated; therefore, higher ash rejections will be reached.

As regards critical oil concentration (20 wt%), a comparison of the agglomeration results obtained with the different type of oils (Figures 1 and 2) reveal that the organic matter recoveries of AT and AV coals as well as ash rejection from the later were improved by using vegetable oils instead of heptane, the amount of the increase depending on the coal. In this way, OMR for AV increased from 80 to 91% and AR from 63 to 67% with GIR. As compared with AT and AV coals, the response of AG coal to agglomeration with heptane was poorer. An organic matter recovery of 55% and ash rejection of 65% were obtained for this coal at an oil concentration of 20 wt%. However, if vegetable oils are used as agglomerants, the organic matter recovery of AG coal was increased to values comparable to those obtained in the agglomeration of AT and AV. Thus, organic matter recoveries of 80 and 71% were achieved in the agglomeration of this coal with SOR and GIR oils, respectively; the ash rejections being 57 and 62%.

From the results obtained in this preliminary work, it can be concluded that sunflower and soyabean vegetable oils are suitable compounds for coal agglomeration.

ACKNOWLEDGEMENTS

This research was carried out with financial support from DGCYT (Research project NAT91-0620). Mr J.M.G. was supported by a predoctoral fellowship provided by FICYT during his work at Instituto Nacional del Carbón, CSIC.

REFERENCES

1. G.R. Couch, *Advanced Coal Cleaning Technology*, IEACR/44, IEA Coal Research, London, 1991.
2. C.E. Capes and K.A. Jonasson, *Interfacial Phenomena in Coal Technology* (Eds. G.D. Botsaris and Y.M. Glazman), *Surfactant Science Series* vol.32, Marcel Dekker, New York, 1989, pp.115-155.
3. C.E. Capes and R.J. Germain, *Physical Cleaning of Coal* (Ed. Y. Liu), Marcel Dekker, New York, 1982, pp. 293-351.
4. D.V. Keller, Jr and W.M. Burry, *Coal Preparation*, 8 (1990) 1.
5. R. Venkatadri, R. Markuszewski and T.D. Wheelock, *Energy & Fuels*, 2 (1988) 145.
6. S.S. Kim, B.I. Morsi and S.-H. Chiang, *Coal Preparation*, 15 (1994) 51.
7. A.B. Garcia, J.M.G. Vega and R.M. Matinez-Tarazona, *Fuel* (in press)
8. R. Petela, *Fuel*, 70(1991) 509.

Mineral Matter Removal by Alkali Leaching and the Characterization of Remained Mineral Matter

J. Wang, Y. Kobayashi, A. Tomita and Z.-G. Zhang

Institute for Chemical Reaction Science, Tohoku University, Sendai 980-77, JAPAN

1. INTRODUCTION

Mineral matter is generally considered to be undesirable and detrimental in coal utilization. In the slagging gasification, the uncontrollable slag deposition on the reactor wall as well as the solidification of molten slag due to the lack of heat may cause serious operation problem. On the other hand, in the fluidized bed gasification or combustion, too much heat causes the agglomeration of dry ash, and this also results in an operational problem. In the catalytic liquefaction or gasification processes, the reaction between catalyst and mineral matter may cause the deactivation of catalyst.

One solution for these problems is coal cleaning prior to the utilization. The absence of mineral matter would eliminate most of the above problems. One possible cleaning method is a chemical approach [1]. CSIRO has developed a cleaning process using NaOH leaching followed by H₂SO₄ washing [2]. The present study first examined the inorganic constituents and the melting behavior of the ultraclean coal prepared by CSIRO. To avoid the use of somewhat expensive NaOH, we attempted to use Ca(OH)₂ as a leaching agent. In spite of a relatively low level of demineralization, there are salient advantages of the Ca(OH)₂ leaching not only in its cheapness, but also in possible effects on the desulfurization and the lowering of ash melting point by remaining Ca species. Additives like limestone are frequently applied to reduce the sulfur emission in fluidized bed processes and to improve the fluidity of the molten slag in entrain bed gasification processes. This paper intends to provide some preliminary results on these aspects.

2. EXPERIMENTAL

2.1. Removal of Mineral Matter

The coal used throughout this study was Newstan coal from Australia. The proximate and ultimate analyses are listed in Table 1. NaOH treatment was carried out in CSIRO. The main procedure was the leaching with an excess of 20% NaOH solution for 30 min at 250°C and an autogenous pressure of 4 MPa. This was followed by H₂SO₄ washing.

The Ca(OH)₂ leaching were carried out in a 300 ml autoclave with a stirrer. Coal (-100 mesh, 15 g) was blended with 150 ml of Ca(OH)₂ suspension. The slurry was heated at 10 K/min to 300 °C. After a predetermined treatment time at a constant temperature, the treated slurry was cooled and filtered, and then the solid mixture was acidified with a 200 ml of 6% hydrochloric acid at a slightly boiling condition for 30 min. Then it was filtered and washed by hot water and distilled water in sequence to yield a sample for analysis. Ash removal rate is calculated from the ash contents in the feed coal and the treated coal.

2.2. Characterization of Ash

Ash samples were prepared by low temperature plasma ashing and by high temperature ashing. The low temperature ashing technique allows mineral matter to be liberated from coal in a relatively unchanged form. The high temperature ashing was conducted at 815°C.

The XRD examinations were performed using CuK α radiation at 30 kV and 30 mA. For the quantitative analyses of elements in ashes, inductive coupling plasma (ICP) associated with atom emission spectrometer technique was employed. The melting behaviors of ash were measured according to ASTM procedure. A triangle sample cone was heated at 5°C/min. A video camera was equipped to record the shape changes of the sample cone.

3. RESULTS AND DISCUSSION

3.1. Removal of ash

The NaOH treatment reduced the ash content of Newstan coal from 9.0 to 0.5% (dry basis), yielding an ultraclean coal.

With respect to the Ca-treatment, the effect of leaching time was first determined. With increasing leaching time, the ash content decreased in the beginning, but there was no further decrease after 30 min. Table 2 presents the effect of leaching temperature on ash removal. The majority of mineral matter was removed at 250-340°C. It can be seen that the ash removal rate became high with an increase of leaching temperature. The effect of the amount of added CaO was also examined. An interesting point was that a better result was obtained with a smaller amount of CaO. This is because more Ca species were remained on coal when an excess amount of CaO was added to the system. The lowest ash content among these experiments was 2.4 %, which corresponds to the removal rate of 73 %. This removal rate was of course lower than that by Na-leaching, but this process seems to be interesting if further optimization can be possible. The main reaction between SiO₂ and Ca(OH)₂ would be the formation of calcium silicate hydrates, (CaO)_x(SiO₂)_y(H₂O)_z, which is soluble in aqueous solution [3].

3.2. Effect of leaching on the characteristics of coal

One of the important characteristics is the property of coal matrix. Table 1 showed the proximate and ultimate analyses of two clean coals obtained by NaOH- and Ca(OH)₂-

Table 1 Proximate and ultimate analyses of Newstan coal and its clean coals.

	Raw coal	Na-coal	Ca-coal*
Proximate analysis (% , dry)			
Ash	9.2	0.5	3.8
Vol. matter	33.7	35.3	32.6
Fixed carbon	57.1	64.2	63.6
Ultimate analysis (% , daf)			
Carbon	83.2	82.3	82.0
Hydrogen	5.4	5.2	5.0
Nitrogen	2.1	2.1	2.3
Sulfur	0.5	0.9	--
Ash analysis (%)			
SiO ₂ **	67.0	30.7	56.3
Al ₂ O ₃	22.5	11.6	7.5
Fe ₂ O ₃	5.5	33.9	3.7
Na ₂ O	1.4	14.1	1.0
TiO ₂	1.0	6.3	1.2
CaO	0.8	1.2	12.4
MgO	0.7	0.6	0.2
SO ₃	1.1	1.6	17.7

* Ca-treatment condition, CaO: 0.5 g/g-coal; Temperature: 340°C, Leaching time: 60 min.

** By difference.

Table 2 Removal of ash from Newstan coal by Ca-leaching*.

Temperature (°C)	Ash content (%)	Ash removal (%)
150	5.6	38
250	2.7	70
340	2.4	73

* CaO added: 0.05 g/g-coal, leaching time: 60 min. Pressure: 1.5, 3.5, 10.5 MPa at 150, 250, 340°C.

leaching. Little changes in volatile matter, carbon and hydrogen contents on the dry ash-free basis were observed after leaching.

Ash analyses for raw coal and treated coals determined by the inductive coupled plasma method are also presented in Table 1. SiO_2 , Al_2O_3 and Fe_2O_3 were the major constituents in the raw coal, and the relative ratio of these oxides drastically changed after treatments. Remarkable increases not only in relative value but also in absolute value of Na_2O and CaO were observed in Na-treated coal and Ca-treated coal, respectively. The amount of remaining alkali may strongly depend on the degree of washing processes. In other words, we can put the optimum amount of these species for the subsequent use.

3.3. X-ray diffraction analysis of ash

As stated above, it is possible to remove most of mineral matter by chemical leaching. However, in the practical use of ultraclean coal, it would be still required to pay an attention to the behavior of the small amount of the remained mineral matter. Thus its characterization was carried out mainly by X-ray diffraction technique. Figure 1 shows the XRD patterns of the low temperature ash (LTA) and high temperature ash (HTA) for raw coal and clean coals. LTA of raw coal contains quartz, kaolinite and small amounts of siderite and pyrite. They turned into quartz and a little hematite and metakaolinite in HTA. Na-treated coal shows quartz peaks with medium intensity with several small peaks which can be assigned to mirabilite, coquimbite, paracoquimbite and aluminium sulfate. All of them have poor crystallinity. In HTA, strong peaks of quartz and hematite appeared. LTA of Ca-treated coal has quartz, kaolinite and bassanite, and its HTA contains only quartz and anhydrite. The calcium sulfates were produced by the interaction of remaining calcium and sulfur oxides evolved from coal during ashing procedure. All of these observations are in accordance with the ash analysis presented in Table 1. The formation of calcium sulfate indicates the possibility of *in situ* sulfur capture by the remaining calcium as expected.

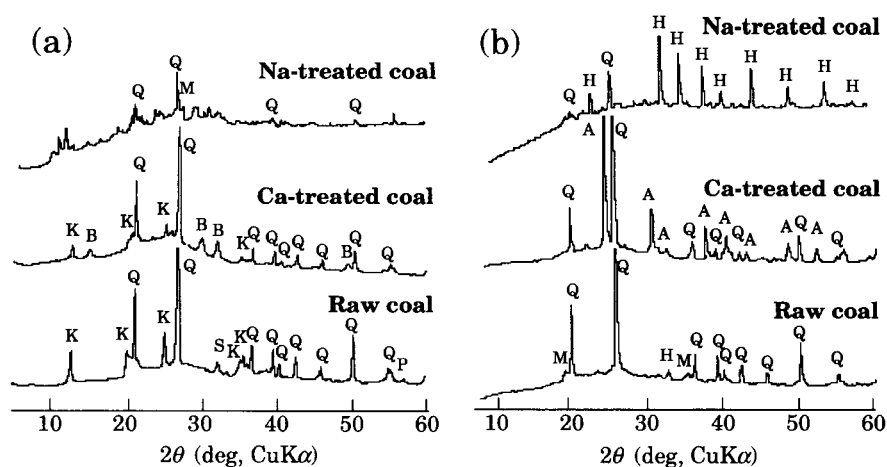


Figure 1 XRD patterns of LTA (a) and HTA (b) for raw Newstan coal and Na- and Ca-treated coal. A: anhydrite, B: bassanite, H: hematite, K: kaolinite, M: metakaolinite, P: pyrite, Q: quartz, S: siderite.

3.4. Melting behavior of ash

Table 3 lists the melting properties for three coals. Raw coal has a flow temperature higher than 1500°C. When it was treated with NaOH or Ca(OH)₂, all the characteristic temperatures were lowered by more than 100°C. This can be expected from the increase of Na, Fe and Ca components in ash (Table 1). This decrease in melting point would be beneficial in handling slag during the high temperature gasification.

Table 3 Melting properties of Newstan coal and clean coals.

Coal	Deformation temp. (°C)	Softening temp. (°C)	Flow temp. (°C)
Raw coal	1460	1490	1510
Ca-coal	1260	1310	1340
Na-coal	1170	1280	1330

The appearance of slag from clean coal was quite different from that of raw coal. The slag from raw coal looked brownish, while the color of Ca-treated coal was pale brown with some greenish tone. The Na-treated coal slag was black, and it has many cavities perhaps due to evaporation of sodium related species and spreaded more than the others.

3.5. Liquefaction and gasification of clean coal

Some preliminary tests of liquefaction and gasification of Na-treated coal were carried out. In liquefaction, coal was mixed with tetralin and synthetic pyrite catalyst, followed by processing with 9.8 MPa hydrogen at 420°C for 1 h. Oil yield was 39% and 46% for raw coal and Na-treated coal, respectively, while the yield of preasphaltene from the Na-treated coal decreased to some extent. The reactivity in the CO₂ gasification was determined at 800°C. The char conversion after devolatilization linearly increased with time in the initial stage. The gasification rate was 0.35 h⁻¹ and 0.75 h⁻¹ for raw coal and Na-treated coal, respectively. This increase is likely due to the catalytic effect of Na species. It can be concluded the pretreatment with NaOH resulted in the better performance in the subsequent utilization in addition to the advantages in better operatability.

4. CONCLUSION

The characteristics of ash remained after the pretreatment with NaOH and Ca(OH)₂ were investigated and it was shown the properties of ash were quite different from those of original ash in many respects. Several advantages can be expected by cleaning: (1) The direct merit related to the decrease of ash content, (2) the lower melting point of ash, (3) a great potential to decrease sulfur evolution, for example, in the fluidized bed processing of Ca-treated coal, and (4) higher reactivities in liquefaction and gasification of Na-treated coal.

ACKNOWLEDGMENTS

NEDO International Joint Research Grant is greatly acknowledged. Mr. I. W. Smith, Mr. C. Thomas and Dr. D. J. Harris of CSIRO, who are the members of the above joint research, kindly supplied the NaOH-treated clean coal.

REFERENCES

1. Wang, Z.-Y., Ohtsuka, Y. and Tomita, A., *Fuel Process. Technol.* **1986**, 13, 279.
2. Waugh, A. B. and Bowling, K. McG. *Fuel Process. Technol.* **1984**, 9, 217.
3. Sanders, J. F., Keener, T. C. and Wang, J. *Ind. Chem. Res.* **1995**, 34, 302.

Demineralization of anthracite char by molten salts

M. Alfaro-Domínguez, F. J. Higes-Rolando and V. Gómez-Serrano

Departamento de Química Inorgánica, Universidad de Extremadura,
06071-Badajoz, Spain

1. INTRODUCTION

Demineralization of coals prior to utilization in conversion processes such as combustion is an important technology as regards coal beneficiation and environmental protection [1]. Techniques of coal demineralization are based on physical or chemical processes. On a small laboratory scale, coals are frequently treated with hydrochloric and hydrofluoric acids at 40 °C [2]. The techniques of significant industrial importance involve the treatment of coals with alkali at temperatures ranging between 150 and 350 °C, at atmospheric pressure or at higher pressures (25-172 atm) [3-5]. The treated coals are leached by using water and mineral acids. Mineral matter removal from anthracite by high temperature chlorination has been recently investigated by Walker and Imperial [6]. In the present work, the demineralization of an anthracite char (AC) by reaction with molten salts at various temperatures is studied. Generally, the molten salts used were a LiCl and KCl mixture containing metallic oxides which differed from the solubility in the molten chlorides. The temperatures were chosen according to the temperature of the LiCl/KCl eutectic and to SiO₂ transition temperatures. Moreover, methods of washing of the samples were tested to remove remaining chlorides and oxides as well as reaction products. Information on composition changes produced because of the treatments of AC and of the subsequent washing of the resulting products was obtained by X-ray diffraction (XRD) and FTIR spectroscopy.

2. EXPERIMENTAL

An anthracite (AN) from Peñarroya (Córdoba, Spain) (particle size = 0.15-0.20 mm, ash content ≈ 40 wt%) was charred at 1000 °C for 2 h in N₂ (purity > 99.998 vol%, flow rate = 100 cm³ min⁻¹), at a heating rate of 5 °C min⁻¹ [7]. Using a porcelain crucible, around 5 g of AC were thoroughly mixed with 5 g of LiCl and KCl or with 4 g of chlorides and 1 g of metallic oxide (CaO, Cu₂O, CoO, ZnO, MgO, NiO or FeO). The LiCl/KCl ratio used was 60/40 mole%, mp = 450 °C [8]. The crucible was placed in a mullite reactor and the system was heated at 470, 600 or 900 °C in N₂. The time of isothermal treatment at maximum temperature was

5 h. After that, the samples were washed with distilled water. A fraction of the resulting products was also washed with 10^{-3} M HCl solution and, eventually, in a few instances with 10^{-2} M NH_4OH solution. Notations indicate the specific component of the mixtures used in the treatments of AC. The symbol W denotes washing with HCl solution. For the sake of brevity, only preliminary results obtained for samples prepared at 900 °C are reported here.

X-ray powder diffraction was obtained through a Philips PW-1700 diffractometer provided with a graphite monochromator, using $\text{CuK}\alpha$ radiation ($\lambda = 1.5406 \text{ \AA}$). The scan range was $2\theta = 7-70^\circ$ and the scan speed was of 1° min^{-1} .

Infrared spectra were recorded on a MIDAC-1012 spectrometer between 4000 and 450 cm^{-1} , with 200 scans being taken and 8 cm^{-1} resolution. Discs were prepared by dispersion of 1.2 mg of sample into 400 mg of KBr. The spectrum of a similar mass KBr disc was subtracted from the spectrum of each sample.

3. RESULTS AND DISCUSSION

Table 1 summarizes the results derived from the X-ray diffraction patterns of the samples. The minority components are not included.

Table 1
Composition changes in the samples (XRD)

Sample	Major components *	Sample	Major components*
AN	Quartz Ankerite Muscovite \approx	AC-ZnO	$\text{LiAlSi}_3\text{O}_8$ - β $\text{LiAlSi}_2\text{O}_6$, etc. Quartz Magnesioferrite
AC	Kaolinite Quartz Muscovite and/or Kaolinite Mullite Oldhamite	AC-Mg	Periclase $\text{LiAl}(\text{SiO}_3)_2$ Quartz Forsterite \approx Magnesioferrite
AC-LiCl+KCl	$\text{LiAlSi}_3\text{O}_8$ - β $\text{LiAlSi}_2\text{O}_6$ Quartz Magnesioferrite	AC-NiO	$\text{LiAlSi}_3\text{O}_8$ - β $\text{LiAlSi}_2\text{O}_6$, etc. Quartz Trevorite Bunsenite
AC-CaO	Gehlenite $\text{LiAlSi}_3\text{O}_8$ - β $\text{LiAlSi}_2\text{O}_6$, etc. Quartz Magnesioferrite	AC-FeO	LiAlSiO_4 Quartz \approx Magnesioferrite Oldhamite
AC-Cu ₂ O	$\text{LiAlSi}_3\text{O}_8$ - β $\text{LiAlSi}_2\text{O}_6$, etc. Quartz \approx	AC-CaO-W	Quartz $\text{LiAlSi}_3\text{O}_8$ - β $\text{LiAlSi}_2\text{O}_6$, etc.

Table 1

Sample	Major components*	Sample	Major components*
	Tenorite \approx		Magnesioferrite
	Copper	AC-MgO-W	Quartz,
AC-CoO	$\text{LiAlSi}_3\text{O}_8$ - $\beta\text{LiAlSi}_2\text{O}_6$, etc.		$\text{LiAl}(\text{SiO}_3)_2$
	Quartz		Magnesioferrite \approx
	CoO		Forsterite

*These are given according to decreasing intensity of the strongest peak for each phase relative to the maximum reflection in the X-ray diffraction pattern.

The FTIR spectra of AC and some samples are shown in Fig. 1. The samples were chosen to make evident the composition changes associated with the chemical treatments of AC and also the washing effect on composition.

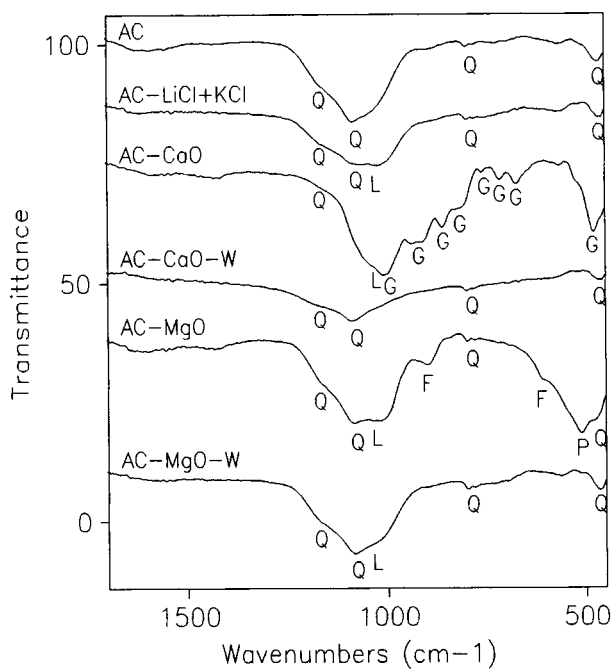


Figure 1. FT-IR spectra of AC and samples treated with molten salts.

The major components of AN (Table 1) are quartz, ankerite, muscovite and kaolinite. The heat treatment of AN resulted in a decrease of muscovite and of kaolinite in AC, and in the formation of mullite, which is a product of

thermal decomposition. The treatment of AC with LiCl+KCl gave rise to the formation of lithium aluminum silicates (LAS). The peak associated with such LAS is the strongest one in the X-ray diffraction patterns of the samples treated with molten salts, but for AC-CaO and AC-MgO. The main component of AC-CaO is gehlenite ($\text{Ca}_2\text{Al}_2\text{SiO}_7$), whereas for AC-MgO is periclase (MgO); although, the amounts of forsterite and magnesioferrite in this sample are significant. Washing with HCl solution caused the complete loss of gehlenite from AC-CaO and a great decrease in LAS. Concerning AC-MgO, MgO was absent from the washed product and the dissolution of LAS was less marked than for AC-CaO.

The results obtained by FTIR spectroscopy are consistent with those provided by X-ray diffraction. The spectra of AC and AC-LiCl+KCl display absorption bands at 1165, 1084, 799, 779 and 467 cm^{-1} , which are ascribable to vibrations modes in quartz (Q). For the latter product a further band is noted at 1025 cm^{-1} , which is associated with LAS (L). Such a spectral feature appears as a shoulder in the the spectrum of AC-CaO. This spectrum also shows bands at 1007, 938, 911, 861, 820, 760, 714, 771 and 478 cm^{-1} due to gehlenite (G). Most bands are absent from the spectrum of AC-CaO-W, in which the presence of only weak bands compared to the AC spectrum is observed. Besides the bands connected with quartz and LAS, the spectrum of AC-MgO presents bands at 895 and 609 cm^{-1} due to forsterite (F), and a strong band at 513 cm^{-1} attributable to periclase (P). These bands disappear from the spectrum of AC-MgO-W and, in addition, the band associated with LAS decreases in intensity in such a spectrum.

The heat treatment of AN and the treatments of AC with molten salts produce significant changes in the composition of the materials, which are greater when using CaO and MgO. Furthermore, the remaining oxides and reaction products can be removed from the samples by washing with HCl solution. The method is more effective for the CaO-treated sample.

REFERENCES

1. K. Kusakabe, M. Orita, K. Kato, S. Morooka, Y. Kato and K. Kusunoki, *Fuel*, 396 (1989) 396.
2. W. Radamacher and A. Hovernath, *Brennstoff-Chemie*, 40 (1959) 97.
3. Battelle Energy Programme Report, July (1974), Battelle, Columbus, Ohio, USA.
4. CFRI Patent Application No. 774 Del (1980).
5. B. K. Mazumdar, *Chem. Eng. World*, 18 (1983) 100.
6. P.L. Walker, Jr. and G.R Imperial, *Fuel*, 74 (1995) 179.
7. M. del Carmen Fernández González, Doctoral Thesis, Universidad de Extremadura, Badajoz (1984).
8. J. J. Lagowski (ed.), *The Chemistry of Nonaqueous Solvents*, VB, Acidic and Aprotic Solvents, Academic Press, New York, 1978.

Effects of Coal Cleaning on Gasification and Combustion Reactivity of Coals and Chars.

D.J. Harris, C.G. Thomas, P.J. Mullins, M.E. Gosnell, E. Gawronski,
P.M. Nicholls and A.B. Waugh

CSIRO Division of Coal and Energy Technology,
PO Box 136 North Ryde NSW 2113 Australia

1. INTRODUCTION

The current worldwide trend of increasing coal-fired electric power generation is expected to continue for the foreseeable future. Research on many current and emerging technologies are required in order to increase process efficiency and minimise production of potential pollutants.

In an International Joint Research Project sponsored by NEDO (New Energy Development Organisation, Japan), collaborative research on 'Clean Coal Power Generation' is being undertaken by six laboratories in three countries. This project focuses on reducing potential pollutants before the coal is used. The project is examining several coal preparation processes, including alkali leaching, acid washing, selective oxidation of sulphur and chemical removal of coal nitrogen. The benefits and consequences of the various coal pre-treatments on the subsequent conversion processes are being assessed from various viewpoints: coal/char reactivity (enhancement or inhibition); the nature of the residual mineral matter; and possible impacts on such things as the total energy balance, process economics and the overall pollutant yield.

2. EXPERIMENTAL

Two roles of CSIRO in this project are: (i) preparation of clean coal samples using an alkali leaching process and distribution of this sample and its parent coal to all of the project participants and (ii) measurement of the gasification and combustion reactivity of the raw and cleaned coal using two novel methods, described below.

2.1. Sample Preparation

A high-volatile bituminous coal from the Hunter Valley region of New South Wales was selected for testing in this program of work.

A split of this coal sample was cleaned using the CSIRO-developed AUSCOAL Ultra Clean Coal process whereby minerals are leached by a caustic soda solution at moderate temperature and pressure (<240°C, 2.5 MPa), followed by a wash using a mild acid at ambient conditions [1]. Chemical analyses of the raw and cleaned samples are given in Table 1.

To produce chars for intrinsic reactivity measurements, the raw and cleaned samples were charred at 1200°C for three hours under flowing argon. The char yields were 73.5% and 68.1% respectively on a dry ash-free basis. The raw coal formed a hard coke during this process. This coke was crushed and sieved to obtain a -1.0 + 0.6mm sample for reactivity measurements. The cleaned coal sample did not coke, presumably due to oxidation of the coking components during the leaching process, and the sample for reactivity measurements was obtained directly by sieving.

Table 1. Analysis of raw and cleaned coal samples

Coal	Proximate (%)				Ultimate (%daf)				
	Moisture (adb)	Ash (db)	Volatile Matter (db)	Fixed Carbon (db)	C	H	N	S (total)	O (diff)
Raw	3.0	9.2	33.7	57.1	83.2	5.4	2.1	0.5	8.8
Cleaned	11.2	0.5	35.4	64.1	82.3	5.2	2.1	0.9	9.5

adb: air-dried basis db: dry basis daf: dry ash-free basis

2.2. Reactivity Measurements

The first of the reactivity measurement techniques uses a small fixed bed reactor [2] to determine the intrinsic reactivity of chars to oxidising gases. Intrinsic reactivity is defined here as the char reaction rate per unit total surface area (N_2 BET) in the absence of any mass transfer limitations. These measurements are being performed for reaction with carbon dioxide, steam and oxygen. The results reported here are for gasification with CO_2 of the two char samples described above.

Another series of measurements are being made, using a laser nanoreactor [3], to determine the combustion reactivity of the raw and clean coal. Essentially, a single particle of coal (~100 μ m dia.) positioned on a nanobalance is heated by focussed laser beams and a mass loss vs time curve is produced. From this curve, the average reactivity and the instantaneous burning rate of the particle (g/g/s) can be directly calculated. To date, particles of vitrinite from the raw and cleaned coal have been studied.

3. RESULTS AND DISCUSSION

3.1. Reactivity of chars to CO_2

The reaction rate of the raw and cleaned char samples with CO_2 is shown as a function of the extent of reaction of the char in Fig. 1. The chars were reacted isothermally at 860°C until approximately 20% weight loss was achieved, at which point the sample was allowed to cool. The temperature dependence of the reaction rate during this cooling period was used to determine the activation energy for the reaction. The surface area of the residual char was determined in order to calculate the intrinsic reactivity of the char at the indicated extent of reaction. Arrhenius plots of the observed reaction rate and the intrinsic reaction rate of the chars are given in Figures 2(a) and 2(b) respectively.

The most striking feature of Fig. 1 is that the cleaned coal has a considerably greater reaction rate than the untreated sample. After approximately 10% weight loss, the cleaned coal has a reaction rate approximately four times that of the untreated sample. The shape of the initial part of the curves in Fig. 1, particularly that for the cleaned coal, is complex showing an initial period of very high reaction rate which diminishes rapidly as a small amount of the carbon is consumed. This behaviour is suggestive of a catalytic reaction which appears to have become more pronounced with the cleaning of the coal. The cleaning process used a sodium hydroxide leach which may have allowed sodium species to be incorporated into the coal (and subsequent char) structure. Complete elemental analyses of the two coal samples were performed by one of the project partners [4] and although these results indicate that the total Na content of the cleaned coal and its char were less (by a factor of about three) than that of the untreated coal, the clean coal had a much greater Na/ash ratio than the untreated coal; an indication that a higher proportion of the coal (and char) Na may be associated with the carbon structure rather than the mineral species. This organically bound alkali is likely to be a more

effective catalyst for the CO₂ gasification reaction than that which is chemically associated with the mineral species [5]. The reasons for the initial period of apparently high reaction rate of the untreated coal char are not yet fully understood and this behaviour is currently being investigated.

For comparative purposes, earlier data on the reaction rate of chars produced from an Australian low volatile coal before and after demineralisation by hydrofluoric acid digestion, are given in Fig. 1 [6]. As for the current work, the cleaned coal char has a higher reaction rate than the untreated sample but, for both samples, the initial peak in the reaction rate curve is absent.

Values for the activation energy, determined from the slope of the Arrhenius plots given in Fig. 2., were 199 and 192 kJ/mol for the untreated and cleaned coal chars respectively. These are considerably less than 240 kJ/mol which is considered to be the appropriate value for uncatalysed C-CO₂ reaction of coal chars [7]. This supports the view that catalysis contributes to the high volatile coal char reactions. Values previously determined for the activation energy for the chars from the untreated and demineralised low volatile coal char were 200 and 256 kJ/mol respectively [6]. The demineralisation process in this case apparently removed some species which had reduced the activation energy in the raw coal char.

The surface area of the untreated char sample before and after reaction with CO₂ to 22% weight loss was 1 and 45m²/g respectively. The corresponding surface areas for the cleaned coal char were 1 and 18m²/g. While the cleaning process itself had no apparent effect on the surface area of the char, despite the loss of coking properties in the clean coal, the subsequent development of the char surface area during reaction differed considerably for the two samples but this does not account for the different reaction rates observed in Fig. 2(a). This is reflected in the intrinsic reaction rates which differed by a factor of twelve (Fig. 2(b)).

The intrinsic reaction rate of the demineralised low volatile coal char can also be seen in Fig. 2(b) to be greater than that of the respective untreated char by a factor of about two at a temperature of 850°C and is significantly less than that of the alkali-leached char which is the subject of the present investigation.

3.2. Combustion reactivity at elevated temperature

Preliminary combustion rate measurements have been made in the laser nanoreactor using a number of single, individually sampled, 100µm particles of vitrinite from the untreated and clean coals. Results indicate that the combustion rate of samples from the cleaned coal have a burning rate, in air and at a controlled temperature of 1600°C, approximately 2-3 times that of similar particles from the untreated coal. Absolute values of the reaction rates measured using this new apparatus were in the range of about 8-12 g/g/s for the untreated coal and 16-32 g/g/s for the cleaned coal samples. Further experiments are required to ensure statistically valid samples are obtained from each of the coals and to allow more detailed interpretation regarding the effects of particle structure, chemical composition and reaction environment on reaction rate measurements using this apparatus.

4. CONCLUSIONS

The work performed in this project to date has shown that the alkali leaching process used to remove the mineral matter from the coal has changed the coking properties of the coal and increased the reactivity to CO₂. Work is underway to determine the relative distribution and mode of association of potential catalytic species in the cleaned coal sample and the effect of the cleaning process on the intrinsic reactivity of the resultant chars to O₂ and H₂O. Work is also being carried out using the laser nanoreactor to extend the range of temperatures and reactant concentrations and to cover the range of maceral types present in the coal.

REFERENCES

1. A.B. Waugh and K.McG. Bowling, Proc. Fourteenth Australasian Chemical Engineering Conference, Adelaide, (1986) 297.
2. D.J. Harris and I.W. Smith, ACS Div. Fuel Chem. Prepr., 34 (1), (1989) 95.
3. C.G. Thomas, M.E. Gosnell, E. Gawronski and P.M. Nicholls, 'Measurement of coal reactivity in the ironmaking blast furnace raceway', This conference (1995).
4. A. Tomita, Tohoku University, Japan, Private communication, (1995).
5. D.J. Harris and D.J. Young, Ironmaking and Steelmaking, 16 (6), (1989), 399.
6. D.J. Harris and J-Y. Chen, unpublished results.
7. N.M. Laurendeau, Prog. Energy Combust. Sci., 4, (1978), 221.

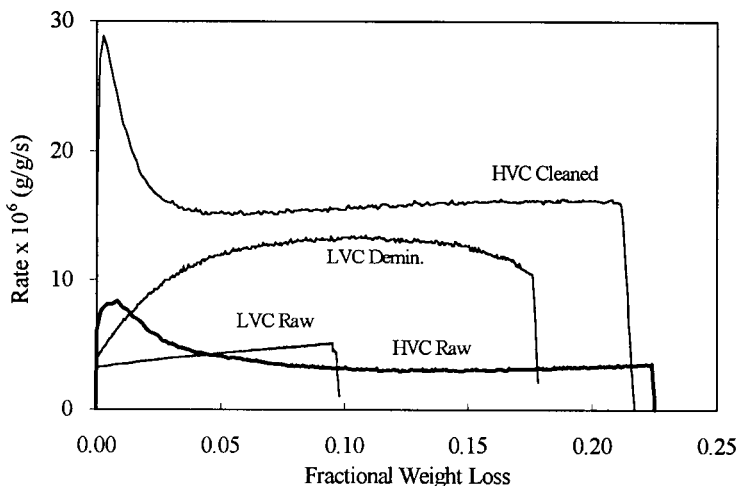


Figure 1. Reaction rate of raw and cleaned high volatile coal char (HVC) with CO₂ at 860°C as a function of extent of reaction. Earlier data for chars from an untreated and acid washed low volatile coal char (LVC) are included.

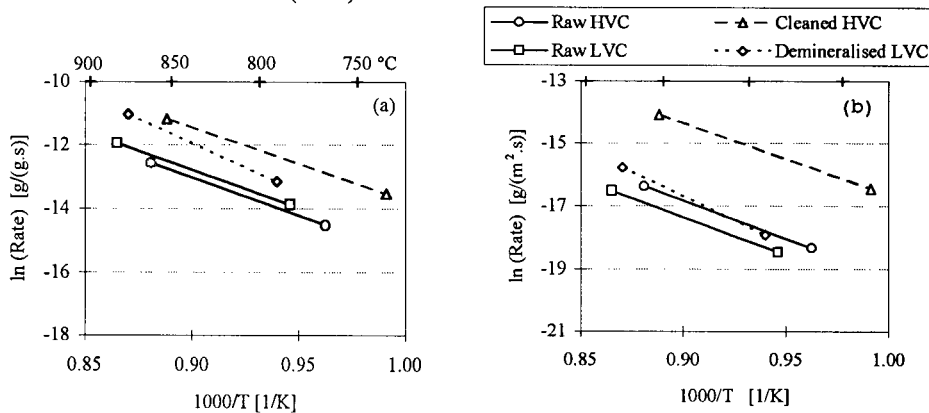


Figure 2. Arrhenius plots of (a) observed and (b) intrinsic reaction rate with CO₂ of raw and cleaned high volatile coal chars (HVC) and low volatile coal chars (LVC).

Rheology of colombian coal-water slurry fuels: Effect of particle-size distribution

J.E. Pulido, C.P. Rojas, G. Acero, M. Durán, M. Orozco

Escuela de Ingeniería Química
Universidad Industrial de Santander (UIS)
A.A. 678, Bucaramanga, Colombia

1. INTRODUCTION

Coal-water slurry fuels (CWSF's) have been prepared and characterized in a research project in Colombia, sponsored by Colciencias and Ecocarbon, in order to evaluate the effects of the different composition variables on the behavior during preparation and pipe line transportation.

The authors have previously presented details describing the characteristics of the slurry fuels prepared with five types of colombian thermal coals and the influence of their chemical composition on the optimum particle-size distribution (PSD) required to prepare highly loaded and workable CWSF's [1-2].

The formulation and design of flow systems of suspensions with high solids content, such as the CWSF's, require a detailed rheological knowledge of the suspension in terms of the governing parameters related to PSD, coal content, surface chemistry of the particles and dispersants used to stabilize the slurries. Important studies on these aspects have been reviewed and carried out experimentally by other authors specially devoted to the correlations between apparent viscosity, solids content and average coal particle-size [3].

One of the targets to obtain an optimum control on the viscosity and flow properties of the CWSF's must be based in correlating the rheological constants for the prevailing model of viscosity law to the characteristic parameters of the particle-size distribution and to the coal content in the slurry. In spite of the effect of PSD on the rheology of highly-loaded coal slurries have been long recognized as significant, the specific influence of the various PSD's on the parameters of the rheological model continues to receive attention to further understanding in order to improve the slurry formulations for a specified purpose on preparation and hydraulic handling.

This paper reports the results of an experimental technique of examining the various PSD's on coal slurry fuel rheology, taking special attention for the effect on the parameters of the rheological model.

2. EXPERIMENTAL

2.1. Materials

The coal used in all the experiments was from Cundinamarca Department, selected by Ecocarbon, and non-beneficiated. Proximate analysis is as follows: % Moisture: 0.82; % Ash: 9.53; % Volatile Matter: 36.84; % Fixed Carbon: 52.81; Higher Heating Value : 13830 BTU/lb.

Ultimate analysis: % Carbon: 74.46; % Hydrogen: 5.25; % Nitrogen: 1.44; % Total Sulfur: 0.73; % Oxygen: 8.84

Dispersant additive used for all the CWSF's was a nonionic ethylene oxide/propylene oxide copolymer.

2.2. Preparation of slurry fuels

Coal samples were firstly reduced to minus 5 mm in a jaw crusher and then ground in a laboratory ball mill where fineness of ground product was controlled by milling time.

Coarse PSD's with geometric mean particle size D_p between 22 and 42 microns were obtained by dry milling. Wet ball milling was used to produce fine PSD's whose geometric mean particle size ranges between 5 and 13 microns. The size distribution characterization of all pulverized coal samples was conducted in a Malvern 2600 Particle Size Analyzer.

The preparation procedure was standardized for all the samples tested. The water was weighed into a 600 ml beaker and the dispersant was dissolved in predetermined amounts. The weighed coal sample was slowly added to the beaker and the contents stirred with a twin rotor stirrer at 600 rpm for 5 minutes after addition of all coal. Weight percent of coal content was ranged between 60% and 70%. Weight percent of dispersant was maintained constant at 0.8% for all preparations.

Slurries with bimodal particle-size distributions were produced by blending coarse and fine grind products and characterized by measuring the weight percent of fine grind component and the blend ratio R_d between the largest and the smallest geometric mean particle diameter of the components.

2.3. Rheological Tests

Rheological tests were conducted in a rotating cilinder viscometer MLW Rheotest II with shear rate varied from 5 to 800 s^{-1} . A computer program, based on an optimized logarithmic regression analysis, was used to process the resulting data of shear stress τ vs shear rate $\dot{\gamma}$ in order to obtain the parameters of the rheological model. The temperature of all the slurries analyzed was maintained at 27°C.

3. RESULTS AND DISCUSSION

3.1. Rheological model

Viscometer measurements on the different slurries prepared as described before indicates that Herschel and Bulkley's law, which is a yield-power law model, is followed in all cases:

$$\tau = \tau_o + K \dot{\gamma}^n \quad (1)$$

where: τ_0 is the yield stress value, K is the flow consistency number and n is the flow behavior index ($=1$ for Newtonian flow, <1 for pseudoplastic material and >1 for dilatant flow).

3.2. Effect of PSD on parameters of rheological model

Variations in n exponent becomes very important since a pseudoplastic flow behavior is always desirable in all CWSF's for an easy hydraulic handling. On the other hand, dilatant flow results detrimental since apparent viscosity increases with shear rate.

Figure 1 shows how the flow index n results affected by variations of the geometric average particle diameter D_p in CWSF's with monomodal PSD. For a constant coal content in the slurry the n exponent decreases with D_p ranging between 13 and 35 microns, besides it exhibits a trend to present a minimum around 25-35 microns.

The coal content in the slurries shown in Figure 1 increases the flow index, specially if D_p is a low value, and the CWSF turns out to have a dilatant behavior for weight percents of coal greater than 60%. It is observed that highly-loaded CWSF's with monomodal PSD should be prepared with geometric average particle diameter close to 25-35 microns in order to obtain a pseudoplastic flow behavior.

CWSF's with bimodal coal particle size distributions also show a decrease in flow index when the ratio R_d , of the largest to the smallest diameters of coarse and fine combined fractions, is increased. As shown in Figure 2, bimodal distributions reduce considerably the flow index by increasing R_d , being a much better way to obtain pseudoplastic highly-loaded CWSF's.

The effect of weight percent of fine grind component on the flow consistency number K and yield stress value τ_0 were followed for bimodal CWSF's prepared at 60% of coal and having two blend ratios R_d at 2.36 and 3.56 respectively. The results are shown in Figures 3 and 4.

A minimum in K and τ_0 was obtained when the weight percent of fine grind component ranges between 35% to 45%. This range also corresponds to a minimum in apparent viscosity and it follows the fact that the optimum network packing of particles is reached. Similar results were obtained for CWSF's with coal weight percents higher than 60% and yield stress values increase proportional to coal content in this case.

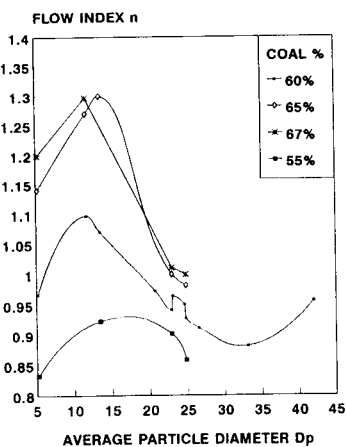


Figure 1. Effect of D_p on flow index for monomodal CWSF

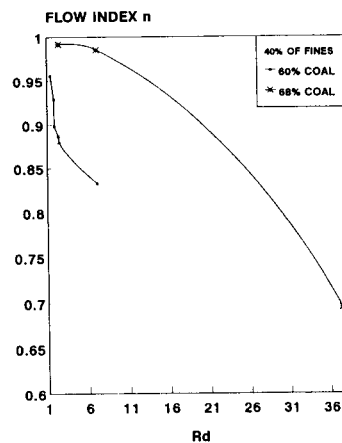


Figure 2. Effect of R_d on flow index for bimodal CWSF

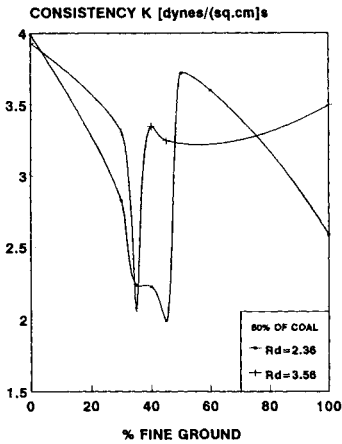


Figure 3. Effect of PSD on consistency K for bimodal CWSF.

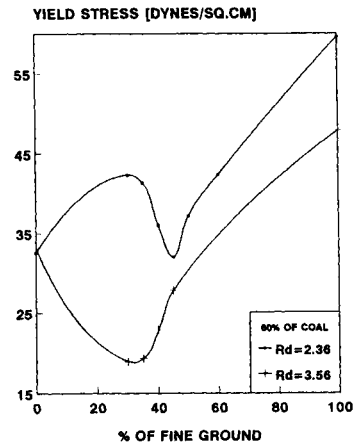


Figure 4. Effect of PSD on yield stress for bimodal CWSF.

4. CONCLUSIONS

Particle size distribution affects the parameters of the rheological model for monomodal and bimodal coal water slurry fuels. In monomodal slurries the flow index n of the model increases with the coal content and tends to exhibit a minimum for geometric average particle diameter ranging between 25 to 35 microns.

In bimodal slurries the flow index decreases with the blend ratio R_d and shows much lower values than monomodal slurries which is a desirable property to reach pseudoplastic behavior.

The yield stress and consistency number also show a minimum when the weight percent of fine grind product in bimodal slurries is in a range between 35% and 45%, which corresponds to a minimum in apparent viscosity and constitutes a way to optimize the formulation of the slurries.

ACKNOWLEDGEMENTS

The authors would like to express their appreciation to Colciencias-Ecocarbon-Fonic in Colombia for the financial support to accomplish this work. Thanks are also extended to Ecopetrol-ICP for facilitating to use the Malvern instrument.

REFERENCES

1. Pulido J.E., Proceedings of the 17th International Conference on Coal Utilization and Slurry Technologies, pp.37-48, Clearwater, Fla. USA, (1992).
2. Pulido J.E., Proceedings of the 12th International Coal preparation Congress, pp.67-72, Cracow, Poland, (1994).
3. Botsaris G.D., Glazman Y.M., in Interfacial Phenomena in Coal Technology, M.Dekker Inc., N.Y., USA, (1989).

Structural Characteristics of Coal Surface and Coal Slurryability

Cheng-Gong Sun, Bao-Qing Li, Wei Yuchi and Bianying Cao

The State Key Laboratory of Coal Conversion, The Institute of Coal Chemistry,
Chinese Academy of Sciences, Taiyuan Shanxi, 030001, P. R. China

1. INTRODUCTION

Coal water slurry as a substitute for oil fuel should be featured with high coal loading and fine rheological behaviour, and this is at least in part determined by the selection of coal. Previous works^[1] have shown that the preparation of concentrated coal water slurry is related to coal surface properties, coal particle size distributions and kinds of additives as well as its processing conditions, but how to predict the slurryability of given type of coal under specified processing conditions directly by basic analyses of coal properties without doing large amount of work is now an important research and still keep unresolved up to now. Unfortunately, little work has been done on this aspect. The present study was undertaken to try to establish the available relations between coal slurryability and coal properties.

2. EXPERIMENTAL

The characteristics of 30 Chinese coals were shown in Table 1.

The carboxyl and phenolic hydroxyl groups on coal surface and the maximum moisture-holding capacity of coal were determined according to the standard procedures which can be found elsewhere^[2]. The analyses results are also shown in Table 1.

The procedures and dispersant used for the preparation of coal water slurry can be found elsewhere^[2]. The coal loading of coal water slurry whose apparent viscosity is 1500mPa.s at a shear rate 28.38 1/S was defined as its maximum coal loading and used as the parameter to evaluate coal slurryability.

3. RESULTS AND DISCUSSIONS

3.1. Dependence of coal slurryability on coal rank

Coal water slurry is a complex two-phase dispersion system formed by coal, water and a little dispersant, its properties are governed by both the coal properties themselves and the processing conditions adopted for its preparation^[1]. In order to evaluate coal slurryability and correlate with coal rank, the preparation of coal water slurry are all carried out under the same specified conditions. Although apparent viscosity of coal water slurry at specified shear rate is often used to evaluate slurry properties under given

conditions, it can not accurately reflect coal slurryability because flow patterns of coal water slurries with different coals are often different from each other. The maximum coal loading of slurry is therefore defined as above and adopted as a parameter to evaluate coal slurryability. As shown in Table 1, the maximum coal loading of coal water slurry is

Table 1
Analyses of coal properties

No. Sample	Ultimate analysis wt. % daf.					Proximate analysis wt. % ad.			Reactive groups mmol/ g coal daf.		MHC wt. %
	C	H	O	N	S	M	A	Vdaf	[COOH]	[Ph-OH]	
1. Hongmiao	71.09	4.46	20.30	0.90	3.25	16.92	17.96	42.62	0.25	2.18	22.30
2. Zhalainuoer	74.68	5.51	17.87	1.57	0.31	22.83	4.02	45.85	0.27	4.60	24.02
3. Kebao	67.06	5.26	24.91	1.60	1.17	17.86	14.03	53.84	0.69	4.76	26.58
4. Sanshan	66.61	5.52	26.16	1.41	0.30	15.35	13.67	56.62	0.83	5.26	27.92
5. Huangxian	73.92	5.36	18.09	1.89	0.74	12.01	8.58	45.27	0.43	4.15	18.20
6. Fanci	65.27	6.22	27.16	0.72	1.16	12.79	14.59	46.44	0.25	4.11	17.39
7. Shenmu	80.93	5.12	12.53	1.10	0.32	7.38	4.31	36.69	0.076	1.74	9.93
8. Jinhuaogong	84.63	4.92	8.62	0.84	0.99	3.01	12.39	31.47	0.035	0.26	4.55
9. Lingwu	79.08	3.98	15.06	0.72	1.16	13.63	9.94	33.50	0.16	4.11	17.50
10. Yanchi	79.88	4.74	13.72	1.18	0.48	11.40	3.73	33.00	0.09	3.20	13.40
11. Daliuta	80.09	5.09	13.51	0.89	0.42	10.03	4.05	38.17	0.095	2.61	13.89
12. Yujialiang	82.53	4.80	11.49	0.94	0.27	5.09	4.91	32.15	0.07	1.53	9.50
13. Dabeyiao	82.39	5.17	10.90	1.34	0.30	5.25	9.49	36.35	0.059	1.50	9.31
14. Wulan	87.93	5.00	3.99	1.26	1.82	0.81	4.75	26.51	0.01	0.09	1.35
15. Fuxing	81.80	5.23	10.17	1.32	1.48	4.62	4.62	10.53	0.023	0.062	5.80
16. Yima	76.22	4.81	17.76	0.95	0.26	11.68	10.87	39.25	0.14	3.11	12.60
17. Jingyuan	82.96	4.64	11.52	0.75	0.13	3.61	6.17	33.96	0.022	0.46	5.10
18. Neimeng	80.18	4.59	13.93	0.85	0.45	11.22	5.08	36.31	0.082	2.23	12.10
19. Meiyukou	82.10	4.74	11.96	0.92	0.28	2.85	13.17	29.34	0.039	0.27	4.60
20. Xiahua yuan	78.39	5.64	13.49	1.25	1.23	2.36	34.75	41.47	0.03	0.46	6.70
21. Huainan	83.73	5.76	8.68	1.54	0.29	1.52	13.37	40.21	0.023	0.48	3.00
22. Yanzhou	81.80	5.50	7.95	1.32	3.43	1.63	3.95	43.73	0.032	0.64	4.10
23. Xiwen	80.94	5.71	7.10	1.60	4.65	1.44	15.77	43.77	0.04	0.53	3.30
24. Kailuan	85.78	5.20	6.99	1.47	0.56	1.10	6.57	34.60	0.00	0.21	2.40
25. Zaozhuang	85.35	4.98	7.62	1.48	0.57	1.62	6.67	36.17	0.00	0.46	2.80
26. Fengfeng	86.26	5.53	5.85	1.62	0.94	0.67	13.55	31.33	0.00	0.27	2.30
27. Luan	90.98	4.72	2.40	1.41	0.49	0.60	25.84	19.51	0.00	0.095	2.60
28. Huobi	89.80	4.48	3.84	1.57	0.31	0.60	13.70	17.21	0.01	0.22	4.60
29. Zibo	91.09	3.57	1.03	1.31	3.00	1.07	14.61	11.63	0.00	0.01	2.85
30. Yangquan	92.61	3.87	1.83	1.26	0.43	1.75	9.38	9.10	0.00	0.00	3.60

dependent on coal rank. For low rank coals such as lignite and subbituminous coals, the maximum coal loadings of their slurries are generally not higher than 60 wt.%, and as high as 76 wt.% for some of higher rank coals. Some necessary correlations between the maximum coal loading and the coal properties were carried out so as to find the possibilities to use coal properties to predict coal slurryability. The results are shown in Fig.1

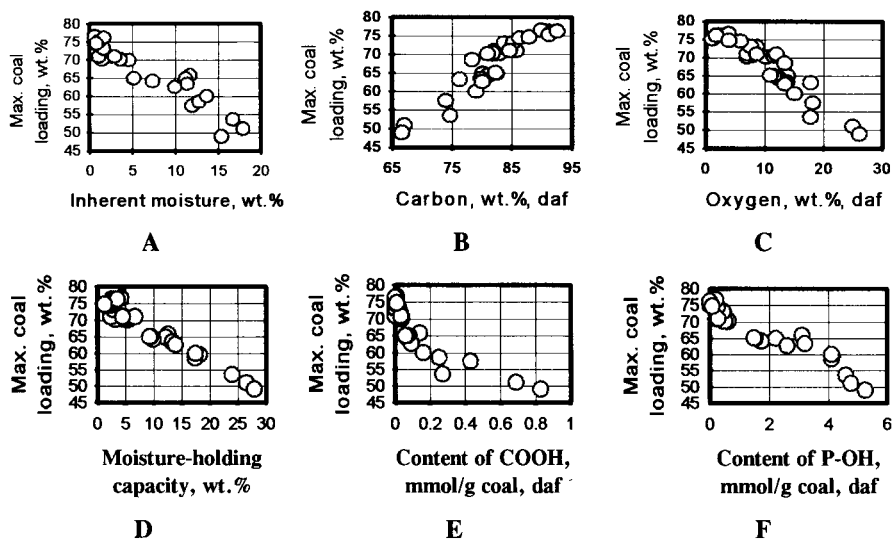


Fig.1 Relations between maximum coal loading of coal water slurry and coal properties

Fig.1 indicates that fine linear relationships exist between the maximum coal loading and inherent moisture content and the maximum moisture-holding capacity of coal over the whole coal rank. For relations with carbon and oxygen content, linear relations are also found when carbon content is not higher than 86 wt.% (daf.) or oxygen content higher than about 5 wt.% (daf.).

Previous research have pointed out that hydrophilicity of coal surface is detrimental to the preparation of highly concentrated coal water slurry^[1,2]. As shown in Fig.1 E, F and D, high content of reactive functional groups on coal surface and their resultant moisture-holding capacity of coal greatly decrease the maximum coal loading of coal water slurry. Compared with phenolic hydroxyl groups on coal surface, carboxyl groups play a far more important role in determining coal slurryability by affecting the moisture-holding capacity of coal^[3,4]. Although mineral matters in coal act as hydrophilic sites on coal surface, no good relation were found with its content here.

3.2. Dependence of the rheological behavior of coal water slurry on coal rank

Both high coal loading and good rheological behavior of coal water slurry are desired for industrial application. The rheological behavior of coal water slurry can be well expressed by the relation between slurry apparent viscosity and shear rate which can be described by the following equation: $V = C S^n$, where V is apparent viscosity of coal water slurry, C , constant, S , shear rate, n , flow index. The flow patterns of coal water slurry can be described by the flow index, n . Its negative value means a shear-thinning behavior of coal water slurry, and its positive value means a shear-thickening behavior. Since the flow pattern of coal water slurry is related to both coal type and the coal loading of slurry which varies greatly from coal to coal, it is difficult to be described under the

same coal content of slurry. Therefore, correspondingly to each coal in Table 1, calculations for flow index, n , are carried out only for the slurry with its maximum coal loading. The relation between flow index, n , and coal rank (described by carbon content of coal) are shown in Fig. 2.

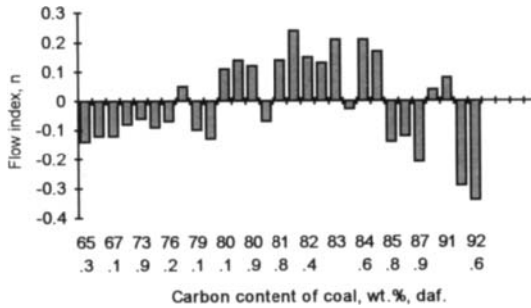


Fig.2 Dependence of rheological behavior of coal water slurry on coal rank

Fig.2 indicates that the rheological behaviour of coal water slurry is related to coal rank. The coal water slurries generally have a shear-thinning behavior when carbon content of coal is lower than about 80 wt.% or higher than 85 wt.% (daf.), however, when carbon content in the range of 80 - 85 wt.% (daf.), coal water slurries are generally featured with a shear-thickening behavior. Some necessary investigations in the effect of coal properties on rheological behavior of slurry will be carried out in another paper.

4. CONCLUSIONS

Both coal slurryability described by the maximum coal loading of coal water slurry and the slurry rheological behavior are dependent on coal rank. For low-rank coals with its carbon content lower than about 80 wt.% (daf.), their slurries generally have a low coal loading but have a shear-thinning behavior, for coals with their carbon content higher than 85 wt.%, a high coal loading and a shear-thinning behavior, for coals with their carbon content in the range of about 80 - 85 wt.%, have a intermediate coal loading (65 - 70 wt.%) but generally have a shear-thickening behavior which is unfavorable for industrial use. Fine linear relationships are found between the maximum coal loading of slurry and inherent moisture content and the moisture-holding capacity of coal over the whole coal rank.

REFERENCES

1. Cheng-Gong Sun and Jia-Shan Wu, *Coal Conversion*, 16(1) (1993) 90
2. Jia-Shan Wu and Yong-Wei Song, *J. Fuel Chemistry and Technology*, 4 (1987) 296
3. R. Kaji et al, *Fuel*, 65 (1986) 288
4. Cheng-Gong Sun and Jia-Shan Wu, *Proceedings of The 17th International Conference on Coal Utilization and Slurry Technologies*, FL U.S.A., 1992, 98

Effect of mineral matters on the properties of coal water slurry

Ya-Xiong Xie, Bao-Qing LI and Cheng-Gong Sun

State Key Laboratory of Coal Conversion, Institute of Coal Chemistry,
Chinese Academy of Sciences, Taiyuan, Shanxi, 030001 P. R. China

1. INTRODUCTION

Coal water slurry (CWS) as an excellent substitute for fuel oil has received more attention in many countries since 1970's. Extensive researches were related to the studies of coal particle size distribution, type of additive and coal properties such as ash content, the amount of inherent water, the degree of coal oxidation, and the quality and quantities of the surface active functional groups. Mineral matters in coal have remarkable influences on CWS properties [1-4]. Different content and composition of mineral matters affect the slurryability of coal due to the great difference of surface properties of coals. However, the effect of mineral matters on CWS has not been systematically studied. In this paper several Chinese coals were demineralized by using various methods. The corresponding changes of rheological behaviour and static stability of CWS were investigated. The function of mineral matters and the added electrolyte on CWS were discussed.

2. EXPERIMENTAL

Three Chinese coals were used in this study. Their characteristics are listed in Table 1 and 2. All CWS were prepared from coals with "Alfred" particle size distribution.

Water-washed and acid-washed coals were prepared by washing coals with deionized water or 1 N HCl under stirring at 60 °C for 3 hr. Deashed coal was obtained by firstly stirring with 3 N HCl at 60 °C for 3 hr and then adding 20% HF at room temperature for 72 hr. After filtration coals were washed by deionized water until no Cl⁻ in washed water for acid-washed and deashed coals, and dried under N₂.

CWS was prepared by mixing coal, additive (1wt% of a typical anion surfactant, dry coal basis) and distill water, and stirring at 3000 rpm for 10 min. Apparent viscosity was measured by NXS-11 rotation viscosimeter. The maximum coal loading (MXCL) was determined when apparent viscosity reaches to 1500 mPa.s with a shear rate of 28.38 1/s. The ion composition and concentration were measured by ICP. The oxygen-containing functional groups in coal were analyzed by Ba(OH)₂ for the sum of acidic groups, Ca(Ac)₂ for carboxyl groups and the difference for hydroxyl groups .

Table 1 Analysis of coal samples

Samples	Oxygen-containing functional group (mmol/g coal, daf)		Proximate analysis (wt%, as received)			Ultimate analysis (wt%, daf)				
	-COOH	-OH	W	A	V	C	H	N	S	O(by diff.)
	Huainan	0.023	0.48	1.52	13.37	40.21	83.73	5.76	1.54	0.29
Changzhi	0.00	0.10	0.60	25.84	19.51	90.98	4.72	1.41	0.49	2.40
Yangquan	0.00	0.00	1.75	9.38	9.10	92.61	3.87	1.26	0.43	1.83

Table 2 Ash composition of coals

Samples	SiO ₂	Al ₂ O ₃	Fe ₂ O ₃	CaO	MgO	K ₂ O	Na ₂ O	SO ₃	TiO ₂
Huainan	38.23	33.41	4.29	13.31	1.31	0.28	0.74	2.80	1.72
Changzhi	48.38	41.04	2.93	1.48	0.20	0.20	0.97	1.51	0.98
Yangquan	59.55	28.97	1.77	1.08	0.66	1.99	0.75	1.00	1.24

3. RESULTS AND DISCUSSIONS

3.1. Effect of Various Pretreatment on CWS Properties

The effects of various pretreatments on slurryability, rheological behaviour and static stability were shown in Fig. 1-2 and Table 3. Water-washing pretreatment did not affect the properties of CWS, while acid-washing significantly enhanced apparent viscosity, reduced the MSC and improved the rheological behaviours. Deashing markedly influenced the properties of CWS by a sharp increase in apparent viscosity and decrease in MXCL. Deashed coal also greatly changed the rheologic properties of CWS. The pseudoplasticity was weakened and even transferred to dilate-plasticity for Yangquan coal (not shown).

The effects of various pretreatment on CWS properties were further studied by the measurement of ion composition and concentration in the supernatant layer of CWS. A typical result was listed in Table 4.

It is found that after acid washing the ion concentration increases markedly, while the ash content was only slightly reduced. It might be that during acid washing the ionic

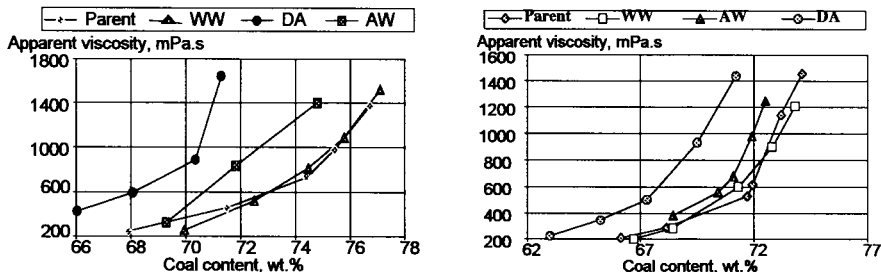


Fig. 1 Relations between coal content and apparent viscosity of CWS under different pretreatment conditions for Changzhi coal (left Fig.) and Huainan coal (right Fig.). WW: Water-washed; DA: Deashed; AW: acid washed.

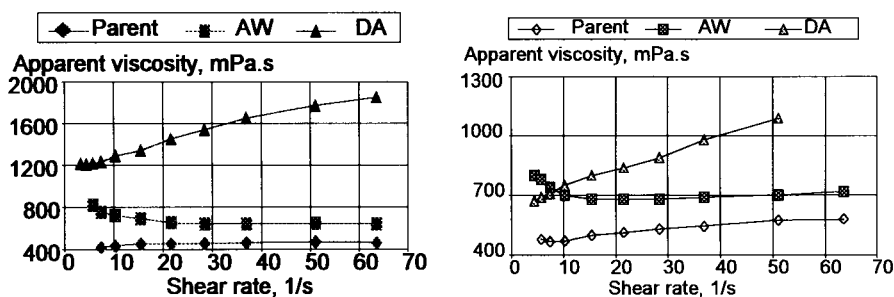


Fig. 2 Effect of coal pretreatment on the rheological behaviour of CWS with Changzi coal (71.3 wt.%) (left Fig.) and Huainan coal (71.3 wt%) (right Fig.)

Table 3 Effect of various pretreatment on static stability

	H-UT	H-WW	H-AW	H-DA	Y-UT	Y-WW	Y-AW	Y-DA
Static stability (days)	13	12	10	6	18	17	17	6

H: Huainan coal; Y: Yangquan, UT: untreated; WW: water-washed; AW: acid-washed; DA: deashed

Table 4 Ion composition and concentration in the supernatant layer of CWS of Huainan coal

Sample	Ioni strenth				Al	Ion comp. and conc. (mg/l)					Ash wt%
	Main valent cation	high	Main valent anion	high		Fe	Mg	Ca	Si		
Untreated	1257		632		29.7	7.3	26.7	204.2	39.5	13.37	
Water-washed	1704		1824		81.2	14.7	19.1	191.2	114.0	/	
Acid-washed	9536		6278		763.8	88.6	21.4	444.6	392.4	10.03	
Deashed	470		84		32.3	6.5	11.5	18.6	5.3	0.28	

exchange occurs, leading to an increase in acidity on coal surface. The pattern of mineral matters, thus, might be changed and they will be dissolved in CWS under strong stirring condition more easily. The effect of acid washing on CWS properties, i.e. increase in apparent viscosity and improvement of rheology, is mainly attributed to the high ion concentration, especially the cation, in CWS. Demineralization by deashing pretreatment dramatically reduced the ash content in coal. Coal with too low ash content will remarkably enhance its hydrophobicity and form huge cross net structure (4), resulting in sharp increase in apparent viscosity and decrease in MXCL and static stability.

3.2. Effect of Electrolyte Addition on CWS Properties

Several chlorides with different metal ions were used to study the effect of electrolyte addition on CWS properties. Fig. 5 showed their influences on apparent viscosity and Fig. 6 indicated the relation between CaCl_2 concentration and the flow patterns for Huainan coal. High-valent cation gave more stronger effect on apparent viscosity. For cation with 2-valent cation the order was $\text{Zn}^{+2} > \text{Ca}^{+2} > \text{Mg}^{+2}$ for Huainan coal. It was found that this order was also related to coal types. Fig. 6 demonstrated that the addition of metal ions can improve the rheologic behaviour of CWS. As ion concentration increased, the dilatopasticity gradually reduced and even totally converted to pseudoplasticity. It was also noted that the conversion in rheological properties of CWS only occurred when the ion concentration increased to a certain extent. Table 5 gave the minimum ion concentrations of various metal cations and the increase of apparent viscosity for this conversion in

rheological properties of CWS of Huainan coal. Although the minimum concentration of Al^{3+} ion is the lowest, it is reasonable to choose 2-valent metal ions as electrolyte for improvement of rheologic behaviour of CWS for Huainan coal due to the slight increase in apparent viscosity.

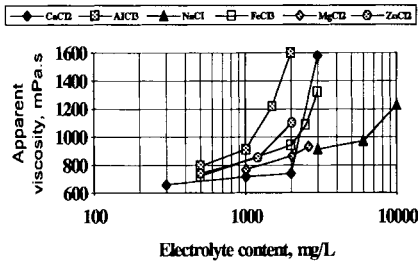


Fig. 5 Effect of different types of electrolytes on the apparent viscosity of CWS with Huainan coal. (coal content: 71.2 wt%)

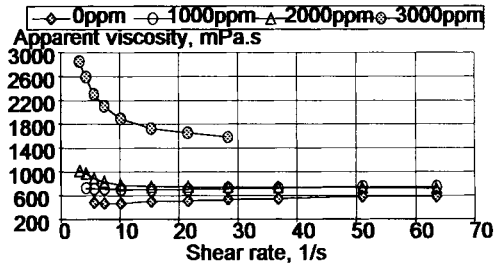


Fig. 6 Effect of $CaCl_2$ concentration on the rheological behaviour of CWS of Huainan coal. (coal content: 71.2 wt%)

Table 5 Minimum concentration of metal ion and corresponding increase in apparent viscosity for conversion of rheological behaviour of CWS for Huainan coal

Ion type	Minimum concentration (ppm)	Increase in apparent viscosity (mPa.s)
Al^{3+}	1850	940
Ca^{2+}	2000	200
Zn^{2+}	2032	560
Mg^{2+}	2017	320
Na^+	6000	430

4. CONCLUSION

Various pretreatment for demineralization was used to study the effects of mineral matters on the CWS properties. Water-washing did not affect CWS properties, while acid-washing significantly increased the apparent viscosity and decreased the MXCL. The high concentration of dissolved inorganic ions, especially high-valent cations was attributed to this behaviour. The damage of CWS properties even more strong after deashing pretreatment, resulting in a sharp increase in apparent viscosity, decrease in MXCL and static stability, and change in rheologic behaviour. The addition of electrolyte can improve the rheological behaviour, but the apparent viscosity also increased. It seems that the effects of mineral matters on CWS properties mainly contribute to their soluble ions.

REFERENCES

1. Atlas, H., Casassa, E. Z., Parfitt, G. D. and Toor, E. W., Proc. Int. Symp. Coal Slurry Fuels Prep. Util., New Orleans, LA, 1985, 1
2. Watanabe, S-I. and Katabe, K-I., Symp. Coal Slurry Fuels Comb. Technol., Orlando, FL, 1984, 67
3. Overseer, J. Th. G., Powder Technol., 37 (1984) 195
4. Schroeder, P. R. and Rubin, A. J., Environ. Sci. Technol., 18 (1984) 264

Real-Time On-line Fugitive Dust Measurement and Control

A Sutton, S Sutton and D G Osborne

CRA-ATD, 1 Research Avenue, Bundoora, Australia

1. BACKGROUND

CRA-ATD have been engaged in research into dust control for the past eight years. The work was initiated and driven by problems encountered with a large open-pit mining operation in Queensland where a coal with high intrinsic moisture, is mined for export. The annual output of the mine is of the order of 10 million tonnes.

Due to the natural dustiness of the coal and the absence of any wet processing, dust is a potential problem at every step in the chain from mining, handling, and stockpiling at the mine and port, to handling by the customer.

It is desirable to minimise the generation of dust for various reasons including the occupational health and safety of workers, the need to maintain environmental standards, reduction of product losses through the handling and transport chain, and enhancing customer acceptability of the product.

Dust is controlled by adding moisture until the coal no longer generates dust on handling. This occurs at moisture levels higher than the dust extinction moisture. The dust extinction moisture (DEM) is defined as the moisture at which a nominal dust number of 10 is achieved. This is indicative of an airborne dust concentration expected in a clean environment.

Coal from different locations, even from different points in a single seam, may have varying dust extinction moistures. Controlling to a single coal moisture level will therefore not effectively control dust. Under such a control system, different parts of a shipment would be either over wet or dusty. The alternative is to add water to a moisture level equivalent to the highest coal dust extinction moisture, eliminating the generation of any dust, which will result in much of the coal being shipped at higher than optimum moisture levels.

The dust extinction moisture must be measured directly, as no correlation with ash, total carbon or moisture holding capacity has been found. This was the reason why CRA-ATD developed a dust-measuring device, which could be used to determine the dust-moisture relationship for coals and therefore the dust extinction moisture.

2. THE DEVELOPMENT OF A LABORATORY DUST TEST

CRA-ATD developed a laboratory test to characterise the dust/moisture relationship as an

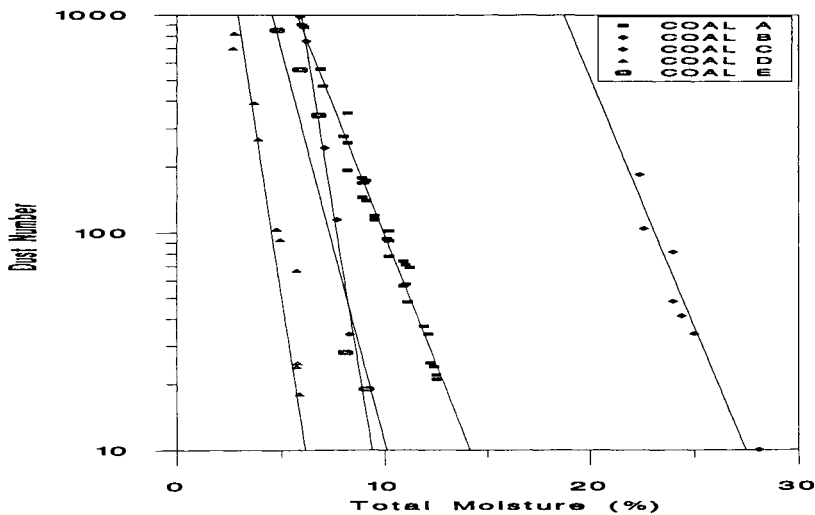
alternative to such tests as ASTM D441¹, ASTM D547-41² and the Jamieson tumbler test³. These previous tests did not provide a dust number that could be used to predict operational dust problems, while the ATD test provides a quantitative measure of the dustiness of a coal.

The ATD test was developed using rotating equipment similar to the Jamieson tumbler, but the procedure was modified by reducing the rotation speed of the drum and operating the unit for a specific time period. A batch test is conducted for each moisture level and the moisture level has been found to remain relatively constant over the test period.

The ATD Tumbler Dust Test uses a stream of air to remove particles which become airborne during the tumbling process. It is a batch test in which dust particles are collected into a pre-weighed filter bag and weighed. From this weight a dust number, calculated as the % mass yield of dust multiplied by 1000, is determined for the test moisture. The test is conducted in a controlled temperature and humidity room. Only 1 kilogram of sample is required for each ATD Tumbler Dust Test. The reproducibility of the test is 10% (relative) which is better than other alternatives.⁴

The ATD Tumbler Dust Test can be repeated with sub-samples at different coal moisture levels to develop a dust extinction curve. Figure 1 shows several examples of dust/moisture curves produced for various Australian coals. The dust extinction curve shows the moisture level at which a coal will no longer produce significant levels of dust during handling, equivalent to a dust number of 10. The slope of the curve provides information on how sensitive the dustiness is to changes in moisture. For example, Coal A and Coal B, show the same level of dustiness, a dust number of 1000, at 8% moisture. However, due to Coal B's increased sensitivity to moisture addition, as shown by the steep gradient of the dust/moisture curve, the moisture required for dust extinction is only 9%, in comparison to the 14% required by Coal A. From this it may be concluded that Coal B would require less water addition to show a significant decrease in dustiness.

Figure 1: Dust Curves for several Australian Coals



3. PILOT SCALE DUST TESTING AT ATD

The pilot scale dust test facility was designed to evaluate the dustiness of coal of normal product size range (up to 50 mm) and to validate results obtained from the laboratory scale tumbler dust test. Results of field trials, in which the aim was to measure levels of dust during bulk material handling, proved to be inconclusive due to variability of external factors, ie prevailing weather conditions, which impact on dust generation. The pilot scale dust test facility provided the large scale testing of coal while controlling the external factors.

The pilot scale facility has a capacity of 12 tonne per hour and was designed to simulate site operations. It consists of a system of conveyors and transfer chutes, and the dust generated from falling coal streams is measured using portable dust monitors. The dust monitors measure the ambient dust concentration generated by a falling coal stream in a fully enclosed, controlled atmosphere room.

4. THE DEVELOPMENT OF ON-LINE DUST MEASUREMENT

The laboratory techniques described are useful for determining the characteristics of the coal, but are of limited benefit for control of operations where the coal type, and hence dust extinction curve, is continually varying. Furthermore, on-site external factors such as mine and plant operating practice and the local environment are also variable. Due to these factors, an on-line dust measuring device was used to monitor dust conditions within coal handling systems.

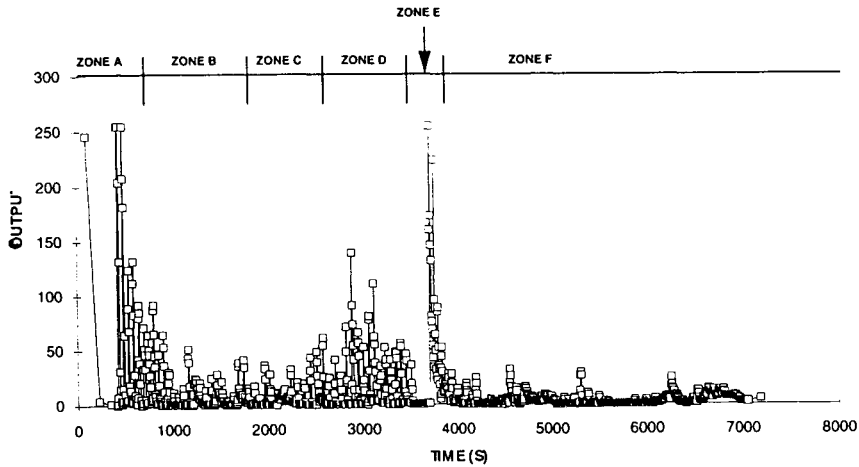
Several commercial dust gauges have been evaluated by ATD for real time on-line monitoring of dust levels during train unloading operations. An optical dust density monitor was selected for on-line monitoring due to its capability of providing a continuous average reading over the path length, had proven reliability in industrial environments, and was sensitive to all particles in the size range of interest.

The most effective of these optical devices has been installed, commissioned and extensively tested. The system was found to be capable of differentiating between different levels of dustiness in the range of interest (0 - 40 mg.m⁻³) and was calibrated against high volume samplers. Due to significant variations in moisture and dustiness of the coal monitored, no correlation for the dust/moisture relationship has been determined for any of the coal types monitored.⁵

The dust monitoring system has been operating for over 12 months at a train receival station in Queensland. Figure 2 shows some of the data collected on a train by train basis. The gauge is also used as a tool by operators for occupational health and safety standards.

The installation of a second dust monitor is underway for a new train receival station at the same location. It is planned to use this gauge to evaluate the design of the new receival station and to determine the extent of modifications required for the upgrading of the dust extraction system of the first train receival station.

Figure 2: Variation in Dust Generation during Coal Discharge



5. ON-LINE DUST CONTROL

Now that an on-line dust monitoring system has been developed, closed loop dust control is a viable option. Previous attempts to control dust on-line have met with limited success due to being based on moisture measurement and control, rather than measurement and control of dust. The aim of the system will be to control dust by adding sufficient water to reach the dust extinction level without unnecessary moisture addition. The dustiness of the coal will be monitored and water will be added in incremental amounts until dust extinction is achieved.

6. CONCLUSIONS

CRA-ATD has developed a laboratory dust test method which is capable of providing accurate and reproducible dustiness measurements of various coal types. Tests have shown that the laboratory scale test method produces results more reliable than those achieved while testing at an intermediate scale. The ATD tumbler dust test is currently under consideration for inclusion in the Australian Standards.

REFERENCES

1. ASTM D441 Tumbler Test for Coal
2. Farrugia T R, Ahmed N and Jameson G J, 1989. *A new technique for measuring dustiness of coal*. J. Coal Qual., Vol. 8, No. 2, pp 51-55
3. Ibid. pp 51-55
4. Box J, Purdon P and Cain D, *Improved handling system operation through dust measurement*. 3rd Japan/Australia Joint Technical Meeting on Coal. Brisbane. 25-26 May.
5. Sutton A, *Dust Monitoring at Dalrymple Bay Coal Terminal*. CRA-ATD Internal Report, January 1995.

CONTROL OF HAZARDOUS METAL EMISSIONS FROM POWER PLANTS VIA PRECOMBUSTION COAL CLEANING

C.J. Lafferty^a, J.D. Robertson^{a,b}, B.K. Parekh^a and F. E. Huggins^c

^a Center for Applied Energy Research, University of Kentucky,
3572 Iron Works Pike, Lexington, Kentucky 40511-8433

^b Department of Chemistry, University of Kentucky,
Rose St., Lexington, Kentucky 40506.

^c Consortium for Fossil Fuel Liquefaction Science, University of Kentucky,
Rose St., Lexington, Kentucky 40506

1. INTRODUCTION

Power Stations in the United States annually produce close to 100 million tons of solid waste by-products (fly- and bottom-ash as well as reject streams from coal cleaning operations) from coal combustion units. Whilst a significant percentage of the by-products are utilized in civil engineering and construction operations, the majority of these materials produced are routinely landfilled, normally at a location geographically close to the power station (in order to minimize transportation costs) where they subsequently come into contact with both subterranean and surface water systems and the potential for the release of metals into the environment exists.

This paper reports the results of preliminary investigations into the fate of various metal species naturally present within coal during coal cleaning and combustion. The research associated with this project is divided into three distinct areas. The first involves the EXAFS investigation of the speciation of various elements present in coal and its associated solid combustion by-products and is the subject of a separate paper to be presented at this meeting. The second area of research involves the quantification of trace element concentrations in coal and its associated solid combustion by-products via the application of Particle Induced X-ray and Gamma-Ray Emission (PIXE/PIGE). The final aspect of the project is the determination of the leachability characteristics of individual elements from coal and its combustion by-products. The overall goal of the project is to determine the effects of coal beneficiation on the concentration, forms-of-occurrence and overall leachability of individual metals from coal and its solid combustion by-products. This paper deals with the development of an appropriate ash leaching procedure for leachability characterization.

2. EXPERIMENTAL

Samples of boiler feed coal, fly ash and bottom ash have been collected from 3 separate power stations in Kentucky. Each power station was selected on the basis of it routinely burning single source coal, so as to eliminate the effects of coal blending on any subsequent mass balances arising from this work.

2.1 TCLP Analysis of Samples

Samples collected from a Western Kentucky power plant burning relatively high-sulfur bituminous coal were each subjected to TCLP analysis, involving the extraction of the solid materials by dilute acetic acid as per standard procedure. The results listed in Table 1 show that the concentrations of metals measured in the extract after 18 hrs of agitation were well below the regulatory limit.

Table 1. TCLP Analysis of Power Station Samples
(Concentration in mg.l⁻¹)

Sample #	Material	Ag	As	Ba	Cd	Cr	Hg	Pb	Se
92269	Coal	<0.01	<0.01	0.242	<0.001	<0.001	<0.0005	<0.01	0.04
92270	Fly Ash	<0.01	0.11	0.312	0.062	0.162	<0.0005	<0.01	0.05
92271	Bottom Ash	<0.01	0.05	0.528	0.029	0.042	<0.0005	<0.01	<0.03
	Regulatory Limit	1.00	5.00	100	1.00	5.00	0.200	5.00	1.00

2.2 Development of Column Leaching Procedure

The results listed in table 1 show that each of the combustion by-products tested are well within compliance for the TCLP procedure and as such it assumed that each material would produce leachate containing 'safe' concentrations of target metals when landfilled. In order to assess the effects of the various coal-cleaning techniques investigated as part of this project, as well as contributing data to assist the interpretation of metal speciation and its effects on leachate composition, it was decided to devise and construct a leaching system capable of generating significant solution concentrations of target metals to aid in data interpretation. A number of different solid waste leaching procedures of varying complexity have previously been used by a number of different researchers as part of several research projects aimed at characterizing the metal release profiles from coal ash and related materials¹. All of these systems have their own inherent advantages and disadvantages however it would appear that no universal 'standard' procedure has been developed to date.

The system devised for this project is best described as a recirculating fixed bed leaching system, integrating a sediment settling stage to prevent column plugging. A known mass of sample (50 g) is placed into a 50 cm glass column fitted with a 70 - 100 μ m glass frit. Deionized water is pumped by a peristaltic pump, upwards through the column of material at a slow speed and passes out the top of the column via 1/8" tubing through a tight fitting stopper. The column effluent is then directed into a 125 mL Erlenmeyer through a tight fitting stopper. The 1/8" inlet stream to the peristaltic pump also comes from the same Erlenmeyer flask but from a shallower depth in the flask, thus any fines that are swept from the column, settle in the bottom of the flask and are not picked up by the pump inlet stream, where they could accumulate and plug the underside of the column frit. The pump flow rate is set such that column throughput is held constant at an estimated 10 column volumes/day. The actual flow rate will be determined at the conclusion of the experiment. The system recirculates the leachate through the column bed allowing each constituent to achieve saturation concentration. The system is sampled by replacing the Erlenmeyer flask at regular intervals with a replacement flask filled

with 100 mL of deionized water. The sample is filtered under vacuum through a $0.45\mu\text{m}$ filter and analyzed for metal content using a combination of directly-coupled and inductively-coupled plasma spectrophotometry. Solution pH, alkalinity and conductivity are also recorded for each sample taken.

The sealed nature of this particular system configuration ensures that water loss from the system through evaporation from the columns and leachate collection containers is eliminated, this will allow for the determination of precise mass balances for each particular species investigated. It will also be possible to investigate the effects of various gas over-pressures on metal release profiles using this particular configuration.

2.3 Preliminary Leaching Results

In order to determine the reproducibility of the leaching system and to optimize the sampling period, a sample of fly ash from the sample set as reported in Table 1. was leached in three identically prepared columns with sampling periods of 5, 10 and 15 days. Table 2. lists some preliminary results obtained from this study.

Table 2 Leachate Analysis of Fly Ash
(Concentration in mg.l^{-1})

Column	Sample	Ca	K	Na	Al	Mo	B
1 (5 Days)	1	644	129	65.0	0.17	13.3	27.0
	2	525	62	30.0	0.05	7.0	14.4
	3	280	33	15.8	0.18	3.5	8.5
	4	165	17.0	8.0	0.91	1.7	6.4
	5	110	10.7	4.5	1.54	0.9	5.4
	6	98	7.1	2.8	2.20	0.4	5.0
	7	54	5.1	2.2	2.75	0.3	4.5
	8	44	3.4	1.4	2.85	0.2	5.0
2 (10 Days)	1	630	127	58	0.17	13.2	20.4
	2	360	61	27	0.22	6.6	9.5
	3	170	35	15	0.75	3.5	7.0
	4	98	20	9	0.85	1.5	6.9
3 (15 Days)	1	633	132	60	0.18	13.5	17.5
	2	225	64	30	0.28	7.0	8.3
	3	118	40	18	0.81	3.8	6.8

The results listed in table 2 show that solution saturation for each of the metals reported has occurred by day 5, furthermore, excellent reproducibility was shown between columns. The results further show that Ca, Na, and K appear to be in a highly soluble form, the concentrations being measured in successive samples rapidly decreasing, note also that the concentrations of Na to K in the leachate are in a 1 : 2 ratio for each sample analyzed (on a mass basis, the ratio calculated on a molar basis being 1 : 1.2) indicating that for the levels measured in solution, both Na and K display similar speciation in the fly ash. Note also that aluminium solubility increases over time, hence it will be necessary to continue sample monitoring over extended periods of time (3 months or possibly longer) to ensure that complete metal release profiles are obtained.

Work is currently underway to assess the leachability characteristics of boiler feed coal as well as fly- and bottom-ash samples from each power station sampled to enable a total mass balance to be calculated for all leachable metals. Future work will include the characterization of the various solid refuse streams derived from the column floatation of high ash coals. The configuration of the apparatus described in this paper will also allow for the leaching of solid coal combustion byproducts with solutions under conditions of controlled solution pH and ionic strength.

ACKNOWLEDGEMENTS

Funding for this work has been provided by the Department of Energy EPSCOR program and is gratefully acknowledged.

REFERENCES

1. Hasset D.J., 1994, Fuel Proc. Tech., **39**, 445-459.

Precombustion Removal of Mercury From Coal by Mild Pyrolysis

T. C. Keener, A.C. Gieske^a, and S.J. Khang^b

^aDepartment of Civil and Environmental Engineering, University of Cincinnati, Cincinnati, Ohio 45221-0071, U.S.A.

^bDepartment of Chemical Engineering, University of Cincinnati, Cincinnati, Ohio 45221-0071, U.S.A.

1. ABSTRACT

The fate of mercury during mild pyrolysis of a high volatile bituminous coal at two temperatures was investigated as a part of an ongoing study. The determination method for mercury content in the original coal sample and the pyrolyzed coal is described. During mild pyrolysis, more than 50% of the parent coal mercury is released at temperatures as low as 300°C with a residence time of 10 minutes. The heating value of the coal is not significantly affected by mild pyrolysis at such low temperatures. A relationship between the residence time, the temperature, and the maximum achievable removal is applied.

2. INTRODUCTION

In the United States, Title III of the 1990 Clean Air Act Amendments specifies that air toxics will be controlled to the maximum extent technically possible (maximum available control technology, or MACT). Most compounds listed as toxic are found in coal and are evolved to the atmosphere when coal is burned. Mercury is present in coal at varying ppm levels and is considered to pose a significant environmental health risk from coal combustion. Material balances on mercury in power plants have shown that only approximately 10% of the total mercury from the coal is found in the fly ash.^[1,2] Other studies investigating the effects of existing control equipment on mercury concentration in flue gases suggest that only 50% to 70% removal can be achieved.^[3,4] Regulations controlling the release of mercury will most likely be promulgated in the future for coal burning power plants.

Mild pyrolysis of coal has been shown to be an economically and technically viable method of desulfurization and denitrification.^[5,6] During mild pyrolysis the majority of trace elements in coal are retained in the solid residue, but volatile elements such as mercury, bromine, and antimony are released in vapor form. Mercury in particular has been shown to be released from coals at the lower temperatures indicative of mild pyrolysis.^[7,8,9] The release of volatile toxic materials from the coal structure before combustion offers the greatest potential for separation of these toxic compounds from the evolved gases and vapors, as the concentrations of these species are at their greatest in the vapor phase during this period. This precombustion removal concept is in line with current attempts at pollution prevention.

3. EXPERIMENTAL

3.1 DETERMINATION OF MERCURY IN COAL AND COAL ASH

Determinations of mercury in coal are difficult because of the intractable nature of the coal matrix, the volatility of mercury, and the varying low levels thought to be present. During the digestion procedure, any organic mercury compounds must be oxidized and mineral mercury compounds must be changed into soluble mercuric salts. This digestion can be achieved by using the ASTM D3684-78 procedure. In the ASTM method, total mercury is determined by combusting a sample of coal in an oxygen bomb with dilute nitric acid absorbing the mercury vapors. The bomb is rinsed into a reduction vessel, and the mercury is determined by the flameless cold vapor atomic absorption technique. The ASTM method was written specifically for fresh coal samples, but should effectively mineralize the pyrolyzed coal samples as well.

3.2 MILD PYROLYSIS METHODOLOGY

Lower Freeport #6A coal mined in Harrison Co., Ohio was used for this study. The coal was sieved to 120 x 150 mesh ($\sim 115\mu\text{m}$) size and stored with CO_2 headspace. Before running the samples for each temperature range, approximately 10 grams of coal were extracted, coned, and separated. Mercury determination was completed on three raw samples to determine a mean ppm mercury value for that sample set. The mild pyrolysis process was carried out in a Lindberg tube furnace with nitrogen flow regulated so that the gas velocity in the heated zone of the tube was approximately 3 cm/s. Each sample was weighed to $0.5\text{gram} \pm 0.1\text{ mg}$, placed in a nickel alloy sample boat, and then purged of any trapped gases in the cool zone of the tube. The sample was heated for a predetermined time and then pulled back into the cool zone of the tube furnace where it remained until room temperature was achieved. The char was analyzed for a final mercury content using the ASTM method.

4. RESULTS AND ANALYSIS

Coal samples were subjected to mild pyrolysis conditions at furnace temperatures of 300°C and 400°C and residence times of 2, 4, 8, and 10 minutes. The initial total mercury in each sample was calculated by multiplying the sample weight and the mean ppm corresponding to that sample set. Percent removal was determined by comparing this initial value with the final mercury content. These results are shown in Table 1.

The mobility of mercury in coal is largely dependent on chemical form, reactor configuration, pressure, particle size, and duration of the mild pyrolysis conditions. The data suggests that under the conditions given in the methodology, the rate of evolution of total mercury is proportional to the fraction of mercury and its compounds remaining in the char at any time multiplied by some reaction rate coefficient dependent on temperature. This can be expressed as a first order homogeneous decomposition with an asymptote dependent on temperature, time, reactor configuration, pressure, heating rate, and particle size:

$$\frac{X}{X_{\max}} = 1 - e^{-kt} \quad (1)$$

Where: X = percent conversion
 X_{\max} = maximum percent available for conversion under a specified set of conditions
 t = reaction time (min)
 k = reaction rate coefficient (min^{-1})

Table 1
 Mercury Removal by Mild Pyrolysis at 300°C and 400°C

Time	300°C			400°C		
	Initial Hg(μg)	Final Hg(μg)	%Removal	Initial Hg(μg)	Final Hg(μg)	%Removal
2	0.3090	0.2563	17.03%	0.2824	0.1698	39.88%
4	0.3447	0.1934	43.89%	0.2086	0.1395	50.28%
8	0.3412	0.1794	47.42%	0.2826	0.1196	57.68%
10	0.3378	0.1655	51.01%	0.2827	0.1196	57.69%

The maximum percent available for conversion corresponding to each temperature can be found by maximizing the regression coefficient obtained when comparing the data with the linear form of equation (1). The slope of this line is the reaction rate coefficient, k. Such analysis of the 300°C and 400°C data showed maximum conversions of 52.68% and 58.23% with reaction rate coefficients of 0.331min^{-1} and 0.501min^{-1} respectively.

Figure 1 shows a plot comparing the measured data with theory. The data given in the figure are experimental values obtained divided by the X_{\max} for that temperature. Plots of the left-hand side of equation (1) using the reaction rate coefficients as determined by theory are represented by the continuous lines. These comparisons show a strong agreement between theory and the measurements.

5. CONCLUSIONS

Given the conditions of the reactor used in this study, mild pyrolysis of coal can achieve up to 51% removal of mercury at temperatures as low as 300°C and residence times of 10 minutes. Furthermore, 57% removal can be achieved at 400°C and eight minutes. These preliminary results show that precombustion removal of mercury from coal by mild pyrolysis can be modeled as a homogeneous reaction with a distinct maximum percent

mercury available for conversion and a distinct reaction rate coefficient for each temperature range. The investigation of this relationship is part of an ongoing study and will become more comprehensive as other temperature ranges are examined.

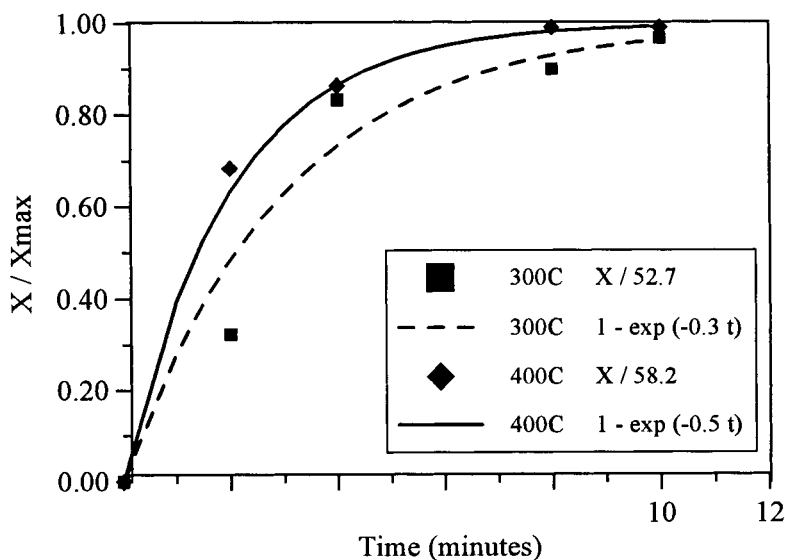


Figure 1. Comparison of Data and Theory

REFERENCES

- Schultz, H., Hattman, E.A., and Booher, W.B., *Am. Chem. Soc.*, 15 (1975), 196.
- Kalb, G.W., *Am. Chem. Soc.*, Ser. 141 (1975), 154.
- Clarke, L.B., *Fuel*, Vol. 72 No. 6 (1993), 731-735.
- Meij, R., *Water, Air, and Soil Pollution*, 56 (1991), 21-33.
- Keener, T.C. Khang, S.J., and Jenkins, R.G., *Fuel Proc. Tech.*, 33 (1993), 33-48.
- Khang, S.J., Lin, L., and Keener, T.C., *Proceedings of World Congress III on Eng. and Environ.*, Vol. 2, Beijing, China (1993), 571-587.
- Karr, C., Jr., (ed), *Analytical Methods for Coal and Coal Products*, 3 volumes Academic Press, 1978.
- Ruch, R.R., Gluskoter, J. J., and Kennedy, E.J., *Il Env. Geo. Notes*, 1971.
- Ebdon, L., Wilkinson, J. R., and Jackson, K.W., *Analyst*, 107 (1982), 269.

Ion exchange properties of brown coals

G.S. Golovin, E.B.Lesnicova, N.I. Artymova

Institute of Fossil Fuels 117912, GSP-1, Leninsky Prospect, 29, Moscow, Russia.

Dens brown coals, containing up to 70% of humic acids and a large amount of functional groups of different nature are practically an unlimited source of ion-exchange materials. Production of efficient and economic ion-exchangers on the base of coals will allow to solve environmental problems by, for example, purification water media from heavy metals [1, 2].

In the work presented as an object for investigation dense brown coal of Beryosovsky deposit has been taken, (table. 1)

Table 1. Characteristics of brown coal and the products of its chemical treatment.

No	Sample	Proximate analysis, wt. %			Ultimate analysis, % daf				Atomic ratio	
		A _d	V _{daf}	S _d	C	H	N	O _d	H/C	O/C
1	Beryosovsky brown coal	7,0	46,1	0,37	71,7	4,81	0,7	22,3	0,81	0,23
2	"-", treated with HCl	3,2	47,4	0,27	70,8	4,87	0,7	23,6	0,83	0,25
3	"-" treated with NH ₃	6,3	43,4	0,26	70,0	4,70	1,52	23,5	0,81	0,25
4	"-", treated with NH ₃ +HCl	1,8	45,5	0,21	68,8	4,7	0,9	23,6	0,82	0,26
5	"-" treated with NaOH+HCl	4,4	44,6	0,31	70,1	4,4	0,8	34,4	0,75	0,26

Dates on functional analysis (table 2) indicate that the most part of oxygen, contained in Kansk- Achinsk coal is presented in the form of functional groups. To determine summed oxy-groups in coal, chemisorption methods with Ba(OH)₂ and Ca(CH₃COOH)₂, based on the ability to exchange hydrogen for barium and calcium ions [3]. The results of chemisorption methods may be veered as a determination of equilibrium exchange capacity of coals on this cations.

To enhance ion-exchange properties of humic substances of coal and obtain materials fit to purify waste waters from heavy metals chemical modification methods have been applied. Initial coal was subjected to alkali and acid treatment under rather mild conditions followed by drying. It was done to partially demineralize and increase the amount of active oxy-groups via the destruction of esteric and other labile bonds existing in coal. Characteristics of the obtained samples are given in tables 1,2.

Table 2. Functional composition of Brown Coal of Beryosovsky Deposit and the products of its chemical treatment, mg-equ/g; daf

No.	Summed oxy-groups	COOH	OH _r	O (unreacted)
1	4.7	0.4	4.3	14.6
2	6.0	1.0	5.0	12.4
3	5.4	0.9	4.5	13.4
4	6.2	1.6	4.6	11.1
5	7.9	2.5	5.4	6.5

Static exchange capacity of coal samples of the initial coal and the products of its chemical treatment determined on the base of Na-ions constitutes 6-8 mg-equ/g daf. It should be noted, that the products of chemical treatment of brown coal, obtained by the methods suggested in the current work, have ion-exchange properties, which are more proximate as compared with those of humic acids; they are of higher mechanical strength. In addition, the process of producing coal cationites excludes the stages of water and filtration of colloid systems, which impede the process of producing humic acids.

The most considerable increase of functional groups has been noted for samples 5, resulted from the consequent alkali and acid treatment of brown coal (table 2). It allowed to view it as the most efficient cationite.

Evaluation of the adsorbability of this materials was performed under static conditions at 20 grad C on model solutions of heavy metal salts.

Analysis of the initial model mixture and that being in contact with the obtained ion-exchangers were performed by plasma photo-metry (table 3).

Table 3. Experimental Data Resulted from Water Purification from Ions of Heavy Metals on Coal Cationite in Static Conditions

Metal Cations	Initial Mixture	Solution volume/sample, V/m				
		1000	500	250	125	63
Metal concentration, mkg/l						
Fe	10000	-	2710	1450	738	386
Ni	12000	-	1850	1133	566	312
Cu	17000	-	3950	2102	1140	755
Zn	17000	-	4435	2358	1204	646
Hg	7100	2100	800	565	432	294
Pb	4000	3000	1820	919	460	236

The dates obtained indicate that the samples show high equilibrium static activity and absorb the metals. With the solutions volume and cationite mass ratio(v/m)- 500, the degree of metal recovery constituted 54-89%. With mass cationite the degree of metal recovery increased till 94-97% at v/m-62.5. It should be noted, that at already v/m-500 ratio value, residual metal concentrations in the solution is considerable lower their MAC.

Maximum value of the summed equilibrium static activity of coal cationite at v/m-500 constitutes 25.8 mg/g, which corresponds to a mean degree of metal recovery ~ 75%. With the stated ratio water volume and coal cationite ion-exchanger will be the most efficient. In the event, when deeper extent of water purification of waste water is needed,

it's expedient to use v/m-125 ratio, for which static activity of coal cationite constitutes 7.8 mg/g, and a mean degree of metal cation recovery does ~ 92%.

Examination of the dynamics of adsorption of heavy metal cations from water solutions coal cationite by coal were performed at a laboratory unit with a fixed bed of ion exchanger.

On the base of preliminary experimental data, the following condition for heavy metals recovery from water solutions have been chosen: flow velocity per a free cross section constituted 1.8 m/hr, the length of a column was 320 mm, cationite mass- up to 42,7 g, column of 18 mm D. The total throughput of water for the column of the stated parameters was 7 L. The water contained salts of the following metals: Ni⁺⁺, Cu⁺⁺, Zn⁺⁺, Hg⁺⁺, Pb⁺⁺. In the course of experimental work the material was periodically sampled. The results obtained were presented in table 4.

From the analysis data it follows that the mean extent of metal recovery constitutes 83-100%, depending on the amount of water passing through the column. In the first period of purification (2 l of solution were passed) the extent of recovery of all metal was close to 100%-, consequently, in increasing the amount of water being passed the mean degree of metal recovery decreased till ~83%.

Table 4. Extent of Water Purification from heave metal ions in dynamic conditions by using coal cationite.

Metal Cations	Water throughput, ml							
	500	1000	1500	2000	3000	4000	5000	7000
	extent of metal recovery, %							
Mg	96	99	99	98	95	87	86	66
Ni	90	99	99	99	99	99	99	97
Cu	100	100	100	100	100	99	97	97
Zn	83	99	99	98	96	93	92	72
Hg	100	100	100	85	80	79	78	62
Pb	100	100	100	100	100	100	100	100
average extent	95	100	100	97	95	93	92	82
dynamic activ. mg/g	1.2	2.4	3.5	4.8	7.2	9.3	11.0	13.9

As a means for the utilisation of worked out coal cationites their combustion is suggested followed by the recovery of the metals absorbed to be used either as a feed stock for further processing, or to remove harmful impurities.

Thus, the results of the investigation carried out has indicated, that brown coals can derive economic and efficient ion-exchange materials fit to be used for purification of iffy waste waters from heavy metals.

REFERENCES

1. N.I. Gamaynov, B.I.Maslennikov, U.A. Shulman/ Ch.T.T. 1991. No 3, h.32-37.
2. Chemistry of the Environment. Editor O.M.Bokris. M. "Chemistry" 1982, p.625-629.
3. New methods of investigation of Humic Acids. USSR Academy of Sciences, Vladivostoc: 1972, 135.

This Page Intentionally Left Blank

A NOVEL COAL BASED PROCESS FOR GROUNDWATER TREATMENT

C.J. Lafferty^a, E.A. McGonigle^{ab}, S. Barry^b, J. Andresen^b and C.E. Snape^b

^a Center for Applied Energy Research, University of Kentucky,
3572 Iron Works Pike, Lexington, KY 40511-8433 USA

^b Department of Pure and Applied Chemistry, University of Strathclyde,
295 Cathedral St., Glasgow G1 1XL, United Kingdom

1. INTRODUCTION.

One of the major issues facing industry today is the removal of heavy metal contaminants from aqueous systems. Whether the intention of metal removal is for the recovery and recycling of the metals in an effort to both protect the environment and offset processing costs or the aim is to completely remove the contaminant species from aqueous solution, the demand exists for treatment processes which can be used to economically process large volumes of water containing low to moderate levels of contamination, particularly where the source of contamination is either unknown or in dispute, hence presenting a difficulty in assigning fiscal responsibility for the remediation process.

Whilst conventional treatment technologies such as pH adjustment and ion exchange resin based processes would be technically suitable for such applications, the process costs involved would preclude all but the most environmentally hazardous scenarios where cost is of secondary importance. Furthermore the use of conventional treatment systems generates secondary waste streams in the form of sludges, acid concentrates and flocs which must be further treated prior to ultimate disposal in a landfill, where preventing the re-release of contaminants to the environment is of ongoing concern and cost.

The ability of low rank coals to form stable complexes with several heavy metal ions has long been recognized^{1,2,3,4,5,6}. This property has been successfully utilized to estimate the concentration of acidic oxygen functional groups present in low rank coals⁵ as well as serving as a convenient means of dispersing metal catalysts across a coal surface prior to liquefaction⁷. The relatively high ion exchange capacity of several low rank coals studied, coupled with the low overall cost of the bulk material, indicates great potential for the utilization of low rank coals as a means to remove a range of metals from aqueous waste streams.

For a number of applications, metal recovery is but the first step of the remediation process. Of equal importance is the permanent immobilization of the adsorbed metals for safe disposal. A unique aspect of the coal-based metal adsorption process described in this paper lies in the characteristics of the adsorbate material. i.e. the coal's inherent calorific and ash contents. Combustion of the ion exchanged coal in an appropriate system would result in the formation of a vitrified non-leachable ash material containing the adsorbed metals in an immobilized non-leachable state which would be intrinsically safe for long term storage or disposal.

One of the potential disadvantages to the use of low rank coal as metal adsorbents lies in the release of humic acids from low rank coals at high pHs in the presence of either sodium or potassium. This results in a the solubilization of a significant percentage of the carboxylic acid sites from the coal as well as producing a dark colored solution which is aesthetically objectionable. Higher rank bituminous coals whilst not displaying

significant cation exchange capacities, as mined, do not release significant concentrations of humic acids when treated with sodium or potassium hydroxide solution. The objective of the research reported in this paper was to attempt to increase the cation exchange capacity of a British bituminous coal through a series of controlled oxidation experiments, whilst at the same time minimizing the formation of soluble humic acid moieties.

2. EXPERIMENTAL

Samples of bituminous Gedling coal mined from the High Hazels seam were supplied by the British Coal Corporation. Samples of a U.S. lignite from the Gulf Coast formation were provided by the Kentucky-Tennessee Clay Company of Mayfield, Kentucky, and used by means of comparison against the oxidized Gedling Coal.

Samples of the Gedling coal were air-oxidized in a laboratory oven for 24 hrs at 150, 200 and 250°C. The ion exchange properties of the fresh and oxidized coals were determined by a combination of barium hydroxide titration (to determine total acid functional group concentration, carboxylic + phenolic) and EDTA titration. The concentration of Cu^{2+} in solution both before and after treatment of a cupric nitrate solution with coal were measured by EDTA titration against a 0.1% PAN indicator to measure 'Cation Exchange Capacity'. Samples of the Gedling coal were also sulphonated via treatment with concentrated sulphuric acid in order to add strongly acidic sulphonic acid sites to the coal. Samples of the oxidized bituminous coal were also characterized using ^{13}C NMR spectroscopy to determine the effects of air oxidation upon oxygen functional group concentrations within the coal. Cross polarization/magic-angle spinning (CP/MAS) spectra were recorded using a Bruker MSL 100 instrument with a contact time of 1 ms.

The cation exchange characteristics of the sample of Kentucky lignite were determined using both batch and column procedures, the principal cation used in these techniques was the Uranyl (UO_2^{2+}) cation, as it is anticipated that the ion exchange properties of the lignite could be integrated into a remediation process for the removal and stabilization of uranium from low level wastes.

3. RESULTS

3.1 Oxidized Coal

Table 1 lists the composition and acid group concentrations of each of the oxidized samples of the Gedling coal.

Table 1. Composition and Acidic Group Concentrations of Oxidized Coals.

Sample	C	H	N % dmmf	S	O	[Acid Groups]* (meq/g)
Fresh	81.7	6.0	1.6	0.7	10.0	0.0
150°C	82.1	5.6	1.6	0.7	10.0	1.5
200°C	76.4	3.3	1.2	<0.1	18.0	2.0
250°C	62.5	1.9	1.6	<0.1	22.9	4.6*

* ^{13}C NMR shows that the increase in acid functional groups between 200 and 250°C measured by barium hydroxide titration is due to an increase in phenol concentration (Fig. 1)

The ^{13}C NMR Spectra of the 200 and 250°C samples are shown in Figure 1. The carboxyl/ carbonyl peak at ca. 194 ppm can clearly be seen on the 200°C sample, similarly the substantial presence of phenolic/ether functionalities can be seen at ca. 160 ppm on the spectrum of the 250°C sample. This indicates that whilst oxidation of the coal at temperatures greater than 200°C results in increases in both cation exchange capacity, as measured by barium hydroxide titration, and oxygen content of the resulting material (Table 1.), this increased oxygen content results from the addition of phenolic functional groups. The intention of this work was to add carboxylic acid functionalities to the coal, it would therefore appear that maximum carboxylic acid group addition occurs at oxidation temperatures lower than 250°C. Note also that all of the aliphatic carbon (ca.25 ppm) detectable within the coal is removed by oxidation at 250°C.

3.2 Sulphonated Coal

Examination of the ^{13}C NMR spectra of the sulphonated coal showed that significant coal oxidation (and hence an increase in carboxylic acid concentration) had occurred in addition to increases in both sulphur content and cation exchange capacity of the sulphuric acid treated coals. This indicates that the sulphuric acid treatment results in significant carbon oxidation upon the coal surface as well as the incorporation of sulphonic acid sites into the coal structure.

The total acid concentration of the sulphonated coals were found to be 6.4 meq/g as measured by barium hydroxide titration. The sulphur concentration of the product material was 4.8% which corresponds to a sulphonic acid content of 1.5 meq/g, when combined with the carboxylic acid content of 2.0 meq/g (as measured from ^{13}C NMR), the total concentration is in excellent agreement with the measured cation exchange capacity of 3.4 meq/g as measured by EDTA titration to quantify the adsorption of copper from a cupric nitrate solution. The difference between the acid functional group concentration and cation exchange capacity (i.e. 1.2 meq/g) is attributed to the incorporation of phenolic functional groups into the coal structure during sulphonation. These total capacities are directly comparable to those of commercially available synthetic ion exchange resins indicating that sulphonated bituminous coals may offer realistic low cost alternatives to synthetic resins in the area of environmental remediation. Further work is currently underway to assess the ion exchange properties of these sulphonated coals using a wide range of metals.

3.3 Lignite

The cation exchange capacity of a sample of western Kentucky lignite was measured using a 10 ppm solution of uranium (as uranyl nitrate) passed through a 10 cm³ column of lignite at 1 column volume per minute. Samples of the effluent were collected at regular intervals and analyzed for residual uranium content using ICP spectroscopy.

Figure 2. shows the concentration of residual uranium as measured in the effluent stream from the column plotted as a function of the number of column volumes. Convention dictates that column breakthrough occurs when $C/C_0 = 0.3$, at this point the total cation exchange capacity of the lignite was 0.23 meq/g after 640 column volumes had been treated. Continuing the experiment until C/C_0 approached 0.95 resulted in a cation exchange capacity of 0.56 meq/g after the treatment of 2500 column volumes.

4. Conclusions

Initial results obtained from the oxidation and sulphonation of a British bituminous coal have shown that cation exchange capacities comparable to those of synthetic resins are achievable with controlled oxidation below 200°C. Oxidation of the coal at temperatures greater than 200°C and sulphonation with concentrated sulphuric acid resulted in the formation of appreciable concentrations of phenolic functional groups within the coal

structure.

Acknowledgements

The work described in this paper originated from a collaborative programme which has been established between the University of Kentucky Center for Applied Energy Research and The University of Strathclyde Department of Pure and Applied Chemistry. One of the authors (E.A.M.) wishes to acknowledge the Center for Applied Energy Research for providing funding for her research in the form of a summer fellowship.

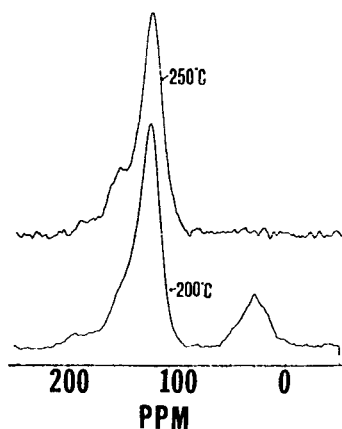


Figure 1. ^{13}C NMR Spectra of Oxidized Coals

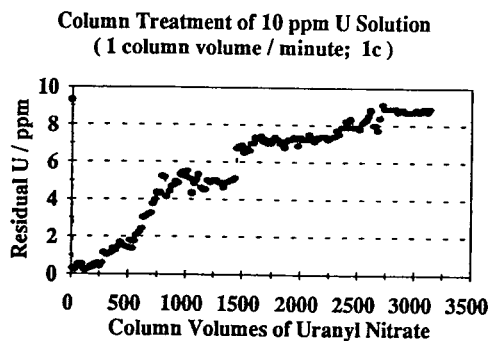


Figure 2. Adsorption of Uranium by W. Kentucky Lignite

REFERENCES

1. Lafferty C.J. and Hobday M.D., 1990, *Fuel*, **69**, 79.
2. Lafferty C.J. and Hobday M.D., 1990, *Fuel*, **69**, 84.
3. Stuart A. D., 1986, *Fuel*, **65**, 1003.
4. Allen S.J., 1987, *Fuel*, **66**, 1171.
5. Schafer H.N.S., 1970, *Fuel*, **49**, 197.
6. Schafer H.N.S., 1970, *Fuel*, **49**, 271.
7. Hatswell M.R., Jackson W.R., Larkins F.P., Marshall M., Rash D. and Egers E.R., 1980, *Fuel*, **59**, 442..

Evaluation of water contamination degree in areas affected by coal related activities - Rio Grande do Sul State, Brazil

I.H. Lagrecia¹; R.B. Binotto¹; E.C. Teixeira²; J.C.D. Sanchez³ and A. Jablonski¹

¹ Laboratório de Geoquímica Ambiental - PPGEMM - UFRGS - Av. Osvaldo Aranha, 99/506
90040-010 Porto Alegre, RS, Brazil

² Fundação Estadual de Proteção Ambiental - FEPAM, RS

³ Fundação de Ciência e Tecnologia - CIENTEC, RS

One of the most significant environmental problems in the Southern Region of Brazil comes from the coal related activities there developed (mining, washing, combustion and coking of coal). This work aims to determine the contamination degree of surface waters, groundwaters and associated sediments affected by coal activities in the Coal region of Rio Grande do Sul State. In order to meet this goal, the following steps were conducted: location of polluter sources, physical-chemical analyses on groundwater and surface waters and extraction tests in sediments. With the obtained results, it was possible to conclude that, in the study area, it was evidenced the contamination of surface waters by direct influence of coal mining and siderurgic activities. With respect to groundwaters, there is a need for more detailed studies that correlate the hydrogeological characteristics of the area with coal wastes disposal time, evaluating more precisely their influence on these waters contamination.

1. INTRODUCTION

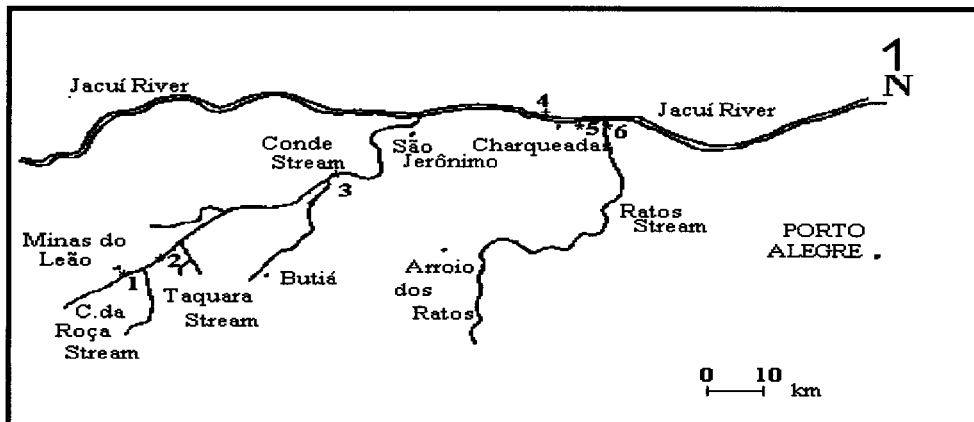
The Brazilian coal reserves amount to 32 billion tons, 87% located in Rio Grande do Sul (RS). In this State, coal production is equivalent to 60% of the overall Brazilian production (5 Mton/year)(11). Candiota and Baixo Jacuí regions, where the greater reserves are located, produced up to 1993 1.2 Mton/year and 720 kton/year, respectively (11). Coal deposits in RS occur in the Paraná Basin, located along the Sul-Riograndense Shield edge, mainly in the southwestern (Candiota) and central (Jacuí River Valley) portions and also in the eastern region (Central Eastern Coalfield)(3). The sedimentation is essentially paleozoic, with more recent overburden and mesozoic volcanism associated. Coal beds occur in the Rio Bonito Formation, Guatá Group, Tubarão Supergroup (12), being inter-related to different kinds of rocks, like conglomerates, quartzzy sandstones, mudstones, siltstones and chalk(3).

Coal processing, since exploitation to utilization, can degrade environmental quality if there is not a control on this activities resulting emissions. Some indications of contamination have been detected in sites of RS, as acidification in surface waters and unadequate disposal of coal wastes, that can change groundwaters quality.

In RS only a few studies related to waters quality in coal affected regions were published until today (6,7,9,10). Among those, one can be highlighted: the work conducted by Machado (9) in Candiota, where it was evidenced contamination in surface and groundwaters by Fe, Mn, Ni, Zn, Al and Cu. Another research was done in Baixo Jacuí region by Luz (8), who used coal ashes from a power plant as a landfill material. The obtained results suggest that this waste disposal did not affect markedly the quality of the groundwaters related to the landfill.

2. EXPERIMENTAL

Waters and surface sediments samples were collected in six points located in Baixo Jacuí Region as shown in the figure below.



• Cities; * Sampling Points

Location of water and sediments sampling points: 1 - Capão da Roça Stream, close to the tailing discharge of the Leão Mine; 2 - Taquara Stream, close to the impounding to Leão washing; 3 - Conde Stream, Butiá Coal Mine; 4 - Jacuí River, Eletrosul storage yard; 5 - Jacuí River, 100m downstream Aços Finos Piratini Siderurgy; 6 - Ratos Stream, Charqueadas

Water samples were taken monthly in Aug/Sep/Oct/92 and in Feb/Mar/Apr/93. With the results, it was possible to conclude that the surface streams that showed greater contamination are those located in areas affected by coal waste disposal and/or coal washery effluents. In this way, additional samples were taken in the Capão da Roça Stream in Nov/94 and Jan/Feb/95, close to the tailings discharge of the Leão Mine washer. The samples destined to metals determination were preserved in $\text{pH} < 2$ with nitric acid, according Standard Methods (13); those destined to dissolved metals analysis were previously filtered in a $0.45 \mu\text{m}$ ester membrane. Surface sediments were collected compositely and wet sieved (teflon sieve frame fitted with polyethylene mesh) for the separation of particles $< 63 \mu\text{m}$ (silt-clay). This fine fraction was dried and ground in agate mortar.

Metals analyses in water and sediments were performed through Flame Atomic Absorption Spectrophotometry (FAAS), after standard digestion procedures (13) and with $\text{HNO}_3/\text{H}_2\text{O}_2$, HF and HClO_4 , respectively.

3. RESULTS AND DISCUSSION

The minimum, maximum and mean of analytical data are shown in Table 1. It can be seen that points 2 (close to Leão Coal Mine) and 3 (close to Butiá Coal Mine) were the most affected by coal mining and/or waste disposal. The effects of pyrite influence can be better seen in points 2 and 3, by the high sulphates concentration, in addition to the acid pH found in the point 2, which is lower than the Brazilian tolerable standard (2).

It was possible to detect an increase in conductivity and total residue values in Aug/Sep/Oct/92 in points 2 and 3, what can be related to stream silting up in winter periods,

that can increase total residue values and enhance the solubility of salts associated to suspended particles.

Table 1. Physical-chemical characterization of surface waters in Baixo Jacuí Region, RS, Brazil.

Param	pH			Dissolved O ₂ (mgO ₂ /l)			Conductivity (uS/cm)			Sulphates (mg/l)			Total Res. (mg/l)		
	min.	max.	X	min.	max.	X	min.	max.	X	min.	max.	X	min.	max.	X
1	5.3	6.2	5.9	-	-	-	350	680	515	-	-	-	3990	76200	32000
2	3.4	4.1	3.6	6.7	10.0	7.3	35.0	490	216	118	216	152	268	9828	2432
3	5.8	6.6	6.1	4.6	10.5	7.8	23.0	385	166	72.0	210	128.7	157	11019	3325
4	6.4	7.2	6.9	7.2	10.6	8.8	36.0	49.0	41.0	3.6	11.8	4.8	72.0	10120	2752
5	6.7	7.3	6.9	6.8	9.6	8.3	33.0	58.0	46.5	3.6	13.8	10.5	61.0	11922	2797
6	6.7	7.4	7.1	7.9	9.8	8.7	34.0	78.0	52.0	1.8	15.0	7.1	123	1459	416

min.: Minimum value ; max.: Maximum value; X: Arithmetic mean; -: not analysed

Jacuí River, in its turn, showed pH values close to neutrality, despite the polluter load it receives. This can be explained by its high self-depuration ability, due to its significant flux, length, and velocity (5). Heavy metals, even not shown here, presented values lower than FAAS detection limits in most points, except for Fe and Mn.

Acid pH associated to high Fe contents in point 2 proves the influence of pyrite associated to coal wastes. Also in this point, it was detected Zn, probably associated to sulphides that, in acid pH, can release it to the water environment. Co and Pb were not detected in waters but in sediments their concentrations surpass the averages for this medium (14). Still in points 2 and 3, it was verified the presence of total and dissolved Mn in water in relatively significant concentrations, probably due to its association with carbonates and oxides (1).

In point 6 (Jacuí River) were detected values of total and dissolved Cr (0.25 and 0.15 ppm) and Ni (0.28 and 0.08 ppm) in water. These elements, besides Cu, were also found in sediments, what can be attributed to anthropogenic influences (probably to siderurgic activities).

Baixo Jacuí groundwaters data presented by Luz (8) and summarized in the Table 2, showed that the coal ashes used in the landfill did not caused significant contamination in the period from 1989 to 1991.

Table 2. Some parameters analysed on groundwaters in Baixo Jacuí Region.

Parameter	P1	P2	P3	Parameter	P1	P2	P3
pH	5.84	6.25	6.83	K (mg/l)	0.72	1.13	2.21
Conduct. (µS/cm)	23.86	34.37	73.37	Na (mg/l)	3.60	4.51	13.77
Sulphates (mg/l)	4.12	3.20	14.92	Si (mg/l)	1.12	0.94	2.75
Total solids (mg/l)	192.00	142.60	343.88	Ca (mg/l)	4.14	1.78	3.85
Dissolved Ox. (mg/l)	3.23	2.44	2.61	Mg (mg/l)	1.57	0.75	1.65
Mn (mg/l)	0.18	0.12	0.16	Fe II (mg/l)	0.06	0.38	0.33
Cu (mg/l)	0.16	0.01	0.03	Fe III (mg/l)	12.13	3.04	11.59
Al (mg/l)	1.73	0.72	3.81	watertable (m)	14.44	11.81	10.79
Cr (mg/l)	0.04	0.02	0.02	ground level(m)	15.04	11.97	11.05
Ni (mg/l)	0.03	0.01	0.03	ash landfill (m)	18.00	15.00	15.00
Pb (mg/l)	0.05	0.01	0.02	piez. deep (m)	4.50	4.50	4.50

After Luz (8)

Although most of parameters (see Table 2) showed higher values for point 3, they are still below the potability international recommended standards (2, 4). This point, with the point 2, presents some trend for waters contamination by Fe II. This ion concentration in these points

can be associated to the lessening of DO. In order to study some further contamination, a monitoring program must be conducted in the forthcoming two years.

4. CONCLUSIONS

Data obtained in this work conducted in Baixo Jacuí Region showed some compromising of surface waters in those points more directly influenced by coal mining and siderurgic activities.

Coal processing influence was evidenced both for high contents of sulphates, Fe, Mn, Zn and acid pH in water close to Leão Coal Mine as for high contents of Pb and Co in surface sediments. The anthropogenic influence of Aços Finos Piratini Siderurgica activities was proved by the high concentrations of Cr and Ni in waters and surface sediments collected immediately downstream to the facility discharge.

With respect to groundwaters, in spite of the results presented by Luz (8) do not indicate contamination by ash disposal, this situation shall be better evaluated once this waste disposal may bring environmental hazards as time passes.

This work is ongoing with more intensive sampling of surface waters through the four seasons of the year, a larger number of metals to be analyzed and sequential extractions in surface sediments in those points more exposed to contamination. In addition, more detailed studies on groundwaters contamination have been conducted, analysing a larger number of sampling points in the Baixo Jacuí Region aquifers.

REFERENCES

- (1) Bowen, H.J.M. 1979. Environmental Chemistry of the elements. NY. Academic Press. 333p.
- (2) Conselho Nacional do Meio Ambiente. 1986. Resolução CONAMA N.20.
- (3) Corrêa da Silva, Z.C. 1989. The classification of south Brazilian Gondwana coals on the basis of different chemical and physical parameters. *Int.J.Coal.Geol.*; 13, p.21-39.
- (4) Custodio, E & Llamas, M.R. 1983. *Hidrologia Subterrânea*. Ed. Omega. Barcelona. 2359p.
- (5) DMAE. 1981. *As águas do Rio Jacuí*. n.36. Porto Alegre. 65p.
- (6) Fiedler, H.D. & Solari, J.A. 1988. Caracterização do impacto ambiental da Mina de Candiota sobre as águas superficiais da região. In: XIII Enc.Trat.Min.Hidrometalurgia, São Paulo. Anais.483-498.
- (7) ELETROSUL. 1986. Relatório de Impacto Ambiental da Usina Termoeletrica de Jacuí I.
- (8) Luz, E.D., da. 1991. Projeto Piloto de disposição controlada de cinzas de carvão. Relatório interno. Centrais Elétricas do Sul do Brasil S.A. - ELETROSUL. 45p.
- (9) Machado, J.L.F. 1985. Mineração de Carvão: Contaminação e Vulnerabilidade dos Mananciais. In: II Simp.Sul-Bras.Geol., Florianópolis. p.539-553.
- (10) Martins, A.F. & Zanella, R. 1990. Estudo Analítico-ambiental na região carboenergética de Candiota, Bagé (RS). *Ciência e Cultura*, 42(314):264-270.
- (11) Ministério de Minas e Energia. 1994. Departamento Nacional de Produção Mineral - DNPM. Informativo Anual da Indústria Carbonífera.
- (12) Schneider, R.L.; Muhlmann, H.; Tommasi, E.; Medeiros, R.A.; Daemon, R.F.; Nogueira, A.A. 1974. Revisão Estratigráfica da Bacia do Paraná. In: *Cong.Bras.Geol.*, 28, Porto Alegre. Anais, 1:41-65.
- (13) Standard Methods for the Examination of Water and Wastewater. 1992. Ed. A. E. Greenberg; L.S.Clesceri and A.D.Eaton. 18th edition.
- (14) Teixeira, E.C.; Pestana, M.H.D.; Sanchez, J.C.D; Fernandes, I.D.1994. Geochemical distribution of Metallic Elements in the mineral matter of Brazilian Coals. *Environ.Tech.*, 25:989-996.

A CRITICAL COMPARISON OF SPECTROPHOTOMETRIC AND POTENTIOMETRIC METHODS FOR THE DETERMINATION OF FLUORIDE AND CHLORIDE IN COAL FLY ASH AND CLAY.

E. Andrés-García; E. Blanco-Gonzalez; M.E. Díaz-García
Dept. of Physical and Analytical Chemistry Faculty of Chemistry
Avda. Julian Clavería, 8 33006-OVIEDO, SPAIN.

INTRODUCTION

Coal and fly ash are currently monitored to control fluoride (and chloride) ground water and air pollution. In fact, fluorine emissions to the atmosphere provide the greatest potential individual source of environmental contamination by trace elements released from the utilization of coals (1). Chlorine, on the other hand, can contribute to the formation of a corrosive atmosphere during combustion and to the formation of acid precipitation, being thus an undesirable species in coal.

Fly ash is a material which is produced in large quantities as a by-product of coal combustion in power plants (5-10 tons/h). This material can not be dumped without cheking that the ground water will not be polluted.

During the last few years a group of laboratories has worked in several intercomparisons in the frame of the BCR-programm to improve their methods for fluorine and chlorine determination, especially for coal analyses (2,3).

In this communication we report on our experience in the certification of fluoride and chloride contents in coal, fly-ash and clay .

ANALYTICAL METHODS USED

Halide Determination

Both fluoride and chloride were analysed using the corresponding ion selective electrode. Alternative

spectrophotometric methods were used. Fluoride was analysed by the Cerium-Alizarin Complexone method and chloride using the mercuric thiocyanate method.

Certified Reference Materials (CKM_s) already certified for F (coal CRMO40) and Cl (coal CRM181) were used to verify the accuracy of the methods. Analyses were done in 5-fold. Replicates were independent and performed at least on two different days on the content of two different sample bottles.

Sample Pretreatment

Dry samples for 2 h at 102 °C in a ventilated oven were thoroughly taken two methods of coal and fly-ash sample pretreatment were considered in order to establish comparative data with respect to analytical accuracy precision, speed and ease of operation: oxygen bomb combustion and alkali fusion.

Clay was dissolved by the alkaly fusion treatment.

RESULTS

Table 1. Shows that the results obtained for fluoride in coal and fly-ash.

TABLE 1
FLUORINE IN SELECTED REFERENCE SAMPLES

SAMPLE	THIS WORK	CERTIFIED VALUE	TECHNIQUE USED*
Coal CRM460	212 ± 6	225 ± 6	ISE-1
Fly-Ash CRMO38	118 ± 11	538 ± 13	SPEC-1, ISE-1
Coal CRM 040	115.3	11.4	ISE-1

*ISE-1 : Ion Selective Electrode after combustion
SPEC-1. Spectrophotometry after combustion

As can be seen, results for fluorine in coal samples by oxygen bomb combustion prior to measurement with the fluoride

ion-selective electrode are generally in acceptable agreement with the certified value. However, at the technical meeting, before the CRM460 were certified, oxygen bomb combustion was considered doubtful for fluoride determination in coal as a wide range of fluoride recoveries were obtained. Results could only be accepted for certification if the total destruction for F^- was confirmed by analysis of the combustion residue.

On the hand, results for fluorine in fly ash samples by this procedure were always erratically lower, by a factor of four or five, than the certified value, and fusion should be systematically used in the case of fly-ash.

Our results for chlorine in coal samples by combustion followed by ion-selective electrode ($178 \pm 20 \mu\text{g/s}$) or spectrophotometric determination ($162 \pm 2.8 \mu\text{g/g}$) were always higher than the recommended values. This appears to be because other species which the chloride ISE senses or that interfere the mercuric thiocyanate spectrophotometric method (such as thiocyanate) could be formed during combustion of coal.

The combustion procedure was considered to be suitable for chloride determination in coal. Due to the scattered values for chlorine found by the participants, the content of chlorine could not be certified and is given as indicative value only ($59 \pm 8 \mu\text{g/s}$). Doubts were thrown on the homogeneity of chlorine in this CRM.

Our results, for chlorine in clay (CRM 461) by fusion-followed by spectrophotometric determination revealed a high spread of values (from 97 to 267 $\mu\text{g/g}$). It was not possible to explain the scattered results found by all other participants and, consequently, this CRM could not be certified for chlorine.

CONCLUSIONS

Te results obtained from this intercomparative exercise on certification of F^- and Cl^- in coal and fly ash revealed that the problem remained of determining the most effective means of sample preparation (2).

Development of experience in analytical techniques and the adaptation of such technique to the analysis of coal, and particularly to fly-ash, was evident throughout the work.

REFERENCES

- (1) K.J. Doolan; *Anal.Chim.Acta*, 202, 61 (1987)
- (2) B.Griepink, H.C. Wilkinson, *Mikrochim. Acta*, III, 25-33 (1989)
- (3) P.Zuevauviller; H. van der Staak; D. van Loenen; W. Lingerak; B.Griepink; *Fresenius. J. Anal. Chem.*, 350, 101-108 (1994)

ACKNOWLEDGMENTS: Authors are gratefully acknowledged to J. Cardin and R. Tarazona from Instituto del Carbón (I.N.C.A.R), Oviedo, for experimental assistance and helpful discussions.

Volatile elements and radionuclides in Highvale and Whitewood Mines, Alberta, Canada

F. Goodarzi^a and T. Gentzis^b

^aGeological Survey of Canada, 3303-33rd Street N.W., Calgary, Alberta T2L 2A7 Canada

^bAlberta Research Council, P.O. Box 8330, Edmonton, Alberta T6H 5X2 Canada

1. INTRODUCTION

Air pollution resulting from fossil fuel combustion has received significant attention recently. Coal contains elements whose concentration may vary significantly both vertically and laterally in a minesite. These elements may be associated either with the mineral matter or the organic matter in coal, could remain in the bottom ash, be mobilized in the fly ash, or be emitted with the flue gas. The distribution of trace elements and their concentration in the above fractions depend on the mode of occurrence and speciation, concentration in coal, boiler type and load, and on operating conditions (Tomza and Kaleta, 1986). Volatile elements, such as Hg, Cd, Pb, F, and Be are of environmental concern (Swaine, 1990).

This study reports on the concentration of Be, Cd, F, Hg, Pb and radionuclides in subbituminous coals used exclusively for power generation in Alberta. One hundred (100) coals from the Highvale Mine and fifty (50) coals from the nearby (12 kms away) Whitewood Mine were analyzed. Coal from the Highvale Mine feeds the 766 MW Keephills and the 1987 MW Sundance power plants, whereas coal from the Whitewood Mine provides the feed for the 570 MW Wabamun plant. Approximately 14 million tonnes of low-sulphur ($S_{\text{tot}} < 0.5$ wt%) are mined every year from six seams in both sites. The trace element geochemistry of the Highvale and Whitewood mines coals has been published by Gentzis and Goodarzi (1995) and Gentzis *et al.* (1995), respectively.

2. EXPERIMENTAL

Determination of Cd and Pb in coal was carried by Atomic Absorption Spectrometry (AAS). Mercury was determined by cold vapour AAS. Fluorine was determined by fusion of the sample with a mixture of Na_2CO_3 : KNO_3 and subsequent measurement by ion selective electrode. Beryllium was determined by AAS. Detection limits are: Cd 0.2 ppm; Pb 2 ppm, F 20 ppm, and Be 0.5 ppm. Total U and Th were measured by Instrumental Neutron Activation Analysis (INAA) and gamma counting, while

^{226}Ra , ^{232}Th , ^{230}Th and ^{228}Th were measured by alpha spectroscopy. Thorium was concentrated by coprecipitation on lanthanum fluoride and purified by anion exchange chromatography, whereas radium was separated by nitrate coprecipitation and purified by cation exchange chromatography.

3. RESULTS

3.1. Cadmium

Cadmium in the Highvale Mine coals ranges from <0.1 to 0.31 ppm in Seam 3 (ash is 17.6%). The element is most likely present in sphalerite, a mineral present in seams 1U and 1L. The Whitewood Mine coals have lower Cd content (0.03 to 0.24 ppm). Compared to numerous U.S. coals (mean is 0.38 ppm; White *et al.* 1984) and world coals (mean of 0.5 ppm; Clarke and Sloss, 1992) the Alberta coals are very low in cadmium (Table 1).

Table 1
Mean values of selected elements in the coals studied

<u>Coal</u>	<u>Elemental Mean (ppm)</u>						
	Be	Cd	F	Hg	Pb	Th	U
Highvale	2	0.2	116	0.1	15	4.7	2.0
Whitewood	<1	<0.1	178	0.4	7	5.4	2.7
World Average*	2	0.5	150	0.1	40	2.0	4.0

*from Clark and Sloss, 1992

3.2. Mercury

Mercury concentration in the Highvale coals ranges from 15 ppb in Seam 2 to 146 ppb in Seam 1. In the Whitewood coals, Hg has a wider range (5 to 845 ppb in Seam 2) but most values are below 170 ppb (world mean is 100 ppb; Table 1). Seam 2 has the highest content, while seams 3, 4 and 5 have the lowest. The distribution of mercury in the two coal successions studied is similar to that of arsenic, pointing to its possible association with epigenetic pyrite.

3.3. Lead

The range is from 2.2 ppm in Seam 4 to 13.5 ppm in Seam 1, Highvale Mine. Lead content in the Whitewood coals is in the 0.3 to 12.0 ppm range, the highest values measured in Seam 1 and the lowest in seams 3 and 4. Samples with less than 20.0% ash (cleaner coals) generally have Pb content less than 10 ppm. Mean values for Pb in these coals are less in western Canadian coals (1 to 22 ppm) (Goodarzi and Swaine, 1993) and in world coals (40 ppm; Table 1).

3.4. Fluorine

The Highvale coals have F content of 23 to 124 ppm, with most values being below 90 ppm. The lowest content was measured in Seam 3 and the highest in Seam 1. Samples low in ash have low F content, pointing to an inorganic association. The element is most likely associated with minerals such as kaolinite, montmorillonite, illite, mica and apatite, all detected in seams 1U, 2, and 4 by XRD. The range of F in the Whitewood coals is from 19.4 ppm to 117.4 ppm, with Seam 1L having the highest content and Seam 6 the lowest. Values are less than 150 ppm, considered to be the world mean (Table 1). The fluorine values may have been higher had we employed the pyrohydrolysis method (also known as the Australian Standard) for F determination (Martinez-Tarazona *et al.* 1993).

3.5. Beryllium

Beryllium content in the Highvale coals is 0.5 to 2.2 ppm and in the Whitewood coals 0.53 to 4.0 ppm. The highest values are found in seams 2 and 3, the lowest in Seam 4. Beryllium content is comparable to that of U.S. coals (mean is 1.5 ppm), and world coals (mean of 2 ppm; Table 1).

3.6. Radionuclides

Uranium content in the Highvale coals is 1.4 to 3.1 ppm and Th content is 3.3 to 6.7 ppm (average: 4.7 ppm) (Table 1). Thorium-232 ranges from 14 to 27 Bqs/kg, ^{234}Th from 19 to 44 Bqs/kg, ^{228}Th from 11 to 37 Bqs/kg, and ^{226}Ra from 21 to 37 Bqs/kg. The range of ^{210}Pb is 20 to 40 Bqs/kg, for ^{210}Po it is 20 to 40 Bqs/kg, and for ^{212}Pb it is 10 to 20 Bqs/kg. In Whitewood coals, U content is 1.3 to 5.7 ppm (average: 2.7 ppm) and Th content is 3.4 to 11 ppm (average: 5.4 ppm) (Table 2). Radionuclide activity is similar to that in the Highvale coals. For example, ^{232}Th ranges from 10 to 40 Bqs/kg, ^{234}Th from 10 to 60 Bqs/kg, ^{228}Th from 10 to 40 Bqs/kg, ^{226}Ra from 20 to 70 Bqs/kg, and ^{214}Bi from 20 to 50 Bqs/kg. Similarly, ^{210}Pb is in the range 10 to 70 Bqs/kg, ^{212}Pb is 10 to 40 Bqs/kg, and ^{210}Po is 10 to 70 Bqs/kg.

Table 2
Variation of radionuclides (Bqs/kg) in the Highvale and Whitewood coals as compared to Canadian feedcoals and world coal

Radionuclides	World Range Salmon (1982)	Canadian Feedcoals Range Evans <i>et al.</i> (1985)	Highvale Coal (Average)	Whitewood Coal (Average)
^{238}U	15-250	13-47	27	35
^{230}Th	-	20-93	B.D.	B.D.
^{226}Ra	1.5-250	9-39	30	40
^{210}Pb	10-50	12-64	20	30
^{232}Th	<7-110	9-23	20	20

B.D. = Below detection limit

4.0 DISCUSSION

The concentration of Be, Cd, F, Hg, Pb, Th and U in both the Highvale and Whitewood coals are within the range of world coal (Clark and Sloss, 1992) and are therefore suitable as feedcoals for use in coal-fired power plants.

The activities of radionuclides (in Bqs/kg) for world coal (Salmon et al., 1982), Canadian feedcoals (Evans et al., 1985), and the Highvale and Whitewood coals are presented in Table 2. It is evident, from the data in Table 2, that the activities of ^{210}Pb , ^{226}Rn , ^{230}Th , ^{232}Th and ^{238}U for the Highvale and Whitewood coals is within the range for Canadian feedcoals and is within the lower range for world coal. Thus indicating that the usage of these coals in coal-fired power plants has little impact on the environment as related to radionuclides.

REFERENCES

1. L.B. Clark and L.L. Sloss, Int. Ener. Agency Report CR/49 (1992) 111pp.
2. D.G. Coles, R.C. Ragaini and J.M. Ondov, Env. Sci. and Technol., 12 (1978) 442.
3. J.C. Evans, K.H. Abel, K.B. Olsen, E.A. Lepel, R.W. Sanders, C.L. Wilkerson, D.J. Hayes and N.F. Mangelso, Final Report, Can. Electr. Assoc. Contract 001G194 (1985) 156pp.
4. T. Gentzis and F. Goodarzi, Ener. Sour., 17 (1995) 57.
5. T. Gentzis, F. Goodarzi and A. Hickinbotham, Ener. Sour. (1995) in press.
6. F. Goodarzi and D.J. Swaine, Int. J. Coal Geol., 24 (1993) 281.
7. B. Hall, O. Lindqvist and E. Lungsrom, Env. Sci. and Technol., 24 (1990) 108.
8. D.H. Klein, A.W. Andren, J.A. Carter, J.F. Emery, C. Feldman, W. Fulkerson, W.S. Lyon, J.C. Ogle, Y. Talmi, R.I. Van Hook and N. Bolton, Env. Sci. and Technol., 9 (1975) 973.
9. H. Lee, T.O. Peyton, R.V. Steele and R.K. White, US EPA Report 600/7-77-082 (1979).
10. M.R. Martinez-Tarazona, G.P. Suarez-Fernandez and J.M. Cardin, Fuel, 72 (1993) 718.
11. J.P. McBride, R.E. Moore, J.P. Winterspoon and R.E. Branco, Oak Ridge Nat. Lab. Report ORNL-5315 (1973).
12. D.F.S. Natusch, J.R. Wallace and C.A. Evans Jr., Science, 183 (1974) 203.
13. L. Salmon, A.E.R. Toureau and A.E. Lally, Sci. Total Env. 35 (1984), 403.
14. I.M. Smith, Int. Ener. Agency Report CR/01 (1987) 87pp.
15. J. Tadmor, J. Env. Radioact., 4 (1986) 177.
16. U. Tomza and P. Kaleta, J. Radioanal. & Nucl. Chem. Lett., 107 (1986) 1.
17. US EPA Report 520/7-79-006 (1979).
18. D.M. White, L.O. Edwards, A.G. Eklund, D.A. Dubose and F.D. Skinner, Radian Corp. Austin, TX (1984) 358pp.

Latest developments in the utilization of coal mining wastes

J. González Cañibano

HUNOSA. Avenida de Galicia,44. Oviedo 33005. Spain

This report summarizes recent studies carried out on coal mining wastes (minestones) of Spain. These studies proved that such wastes can be used as filling materials in reinforced earth structures, capping layers of roads, substratum in hydroponic cultures and fuel.

1. INTRODUCTION

As a consequence of the many and different problems arisen by coal mining wastes, in most countries concerned several researches have been carried out in order to use such wastes as raw material in different fields: mine filling, brick manufacturing, obtaining of cement, construction of road, highway and railway embankments, etc. (1).

However and because of the fact that the above-said applications do not solve once and for all the problems related to mining coal wastes and that these show other properties which were not being used, several studies have been carried out -the results of which are summarized in this report- with the aim of searching for new industrial applications which should help to solve and/or minimize the problems arisen by wastes, to create new business and jobs, to make a better use of materials and energy that were being wasted, etc.

2. REINFORCED EARTH

Throughout 1993-1994 a study was carried out in order to prove the technical feasibility of the utilization of coal mining wastes as a filling material in reinforced earth structures. In this study, besides determining the geotechnical and electrochemical properties of the aforementioned materials, corrosion tests were carried out on different reinforcing elements and a full scale filling with reinforced-earth walls was constructed for the purpose of confirming the results obtained both in laboratory tests and in corrosion tests and determining the placing conditions of minestones. The reinforced earth walls were of two types: a) Freyssisol system with prestressed concrete flakes and Parawebb-SS reinforcements like the ones that were used in the corrosion tests and b) geomesh wall using the Arco process.

The filling was 20 m long, 10 m wide and 2 m high. Coal mining wastes from

two heaps were used as filling material. Besides the reinforcing elements corresponding to the two walls, 16 metal band pieces of 1 m were placed inside the filling. The said pieces were like the ones that were used in corrosion tests. In order to determine whether coal wastes originated combustion processes inside the filling, 7 thermocouples were placed at different heights. After completing the construction, in order to simulate real traffic, the filling was subjected to 3,085 passes of a truck having an axle of 10.5 tons.

Control tests were carried out before and after the construction of the structure. The behaviour of the minestones proved completely satisfactory.

In 1994, in the Ujo-Caborana road (Asturias, Spain), a reinforced earth structure was constructed using 120,000 t of coal mining wastes.

3. CAPPING LAYERS

Researches are being carried out since a few years in the field of the utilization of alternative materials such as coal mining wastes for their utilization in capping layers of roads (bases and subbases). This would allow the traditional materials to be reserved for those uses in which it is more difficult to replace them and, moreover, meets the environmental requirement of using wastes as raw material.

3.1. Minestones stabilized with cement

Since from the characteristics and properties of unburnt minestones it is deduced that their use in the upper layers of roads is not advisable without a previous treatment, researches were carried out in order to determine both the feasibility of their use, after stabilizing them with cement, in bases and subbases and the optimum conditions for their utilization.

The laboratory tests, which produced successful results, led to the construction of a 4.5 km long subbase in the Baiña-Mieres section of the Oviedo-Campomanes highway (Asturias-Spain) in which 53,000 t of washery coal wastes stabilized with 6% of cement were used.

3.2. Aggregates

In order to obtain aggregates from minestones, a study was carried out and it proved that:

- Burnt minestones, after they are grinded to sizes smaller than 50 mm, can be used as a material for subbases bearing any type of traffic and also as artificial ballast.
- Unburnt minestones, after removing the sizes smaller than 25 mm and after grinding them up to sizes smaller than 50 mm, can be used as a subbase material in roads designed to bear light and medium traffic.

With this view, a plant has been constructed in Asturias. It is located at the foot of the Reicastro Heap and produces granular materials from minestones whose properties are summarized in Table 1.

The plant started production in November 1993 and has supplied 86,400 t of aggregates.

Table 1
Geotechnical properties of burnt minestones

Test	Value
Plasticity	Non plastic
Sand equivalent	65-78
Modified Proctor	
• Maximum density	1.95-1.98 g/cm³
• Optimum moisture	11.5-13.5 %
C.B.R. Index. Modified Proctor	50-110
Los Angeles	< 35
Specific weight	2.62-2.64 g/cm³

4. FUEL

Coal mining wastes, with coal distributed throughout their mass, show a higher calorific value ranging from 1,000 kJ/kg to 9,000 kJ/kg depending on the type of waste and on the coal produced by the coal basin, which means that very important quantities of energy are being wasted.

The studies carried out in order to make use of such energy proved the technical feasibility of combustion of coal mining wastes in fluidized bed. The influence of the different operating variables involved in the process, i.e., combustion temperature, bed height, fluidization speed, addition of limestone, etc. have also been studied.

HUNOSA has constructed in Mieres (Asturias, Spain) a power station which started operating in 1994 equipped with circulating fluidized bed boiler with an output of 50 MWe and where a mixture of coal mining wastes from heap (60%), wood wastes and run of mine coal (40%) are used as a fuel. This makes possible an annual consumption of about 250,000 t of coal mining wastes with an ash content of 80%.

5. SUBSTRATUM IN HYDROPONIC CULTURES

In 1993 was started a project in which two lines of greatest interest are being developed. For the first time in the world, coal mining wastes are used as:

- Substratum in hydroponic cultures for the production of vegetables
- Basic component for growing ornamental plants in containers by means of fertilizing irrigation.

The results obtained led to undertake the construction of a greenhouse with a surface area of 10,000 m² for the production of tomatoes using the hydroponic culture technique and where coal mining wastes will be used as a substratum because of the fact that the tests that were carried out resulted in crops amounting to the same quantities as those obtained using traditional substrata, such as rock wool and perlite, that are more

expensive than coal mining wastes.

On the other hand, an installation of 20,000 m² is going to be constructed for the production of ornamental plants using coal wastes as a basic component for their growth.

Photo 1 shows a tomato plantation in hydroponic culture in which coal mining wastes are used as substratum.

REFERENCES

1. J. González Cañibano and R. Madera; 9th Mining and Metallurgy International Congress. Vol. 4, 397. León (Spain), 24th-28th of May 1994.
2. F. Pardo, J. González Cañibano and M. Torres. III National Symposium on Road Geotechnics. Vigo (Spain), 28th-30th of September 1994, 531.
3. S. Esteras, R. Jiménez, J.L. Ibarzábal, J. González Cañibano and A. Ruíz. Civil Engineering, nr. 957 (1994).



Photo 1. Tomato plantation using coal mining wastes as substratum in hydroponic culture.

Application of coalcontaining waste in production of brick and expanded clay aggregate

E.J.Galpern

Institute of Industrial Construction

F1.81,151, 50-years USSR str., 340100, Donetsk, Ukraine

The past years the waste of coal extraction and preparing are applied in the production of burning building materials, such as ceramic brick, expanded clay aggregate and agglomerite, as well as main raw material and additions.

1. OBJECTS OF INVESTIGATIONS

The technology of waste preparation comes to the raw material crumbling up to a certain size and to the half finished product preparation. The process excess carbon and sulfur elimination, which are obstructing to the normal agglomeration or swelling of mineral component of the waste represents the main complicity at a such preparation. That decreases considerably the quality of finished production. The ceramic brick with carbon not completely burned off in the form of coke residue, as a rule, is characterized by a low frost-resistance.

The swelling at burning of granulated waste containing more than 1,5-3% of carbon is decreased in 2-3 times that does not permit to obtain porous aggregates with a poured density less than 500 kg/m³.

The process of surplus carbon elimination needs considerable time expense that decreases productivity of the process and it's technical and economic indexes.

The rock produced by mines and coal-preparation factories is characterized by carbon content by a high-degree of heterogeneity. That's why the elaboration of methods of considerable carbon content decreasing before stage of raw material mixture preparation and the stabilization of this index are the main problems of technology.

To regulate the carbon content in furnace charge, it is necessary first of all to know it's distribution in raw material.

It has been known that with rocks size increasing the carbon content is decreased in it, that is related to elevated coals size which are more crumbled up at the extraction than clay and sandy-clay rocks, and they come into smaller fractions.

Especially it is characteristic for rocks accompanying high-rank coals.

It has been also known that the coal and coal-mineral aggregations as well as the rock saturated by coal, have a less density than "pure" rock and they are concentrated in preparation waste by density less than 2200 kg/m³.

These well-known properties of carbon distribution in the waste of coal extraction and preparation were not used in technology of raw material preparing for production of building materials until last time.

To develop this direction we have carried out investigations of matter composition and technological properties of separate fractions size and density of the rock of a series of the largest coal preparation factories of Donetsk basin.

2. EXPERIMENTAL

The results of analysis realized showed that the main carbon mass is concentrated in rock fractions by size less than 30-40 mm and density less than 2400 kg/m³. The oxides distribution in the mineral part of some classes of sizes and density is practically the same, excluding fraction by density of more than 2,6-2,8 kg/m³, in which considerable quantities of iron oxide (up to 60%) and sulfur (up to 30%) are concentrated.

The X-ray phasic analysis of coal preparation waste 46 factories of Donetsk region demonstrated that hidromica, caolinite and quartz are the principal rock-forming minerals. In the rocks of 19 factories a considerable predomination of hidromica takes place, rocks of 7 factories are characterized by kaolinite predominate, in other ones the kaolinite and the hidromica are in equal parts.

The regularities of carbon distribution established experimentally in the coal preparation waste and technological characteristics of separate fractions of rock size and density demonstrated the necessity of utilization of these properties of raw material at its preparing to be used in the production of building materials.

One of such solutions was an isolation from the rock total mass of low-carbonous fractions ($C_{org} \leq 3-8\%$) with their following processing into ceramic brick, expanded clay aggregate and agglomerate by technological schemes, accepted in these productions.

By second solution the raw material was divided by carbon content by fractionating by size or density, high carbonous part of raw material ($C_{org} \geq 18\%$) was burned off in furnaces of low temperature fluidized bed with using of the heat in main technological process or in boiler-utilizator. The mineral residua obtained after burning off ($C_{org} \leq 2\%$) and low-carbonous part of raw material ($C_{org} \leq 6-10\%$) were proportioned in needed ratio, together were crumbled up and the half-finished product the brick or the granulate was prepared from the obtained mixture.

The efficiency of this variant of technology is conditioned by that waste organic part is used as low-grade fuel for obtention of technological heat or vapor, and the mineral one - for obtaining of main product. The method permits to regulate enough precisely the carbon content in raw material mixture, serving in preparation of half-finished product by mixing in given proportion of the mixture components.

The process of burning of rocks high-carbonous fractions in low-temperature fluidized bed is well studied and verified on the industrial furnaces installations. The carbon essential mass (80-90%) is burned off for 5-7 minutes in this bed at temperature 800-900° C. The ash residua contain not more than 1,5-2% of carbon.

3. CONCLUSIONS

The building materials of high quality have been obtained from raw material mixtures on the basis of waste, such as: ceramic brick by resistance at pressing of 15 MPa, frost-resistance more than 25 cycles; expanded clay aggregate gravel with poured density of 450 kg/m³, strength at pressing in cylinder of 2,2 MPa and frost-resistance of more than 15 cycles; agglomerite with poured density up to 600 kg/m³.

The ash residua of the rock high-carbonous fractions burning can be successfully used in production of binding materials, silica brick, and as a small aggregate in concretes.

The projects of enterprises by waste processing into building materials using described methods of raw material preparation have been elaborated. Thus, in the project of shop on expanded clay aggregate gravel production by power of 174 000 m³ per year the obtention of 5-7 tons of vapor per hour at burning of high-carbonous fraction of the raw material is envisaged.

The substitution of clay raw material or waste of coal preparation in the production of building materials provides an important economy of fuel and raw material resources, it permits to ameliorate ecological situation in coal-extraction regions, and also to reduce the deficiency of materials in building.

This Page Intentionally Left Blank

Phase composition of coal mining and preparation wastes and its role in determining the trends of their usage.

G.B.Skripchenko^a, R.Ya.Kleyman^a, M.Ya.Shpirt^a, I.M.Shchadov^b

^aFossil Fuel Institute, 29, Leninsky prospect, 117910, Moscow, Russia

^bStock Company "Vostsibugol", 4, Sukhae - Bator street, 66474, Irkutsk, Russia.

Coal wastes, on the one hand, are a valuable mineral raw, on other hand, they are nothing else, but wastes of mining coal, inflicting damage to the environment. Researches, performed in Russia and abroad, have indicated that coal wastes may be utilised in different ways: either as the major raw, or fuel mineral additions [1].

In practical examination to determine trends of coal wastes processing conventional analysis are used - chemical and petrographic ones, but they do not yield enough information to determine the trends of their utilisation.

It is difficult to make any forecasts concerning coal waste utilisation on the base of the results of chemical analysis, as its data do not reflect the fact, of occurrence of one and the same oxide as useful, neutral, or undesirable for processing. For example, iron oxide may occur in hydromica, siderite, pyrite; aluminium oxide may be an inclusion of kaolinite, hydromica, montrillonites and feldspars.

More reliable in this respect are the data on phase composition of coal wastes, which are obtained, for example, in the result of petrographic analysis. But coal wastes are specified as multicomponent associations: they may include different classes (8 - 10) of minerals both argillaceous (kaolinite, hydromica, montmorillonites, chlorites, feldspars) and non-argillaceous (quartz, pyrite, calcite, siderite, dolomite, gypsum and others) ones. Therefore, petrographic analysis of phase composition is also not sufficiently informative concerning detailed determination of the components, - such as argillaceous minerals, playing this or that role in technological processes.

The application of X-ray analysis allows to completely solve the problem stated and to determine a set of minerals existing in coal wastes, their ratios and absolute quantity.

Taking into account the specified composition of coal wastes, complex method have been developed, allowing to quantitatively determine the major mineral components composing them [2 - 5]. The methods include several steps:

- 1) preparation of specimens for the analysis by using physical, chemical, and thermal methods of simplification of their composition in order to qualitatively identify individual components;

- 2) establishment of relationship between the intensities of characteristic reflection bands of minerals and their mass concentrations in mixture;

- 3) quantitative assessment of content of minerals and compiling of the general balance (on the base of determination of proportion of characteristic reflection bands intensities of minerals, calculation coefficients and chemical analysis data).

Thus, in the process of determination of composition of coal wastes a consequent information is obtained about a qualitative composition of the specimen, relationship

of its main components and, finally, about the quantity of the components. The data obtained are of technological importance at the stages of trying out the processes of treatment.

Ranges of detection for argillaceous minerals are 5 - 7 % , quartz - 1.5 %, pyrite, siderite, calcite, dolomite - 1.5 - 3.0 %. The accuracy of determination for argillaceous and non-argillaceous minerals is 2 - 5 % and 1.5 - 2.5 % correspondingly.

By using the method suggested the composition of samples of mining and preparation wastes has been determined for many open pits and preparation factories of the main coal basins of Russia (Kuznetsky, Donetsk, Kansk-Achinsk, Pechorsky, Irkutsky, Submoskavian, South-Yakutsky, Sakhalinsky) as well as CIS Countries [6, 7].

The examination performed has indicated, that for different basins different combination of minerals (quantitative and qualitative) is observed. Table 1 presents the ranges of mineral contents for a number of basins.

Table 1
Content of minerals for coal wastes of different basins of Russia (wt. %)

Mineral	Basins		
	Kuznetsky	Donetsky	Kansk-Achinsky
Kaolinite	6 - 25	6 - 30	19 - 35
Chlorite		3 - 9	
Hydromica	16 - 40	24 - 55	13 - 17
Montmorillonite		0 - 15	18 - 30
Quartz	6 - 41	11 - 33	21 - 35
Feldspars	4 - 15	2 - 13	3 - 14
Siderite	1 - 10	0 - 5	2 - 7
Calcite	1 - 9	2 - 7	1 - 7
Dolomite	2 - 7	0 - 2	
Pyrite	0 - 3	3 - 9	1 - 2

The quantitative data obtained allow to determine phase composition of coal wastes for coal wastes for individual enterprises, as well as the nature of mineral distribution for basins, ranges of their occurrence, prevailing minerals.

Knowledge of phase composition of coal wastes, obtained by means of X-ray analysis, allow to choose optimum trends of their usage depending on mineral relationship: production of bricks, agloporite, fire resistant materials, special ceramics and others. Hereat, of great significance is the content of organic carbon, sulphur, oxides of iron, aluminium, calcium and magnesium and others.

Table 2 presents the limiting values for phase composition and carbon and sulphur limits for different routes of coal waste processing.

Table 2
Limiting factors for different trends of using coal wastes

Trend of usage	Phase composition	Content of organic carbon	Sd_t
Brick	Kaolinite + hydromica + montmorillonite > 40, pyrite < 2.2, calcite and dolomite < 10	< 8	< 1.5
Agloporite	Kaolinite + hydromica + montmorillonite > 40, pyrite < 3.7	8 - 12	< 2.0
Hydrotechnical construction	Hydromica + quartz + feldspars > 80, pyrite < 1.5, siderite < 5, kaolinite < 10	< 20	< 0.5
Fire-resistant materials	Montmorillonite < 10, pyrite < 1.5, calcite and dolomite < 3, siderite < 5	8 - 12	< 0.5

It should also be noted, that in using new forms of raw, as well as in utilising coal wastes for the production of building materials, the presence of natural radionuclides (NRN) in them is necessary to be determined. Hereat, the content of natural radioelements in construction materials should not exceed (Bq/kg): ^{40}K - 4810, ^{232}Th - 259, ^{226}Ra - 370 to secure radioelement safety of the population. In the assessment of coal wastes as the raw for brick production, implied to build residential houses for a mixture of radioelements stated the following condition should be fulfilled: $C_{\text{Ra}}/370 + C_{\text{Th}}/250 + C_{\text{K}}/4810 < 1$.

REFERENCES

1. M. Ya. Shpirt, Wasteless Technology. Utilisation of Fossil Fuel Mining and Processing Wastes. Russia, Moscow, 1986.
2. R. Ya. Kleyman, G. B. Skripchenko, M. Ya. Shpirt et al., Solid Fuel Chemistry, No 2 (1986) 27.
3. Yu. V. Itkin, R. Ya. Kleyman, G. B. Skripchenko et al., Solid Fuel Chemistry, No 3 (1988) 111.
4. R. Ya. Kleyman, G. B. Skripchenko, M. Ya. Shpirt et al., Solid Fuel Chemistry, No 3 (1989) 130.
5. R. Ya. Kleyman, G. B. Skripchenko, M. Ya. Shpirt et al., Solid Fuel Chemistry, No 6 (1991) 135.
6. M. Ya. Shpirt, R. Ya. Kleyman, G. B. Skripchenko et al., Solid Fuel Chemistry, No 4 - 5 (1994) 169.
7. G. S. Golovin, G. B. Skripchenko, I. M. Shchadov, Solid Fuel Chemistry, No 6 (1994) 57.

This Page Intentionally Left Blank

Briquetting of brown coal with hydrolized lignin

V.I.Saranchuk, L.Ja.Galushko, L.V.Pashchenko and V.A.Khazipov

L.M.Litvinenko Institute of Physical, Organic and Coal Chemistry

National Ukrainian Academy of Sciences

R.Luxemburg street, 70, 340114, Donetsk, Ukraine

In present the briquetting of coal fines becomes one of priory directions in the solution of problem of provision of needs of people with solid fuel because of deficiency in energetic resources in Ukraine [1]. One of possible ways of developing production of briquets as consumer fuel is the utilization of secondary material resources as additions, in particular, waste products of hydrolysis production-lignin [2].

1. OBJECTS AND METHODS OF INVESTIGATIONS

The aim of the work was studying of possibilities of hydrolized lignin utilization ($C^{daf}=59,9\%$) as addition from 10 up to 50% at brown coal briguetting of Ukraine ($C^{daf}=62,3\%$, $A^d=20,7\%$).

The presence of chemical interacting between brown coal and lignin at briquetting has been established by methods of X-ray structural analysis, EPR and IR-spectroscopy, derivatography and analysis on oxygen functional groups contain.

2. EXPERIMENTAL

The data of radiostructural analysis testify the better ordering of lignin

structure comparing to brown coal: the greater ratio of height of principal diffractonal maximum to the width (8,1 and 1,0 respectively).

At pressing the lignin structure is underwent to more considerable reconstruction than the brown coal structure: the height of principal diffractonal maximum of lignin is decreased in two times greater than brown coal one, the value of interlayer distance and the banches thickness is considerably decreased.

The change of phenol and carboxylic functional groups contain indicates the carryng out of chemical processes at comun briquetting of brown coal and lignin, as well as the paramagnetic centers contain increasing in briquets by comparison with their additive quantity.

The change of intensities of adsorption bands on IR-spectra of briquets in the region of 3400 , 1700 , 1650 , 1280 and 1200-1000 cm^{-1} , the change of durability and quantity of hydrogen bonds in briquets by comparison with brown coal and lignin indicate the reconstruction of structure at mixtures briquetting, depending on their composition. The great contain of polar groups in lignin structure and elevated quantity of hydrogen bonds in brown coal structure favorise a more resistant contact of coal grains with lignin at briquetting owing to specific and no-specific interacting.

It has been established by method of derivatography that at briquets heating containing mixtures of coal and lignin the maximum separation of organic matter decomposition and displacement of maximum of water isolation in more high temperature region.

The introduction in briquets of brown coal from 10 up to 50% of lignin leads to the increasing of resistance of confinement of bonded water in briguets. In this case the deviation of additive rate of briguets organic mass decomposition on the side of increasing of thermal stability that could testify structurizing role of lignin in brown coal briguets an hardening of intermolecular interaction at common briguetting of brown coal with lignin. The greatest deviations from additivity are those of briguets with lignin contain of 10-20% (Figure).

It has been established that the addition of lignin 20% to the brown coal is the most optimal at briquetting. The industrial testing showed that the addition of lignin 20% ameliorates the briquets quality by all the indexes, in this case the briquets mechanic resistance is increased from 70,0 up to 79,1%.

At storage of brown coal briquets on the storehouses more than 40% of them are distructed and become coal fines. It has been established with a help of research works carried out, that chemical transformations leading to the change of structural-group composition, paramagnetic centers and oxygen-containing groups take place in

briquets at storage.

The lignin is more underwent the change at storage than brown coal. The composition changes are minimal at storage of briquets with lignin contain of 20%. Besides, the investigations demonstrated that the increasing of lignin quantity in briquets from 10 up 50% leads to the growth of water-absorption from 19,4 up to 39,9%, that's why additions of lignin to the coal should not be great- 10-20%. To study the briquets state at storage the piles were embedded.

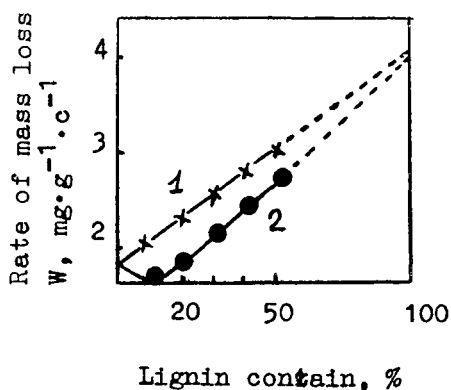


Figure. Dependence of the decomposition rate of briquets organic mass, calculated by rule of additivity (1) and factual one (2) on the lignin contain.

After one month of storage the lowest contain of fines (< 25mm) and water-absorption were in the pile from briquets with addition of lignin 20%, when the mass loss of briquets with a higher lignin contain and without it consisted of 30-40%.

3. CONCLUSIONS

Thus, it has been established that the addition to the brown coal of 20% of hydrolizing industry waste lignin - is the most optimal at briquetting and storage. The lignin plays a structurizing role and reinforces intermolecular interactions. The brown coal briquets with additions up to 20% of lignin are less underwent the destruction

at atmospheric action than without additions and with a higher contain of lignin and they could be stored practically without changes up to half-year.

REFERENCES

1. T.Sviatets. Technological utilization of brown coals, Moskow, Nedra. 1985, 207 p.
2. V.Saranchuk, L.Pashchenko, V.Khazipov. Coal of Ukraine, 1992 , p.53

Experimental study on the characteristics of gangue briquetting combustion in industrial boilers

Zhang Bailiang, Zhang Quanguo and Liu Shengyong

Energy Engineering Laboratory, Henan Agricultural University, Zhengzhou, HN450002, People's Republic of China

It is recognized that the gangue briquetting combustion (GBC) in some fixed-bed furnaces is an efficient method in order to save resources and avoid polluting environment in China^{1,2}. Therefore, a suitable combustion-promoting additive is indispensable for GBC to be very reliable and efficient. In China biomass from agriculture and forestry may be an appropriate additive because it is widely available and relatively cheap. To examine the combustion-promoting effect of biomass additives on gangues the relations between the biomass content and the volatiles or combustion weightless rate (CWR) of gangue briquettes have been examined in this paper.

1. EXPERIMENTAL

1.1. Gangue Briquette Samples

The proximate analyses of coals, gangues, maize straw and saw dust are given in Table 1. Sampling, size reduction, division and mixing of the sample was carried out according to Chinese Standards GB212, GB474 and GB475. All of the briquettes were briquetted satisfactorily at 14.7 MPa and the optimum moisture (10%), to give cylindrical samples (Diameter = 21mm, Length = 18mm, Single mass = 10g).

1.2. Measurement

According to Chinese Standard GB212, all of the experiment on the volatiles (air dry basis) of the briquette samples were carried out using SX 2-4-10 Resistance Furnace, TG328B Photoelectric Balance, china crucible and dryer etc³. The measurements of CWR of gangue briquettes were carried out in a constant temperature combustion apparatus using a temperature of 850°C. CWR is defined as follows:

$$\text{CWR} = (\text{A} - \text{B}) / \text{A} \times 100$$

Where A is the original mass of the gangue briquettes to enter into the combustion apparatus, B is the mass of the remainder when the gangue briquettes burn for 30 minutes or 45 minutes inside the combustion apparatus.

Table 1 Proximate analyses of the samples

	Pingdingshan gas coal	Dengfeng meagre coal	Gangues	Maize straw	Saw dust
Moisture (as fired basis, wt %)	5.9	5.8	3.9	13.2	11.4
Ash (dry basis, wt %)	28.4	22.9	73.8	8.7	2.0
Volatiles (dry, ash free basis, wt %)	22.3	12.7	8.8	74.5	76.0
Fixed carbon (as fired basis, wt %)	46.1	62.6	18.2	8.1	12.9
Calorific value (as fired basis, MJkg ⁻¹)	23.39	23.00	6.57	12.56	15.24

2. RESULTS AND DISCUSSION

2.1. Influence of Biomass Additives on the Volatiles of Gangue Briquettes

The relation between the mix share of biomass additives and the volatiles of the gangue briquettes are shown in Fig. 1, which shows that the volatiles of gangue briquettes increases obviously as the biomass content adds.

When the mix share of biomass additives is 4% the volatiles of the gangue briquettes are 11.7% (i. e. biomass is maize straw) and 12.7% (i. e. biomass is saw dust) respectively, being close to the volatiles of Dengfeng meagre coal (11.9%). It makes the ignitibility of the gangue briquettes come up to that of meagre coals (i. e. lower grade bituminous coals).

When the content of biomass additives is 10%, the volatiles of the gangue briquettes are close to that of Pingdingshan gas coal (17.2%). They are 15.4% (mixing maize straw additives) and 19.4% (mixing saw dust

additives) respectively, which makes the ignitibility of the gangue briquettes in furnaces be close to high grade coals in industry and can meet the needs of various industrial furnaces for the performance of fuels.

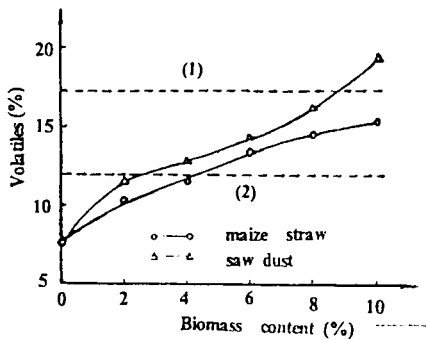


Fig1. The relation between the volatiles of gangue briquettes and the biomass content. (1), the volatiles of Pingdingshan gas coal briquettes; (2), the volatiles of Dengfeng meagre coal briquettes.

2. 2. Influence of Biomass Additives on CWR of Gangue Briquettes

CWR is a significant parameter judging the combustion process of the gangue briquettes. The larger CWR is, the faster the burning rate and the

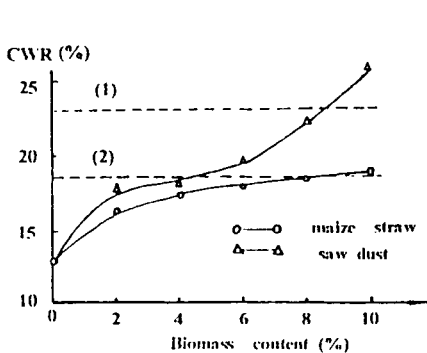


Fig2. The relation between CWR and the biomass content. Burning time: 30 min, Temperature: 850°C. (1) CWR of Pingdingshan gas coal briquettes; (2) CWR of Dengfeng meagre coal briquettes.

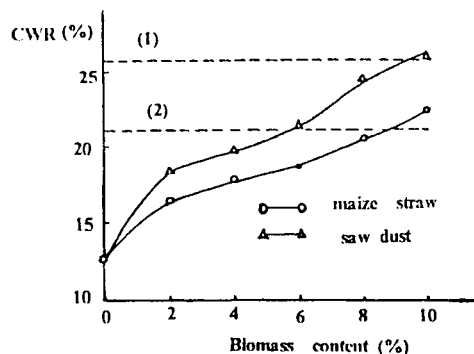


Fig3. The relation between CWR and the biomass content. Burning time: 45 min, Temperature: 850°C. (1) CWR of Pingdingshan gas coal briquettes; (2) CWR of Dengfeng meagre coal briquettes.

more complete the combustion process of the gangue briquettes will be. Fig.

2 and Fig. 3 are the relation curves between CWR and the mix share of biomass additives. Obviously, CWR increases as the biomass content adds, which shows that biomass may make the complete combustibility and CWR be higher to the advantage of GBC.

When the gangue briquettes burn for 30 minutes inside the combustion apparatus using a temperature of 850°C , CWR of the gangue briquettes with saw dust additives of 6% or maize straw additives of 8% is 19.7% or 18.4% approaching that of Dengfeng meager coal (CWR = 18.5%), When the mix share of saw dust reaches 10%, CWR of the gangue briquettes is 25.8% exceeding that of Pingdingshan gas coal (CWR=23.0%) and coming up to the combustion property of high grade bituminous coals in industry. the experimental result shown in Fig. 3 is similar to that shown in Fig. 2.

3. ACKNOWLEDGEMENT

The authors thank Henan Province Environmental Protection Bureau of China for providing some financial assistance.

REFERENCES

1. Hanchen, W. Coal Processing and Comprehensive Utilization, 1(1992)7.
2. Quanguo, Z. Resources Economization and Utilization, 3(1991)23.
3. Yen, S. Power Fuel Analysis, Power Publisher, Beijing, China, 1984.

Metalliferous coals: a new potential source of valuable trace elements as by-products

V.V. Seredin^a and M.Y. Shpirt^b

^aInstitute of the Geology of Ore Deposits, Petrography, Mineralogy and Geochemistry (IGEM), Russian Academy of Sciences, 35 Staromonetnyi, 109017, Moscow, Russia*

^bInstitute of Solid Fuel, 29 Leninskiy pr., 117910, Moscow, Russia

Reported are new data on metalliferous coals, which are high in several valuable trace elements (VTE) and were found in a number of Siberian and Russian Far East deposits. The paper reports VTE concentration levels and their modes of occurrence in the metalliferous coals and demonstrates the possibility for extraction of rare and noble metals as by-products.

1. VTE CONCENTRATION LEVELS AND GEOCHEMICAL TYPES OF THE METALLIFEROUS COALS

The data cited in Table 1 indicate that the VTE contents of the metalliferous coals are 1 - 3 orders of magnitude higher than those of the ordinary coals [5,6,], and the VTE contents in the ashes of the former coals are comparable with or higher than those of the conventional-type ores. Metalliferous coal seams often contain VTE of a variety of types and, hence, can be regarded as a complex raw material. Seams with the following VTE assemblages were detected on the Russian coal deposits: Ge - Ga (Rakovka), Ge - W (Bikin, Shkotovo,), Ge - W - Mo (Pavlovka), Ge - W - REE, Ge - Zr - REE (Black Stone), Nb - Zr - REE (Shevyakova, Sibirinskii), Ag - Au - PGE (Bikin), Au - PGE (Zavyalovskaya), Au - PGE - REE (Pavlovka). The occurrence, on some of the deposits, of spatially separated seams and seam groups of diverse geochemical types allows for the selective mining and processing of metalliferous coals with different VTE.

*Research grant from the Russian Foundation for Fundamental Research, project no. 93-05-08847; sponsoring agency - Primorskugol Far Eastern Coal Company.

Table 1

VTE concentration ranges in the metalliferous coals from some Russian coal deposits (Ag, Au, PGE in ppm, other VTE: coal in ppm, ash in wt %)

VTE	Contents		Deposits
	coal	ash	
Ag	3 - 40	20 - 120	B, Bl, P, Shk
Au	0.1 - 1.2	0.5 - 10.2	B, P, Rt, Z
PGE	0.2 - 1.4	0.5 - 13.6	B, P, Rt, Z
Ga	30 - 100	0.01 - 0.05	R
Ge	100 - 3200	0.1 - 0.8	B, Bl, P, R, Shk
REE + Y	500 - 1500	0.2 - 1.1	Bl, P, R, Rt, Shv, S
Nb	50 - 250	0.07 - 0.2	Bl, Shv, S
Zr	200 - 1100	0.2 - 0.7	Bl, Shv, S
Mo	100 - 500	0.1 - 0.3	P
W	100 - 600	0.1 - 0.6	Bl, P, R,

Deposits: B - Bikin, Bl - Black Stone, P - Pavlovka, R - Rakovka, Rt - Rettichovka, S - Sibirginskii, Shk - Shkotovo, Shv - Shevyakova, Z - Zavyalovskaya

2. MODES OF OCCURRENCE OF VTE IN THE METALLIFEROUS COALS

Analysis of VTE distribution in gravity fractions, experiments on acid leaching and extraction of humic acids, and SEM-EDS analysis have demonstrated that most of the elements examined occur in the metalliferous coals in two principal forms: fine-dispersed authigenic minerals and compounds sorbed on organic material and mineral particles.

2.1. Mineral forms

Fine-dispersed (0.5 - 10 mkm) VTE and VTE-bearing minerals are present in most of the examined types of metalliferous coals in assemblage with pyrite, barite, and alkali chlorides (halite and sylvite). Specific morphologies and chemistries of these minerals and their relationships with the organic and mineral matters of the coals indicate their authigenic origin.

Approximately 50 mineral varieties have been detected by the present time. The most interesting of them are platinum minerals (cooperite, isoferroplatinum, and native platinum), all of them have not been previously detected in coals with even very high abundances of these metals [7], and unusual REE-bearing minerals, which selectively concentrate individual REE.

Platinum minerals were determined in the coals and fossil wood in assemblage with sulfides, native metals, and intermetallic compounds of

Fe, Ni, Co, Cu, Zn, Sn, Bi, Ag, and Au. These minerals often fill in microfractures in fossil wood on the Pavlovka deposit.

REE minerals of the enriched coals are dominated by phosphates, aluminophosphates, and fluorcarbonates, whereas phosphorus- and fluorine-free phases (perhaps oxides and hydroxides) occur more rarely. Of these phases, a special attention is deserved by the minerals of predominantly individual REE. For example, the REE-bearing coals contain minerals consisting mainly of Gd with minor (1 - 2%) Sm and Eu, and minerals of Dy (containing 1.5 - 3.0% Gd and Tb). Fe-Nd and Fe-Dy phases were found in assemblage with halite. A mineral containing, in addition to Sm, only Cl and O was encountered in fossil wood as an overgrowth on fungal hyphae. The occurrences of such minerals in the coals and fossil wood points up to the existence of a natural mechanism thorough separating REE in organic materials.

2.2. Sorbed forms

Many VTE occur in the examined metalliferous coals as a variety of organic compounds or are sorbed on clay and, to a lesser extent, other mineral particles. Our experiments indicate that the ratios of the forms vary significantly for different VTE. Moreover, the percentages of the sorbed forms and their relationships with the mineral forms can vary remarkably even for the same elements as a function of ash contents and metamorphic rank of the coal organic matter.

For example, it was established that 75 - 96% of the total germanium contents of the metalliferous lignites occur in the form of complex humates, and 3 - 24% are germaniumorganic compounds. The percentages of these forms in the subbituminous coals are 28 - 60 and 38 - 70%, respectively. The bulk of germanium (85 - 90%) in the coaly clays occurs as complex humates and mere 2 - 9% are contained as germaniumorganic compounds. No more than 10% Ge is contained in silicogermanates, as an isomorphous component of pyrite, and all other forms [8].

The REE-bearing lignites and subbutuminous coals contain 30 - 40% of the total REE as complex humates and fulvates, which can be extracted with a NaOH solution. No less than 40 - 50% REE are thought to be contained in these coals as undetermined organic compounds, with the rest percentage falling on authigenic minerals and sorbed on the clay particles. The latter form, which was noted for the preferential concentration of LREE, seems to be the most important in coaly-clay and clay rocks of the partings and near-contact zones of the enriched seams.

Supposedly sorbed forms of noble metals, which pass into solution on the oxidation of the organic matter with HNO₃, were found in the metalliferous lignite and fossil wood. The percentages of such soluble compounds are: fossil wood: Au - 88%, Pt - 77%, Pd - 33%; lignite: Au - 40 - 70%, Pt - 20 - 66%, Pd - 0 - 65%.

Hence, the predominant VTE occurrence in the metalliferous coals in the form of sorbed compounds and authigenic minerals definitely indicates that they had been transported in the coal-accumulation basins in soluble forms. The origin of thick (up to 10 m) metalliferous coal seams evidently was only possible if the organic matter had been previously enriched during the peat-accumulation stages.

3. TECHNOLOGICAL ASPECTS OF METALLIFEROUS COAL TREATMENT

As is evident from our calculations, the recovering of VTE from metalliferous coals is profitable if the conventional techniques of organic matter utilization (preparation and combustion) are used. Our experiments demonstrate that 50 - 80% VTE pass into preparing concentrates of the coals, because VTE occur in the metalliferous coals as fine-grained minerals and sorbed forms. The VTE contents recalculated to their contents in the concentrate ashes are higher than those in the ashes of the coals themselves, because compounds of such ash-forming elements as Si, Al, Fe, etc. are generally incorporated in the concentrates in a lesser degree than nearly all VTE. Hence, the usually employed preparing procedure of metalliferous coals simultaneously serves as their dressing for VTE.

According to our thermodynamic calculations and experimental data, the studied VTE distribute between the fly ash and slag on combustion and cooling of the gaseous products to 100 - 120°C. Some VTE form gaseous compounds in the high-temperature zone and enrich the fly ash, whereas the others do not and concentrate in the slag. On this basis, VTE are classified into two groups: (1) Ge, Ga, Mo, W, Ag, Au (?), PGE (?); (2) REE and Y, Zr, Nb.

We worked out specified combustion regimes for each element of the two groups to attain their maximum possible enrichment in the fly ash and slag at satisfactory yields of the products. Studies performed on both pilot and industrial installations show that a combination of preparation and combustion methods of the metalliferous coals allow for a 16 - 25 times higher enrichment of the group 1 VTE in the fly ash and 5 - 10 times higher enrichment of group 2 VTE in the slag-fly ash mixtures with regard to their contents in the initial coals. If a metalliferous coals are high in a number VTE, their fly ash or a slag-fly ash mixture will be enriched in several VTE.

Additionally, specified combustion regimes of metalliferous coals were worked out that form such VTE compounds in the slags and fly ashes, which can be nearly completely extracted with weak (5 - 10%) solutions of mineral acids.

Hence, we consider metalliferous coals, as R. Finkelman and R. Brown [9] do, to be a new promising source of VTE as a by-product.

REFERENCES

1. M. Shpirt, *Physical and Chemical Fundamentals for Processing of Germanium Raw Materials, Metallurgiya, Moscow, 1977 (in Russian).*
2. V. Seredin, *Transact. USSR Acad. Sci., V.320, No 6 (1991) 1446-1450.*
3. V. Seredin, *Transact. Russian Acad. Sci., V.335, No 5 (1994) 634-636.*
4. V. Seredin, M. Povarennykh, M. Shpirt, *Abs. VII IPC (1994) 110.*
5. V. Valcovic, *Trace Elements in Coal, CRC Press Inc., Boca Raton, 1983.*
6. Y. Yudovich, *Trace Elements in Fossil Coal, Nauka, Leningrad, 1985, (in Russian).*
7. E. Van der Flier-Keller, *Econ. Geol., V.86, No 2 (1991) 387-395.*
8. M. Shpirt, V. Kler, I. Pertsikov, *Inorganic Components of Solid Fuels, Chemistry, Moscow, 1990. (in Russian).*
9. D.C. Peters (eds.), *Geology in Coal Resource Utilization, TechBooks, 1991.*

Analysis of forms of sulphur within coal, and minor and trace element associations with pyrite by ICP analysis of extraction solutions.

P. F. Cavender and D. A. Spears

Department of Earth Sciences, Dainton Building, University of Sheffield, Sheffield, S3 7HF, United Kingdom.

1. INTRODUCTION

A considerable amount of attention has been paid to the standard methods of analysis of total sulphur and forms of sulphur within coal. Both the British Standard [1,2] and the American standard [3,4] are similar in principal with the major problem being their indirect measurement of organic sulphur. This paper briefly reviews the standard methods and their problems, it then goes on to describe an alternative method which has been used to determine trace element associations as well as forms of sulphur.

2. STANDARD METHODS OF ANALYSIS OF TOTAL SULPHUR AND FORMS OF SULPHUR IN COAL

In both the British Standard (BS) method [1] and the American standard (ASTM) method [3] of the analysis of forms of sulphur in coal, a hydrochloric acid extraction is used to determine sulphate sulphur and a nitric acid extraction is used to determine pyritic sulphur. Alternative low-temperature (eschka mixture) and high-temperature methods are suggested in the BS [2] and ASTM [4] standards to determine total sulphur in coal. Organic sulphur in the standards is determined by difference.

Many workers have reviewed and investigated the problems with these standard methods of analysis [5-8], and a number of problems have been suggested. These include:

- a) density separation of pyrite during storage and unrepresentative sub-sampling;
- b) evolution of other acid species during the high-temperature determination of total sulphur;
- c) incomplete dissolution of sulphate during the HCl extraction;
- d) partial dissolution of pyritic and organic sulphur by the HCl extraction;
- e) magnetite (if present) is determined as pyritic iron and therefore pyritic sulphur;
- f) incomplete dissolution of pyrite during the HNO₃ acid extraction;
- g) the presence of iron sulphides not in the form of FeS₂;
- h) the presence of other sulphide minerals;
- i) the partial dissolution of organic sulphur by the HNO₃ extraction;
- j) error accumulation during the calculation of organic sulphur by difference;
- k) the presence of elemental sulphur which will ultimately be expressed as organic sulphur.

Many alternative methods have been suggested for the analysis of forms of sulphur in coal, and these have been reviewed elsewhere [5,9,10]. However a considerable number of these methods use complex analytical equipment which may not be readily available. It is usual for the validity of these new methods to be compared to results from the use of the standard methods, the procedures which they are actually attempting to improve upon. Although many problems exist with these methods, they are still perhaps the best available [5].

3. ALTERNATIVE METHOD OF ANALYSIS USING ICP-AES

During a study of sulphur and forms of sulphur in the Parkgate Seam, East Pennine Coalfield, UK, an alternative method of analysis was developed based on the BS Method [1]. The seam is from the Langsettian (Westphalian A), it is a multi-bed seam with a number of mappable plies and the variation in sulphur in the seam is almost entirely due to the concentration of pyrite [11].

Coal samples were processed with an additional distilled water extraction prior to hydrochloric acid and nitric acid extractions. This was done to determine water soluble sulphate sulphur as well as acid soluble sulphate sulphur. A single coal sample of approximately 1.0g was used instead of two sub-samples as suggested in the BS Method [1], 40ml of 5N HCl was used in the acid soluble sulphate sulphur procedure and 40ml of 2N HNO₃ to determine pyritic sulphur. The three resulting extraction solutions were then made up to volume for ICP-AES (inductively couple plasma atomic emission spectrometry) analysis. The resulting coal residue was analysed for total sulphur using the BS high-temperature method [2] which gives a direct determination of organic sulphur [12]. Organic sulphur was also determined by difference [1]. A similar method based on the use of ICP-AES has been proposed elsewhere [13], but data other than forms of sulphur were not discussed.

Extraction solutions were analysed for a number of major, minor and trace elements. Sulphate sulphur was calculated by addition of the sulphur present in the distilled water and the hydrochloric acid extraction solutions. The standard methods of analysis [1,3] calculate pyritic sulphur by determining pyritic iron and then recalculating it as pyritic sulphur assuming the 1:2 stoichiometry of pyrite (FeS₂). The use of ICP-AES analysis on the nitric acid extraction solution allows both iron and sulphur to be analysed and therefore the nature of the pyrite, as well as the amount of pyritic sulphur to be determined. All determinations show close accordance with the standard methods of analysis.

The advantages of this method of analysis over the standard methods include:

- a) a quicker and more convenient procedure using small sample weights if necessary [13];
- b) distinction of both water and acid soluble sulphates;
- c) the determination of the form of pyrite by the measurement of both sulphur and iron in the nitric acid extraction solution;
- d) the determination of the relationship between trace elements and pyrite by elemental correlations.

4. PYRITE COMPOSITION

Since both sulphur and iron have been determined in the nitric acid extraction solution the ratio of these elements can be calculated to investigate the composition and stoichiometry of

the pyrite. Figure 1 shows pyritic iron plotted against pyritic sulphur. The plot of actual data points is not the same as the theoretical line for pyrite. This deviation may be due to a number of factors such as: dissolution of non-pyritic iron in the residue (after the HCl procedure) producing excess iron. This appears unlikely however, as the correlation coefficient is extremely high and also because the ash content of the samples is variable which would reduce the correlation coefficient. The relationship may also be due to iron sulphide species with a stoichiometry of less than 1:2 iron to sulphur.

It appears from this relationship that organic sulphur is not significantly affected by the nitric acid extraction procedure as no excess sulphur has been determined over FeS_2 . Although it should be noted that organic sulphur is relatively minor when compared to pyritic sulphur in many samples [11]. Nevertheless the regression equation passes very close to the origin demonstrating little dissolution of organic sulphur (when $\text{Fe} = 0$, $\text{S} = 0.04\%$. Organic sulphur = $1.09 \pm 0.36\%$).

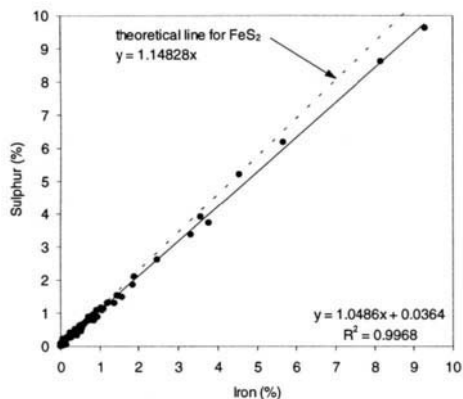


Figure 1. Relationship between iron and sulphur in the nitric acid solutions.

5. TRACE ELEMENT ASSOCIATIONS WITH PYRITE

Various potentially hazardous elements such as arsenic, lead, and mercury have commonly been cited as being associated with pyrite in coals [14,15]. The trace elements associated with pyrite have been determined by correlation of the concentration of these elements with pyritic iron present in the nitric acid extraction solution. Various elements have been found to have high positive correlations with pyrite including arsenic and lead. In addition cadmium has a positive correlation with pyritic iron (Fig. 2). Cadmium is commonly cited as being associated with sphalerite [14], however it has been found to be associated with pyrite also [16].

Although boron has an organic association in coal [14,15], it was found to have a highly positive correlation with pyrite in the Parkgate Seam (Fig. 3). This relationship is attributed to fact that both sulphur and boron increase in concentration in more saline waters, so the same swamp chemistry which causes high amounts of sulphur will also cause high amounts boron. The fact that these two elements should have a positive correlation has been noted previously [17].

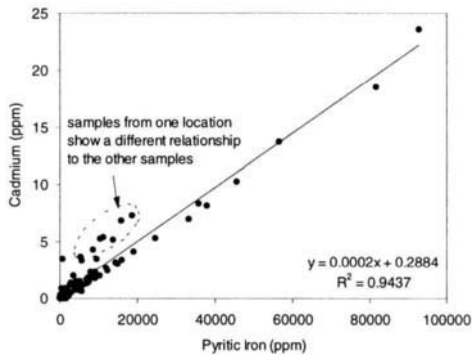


Figure 2. Cadmium plotted against pyritic iron for nitric acid extraction solutions from samples of the Parkgate Seam.

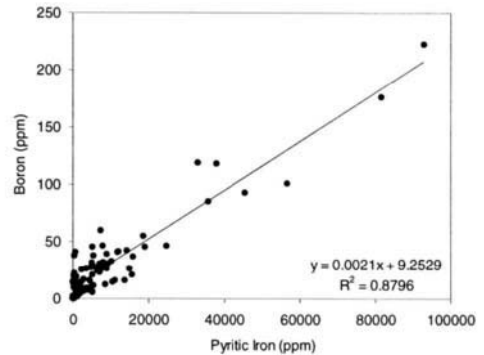


Figure 3. Boron plotted against pyritic iron for nitric acid extraction solutions from samples of the Parkgate Seam.

ACKNOWLEDGEMENT

Acknowledgement is made to the British Coal Utilisation Research Association Ltd. and the UK Department of Energy for a grant in aid of this research, but the views expressed are those of the authors and not necessarily those of BCURA or the Department of Energy.

REFERENCES

1. British Standards Institution, BS 1016: Part 6, 1977
2. British Standards Institution, BS 1016: Part 11, 1977
3. American Society for Testing and Materials, D2492, 1988
4. American Society for Testing and Materials, D3177, 1988
5. Markuszewski, R., *J. Coal Qual.* 1988, **7**, 1
6. Friedman, S. in 'Proceedings of the 1st international conference on the biological processing of coal', 1990, pp.1-14
7. Norton, G. A., Peters, R. E. and Chriswell, C. D., *Fuel Sci. Tech.* 1994, **12**, 749
8. Bottrell, S. H., Louie, P. K. K., Timpe, R. C. and Hawthorne, S. B., *Fuel* 1994, **73**, 1578
9. Davison, R. M., *Fuel* 1994, **73**, 988
10. Calkins, W. H., *Fuel* 1994, **73**, 475
11. Cavender, P. F., and Spears, D. A. in Symposium Series No. 138, Institute of Chemical Engineers, 1995, in press.
12. Riley, J. T., Ruba, G. M. and Lee, C. C. in 'Geochemistry of sulfur in fossil fuels', Symposium Series 429, American Chemical Society, 1990, pp.231-240
13. Eames, J. C. and Cosstick, R. J., *Analyst* 1992, **117**, 1581
14. Finkleman, R. B., in 'Atomic and nuclear methods in fossil energy research' (Eds R. H. Filby, B. S. Carpenter and L. Ragaini), 1982, pp.141-149
15. Finkleman, R. B., *Fuel Proc. Tech.* 1994, **39**, 21
16. Swaine, D. J., 'Trace Elements in Coal', Butterworths, London, 1990.
17. Banerjee, I. and Goodarzi, F., *Sed. Geol.* 1990, **67**, 297

Origin and fate of sulphur in Spanish coals

R. Gorchs^a, C. Catalan^a, J. Campà^a, P. Danishfar^a, L. Cabrera^b and F.X.C. de las Heras^a

^aEscola Universitària Politècnica de Manresa (UPC), Av Bases de Manresa 61-73, 08240-Manresa, Catalonia, Spain.

^bDepartament de Geologia Dinàmica, Geofísica i Paleontologia. Universitat de Barcelona. C. Martí i Franquès, 08028-Barcelona, Catalonia, Spain.

1. ABSTRACT

The presence of abundant sulphate in sedimentary reducing conditions derives into a massive microbiological sulphate-reduction process that generates (poly)sulphides able to be combined with the sedimentary iron forming pyrite or with the sedimentary organic matter forming organic sulphur compounds (OSC).

Analysis of pyritic and non pyritic (mostly sulphatic) iron, together with pyritic, sulphatic and organic sulphur have been carried out. From the results, first, we have defined a certain degree of weathering (DOW) related to the increase of iron sulphate. Second, we have assessed a degree of pyritisation (DOP) in order to recognize their geochemical implications. Finally, in such Spanish coals, iron limitation in depositional environments with very good availability of sulphur and organic matter, is usually related to high values of DOP and can derive into a massive presence of organic sulphur such as in Mequinensa lignite. In our study, we describe OSC of the soluble fraction extracted from this exceptional coal. Gas chromatography-mass spectrometry is used to elucidate organosulphur functionalities present in the biomarkers such as thiolanes, thiophenes and heteroaromatics containing sulphur, their distribution suggests organic matter origin, depositional palaeoenvironment and degree of coalification.

2. EXPERIMENTAL

2.1. Low rank coals.

Utrillas subbituminous coals (Estercuel and Portalrubio) were taken from the Maestrazgo basin, located in the Iberian Range linking zone with the southernmost sector of the Catalan coastal range, deposited during middle Albian (Lower Cretaceous, ca. 105 Ma)[1]. Fígols lignite belongs to the Tremp Formation (Eastern Pyrenees) and was deposited during Late Cretaceous (ca. 70 Ma) in a marine influenced zone [2]. Calaf lignite belongs to La Segarra Lacustrine System (Eastern Ebre basin) and was deposited during early Oligocene (ca. 35

Ma)[3] in a lacustrine basin. The Mequinensa coal bearing sequence is included in the Monegros Lacustrine System (SE Ebre basin) and was deposited during late Oligocene (ca. 30 Ma). Evaporitic facies were developed mainly in the marginal lacustrine zones while carbonate and lignite deposits were dominant in inner lacustrine areas [3]. Rubielos lignite was taken from a basin located in the southern part of the Iberian chain and belongs to a Miocene lacustrine system (ca. 13 Ma)[4].

2.2. Analytical procedure.

Elementary analysis (C and S) was carried out in an elementary analyzer (Carlo Erba 1106). Pyritic and sulphate sulphur as well as pyritic and non pyritic iron were determined according to the ASTM D2492-90 method. Organic sulphur was obtained as a difference between total and sulphate plus pyritic sulphur.

The extraction procedure has been described elsewhere [5]. In short, lignites were Soxhlet extracted with $\text{CH}_2\text{Cl}_2\text{:MeOH}$ (2:1). The neutrals were further extracted and divided into aliphatic, aromatic and polar fractions. All these fractions were submitted to gas chromatography-mass spectrometry performed using a Fisons MD-800 instrument with a DB-5ms column.

3. RESULTS AND DISCUSSION

3.1. Sulphur distribution, origin and fate.

Results obtained are described in Table 1, where organic matter is described by %C, sulphur (%S) is divided into pyritic (S py), sulphatic (S su) and organic (S or). Iron is divided into pyritic (Fe py) and non pyritic (Fe np) all calculated on a d.a.f. basis. Degree of weathering (DOW) defined as $\text{DOW}\% = \text{Ssu} \cdot 100\% / (\text{Ssu} + \text{Spy})$ is a parameter suggested to measure how advanced is the weathering for a pristine coal after storage, the percentages of non pyritic iron and sulphate shows a good correlation, close to the stoichiometric ratio between S and Fe (1.08 in %w/w), except for Calaf were a high amount of non iron sulphate could be present in the collected coal. Whereas in Rubielos the high amount of non pyritic iron could be combined to anions other than sulphate. From the above results, it is corroborated that pyrite is weathered mostly to iron sulphate and elementary sulphur in further steps [6]. Elementary sulphur has been detected in trace amounts for the most weathered Mequinensa coal (58%) by flash pyrolysis. This, represents a short deviation for the DOW% and the organic sulphur (S or) measured as a difference. Coal-bearing seams depending on the degree of weathering, due to the subaerial exposure to the atmosphere and storage generates iron sulphate as a degradation process during pyrite oxidation. It also can generate elementary sulphur. Indications for the presence of sulphate other than iron sulphate in coals is given for Calaf, and another forms of iron than pyrite in Rubielos.

The degree of pyritisation (DOP) defined previously [7], it is considered in our case as $\text{DOP}\% = (\text{Fe py} + \text{S su} \cdot 0.93) \cdot 100\% / (\text{Fe py} + \text{Fe np})$ where 0.93 is the stoichiometric ratio between atomic Fe and S, therefore the numerator includes all iron coming from the initial pyrite after weathering (excepts elemental sulphur), and the denominator is total iron.

Iron is usually limiting for lakes [8]. In our samples Rubielos is an exception where atomic ratio Fe/S is higher than 0.93 and sulphur is limiting. It corresponds to the lower DOP (56%). The rest of coals have DOP close to 100% probably related to more anoxic conditions

as it has been described [9].

Organic matter was very abundant for all coals. When representing DOP versus %C it shows no good correlation because all iron was pyritised independently of the amounts of organic matter, as it has been shown for lakes [8]. When representing DOP versus %S there is no relationship [9,10]. In our case, %C and %S are not coupled, because sulphur comes only in a minimum percentage from the same organic matter and mostly from the lixiviates of the lake catchment area or from direct marine influence.

Sulphur incorporation in ancient lakes that further generated sulphur-rich low rank spanish coals was generally due to the lixiviation through riverine systems of sulphate salts widespread in the catchment area (Triassic and Liassic gypsum) into the lacustrine basins or from direct marine influence [1-4]. All these coals are below the normal marine line ($S/C < 0.36$), although giving higher values than 0.02 previously reported for acid lakes [8]. Exceptionally, S is limiting in Rubielos coal. Organic sulphur is important in extreme cases with very low availability of iron [8](Calaf and Mequinensa, $Sor/C > 0.04$). For this reason, OSC from Mequinensa are further described.

Table 1. Elementary analysis of C and S (d.a.f.). Pyritic (S py), sulphatic (S su), organic sulphur (S or), pyritic iron (Fe py) and non pyritic iron (Fe np) contents are calculated on d.a.f. basis. DOW (degree of weathering) and DOP (degree of piritisation) are defined according to the text.

Sample	% C	% S	S py	S su	S or	Fe py	Fe np	DOW	DOP
Portalrubio	73.5	3.5	1.3	0.6	1.7	1.1	0.6	32	97
Estercuel	73.2	5.3	1.9	0.3	3.1	1.7	0.3	14	99
Fígols	64.1	7.4	3.2	0.92	3.2	2.8	0.75	22	103
Calaf	53.1	15.1	1.7	7.6	5.8	1.5	1.1	40	-
Mequinensa	60.6	13.4	0.5	0.7	12.2	0.4	0.6	58	105
Rubielos	52.9	4.3	3.3	0.7	0.3	2.9	3.4	28	56

3.2. Organic sulphur compounds. Biomarker information.

The sulphur-containing compounds of the Mequinensa lignite (type III-S) [11] are related to anoxic conditions of deposition. They are represented by mixtures of linear C_{21} and C_{29} - C_{32} thiophenes, probably originated by sulphur incorporation in higher plants. Mequinensa lignite, to the best of our knowledge, is the first coal investigated containing non-aromatic OSC in the organic soluble extract. Together with such linear compounds, polycyclic thiolanylhopanes with maximum at C_{35} as it is shown in Fig. 1 are present in the aromatic fraction. They are related to eubacteria probably deposited in a carbonate-evaporitic palaeoenvironment [12] that further generated coal. High abundance of (alkyl)benzothiophenes also shown in Fig. 1 are associated to such specific depositional environment [13]. They also refer to a low degree of maturation [14]. The same indication is given by the dibenzothiophene ratio ($DBR=0.91$) according to their low degree of coalification ($\%R_0$ 0.4).

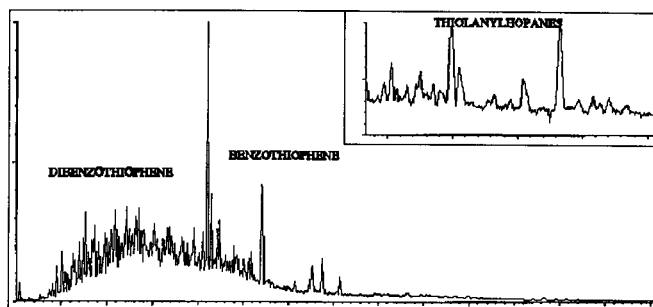


Figure 1. Total ion current chromatogram showing the distribution of organic sulphur compounds present in the aromatic fraction from Mequinensa lignite.

4. CONCLUSIONS

The distribution of Fe and S in Spanish low-rank coals with high amount of organic sulphur has been studied and their origin proposed. OSC from Mequinensa are described and organic matter input, depositional palaeoenvironment and degree of coalification suggested.

REFERENCES

1. X. Querol, S. Chinchón and A. López-Soler, *Int. J. Coal. Geol.* **11** (1989) 171.
2. V. Masachs and L. Via, *Itineraris Geològics* (ed., Masachs) Manresa (1980) 121.
3. L. Cabrera and A. Sáez, *J. Geol. Soc. London*, **144** (1987) 451.
4. P. Anadón, L. Cabrera, R. Julià, E. Roca and L. Rosell, *Paleogeogr. Paleoclimatol. Paleocol.* **70**, (1989) 7.
5. F.X.C. de las Heras, *Geoquímica orgànica de conques lacustres fòssils*. Institut d'Estudis Catalans XCVII, Barcelona (1991) 291.
6. L.M. Stock and R. Wolny, *Geochemistry of Sulfur in Fossil Fuels* (eds., Orr and White) ACS 429, Washington (1990) 241.
7. R.A. Berner, *Amer. J. Sci.* **268**, (1970) 1.
8. R. Carignan and A. Tessier, *Geochim. Cosmochim. Acta* **52** (1988) 1179.
9. S.E. Calvert and R.E. Karlin, *Geochim. Cosmochim. Acta* **55** (1991) 2483.
10. J.P. Chanton, C.S. Martens, C.K. Paull and J.A. Coston, *Geochim. Cosmochim. Acta* **57** (1993) 1253.
11. J.S. Sinninghe Damsté, F.X.C. de las Heras and J.W. de Leeuw, *J. Chromat.*, **607** (1992) 361.
12. J.S. Sinninghe Damsté and J.W. de Leeuw, *Geochemistry of Sulfur in Fossil Fuels* (eds., Orr and White) ACS 429, Washington (1990) 417.
13. J.O. Grimalt, M. Grifoll, A.M. Solanas and J. Albaigés, *Geochim. Cosmochim. Acta* **55** (1991) 1903.
14. R.P. Philp and A. Bakel, *Energy & Fuels* **2**, (1988) 59.

The Sulfur Geochemistry of Some Australian Brown Coals

Z. Song^a, B.D. Batts^a and J.W. Smith^{a,b}

^aSchool of Chemistry, Macquarie University, Sydney, NSW, Australia 2109

^bCSIRO Division of Petroleum Resources, North Ryde, NSW, Australia 2113

1. INTRODUCTION

The separation of sulfur in coal into inorganic sulfate, pyritic, acid volatile sulfide, elemental and organic may be routinely accomplished. $\delta^{34}\text{S}$ values for these forms of sulfur are not so frequently measured. The isotopic evidence presented by the inorganic forms can often be interpreted in terms of fresh water and marine environments, changes of the latter with time, and sulfate reduction in closed and open systems. Understanding of the $\delta^{34}\text{S}$ organic data is less advanced. In bituminous coals where marine influence has been minimal and total sulfur contents are <1%, recognisable patterns in isotopic distributions in organic sulfur have been described. At sulphur content >1% the isotopic data appears to be largely at random^{1,2,3,4}. Although few samples have been analysed, the $\delta^{34}\text{S}$ organic data for coals of low rank appears to exhibit a similar randomness regardless of sulfur content⁵.

In this work partitioning of the organic sulfur in three brown coals is effected. Interest in the organic forms of sulfur in carbonaceous sediments is considerable because their rate of maturation may depend on the concentration, and distribution of the relatively weak sulfur linkages in these. In this regard, since structure stabilities are readily assessed by hydrous pyrolysis, this technique has found increasing application^{6,7}. Finally an isotopic comparison of organic compound types within and between coals is made.

2. EXPERIMENTAL

2.1 Hydrous Pyrolysis of Model Compounds

Thirteen compounds containing S-linkages likely to occur within coal structures were reacted with excess water in sealed glass tubes for 66 hours at temperatures of 200°, 230°, 270° and 330°C. Additional reactants included were cadmium acetate to precipitate H_2S as formed and a low S brown coal to provide active H^+ to cap reactive sites as formed. It has been shown previously that carbonaceous materials play a major role in promoting hydrous pyrolytic reactions⁷. After cooling in liquid nitrogen the tubes were opened under dichloromethane (DCM) and their contents Soxhlet extracted with DCM/methanol to recover unreacted parent material. The solid residue was dried and then reacted with HCl. H_2S released from the cadmium sulfide was trapped as Ag_2S and weighed. Finally the sulfur content of the HCl reacted residue was determined by reaction with Eschka mixture.

The BaSO₄ recovered was dried and weighed. See Figure 1.

Only the data relating to the H₂S formation are reported here. These data are shown in Figure 2. Differences in the reactivities of the various sulfur linkages are demonstrated. Benzothiophene, dibenzothiophene, diphenyl sulfide and thianthrene were shown to be virtually unreactive under the reaction conditions used.

2.2 Reactions of Coals

The three brown coals studied, Loy Yang and Anglesea from Victoria and Lochiel from South Australia contained 0.2, 2.9 and 2.3% organic sulfur (air dried basis) respectively. The coals were separated into the components as shown in Figure 1 and the organic solvent insoluble fractions hydrous pyrolysed. ³⁴S/³²S ratios were determined for all products. Detailed experimental results are listed in Table 1.

3. DISCUSSION

3.1 Hydrous Pyrolysis

Three reactivity profiles, similar to those displayed in Figure 2 for model compounds, were constructed for the sulfur in the three coals. A comparison of these data illustrates the differences between these coals and shows

- the Lochiel coal to have high reactivity similar to that of mercaptans, disulfides and thiazoles and only a small content of unreactives, that is compounds such as benzothiophene, dibenzothiophene and diphenyl sulfide.
- the two Victorian coals, although differing largely in sulfur contents, have a similar intermediate reactivity. This could suggest a composition like the Lochiel coal, but with a higher proportion of the unreactives. Alternatively these coals may be comprised of other sulfur-compound types of relatively moderate reactivity, that is methyl substituted thiophenes and/or thiolanes.

It is expected that gas chromatography-mass spectrometry (gc-ms) analyses of the pyrolysates from the organic solvent insolubles and of the soluble products of hydrous pyrolysis (⑦, Fig. 1) will assist in these structure conformations.

3.2 Isotopic Data

These show little variation within the coals indicating essentially a single source of sulfur for each coal. Large variations exist between coals which are unrelated to total organic sulfur contents. A slight tendency for the H₂S generated in highest yields at 330 °C to be enriched in ³⁴S is not paralleled by changes in the composition of corresponding residues. The constancy of the isotopic difference between generated H₂S and unreacted sulfur at all stages is not understood at this stage.

4. CONCLUSIONS

Major differences exist in response of sulfur-containing coals to hydrous pyrolysis. In the Lochiel coal the sulfur is generally in a highly reactive form and unreactive sulfur-forms

such as benzothiophenes can only be in very low concentrations. Explanations for the lower reactivities of the other coals are advanced. Sulfur isotopic data, whilst further illustrating differences between coals, appears at this stage to be of limited value in the interpretation of hydrous pyrolysis data but they do indicate the possibility of a single source of sulfur for each coal.

REFERENCES

1. J.W. Smith and B.D. Batts, *Geochim. Cosmochim. Acta*, 38 (1974) 121.
2. F.T. Price and Y.N. Shieh, *Econ. Geol.*, 74 (1979) 1445.
3. L.M. Westgate and T.F. Anderson, *Int. J. Coal Geol.*, 4 (1984) 1.
4. J.W. Hunt and J.W. Smith, *Chem. Geol.* 58 (1985) 137.
5. K.W. Gould, T.D. Gilbert and J.W. Smith, *Proc. 1985 Int. Conf. Coal Sci.*, 811.
6. M.D. Lewan, "Organic Geochemistry"; Edited M. H. Engel and S. A. Macko, 1993 419 Plenum Press.
7. J.W. Smith, B.D. Batts and T.D. Gilbert, *Org. Geochem. J.*, 14 (1989) 365.

Table 1.
 $\delta^{34}\text{S}$ (‰). Samples Number as per Figure 1.

Coal	React. Temp. (°C)	Sulfur Conv. to H ₂ S (%)	H ₂ S Formed ⑤	Resid. Coal ⑥	H ₂ S - Coal resid.
Anglesea	200	16.2	+18.8	+22.5	+5.7
	230	27.8	+19.4	+23.0	+3.6
	270	44.8	+19.7	+21.9	+2.2
	330	52.2	+19.9	+22.1	+2.2
Asphaltenes (①) +20.9‰, Pyritic + SO ₄ (④) +16.4‰					
Lochiel	200	36.7	-3.4	+3.8	+7.2
	230	50.8	-2.2	+3.1	+5.3
	270	77.0	-0.5	+4.1	+4.6
	330	91.1	-1.4	+4.7	+6.1
Asphaltenes (①) +1.0‰, Pyritic + SO ₄ (④) -7.6‰; Acid volatile sulfide (③) -3.6‰;					
Loy Yang	200	12.5	+12.3	+9.7	-2.6
	230	28.9	+12.3	+15.2	+2.9
	270	42.7	+13.1	+13.3	+0.2
	330	49.3	+15.0	+14.4	-0.6
Asphaltenes (①) +13.0‰, Pyritic + SO ₄ (④) =2.1‰					

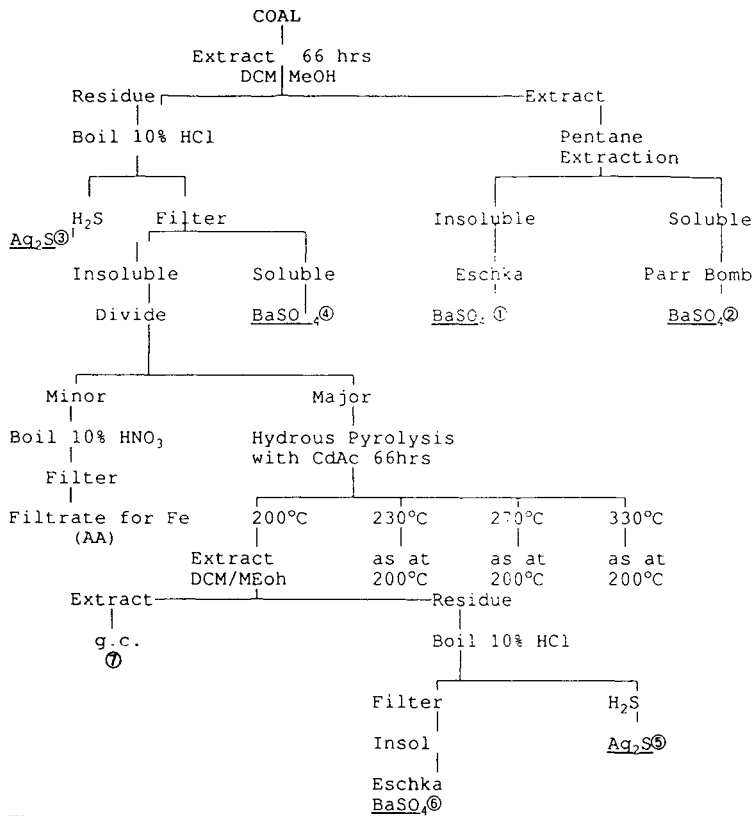


Figure 1.
Separation Method.

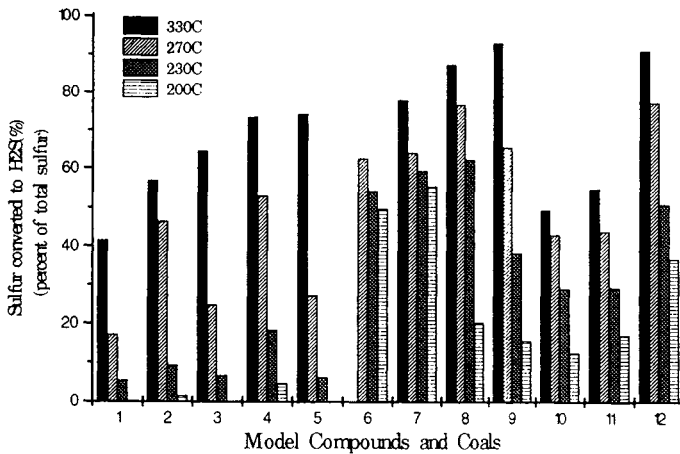


Figure 2.
Amounts of Sulfur released by Hydrous Pyrolysis from Model Compounds and Coals.
1. Pentamethylene Sulfide 2. 2,5-Dimethylthiophene 3. Bithiophene 4. 2-Methylthiophene
5. Thiophene 6. Nonylmercaptan 7. Butyl Disulfide 8. 2,5-Dimethylbenzothiazole 9. Benzothiazole
10. Loy Yang Coal 11. Angelsea coal 12. Lochiel coal.

Thermal behaviour of sulphur forms in Spanish low-rank coals.

Ana J. Bonet, José V. Ibarra and Rafael Moliner

Instituto de Carboquímica, C.S.I.C., P.O. Box 589, 50080-Zaragoza, Spain

1. INTRODUCTION

The development of new tactics for the removal of the sulphur compounds from coal depends, in part, upon a knowledge of their chemical constitution. It is generally assumed that the sulphur in coal is distributed among organic sulphur, sulphatic sulphur and pyritic sulphur compounds. The organic sulphur value of coal is derived as the difference between the total sulphur content of coal and the amount of pyritic plus sulphatic sulphur. Elemental sulphur, which would be accounted for as "organic sulphur", has been mentioned only in a few references in the literature [1].

In this paper, the thermal behaviour of the different sulphur forms, including elemental sulphur, of a series of Spanish-low rank coals has been investigated, by means of temperature programmed degradation (TPD) and X-ray based spectroscopic techniques. The thermal evolution of volatile sulphur compounds was followed by sulphide electrode and FTIR spectroscopy and the speciation of organic sulphur forms by XPS. The influence of coal rank, pyrite content and operating conditions on the thermal stabilities of sulphur structures were also established.

2. EXPERIMENTAL SECTION

A series of low rank coals with high sulphur contents were studied. They were selected from the Teruel and Mequinenza basins on the basis of their different sulphur form content (mainly, pyritic and organic). The samples were ground to less than 200 μm . The main characteristics of some of the selected coals are given in Table 1. Analyses of sulphur forms were carried out according to ASTM method D-2492. Mequinenza coal (M6) was chosen for its high organic sulphur content. The AA6-F, EC4-F and AA5-F samples are freshly mined while the AA6, EC10 and AA5 coal samples have been stored under laboratory conditions for up to five years since collection and contain high amounts of sulphatic sulphur.

Elemental sulphur (S^0) was determined by extracting the coal samples (20 g) in a Soxhlet with tetrachloroethylene (PCE) (200 ml) at its boiling point (120°C) for up to six hours. The S^0 contents in PCE extracts were determined using Gas Chromatography. The sulphur quantization was carried out using a Varian 3400; split-splitless injector running in splitless way and FID-FPD detector. A column of 50m x 0.25mm i.d. covered with a 0.4 μm film of CP-sil-5 CB chemically bonded phase was used. Detector and injector temperature: 300°C,

initial temperature of 120°C (2 min); heating rate of 40°C/min up to 240°C.

Table 1.
Main characteristics of coal samples.

	AA6	AA6-F	AA5	AA5-F	EC-8	EC-10	EC4-F	M6
Oxidation state	W ^c	F ^c	W	F	W	W	F	W
% C ^a	65	71.7	69.6	73.7	79.1	74.5	79.2	69.6
% S _T ^b	7.48	7.40	6.44	5.28	3.19	6.68	2.94	9.83

a) daf

b) air dried basis

c) W:weathered; F:fresh

Pyrolysis runs were carried out in a swept fixed bed reactor (30 cm length, 2 cm i.d.) with the coal samples placed into a quartz tube and heated up to 850°C at a heating rate of 5°C min⁻¹. The tar produced was trapped at 0°C, and the evolved gas was swept with N₂ to the sulphur detector system. Sulphide electrode (SE) and infrared spectroscopy (FTIR) were used as sulphur detectors, both coupled on-line with the reactor system. More experimental details have been previously described [2].

Coal samples with different pyrite contents were obtained by separation into density fractions ($d=1.4-2.8 \text{ g cm}^{-3}$) with defined limits by float-sink using mixtures of liquids of different density (bromoform, xylene and perchloroethylene). Morphological studies and the determination of organic sulphur in the coal or char matrix were conducted with a scanning electron microscope (SEM) coupled to a Si-Li detector and a processor for energy-dispersive X-ray analysis (EDX).

3. RESULTS AND DISCUSSION

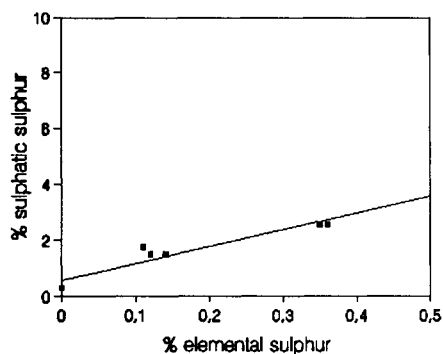


Figure 1. Sulphatic sulphur v.s. elemental sulphur content.

3.1. Elemental sulphur.

From the sulphur forms present in coal, only elemental sulphur was shown to be extracted by PCE [3]. Table 1 summarizes the results for PCE extractions of samples taken from seven different coals as a function of weathering evaluated by the sulphatic sulphur content.

AA6-F, EC4-F and AA5-F coal samples produced only trace amounts of S⁰. PCE extracts of weathered coals always contained S⁰. The linear correlation between the elemental sulphur and the sulphate content of coal (Figure 1) suggests that both sulphur forms are the result of weathering reactions in coal. The absence of S⁰ in PCE extracts of M6

coal, which has been exposed to an air oxidation process but does not contain pyritic sulphur, can be explained on the basis that the pyrite oxidation is the source of both S^0 and sulphate in coal, as appears in literature.

3.2. Changes in sulphur forms during coal pyrolysis.

The study of the evolution of sulphur forms in chars obtained at different temperatures shows how the sulphate content decrease markedly over 400°C in chars from weathered coals. Other species except iron sulphates (mainly calcium sulphates) remain in chars. Pyrite seems to be stable up to 450°C but it is entirely decomposed over 550°C . Sulphides begin to appear coinciding with the pyrite decomposition to pyrrhotite and they increase with temperature of pyrolysis. At temperatures as low as 600°C a high percentage of the organic sulphur has already been removed between 30-55% for Teruel coals and 75% for Mequinenza coal. This removal is greatly influenced by the weathering and pyrite content of the samples. For the studied coals, total sulphur removal between 35 and 65% has been achieved by low temperature pyrolysis (600°C).

3.3. Evolution of sulphur compounds during pyrolysis.

The H_2S evolved from the pyrolysis of Teruel coals (Figure 2a) shows the presence of two peaks related to the decomposition of organic sulphur in thermally labile structures (250 - 450°C) and to the decomposition of pyrite into pyrrhotite (500 - 650°C), respectively.

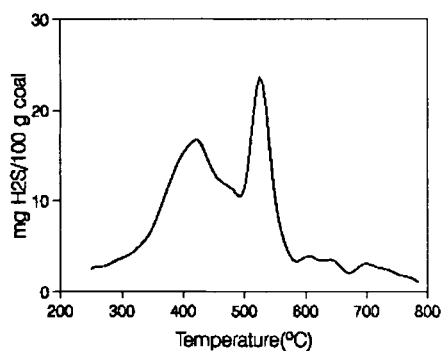


Figure 2a. H_2S evolution with pyrolysis temperature for EC8 coal.

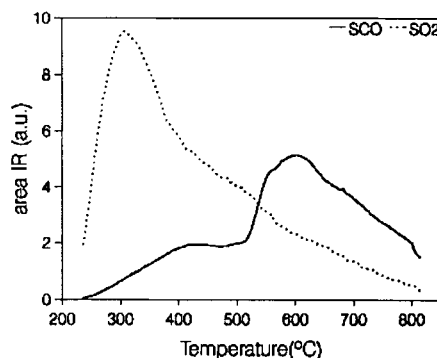


Figure 2b. Evolution of oxygenated sulphur forms for AA6 coal.

Evidence of the capture by the coal matrix of sulphur from pyrite decomposition as well as the influence of the coal organic matter on the decomposition of pyrite was obtained by SEM-EDX and XRD using float-sink coal fractions with different organic matter and pyrite contents. These findings demonstrate that desulphurization by pyrolysis has to be considered individually for each coal, depending on its rank, degree of weathering and distribution of sulphur forms, since the interactions observed greatly limit the efficiency of desulphurization.

The evolution of oxygenated sulphur compounds (COS and SO_2) during pyrolysis was followed by FTIR spectroscopy (Figure 2b). The evolution of COS shows a similar trend to that of H_2S . Therefore, the study of this evolution can be used to follow the decomposition

of sulphur forms of coal during pyrolysis. The evolution of SO₂ seems to be related to the decomposition of sulphates coming from the weathering of coal.

3.4. Speciation of organic sulphur forms in chars.

Determination of the distribution of organic sulphur forms in these coals and their evolution during low temperature pyrolysis was carried out by X-Ray Photoelectron Spectroscopy (XPS). For the correct assignation of S 2p binding energies (BE) to different sulphur forms, model compounds, including pyrite concentrates and coal organic matter fractions, were used [4].

In Mequinenza coal, a noticeable contribution of sulphidic sulphur was observed. This unstable sulphur form vanishes simply by heating up to moderate temperatures (400°C). Starting from 400°C, thiophenic sulphur is the major organic sulphur form and little changes are produced with increasing temperature of pyrolysis. Sulfoxide structures have also been detected in proportions close to 20%. They remain stable at the assayed temperatures.

Coals from Teruel show the presence of oxidized sulphur (S⁶⁺) that can be attributed to sulphonic structures but also iron sulphates from the pyrite oxidation. This last assignation is supported by the marked decrease observed for the S⁶⁺/S²⁺ ratio in the temperature range of sulphate decomposition. Above 600°C, when pyrite has already decomposed, thiophenic sulphur is the major organic sulphur form in char (over 80%) though sulphone structures have also been detected. The marked increase of the sulphur to carbon ratio observed for high temperature chars in relation to starting coals and low temperature chars suggests that the organic sulphur could be incorporated to char from pyrite decomposition mainly as thiophenic structures.

Acknowledgements.

The authors wish to thank the ECSC (Project 7220-EC/756), CICYT and DPT for financial support. A.J.B. also thanks CONAI of the DGA for a grant.

REFERENCES

1. Duran J.E., Mahasay S.R., Stock L.M., Fuel 65, 1167-1168, 1986
2. Ibarra J.V., Bonet A.J., Moliner R., Fuel 73, 933-939, 1994
3. Huggins F.E., Vaidya S.V., Shah N., Huffman G.P., Fuel Proc. Technology, 35, 233-257, 1993
4. Fierro J.L.G., Palacios J.M., Moliner R., Ibarra J.V., 7th International Conference on Coal Science, (K.H. Michaelian Ed.), Banff, Canada, IEA, Vol. I, 489-492, 1993

INTERPRETATION OF AP-TPR PROFILES BY NON-ISOTHERMAL KINETICS

H. Van den Rul, I. I. Maes, J. Yperman, D. Franco, J. Mullens and L. C. Van Poucke

Laboratory of Inorganic and Physical Chemistry, Limburgs Universitair Centrum, B-3590 Diepenbeek, Belgium

The two peaks in the AP-TPR (Atmospheric Pressure - Temperature Programmed Reduction) spectrum of cystein are resolved and interpreted in terms of the non-isothermal kinetics theory.

1. INTRODUCTION

In this work, cystein is taken as the investigated sample, as a model compound for sulfur functionality description in coal. During an AP-TPR experiment, a sulfur containing solid sample is heated by a linear temperature programme, in a reducing environment and under atmospheric pressure [1]. Maximum evolution of H₂S occurs at discrete temperatures, characteristic for the different sulfur functional groups, resulting in a spectrum with overlapping peaks. Applying the non-isothermal kinetics theory to such a spectrum is a means for resolution of the peaks that takes into account the chemical relevance.

The rate of solid state reactions of the type A(s) → B(s) + C(g) in non-isothermal conditions can be expressed in the form

$$\frac{d\alpha}{dT} = k(T)f(\alpha) = A \exp\left(-\frac{E}{RT}\right)f(\alpha) \quad (1)$$

Or by integration

$$g(\alpha) = \int_0^{\alpha} \frac{d\alpha}{f(\alpha)} = \frac{A}{\beta} \int_0^T \exp\left(-\frac{E}{RT}\right) dT = \frac{AE}{\beta R} p(x) \quad (2)$$

Where α = conversion degree, $f(\alpha)$ and $g(\alpha)$ are functions depending on the reaction mechanism, $x = E/RT$, $p(x)$ is the temperature integral, β is the heating rate and it is assumed that the rate constant $k(T)$ can be described by the Arrhenius equation.

The most commonly used models in non-isothermal kinetics are summarized in table 1.

The AP-TPR spectrum of cystein at a heating rate of 5.1 °C/min shows two overlapping peaks. It is assumed that cystein transforms into two independent products, which then release sulfur in the form of H₂S during the experiment. In this way, the two peaks can be analysed separately.

Table 1
Most commonly used kinetic models

Name	$f(\alpha)$	Name	$f(\alpha)$	Name	$f(\alpha)$
Pn	$n\alpha^{1-1/n}$	D1	$1/(2\alpha)$	D4	$1.5[(1-\alpha)^{-1/3}-1]^{-1}$
An	$n(1-\alpha)[- \ln(1-\alpha)]^{1-1/n}$	D2	$[- \ln(1-\alpha)]^{-1}$	Fn	$(1-\alpha)^n$
Rn	$n(1-\alpha)^{1-1/n}$	D3	$1.5(1-\alpha)^{2/3}[1-(1-\alpha)^{1/3}]^{-1}$	SB(m,n,r)	$\alpha^m(1-\alpha)^n[- \ln(1-\alpha)]^r$

2. EXPERIMENTAL

40.0 mg of cystein (Aldrich-Chemie) is recorded in AP-TPR experiments at heating rates of 1.9, 2.9 and 5.1 °C/min, at a constant flow of H₂ (50 ml/min) and in the presence of a reducing mix.

3. RESULTS AND DISCUSSION

3.1. RESOLUTION OF THE OVERLAPPING PEAKS

For the resolution of three overlapping peaks of a glassy alloy in a DSC experiment, Wagner et al. [2] describe each experimental peak by the sum of two Gaussian functions, which best fit the experimental data:

$$f(T) = a [H(T_M - T) \exp(-b_1(T - T_M)^2) + H(T - T_M) \exp(-b_2(T - T_M)^2)] \quad (3)$$

Where $H(T_M - T)$ and $H(T - T_M)$ are forms of the Heaviside unit function and T_M is the temperature at the maximum of the peak.

The entire spectrum is then expressed by the sum of the individual functions.

The same approach is used for resolving the two peaks in the AP-TPR spectrum (rate of evolution of S) of cystein at a heating rate of 5.1 °C/min, and this for three experimental data sets. Figure 1 shows the separation of the two peaks for one set.

3.2. KINETIC ANALYSIS

As previously mentioned, it is assumed that the peaks refer to two independent reactions, so they can be analysed separately.

At first, the procedure of Stander and van Vuuren [3] is performed on the three experimental data sets at 5.1 °C/min. This method is based on the principle that B_i in equation (4) should theoretically be constant for every experimental data point for the right E, A and model function $f(\alpha)$.

$$\ln f(\alpha_i) - \ln p(x_i) = \ln \frac{AE}{\beta R} = B_i \quad (4)$$

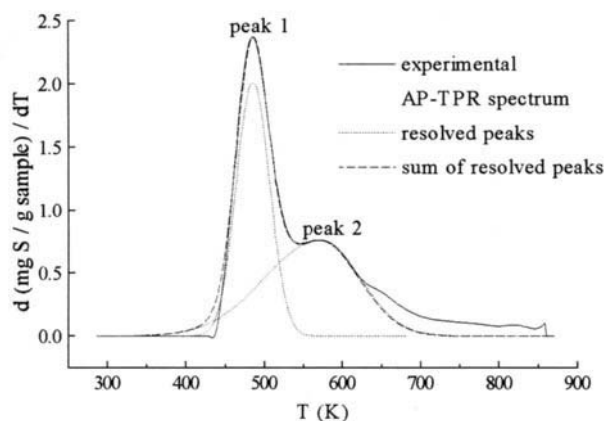


Figure 1: Separation of two peaks in the AP-TPR spectrum of cystein at a heating rate of 5.1 °C/min

Comparison of simulated curves, based on the obtained parameters, with the experimental curves, shows no good agreement. The temperature-interval of the simulated curves though is in the same region as the experimental ones. Therefore, the Stander - van Vuuren parameters are taken as initial parameters for a non-linear regression analysis with a Marquardt algorithm [4], optimising the kinetic parameters for different assumed models. Excellent fits are obtained for the SB(m,n,r) model.

It is seen that different (E, A, m, n, r) parameter sets fit each of the two experimental peaks equally well. However, when calculating k_M , the rate constant at the maximum peak temperature, this is nearly a constant for the different parameter sets and for the different experimental data sets. In fact, this is an illustration of the kinetic compensation effect, observed in many kinetic studies [5] and expressed by

$$\begin{aligned} \log A &= 1.1 \cdot 10^{-4} E - 0.55 && \text{for peak 1} \\ \log A &= 0.9 \cdot 10^{-4} E - 1.01 && \text{for peak 2} \end{aligned}$$

As a consequence of this mutual correlation of E and A, both peaks can be described by several apparent kinetic parameters, instead of the appropriate ones.

Málek [6] has described a solution for this problem, when the true activation energy is known. He recommends the use of the isoconversional method to determine the activation energy. This method uses several measurements of the same product at different heating rates and results in a series of activation energies, depending on the degree of conversion. The isoconversional KinTool software of Vyazovkin[7] is therefore applied to three AP-TPR cystein curves at heating rates 1.9, 2.9 and 5.1 °C/min. For $\alpha < 0.25$, a constant activation energy of 1.75 Jmol^{-1} is obtained from this analysis. Considering the fact that in the beginning of the spectrum ($\alpha < 0.15$) the contribution of the second peak is negligible compared to the first peak, it can be assumed that the 'true' activation energy of the first peak is 1.75 Jmol^{-1} . Málek finds the most probable kinetic model now by investigating the characteristics of two special functions [6]. From this approach it is concluded that the SB(m,n) model is the most

suitable for describing the experimental data of the first peak. The parameters A, E, m and n calculated by Málek's method don't give excellent fits, so the non-linear Marquardt regression was again used for optimising the parameters (E was held constant at 1.75 Jmol⁻¹). The results can be found in table 2.

Table 2

Kinetic parameters calculated by Málek's method for the most suitable model SB(m,n) compared with excellent fitting parameters.

	Parameters of Málek's method				Excellent fitting parameters			
	E/Jmol ⁻¹	A/min ⁻¹	m	n	E/Jmol ⁻¹	A/min ⁻¹	m	n
dataset 1	1.75	5.13	0.951	0.951	1.75	0.330	0.810	0.925
dataset 2	1.75	0.347	1.04	0.965	1.75	0.311	0.790	0.900
dataset 3	1.75	0.530	0.962	0.950	1.75	0.312	0.790	0.900

4. CONCLUSION

For both separated peaks in the AP-TPR spectrum of cystein, a set of kinetic parameters is obtained, with the general SB(m,n,r) model as the best fitting model. The pre-exponential factor and the activation energy are correlated, expressed by the kinetic compensation effect.

For the first peak, the true activation energy can be assumed to be equal to the isoconversional result at the beginning of the peak. With this information the most probable kinetic model and the kinetic parameters are determined by Málek's method. This shows that the SB(m,n) model is best suited to describe the experimental first peak, but the calculated kinetic parameters can not simulate the experimental peak exactly. The parameters are therefore optimised by non-linear regression.

REFERENCES

1. J. Yperman, D. V. Franco, J. Mullens, G. Reggers, M. D'Olieslaeger, L. C. Van Poucke, S. P. Marinov, NATO ASI Series C, C. E. Snape Ed., Vol. 455 (1995) 449.
2. C. Wagner, J. Vázquez, P. Villares and R. Jiménez-Garay, Materials Letters, 18 (1994) 280.
3. P. P. Stander, C. P. J. van Vuuren, Journal of Thermal Analysis, 41 (1994) 493.
4. P. R. Bevington, Data Reduction and Error Analysis for the Physical Sciences, McGraw-Hill book company, New York, 1969.
5. N. Koga, Thermochemica Acta, 244 (1994) 1.
6. J. Málek, Thermochemica Acta, 200 (1992) 257.
7. S. Vyazovkin, V. Goryachko, International Labmate, 17 (1992) 21.

Acknowledgement

This work is financed with a specialization grant of the 'Vlaams Instituut voor de bevordering van het wetenschappelijk-technologisch onderzoek in de industrie (IWT)'.

A study of the organic sulphur distribution in solid fuels by means of Atmospheric Pressure Temperature Programmed Reduction (AP-TPR)

J. Yperman^a, D. Franco^a, J. Mullens^a, L.C. Van Poucke^a, C.E. Snape^b and S.C. Mitchell^c

a) Lab of Inorganic and Physical Chemistry, Limburgs Universitair Centrum, Universitaire Campus, B-3590 Diepenbeek, Belgium

b) Department of Pure and Applied Chemistry, University of Strathclyde, Glasgow G1, 1XL, UK

c) School of Chemistry, University of Leeds, Leeds, UK

1. ABSTRACT

A selection of low rank coals have been analysed by Atmospheric Pressure Temperature Programmed Reduction and the results are compared with those from the high pressure TPR technique. For purposes of comparison a relatively immature Type 1 kerogen has also been investigated.

2. INTRODUCTION

Sulphur is present in all solid fuels, both as inorganic compounds (mainly pyrite) and as a part of the organic matrix. Further information on the nature and distribution of organic sulphur forms is needed to improve current understanding of processing (liquefaction, pyrolysis and combustion) and the geochemistry of solid fuels formation. Instrumental quantification techniques such as ¹³C NMR, EPR, X-ray photoelectrospectroscopy (XPS) and X-ray absorption spectroscopy (K and L-edge XANES) and chemical quantification methods (pyrolysis, oxidation (CAPTO) and reduction (TPR)) for the sulphur functional groups distribution have previously been investigated. Indeed, Temperature Programmed Reduction (TPR), which is based on the principle that different organic sulphur forms present in solid fuels have different characteristic reduction temperatures at which hydrogen sulphide (H₂S) evolves has also been extensively studied. However only limited success has been achieved thus far, primarily because of poor sulphur balances with virtually all the thiophenic sulphur remaining in the char. This drawback has recently been overcome by the Strathclyde group using a well-swept fixed bed reactor at relatively high hydrogen pressures (up to 150 bar). Similarly, its atmospheric pressure counterpart by the LUC group, also has considerable potential in light of improvements in reactor design that minimise secondary reactions and thus improve sulphur balances. In this contribution the results obtained by the two techniques are compared for two lignites and two kerogens. In addition the effect of LiAlH₄ treatment is discussed for the Kimmeridge kerogen.

3. EXPERIMENTAL

3.1. Samples

The analyses of the kerogens and lignites are listed in Table 1. For the kerogens pyrite was removed from the samples, using LiAlH₄.

Table I.
Analyses of the lignites and kerogens (% dmmf) [3]

Sample	Mequinenza	Rasa	GoydnuK	Kimmeridge
C	66.4	80.2	56.1	55.5
H	5.8	5.2	7.6	6.2
N	1.6	1.2	0.9	2.1
S Total (% db)	9.0	11.8	3.3	8.3
pyritic	0.5	0.4	n.d.	n.d.
sulphatic	0.5	< 0.1	n.d.	n.d.
organic	8.0	11.4	n.d.	n.d.

3.2. Apparatus

The AP-TPR apparatus has been described previously [1,2]. About 20 mg sample was placed in the reactor. A hydrogen sweep gas with a flowrate of 50 cm³/min was used. The reactor was heated at 5°C/min upto 1000°C. First derivative plots (i.e. instantaneous hydrogen sulphide concentration vs. temperature) obtained from the ion-selective electrode output were smoothed using the Savitsky-Golay-Gorry procedure [4,5] and the total amount of H₂S evolved, was determined by integration of the peak area.

4. RESULTS

In both the atmospheric and high pressure systems, all the characteristic reduction temperatures found for the non-thiophenic forms are well-resolved from that of dibenzothiophene. Further, the reduction temperatures of poly/disulphides and thiols are much lower than those of both aliphatic and aromatic sulphides. Although thiophene and benzothiophene calibrants have not been synthesised their T_{max} will probably overlap bands from polynuclear diaryl sulphides [2].

4.1. Lignites

Figure 1 shows the AP-TPR profiles of the Mequinenza lignite (a) and the Rasa lignite (b). The H₂S recoveries are 60 and 70% for Rasa and Mequinenza lignites, respectively, with virtually all the sulphur not observed (little tar is obtained from AP-TPR) remaining in the chars. Thus figure 1 indicates that thiophenic sulphur is the dominant form in Rasa lignite (ca 80%, assuming the non-observable sulphur in the char arises from thiophenic forms) consistent with the high pressure findings [3]. In contrast, Mequinenza appears to contain a much higher proportion of sulphidic sulphur (ca 50%, again assuming the non-observable sulphur is thiophenic). This apparent discrepancy with the high pressure result [3] would suggest that, in this case, sulphides have been converted to thiophenes to a much lesser extent in AP-TPR, consistent with the findings for immobilised substrates [2]. At this moment a correct pre-treatment of the lignites is under investigation in order to increase the sulphur yield, and consequently to get more insight in the sulphur groups distribution.

4.2. Kerogen

The AP-TPR for both kerogens samples are shown in figure 2. For both samples a 100% sulphur recovery is obtained. For GoydnuK oil shale (Fig. II a) the organic sulphur is mainly present in non-thiophenic sulphur. For Kimmeridge the thiophenic sulphur (560-1000°C) dominates the AP-TPR profile (Fig. II b) but there remains a contribution from the non-

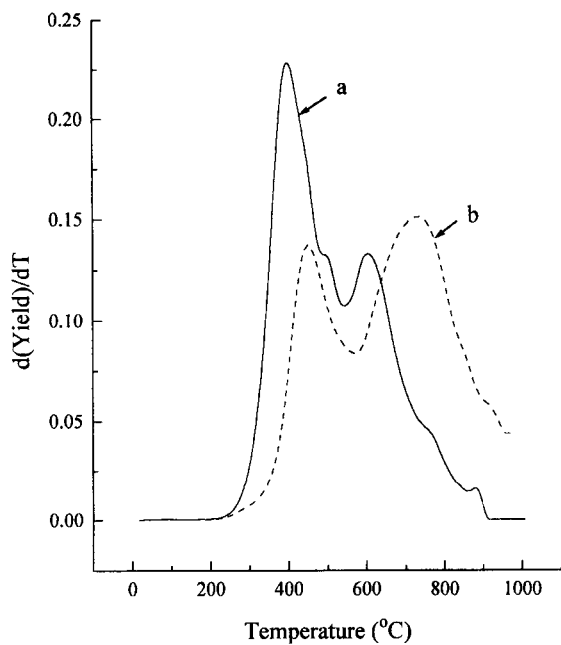


Fig. 1 AP-TPR profiles of the lignites (Mequinenza (a) and Rasa (b))

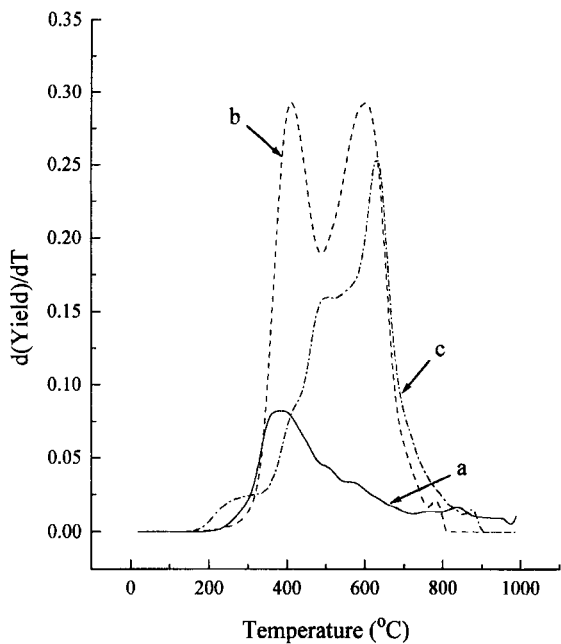


Fig. 2 AP-TPR profiles of the Goydnuk oil shale (a), Kimmeridge raw (b) and Kimmeridge after LiAlH_4 (c)

thiophenic sulphur forms.

The evidence for the reduction of organic sulfur compounds is scarce by the use of LiAlH_4 but, there is still a possibility that cleavage of disulphide and polysulphide linkage can occur, yielding methyl thioethers and thiolgroups, respectively. Fig. 2 c shows the AP-TPR profile of the Kimmeridge kerogen treated with LiAlH_4 . From these results it is clear that besides pyrite also organic sulfur forms are removed during this treatment. Together with this desulphurization, the formation of thiols has been identified for this kerogen, suggesting the initial presence of disulphide and polysulphide linkages in these samples.

REFERENCES

1. J. Yperman, D.V. Franco, J. Mullens, L. Van Poucke, G. Gryglewicz, S. Jasienko, Fuel, accepted
2. K. Ismail, S.C. Mitchell, S.D. Brown, C.E. Snape, A.C. Buchanan III, P.F. Britt, D.V. Franco, I.I. Maes and J. Yperman, Energy and Fuel, accepted
3. S.C. Mitchell, C.E. Snape, R. Garcia, K. Ismail, and K.D. Bartle, Fuel, 1994, 73, 159
4. A. Savitsky and M.J.E. Golay, Analytical Chemistry, 1964, 36, 1627
5. P. Gorry, Analytical Chemistry, 1990, 62, 570

Acknowledgement

The Authors like to thank M. Vanhamel and J. Kaelen for technical assistance with the TPR experiments. The research was supported by the European Coal and Steel Community (contract No 7220:EC-025)

Study of the sulphur functionalities and physical characteristics of a Bulgarian lignite by desulphurization techniques

I.I. Maes^a, D.V. Franco^a, J. Yperman^a, J. Mullens^a, L.C. Van Poucke^a, S.C. Mitchell^b and S.P. Marinov^c

^aLaboratory of Inorganic and Physical Chemistry, Limburgs Universitair Centrum, B-3590 Diepenbeek, Belgium.

^bSchool of Chemistry, University of Leeds, Leeds LS2 9JT, U.K.

^cInstitute of Organic Chemistry, Bulgarian Academy of Sciences, Sofia 1040, Bulgaria.

Abstract: A complete knowledge and understanding of the thermal reactivity of sulphur forms in coal is crucial for the development of new, efficient desulphurisation techniques. This contribution reports on seven selective desulphurization treatments of a Bulgarian lignite. The impact of individual treatments on the sulphur distribution was monitored by AP-TPR and XANES techniques. Complementary data concerning the physical impact of the treatments was obtained by DTA and SEM-EDX.

1. Experimental

Maritza Iztok, a Bulgarian lignite (I) (Table 1) was subjected to the following treatments: BuLi/TMEDA+BuOH followed by alkaline (II) and acidic (III) hydrolysis, Bu-ONa (IV), HNO₃ by both a low (V) and a high temperature (VI) ASTM (D 2492) method, molten caustic (VII) and a hydrothermal treatment (VIII). Desulphurization treatments, AP-TPR and K-edge XANES experimental details are described elsewhere [1,2].

2. Results

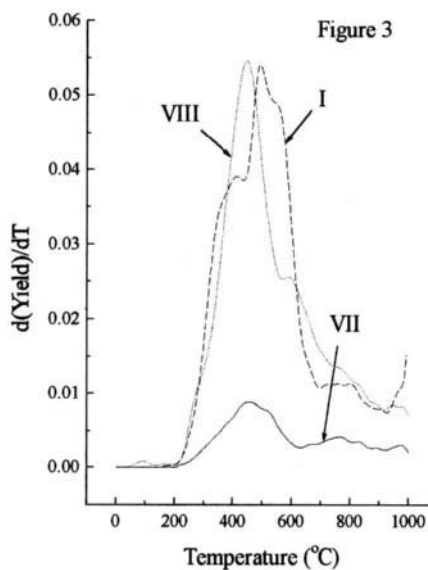
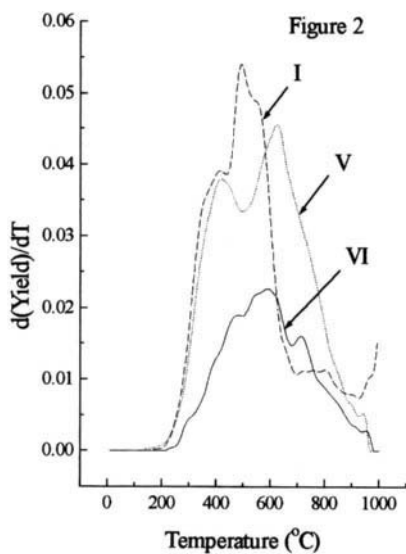
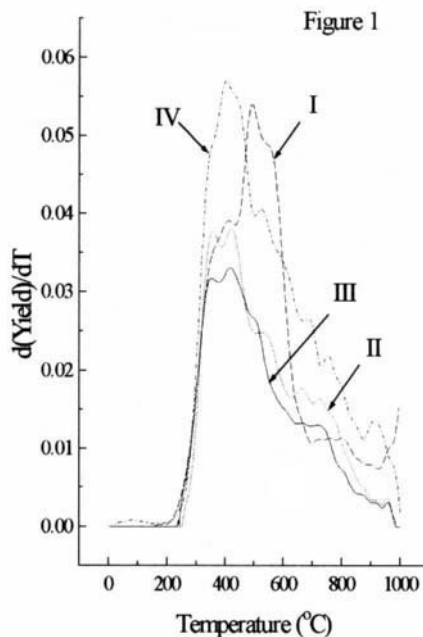
The characteristics of the products following the different chemical treatments of the Maritza Iztok lignite are given in Table 2. The AP-TPR and XANES spectra are presented in Figures 1-3 and 4 respectively. The DTA burning profiles of the treated samples are shown in Figure 5.

The AP-TPR profile of the untreated lignite (I) shows two main peaks at 410 and 495°C which, from model compound studies [3] can be attributed to the reduction of the Ar-S-R groups and pyrite. The leading shoulder at 350°C can be assigned to aliphatic sulfides, whilst the shoulder at 550°C corresponds to the reduction of sulphatic and arylsulphide groups [3]. The broad band observed between 670 and 820°C occurred in the region of 1-2 ring thiophene reduction. It is worth noting that the corresponding XANES spectrum also indicated the presence of sulfoxides in the lignite (Figure 4).

The BuLi/TMEDA + BuOH treatment followed by alkaline (II) hydrolysis was found to be a more effective desulphurization method than the acidic (III) variant. The AP-TPR spectra in Figure 1 show for both treatments the disappearance of the peaks at 495 and 550°C, indicating the removal of practically all the inorganic sulphur. The effective cleavage of sulphur ether groups and disulphide bridges resulted in an observable increase in the reduction of simple thiophenic compounds in the range of 650-800°C. XANES spectra confirmed the significant decrease in the sulphate content and indicated the formation of sulphones during

Table 1: Analyses of the Bulgarian lignite (I)

Ultimate Analysis*, wt%	
C	59.80
H	6.41
N	0.67
O(diff)	30.67
Proximate Analysis , wt%	
Moisture	7.5
Ash°	14.5
Volat. Mat.*	60.0
Fixed C*	38.6
Sulphur Analysis°, wt%	
Total	3.57
Pyritic	0.62
Sulphatic	0.85
Organic	2.10
* : dry ash free basis ° : dry basis	



Figures 1-3: AP-TPR spectra of the treated samples

Table 2 : Analyses of the treated samples of Maritza Izток lignite

Treatments :	II	III	IV	V	VI	VII	VIII
Proximate Analysis, wt%							
Moisture	4.2	4.6	6.5	6.5	3.1	4.2	4.5
Ash [°]	2.4	8.1	5.3	13.1	14.0	2.6	15.7
Volat. Mat.*	64.1	62.3	56.8	61.5	62.5	46.8	51.0
Fixed C*	35.8	37.3	42.8	37.4	36.7	53.0	48.1
Total Sulphur*, wt%	1.86	2.15	2.83	2.16	2.17	0.63	2.65
Desulphurization, %	47.9	39.8	20.7	39.5	39.2	82.3	25.8
Recovery AP-TPR, wt%	70	66	82	95	77	57	67

*: dry ash free basis °: dry basis

treatment. The corresponding burning profiles for the lignite samples were considerably different for both BuLi methods. A significant development of porosity generated by the alkaline method resulted in a shift towards a lower burning temperature (Figure 5, profiles II and III).

Treatment with BuONa (IV) removed only part of the pyritic and sulphatic sulphur. The main peak observed in the AP-TPR spectrum reflects the presence of disulphides and aryl-acyl sulphides. XANES analysis (Figure 4, spectrum IV) clearly shows that a considerable proportion of the organic sulphur groups were oxidised to sulfoxides and sulphones.

Both nitric acid treatments successfully removed the majority of the pyritic and sulphatic sulphur. The high temperature treatment (VI) (boiling temp., 30 min) had a greater effect on the distribution of organic sulphur groups than the low temperature treatment (V) (room temp., 24 hrs) (Figure 2). Once again, XANES analysis revealed the formation of sulphones from organically bound sulphur. Further investigation by SEM indicated that the surface of the products was more porous than for the original lignite, which would explain the increased rate of burning.

The highest level of sulphur removal was obtained using the molten caustic (VII) treatment. The overall AP-TPR response (Figure 3) and recovery indicated that no specific sulphur functionality was selectively desulphurized. Indeed, the removal of organic sulphur was accompanied by a significant decrease in mineral constituents, mainly Ca, Al and Si as observed by SEM-EDX analysis.

Hydrothermal treatment (VIII) resulted in the removal of only 25.8% of the sulphur. The AP-TPR results (Figure 3) suggest the removal of part of the pyritic and sulphate sulphur. The maximum at 450°C indicates the presence of mainly aryl-acyl sulphides. Surprisingly, the hydrothermal treated sample exhibits the highest maximum burning temperature shift of all treated samples.

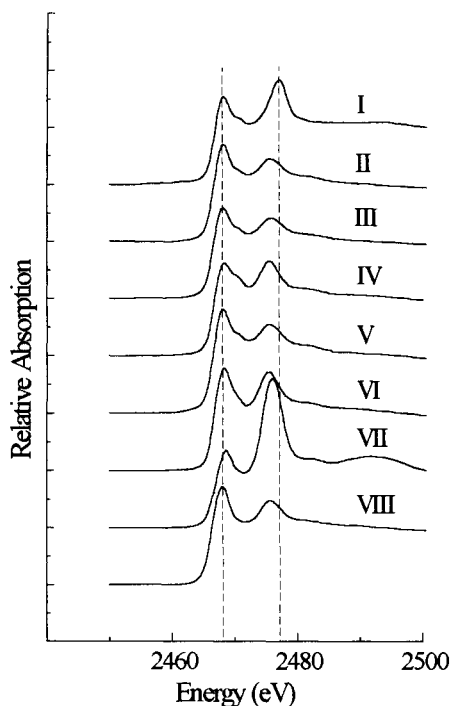


Figure 4: K-Edge XANES spectra of the treated samples

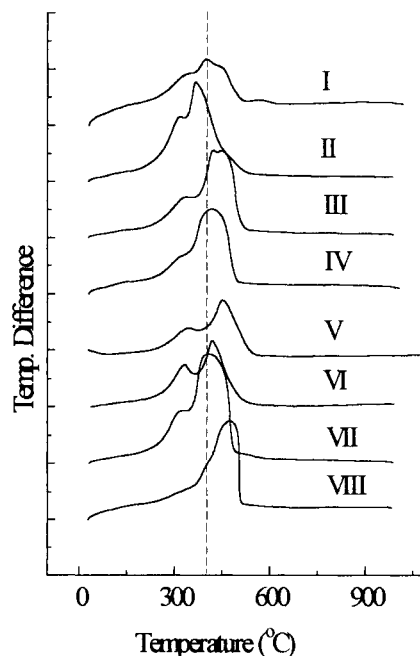


Figure 5: DTA Burning Profiles of the treated samples

3. Conclusions

The AP-TPR and XANES techniques offers a promising approach for monitoring the changes in sulphur functionalities induced by chemical desulphurization of coal. All the treatments used in this work resulted in an increase in porosity and improved the burning characteristics of the lignite studied.

References

- [1] J. Yperman, D.V. Franco,, J. Mullens, G. Reggers, M. D'Olieslaeger, L.C. Van Poucke and S.P. Marinov, NATO ASI, Series C, Vol.455 (1995) 449.
- [2] S.C. Mitchell, Ph.D Thesis, Univerity of Strathclyde, 1994.
- [3] K. Ismail, S.C. Mitchell, S.D. Brown, C.E. Snape, A.C. Buchanan III, P.F. Britt, D.V.Franco, I.I. Maes and J. Yperman, Energy & Fuels (1995), in press.

Acknowledgements

The authors would like to thank Mrs. M. Vanhamel and Mr. J. Kaelen for their technical assistance with the AP-TPR experiments. This research is financed with a specialisation grant of the "Vlaams Instituut voor de bevordering van het Wetenschappelijk-Technologisch onderzoek in de industrie (IWT)".

A study of sulphur and nitrogen in two high sulphur coals

Z. Zhu^a, Y. Gu^{a,b}, S.C. George^b, M.A. Wilson^b, F.E. Huggins^c and G.P. Huffman^c

^aInstitute of Coal Chemistry, Chinese Academy of Sciences, Taiyuan, China

^bCSIRO Division of Petroleum Resources and Australian Petroleum Cooperative Research Centre (APCRC), PO Box 136, N. Ryde, NSW 2113, Australia

^cChemical and Materials Engineering Department, University of Kentucky, Lexington, Kentucky, KY 40506, USA

1. INTRODUCTION

Sulphur and nitrogen-containing compounds in coals are of great importance due to the SO_x and NO_x emission problem during coal combustion and other problems such as poisoning during catalytic processing and instability during storage of liquid products. A previous report [1] addressed the distribution of sulphur and nitrogen-containing compounds in organic solvent-extracted Chinese high sulphur bituminous coal (Guiding, GD, 11.7% total sulphur). The present paper provides further details using XPS and XANES spectroscopies on this coal and new findings for a Spanish lignite (Mequinenza, MQ; 13.6% total sulphur). Gas chromatography mass spectrometry is also used to look for sulphur compounds in extracts from the coals.

2. EXPERIMENTAL

The MQ coal (H/C 0.89) was stored under argon in a container until crushing (-80 mesh) in air to measure. No special storage conditions were employed for the GD coal (H/C 0.83).

The XPS data were obtained on a Perkin-Elmer PH15300 ESCA system using Mg K α radiation with 250watts. The spectrometer was run at an analyser pass energy of 71.55eV. A binding energy correction was made to account for sample charging based on the C1s peak at 284.6eV. The S2p and N1s peaks were curve resolved using a 70% Gaussian 30% Lorentzian line shape and various FWHM (within the limits 1.8-2.1eV) and using peak positions of sulphur and nitrogen forms as reported elsewhere [2,3].

The XANES spectra was obtained at the National Synchrotron Light Source, Brookhaven National Laboratory, New York, on beam-line X-19A. The synchrotron is normally run at 2.53GeV and a current between 110 and 250mAmps. The data were collected from 2.42keV to 3.2keV with steps of 0.1eV/step over the XANES region from 2.46-2.49keV. Elemental sulphur was used as the primary energy calibration with a main peak position at 2.472keV. The spectra were fitted using a least-squares minimisation routine that fits a

mixed Lorentzian-Gaussian function to the peak shape and an arctangent function for the absorption edge-step(s).

Coal samples were extracted using dichloromethane/methanol (93:7). Asphaltenes were precipitated and the soluble maltenes were fractionated by column chromatography on alumina and silica gel [4]. Gas chromatography-mass spectrometry of the aliphatic and aromatic hydrocarbon fractions was carried out on a VG AutoSpec Ultima interfaced to a Hewlett Packard 5890 using splitless injection and DB1 and DB5 60m capillary columns.

3. RESULTS AND DISCUSSION

The curve resolved S2p XPS spectra of GD coal is shown in Figure 1 and the numerical result in addition to that of the MQ coal are listed in Table 1. The resolved peaks were assigned as follows. Approximate binding energies (eV) are: 162.0 organic sulphides, 164.2 thiophenes, 168.1 sulphones, 168.9 sulphoxides, 169.3 sulphate. In both coals the organic sulphides (ie. alkyl-, aryl-sulphides and di/polysulphides) and thiophenic sulphur are the dominant forms, but there is a significant difference in their relative levels. In the MQ coal, the sulphides are the most abundant form with 62% of total sulphur constituents; this value is in good agreement with the results from Calkins *et al.* by XPS [5] and flash pyrolysis [6]. The results differ from those obtained with K-edge XANES [7] in that they indicate a greater organic sulphide and a lesser thiophene content. For the GD coal (Table 1), thiophenic sulphur (52%) is more abundant than organic sulphides (30%), but again XPS appears to show a greater organic sulphide and a lesser thiophene content with respect to XANES. A typical XANES spectrum for GD coal is shown in Figure 2.

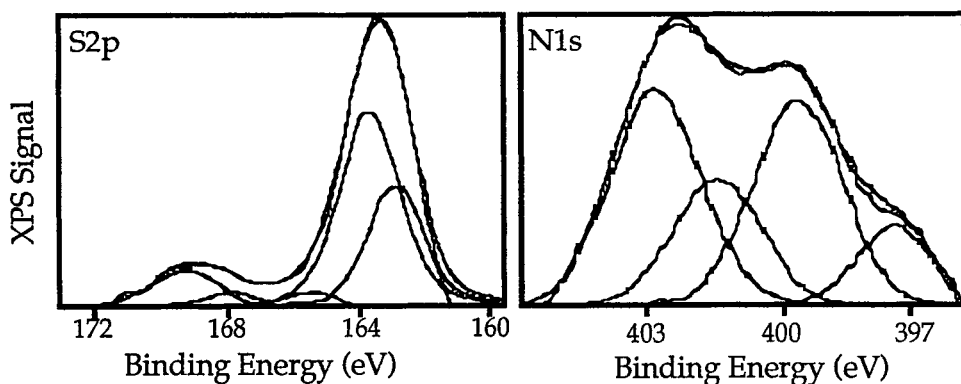


Figure 1 The curve resolved S2p and N1s XPS spectra of GD coal.

The curve resolved N1s XPS spectra of GD coal is shown in Figure 1 and the numerical results in addition to that of the MQ coal are listed in Table 2. The assignments are made as follows. Approximate binding energies (eV) are: 398.7 pyridinic, 400.3 pyrrole, 401.4 quaternary, ca 403 N-oxide. For MQ coal, pyrrolic nitrogen is the most abundant form followed by pyridinic nitrogen, which is

similar to previous analyses for other coals [3]. A higher level of N-oxide type nitrogen and a lower level of pyrrolic and pyridinic nitrogen were observed in the GD coal.

Table 1

The percent of organic sulphur forms by XPS and XANES

Coal	Analytical technique	Pyrite	Sulphides	Thiophenes	Sulphoxides	Sulphones	Sulphate
MQ	XPS	-	62	32	-	2	4
	XANES ^a	-	43	42	9	0	5
GD	XPS	-	30	52	3	4	11
	XANES	11 ^b	13	68	4	-	4

a: Reference [7].

b: The value has been estimated from Mössbauer spectroscopy.

Table 2

The percent of organic nitrogen forms by XPS

Coal	N-oxide	Quaternary	Pyrrolic	Pyridinic
MQ	16	11	52	21
GD	36	20	33	11

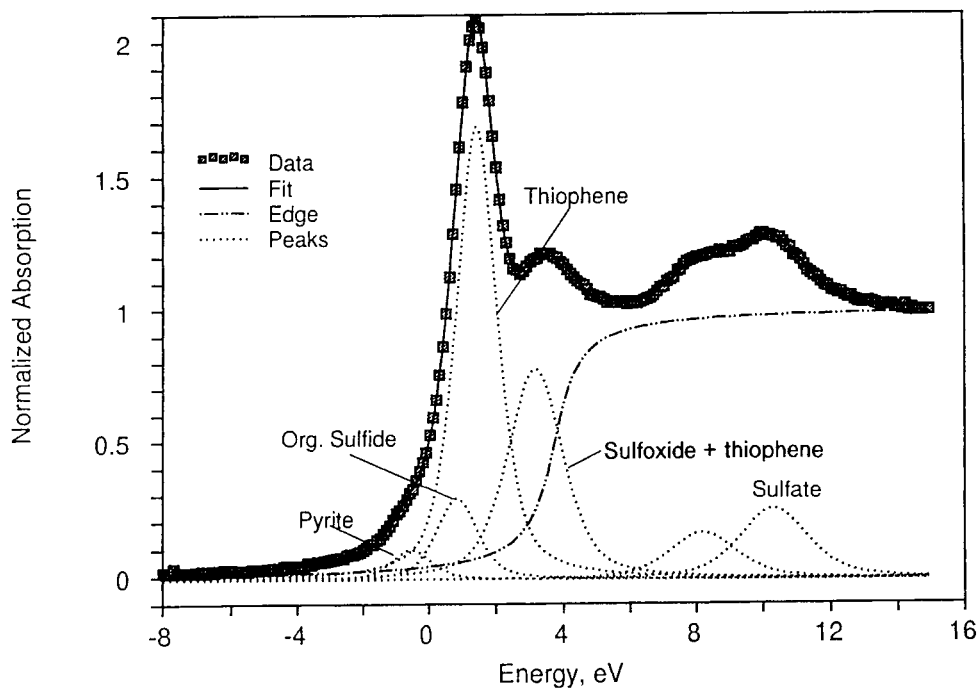


Figure 2 Least-squares fit of XANES data for GD coal.

The molecular and gross composition of the coal extracts, in part, corroborates the XPS and XANES data. No aliphatic sulphur compounds were detected in GD coal. Most of the organic sulphur in the extract of GD coal is present in aromatic groups, notably C₀-C₄ dibenzothiophene and C₀-C₃ alkylbenzothiothiophene homologues. In particular, 4-methyldibenzothiophene is the most abundant compound in the extractable fraction of GD coal. MQ coal also contains these and other aromatic sulphur compounds, but in addition contains significant amounts of alkylthiophenes, including 2-alkyl-5-methylthiophenes. These homologues have also been detected in the flash pyrolysates of MQ coal [8]. No aliphatic sulphides were detected by GC-MS of the extractable fraction of MQ coal, although XPS and XANES data suggest that sulphides form a major fraction of the organic sulphur. Aliphatic sulphides could not be detected in solvent extracted MQ coal by low voltage, high resolution MS using a direct insertion probe [7] either and it is likely that this discrepancy reflects the selectivity of solvent extraction. Further studies will be directed at identifying the organic sulphides in these coals by expansion of the coal lattice with solvents such as pyridine and mild chemical treatment.

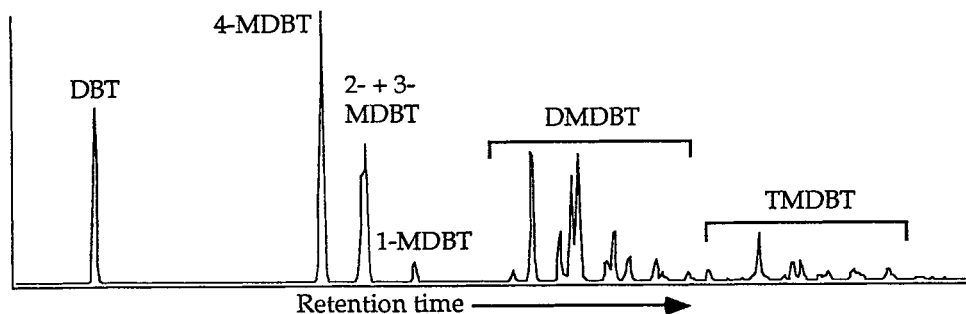


Figure 3 Added m/z 184+198+212+226 mass chromatogram, showing the distribution of dibenzothiophene (DBT) and its alkylated homologues in GD coal.

REFERENCES

1. X. Wang, W. Xue, J. Zhu, Y. Gu, P. Peng, G. Sheng and J. Fu, Proceedings of International Conference on Coal Science II, Banff, Alberta, Canada, (1993) 219.
2. S.R. Kelemen, G.N. George and M.L. Gorbaty, *Fuel*, **69** (1990) 939.
3. S.R. Kelemen, G.N. George and P.J. Kwiatek, *Energy & Fuels*, **8** (1994) 896.
4. S.C. George, S.M. Llorca and P.J. Hamilton, *Org. Geochem.*, **21** (1994) 235.
5. W.H. Calkins, R.J. Torres-Ordonez, B. Jung, M.L. Gorbaty, G.N. George and S.R. Kelemen, *Energy & Fuels*, **6** (1992) 411.
6. R.J. Torres-Ordonez, W.H. Calkins and M.T. Klein, In: *Geochemistry of Sulfur in Fossil Fuels*, W.L. Orr, C.M. White, Eds., ACS Symposium Series 429, Washington DC, 1990, 287.
7. C.M. White *et al.*, *Energy and Fuels*, **8** (1994) 155.
8. J.S. Sinninghe Damsté, F.X.C. de las Heras and J.W. de Leeuw, *J. Chrom.*, **607** (1992) 361.

Changes in the Forms of Nitrogen and Oxygen during Rapid Coal Pyrolysis

Mathew Watt, William Allen, and Thomas Fletcher

Department of Chemical Engineering, Brigham Young University, Provo, UT 84602 USA

1. INTRODUCTION

During coal combustion fuel nitrogen is the major source of nitrogen oxide pollution. This makes the study of nitrogen in coal and coal pyrolysis products an important area of study for the design and implementation of NO_x control strategies. It has long been felt that nitrogen is located within the nitrogen macromolecule as pyridinic and pyrrolic structures with some amines forms [1-2]. Only recently with the use of X-ray photoelectron spectroscopy (XPS) and X-ray absorption near-edge spectroscopy (XANES) has the pyridinic and pyrrolic forms of nitrogen been confirmed [3-4]. As shown in Fig. 1, these methods have shown approximate amounts of the different nitrogen functional groups. How these forms are released during pyrolysis, however, is poorly understood.

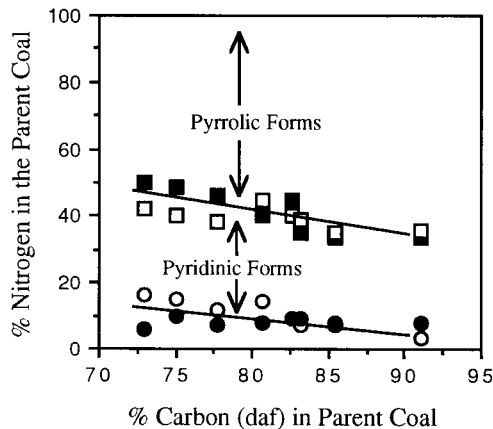


Figure 1. XPS and XANES data showing nitrogen functional forms in coal.

Very little has been done in the study of nitrogen forms in coal pyrolysis products. Kelemen et. al. [4] have studied a limited number of chars with the use of XPS and found that the levels of quaternary nitrogen went down while the forms of pyridinic nitrogen went up. Other studies have shown similar results [5]. The chars used in these studies were produced at low heating rates and temperatures and may not be applicable to the high heating rates and temperatures encountered in commercial pulverized coal furnaces.

It has been found that at high heating rates and temperatures, nitrogen release during pyrolysis is a function of coal rank. Figure 2 shows nitrogen release data from single particle entrained flow experiments, where char samples were collected immediately after pyrolysis in a laminar flow flat flame burner [6]. It is apparent that large differences in the nitrogen volatiles occur over a range of coal rank and among coals of the same rank.

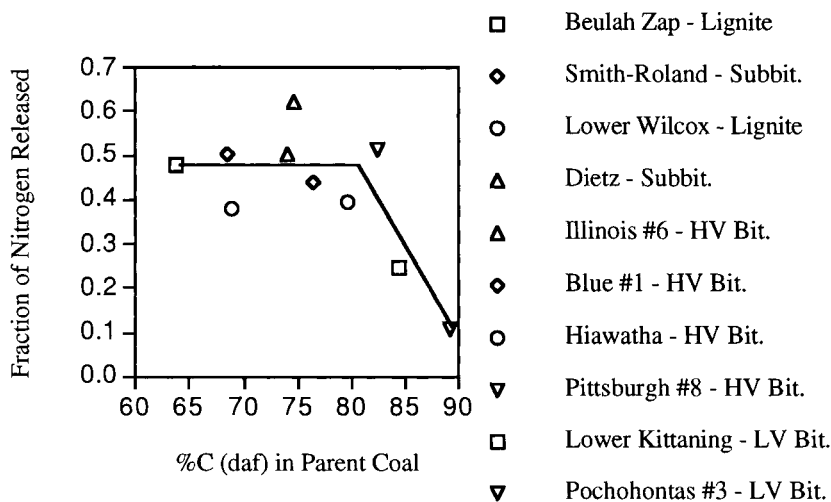


Figure 2. Fractional nitrogen release as a function of coal rank [6].

Comparing the XPS and XANES data of Fig. 1 and the nitrogen volatile data of Fig. 2 does not give any clear picture of the reasons for the major differences in nitrogen release between different coals. This study explores how nitrogen functional groups react during rapid pyrolysis. Analysis of pyrolysis products, such as tars and chars are analyzed using X-ray photoelectron spectroscopy (XPS). Insights into the pyrolysis reactions of nitrogen species are discussed.

2. EXPERIMENTAL

Coals were pyrolyzed at atmospheric pressures in a drop tube reactor [7]. Pulverized coal pyrolysis experiments were performed in 100% Nitrogen at temperatures of approximately 1000 K and at heating rates of 10^4 K/s. Residence times were varied between 70 and 200 ms within the reactor to obtain chars and tars that corresponded to different amounts of pyrolyzed mass release. A water cooled, nitrogen quench, transpiring wall collection probe was used to obtain samples of chars and tar. Tar and char were separated aerodynamically using a virtual impactor and cyclone, in a manner similar to that used by Fletcher [8].

Additional pyrolysis experiments were performed by injecting entrained pulverized coal particles through a methane/hydrogen/air flat flame burner operating under fuel-rich conditions. This allowed for char and tar samples to be produced at temperatures of 1500 to 1700 K with heating rates of 10^5 K/sec. The flat flame burner experiments used a collection system similar to that used in the drop tube experiments.

The coals used in this study are shown in Table 1. The coals were chosen due to the well-characterized nature and the large literature information available. Other investigators have also used some of the chosen coals in their investigations of nitrogen evolution during pyrolysis [4-6, 8-9]. Chars and tars were analyzed for the different coal nitrogen and oxygen compositions at Exxon Research using established techniques [4].

3. RESULTS & DISCUSSION

As noted in Fig. 3, for the Wyodak chars, the forms of nitrogen found by XPS do not change much as a function of mass release. The major changes show that the pyridinic forms of nitrogen increase slightly while the quaternary forms decrease slightly. It is thought [4] that

a portion of the quaternary nitrogen forms are protonated nitrogen functionalities. As pyrolysis takes, it is possible that the hydrogen is scavenged from the nitrogen to form other pyrolysis products. The functional form of nitrogen would then increase pyridinic nitrogen and decrease quaternary nitrogen, as analyzed by XPS.

Table 1. Elemental analysis of coals examined

Coal	Rank	Coal ID	%C (daf)	%H (daf)	%N (daf)	%S+O (daf)	%Ash (mf)
Wyodak	Subbit.	Argonne Prem.	85	5.4	1.6	7.2	19.8
Blind Canyon	HV Bit.	Utah Power	81	5.8	1.6	11.1	4.7
Pittsburgh #8	HV Bit.	PSOC 1551D	84	5.5	1.7	8.2	4.1
Illinois #6	HV Bit.	PSOC 1493D	77	5.0	1.5	17.0	15.1
Pocahontas #3	LV Bit.	PSOC 1508D	91	4.6	1.6	3.3	15.9

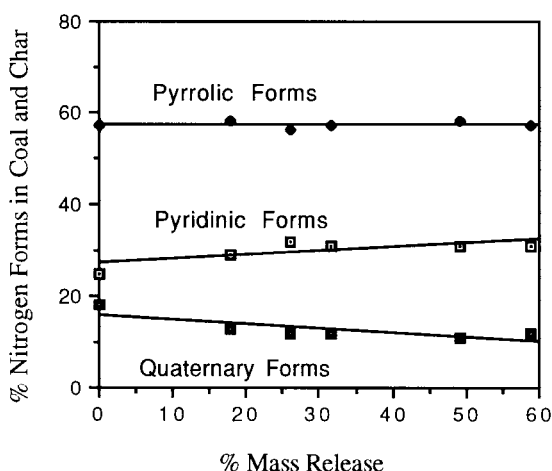


Figure 3. XPS forms of nitrogen found in Wyodak chars as a function of mass release

It is interesting to note that quaternary forms of nitrogen are present in all of the chars. These forms must be relatively stable, since pyrolysis conditions for these samples were relatively harsh; the quaternary forms may not only be protonated pyridines. If such were the case, very little quaternary nitrogen groups would be left in the char with 60% mass release.

Oxygen analysis was also performed on the Wyodak char samples using XPS, shown in Fig. 4, showing that oxygen is lost preferentially at the beginning of pyrolysis and then is released at the same rate as total mass is released. It is possible that the oxygen chemistry is somehow coupled to the nitrogen volatile chemistry in some form. Oxygen has a strong affinity for hydrogen, and pyrolysis products could include species such as H₂O and phenols. Further investigation of the solid phase chemistry is necessary before any such speculated mechanisms can be verified.

4. SUMMARY AND CONCLUSIONS

The use of XPS was used to determine how nitrogen functional forms in chars change during pyrolysis. It was found that only small changes occur in the overall functional forms of nitrogen. The quaternary nitrogen forms decrease slightly and pyridinic nitrogen forms increase almost the same amount. This seems to show, as has been indicated previously [4],

that many of the quaternary XPS forms are protonated pyridines. Not all the quaternary nitrogen forms are lost during pyrolysis, showing that some quaternary forms are more stable than previously thought. It is thought that coal organic oxygen may play a role in fuel nitrogen chemistry. Additional analytical methods are needed, such as ^{15}N NMR [10], to determine the forms of nitrogen in coal that affect coal-dependent nitrogen pyrolysis behavior.

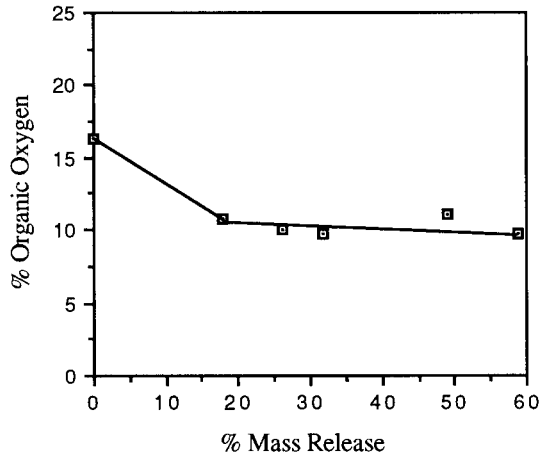


Figure 4. % Organic oxygen present in the Wyodak chars as a function of mass release.

REFERENCES

1. Pohl, J.H. and A.F. Sarofim, *16th Symposium (Int.) on Combustion*, p. 491 (1977)
2. Solomon, P.R. and M.B. Colket, *Fuel*, **57**, 749 (1978)
3. Mullins, O.C., Mitra-Kirtley, S., Elp, J. V., Cramer, S. P., *Applied Spectroscopy*, **47**(8), 1268 (1993)
4. Kelemen, S. R., M. L. Gorbaty, and P. J. Kwiatek, *Energy & Fuels*, **8**, 896 (1994)
5. Wojtowicz, M. A., J. R. Pels, and J. A. Moulijn, Submitted to *Fuel*, (1993)
6. Mitchell, R.E., Hurt, R. H., Baxter, L. L., Hardesty, D. R., *Compilation of Sandia Coal Char Combustion Data and Kinetic Analyses*, Milestone Report, Sandia Report SAND92-8208, (1992).
7. Monson, C. R., Germane, G. J., *Energy & Fuels*, **7**(6), 928, (1993)
8. Fletcher, T. H., *Comb. & Flame*, **78**, 223 (1989).
9. Freihaut, J.D., W.M. Proscia, and J.C. Mackie, *Comb. Sci. Tech.*, **93**, 323 (1993)
10. Pugmire, R. J., "Project 1A. NMR Analysis of Coal and Char Structure," *Advanced Combustion Engineering Research Center, 9th Year Progress Report*, **2** (1995)

ACKNOWLEDGMENTS

This work was sponsored by the Advanced Combustion Engineering Research Center at Brigham Young University. Funds for this center are received from the National Science Foundation, the State of Utah, 40 industrial participants, and the U.S. Department of Energy. We would also like to thank Dr. Simon Kelemen at Exxon Research for performing the XPS analyses.

Change in char nitrogen functionality during iron-catalyzed nitrogen removal

Y. Ohtsuka, T. Watanabe, H. Mori, and K. Asami

Research Center for Carbonaceous Resources, Institute for Chemical Reaction Science,
Tohoku University, Sendai 980-77, Japan

1. INTRODUCTION

The NO_x emitted in coal combustion originates mostly from the nitrogen present in the coal. Efficient conversion of coal nitrogen to N_2 in the pyrolysis process preceding combustion would thus contribute to the reduction of the NO_x emissions. This method would also be effective for reducing the N_2O emissions in the fluidized bed combustion of coal. We have recently found that, when brown coal with inexpensive iron is heated in an inert atmosphere, a large amount of coal nitrogen can be converted to N_2 [1,2]. It is probable in the iron-catalyzed nitrogen removal that fine iron particles react with the nitrogen in the char matrix because of the high reactivity and large mobility. Therefore the present work focuses mainly on making clear the effect of the iron catalyst on the functionality of char nitrogen. Since X-ray photoelectron spectroscopy (XPS) is the most successful technique to study the functionality of nitrogen in coal and char [3], this technique is used to examine the change in char nitrogen functionality during pyrolysis.

2. EXPERIMENTAL

Loy Yang coal of size fraction 150 – 250 μm is used. The ultimate analysis (wt% daf) is: C, 65.9; H, 4.7; N, 0.60; S, 0.27; O (diff.), 28.5. Fine particles of FeOOH are precipitated onto coal from an aqueous solution of FeCl_3 by using $\text{Ca}(\text{OH})_2$ powder as a precipitating agent. The details of catalyst preparation have been described elsewhere [4]. Pyrolysis experiments are carried out with a fluidized bed reactor attached with a transparent electric furnace [2]; 5 g of the sample is heated in a stream of He at about 700 K/min up to 900°C. Evolved N_2 recovered in a plastic bag is analyzed by gas chromatography, and the amounts of HCN and NH_3 dissolved into deionized water are determined by specific ion electrode analysis. The nitrogen contents in both solid char and liquid products comprising tar, oil, and water are determined by the conventional combustion methods.

The N 1s XPS spectra of the char samples after pyrolysis are measured using a Mg-K α X-ray source. A long acquisition time (several hours) is used to ensure good resolution, and the binding energy is referred to the Ag 3d peak at 367.9 eV. In order to examine depth profiles of the spectra, the char samples are exposed to Ar ion bombardment. Least-square curve fitting of all the spectra is performed using Gaussian peak shapes.

3. RESULTS AND DISCUSSION

3.1. Nitrogen distribution during pyrolysis

The change in nitrogen distribution at 900°C with iron loading is illustrated in Figure 1, where nitrogen mass balance falls within the reasonable range 100 – 107 %. The liquid material comprising tar, oil, and water is the main N-containing product for the original coal, as is denoted as liq.-N in the figure, and NH₃ is dominant among the evolved gas. It is shown that NH₃ is the dominant gas product in the pyrolysis of coal at low heating rate [5]. The presence of the iron catalyst even at a small loading of 0.7 wt% changes drastically the nitrogen distribution; a large amount of N₂ evolves at the expense of other products, nitrogen conversion to N₂ reaching 50 – 60 % at 0.7 – 2.8 wt% Fe. Conversion to char nitrogen (as char-N) is much lower in the presence of the iron. The decreased conversion is caused by the decreased nitrogen content in the char, since char yield is unchanged by catalyst addition.

The increased amounts of N₂ by iron addition, about 3.0 mg-N/g-coal, are almost twice as large as the decreased amounts of volatile nitrogen (NH₃, HCN, and liq.-N) irrespective of iron loading. This observation shows that, even if all the volatile nitrogen decreased is converted to N₂ through secondary decomposition reactions over the catalyst surface, almost half of N₂ formed in the presence of the catalyst comes from char-N (and/or the precursors). This means that the iron catalyst can promote solid-phase nitrogen removal reactions. Surely, fine iron particles catalyze considerably the formation of N₂ from N-enriched carbon during heat treatment in an inert atmosphere [6].

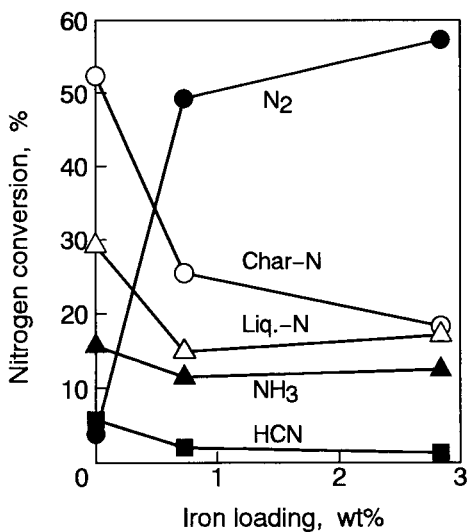


Figure 1. Effect of iron catalyst on nitrogen distribution at 900°C.

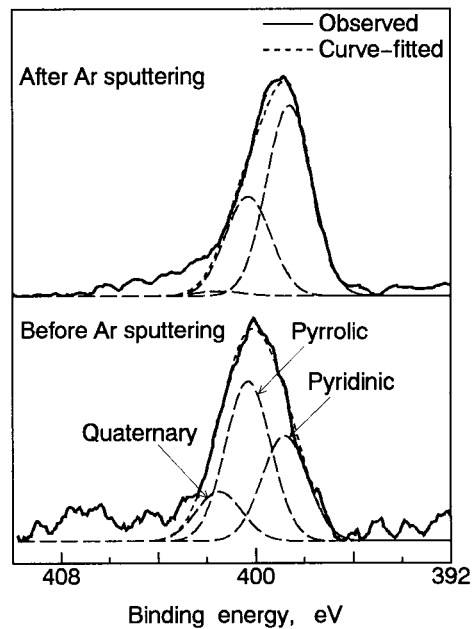


Figure 2. N 1s XPS spectra for Fe-bearing chars after pyrolysis at 900°C.

3.2. Char nitrogen functionality

Figure 2 shows the typical examples of N 1s XPS spectra for iron-bearing chars after pyrolysis at 900°C. When the atomic ratios of N/C determined by both XPS measurements and elemental analysis are compared for several coals and chars with and without the iron catalyst, there is the excellent surface:bulk correlation in the range of N/C of < 0.03. As is seen in Figure 2, very good curve resolution is observed in most cases, and pyridinic, pyrrolic, and quaternary nitrogen can be resolved at 398.7, 400.3, and 401.4 (± 0.1) eV, respectively [7,8].

Figure 3 shows the results of curve resolution analysis for these three nitrogen forms. When XPS spectra are measured without Ar sputtering, pyrrolic nitrogen is the dominant species without the iron, and pyridinic nitrogen succeeds it, quaternary nitrogen being minor. Compared with the spectrum for the original Loy Yang coal, the ratio of pyridinic to pyrrolic nitrogen is higher after pyrolysis and the quaternary nitrogen is lower. These observations are in agreement with previous findings for the char samples after mild pyrolysis of other coals [7]. It is suggested that the quaternary nitrogen species are pyridinic forms associated with hydroxyl oxygen and decreased by loss of oxygen functional groups on pyrolysis [7].

It is noteworthy that the ratios of pyrrolic to pyridinic nitrogen are lower in the iron-bearing chars, as is shown in Figure 3. Since their nitrogen contents are less than half of that in the original char, the absolute amounts of pyrrolic and pyridinic functionalities are much lower in the presence of the iron. These findings show that the catalyst can promote the nitrogen removal from pyrrolic nitrogen more selectively than from pyridinic nitrogen. The quaternary nitrogen increases linearly with increasing iron loading (Figure 3). The Fe 2p3/2 XPS spectra of the iron-bearing chars reveal that iron oxides such as Fe_3O_4 and Fe_2O_3 are the dominant species, and the intensities are larger at a higher iron loading, although the X-ray diffraction measurements show that $\alpha\text{-Fe}$ and Fe_3C alone are the bulk species. It is suggested that quaternary nitrogen may be formed by interaction between pyridinic nitrogen forms and lattice oxygen atoms in surface oxides and/or adsorbed oxygen species.

Figures 2 and 3 also show the results after Ar sputtering in order to clarify the depth profiles of char nitrogen functionalities. The binding energies of C 1s peak and the N/C ratios for the original samples before pyrolysis are changed largely by exposing them to Ar ion bombardment. However, there are no significant changes in both values for the pyrolyzed chars with and without the iron. This means no significant damage to char structure by Ar sputtering.

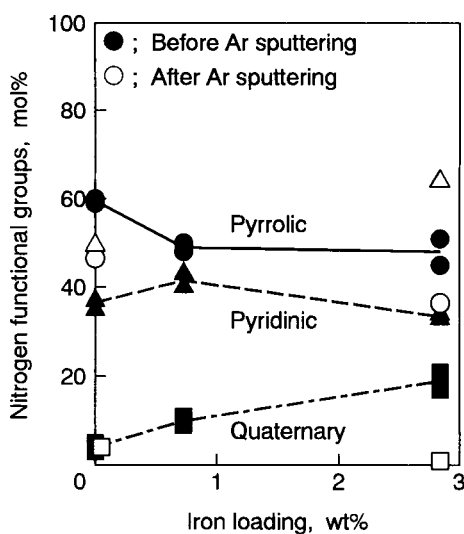


Figure 3. Effects of iron loading and Ar sputtering on char nitrogen functionality.

As is seen in Figure 3, in the original char, quaternary nitrogen is unchanged after sputtering, whereas the ratio of pyrrolic to pyridinic nitrogen is lower, showing a higher concentration of pyrrolic nitrogen at the outermost layer. Figures 2 and 3 indicate that the nitrogen functionalities of the iron-bearing chars change drastically after Ar sputtering; pyridinic nitrogen becomes major, and quaternary nitrogen almost disappears. The XPS intensities of iron oxides also decrease remarkably, whereas those of α -Fe and Fe_3C increase largely, which means easy removal of surface oxides. Therefore the quaternary nitrogen species at the outermost layer in the presence of the catalyst would be pyridinic forms associated with iron oxides, as suggested above. The comparison of the N 1s spectra after Ar sputtering for the original and iron-bearing chars points out the lower ratios of pyrrolic to pyridinic nitrogen in the latter chars. It can be concluded that the iron catalyst promotes the nitrogen removal from pyrrolic nitrogen to a larger extent than from pyridinic nitrogen, irrespective of the depth of coal sample.

The presence of Fe_3C as the bulk species shows that metallic iron with the fine size of 20 – 30 nm can readily react with the carbon in the char matrix because of the high mobility and large reactivity. Fine iron particles would also react with pyrrolic and pyridinic nitrogen forms in the char substrate to form interstitial iron nitrides, which are subsequently decomposed to iron species and N_2 .

4. CONCLUSION

The presence of the iron catalyst precipitated onto brown coal lowers the ratio of pyrrolic to pyridinic nitrogen in the char after pyrolysis at 900°C. Since residual nitrogen in the char decreases with the formation of N_2 during the iron-catalyzed pyrolysis, it is probable that the catalyst promotes the preferential nitrogen removal from pyrrolic nitrogen forms.

ACKNOWLEDGEMENT

The authors gratefully acknowledge the assistance of Miss Ayumi Shoji in carrying out experiments. This research is supported in part by the NEDO International Joint Research Grant.

REFERENCES

1. Y. Ohtsuka, H. Mori, K. Nonaka, T. Watanabe and K. Asami, *Energy Fuels*, **7** (1993) 1095.
2. Y. Ohtsuka, H. Mori, T. Watanabe and K. Asami, *Fuel*, **73** (1994) 1093.
3. R.M. Davidson, IEAPER/08, IEA Coal Research, London, 1994.
4. K. Asami and Y. Ohtsuka, *Ind. Eng. Chem. Res.*, **32** (1993) 1631.
5. R. Bassilakis, Y. Zhao, P.R. Solomon and M.A. Serio, *Energy Fuels*, **7** (1993) 710.
6. T. Watanabe, Y. Ohtsuka and Y. Nishiyama, *Carbon*, **32** (1994) 329.
7. S.R. Kelemen, M.L. Gorbaty and P.J. Kwiatek, *Energy Fuels*, **8** (1994) 896.
8. M.A. Wójtowicz, J.R. Pels and J.A. Moulijn, *Fuel*, **74** (1995) in press.

XPS Evidences for Changes in the Nitrogen Forms in Result of Hydrolysis of Model Chars.

Z.Piwowska^a, K.Stańczyk^b and R.Dziembaj^a

^a Faculty of Chemistry, Jagiellonian University, ul. Ingardena 3, 30-060 Kraków, Poland

^b Institute of Coal Chemistry, Polish Academy of Sciences, ul. Sowińskiego 5, 44-102 Gliwice, Poland

1. INTRODUCTION

Determination of the nitrogen forms in coals has got increased significance resulting from many attempts to find relationships between given nitrogen functionalities and NO_x emission during coal combustion.

Non-destructive techniques (XPS, XANES), making it possible to determine the forms of nitrogen in coals and chars, have shown that most of the nitrogen in coal is present in a form of ring compounds as pyrrolic, pyridinic and quaternary structures.

In the previous studies [1-3], undertaken to characterize these forms in the course of pyrolysis and gasification, an assumption was made that the nitrogen forms survived the carbonization procedure.

Our previous work [4] however, has revealed the transformation of nitrogen functionalities during low temperature carbonization. The aim of the present work was to establish influence of the reducing hydrogen atmosphere on the state of nitrogen forms in the course of hydrolysis.

2. EXPERIMENTAL

Carbonization of the nitrogen compounds was carried out in a fixed-bed reactor in the argon or hydrogen flow. The apparatus is described elsewhere [5]. The model chars were prepared from the following precursors: polyvinylpyrrolidone (Prolabo), symbol PVPI, acridine 99% (Aldrich), ACRI and 9-aminoacridine 97% (Merck), AMAC. The nitrogen compounds were heated to 300°C at 15K min⁻¹ and then to 460°C at 5K min⁻¹ under 5MPa of argon and kept at 460°C for three hours. The chars were subjected for further heating with the heating rate of 5K min⁻¹ under 5MPa of hydrogen at 600°C or 800°C for 15 minutes.

XPS analyses of the chars were carried out in a VSW ESCA 100 spectrometer using MgK α radiation (1253.6 eV). All spectra were obtained at an analyser pass energy 44 eV in the fixed analyser transmission mode. The operating pressure was below 3 \times 10⁻⁶ Pa. Char specimens were mounted by pressing the powder onto an indium foil. They were continuously cooled by liquid N₂ during the measurements. The required acquisition time for obtained the N 1s spectra of sufficient quality was 2.5 hours.

3. RESULTS AND DISCUSSION

The analyses of the model chars are listed in Table 1. The nitrogen content of the chars calcined at 460°C does not change after further hydrolysis at 600°C but it is strongly reduced after the hydrolysis at 800°C.

Table 1

Elemental analysis of chars carbonized at 460°C and calcined under hydrogen at 600 or 800°C.

% wt	PVPI			ACRI			AMAC		
	460	600	800	460	600	800	460	600	800
N	9.4	8.5	4.9	8.2	9.0	5.6	8.5	8.5	5.6
C	81.8	83.0	86.5	85.9	86.7	86.6	83.7	83.5	82.7
H	3.1	2.4	1.3	3.3	2.7	1.3	2.9	2.5	1.2

The N 1s spectra of the chars obtained from PVPI, ACRI and AMAC are presented in Figures 1-3, respectively. For all chars hydrolyzed at 600°C three types of nitrogen forms are observed: pyridinic (398.3 eV), pyrrolic (400.3 eV) and quaternary (401.3 eV). Spectra of chars prepared at 800°C are broader and it is necessary to include a peak at 403.0 eV which is interpreted as N-oxide.

Distribution of these nitrogen forms is shown in Table 2. In all chars obtained at 460°C the most abundant is pyrrolic one. After 600°C hydrolysis the ratio of pyridinic to quaternary nitrogen increases (in case of AMAC it remains similar) and after 800°C hydrolysis clearly decreases. Moreover, the amount of quaternary structures in chars hydrolyzed at 600°C is lower or the same as the chars carbonized only at 460°C. This is an opposite change to this observed after pyrolysis [4]. In the chars hydrolyzed at 800°C small amount of N-oxides appears.

Table 2

Distribution of nitrogen structures in chars carbonized at 460°C and calcined under hydrogen at 600 or 800°C.

		pyridinic nitrogen	pyrrolic nitrogen	quaternary nitrogen	N-oxide	pyrrolic / pyridinic	pyridinic / quaternary
PVPI	460	34	48	18		1.4	1.9
	600	41	46	13		1.1	3.1
	800	29	38	27	6	1.3	1.1
ACRI	460	40	48	12		1.2	3.3
	600	45	45	10		1.0	4.5
	800	35	46	16	3	1.3	2.2
AMAC	460	41	47	12		1.1	3.4
	600	41	46	13		1.1	3.2
	800	31	41	21	7	1.3	1.5

In the paper concerned the chars pyrolyzed under argon it was stated [4] that the amount of quaternary nitrogen increases with the increase of pyrolysis temperature. The same tendency is observed for hydrolysis, however, in the chars obtained under hydrogen the quantity of these structures is lower in comparison with pyrolysed chars. With the increase of pyrolysis

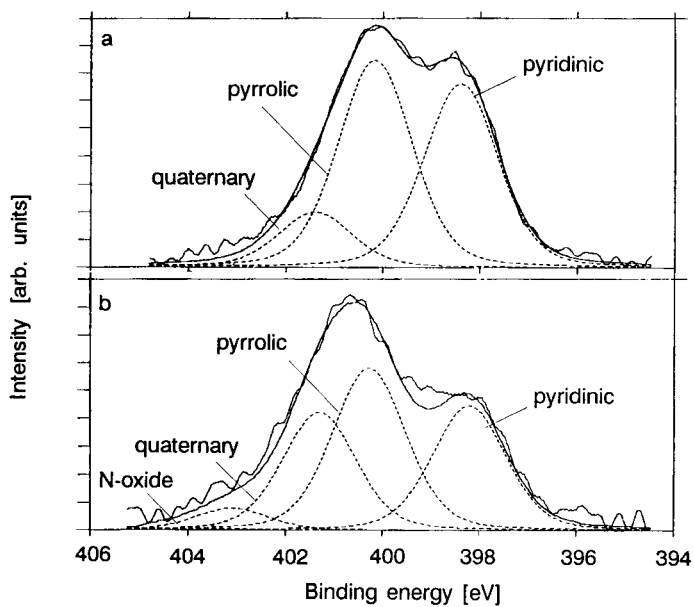


Figure 1. N 1s spectra of PVPI chars calcined under hydrogen at 600°C (a) and 800°C (b)

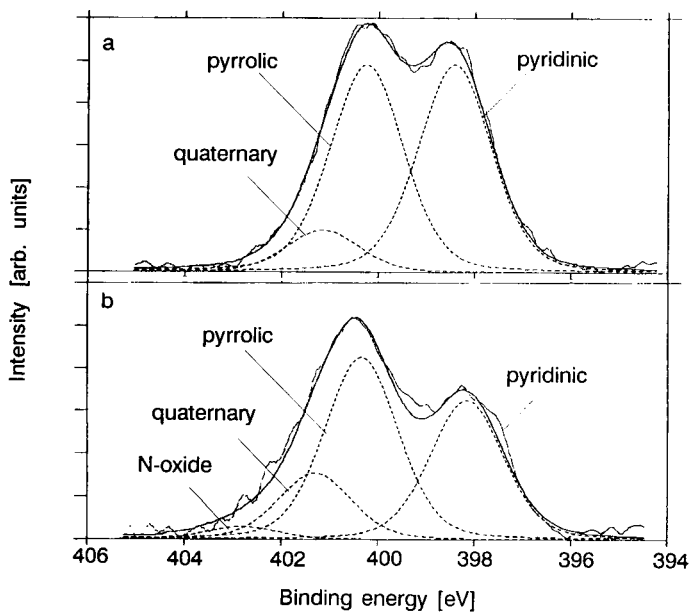


Figure 2. N 1s spectra of ACRI chars calcined under hydrogen at 600°C (a) and 800°C (b)

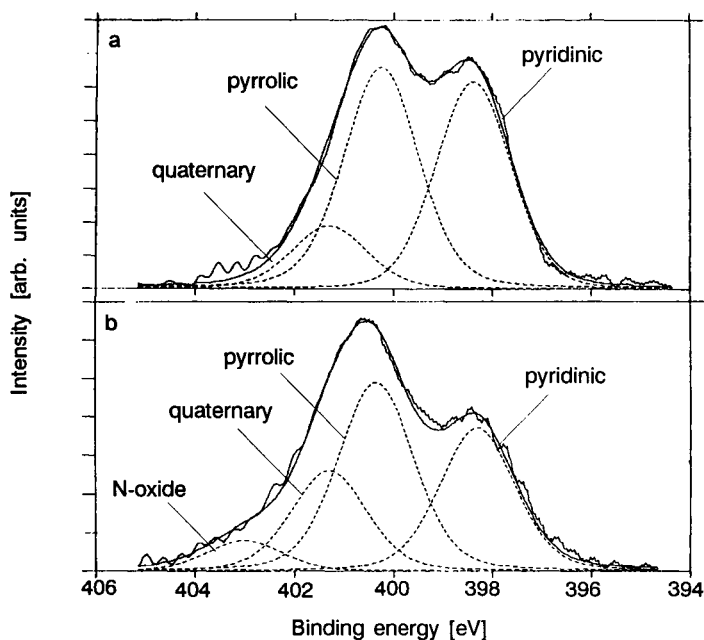


Figure 3. N 1s spectra of AMAC chars calcined under hydrogen at 600°C (a) and 800°C (b)

temperature the amount of pyridinic and pyrrolic forms decreases. This decrease is stronger for the pyrrolic forms in case of the inert pyrolysis, but smaller in case of the hydrolysis.

It may be concluded that pyridinic nitrogen is transformed into quaternary during pyrolysis. Hydrogen stabilizes the pyridinic forms so in chars hydrolyzed at 600°C the pyridinic/quaternary ratio is higher than in case of the chars pyrolyzed in argon. Smaller amount of quaternary and higher quantity of pyridinic nitrogen in chars obtained in hydrolysis, in comparison with pyrolysis, is reported also in studies performed on coal [6]. However, the explanation presented there can not be applied in the case of the model chars study. It seems rather, that pyridinic nitrogen is transformed into quaternary (understood as protonated pyridinic form in the interior of aromatic carbon layers). With temperature increase up to 800°C they transform to pyridinic N-oxide.

REFERENCES

1. W.X.Wang and K.M.Thomas, *Fuel*, 71 (1992) 871.
2. W.X.Wang and K.M.Thomas, *Fuel*, 72 (1993) 293.
3. K.Stańczyk and J.P.Boudou, *Fuel*, 73 (1994) 940.
4. K.Stańczyk, R.Dziembaj, Z.Piwowska and S.Witkowski "Transformation of nitrogen structures in carbonization of model compounds determined by XPS", *Carbon*, accepted.
5. K.Stańczyk and P.Dyla, *Przemysł Chemiczny*, 67 (1988) 326.
6. S.R.Kelemen, M.L.Gorbaty and P.J.Kwiatk, *Energy & Fuels*, 8 (1994) 896.

Promotion of Nitrogen Removal during Coal Pyrolysis by Using Iron Catalyst Impregnated by Solvent Swelling Method

J.-i. Hayashi^a, K. Kusakabe^a, S. Morooka^a and E. Furimsky^b

^aDepartment of Chemical Science and Technology, Kyushu University, 6-10-1, Hakozaki, Higashi-ku, Fukuoka 812-81, Japan

^bCanada centre for Mineral and Energy technology (CANMET), Energy Research Laboratories, 555 Booth Street, Ottawa, Ontario, K1A, OG1 Canada

1. Introduction

Recently the fate of coal nitrogen during pyrolysis has been extensively investigated. [1-3] Nitrogen evolved as HCN, NH₃ and tar in the initial pyrolysis period is the primary contributor to NO_x generated in following combustion stage, while a portion of nitrogen in char is also converted into NO_x. Thus the selective conversion of coal nitrogen into N₂ in the pyrolysis stage is effective for suppressing NO_x emission.

Ohtsuka et al. [4,5] introduced an iron precursor, FeOOH, into the matrix of a brown coal from an aqueous FeCl₃ solution and found that the iron catalyst significantly enhanced the evolution of N₂ during a pyrolysis in an inert atmosphere. The selective increase of N₂ was balanced by the reduction of nitrogen evolved as HCN, tar and that fixed in char. Iron catalyst precursors should be located in micropores prior to pyrolysis to contact the coal matrix at molecular level for promoting pyrolytic removal of coal nitrogen. Brown coals contain much carboxyl groups as cation exchange sites. Fe³⁺ ions are easily incorporated into the coal matrix via ion exchange. However, it is difficult to apply the ion exchange method to higher rank coals which are poorer in carboxyl groups and are less microporous than are brown coals.

In the present study, two organometallic iron precursors, ferric acetate and ferrocene, were impregnated into three coals of different ranks swollen in polar organic solvents. The iron-impregnated coals as well as the original ones were subjected to slow and atmospheric pyrolysis. The effect of the incorporated iron species on the fate of nitrogen was quantitatively examined.

2. Experimental

Yallourn brown coal (YL), Wyoming sub-bituminous coal (WY) and Illinois No.6 coal (IL) were pulverized, sized to 0.074 - 0.125 mm and dried *in vacuo* at 80°C. Ferric acetate, Fe(OH)(CH₃COO)₂, and ferrocene, Fe(C₅H₅)₂, were used as the iron precursors. Ferric acetate was dissolved in ethanol or ethanol/THF (1:1 by weight) binary solvent, and ferrocene in THF. Ferric chloride, FeCl₃, was also used to incorporate Fe³⁺ into the YL coal by ion-exchange method. 3-4 g of each coal sample was added to the solution containing a prescribed amount of the respective iron precursor. The mixture was quiescently kept in a flask for 12 h at 30°C. The solvent was then slowly evaporated at 70°C for 5 h into a nitrogen flow under atmospheric pressure, followed by vacuum drying. Ferric acetate impregnated from ethanol and ethanol/THF solutions are respectively abbreviated as FeAc(EtOH) and FeAc(EtOH/THF) hereafter. Table 1 shows the amount of iron impregnated into coals. The amount of impregnated ferrocene as iron was initially 3.7-3.8 wt% of dry coal. During the pyrolysis of ferrocene-impregnated coals, however, about 50% of ferrocene was desorbed from the coals at the low temperature region below 300°C with no decomposition. The amount of ferrocene remaining in the coals was shown in Table 1.

The raw and iron-impregnated coals were pyrolyzed in a fixed-bed reactor. A coal sample of ca. 0.6 g was fixed in the quartz tube reactor. The pyrolysis was conducted in an atmospheric

flow (0.6 L/min) of helium under a heating rate of 10°C/min from 20°C to 1000°C. The temperature was held at 1000°C for 40 min. Pyrolysis gas was continuously introduced into an FT-IR gas analyzer and injected into an TCD gas chromatograph at 2.5 or 3-minute intervals. The concentration of H₂O, CO, CO₂, NH₃, HCN and N₂ was determined.

3. Results and discussion

Figure 1 shows the evolution profiles of N₂ from the raw and iron-impregnated coals. The N₂ evolution from the IL coal was obviously promoted in the presence of iron species from both precursors. The temperature where N₂ formation started was ca. 600°C for the iron-impregnated coals and was lower by 100°C than that for the raw coal.

However, the impregnation hardly changed the temperature at which the evolution rate reached the maximum, T_{max} . The impregnation of ferrocene promoted the N₂ evolution most significantly. The final N₂ yield, 0.72 wt%, was 2.6 times higher than that for the raw coal. On the other hand, FeAc/EtOH was far less effective than that of ferrocene, although the amount of iron loaded from FeAc/EtOH was 2.4 times that of ferrocene. Ferrocene and FeAc was respectively decomposed at 250-400°C and 250-350°C, which were confirmed by the evolution of cyclopentadiene from the former and acetic acid from the latter. When N₂ evolution began at 600°C, iron is considered to exist as oxides and metal [4,5] for both precursors, and hydroxide was also possible in case of ferric acetate.[6] The difference in catalytic activity may be originated from the difference in dispersivity of the precursors.

The swelling ratio of the IL coal in ethanol was only 1.1 at 30°C, while that in THF was 1.7 at the same temperature. The swelling ratio is a measure for the expansion of micropores and has a strong relationship with the penetration of reagents into coal. Since the swelling ratio of the IL coal was 1.5 in the mixed solvent, the diffusion of ferric acetate into the coal matrix should be much increased than in ethanol. As indicated in Fig.1(a), the N₂ evolution was actually enhanced. To compensate the amount of iron impregnated, the increment of N₂ is normalized by the amount iron impregnated on molar basis. For the IL coal, for instance, the values for the ferrocene, Fe(EtOH/THF) and Fe(EtOH) coals are respectively 1: 0.8: 0.24, indicating that sufficient swelling increased dispersivity and activity of the iron catalyst. Thus the overall activity of iron from FeAc(EtOH/THF) was about 3.3 times higher than that from FeAc(EtOH).

The impregnation of ferrocene and FeAc also promoted the N₂ formation from the WY and YL coals. As shown in Fig.1(b), the N₂ evolution from the iron-impregnated YL coals suddenly began at about 580°C, and the evolution rate quickly increased to the first maximum at 620-630°C. The evolution profiles were more complicated than those with the IL coal. Three peaks were observed for the YL coal samples including the raw coal. The value of T_{max} was different for each coal sample prepared differently. The introduction of Fe³⁺ ions by ion exchange method was as effective as the impregnation of FeAc (EtOH) and FeAc (EtOH/THF) for promoting the N₂ evolution and was less effective than that of ferrocene. The evolution rate of N₂ from the ferrocene-impregnated YL was larger than that from any other YL coals at a temperature range of 580-900°C. For the ferrocene-impregnated YL coal, these peaks were observed at T_{max} = 620, 740 and 900°C. For the other YL coals only the lowest and medium T_{max} appeared at 600-800°C. It is clear that iron species derived from ferrocene behave

Table 1. Combinations of iron precursor and solvent

Coal	Precursor	Solvent	Fe loading [wt%, db]
IL ^{a)}	FeAc	EtOH	4.17
	FeAc	EtOH/THF	1.95
	Ferrocene	THF	1.75
WY ^{b)}	FeAc	EtOH	3.77
	Ferrocene	THF	1.74
YL ^{c)}	Fe ³⁺ exchange	H ₂ O	1.96
	FeAc	EtOH	3.86
	FeAc	EtOH/THF	2.03
	Ferrocene	THF	1.80

a) C: 75.6, H: 5.3, N: 1.4 wt%, daf., Ash: 13.0 wt%, db.

b) C: 73.8, H: 5.1, N: 1.0 wt%, daf., Ash: 6.0 wt%, db.

c) C: 65.9, H: 4.9, N: 0.65 wt%, daf., Ash: 2.0 wt%, db.

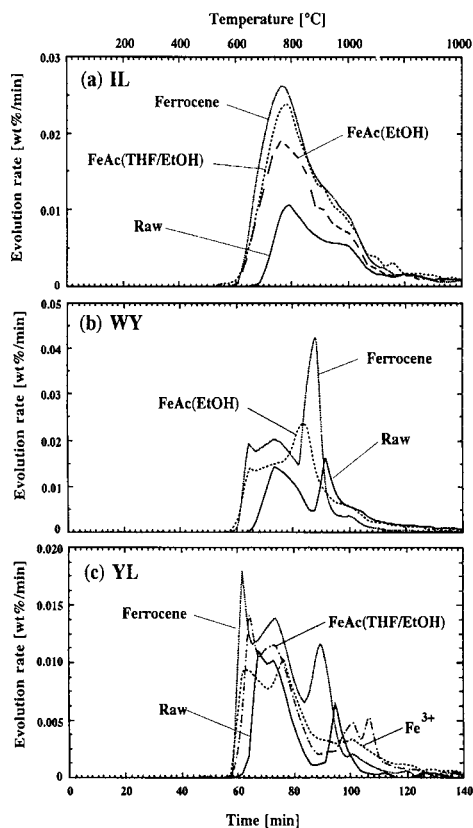
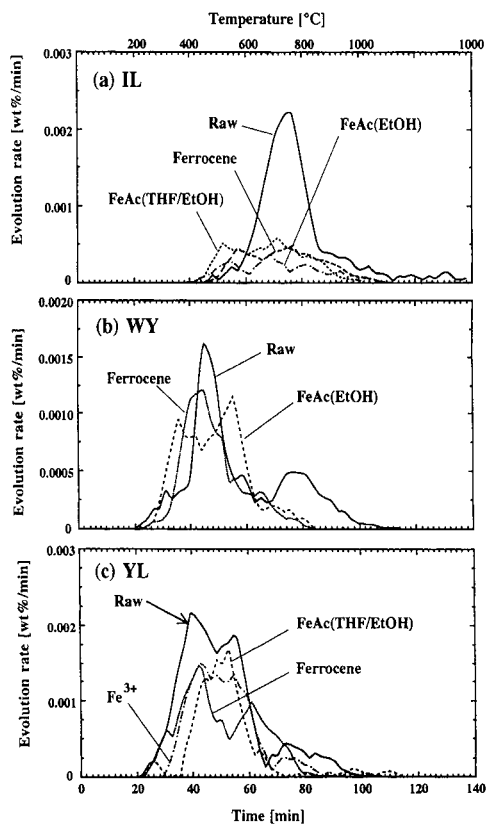
Figure 1. Evolution profiles of N_2 

Figure 2. Evolution profiles of HCN

differently in the N_2 formation above 800°C from those initially bound to carboxyl groups. The original and ferrocene-impregnated YL and WY coals gave similar evolution profiles for N_2 , suggesting that the chemical form and catalytic effect of iron derived from ferrocene were similar with these coals and were quite different with the IL.

Figure 2 shows the evolution profiles of HCN. For the IL coal, the impregnated iron considerably suppressed the HCN evolution above 600°C . The temperature region where the HCN evolution was suppressed was well coincided with that where the N_2 evolution was accelerated. This indicates that the generation of HCN as well as that of N_2 was affected by the catalytic activity of iron. The HCN evolution from the iron-impregnated coals was not affected by combinations of precursor and solvent. Two different explanations are possible for the reduction of HCN emission. This implies that the iron was concerned with the secondary conversion of HCN to N_2 while HCN diffuses through the porous structure impregnated with iron, rather than that the HCN formation itself is suppressed in the presence of iron. The suppression of HCN evolution was also observed for the WY and YL coals. The evolution rate of HCN from the raw WY coal showed two peaks at $450\text{--}600^\circ\text{C}$ and $700\text{--}900^\circ\text{C}$. The peak area at the lower temperature was much larger than that at the higher temperature. The formation of HCN above 700°C was effectively suppressed in the presence of iron, but that below 600°C was not so changed. Impregnated iron was activated for N_2 evolution at about

600°C, which was higher than the low temperature peak of HCN evolution. This can be the major reason of less significant reduction of HCN yield for the WY coal than that for the IL coal from which the HCN evolution began at 600°C. However, it is also a fact that the iron impregnated into the YL coal suppressed the HCN formation to some extent even at 300-450°C. This indicates that the impregnated iron influenced the pyrolysis behavior of the coal in this temperature region where tar formation was the major event.

NH₃ was evolved in the temperature ranges of 400-900°C from the IL raw coal and 300-800°C for the WY and YL raw coals. The evolution profiles evidently reveal that iron derived from both precursors suppressed the NH₃ evolution above 600°C. At above 500°C, the impregnated iron significantly suppressed the NH₃ emission. The extent of NH₃ reduction was hardly varied by varying the combinations of precursors and solvents.

Figure 3 shows the nitrogen distribution in the pyrolysis products. The higher the N₂ yield, the lower the nitrogen content in char. The increase in N₂ yield due to the impregnation of iron was canceled out by the decrease in nitrogen emitted in HCN, NH₃, tar and that fixed in char. This suggests that the N₂ formation in the presence of iron catalyst is promoted by; (1) secondary conversion of HCN, NH₃ and N-containing tar primarily generated in coal micropores into N₂, (2) conversion of HCN, NH₃ and N-containing tar precursors into N₂-forming precursors, and (3) additional conversion of char nitrogen into N₂. At present, however, we cannot specify the mechanism. Chemical forms of nitrogen as well as iron species should be determined during the reaction path from coal to char in future works.

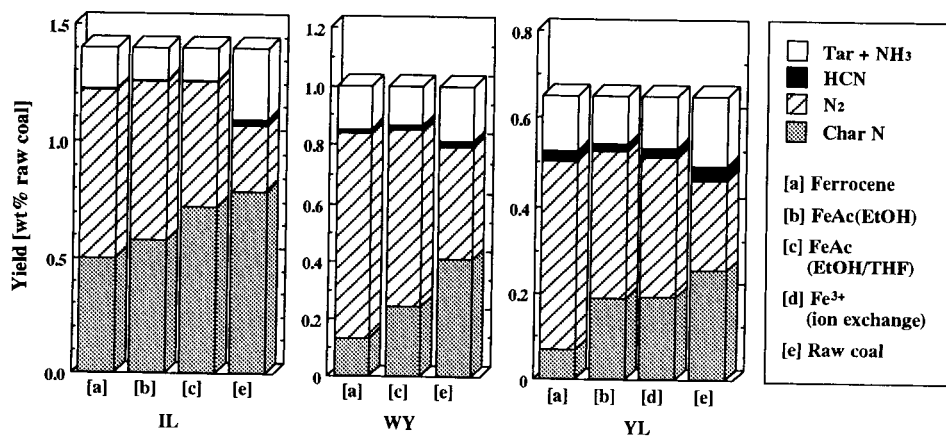


Figure 3. Distribution of coal nitrogen in pyrolysis products

Acknowledgment

This study was conducted under the Japan-Canada Joint Research Program "Developing Advanced Coal Utilization Processes to Minimize Environmental Impact" (Project No. 04044086) by the Ministry of Education, Science and Culture, Japan.

References

- [1] J.C. Chen, S. Niksa, *Energy Fuels*, 6 (1992) 264.
- [2] R. Bassilakis, Y. Zhao, P.R. Solomon, *Energy Fuels*, 7 (1993) 710.
- [3] S. Kambara, T. Takarada, Y. Yamamoto, T. Kato, *Energy Fuels*, 7 (1993) 1013.
- [4] Y. Ohtsuka, H. Mori, K. Nonaka, T. Watanabe and K. Asami, *Energy Fuels*, 7 (1993) 1095.
- [5] Y. Ohtsuka, H.; Mori, T. Watanabe, K. Asami, *Fuel*, 73 (1994) 1093.
- [6] H. Yamashita, Y. Ohtsuka, S. Yoshida, A. Tomita, *Energy Fuels*, 3 (1989) 686.

Formation of N₂ during the fixed-bed pyrolysis of coals

Zhiheng Wu,^a Yasuo Ohtsuka,^a and Edward Furimsky^b

^aResearch Center for Carbonaceous Resources, Institute for Chemical Reaction Science, Tohoku University, Sendai 980-77, Japan

^bEnergy Research Laboratories, CANMET, Natural Resources Canada, Ottawa, Ontario, Canada KIA OG1

1. INTRODUCTION

Research on the fate of the nitrogen in coal during pyrolysis has attracted increased attention, since it is related with the NO_x and N₂O emissions during subsequent combustion. It has been reported that coal nitrogen is initially released as tar [1], which is then converted to HCN and NH₃ through secondary decomposition reactions [2-4]. However, little attention to N₂ has been paid so far [5]. We have recently found that N₂ is the dominant product in slow heating rate pyrolysis of a subbituminous coal [6], and that the finely dispersed iron catalyst promotes drastically the formation of N₂ from a brown coal [7]. If coal nitrogen can be removed efficiently as N₂ during pyrolysis, this method would contribute to the reduction of the NO_x and N₂O emissions, since such pollutants originate mostly from coal nitrogen.

Therefore the present study aims at making clear the influence of coal type, pyrolysis conditions, demineralization, and iron catalyst on the formation of N₂ during the fixed-bed pyrolysis of several coals with different ranks.

2. EXPERIMENTAL

The analyses of five coals with size fraction 150-250 μm are shown in Table 1, where the nitrogen contents in most coals are around 2%. Two coals, ZN and NS coal, were demineralized at elevated temperatures with HCl and NaOH, respectively. The high temperature ashes from the original and demineralized coals were characterized by X-ray diffraction (XRD) analysis. A nanophase iron oxide catalyst with mean particle size of 3 nm was added onto coal by mixing them in deionized water, the nominal loading being 5 wt% as iron metal.

Pyrolysis experiments were performed with a quartz-made fixed-bed reactor; about 0.5 g of the sample, held in a graphite cell, was heated under a flow of high pure He at 400 K/min up to 1000°C, and soaked for 2 min, unless otherwise stated. Before every run, special care was taken to ensure that the entire system was free from any leakage. Pyrolysis products were separated into gas, liquid, and char [7]. Coal nitrogen evolution was monitored mainly in terms of N₂ and the nitrogen in the char (denoted as char-N).

3. RESULTS AND DISCUSSION

3.1. Relationship between coal rank and nitrogen distribution

The influence of coal type on nitrogen distribution at 1000°C is illustrated in Figure 1, where the sum of nitrogen conversions to NH_3 , HCN, and liquid products is determined by difference and denoted as "other". The analysis of the nitrogen in "other" with some samples ensured that nitrogen mass balance fell within the reasonable range 98 – 102 %.

As is seen in Figure 1, nitrogen distribution depended strongly on the coal type. It tended that higher conversion to N_2 resulted in lower conversion to char-N, but there seemed no linear relationship between the carbon content in coal and conversion to N_2 . The conversion ranged 13 – 48 %, and N_2 was the dominant product with ZN, OM, and IL coal. The conversion with OM coal was almost the same as that observed in the pyrolysis at a slow heating rate of 10 K/min [6]. It is noteworthy that about 50 % of coal nitrogen is converted to N_2 with ZN coal. The effects of pyrolysis temperature and heating rate on the formation of N_2 will thus be examined with ZN coal as follows.

3.2. Effect of pyrolysis conditions on the formation of N_2 from a low rank coal

Figure 2 shows the effect of pyrolysis temperature on nitrogen conversion with ZN coal. Any appreciable amount of N_2 was not formed at 600°C. When the temperature was raised to 800 and 1000°C, conversion to N_2 increased linearly with increasing temperature, reaching about 50 % at 1000°C. On the contrary, conversion to char-N decreased with temperature. Such the relationship between the formation of N_2 and nitrogen retention in the char was also observed during the iron-catalyzed pyrolysis of a brown coal [7]. There was no significant temperature dependence on the evolution of NH_3 or HCN; conversion to NH_3 or HCN in the range of 600 – 1000°C was 5 – 8 % or 1 – 2 %, respectively. These findings show that N_2 comes not from NH_3 and HCN but from char-N and/or the precursors.

When the char after pyrolysis of ZN coal at 600°C was heated again from room temperature up to 1000°, NH_3 and HCN were not formed significantly, but the amount of N_2 evolved was almost the same as that observed with the original coal. Therefore it is probable that the formation of N_2 proceeds through solid phase reactions.

Lower conversion to N_2 was observed at a higher heating rate in the range of 10 – 1300 K/min, but the rate dependence was small. A higher heating rate means a shorter soaking time in the temperature region where N_2 evolves, resulting possibly in lower conversion to N_2 .

3.3. Influence of demineralization on nitrogen conversion

The effect of demineralization on nitrogen conversion for two coals is shown in Table 2, where the efficiency of removal of mineral matter was much higher with NS coal, and the ash content in the demineralized coal was decreased to 0.5 %. For ZN coal, interestingly, conversion to N_2 decreased remarkably by demineralization, whereas conversion to char-N increased largely. Furthermore, it is noted that the decreased amount of N_2 by demineralization is almost the same as the increased amount of char-N. The observation supports the above-mentioned conclusion that N_2 comes from char-N. For NS coal, on the other hand, demineralization had only a small effect on conversions to N_2 and char-N, although the ash

content was quite different before and after demineralization.

The XRD measurements of high temperature ashes revealed that large amounts of Ca and Fe species were inherently present in ZN coal and removed mostly by demineralization, whereas SiO₂ was the major component in NS coal. Since ZN coal contained larger amounts of oxygen functional groups (Table 1), most of Ca and Fe species in the coal would exist in the ion-exchangeable forms. Such the exchangeable metal cations would thus play very important roles in the formation of N₂ during pyrolysis.

3.4. Catalytic effect of a nanophase iron oxide

The iron catalyst promoted the evolution of N₂ for all the coals used in the present study. However, the catalytic effect was dependent on the coal type, and the largest effect was observed for LY coal; conversion to N₂ increased from 13 % without iron to 35 % with iron, and conversion to char-N decreased correspondingly. The different effectiveness would be caused by the different degree of catalyst dispersion. When the iron catalyst was precipitated onto LY coal from an aqueous solution of FeCl₃ and then the resulting sample was pyrolyzed at 900°C with a fluidized bed reactor, conversion to N₂ reached 50 – 60 % [7]. The size of iron particles after pyrolysis was as small as 20 – 30 nm, whereas it was > 100 nm for the nanophase catalyst physically mixed with coal. It is evident that catalyst dispersion is one of the key factors in controlling the conversion of coal nitrogen to N₂.

4. CONCLUSION

Nitrogen conversions to N₂ and char nitrogen in the fixed bed pyrolysis of coals at 1000°C are strongly dependent on the coal type, and at the highest 50 % of coal nitrogen can be converted to N₂. Conversion to N₂ increases linearly with increasing pyrolysis temperature in the range of 600 – 1000°C, but contrarily nitrogen retention in the char decreases with temperature. When a low rank coal containing large amounts of exchangeable metal cations is demineralized by acid washing, conversion to N₂ decreases drastically. A nanophase iron catalyst promotes the formation of N₂.

ACKNOWLEDGEMENTS

The present work is supported in part by the NEDO international Joint Research Grant.

REFERENCES

1. P.R. Solomon and M.B. Colket, *Fuel*, **57** (1978) 749.
2. P.F. Nelson, M.D. Kelly, and M.J. Wornat, *Fuel*, **70** (1991) 403.
3. J.C. Chen, C. Castagnoli, and S. Niksa, *Energy Fuels*, **6** (1992). 264.
4. R. Bassilakis, Y. Zhao, P.R. Solomon, and M.A. Serio, *Energy Fuels*, **7** (1993) 710.
5. S. Kambara, T. Takarada, Y. Yamamoto, and K. Kato, *Energy Fuels*, **7** (1993) 1013.
6. Y. Ohtsuka and E. Furimsky, *Energy Fuels*, **9** (1995) 141.
7. Y. Ohtsuka, H.Mori, T.Watanabe, and K.Asami, *Fuel*, **73** (1994) 1093.

Table 1
Analyses of coals

Coal (Country)	Ultimate analysis (% daf)					Ash (% db)
	C	H	N	S	O	
LY (Australia)	65.9	4.1	0.7	0.3	29.0	0.6
ZN (China)	72.0	5.0	1.7	0.4	20.9	4.1
OM (Canada)	74.0	5.3	1.8	0.6	18.3	12.6
IL (U.S.A.)	76.5	5.3	1.6	3.5	13.1	9.0
NS (Australia)	81.2	5.5	2.2	0.8	10.3	8.2

Table 2
Effect of demineralization on nitrogen conversion at 1000°C

Sample	Ash (% db)	Nitrogen conversion (%)	
		N ₂	Char-N
ZN-Raw	4.1	48	37
ZN-Dem	0.8	13	68
NS-Raw	8.2	14	63
NS-Dem	0.5	16	68

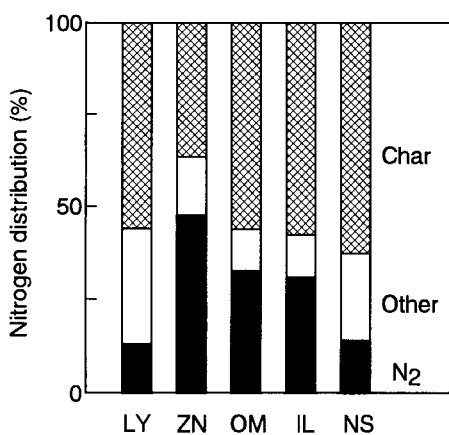


Figure 1. Nitrogen distribution at 1000°C for different coals.

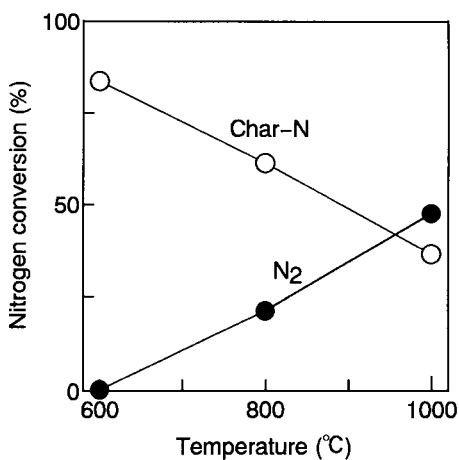


Figure 2. Temperature dependence of nitrogen conversion for ZN coal.

Regularities of chlorine concentration and form location in Russian coals

Iu.N. Zharov

Fossil Fuels Institute, 29 Leninsky prospekt Moscow, GSP-1, 117910, Russia

Chlorine has been studied mainly in Russian coals from Pechersky, Kuznetsky, Lensky, Sachalinsky and some other basins and fields of the North-East and Primorje.

Chlorine is investigated in coals by prospecting works together with other elements in saueple duplicates from pores and mining opening, In quality specifications of solid fuel supplied to consumers, the obligatory determination of element content is not get prided.

The attention of specialists to chlorine is stimulated because of unpleosand properties of galoid and its compounds, what takes place by widly coal use, Burning and technological treatment of solid fuel is accompanied by instruments corrosion, output decrease and products composition change and increase of toxic component emission.

Chemical analyse of chlorine in coals and brown coals (GOST 9326-77) is the basic valuation method of its content, corresponding to the international standard JSO 587-1974, Supersensitive (up to 0.001%) neutron-activation method of chlorine determination is not widely used today by mass determination.

In spite of biogene accumulation ability, the high modility of chlorine doesnt allow it to accumulate selectively at different stages of peat-coal forming process.

In the rank peat - brow coal - coal chlorine is even dishibuted, isnt concentrating noticeable in organic of mineral matters.

Geological age and matters composition of coal controls chlorine accumulation weakly. Jts average content at objects, here special determinations have been conducted, is 0.05-0.1%, what corresponds to element clark in brow coals and coals. The minimal content of chlorine is more often to meet in highly transformed coals and anthracites (Table.1).

The high chlorine contens, exceeding 0.4-0.6% are founded in salty coals, refined simultaneously of water soluble natrium and potassium. However in Russia fields of salty coals has not been discovered. Today relate high accumulations are found in coals of Kansko-Achinsk, Sachalinsky, Arkagalinsky and Bikinsky basius (1,2). Investigated coals relate in accordance with geochemical value of saltness K/Na - 0.3-0.6 to weakly salty category.

Maximal salt accumulation takes place at local areas of some mine seams and deep coal horizons, refined of highly mineralized waters (>10 g/l).

Table 1

Chlorine content in coals from Russian basins and fields (% for dry coal basis)

Basin, Field	Coal Characteristic			Chlorine content		
	Age	Mark	Ash, %	Min	Max	Average
Pechorsky	P	Д-Ж	8-30	0.031	0.07	0.04
Kuznetsky	C ₃ -P	Д-Т	20-25	0.005	0.079	0.038
Kansko-Achinsky	J ₁₋₂	Б	9-12	0.04	0.07	0.05
Lensky	J ₃ -K ₁	Б-Д	10-13	0.03	0.1	0.045
Partizansky	K	Ж-Т	26-39	0.028	0.094	0.068
Razdolnensky	K	Д	30-34	0.05	0.081	0.065
Uglovsky	P	Б	18-38	0.044	0.082	0.056
Pavlovskoe	P	Б	10-25	0.043	0.06	0.05
Arkagalinsky	K ₂	Д	10-25	0.02	0.57	0.21
Sachalinsky	N	Б-Д	15-20	0.019	0.717	0.045
Anadirsky	P ₂	Б	15-20	0.11	0.33	0.18

Early it was demonstrated, Heat in coals of different saltness the content of sodium and potassium submit a normal low of distribution (3). The statistic analyse of experimental date shows that chlorine distribution with all so connected from saltness degree of coal, but corresponds to lognormal distribution.

In opinion of L.A.Janochkina (1966) and Gr.Eskenazy (1969) the logarythmic typ of distribution function demonstrates a sufurrority of one migration method and final fixation form of chemical element in nature. The lognormal chlorine distribution in coals in this case cau be explained through its migration in composition of water soluble haloid compounds with resulting deposition of NaCl and partial KCl, MgCl₂, CaCl₂ or through chlorine moving in forms binding with organic and mineral maffer.

Chlorine moving in peat and coal fields as a water soluble haloid form resulted its binding with alkali elements. Its stated, that function of correction of Cl-Na content in coals corresponds to lineai. In weakly salty and not salty coals chlorine quantity doesut correlate with gross content of sodium and potassium.

Chlorine, sodium and potassium concentrations, specially in not salty coals, are independent values and its accumulation occured on differt wags. The last statment corresponds to results of chlorine valuation in coals of Ukraina (4). In tab. 2 the results of chlorine, sodium and potassium are extraction from weakly salty and not salty brow coals of Arkagalinsky basin up to 8% of chlorine, 52-59% of sodium and 8-33% of potassium are transformed into water extract, So it can be supposed, that in the investigated coals chlorine is mainly in following forms: 1) as mineral form in cmposition of water soluble galit and silvin, 2) as mineral and (or) organic

form in composition of not water soluble chlorine oxides and organic complex. In several coals chlorine content forms are different (6,7). It seems that coals with chlorine as a galit form predominate.

Table 2

Chlorine, sodium and potassium extraction from coals

Denomination	Content in dry coal, %					
	Chlorine		Sodium		Potassium	
	General	Water soluble	General	Water soluble	General	Water soluble
1 Not salty brown coal of "Buchta Ugolnaja" field	0.05	0.05	0.07	0.05	0.07	0.02
2 Not salty and weakly salty coal of Anadirsky field	0.02	0.02	0.15	0.09	0.07	0.02
3 Weakly salty coal of Arkagalinsky basin	0.02	0.02	0.08	0.01	0.01	0.01
	0.37	0.37	0.37	0.36	0.02	0.02
	0.40	0.40	0.29	0.29	0.02	0.02
	0.05	0.05	0.10	0.10	0.02	0.02
	0.13	0.03	0.51	0.30	0.06	0.02
	0.14	0.00	0.52	0.29	0.17	0.02
	0.04	0.00	0.59	0.31	0.37	0.03

REFERENCES

1. V.R.Kler, E.P.Dik, Iu.N.Zharov. Studing of salty coals. Prospecting and protection of depth, N2, 1987, p.30-34
2. A.M.Mingaleeva, T.M.Thcherbakova, V.K.Prjanishnikov. To question about saltness of ash of Berezovsky seam coal. Coal, N7, 1984, p.53-55
3. V.R.Kler, Iu.N.Zharov, J.J.Slivinskaja. About potassium and sodium distribution in coals. Reports of Academy of science of the SU, v.298, N4, p.936-939
4. A.V.Ivanova, L.B.Zaitceva. Genesis problem of salty coals of the West Donbass. Geological Institute of Ukraina. Preprint 82-17, 1982, p.53
5. V.R.Kler, E.P.Dik. Studing of mineral components of power sull coals. Prospecting and protection of depths, N4, 1981, p.32-35
6. Ja.E.Yudovitch, M.P.Ketric, A.V.Merz. Admixthere elements in fossil coals "Science" Leningrad, 1985, p.134-140
7. L.Ya.Kizilshstein, Yu.A.Fedorov, A.G.Lutochin, V.V.Galtchikov. Sodium in Donbass coals. Prospecting and protection of depths, N2, 1984, p.33-36

This Page Intentionally Left Blank

ORGANIC SULFUR REMOVAL FROM COAL BY RAPID PYROLYSIS WITH ALKALI LEACHING AND DENSITY SEPARATION

Katsuyasu Sugawara, Keiko Abe and Takuo Sugawara

Division of Materials Process Engineering, Mining College, Akita University,

1-1 Tegata Gakuen-cho, Akita city, Akita Pref., 010 JAPAN

1. INTRODUCTION

As well as the need for highly efficient utilization processes for the limited reserves, there is a need to urgently develop various cleaning technologies to suppress the air pollution and acid rain problems resulting from the use of high sulfur coals. The authors have conducted experiments and simulation studies on the desulfurization of coal paying attention to establishment of appropriate processing technology to meet various types of coal produced from any mine^{1,2}.

The purpose of this study is to elucidate the effects of density distribution of coal and of pretreatment by use of alkali solution on the desulfurization behavior under the rapid pyrolysis condition. The desulfurization characteristics was investigated from view point of differential concentration of macerals with the use of density-separated coals. The alkali leaching samples were obtained by heat treatment in a nitrogen atmosphere after the immersing coal samples in a saturated alkali aqueous solution. The alkali-leached samples were, then pyrolyzed rapidly in a nitrogen stream by using a free-fall pyrolyzer.

2. EXPERIMENTAL

Table 1 shows proximate, ultimate and sulfur-form analyses of sample coals used: Muswell Brook (Australia), PSOC 592 (U.S.A.), Nan Tong and Fu Rong (China). The particle size of the samples ranges in 0.3-0.4 mm.

The sample was fractionated into three density groups by sink-float in zinc chloride aqueous solution³. The separated samples were repeatedly washed to remove zinc chloride.

The sample coals were immersed in a saturated aqueous solution of potassium hydroxide for 24 h with agitation at room temperature. The wet alkali immersed samples were heated at 523 K for 4 h in a nitrogen atmosphere after filtration from potassium hydroxide solution.

The density-separated samples and alkali treated samples were pyrolyzed rapidly in a nitrogen atmosphere in a free fall pyrolyzer. The reactor was a fused silica tube (i.d. 36 mm) and the reactor temperature was controlled by an electric furnace composed of five sections. This apparatus enables coal particles in nitrogen gas (at 2.0 liters NTP/min) to be heated at rates from 10^3 to 10^4 K/s. The temperature was 1233 K in the isothermal section of the reactor. The details of the free fall pyrolyzer were described elsewhere². Residence time and temperature of coal particle in the reactor were estimated by solving simultaneous equations of momentum and heat balance equations².

3. RESULTS AND DISCUSSION

The four samples were fractionated into three groups by a sink-float method and each group was pyrolyzed rapidly. Table 2 shows yield and sulfur form analyses of density-separated samples. Figure 1 shows change in extent of organic sulfur removal during rapid pyrolysis of density-separated coals. The extent of organic sulfur removal is defined as $[(S_{org})_{coal} - (S_{org})_{char}] / (S_{org})_{coal} \times 100$ [%]. The lowest density group of Muswell Brook, PSOC 592 and Nan Tong coals were desulfurized higher than other groups. Exinite and vitrinite which are concentrated in the lowest density group played an important role on the release of organic sulfur from the solid phase during rapid pyrolysis. The highest density group of Fu Rong coal containing the highest organic sulfur showed the highest removal of organic sulfur. This result might be related to the existence of elemental sulfur generated from pyrite⁴.

Figure 2 represents the effects of treatment time and temperature in alkali treatment on organic sulfur content in alkali-treated coal and char of Muswell Brook. A in Fig.2 indicates organic sulfur contents of parent coal and rapid pyrolysis without alkali treatment. The effect of time in alkali treatment at 523 K is shown in B, C and D. Though a treatment time more than 2 h was not effective for reducing organic sulfur in alkali treated coal, the organic sulfur content of rapid pyrolysis char remarkably decreased with treatment time. It was found that the combined process of rapid pyrolysis with alkali leaching was successful to reduce the organic sulfur. However, treatment at 473 K, lower by 50 K for 4 h with alkali treatment did not contribute to efficient decrease in organic sulfur in pyrolysis char.

Figure 3 shows the change in organic sulfur content of density separated coals for Muswell Brook, PSOC 592 and Nan Tong coals during rapid pyrolysis with alkali treatment. Combined process of rapid pyrolysis with alkali treatment was effective for the lowest density group than for highest density group.

Table 1 Analyses of sample coals [wt%, d.b.]

Sample	C	S	VM	Ash
Muswell Brook	77.5	0.8	41.1	8.3
PSOC 592	77.3	2.1	37.0	12.4
Nan Tong	73.6	4.1	17.0	17.8
Fu Rong	69.7	5.2	10.5	21.6

Table 2 Yield and analyses of density separated samples

Sample	Group (Density g/cm ³)	Yield	S	Pyritic	Sulfate	Organic
		[wt%, db]		[wt% of total sulfur]		
Muswell Brook	I (under 1.26)	24	0.6	2	4	94
	II(1.26-1.40)	61	0.6	4	3	93
	III(over 1.40)	15	0.7	45	2	53
PSOC 592	I(under 1.32)	10	2.1	2	0	98
	II(1.32-1.40)	66	1.9	4	1	95
	III(over 1.40)	24	1.6	8	2	90
Nan Tong	I(under 1.30)	18	3.5	4	0	96
	II(1.30-1.42)	47	3.6	12	0	88
	III(over 1.42)	35	4.9	66	0	34
Fu Rong	I(under 1.40)	17	1.1	43	4	57
	II(1.40-1.50)	39	1.3	54	2	44
	III(over 1.50)	44	10.2	88	0	12

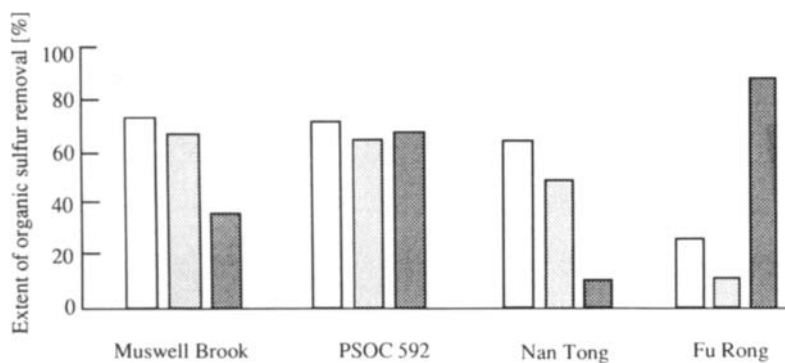


Fig.1 Change in extent of organic sulfur removal with density separated coals

□ Group I, □ Group II, ■ Group III

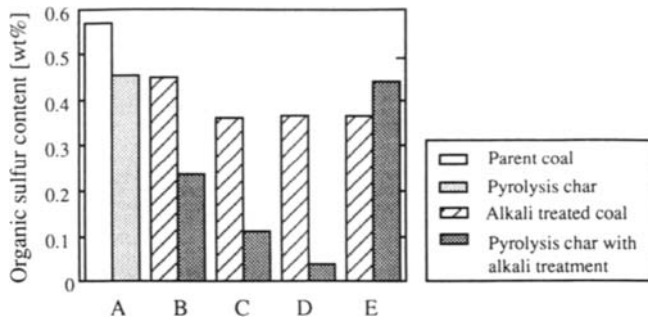


Fig. 2 Effect of alkali leaching condition on organic sulfur content of Muswell Brook coal. Treatment conditions : B, 523K, 1 h; C, 523K, 2 h; D, 523K, 4 h; E, 473K, 4 h.

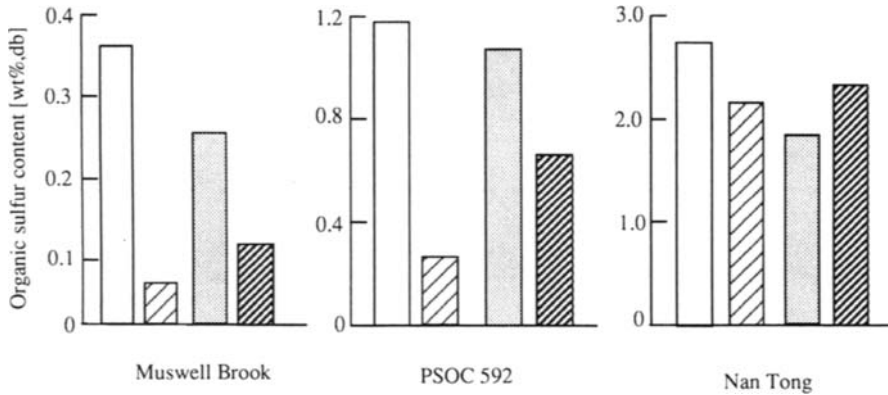
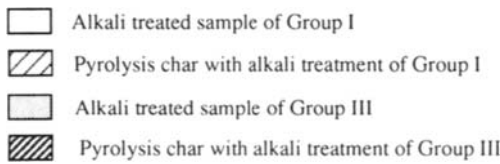


Fig.3 Change in organic sulfur content with alkali treatment and rapid pyrolysis



REFERENCES

- 1) Sugawara, K., Tozuka, Y., Sugawara, T. and Nishiyama, Y., *Fuel Processing Technology*, 37, 73 (1994)
- 2) Sugawara, T., Sugawara, K., Nishiyama, Y. and Sholes, M. A., *Fuel*, 70, 1091 (1991)
- 3) Sugawara, K., Tozuka, Y., Kamoshita, T., Sugawara, T. and Sholes, M. A., *Fuel*, 73, 1224 (1994)
- 4) Stock, L.M., Wolny, R. and Bal, B., *Energy Fuels*, 3, 651 (1989)

OXIDATIVE PRETREATMENTS FOR THE ENHANCED REMOVAL OF ORGANIC SULFUR FROM COAL

S.R. Palmer, E.J. Hippo and Y. Liu.

Department of Mechanical Engineering and Energy Processes, Southern Illinois University at Carbondale, Carbondale, Illinois 62901.

1. INTRODUCTION

In previous studies the selective oxidation of coal with peroxyacetic acid (PAA) was examined as a desulfurization strategy (1,2). These studies showed that most of the pyritic sulfur and up to 20% of the organic sulfur in coal could be removed under relatively mild conditions. Removing more of the organic sulfur required increasing the level of oxidation, and this led to extensive dissolution of the coal and low BTU recoveries. Due to these problems the selectively oxidized coals were investigated for further desulfurization under a variety of conditions ranging from mild pyrolysis at 250°C to supercritical alcohol(SCA)/base mixtures at 450°C, with the selective oxidation reaction being used as a pretreatment (3,4). Using these combined treatments it was established that significant levels of sulfur removal (up to 95%) could be obtained (1).

To determine if this behavior could be repeated with other oxidants, aliquots of an Illinois No.6 and an Indiana No.5 coal were initially oxidized with air, alkaline oxygen, nitric acid, hydrogen peroxide, potassium permanganate and sodium dichromate, as well as with the original oxidant PAA. The preoxidized coals were then desulfurized using a methanol solution of sodium hydroxide at 350°C. Various oxidation conditions and oxidant concentration were also investigated. Products derived from PAA oxidation and subsequent desulfurization together with the original coal were examined for sulfur forms using XANES.

2. EXPERIMENTAL

2.1 Coal preparation

Two coal samples were obtained from the Illinois Coal Basin Sample Program (IBCSP), IBC-101 and IBC-106. 500g aliquots of each coal were micronized and stored under nitrogen. Proximate and ultimate analysis of each coal gave: IBC-101 14.8% moisture, 10.5% ash, 69.3% C, 5.18% H, 1.31% N, 4.36% S, 40.7% vol. matter and 48.8% fixed carbon. IBC-106 10.5% moisture, 9.0% ash, 71.9% C, 4.93% H, 1.67% N, 3.77% S, 39.7% vol. matter and 51.3% fixed carbon. (On a moisture free basis except for moisture.)

2.2 Oxidation pretreatments

All oxidative pretreatments were performed on 5 grams of micronized coal. The nitric acid, hydrogen peroxide, peroxyacetic acid, potassium permanganate and the sodium dichromate oxidations were performed in a magnetically stirred 250mL flask with 150mL distilled water under two different conditions. These conditions were 24 hours at room

temperature (21°C) and 100°C for 1 hour respectively. The amount of oxidant used in each experiments was 10mmoles of oxygen equivalent. After oxidation the solid coal product was collected by filtration and washed with distilled water. The permanganate oxidation products were treated with conc. HCl and then more distilled water to dissolve manganese dioxide. The alkaline oxygen oxidations were performed at 100°C for 24 hours using an alkaline coal slurry (5g coal, 150mL distilled water, 0.2g NaOH) with an oxygen flow rate of 25mL per minute. After oxidation the coal products were filtered, washed with dil. HCl and then distilled water. Air oxidations were performed in an oven at 160°C for 24 hours. The air oxidized coals received no other treatment prior to the desulfurization reaction with base/methanol.

2.3 Base desulfurization reaction

2g of the preoxidized or unoxidized (control) coal was placed in a 10 mL stainless steel micro-reactor together with 33 mmoles of sodium hydroxide slurried in 5mL of methanol. The microreactor was then purged with argon, sealed and immersed in the fluidized sand bath for one hour at 350°C. After reaction the microreactor was cooled in cold water and the contents washed with dil. HCl and then distilled water at the filter. All samples were submitted for carbon and sulfur analysis after drying in a vacuum oven overnight.

2.4 XANES

Selected samples were examined by Professors G.P. Huffman and F.E. Huggins at beam line X-19A at the National Synchrotron Light Source at Brookhaven National Laboratory, NY. Descriptions of this technique can be found elsewhere (5,6).

3. RESULTS AND DISCUSSION

Figure 1 illustrates the desulfurization of the IBC-101 coal, both after oxidation, and after combined oxidation and base/alcohol treatment. Figure 2 gives the same information for the IBC-106 coal. It can be seen that significant amounts of sulfur can be removed from this coal by applying a combination of an oxidative pretreatment with a subsequent desulfurization reaction. Although the combined process can be viewed in terms of a preoxidation step and a desulfurization step, it is clear from Figures 1 and 2 that sulfur removal is achieved in both stages.

The original unoxidized coals were first desulfurized using the standard base/methanol procedure to provide the baseline desulfurization behavior prior to any preoxidation. As shown in Figures 1 and 2 both the IBC-101 and IBC-106 coals can be significantly desulfurized without any preoxidation. Indeed, sulfur removal levels of around 50% can be obtained for both the IBC-101 and IBC-106 coals. However, significantly higher levels of sulfur removal are obtained if the coals are preoxidized first.

It is interesting that the levels of desulfurization achieved using the peroxyacetic acid (PAA) pretreatment are not significantly higher than those obtained with other oxidants. This was unexpected since peroxyacetic acid is reported to be able to selectively oxidize organic sulfur species, and it was expected that the other oxidants would not be able to duplicate this ability. Indeed, it appears that all of the oxidants examined, even air and alkaline oxygen, can lead to desulfurized products with similar sulfur contents as those derived from PAA pretreated coals. This is a significant finding for it means that very inexpensive oxidants such as air, oxygen and nitric acid could be used instead of peroxyacetic acid. This would dramatically reduce the cost of any commercial process designed around this strategy.

The amount of sulfur typically removed from the IBC-101 coal during the oxidative pretreatment with most of the oxidants is around 10%, while for the IBC-106 coal about 16% of the sulfur is typically removed. In general, the conditions of time and temperature under

which the oxidants were employed did not seem to significantly influence the level of sulfur removal obtained in the pretreatment step or the desulfurization step. In some cases, increasing the amount of oxidant available for oxidation was found to increase the amount of sulfur removed in the preoxidation step.

The results of the XANES analysis of a more severely PAA oxidized IBC-101 coal and the subsequent base desulfurized product derived from it, are compared to the data for the original coal in Figures 3 and 4 respectively. It can be seen from Figure 3 that most of the sulfur forms in the original coal are converted to oxidized sulfur species upon PAA oxidation. All of the pyrite and nearly all of the thiophenic and sulfide sulfur is converted to sulfate, sulfoxide, sulfone and sulfonic acid functionalities. Presumably the sulfate comes from pyrite oxidation. Under milder reaction conditions organic sulfides are apparently converted to their sulfones, but thiophenic sulfur forms appear to be unchanged. Examination of Figure 4 reveals that the desulfurization treatment (alcohol/base treatment at 350°C of the PAA oxidized coal) virtually eliminates all of the oxidized sulfur forms that were produced during the oxidation. Indeed the only significant sulfur form remaining after this combined treatment is thiophenic sulfur and this has been reduced from a concentration of 2.2% in the original coal to only 0.65% in the desulfurized product. Although most of the oxidized thiophenic sulfur is removed during the base treatment, some apparently reverts back to the thiophenic structure during this process.

4. CONCLUSIONS

The conclusion that can be made from this study is that inexpensive oxidants appear just as good as, if not superior to, expensive oxidants such as hydrogen peroxide, peroxyacetic acid, potassium permanganate and sodium dichromate for the oxidative pretreatment step in a desulfurization process. It appears that any oxidation prior to base/alcohol desulfurization enhances the removal of sulfur from coal. Typically the oxidative pretreatments remove about 10% of the sulfur from the IBC-101 coal and about 15% of the sulfur from the IBC-106 coal. After combined oxidation and desulfurization the average sulfur removal for the 101 coal is around 60% with the highest level being 70%. For the IBC-106 coal the average level of desulfurization is 65% with the highest level being 74%. XANES analysis clearly shows the conversion of divalent sulfur forms to their oxidized counterparts upon PAA oxidation and the successful removal of the majority of these oxidized sulfur forms during the base/alcohol desulfurization stage.

5. ACKNOWLEDGEMENTS

This work was supported by the New Energy Development Organization (NEDO) through the International Co-operative Research Program of Japan, the Illinois Department of Energy and Natural Resources through its Coal Development Board and Illinois Clean Coal Institute. Coal samples were provided by the Illinois Basin Coal Sample Program (IBCSP). We would like to thank Dr Ken Ho our ICCI project manager and Professors G.P. Huffman and F.E. Huggins for performing the XANES analysis.

6. REFERENCES

1. S.R. Palmer, E.J. Hippo, and X.A. Doria, *Fuel*, 1994, 73, 161-169.
2. S.R. Palmer, E.J. Hippo, M.A. Kruge and J.C. Crelling, *Coal Prep.* 1992, 10 93-106.

3. S.R. Palmer, E.J. Hippo, and X.A. Doria, Proceedings of the Ninth Annual International Pittsburgh Coal Conference, 1992, 77-82.
4. S.R. Palmer, E.J. Hippo, and X.A. Doria, Fuel, 1995, 74, p193-200.
5. G.P. Huffman, F.E. Huggins, N. Shah, S. Mitra, R.J. Pugmire, B. Davis, F.W. Lytle and R.B. Greigor. Energy & Fuels, 1989, 3, p200-205.
6. M.M. Taghiei, F.E. Huggins, N. Shah and G.P. Huffman. Energy & Fuels, 1992, 6, 293-300.

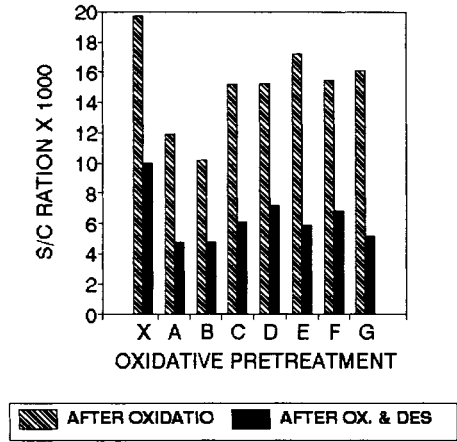
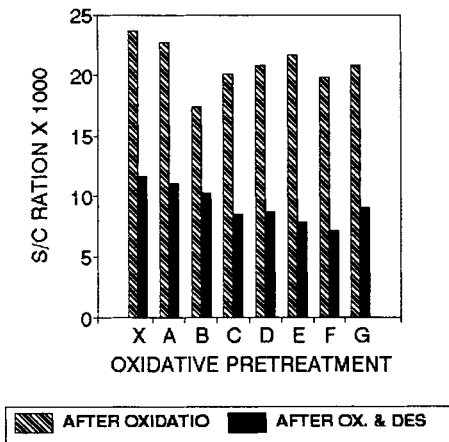


Figure 1. S/C ratios of the IBC-101 coal after various 24hr pretreatments. X = no oxidation, A = air 160°C B = alk. O₂/100°C, C = nitric acid/RT D = H₂O₂/RT, E = PAA/RT, F = KMnO₄ G = Cr₂O₇/RT (RT = room temp.)

Figure 2. S/C ratios of the IBC-106 coal after various 24hr pretreatments. X = no oxidation, A = air 160°C B = alk. O₂/100°C, C = nitric acid/RT D = H₂O₂/RT, E = PAA/RT, F = MnO₄/RT G = Cr₂O₇ (RT = room temp.)

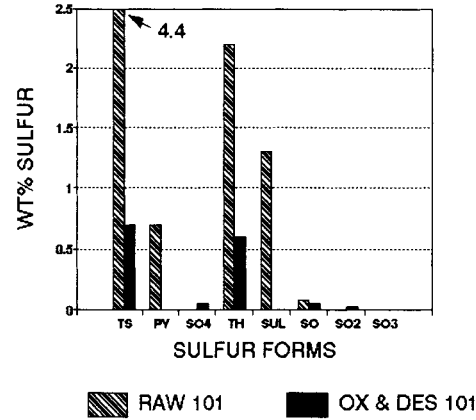
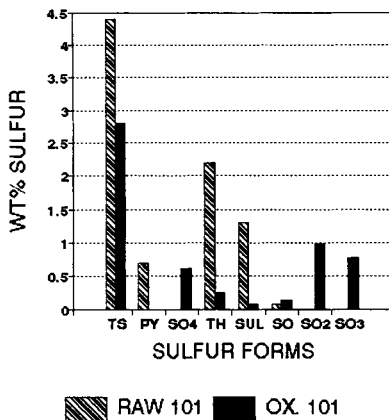


Figure 3. Sulfur forms distribution of IBC-101 before and after PAA oxidation.

Figure 4. Sulfur forms distribution of IBC-101 before and after desulfurization.

Effect of nitric acid attack on the organic sulphur content of coals

R. Álvarez Rodríguez. and C. Clemente.

Mining School, Polytechnical University,
21 Rios Rosas St., 28003 Madrid, Spain.

1. INTRODUCTION

Nitric acid attack on coal is used to determine the forms of sulphur in coals (1), as has also been studied as a possible way of removing sulphur from them (2), (3). The object of this work has been to study the behaviour of organic sulphur during nitric acid attack, for which four Spanish coals of different range and characteristics were used.

In order to determine the organic sulphur, the standard ASTM D 2492-90 (4) was used, that does this through the difference between the total sulphur and the sum of the sulphide and sulphate sulphurs. For sulphide sulphur it makes use of an attack with nitric acid 2N.

As in the case of some coals, as may be seen in this same work and in others by the authors (3), there are very fine inclusions in sulphides or sulphates, which are totally surrounded by carbonaceous matter so they may not be affected by the nitric attack when determining the sulphide sulphur, the coal submitted to this analysis has been finely grinded in order to eliminate this possible interference, in spite of many of the samples being smaller than 0.25 mm. The total sulphur was determined using a Leco apparatus.

2. EXPERIMENTAL

The Spanish coals used have been, in increasing order of coal rank, a coal from Mequinenza with a very high organic sulphur content, crushed and sized to -0.25 mm, a coal from Puertollano with a very low organic sulphur content, using the lesser fraction of 0.25 mm produced by natural decay, a coal from La Robla with a mean organic sulphur content, obtained from flotation, with a grain size smaller than 2.38 mm. and a coal from Fabero, also with a mean organic sulphur content, from flotation, with grain size smaller than 0.5 mm, even though it is considered as practically smaller than 0.25 mm., as 84 % of its weight is in sizes under that dimension. Table 1 shows its characteristics.

The attacks were performed using 50 g of coal and 500 cm³ of nitric acid solution (except in the case of the lower rank coal, in which the intensity of the attack made it advisable to use only 25 g of coal, with the same amount of acid solution), using a flask with several openings, submerged in a thermostatic bath, and stirred by a mechanical stirrer. The flask also had a flow-back cooler which prevented any losses due to evaporation of the liquid and allowed the removal of the gases produced during the attack.

Table 1
Characteristics of the coals studied

	Mequinenza	Puertollano	La Robla	Fabero
% Ash	27.6	40.6	17.0	24.2
% Vol. Matt.	47.45	21.18	12.03	6.60
kJ/kg	21,060	18,800	29,000	24,900
% Total S	9.51	1.18	2.37	1.78
% Organic S	8.34	0.27	0.85	0.69
% S _o ash free	11.52	0.46	1.02	0.91

A temperature of 90° C and two concentrations of acid were used, at 20 % w/w (approximately 3.55 N) and at 30 % w/w (approximately 5.42 N).

After the attack, the coals were filtered, washed, dried and grinded for analysis.

3. RESULTS AND DISCUSSION

The results obtained from the Mequinenza coal are shown in Figure 1, where the variation curves of the organic sulphur are represented, expressed on a dry, ash free basis, for cases of an attack with 20 and 30 % of nitric (○ and • respectively). There is also shown the variation of the inorganic sulphur content, considered as the sum of the sulphate sulphur and the sulphide obtained through application of the aforementioned standard ASTM, expressed on dry basis, although with ashes (□ and ▲ for 20 % acid and 30 % acid, respectively).

The form of expressing the results of the organic sulphur on the ash free basis is to allow an adequate comparison, as in the attack there is a variation in the ash content and this may mask the results on the organic sulphur, if expressed only on dry basis.

In the Mequinenza coal, it was observed that, as there was a rapid attack on the small

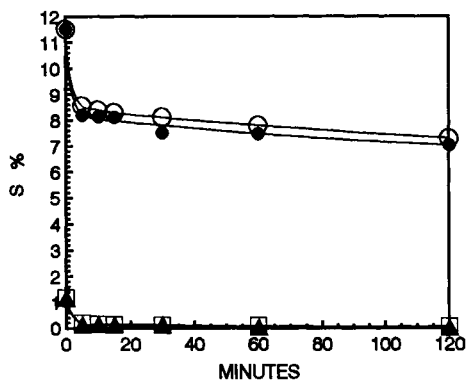


Figure 1. Mequinenza coal. S_{org} ash free (○, ●), S_{inorg} dry basis (□, ▲).

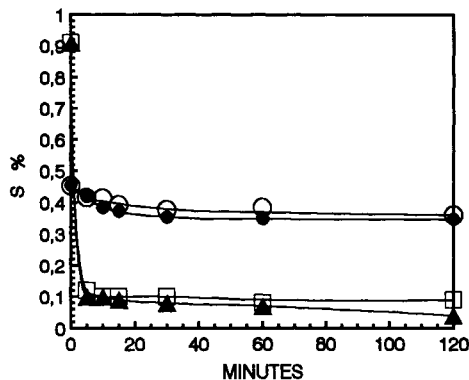


Figure 2. Puertollano coal. S_{org} ash free (○, ●), S_{inorg} dry basis (□, ▲).

amount of inorganic sulphur which immediately dropped to most low levels. The organic sulphur also underwent a rapid initial attack, which was greater in the case of the acid at 30 % than with the acid at 20 %, which allows a considerable decrease in the organic sulphur content within the first five minutes. The attack still continued thereafter, although much slower, with an almost constant real rhythm for the two hours the test lasted.

Due to the low initial level, much later than the first five minutes of the attack, of the inorganic sulphur, and to the high level of the organic sulphur, which allows greater precision in its determination, there is really no doubt that the nitric attack makes the organic sulphur content decrease, due to a preferential attack on the molecules that contain this element.

This behaviour suggests that there is a rapid attack on the surface of the grains and in the easily accessible pores, which justifies the great initial drop in organic sulphur content, and slower thereafter, when the acid has to penetrate inside the grains or wait until their size breaks down.

Figure 2 shows the case of the Puertollano coal, of higher rank than the previous one, with very low organic sulphur content and a comparatively high inorganic sulphur content, in the case of attack with 20 % and 30 % acid. A sharp initial drop was noted in the inorganic sulphur, to levels of 0.1 % and a much slower drop thereafter as a result of some very fine inclusions. The organic sulphur drops fairly rapidly at the beginning, although not so sharply as in the previous case, and after that, it practically tends to almost stabilise, although not completely, something which is difficult to specify if only this case is considered, due to the low organic sulphur content and thus greater lack of precision in the results. The attack is deduced to be much slower now, due to the greater degree of evolution of the coal.

Figure 3 shows the case of La Robla coal, in which a small relative drop is appreciated in the organic sulphur in the attack with 20 % acid, which reaches somewhat more than 5 % and a greater reduction in the case of 30 % acid attack (which reaches approximately 9 %),

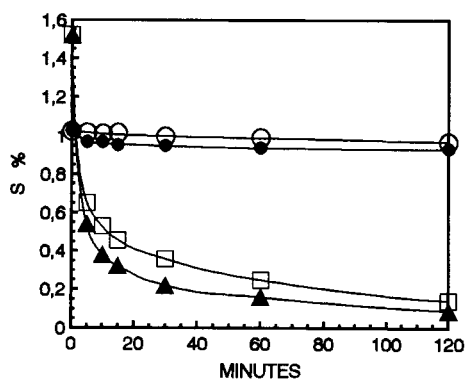


Figure 3. La Robla coal. S_{org} ash free (○, ●), S_{inorg} dry basis (□, ▲).

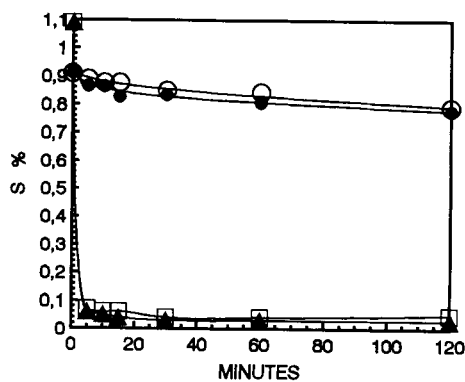


Figure 4. Fabero coal. S_{org} ash free (○, ●), S_{inorg} dry basis (□, ▲).

in which case a greater initial decrease is noted. This situation corroborates what has been stated in the previous cases by supporting the intervention of a mechanism of surface attack.

This graph also clearly shows the effect of a much slower attack on the inorganic sulphur, giving inorganic sulphur content curves which show a gradual reduction of same, indicating protection of the inclusions by the coal, something which is much more apparent due to the

larger size of the grains in this sample in comparison with the previous ones.

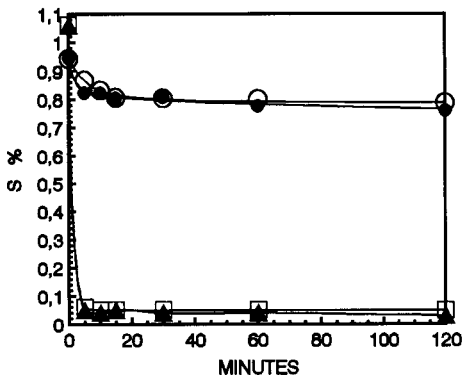


Figure 5. Fabero, -0.125mm . S_{org} ash free (\circ , \bullet), S_{inorg} dry basis (\square , \blacktriangle)

sulphur is much sharper due to the greater surface area reacting. The behaviour of the inorganic sulphur is very similar to the previous case.

Figure 4 shows the results of the Fabero coal which, as mentioned, has approximately 84 % of grains under 0.25 mm. In this coal, the inorganic S decreases rapidly and becomes asymptotic at once, while the organic sulphur decreases relatively quickly in the initial stages, although not very sharply, and it then decreases more slowly. Reduction levels of approximately 13 and 14% are reached (within 2 hours).

A 0.125 mm sieving was carried out on this sample and the products smaller than that size were analyzed, to demonstrate the size influence on the sulphur content.

The results are shown in Figure 5, which follows the same trend as the previous one, except that from it one may deduce that in these sizes the influence of the acid concentration may be masked by analytical errors. It also shows how the initial decrease of the organic

4. CONCLUSIONS

The attack with nitric acid makes the organic sulphur content of the coal to decrease.

Basically, the attack takes basically on the surface, so the finer the coal grain size is, the greater the decrease.

The most important decrease in organic sulphur takes place in the first minutes of the attack, and slows down afterward.

The lesser rank coals suffer a greater attack on their organic sulphur.

The greater the concentration of acid, the more reduction of organic sulphur there is, even if there is not a very acute difference between 20 % and 30 % of acid.

The decrease in inorganic sulphur content depends on the accessibility of same to attack, because of that being more or less protected by carbonaceous material. This makes very fine grinding of the coal advisable before determining this.

REFERENCES

1. Riley, J.T. and Ruba, G.M., Fuel, **68** (1989) 1594.
2. Lukać, J. Álvarez R., Turcainova, L. Clemente, C. and Gómez-Limón, D., Fuel Proc. Tech., **36** (1993) 277.
3. Álvarez, R. Clemente C. and Gómez-Limón, D., Fuel, pending publication.
4. ASTM, Standard Test Method for Forms of Sulphur in Coal (D 2492-90). Volume 05.05, 279 (1992).

Chemical desulphurization methods of organic sulphur of Eocene coal, Jaintia Hills, Meghalaya

M. Ahmed^a and A. Rahim^b

^aDepartment of Geological Sciences, Gauhati University, Guwahati-781014, India

^bDepartment of Chemistry, Gauhati College, Guwahati-781021, India

1. INTRODUCTION

In the Bapung coalfield of Jaintia Hills, Meghalaya, the Lakadong sandstone member of Shella Formation of Jaintia Group (Eocene) includes three persistent coal seams ranging from 1 to 3 metres in thickness along with interseam sandstones and shales [1].

The Bapung coal (Bituminous type) contains very high amount of organic sulphur, which includes different ring structured sulphur compounds like dibenzo-thiophene (DBT), benzo-thiophene (BT), thiophenol (TP) and alkyl sulphides [2].

The removal of organic sulphur is difficult by chemical means and the organic sulphur of Bapung coal is the main barrier for using the coal for domestic and other industrial applications as fuel.

The present investigation aims to find out a suitable chemical method to remove the organic sulphur from the coal.

2. EXPERIMENTAL

The coal samples [3] are first digested with 1:3 nitric acid solution for 24 hours at room temperature with occasional stirring. Nitric acid dissolves out all the inorganic sulphur (i.e. both the pyritic and the sulphate sulphur) from the coal. After the digestion period, the coal mixture is filtered and washed with water. The residual coal contains only the organic sulphur compounds associated with the coal structure.

The inorganic sulphur free coal is now treated with different reagents under different reaction conditions to remove organic sulphur from the coal.

2.1. Treatment with organic solvents

The organic solvents used in the investigation are -

- (i) Ethyl alcohol : Xylene (1:1 = v/v),
- (ii) Rectified Xylene,
- (iii) Rectified alcohol and
- (iv) Benzene : Pyridine (1:1 = v/v).

2.2. Treatment with Inorganic solvents

The following inorganic solvents are used for coal desulphurization -

- (i) 2(N) Na_2CO_3 solution,
- (ii) 5% KOH : Methanol (1:1 = v/v),
- (iii) NaOH : Na_2SO_3 (1:1 = v/v) normal solution and
- (iv) 2(N) NaOH solution

The coal is treated separately with all these reagents, in case of organic solvents digestion is carried out at room temperature for 24 hours and in case of inorganic solvents viz. (i) 2(N) Na_2CO_3 solution, (ii) 5% KOH: Methanol (1:1 = v/v), (iii) 2(N) NaOH solution, digestion is carried out at boiling temperature for 3 hours and with (iv) NaOH: Na_2SO_3 (1:1 = v/v) normal solution, digestion is carried out at room temperature for 24 hours. After the digestion period is over, the coal mixture is filtered and washed with water. The residual coal is taken to determine the total organic sulphur by the standard procedure (Eschka mixture method).

The leachants of the coal with both organic and inorganic solvents except NaOH: Na_2SO_3 (1:1 = v/v) normal solvent, are collected and treated with chemical reagents to determine the amount of organic sulphur leached and percentage of desulphurization is calculated.

3. RESULTS AND DISCUSSION

The organic solvents- Benzene : Pyridine (1:1 = v/v) and Ethyl alcohol : Xylene (1:1 = v/v) remove organic sulphur to the extent of 40.41% and 35.19% respectively. The other organic solvents are less effective, which can remove organic sulphur upto 16.53% only (Table 1).

The inorganic solvent 2(N) NaOH solution removes organic sulphur upto 67.20% (Table 3). The other inorganic solvents are less effective, which can remove organic sulphur upto 9.17% only (Table 2).

The hot alkali solution reacts with sulphur compounds in two steps - (i) in the first the bi-valent sulphur compounds are oxidised to sulphones and (ii) in the second, these sulphones containing '-SC₂' group get hydrolysed by the boiling alkali solution to form SO₃⁻ ion and eliminates from the ring structure.

During the alkali desulphurization, the compact coal structure is opened up to give a product having a spongy like morphology. The porous structure allows the alkali solution to penetrate the coal particles and subsequently reacts with the sulphur bridged functional groups of the coal molecule.

This alkali desulphurization process has a potential technology for removing higher amount of organic sulphur and also some trace metals associated in coal.

The total sulphur reduction obtained by treatment with 1:3 nitric acid and 2(N) NaOH solution is found to be 86.48% (on total sulphur basis) for Bapung coal.

4. CONCLUSIONS

The desulphurization method by alkali solution for removal of organic sulphur will be beneficial for industrial and other purposes using coals of Meghalaya and Assam, both having high organic sulphur.

The two steps treatment of coal that is first with 1:3 nitric acid and secondly with 2(N) NaOH solution will be a viable process for coal desulphurization, and may be recommended for coal desulphurization having high organic sulphur.

Table 1
Desulphurization of organic sulphur from coal with different organic solvents

Chemical reagents used	Sample No.	Coal basis (%)			Org. sulph. basis
		Total Org.sulp.	Org. sulph. leached	Org. sulph. left	P.C.of Org. sul.leached
1. Ethyl alcohol : Xylene (1:1 =v/v)	1	3.18	0.67	2.51	21.07
	4	2.86	0.89	1.97	31.12
	9	2.42	0.85	1.57	35.19
2. Rectified Xylene	3	2.06	0.16	1.90	7.77
	4	2.86	0.45	2.41	15.73
	9	2.42	0.40	2.02	16.53
3. Rectified alcohol	3	2.06	0.15	1.91	7.28
	4	2.86	0.24	2.62	8.40
	9	2.42	0.20	2.22	8.26
4. Benzene : Pyridine (1:1=v/v)	1	3.18	0.83	2.35	26.10
	2	3.32	0.85	2.47	25.60
	9	2.42	0.98	1.44	40.41

Table 2
Desulphurization of organic sulphur from coal with different inorganic solvents

Chemical reagents used	Sample No.	Coal basis (%)			Org. sulph. basis
		Total Org.sulp.	Org. sulph. leached	Org.sulp. left	P.C.of Org. sul.leached
1. 2(N) Na ₂ CO ₃ solution	1	3.18	0.29	2.89	9.17
	2	3.32	0.30	3.02	9.04
	9	2.42	0.18	2.24	7.44
2. NaOH:Na ₂ SO ₃ (1:1=v/v) normal solution	1	3.18	0.27	2.91	8.50
	2	3.32	0.27	3.05	8.13
	9	2.42	0.16	2.26	6.61
3. 5% KOH:CH ₃ OH (1:1=v/v) solution	1	3.18	0.24	2.94	7.55
	4	2.86	0.20	2.66	6.99
	9	2.42	0.17	2.25	7.02

Table 3
Desulphurization of organic sulphur with 2(N) NaOH solution

Sample No.	Coal basis (%)			Org. sulphur basis
	Total org. sulphur	Org. sulph. left	Org. sulph. leached	P.C. of org. sulph. leached
1	3.18	1.47	1.71	53.77
2	3.32	3.00	0.32	9.64
3	2.06	1.92	0.14	6.80
4	2.86	1.15	1.71	59.79
5	2.50	0.82	1.68	67.20
6	2.50	1.91	0.59	23.60
7	2.19	1.90	0.29	13.24
8	2.23	1.94	0.29	13.01
9	2.42	0.92	1.50	61.98

REFERENCES

1. M. Ahmed and J.P. Bora, J. Assam Sci. Soc. 24(1981) 1.
2. S.N. Debey and C.N. Das, J. Mines, Metals & Fuels, 29(1981) 280.
3. M. Ahmed and A. Rahim, Proc. 7th I.C.C.S. 2(1993) 81.

Novel Methods for the Organic Desulfurisation of Coal

K. Singh and W.R. McWhinnie

Department of Chemical Engineering and Applied Chemistry, Aston University, Aston Triangle, Birmingham B4 7ET, England.

Microwave heating is shown to greatly accelerate the reaction of $\text{Fe}_3(\text{CO})_{12}$ with thiophene which leads to the removal of sulfur from the ring. Organotellurium compounds are evaluated as "sulfur models"; tellurophene is shown to undergo a similar reaction with $\text{Fe}_3(\text{CO})_{12}$ as does thiophene, but in better yield. Dibenzotellurophene, unlike dibenzothiophene, undergoes a detelluration reaction in the presence of $\text{Fe}_3(\text{CO})_{12}$. Intermediate compounds are recognised, and the structure of the product ferrole confirms that the integrity of the organic group is retained.

Experiments with cyclic telluroethers and $\text{Fe}_3(\text{CO})_{12}$ also give detelluration products. The possible significance of these results to coal desulfurisation is discussed.

1. INTRODUCTION

In 1960 Stone et al¹. reported that at elevated temperatures iron carbonyls underwent a novel reaction with thiophene which resulted in the removal of sulfur and its substitution with an $\text{Fe}(\text{CO})_3$ group but initial yields were low (5%). The possible importance of this chemistry to the removal of sulfur from coal and oil derived liquids was recognised and a significant series of papers has appeared in the literature. In particular Rauchfuss and co-workers² have shown that the iron initially enters the thiophene or benzothiophene ring to give a thiaferrole. Although the benzothiophene derivative undergoes oxidative demetallation it does not result in organic sulfur removal. Angelici and co-workers have also made important contributions in their efforts to understand the mechanisms of heterogenously catalysed hydrodesulfurisation reactions of thiophene compounds: they also have recognised the importance of the initial formation of a thiametallo-cyclic compound.³ Unfortunately since it is a better coal model, dibenzothiophene shows limited reactivity in the presence of iron carbonyls; however it will co-ordinate to iron in an η^1 -fashion in the complex $[\text{Fe}(\text{dbt})(\text{CO})_2(\text{cp})][\text{BF}_4]$ ⁴ where dbt = dibenzothiophene and cp = C_5H_5^- . It has been suggested that a very electron rich metal centre is required if insertion of the metal atom into the thiophene ring is to occur⁵, and recent work by the Rauchfuss group establishes that two metal centres are required if sulfur is to be removed from the ring⁶. In this paper it is proposed to investigate tellurophene derivatives on the grounds that they are chemically similar to thiophenes but contain weaker carbon to chalcogen bonds and may therefore be expected to be more reactive. Following

the commencement of these studies Angelici et al. published a paper in which their investigations had been extended to selenophene derivatives⁷.

2. EXPERIMENTAL

2.1. Syntheses

Tri-iron dodecacarbonyl was obtained from Aldrich and used as received. Thiophene was distilled from CaH_2 prior to use and tellurophene⁸, dibenzotellurophene⁹, and 3,4-benzo-1-telluracyclopentane¹⁰ were prepared by literature methods. n-Pentane was HPLC grade and all reactions were carried out under an atmosphere of pure argon using standard Schlenk techniques.

Tri-iron dodecacarbonyl was reacted with thiophene over 15 h following the original method of Stone *et al.*¹. The reaction was repeated by sealing the reactants, together with a small quantity of magnetite (0.5 g), in a stout Teflon container which was placed in a domestic microwave oven (Sharp-Carousel) and heated for 50 min. In both cases the reaction mixtures were worked up using column chromatography. A similar microwave experiment was conducted using benzothiophene which gave a 39% yield of the benzothiaferrole after 1 h compared with a 49% yield after 18 h reflux³.

The Reaction of Tellurophene with Tri-iron Dodecacarbonyl

Tellurophene (3.0 g), $\text{Fe}_3(\text{CO})_{12}$ (3.0 g), and n-heptane (100 cm³) were heated under reflux for 2.5 h. After 45 min the colour became violet, and then changed to orange after 1.5 h following which no other change occurred. Filtration afforded an orange solution and a black solid residue. Removal of the solvent gave orange crystals, mp 51°C; $\text{C}_{10}\text{H}_4\text{Fe}_2\text{O}_6$, found: C,36.2; H,1.21%, requires: C,37.0; H,1.38%.

The reaction was repeated, but stopped at the point of formation of the violet solution. Chromatography through tlc grade silica gave three components which were eluted with pentane to give unreacted $\text{Fe}_3(\text{CO})_{12}$, the above orange solid and a dark red powder which was recrystallised from boiling heptane to give violet, plate-like crystals of mp 42°C; $\text{C}_{10}\text{H}_4\text{Fe}_2\text{O}_6\text{Te}$ found: C,26.0; H,0.91%, requires: C,26.1; H,0.90%.

The Reaction of Dibenzotellurophene with Tri-iron Dodecacarbonyl

Dibenzotellurophene (1.93 g), $\text{Fe}_3(\text{CO})_{12}$ (1.16 g), and heptane (100 cm³) were refluxed for 2.5 h during which time the colour of the solution gradually changed from dark green to orange. After cooling, the solution was filtered to remove a brown residue; the deep orange filtrate was evaporated to dryness to give a brown solid. The brown solid was chromatographed on tlc grade silica giving a main purple band preceded by a small yellow band. Elution with pentane gave first a yellow material (dibenzotellurophene) and a dark red powder which, on recrystallisation from boiling heptane, gave violet crystals of a dibenzoferrole, mp 176°C; found: C,50.2; H,1.93%, $\text{C}_{18}\text{H}_8\text{Fe}_2\text{O}_6$ requires: C,50.1; H,1.85%.

The Reaction of 3,4-Benzo-1-telluracyclopentane with Tri-iron Dodecacarbonyl

3,4-Benzo-1-telluracyclopentane (1.93 g), $\text{Fe}_3(\text{CO})_{12}$ (2.80 g), and heptane (100 cm^3) were heated and stirred under reflux for 3 h during which time a colour change from dark green to purple occurred. After cooling, the solution was filtered to separate a black solid from the intensely purple filtrate. The filtrate was taken to dryness under vacuum to give a purple solid and a red oil. The mixture was dissolved in pentane (10 cm^3) and chromatographed on tlc grade silica to give two components. Elution with pentane and removal of solvent gave, first, purple crystals, and secondly, a small quantity of a red-brown material of mp 76°C. The purple compound was shown to be $\text{Fe}_3\text{Te}_2(\text{CO})_9$ (MS, FTIR), found: C,16.6; H,0.09%, requires: C,16.0; H,0.00%. The red compound was $\text{C}_{19}\text{H}_{16}\text{FeO}_3$, found: C,65.2; H,4.78%, requires: C,65.5; H,4.60%.

All compounds mentioned in this paper gave satisfactory MS, NMR and FTIR data which were entirely consistent with the proposed formulations.

2.2 Physical Measurements

^1H , ^{13}C , and ^{125}Te NMR spectra were obtained with a Bruker AC-300 instrument for CDCl_3 solutions using TMS (^1H , ^{13}C) and Me_2Te (^{125}Te) as standards. Infra-red spectra were recorded with a Biorad FTS-40A spectrometer. EI, CI and FAB mass spectra were obtained from the EPSRC service at University College, Swansea. Single crystal X-ray data were collected using an Enraf-Nonius CAD4 diffractometer operating in the ω -2 θ scan mode using $\text{MoK}\alpha$ radiation.

3 RESULTS AND DISCUSSION

3.1 Thiophene Experiments

The original work of Stone *et al.*¹ was repeated, and the expected ferrole, $\text{C}_4\text{H}_4\text{Fe}_2(\text{CO})_6$ together with FeS were identified as products (5% yield); in addition, a small quantity of a trimeric product not specifically identified by Stone *et al.* was shown to be: $\text{C}_4\text{H}_4\text{Fe}(\text{CO})_2[\text{Fe}(\text{CO})_3]_2$. The most interesting observation was that the same yield of the same products could be obtained in 50 minutes in the microwave oven using magnetite as the microwave receptor. Rauchfuss *et al.*³ were unable to remove sulfur from benzothiophene using this chemistry, the reaction affording the intermediate benzathioferrole. Unfortunately, microwave heating did not drive the reaction to the desulfurisation stage, but it did achieve similar yields of products in 1 h opposed to 18 h. It is therefore established that microwave heating can be effective in desulfurisation techniques based on organometallic reagents.

Unfortunately, benzothiophene and dibenzothiophene are much better models of organic sulfur in coal than is thiophene and it is clear that both molecules show different behaviour to thiophene in the presence of tri-iron dodecacarbonyl³. It was decided therefore to explore the analogous tellurium compounds, since these materials show similar chemical behaviour to the thiophenes but the carbon chalcogen bond strength will be less.

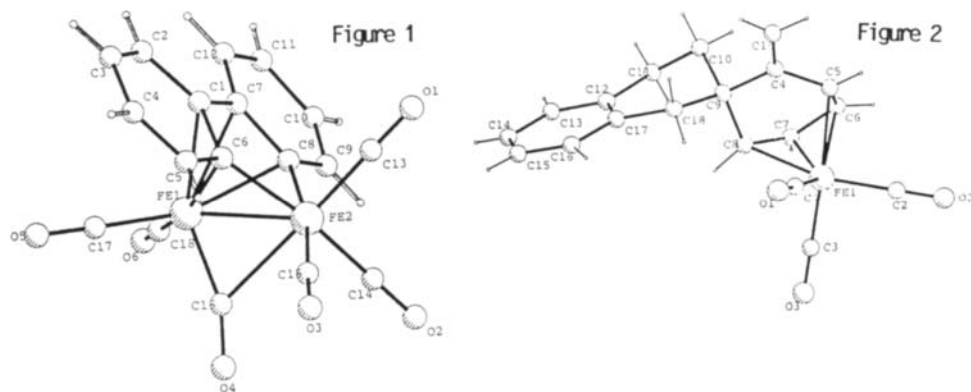
3.2 Tellurium Heterocyclic Compound Experiments

The reaction of tri-iron dodecacarbonyl with tellurophene affords the ferrole $\text{C}_4\text{H}_4\text{Fe}_2(\text{CO})_6$ via the intermediate telluraferrole (see experimental section); in fact, if the ferrole is the desired product the tellurophene route is much more

efficient. Tellurium is deposited as FeTe. More importantly, dibenzotellurophene has been shown to undergo a detelluration reaction with tri-iron dodecacarbonyl with the implication that the failure to see this step in the sulphur case arises from the strength of the C-S bond. Confirmation of the removal of tellurium is provided by the crystal structure of the dibenzoferrule, a new compound (fig. 1).

The opportunity has also been taken to examine organotellurium compounds which are models for thioethers, in particular 3,4-benzo-1-telluracyclopentane. The reaction with tri-iron dodecacarbonyl is complex, but two clearly defined products have been identified namely the previously described cluster compound $\text{Fe}_2\text{Te}_2(\text{CO})_9$ ¹¹ and a novel organometallic compound, $\text{C}_{16}\text{H}_{16}\text{Fe}(\text{CO})_3$ which contains an unsymmetric dimer of the organic fragment of the initial organometallic compound (structure in fig. 2). This is in contrast to the thermal decomposition of 3,4-benzo-1-telluracyclopentane which, following tellurium extrusion, forms the symmetric dimer.

The encouraging feature of this work is that it has been shown that both "ether"-like and "aromatic" tellurium may be removed by use of organometallic reagents. This encourages belief that it should be possible to define reagents to remove sulfur from realistic model compounds for sulfur in coal.



4 REFERENCES

1. H.D. Kaesz, R.B. King, T.A. Manuel, L.D. Nichols, and F.G.A. Stone, *J. Amer. Chem. Soc.*, 82 (1960) 4749.
2. A.E. Ogilvy, M. Draganjac, T.B. Rauchfuss, and S.R. Wilson, *Organometallics*, 7 (1988) 1171.
3. J. Chen, L.M. Daniels, and R.J. Angelici, *J. Amer. Chem. Soc.*, 113 (1991) 2544.
4. J.D. Goodrich, P.N. Nickias, and J.P. Selegue, *Inorg. Chem.*, 26 (1987) 3424.
5. S. Harris, *Organometallics*, 13 (1994) 2628.
6. A.E. Ogilvy, A.E. Skaugest, and T.B. Raufuss, *Organometallics*, 8 (1989) 2739.
7. C.J. White, T. Wang, R.A. Jacobsen, and R.J. Angelici, *Organometallics*, 13 (1994) 4474.
8. W. Lohner and K. Praefcke, *Chem. Ber.*, 111 (1978) 3745.
9. J.D. McCullough, *Inorg. Chem.*, 9 (1975) 2285.
10. R.F. Ziolo and W.H.H. Gunther, *J. Organometal. Chem.*, 146 (1978) 245.
11. D.A. Lesch and T.B. Rauchfuss, *Inorg. Chem.*, 20 (1981) 3583.

Coal Desulphurization with Hydroiodic Acid and Microwaves*

A.C. Ferrando, J.M. Andrés and L. Membrado

Instituto de Carboquímica, CSIC,
Poeta Luciano Gracia 5, 50015-ZARAGOZA, SPAIN

Introduction

The use of high-sulphur coals for energy production requires a cleaning stage to meet environmental regulations. Most times this cleaning is carried out over the flue gases, but chemical desulphurization has also received attention. Most methods for the chemical desulphurization of coal have relied on the treatment of coal with caustics in oxidizing atmospheres^{1,2}, but this method is of difficult application to low-rank coals due to the high amount of phenolic and humic materials released during the treatment³.

When studying the application of microwaves to coal processes we found that hydroiodic acid allowed sulphur to be removed from the coal when used in a sealed reactor with a reducing atmosphere. In this paper we present this novel and alternative treatment of coal with hydroiodic acid, which allows the complete elimination of pyritic sulphur at mild conditions.

Experimental

The reactions were carried out using a microwave digestion equipment (MLS-1200 Mega, Milestone SL) provided with a 500mL sealed reactor whose internal parts were made of a fluorinated polymer (TFM, Hoescht AG). The reactor can withstand up to 260°C and 60bar for limited periods of time, using an inner thermocouple for temperature control.

All experiments were carried out placing 5g of coal in the vessel, adding the acidic solution to it and bubbling argon for 5 minutes to obtain an inert atmosphere prior to closing the reactor. The required volume of hydrogen was added with a gas syringe through a port provided with a rubber septum. After the experiment was complete, the reaction mixture was allowed to cool to 40°C and the reactor opened. The reaction mixture was diluted with water and filtered through a Gooch crucible. After washing with water, the crucible was dried in a vacuum oven for 24h. at 50°C and weighed.

The base coal for the experiments was a sample from the "Sierra de Arcos" mine, located in the Teruel mining district, north zone, in Spain, with 1.56% of sulphate sulphur, 1.95% of pyritic sulphur and a calculated organic sulphur of 2.80%, for a 6.31% of total sulfur content. As the treatment with hydroiodic acid causes the removal of some mineral matter, a soft demineralization of the SA coal was carried out using concentrated hydroiodic acid at 25°C for 2hrs, which caused a weight loss of 12.76%. The analyses of the resultant product were taken as a base for the calculations, which were done using the "as received basis" for each product obtained. To avoid false interpretation of the yields obtained, mass balances for each sulphur form were calculated, making the results independent of the behaviour of the mineral matter of the coal.

* The work presented here has been funded by EC (CECA 7220-EC/759), CICYT (AMB-1221/92-CE) and CSIC (584). A patent has been applied for

Concentrated acids used in this work were reagent grade. Concentrated hydroiodic acid usually contains iodine, which was reduced by addition of small amounts of hypophosphorous acid until discoloration of the remaining solution. The iodine-free acid so obtained was stored under argon.

Results and Discussion

A simple factorial design was used to obtain initial information about the process, considering three variables: time of irradiation (1-5min), hydrogen volume injected (1-5mL) and concentrated hydroiodic acid volume(25-75mL). A 1000W microwave power for very quick heating was selected and the maximum temperature allowed was 230°C, to keep the reaction mixture below the safety limit established by the manufacturer of the reactor.

The statistical analysis of the results shows that time of irradiation is the main factor affecting the yield of the reaction, mainly to the desulphurization process. Sulphur and sulphur forms removal strongly increase with increasing time. Short irradiation times did not raise the temperature of the mixture to the levels attained for longer irradiation times, so it is possible to infer the influence of temperature in the yield of the desulphurization process.

The strong effect of time and the nonlinearity observed mask the effect of the other variables. As their significance is important to the development of the method, the design was divided into two blocks, one for short times and the other for longer times. The statistical analysis showed a positive effect of hydrogen in both cases, this effect being greater for shorter times. The effect of the volume of acid is related to the heating of the mixture: at short times, lower volumes allow higher temperatures, so the effect is negative, while for longer times, the temperature reaches the maximum allowed and it is the phase change to vapor that causes low volumes of acid to give poorer yields, as the remaining amount of liquid is not enough to completely cover the coal. The effect of this variable can be neglected by carrying out the reaction with appropriate volumes of reagent, so the volume was fixed to 75mL for subsequent experiments.

The balances for the sulphur forms show that organic sulphur seems to increase (negative removal) in some experiments. An explanation for this behaviour is the formation of elemental sulphur, which can be detected by extraction with carbon disulphide.

The results obtained showed that the desulphurization of coal with hydroiodic acid is possible, so subsequent series of experiments were carried out to establish the effect of longer times, maximum temperature allowed, gaseous environment and kind of acid on the desulphurization process. For these series, the conditions which yielded the best results, 230°C as maximum temperature, reaction time of 5 min., injection of 5mL of hydrogen and 75mL of hydroiodic acid were used as a reference, modifying one variable at a time.

The effect of time in the desulphurization process is shown in Figure 1. The removal of total sulphur depends on the behaviour of the sulphur forms. More than 99% of pyritic sulphur is removed in 10 or more minutes of irradiation, which combined with an organic sulphur removal of 64.7% in the best case (20 min.) allows 80.1% of the total sulphur of the coal tested to be removed. Lengthening the time of irradiation from 15 to 20 minutes did not significantly increase the sulphur removal,

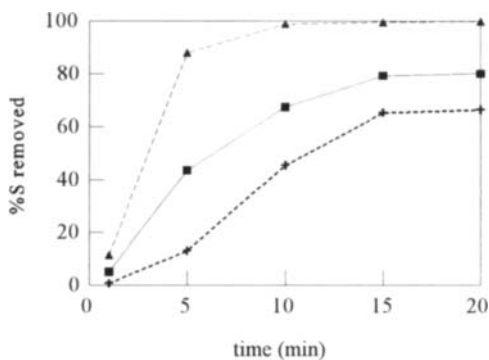


Figure 1. Desulphurization vs. time.

■ S_{total}, ▲ S_{pyritic}, + S_{organic}

establishing a limit of desulphurization for the coal tested. Total sulphur removal strongly depends on the nature of the organic sulphur bonds. In low-rank coals, a considerable amount of aliphatic sulphur compounds can be found, so organic sulphur removal can be high. For higher rank coals, where aromatic sulphur compounds are in larger amounts, lower yields can be expected for the removal of organic sulphur. So, the limit for the sulphur removal can be expected to be dependent on the coal treated, yielding good results for coals with pyritic sulphur as the main sulphur form.

The study of the effect of time was completed studying the effect of the maximum temperature allowed while fixing the time of reaction to 5 minutes. The balances for the sulphur forms are shown in Figure 2. The lower maximum temperatures 125 and 150°C did not show significant differences in the yields of the desulphurization process. The next two temperatures 175°C and 200°C allow a deeper attack to the coal by hydroiodic acid with greater sulphur removal. In these experiments, the removal of sulphur is mainly done by elimination of pyritic sulphur, but the removal of the organic sulphur increases with increasing temperature. Raising the temperature to 230°C produces a qualitative leap in the desulphurization yields as much more pyritic sulphur is removed but the elimination of organic sulphur is considerably less than that of the previous experiments, which could be attributed to the transformation of pyritic sulphur to elemental sulphur. Finally, setting the maximum temperature at 250°C allows high yields for the elimination of sulphur, due to an increase in the organic sulphur removal. From the data presented here, neither the pyritic sulphur nor the organic sulphur removal seem to be simple processes, and further experimentation, including quantification of elemental sulphur, is needed.

The effect of the gaseous environment on the yield from the treatment was established in experiments with air and with 50% of hydrogen in argon, that were carried out and compared with those obtained for 1 and 5mL of hydrogen. The balances for the reactions are shown in Figure 3. The use of air considerably increases the elimination of organic sulphur, though the overall yield is in between those obtained for the experiments with 1 and 5mL of hydrogen. The results using air were quite surprising as the liquid phase, once filtered, produced a yellow precipitate which was identified as elemental sulphur. This behaviour made the comparison with the other experiments difficult, as the experiment with 1mL of hydrogen shows a similar behaviour (increase of organic sulphur content) but elemental sulphur seems to remain in the product, not in solution. The desulphurization yields obtained for the experiments with hydrogen shows that hydrogen is important for the organic sulphur removal.

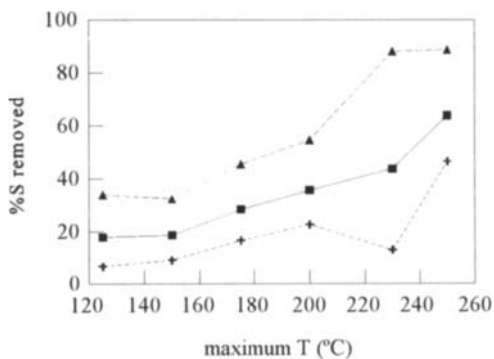


Figure 2. Desulphurization vs Temperature

■ S_{total}, ▲ S_{pyritic}, + S_{organic}

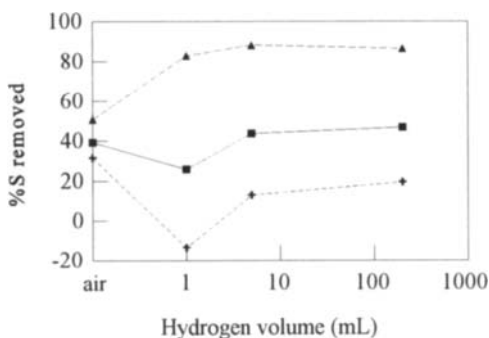


Figure 3. Desulphurization vs H₂ volume

■ S_{total}, ▲ S_{pyritic}, + S_{organic}

The last set of experiments were devoted to determine if other acids besides hydroiodic acid could be used and what effect the concentration of this acid has on the desulphurization yields. For comparison purposes concentrated hydrochloric and orthophosphoric acids were used, showing desulphurization yields lesser than those obtained with concentrated hydroiodic acid. The effect of the concentration of the hydroiodic acid was investigated comparing concentrated hydroiodic acid with 1/2 and 1/4 dilutions. Reducing the concentration of the acid to 1/2 produces a reduction in the removal of pyritic sulphur but increases the

elimination of the organic sulphur. Further reduction of the concentration of the reagent leads to lower desulphurization yields, with no removal of organic sulphur. In addition to these experiments two more experiments were carried out to test the behaviour of the system. The former tried to establish if hydroiodic acid, an expensive reagent, could be used as a catalyst while maintaining the acidity of the media with hydrochloric acid, a cheaper reagent. While the overall desulphurization yield was not good, pyritic sulphur elimination was significant. In the latter experiment, elemental iodine was added to the mixture to assess if the oxidizing ability of iodine plays a role in the desulphurization process. Results clearly show that iodine enhances sulphur removal, the effect being more pronounced for organic sulphur than for pyritic sulphur. All these experiments demonstrate that the process depends exclusively on the particular behaviour of the hydroiodic acid, with acidity, nucleophilic ability and redox potential playing a role in the desulphurization process.

The results presented allow us to conclude that chemical desulphurization of coals with hydroiodic acid is possible, and that this desulphurization process mainly removes pyritic sulphur, together with moderate amounts of organic sulphur. Sulphur is removed as hydrogen sulphide, though elemental sulphur is also obtained but not separated from the product. Future work will deal with model compounds to assess the ability of hydroiodic acid to remove different kind of sulphur bonds, including pyritic sulphur, and to try to establish the mechanisms that play a role in the overall process.

REFERENCES

- 1.- Meyers, R.A., "Coal Desulfurization", Marcel Dekker, New York, 1977.
2. IEA Coal Research, "The Problems of Sulphur", Butterworths, London, 1989.
3. Chriswell, C.D., Markuszewski, R. and Jewell, D.V., in "PROCESSING AND UTILIZATION OF HIGH-SULFUR COALS IV", Dugan, P.R., Quigley, D.R. and Attia, Y.A. Eds., Elsevier, Amsterdam, 1991, p. 407-424.

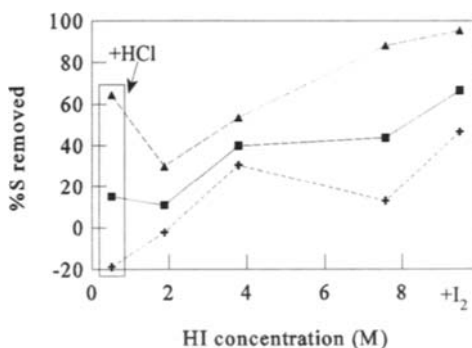


Figure 4. Desulphurization vs HI conc.

■ S_{total}, ▲ S_{pyritic}, + S_{organic}

Oxydesulphurization of coal using trona mineral

S. Yaman and S. Küçükbayrak

Istanbul Technical University, Chemical and Metallurgical Engineering Faculty, 80626, Maslak, Istanbul, Turkey

In this study, the desulphurization of coal by oxydesulphurization method using raw trona mineral was investigated. The experiments were carried out on a Turkish lignite sample which has both high pyritic and high organic sulphur contents. Some experimental parameters such as temperature, partial pressure of oxygen, concentration and time were investigated.

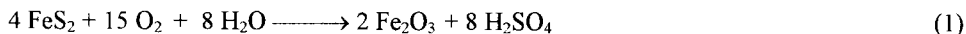
1. INTRODUCTION

Some physical, chemical and biological methods have been developed to desulphurize high sulphur coals. To remove the sulphur bonded with the organic structure of coal, chemical desulphurization methods must be used.

The economic applicability of a chemical desulphurization method depends on the price and abundance of reagents used. Since most of the reagents are expensive and unrecoverable, to use these chemical methods economically seem impossible. Many investigations have been conducted to study the alternative reagents.

One of the chemical desulphurization processes is oxydesulphurization. This process is a chemical technique by which all rank of coal can be desulphurized in acidic or basic solutions containing dissolved oxygen under pressure..

When the solution has a neutral pH at the beginning of the oxydesulphurization process, as the reactions proceed, H₂SO₄ forms and the solution becomes acidic [1,2].



The acidity of the solution causes some corrosive effects on the equipments. In this study the addition of trona mineral to the reaction medium as neutralizing and desulphurizing agent was investigated.

2. EXPERIMENTAL

The experiments were performed in a 1-liter magnetically stirred autoclave made of Type 316 stainless steel. In the experiments a hard lignite sample (-250 µm) from Gediz area (a region in the west of Turkey), was used. The analysis of the lignite sample is shown in Table 1.

Table 1
Analysis of the Lignite Sample from Gediz

Moisture (%)	-----Moisture Free-----									
	Volatile Matter (%)	Fixed Carbon (%)	Ash (%)	Calorific Value (MJ/kg)	C (%)	H (%)	S _T (%)	S _P (%)	S _O (%)	S _S (%)
1.84	30.74	37.36	31.90	22.90	64.74	5.02	7.38	2.85	4.16	0.37

where,

S_T : Total sulphur ; S_P : Pyritic sulphur ; S_O: Organic sulphur ; S_S : Sulphate sulphur

The trona solution used, was prepared by dissolving in water the required amount of trona mineral having a particle size of -250 µm. In order not to increase the mineral matter content of the lignite sample, the solution was used after the filtration. The chemical composition (%) of the trona mineral is as follows: Na₂CO₃: 45.92 ; NaHCO₃: 37.85 ; H₂O:15.37 ; SiO₂: 0.184; CaO: 0.075; MgO: 0.080; Al₂O₃: 0.036; Others:0.485

The total alkalinity originating from Na₂CO₃ and NaHCO₃ contents of the solution was represented as an alkaline concentration equivalent to Na₂CO₃.

For each experiment, 10 g lignite sample and 200 ml extraction solution with the desired concentration were filled into the reactor. Afterwards the partial pressure of oxygen is established, the heating has been started. After the desired period, the autoclave content filtered and washed with the hot distilled water until the washings get a neutral pH. The extracted coal was dried in a vacuum oven under nitrogen atmosphere at 373 K for 24 hours. After weighing, the required analyses were carried out according to ASTM Standards.

The effect of the partial pressure of oxygen on the total sulphur content of sample was investigated in the range of 0-1 MPa by leaching the lignite sample with a 0.15 M Na₂CO₃ equivalent alkaline solution for 15 min at 423 K and 473 K.

To study the effect of the alkaline concentration, the lignite sample was leached at 0-0.3 M equivalent alkalinity of Na₂CO₃ under 1 MPa oxygen partial pressure at 423 K for 30 min.

To investigate the effect of temperature, some experiments were performed between 423-473 K under 1 MPa partial pressure of the oxygen with an equivalent alkalinity of 0.10 M Na₂CO₃ for 60 min.

The effect of reaction time on the total sulphur content of sample was studied for 2.5-60 min. In these experiments, the conditions of experiments were chosen as an equivalent alkalinity of 0.10 M Na₂CO₃ and 1 MPa partial pressure of the oxygen at 423 K and 473 K.

3. RESULTS AND DISCUSSION

The effect of oxygen partial pressure on the total sulphur content of the sample is shown in Figure 1. Some reductions were observed in the total sulphur content of the sample with the increasing partial pressure of oxygen at the temperatures of 423 and 473 K. Total sulphur contents decreased to 6.20 % at both temperatures without oxygen pressure.

Under 1 MPa partial pressure of oxygen, total sulphur contents were decreased to 4.33 % at 423 K and to 3.40 % at 473 K. These correspond to 43.2 % and 64.9 % removals of the total sulphur content. The increase in the partial pressure of oxygen from 0 to 1 MPa also improved pyritic and organic sulphur removals. Pyritic sulphur removal increased from 27.7 % to 79.1 % and organic sulphur removal increased from 7.8 % to 14.9 % at 423 K, while at 473 K, pyritic sulphur removal increased from 26.9 % to 82.8 % and organic sulphur removal increased from 9.9 % to 50.2 %. Solid product yield was not affected negatively at 423 K. But at 473 K, the increase in the partial pressure of oxygen from 0 to 1 MPa led to reduction in solid product yield from 95.4 % to 76.2 %. Partial pressure of oxygen did not show any effect on the calorific value recovery.

The effect of alkaline concentration on the total sulphur content of the sample is seen in Figure 2. Although, the increase in the concentration up to 0.10 M provided some decreases in the total sulphur content, more concentrated solutions led to an increasing effect on the total sulphur content. The optimum concentration was seen as 0.10 M equivalent Na_2CO_3 . 37.3 % of the total sulphur content was eliminated using only water and 46.4 % of the total sulphur content was eliminated using a solution containing 0.1 M equivalent Na_2CO_3 . Alkaline concentration of 0.1 M equivalent Na_2CO_3 improved pyritic and organic sulphur removals from 76.4 % to 85.9 % and from 8.3 % to 15.5 %, respectively. Solid product yield and calorific value recovery were not affected considerably at 423 K.

Figure 3 shows that the total sulphur content of the sample decreased with increasing temperature. Total sulphur contents were determined as 3.99 % at 423 K, 3.52 % at 448 K and 3.04 % at 473 K. Pyritic sulphur removals decreased from 92.0 % to 87.5 % and organic sulphur removals increased from 14.5 % to 51.9 % with increasing temperature from 423 K to 473 K. As the coal structure decomposed at high temperatures, organic sulphur could be removed at high temperatures. The reaction of pyritic sulphur under process conditions is exothermic. Therefore, high temperature had negative effect on the pyritic sulphur removal. Solid product yield decreased to 79.3 % from 96.8 % and calorific value recovery decreased to 55.1 % from 86.6 %, as the temperature increased from 423 K to 473 K.

Figure 4 illustrates the effect of time on the total sulphur content. The results indicate that the total sulphur content decreased with time but changed little beyond 30 min. After 60 min, total sulphur removals were 47.7 % at 423 K and 67.3 % at 473 K. Pyritic sulphur removals were 92 % at 423 K and 87.5 % at 473 K, for 60 min. Organic sulphur removals were 14.5 % at 423 K and 51.9 % at 473 K for the same period. The extents of the calorific value recovery were 77.6 % for 10 min, 59.4 % for 30 min and 55.1 % for 60 min at 473 K. The solid product yield was also decreased depending on time.

REFERENCES

1. K.C. Chuang, R. Markuszewski and T.D. Wheelock, *Fuel Proc.Tech.*, 7 (1983) 43.
2. S.S. Akhtar and K.R. Cliffe, *Proc.of the Int.Conf.on Coal Science*, Vol. II, Japan, Tokyo, 1989.

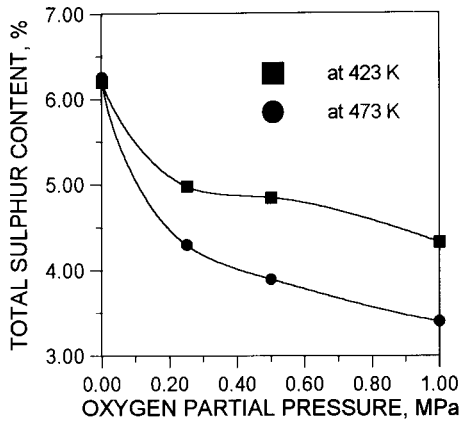


Figure 1. Effect of partial pressure of oxygen

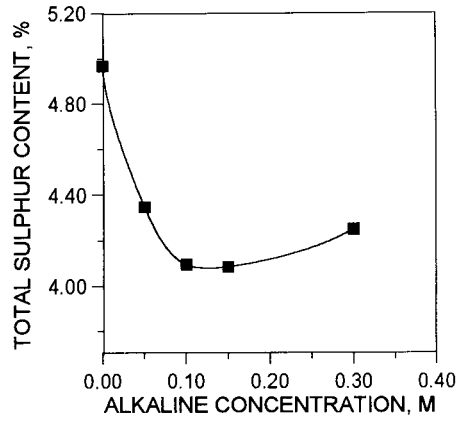


Figure 2. Effect of alkaline concentration

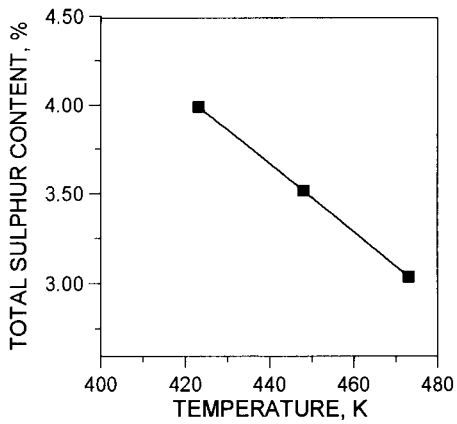


Figure 3. Effect of temperature

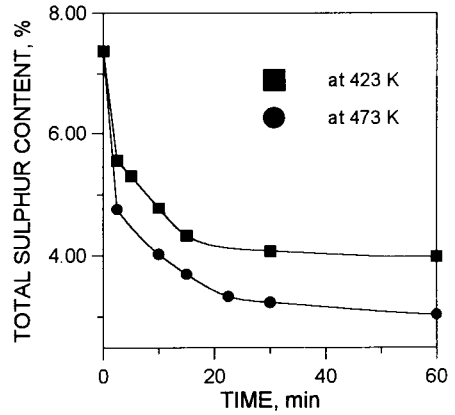


Figure 4. Effect of time

SOLUBILIZATION AND DESULPHURIZATION OF HIGH SULPHUR COAL UNDER MILD CONDITION WITH TRIFLUOROMETHANE SULPHONIC ACID

Kiyoyuki SHIMIZU, Yoshihiro IWAMI*, Toshiaki HAMADA*,
Akira SUGANUMA* and Ikuo SAITO

Energy Resources Dept., National Institute for Resources and Environment, AIST. 16-3 Onogawa, Tsukuba, Ibaraki 305, Japan.

*Department of Industrial Chemistry, Faculty of Science and Technology, Science University of Tokyo, Noda, Chiba 278, Japan

KEYWORDS: Coal Desulphurization, Solubilization, Superacid

INTRODUCTION

Liquid Brønsted super acid, trifluoromethane sulphonic acid (TFMS), can be a catalyst for hydrogen transfer, alkylation and transalkylation at low temperatures under the atmospheric pressure (ref. 1-4). It has been reported that TFMS cleaves the chemical bond in coal through the generation of carbonium ion, having the advantage of no direct reaction with hydrocarbon, and can be easily removed from the coal by neutralization (ref. 5). We have previously reported coal depolymerization/solubilization in the presence of pentane by the aid of TFMS without hydrogen at 150°C gave 90% soluble in pyridine (ref. 6).

In the present paper, the activity of TFMS was examined on the coal desulphurization as well as solubilization. Desulphurization of high sulphur coal is studied in the acid-catalyzed depolymerization reaction by the aid of super acid, TFMS, without gaseous hydrogen at milder conditions.

EXPERIMENTAL

A lignite coal, Mequinenza coal (C:63.2, H:6.1, N:0.9, Odiff:17.8, S:12.0% daf base, ash:12.5%, <0.25mm) was used in the present study. This sample coal was treated with a nitric acid solution (25vol%) for 24h at room temperature to remove inorganic sulphur (FeS₂ and FeSO₄, and so on). The sulphur content in coal was determined according to JIS M8813-1976 method by a Heraeus CHN-O-PAPID. Coal and solvent (toluene or isopentane) were placed in the ice cooled stainless autoclave (100ml), and TFMS was added dropwise to its coal/solvent slurry under stirring. The autoclave was heated to 150°C or 200°C at a heating rate of 1.5°C/min under autogeneous pressure of 6.1-6.9MPa for 3hr. After the reaction, the contents in the autoclave were gradually neutralized with an aqueous solution (5

wt%) of Na_2CO_3 . The products were filtered and washed in water-methanol solution under ultrasonic irradiation. Washing with methanol aqueous solution(10-50vol%) was repeated 10 times. It was heated at 100°C for 24h in a methanol solution(50vol%) with bubbling of nitrogen gas to remove TFMS completely. The products were extracted with hexane, benzene and THF, with a Soxhlet extractor, respectively. Gas products trapped at -5°C by depressurising the autoclave were analyzed by gas chromatography(Gasukuro Kogyo Model 312).

RESULTS AND DISCUSSION

The conversion and desulphurization of the treated coal are shown in Table 1. Acid catalyzed reaction in the presence of TFMS without solvent at 200°C(None-4-200) gave 19.8% desulphurization. The reaction with TFMS and isopentane(I-6-200) showed desulphurization of 23.4%. The reaction with toluene and TFMS of 45.2mmol/g-coal at 150°C gave 27.2% desulphurization in spite of the reaction temperature being lower. Desulphurization of T-4-150 was higher than I-6-200 in spite of the reaction condition of T-4-150 being milder. It is suggested that toluene plays an more important role as a solvent in the desulphurization reaction of coal when compared with isopentane. It should be noted that the reaction with TFMS of 45.2mmol/g-coal and toluene at 200°C(T-4-200) drastically increased the desulphurization up to 48.7%, indicating that higher reaction temperature promoted the cleavage of C-S bond in the acidic reaction conditions.

Table 1 Desulphurization and reaction conditions.

Run.No.	Reaction conditions			Desulphurization (%)
	Temp. (°C)	TFMS (mmol/g-coal)	N_2 (atm)	
None-4-200	200	45.2	20	19.8
I-6-200	200	67.8	40	23.4
T-4-150	150	45.2	20	27.2
T-4-200	200	45.2	20	48.7

Run.No.:solvent - amount of TFMS - Temperature
 none:no solvent, I:Isopentane, T:Toluene
 1)Desulphurization

The effects of TFMS concentration on desulphurization of Mequinenza coal are shown in Figure 1. TFMS of 11.3mmol(1ml) per 1g coal(T-1-200) allowed desulphurization of 34%. The desulphurization gradually increased with the concentration of TFMS up to 45.2mmol/g-coal where the desulphurization was saturated. The reaction with TFMS and toluene increased the desulphurization of coal, which depended on the TFMS concentration. However, increased TFMS(67.8mmol/g-coal) did not further accelerate desulphurization.

The solubility of the treated coals is summarized in Figure 2. The HNO_3 -MQ was 7wt% soluble in benzene and 33wt% soluble in THF. The product from the reaction with TFMS alone without solvent(None-4-200) was almost insoluble in any solvent. However, the reaction with TFMS and isopentane increased the solubil-

ity of the coal and its HS, HI-BS and BI-THFS yields were 20, 17 and 19wt%, respectively. 11.3mmol/g-coal of TFMS(T-1-200) did not essentially increase the solubility of coal. In contrast, TFMS of 22.6mmol/g-coal(T-2-200) rapidly increased solubility in any solvent, and T-4-200 showed high solubility such as 86wt% soluble in THF, 76wt% soluble in benzene and 50wt% soluble in hexane.

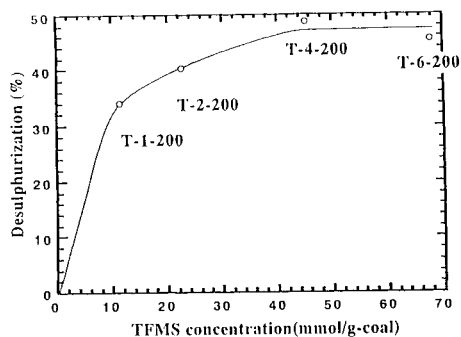


Figure 1 Effect of TFMS concentration on desulphurization of Mequinenza coal at 200°C.

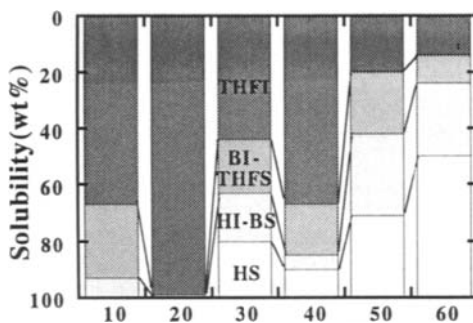


Figure 2 Solubility of the treated coals.

(a)HNO₃-MQ (b)None-4-200 (c)I-6-200
(d)T-1-200 (e)T-2-200 (f)T-4-200

Table 2 summarizes the gaseous products. These products found during the reaction with TFMS were mainly divided into 3 groups, hydrocarbon gases(C₃H₈, C₄H₈, C₄H₁₀), CO/CO₂ and hydrogen sulphide(H₂S). The produced gases from the None-4-200 were principally CO/CO₂. Isopentane(I-6-200) produced the hydrocarbon which comprises 39.7% of introduced isopentane and hydrogen sulphide as well as CO/CO₂. The reaction with toluene gave more hydrogen sulphide and much less hydrocarbon gas. The amount of produced hydrogen sulphide is correlated with the desulphurization which is calculated from sulphur content in the treated coal. This results suggested that the sulphur in coal was mainly released as hydrogen sulphide.

Table 2 Yields of produced gases during the acid-catalyzed coal desulphurization reaction with TFMS at 200°C.

	g/g-coal			Desulphurization (%)
	Hydrocarbon	CO ₂ +CO	H ₂ S(*)	
None-4-200	trace	0.060	trace(-)	19.8
I-6-200	0.994	0.031	0.006(8.5)	23.4
T-2-200	0.021	0.017	0.018(25.5)	40.4
T-4-200	0.044	0.009	0.023(28.7)	48.7
T-6-200	0.132	0.014	0.020(26.5)	45.5

Hydrocarbon:C₃H₈, C₄H₈, C₄H₁₀

(*)Desulphurization was calculated by amount of H₂S gas(%)

None-4-200 exhibited the lowest desulphurization and solubility. In contrast, T-4-200 showed the best desulphurization and solubility, suggesting that toluene and isopentane have two important roles. One is to donate hydrogen to coal for desul-

phurization during the acid-catalyzed depolymerization. The other is to promote the solubilization of the treated coal. The high solution of coal constituent molecules containing sulphur in solvent would give efficiently desulphurized and depressed negative cationic polymerization.

It is known that the extent of cationic reaction is a function of the acidity of the system(ref. 7). Consequently, HF/TaF₅ is favorable for production of carbonium ion because acidity of HF/TaF₅ ($H_0 = -18.85$) is at least more than 17800 times that of TFMS($H_0 = -14.6$)(ref. 8). HF/TaF₅ does not cleave the S-C bond of sulphur containing compounds in the presence of isopentane at 75°C. However, the present reaction condition with TFMS at 200°C could cleave the S-C bond in coal even under the lower acidic reaction condition. It is suggested that temperature as well as acid concentration would be required to cleave the S-C bond. Protonation of the sulphur containing compounds could easily take place at the lone pair electron of the sulphur, but the cleavage of S-C bond of the protonated compound would be need higher reaction temperature.

Sulphur in coal is mainly released as H₂S although hydrogen gas and conventional hydrogen donor solvent were not used in the present reaction. Evolution of hydrogen gas was hardly observable in the reaction with TFMS, thereby hydrogen of H₂S may be derived from toluene and coal molecules through hydrogen transfer at their cationic polymerization.

CONCLUSIONS

- 1) Trifluoromethane sulphonic acid(TFMS) was found to desulphurize coal in the presence of hydrocarbon without gaseous hydrogen at 150-200°C for 3h under autogeneous pressure of 2.6-6.6MPa.
- 2) Toluene provided 48.7% desulphurization and higher solubility(86wt% soluble in THF, 76wt% soluble in benzene and 50wt% soluble in hexane).
- 3) Sulphur in coal was released as H₂S.

ACKNOWLEDGMENT We wish to thank Instituto de Carboquimica, CSIC for providing the sample coal.

REFERENCES

1. H.Kumagai, M.Shimomura, and Y.Sanada, Fuel Process. Technol., 13, 97(1986)
2. H.Kumagai and Y.Sanada, Fuel Process. Technol., 14, 171(1986).
3. M.Farcausiu, Fuel Process. Technol., 14, 161(1986).
4. D.Frankel, V.R.Pradhan, J.W.Tierhey and I.Wender, Fuel, 70, 64(1991).
5. M.Farcausiu, T.R.Forbus and B.R.Rubin, Energy & Fuels, 1, 28(1987).
6. K.Shimizu, H.Karamatsu, A.Inaba, A.Suganuma and I.Saito, Fuel submitted for publication.
7. Wristers, J., J. Am. Chem. Soc. 99, 5051(1977)
8. G.A.Olah, G.K.Surya Prakash and S.Jean, Superacids; Wiley: New York, 1985, p9.

Microbial desulfurization of different coal types*

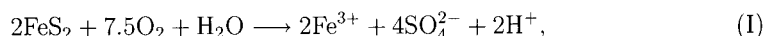
Gunnel Olsson^a, Olle Holst^b and Hans T. Karlsson^a

^aDepartment of Chemical Engineering II, ^bDepartment of Biotechnology, Chemical Center, Lund University, P.O.Box 124, S-221 00 Lund, Sweden

Microbial desulfurization of seven different coals by the thermophilic archaea *Acidianus brierleyi* was investigated. The objective was to elucidate the impact of coal composition on the degree of sulfur removal and jarosite formation.

1. INTRODUCTION

Microbial processing of coal is one of the options for control of sulfur emissions. Extensive work has been undertaken over the past decade to investigate the capability of different microorganisms to remove sulfur from coal [1]. Amongst the different sulfur forms present in coal, pyritic sulfur is readily oxidized microbiologically according to the following overall reaction:



a well established reaction basically representing the removal of inorganic sulfur from coal. If jarosite formation is not controlled, some of the solubilized sulfur precipitates back on the coal surface as, e.g., $\text{HFe}_3(\text{SO}_4)_2(\text{OH})_6$. Furthermore, some microorganisms are claimed to remove organic sulfur from coal, a matter of subject still controversial [2].

In the present study seven different coals were compared with respect to extent of sulfur removal and jarosite formation when processed with *A. brierleyi*. All coals were of low-sulfur type with a sulfur content ranging from 0.6 % through 1.8 %. Of the sulfur, between 33 % and 98 % was reported as organic sulfur; estimated as difference.

2. EXPERIMENTAL

Batch experiments were performed with microorganisms obtained from Deutsche Sammlung von Mikroorganismen (DSM). The major part of the study was carried out with *Acidianus brierleyi* (DSM 1651) at 70 °C. Furthermore, experiments with *Thiobacillus ferrooxidans* (DSM 585) were performed at 35 °C. For both the microorganisms the pH was set at its optimal value of two.

Seven different coals obtained from European Centre for Coal Specimens (SBN) were investigated. The distribution of different sulfur forms in the unprocessed coals is shown in

*The work was financially supported by the Swedish National Board for Industrial and Technical Development.

Table 1

Sulfur distribution in unprocessed coals, and sulfur removal and jarosite formation after 15 days of microbial processing (analyses on a dry basis).

Coal type*	101DE06	106DE20	134GB04	135GB14	171US34	177US41	516BE30
S_{tot} (%)	1.82	0.75	0.60	0.70	0.83	1.38	0.84
S_{org} (%)	1.01	0.73	0.58	0.67	0.73	0.46	0.54
S_{pyr} (%)	0.77	0.02	0.01	0.02	0.03	0.87	0.30
S_{sul} (%)	0.04	0.00	0.01	0.01	0.07	0.05	0.00
S_{∞} (%)	1.13	0.75	0.58	0.69	0.57	0.76	0.66
η_{tot} (%)	38	0	4	1	31	45	21
η_{jar} (%)	17	1	20	1	10	8	8

* according to classification by SBN

Table 1. All coals were ground down to less than 100 μm corresponding to a mass-median diameter of about 20 μm before each experiment.

Each experimental run was made with a coal slurry containing about 6 weight percent coal and lasted for 15 days. Samples were intermittently withdrawn from the reactors for analyses. The samples of coal slurry were filtered and dried. Jarosite precipitated on the coal surfaces was removed in boiling 5 M hydrochloric acid. The total sulfur content of the coal was determined before and after removal of jarosite using a Leco sulfur analyzer.

3. RESULTS

The percentage total sulfur removal from the coals (η_{tot}) has been defined as a gross value when jarosite is absent. The gross removal thus represents the potential removal efficiency provided complete inhibition of jarosite formation. The net removal can simply be estimated as $\eta_{net} = \eta_{tot} - \eta_{jar}$, where η_{jar} is the percentage coal sulfur converted to jarosite. The achieved sulfur removals are displayed in Table 1 for the seven different coals. As can be seen up to 45 % total sulfur removal was obtained in the best case. For the coals containing a negligible fraction of inorganic sulfur, no or very little of the sulfur was removed. The values of η_{tot} given in Table 1 correspond to the conditions attained after 15 days of microbial treatment.

Concurrently with the removal of sulfur, solubilized sulfur precipitated back on the coal surface in the form of jarosite. As seen from the table the jarosite formation was substantial. The rate of jarosite formation was seen to follow the rate of sulfur removal. For one of the coals (134GB04) massive jarosite formation was obtained because of dissolution of a large portion of the ash. In this case the jarosite was produced from the medium and the ash in spite of lack of sulfur removal from the coal.

4. DISCUSSION

The efficiency of microbial processing of coal depends on three factors, namely the rate of sulfur removal, the extent of sulfur removal, and the formation of jarosite. Each coal contains one part sulfur available for removal during microbial processing. The remaining

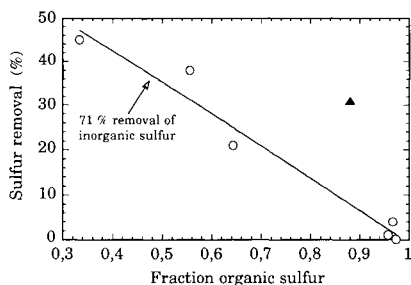


Figure 1. Weight percent sulfur removed as a function of the organic sulfur in the coal.

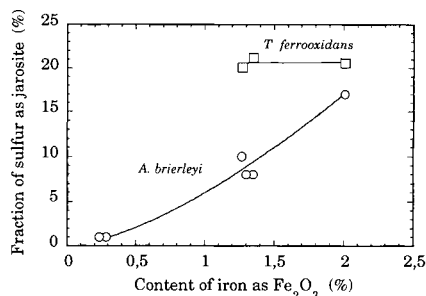


Figure 2. Weight percent jarosite produced as a function of the iron content of the coal.

sulfur (S_{∞}) is considered as unavailable even when exposed to microorganisms during an extended period of time. It should be noted that $S_{\infty} < S_{org}$ implies that some organic sulfur most likely has been removed. As can be seen from Table 1 only one of the coals fulfil this condition. Furthermore, if the difference $S_{in} - S_{\infty}$ is greater than zero it represents the amount of the inorganic sulfur not removed; S_{in} is the sum of sulfatic and pyritic sulfur.

The available sulfur can in most cases be deduced to pyritic and sulfatic sulfur, the latter only representing a minor fraction of the total sulfur. Hence, the unavailable sulfur consists of organic and some pyritic sulfur. During microbial processing of a coal the sulfur remaining in the coal versus time decays gradually to approach the level of the unavailable sulfur. Data for such experiments can generally be represented by a first-order rate expression with respect to the available sulfur remaining in the coal. The half-life time of the available sulfur can be estimated from $t_{1/2} = \ln(2)/k_1$, where k_1 is the first-order rate constant. Typically, the half-life time is several days. Our studies show that the half-life time ranges from 2.2 to 3.2 days for *A. brierleyi*. In a comparative study the half-life time was 40 % higher for *T. ferrooxidans* than for *A. brierleyi* [3]. First-order rate constants taken from the literature for *T. ferrooxidans* indicate a half-life time ranging from 2.2 to 96 days [4], depending on conditions and the way by which the rate constant was determined.

Investigating the data for sulfur removal reveals that mostly inorganic sulfur is removed, possibly except for coal 171US34. To analyze the potential for removing different sulfur forms the following procedure may be followed. First, since sulfatic sulfur (S_{sul}) is present in small amounts it is lumped with pyritic sulfur (S_{pyr}) into inorganic sulfur (S_{in}) present in the coal before microbial processing. The total sulfur present in the coal before microbial processing can then be represented as the sum of inorganic and organic sulfur:

$$S_{tot} = S_{in} + S_{org} \quad (1)$$

The total removal is related to the removal of organic sulfur and inorganic sulfur, respectively, as follows:

$$\eta_{tot} \cdot S_{tot} = \eta_{in} \cdot S_{in} + \eta_{org} \cdot S_{org} \quad (2)$$

Using Equations 1 and 2 the total sulfur removal as a function of the fraction organic sulfur in the coal before processing can be written as:

$$\eta_{tot} = \eta_{in} + \frac{S_{org}}{S_{tot}} \cdot (\eta_{org} - \eta_{in}) \quad (3)$$

Data for the seven coals have been plotted in Figure 1 according to Equation 3. All coals except 171US34 (filled symbol) seem to follow a straight line as predicted by Equation 3. A least-square fit leads to $\eta_{in} = 71 \pm 6 \%$ and $\eta_{org} = 0 \pm 3 \%$, respectively. Furthermore, the removal of organic sulfur from coal 171US34 was 22 - 35 %, the limits given from the assumption of 100 % and 0 %, respectively, removal of inorganic sulfur.

The formation of jarosite on the coal surface depends on temperature, media composition, type of microorganism and type of coal [4]. Jarosite is produced concurrently with the removal of sulfur from the coal. However, cases have been seen in which jarosite formation accelerated after most of the sulfur had been removed from the coal [5].

By investigating the impact of different parameters on the jarosite formation it was found that the total iron content of unprocessed coal is most significant. Theoretically, the molar ratio Fe/S_{in} in coal would be 0.5 if all the iron exists as pyrite. However, the iron content varied widely and the ratio Fe/S_{in} ranged from 0.6 to 5.7 when comparing the different coals. Furthermore, it was found that the iron content rather than the Fe/S_{in} ratio governs the jarosite formation.

The percentage of the coal sulfur converted to jarosite was thus plotted as a function of the total iron content expressed as weight percent Fe_2O_3 as shown in Figure 2. Based on reasons previously discussed, coal 134GB04 was excluded from the plot. Figure 2 also includes a few data points for *T. ferrooxidans* as a comparison. The data points for *A. brierleyi* were fitted to the following equation:

$$\eta_{jar} = 6 \cdot (Fe_2O_3)^{3/2} \quad (4)$$

where (Fe_2O_3) represents the iron present in the coal before processing expressed as weight percent Fe_2O_3 on a dry basis.

A possible explanation of the clear impact of the iron content on the jarosite formation is that jarosite is not precipitated but rather produced by reaction of dissolved sulfate with iron sites on the coal surface.

REFERENCES

1. L. Larsson, G. Olsson, H.T. Karlsson and O. Holst, *Biological Degradation and Bioremediation of Toxic Chemicals* (G.R. Chaudhry, ed.), Dioscorides Press, Portland, Oregon, Chapter 23 (1994) 493.
2. P. Bos, F.C. Boogerd and J.G. Kuenen, *Environmental Microbiology* (R. Mitchell, ed.), Wiley, New York (1992) 375.
3. G. Olsson, B-M. Pott, L. Larsson, O. Holst and H.T. Karlsson, *J. Ind. Microbiol.* 14 (1995) (in print).
4. G. Olsson, L. Larsson, O. Holst and H.T. Karlsson, *Chem. Eng. Technol.* 16 (1993) 180.
5. B-M. Pott, G. Olsson, L. Larsson, H.T. Karlsson and O. Holst, *J. Resource and Environ. Biotech.* (accepted for publication).

Biological sulphur removal by *thiobacillus thiooxidans* in fine coal coming from a flotation washing plant

G. González Benito ^a, G. Osorio^a, D. Bonilla^b, .

^aDepartment of Chemical Engineering, Faculty of Sciences, University of Valladolid, 47011 Valladolid, Spain.

Tfn: + 34 (9)83 42 31 70 Fax: + 34 (9)83 25 72 93

@mail: gerardo@cta.uva.es

^b S.A. Hullera Vasco-Leonesa, La Robla, 24640 León, Spain.

Biological removal of sulphur from coal by means of a pure culture of *Thiobacillus thiooxidans* NCIMB 8373 was studied. The coal used (Ciñera-Matallana coalfield, León, Spain) was classified for ASTM to have a rank like semi-anthracite. The two fine coal used come from two different flotation stages of the coal washing process. One was from the effluent and the other from flotation froth.

The influence of several parameters: pH, addition of nutrients to the slurry, slurry concentration and type of coal (stage of washing, different size) was studied.

About 15% removal of sulphur was obtained operating with a pH of 3.6, using a slurry concentration of 20% wt/v. The diameter of coal particles was less than 15 μm .

1. INTRODUCTION

More of production of coal is employed in combustion and coking; however, this application presents several environmental problems. Coal contains substantial amounts of sulphur, nitrogen, including significant quantities of toxic impurities which yield sulphur oxides, nitrogen oxides and compounds of toxic metals. Recently researches have focused on eliminating sulphur as a principal cause of *acid rain*. Sulphur is present in coal as four different forms: Pyritic, organic sulphur (it cannot be removed by physical methods), sulphate sulphur (it does not present atmospheric pollution, since is soluble), and elemental sulphur (it occurs in amounts very low).

Physical coal cleaning can remove a part of the pyritic sulphur when it is present as macroscopic particles, but not when the pyritic sulphur is present as microscopic particles or when it is there as organic sulphur. Chemical methods to remove organic sulphur have been examined, however they are too expensive and generally alter the coal characteristics. A method that could be complementary and/or alternative to traditional desulphurization methods is a biological process based on the action of specialized microorganisms, which obtain energy from oxidising the sulphur contained in coal.

* To whom all correspondence should be addressed

A great number of microorganisms have been identified which selectively remove sulphur from coal. In this work we have studied the influence of certain parameters in sulphur removal by a pure culture of *Thiobacillus thiooxidans*¹, that is not enough investigated in coal desulphurization. The influence of sulphur concentration and size of coal, nutrients, pH and slurry concentration was analyzed.

2. EXPERIMENTAL

2.1. Microorganism

The strain employed was *Thiobacillus thiooxidans* NCIMB 8343 (ATCC 19377). The microorganism was maintained on slants tubes containing (g·dm⁻³ distilled water): NH₄Cl, 0.1; KH₂PO₄, 3.0; MgCl₂·6H₂O, 0.1; Na₂S₂O₃·5H₂O, 5.0; bacteriological agar, 20.0. The pH of the medium was adjusted to 4.2 prior to sterilization (120°C for 15 min.), and was incubated at 30°C for ten days.

T. thiooxidans was grown in a liquid medium where sulphur (0.3 g·dm⁻³) was substituted for sodium thiosulphate. Sulphur must be sterilized separately (100°C, 30 minutes for three consecutive days). Cultures (100 cm³ liquid medium) were grown aerobically in 250 cm³ flask continuously shaken in a rotary shaker (200 rpm) at 30°C for six days.

2.2. Coal

The coal used was classified for ASTM to attend rank like Semianthracite. It was extract from Cifera-Matallana coalfield, located at Leon, Spain (Hullera Vasco-Leonesa S.A.). Coal fines used were assigned to produce power, and had convenient size to avoid coal grinding stage that would rise production costs. Two samples of fine coal with different sizes coming from froth flotation process of the washing plant, were studied. One was from the effluent and the other from the flotation froth, hereafter named E and F respectively.

2.3. Experiments

Coal's slurry was prepared with distilled water at the desired concentration (coal weight/liquid volume). The coal had a high carbonate concentration and it was necessary to realize a pretreatment with HCl 5M, to its elimination; then, pH was adjusted at required value depending of the experience. The slurry was sterilized (120°C for 15 min). The flasks containing slurry were inoculated with *T. thiooxidans* previously grown. This inoculum was prepared by filtering and centrifuging at 6000 rpm for 15 minutes, then, it was washed several times with H₂SO₄ 10⁻³ M and water. Starting cell concentration were about 10⁸ microorganisms per mL. Flasks (500 cm³ with 220 cm³ slurry) were incubated at 30°C in a rotary shaker (200 rpm). Samples were periodically removed, centrifuged and filtered to test for sulphate concentration in order to follow the performance of the desulphurization process. After about 25 days, the coal treated was filtered, washed with distilled water and dried; then, it was analyzed its content in total and sulphur forms, % ash, and heating value.

2.4. Analytical methods

Sulphate was determined by HPLC. Total sulphur content in coal was determined using an automatic analyzer, LECO SC-32, contrasted with the standard ISO 334². Forms of sulphur in coal were determined using ISO 157 procedure³. It must be remark that the values of organic sulphur are not precise because of its were calculated by difference between total and pyritic sulphur. Gross calorific value was determined using an Isothermal Calorimetric Bomb,

LECO AC-300. Ash concentration was determined by standard method⁴. Cell concentration was determined by two methods: direct microscopic enumeration in a hemacytometer Thoma using a NIKON microscope and by protein concentration (Lowry method)⁵.

3. RESULTS

3.1. Preliminary tests

Preliminary tests were made carried out with different values of pH (3.0, 3.6, 4.2, 5.0). The coal used was effluent (E) with characteristics were shown in the table. Results suggest that the pH more adequate is closed to 3.6, achieving the higher desulphurization (15.36 %) for both pyritic and organic sulphur.

On the other hand, several experiences were carried out working without nutrients in the culture medium. The slurry only had distilled water and coal. Results obtained for the coal F are shown in the table and as it can be seen, the addition of nutrients did not improve the percentage of desulphurization.

Therefore, all experiences carried out after were realized without addition of nutrients and with an initial pH value close to 3.6.

3.2. Influence of slurry concentration

The content of solids in the growth affects to mass and oxygen transfer and therefore to the overall yield of the process. With the purpose of analyzing this influence, it was carried out the bioleaching with different concentration of coal (15, 20, 25% wt/v for coal E). Results obtained, shown in the table, indicate that the best yield on the desulphurization was obtained for a slurry concentration of 20% wt/v.

3.3. Influence of cleaning stage

Finally, the influence of type and size of the coal on the desulphurization process was analyzed. It was worked with coal samples, E and F, corresponded to the same coal, but present different characteristics. Even though the sample E had got less sulphur than F, it was found that the percentage of desulphurization was highest in samples E (15.36% vs 3.7% in total sulphur). It could consider that this substantial difference is due to two causes:

- Size: Samples E were smaller (less than 15 μm) than samples F (less than 500 μm), so, the transport phenomena rate did not control the process, and microorganisms reach readily sulphur contained in coal's matrix.

- Different stage of coal washing process: Samples E were effluent's coal and F were flotation froth, and a possible effect of chemicals products added to the process could happen.

4. Discussion

The results of the biodesulphurization of fine coal coming from a washing process with *Thiobacillus thiooxidans* NCIMB 8343 indicate that the more adequate value of the initial pH is 3.6 achieving a percentage of desulphurization about 15% for a slurry concentration of 20% wt/v and a diameter of particles less than 15 μm . In this operating conditions, we found that the sulphur removal take place from the pyritic form. Moreover, the addition of nutrients to the culture medium was considered no necessary.

On the other hand, it is essential to indicate that this low value in the removal of sulphur can be due to the coal is coming from washing process therefore a significant amount of sulphur has just been removed in this process.

Table1
Biological desulphurization of coal

	Sample E (Effluent)						Sample F (Froth)				
	Samples treated						Samples treated				
	E*	E1	E2	E3	E4	E5	E6	F*	F1	F2	F3
pH		3.0	3.6	4.2	5.0	3.6	3.6		3.6	3.6	3.6
% Slurry		20	20	20	20	15	25		10	20	20
Nutrients		no	no	no	no	no	no		no	no	yes
Size μm)	< 15	< 15	< 15	< 15	< 15	< 15	< 15	<500	<500	<500	<500
Ash (%)	39.8	37.63	37.7	37.82	38.4	37.70	37.82	17.9	15.81	15.90	15.81
G.C.V (MJ/Kg)	20.09	20.84	20.57	20.77	20.30	20.70	20.77	28.6	20.27	20.25	20.23
KgS/GJ	0.64	0.56	0.55	0.56	0.57	0.55	0.55	0.77	0.75	0.74	0.75
Total Sulphur (%)	2.14	1.88	1.81	1.87	1.87	1.85	1.85	2.68	2.60	2.58	2.61
Pyritic S.(%)	1.18	1.03	1.00	1.05	1.17	0.98	0.98	1.84	1.76	-	1.76
Organic S.(%)	0.81	0.85	0.74	0.82	0.70	0.87	0.87	0.79	0.84	-	-
Sulphate S.(%)	0.15	-	-	-	-	-	-	0.05	-	-	-
%Removal of S.											
Total S		12.46	15.36	12.94	12.88	13.86	13.69		2.94	3.72	2.49
Pyritic S.		12.98	15.61	11.37	0.85	16.96	16.79		4.35	-	4.35
Organic S.		-	9.34	-	14.26	-	-		-	-	-

* Coal untreated

Acknowledgements

The authors thank S.A. Hullera Vasco-Leonesa for supplying fine coal samples and helping in some coal analyses.

REFERENCES

1. *Bergey's Manual of Systematic Bacteriology*, Vol 3, 1989.
2. **ISO 334:1975**: Coal and Coke- Determination of total sulphur- Eschka method.
3. **ISO 157:1975**: Hard coal - Determination of forms of sulphur.
4. **ISO 1171:1981**: Solid minerals fuels - Determination of ash.
5. **Lowry O H**: *Journal of Biological Chemistry*, 193, 265-275, 1951.

BIODESULPHURIZATION OF COALS FROM THE NORTH OF LEÓN (SPAIN). OPTIMIZATION OF PROCESS VARIABLES.

O. Martínez, A. Aller, J. Alonso, E. Gómez, A. Morán

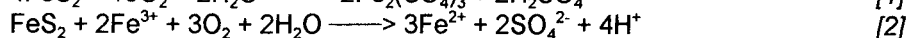
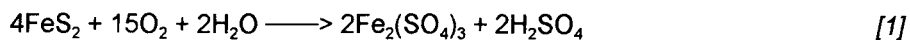
Dept. of Chemical Engineering. University of León. Jesús Rubio, 2; 24004 León (Spain).

1. INTRODUCTION

Sulphur compounds removal from coals may be carried out with several procedures, which differ according to whether they take place before, during or after the coal burning. They are based usually on procedures of chemical and physical split-off of mineral sulphur from the coal. It is hampered by the difficulty of removal of organic sulphur together with the high energy input required. The sulphur removal techniques during the coal combustion apply to combustion in fluidized bed (1). Sulphur dioxide suppression after the combustion process has been carried out recently (2).

Biological cleansing of coals is applicable before the coal combustion, though biological procedures for the desulphurization of combustion exhaust have been suggested lately (3). This sulphur removal before the coal combustion may take place, either through catalyzed dissolution of the pyrite, or through the modification of the flotation properties of the pyrite by means of contact with microbiological species (4).

The pyritic sulphur oxidation of coals is a natural process that happens quite slowly. This process causes acid drainage from coal mines (5). The process is quickened when there are certain kinds of microorganisms in this environment, which starts the coal pyrite oxidation. One of the most studied and used bacteria is *Thiobacillus ferrooxidans*, which is able to take energy by oxidizing reduced forms of iron and sulphur. This bacterium is autotrophous, acidophilous and mesophilous (6), and can be isolated from natural mine sludges, where its catalytic activity takes place. It is postulated that the pyrite oxidation mechanism (7) is triggered by direct bacterial attack [1] on the pyrite cores, and by indirect attack [2] by the ferric ion produced by the bacterium [3], according to the following reactions:



The readiness with which bacteria can reach the coal pyrite cores depends on the latter's distribution throughout the coal, on the bacterial concentration and on the mobility of microorganisms, which is favoured in an aerobian aqueous culture medium (8, 9).

2. MATERIAL AND METHODS

A run-of-mine low-volatile content coal from the Hullera Vasco-Leonesa of La Robla (León, Spain) was chosen as raw material for the biodesulphurization. This coal has 1.90% of total sulphur, 1.20% of which is pyritic sulphur, 0.63% is organic sulphur, and 0.7% is sulfate. The bacterial culture used was selected among several ones coming from acid water of coal mines, by growth of sludges and water samples in 9K salt medium (10). Biodesulphurization tests have been carried out in 100-mL-shaken flasks, with 50 mL of coal pulp, and in 2-L-reactor flasks, with 1 L of coal pulp. Temperature has been controlled in thermostatable bath.

The results of sulphur removal from coal have been measured with spectrophotometric analysis of dissolved iron, and with analysis of forms of sulphur, according to standardized methods.

3. RESULTS AND DISCUSSION

3.1. Selection and adaptation of bacterial culture

ATCC and mine's acid water bacterial strains —isolated from natural environments— have been cultured and enriched in 9K salt medium, the latter having proved to grow rather more profusely than the former. At the same time the selected culture has been set to adapt to the coal pulp through successive sowings, in order to increase its output in the biodesulphurization process. Therefore a very rich in bacterial mass coal pulp is obtained, which used as inocule, renders the advantage of absence of mineral salts to be added to the desulphurizing coal. The results thus obtained are shown in figure 1, which indicates that the lag phase becomes shorter as the culture adapts itself to its medium. According to these results it can be inferred that a significant desulphurization takes place after ten days of process, after which time span is considered the end of process for the following tests.

3.2. Process variables optimization

Coal pulps were treated in shaken flasks at pH ranging from 1.0 and 3.0 and temperatures between 20 and 40 °C, in order to find out the best pH and temperature for the biodesulphurization process. For the pH to be kept in its values a sulphuric acid addition during the first days was required, owing to the acid neutralization capacity of coal mineral matter. The results thus obtained, plotted in figure 2, show that the optimal pH and temperature values are 2.0 and 35 °C respectively. Under these conditions a total sulphur removal of around 50% is achieved.

Afterwards, keeping the above mentioned pH and temperature values, desulphurization tests in reactor flasks containing coal pulps in w/w (weight/weight) concentration between 5 and 20% and particle size <0.125 mm were carried out. These results are displayed in figure 3. Pulp concentration of 15% renders the optimal desulphurization output. On the other hand, after the sulphur and forms of sulphur analysis, it can be established that about 50% of total sulphur and over 90% of pyritic sulphur is disposed of, remaining only the organic sulphur. Also noteworthy is the remarkable sulphur removal from the non-inoculated sample, leading to consider that there is a strong chemical pyrite oxidation, and/or a biological sulphur removal carried

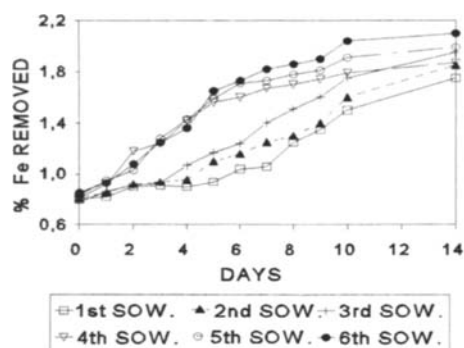


Figure 1. Culture adaptation for coal pulp.

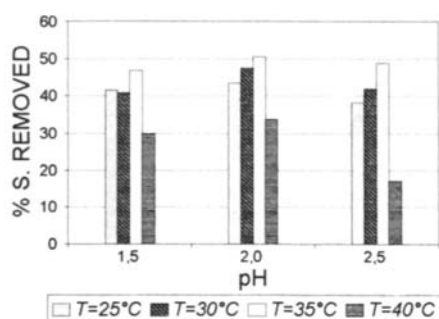


Figure 2. Optimization of pH and temperature.

out by the coal's own bacteria. On tests with sterile coal samples, a 30% of pyritic sulphur removal was observed, whereas with the non-inoculated blank sample, nearly 50% of pyritic sulphur removal was attained. This difference shows the amount of desulphurization carried out by the coal's accompanying bacteria.

3.3. Coal's technological properties modification

As a result of an acid pH, besides the consequent removal of most of pyritic sulphur, a good deal of coal's mineral matter is cleared away, which is highlighted by the ash content reduction (around 15%) of the treated coal. The dissolution of the mineral matter's carbonates produces carbon dioxide, which is a bacterial nutrient.

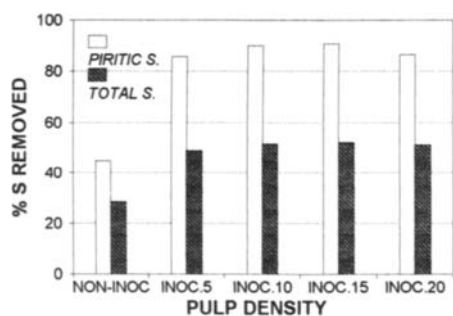


Figure 3. Sulfur removed for different coal pulp concentrations.

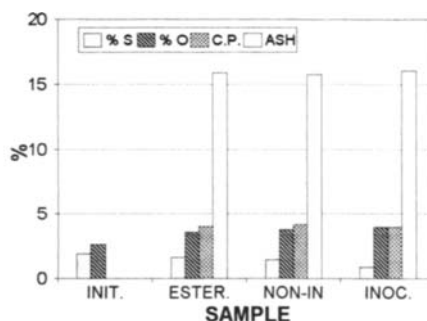


Figure 4. Modification of coal properties after the biodesulphurization.

Besides, there is an estimated slight reduction of 4% of calorific power. These results are drawn in figure 4. In tests carried out at higher temperatures, a bigger mineral matter removal and more calorific power loss happen, as well as a sinking in the desulphurization output as an effect of temperature deviation from the optimal one upon the bacterial growth.

Together with the sulphur clearance, an increase of the amount of oxygen in coal is produced, though the content of organic carbon, hydrogen and nitrogen is not altered, which shows that a minimal degradation in coal's carbonous structure is produced asside effect.

5. CONCLUSIONS

The biodesulphurization output produced on coal pulps by means of an autoctonous bacterial culture is higher than that produced by collection cultures. Moreover, the inherent bacteria of coal help to this performance improvement.

Working with coal particles <0.125 mm at pH 2.0, temperature of 35 °C and pulp density of 15%, a higher biodesulphurization rate is achieved.

The coal quality is improved in the process of biodesulphurization as a pre-combustion stage, due to both pyritic sulphur and mineral matter removal. On the contrary, this process brings about the drawback of a small loss in the coal's energetic power.

REFERENCES

- (1) Pis, J.J., Escudero, J.B. Combustión del carbón en lecho fluidizado. *Energía*. 25 (10): 650-652 (1979).
- (2) Hjalmarsson, A.K. Fig installations on coal-fired plants. In: *Technologies and Strategies for Reducing Sulphur Emissions. Biodesulphurisation-2*. Rugby, UK: Institution of Chemical Engineers (1991).
- (3) Dasu, B.N., Deshmane, V. et al. Microbial reduction of sulphur dioxide and nitric dioxide. *Fuel*, 72 (12): 1705-1714 (1993).
- (4) Ohmura, N., et al. Desulfurization of Coal by Microbial Column Flotation. *Biotechnology and Bioengineering*. Vol 44: 125-131 (1994).
- (5) Gómez, E. El drenaje ácido de aguas de minas en actividades mineras de la provincia de León. León, Universidad: Tesis doctoral. 260 pgs. (1989).
- (6) Bergey's. *Manual of determinative bacteriology*. Baltimore, USA. Waverleys Press. 8th Edition (1975).
- (7) Monticello, D.J.; Finnerty, W.R. Microbial Desulphurization of Fossil Fuels. *Ann. Rev. Microbiol.* 39: 371-389 (1985).
- (8) Reed, L. Focus of research in coal bioprocessing. In: *Bioprocessing and Biotreatment of Coal*. (Wise, D. L.) Ed. Marcel Dekker, Inc., New York: 1-27 (1990).
- (9) Kargi, F., and Robinson, J.M. Microbial Coal Desulphurization. *Enzyme Microb. Technol.*, 4 (1): 13-19 (1982).
- (10) Silvermann, M.P.; Lundgren, D.G. Studies on the Chemilitotrophic bacterium *Ferrobacillus ferrooxidans*. *J. Bacteriol.* 77: 642-647 (1959).

Microbial Degradation of Illinois No.6 Coal by Means of Comatabolism with Phenols

Y.Kabe, T.Furuta, M.Takai, K.Higashi, S.Katoh and T.Kojima

Faculty of Agriculture, Tmamagawa University, Tokyo 194, Japan

1. Introduction

Since the phenomenon of microbial solubilization of weathered lignite was found by Cohen et.al.¹⁾, microbial degradation of coal has been studied actively, and various mechanisms have been proposed. Two different approaches have been made to elucidate the mechanism of microbial degradation of coal. One of them is the research of biodegradation of condensed multi ring aromatic hydrocarbon such as anthracene and phenanthrene as model compounds, which has been made as earlier as 1950s^{2),3)}. Another approach is lowering the molecular weight of coal, which is comparatively new. In order to lower the molecular weight of coal, either ether or methylene bridged linkage must be cleaved. This second approach could be subdivided into the following three, 1)depolymerization of lignite^{4),5)}, 2)cleavage of ether linkage of lignin dimer⁶⁾, of which structure is close to that of coal, 3)cleavage of ether linkage of diphenylether as a model compound of coal by Pfeifer et. al.^{7),8)}.

Thus, there is a fair prospect of biodegradation of coal, but in order to develop practically, furthermore many sided research must be made. Therefore, in this study for the purpose of the beneficial utilization of coal, many sided research have been carried out to examine simultaneous abilities of cleavage of aromatic ring, degradation of lignin and water soluble coal with four *Aspergillus* species, of which two species were isolated as coal assimilative microbes and another two species were isolated as lignin assimilative microbes.

Because lignin and water soluble coal are macromolecule having complex structure, it is considered that biodegradation of these substances are very difficult. For this reason, cometabolism with phenols was adopted to accelerate microbial degradation of lignin and coal.

2. Experimental

Microorganisms used were four *Aspergillus* species, of which two strains, FKS1 and FKS7 were isolated from weathered pine tree sample and another two strains, FHS3 and FHS5 were isolated from soil containing coal. Of these four strains, FHS3 and FHS5 were identified as *As. versicolor* and *As. fumigatus*, respectively.

These fungi were cultivated in the media containing coal or the related substances as a sole source of carbon and energy and mineral solution(NH₄NO₃:2.5g, NaHPO₄:1.0g, KH₂PO₄:0.5g, MgSO₄:0.24g, MnCl₂:0.13g, a slight amounts of CaCl₂, ZnSO₄, FeSO₄ and CuSO₄, and distilled water:1L), and 10 ml of media were put in L shaped test tube(i.d.:16mm, L:120mm, H:90mm) and reciproskated in the speed of 120rpm, at 30°C.

A kind of coal mainly used was Illinois No.6 coal, in addition, Wandoan coal, Daton coal and Shenyan coal were occasionaly used. Coal was ground to particle size of 63-106 μ m and used without further treatment, or used as water soluble coal with treatment of nitric acid oxidation according to the procedure reported by Crawford et.al.⁶⁾. Water soluble coal were divided three components called water soluble Illinois No.6 coal A, B and C precipitated at 1700 cm⁻¹ of -COOH increased in turn.

The following commercial reagents were used as coal related substances without further purification ;lignin, phenol, guaiacol, veratric acid and acetoveratrone.

Growth was expressed by apparent volume of mycelia in L shaped test tube on standing for 1 hr.

Concentration of lignin or water soluble coal was mainly measured by UV spectra using UV spectrophotometer UV-240 (Shimazu Co.).

3. Results and discussion

3.1. Degradability of lignin and the related compounds.

In order to examine whether aromatic ring was cleaved by four *Aspergillus* strains FKS 1, FKS7, FHS3 and FHS5, cultivations were carried out in the media containing lignin, phenol, guaiacol (2-methoxyphenol), veratric acid (3,4-dimethoxybenzoic acid) and acetoveratrone (3,4-dimethoxyacetophenone) as a sole source of carbon and energy. Here, guaiacol, veratric acid and acetoveratrone were used considering as intermediates produced in the degradation of lignin, which had been examined by Cespedes et.al.⁶⁾. As shown in Fig. 1, in the medium containing lignin, all of four strains slightly grew more than in that containing no carbon source, and all of them remarkably grew in media containing phenol, guaiacol and veratric acid. In the medium containing acetoveratrone, FKS1 and FHS3 significantly grew, whereas FKS7 and FHS5 grew only to the level of no carbon source.

Measuring concentration of compounds, phenol, guaiacol and veratric acid were expended

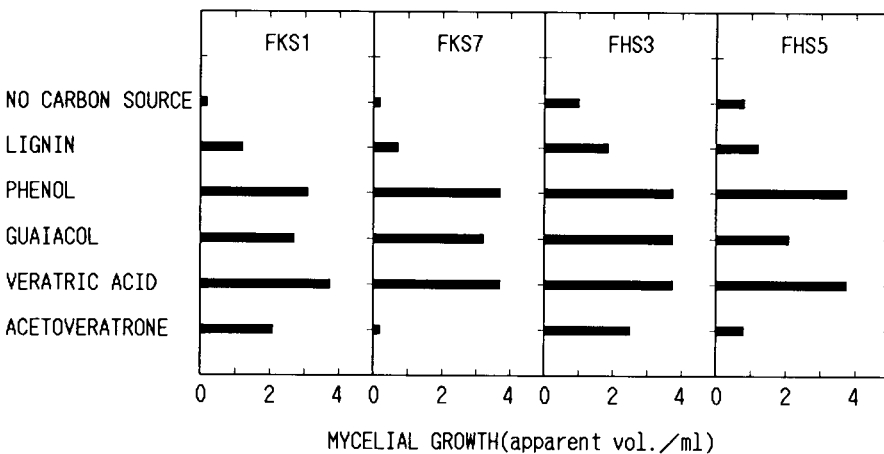


Figure 1. The growth of four *Aspergillus* species in the media containing lignin and the related compounds.
10 ml, lignin:2000ppm. others:500ppm, pH7, 30°C, 120rpm, 2weeks.

by all of four strains within 2 weeks. In the medium containing acetoveratrone, it was expended almost perfectly with FKS1, but the color of the culture changed to yellowish brown and a new absorption maximum appeared at 300nm, and some new spots also appeared in TLC. Therefore, it was suggested that it was not perfectly decomposed, but converted to some new colored substances. With FHS3, it was expended almost perfectly after 8 days, and the color of the culture changed to slightly pink, however, as neither new absorption maximum nor spot in TLC was observed, it was appear that it was perfectly decomposed.

3.2 Degradability of coal

Cohen et al.¹⁾ reported that water soluble black substance was produced when some broken pieces of weathered lignite were put on *Polyporus versicolor* grown thick on the nutrient medium. Saiki et al.⁹⁾ also found similar phenomenon using Joban coal (brown coal) oxygenated with hydrogen peroxide. In this study, similar experiment was attempted, in which Wandoan coal (subbituminous coal), Daton (bituminous coal), Shenyan coal (lignite) and Illinois No.6 coal (subbituminous coal) were used without any treatment. Then, small pieces of Daton and Illinois No.6 coal on FKS1 and FHS3 strains were covered by drops of water, especially around Illinois No.6 coal, 5-10mm drops of water were formed after a few days. These color were not black like that reported Saiki et al.⁹⁾, but slightly yellowish brown. Therefore, it was appear that coal were little degraded. However, it was considered that these drops of water were resulted to undergo some actions of both two strains to solubilize and assimilate coal.

Taking notice of this phenomenon with Illinois No.6 coal, cultivation suspending its fine powder as a sole source of carbon were attempted, but remarkable growth of four strains were not observed.

Subsequently, degradability of water soluble Illinois No.6 coal A and C were examined. FKS1 and FHS3 grew to the level of lignin with A, and grew with C more than with A which was little oxidized by H_2O_2 .

3.3 Effect of phenol addition

As it is considered that assimilation rate of lignin or water soluble coal is not fast because of high molecular substances, addition of phenol to these media was examined to support rapid growth. The result on lignin was in Fig.2. Here, pH was adjusted to 5 which was not well suited for assimilation of phenol (compare of Fig.1 at pH7), but FKS1, FKS7 and FHS3 grew well in mixed medium of lignin and phenol, Especially, the effect was noteworthy for FKS1.

The effects of phenol addition to water soluble Illinois No.6 coal on growth of FKS1 and FKS7 were also remarkable, data are not shown here.

In Fig.3, UV spectra of cultures containing lignin and water soluble Illinois No.6 coal C with FKS1 were shown. Spectra drawn with dotted line are those noninoculated and shaken for the same incubation period. In noninoculated media in phenol addition, absorption of phenol at 270nm was observed, it was disappeared in both cultures containing lignin and water soluble coal with FKS1, and concentration of lignin and water soluble coal in each culture inoculated decreased more than in that noninoculated. Moreover, when excess of mycelia was inoculated, color of lignin in the culture changed to colorless.

As above mentioned, both phenol and lignin or water soluble coal became liable to be degraded by means of cometabolism. Therefore, *Aspergillus* FKS1 strain would be available to treat waste containing water soluble coal.

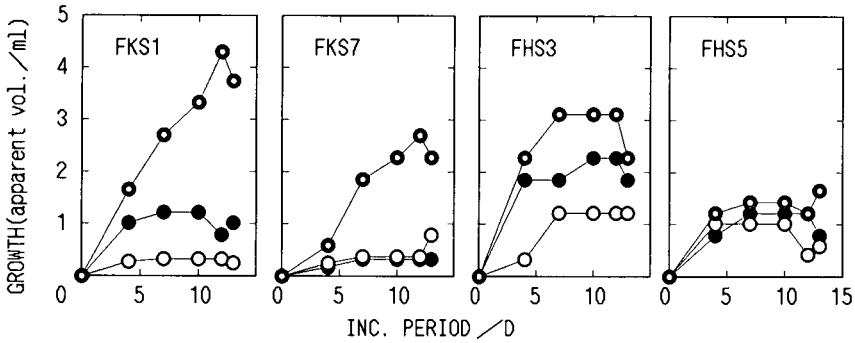


Figure 2. Effect of phenol addition to media containing lignin on the growth of four *Aspergillus* species.

●:lignin 2000ppm, ○:phenol 500ppm, ⊙:lignin + phenol 10mL, pH5, 30°C, 120rpm.

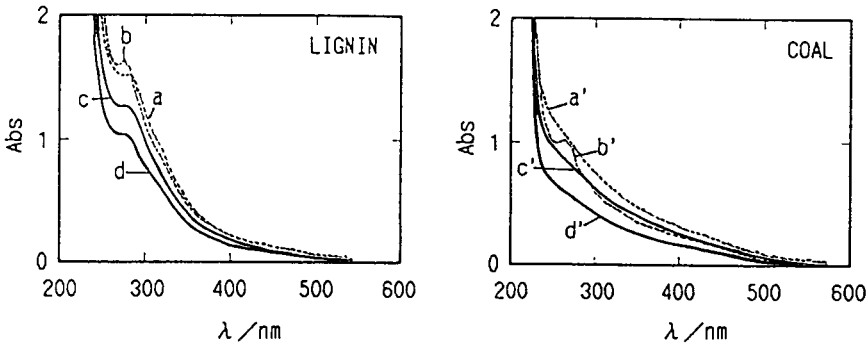


Figure 3. Effect of phenol addition on the decrease of lignin and water soluble coal concentration with the growth of *Aspergillus* FKS1.

a:lignin(noninoculum), b:lignin + phenol(noninoculum)

a':coal ("), b':coal + " (")

c:lignin(inoculum), d:lignin + phenol(inoculum)

c':coal ("), d':coal + " (")

Incubation:pH5(lignin),pH7(coal), 30°C, 120rpm, 2weeks.

Dilution:1/25 with water adjusted to pH2(lignin) and pH9(coal).

References

- 1) Cohen, M.S., et al., Appl. Environ., vol.44, p.23, 1982.
- 2) Rogoff, M.H., et al., J. Bactriol., vol.74, p.108, 1957.
- 3) Rogoff, M.H., et al., J. Bactriol., vol.74, p.264, 1957.
- 4) Gupta, R.K., et al., Appl. Biochem. Biotech., vol.24/25, p.899, 1990.
- 5) Crawford, D.L., et al., Fuel, vol.70, p.577, 1991.
- 6) Ces peds, R., et al., Arch. Microbiol., vol.158, p., 1992.
- 7) Pfeifer, F., et al., Arch. Microbiol., vol.152, p.519, 1989.
- 8) Pfeifer, F., et al., Arch. Microbiol., vol.159, p.323, 1993.
- 9) Saiki, H. et al., Proc. 1st Conf. Coal Utiliz. Tec., p. 264, 1991.

Biological treatment of coals for their conversion to methan.

S.Shumkov and S.Terehova

Scientific Technical Mining Assotiation (NTGA)

Taganskaya 58, str.1,109147 Moscow, Russia

In the investigations on coals conversion to methan that we have began to carry out during the last years we took into consideration published earlier by many investigators results of solubilization and bituminous and subbituminous coals conversion to methan. However, it was interesting for us theoretically and practically to investigate coals bioconversion to methan.

For coals treatment there were used anaerobe enrichment assotiations of microorganisms from decomposed traces of plants, lake's sapropel and coal's waste. The microbe assotiations included hydrolitic, fermented and methan-produced bacterias [1]. Enrichment cultures are characterised by high level of hydrolitic microorganisms, which use cellulose, lignin-cellulose, starch and pepton as the only source of carbon and energy. Among fermented microorganisms were prevaled those cultivated on glucose.

Coals with different degree of carbonization from brown coal to anthracite were treated with anaerobic enrichment microorganisms assotiation. Brown coal gave very low methan level (Fig.1), possibly because of the fact that microorganisms were obtained from coal which hasn't been preliminarily treated. The highest methan level - 50% - was obtained from anthracite.

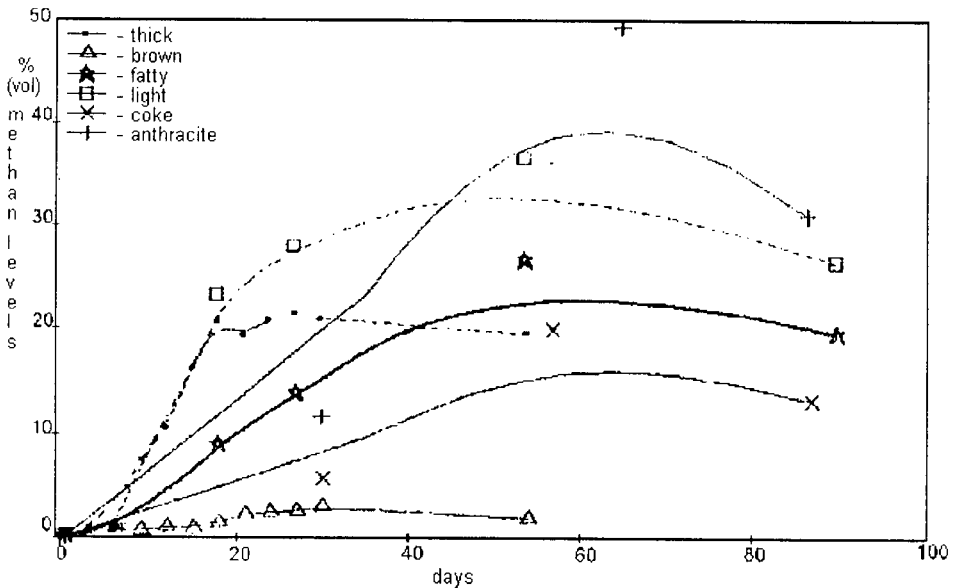


Figure 1. The production of methane from coals with different metamorphism degree treated with enrichment microbe assotiation.

Light and fatty coals with low reactionary ability under the low temperature oxidation by air oxygen which have special place in the carbonization rank are the least capable to methane production. Many investigators suppose [2] that under the oxidation of coals with low metamorphism stage the processes of structure concentration are predominated owing to polymerization and polycondensation of coal's oxygen groups. Under the oxidation of coals with more highly metamorphosed stage the processes of destruction with splitting of oxidation gaseous products and radical production are prevailed. The limits of two coals groups oxidizing on different mechanisms lies between fatty and coking coals. This coals have low ability to methane production and this ability increases as to coals with low metamorphism stage as to anthracites. (Fig.2).

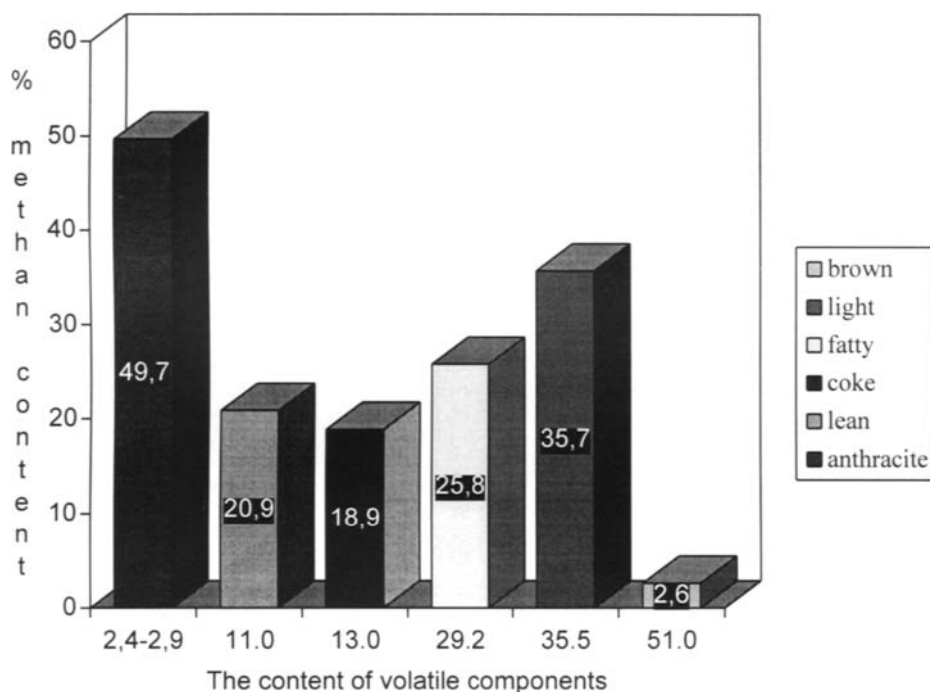


Figure2. The dependence of bioconversional coals methane levels on their metamorphism degree.

Biogas except methane was consisted of carbon dioxide, hydrogen (up to the 8% (Vol.) on the 15-th day of investigations), as well as ethane, propane, butane, pentane and their isomers, totally 1,5%.

After the investigations on coal's conversion to methane the liquid fraction was separated and analysed through the ultra-violet spectroscopy method. The liquid phase of coal's control patterns not treated with microorganisms was analysed as well.

For treated coals of K-mark and anthracite A in the $46 \cdot 10^3 \text{ cm}^{-1}$ spectrum zone the distinctions in comparison to control patterns are observed. (Fig.3). This distinction can be caused by the fact that microorganisms use

functional groups for methane production. Greater distinctions in optical density of solutions over anthracite than over coal of K-mark are conform to the fact that anthracite produced greater methane level.

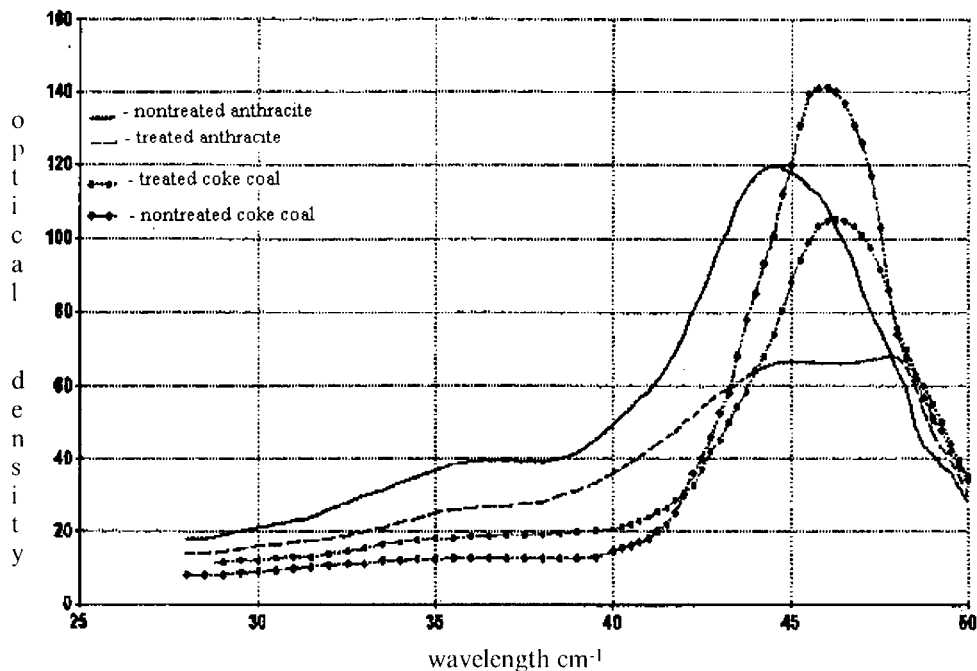


Figure 3. Ultra-violet water phase spectrums of treated with microorganisms and nontreated coals.

In the $34-40 \cdot 10^3 \text{ cm}^{-1}$ zone the significant differences in the water medium spectrum of treated anthracite and K-mark coal were observed. For anthracite the optical density was lower than in the control experiment, for K-mark coal there was vice versa. In this spectrum zone only anthracite functional groups passed into solution are spent for boigas production.

After the separation and analyses of water medium the coals were treated with 0,1N HCl solution on the method [3] in which was shown that after coal's treatment the aromatic compounds pass into solution. This compounds contain carbonic, carboxylic and hydroxilic groups which are the legends of complex ferric salts. The ions of iron pass into solution as well. In hydrochloric acid atracts of treated coal and anthracite the optical density was lower than in the control patterns. Coal's contact surface after microbiological treatment is lack of lowmolecular compounds. The Fe^{2+} and Fe^{3+} ions are absent in the solution.

Coal's patterns after boiprocess and control patterns were dried and separated into fractions. Through the X-ray analyses was determined that in organic part of coal the interstratum distance in turbostratum carbon zone was increased and also it was determined the presence of conformical transformations in aliphatic fragments of coal's macromoleculs that is index of microvoltages value balanced in macromolecular associations. The observed distotions belong

to abnormal and indicate about developed destruction process in edge parts of coal's macromolecules.

In the light coal's patterns the main components of mineral fase were pyrites and quartz and in small amounts kaolin and calcite were present. After bioprocess the calcite and pyrites were absent, but new phases not identified yet were appeared in the coal.

In the coal's bioprocess the dynamic of methanogeneses intermidiate products such as acetic, propionic and butiric acids was studied. The maximum concentrations of this acids reached 4,2; 1,3 and 2,4 mkg/ml correspondenly. The presence in the medium after the end of methanogeneses of volatile fatty acids - methan forerunners - testifies about the possible increase of methan level by optimization conditions of coal's bioprocess.

REFERENCES

1. B.B. Namsarayev and L.Y. Dulov (eds.), Microorganisms introduction into nature, RAS, Moscow (1994) 71-72.
2. V.I. Saranchuk, Oxidation and selfinflammability of coal, Naukova dumka, Kiev (1982).
3. N.G. Korgenevskaya and S.L. Hylno, Ukranian Academy of Sciences reports, 2 (1989) 39.

Some properties of lignite bioconversion products

Yu.G.Golovin, M.L.Shchipko, B.N.Kuznetsov, V.V.Golovina and A.O.Eremina

Institute of Chemistry of Natural Organic Materials, Siberian Division of Russian Academy of Sciences, Academgorodok, Krasnoyarsk, 660036, Russia

Biobeneficiation of low grade coals is a good alternative for some ways of their chemical processing. Biotechnological processes of coal conversion can be applied for the production of improved solid fuels, liquid and gaseous products depending on the type of used strains aerobic bacteria. The possibility of biological transformation of Kansk-Achinsk lignite with the formation of coal derived fuel suspension, fuel gas and binder for briquettes production has been shown [1]. The present paper is devoted to the study of physical and chemical properties of products obtained by biotechnological processing of Kansk-Achinsk lignite. Chemical analysis, IR spectroscopy, EPR and X-ray methods were applied for study the composition and structure of initial materials and reaction products.

1. EXPERIMENTAL

Active biological substance for lignite degradation was isolated from coal-adaptive strains - Acinetobacter and Pseudomonas. Biocenosis of microorganisms mainly consisted of Acinetobacter SP10, Pseudomonas SP2 and Pseudomonas SP57 strains in quantity of 6×10^9 - 8×10^9 , 3×10^9 - 4×10^9 , 2×10^9 - 3×10^9 of cells/g of each strain respectively. In the technological cycle the indicated biocenosis has been used as water lignite inoculum containing 30-40 g/l of raw biomass matter. The bioconversion process was carried out in flotation installation with air consumption during experiments made up 16-20 l/min at room temperature for 72 hour.

The elemental composition of initial lignite and reaction product was determined by conventional coal analysis measures up to ISO and ASTM requirements. The content of functional groups was defined by chemical methods [2].

IR analyses was carried out with standard pellets (13 mm in diameter) obtained by dispersing 3,5 mg of sample into 3000 mg of potassium bromide. IR spectra were obtained by using Specord IR-75 spectrometer. EPR spectra were recorded by using RE-1307 (λ -3 cm, X-range) and RE-1308 (λ -8 cm, Q-range) spectrometers. X-ray measurements were carried out using DRON-2 with monochromatic copper $K\alpha$ -radiation. The model of turbostrate regulation of block carbon has been applied for spectra interpretation. In order to calculate X-ray structural parameters the well-known Warren-Franklin equations have been used [3].

The values of dynamic viscosity of suspension formed during lignite bioconversion were measured using "Rheotest" apparatus.

Kansk-Achinsk lignite with ash content 5,3 % relative to the dry weight and elemental composition (in weight %): C - 74,61; H - 5,02; S - 0,54; N - 0,50; O - 19,33 has been used as initial raw material.

2. RESULTS AND DISCUSSION

The vital activity of aerobic microorganisms is accompanied by the evolution of carbon dioxide. Due to CO_2 removal the weight of lignite organic matter was decreased with time.

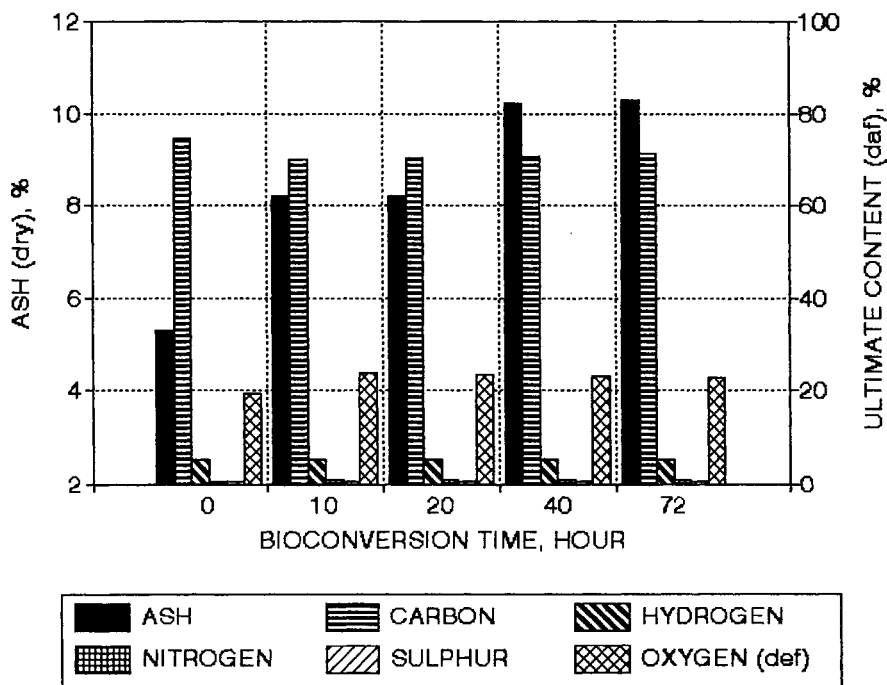


Figure 1. Proximate and ultimate analysis of initial lignite and bioconversion products, obtained at different time of treatment.

The rate of variation of carbon content in lignite was used for estimation the process productivity. Presented in Figure 1 and Figure 2 data show that under used conditions the bioconversion process is finished almost completely during the period of time 40-50 hour. The rate of lignite conversion was increased at first with the maximum corresponding to 20-25 hour, and then its value was decreased. The main part of bioconversion products is diffused to liquid phase, resulting to the increase of suspension viscosity. Data on fluidity changes with time (Figure 2, curve 2) also confirm that the most intensive variation of the reaction mixture composition takes place during the first 40 hours.

Presented in Figure 1 and Figure 3 data illustrate the variation of the elemental composition of suspended organic matter with time. In the initial period of time, corresponding to the high rate of bioconversion, the content of oxygen and hydrogen in organic products was increased. This fact can be explained by the accumulation of microorganisms in the suspension. Nitrogen compounds were accumulated in the suspended organic matter only during the first twenty hours.

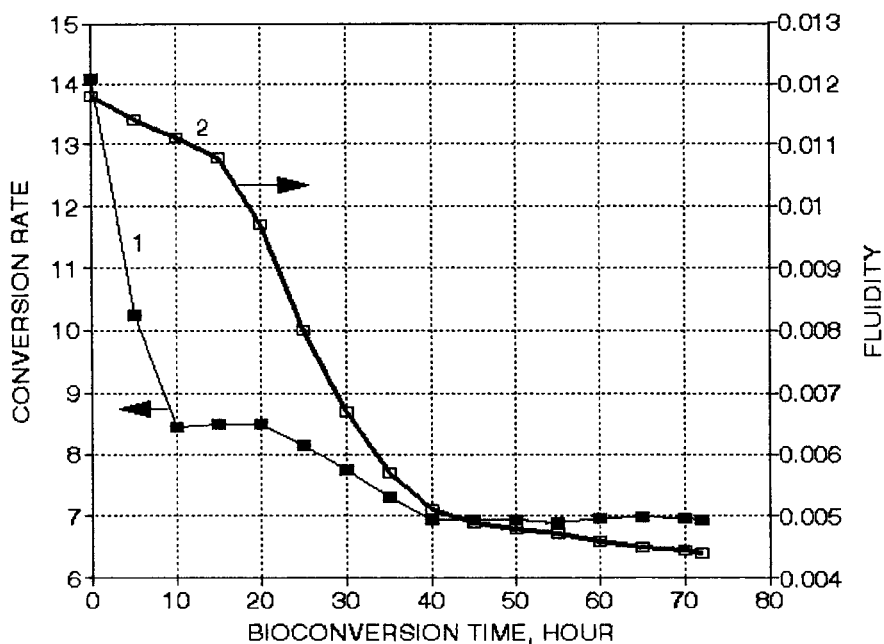


Figure 2. Variation of conversion rate and fluidity of reaction mixture with lignite bioconversion time. Curve 1 - carbon (%) / ash (%), curve 2 - fluidity ($\text{m}^2/\text{kg}\cdot\text{s}$).

The obtained results suggest that at the first stage of bioconversion process the accumulation of microorganisms biomass takes place in the suspension during 0-20 hours, with the further exhaust of resources of vital activity in the second stage of lignite biotransformation during the next 20-50 hours.

The EPR spectra of investigated samples of initial and biologically treated lignite show that in all cases the value of g-factor is low and cannot be quantitatively evaluated. The concentration of paramagnetic centers was increased during the first ten hours up to value $4,2 \cdot 10^{10}$ spn/g, which was by 2,5 times higher than that in the initial lignite. The observed changes in concentration of PMC with time can be connected with the formation and destruction of aroxyl radicals and free aliphatic radicals, according to [3].

The comparison of IR spectra of lignite bioconversion products, obtained at different reaction time, show that intensity of absorption band in the region $2700-3000 \text{ cm}^{-1}$, corresponding to valance vibrations of aliphatic OH-groups [4], goes through small maximum at the time of treatment 20-35 hour. The absorption band at 1450 cm^{-1} , which can be referred to the vibrations of CH-group or carbonate- carboxylate-groups, is appeared during lignite bioconversion and its intensity is increased with time. Taking into account the data of chemical analysis it was found that the intensity of this band has a good correlation with concentration of carbonate and carboxylate groups in studied samples.

Some information, concerning the regularity of carbon layers in biotreated lignite, was obtained from X-ray spectra analysis in the region of 002 graphite band. The value of mathematical expectation of interplane distance (σ) shows that the sample, biotreated during 72 hours, differs from the others samples by less interplane distance (by 3,5 % relative).

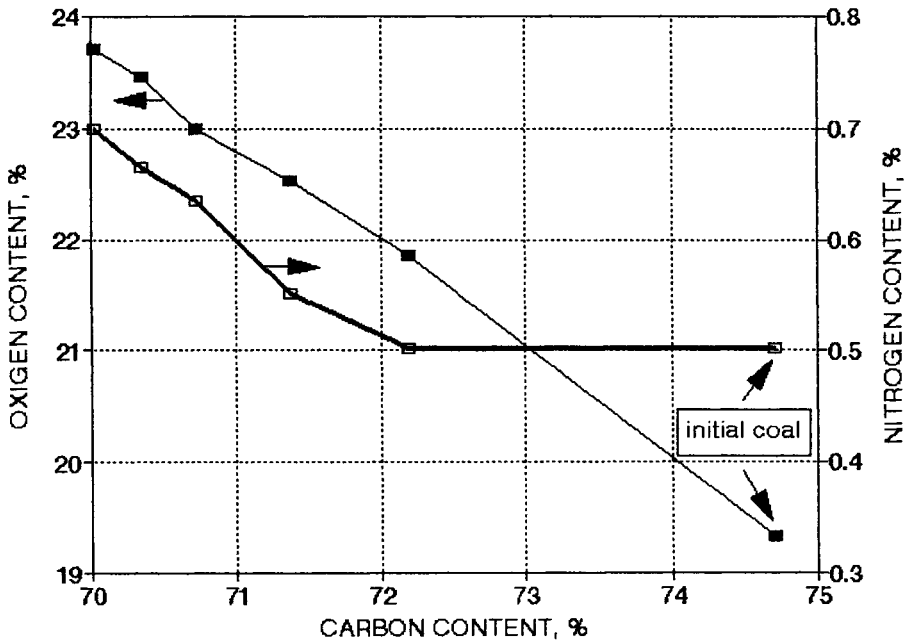


Figure 3. Some relations between content of carbon, oxygen and nitrogen in initial lignite and bioconversion products.

With using of chemical analysis and spectral methods the main stages of lignite bioconversion were defined. During the first 20 hours the rate of lignite conversion was increased with the growth in reaction products H, O, N, S elements content and oxygen-containing functional groups. The extensive oxidation of aliphatic fragments of lignite was detected. At the second stage the rate of lignite bioconversion becomes slower and the carbonization of organic matter took place with the growth of carbon content relative to other elements. The duration of this stage was 20-30 hours and than the chemical composition of products remained practically stable.

REFERENCES

1. Demidov Yu.V., Drudzh P.V. Perspectives in the development of lignite biotechnology M., TsHIEIupol, 1991, (in Russian).
2. Standard laboratory test for coal and coke. (C.Karr, Ed), Academic Press, N.-Y., 1978.
3. Sklyar M.G. Physical-chemical bases of coal baking. M., Metallurgy, 1984, (in Russian)
4. Smith A.Lee Applied infrared spectroscopy. John Wiley & Sons, N.-Y., 1979.

SECTION C

COAL AND THE

ENVIRONMENT

Sub-section C.2

Utilization and

post-utilization aspects

This Page Intentionally Left Blank

A Two Mixture Fraction Approach for Modeling Turbulent Combustion of Coal Volatiles and Char Oxidation Products

Daniel V. Flores and Thomas H. Fletcher

Chemical Engineering Department, Brigham Young University, Provo, Utah, USA 84602

1. INTRODUCTION

In many comprehensive turbulent coal combustion codes, one progress variable is used to treat coal combustion products [1-3]. Gas phase reactions between coal combustion products and inlet oxidizers (e.g., air) are often assumed to be mixing-limited, and treated using an assumed-shape PDF. The use of one progress variable for the coal combustion products means that the composition of the coal off-gas is the same as that of the parent coal and is constant throughout both devolatilization and char oxidation. Therefore, to characterize the chemistry in turbulent environments, one mixture fraction is used for the oxidizer streams (primary versus secondary air) and another for the coal off-gas. However, it is well known that coal volatiles are released from the coal particle at a faster rate than char oxidation products. Since the coal volatiles are generally enriched in hydrogen and oxygen, compared to the coal char, the use of distinct mixture fraction variables for volatiles and char off-gases is warranted, in which case, a total of three mixture fractions are needed.

Two studies directly related to multiple mixture fractions for coal are found in the literature. Brewster, et al. [4] developed a generalized theory that includes several mixture fractions to describe the gas phase turbulence/chemistry interactions. Brewster and coworkers showed that accounting separately for devolatilization and char oxidation products resulted in a drastic difference in the gas temperature predictions compared to calculations using one mixture fraction for coal combustion products. Similarly, Eddings, et al. [5] used different mixture fractions to account for devolatilization and char oxidation products separately. Eddings' new method predicted trends of NO_x emissions as a function of coal type for a laboratory scale furnace, whereas the one coal mixture fraction approach was unsuccessful.

In the present work, one mixture fraction is used to distinguish between primary and secondary air streams, and two progress variables are used to treat mixing between oxidizers and pulverized coal combustion products. The source terms of char off-gases and volatiles to the gas phase are obtained from Lagrangian treatments of particle trajectories and reactions. The Chemical Percolation Devolatilization (CPD) model [6] is used for devolatilization rates, and char oxidation rates are taken from Hurt and Mitchell [7]. The total devolatilization yield is as estimated by the CPD model. The elemental composition of the char is taken from elemental composition data for fully-devolatilized chars in a flat flame burner [8]. The elemental composition of the volatiles is calculated by mass balance from the volatiles yield and the elemental composition of the char.

The computer code used for these calculations was PCGC-3 (Pulverized Coal Gasification and Combustion, 3-Dimensional) [3].

2. THEORY

2.1 Major Gas Species

The mixture fractions to be used are defined as follows:

$$f_1 = \frac{m_s}{m_p + m_s} \quad (1)$$

$$f_2 = \frac{m_v}{m_p + m_s + m_v} \quad (2)$$

$$f_3 = \frac{m_c}{m_p + m_s + m_v + m_c} \quad (3)$$

where m_p , m_s , m_v and m_c represent the mass of gas originating from the primary gas stream, secondary gas stream, coal volatiles, and char oxidation products, respectively. Each mixture fraction may vary from zero to unity. On the other hand the enthalpy h is partitioned into the adiabatic enthalpy of the mixture $h(f_1, f_2, f_3)$ and an average residual energy (h_r) as described by Smoot and Smith [2].

In this research, a simplification is made to the model proposed by Brewster, et al. [4] in order to reduce the computational time requirement. The fluctuations due to turbulence in the char off-gases are neglected (i.e., $g_{f_3} = 0$). This simplification is justified as follows:

1. The char off-gas is defined to be the mass of char that ends up in the gas phase. For example, the carbon in the CO or CO₂ produced from char oxidation is accounted for in f_3 , but the oxygen is not included in f_3 because it probably comes from the primary or the secondary air streams. The oxidizer and C from char combustion are therefore mixed as soon as reaction occurs, and fluctuations are not needed.
2. The char reactions are thought to be slow enough to be independent of temperature and concentration fluctuations.
3. Experience in calculations has shown that the turbulent fluctuations are only significant (>5% of the mean) in the near-burner regions, where devolatilization occurs.

With this simplification, the gas phase properties are still calculated by convolution over the clipped Gaussian distribution, as follows:

$$\tilde{\beta}(f_1, f_2, \tilde{f}_3, \tilde{h}_r) = \int_{-\infty}^{\infty} \int_{-\infty}^{\infty} \beta(f_1, f_2, \tilde{f}_3, \tilde{h}_r) \tilde{P}(f_1, f_2) df_1 df_2 \quad (6)$$

and the joint probability distributions are separated, as in previous calculations. In order to model the chemistry/turbulence interaction, transport equations for the Favre-averaged mixture fractions and their variances need to be solved. The equations for the mixture fractions are:

$$\nabla \cdot (\bar{\rho} \tilde{u} [\tilde{f}_1 (1 - \tilde{f}_2) (1 - \tilde{f}_3)] - D_f' \nabla [\tilde{f}_1 (1 - \tilde{f}_2) (1 - \tilde{f}_3)]) = 0 \quad (7)$$

$$\nabla \cdot (\bar{\rho} \tilde{u} [\tilde{f}_2 (1 - \tilde{f}_3)] - D_f' \nabla [\tilde{f}_2 (1 - \tilde{f}_3)]) = \bar{S}_p^{\tilde{f}_2} \quad (8)$$

$$\nabla \cdot (\bar{\rho} \tilde{u} \tilde{f}_3 - D_f' \nabla \tilde{f}_3) = \bar{S}_p^{\tilde{f}_3} \quad (9)$$

where $\bar{S}_p^{\tilde{f}_2}$ and $\bar{S}_p^{\tilde{f}_3}$ are the rates of production of the volatiles and char off-gases, respectively. Descriptions of the transport equations for the variances g_{f_1} and g_{f_2} may be found elsewhere [8].

2.2 NO_x

The NO_x submodel used in PCGC-3 [9] was modified in order to differentiate between the nitrogen evolved with the volatiles and that evolved with the char off-gas. The solution procedure of the new submodel is unchanged; the NO_x equations are decoupled from the solution of the major variables and calculated in a post-processor. Conservation equations are solved for the three main species in the reaction mechanism (NO, HCN and NH₃). The global rate expression for fuel NO is taken from DeSoete [10]; thermal NO calculations are based on parameters reported by Bowman [11] and by Miller and Bowman [12]. The mean values of the gas phase reactions are obtained by convolution over the fluctuating mixture fractions [9]. It is assumed that the local fractional conversion x_i (where $i = \text{NO, HCN or NH}_3$) is not affected by the turbulent fluctuations. Thus, the local instantaneous concentrations (for the PDF solution) can be calculated from the fractional conversion obtained using the Favre-averaged concentrations (from the

conservation equations). This is an iterative procedure. Moreover, in the new approach the nitrogen evolved with the volatiles appears in the gas phase either as HCN or as a user-specified partition (α) between HCN/NH₃. The nitrogen evolved from the char is assumed to appear as NO and N₂ only; the partition (ζ_{char}) is user-specified. The recommended value for ζ_{char} is taken from Pershing and Wendt [14], who showed that about 15 % of the nitrogen contained in the char is converted to NO.

3. RESULTS AND DISCUSSION

Calculations were made using PCGC-3 to compare the use of one versus two coal product mixture fractions. The results are shown in Figure 1 for the BYU Controlled-Profile Reactor [15], a two-dimensional down-fired laboratory furnace. In this simulation, 11.4 kg/hr of pulverized Utah Blind Canyon HVBB coal burned in air at atmospheric pressure at a stoichiometric ratio of 1.15.

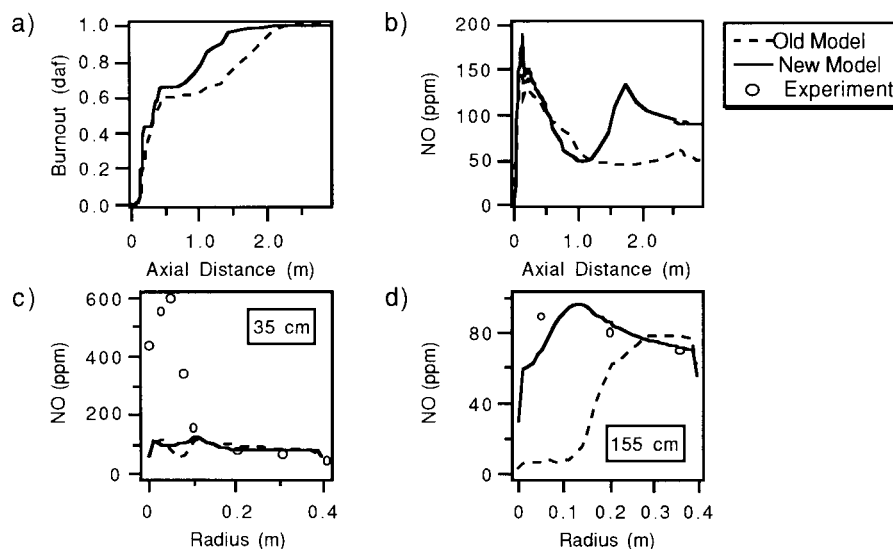


Figure 1. Radially-averaged profiles of (a) coal burnout and (b) NO concentration using one and two mixture fractions for coal reaction products. Radial profiles of NO concentrations versus experimental data (c and d). Predictions are of the BYU controlled profile reactor, Stoichiometric ratio of 1.15 and Swirl No. of 1.4 [15, 16]

Radially-averaged predictions of coal burnout are shown in Figure 1a for the one versus the two coal product mixture fraction approach. The calculated burnout profiles from the two methods seem to be very similar (within 10%). Calculated temperatures and major species concentrations (not shown here) using the two methods are in general agreement with each other and with measurements.

Radially-averaged predictions of NO concentrations are shown as a function of axial distance in Fig. 1b. The most significant differences between the two predictions are found in the char burnout region (at an axial distance of 1 m), where the new model uses a different nitrogen release mechanism, as explained above. The two predictions seem to be more similar near the burner, where devolatilization predominates.

Radial profiles predicted by the two models at two different axial locations are shown in Figs. 1c-d together with measurements reported by Sanderson [16]. In the region near the burner (35 cm from the inlet), both models give similar predictions, which agree with the measurements away from the centerline (after 0.1 m). However, drastic differences between predictions and measurements of NO occur along the centerline. This region is highly recirculating, and the accuracy of the measurements made with sampling probes [16] is questionable. Further down in the reactor (155 cm from the inlet), the new model shows a better agreement with the data. This difference exists because the new model accounts for the NO formed from char oxidation separately from the NO formed from devolatilization products

4. SUMMARY AND CONCLUSIONS

Predicted temperatures and major gas species concentrations between the one and two coal mixture fraction approaches are not very different. However, the predictions for NO were significantly better using two coal mixture fractions. The results shown here indicate that the incorporation of improved physical models (i.e., the two coal gas mixture approach) significantly affects predictions, and should therefore be used instead of the previous approach that assumed uniform coal off-gas composition. There is a significant need for detailed experimental data regarding the yield and composition of volatiles versus char as a function of coal type and operating conditions. A better understanding of the conversion of char nitrogen to NO as a function of coal type and operating conditions is also needed.

REFERENCES

1. Smith, P.J., Fletcher, T.H. and Smoot, L.D., 18th Symp. (Int.) on Combustion, 1285, (1981).
2. Smoot, L.D., and P.J. Smith. Coal Combustion and Gasification, Plenum. New York, 321, (1985).
3. Brewster, B.S., Scott C. Hill, Predrag T. Radulovic and L.D. Smoot, in Fundamentals of Coal Combustion, Elsevier, Amsterdam, 567 (1993).
4. Brewster, B.S., L.L. Baxter, and L.D. Smoot, Energy & Fuels, **2**, 362, (1988).
5. Eddings, E.G., P.J. Smith, M.P. Heap, D.W. Pershing, and A.F. Sarofim, in Coal-Blending and Switching of Low-Sulfur Western Coals, New York. The ASME, 169-184, (1994)
6. Fletcher, T.H., Kerstein, A.R., Pugmire, R.J. Solum, M.S., and Grant, D.M., Energy and Fuels, **6**, (4), 414-431 (1992).
7. Hurt, R.H. and Mitchell, R.E., 24th Symp. (Int.) on Combustion, 1243 (1992).
8. Mitchell, R.E., Hurt, R.H., Baxter, L.L. and Hardesty, D.R., Compilation of Sandia Coal Char Combustion Data and Kinetic Analyses. Sandia Nat. Labs., (1992), SAND92-8208 UC-361.
9. Bowman, C.T., Prog. in Energy and Comb. Sci., **1**, 1 (1975).
10. DeSoete, G.G., 15th Symp. (Int.) on Combustion, 1093 (1975).
11. Boardman, R.D. and L.D. Smoot, AIChE J., **34**, 1573, (1988)
12. Miller, J. A.; Bowman, C. T., Prog. Energy Combust. Sci., **15**, 287 (1989).
13. Smith, P.J., Hill, S.C. and Smoot, L.D., 19th Symp. (Int.) on Combustion, 1263 (1982)
14. Pershing, D.W. and J.O.L. Wendt, Ind. Eng. Chem. Process Des. Dev., **18**, 60 (1979)
15. Eatough, Craig N., Ph.D. Dissertation, Mech. Eng. Dept., Brigham Young Univ., Provo, UT, (1991)
16. Sanderson, David K., M.S. Thesis, Mech. Eng. Dept., Brigham Young Univ., Provo, UT, (1993)

Experimental study and modeling of the influence of the inlet NO concentration in the natural gas reburning process

R. Bilbao, A. Millera and M.U. Alzueta

Department of Chemical and Environmental Engineering, Faculty of Science,
University of Zaragoza, 50009 Zaragoza, Spain.

1. INTRODUCTION

Significant NO and NO₂ (NO_x) amounts can be produced during coal combustion. Because of the different harmful effects of NO_x and the legislation about their emissions, several NO_x reduction methods have been proposed. Among the different methods, reburning with natural gas is an attractive technique that can be applied to existing or new coal boilers, with few modifications and low investment costs. The reburning process divides the boiler into three zones. In the primary zone, the main combustion of coal is produced and the NO_x and other typical combustion products are generated. Downstream, natural gas is injected into the so-called reburning zone in order to create a reducing environment where the NO_x are broken down by the action of hydrocarbon radicals. Afterwards, air is injected into the burnout zone in order to eliminate any remaining fuel fragment.

In each zone, there are different influencing variables that affect the final NO_x reduction reached in the reburning process. One of the most important variables is the NO concentration proceeding from the primary zone, (NO)_p, because this is responsible for the necessity of a NO_x reduction method. The (NO)_p value will influence the final concentration of NO and other nitrogenous species.

There are some discrepancies with respect to the efficiency of the reburning process for different (NO)_p concentrations. While some authors [1, 2] consider this process ineffective for NO concentrations lower than 150 ppm, Fujima et al. [3] obtained significant reductions for lower (NO)_p values.

Owing to these discrepancies and to its significance, the influence of the (NO)_p on the NO and HCN concentrations at the outlet of the reburning zone has been analyzed. The study has been performed from both experimental and theoretical points of view.

2. EXPERIMENTAL METHOD AND RESULTS

The reburning experiments were carried out in a bench scale installation [4], which includes a reaction system, a gas feeding system and a gas analysis system. The reaction system includes a tubular ceramic reactor heated by an electric furnace that allows us to reach temperatures up to 1500 °C. A gas mixture simulating the gas composition exiting from the primary zone is introduced into the reburning reactor. Mass flow meters were used to control the flow rates of N₂, O₂, CO₂, NO and natural gas. Steam was added to the gas by passing it through a water container where the temperature is controlled and the desired level of moisture is reached.

The analysis of the products at the outlet of the reburning zone was performed using different methods. The contents of NO_x (NO and NO₂), O₂, CO and CO₂ were measured by continuous analyzers. O₂, H₂, N₂, CO, CO₂, CH₄ and other hydrocarbons were determined

by gas chromatography. The concentration of NH_3 was determined by passing a known volume of gas through an aqueous acid solution, which was subsequently analyzed using the Nessler colorimetric method [5]. The concentration of HCN was also determined by collecting it in an aqueous basic solution and analyzing it using the barbituric-pyridine method [5].

The study of the influence of $(\text{NO})_p$ has been performed varying this concentration between 100 and 1200 ppm. The temperature ranged between 1200 and 1450 °C, and concentrations of 2 % oxygen and 1.7 % natural gas have been used. These values have been chosen because they correspond to operating conditions that allow us to obtain high efficiencies in the process. A flow rate of 900 Nl/h was considered, which corresponds to residence times ranging between 160 and 190 ms.

Figure 1 shows the NO reduction obtained for different temperatures and $(\text{NO})_p$ values. It can be observed that significant NO reduction can be achieved, even for the lowest $(\text{NO})_p$ values. The reduction increases slightly when $(\text{NO})_p$ increases and it also increases with the temperature when this ranges between 1200 and 1400 °C. For higher temperatures (1450 °C) a lower reduction is obtained, which could be due to the NO thermal formation.

Besides the NO reduction values, it is also interesting to analyze the concentrations of other nitrogenous species at the outlet of the reburning zone. This analysis has been performed through the results of the most abundant compound (HCN) and of the total fixed nitrogen ($\text{TFN} = \text{NO} + \text{HCN} + \text{NH}_3$). Figure 2 shows the results obtained for a temperature of 1200 °C. It can be observed that the HCN concentrations at the outlet of the reburning zone are higher than those corresponding to NO ones. An increase in the concentration of $(\text{NO})_p$ produces a slight increase in the output NO concentration and a more appreciable increase of the concentration of HCN, although it is important to take into account that the HCN formed in the reburning zone reacts nearly in its totality in the postcombustion zone. Figure 3 shows the TFN results obtained for different temperatures and $(\text{NO})_p$ values. It is observed that the TFN values decrease when the temperature increases. For higher temperatures, the TFN value is not very dependent on the $(\text{NO})_p$ concentration, while for lower temperature the TFN values increase when $(\text{NO})_p$ increases.

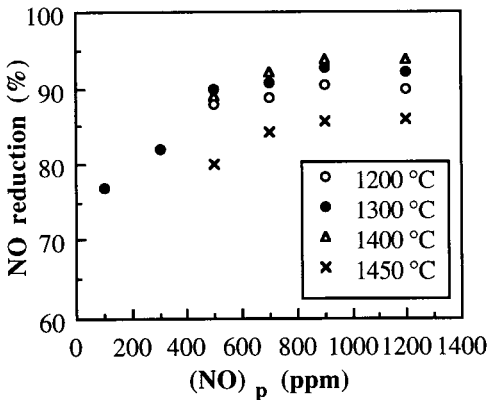


Figure 1. NO reduction versus $(\text{NO})_p$.

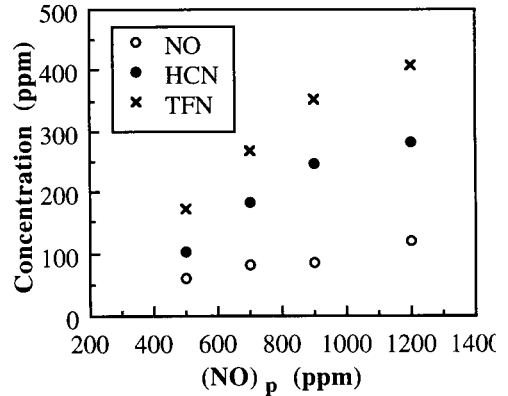


Figure 2. Concentration of NO, HCN and TFN versus $(\text{NO})_p$. $T = 1200$ °C.

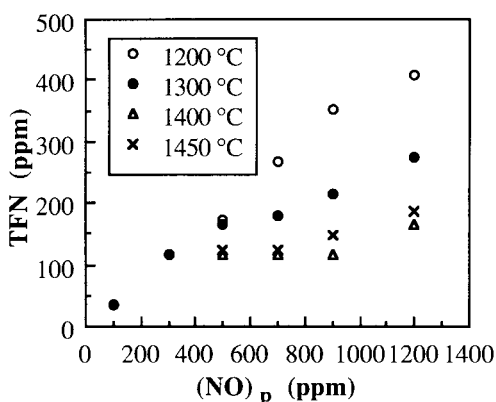


Figure 3. TFN concentration versus $(NO)_p$.

3. KINETIC MODEL AND EXPERIMENTAL VERIFICATION

The chemistry of the reburning process involves a large number of reactions of formation and consumption of many nitrogenous and hydrocarbon species. Many of these species are very reactive and are present only in very low concentrations and during short periods of time.

Different kinetic models have been reported to describe the reburning zone with natural gas. Depending on their complexity and description level, these models can be classified as detailed, simplified and reduced models.

In this work it has been considered useful to obtain a simplified kinetic model to predict the influence of the main operating variables on the concentrations of the different species. This model must be as simple as possible in order that it can be applied with a reasonable computational time even with the joint use of complicated flow models and should not include fitting parameters.

The starting point was a detailed kinetic model composed by the reactions proposed by Kilpinen et al. [6] and by Glarborg and Hadvig [7]. This initial model consists of 298 elementary reactions and 48 chemical species. Using different reaction rate analyses and excluding the species whose concentration was always lower than 1 ppm, a simplified model was obtained. This model consists of 87 elementary reactions and 38 chemical species [8]. It takes into account the reactions corresponding to the natural gas decomposition and oxidation, the interaction between NO and hydrocarbons, and the conversion of the intermediate nitrogenous species.

The model has been solved using the chemical kinetic software CHEMKIN [9]. For each elimination carried out, the results obtained with the simplified model were compared with those obtained with the detailed model. The experimental verification of the model has been performed through the concentrations of NO, HCN, NH₃, CO and CO₂. Some examples of the NO and HCN concentrations, which can be considered as the most relevant nitrogenous species, are shown in Figures 4 and 5. In general, a good agreement is achieved. For the highest $(NO)_p$ concentrations, some discrepancies in the NO and HCN concentrations are observed, although the TFN amount is well predicted. For the higher temperatures, a good agreement is achieved for the HCN concentrations, while the NO concentrations predicted are higher than those obtained experimentally. The NH₃, CO and CO₂ concentrations calculated with the model agree with those obtained experimentally.

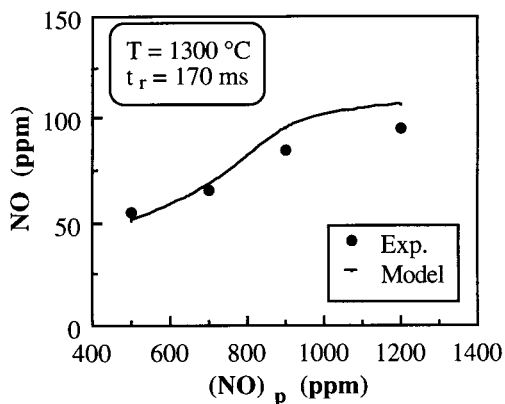


Figure 4. Experimental and calculated NO versus $(NO)_p$.

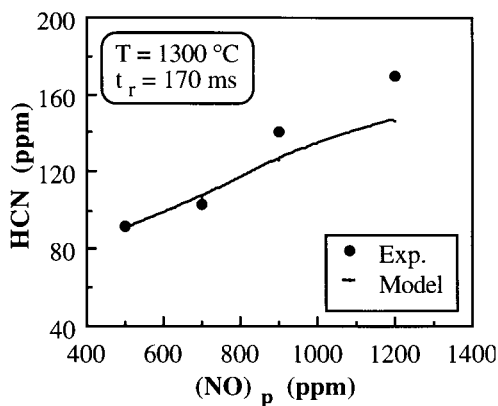


Figure 5. Experimental and calculated HCN versus $(NO)_p$.

ACKNOWLEDGEMENTS

The authors express their gratitude to the ENAGAS, ENDESA and SEVILLANA companies, to OCIGAS, OCIDE and CICYT (Project AMB92-0888) for providing financial support for this work and also to MEC (Spain) for a research grant awarded to M.U. Alzueta.

REFERENCES

- [1] S.L. Chen, J.M. McCarthy, W.D. Clark, M.P. Heap, W.R. Seeker and D.W. Pershing, Proceeding of the 21st Symp. (Int.) on Combustion, The Combustion Institute, Pittsburgh, 1986, p. 1159.
- [2] W.S. Lanier, J.A. Mulholland and J.T. Beard, Proceedings of the 21st Symp. (Int.) on Combustion, The Combustion Institute, Pittsburgh, 1986, p. 1171.
- [3] Y. Fujima, Y. Takahashi, T. Kunimoto and S. Kaneko, Proceeding of the Reburning Workshop, Örenäs Slott, Sweden, 1990, p. 225.
- [4] R. Bilbao, A. Millera and M.U. Alzueta, Ind. Eng. Chem. Res., 33 (11) (1994) 2846.
- [5] L.S. Clesceri, A.E. Greenberg and R.R. Trussell (Eds.), Standard methods for the examination of water and wastewater, APHA-AWWA-WPCE, Washington, 1989, Chapter 4, pp. 20, 111.
- [6] P. Kilpinen, P. Glarborg and M. Hupa, Ind. Eng. Chem. Res., 31 (1992) 1477.
- [7] P. Glarborg and S. Hadvig, Report Nordic Gas Technology Centre, Horsholm, Denmark, 1991.
- [8] M.U. Alzueta, Ph. D. Thesis, University of Zaragoza, Spain, 1994.
- [9] R.J. Kee, J.A. Miller and T.H. Jefferson, Report No. SAND80-8003, Sandia National Laboratories, Livermore, 1989.

NO_x Reduction Using Coal Pyrolysis Gas as Reburn Fuel: Effects of Pyrolysis Gas Composition

H. Spliethoff, U. Greul, H. Rüdiger, H.-C. Magel, U. Schnell, K.R.G. Hein
 Institut für Verfahrenstechnik und Dampfkesselwesen
 Universität Stuttgart, Germany

C.-Z. Li, P.F. Nelson
 CSIRO Division of Coal & Energy Technology
 PO Box 136, North Ryde, Australia

1. INTRODUCTION

Reburning or fuel staging has been demonstrated to be an effective method for reducing NO_x from stationary combustion sources. Natural gas or methane is usually used as reburn fuel, but coal pyrolysis gas has recently been demonstrated to be even more effective. Using coke oven gas as reburn fuel at a 150 MW_{el} power station, minimum emissions of 150 ppm NO_x at 6% O₂ could be achieved /1/. The investigations in this study concern the reburning efficiency of a pyrolysis gas produced in an entrained flow or fluidized bed reactor. Pyrolysis experiments have been performed for a series of Australian and German coals and combustion studies in a two-stage fuel splitting and staging reactor.

2. PYROLYSIS RESULTS

The bench scale fuel staging and splitting facility of the IVD is shown in ref. /2/. The pyrolysis of coal can be investigated in an entrained flow or in a fluidized bed reactor, the pyrolysis gas then being utilized in the combustion reactor as reburn fuel. For baseline investigations each of the reactors can be operated separately. For the process of fuel splitting and staging the pyrolysis and combustion reactors were operated simultaneously. The maximum temperature of the entrained flow pyrolysis reactor is 1300°C. The hot gas filtration and the pyrolysis gas pipes to the combustion reactor are heated beyond temperatures of 500°C. Detailed analysis of the coals and the reburn fuels are given in ref. /3/.

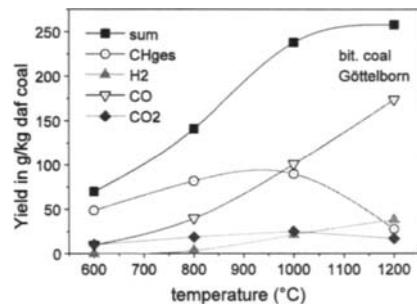


Figure 1: Pyrolysis gas composition for a bituminous coal (Göttelborn)

The effect of pyrolysis temperatures between 600 and 1200°C has been studied at the en-

trained flow reactor. The gaseous species are shown in figure 1 for a bituminous coal. Hydrocarbon production is maximum between 800 and 1000°C. Hydrogen shows a strong increase at temperatures higher than 800°C. At 1200°C the hydrogen yield is about 10 g/kg daf, the share in the pyrolysis gas volume, however, is nearly 70%. Carbon monoxide production increases as well, together with the reaction temperature. The CO formation is caused by oxygen in the fuel (105 g per kg daf) and by oxygen (0.5 g per kg daf) out of air in the bulk material. Carbon dioxide is released over the whole temperature range in the same concentration.

The pyrolysis of brown coals results in higher gas yields, as shown in figure 2. The high yield of CO and CO₂ is given through the high ratio of oxygen in the brown coal. Like in the case of hard coals, there is a peak of hydrocarbons between 700 and 800°C of reactor wall temperature and also an increase of the hydrogen values at higher temperatures. The tar yield of both coal types is approximately the same over the whole temperature range.

Figure 3 gives information about the total yield in coal pyrolysis of a bituminous coal. In the investigated range of temperatures, the gas yield increases with rising reaction temperatures. The tar yield decreases with higher temperatures, and at 1200°C the tar is totally cracked. The char yield sinks from 68% at 600°C to 51% at 1200°C. The soot is formed by a tertiary process at high temperatures. The difference in the mass balance at 1200°C arises from difficulties in the determination of soot.

For the prediction of pyrolysis yields, a functional group model for coal devolatilization developed by Solomon et al. /4/ has been applied. Based on the coal's functional group composition the model permits to calculate in detail the composition of the volatile species and of char. The predicted decrease of the tar concentration does not correspond to the measured values because the model does not account for any secondary reactions, and the residence time in the pyrolysis reactor is about 1.5 seconds.

Figure 4 shows nearly the same behaviour for brown coals. The total gas yield is increasing

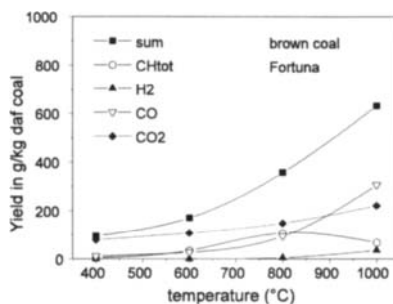


Figure 2: Pyrolysis gas composition for a brown coal (Fortuna)

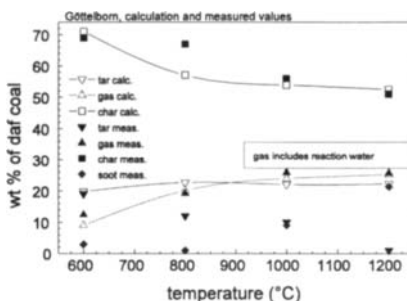


Figure 3: Mass balance of pyrolysis (bituminous coal Göttelborn) - comparison of measurements and calculations

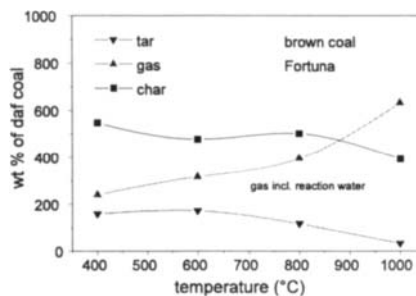


Figure 4: Mass balance of pyrolysis - brown coal Fortuna

with rising temperatures, dominating the products at 1200°C. The remaining char is about 33%.

Figure 5 gives the behaviour of the fuel nitrogen for the pyrolysis in the entrained flow reactor. The main part of the fuel nitrogen remains in the char. The nitrogen release however is lower than the weight loss of the coal. Due to neglect of secondary pyrolysis reactions, the model predicts tar N also for higher temperatures.

At CSIRO the evolution of nitrogen was investigated in more detail in a lab-scale fluidized bed reactor as a function of temperature. For the Göttelborn coal the concentration of HCN in the pyrolysis gas continuously increases with the temperature, whereas for NH_3 a maximum is observed at a temperature of 800°C (figure 6). The decline of NH_3 at higher temperatures may be caused by the destruction on reaction surfaces.

3. RESULTS OF COMBUSTION TESTS

Figure 7 shows the results of fuel staging for different reburn fuels with Göttelborn coal as primary fuel. Based on the experience with synthetic reburn fuels, the experiments have been carried out with a sufficient residence time of about 1.5 seconds in the secondary fuel rich reduction zone. There is only a small difference in NO_x reduction between methane and synthetic gas mixtures as reburn fuel. The deviation was less than 10% at all investigated stoichiometries. The use of pyrolysis gas improves the reburning efficiency and shifts the optimum air ratio from $\lambda_2 = 0.75$ for methane to 0.9 for pyrolysis gas with tar.

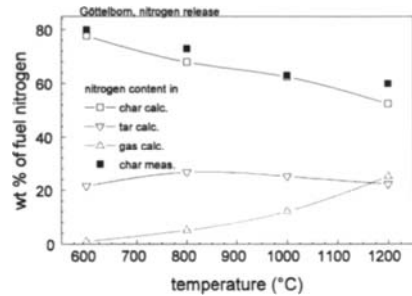


Figure 5: N-balance for a bituminous coal (Göttelborn) - calculation and measurements

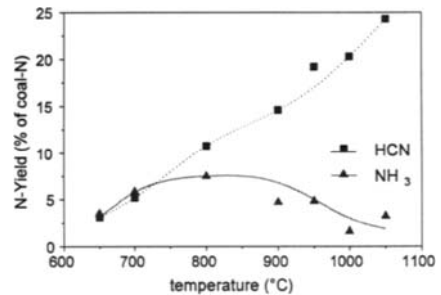


Figure 6: NH_3 , HCN yield (Göttelborn)

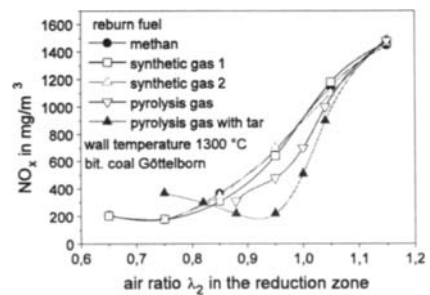


Figure 7: Comparison of different reburn fuels

The influence of the pyrolysis reactor temperature on the efficiency of the reburn fuel is shown in figure 8. A bituminous coal (Göttelborn) was used as primary fuel in the combustion reactor and in the pyrolysis for the production of the reburn fuel. The optimum temperature of the pyrolysis reactor for NO_x reduction is 800°C. For the best reduction a certain

share of pyrolysis gas to rapidly achieve an understoichiometric air/fuel ratio and also a certain share of tar for the reduction of NO are necessary.

The effect of temperature variation in the pyrolysis reactor is shown in figure 9 for a brown coal. The utilization of brown coal as primary fuel results in lower baseline emissions. Despite lower combustion temperatures of about 1000°C, NO_x emissions below 200 mg/m³ can be achieved when reburning is applied. The reduction efficiency is optimum for a pyrolysis gas produced at 800°C.

4. CONCLUSIONS

Fuel staging or reburning is an efficient method to reduce NO_x emissions from bituminous and brown coals. With coal pyrolysis gas as reburn fuel the NO_x reduction can be further improved. The German emission standards of 200 mg/m³ at 6% O₂ could be achieved at the test facility. The optimum pyrolysis temperature for maximum NO_x reduction was determined at 800°C. At this temperature the pyrolysis gas contains maximum concentrations of tar, hydrocarbons, and NH₃.

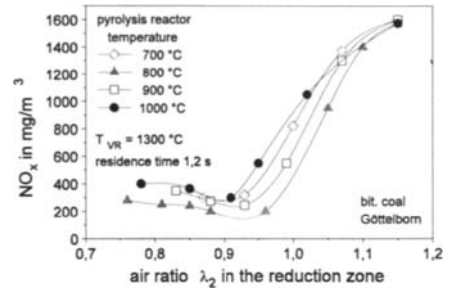


Figure 8: Effect of pyrolysis temperature for a bituminous coal (Götteleborn)

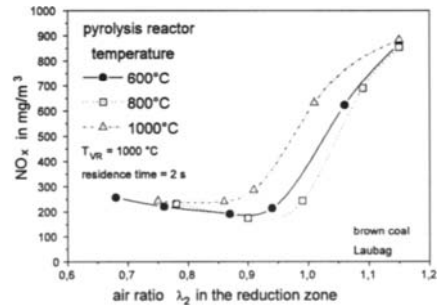


Figure 9: Effect of pyrolysis temperature for a brown coal

REFERENCES

1. Spliethoff, H.: "Large Scale Trials and Development of Fuel Staging in a Slag-Tap Furnace". 1991 Joint Symposium on Stationary Combustion NO_x Control, Washington D.C., 1991
2. Spliethoff H., Rüdiger H., Greul U., Spliethoff H., Hein K.R.G.: *Kombinierte Minderung der NO_x-Bildung und Reduzierung von gebildetem NO_x bei der Verbrennung von Steinkohle, Phase 3*. Abschlußbericht Forschungsvorhaben 0 326 535 C, 1994
3. Greul, U., Rüdiger, H., Spliethoff, H., Hein, K.R.G.: Use of Pyrolysis Gas as Reburn Fuel, 3rd European Conference on Industrial Furnaces and Boilers, Lisbon, April 1995
4. Solomon P.R. et al.: "A characterization method and model for predicting coal conversion behaviour". In: *Fuel*, Vol. 72 No. 4, 1993

The effect of reburning coal properties on the reduction of NO in a drop-tube furnace

E. Hampartsoumian^a, H. Liu^a, B. M. Gibbs^a and J. P. Smart^b

^aDepartment of Fuel and Energy, The University of Leeds, Leeds LS2 9JT, United Kingdom

^bNational Power PLC, Swindon, SN5 6PB, United Kingdom

The reburning performances of thirteen coals of different rank were investigated in an isothermal drop-tube furnace. The experimental data were correlated with coal properties including volatile matter, fuel nitrogen content and, as a measure of reactivity, carbon burnout.

1. INTRODUCTION

Reburning or fuel staging is an in-furnace NO_x control strategy that removes NO_x from the combustion products after it is formed. Previous studies have shown that gaseous hydrocarbon fuels are effective reburning fuels for the reduction of NO_x [1,2]. More recently, it has been demonstrated in laboratory and pilot-scale combustors that coals can also reduce NO_x by reburning [3-5]. However, there are some uncertainties concerned with coal reburning related to physical and chemical properties of the reburn fuels, geographical origin and morphology [6]. Some characteristics such as volatile matter content, reactivity and rank are coupled and cannot be easily evaluated separately. The aim of this study is to investigate the influence of the reburning coal type on the reduction of NO. The methodology is based on characterising a set of bank coals experimentally and to develop useful correlations of their reburn characteristics. Although such correlations may be sensitive to the experimental apparatus used, we can use them to predict qualitatively, if not quantitatively, the reburn characteristics of other coals not included in these tests.

2. COAL SELECTION AND EXPERIMENTAL SYSTEM

A suite of thirteen coals of varying geographical locations were chosen on the basis of rank, reactivity, volatile matter and fuel nitrogen content. Since bituminous coals are expected to be effective reburn fuels, the majority of coals chosen were of this type. Table 1 shows the proximate analysis, ultimate analysis and other details of the coals selected. The reactor comprised a heated 40 mm (id) × 1.8 m drop-tube furnace incorporating a natural gas pre-combustor, an ammonia doping system (to produce between 650 - 720 ppmv NO by reaction with excess oxygen from the pre-combustor) and a calibrated coal supply/injection system. The drop-tube reactor simulated the primary zone and reburn zone of the reburning process. All the results presented are for an average reburn zone gas temperature of 1373K and a pre-combustor burner air/fuel equivalence ratio, SR₁, of 1.20 or 1.08 to give an oxygen concentration of around 3.9% and 1.5% (dry basis) respectively at the coal injection point

Table 1
Reburn fuel types and physical and chemical properties.

Reburn Fuel & Country of Origin	Symbol	Proximate (% dry)			Elemental (% dry, ash free)			
		V.M.	Ash	F. C.	C	H	N	S+O*
UK Anthracite	▲	7.6	4.2	88.2	92.3	3.5	1.3	2.9
UK Semi-anthracite	▽	13.9	16.9	69.2	91.4	4.5	1.5	2.6
UK Bituminous 1	●	37.9	5.4	56.7	79.0	5.3	1.4	14.3
UK Bituminous 2	◆	37.4	3.7	58.9	82.4	5.2	1.8	10.6
UK Bituminous 3	○	30.4	17.8	51.8	83.2	5.8	1.7	9.3
UK Bituminous 4	▼	19.7	5.9	74.4	90.3	4.4	1.5	3.8
UK Bituminous 5	◐	39.0	4.3	56.7	85.1	5.9	2.1	6.9
Colombian Cerrejon Bituminous	□	39.7	4.4	55.9	81.2	5.4	1.6	11.8
Indonesian Tanjung Sub-Bituminous	⊞	33.1	3.8	63.1	82.4	5.4	1.3	10.9
US Pittsburgh #8 Bituminous	◇	39.4	11.5	49.1	83.2	5.3	1.6	9.9
German N. Waltsam Bituminous	⬧	32.4	3.8	63.8	83.1	5.0	1.8	10.1
Australian Buchanan Bituminous	■	30.0	17.0	53.0	81.9	5.2	1.8	11.1
Egyptian El-Maghara Lignite	◑	45.3	10.2	44.5	76.2	5.5	1.2	17.1

* by difference

prior to feeding any reburning fuel. Carbon conversion efficiencies of the reburn coals were determined from gas analysis and solids sampling using the ash tracer method and NO reduction efficiencies from the initial and final NO concentration when the reburn fuel is injected into the furnace.

3. RESULTS AND DISCUSSION

Figure 1 shows the NO reduction achieved for all sixteen fuels against reburn zone stoichiometry, SR_2 , for a primary stoichiometry $SR_1=1.20$. The effect of reducing SR_2 varied with coal type. Typically, the NO reduction efficiency increased by about 15% (absolute) for the more reactive bituminous coals for a decrease of SR_2 from 1.1 to 1.0 but only about 5% for the less reactive coals such as anthracite. The data show that it is possible to reduce NO by reburning even in lean burned gases. The relationship between NO reduction and burnout of the reburn fuels is shown in Figure 2 for $SR_1=1.20$ and 1.08 (the latter for eight coals). The burnout of a particular coal will depend on its reactivity (which is also related to rank). The reactive coals are expected to be the more effective reburn fuels since they can more readily provide hydrocarbon radicals which are mainly responsible for NO reduction under reburning conditions. Other coal parameters influenced by rank may also be expected to have an effect on the NO reduction efficiency. Figure 3 shows the relationship between volatile matter and the normalised NO reduction (to account for the differences in burnout between different fuels) for all reburn fuels defined as:

$$\text{Normalised NO reduction, \%} = \left(\eta_{\text{NO}} / \eta_{\text{C}} \right) \times 100 \quad (1)$$

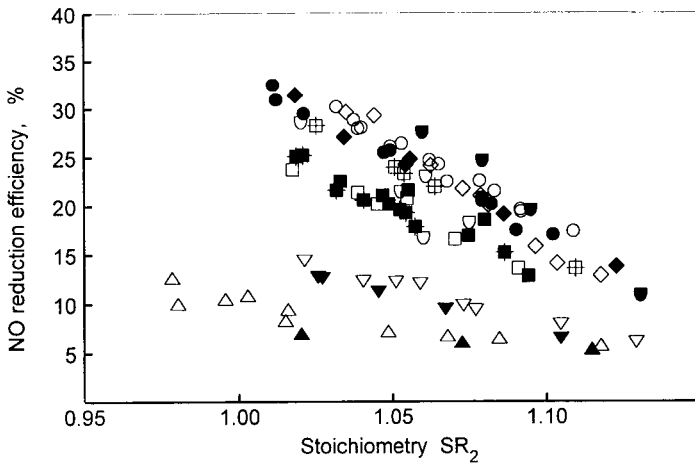


Figure 1. Effect of coal type on NO reduction efficiency as a function of overall stoichiometry; symbols as Table 1, reburn zone gas temperature 1373 K, particle residence time 360 ms, $SR_1=1.20$

where η_{NO} , η_C are the NO reduction efficiency and carbon conversion efficiency respectively.

3.1. Correlation of experimental data

The experimental data corresponding to the fixed reaction zone temperature of 1373 K and total gas residence time of 360 ms for all sixteen fuels were analysed using multi-variate analysis. Correlation coefficients of the NO reduction achieved with carbon conversion efficiency, volatile matter, stoichiometry SR_1 , SR_2 and rate of coal-bound nitrogen input into the reactor were 0.265, 0.675, -0.631, -0.557, 0.344, respectively. The greater importance of volatile matter and stoichiometry relative to carbon conversion efficiency and fuel nitrogen input is evident. However, when the data are correlated for a specific primary stoichiometry, a much higher correlation coefficient of 0.695 is obtained for carbon conversion efficiency confirming the importance of this parameter on the NO reduction. Linear regression analysis of all the data yielded the following expression (with an acceptable squared correlation coefficient of 0.85).

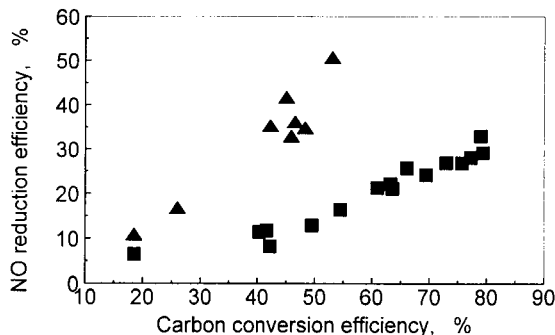


Figure 2. NO reduction efficiency versus Carbon conversion efficiency ; ■ $SR_1=1.20$, $SR_2=1.04$ All fuels; ▲ $SR_1=1.08$, $SR_2=0.95$ (UK Bit1, UK Bit3, Pet. Coke, UK semi-anthracite, Cerrejon, Pitts#8, Walsam, Buchanan).

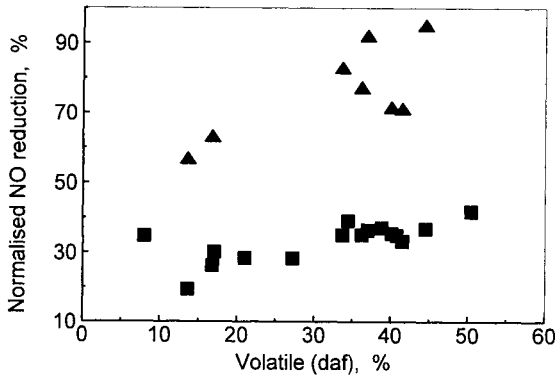


Figure 3. Effect of fuel volatile content on normalised NO reduction efficiency (symbols as Fig5)

$$\eta_{NO} = 150 - 40.4 SR_2 - 104 SR_1 + 0.238 V + 0.243 \eta_c + 0.983 N \quad (2)$$

where N is the rate of fuel nitrogen input (mg/min) and V the wt% volatile content (daf basis).

4. CONCLUSIONS

High volatile and reactive coals were found to be the most effective of the reburn fuels tested with the NO reduction showing a strong dependence on carbon burnout. The NO reduction efficiency achieved for all the reburn fuels tested was correlated with volatile matter, carbon conversion, stoichiometries and fuel-bound nitrogen and a regression equation was determined.

Low reactivity coals, such as anthracite and semi-anthracite, need higher reburning zone temperatures and longer residence times to achieve good burnout and hence NO reduction.

REFERENCES

1. B. A. Folsom., T. M. Sommer and R. Payne, Demonstration of Combined NO_x and SO_2 Emission Control Technology Involving Gas Reburning, Proceedings of the AFRC/JFRC International Conference on Environmental Control of Combustion Processes, Hawaii, 1991
2. R. W. Borio *et al*, Reburn Technology for NO_x Control in a Cyclone -Fired Boiler, Proceedings of the ASME 1991 International Joint Power Generation Conference, California, 1991
3. Chen S. L., McCarthy J. M., Clark W. D., Heap M. P., Seeker W. R. and Pershing D. W., Bench and Pilot Scale Process Evaluation of Reburning for in-furnace NO_x reduction, Twenty-first Symposium (International) on Combustion, The Combustion Institute, 1988.
4. J. P. Smart and D. J. Morgan. Fuel, Vol. 73, No. 9, 1994
5. A. Kicherer, H. Spliethoff, H. Maier and K. R. G. Hein, Fuel, 73, No. 9, 1994
6. R. Boardman and L. D. Smoot (eds), Chapter 6 in Fundamentals of Coal Combustion for Clean and Efficient Use, Elsevier Science Publishers B. V., 1993

ACKNOWLEDGEMENTS

The authors acknowledge the UK EPSRC for a grant in aid of this work and the Sino-Britain TC programme for providing of studentship.

PRIMARY MEASURES FOR REDUCTION OF NO_x IN LOW VOLATILE COALS COMBUSTION

A. Plumed¹, L. Cañadas¹, P. Otero², M. I. Espada², M. Castro³, J.F. González⁴, F. Rodríguez⁵

1 E.S. Ingenieros Indust.de Sevilla, D.I.Q.A. Reina Mercedes s/n. 41012, Sevilla. SPAIN.

2 ENDESA - C.T. Compostilla. Apdo. 35, 24400 Ponferrada, Lcón. SPAIN.

3 UNION FENOSA - C.T. La Robla. La Robla 24640, Lcón. SPAIN.

4 ENDESA-DIVISION I+D. Suero de Quiñones 36-38. 28002 Madrid, SPAIN.

5 INERCO. Edf. Renta Sevilla 7^op. Avda. Innovación s/n, 41020 Sevilla. SPAIN.

1. INTRODUCTION

An important fraction of the coal produced at the Northern Spanish mining regions of Asturias and Lcón are anthracites and other low volatile coals. More than 4.700.000 Tn/year of this coal is burnt at Compostilla (% Volat.: 7,2; %N:1,0) and La Robla (% Volat.: 10,7; %N:1,7) power stations.

Arch-fired furnaces (Figure 1) have been designed for industrial firing of low volatile coals as they account for the problems of low ignitability and combustibility of this type of fuels. The characteristic high temperature levels and residence times of these combustion systems, besides the higher char-volatile ratio of low volatile coals, determine higher NO_x emission levels than for bituminous coal firing.

As a consequence of this situation a wide research project concerning the reduction, by the sole use of combustion measures, of nitrogen oxides emissions in power plants burning anthracites is currently being performed. This report summarizes the main results obtained in the first phase of this Project, developed at the 7 Units (1932 MW) of the above mentioned power stations of Compostilla (ENDESA) and La Robla (UNION FENOSA).

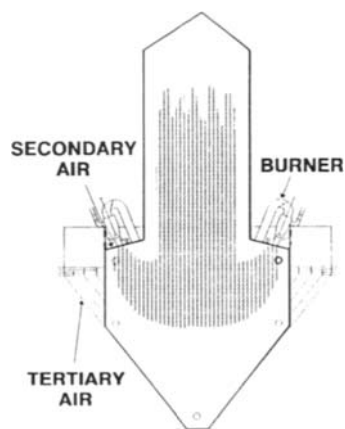


Figure 1. Arch-fired boiler.

2. TESTING PROGRAMME

The historic performance in relation to NO_x emissions of the seven units involved in the Project was very diverse. Hence, the first objective of the trials was to take a "picture" of the current NO_x levels of all the units to evaluate these differences. Afterwards, several

modifications were introduced or observed during the tests, consisting of variations of operational parameters, as excess air, boiler load, number and distribution of active burners, secondary and tertiary air dampers openings and combustion air temperatures, and characteristics of coal, as moisture, nitrogen and volatile contents. Other factors were also considered such as the fouling condition and design of the boiler. Likewise, possible adverse impacts as increases in fly ash carbon contents were evaluated.

3. RESULTS AND DISCUSSIONS

An extensive programme of combustion tests was conducted, confirming not only the different performance of the units with respect to NO_x emissions, but also the significant reduction of these levels for each boiler through primary measures.

Due to the important number of data collected, a statistical approach to the problem has been applied in order to determine the contribution of different operational and coal variables on NO_x emissions. This study, performed by the use of the computer package Statgraphics 7.1, has permitted the achievement of different correlations, from which it is possible to establish the importance of some parameters that affect NO_x production in arch-fired furnaces:

- I) Coal characteristics (fixed carbon/volatile content ratio, nitrogen content, inherent moisture, total moisture).
- II) Oxygen excess of combustion.
- III) Thermal levels of combustion (defined by the gases temperature at the exit of the furnace and furnace peak temperature).

In the cases where the variations of these parameters are significant, increases in fixed carbon/volatile ratio, nitrogen content, oxygen excess or thermal levels imply higher NO_x emissions. On the contrary, increases in inherent moisture bring about lower NO_x emissions. The effect of total moisture is not very clear as depending on the specific situation its influence is different. These results basically confirm the trends shown in bibliography¹ for NO_x production at a pilot plant level when coal characteristics and operational parameters are modified.

Quantitative effects of the above mentioned factors plus other operational variables, as oil support or air dampers openings, that the statistical analysis could not take into account, have been evaluated by means of a programmed cases study. The observed variations in NO_x emissions, from tests performed during the commercial operation of the power units, are explained by changes in several of these factors. Individual effects can be hardly established in some cases; nevertheless it is possible to extract from these trials some very interesting generic results:

- a) The important differences between NO_x emissions levels, 900–2500 mg/Nm³ (d.b., 6% O_2) at full load, of the Project arch-fired units may be ascribed to typical features of their designs (furnace volumes, heat exchanging surfaces) with regard to the thermal levels that they determine. This fact explains the significant higher NO_x levels of Compostilla 2 and La Robla 2 units. (Figures 2 and 3).
- b) As a general rule NO_x emissions are found to diminish for decreases in unit load or

oxygen percent at the exhaust of the furnace. These reductions may be as high as 30% and 20%, respectively (Figures 2 and 3).

- c) Combustion modifications that contribute to increase the richness in the initial flame region^{2,3}, such as operations with burners out of service or higher ratios of tertiary to secondary air, also imply lower levels of NO_x emissions. In this sense, the differences of more than 30% in NO_x emissions levels for Compostilla Boilers 4 and 5 at low load may be explained by the operation with a higher number of burners out of service (4 more) in the last case.
- d) For an identical number of burners in service it has been found (Compostilla 2, 105 MW) that the operation with a lower number of burners located at the centre of the furnace (area of higher temperatures) determines a reduction of around 24% in NO_x concentrations.
- e) Depending on the slagging condition of the furnace, which is correlated with the measured thermal levels, differences in NO_x as high as 17% (Compostilla 5, 260 MW) have been reported.
- f) Other factors with influence, although not exactly quantified, on NO_x emissions are oil support, openings of central air dampers and coal fineness. The effects of variations of these parameters on NO_x concentrations, together with the degree of additionality of the other reported impacts, will be further investigated in the second phase of this Project.
- g) Lower NO_x emissions do not necessarily imply higher fly ash carbon contents (Figure 3). In this sense, the trials performed within this Project show that, for certain firing patterns, optimization of combustion in both directions is possible.

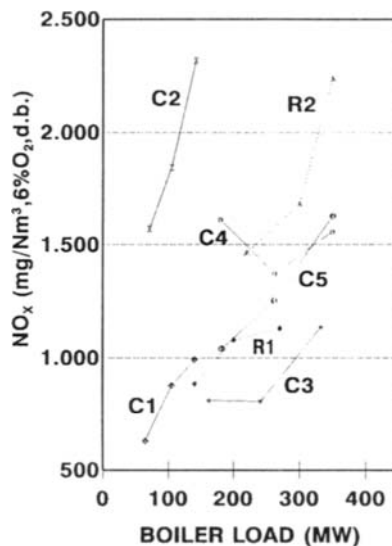


Figure 2. NO_x emissions vs. boiler load for Compostilla (C) and La Robla (R) power units.

4. CONCLUSIONS

Combustion of anthracites and other low volatile coals in arch-fired boilers determines, due to its special characteristics, high levels of NO_x emissions. Tests performed at Compostilla and La Robla arch-fired units have shown a very diverse situation, with NO_x emissions ranging from 900 to 2500 mg/Nm³ (dry gas, 6% O₂). These wide variations may be basically ascribed to the thermal levels of the furnaces determined by their specific design patterns. Nevertheless there are other factors as certain coal properties and operation conditions which have also been found to contribute to the reported NO_x emission levels. In

this sense modifications of combustion features as boiler loads, oxygen excess, burners out of service, tertiary to secondary air ratio and distribution of burners in service may result in reductions in NO_x emissions of around 20–30%. The trials reported here have also shown that "low- NO_x " operation does not necessarily imply higher fly ash carbon contents.

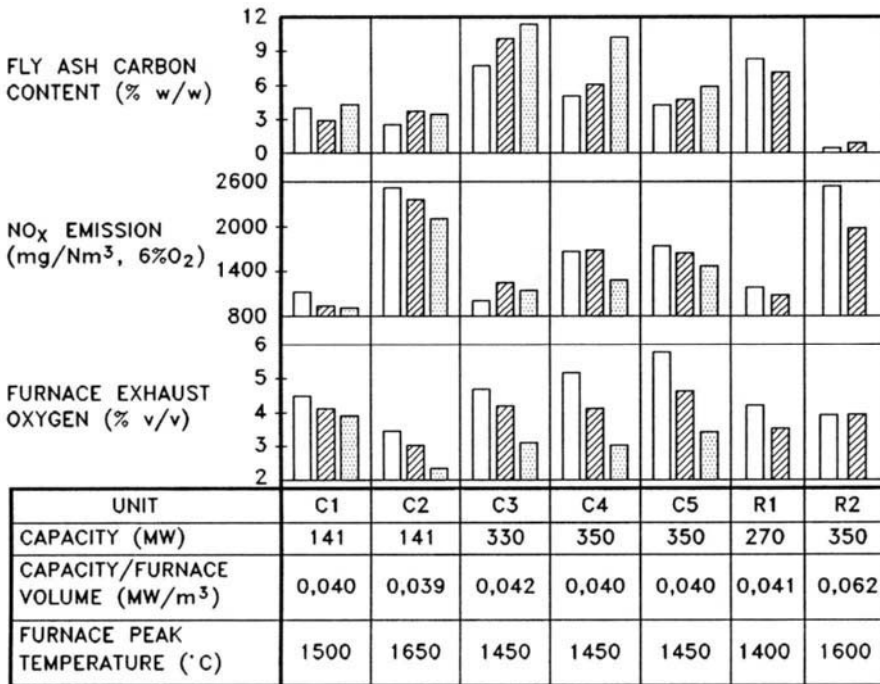


Figure 3. NO_x and fly ash carbon content at different furnace exhaust oxygen levels for Compostilla (C) and La Robla (R) power units (results in dry basis) (temperatures by optical pirometry)

5. ACKNOWLEDGEMENTS

The authors gratefully acknowledge the financial support of OCIDE, OCICARBON and ECSC. Further they would like to thank ENDESA and UNION FENOSA for permission to publish this paper.

REFERENCES

1. S. MIYAMAE; T. KIGA and K. MAKINO. Proc. of Joint Symposium on Stationary Combustion NO_x Control. pp 3-111/3-123 (1989).
2. T.W. SONNICHSEN and J.E. CICHANOWICZ. Proc. of Joint Symposium on Stationary Combustion NO_x Control. pp 237/268 (1981).
3. N.A. BURDETT. Journal of the Institute of Energy. pp 103/107 (1987).

NO_x reduction by coal briquets.

A. García-García, M.J. Illán-Gómez, A. Linares-Solano and C. Salinas-Martínez de Lecea.

Departamento de Química Inorgánica. Universidad de Alicante. Spain.

1. INTRODUCTION.

Reducing air pollution caused by NO_x is currently an urgent and serious challenge. Selective catalytic reduction with ammonia is still the most suitable process which has already been proved in large scale systems. However, the drawbacks originated by this technology lead to the search of other less problematic alternatives⁽¹⁾. From a practical point of view, an abatement method based on a solid reducing agent which does not require any additional gaseous streams would be very desirable. Carbon has always been considered a powerful NO reducing agent. The uncatalyzed and catalyzed NO reduction by activated carbons has been recently investigated⁽²⁻⁷⁾. For a practical point of view the use of a cheaper carbon material and the presence of oxygen have to be considered.

In this study, the possibility of using bindered carbons (from coals) to reduce NO_x emissions is examined. Moreover, the novel manufacture method proposed in this work, presents the advantage of using as binder agent, humic acid, containing potassium which will act as an inherent catalyst. The system catalyst-binder-coal stays intimately joined by a moulding stage and subsequent pyrolysis. Therefore, the objectives are to analyze the effect of pyrolysis temperature and potassium content in the NO reduction in the presence of oxygen. Complementary study carried out includes the analysis of the behaviour of different coals and reactor type.

2. EXPERIMENTAL SECTION

Bituminous coals have been used to perform the NO_x reaction. The results presented in this paper are focused on a bituminous coal from Puertollano (A3N sample). The particle size chosen was 0.1-0.2 mm to facilitate the agglomeration step. The coal was impregnated with the humic acid (liquid with a density of 1.12 g/cm³ and a potassium content of 0.049 g/cm³) in a ratio humic acid/coal of 12 ml per 10 g. The mixture was kept in stirring for thirty minutes. After this, the mixture was dried in an oven at 110 °C for one hour approximately. The paste obtained was pressed at 1-2 Kg/cm². The cylinder-shaped piece was dried at 110 °C, and pyrolyzed for two hours in a fixed-bed horizontal oven in N₂ atmosphere (flow rate 80 ml/min). The pyrolysis temperatures studied were 400, 500, 600 and 700 °C respectively. After the pyrolysis, a test was conducted to determine mechanical resistance of the briquets. The briquets described in this papers have a satisfactory resistance value. The amount of potassium was determined after the pyrolysis step by AES-ICP.

The NO_x reduction was performed in a U-shaped quartz microreactor coupled to a gas chromatograph (Hewlett Packard 5890 Serie II) and a chemiluminiscent analyzer (Thermo

Environmental Inc. 42H). The reaction was analyzed in the following reactant gas mixture atmospheres: i) 0.5% NO/He, ii) 5% O₂/He and iii) 0.5% NO+5% O₂/He (NO and O₂ proceed from different gas cylinders). Additional experiments (for comparison purpose) have been carried out using also 0.5% NO and 5% O₂ previously mixed in one cylinder. The gas flow rate was 60 ml/min. The briquets were ground to 2.0-2.83 mm to introduce them in the microreactor. No diffusional problems were checked using other small fractions (0.1-1.2 and 1.2-2.0 mm). The microreactor was packed with approximately 300 mg of sample. Isothermal reactions at 300 °C were followed for six hours. TPD experiments were conducted after the reactions, by analysis of the gas evolution with the gas chromatograph.

3. RESULTS AND DISCUSSION

The effect of oxygen in the NO reduction activity has been investigated for a sample containing 4.7 potassium wt%. Table 1 presents the NO reduced over a 6 hour period and the CO₂ evolved for the three atmospheres studied. An important enhancement of NO reduction in the presence of oxygen is observed which is in agreement with the results of Tomita and coworkers⁽⁸⁾ and the proposed mechanism for the reaction⁽⁹⁾. The observation that CO₂ evolution is quite comparable in a NO+O₂ mixture than in the O₂ atmosphere is noteworthy and needs comments. This may suggest : i) that oxygen from the NO reduction by carbon does not evolve as CO₂, (probably as CO and/or increasing the oxygen content of the carbon-potassium system) ii) that the C-O₂ reaction is inhibited in the presence of NO, and iii) that the carbon reactivity at given temperature (300°C) controls the amount of CO₂ evolved. The weight loss of carbon substrate (during 3 hours) has been followed by thermogravimetric analysis. The results were: 2.04 and 1.45% in NO+O₂ and O₂, respectively, that correspond to 1582 and 1124 μmol of CO₂/gC (assuming that carbon conversion is only due to CO₂ evolution). These weight losses discard points ii) and iii) and indicate that point i) is the most reasonable. Furthermore, both CO evolution and oxygen retention seems to occur. The former can be deduced because, in spite of the reactivity is higher in the NO+O₂ mixture than in O₂/He, the CO₂ evolution is lower (see Table 1). The latter will be discussed below.

Table 1

Data from reactions (at 300 °C) in different atmospheres for sample A3N-4.7(700°)

Reaction atmosphere	NO _x red. (μmol/gC)	CO ₂ evolved (μmol/gC)
NO	80	46
O ₂	--	1355
NO+O ₂	1276	1205

Figure 1 presents the TPD profiles of the sample A3N-4.7 after NO, O₂ and NO+O₂ reaction at 300 °C. After NO exposure, no significant changes are noted comparing with the corresponding TPD of the untreated sample (not shown in the Figure). This is reasonable observing the low NO conversion showed by the sample in this atmosphere. On the contrary, both the CO₂ and the CO profiles are affected by the other reactive gas mixtures, mainly in NO+O₂. A well defined CO₂ peak appears at 600°C after NO_x reaction that may correspond

to K_2CO_3 decomposition previously formed during the reaction. Although the reason that favours carbonate formation in NO_x and not in O_2 is not well understood, it could be related to the formation of potassium superoxide. Only in the $NO+O_2$ mixture, potassium superoxide has been confirmed, and hence its reaction with $CO_2^{(10)}$ (evolved during reaction) may be possible. The Figure also shows that CO evolution is larger for the NO_x reacted sample than for the sample reacted in the other two gas mixtures. Both CO and CO_2 profiles indicate that an oxygen enrichment has occurred on sample, both on the catalyst and on the carbon surface.

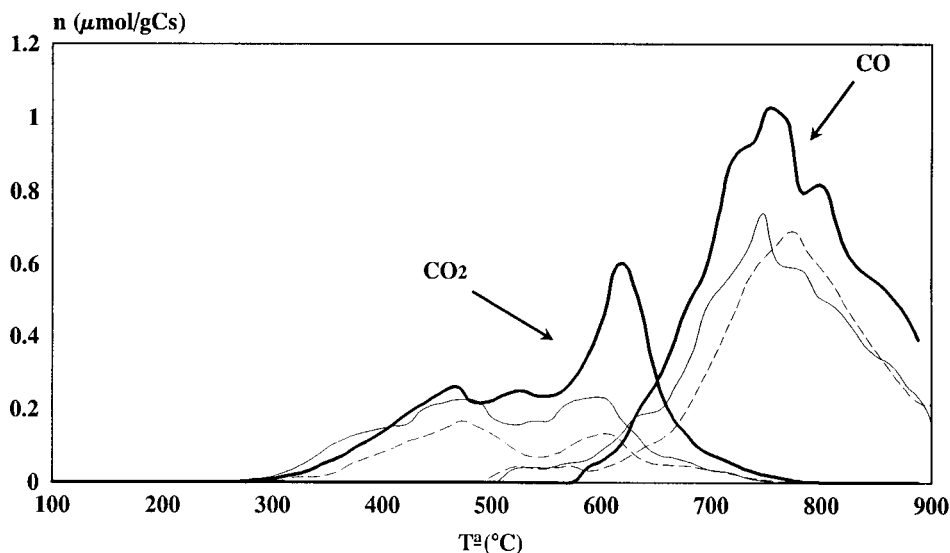


Figure 1. TPD profiles of sample A3N-4.7(700°) after exposure in different reactant mixtures for 6 hours at 300°C, (---) 0.5% NO/He , (—) 5% O_2/He and (—) 0.5% $NO/5\% O_2/He$.

The effect of the temperature of the pyrolysis treatment conducted during sample preparation has been investigated in the range from 400-700°C. No effect was found in the NO_x reduction activity except for the lower temperature (400°C), at which a lower activity (50% less) has been found. In spite of the increasing amount of potassium as temperature increases, due to the larger volatile matter loss during the treatment, the sample prepared at 500, 600 and 700 °C exhibit the same activity.

The effect of potassium is clear comparing the activity for NO_x reduction of the parent coal with that of one sample containing 4.7 wt% of potassium (242 and 1276 μmol NO reduced/gC, respectively). However no clear effect has been found, for the moment, of the potassium content. Increasing the metal loading from 4.7 up to 14%, using KOH as potassium precursor, no increase in activity was observed.

4. CONCLUSIONS

Coal briquets prepared by humic acid impregnation, pressing and pyrolysis have an adequate mechanical resistance and can be used as NO_x reductants. In the presence of oxygen the carbon NO reduction activity is considerably enhanced. The potassium introduced with the binder has catalytic effects. A larger amount of potassium added as KOH does not increase the reduction activity. The role of the alkali in the global process involved in NO_x reduction in the presence of oxygen remains still unclear.

ACKNOWLEDGEMENTS. The authors thanks EC (CECA -7220-ED/053), OCICARBON (C23-435) and DGICYT (AMB92-1032-C02-02) for financial support.

REFERENCES

1. Bosch, H., and Hanssen, F., *Catal. Today* **2**, 369 (1988).
2. Illán-Gómez, M.J., Linares-Solano, A., Salinas-Martínez de Lecea, C., and Calo, J.M., *Energy and Fuels* **7**, 146 (1993).
3. Illán-Gómez, M.J., Linares-Solano, A., Radovic, L.R. and Salinas-Martínez de Lecea, C., *Energy and Fuels* **9**, 97 (1995).
4. Illán-Gómez, M.J., Linares-Solano, A., Radovic, L.R. and Salinas-Martínez de Lecea, C., *Energy and Fuels* **9**, 104 (1995).
5. Illán-Gómez, M.J., Linares-Solano, A., Radovic, L.R. and Salinas-Martínez de Lecea, C., *Energy and Fuels* **9**, 112 (1995).
6. Illán-Gómez, M.J., Linares-Solano, A., Radovic, L.R. and Salinas-Martínez de Lecea, C., "NO reduction by activated carbons. 5. Catalysis by iron". *Energy and Fuels*, in press.
7. Illán-Gómez, M.J., Linares-Solano, A., and Salinas-Martínez de Lecea, C., "NO reduction by activated carbons. 6. Catalysis by transition metals" *Energy and Fuels*, submitted.
8. Suzuki, T., Kyotani, T. and Tomita, A., *Industrial Engineering Chemical Research* **33**, 2 (1994).
9. Illán-Gómez, M.J., Linares-Solano, A., Radovic, L.R. and Salinas-Martínez de Lecea, C., "NO reduction by activated carbons. 7. Some mechanistic aspects of the uncatalyzed and catalyzed reaction." *Energy and Fuels*, submitted.
10. Greenwood N.N. and Earnshaw, A. *Chemistry of the Elements*. Ed. Pergamon Press. (1984).

COAL-BASED ACTIVATED CARBONS: NO_x AND SO₂ POSTCOMBUSTION EMISSION CONTROL

John M. Stencel and Aurora M. Rubel

Center for Applied Energy Research, University of Kentucky, 3572 Iron Works Pike, Lexington, KY 40511 USA

1. ABSTRACT

A coal-based activated carbon was used to adsorb nitric oxide (NO) and SO₂ at temperatures between 20-140°C. At a relative NO/SO₂ ratio of 40/1, the rate of NO uptake and the conversion of NO-to-NO₂ was decreased by approximately 15% as compared to the case when no SO₂ was present. Adsorbed NO₂ consisted of two species, the more strongly bound of which could be removed by desorption at temperatures between 100-150°C. Adsorbed SO₂ also consisted of two species, the more strongly bound of which required a temperature of 300°C to desorb. The concentration of the more weakly held SO₂ decreased in the presence of adsorbed NO₂ while the overall concentration of adsorbed SO₂ increased in the presence of NO₂ as compared to without NO₂. The data suggest that the sites which catalyze NO → NO₂ are either poisoned or eliminated by adsorbed SO₂.

2. INTRODUCTION

Because of environmental regulations pertaining to the control of SO₂ and NO_x emissions, there has been considerable research and development on processes and materials that effectively remove these gases from stationary fossil fueled power plants. The most commercially proven NO_x control technology is selective catalytic reduction (SCR). The application of SCR can decompose NO_x at the very high space velocities that are needed in power plants but there are a number of environmental issues that have to be considered when using this technology (1-3).

For SO₂, the most commercially applied technologies rely on the use of disposable sorbents containing calcia. Newer technologies are applying recyclable SO₂ sorbents to produce sulfur-containing commodities, although the quality of these products are, in general, yet to be optimized (4-6).

Recently, research into the use of activated coke or carbons has shown their potential application for SCR reactions, SO₂ oxidation to SO₃ with the subsequent formation of H₂SO₄, and selective adsorption of NO_x and SO₂ (4-9). There is no known correlation between the SO₂ uptake capacity and a carbon's BET N₂ surface areas (10). The amount of SO₂ or NO adsorbed on carbon

can be greatly enhanced by the presence of O_2 (11,12); in the presence of H_2O , SO_2 adsorption is enhanced whereas NO adsorption can be decreased (11,12) Both NO and SO_2 can be physically or chemically bonded to carbon, with the relative amount of each depending on the chemical nature of the carbon surface (11-13).

Overall, there is very little published information available which describes interactions and mechanisms of interactions of $NO + SO_2$ over activated carbons under conditions relevant to coal combustion emissions control. In atmospheric chemistry related studies (14), surface reactions of NO_2 with SO_2 over carbon have been described to depend on the types of carbon and 'sites on the surface'; adsorbed $HONO$, sulfate, NO and NO_2^- were suggested as surface species. It is the purpose of this communication to examine in further detail the fundamentals of SO_2 and NO/NO_2 interactions over activated carbon.

3. EXPERIMENTAL

Adsorption and desorption experiments were conducted using a Seiko TG/DTA 320 coupled to VG Micromass quadrupole mass spectrometer (MS). The two computer-controlled instruments were coupled by a heated ($170^\circ C$) fused silica capillary transfer line leading from above the sample pan in the TG to an inert metrasil molecular leak which interfaced the capillary with the enclosed ion source of the MS.

The conditions of the NO and SO_2 adsorption and desorption experiments included the use of 20-30 mg of activated carbon, 200 ml/min total gas flow rate with a composition of 1% NO , 0.025% SO_2 , 5% O_2 , 15% CO_2 , 25% N_2 , and balance He, adsorption temperatures between 20 - $140^\circ C$, and desorption temperatures up to $350^\circ C$ under a He purge. During adsorption and desorption experiments, thermal gravimetric (TG) measurements were used to measure weight increase and decrease. The MS data from these experiments were compared and standardized with the use of mixtures of pure gases.

The carbon used during this study was commercially prepared from coal by steam activation. It was subjected to ultimate and proximate analyses using LECO instrumentation, BET N_2 surface area measurement using a Quantachrome Autosorb-6 and Hg porosity analyses using a Quantachrome Autoscan over a pressure range of $0-4.14 \times 10^8 N/m^2$. The properties of this carbon from these measurements were: % ash = 2.2; % C = 90.6; %N = 1.3, %S = 0.7; %H = 0.6; %O (by diff.) = 6.8; pH = 7.4; N_2 surface area = $460 m^2/g$; total pore volume = 0.69 ml/g.

4. RESULTS AND DISCUSSION

Adsorption/desorption profiles over the activated carbon using the reactant concentrations listed above and at various temperatures are displayed in Figure 1. A rapid increase in the weight of the carbon was

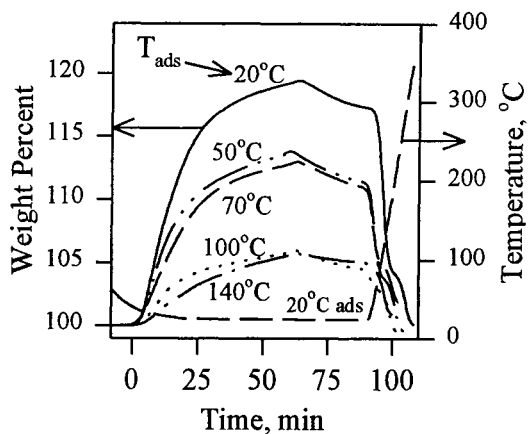


Figure 1. Ads/desorption weight curves vs. T_{ads} .

observed immediately upon introducing the gaseous mixtures; the initial rate increase of weight decreased as the temperature of adsorption was increased. After attaining a nearly constant weight level, the gas flowing over the sample was switched to He, at which time sample weight decreased. The amount of this decrease was sensitive to the adsorption temperature and amounted to approximately 15-40% of the total uptake between adsorption temperatures between 20-100°C, respectively. This weight loss is related to the desorption of weakly held, reversibly adsorbed (RA) nitrogen oxide species.

After attaining a nearly constant weight during He purging, the temperature of the samples was increased to 350°C under a linear temperature ramp. Subsequently, the weight of the samples returned to their original, pre-adsorption values as a consequence of desorption of the irreversibly adsorbed (IA) species.

In Figure 2 are presented the weight increases of the carbon relative to NO and SO₂ uptake at different adsorption temperatures. The amount of adsorbed nitrogen oxide decreased with increasing adsorption temperature whereas the amount of adsorbed SO₂ was insensitive to temperature range of 20-140°C.

During the adsorption of NO + O₂ and NO + O₂ + SO₂ mixtures, significant reaction exotherms have been measured. The value of this exotherm was near 2 kcal/(g adsorbate) independent of the adsorption temperature between approximately 20-80°C. These data, in conjunction with MS data suggests that NO₂ forms at the carbon surface as a consequence of NO + 1/2O₂ → NO₂ (9).

Curves representing the differential of weight loss during temperature induced desorption are presented in Figure 3. The maximum in weight loss between 50-170°C is associated with the evolution of NO₂ and the maximum between 250-320°C is associated with the evolution of SO₂. No sulfur-containing species was detected below a desorption temperature of 250°C. Hence, there is a significant separation between the desorption temperature of nitrogen and of sulfur oxide specie. This separation implies that NO_x and SO₂ could be removed from a flue gas stream and sequestered into two independent gas streams under a temperature swing process.

The position of the NO₂ evolution peak in Figure 3 varied between 100-150°C whereas the position of the SO₂ evolution peak was constant at approximately 300°C. These differences are probably associated with the physical and/or chemical forms of the adsorbed specie. For nitrogen oxides, the formation of NO₂ at the surface leads to NO₂ condensation within the carbon's porous network. It

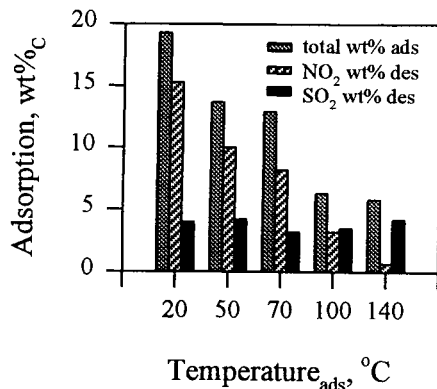


Figure 2. Total adsorption, NO₂ and SO₂ desorption.

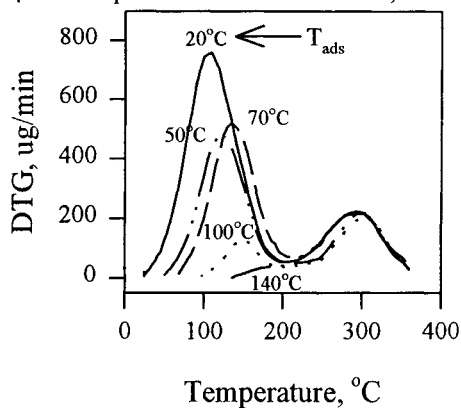


Figure 3. DTG curves during thermal desorption.

is also possible that N_2O_4 is formed at the surface, $2(NO_2) \rightarrow N_2O_4$, the heat of formation for which is approximately 1/4 of the heat of formation for the reaction $NO + 1/2 O_2 \rightarrow NO_2$. If O_2 is not present as a reactant, the exotherm associated with adsorbing NO_2 onto carbon is 1/3-to-1/4 of the value of the exotherm during $NO + 1/2 O_2$ adsorption. In the copresence of O_2 , no exotherm is observed during NO_2 adsorption. Hence, the interaction of nitrogen oxides with the carbon surface is complex and depends on the reactants and the chemical form of the surface.

The overall capacity and rate of NO uptake is decreased by about 15% when adsorbing $NO + SO_2 + O_2$ mixtures (with relative concentrations defined above) in comparison to adsorbing $NO + O_2$ mixtures. This difference implies that the SO_2 interferes with sites on the carbon which convert NO to NO_2 . These surface reactions, however, still lead to condensed NO_2 within the pores of the carbon. It is suggested that the RA species is primarily located in the mesopores or near the mouth to the micropores, whereas the IA species would be located primarily in the micropores where the interaction with the walls of the pore lowers the energy of NO_2 species. The interaction of SO_2 is stronger than the interaction of NO_2 with the carbon. However, the presence of NO_2 increases the amount of SO_2 species which is adsorbed. With NO_2 , it is possible that a SO_3 species is formed, the interaction of which within the carbon would be greater than any SO_2 species. However, no SO_3 has been observed during desorption. Future spectroscopic examination of adsorbed SO_2 and NO is expected to provide further information about these type of interactions.

REFERENCES

1. H. Bosch and F. Janssen, *Catal. Today*, **2**,369(1988).
2. T. Grzybek and H. Papp, *Appl Catal. B, Environ.*, **1**, 271(1992)
3. F.Radtke, R.A. Koepfel and A. Baiker, *Appl. Catal. A*, **107**, L125(1994).
4. Clean Coal Technology Demonstration Program, Prog. Update, OSTI/NTIS, March 1994.
5. C.-Y Cha, *Res. Chem. Intermed.* **20**, 13(1994).
6. S.K. Gangwal, G.B. Howe, J.J. Spivey, P.L. Silveston, R.R. Hudgins and J.G. Metzinger, *Environ. Prog.* **12**, 128(1993).
7. Catalytic Reduction of Nitric Oxide over Activated Carbons, by S.N. Ahmed, R. Baldwin, F. Derbyshire, B. McEnaney and J.M. Stencel, *Fuel*, **72**, 287(1993).
8. Activated Carbons for the Removal of Nitric Oxide, by S.N., Ahmed, J.M. Stencel, F. J. Derbyshire and R. M. Baldwin, *Fuel Proc. Technol.* **34**, 123(1993).
9. A.M. Rubel, S.N. Ahmed and J.M. Stencel, Reprint, AIChE Nat'l. Mtg., paper 77b, 8/15-18/93, Seattle, WA.
10. A.I. Foster, H.J. Linney, S.R. Tennison, R.A. Cory and D.P. Swan, *Fuel*, **72**, 337(1993).
11. J. Sawadzki, *Carbon*, **25**, 431(1987).
12. C. Moreno-Castilla, F. Carrasco-Marin and J. Rivera-Utrilla, *Fuel*, **69**, 354(1990).
13. F. Carrasco-Marin, E. Utrera-Hidalgo, J. Rivera-Utrilla and C. Moreno-Castilla, *Fuel* (1991).
14. F. De Santis and I. Allegrini, *Atmos. Environ.* **26A**, 3061(1992).

Reduction of NO with carbons using copper based catalysts

C. Marquez-Alvarez^a, I. Rodríguez-Ramos^a and A. Guerrero-Ruiz^b

^aInstituto de Catálisis y Petroleoquímica, C.S.I.C., Cantoblanco, 28049 Madrid, Spain

^bDepartamento de Química Inorgánica y Técnica, Facultad de Ciencias, U.N.E.D., 28040 Madrid, Spain

The presence of oxygen functional groups on the surface of carbons, as well as their surface structure and porosity, and the oxidation state of copper have been related to the catalytic performance of Cu/carbon systems for the NO reduction by carbon and the NO+CO reaction. The co-feed of oxygen inhibits the NO reduction with CO, while the NO reaction with carbon is enhanced.

1. INTRODUCTION

At present, the removal of NO by catalytic reduction processes using reducing gases like hydrocarbons, CO, H₂ and NH₃ is largely applied [1,2]. Carbon (activated carbons, graphites, coal-chars,...) would be another candidate to be used as reductant for the NO elimination due to its low cost. Moreover, carbon materials can participate in the reduction process both as a catalyst [3] and as a catalyst support for the active phase (metal or oxide) [4]. Copper based catalysts have been shown to be efficient for reactions of NO removal [5], and particularly for the catalyzed C+NO reduction [6]. This latter reaction is also interesting because soot is frequently generated in oil burners and diesel engines and it can be considered as another polluting component of exhaust gases.

The aim of this work is to provide evidence of the C+NO reaction catalyzed by copper. Reactivity of three carbons, two graphites exhibiting different surface area and an activated carbon, with NO has been explored in order to understand the role of oxygen surface groups and porosity in the copper catalyzed reaction. Furthermore, the catalysts were tested under a C+NO+O₂ mixture to obtain information about the competitive C+NO and C+O₂ reactions. Also, the catalytic reduction of NO with CO, both in the presence and in the absence of an excess of oxygen, has been analyzed. Particular attention has been paid to the chemical nature of the copper ions under the different reaction conditions. To shed light on this matter, spent catalysts were studied by X-ray diffraction (XRD).

2. EXPERIMENTAL

The carbon supports were two high-purity graphites (LT10, $S_{\text{BET}} = 15 \text{ m}^2/\text{g}$ and HSAG, $S_{\text{BET}} = 306 \text{ m}^2/\text{g}$) supplied by Lonza Ltd, and a purified Merck activated carbon (AC, $S_{\text{BET}} = 976 \text{ m}^2/\text{g}$). Details about characteristics of these samples have been given elsewhere [7]. Carbon supported copper catalysts were prepared by impregnation of the supports with ethanolic solutions of copper nitrate [8]. In all cases copper loading was closed to 5%. X-ray diffraction (XRD) was recorded on a Seifert 3000P diffractometer using Ni filtered Cu K_{α} radiation ($\lambda = 0.15406 \text{ nm}$) and a graphite monochromator.

Catalytic activity measurements were carried out in a fixed-bed flow reactor, which was an U-shaped quartz tube with an inner diameter of 4 mm. Before introducing the reactants, the samples (ca. 250 mg) were "in situ" dried under a helium flow at 573 K for 1 h. Then the reactant mixtures, adjusted by Brooks mass flow controllers, were passed through the catalytic bed. The composition of the effluents was determined by a gas chromatograph, Varian 3400, equipped with a switched dual columns system (Porapak Q + Molecular sieve) and with a thermal conductivity detector.

3. RESULTS AND DISCUSSION

The reaction of NO on carbon supported copper catalysts is not a typical heterogeneous catalytic process because the reducing agent is the support, and given sufficient time, this carbon support would be consumed. However, we have been able to achieve quasi-steady-state NO activities because of the very low quantity of NO reactant introduced into the reactor. Table 1 presents the NO conversions and the selectivities measured on the supported copper catalysts contacted with a mixture of 3%NO/He at 573 K and 673 K. Very low conversions were achieved with the Cu/LT10 sample. This behaviour can be understood considering the low surface area of this support (LT10) and consequently its lower reactivity. Also, the average copper oxide particle size is expected to be very high. On the other hand, NO conversions over Cu/AC are lower than for Cu/HSAG. Therefore, neither the high surface area of AC nor its microporosity seem to be a key factor for the NO reduction with carbon. Given that the HSAG sample has the surface covered by oxygen groups and that the AC sample does not possess such complexes [7], it is possible to conclude that these functional groups play an important role in this copper catalyzed reduction. Moreover, it can be observed (Table 1) that N_2O appears at lower reaction temperatures (573 K), while the selectivity to N_2 is practically total at higher temperatures (673 K). A non catalyzed reaction between the carbon surface groups and NO might be working at 573 K, and N_2O would be produced, as already detected by TPSR of NO [8]. However, at 673 K, the copper catalyzed reaction between C and NO would be the only one taking place. Finally the co-feed of oxygen increases the yield for NO transformation to N_2 , particularly at 573 K. Nevertheless, the oxygen has two other effects: generation of NO_2 by the equilibrium reaction ($2\text{NO} + \text{O}_2 \rightleftharpoons 2\text{NO}_2$), and consumption of carbon by

Table 1
Catalytic behaviour under various reaction conditions of the different catalysts

Catalyst	Reactant Mixture	T _{reac.} (K)	Conversion (%)		Selectivity (%)			
			NO	CO	N ₂	N ₂ O	CO	CO ₂
Cu/LT10	3%NO/He ^a	573	4	-	89	11	0	67
		673	5	-	95	5	0	100
	2%NO+2%CO/He ^a	573	100	97	96	4	-	100
Cu/HSAG	3%NO/He ^a	573	57	-	66	34	0	75
		673	100	-	100	0	0	96
	3%NO+5%O ₂ /He ^a	573	100	-	47	5	0	>100
		673	57	-	75	0	0	*
	2%NO+2%CO/He ^b	573	100	96	98	2	-	96
		673	100	98	100	0	-	99
	2%NO+2%CO+ 5%O ₂ /He ^b	573	100	100	2	1	-	100
		673	100	100	2	1	-	100
	Cu/AC	3%NO/He ^a	573	18	-	82	18	0
673			26	-	99	1	0	100
2%NO+2%CO/He ^b		573	100	87	95	5	-	91
		673	100	95	99	1	-	99

* All the oxygen is consumed giving CO₂, ^aGHSV = 4000 h⁻¹, ^bGHSV = 40000 h⁻¹

combustion ($C + O_2 \rightarrow CO_2$).

As for the $2NO + 2CO \rightarrow N_2 + CO_2$ reaction, all the carbon supported copper catalysts are very active, as it can be seen in Table 1. Note that conversions of NO and CO, and selectivities to N₂ and CO₂ are closed to 100%. This behaviour is distinct to that of other supported copper catalysts. On the other hand, this reaction is suppressed in the presence of oxygen and the CO oxidation becomes predominant (Table 1).

Some important differences in the catalytic phase working under these various reactant mixtures can be detected by XRD. Figure 1 indicates that CuO and Cu₂O coexist when catalysts are submitted to NO and NO+O₂ mixtures at 573 and 673 K. Under these conditions the copper oxides must be assumed as the active catalytic phases. However, metallic copper is stabilized under NO+CO stoichiometric mixture. This latter phenomenon does not take place over other supported copper catalysts.

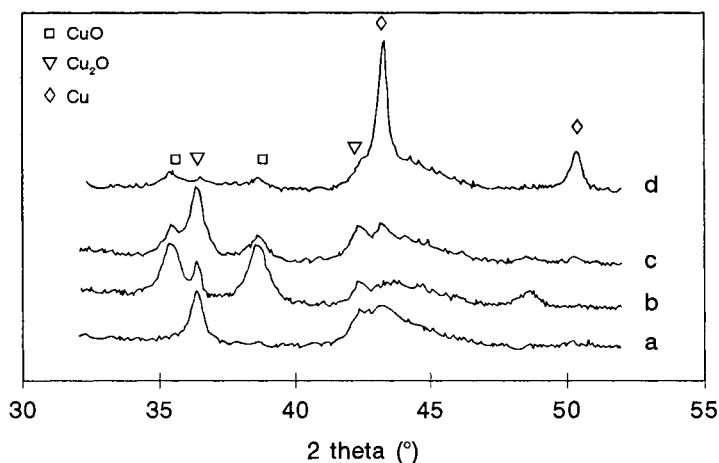


Figure 1. Copper phases detected over the Cu/HSAG catalyst after reaction under different conditions: a) He at 573 K for 2h, b) 3%NO/He at 773 K for 6h, c) 3%NO+5%O₂/He at 773 K for 6 h, d) 2%NO+2%CO/He at 773 K for 6 h.

Therefore, the high efficiency of Cu/carbon catalysts for the NO reduction by CO can be explained as due to this particular stabilization of Cu⁰ on carbon materials.

Acknowledgements

This work was supported by CAM (project no. 060/92). C.M.A. wish to thank a grant from the Comunidad de Madrid and assistance by Fundaci3n Caja Madrid.

REFERENCES

1. M. Shelef, *Chem. Rev.*, 95 (1995) 209.
2. H. Bosch and F.J.J.G. Janssen, *Catal. Today*, 4 (1988)1.
3. H. Teng, E.M. Suuberg and J.M. Calo, *Energy Fuels*, 6 (1992) 398.
4. F. Kapteijn, S. Stegenga, N.J.J. Dekker, J.W. Bijsterbosch and J.A. Moulijn, *Catal. Today*, 16 (1993) 273.
5. M. Iwamoto and H. Hamada, *Catal. Today*, 10 (1991) 57.
6. H. Yamashita, H. Yamada and A. Tomita, *Appl. Catal.*, 78 (1991) L1.
7. A. Guerrero-Ruiz and I. Rodr3guez-Ramos, *Carbon*, 32 (1994) 23.
8. C. Marquez-Alvarez, I. Rodr3guez-Ramos and A. Guerrero-Ruiz, submitted for publication.

NO REDUCTION BY ACTIVATED CARBONS. SOME MECHANISTIC ASPECTS OF UNCATALYZED AND CATALYZED REACTION

M^a J. Illán-Gómez, Angel Linares-Solano, L. R. Radovic* and C. Salinas-Martínez de Lecea.

Department of Inorganic Chemistry, University of Alicante, Spain

* Department of Materials Science and Engineering, Fuel Science Program, Penn State University, University Park, PA 16802, USA

INTRODUCTION

Because of society's increasing environmental awareness, removal of NO_x from both stationary and mobile sources has been the subject of very intense research and development efforts in the recent past. Novel burner and engine design, adsorption and thermal destruction are some of the more straightforward approaches that can be used to resolve this increasingly serious environmental problem. Catalysis is another approach, and it turned out to be quite a challenge [1,2]. The use of carbon as a reducing agent [3], catalyst [2,3], and/or catalyst support [4-12] offers obvious potential advantages, including (a) very efficient, *in situ* oxygen scavenging capability, and (b) elimination of the environmentally problematic 'slip' of the gaseous reducing agent (e.g., ammonia). The virtues of carbon-based catalysts have thus been scrutinized in considerable detail, especially during the last decade.

We have recently concluded a comprehensive study of both uncatalyzed [13] and catalyzed (alkaline, alkaline-earth, transition metals) NO reduction with activated carbons [7-11]. The objective of this paper is to summarize our current understanding of the mechanism of the NO-carbon reaction, both in the presence and absence of catalysts, as well as to reconcile our findings and conclusions, as much as possible, with those available in the literature.

EXPERIMENTAL SECTION

The details of the experimental procedures are described elsewhere [7-11,13]. Briefly, we performed both temperature-programmed reaction (TPR) and isothermal kinetic studies in a fixed-bed flow reactor. The reactor effluents were analyzed in detail by gas chromatography. The carbons used were loaded with

alkali, alkaline earth and transition metals mostly by excess-solution impregnation but also, in selected cases, by incipient wetness impregnation and ion exchange. In all cases, prior to the NO reduction experiments the samples were subjected to an *in situ* heat treatment in He, at 50 °C/min to 900 °C for 10 minutes. Metal catalyst loadings were determined in all cases by atomic absorption spectroscopy.

RESULTS AND DISCUSSION

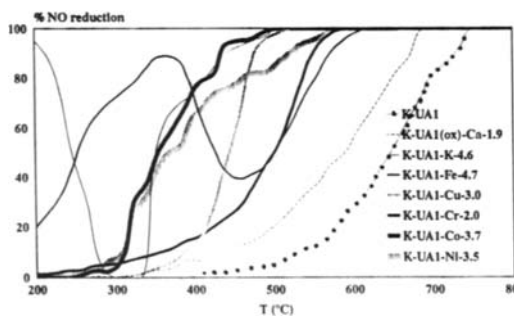


Figure 1. Temperature-programmed reaction (TPR) profiles of NO reduction for activated carbon and catalyst-loaded carbons.

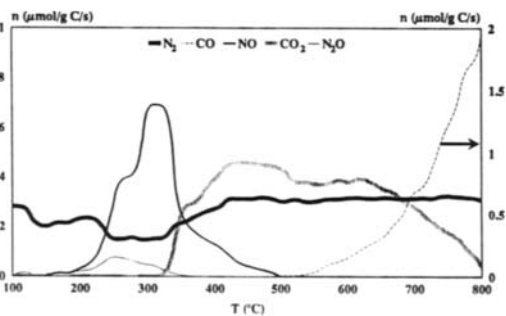


Figure 2. TPR gas composition profiles during potassium-catalyzed NO reduction.

Figure 1 shows typical TPR profiles for NO reduction with pure and metal-loaded carbons. The extent to which the metals exhibit a catalytic effect is seen to vary in a remarkable way. The temperature sensitivity of NO reduction is especially affected by the catalyst's presence. Potassium is the most effective catalyst: its presence on the carbon surface is responsible for carbon's high NO removal capability at low temperatures (~ 200 °C) and for the lowest temperature at which 100% NO reduction is achieved ($T_{100} \sim 500$ °C). Cobalt and nickel are similarly effective at 350–500 °C, even though they exhibit no activity at low temperatures. Copper is inactive at low temperatures (< 450 °C), but its high temperature sensitivity (activation energy) makes it quite effective at 450–500 °C. The behavior of iron is particularly interesting: in a way similar to potassium, it exhibits distinct low-temperature and high-temperature activity regions; in comparison with potassium, however, these regions are shifted to much higher temperatures. The TPR profiles of chromium- and calcium-loaded carbons are similar to that of the metal-free carbon; these are the least effective catalysts, exhibiting appreciable NO reduction capability only at temperatures in excess of 500 °C.

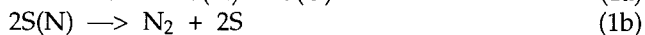
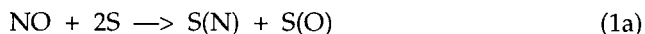
The analysis of reaction products in TPR experiments (Figure 2) clearly reveals three stages, especially in the presence of very active catalysts such as potassium. (i) In the first stage (typically, $T \leq 300$ °C), N_2 and/or N_2O are the only

products; oxygen is retained on the catalyst/carbon surface. (ii) In the second stage, N₂ continues to evolve, but CO₂ evolution occurs as well and the rate of NO reduction is enhanced. (iii) In the third stage (typically, T > 500 °C), N₂ evolution becomes constant and CO becomes the dominant oxygen-containing product.

A detailed analysis of the effects of various catalysts on the NO reduction by carbon shows that alkali, alkaline-earth and transition-metal catalysts appear to enhance NO chemisorption to different extents and intervene with varying degree of effectiveness in the oxidation-reduction (redox) cycle which shuttles oxygen from NO, via the catalyst and the carbon surface, to CO₂ and CO. This mechanism is analogous to that which is operative in other carbon gasification reactions [14]. While this NO reduction mechanism is common to all the catalysts studied, the active sites that retain and transfer oxygen to the carbon are different, depending on the nature of the chemical species involved in each case. The oxygen balances obtained from the gas evolution during TPR are helpful in suggesting the probable species involved. The proposed redox cycles are: CaO/CaO(O), K_xO_y/K_xO_{y+1}, Fe(or Fe_xO_y)/FeO(or Fe_xO_{y+1}), and Co(or CoO or Co₃O₄)/Co₂O₃. For the sake of completeness, and admittedly with little experimental evidence provided in this study, we propose that the remaining catalytic cycles are the following: Cu/CuO(or Cu₂O), Cr₂O₃/CrO₂, and Ni/NiO.

CONCLUSIONS

Under typical reaction conditions in both catalyzed and uncatalyzed NO reduction on carbon, only the following reactions involving NO seem to be kinetically significant:



In the above reactions S denotes a surface site. In the uncatalyzed reaction, this is a carbon reactive site. In catalyzed NO reduction, this is a reduced catalytic site (e.g., K_xO_y; CaO; Fe_xO_y or Fe). If the catalyst is effective in reducing the activation energy of adsorption of NO (e.g., most notably in the case of potassium), the chemisorption process can occur at low temperatures and then it is not accompanied by the formation of surface oxides. Both N₂ and N₂O can be produced at these low temperatures (reactions 1b and 2). Severe catalyst deactivation is observed, however, under these conditions which are best characterized by oxygen accumulation on the surface. The transfer of oxygen from the oxidized catalytic site (e.g., K_xO_{y+1}; CaO(O); Fe_xO_{y+1} or FeO) to the carbon is crucial for maintaining high steady-state catalytic activity (reaction 3). Upon

restoration of the reduced catalytic site, the remaining kinetically significant reactions are the same ones that characterize well the oxygen-carbon reaction (reactions 4 and 5).

The mechanism proposed above is analogous to one of the mechanisms postulated for the selective catalytic reduction by hydrocarbons [15] and also analogous to that of alkali- and alkaline-earth-catalyzed gasification of carbon.

ACKNOWLEDGMENTS

This study was made possible by the financial support from DGICYT (project AMB92-1032-CO₂-O₂) and OCICARBON (C-23-435), Spain. The thesis grant for M.J.I.G., an invited research grant to L.R.R. from Generalitat Valenciana, as well as a postdoctoral research grant to M.J.I.G. from the Ministry of Education and Science (Spain) are also gratefully acknowledged.

REFERENCES

1. Spitznagel, G. W.; Hüttenhofer, K.; Beer, J. K. In *Environmental Catalysis*; J. N. Armor, Ed.; American Chemical Society: Washington, DC, 1994; p. 172.
2. Jüntgen, H.; Köhl, H. In *Chemistry and Physics of Carbon*; P. A. Thrower, Ed.; Marcel Dekker: New York, 1989; Vol. 22, p. 145.
3. Bosch, H.; Janssen, F. *Catal. Today* **1987**, *2*, 369.
4. Kapteijn, F.; Stegenga, S.; Dekker, N. J. J.; Bijsterbosch, J. W.; Moulijn, J. A. *Catal. Today* **1993**, *16*, 273.
5. Okuhara, T.; Tanaka, K.-I. *J. Chem. Soc. Faraday Trans. I* **1986**, *82*, 3657.
6. Imai, J.; Suzuki, T.; Kaneko, K. *Catal. Lett.* **1993**, *20*, 133.
7. Illán-Gómez, M. J.; Linares-Solano, A.; Radovic, L. R.; Salinas-Martínez de Lecea, C. *Energy Fuels* **1995**, *9*, 97.
8. Illán-Gómez, M. J.; Linares-Solano, A.; Radovic, L. R.; Salinas-Martínez de Lecea, C. *Energy Fuels* **1995**, *9*, 104.
9. Illán-Gómez, M. J.; Linares-Solano, A.; Radovic, L. R.; Salinas-Martínez de Lecea, C. *Energy Fuels* **1995**, *9*, 112.
10. Illán-Gómez, M. J.; Linares-Solano, A.; Radovic, L. R.; Salinas-Martínez de Lecea, C. *Energy Fuels* **1995**, in press.
11. Illán-Gómez, M. J.; Linares-Solano, A.; Salinas-Martínez de Lecea, C. *Energy Fuels* **1995**, in press.
12. Imai, J.; Kaneko, K. *J. Colloid Interf. Sci.* **1992**, *148*, 595.
13. Illán-Gómez, M. J.; Linares-Solano, A.; Salinas-Martínez de Lecea, C.; Calo, J. M. *Energy Fuels* **1993**, *7*, 146.
14. Mims, C. A. In *Fundamental Issues in Control of Carbon Gasification Reactivity*; J. Lahaye and P. Ehrburger, Eds.; Kluwer Academic Publishers: Dordrecht, 1991; p. 383.
15. Iwamoto, M.; Yahiro, H. *Catal. Today* **1994**, *22*, 5.

ACTIVE CARBON MONOLITHS AS CATALYST SUPPORTS FOR SCR (SELECTIVE CATALYTIC REDUCTION) OF NO_x WITH AMMONIA

J. TRAWCZYŃSKI and M. KUŁAŻYŃSKI

Institute of Chemistry and Technology of Petroleum and Coal, Wrocław Technical University
50-344 Wrocław ul. Gdańska 7/9, Poland

Active carbon in the form of monoliths with "honeycomb" structure has been performed as a catalyst support. The activity of carbon supported copper, copper-chromium, chromium, and iron catalysts for reduction of nitric oxide in exhaust gases with ammonia has been investigated. The effect of chemical composition of active phase supported on active carbon on catalyst activity was evaluated. Iron based catalyst were found to be the most active for denitrogenation at low temperatures.

1. INTRODUCTION

Several techniques have been developed to reduce the nitric oxides emission. The selective catalytic reduction has been particularly extensively investigated and successfully applied in industrial practice to reduce NO_x content in flue gases of industrial boilers. Active carbon based catalysts compete against vanadia-titania based catalysts. SCR process proceeds on these latter catalyst at temperatures between 620-720 K [1]. Carbon based catalysts are active at temperatures about 360-473 K [2], so that NO_x removal is possible downstream of the flue gases desulfurization and regenerative reheating of the washed flue gases. Conventional active carbon is manufactured in the form of granules or pellets. This form of the support (catalyst) have some obvious disadvantages such as high pressure drop, sensitivity on the pollution with dust, etc. Preshaped catalysts in monolithic structures are found to have a great advantage - low pressure drop and low sensitivity on the dust included in the purified gas. We have manufactured active carbon in the monolithic form, consisting of a honeycomb array of parallel channels. The purpose of the presented paper is to examine the different types of active phases supported on the "honeycomb" shaped active carbon support.

2. EXPERIMENTAL

Active carbon in the form of monoliths of the "honeycomb" structure has been utilized as a catalyst support. Monoliths (external dimensions: 12 x 12 x 80 mm, cell parameters: 1.8 x 1.8 mm, wall thickness: 1.2 mm) made of active carbon, manufactured in our laboratories, has been used. The following parameters were characteristic for the

active carbon support elements: specific surface area 350 m²/g, pore volume 0.30 cm³/g. Catalysts were prepared by the impregnation of the monoliths with solution of selected metal salts. After impregnation catalysts were dried and heated in the inert atmosphere at the temperature of 673K. Content of the active phase is expressed by the molar ratio of carbon to active compound, C/X and catalysts on the basis of chromium, copper and iron compounds with C/X ratio of 100 and 200 were prepared. Catalysts containing combination of both copper and chromium oxides were also prepared (Cu/Cr = 1:1 (cat. C-1); 2:1 (cat C-2); 1:2 (cat. C-3)). For activity comparison catalyst containing 8% WO₃ on TiO₂ was used. Catalyst activity was tested in the reaction of the selective catalytic reduction of nitric oxide with ammonia. Catalytic activity tests were carried out using laboratory apparatus consisting of three sections: gas mixing section followed by a reactor section and a gas analysis section. The reactant gas contained equal amounts of nitric oxide and ammonia diluted in a mixture of air, nitrogen and water steam. Composition of the model gas represented composition of stack gases. Conditions of the catalyt activity test are listed in the Table 1.

Table 1.
Parameters of the measurements of the catalytic activity

Nitric oxide	1000 ppm
Nitrogen	86 %
Oxygen	8 %
Steam	6 %
Temperature	373-473 K
GHSV	3300 h ⁻¹
NO:NH ₃ ratio	1:1

2. RESULTS

The results of investigations showed that active carbon is more active as a catalyst of the reduction of nitric oxide with ammonia than typical catalyst of this reaction - tungsten oxide supported on titania (Figure 1). The latter is apparently active in much higher temperatures (620-650 K). Carbon supported catalysts can not work at such high temperatures due to quick oxidation of carbon at temperatures above 490 K.

Deposition some metal salts of active carbon support leads to very active catalysts (Figure 2 and 3). Activity of these catalysts is strongly influenced by the its chemical composition (type of metal and type of salt). Among examined catalysts the one prepared on the basis of ferrous compounds appeared to be the most active (Figure). Deposition of copper, chromium and ferrous salts leads to catalysts that show activity at relatively low temperatures in the following order: ferrous > copper-chromium > chromium > copper. At low temperatures elaborated catalysts exhibits significantly higher activity than titania supported tungsten oxide.

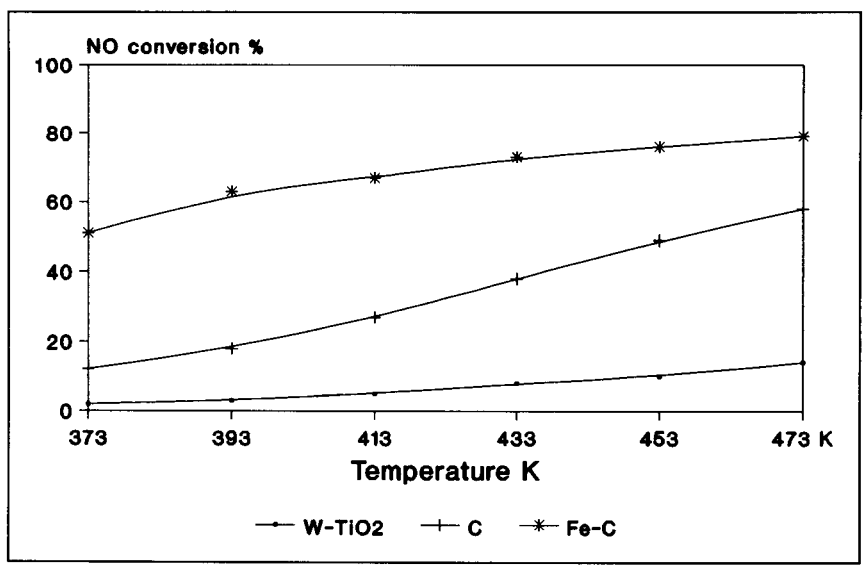


Figure 1. NO conversion as a function of temperature.

Deposition of ferrous salts on monolithic active coal support leads to the most active catalysts of nitric oxide reduction (Fig. 3). It allows to obtain over 50 % of conversion at low temperature as 373 K. Ferrous catalysts supported on inorganic oxides like alumina, silica or zirconia have been investigated in the selective reduction of nitric oxide for many years [1]. However only active carbon support enable manufacturing catalyst active at such low temperature.

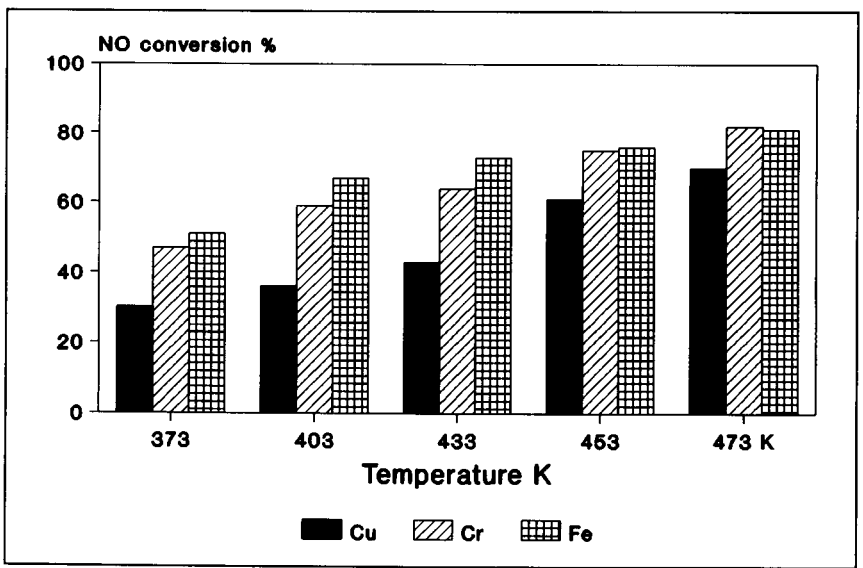


Figure 2. NO conversion on the copper, chromium and ferrous catalysts supported on monolithic activated carbon.

Mixed copper - chromium catalysts also exhibits a high NO reduction activity. Catalyst with the highest content of chromium (cat. C-3) almost complete converts nitric oxide at temperature 473 K. At lower temperature however, the highest activity exhibits catalyst C-1 containing equal amounts both metals. For catalyst C-1 we observed the almost 50 % conversion of nitric oxide at temperature 373 K. It seems that binary copper - chromium catalysts are more active than the single component copper or chromium catalysts. Copper - chromium catalysts are proposed for catalytic process of automotive emission control involving nitric oxide reduction with simultaneous carbon oxide oxidation [3].

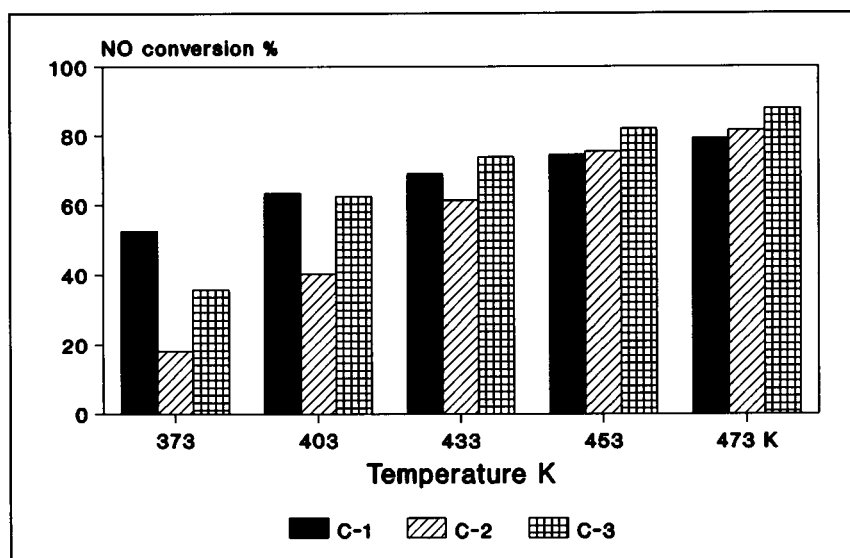


Figure 3. NO conversion on the binary copper-chromium catalysts.

The results of investigations clearly demonstrated that catalysts supported on active carbon monoliths are very active in reduction of NO with ammonia at low temperatures. Because of their advantageous properties catalysts on monolithic supports are favored over packed beds in purification of flue gases. As it was above shown monolith made of active carbon enable manufacturing very active catalyst for reduction of nitric oxides in such processes.

REFERENCES

1. H. Bosch and F. Janssen, *Catalysis Today*, 2 (1988) 431.
2. E. Richter, *ibid*, 7 (1990) 93.
3. S. STEGENGA, R. van SOEST, F. KAPTEIJN, J.A. MOULIJN, *Applied Catalysis B: Environmental*, 2 (1993) 257.

The performance of a new monolithic SCR catalyst in a life test with real exhaust gases. Effect on the textural nature.

J. Blanco^a, P. Avila^a, M. Yates^a, A. Bahamonde^a, J. Belinchon^a, E. Medina^b and A. Cuevas^b.

^aInstituto de Catálisis y Petroleoquímica (CSIC), Camino de Valdelatas s/n, Campus Universidad Autónoma, Cantoblanco, 28049 Madrid, Spain.

^bUnión Electrica Fenosa S.A., Capitán Haya 53, 28020 Madrid, Spain.

The catalysts for NO_x abatement technology in coal fired power plants are usually based on vanadia and tungsta supported on titania [1]. The catalyst described here also incorporates 50% by weight of a natural magnesium silicate, α -sepiolite, as a binder which reduces the cost of the final product. Over a 5000 h exposure period to real exhaust gases from a coal fired power plant no adverse effects on the activity or service life of the catalyst were found.

The textural stability of the catalyst after thermal treatments up to 800°C was also analysed to determine at what temperature the phase change of the titania from anatase→rutile occurred, since this greatly reduces the activity of the catalyst.

Key words: Monolithic catalyst, Selective Catalytic Reduction.

1. INTRODUCTION

In industrialised countries approximately 35% of the total nitrogen oxides emissions originate from power plants. Due to the concern for the environment, the use of Selective Catalytic Reduction (SCR) units to reduce these NO_x emissions has become not only a necessity but a legal requirement [2]. However, the average costs of these systems can be quite high [3] and thus cheaper catalysts are sought. The cost of an SCR catalyst is derived from two main sources: the cost of the primary materials or the short duration of the catalyst in operation. In this paper a less expensive monolithic catalyst which maintained good long term stability/activity is described.

2. EXPERIMENTAL

The monolithic catalyst developed for this study was fabricated from a dough containing the vanadium and tungsten salts impregnated on a titania precursor and the α -sepiolite by a method described elsewhere [4]. The monolithic catalyst was produced with a square cell shape with a cell density of 8 cells/cm². The wall thickness was 0.089 cm with an open

section of 0.070 cm^2 and cross section of 0.1253 cm^2 , giving a bulk density of 0.64 g/cm^3 and a geometric surface area of $846 \text{ m}^2/\text{m}^3$. Units of this monolithic catalyst were placed in parallel with the SCR installation of a coal fired Power Plant in a low dust configuration running at 320°C with addition of fly ash. Samples were recovered for catalytic activity and textural characterization after 500, 1000, 1500, 3000 and 5000 h respectively.

The catalytic activity measurements were made at laboratory scale in a simulated flue gas mixture in isothermal conditions, described elsewhere [5]. The test was carried out at 350°C , 900 torr pressure, Area Velocity = 7.9 Nm h^{-1} and a feed composition of $[\text{NO}] = [\text{NH}_3] = 1000 \text{ ppm}$, $[\text{O}_2] = 3\%$ with N_2 as balance. The analyses of NO and NO_2 at the inlet and outlet of the reactor were made by chemiluminescence in a Luminox 201B (BOC) and the NH_3 was determined by nondispersive infrared spectroscopy in a Luft model (ADC).

The porosities were measured by mercury intrusion porosimetry (MIP) using a Micromeritics Poresizer 9320, taking the contact angle and mercury surface tension as 140° and 480 mNm^{-1} , respectively. Nitrogen adsorption isotherms were determined on samples previously outgassed at 140°C on a Micromeritics 1310 ASAP. The surface areas were calculated using the BET method taking the area of the nitrogen molecule as 0.162 nm^2 .

Thermal gravimetric analysis (TGA) was carried out on a Netzsch STA409EP instrument in an air flow of 75 ml min^{-1} and a heating rate of 5°C min^{-1} from ambient to 1200°C . X-ray diffraction (XRD) patterns were recorded on a Philips PW1710 powder diffractometer using $\text{CuK}\alpha$ radiation ($\lambda = 0.1518 \text{ nm}$).

3. RESULTS AND DISCUSSION

3.1 Exposure to real exhaust gases

With thermal treatment at 350°C in air over the 5000 h test period the porosity and surface area of the material was unaffected, remaining at the levels of the fresh catalyst: BET nitrogen surface area of *ca.* $90 \text{ m}^2\text{g}^{-1}$ and MIP pore volume of *ca.* $0.45 \text{ cm}^3\text{g}^{-1}$. On exposure to exhaust gases the surface areas and the pore volumes were progressively reduced due to the deposition of fly ash and sulphates on the monoliths. This was corroborated by the increase in the weight loss with exposure time observed from the TG measurements in the temperature range of 700° to 1000°C , attributed to the decomposition of the sulphate species. These variations are presented in Figure 1. It should be noted that the fall in the BET surface area was more severe than the reduction in the MIP pore volume. This indicated that the major loss in area was probably due to blocking of the smaller mesopores which greatly contributed to the surface area but not to the pore volume as measured by the MIP technique.

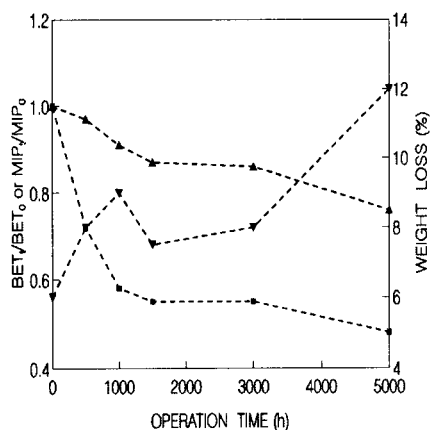


Figure 1. Change in SA_{BET} -■-, TPV_{MIP} -▼-, and Weight Loss -▲- with exposure time.

From the porosimetry curves, presented in Figure 2, it should be noted that although the total pore volumes were reduced with increasing exposure times the pore size distributions remained largely unchanged. These two findings led to the conclusions that: the deposition of the fly ash and sulphates took place mostly in the smaller mesopores of less than 6nm diameter and thus did not effect the pore size distributions; and the deposits on the external surfaces were nonporous, leading to the reduction in the total pore volumes since the results are calculated on a per gramme of sample basis.

Although reductions in the surface areas and pore volumes took place with increasing exposure time, the initially high catalytic activity was maintained practically constant over the entire 5000 h exposure period. The NO conversion of the fresh catalyst was approximately 95% with an ammonia slip of 15 ppm. Furthermore, the undesirable oxidation of SO₂ to SO₃ was negligible over the whole test at below 0.01%.

3.2 Thermal stability up to 800°C

The catalytic activity of SCR catalysts based on vanadia supported on titania is greatly reduced if the titania undergoes the phase change from anatase→rutile. This phase change has been shown to occur at *ca.* 1000°C for the titania utilised in the fabrication of these monoliths [6]. However, in the presence of vanadia the phase change takes place at lower temperatures [7]. Thus, samples of the fresh catalyst were heat treated at 500°, 600°, 700° and 800°C for 4 h and then analysed by X-ray diffraction and MIP, in order to define the thermal stability of the anatase phase. The results from these two techniques are presented in Figures 3 and 4 respectively.

From the diffractogrammes, presented in Figure 3, the higher intensities of the XRD peaks for anatase, marked A, with heat treatment from 500° to 700°C were due to the increased crystallinity of this phase. However, with treatment at 800°C the almost total absence of these peaks and the presence of those due to rutile, marked R, indicated that the phase change was almost complete.

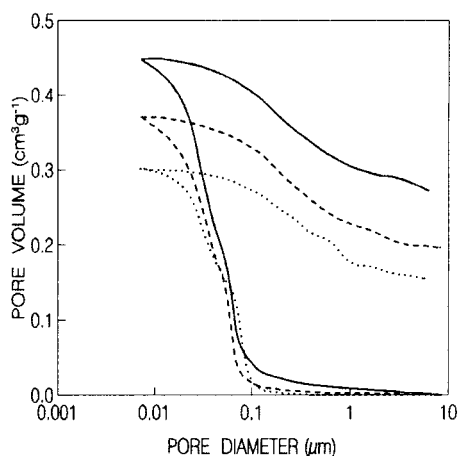


Figure 2. MIP curves of catalyst exposed for 0 h —, 3000 h - - and 5000 h ···.

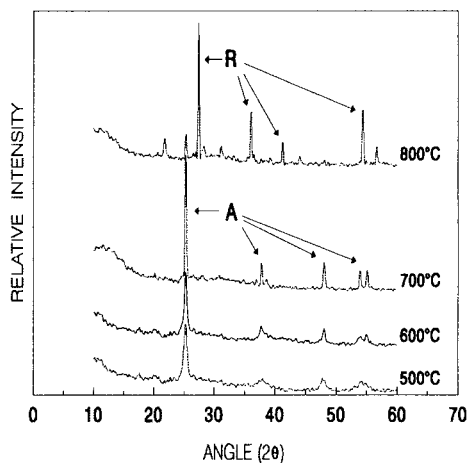


Figure 3. XRD analysis of catalyst heated at various temperatures for 4 h.

The changes in crystallinity of the titania phase with heat treatment led to variations in the porosities of the materials. From the MIP curves presented in Figure 4 these variations may be appreciated. With heat treatments between 500° to 700°C although there was a slight rise in the total pore volume, the bimodal distribution centred around pores of *ca.* 0.08 and 0.04 μm was preserved. After treatment at 800°C the anatase \rightarrow rutile phase change caused a shift in the average pore size to *ca.* 0.8 μm .

However, it should be noted that probably due to the presence of the binder the total pore volume remained practically constant for all the heat treatments, even when the titania phase underwent the phase change from anatase \rightarrow rutile.

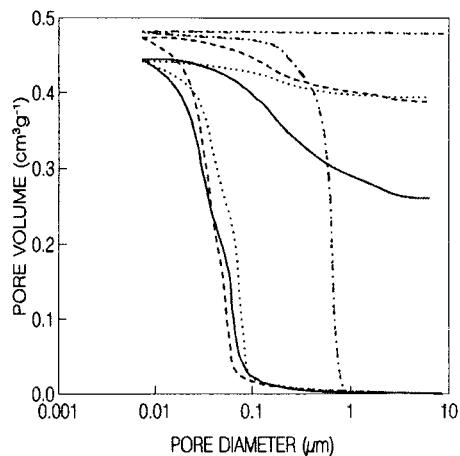


Figure 4. MIP curves of catalyst heated to 500° —, 600° --, 700° ... and 800°C ···.

4. CONCLUSIONS

From the results it may be seen that although this monolithic catalyst displayed a reduction in its surface area and pore volume, calculated on a per gramme basis, with increased exposure time to real exhaust gases during a 5000 h test, it maintained excellent performance for the reduction of nitrogen oxides with ammonia, calculated on a geometric area basis. Additionally the thermal stability up to 700°C of the anatase phase when α -sepiolite is used as a binder was also confirmed.

The results demonstrate the high potential for the adoption of this catalyst to be used commercially in the control of NO_x emissions from Power Plants. Apart from the excellent activity results over the 5000 h test period the much lower cost of the primary materials leads to economical advantages in comparison with catalysts currently in use.

REFERENCES

1. H. Bosh and F. Janssen, *Catal. Today*, 2 (1988) 369.
2. Directiva del Consejo (88/609/CEE), 24 noviembre (1988).
3. J. Blanco, P. Avila, A. Bahamonde and M. Yates, *Latin American Applied Research*, (in press).
4. J. Blanco, P. Avila, A. Bahamonde, C. Barthelemy, C. Chacón and J.M. Ramos, Spanish Patent No. 8 803 453 (1989).
5. A. Bahamonde, PhD. Thesis, Universidad Complutense, Madrid (1992).
6. J. Blanco, P. Avila, M. Yates and A. Bahamonde, Elsevier "Studies in Surface Science and Catalysis", (in press).
7. T. Machej, J. Haber, A.M. Turek and I.E. Wachs, *Appl. Catal.* 70 (1991) 115.

ECOLOGICAL ASPECTS OF DIFFERENT TYPES COAL FUEL USE

S.A.Kudashkina, E.P.Volynkina, M.B.Shkoller

"Carbonic Materials" Laboratory,Zabsib Corp.,Novokuznetsk,654043,RUSSIA

1. INTRODUCTION

One of the main sources of air pollution in large industrial cities is heat and power devices. The products of coal combustion greatly influence on environment and on man's organism. Tendency to increasing the quantity of coal used by heat power engineering makes problem of reduction of harmful substances in products of its combustion to be the most important and urgent. Such measures as coal combustion in boiling layer, pregasification, use of desulphurizing systems and selective catalitic treatment of smoke gases are known and are widely used in large industrial devises [1].

At the same time the large number of middle- and small-size boiler plants are tested in some countries using the traditional method of coal combustion in layer. The content and quantity of removals during layer method of combustion is defined to a large extent by type of fuel which is used. The change of unprepared raw coal into graded or lump coal by means of fuel briquetting limits the heat losses during its combustion in layer burners upto 40% and 60 - 90%, respectively [2], that gives the reduction in content of harmful ingredients in gaseous products of coal combustion.

In Russia the range of boiler houses with layer system of coal combustion in common number of boiler plants is more than 70% [2]. So the main part of boiler houses use the smoke coals of 50-60 - 0 mm size for the combustion (with the emission of volatile substances upto 40%) because of disadvantage of prepared - agglomerated, graded and briquetted fuel, that is the reason of high dust removals into the atmosphere, toxic and cancerous combinations.

In Novokuznetsk, being the large industrial centre of Kuznetsk coal basin the smoke coal of B grade, with emission of volatile substances upto 40% and particles content less than 6 mm in size upto 80%, is burned preferably in 167 city boiler plants, generating heat and vapour and also in house stoves. The investigation carried out by us showed that every year the boiler houses and house stoves remove 2000 tons of dust, 6000 tons of sulphur oxides and carbon each of them, 3000 tons of nitrogen oxides, 70 tons of cyanide hydrogen, 35 tons of ammonia, 7 tons of phenol and 100 kgs of 3-4-benz(a)pyrene into city atmosphere.

During this work the influences of different types of fuels, prepared from coal of B grade,traditionally used in Novokuznetsk on emission wide variety of different pollutants in process of combustion in layer were being investigated.

2. EXPERIMENTAL

Combustion of fuel is carried out on closed boiler device with layer refinement according to the method described in [3]. The procedure of the test included: fuel sample charging (10kg) at a certain thermal state of the furnace, poking in a fixed time

intervals and combustion product sampling within 60 min from the moment of charging. Pollutant concentrations in flue gases were determined according to the existing methods [4].

The following types of fuels have been investigated:

- the coal of B grade in unprepared form of 60-0 mm size;
- coal of the same grade of 60-6 mm size;
- coal of the same grade of 60-0 mm washed upto 8% of ashness (concentrate);
- coal of the same grade concentrate of 60-6 mm size;
- coal of the C grade of 60-0 mm size;
- mixture of coal of B grade with coal of C grade in ratio of 1:1 and 60-0 mm size;
- the same mixture of 60-6 mm size;
- briquettes, produced from coal of B grade with use of oil binder;
- briquettes, produced from coal of B grade with use of oil binder and Ca containing the additives;
- briquettes, produced from coal of B grade with use of coal tar;
- briquettes produced from coal of B grade with use of combined binder made of wastes from city water treatment plants, Ca containing the additives and coal tar.

Table 1 gives quality characteristics for investigated fuels.

Table 1.
Quality of fuels.

Fuel	W_a^d %	A^d %	$V_{vol}^{d,t}$ %	S^d %	$C^{d,t}$ %	$H^{d,t}$ %	$N^{d,t}$ %	$O^{d,t}$ %	Heat of combustion, mJ/kg	
									Q_c	Q_s
Coal B	2.1	16.0	40.2	0.3	83.3	6.0	2.6	7.4	23.92	34.97
Coal C	1.9	18.0	13.0	0.2	92.3	3.0	1.8	2.8	27.36	34.76
CoalB+oil binder	2.0	15.2	43.4	0.5	83.2	6.6	2.6	7.6	24.33	35.65
CoalB+oil bind.+CaO	1.7	18.6	44.6	0.5	83.0	6.5	2.4	7.9	23.37	35.43
CoalB+coal tar	2.3	18.8	39.8	0.32	82.9	5.5	2.3	8.9	22.59	33.97
CoalB+comb.bind.	2.0	21.6	39.6	0.33	81.4	5.0	2.3	11.3	21.38	32.65

3. RESULTS AND DISCUSSION

Table 2 contains the result of investigation.

It is stated that the largest quantity of deleterious substances is evolved during combustion of raw coal B of 60-0mm size, which is characterized by a high volatile matter content (40.2%). It should be noticed, that coal of such a quality is the most suitable fuel for boiler plants due to its low ignition temperature and high combustion rate.

The application of a graded coal of 60-6mm size of the same rank allows to make dust emissions 2.5 times lower and CO emissions 5 times lower; practically to make null the evolution of CH₄ and H₂; to reduce the emissions of ammonia, hydrogen cyanide, hydrogen sulphide, oxides of sulphur and nitrogen. Coal washing (upto A - 8%) reduces to some extent the emissions of CO, CH₄, H₂, ammonia, sulphur and nitrogen oxides, but does not practically influence the emissions of dust and

benzopyrene. Washed coal grading gives the possibility of reducing 4 times dust emission, of eliminating emission of CO, CH₄, and of decreasing considerably the emissions of SO₂ (7 times) and NO_x (150 times).

Table 2.

Specific emission values for combustion of different types coal fuel on closed boiler device, kg/tonne of fuel.

Fuel, size	Dust	SO ₂	NO _x	CO	C ₂₀ H ₁₂ x10 ²	NH ₃	CH ₄	C ₆ H ₅ OH x10 ²	H ₂ S
CoalB,60-0mm	52.0	30.0	45.0	178.0	198.0	0.20	30.0	2.0	10.0
CoalB,60-6mm	21.0	27.0	6.1	34.0	213.5	0.11	0	2.0	0.2
CoalB,conc.,60-0mm	50.0	13.7	8.7	58.0	199.5	0.10	1.6	1.0	0.3
CoalB,conc.,60-6mm	12.0	4.4	0.03	0	320.0	0	-	-	-
CoalC,60-0mm	7.1	11.0	0.8	9.5	2.3	0.03	0	1.0	0.4
Blend:B+C(1:1),60-0mm	32.0	-	4.0	170.0	128.0	-	30.0	-	3.0
Bend:B+C(1:1),60-0mm	11.0	19.0	0.8	1.4	21.3	0.10	0	1.0	1.0
CoalB+oil binder	46.0	28.2	7.1	130.0	235.0	0.10	5.7	2.0	2.0
CoalB+CaO+oil binder	34.0	20.0	0.2	0	14.0	0.10	0	1.0	3.0
CoalB+coal tar	15.3	10.2	4.4	46.0	1085.2	1.5	2.2	2.0	0.4
CoalB+comb.binder	1.3	5.5	1.2	0	38.8	0.08	0	1.0	0.9

There should be mentioned the tendency to some increase of benzopyrene emissions in going from raw coals to graded ones, which is observed both for unwashed fuels and for concentrates. It appears to be the result of secondary thermochemical transformations in organic coal mass inside large coal grains.

Using raw coal C instead of raw coal B, the former being characterized by a low volatile matter content (13.0%), will allow to improve considerably the ecological parameters of fuel combustion process: dust emission is to become 7 times less; CO, CH₄ and H₂ is practically vanish; the emission of benzopyrene - 86 times less; of sulphur oxides - 3 times less, of nitrogen oxides - 56 times less. Coal C, however, is characterized by a lower efficiency of combustion in spreader stokers as compared to coal B due to its low combustion rate. An essential reduction of deleterious emissions, combined with a good workability, is achieved by the application of fuels obtained from coal blends (B+C): dust emissions become 5 times less, incomplete combustion products (CO, CH₄, H₂), practically disappear, benzopyrene emissions are 10 times less, sulphur oxides emissions - 1.6 times less, nitrogen oxides emissions - 55 times less.

The tests showed, that making use of briquetted coals did not always permit to improve essentially combustion process ecology, which to a considerable extent depended not only on briquetted coal rank, but also on binder type. Thus, during combustion of briquetted coal B with oil binders dust emissions are insignificantly reduced, probably, due to intensive soot formation in the process of petroleum product destruction; the values of incomplete combustion products and sulphur oxide emissions also slightly change, and benzopyrene emissions even increase.

A considerable reduction of benzopyrene emissions is achieved, when briquettes are prepared with catalytic additives on the base of Ca (slaked lime). In this case incomplete combustion products practically disappear and emissions of sulphur and nitrogen oxides are essentially reduced.

Utilisation of hydrophobic by-products of coke production, for example, coal tar in comparison with initial raw coal allows to reduce considerably (3 times) dust emissions, to make 4 times less the emissions of incomplete combustion products, 3 times less sulphur oxides emissions and 10 times less nitrogen oxides emissions. Benzopyrene emissions, however, may essentially increase.

Finally, the application of a combined binder on basis of wastes from city water treatment plants, coal tar and Ca containing the additives gives an extra reduction of dust emissions in 502 times, NO_x - in 14 times, considerable reduction of 3-4-benz(a)pyrene and also removal of CO.

The economic calculations which have been made showed that the technology of fuel briquettes production with use of biological binder are characterized by less capital and maintenance costs than traditional technology of coal briquetting with use of oil binder mainly because of elimination of coal drying stage. In 1994 the strategy on reduction of removals from boiler plants in Novokuznetsk had been developed by us together with American specialists in sphere of power engineering, in frames of works, being carried out Project for nature protection policy and technology of USA Agency on international development according to the results of our investigations, short-term programme of worked out strategy contains the creation of experimental-industrial briquetting devices together with change of boiler devices into graded coals. Such an installation will give the possibility to work for a certain period the technology of production from smoke coal fuel of high ecological purity being suggested by us.

4. SUMMARY

So the results of carried out investigations showed that large reduction of removals of harmful substances during use of smoke coal can be achieved by its briquetting. In case of use of briquetted fuel the wide possibilities of correct regulation by formation of ecologically dangerous combinations directly during the process of combustion by addition of different kinds of admixtures into briquette composition are opened. Briquette composition developed with use of combined binder produced on the basis of wastes from city water treatment plants, coal tar and Ca containing the additives worked out by us allows to get fuel from smoke coal of sufficient mechanical durability and high ecological purity.

REFERENCES

1. D.J.Smith, Power Eng.Int., 1994, 2,N1.
2. Бунин Г.М., Теплоэнергетика, 1988, 6.
3. E.P.Volynkina, M.B.Shkoller, C.A.Kudashkina, Proc. of 7-th ICCS, September 1993.
4. Сборник методик по определению концентраций загрязняющих веществ и промышленных выбросов, Ленинград, МЕТЕОИЗДАТ, 1987.

Role of Coal Maceral Composition in Reducing Sulfur Dioxide and Oxides of Nitrogen Emissions from Pulverized Coal Flames

S. Rajan^a and J.K. Raghavan^b

^aDepartment of Mechanical Engineering and Energy Processes, Southern Illinois University at Carbondale, Carbondale, Illinois 62901-6603 USA

^bBattelle Columbus Laboratories, Columbus, Ohio USA

1. INTRODUCTION

With the wide variety of coals of different petrographic origin currently in use, a primary concern of large scale utility and industrial size coal fired plants is the acid rain precursor emissions such as oxides of nitrogen and sulfur dioxide. These emissions are influenced by fuel nitrogen and fuel sulfur content as well as combustion temperatures and combustion histories. Recent investigations have shown that the volatiles evolution and char combustion patterns are dependent not only on coal chemical composition, but also on its maceral composition. Thus, it is reasonable to expect that through a combination of effects, controlled by the petrographic distribution of fuel sulfur and nitrogen as well as the individual reactivities of the coal macerals themselves, the production histories of the oxides of sulfur and nitrogen and their final emission levels will be influenced by the coal petrographic composition. The present paper investigates these interactions.

2. EXPERIMENTAL COMBUSTION EQUIPMENT AND PROCEDURE

A number of coals were selected from the Pennsylvania State University Coal Bank, which had as far as possible the same total sulfur content and were of the same rank (high volatile bituminous). The variation in the total sulfur content of the coals was less than 6 percent. Simultaneously, it was desired to maintain the fuel sulfur content as constant as possible among the selected coals. Of the seven coals selected, the nitrogen content of three of the coals varied less than 2% while the maximum variation was 20% from the mean. The coals were also selected to provide a wide distribution in the maceral composition so that the parametric effect of these macerals could be investigated.

For comparison purposes, it is desirable to minimize the specific influence of a particular furnace design such as flow patterns, turbulence characteristics, etc. Hence, a Meker type burner capable of sustaining an unaugmented coal-dust-air flame was selected as the test apparatus over other laboratory devices. The design of the Meker burner is similar to that used by other workers (1, 2). A schematic of the test apparatus is shown in Figure 1. The test coal, ground to <325 mesh, is fed from a fluidized bed coal dust feeder and a stable coal-dust-air flame is established at the mouth of the 6.3 cm diameter burner. Gas and particulate samples were extracted at different heights of the coal flame, using a 0.46 cm, i.e., S.S. water cooled probe. Samples from the probe were carried by 0.625 cm o.d. heated Teflon tubing through in-line filters for particulate collection. The gas samples from the flame were analyzed for CO, CO₂, O₂, SO₂ and NO_x concentrations. The flame temperatures at the different positions in the flame at specified heights from the stabilizing S.S. screen, were measured using a 0.127 mm grounded Pt/Pt 13% Rh thermocouple.

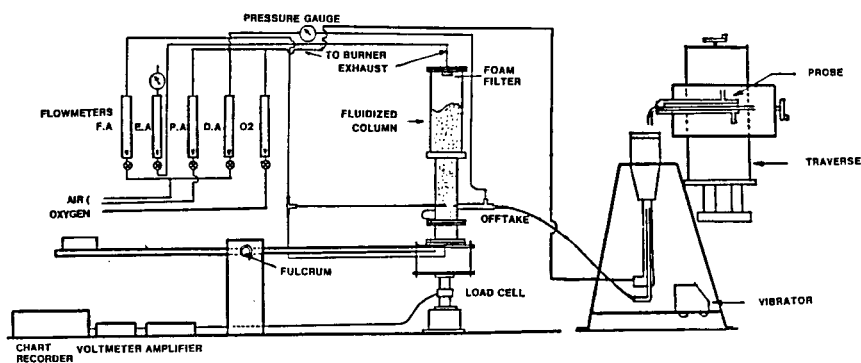


Figure 1 Schematic of Experimental Burner System

3. RESULTS AND DISCUSSION

Table 1 shows the organic maceral compositions of the coals tested. This data was supplied with the coals when purchased from the Penn State Coal Bank and was not measured in this investigation. The liptinitic macerals contain a variety of sub-maceral groups and are generally richer in hydrogen content than other maceral groups. The hydrogen content of vitrinites is intermediate between that of the liptinites and the inertinite macerals. Oxygen contents of the vitrinites are often higher than that of liptinite. The trends in hydrogen content also reflect the volatile matter content of the maceral groups. These compositional differences influence the combustion and emissions data of the coals.

Table 1 Maceral Composition of Constant Sulfur Coals (dry basis)

Sample I.D. #	Vitrinite (wt.%)	Inertinite (wt.%)	Liptinite (wt.%)	Mineral Matter (wt.%)
PSOC 828	54.2	22.3	15.9	7.6
PSOC 672	72.2	12.8	0.5	14.5
PSOC 832	51.1	20.9	18.6	9.3
PSOC 796	89.1	2.7	2.9	5.2
PSOC 831	75.6	15.2	4.7	4.6
PSOC 671	75.8	7.3	0.7	16.2
PSOC 1109	19.1	2.8	49.6	28.5

To evaluate the influence of maceral composition, the test conditions for the various coals were kept the same. To secure a stable flame at the burner mouth without oxygen enrichment, it was necessary to use a fuel rich mixture with a whole coal equivalence ratio of 3.25. The corresponding coal concentration varied from about 322 to 364 mg/liter of air. The cold gas velocity was maintained fairly constant at about 10 cms/sec.

3.1 Influence of Maceral Composition on Flame Temperature Profiles

Figure 2 shows the flame temperature profiles for three of the coals tested. PSOC 796 has the highest vitrinite content of 89.1% and nominal amounts of inertinite and liptinite. The coal with the highest liptinite content was PSOC 1109, and it has the lowest vitrinite content,

while PSOC 828 had the highest inertinite content of the coals tested. The individual temperature profiles are all highest near the flame stabilizer grid and gradually decrease at further distances downstream due to cooling and gas dispersion effects. Also, the volatiles release and combustion are most pronounced near the burner mouth.

Distinct differences may be observed in the flame temperature profiles of these coals specifically between PSOC 828 and 796 on the one hand, and 1109 on the other. Although the vitrinite contents are different, both PSOC 828 and 796 exhibit similar temperature profiles with a maximum value of around 2000°F near the burner mouth. For the first 0.5 cm, the profiles are identical; however, the temperature profile of PSOC 828, which contains a higher fraction of liptinites is higher in the 0.5 to 1.5 cm region. It was also observed that at about 3.0 cm, the temperature from the high vitrinite 796 coal was beginning to drop off more sharply. In contrast, the very high liptinite coal PSOC 1109 yielded much lower temperatures throughout the flame, which remained fairly steady and did not drop off so rapidly as compared to the other two coals.

As is generally accepted, liptinites being high hydrogen content fuels are necessary for good combustion. However, the temperature profiles indicate that too high a liptinite content may not be desirable to achieve high flame temperatures, and liptinite contents of about 5 to 10% may be the optimum value for good combustion performance.

3.2 Effect of Macerals on Combustion Characteristics

Figures 3-5 show the gaseous emissions profiles for the high vitrinite, high inertinite and high liptinite flames. Peak carbon dioxide levels for PSOC 796 and 828 are of the same order of magnitude, consistent with the temperature profiles discussed above; however, oxygen utilization for high vitrinite PSOC 796 is lower at further distances downstream. Also carbon monoxide levels are somewhat lower. For the high liptinite coal PSOC 1109, carbon dioxide levels were the lowest as seen from Figure 5, being on the order of 6%. PSOC 828 also had the highest amount of volatiles, and as observed from Figures 3 and 4, the peak carbon dioxide levels are reached closer to the burner grid, in the devolatilization region. This data suggests that a mixture of vitrinite, liptinite and inertinite in the right proportion, is more to be desired in coals in order to obtain peak combustion performance, and good carbon burnout.

3.3 Effect of Maceral Composition on Oxides of Nitrogen and Sulfur Dioxide Emissions

Figure 6 and 7 highlight the important differences resulting from maceral composition on the sulfur dioxide and oxides of nitrogen measured from the high vitrinite and high liptinite flames. Although the total sulfur content of the flames is the same, the combustion conditions as described above, result in somewhat different concentrations of these emissions from the flames. Even though the temperature is lower, PSOC 1109 produced somewhat higher sulfur dioxide levels than high vitrinite PSOC 796, Figures 6 and 7. Also the evolution profiles can be seen to be quite different. Peak values of sulfur dioxide are reached close to the end of the devolatilization region, followed by a reduction of sulfur dioxide values. This is considered to be brought about by a char reduction mechanism in the case of PSOC 796, which produces a porous char unlike that of PSOC 1109. The data further suggests that the sulfur distribution in PSOC 1109 may be highly concentrated in the volatiles fraction of the coal similar to that of 796, but without the benefit of the char reduction mechanism.

While the oxides of nitrogen profiles are similar to the sulfur dioxide profiles, PSOC 1109 exhibited higher levels of fuel nitrogen conversion than PSOC 796, even though the latter coal had slightly higher fuel nitrogen and higher gas temperatures. This suggests that in high liptinite coals, fuel bound nitrogen escapes the coal particle much easier and is converted to its oxides more readily than in high vitrinite coals. High vitrinite coals possibly retain much of the fuel nitrogen in the char mass and depend on the char burnout for complete oxidation.

REFERENCES

1. Milne, T.A. and Beachey, J.E., "The Microstructure of Pulverized Coal-Air Flame 1. Stabilization on Small Burners and Direct Sampling Techniques," *Combustion Science and Technology*, Vol. 16, 123-128, 1977.
2. Altenkirch, R.A., Peck, R.E. and Chen, S.L., "The Appearance of Nitric Oxide and Cyanide in One-Dimensional Coal Dust/Oxidizer Flames," *Combustion Science and Technology*, Vol. 20, 49-58, 1979.

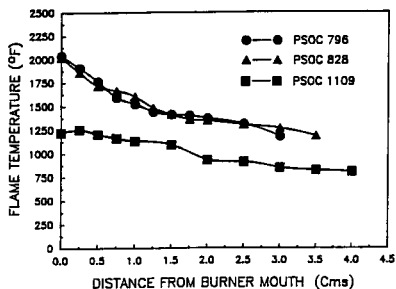


Figure 2 Measured Temperature Profiles for PSOC 796, 828 and 1109 Coals

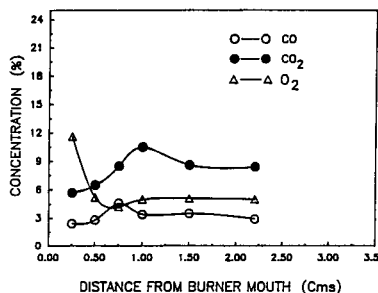


Figure 3 Carbon Dioxide, Carbon Monoxide and Oxygen Profiles for High Vitrinite PSOC 796 Coal

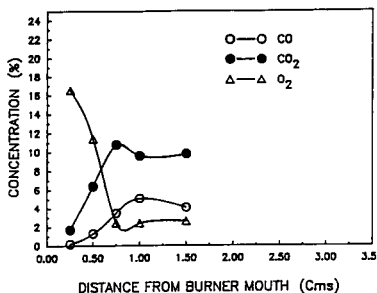


Figure 4 Carbon Dioxide, Carbon Monoxide and Oxygen Profiles for High Vitrinite PSOC 828 Coal

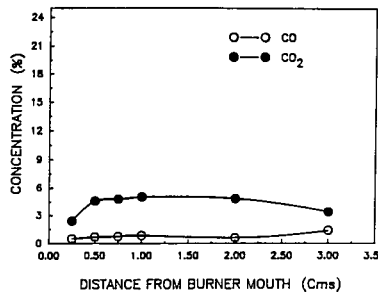


Figure 5 Carbon Dioxide, Carbon Monoxide and Oxygen Profiles for High Vitrinite PSOC 1109 Coal

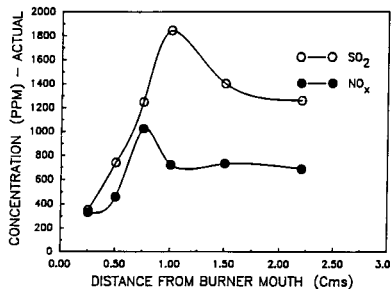


Figure 6 Sulfur Dioxide and Oxides of Nitrogen Profiles for High Vitrinite PSOC 796 Coal

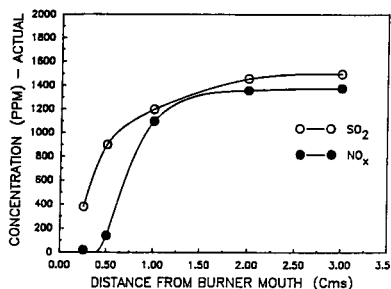


Figure 7 Sulfur Dioxide and Oxides of Nitrogen Profiles for High Liptinite PSOC 1109 Coal

Sorbent Characterization for Boiler Injection Process

J. Adánez, J.A. de Diego, V. Fierro, L.F. de Diego and F. García-Labiano

Instituto de Carboquímica (C.S.I.C.)
P.O. Box 589, 50080 Zaragoza (Spain)

1. INTRODUCTION

Sulphur dioxide emissions from coal-fired utility boilers are an important contributor to the acid rain. The injection of calcium-based sorbents into the post-flame zone are used to reduce these emissions. The main disadvantage of this process is the low calcium-utilization efficiencies due to the adverse conditions existing in the boilers: high temperature and low residence times. In this sense, the knowledge of the process, and especially the evolution of the porous system of the sorbents and its influence in their sulfation capacity, is basic for the design of the sorbent injection in pulverized-coal boilers.

In this work, the main variables affecting the sorbent sulfation have been studied through the knowledge of the sulfation conversion and the evolution of the porous system of the sorbent in different conditions.

2. EXPERIMENTAL

A drop tube system has been used to simulate the conditions existing in a pulverized coal-fired boiler, with a reacting gas mixture of 76% N₂, 15% CO₂, 2% O₂, 7% H₂O and a variable SO₂ concentration. A volumetric syringe type feeder with an entraining system for the solids, was used. The particle feeder was capable of injecting sorbent as small as 10 μm at a rate between 0.1 and 1 g/min.

The reacting mixture and the sorbent entered at the top of the reactor and passed downward through an annular 4.2 cm ID x 200 cm fused alumina reactor tube. At the gas exit line, the SO₂ and CO₂ concentration were continuously measured by two IR analyzers. The sorbents were collected in a high efficiency cyclone, which was heated to avoid the hydration of the reacted sorbent. A TG method [1] developed for the analysis of reaction products in coal combustion processes with limestone addition was used to determine the Ca(OH)₂, CaCO₃, CaO and CaSO₄ content of the sorbent after reaction. The porous system of the reacted solids was measured by N₂ physisorption at 77 K, determining BET surface areas and incremental surface areas BJH.

2.1 Materials

Five sorbents of different characteristics have been employed: 3 limestones (LIM1, LIM2, LIM3), a commercial calcium carbonate (CCC) and a commercial calcium hydroxide (CCH). Figure 1a shows the porous system of the sorbents calcined at 1000 °C, 15% of CO₂ and 1 second of residence time. Two different types of porous systems can be distinguished: LIM1, LIM2 and CCC show a porous system mainly composed by pores under 200 Å; and the CCH and LIM3 show a more widespread distribution, with pores up to 600 Å.

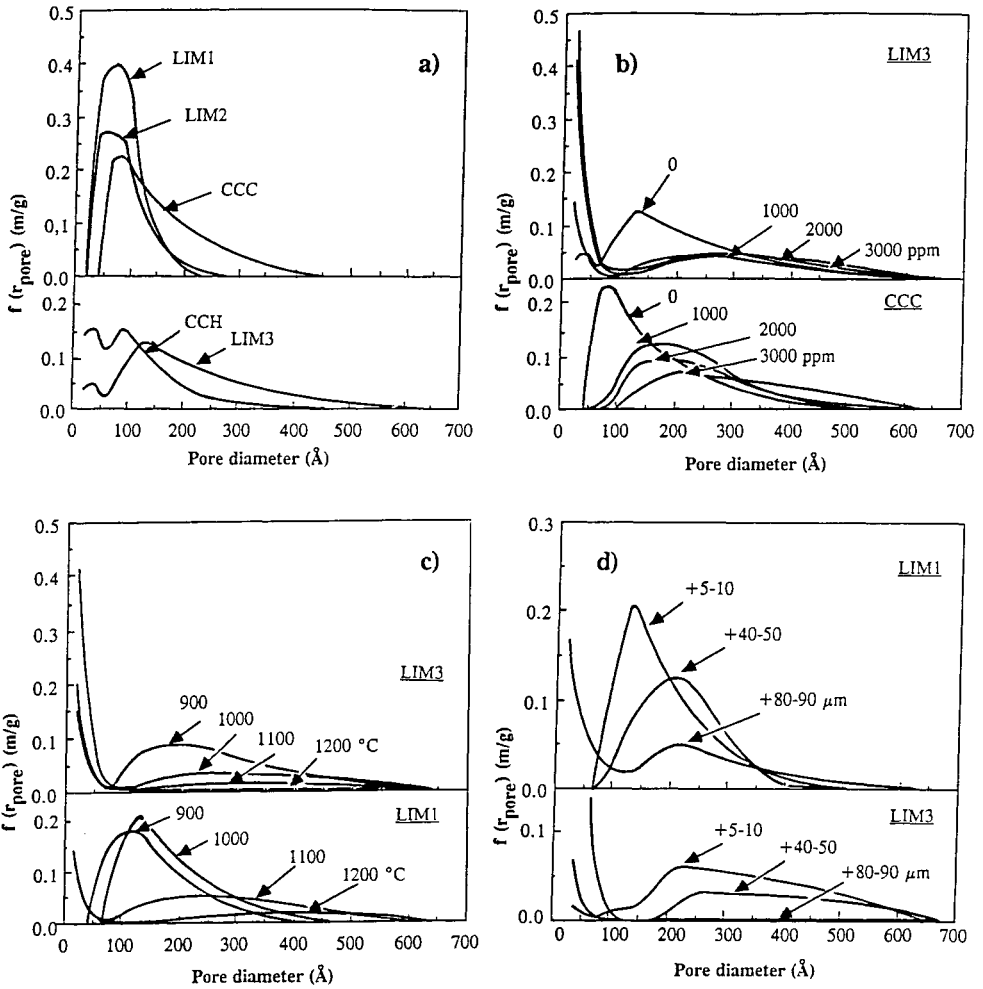


Figure 1. Evolution of the porous system of sorbents at different operating conditions.

3. RESULTS AND DISCUSSION

In addition to the sulfur conversion, important information about the processes happening inside the sorbent during sulfation is obtained when studying the porous system of the sorbent, as shown in Figure 1 for different operating variables.

3.1 Effect of the Ca/S molar ratio

The Ca/S molar ratio in the feed is a basic parameter affecting the sulfur retention in the boiler. Figure 2a shows the Sulfur Retention (SR) obtained in the reactor as a function of the Ca/S molar ratio for the five sorbents. As expected, an increase in the Ca/S molar ratio produced an increase in the sulfur retention, which was different for each sorbent used. The highest retentions were obtained with the LIM3 and CCH sorbents.

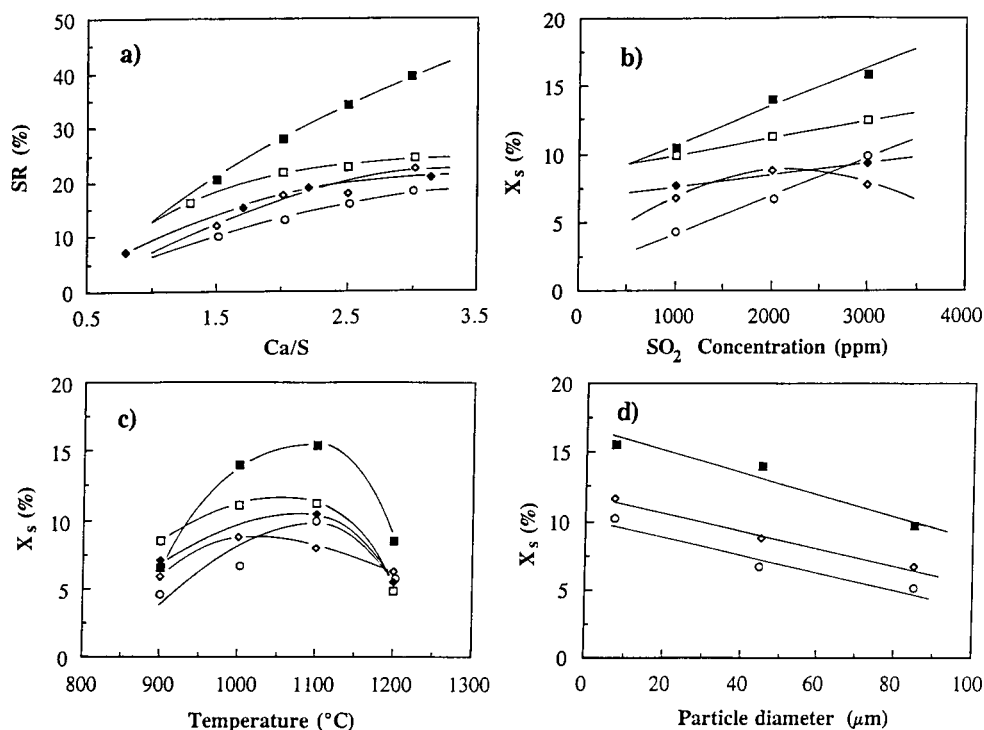


Figure 2. Effect of the operating conditions on SR and sulfur conversion.
(LIM1 \circ , LIM2 \diamond , LIM3 \blacksquare , CCC \blacklozenge , CCH \square)

3.2 Effect of the SO_2 concentration

The SO_2 concentration in the boiler will depend on the sulfur content of the coal used. In the experimental work, three different SO_2 concentrations were used: 1000, 2000 and 3000 ppm. Figure 2b shows the sorbent conversion obtained at different C_{SO_2} . An increase in the SO_2 concentration gave an increase in the sorbent conversion in all cases excepting for the LIM2 sorbent, where a maximum with the concentration was obtained.

Figure 1b shows, the density of incremental surface area BJH as a function of the pore diameter in the sulfation of the LIM3 and CCC sorbents when using different SO_2 concentrations. In the commercial calcium carbonate (CCC), a progressive decrease in the number of the smallest pores can be appreciated when increases the SO_2 concentration. This is not only due to the total pore blockage of the smallest pores but also the formation of pores of higher size by sinterization. Opositely, for the limestone LIM3, the smallest pores are becoming narrower but they never totally dissappear. This can be due to the different pore shape (plate or cilindric) formed in the different sorbents [2] [3].

3.3 Effect of the temperature

The combustion chamber temperature determines the location of the limestone injection points in the boiler, in order to achieve the maximum sorbent utilization. In the work carried out, a maximum was obtained in the sulfation conversion at temperatures between 1050 to 1100 °C, as shown in Figure 2c. These results agree with the obtained by other authors [4] [5].

Figure 1c shows the evolution of the porous system of the sorbents when working at different temperatures. For the less reactive sorbents (LIM1, LIM2 and CCC), an increase in the porous surface with the temperature was initially found due to the calcination process, decreasing later at temperatures about 1100 °C, due to the pore blockage by higher sulfation. At 1200 °C, a decrease in the density surface area was found in all the range of pore size, although some small pores are being formed by sulfate decomposition. A different behaviour was showed by the most reactive sorbents (CCH and LIM3), where a decrease in the density of surface area was found in the range of 100 to 600 Å with increasing temperature due to pore shrinking. Since small pores were found in all cases after sulfation, a dominant process of the pore shrinking over the pore blockage can be observed.

3.4 Effect of the reaction time

Low residence times (< 2 s) are normally given for the sorbent injected in pulverized coal boilers. Different processes take place inside the sorbent during this time: heating, calcination, sulfation and sinterization. The effect of the residence time, varying from 0.4 to 1.5 s, on the SO₂ retention was studied. It must be noted how about the 70% of the final sulfation is reached in the first moments of the reaction (times lower than 0.4 s).

3.5 Effect of the sorbent particle size

The sulfation capacity of a sorbent strongly depends on the particle size, because the pore blockage makes impossible the sulfation of the inner parts of the sorbent. Three particle size fractions of the limestones (LIM1, LIM2 and LIM3) were selected to study the effect of the particle size on the sulfation process: +5-10 μm, +40-50 μm, +80-90 μm.

In all cases, an increase in the particle size produced an decrease in the sulfation conversion, as shown in figure 2d. Figure 1d shows the density of incremental surface area BJH as a function of the pore diameter for different particle sizes and for two sorbents of different reactivity. For LIM1, the particle size of +5-10 μm, showed the no existence of pores smaller than 80 Å due to the pore blockage and sintering suffered during the sulfation process. The particles of +80-90 μm showed an appreciable amount of pores of small size due to the small sulfation conversion and the lower sintering time by the lower calcination conversion reached during the residence time in the reactor.

For the most reactive sorbents, as LIM3, pores of small size, under 80 Å were found for the three sizes. It must be noted the small density of incremental surface area BJH found for the +80-90 μm particles where the porous system have not yet been developed due mainly to the small calcination conversion reached at this reaction time.

4. CONCLUSIONS

A direct relation between chemical structure (calcium hydroxide-calcium carbonate) and sorbent reactivity was not found. In this way, the sorbents with a widespread pore size distribution with pores above 100 Å showed the highest reactivity and sulfation capacity, maintaining pores of small size (under 80 Å) at all times and operating conditions. In the less reactive sorbents, the pores under 80 Å became blockage during sulfation, being more sensitive to the effect of the different operating variables affecting the sulfation process.

REFERENCES

1. S.A. Mikhail, A.M. Turcotte, *Thermochim. Acta.* **166** (1990) 357
2. K.R. Bruce, B.K. Gullett, L.O. Beach, *AIChE J.* **35** (1989) 37
3. D. Beruto, L. Barco, A.W. Searcy, G.J. Spinolo, *J. Am. Ceream. Soc.* **63** (1980) 439
4. C.R. Milne, G. Silcox, D. Pershing, D.D. Kirchgessner, *I.E.C. Res.* **29** (1990)2201
5. S.J. Bortz, P. Flament, EPA-600/9-85-020b. Washington (1985)

ABATEMENT OF SO_x ON MONOLITHIC CARBON CATALYST

M. KUŁAŻYŃSKI, J. TRAWCZYŃSKI and B. RADOMYSKI

Institute of Chemistry and Technology of Petroleum and Coal, Wrocław Technical University
50-344 Wrocław ul. Gdańska 7/9, Poland

The investigation on catalytic desulfurization of flue gas model on monolithic active carbon catalysts have been performed. Active carbon in the form of monoliths with "honeycomb" structure has been performed as a catalyst support. The activity of carbon catalyst and carbon supported vanadium catalysts for flue gas desulfurization has been investigated. The effect of chemical composition of active phase supported on active carbon on catalyst activity was evaluated. Vanadium pentoxide based catalyst were found to be the most active for desulfurization at low temperatures.

1. INTRODUCTION

Active coke and active carbon are often used for desulfurization of flue gases [1-3]. For these purposes the carbon is converted into the form of grains or tablets. After the formation the processes of carbonization and activation are carried out to obtain an active carbon [4].

The application of active carbon in such a form is rather troublesome, particularly for the cleaning of gases containing considerable amounts of dust. Conventional active carbon is manufactured in the form of granules or pellets. This form of the support (catalyst) have some obvious disadvantages such as high pressure drop, sensitivity on the pollution with dust, etc. The cleaning processes for dust containing gases requires the deep dedusting and creates very high gas flow resistance throughout the catalyst bed. However, these drawbacks can be eliminated by application of carbon in the form of monolithic "honeycomb". The resultant catalyst in the form of thin-wall blocks with longitudinal channels enables very low gas flow resistance, is easy regenerable, and leads to a substantial elongation of the catalyst's life-time. Such catalysts can be effectively used for high dusty gases.

The geometry of active carbon monoliths in the form of honeycombs guarantee the highest surface at the specific volume of the catalyst. The advantages of monolithic catalyst are:

- Considerably lower butting face (catalysts of granular form should have a thin bed and a very high butting face to minimize the pressure drop through the bed),
- Elimination of plugging of catalyst's channels by the dust contained in the cleaned gas even at relatively high dust concentration,

- Operation at higher gas flow rates,
- Apparent limitation of abrasion,
- The gas flow distribution in the catalyst bed and temperature distribution is more uniform and time of residence is appropriate.

Investigation of catalytic desulfurization of the flue gas on model the monolithic active carbon catalysts have been performed. Vanadium pentoxide was used as catalyst's activators.

2. EXPERIMENTAL

Catalysts were supported on active carbon shaped in the form of monolithic honeycomb. The carries were manufactured from the coal, which was properly prepared, dried, carbonized, and then activated.

Support was prepared as rectangular blocks of the following external dimensions: 12 x 12 x 80 mm. Monoliths (cell parameters: 1.8 x 1.8 mm, wall thickness: 1.2 mm) made of active carbon, has been used. The following parameters were characteristic for the active carbon support elements:

specific surface area:	350 m ² /g,
pore volume:	0.30 cm ³ /g
density:	0.60 g/cm ³
surface area of pores with radius <5nm:	24 m ² /g

Monoliths were impregnated with oxalic acid solution of vanadium pentoxide. After the impregnation, the catalysts were dried at 386K and subsequently calcined at 773K for 4 hours in the oxygen-free atmosphere.

Following catalysts were prepared:

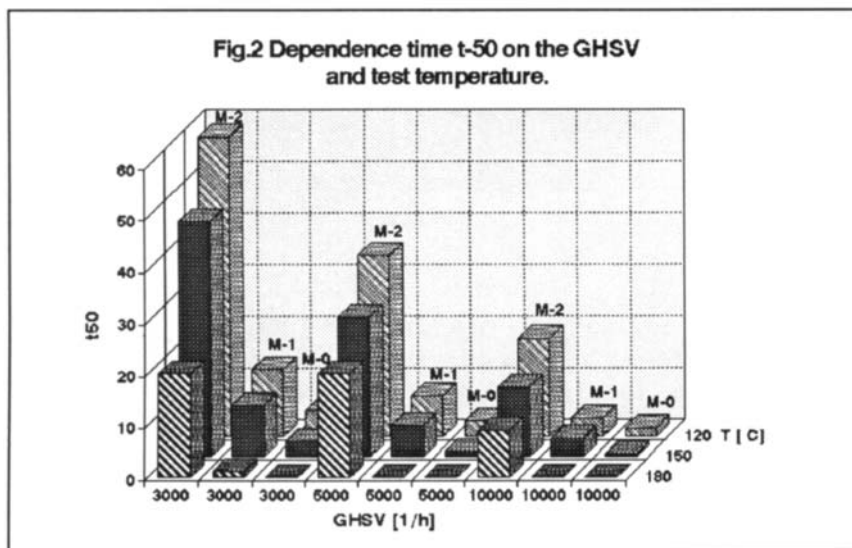
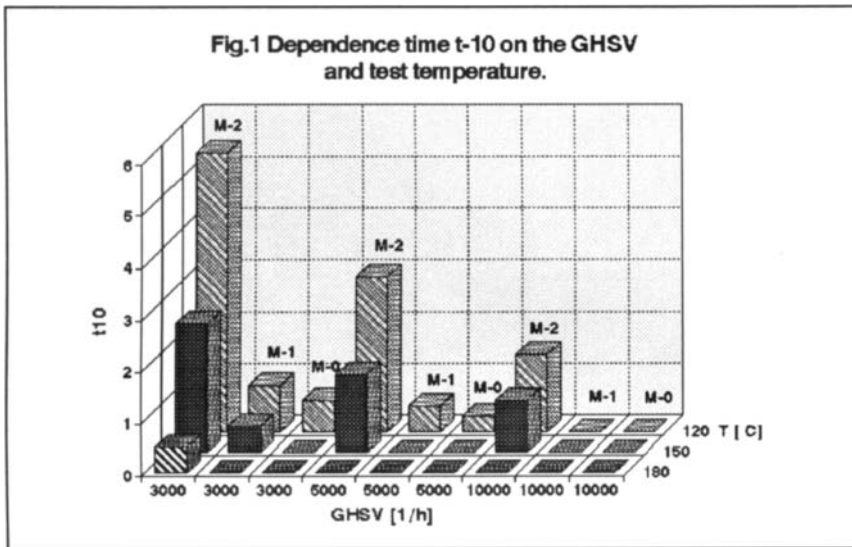
M-0 -	0% V ₂ O ₅
M-1 -	0.1% V ₂ O ₅
M-2 -	1% V ₂ O ₅

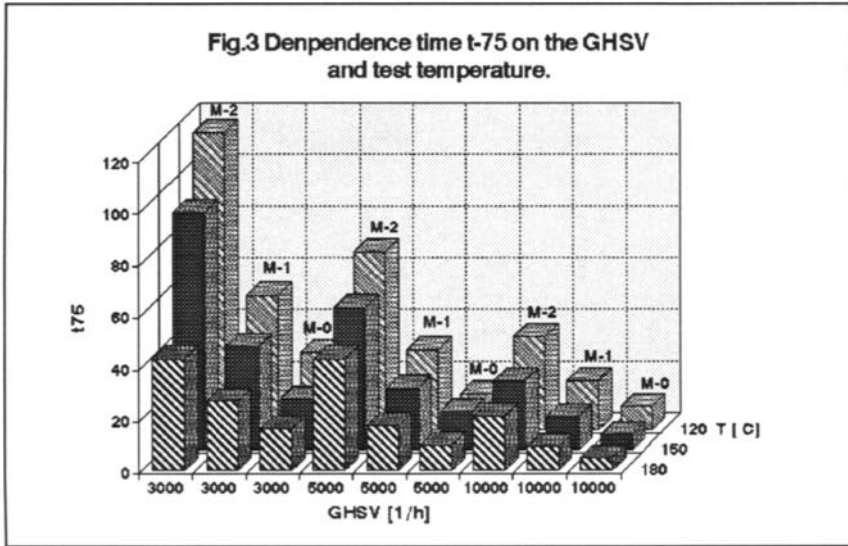
The activity in desulfurization was determined in the laboratory scale with a flow reactor. 15 cm³ of the catalyst was introduced to the electrically heated reactor. The analysis was performed using the MSI-2500 and Bacharach gas analyzers. Conditions of the catalyst activity test are listed below:

Sulfur dioxide	2000 ppm
Nitrogen	86 %
Oxygen	8 %
Steam	6 %
Temperature	393-453 K
GHSV	3000 - 10 000 h ⁻¹

3. RESULTS

The relationship between the volumetric flow rate and the sulphur dioxide content was determined for various test temperatures. The results of activity tests are given in Figs. 1, 2, and 3. They contain the data of t_{10} , t_{50} , and t_{75} (in minutes) for various volumetric flow rates and test temperatures. t_{10} , t_{50} , and t_{75} correspond to the times, when the concentration of sulfur dioxide in the outgoing gas is equal 10, 50, and 75% of the value of input concentration, respectively.





The resultant catalyst in the form of thin-wall blocks with longitudinal channels enables very low gas flow resistance, is easy regenerable, and leads to a substantial elongation of the catalyst's life-time. Such catalysts can be effectively used for high dusty gases.

The active carbon in the monolithic form of honeycomb structure is an excellent catalyst carrier for flue gas desulfurization. The structure of the new elaborated catalyst is very beneficial advantageous particularly for the desulfurization of flue gases of high dust concentration.

REFERENCES

1. E.Richter, K.Knablauch; "Aktivkoks-Verfahren der Bergbau - Forschung zur SO₂ und NO_x - Entfernung aus Feuerungsabgasen"
Haus der Technik Vortragsveroeffentlichungen **505**, 1986, 51-55
2. K.Knablauch, E.Richter; "Umweltschutz und Wertstoffgewinnung mit Kohlenstoffhaltigen Adsorptionsmitteln" Erdöl-Erdgas-Kohle, **102**, 1986, 276
3. A.Vass, T.Stor, H.P.Boehm; "Carbon-catalysed oxidation reactions",
Proc.4th Int. Carbon Conf., Baden-Baden 30.06.-04.07.1986, 411-413.
4. E.Richter, G. Ritter; "Aktivkoks und Herdofenkoks zur Reinigung von Verbrennungsabgasen", Berichte DGMK, Sept. 1990, Münster.

Effect of alkaline metal oxides on the adsorption of SO₂ by activated carbons

M.A. Alvarez-Merino, F. Carrasco-Marín and C. Moreno-Castilla.

Departamento de Química Inorgánica, Facultad de Ciencias, Universidad de Granada.
18071 Granada, Spain.

1. INTRODUCTION

Activated carbons are often used for flue gas desulphurization because of their ability to adsorb SO₂. In previous papers [1,2] we have investigated the effect of porosity and surface chemical nature of activated carbons on their capacity to adsorb SO₂ in flowing air. Results found showed that in such conditions the SO₂ adsorption process was governed mainly by a suitable developed microporosity (that which was accessible either to benzene or n-hexane) and to a less extent by an adequate surface basicity of the adsorbent as measured by HCl titration.

The objective of the present work is to ascertain the effect of different alkaline metal oxides supported on an activated carbon on its SO₂ adsorption process in flowing air and how they affect to the different SO₂ adsorption-desorption cycles.

2. EXPERIMENTAL

Activated carbon used in this study was prepared from a Spanish bituminous coal pyrolyzed in a N₂ flow at 1273 K. This sample was activated in a CO₂ flow at 1123 K for 18 h in order to get a 31% burn-off and it will be referred to in the text as A31. Different portions of this activated carbon were impregnated with aqueous solutions of nitrates of Li, Na, K, and Rb in order to obtain around 3% metal loading. The metal content of the activated carbon was determined by burning a known quantity of the sample at 773 K in a thermobalance.

All samples used were characterized by benzene adsorption at 303 K following an experimental procedure described elsewhere [3]. Prior to the adsorption experiments the samples were heated in N₂ flow up to 773 K (the initial conditions for the SO₂ adsorption experiments) in order to decompose the precursor nitrate and obtain the corresponding alkaline oxide.

The adsorption of SO₂ was followed isothermally at 298 K in a TGA equipment under dynamic conditions, by passing dry air (60 cm³.min⁻¹) containing 2 vol % SO₂ over the sample. Prior to an adsorption run, the sample was heated at 773 K in a N₂ flow (100 cm³.min⁻¹) for 5 min. The sample was then cooled to the adsorption temperature, 298 K, and the N₂ flow was changed to the air-SO₂ flow, following the increase in weight of the sample during 3 h. The amount of SO₂ adsorbed after this time, W_e, was taken as the SO₂ adsorption

capacity of the activated carbon. Once reached this time, the air-SO₂ flow was changed to N₂ and the temperature was raised to 773 K at a heating rate of 20 K.min⁻¹ to remove the adsorbed SO₂. After that, the sample was cooled to the initial adsorption temperature and a new adsorption run was carried out. This process was performed three times for each sample.

3. RESULTS AND DISCUSSION

The Dubinin-Stoeckli [3,4] equation was applied to the benzene adsorption isotherms. However, before applying this equation the experimental benzene adsorption isotherms were corrected for the adsorption on mesopores by using the Dubinin-Zaverina equation. Thus, according to Dubinin [5], for microporous activated carbons containing mesopores the experimental values, *a*, of the adsorption isotherms are composed of the adsorption in micropores, *a_{mi}*, and in mesopores

$$a = a_{mi} + S_{me} \gamma \quad (1)$$

where *S_{me}* is the surface area of the mesopores and γ the adsorption of the vapour at a given temperature per unit mesopores surface area of the adsorbent and it is obtained for benzene adsorption from equation (2)

$$\gamma = 9.16 \times 10^{-3} \times \exp\left(-\frac{A}{6.35}\right) \frac{mmol}{m^2} \quad (2)$$

where $A = RT \ln (P_0/P)$.

Table 1
Metal content and textural characteristics of samples.

Sample	Metal content (%)	<i>S_{me}</i> (m ² .g ⁻¹)	<i>W₀</i> (cm ³ .g ⁻¹)	δ (nm)	<i>L₀</i>
A31	---	116	0.22	0.106	0.79
A31Rb	2.7	88	0.20	0.120	1.07
A31K	2.4	86	0.20	0.119	1.11
A31Na	3.0	85	0.18	0.119	1.17
A31Li	2.9	86	0.18	0.120	1.31

Results obtained after applying the above equations, for *S_{me}*, the micropore volume, *W₀*, the micropore width at the distribution curve maximum, *L₀*, and the dispersion of the

micropore distribution, δ , are compiled in Table 1 for all samples used. The value of S_{me} decreases after supporting the metal oxides on the activated carbon A31 due to a partial blocking of the mesopores by the metal oxides particles, however the value of S_{me} of these samples remains constant because the different alkaline metal oxides were equally accessible to the mesoporosity. The micropore volume, W_0 , also decreases when the alkaline metal oxides are supported on A31, being this decrease higher for the smaller alkaline metals Li and Na, which makes to increase the value of L_0 from Rb to Li. This indicates that Li and Na block the smaller micropores of the activated carbon in a greater extent than K and Rb.

The SO_2 adsorption capacity of the activated carbons, W_e , are compiled in Table 2. These results show that the presence of the alkaline metal oxides does not enhance the SO_2 adsorption capacity of the samples, and even in samples A31Na and A31Li the value of W_e is lower than in the other cases, which is due to in these two samples the micropore volume, W_0 obtained from benzene adsorption is lower. Therefore, at the experimental conditions used the SO_2 adsorption capacity of samples containing alkaline metal oxides is mainly governed by the microporosity of the samples accessible to benzene as was found before for other activated carbons, which did not contain these metal oxides [2].

Table 2
 SO_2 adsorption capacity, W_e , of the activated carbons after different adsorption-desorption cycles.

Sample	W_e g SO_2 /g carbon		
	1st cycle	2nd cycle	3rd cycle
A31	0.23	0.21	0.19
A31Rb	0.23	0.20	0.18
A31K	0.23	0.20	0.18
A31Na	0.19	0.16	0.15
A31Li	0.19	0.15	0.11

In all cases, W_e decreases from the first to the subsequent adsorption cycles, presumable due to a blockage of the narrower micropores by the SO_2 molecules not released during the desorption cycles.

During the desorption step the SO_2 was desorbed at two different temperatures in the case of samples A31, A31Li and A31Na (see Figure 1 as an example), however in the case of samples A31K and A31Rb (see Figure 2) a third peak appears at higher temperatures which can be associated to a partial sulfidation of the metal oxide particles during the desorption run due to the higher basicity of the potassium and rubidium oxides.

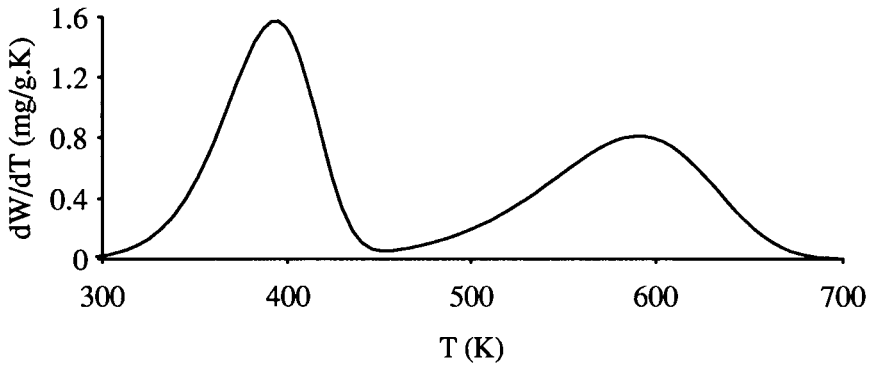


Figure 1.- Differential weight loss during the first desorption cycle of SO_2 from sample A31Na.

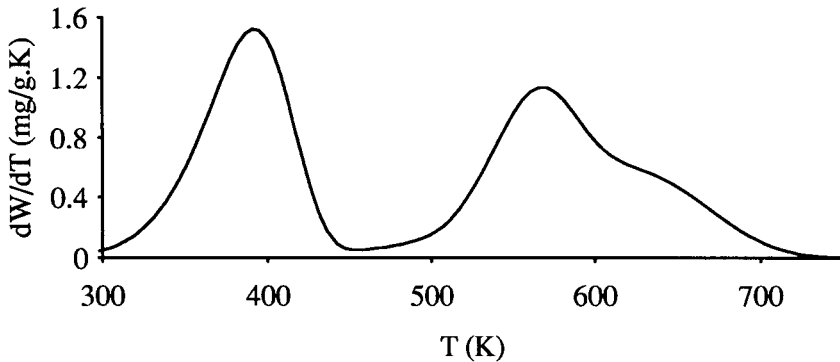


Figure 2.- Differential weight loss during the first desorption cycle of SO_2 from sample A31K.

REFERENCES

1. F. Carrasco-Marin, E. Utrera-Hidalgo, J. Rivera-Utrilla and C. Moreno-Castilla, *Fuel*, 71 (1992) 575.
2. C. Moreno-Castilla, F. Carrasco-Marín, E. Utrera-Hidalgo and J. Rivera-Utrilla, *Langmuir*, 9 (1993) 1378.
3. C. Moreno-Castilla, F. Carrasco-Marín and M.V. López-Ramón, *Langmuir* 11 (1995) 247.
4. R. C. Bansal, J. B. Donnet and F. Stoeckli, *Active Carbon*; Marcel Dekker, Inc, New York, (1988).
5. M. M. Dubinin, *Carbon*, 23 (1985) 373.

Sulfur dioxide capture by calcium containing carbon

M.C. Macías-Pérez, A. Linares-Solano and C. Salinas-Martínez de Lecea.

Department of Inorganic Chemistry. University of Alicante, Alicante, Spain.

1. INTRODUCTION

Sulfur dioxide is one of the major pollutant produced from fossil fuelled combustion sources. The addition of Ca compounds to coal combustors and flue gas desulphurisation processes (FGD) have been successfully employed in thermal power stations (1). The retention of SO₂ in gaseous streams by calcium containing samples has also being investigated in our laboratory. Previous results on the SO₂ capture by limestone have shown that there is a clear relationship between CaO dispersion and SO₂ retention at 300 °C (2). The improvement of CaO dispersion will be a challenge to reach for practical application and the use of activated carbons as supports for calcium species should be exploited with this purpose. The aim of this study is to analyze the effect of the activated carbon properties on the calcium loading, dispersion and SO₂ retention. The effect of the calcium content will be also analyzed, keeping constant the nature of the calcium precursor used.

2. EXPERIMENTAL

Two commercial activated carbons, C0 and C1, were used. Their textural characteristics were determined by physical adsorption of gases (CO₂ at 0 °C and N₂ at -196 °C). The apparent surface area and the pore volumes (micro, supermicro and mesopore) were worked out by applying BET and DR equations to N₂ and CO₂ adsorption isotherms respectively. The samples were impregnated with calcium acetate solutions to introduce different amount of Ca ranging from 3 to 20 Ca wt%. Ca content was determined by dissolving the ashes of the sample in hydrochloric acid and measuring the Ca concentration of the solution by AES-ICP. CaO dispersion was measured by CO₂ chemisorption at 300 °C after thermal treatment of the calcium-carbon samples in N₂ at 880 °C (3).

Measurements of SO₂ retention were followed by TG at 25 °C and 300 °C. About 10 mg of sample were placed in a platinum crucible. Prior to the retention run, the sample was heated at 20 °C/min to 880 °C in N₂ flow (60 ml/min) for 10 min. Subsequently, the sample was cooled to the desired temperature and the N₂ flow was changed to a gas mixture containing 0.3 vol% SO₂ in He, at the same flow rate. The amount of SO₂ retained by the sample during 1.5-2h of treatment, was determined by the increase in weight, measured after changing the reaction mixture to the N₂ flow to avoid any buoyancy effect.

3. RESULTS AND DISCUSSION

3.1 Activated carbon samples.

Table 1 compiles some characteristics of the original activated carbons. The amount of SO₂ (mg SO₂/g) retained at 25 °C (R1) and 300 °C (R2) are also included.

The SO₂ retention on the activated carbons depends on their textural properties.

Table 1. Activated carbon properties and SO₂ retention.

SAMPLE	S _{BET} (m ² /g)	V _{MC} ^a (cm ³ /g)	V _{MC+SP} ^b (cm ³ /g)	V _{MESO} ^c (cm ³ /g)	Ca wt%	mg SO ₂ /g	
						R1	R2
C0	767	0.241	0.278	0.157	1.99	30.5	14.08
C1	1656	0.230	0.631	0.31	0.39	70.23	26.38

a) V_{MICRO} is deduced applying DR equation to CO₂ adsorption isotherm.

b) V_{MICRO+SUPERMICRO} is deduced applying DR equation to N₂ adsorption isotherm.

c) V_{MESO} is deduced from the amount adsorbed from 0.2 to 0.7 relative pressure.

Sample C1 with the larger specific surface area and wider porosity exhibits the higher SO₂ retention independently of the temperature.

Conflicting reports have been published on the effect of the properties of the activated carbon. SO₂ is adsorbed onto activated carbons in two different forms (4), one weakly bonded on the surface of the carbonaceous matrix or physisorbed, and the other more strongly bonded or chemisorbed. In the former the adsorption is directly related to the specific surface area (5) or to the micropore volume (6), while in the second the chemical nature of the surface, specially basic groups (7) or the inorganic impurities are the main factors. Both processes are affected by temperature, decreasing the SO₂ physisorbed with increasing temperature. In our case, at 25 °C the physisorption process will be the main responsible for SO₂ retention while at higher temperatures (300 °C) chemisorption becomes more important. The larger calcium content originally present in both samples also contribute to the SO₂ retention at 300 °C.

3.2 Ca containing activated carbons.

The results for calcium containing activated carbons are included in Table 2. Samples nomenclature includes the activated carbon, and the maximum wt% of Ca that could be loaded from a given calcium acetate solution. The table compiles the initial calcium percentage (Ca₀ wt%), the calcium percentage after heat treatment of the sample (Ca wt%), the CaO dispersion, (d = mol CaO₂/mol CaO), and the sulfur dioxide retention values at 25 °C (R1) and 300 °C (R2), expressed as mg SO₂ per g of sample.

The calcium content of the samples (Ca₀ wt%) increases, as expected, with the concentration of the solution used. However, it reaches a maximum independently both of the concentration of the solution used to impregnate the samples and of the porosity of the activated carbon used. The maximum level, which does not reach a 10wt%, is only slightly larger for sample C1. This saturation level, which constitutes an important drawback for the present work, shows the difficulty to introduce large amounts of calcium by impregnation. CaO dispersion is quite constant for each activated carbon although slightly higher for C1 than for C0 series, probably as a consequence of the higher specific surface area of C1. As it is shown in previous publications (8), during an impregnation process with a calcium acetate solution, two sequential processes occur; first the Ca ions are ion-exchanged with the available protons of the carboxylic groups on the carbon surface. Second, if the amount of the calcium exceeds the available carboxylic groups, then the calcium loading by impregnation forces the formation of calcium acetate crystals. Therefore, the loading by a calcium impregnation process depends on the surface chemistry and on the textural properties of the carbon sample, which in turn affects dispersion as well. In general, as the Ca wt% increases there is a decrease in dispersion. However, in our case, specially in the C1 series, this is not observed presumably as a consequence of its high available surface area and high amount of

carboxylic groups.

Table 2. SO₂ retention (mg SO₂/g) on Ca containing activated carbons.

SAMPLE	Ca ₀ wt%	Ca wt%	d	R1	R2
C0-A3	4.86	5.72	0.35	29.3	37.91
C0-A5	6.51	7.80	0.36	42.8	53.88
C0-A10	8.58	11.64	0.35	71.5	88.55
C0-A15	8.75	12.17	0.33	---	88.7
C0-A20	9.03	12.37	0.31	---	86.96
C1-A3	2.90	3.5	0.40	---	38.03
C1-A5	4.45	5.71	0.38	---	50.76
C1-A10	8.33	12.15	0.41	86.02	122.97
C1-A15	9.47	14.35	0.41	---	143.52
C1-A20	9.14	13.57	0.41	---	131.6

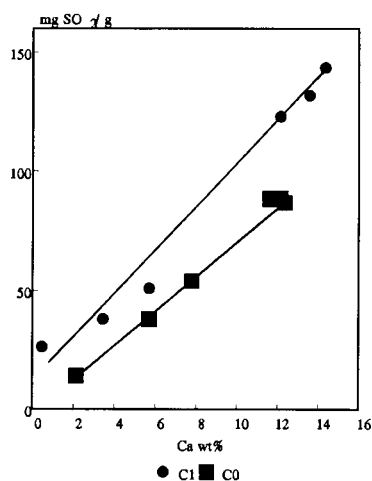


Figure 1. SO₂ retention versus Ca content.

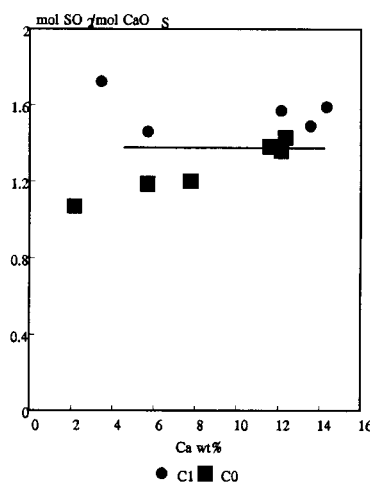


Figure 2. SO₂/CaO versus Ca content.

As can be observed in Table 2 the effect of the SO₂ retention temperature in samples with calcium is opposite to that observed on the two parent carbon samples. Upon heat treatment of the calcium containing sample prior to the SO₂ retention, the calcium compound is decomposed to CaO. Once the SO₂ contacts the CaO-carbon sample CaSO₃ formation occurs (9). Note that the SO₂ retention increases with increasing temperature as a consequence of this SO₂-CaO reaction.

The effect that calcium has on SO₂ retention is clearly observed in Figure 1, where the SO₂ uptake at 300 °C is plotted as a function of the Ca content. The SO₂ removal increases proportionally to the wt% of Ca content, being slightly higher in C1 series, probably because its wider porosity (note that this was also observed in Table 1 comparing these two samples), and also because its higher CaO dispersion. Because the CaO dispersion is practically constant for both series, the surface of CaO (CaO_s) must increase in the same proportion as does the calcium content. Thus in both cases the addition of about 10 wt% calcium increases the SO₂ retention on activated carbon by a factor of five.

Considering the retention of SO₂ as a surface process, the ratio mol SO₂/mol CaO_s should be constant and equal to 1. Figure 2 shows the evolution of this ratio as a function of the activated carbon used and of the wt% of Ca content. A constant value can be observed in both carbon series (except for the two lowest calcium content samples, presumably because lack of precision on the determination of SO₂ retention and/or CO₂ chemisorption), but the molar ratio is higher than unity which means that SO₂ is not exclusively retained in the CaO by surface CaSO₃ formation. Additionally some bulk CaSO₃ seems to form or some SO₂ may be retained at the carbon surface.

4. CONCLUSIONS

SO₂ retention for unloaded calcium samples decreases with temperature, as correspond to a physisorption process while calcium added to activated carbons considerably increases SO₂ retention at higher temperature. The retention increases linearly with calcium content and the surface of the CaO particles seems to be a factor controlling the SO₂ retention. A limiting aspect is that the amount of calcium introduced by impregnation in the activated carbons seems to reach a maximum, independently of the concentration of the impregnation solution used. This aspect needs further investigations.

ACKNOWLEDGEMENTS. The authors thanks EC (CECA -7220-ED/053), OCICARBON (C23-435) and DGYCYT (AMB92-1032-C02-02) for financial support.

REFERENCES

1. The problems of sulphur, IEA Coal Research, edited by Butterworths, U.K., 1989.
2. M.J. Muñoz-Guillena, A. Linares-Solano, C. Salinas-Martínez de Lecea, Applied Surface Science, 81 (1994) 417.
3. A. Linares-Solano, M. Almela-Alarcón, C. Salinas-Martínez de Lecea, J. Catal., 125 (1990) 401.
4. J. Zawadzki, Carbon, 25 (1987) 431.
5. P. Davini, F. Morelli, R. Tartarelli, La Chimica e l'Industria, 49, No 4 (1977) 235.
6. C. Moreno-Castilla, F. Carrasco-Marín, E. Utrera-Hidalgo, and J. Rivera-Utrilla, Langmuir, 9 (1993) 1378.
7. P. Davini, Fuel, 68 (1989) 145.
8. A. Linares-Solano, C. Salinas-Martínez de Lecea, D. Cazorla-Amorós and J.P. Joly, Energy and Fuels, 4 (1990) 467.
9. M.J. Muñoz-Guillena, M. C. Macías-Pérez, C. Salinas-Martínez de Lecea and A. Linares-Solano, Carbon 94, (1994) 508.

Simple desulfurization technology using limestone supported in coal briquette

S. Uemiya, K. Itoh, and T. Kojima

Department of Industrial Chemistry, Seikei University,
3-3-1 Kichijoji Kitamachi, Musashino-shi, Tokyo 180, Japan

The behavior of sulfurous acid gas emission from a coal briquette consisting of high-sulfur coal and limestone was studied. Sulfur retention was affected by Ca/S, surrounding temperature, and heating rate during combustion. The suitable temperature for efficient sulfur capture was 973-1073 K, while sulfur retention was not improved by the further addition of limestone beyond Ca/S of 2. Rapid heating led relatively high degrees of sulfur retention because sulfurous acid gas evolved during the combustion of volatile matter could also be captured by calcined limestone.

1. INTRODUCTION

The release of sulfurous acid gas to the atmosphere accompanied by combustion of coal leads to both severe local air pollution in developing countries and international acid rain problem. Various desulfurization processes have been constructed, but they are applied only to large scale boilers and furnaces such as power plants; therefore, development of a cost-effective countermeasure for the release from domestic and small scale use of coal is demanded.

As one of the developing countermeasures, our attention is focused on fuel briquettes consisting of coal, limestone, and their binder. Several studies have been reported on the behavior of sulfurous acid gas emission and the selection of coal and binder for a smokeless briquette [1]. The optimum mixing procedure, quantity and distribution of limestone in a briquette, however, have not been acquired yet. In this study, we intend to reveal the effects of added-Ca/S molar ratio, furnace temperature, and heating rate during combustion on the behavior of sulfurous acid gas emission from a briquette of high-sulfur coal with limestone.

2. EXPERIMENTAL

2.1. Sample

Illinois No. 6 coal and Chichibu limestone occurring in Japan were used in this study. Proximate and ultimate analyses of the coal and chemical composition of the limestone are summarized in Tables 1 and 2. A spherical coal briquette was prepared in the following manner. The coal and limestone were ground to have particle sizes below 125 and 600 μm , respectively. Weighted amounts of the coal and limestone were mixed in sufficient amount of water at room temperature. The slurry thus obtained was dried and successively molded to about 20 mm (ca. 2 g) without any binder.

Table 1
Proximate and Ultimate Analyses of Coal

Proximate (wt%, as received)	
Fixed carbon	44.3
Volatile matter	37.7
Ash	11.2
(Moisture (wt%))	6.8
Ultimate (wt%, dry)	
C	69.2
H	4.9
N	1.28
C-S	3.27
O (difference)	10.0
T-S	3.41

Table 2
Chemical Properties of Limestone

Moisture (wt%)	0.1
Ignition Loss (wt%)	35.5
Elemental(wt%)	
CaO	63.27
MgO	0.92
Al ₂ O ₃	0.28

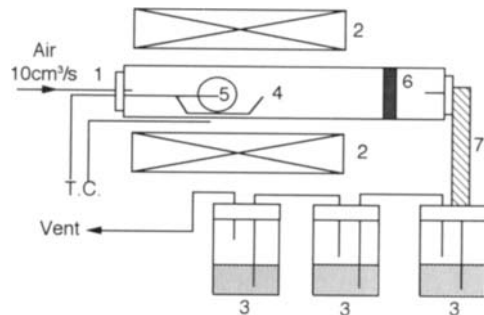


Fig.1 Experimental apparatus

1, Reaction tube; 2, Electric furnace;
3, Absorption bottle; 4, Ceramic boat;
5, Sample; 6, Quartz wool; 7, Ribbon heater

2.2. Apparatus and procedure

A schematic diagram of experimental apparatus is shown in Figure 1. To reveal the effect of heating rate on the behavior of sulfurous acid gas emission, two types of experimental procedure, abbreviated to rapid heating and constant-rate heating, were adopted. The briquette sample prepared was put onto a ceramic boat in the unheated section of a quartz reactor tube in the both cases. In case of rapid heating, the boat was moved quickly to the isothermal section kept at experimental temperature in advance and the sample was completely burnt out in a stream of air. On the hand, the furnace was not heated in advance in case of constant-rate heating. The sample on the boat was set to the central section of unheated reactor. The furnace was heated to experimental temperature at the moderate heating rate of 10 K/min. In both cases, tar was trapped by quartz wool packed in the unheated section. After the combustion of briquette, trapped tar was also burned out completely. Sulfurous acid gas in the flue gas during the combustion of the briquette and tar was absorbed in hydrogen peroxide solution and its concentration was quantitatively analyzed in Arsenazo III (C₂₂H₁₈As₂N₄O₁₄S₂)-titration method (JIS K 0103). When time variation of sulfurous acid gas emission was investigated, the hydrogen peroxide solution was periodically exchanged. Temperature at the center of a briquette was continuously measured during the combustion.

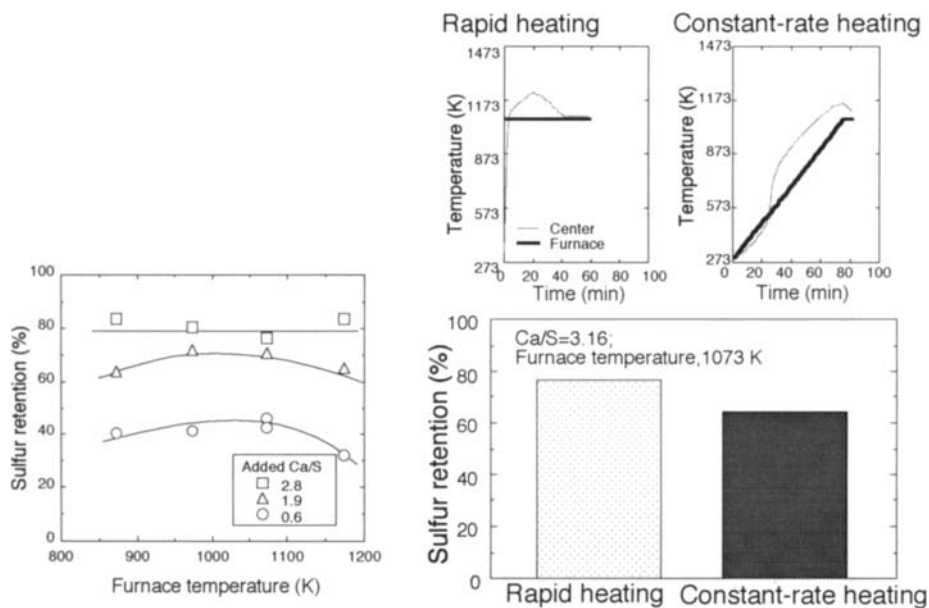


Fig.2 Effect of furnace temperature Fig.3 Effect of heating rate on the behavior of sulfurous acid gas emission and temperature during combustion.

3. RESULTS AND DISCUSSION

Figure 2 shows sulfur retention in case of rapid heating. The degree of sulfur retention increased with an increase in added-Ca/S molar ratio and attained to relatively high values, 60-70%, at Ca/S molar ratio of 1.9 in the temperature range of 873 to 1173 K. These high degrees of sulfur retention are sufficient for practical use of a coal briquette in developing countries. However, the degree attained to a plateau value, 80% beyond Ca/S of 2.

It is also found from Fig. 2 that the suitable surrounding temperature for desulfurization was around 973-1073K, which is lower than that in bubbling fluidized bed coal combustion, 1073-1173 K [2]. The suitable temperature may be dependent on the way of combustion and the type of furnace.

The effect of heating rate on sulfur retention is shown in Fig. 3. Note that rapid heating led comparatively high degree of sulfur retention. Time variations in surrounding temperature, namely furnace temperature, and in the center of briquette are also shown in Fig. 3. In case of rapid heating, temperature in the center of the briquette increased rapidly due to not only the high surrounding temperature but also the combustion of volatile matter. On the other hand, the combustion of volatile matter occurred from comparatively low temperature of around 500 K for constant-heating.

Time variation in the emission of sulfurous acid gas during the combustion for a briquette with limestone at Ca/S of 3.16 was compared with that of a briquette without limestone. The results are shown in Fig 4. From the results of the briquette without limestone, a large amount of sulfuric acid gas was evolved during 0-5 min. for rapid heating and 20-30 min. for constant-rate heating. These periods must be

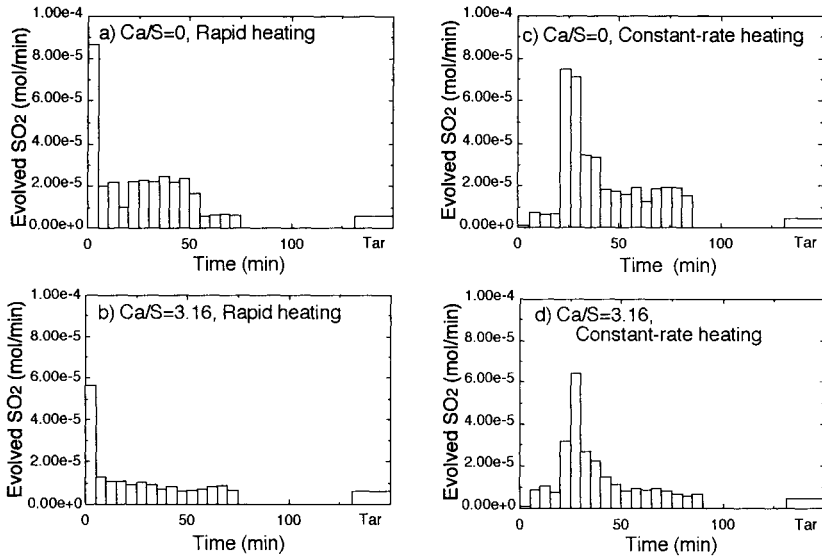


Fig.4 Time variation in sulfurous acid gas emission.
Coal weight, 2 g; Furnace temperature, 1073 K

corresponding to combustion of volatile matter, taking aforementioned findings for the temperature variation of the center of a briquette into consideration. We may conclude that most of uncaptured sulfurous acid gas was evolved mainly during the combustion of volatile matter. Thus, the difference in sulfur retention between rapid heating and constant-rate heating cases was possibly resulted from the different state of added limestone. Namely, added limestone did not calcine at the ignition stage of devolatilization in case of constant-rate heating and consequently it could not capture the sulfurous acid gas, while in case of rapid heating, limestone calcined and reacted efficiently with the sulfurous acid gas, resulting in comparatively high degree of sulfur retention.

4. CONCLUSIONS

Briquetting of high-sulfur coal with limestone depressed sulfurous acid gas emission during combustion; for instance the degree of sulfur retention attained to 78% at 1073 K and added-Ca/S of 2.8. The combustion temperature suitable for desulfurization was between 973 and 1073 K. Plenty of sulfurous acid gas was evolved during the combustion of volatile matter. When the briquette was burnt in rapid heating rate, added limestone simultaneously decomposed and captured sulfurous acid gas efficiently.

REFERENCES

1. P. Burchill, G.D. Hallam, A.J. Lowe and N. Moon, Fuel Process Technology, 41 (1994) 63.
2. M. Valk, E.A. Bramer and H.H.J. Toissant, Proceedings of the 9th International Conference on Fluidized Bed Combustion, ASME, Boston, 2, 784 (1987).

Sulphur retention in circulating fluidized bed coal combustion. Modelling and simulation.

J. Adánez, L.F. de Diego, F. García-Labiano and P. Gayán.

Instituto de Carboquímica (C.S.I.C.), P.O. Box 589, 50080 Zaragoza, Spain

1. INTRODUCTION

Circulating fluidized bed coal combustion (CFBC) with sorbent addition allows the combustion of coals of different rank even with high sulphur and ash contents in a clean way. High combustion efficiencies together with high sulphur retentions are the principal objectives to be reached.

To optimise the process and make predictions about the combustor behaviour in a broad range of operating conditions it is necessary to make a mathematical model of the process. This model was developed integrating hydrodynamic and sulfation kinetic submodels. The model was validated previously [1] with experimental results obtained in pilot plant and good fitting was found.

2. MODEL DESCRIPTION

Riser hydrodynamic was modelled taking into account previous work [2,3]. In this work the bed was divided in two regions. A dense region with constant voidage of 0.82 in which the solids present were perfectly mixed, and the dilute region, was considered with a core-annulus structure with a net dispersion of solids from the core to the annulus. The axial voidage profile in the dilute region was analysed with an exponential decay model.

To calculate the hydrodynamic properties of the bed, mean particle size and density of solids in the bed (partially sulphated limestone, coal and ashes) were used. The size distribution of ashes and limestone in the bed is calculated considering that the ashes had the same size distribution as the coal particles fed into the boiler, and then a fraction of them, P_r , had a breakage giving fines with a function of size distribution $P_f(r)|_{ash}$. With this initial assumption the mean particle size and density of the solids present in the bed were calculated and the hydrodynamic model was solved. Then, taking into account the collection efficiency of solids by the cyclone, the composition and size distribution of solids in the recirculation stream were calculated. This process was repeated iteratively until the convergence on the ash fraction in the bed was reached.

The axial solid distribution in dilute region of CFB was determined with the exponential decay model of Kunii and Levenspiel [4] modified by Adánez et al. [2] by the following equation:

$$(1 - \varepsilon) = \left[(1 - \varepsilon^*) + (\varepsilon^* - \varepsilon_{Ro}) \exp(-a h_f) \right] - K \quad (1)$$

The K constant was calculated [2] as a function of the solid circulation flux, the solid flux above TDH and the solid downward velocity. The main parameter in this model is the decay constant "a", which was calculated with the following equation [2]:

$$a (u_o - u_t)^2 D^{0.6} = 0.88 - 420 d_p \quad (2)$$

In the dilute region the solids rise through the core with a voidage ϵ_c and descend through the annulus at a velocity of 1m/s in a denser suspension. A modified Rhodes model [5] was used in which the flowrate of solids transferred from the core to the annulus is proportional to the solid concentration present in the core and to the interface surface. The solid dispersion constant was calculated as a function of the operating conditions [3]. Plug flow of gas was considered in the bed and perfect mixing to the solids.

The solution of the hydrodynamic model indicates, at each bed height, the following aspects: mean voidage, wall and core voidage, core radius, upward solids flow in the core, downward solids flow in the wall and external circulation solid flux. Then, to calculate the mean residence times of particles it is necessary to know all the solid fluxes in the system. The solid fluxes are dependent on the recovery efficiency of solids by the cyclone.

The mean residence time is defined as a function of the volume of solids in the bed (V_e), the volume of solids of size r_i ($V_e(r_i)$), the volumetric flow rate of solids leaving the fast column (v_4), and the volumetric flowrate of solids recirculated to the fast column (v_1), by the following expression:

$$\tau(r_i) = [v_4 / V_e - v_1(r_i) / V_e(r_i)] \quad (3)$$

Different SO_2 generation rates depending on the height in the bed were considered. These differences were due to differences in the char combustion rate because of the existence of axial oxygen concentration profiles due to the plug flow in the bed. Moreover, the place of coal devolatilization must be taken into account because the combustion of volatiles consumes O_2 . The model of coal combustion utilised corresponds to that proposed by Adánez et al. [6].

The SO_2 disappearance rate will depend on the SO_2 concentration in the differential element considered in each region. Moreover, the sulfation reactivity depends on the SO_2 concentration and the reaction time for each size and it is expressed by the equation:

$$dX_s / dt = K_c^0 C_{sup} \exp(-K_c^0 C_{sup} t / X_{s,max}) \quad (4)$$

In a differential element of the reactor for a SO_2 concentration and a limestone particle size, the mean reactivity for each size of limestone particle will depend on the age distribution of the limestone particles: for perfect mixing of solids in the bed $E(t)$ depends on the mean residence time using the following equation:

$$\left(\frac{dX}{dt}\right)_\phi = \int_0^\infty \left(\frac{dX}{dt}\right)_\phi E(t) dt \quad \text{where} \quad E(t) = e^{-t/\tau} / \tau \quad (5)$$

For model solving the mean conversion in the bed achieved for each limestone cut size was assumed. With these conversions the hydrodynamic submodel was solved iteratively. The axial SO_2 concentration profiles were obtained by solving the coal combustion model in CFB previously developed [6]. When the SO_2 generation rates were determined, the SO_2 retention was calculated dividing the bed into compartments (400 in dense region and 100 in dilute region). In each of them the SO_2 in the outlet was determined iteratively calculating $C_{SO_2,f}$ and the mean conversion of each limestone cut size in the compartment. The mean conversions in the bed for each limestone size were compared with those previously assumed and the process was repeated iteratively using as convergence criterion the mean conversion of each limestone cut size.

3. RESULTS AND DISCUSSION

The simulation was made considering a reactor with 6 m high and 20 cm of diameter. The

excess air was 15% with a 20% introduced as secondary air at 2.5 m high. The pressure drop in the bed was 8000 N/m^2 . A lignite with a particle size distribution less than 2 mm and a limestone with particle size distribution between 0 and 0.8 mm were used. Moreover the efficiency of solids recovery is the resultant of the standard curve of a high gas throughput cyclone.

Pressure drop: The effect of different pressure drop in the combustor have been simulated in the Figure 1, which represents the sulphur retentions (SR) as a function of the air velocity. The pressure drop is important in the retention prediction because increases the retention when increases the pressure drop, due to an increase of mean residence time of solids in the bed.

Bed height: Figure 2 shows the effect of different bed heights between 5 and 8 m on sulphur retention as a function of air velocity using the same pressure drop to combustor height ratio. It can be seen, that an increase in the combustor height gives a slight increase in sulphur retention.

Secondary air: Figure 3 shows, the SR obtained as a function of Ca/S molar ratio using different percentages of secondary air. As can be seen, an increase in percentage of secondary air shown an increase in the retention. Moreover, the effect of the introduction height of secondary air was analysed, it was found a little effect on the retention, being negligible at high velocities. From the point of view of sulphur retention, the percentage must be high inside the range studied, while heights of introduction of 2.5 m are enough in the operating conditions analysed.

Sulphur in coal: The sulphur coal content is distributed in different way between char and volatiles. For this reason the effect of the form of sulphur distribution was analysed and a poor effect on sulphur retention was found.

Besides, it was studied the effect of sulphur on SR. Figure 4 shows the SR as a function of Ca/S molar ratio using a lignite with three different sulphur contents from 3 to 9%. It was observed that for a fixed Ca/S molar ratio, it can be reached more retentions increasing sulphur contents due to the bigger SO_2 concentrations present in the bed.

Particle size distribution: The particle size distribution of the limestone fed can be very different, therefore the combustor behaviour was simulated using several Rosin-Ramler limestone feed distributions between 0 and 0.8 mm.

It has been found a great effect of the form of the particle size distributions on the sulphur retention predictions. Moreover, there is a range of values of n (2-3) which shows the best sulphur retentions in the system, because these distributions have particle sizes so large that can be recovered by the cyclones, but enough fine that can reach high particle conversions, as can be seen in Figure 5. With the bigger values of n , in which the distribution has a great proportion of coarse particles, high retentions are assured because high sulphation particle conversion are reached.

Cyclone: The effect of the recovery efficiency curve of cyclone on SR was simulated. Figure 6 shows the predicted sulphur retentions (SR) obtained when working with the different curves of the cyclone, increasing the retentions when the efficiency of the solids recovered by the cyclone increases. From these results, it can be said that the knowledge of the curve of recovery of solids by the cyclone is an important parameter in the modelling and operation of circulating fluidized bed combustors.

REFERENCES

- 1- Adánez J., De Diego L.F., Gayán P., Armesto L., Cabanillas A.: Eurotherm Seminar n° 38. Marseille (1994).
- 2- Adánez J., Gayán P., García-Labiano F., De Diego L.: Powder Tech. 81(3), 25 (1994).
- 3- De Diego L.F., Gayán P., Adánez J.: Powder Technol. (accepted).
- 4- Kunii D., Levenspiel O.: Powder Technol. 61, 193 (1990).
- 5- Rhodes M.J.: Powder Technol. 60, 27 (1990).
- 6- Adánez J., De Diego L.F., Gayán P., Armesto L., Cabanillas A.: Fuel (in press).

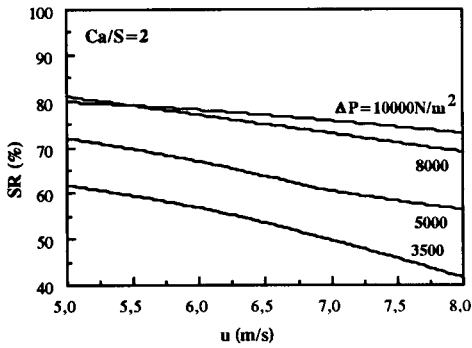


Figure 1. Effect of air velocity on sulphur retention using different pressure drops.

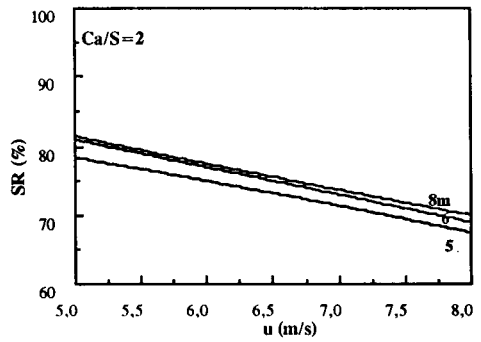


Figure 2. Effect of air velocity on sulphur retention using different bed heights.

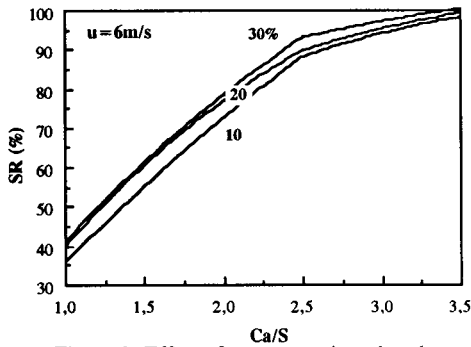


Figure 3. Effect of percentage introduced as secondary air on sulphur retention.

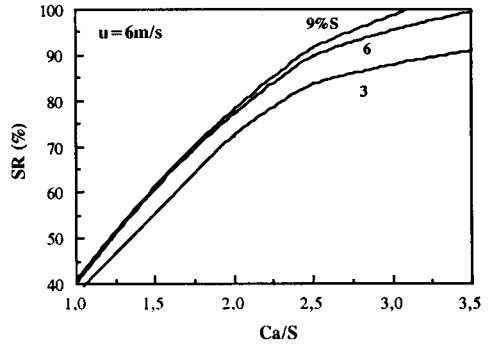


Figure 4. Effect of Ca/S molar ratio on sulphur retention using different sulphur contents.

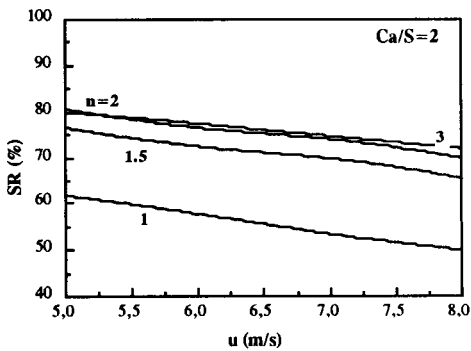


Figure 5. Effect of air velocity on sulphur retention using different particle size distributions.

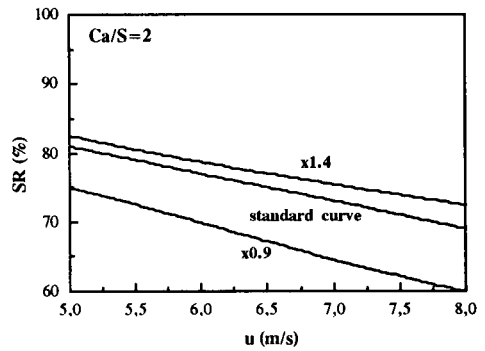


Figure 6. Effect of air velocity on sulphur retention with different curves of cyclone.

Flue gas desulfurization in a circulating fluidized bed

R. Ortiz de Salazar^a, P. Ollero^b, A. Cabanillas^a, J. Otero-Ruiz^a, L. Salvador^b.

^aCIEMAT – Tecnología de Combustión y Gasificación. Avda. Complutense 22, 28040 Madrid.

^bAICIA. Avda. Reina Mercedes s/n, 41080 Sevilla.

KEYWORDS: FGD, CFB, SO₂ abatement.

1. INTRODUCTION

In the last years major concern has been drawn upon SO₂ emissions from combustion power plants. SO₂ emission standards for new and existing coal-fired plants were introduced in the EC on 24 Nov. 1988¹. Spain, as EC member country is legally bound to meet these targets. There is a moratorium for Spain, though. It should not fully comply with the directive until 2003. Therefore, SO₂ removal from the flue gases is and will become necessary to meet environmental regulations in the future, as fuel switching, cleaning and/or blending may not be sufficient as regulations are made stricter.

Nowadays there are many ways of reducing SO₂ emissions from coal utilization: wet or dry scrubbers or slurry sorbent injection, high or low temperature processes...^{2,3} This project develops a Flue Gas Desulfurization (FGD) system using a Circulating Fluidized Bed (CFB) as a dry scrubber, taking advantage of the special gas–solid contact characteristics of this technology^{4,5}.

In a first phase a CFB pilot plant for FGD has been built up at CIEMAT, Madrid. This desulfurization system cleans the flue gases (200 Nm³/h) produced in a CFB combustor. These exhaust gases are conditioned to simulate those produced in a pulverized coal power plant. The conditioning implies adjusting gas temperature and dust load. This first phase has a duration of two years. In this paper we present the objectives and design of the operational tests.

Soon the process will be scaled to a plant of 15000 Nm³/h to be built up in a commercial power plant. The design, built-up and operational tests of this plant will be carried out during the second phase of this project.

2. OBJECTIVES

The main objective of this project is to evaluate the technology of desulfurization in a CFB at low temperature using calcium hydroxide as sorbent. This means establishing the maximum SO₂ abatement to be achieved in the plant and its

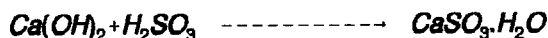
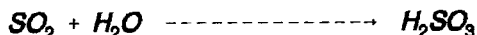
approximation to maximum solid conversion⁶, and measuring the consumption of sorbent, power and water.

The second objective, closely related to the previous, is the design of an industrial plant and the establishment of working parameters (Ca/S ratio, approximation to adiabatic saturation temperature, solid recirculation...).

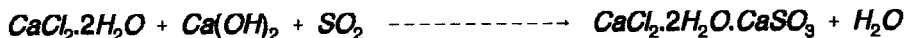
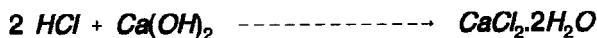
3. PROCESS DESCRIPTION

Acidic gases in the combustion effluent can be removed in a purposed designed vessel after the furnace. Post furnace sorbent injection offers great residence time and better control of gas temperature, thus enhancing sulphur capture. There is also the option of injecting water or steam to promote the reactions. The main disadvantage of this technique is that sorbents need to be more reactive and hence more expensive than those used for in-furnace desulphuration.

In this project Ca(OH)₂ will be used as sorbent in a circulating fluidized bed reactor. The flue gases leaving the combustion chamber and energy recovery circuit enter the desulphuration reactor at a relatively low temperature. Acidic gases are then removed by dry reactive particles (Ca(OH)₂) injected into the fluidised bed. The reactions that take place are:



If HCl is present it is removed by Ca(OH)₂ at a temperature > 120 C. The reaction product is very hygroscopic and cannot be handled at lower temperature. SO₂ is also removed at this temperature by the following reactions:



These reactions are temperature dependent. Generally they are more effective as the flue gas temperature approaches the adiabatic water saturation temperature.

The desulphuration resultant residues are calcium sulphite, unreacted sorbent and flyash. These residues are recirculated to improve sorbent utilisation.

4. EXPERIMENTAL PLANT

The flow diagram of the experimental plant built in CIEMAT, Madrid, is shown in

figure 1.

Flue gas entering the CFB scrubber is humidified and cooled to within 20–30°C of the adiabatic saturation temperature with a water spray. Then it flows vertically upward through the bell plate and through the bed of fresh reagent and recirculated material, where the SO₂ retention takes place. The gases leaving the reactor are cleaned of particles in the bag filter.

The solids collected in the filter are recirculated to the CFB absorber by means of a screw feeder. By this way unused sorbent remains in the process for a long residence time and conversion increases.

An electrical heater and an ash feeder are used to condition the exhaust gases produced in a CFB combustor, so that they simulate those produced in a pulverized coal power plant.

5. FUTURE ACTIONS

The cleaning performance of the CFB absorber will be evaluated at two ranges of SO₂ concentration in the flue gases: 500–1000 ppm and 2500–3500 ppm. In both cases the coals used to generate the gas are actually being used in Spanish pulverized coal power plants.

Different Ca/S ratios, approximations to adiabatic saturation temperature, solid recirculations and fluidization velocities will be tried in a factorial design. Experimental tests will begin in May 1995.

REFERENCES

1. 88/609/EC
2. Takeshita, M., Soud, H. 'FGD performance and experience on coal-fired plants', IEACR/58, IEA Coal Research, July 93.
3. Pan, Y.S. 'Recent advances in flue gas desulfurization technologies', DOE/PETC/TR-91/4.
4. Porter, D. 'Dry removal of gaseous pollutants from flue gases with the circulating fluid bed scrubber'. Low Cost Emission Control Systems Seminar, IMeChE, London, 20th Oct. 1994.
5. Keene, T.C. et al. 'The use of a circulating fluidized bed absorber for control of sulfur dioxide', AIChE Annual Meeting, Washington D.C., Nov.27– Dec. 2, 1988.
6. Irabien, A. et al. 'Kinetics of flue gas desulfurization at low temperatures: nonideal surface adsorption model', Chem. Eng. Sc., Vol.47, N°7, pp 1533–1543, 1992.

This work is supported by the ECSC and OCIDE- PIE.

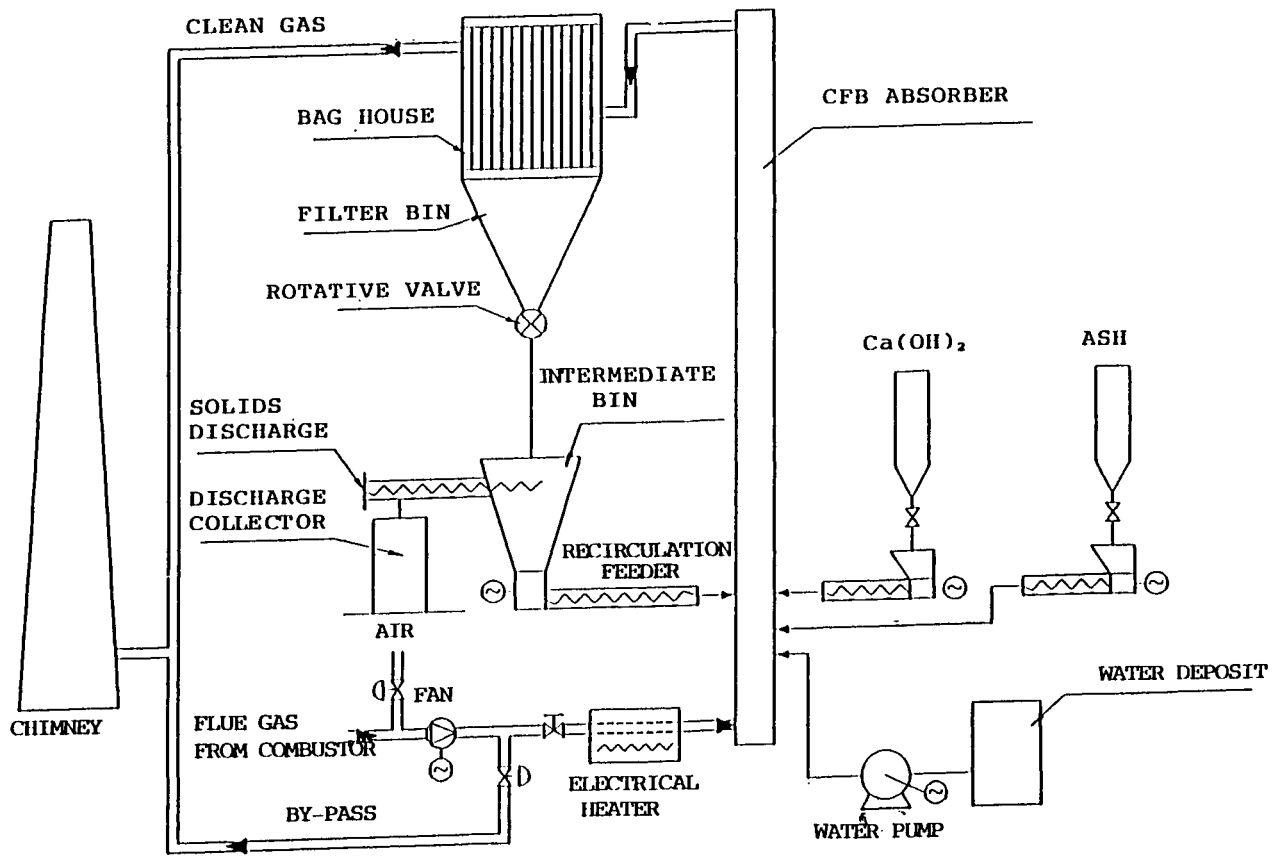


FIG. 1. CIRCULATING BED ABSORBER. FLOW DIAGRAM.

REGENERATIVE DESULFURIZATION IN COAL CONVERSION PROCESSES APPLYING THE INTERCONNECTED FLUIDIZED BED SYSTEM

O.C. Snip, R. Korbee, J.C. Schouten and C.M. van den Bleek

Delft University of Technology

Department of Chemical Process Technology, Section Chemical Reactor Engineering

Julianalaan 136, 2628 BL, Delft, The Netherlands

1. INTRODUCTION

At Delft University of Technology (DUT), synthetic sorbents have been developed for high temperature regenerative removal of SO_2 and H_2S in fluidized bed combustion of coal (FBC) and coal gasification, respectively. The work presented in this paper is focused on the development of an IFB reactor specifically for regenerative sulfur capture in FBC.

The synthetic sorbent that was developed at DUT consists of 8-9 wt% CaO , highly dispersed on a $\gamma\text{-Al}_2\text{O}_3$ carrier. The formation of calcium aluminates enables regeneration at a relatively low temperature of 850°C (combustor temperature), thereby rendering a highly integrated and energy efficient process. The sorbent was extensively tested and appeared to be technically suitable for a regenerative desulfurization process, having a lifetime of about 200 cycles under fluidized bed operation.

In order to minimize the problem of particle attrition due to high velocity collisions in conventional pneumatic transport systems, a new type of reactor is presently being developed at DUT based on IFB technology [1].

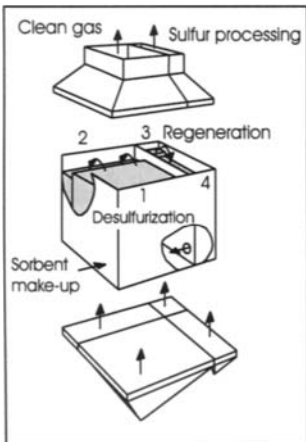


Figure 1. IFB reactor.

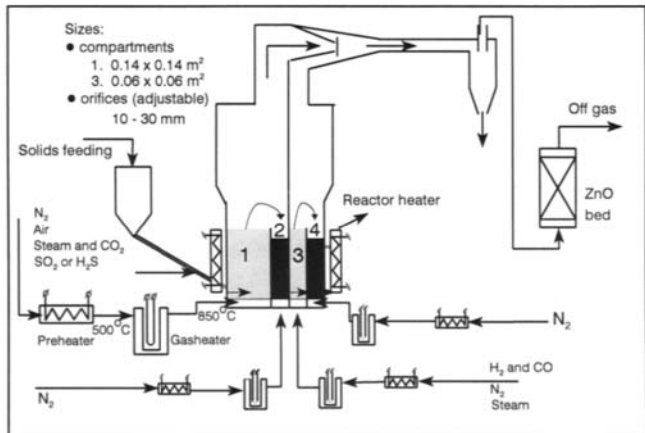


Figure 2. Schematic view of the IFB pilot plant.

The IFB reactor consists of four compartments (Figure 1): two chemical reactors (combustor

and regenerator) and two transport compartments. Differential aeration is applied to supply the driving force for solids circulation. Next to cold models for hydrodynamic studies, an IFB pilot plant (Figure 2) was designed and constructed at DUT to investigate process performance at various operating conditions. Coal combustion is simulated by feeding a specified mixture of gases at the operating temperature to the reactor. The sorbent is regenerated in a mixture of reductive components (H_2 and CO) in nitrogen.

2. IFB MODEL

A model predicting overall reactor performance was set up, integrating hydrodynamic and chemical sub-models. First, the Circulation Rate of Solids (CRS) is calculated as a function of the hydrodynamic parameters. Then the calculations are performed for the sulfur capture and regeneration process, resulting in a prediction of the overall sulfur retention of the IFB pilot plant as currently operated at DUT. In the following sub-sections, the individual sub-models are shortly presented.

2.1 Hydrodynamics

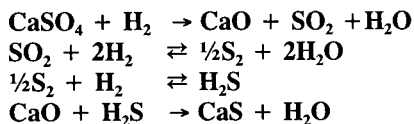
In an earlier paper a hydrodynamic IFB model was developed and verified. This model predicts the solids and gas flow from a dense bed through an orifice into a lean bed. Thereby, it is possible to calculate the CRS as a function of hydrodynamic parameters such as fluidizing velocities, characteristic dimensions of the IFB system and particle properties. For a full derivation of the model, experimental verification and model sensitivity analysis, the reader is referred to Korbee *et al.* [1].

2.2 Sulfur capture and regeneration

Both sulfur capture and regeneration are modelled on the basis of a few assumptions concerning the hydrodynamics of the fluidized compartments 1 and 3. It is assumed that the gas and solids phases are ideally mixed. This assumption holds for both solids and gas phase due to the relatively large sorbent particles used in the pilot plant facility (and generally in FBC) resulting in a slugging and/or slow bubbling regime with relatively good mixing and contact between both phases.

The sulfation is assumed to proceed through the formation of SO_3 and is further described by an unreacted shrinking core model, the SURE2 model [2]. In this model, the rate of sulfation is assumed to be first order in the SO_3 concentration at the core radius and first order in the outer surface of the core. The model adequately predicts the sorbent sulfation behaviour and is based on experimental work in different reactor equipment.

The kinetic model for the regeneration is based on two gas-solid reactions and two gas phase equilibria:



The regeneration reactions are considered to be first order in the outer surface area of the sorbent particles and first order in the gas concentrations [4]. The appropriate kinetic parameters were obtained from fluidized bed regeneration experiments.

3. RESULTS

The results presented in this paper are obtained as an operational analysis of the experimental facility in Figure 2. The sorbent main properties are: $\rho_p = 1400 \text{ kg/m}^3$ and $d_p = 2 \text{ mm}$. With respect to hydrodynamics, the results are expressed in terms of the Circulation Rate of Solids. It is shown that desulfurization is directly related to IFB hydrodynamics.

3.1 Hydrodynamics

A thorough discussion of the influence of the hydrodynamics on the CRS is found in Snip *et al.* [3]. The hydrodynamics are only briefly explained here and aim to give an understanding of IFB principles.

The size of the connecting orifice is found to have an important influence: increasing the size of the orifice clearly results in higher solids flows (Figure 3), with a maximum solids flow at the conditions of minimum fluidization in the dense bed.

Other important considerations are the bed heights in the IFB system and the height at which the orifice is inserted between the separating wall. In Figure 3 it is further shown that in a given IFB reactor, the CRS can be controlled by the gas velocity in the dense bed (transport bed).

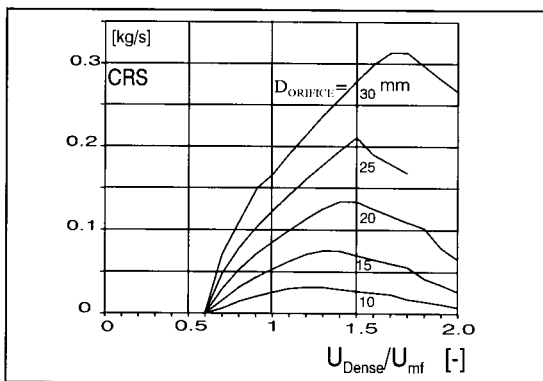


Figure 3. Solids flow vs. gas velocity in dense bed, for indicated orifice diameters.

3.2 Desulfurization

For different inlet SO_2 concentrations (corresponding to 1-3 wt% sulfur in the coal), the sulfur retention (fraction of sulfur captured) was calculated as a function of CRS (Figure 4). The input parameters are chosen in such a way that regeneration of the sorbent is not rate-limiting in the process. Obviously, sulfur retention is enhanced with increasing sorbent circulation since the latter corresponds to increasing the Ca/S ratio.

At a low CRS, the influence of an increasing sorbent flow is strong, while at higher CRS, sulfur retention diminishes to a nearly constant value. This is explained by the fact that the sulfur capture rate is assumed to be dependent on the degree of sulfation of the sorbent. Therefore at higher

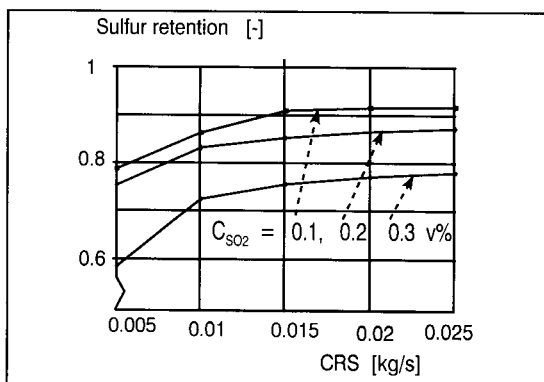


Figure 4. Calculated sulfur retention versus CRS, in IFB pilot plant.

sorbent conversion (low CRS), the influence is stronger.

These results show that the influence of the hydrodynamic parameters is translated to the CRS-dependency of sulfur retention and therefore can be used to comply with process requirements. This is done either in the design of an IFB system or by means of operation :

IFB design

The size of an orifice clearly influences IFB performance: increasing the size of the orifice (increasing CRS while keeping operational parameters constant) will result in a higher sulfur retention, with the previously described limitations at high sorbent conversion. Increasing the height of the inserted orifice will result in a decreasing CRS and consequently a lower sulfur retention. All hydrodynamic parameters should be carefully chosen in order to fulfil the requirements of the process.

IFB operation

The most important operating parameter is the aeration rate of one of the dense beds. Adjusting the gas velocity (preferably operating the dense bed in a de-fluidized, moving-bed mode) allows control of the CRS and therefore sulfur retention.

4. CONCLUSIONS

A mathematical model is used for an operational analysis of the DUT IFB pilot plant facility. The influence of hydrodynamic parameters on the CRS and subsequently on the sulfur retention is determined. Orifice dimensions and position (height in the separating wall) greatly influence the CRS. The size can be chosen in such a way that the attainable range of CRS (controlled by the rate of aeration of one of the transport beds) meets the process requirements. The modelling results show that the IFB system can be effectively used in a regenerative desulfurization process. The results and conclusions will be experimentally verified in the DUT IFB facility in an extensive experimental program to increase insight in the regenerative desulfurization process carried out in an IFB reactor. This will allow optimal design of future facilities of commercial scale.

REFERENCES

1. Korbee, R., Snip, O.C., Schouten, J.C., Van den Bleek, C.M., Chem. Eng. Sci., 49 n. 24B (1995) 5819.
2. Wolff, E.H.P., A.W.G. Gerritsen, Van den Bleek, C.M., Canadian Journal of Chemical Engineering, 71 (1993) 83.
3. Snip, O.C., Korbee, R., Schouten, J.C., Van den Bleek, C.M., AIChE Annual meeting, Preprints on Fluidization and Fluid-Particle Systems, San Francisco (1994).
4. Korbee, R., Grievink, J., Schouten, J.C., Van den Bleek, C.M., Proc. 12th Int. Conf. on Fluidized Bed Combustion, San Diego, USA, 1143 (1993).

ACKNOWLEDGEMENT

The authors wish to acknowledge the financial support from the Commission of the European Communities (contract no. JOUF-CT91-0063 (DTEE)) and the Delft University Stimulation fund 'Beek' (contract no. 1-71925).

Laboratory testing of different SO₂ sorbents for dry sorbent injection

A. B. Fuertes and M. J. Fernandez

Instituto Nacional del Carbón, C.S.I.C., Apartado 73, 33080-Oviedo

1. INTRODUCTION

Dry sorbent injection technology (DSI) is a relatively recent alternative to wet scrubbing and spray drying. In general three DSI approaches have been extensively investigated [1]: i) Furnace injection of calcium-based sorbents (limestone or hydrated lime at a temperature region of around 1200°C), ii) Low temperature (70-100 °C) duct injection of hydrated lime at high relative humidity and iii) Low temperature (120-175°C) duct injection of sodium-based sorbents (i.e. sodium carbonate and sodium bicarbonate). Recently, especial attention has been given to injection of different kinds of sorbents in the flue gases at temperatures around 400-600°C [2, 3]. The sorbent injection in this temperature window (existing in the economizer) avoids the problems derived from the impact of sorbent particles on tube banks and allows the utilization degree of some sorbents to be improved.

This paper reports results of different tests for several candidate sorbents to be used in the 300-600°C temperature window. Especial emphasis is placed in the analysis of the sulfation of sodium carbonate at different temperatures and SO₂ concentrations.

2. EXPERIMENTAL

The experiments were performed in a fixed bed reactor using a simulated combustion gas mixture. The fixed bed reactor is a vertical packed bed formed by sorbent particles dispersed in silica sand. The entire bed is supported on a 2 cm diameter fritted quartz plate contained in the quartz cylinder. The main characteristics of the fixed bed reactor and experimental conditions are given in Table 1. For these experimental conditions, the Peclet number values for this fixed bed reactor are in the range of 70-100. This suggests that the effect of gas dispersion can be neglected so that a plug flow model is a reasonable assumption.

Eight classes of sorbent have been tested: Calcium hydroxide (HCa), calcium acetate (ACa), dolomite (D), magnesium hydroxide (HMg), magnesium acetate (AMg), sodium acetate (ANa), sodium bicarbonate (BNa) and sodium carbonate (CNa). The dolomite is the only natural sorbent, being the rest analytical reagent grade. All the particles were below 53 μm. Prior to testing, the reactor was by-passed, and the test gas SO₂ concentration was established. During the experiment the gas passed from the fixed bed reactor via the water trap to SO₂ analyzer (IR Beckman 880). SO₂ absorption in the fixed bed reactor was calculated by integration of SO₂ concentration/time curve.

Table 1. Fixed-bed characteristics and experimental conditions.

Fixed-bed characteristics	
Silica sand size range (μm)	180-355
Bed height (cm)	3
Sorbent/inert ratio (g/g)	1/173, 1/100
Bed porosity	0.44
Sorbent size (μm)	20-53
Experimental conditions	
Gas composition (%vol)	
O ₂	5
CO ₂	15
H ₂ O	10
SO ₂ (ppm)	900-3200
Temperature range ($^{\circ}\text{C}$)	300-600
Gas flow rate (STP l/min)	~ 0.5

3. RESULTS AND DISCUSSION.

3.1. Sorbent selection

In Figure 1 the sulfation capacity (mol SO₂/mol sorbent) of the tested sorbents is indicated. Calcium and magnesium sorbents show very low sulfur capture under the studied conditions. From these results, only Na-based sorbents (mainly sodium carbonate and sodium

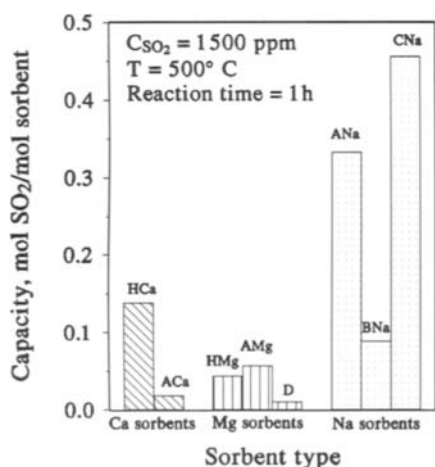


Figure 1. Sulfur capacity of the different type of sorbents.

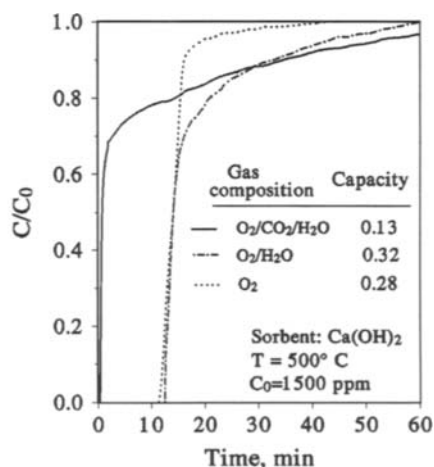


Figure 2. Influence of gas composition on sulfur capture.

acetate) are reliable candidates to be used under the economizer conditions. The differences in sulfur capture can be explained as a result of possible equilibrium constraints and competing reactions such as carbonation and hydration. This fact is illustrated in Figure 2 where the breakthrough curves corresponding to $\text{Ca}(\text{OH})_2$ sulfation under different gas compositions are displayed. Thus, it is observed that the presence of CO_2 in the gas composition strongly inhibits the sulfur capture. It can be considered that under these reaction conditions, the dehydration of $\text{Ca}(\text{OH})_2$ occurs and simultaneously the recarbonation of CaO rapidly takes place, inhibiting the sulfation reaction. On the other hand, it is observed that the presence of H_2O hardly have influence on sulfur capture under these conditions.

Surprisingly, sodium bicarbonate shows a lower degree of sulfur capture than sodium carbonate. This fact is contrary to the results obtained during sulfation at lower temperatures (around 150°C) [4]. During these experiments sodium bicarbonate rapidly decomposes into sodium carbonate. The sodium carbonate formed presents a high surface area and consequently high reactivity. However, at temperatures above 300°C , a loss in surface area due to sintering is observed. The effect of sintering on reactivity and sulfur capture could therefore explain the low sulfur loading observed for sodium bicarbonate.

3.2. Sodium carbonate- SO_2 reaction under economizer conditions

Different studies indicate that sodium sorbents, mainly sodium bicarbonate, have great activity in sulfur capture at temperatures around $120\text{--}175^\circ\text{C}$ [5]. However, in this study we demonstrate that sodium sorbents (i.e. sodium carbonate) can be also efficiently used at temperatures around 550°C . The overall reaction between SO_2 and sodium carbonate can be

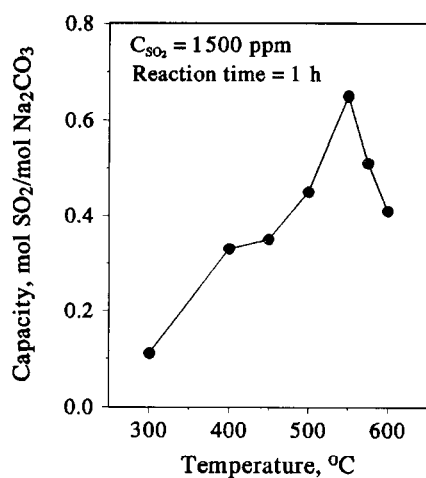


Figure 3. Variation of Na_2CO_3 sulfur capacity with temperature.

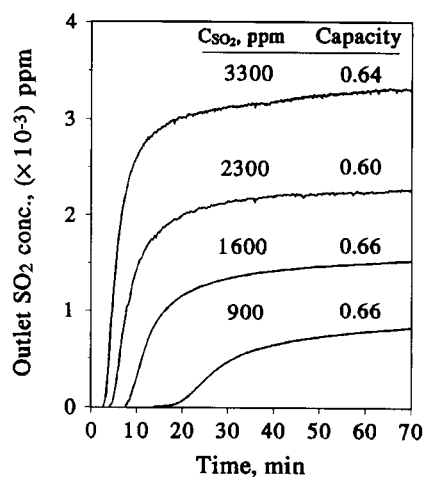
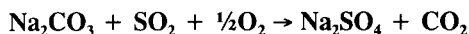


Figure 4. Influence of SO_2 concentration on the Na_2CO_3 sulfur capture ($T = 550^\circ\text{C}$).

written as



The sulfur capture of sodium carbonate is strongly dependent on reaction temperature. In Figure 3 the variation of sorbent sulfur capacity with reaction temperature is represented. The sulfur capture increases from 0.11 mol SO₂/mol sorbent at 300°C to 0.66 mol SO₂/mol sorbent at 550°C. A maximum in sulfur capture is found at this temperature. At higher temperatures the sulfur capture decreases.

The modification of SO₂ concentration does not have any influence on sulfur capture, as observed in Figure 4 where the breakthrough curves for different SO₂ concentration levels between 900 ppm and 3300 ppm are showed.

4. CONCLUSIONS

Our observations indicate that several competing processes contribute to the sulfur capture of the tested sorbents. This fact suggests that simulation of boiler conditions is required for meaningful evaluations.

From all tested sorbents, sodium carbonate presents the higher sulfur loading under the experimental conditions utilized (temperatures around 550°C and gas composition typical of combustion flue gases).

The sodium carbonate presents a maximum in sulfur capture of 0.66 mol SO₂/mol sorbent at a temperature of 550°C. This fact suggests that this sorbent is a good candidate to be utilized under economizer conditions. Additionally, it has been detected that the change in SO₂ concentration between 900 and 3300 ppm does not have any influence on sulfur capture.

ACKNOWLEDGEMENTS

The financial assistance of the DGCICYT (PB91-0101) is gratefully acknowledged.

REFERENCES

1. M. Takeshita and H. Sound, FGD performance and experience on coal-fired plants, IEA Coal Research, IEACR/58, IEA, London, 1993.
2. P. V. Smith, in Processing of High Sulfur Coals IV, Ed. by P. R. Dougan, D. R. Quigley and Y. A. Attia, Elsevier, Amsterdam, 791, 1991.
3. S. M. Dalton and B. C. Syrett, in Desulphurization in Coal Combustion Systems, IChemE SYMPOSIUM SERIES No. 106, The Institution of Chemical Engineers, London, 161, 1989.
4. T. C. Keener and S. J. Khang, Chem. Engng. Sci., 48 (1993) 2859.
5. M. Hartman, Int. Chem. Eng., 18 (1978) 712.

Advanced flue gas treatment system using LILAC absorbent prepared from flyash

Tomohiro Ishizuka*, Tsutomu Ueno*, Atsushi Tatani**, Shinichiro Kotake**

*Hokkaido Electric Power Co., Inc.

Utsukushigaoka 4-9-2-1, Toyohira-ku, Sapporo Japan

**Mitsubishi Heavy Industries Ltd.

5-1, Marunouchi 2-chome, Chiyoda-ku, Tokyo Japan

The new FGD process called LILAC process has been developed jointly by Hokkaido Electric Power Co., Inc. and Mitsubishi Heavy Industries Ltd.

The system is characterized by the use of a highly active absorbent which is prepared from lime, gypsum and flyash by aging in hot water. For development of the semi-dry LILAC process, improvement of the sprayer and the atomizer as well as the absorbent was a key point. The results of demonstration test for semi-dry LILAC process are described. And the features of different types of FGD system are compared in terms of desulfurization efficiency, utilities, and construction space and costs.

1. INTRODUCTION

Among environmental problems, SO_x and NO_x from the flue gas is one of the most important and effective countermeasures for protection of clean air from pollution.

Installation of the desulfurization and denitrification equipment is costly and is difficult to adopt by countries other than the industrially developed ones. For that reason, the demand for a more simplified and low cost FGD system is increasing.

Hokkaido Electric Power Co., Inc. (HEPCO) has found that a solid compound prepared from coal flyash, lime and gypsum possesses a high desulfurization ability. The absorbent was named as LILAC absorbent and HEPCO and Mitsubishi Heavy Industries Ltd. (MHI) have jointly developed a new FGD system called LILAC FGD process. A demonstration test for a semi-dry LILAC process using the absorbent in the slurry form for the flue gas from a commercial coal-fired boiler has performed from October 1991 to March 1994. This paper shows the outline of the LILAC process as well as the results of the demonstration test.

2. LILAC SYSTEM

2.1 Properties of Equipment

The process flow of the semi-dry desulfurization system is shown in fig. 1. In LILAC process, the absorbent in the form of slurry is sprayed into the flue gas to react with SO₂. The gas temperature

decreases due to evaporation of the water from the slurry as the gas is approaching the outlet. At the outlet, the temperature of gas is slightly above the dew point of the gas. Therefore, the particles are dry at the outlet of the sprayer. SO₂ is fixed in the form of CaSO₃ or CaSO₄ in the spent absorbent. A part of the spent absorbent is supplied to the absorbent preparation unit as a source to produce active absorbent.

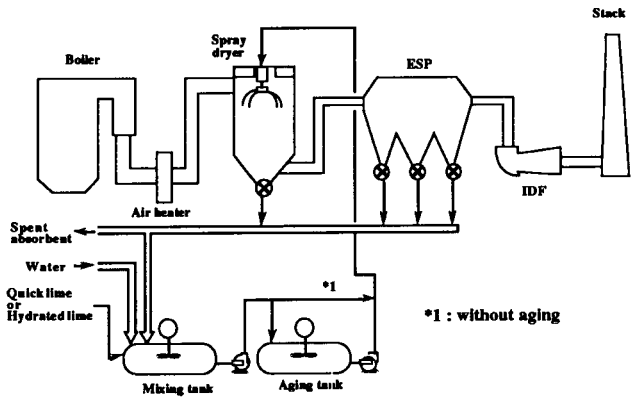


Figure 1 Process flow of LILAC FGD system

For the demonstration plant, a high-speed spray dryer and a light weight rotary atomizer were adopted. For dust collection, use of both electrostatic precipitator and bag filter was verified. The sprayer is required to scrub a large volume of a low approach temperature gas in stable operation without causing accumulation of solids in the spray dryer tower. A small size atomizer installed at the top of the spray dryer permits easy maintenance access, simplified top frame structure and to reduce electric power consumption.

2.2 LILAC absorbent

The absorbent is prepared from a mixture containing flyash, lime and gypsum or the spent absorbent. There are two types of the preparation methods of LILAC absorbent. Raw materials are mixed and hydrated in hot water at 95°C for 15 min, followed by aging at 95°C for 12h. During the aging period, porous compounds such as calcium silicate and ettringite are formed. In addition, an absorbent containing a large amount of Ca (85~95% as Ca(OH)₂) which is prepared without aging process of 95°C and 12h, but hydration of only 15min during mixing of the raw materials was developed to lower the equipment cost. Two kinds of slurry LILAC absorbents that are prepared by the methods mentioned above are adopted in demonstration test as follows.

LILAC-50 : 50% of Ca(OH)₂ contents, 95°C and 12h aging

LILAC-85 : 85% of Ca(OH)₂ contents, 95°C and 20min aging

3. DEMONSTRATION TEST

A demonstration plant capable of treating 10,000 m³N/h of flue gas at the maximum from No.2 coal-fired boiler unit of Tomato-atsuma power station(HEPCO) was constructed and put into operation in October 1991 to test the spray drying process. The test has been completed in March 1994.

The demonstration test was carried out with a 7.5 kW rotary atomizer and a spray dryer having a 2.8m tower diameter. The results showed that mixing of the sprayed particles and flue gas was sufficient to obtain high efficiency of sulfur removal. And a stable continuous operation was performed without the build up of solids.

The relation between desulfurization efficiency and Ca/S molar ratio for three kinds of absorbents is shown in fig.2. The hydrated lime absorbent showed the desulfurization efficiency of about 55% under the conditions of the approach temperature 15-17°C and Ca/S molar ratio 1.2. LILAC-50 absorbent achieved much higher efficiency of about 75% under the same conditions. The efficiency is comparable to that of the wet system. LILAC-85 absorbent showed the ability in between those of LILAC-50 and hydrated lime. Although the ability of LILAC-85 absorbent is not high as compared to the LILAC-50 absorbent, it has the advantage of a simplified preparation method in which no further aging period is required after hydration during mixing of raw materials for 15 min.

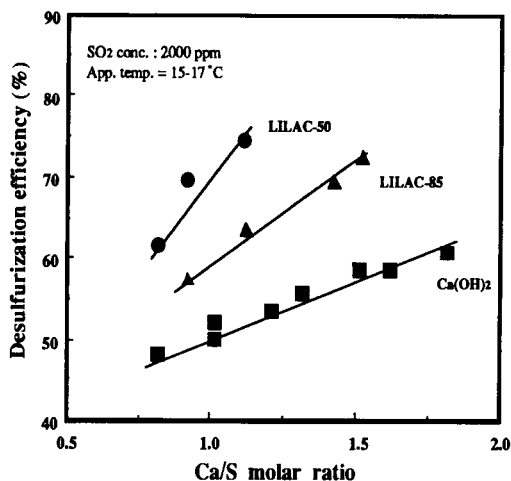


Figure 2 Desulfurization efficiency vs Ca/S on various absorbent

The relation between desulfurization efficiency and inlet SO₂ concentration is shown in fig.3. The desulfurization efficiency of LILAC-50 absorbent is high and keeps constant with an increase in the inlet SO₂ concentration. The desulfurization efficiencies for both LILAC-85 and hydrated lime decreased as the inlet SO₂ concentration increased. As shown in fig.3, when a higher desulfurization efficiency is desired LILAC process is more feasible than hydrated lime process. Selection of the absorbent depends upon the desulfurization efficiency required.

4. SYSTEM COMPARISON

For selecting the optimum FGD system, the points to be taken into account are (1) capacity of the equipment, (2) fuel type, (3) absorbent cost, (4) desulfurization efficiency required, (5) plant availability, and (6) disposable or salable by-products. Features of different systems, the wet limestone/gypsum FGD system, and semi-dry systems using hydrated lime, LILAC-85 and LILAC-50, are compared in terms of desulfurization efficiency, utilities, construction space, and construction cost, and summarized in Table 1.

The wet limestone/gypsum system is suitable for large size plants requiring 90

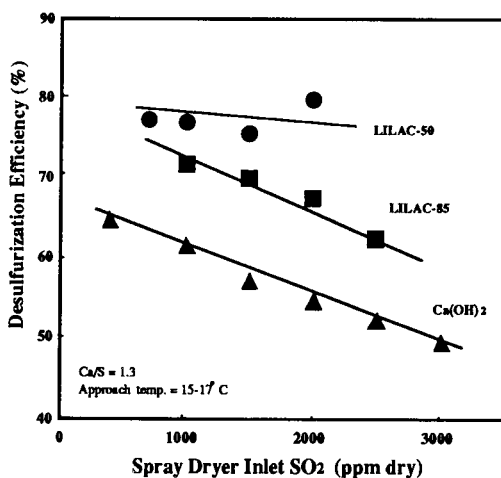


Figure 3 Effect of SO₂ concentration on SO₂ removal

to 95 % sulfur removal efficiency, and is also applicable for fuels such as coal, heavy oil, orimulsion, etc., which have a wide range of sulfur content. Because of these merits, the wet limestone/gypsum system is widely adopted at present in spite of its high initial cost.

The semi-dry system using lime is suitable in a place where supply of quick lime or hydrated lime can be assured at a stable price since the capital cost is much lower than that of the wet system.

The semi-dry system using LILAC-50 absorbent has 80-90% desulfurization efficiency at almost the same Ca/S ratio as that of the wet limestone/gypsum system. The semi-dry system using LILAC-85 absorbent has the advantage of achieving the desulfurization efficiency higher than that of the semi-dry system using hydrated lime.

Table 1 Comparison Between Wet-FGD (Lime-Gypsum) and Spray-Dry FGD System

FGD System	Wet System	Spray Dry System			Remarks
		Lime	LILAC-85	LILAC-50	
De SO _x Efficiency	Ca/S=1.05 90% outlet gas temp. =90 °C	Ca/S=1.5 65% App. Temp.= 12°C	Ca/S=1.4 70% App. Temp.= 12°C	Ca/S=1.1 80% App. Temp.= 10°C	SO _x Conc.: 2,000ppm
Utility Consump.					Calc. Condition
Electric Power	1600KW	820KW	880KW	960KW	Gas Volume:
Water	16.8 t/h	14 t/h	14 t/h	14 t/h	300,000m ³ /h
Absorbent	Limestone(CaCO ₃) 2.5 t/h	Quick Lime(CaO) 2.0 t/h	Quick Lime(CaO) 1.9 t/h Fly-Ash, Byproduct	Quick Lime(CaO) 1.5 t/h Fly-Ash, Byproduct	SO _x Conc.: 2,000 ppm
Required Area	270 m ²	190m ²	200m ²	210m ²	
Initial Cost	100	65	70	80	

5. PRACTICAL USE OF LILAC FGD SYSTEM

Above mentioned, LILAC absorbent have several advantages compared with conventional FGD system such as wet-type method on operation or costs. Being evaluated those advantages, the LILAC system has adopted to Green Aid Plan as international support in energy and environment for developing countries promoted by Ministry of International Trade and Industry in Japan. And a commercial plant of LILAC system was installed at Huangdao Power station in People's Republic of China. The system is required lower costs to be installed in developing countries. For that reason desulfurization efficiency in specification is established on 70% at Ca/S=1.4 that would be rather low.

The system is now under the demonstration test and would be delivered to China on Oct. 1997.

6. CONCLUSION

The LILAC FGD system is applicable to various types of flue gas treatment for its flexibility in the preparation of different forms of the absorbent. This system is capable of achieving a high desulfurization efficiency without waste water treatment which is usually required in a wet type FGD system like the limestone/gypsum method. Because of omission of the waste water treatment unit, the LILAC system is composed of simplified equipment, and therefore, its capital and operational costs are low.

We hope the LILAC system would make a large contribution towards the settlement of global air pollution problems.

KINETIC STUDIES ON LOW TEMPERATURE, DRY FLUE GAS DESULPHURIZATION

Aichinger G., Brunner Ch., Khinast J., Seebauer V., Staudinger G.

*Department of Apparatus Design and Particle Technology, Graz University of Technology,
Inffeldgasse 25/II/1, A-8010 Graz, AUSTRIA*

Garea A., Fernandez I., Viguri J.R., Irabien A.

*Departamento de Química, E.T.S.I.I. y T. Universidad de Cantabria, Avda Los Castros s/n,
39005 Santander, SPAIN*

Industrial, hydrated lime - $\text{Ca}(\text{OH})_2$ - is a common sorbent for low temperature, dry flue gas desulphurization. The influence of the reaction conditions and the use of impregnated fly ash/lime mixtures on kinetics and desulphurization capacity of lime were investigated. Sorbent samples were exposed to synthetic flue gas in two different reactors. The SO_2 breakthrough curve was monitored in a sand bed integral reactor, which is outlined in more detail by Ortiz et al. [1]. A thermobalance was used to record the weight change of the sample during reaction with SO_2 . The samples were analysed using thermogravimetry, ion chromatography, X-ray diffraction and SEM. BET surface areas were measured by means of N_2 -adsorption technique.

The objective of the thermobalance experiments was to observe the reaction kinetics under differential conditions by recording the weight change during the reaction of $\text{Ca}(\text{OH})_2$ with SO_2 . Although very low sample weights, between 3 and 17 mg, were used, reaction conditions were not differential during the first ten seconds. To distinguish between the weight gain by water adsorption and the weight gain by the SO_2 -reaction, the samples were first exposed to a $\text{H}_2\text{O}/\text{N}_2$ /air mixture with the same humidity as the flue gas. Then part of the N_2 was replaced by CO_2 and SO_2 to form synthetic flue gas.

The investigated parameters were humidity, temperature, SO_2 -concentration and the presence of CO_2 . The influence of these four parameters on the conversion of $\text{Ca}(\text{OH})_2$ in the thermobalance is expressed by different graphs of weight gain over time, as illustrated in Figs. 1 - 4.

The initial reaction rate was similar for all conditions. It ranged from $2 \cdot 10^{-3}$ - $7 \cdot 10^{-3}$ $\text{mg}/(\text{mg}_0 \text{ s})$. After the initial uptake the reaction rate bent off sharply or gradually, depending on the reaction conditions. In all cases the reaction rate decreased by three orders of magnitude over two hours reaction time.

The most crucial parameter for the reactivity of lime is relative humidity, Hr. It was varied by changing the partial pressure of water. Temperature and concentrations of the other flue gas components were kept constant. Figure 1 shows the impact of increased humidity for enhanced calcium conversion. This suggests that the reaction occurs in the adsorbed water phase. At a relative humidity of 20%, the lime surface is covered by a monolayer of adsorbed

water, which was also reported by Klingspor et al [2]. At such low humidities the mobility of the adsorbed water molecules may be too limited for dissolution of SO₂ and calcium. As the water film thickness increases with humidity, the desulphurization reaction works better.

Temperature was less influential than relative humidity, as shown in Figure 2. The influence of SO₂-concentration was also small, particularly at 3500 ppm and above, see Figure 3. Figure 4 shows that the presence of CO₂ caused a small weight gain, SO₂ caused a much higher weight gain and CO₂ + SO₂ caused a slightly higher weight gain than SO₂ alone. This may raise the impression that part of the weight gain during flue gas treatment is caused by recarbonatization of lime. Thermogravimetric product analysis showed, however, that the fraction of CaCO₃ did not increase. Thus the presence of CO₂ had no influence on the SO₂ capture.

Far better results were achieved when impregnated fly ash/lime mixtures were used. Figure 5 shows the relative weight gain of an ash/lime mixture (3:1 by weight) and lime alone. The weight gain of the ash/lime mixture was related to the lime fraction. Additional experiments showed, that the lime capacity in terms of SO₂ capture was improved by a factor of 2.3 to 3.6. The influence of humidity and temperature on the reaction kinetics was similar to that of lime.

To compare the sand bed reactor results with the thermobalance results, the relative weight gain data of the thermobalance must be interpreted in terms of calcium conversion. Conversion data from thermobalance experiments are listed in Table 1 based on the assumption that CaSO₃ · ½H₂O was the only solid reaction product. These data are in comparable range with the sand bed reactor data, see also Table 1. With short reaction times the conversion levels were generally higher in the thermobalance than in the fixed bed reactor because of integral conditions in the sand bed reactor.

Large samples of 1 g were produced in the sand bed reactor and analysed with respect to composition and surface area. X-ray diffraction and ion chromatography showed almost exclusive formation of CaSO₃ · ½H₂O. In contrast, thermogravimetric analysis allowed the interpretation that part of CaSO_x consisted of CaSO₄ · xH₂O. The extent of CaSO₄ · xH₂O formation has not been clarified yet.

The specific BET-surface area of the used lime was about 18 m²/g. This would correspond to the specific surface of particles with 0.12 μm diameter. Conventional particle size measurements were not meaningful because complete dispersion of the powder was not possible. SEM photographs at 20.000-fold magnification showed that such small submicron particles exist within aggregates of 5 to 20 μm diameter. However, many particles with diameters from 0.1 to 1 μm were also detected. This led to the conclusion that total surface area is the sum of external submicron particle surface area and internal particle porosity.

The BET-surface area decreased over the course of reaction to about 14 m²/g for conversions below 15% and to 9 m²/g for higher conversions around 30%. The higher molar weight of the reaction product alone contributes to specific surface area reduction, e.g. a 30% conversion of Ca(OH)₂ to CaSO₃ · ½H₂O involves a reduction of the specific surface area from 18 m²/g reactant to 14.7 m²/g product keeping the same absolute surface area.

True surface area loss may be attributed to loss of internal particle surface, while the remaining surface comes from submicron particles.

When fly ash and lime were mixed in hot water under pressure for several hours, part of the lime was incorporated into Ca-Al-Si-composites as detected by X-ray diffraction. The BET-surface area of a tested impregnated ash/lime mixture was the same as for lime: 18 m²/g. The surface area was made up of a calcium-containing, web-like matrix with a very high surface area and big, sphere-like ash particles of 50 µm diameter with a low surface area, about 0.04 m²/g. The surface enlargement of the calcium containing solid explains the increased desulphurization capacity of calcium in the impregnated mixtures.

According to SEM-photographs the chemical reaction did not alter the matrix structure of sulphurized ash/lime agglomerates. CaSO₃ · ½H₂O was the predominate reaction product. Sulphurized Ca-Al-Si-composites were not detected.

ACKNOWLEDGEMENTS

Thanks are due to the Ministerio de Educacion, Spain, and to the Bundesministerium fuer Wissenschaft und Forschung, Austria, for authorizing the exchange project "Acción Integrada No. HU93-017" and for the financial support.

REFERENCES

1. Ortiz I., Garea A., Fernandez I., Oliván A.M.O., Viguri J.R., Irabien A.; "On the Kinetic Modelling of the FGD Reaction at Low Temperatures"; SO₂ Control Symposium; National Technical Information Service, Springfield, Virginia, USA, 1993.
2. Klingspor J., Karlsson H.T., Bjerle I.; "A Kinetic Study of the Dry SO₂-Limestone Reaction at Low Temperature"; Chem. Eng. Commun., 22 (1983), p. 81-103.

Table 1

	Thermobalance		Sand Bed Reactor	
Temperature	80°C		80°C	
Relative humidity Hr	35%		35%	
SO ₂ -concentration dry	4200 ppm		4000 ppm	
Reaction time	10 min	55 min	10 min	55 min
Conversion to CaSO ₃ · ½H ₂ O	5.9%	8.1%	1.9%	6.3%
Temperature	67°C		70°C	
Relative humidity Hr	40%		51%	
SO ₂ -concentration dry	5000 ppm		4000 ppm	
Reaction time	10 min	48 min	10 min	48 min
Conversion to CaSO ₃ · ½H ₂ O	6.3%	8.3%	7.1%	12.3%
Temperature	67°C		66°C	
Relative humidity Hr	70%		70%	
SO ₂ -concentration	5000 ppm		5000 ppm	
Reaction time	10 min	60 min	10 min	60 min
Conversion to CaSO ₃ · ½H ₂ O	18.5%	23.6%	8.4%	25.1%

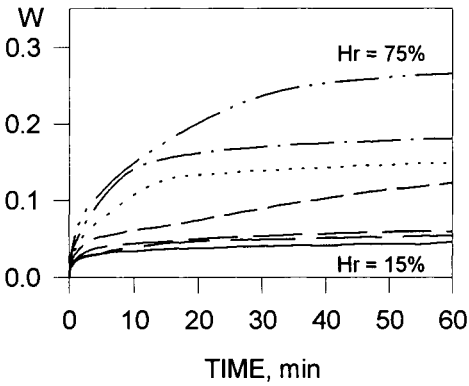


Figure 1. Relative weight gain of lime in a thermobalance at 80°C and humidities Hr between 15% and 75% at 10% steps. Sample weight: 3.3 mg. 3500 ppm SO₂, 9% CO₂, 7% O₂, N₂ wet.

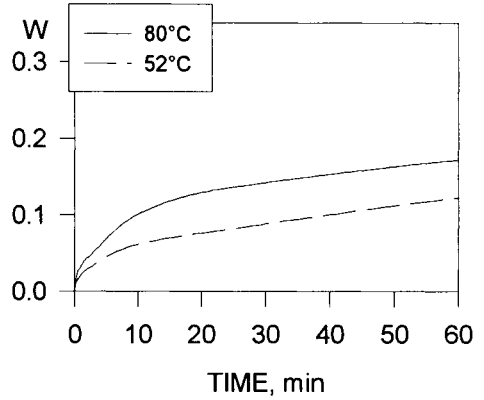


Figure 2. Relative weight gain of lime in a thermobalance at 70% Hr at 52°C and 80°C. Sample weight: 14 mg. 5000 ppm SO₂, 12% CO₂, 2% O₂, N₂ dry.

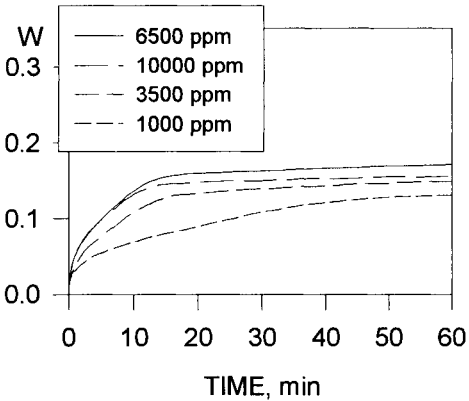


Figure 3. Relative weight gain of lime in a thermobalance at 80°C and 55% relative humidity at different SO₂ concentrations. Sample weight: 3.3 mg. 9% CO₂, 7% O₂, N₂ wet

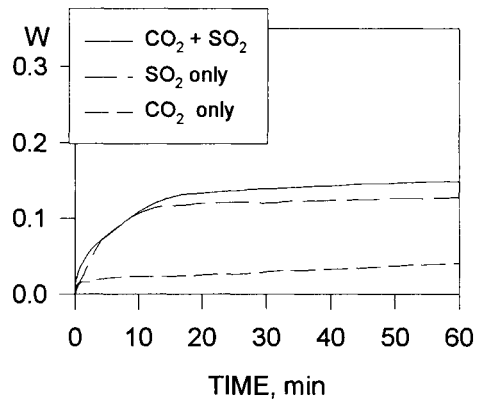
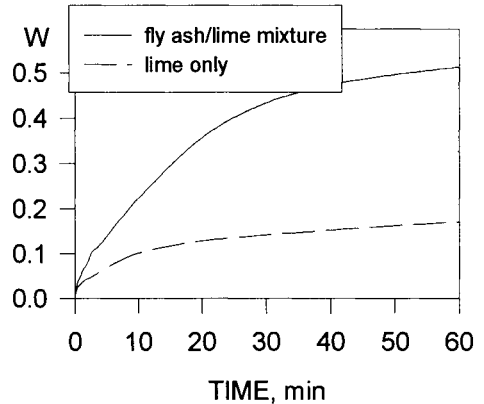


Figure 4. The influence of CO₂ at 80°C and 55% relative humidity. Weight: 3.3 mg (3500 ppm SO₂), (9% CO₂), 7% O₂, N₂ wet

Figure 5. Relative weight gain related to the lime fraction of an impregnated fly ash/lime mixture (3:1 by weight) and pure lime in a thermobalance at 80°C, 70% relative humidity. Sample weight: 14 mg. 5000 ppm SO₂, 12% CO₂, 2% O₂, N₂ dry



Desulfurization rate at low temperatures using calcium hydroxide and fly ash

A. Garea, J.R. Viguri and J.A. Irabien

Departamento de Química. E.T.S.I.I. y T. Universidad de Cantabria.
Avda. Los Castros s/n. 39005 Santander. SPAIN

The direct injection of dry sorbents into the flue gas duct offers a good alternative for controlling sulphur dioxide emissions at low temperature with a technology relatively simple compared to semi-dry or wet methods. Coal combustion fly ash, mixed with $\text{Ca}(\text{OH})_2$ has an increasing utilisation as flue gas desulfurization (FGD) solid sorbents with potential use as reagent for in-duct injection systems. In this work starting from commercial calcium hydroxide and coal combustion fly ash mixtures, kinetic experiments have been performed in a fixed bed reactor at different temperatures, concentration of SO_2 and humidities as reaction conditions. The experimental kinetic results were fitted to two kinetic models for the reaction rate and predict satisfactorily well the experimental results.

1. INTRODUCTION

In - duct injection systems work with a dry powdered sorbent introduced into the humidified flue gas duct, downstream of the air preheater and ahead of the particulate collector. Due to the residence time of the solids in the injection process is short (1-3 seconds) a reactive sorbent must be used in order to achieve acceptable levels of SO_2 removal [1].

A great deal of effort has been devoted to improve sorbent reactivity by substituting conventional high calcium content hydrated lime with other sorbents. Alternatives investigated have included sodium based solids, reactivation of spent solids, and mixtures of alumina/Ca sorbents containing metal oxides [2-3]. Sorbents obtained by mixing with fly-ash, have demonstrated to provide significantly higher conversion of calcium compared to the conversion obtained using $\text{Ca}(\text{OH})_2$ with an attractive use both economically and environmentally, because fly-ash is the most voluminous by-product from coal fired power plants [4].

The study of the desulfurization yield of sorbent prepared with commercial $\text{Ca}(\text{OH})_2$ and fly-ash has been the main interest of this work in order to establish the kinetic behaviour of the SO_2 - $\text{Ca}(\text{OH})_2$ reaction for the design, simulation or optimisation routines in FGD processes at low temperature.

2. EXPERIMENTAL SECTION

The sorbents were prepared using commercial Ca(OH)_2 obtained from Calcinor S.A. and ASTM Class F coal fly-ash collected in an electrostatic precipitator of Pasajes (Guipuzcoa-Spain), a bituminous coal fired power plant. Sample preparation has been described elsewhere [5]. The properties of the material for the kinetic experiments are fly ash/ Ca(OH)_2 initial weight ratio=3/1 g/g, specific surface =18,4 m^2/g , $d_p < 60 \mu\text{m}$ and a Ca content of $3.092 \cdot 10^{-3}$ mol Ca/g reactive.

The reaction between the solid and SO_2 is performed in a glass-made jacketed fixed bed reactor, where the solid is dispersed in an inert silica sand (sorbent/inert ratio: 1/30). The flue gas generated by mixing gases from cylinders was passed through the sample at 885-932 Ncm^3/min with a composition of 2000-5500 ppm SO_2 , 12 % CO_2 , 2% O_2 , 40-90 % relative humidity (H_R) and balance N_2 . The reaction temperature was 52-72°C with 1 h as reaction time.

The flue gas is passed through the humidification system where the gas is in contact with water vapour produced at a steady rate in two absorbers of 250 ml each. After water saturation, the humidified SO_2 flows to the reactor through a system of preheated pipes. The reactor is maintained at the reaction temperature by means of hot water passing through the jacket[6].

The concentration of SO_2 in the gas phase was continuously measured by introducing the gas sample into a infrared gas analyser. The reaction solid product is sieved to separate the spent sorbent from the inert silica sand ($d_p > 150 \mu\text{m}$). The sorbent without inert is analysed using the TG analysis, in a Perkin-Elmer TGA-7 unit, with high temperature furnace. Synthetic air was used as carrier gas (30 ml min^{-1}) in order to oxidise the CaSO_3 formed in the FGD reaction to CaSO_4 . This analysis allows the calculation of the amount of SO_2 that has reacted in the bed as SO_4^{2-} due to the decomposition of sulfate species to SO_3 between 850 °C - 1300 °C. Starting from the number of calcium mol in the bed, the solid conversion is presented as reacted mol SO_2 referred to Ca [7].

3. RESULTS AND DISCUSSION

The system of equations describing the adsorption of a component from a moving gas stream by a fixed solid in a packed bed consists of two partial differential equations from material balances in the gaseous and solid phases, with r_R defined respect to the reactive surface (mol $\text{SO}_2/\text{m}^2\text{solid}\cdot\text{time}$).

$$u \frac{\partial C}{\partial z} + \varepsilon \frac{\partial C}{\partial t} + \frac{Se W}{V_R} r_R = 0 \quad (1)$$

$$\frac{\partial x_s}{\partial t} = v Se M_S r_R \quad (2)$$

The procedure followed consisted on the integration of equations (1) and (2), once the kinetic model of the reaction rate has been defined and comparison of the obtained results with the experimental data studying the influence of the SO_2 concentration, temperature and relative humidity on the proposed kinetic models (Figures 1-2). The optimisation of the kinetic parameters has been performed using the minimum standard deviation as criteria.

3.1. Non ideal surface adsorption model with x_S exponential dependence

The first proposed model for the reaction rate include a non ideal surface adsorption kinetic model with two fitting parameters K and g , previously applicated to the $\text{SO}_2\text{-Ca(OH)}_2$ reaction [8-9]. The kinetic expression (eq.3), with the solid conversion x_S , is:

$$r_R = K \frac{1}{g} C [\exp(-gx_S) \cdot \exp(-g)] \quad (3)$$

The experiments show no influence of oxygen and carbon dioxide concentration, an a first order dependence of SO_2 concentration and an Arrhenius type relation for the temperature (K), obtaining the value for the parameters, preexponential factor (A) and ideal adsorption energy ($-E_{\text{ads}}^0$) showed in Table 1. A linear relation of the reaction parameter (g) with the temperature has been obtained attending to the g value that corresponds the minimum σ at each temperature. The parameter g is independent of the relative humidity for values from 55% to 90% with an average value of $g=5.82$, obtaining a significant influence of H_R in the reactivity at values less than 50%.

Table 1.

Kinetic models optimised parameters and its dependence with reaction conditions.

Reaction variable	Non-ideal adsorption models	
	Exponential dependence	Potential dependence
SO_2 Concentration	$g=3$ and $K=13508$ ($\sigma=4.4\%$)	$B2=2$ and $K=3421$ ($\sigma=4.5\%$)
Temperature	$K=A \exp[-E_{\text{ads}}^0/RT]$ ($\sigma<3.2\%$) $A=5.82 \cdot 10^{12}$ and $-E_{\text{ads}}^0=12576$ $g=-3.77 + 0.16 T$	$B2=4$ and $K=4300$ ($\sigma=3.4\%$)
Relative Humidity	$g=5.82$ ($\sigma=8.6\%$)	$B2=9.315-7.945 H_R$ ($\sigma<4.5\%$)

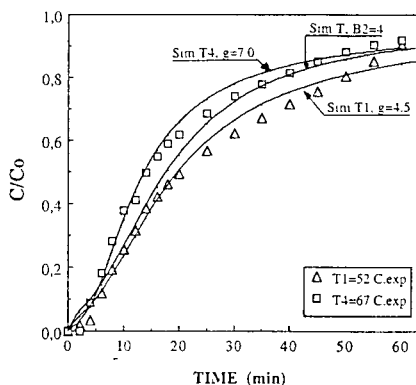


Figure 1. Experimental and simulated curves. Influence of the temperature

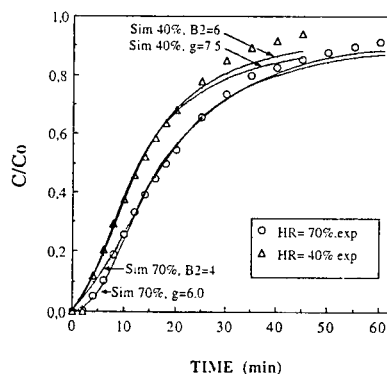


Figure 2. Experimental and simulated curves. Influence of the relative humidity

3.1. Non ideal surface adsorption model with x_s potential dependence

A potential model based in the Freundlich isotherm has been applied to the kinetic experiments. The kinetic expression is:

$$r_R = K C^{B1} (1 - x_s)^{B2} \quad (4)$$

In order to compare kinetic models (exponential and potential dependence) with similar number of fitting parameters the parameter B1 is maintained constant in the value of 1, reported previously in the literature [10], and optimising K and B2.

This model predicts satisfactorily well experimental results at different SO₂ concentrations. From the adjustment of the experiments at different temperatures it has shown no influence of the temperature in the kinetic constant in the range studied; although K has the same magnitude than in the previous fitting, the B2 parameter is higher due to the less humidity (70% in front of 90%). The dependence of B2 with the humidity leads to a linear expression. In Table 1 are summarised the optimised parameters and its dependence for each model with the reaction conditions. In Fig. 1-2 are shown the experimental and simulated behaviour of SO₂ concentrations.

4. CONCLUSIONS

The present study has investigated how the reaction variables: SO₂ concentration, temperature and relative humidity influence the kinetic behaviour of the solids produced by slurring fly ash with Ca(OH)₂, testing for reactivity toward SO₂ in a packed-bed reactor. The influences of these variables were examined by solving the differential equations in order to describe the system with two proposed kinetic expressions, obtaining the optimised parameters values which fit satisfactorily well the experimental results.

Acknowledgement

This work has been supported by a Spanish CICYT Project No. AMB94-0991-CP.

REFERENCES

1. L.J. Muzio and G.R. Offen, JAPCA, 37 (1987) 642.
2. J. Klingspor, H. Karlsson and I. Bjerle, Chem. Eng. Commun., 22 (1983) 81.
3. K. Svoboda, J. Nannes, W. Lin and C.M. van den Bleek, IChemE Symp.Ser., 131 (1993) 253.
4. J.R. Peterson and G.T. Rochelle. Environ. Sci. Technol., 22 (1988) 1299.
5. A. Garea, M.J. Renedo, J. Fernandez, M.I. Ortiz, J.R. Viguri and J.A. Irabien, Thermochim. Acta (1995) In press.
6. A. Irabien, F. Cortabitarte, J. Viguri, I. Ortiz, Chem. Eng. Sci., 45 (1990) 3427
7. M.I. Ortiz, A. Garea, A. Irabien, F. Cortabitarte, Powder Technol., 75 (1993) 167.
8. A. Irabien, F. Cortabitarte, M.I. Ortiz, Chem. Eng. Sci. 47 (1992) 1533
9. A. Irabien, M.I. Ortiz, F. Cortabitarte, F., A. Garea, J.R. Viguri, IChemE Symp. Ser. 131, Desulphurisation 3, Sheffield, U.K., 229 (1993).
10. C. Jorgensen, J.C.S. Chang and T.G. Brna, Environ. Progress., 6 (1987) 26

A Mathematical Model of a Spray-dryer Flue Gas Desulfurization System

A.Abad, P.Ollero, and L.Salvador

Departamento de Ingeniería Química y Ambiental, Escuela Superior de Ingenieros
Avda.Reina Mercedes s/n, 41012-Sevilla, University of Seville, Spain

1. INTRODUCTION

At a pilot plant installed at the Los Barrios Power Plant [1] (Cádiz, Spain), a research project was carried out to study, among other things, the desulfurization of flue gas by means of a spray dryer under different operating conditions. At the same time, and as a tool for evaluating the experimental results and for reaching reliable conclusions, we developed a spray dryer simulation model based on a theoretical approximation to the behaviour of these desulfurization units. This mathematical model was translated into a computer code, creating a computer simulation tool that will allow us to investigate some spray dryer design parameters and their operational conditions.

2. BASIC CHARACTERISTICS OF THE SPRAY DRYER MODEL

The MODSDSE model (Modelo de Spray Dryer de la Universidad de Sevilla) is based primarily on the SPRAYMOD-BAMA model [2] which, in turn, has two other close predecessors, SPRAYMOD and SPRAYMOD-M. However, MODSDSE incorporates a series of modifications that enhance the predictive capacity of the models on which it is based. Among them, we should mention that the model:

- incorporates the recirculation of solids generated in the desulfurization unit.
- considers the effect of the fly ash load at the the desulfurization unit input.
- takes into account the heating that the slurry undergoes and, therefore, that the cooling of the gas is not strictly adiabatic.
- calculates the mass transfer coefficient estimating the thickness of the liquid film by means of a physical model of particle distribution in the droplets.
- prolongs the drying process to the dry absorption stage, considering that this process does not cease until the humidity equilibrium is reached with the gas.
- models the evolution of the solid agglomerate porosity during the reaction in the dry stage.

2.1. Recirculation modeling

The possibility of simulating the operation of a spray dryer with partial recirculation of the product is perhaps the most relevant contribution of MODSDSE. When there is

recirculation, the composition of the feed slurry is not known a priori because it contains fresh lime and recirculated product with partially converted lime. The model resorts to an iterative process in which, based on an estimate of the free lime in the recirculated product, calculates the desulfurization and the composition of the resulting product, and iterates until convergence.

The inert matter recirculated with the product -- mainly ashes and reaction products - - will form part of the slurry droplets and constitute a resistance to lime diffusion. In the wet absorption stage -- the most important one in the overall process -- this effect implicitly appears in the absorption velocity equation in the mass transfer coefficient for lime dissolution (K_s). Applying the film theory and introducing a correcting factor to take into account the inhibiting effect of the inert matter, the model uses this expression:

$$K_s = \frac{(D_{BL}/RF)}{\delta} \quad (1)$$

where D_{BL} is the diffusivity of the lime, δ the thickness of the diffusion film, and RF the volumetric ratio of the total solid (lime + reaction product + ash) and the unconverted lime.

3. MODEL VALIDATION

The MODSDSE model has been validated comparing its predictions with experimental data from the bibliography [2] (without recirculation) and the Los Barrios Pilot Plant (with recirculation). Figure 1 shows this comparison, which corresponds to a series of tests executed at the Los Barrios plant. We can observe that the tendencies described by the MODSDSE predictions are, in general, similar to the experimental tendencies. The difference observed between the predictions and the experimental data ranges between 0 and 14 efficiency percentage points, with an average value of 3.84. If we take into account that in the experimental tests there were many incidents and deviations in respect to the operating conditions established for each test, this concordance is very satisfactory.

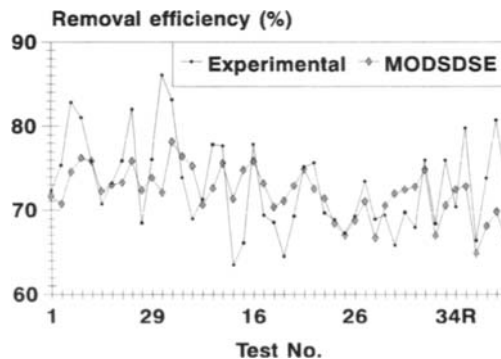


Figure 1. Comparison of the MODSDSE predictions with the Los Barrios experimental results.

4. SENSITIVITY ANALYSIS BASED ON THE MODEL

One of the main utilities of the model is the possibility of carrying out a quick, detailed analysis of the influence of certain operating parameters on the behaviour of the spray dryer. Since the introduction of recirculation modifies the way some parameters act, we have made two similar sensitivity analyses that reflect the operation modes with and without the partial recirculation of the reproduct. Also, we have considered two basic scenarios to carry out these analyses: low and high SO₂ concentration in the gases, giving us a total of four analyses performed.

4.1. Analysis results

Figure 2 shows a summary of the sensitivity analysis carried out with the model. The results shown were obtained assuming that the approximation to the adiabatic saturation temperature is controlled, so the conclusions are strictly applicable only to this mode of operation. In view of these results, we can make two general observations:

- the recirculation produces an average increase of 12 yield points and, obviously, a larger amount of lime utilization; this improvement is due to an increase in the internal Ca/S ratio and in the solid-liquid interface area.
- the concentration of SO₂ in the gases not only limits the yield that can be reached, but also determines the effect that other parameters have on desulfurization.

In relation with the three parameters considered explicitly in the analysis -- perhaps the least studied in the bibliography -- the conclusions reached are shown below.

- **Fly ash load in the combustion gas, Z (mg/Nm³)**

Fly ash capture before desulfurization has positive and negative implications on the overall pollution control system and is, in fact, an alternative that is not always adopted. The tests carried out at the Los Barrios pilot plant show that the reduction of the fly ash load has a favorable effect on the spray dryer behaviour, that has been analyzed with the MODSDSE model under different operating conditions. Reducing the ash load from 7000 to 1000 mg/Nm³ gives an increase in desulfurization efficiency similar to that which would be obtained by reducing ΔT 3 or 4° C (with the same Ca/S), or increasing Ca/S between 4 and 7 decimal points (with a constant ΔT). This would mean a reduction in lime consumption of between 30 and 50%.

- **Droplet diameter, DO (μm)**

Droplet size has an appreciable effect on desulfurization efficiency that is somewhat more complex than what it seems at first sight. An increase in droplet size reduces the interface area for matter transfer but, at the same time, increases the duration of the wet absorption stage. These effects have an opposite influence on SO₂ elimination and the net result on efficiency depends on the conditions under which the absorber operates. In the scenarios analyzed (figure 2), we observe, in general, an increase in efficiency as the droplet size increases, although its magnitude is quite variable, being almost zero when it operates with recirculation and at low SO₂ levels (400 ppm). The greater or lesser importance of the size of the droplet and, consequently, of the atomizer design, will depend on the operating conditions of the unit.

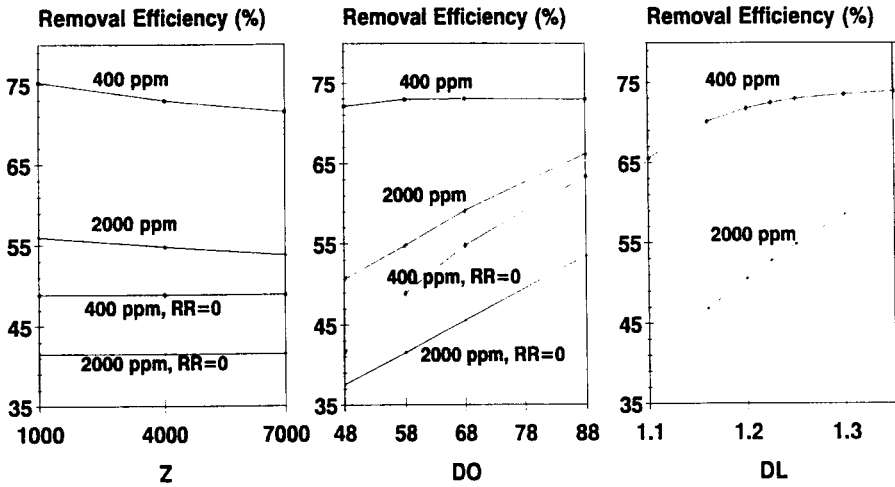


Figure 2. The effect of some operating parameters on desulfurization: Z, fly ash load (mg/Nm³); DO, average droplet size (μm); DL, slurry density (kg/m³). Different basic cases: without recirculation (RR=0) (at 400 and at 2000 ppm of SO₂) and with recirculation (at 400 ppm and at 2000 ppm of SO₂).

- Recirculation ratio (RR) and slurry density (DL)

An increase in the slurry density (equivalent to a greater recirculation ratio) leads to an increase in the internal Ca/S ratio and a decrease in the duration of the wet stage. These two factors have opposite effects on absorption efficiency and the net result will depend on the value of the mass fraction of lime in the recirculated product. On the operational level analyzed, the increase in slurry density always leads to a greater elimination of SO₂.

REFERENCES

1. L.Cañadas et al., A Flue Gas Desulphurisation and Electrofiltration Pilot Plant: Design and Objectives, World Energy Research Symposium, Florence, July 1994.
2. H. S. Shih, Simulation of SO₂ Removal via Hydrated Lime Slurries in a Spray Dryer Absorber Flue Gas Desulfurization System, Dissertation, University of Alabama, 1989.

Recovery of lime from coal gasifier waste containing calcium sulfide

S. B. Jagtap and T. D. Wheelock

Ames Laboratory and Department of Chemical Engineering, Iowa State University, Ames, Iowa 50011-2230, U.S.A.

INTRODUCTION

Calcium-based materials hold great promise as sorbents for reduced sulfur compounds at high temperature. Such materials are needed for hot gas clean up or for direct addition to coal gasifiers in several types of integrated coal gasification, combined-cycle (IGCC) power generation systems under development. Calcium-based materials are suitable for this application because they are inexpensive, readily available, and effective at high temperature because very stable CaS is formed [1,2]. However, their use has been hindered by the lack of a suitable regeneration process for converting CaS back to CaO. In principle, the regeneration of CaO could be accomplished by oxidation of CaS particles with air at high temperature. Indeed, previous work had shown that CaS particles can be converted to CaO by oxidation at 1450 to 1550°C [3,4]. Unfortunately, such temperatures are not achieved easily and the CaO would probably be dead burned and unreactive so that it could not be reused. Attempts to oxidize CaS at lower temperature produced particles containing both CaO and CaSO₄ [3,5,6]. But the formation of CaSO₄, which occupies a larger volume than CaS, led to plugging of particle pores and incomplete conversion of CaS.

Recently it was discovered in our laboratory that CaS particles can be converted rapidly and almost completely to CaO by a cyclic process which exposes the material alternately and repeatedly to oxidation and reduction at 900 to 1100°C. During oxidation with air a small portion of CaS is converted to CaSO₄ which upon treatment with a reducing gas is converted to CaO. By repeating the cycle numerous times, individual particles are converted completely to CaO. Such a process can be carried out in a fluidized bed reactor which either has both oxidizing and reducing zones or is supplied with gas that is alternately oxidizing and reducing [7].

The cyclic oxidation/reduction process for converting CaS to CaO has been demonstrated with a thermogravimetric analysis (TGA) systems, and the results are reported below. The effects of temperature and gas composition on the overall rate of conversion are indicated as well as the effect of subjecting typical sorbent materials to repeated sulfidation and regeneration.

EXPERIMENTAL METHODS

Calcium sulfide powder (99% pure from Cerac, Inc.) and reagent grade CaCO_3 powder were utilized as well as two samples of crushed limestone having the following compositions: Sample A, 52.0% CaO , 2.8% MgO , 1.1% SiO_2 ; Sample B, 49.3% CaO , 1.0% MgO , 2.9% SiO_2 . The powdered materials were briquetted with a hydraulic press which produced flat discs having a diameter of 6.35 mm and thickness of 1-2 mm. For some experiments the discs were used directly, whereas for other experiments the discs were crushed first, and the particles were sized by screening.

For demonstrating the cyclic oxidation/reduction process, a single disc of pure CaS was placed in a quartz basket which was suspended inside of a 25 mm diameter tubular quartz reactor from a calibrated electrobalance. As the reactor was heated by a temperature-controlled electric furnace, nitrogen was passed through the reactor at a flow rate of 1.0 liter/min. measured at room temperature and pressure. When the sample reached the required temperature, the gas composition was changed at 1.0 min. intervals in order to subject the material to the cyclic treatment. As a run progressed at a constant temperature, the weight of the sample was recorded continuously, and when the sample approached a constant weight, the run was discontinued.

For demonstrating repeated sulfidation and regeneration of typical sorbents, a number of crushed and sized particles of either pure calcium carbonate or limestone were placed on a quartz pan which was suspended inside of the tubular reactor. The sample was heated and calcined in a stream of nitrogen to decompose carbonate minerals, and the material was sulfided by treatment with the following mixture: 10% SO_2 , 15% CO , and 75% N_2 . Sulfidation was followed by regeneration using the oxidation/reduction treatment described above.

EXPERIMENTAL RESULTS AND DISCUSSION

A preliminary series of experiments was conducted with the TGA apparatus to determine the effects of gas composition and temperature on the overall rate of conversion of CaS to CaO by the cyclic oxidation and reduction process. Single discs of pure CaS were treated alternately and repeatedly to oxidizing and reducing gas mixtures at constant temperature, and the progress of the reactions was observed by recording the weight of each disc continuously. A 2 min. cycle time was used with 1 min. devoted to oxidation and 1 min. to reduction. Temperature, oxygen concentration, and the type of reducing gas and its concentration were varied among different runs. The conversion of CaS to CaO was determined throughout each run from the loss in weight of the reacting disc.

By conducting a number of runs at 1050°C in which either the O_2 concentration or the type and concentration of reducing gas were varied among runs, it was established that an O_2 concentration of 20% in conjunction with one of the following reducing gas concentrations gave the highest overall rate of reaction: 2% propane, 5% natural gas (principally CH_4), or 30% CO . Small deviations from these concentrations did not have a large effect on the rate of conversion.

The optimum reducing gas concentration seemed to be related to the stoichiometric quantity of reducing gas required to convert CaSO_4 to CaO and SO_2 . The stoichiometric conversion of one mole of CaSO_4 requires either 0.1 mole propane, 0.25 mole methane, or 1.0 mole CO. With less than the optimum concentration of reducing gas, the rate of conversion of CaSO_4 to CaO increased with an increase in reducing gas concentration which was to be expected. For concentrations greater than the optimum value, the rate of conversion of CaSO_4 to CaO was probably depressed by the simultaneous conversion of part of the CaSO_4 to CaS .

After establishing the optimum gas composition, additional runs were conducted to establish the optimum temperature. In one set of runs, 20% O_2 was used for oxidation and 5% natural gas for reduction while the temperature was varied from 960 to 1100°C among runs. During each of the runs, the overall rate of conversion was nearly constant until the material was almost completely converted. The rate of conversion was observed to increase with each increase in temperature so that the maximum rate was observed at 1100°C. At this temperature a disc of CaS was completely converted to CaO in 40 min. which corresponded to an overall average rate of conversion of 2.5%/min. This rate was three times that observed at 960°C.

The temperature was also varied during another set of runs which was similar to the preceding set except that 30% CO was used in place of 5% natural gas. In this set the maximum rate of conversion was also observed at 1100°C, but it was slightly lower than that observed with 5% natural gas.

Since the preliminary experiments were highly encouraging, further experiments were conducted to see whether or not various sulfur adsorbents would retain their reactivity when subjected to repeated sulfidation and regeneration. The adsorbents were derived from pure calcium carbonate and two different limestones. Since the pure calcium carbonate was obtained as a fine powder, it was first pelletized and crushed to prepare particles in the range of 0.83 to 1.17 mm. Limestone particles of a similar size were prepared by screening the as received materials which had been crushed previously. The materials were calcined to decompose the carbonate minerals. In each experiment a number of particles were subjected to a series of sulfidation and regeneration cycles at 1100°C. During the sulfidation phase of each cycle, CaO was converted to CaS by passing a gas mixture containing 10% SO_2 and 15% CO over the particles until the material approached a constant weight. Then the sorbent was regenerated by subjecting the particles to the oxidation/reduction cyclic treatment to convert CaS back to CaO . For the regeneration step 10% O_2 was used for oxidation and 30% CO for reduction, and the treatment was continued until the material approached a constant weight.

In one run the sorbent derived from pure CaCO_3 was subjected to four sulfidation and regeneration cycles. During the first part of each cycle CaO seemed to be converted completely to CaS , and during the second part CaS seemed to be completely converted back to CaO . The time required for sulfidation was 18 min. for each of the first three cycles and 14 min. for the fourth cycle, whereas the time required for regeneration was 20 min. for the first cycle, and it decreased to 14 min. for the fourth cycle.

In a second run in this series the sorbent derived from limestone A was subjected to five sulfidation and regeneration cycles. Again during each cycle the conversion of CaO to CaS and the regeneration of CaO appeared complete. For the first three cycles the time required for sulfidation was 14 min., and for the last two cycles it was 12 min. For the first cycle the regeneration time was 36 min. and for most of the remaining cycles it was 34 min.

In a third run in this series the sorbent derived from limestone B was subjected to seven sulfidation and regeneration cycles. With this less pure material the conversion of CaO to CaS was 85-86% during each cycle while the regeneration of CaS was complete. For the first four cycles the time required for sulfidation was 24 min., and for the last three cycles it was 20 min. Interestingly, the time required for regeneration was 20 min. for the first cycle, and it decreased steadily from one cycle to the next until only 10 min. was required for regeneration in the final two cycles.

In all three of the preceding experiments the maximum levels of sulfidation and regeneration remained constant from one cycle of sulfidation and regeneration to the next. Furthermore, the cycle time decreased between the first and last cycles of each run. Therefore, the reactivity of the materials appeared to increase with repeated sulfidation and regeneration.

CONCLUSIONS

The experimental results showed that CaS can be converted to CaO by a cyclic oxidation/reduction process. The overall rate of conversion depends on reaction temperature and the concentration of oxygen during the oxidizing phase and the type and concentration of reducing gas during the reducing phase. The repeated sulfidation and regeneration of typical calcium-based sorbents seems to enhance the reactivity of the materials.

ACKNOWLEDGMENT

Support for this project was provided by a Department of Energy, Ames Laboratory Directed Research and Development Grant.

REFERENCES

1. P.R. Westmoreland and D.P. Harrison, *Environmental Science & Technology*, 10 (1976) 659.
2. J.H. Swisher and K. Schwerdtfeger, *Journal of Materials Engineering and Performance*, 1 (1992) 399.
3. R.J. Torres-Ordoñez, J.P. Longwell, and A.F. Sarofim, *Energy & Fuels*, 3 (1989) 506.
4. D.C. Lynch and J.F. Elliot, *Metallurgical Transactions B*, 9B (1978) 691.
5. D.C. Lynch and J.F. Elliot, *Metallurgical Transactions B*, 11B (1980) 415.
6. J. Abbasian, A. Rehmat, and D.D. Banerjee, *Ind. Eng. Chem. Res.*, 30 (1991) 1990.
7. T.D. Wheelock and T. Riel, *Chemical Engineering Communications*, 109 (1991) 155.

^{29}Si -NMR study of the absorbent for flue gas desulfurization

Hideshi Hattori, Nariyasu Kanuka, and Ryu-ichi Kanai

Center for Advanced Research of Energy Technology, Hokkaido University, Sapporo 060, Japan

1. INTRODUCTION

The flue gas from a coal fired boiler contains a high concentration of SO_2 which should be removed before emitted from a chimney for protection of environment from pollution. A wet desulfurization system is commonly adopted for flue gas desulfurization (FGD), and exhibits a high utilization efficiency of Ca component in the absorbent, but needs a large amount of water. As dry FGD systems, a duct injection and a slurry spraying are adopted. The efficiency, however, is not so high as compared to a wet FGD system.

Recently, the SO_2 absorbent which exhibits a high utilization efficiency of Ca component in a dry FGD process was prepared from a coal fly-ash, $\text{Ca}(\text{OH})_2$, and CaSO_4 by hydrothermal reaction. The dry FGD process using this absorbent has been commercially operated since 1991. The process is schematically illustrated in Fig.1.

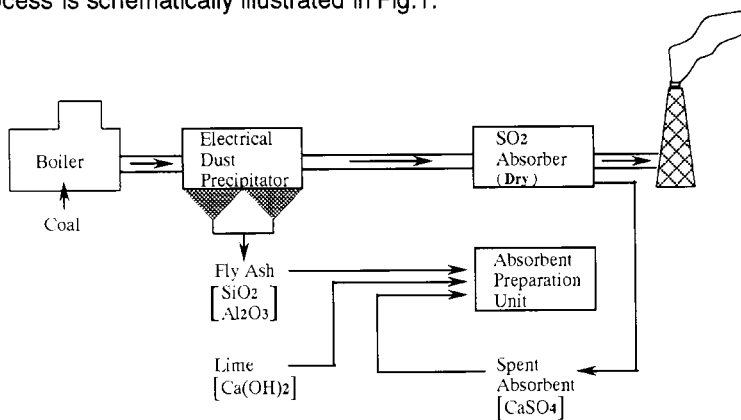


Fig. 1 Process flow of FGD for coal fired boiler

A coal fly-ash collected at the electrostatic precipitator is mixed with $\text{Ca}(\text{OH})_2$ (lime) and CaSO_4 (gypsum), and transferred to the absorbent preparation unit where hydrothermal reaction is taken to produce active absorbent. The absorbent is extruded into granules, dried, and placed in the SO_2 absorber where SO_2 is removed from dirty flue gas to emit a clean flue gas. SO_2 is fixed in the form of CaSO_4 . The utilization efficiency of Ca component converting into CaSO_4 exceeds 90%.

In the present paper, we study the structural changes of the absorbent during the hydrothermal reaction and SO_2 absorption by ^{29}Si -MASNMR using a model absorbent of

calcium silicate hydrate to elucidate the mechanisms for a high utilization efficiency of Ca component. It is revealed that the structural changes during the absorption of SO_2 enable Ca component present in a bulk to be exposed to the flue gas.

2. EXPERIMENTAL METHODS

2.1. Preparation of the absorbent

For preparation of a model absorbent of calcium silicate hydrate, a mixture of $\text{Ca}(\text{OH})_2$ and $\text{SiO}_2 \cdot x\text{H}_2\text{O}$ was heated at 363K for 20h in a water with stirring. The resulting slurry was filtered, washed with water and dried at 373K and then 473K for 3h. The ratio CaO/SiO_2 was adjusted to 1.4 (mol/mol). The absorbent prepared using fly-ash was prepared as follows. To a hot water at about 343K, CaO, fly-ash and spent absorbent (CaSO_4 source) were added and stirred with a mill. The slurry was hydrated for 12 h at 363K and then dried at 473K for 1 h. A physical mixture of $\text{Ca}(\text{OH})_2$ and $\text{SiO}_2 \cdot x\text{H}_2\text{O}$ was prepared by grinding the compounds in a mortar.

2.2. Reaction procedures

The desulfurization was carried out at 303 K in a flow reactor with a model flue gas composed of SO_2 1000ppm, NO_x 1000ppm, O_2 10%, H_2O 10%, and He balance. The flow rate was 200 ml/min using 0.5 g of the absorbent. The concentrations of SO_2 and NO_x were measured by infrared spectroscopy and chemiluminescence, respectively.

2.3. NMR measurement

^{29}Si -MASNMR spectrum was measured for the powdery sample on a Bruker MSL-200 in the mode of high power decoupling. The main conditions for measurement were as follows; observed frequency 39.8Mhz, observed spectral width 10kHz, pulse width (90° pulse) 4.0 ms, pulse interval 7 s(10 ms delay), data points 8192, line broadening factor 30Hz, accumulation 5000, reference of ^{29}Si chemical shift Q^4 (11.72ppm).

3. RESULTS AND DISCUSSION

The percentages SO_2 removal are plotted against the time on stream in Fig. 2 for the calcium silicate hydrate, the absorbent prepared from fly-ash, and the physical mixture. For both the calcium silicate and the absorbent prepared from fly-ash, SO_2 removal kept 100% for the initial 1 h, and then decreased gradually to about 30 %, and kept this level for a long time on stream. The physical mixture scarcely absorbed SO_2 except for the initial few min. The $\text{Ca}(\text{OH})_2$ became active by combination with SiO_2 . There seem to be two different mechanisms for absorption of SO_2 , one occurring in the initial stage of the time on stream which results in 100% SO_2 removal, and the other in the later stage of the time on stream which results in about 30% SO_2 removal.

The presence of NO_x and H_2O is required for SO_2 absorption. Without NO_x or H_2O , SO_2 absorption was not appreciable.

^{29}Si -MASNMR spectra for the calcium silicates prepared with different hydration period are shown in Fig. 3 together with that for the raw material silicic acid. The peak at -112 ppm observed for the silicic acid is assigned to the cross-linked framework(Q^4). After hydration of 20min, Q^4 peak disappeared, and two peaks appeared at -83 ppm and -79 ppm which are assigned to middle group in chain (Q^2) and chain end group (Q^1), respectively. On prolonging the hydration time to 12h, the peaks did not change much in both intensity and chemical shift, only a slight broadening of the peaks was observed. It is indicated that Si-O-Si

bonds of Q^4 structure rapidly cleave and convert into straight chain Si-O-Si as hydration with $Ca(OH)_2$ starts.

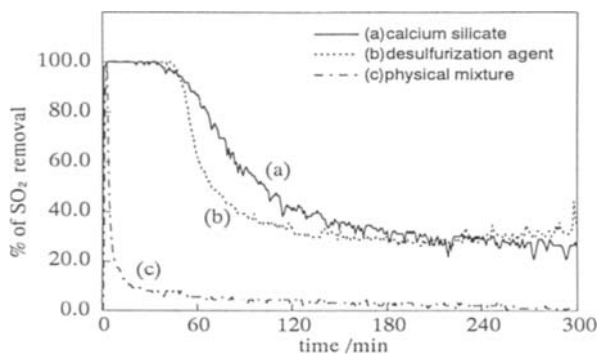


Fig. 2 The percentage SO_2 removal vs. time on stream

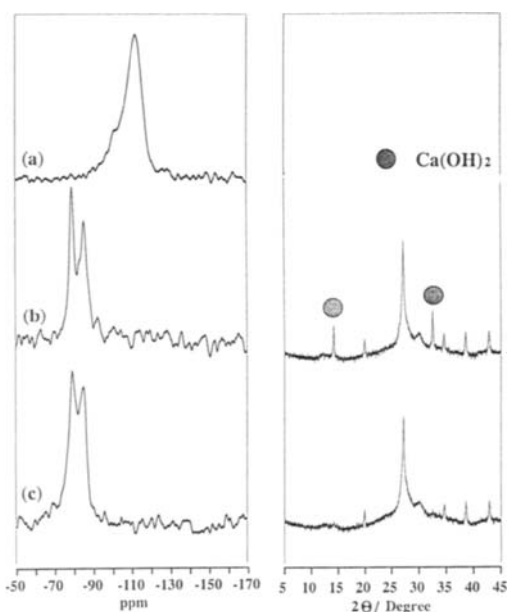


Fig. 3 ^{29}Si -MASNMR spectra and XRD patterns of the sample hydrated for different period. (a) silicic acid, (b) hydrated for 20min, (c) hydrated for 12h

From the intensity ratio of Q^2/Q^1 , the averaged chain length of the silicate can be calculated. One silicate chain was calculated to consist of about 4 SiO_4 tetrahedra regardless the hydration time.

To examine the structural change during desulfurization, ^{29}Si -MASNMR spectra were measured for the samples being allowed to react for different time on stream and, shown in Fig. 4. The percentages of SO_2 removal in 1h, 1.5h, 5h, and 20 h were 100%, 100%, 58%, 27%, and 10%, respectively. The samples reacted for 1h and 1.5h, which still kept high SO_2 removal, showed the peaks for Q^1 and Q^2 . As the reaction proceeded, the peak intensity for Q^1 slightly decreased. In this period, the Ca ions interacting with non-cross linked O of Q^1 participate in the SO_2 removal. For the samples reacted for 5h and 20 h, which showed low SO_2 removal, the appearance of the peaks for Q^3 and Q^4 with concomitant decrease in the peak intensity for Q^1 and Q^2 was observed. In the period where the SO_2 removal level is low, the Ca ions interacting with non-cross linked O of Q^2 participate in the SO_2 removal.

The surface area of the sample did not change much with the time on stream, though $CaSO_4$ was accumulated on the sample. It is suggested that the original surface present on the sample before SO_2 absorption decreases with the formation of $CaSO_4$, and a new surface appears with the formation of silica framework as the SO_2 absorption proceeds.

The structural change of the absorbent during SO_2 absorption is illustrated in Fig. 5. In the initial stage of the reaction, SO_2 is absorbed by the CaO component located on the

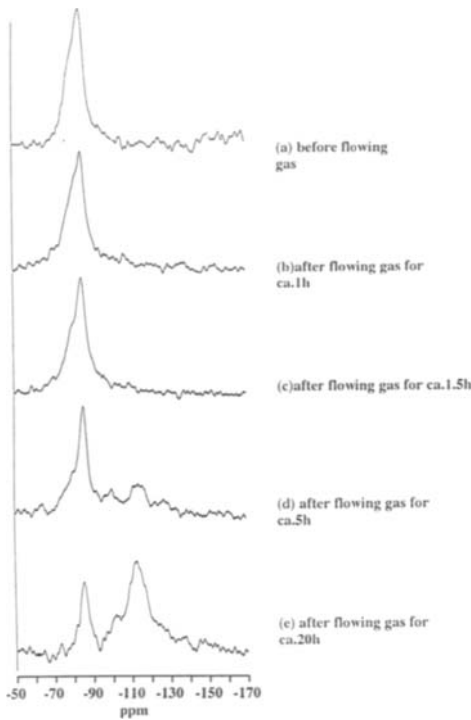


Fig. 4 ²⁹Si-MASNMR spectra of calcium silicate used for different time on stream

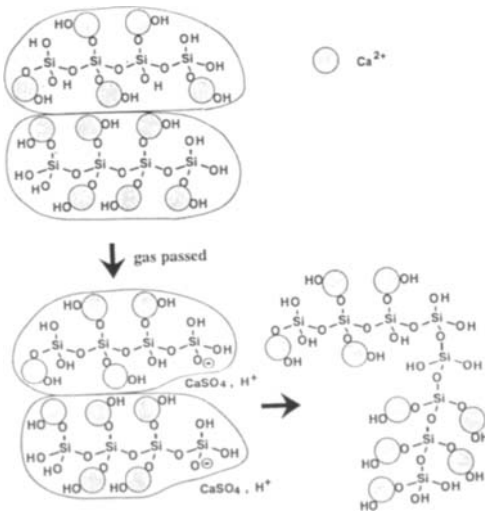


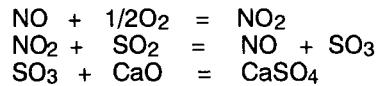
Fig. 5 Model for structural change during desulfurization

outer surface of the particles consisting of several silicate chains. The high SO₂ removal observed in the initial stage of the reaction proceeds by this mechanism.

As CaO component converts to CaSO₄ and expelled from the particle, Si-O-Si bonds begin to form. The formation of new Si-O-Si bonds results in exposure of Ca component located in a bulk to the surface. In this way the Ca component located in the bulk of the absorbent becomes utilized for SO₂ absorption, and therefore, the utilization efficiency of Ca is able to exceed 90%. The low SO₂ removal observed in the later stage of reaction which persists for a long period proceeds by this mechanism.

When simple Ca(OH)₂ is used, CaSO₄ is formed on the outer surface of the particles, and the CaSO₄ layers cover the unreacted Ca(OH)₂ to be inactive. In the case of the absorbent of calcium silicate, SO₂ absorption is accompanied by the structural change in Si-O-Si framework, which enable Ca component in the bulk to expose to the gaseous SO₂. As a result, a high Ca utilization efficiency is attained.

Finally, the role of NO which is required for SO₂ absorption is suggested to be a catalyst. The SO₂ proceeds through the following reactions.



The NO and NO₂ act as catalyst for the SO₂ absorption to form CaSO₄.

Design of a Hot Gas Desulphurisation Plant

V. Artos, Y. Benito, P. García and J. Otero-Ruiz

Centro de Investigaciones Energéticas Medioambientales y Tecnológicas (CIEMAT)
Avda. Complutense 22, 28040 Madrid, Spain

1. ABSTRACT

This paper describes the main characteristics of a gas processing plant installed at CIEMAT (Madrid, Spain) to perform studies of hot gas desulphurisation. The plant can treat up to $5.5 \cdot 10^3 \text{ Nm}^3/\text{s}$ of a mix of gases simulating the composition of the flue gases from coal combustion or gasification processes. It is designed to operate at a maximum temperature of 973 K and a pressure of 30 bar. Gas samples taken at different points are conditioned and analysed on-line by gas chromatography.

2. INTRODUCTION

In the last decade the electric utility industry and industrial research organisations have sponsored a major effort towards the development of new clean coal technologies for the production of electric power.

As a result of these research, development, and demonstration programs, the Integrated Gasification Combined Cycle (IGCC) technology is approaching technical and economical maturity. IGCC uses coal gasification, followed by gas cleanup, to provide a clean fuel for a gas turbine.

For such advanced power generation systems there is the need to remove dust, sulphides, ammonia, cyanides, and halides from the fuel gas, to avoid damage of the turbines and reduce pollutant emissions. Two different technologies may be used to remove these pollutants:

1. Cold Gas Cleaning Up (CGCU): a well developed process in which the gases are cooled down to 313 K, its based on wet gas cleaning systems by means of scrubbers. This process has an adverse effect on the cycle efficiency.
2. Hot Gas Clean Up (HGCU): a process still under development, which cleans the gasifier outlet gases at temperatures in the range of 573-873 K and at pressures of 10-25 bar.

Calculations performed by Verweij et al. (1) show that the application of HGCU results in efficiency improvements in the range of 2-3 % depending on the system configuration.

Hydrogen sulphide removal at high temperatures is based on absorption in a solid compound. Two types of solids are studied:

1. Non-regenerable solids such as limestone or dolomite, which are introduced into the gasifier at temperatures of 1073-1273 K (insitu desulphurisation). This method has the main drawback that it generates a big quantity of solid wastes requiring an expensive treatment to transform the CaS in the more stable CaSO_4 before deposition. In addition these solids are not appropriate to use under the conditions existing in moving or entrained flow gasifiers.
2. Regenerable sorbents which are brought in contact with the flue gases in an external bed, after removing the particles.

Currently metal oxides are studied as regenerable sorbents. In addition to demonstrate low H₂S concentrations (less than 100 ppm) in the outlet streams these sorbents must be stable and easily regenerable, and the sulphidation and regeneration kinetics should be fast. They also must demonstrate a very long life and maintain low costs in their production and disposal (2).

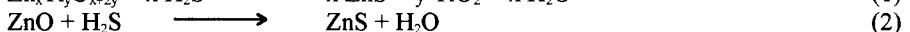
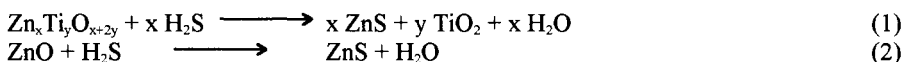
CIEMAT collaborates with three other European research organisations (CTDD British Coal -United Kingdom-, Kema -Holland- and Rheinbraun -Germany-) and, TGI (Tecnología y Gestión de la Innovación S.A.) and UPC (Universitat Politècnica de Catalunya) from Spain in a ECSC (European Coal and Steel Community) project entitled Hot Gas Desulphurisation for Advanced Power Generation Systems. The main objective in this project is to gain experience about the hot gas desulphurisation processes, to collaborate in the development of the technology in Europe, and to evaluate the performance of several commercially available sorbents over a range of conditions relevant to various combined cycle coal gasification technologies. For these investigations CIEMAT installed a Hot Gas Desulphurisation Plant with a fixed/fluidised bed reactor, designed to operate at high temperatures and high pressures. This paper presents the main characteristics of this plant.

2. HOT GAS DESULPHURISATION

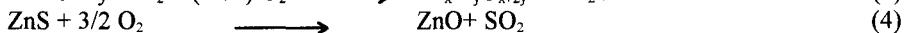
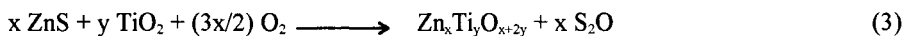
In this project, CIEMAT evaluates the performance of commercially available sorbents with two simulated gases representing the compositions of the gases produced by the ELCOGAS IGCC (50 % CO, 20 % H₂, 4 % CO₂, 9 % N₂, 1 % H₂S and 10 % H₂O) from Spain and the Air Blown Gasification Cycle ABGC (16 % CO, 15 % H₂, 8.5 % CO₂, 45.2 % N₂, 0.05 % H₂S, 15 % H₂O, 0.2 % NH₃ and 0.05 % HCl) developed by the CTDD British Coal from the United Kingdom. Two zinc oxide based sorbents were selected according to published information to use with these gases:

- A Zinc Titanate provided by the Research Triangle Institute (RTI) in USA for fluidised bed studies, This solid has a ZnO to TiO₂ molar ratio of 1.5 and a particle size between 100-300 μm.
- Z-Sorb provided by the Phillips Petroleum Company (USA) for fixed bed studies. Phillips supplies the sorbent as cylindrical pellets of 3.2 mm diameter and (6-10) mm long.

During sulfidation the reactions that may occur with zinc titanate or zinc oxide are:



The sorbent is then regenerated with air diluted with N₂ following reactions (3) and (4) for zinc titanate and zinc oxide respectively:



A parametric study is conducted to evaluate influence of the operating variables in the desulphurisation process. At a pressure of 25 bar the sorbent is tested at absorption temperatures from 723 K to 973 K and absorption gas space velocity from 0.8-1.7 s⁻¹. During the regeneration step the influence of temperature (773-973 K), gas space velocity (0.3-0.6 s⁻¹) and O₂ content in the regeneration gas (1-2%) are evaluated. To conduct this studies CIEMAT installed a bench scale plant which operates at temperatures up to 973 K and pressures of 30 bar with a maximum flow rate of 5.5 10⁻³ Nm³/s. A flow diagram of this plant is represented in Figure 1.

2. Hot Gas Desulphurisation Plant

2.1.1. Gas Supplying Unit

This unit supplies six different gases to the plant (Air, H₂, H₂S in N₂, CO, CO₂, and N₂ in this project). Each gas is supplied to the plant through two lines. When the gas of the first line terminates, the system gives an alarm and changes automatically to the second line. This mechanism allows continuous operation of the plant for several days, if necessary. These gases are then mixed to simulate the desired gas composition. A battery of twelve mass flow controllers, operated by a personal computer, is used to adjust the composition and flow rate of the simulated gas. For security reasons it is impossible to introduce air into the plant whenever H₂ or CO is fed. The unit is designed to work with a maximum flow rate of $5.5 \cdot 10^3 \text{ Nm}^3/\text{s}$ and under a pressure of 75 bar. The rest of the plant is designed for pressures up to 30 bar.

2.1.2. The Inlet Gas Conditioning Unit

In this unit the gases are heated up to the process temperature in two steps. After the first step in the preheater (EH1) the gases reach a maximum temperature of 673 K. Next, vapourised water from a steam generator (EH2) can be added to the main gas stream. Gas pollutants like chloride or ammonia can be introduced as well at this point with the water. Then, in the second step the gas is heated further in a superheater (EH3) up to a maximum temperature of 973 K. The pipelines going to the reactor are heated electrically (EH4). Security valves are installed in each furnace. Separate controllers are used for each of the heating elements.

2.1.3. The Pressure Reactor

The reactor, manufactured by Autoclave Engineers, is built of Incoloy 800. It has a height of 1 m and an internal diameter of 80 mm. The inlet and outlet lines can be interchanged, which allows the operation under fixed or fluidised bed conditions. Inside the reactor the sorbent is contained in a removable cage. The bottom of this cage is a distributor of α -alumina. The reactor is heated by a four-zone furnace equipped with separate temperature electronic controllers. The temperature profile inside of the reactor is determined by 11 type K thermocouples, one of which is mounted at the bottom of the reactor to measure the outlet temperature of the gases in case that the reactor works as a fixed bed (equally, the same thermocouple measures the inlet gas temperature under fluidised bed conditions). The other 10 thermocouples are placed at different heights in the bed. A differential pressure monitor is used to detect plugging across the reactor. Security valves are also installed in both sides of the reactor.

2.1.4. The Outlet Gas Conditioning Unit

The exit gases from the reactor are cooled down to 473 K in a heat exchanger (HE1). Following this, a refrigerated pot is installed to remove the sulphur condensates. Two 50 μm filters avoid that particles reach the pressure control valve. The gases are finally cooled to ambient temperature in (HE2) before they exit to the atmosphere.

2.1.5. Process Control and Data Acquisition Unit

Flow rate and composition of the inlet gases as well as temperatures and pressures are automatically controlled during the process. A personal computer operates the mass flow controllers to adjust the required gas flow and composition. PID controllers with two alarm levels are used to control temperatures and pressures. A PLC with 64 input and 48 output signals supervises all the alarms of the process, allowing uninterrupted operation of the test

facility. Other functions of the PLC are the control of the plant valves and actuators and the communications with the PC. Real time data acquisition is performed by the personal computer. The collected data can be graphically displayed to the screen and logged to a disk. The computer also records the alarms produced during the test.

2.1.6 Gas Analysis System

Gas samples are taken in five points along the plant (CG1 to CG5) and continuously analysed by a Hewlett Packard Gas Chromatograph equipped with two detectors. A Thermal Conductivity detector is used to analyse H_2 , CO , CO_2 , O_2 , N_2 , and high concentrations of H_2S and SO_2 . Low concentrations of H_2S and SO_2 , and COS are detected in a Flame Photometric Detector. The sampled gas is maintained at temperatures over 433 K to avoid sulphur condensations on the lines. The analysis results are collected and processed by a personal computer with a Hewlett Packard data acquisition software.

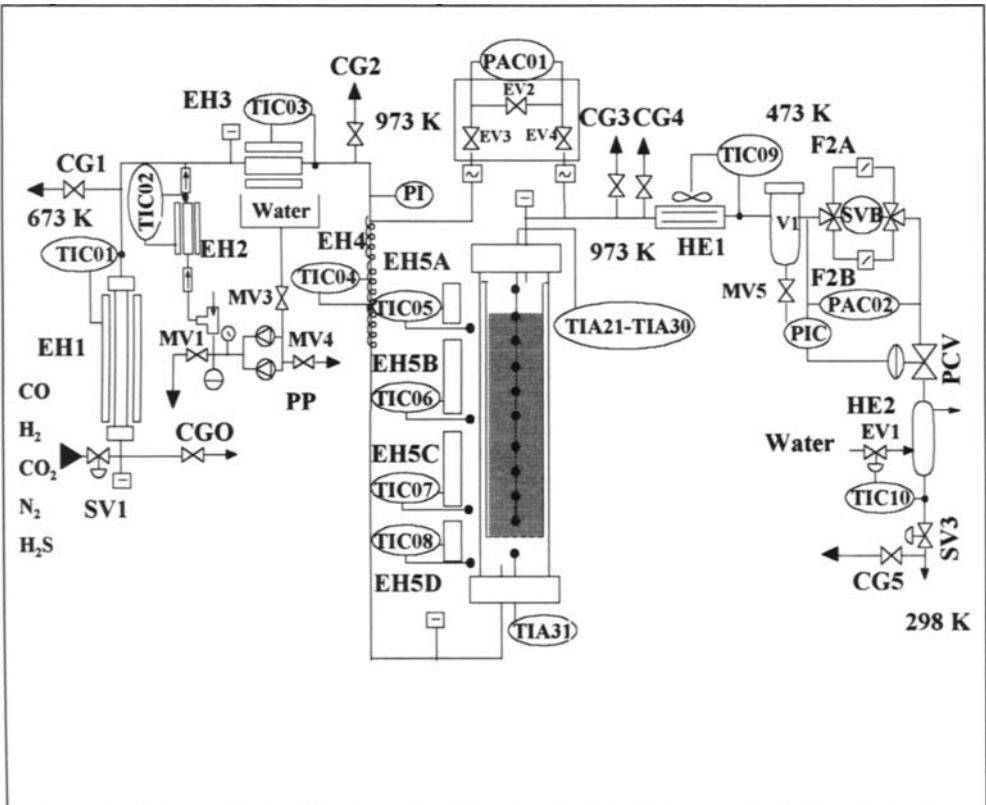


Figure 1. Diagram of Ciemat's Hot Gas Desulphurisation Plant

REFERENCES

1. K. Verweij, J. Staverman and W. Boender, *Modern Power Systems*, November (1993), 57.
2. Cicero D.C., (DOE/METC/C-94/7157), *Proceeding of the Coal Fired Power Systems 94--Advances in IGCC and PFBC Review Meeting*, Morgantown (West Virginia), (1994), 219.

Hot gas desulfurization using zinc-ferrite regenerable sorbents

C.Cilleruelo^a, E.García^a, R.Moliner^a and J.V.Ibarra^a

^aInstituto de Carboquímica, Poeta Luciano Gracia 15, 50015 Zaragoza, Spain

M.Pineda^b, J.L.G.Fierro^b and J.M.Palacios^b

^bInstituto de Catálisis y Petroleoquímica, Campus Universidad Autónoma, Cantoblanco, 28049 Madrid, Spain

1. INTRODUCTION

An integrated gasification combined cycle (IGCC) power system employing hot-gas desulfurization of coal-derived gas is the most promising advanced technology for producing electric power from coal. Recent developments in hot-gas desulfurization technologies have focused on regenerable metal oxide sorbents to remove reduced sulfur species (H_2S , COS) from coal gas. In this paper zinc ferrite sorbents have been tested in the process of H_2S retention at high temperature.

2. EXPERIMENTAL

2.1. Sorbents preparation

Four types of samples with three different Fe:Zn ratios were prepared. Type 1 samples were obtained by calcination of commercial bulk oxides. Type 2 samples (FZ2) were similar to type 1 although after calcination they were mixed in the proportion 10:90 with Al_2O_3 (particle diameter = 0.4–0.6 mm). Types 3 and 4 were prepared by impregnation of Al_2O_3 with aqueous solutions of $Zn(NO_3)_2$ and $Fe(NO_3)_3$ of the appropriate concentrations. Water was removed in a rotary evaporator at 65°C and the samples were then dried overnight at 120°C. All samples were finally calcined at 650°C for 16h. Three different Fe:Zn stoichiometries (between 0.8 and 1.2) were considered for each type of sample.

Morphological studies and element distributions of the fresh, sulfurized and regenerated samples were carried out by Scanning electron microscopy (SEM-EDX). The textural properties were characterized by N_2 adsorption at 77 K, Hg porosimetry, X-Ray diffraction (XRD) and X-ray photoelectron spectroscopy (XPS). Table 1 summarizes the method of preparation and some relevant textural parameters for the fresh and sulfurized zinc-ferrites of 1:1.2 stoichiometry. The regenerated samples considered for the morphological study were zinc-ferrites of 1:1 stoichiometry.

Table 1.
Labelling and textural parameters of fresh and sulfurized samples of 1:1.2 stoichiometry

Sample	Support (wt%)	Method	$S_{\text{BET}}(\text{m}^2/\text{g})$		$V_p(\text{cm}^3/\text{g})$		$D_p(\text{nm})$	
			a)	b)	a)	b)	a)	b)
FZ1	none	bulk	81	11	0.28	0.31	8.2	8.7
FZ2	$\gamma\text{-Al}_2\text{O}_3(90\%)$ $d_p=0.4\text{-}0.6\text{mm}$	mixing	162	139	0.37	0.51	7.6	7.5
FZ3	$\gamma\text{-Al}_2\text{O}_3(90\%)$ $d_p=0.4\text{-}0.6\text{mm}$	impregnation	166	152	0.76	0.68	6.8	6.9
FZ4	$\gamma\text{-Al}_2\text{O}_3(90\%)$ $d_p<0.2\text{mm}$	impregnation	164	151	0.50	0.77	6.9	6.9

a) fresh b) sulfurized

2.2. Study of H_2S retention

The sulfidation performance of the zinc ferrite sorbents was investigated, in terms of breakthrough curves, in a 1cm i.d. stainless steel fixed-bed vertical microreactor. Gas analyses at the inlet and outlet were performed by mass spectrometry using a quadruple mass analyser. Sulfidation runs were carried out at 540°C using 2g samples, corresponding to a bed depth of 3.8cm and total gas flow of $70\text{cm}^3/\text{min}$ (0.5% vol H_2S in N_2).

The sulfurized sorbents were regenerated at 680°C , in a fixed-bed microreactor of 1.6 cm i.d., with an air/steam mixture (3% O_2 , 30% H_2O). The results obtained in this study for the FZ1 sample with a stoichiometry of 1:0.8 are shown in Figure 1 and 2.

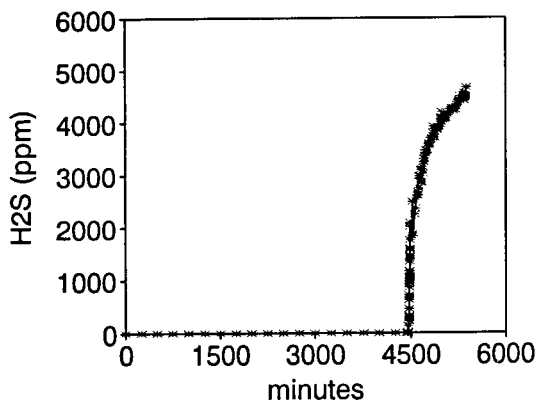


Figure 1. H_2S breakthrough curve for FZ1 (1:0.8) sorbent.

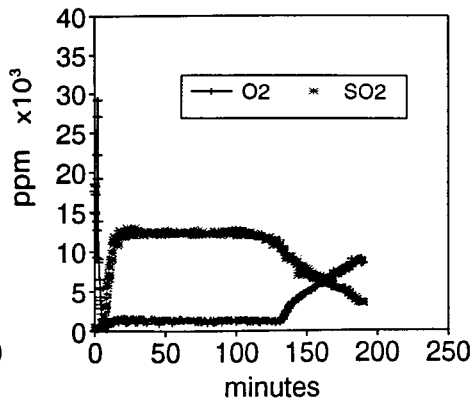


Figure 2. SO_2 and O_2 evolution with regeneration time for the same sample.

The kinetics of H₂S retention by zinc ferrites was performed on 10mg samples in thermobalance under isothermic conditions. The intrinsic rate constants were deduced from the results on the smallest particles (50 μ) using a grain model under conditions of chemical control of the reaction. Tests were carried out in the temperature range of 540-650°C and the intrinsic rate constants obtained were adjusted to the Arrhenius equation in order to obtain activation energies. The results are shown in Table 2.

Table 2.

Kinetic constants at different temperatures for H₂S retention by zinc ferrites

Sample	Temperature °C	k cm/s $\times 10^{-5}$	k' s ⁻¹	Ea cal/mol	A s ⁻¹
FZ1(1:0.8)	540	3.54	31.9	3166.7	228.86
	600	4.37	39.4		
	650	4.42	39.9		
FZ1(1:1)	540	4.20	35.9	3075.94	235.09
	600	4.23	40.3		
	650	4.34	45.0		
FZ1(1:1.2)	540	3.37	30.4	2369.14	130.16
	600	3.69	33.3		
	650	4.01	36.2		

3.RESULTS AND DISCUSSION

3.1.Characterization of fresh and sulfurized samples

The morphological characteristics obtained by SEM micrographs in the fresh sorbents showed that bulk samples FZ1 are constituted by aggregates of very small particles with porosity associated mainly to interparticular voids. However, the impregnated samples (FZ3 and FZ4) are made up of large alumina particles on which the active ingredient is spread with a high degree of dispersion. FZ2 samples exhibit an intermediate situation with large alumina particles and small zinc ferrite particles deposited on them.

Sulfurized bulk samples (FZ1) presented a decrease of almost one order of magnitude in the BET area although the decrease in the pore volume and the parallel increase of pore diameter were small. This means that the smaller particles of the original Zn and Fe oxides disappeared in the course of sulfidation and larger metal sulfide structures were formed. Similar effects are observed in the mixing samples (FZ2) although the changes are much less pronounced because only one tenth of the metal oxides was present with respect to the bulk samples. In relation to impregnated samples, the change in the textural properties was very small suggesting that no pore occlusion took place during the incorporation of Fe and Zn. The low efficiency of the impregnated samples was associated not only to the low metal content, but also to the formation of aluminates by interaction with the support.

The characterization of the regenerated bulk samples showed an almost complete recuperation of active phase (zinc ferrite) as well as a remarkable sintering process which produced a great diminution in specific surface area ($6\text{m}^2/\text{g}$) and an increase of the pore diameter (13.8nm).

3.2. Sulfidation and regeneration cycle

Zinc-ferrites were able to remove hydrogen sulfide up to less than 10ppm according to literature (1). Bulk samples (FZ1) showed the best behaviour in the sulfidation reaction with breakthrough times, correspondent to 500 ppm, between 200 and 4500 minutes (Figure 1). The fast increase in the outlet H_2S concentration after the breakthrough point indicates a bed exhaustion and a favourable sorption process with a narrow front moving along the bed.

Regeneration times were related to the sulfidation times. The stoichiometry 1:0.8 presents for all types the highest relations of sulfidation/regeneration cycle time because this stoichiometry presents the highest sulfidation time but at the same time the lowest regeneration time. These facts would indicate that the increase in iron content in the stoichiometry of the ferrite has a positive effect in the operation time (sulfidation/regeneration cycle).

3.3. Kinetic studies

The increasing values of activation energy observed in Table 2, indicate an impediment in the chemical reaction with decreasing zinc oxide contents in the samples. These results agree with the thermodynamic studies by Shrodt et al. (2). According to them the iron oxide presents an unfavourable thermodynamic for attempting high efficacy in desulfurization process in comparison with zinc oxide.

The low activation energies found in this work suggest that an adsorption-desorption mechanism could be involved in the sulfidation reaction, wherein H_2S is dissociatively adsorbed on the Fe surface and hydrogen is desorbed as the product gas. Reaction control by this mechanism has been also suggested by Tamhankar et al. (3) in the studies on iron oxide- H_2S reaction, wherein activation energy for reaction is found to be low and the controlling step is considered to be the decomposition of H_2S .

Acknowledgements

The authors wish to thank the ECSC (Project 7220-EC/756) for financial support.

REFERENCES

1. Gupta R., Gangwal S.K., *Energy & Fuels*, 6, 21-27, 1992.
2. Schrodt J.T., Hilton G.B., Rogge Ch.A., *Fuel*, 54, 269-272, 1975.
3. Tamhankar S.S., Hasatani M., Wen C.Y., *Chem. Eng. Sci.*, 1981, 36, 1181-1191.

Influence of physical properties of iron oxide sorbents on their reactivity for high temperature removal of hydrogen sulfide

S. Kushiyama, R. Aizawa, S. Kobayashi, I. Uemasu, K. Mizuno, M. Kaiho and Y. Yamashita

National Institute for Resources and Environment,
16-3 Onogawa, Tsukuba, Ibaraki, Japan

1. INTRODUCTION

Iron oxide is a material most frequently utilized in the preparation of sorbents for hot coal gas desulfurization. A great number of studies have been reported on the various aspects of its performance, including thermodynamics (1,2), kinetics (3,4) and durability (5), but the factors affecting the reactivity of iron oxide-based sorbents seem not to be fully understood. In this study an emphasis is placed on the influence of physical properties and impurities in the sorbents prepared. The influence of water in the reaction gas mixture is also investigated.

2. EXPERIMENTAL

The materials used were natural iron oxide minerals, namely ochers, red iron oxide (RIO) and iron ores, and synthetic pure α -Fe₂O₃, all of which were first pelletized and calcined at temperatures above 600°C, and then crushed and sieved into 0.59/0.84mm of particle size. The properties are listed in Table 1.

Table 1
Properties of sorbents calcined at 600°C or 900°C

	Composition (wt.%)				Surface area (m ² /g)	Fe ₂ O ₃ cryst. size (nm)
	Fe ₂ O ₃	SiO ₂	Al ₂ O ₃	CaSO ₄		
Ocher(Niwasaka)	71.9	12.4	3.0	12.5	114 (19)	13 (33)
RIO	89.0	7.5	1.9	0.4	12 (5)	140 (150)
Iron ore(Newman)	96.0	2.6	1.3	0.0	4 (1)	120 (160)
pure α -Fe ₂ O ₃	99.9	-	-	-	-	(>200)

The values for 900°C calcination are shown in parentheses.

Desulfurization reactions were carried out by a fixed bed reaction apparatus equipped with a quartz reactor of 6mm inner diameter using a reaction gas mixture of 0.5% H_2S -20% H_2 - N_2 (balance) or 0.5% H_2S -10% H_2O -20% H_2 - N_2 , at the condition of; temperature 500°C, GHSV 10,000 hr⁻¹, pressure 1.4 atm. The average degree of sulfidation of sorbent bed, which was defined as the mol ratio of the total amount of H_2S uptake to the amount of Fe loaded in the reactor, at the time when the reactor outlet H_2S concentration reached 300ppm, was taken as a measure of reactivity. Reactions using an electrobalance system were also conducted to measure the reaction rate of sorbent particles or powders.

3. RESULTS AND DISCUSSION

3.1. REACTIONS IN THE ABSENCE OF WATER

As described in a previous paper (6), the reactivity with the gas mixture containing no water is strongly controlled by intraparticle diffusion, namely the pore size distribution or effective diffusivity of sorbent particles being one of the dominant factors. Surface area or Fe_2O_3 crystallite size has only a little influence. However, as can be seen in Figure 1, the relation between the reactivity and the effective diffusivity is markedly different according to the types of sorbents. Ochres exhibit much higher reactivity compared to the other sorbents at the same level of diffusivity.

Scanning electron microscopic (SEM) examination of the sulfided particles shows that, for all the sorbents, except ochers, a dense layer of ca. 10 μm thickness of iron sulfide (pyrrhotite) is formed around the outer surface of the particles as illustrated in Figure 2 (left side). This indicates a severe limitation of the gas diffusion into the particles, and thus explains the lower reactivity.

A careful examination of the SEM image suggests the presence of very fine SiO_2 particles (at least less than 1 μm) in the ochers, leading to the idea that it might prevent the sintering or agglomeration of fine particles of iron sulfide. To confirm this, powdered RIO was wet-mixed with a solution of silica sol prepared by sol-gel method (7), and the resulting silica (6wt%) -coated RIO was formed into 0.59/0.84mm

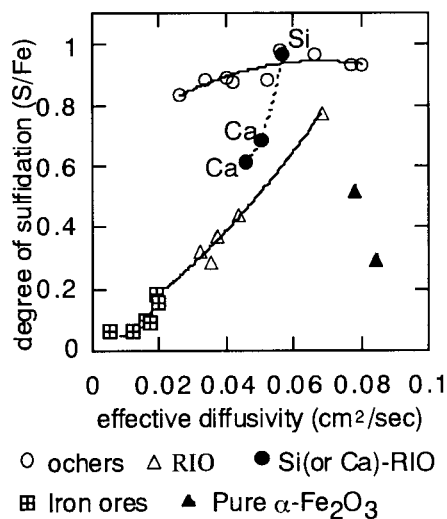


Figure 1. Relation between De and average degree of sulfidation of sorbent bed at the breakthrough of 300ppm

particles as usual. As shown in Figure 1, this sorbent (plotted with the mark ●) actually gives a high reactivity comparable to the others. In the figure, the results of 10wt% of CaSO_4 addition (prepared by mixing with an aqueous suspension of powdered CaSO_4) are also shown, but the effect is not so remarkable as that of the silica-coated one. It is worth noting that the pore size distribution of these preparations are considerably different from that of RIO, and the silica-coated RIO shows a similar distribution as the others.

3.2. REACTIONS IN THE PRESENCE OF WATER

The results of the breakthrough experiments are listed in Table 2. The reactivity with the gas mixture containing 10 vol% of water is greatly different

Table 2

Influence of water on the degree of sulfidation of the sorbents calcined at 900°C

water content in reaction gas	degree of sulfidation at breakthrough (S/Fe atomic ratio)				
	ocher	RIO	SiO_2 -RIO	CaSO_4 -RIO	pure $\alpha\text{-Fe}_2\text{O}_3$
0 vol%	0.95	0.31	0.96	0.68	0.52
10 vol%	0.25	0.67	0.64	0.70	0.86

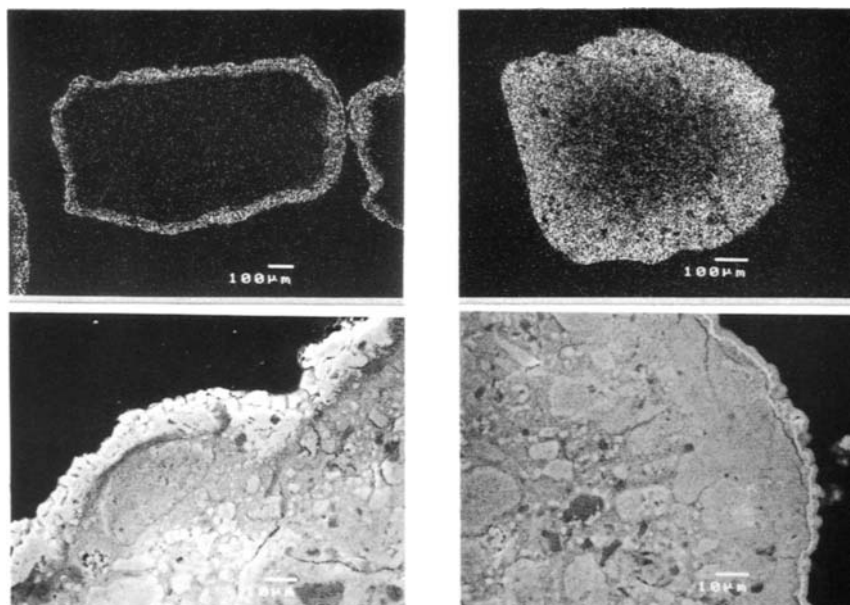


Figure 2. Sulfur(above), SEM(below) image of RIO particles sulfidated in the absence(left) and in the presence(right) of water vapor

from that observed in the previous section. The pure α -Fe₂O₃ shows the highest performance followed by RIOs, and the ochers are the least effective. Almost no correlation exists between the reactivity and the diffusivity of sorbent particles. This may be partly explained by the lower rate of sulfidation in the presence of water as compared to that in its absence, as shown in Figure 3. It is also a point of interest that, except for iron ores, no such a dense layer of iron sulfide as observed in the reactions without water is formed (see Figure 2. right side), and the sulfidation proceeds well deep inside the particles.

As for the ochers, the crystallite size or surface area varies remarkably by the temperature of calcination, and it influences the reactivity; namely the degree of sulfidation of 600°C (surface area: 114 m²/g), 900°C (19 m²/g) and 1,000°C (1 m²/g) calcinations being 0.81, 0.25 and 0.23, respectively. However, the fact that the reactivity of pure α -Fe₂O₃ is very high despite the largest crystallite size and the very low surface area among the sorbents (see Table 1, 2) requires another explanation. The pure α -Fe₂O₃ was prepared by calcining a pure goethite, α -FeOOH, which is the same iron species as found in the ochers before calcination. It is therefore probable that some sort of impurities or the morphology of Fe₂O₃ grains is an important factor to be considered. Further study is necessary to clarify these aspects.

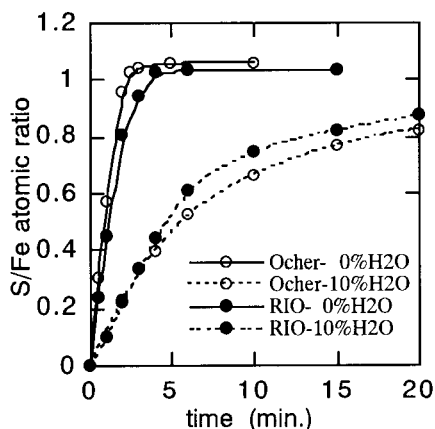


Figure 3. Reaction rate of sulfidation of powdered sorbents calcined at 900°C

REFERENCES

1. P.R.Westmoreland and D.P.Harrison, *Environ. Sci. Technol.*, 10 (1976) 659
2. "Chemistry of Hot Gas Cleanup in Coal Gasification and Combustion", MERC/SP-78/2 (1978)
3. S.S.Tamhankar, M.Hasatani and C.Y.Wen, *Chem. Engng. Sci.* 36 (1981) 1181
4. T.Suzuki and M.Ishida, *Kagaku Kogaku Ronbunshu*, 8 (1982) 327
5. H.Shirai, M.Kobayashi, T.Nakayama, H.Matsuda and T.Tanaka, *Research Report (Central Research Institute of Electric Power Industry): W89040* (1990)
6. S.Kushiyama, Y.Koinuma, S.Kobayashi, R.Aizawa and K.Mizuno, *Nippon Enerugi Gakkai-shi*, 73 (1994) 737
7. K.Kamiya, T.Yokoo and S.Sakka, *Yogyo Kyokai-shi*, 92 (1984) 242

Reaction of hydrogen sulfide with limestone particles

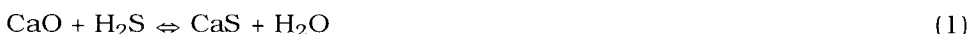
S.Y. Lin^a, A. Al-Shawabkeh^a, M. Horio^b, H. Matsuda^a and M. Hasatani^a

^aDepartment of Energy Engineering & Science/Chemical Engineering, Nagoya University, Furo-cho, Chikusa-ku, Nagoya 464-01, Japan

^bDepartment of Chemical Engineering, Tokyo University of Agriculture and Technology, Koganei, Tokyo 184, Japan

INTRODUCTION

Hydrogen sulfide (H₂S) removal from a coal gasifier by limestone injection seems economical because of its technical simplicity and high efficiency. Depending on whether the carbon dioxide (CO₂) partial pressure is lower or higher than its equilibrium value, H₂S can be captured by either calcined limestone, reaction (1), or limestone, reaction (2), respectively.



Although numerous studies on both reactions (1) and (2) had been done (Fenouil et al., 1994; Borgwardt and Roache, 1984; Iisa et al., 1992), the superior H₂S-reactivity of calcined limestone over limestone still have not been fully elucidated. Accordingly, the current experimental work was mainly aimed at interpreting this superior reactivity through examining the forming product layer (CaS) by the aid of TGA, XRD, SEM and BET techniques. A simple method to enhance the reactivity of limestone at high partial pressures of CO₂ was also proposed.

1. EXPERIMENTAL

A 0.84–1 mm limestone (Chichibu, Japan) was used in all the sulfidation runs performed in a thermogravimetric analyzer (TGA-50, Shimadzu Corporation, Kyoto, Japan). The pore-structure characteristics of the samples were examined using a Micromeritics surface area analyzer which utilized the BET low-temperature N₂ adsorption technique (ASAP 2000) both before and after sulfidation. The sulfidation products were identified via an X-ray powder diffractometer. A scanning electron microscopy (SEM) was also utilized for examining the CaS surface morphology.

2. RESULTS AND DISCUSSION

The XRD patterns depicted in Figure 1 indicated that CaS was the only sulfidation product. The superior reactivity and final H₂S-capacity of calcined limestone over limestone are shown in Figure 2. This superiority

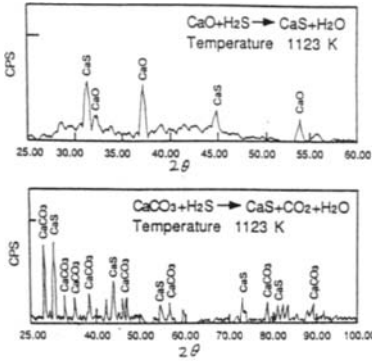


Figure 1. XRD patterns of sulfated limestone samples.

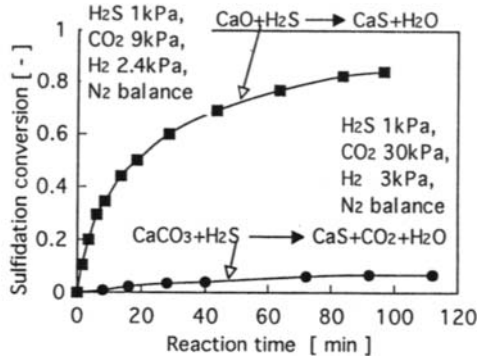


Figure 2. Conversion–time curves of limestone and calcined limestone.

might be attributed to the smaller particle sizes and higher porosity of the CaS produced via reaction (1), compared to reaction (2), as shown in the SEM photos depicted in Figure 3. Another reason is that the specific surface areas of CaS (S_{CaS}) formed via reaction (1) were found to be larger than those formed via reaction (2). The S_{CaS} values, calculated using Equation (3), are listed in Table 1.

$$S_{CaS} = \frac{(S_t - (1 - X) S_o)}{X} \quad (3)$$

The effects of H₂ and H₂O vapor on both reactions (1) and (2) are shown in Figures 4–7. It may be noticed that increasing the H₂O vapor content resulted in reducing only the initial sulfidation rate of calcined limestone, while both the initial sulfidation rate and final capacity were remarkably reduced with limestone (Figures 4 and 5).

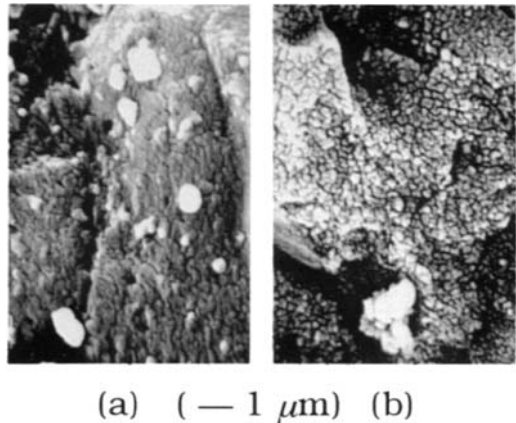


Figure 3. SEM photos of CaS formed by sulfidation of limestone (a) and calcined limestone (b).

As may be seen in Figure 6, the presence of H_2 hinders the sulfidation rate of calcined limestone *only* with CO_2 existence. This inhibiting effect is most likely due to the sintering effect of H_2O formed via the reaction between H_2 and CO_2 . Due to the same reason, H_2 dramatically inhibited the sulfidation rates of limestone as shown in Figure 7.

Table 1.
Specific surface areas of CaS

Sulfidation	$S_0 \times 10^{-3}$ [$m^2 \text{ kg}^{-1}$]	$S_t \times 10^{-3}$ [$m^2 \text{ kg}^{-1}$]	X [-]	$S_{CaS} \times 10^{-3}$ [$m^2 \text{ kg}^{-1}$]
Limestone	0.19	2.48	0.75	3.20
Calcined limestone	30.0	6.48	0.91	4.10

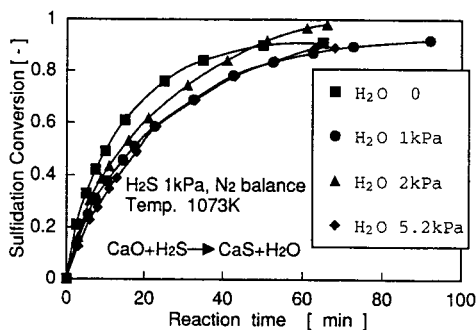


Figure 4. Conversion-time curves of calcined limestone at different H_2O concentrations.

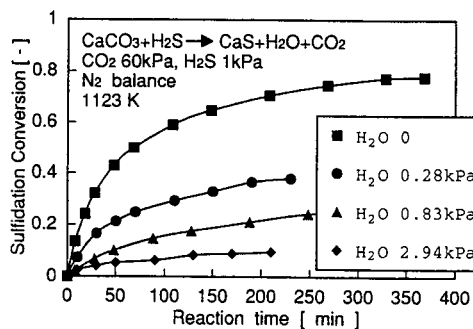


Figure 5. Conversion-time curves of limestone at different H_2O concentrations.

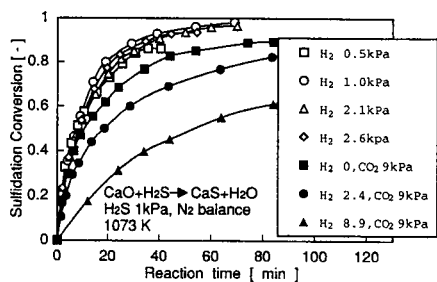


Figure 6. Conversion-time curves of calcined limestone at different H_2 concentrations.

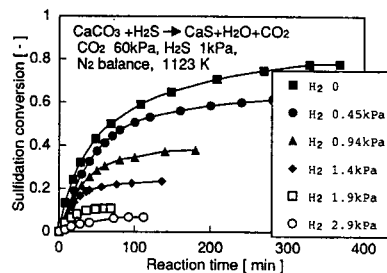


Figure 7. Conversion-time curves of limestone at different H_2 concentrations.

The H_2S -reactivity of limestone was enhanced by a simple repeated calcination/carbonation cycle during sulfidation as illustrated in Figure 8. The calcination/carbonation cycle was controlled by a programmed change of the reaction temperature between T1 and T2 (i.e. below and above the decomposition temperature of limestone). Thus, the reactivity towards H_2S could be increased from 5 to about 72% within 70 min reaction at 1123 K as Figure 9 shows. The reason for this enhancement is still under study. One possible explanation might be the formation of new pores as a result of changes in the particles structure accompanying the successive calcination/carbonation transformations.

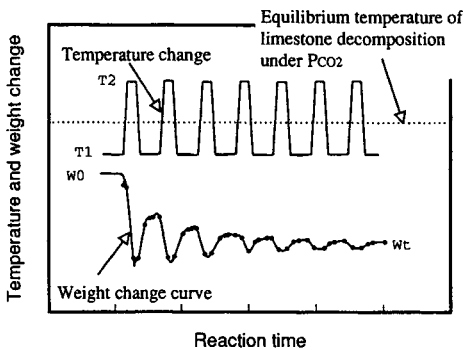


Figure 8. Conceptual illustration of the repeated calcination/carbonation cycle during sulfidation.

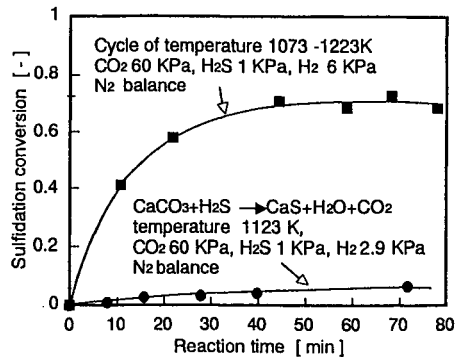


Figure 9. Effect of repeated calcination/carbonation treatment on limestone sulfidation.

3. CONCLUSIONS

The superior H_2S -reactivity and final capacity of calcined limestone over those of limestone were ascribed to its higher porosity and larger specific surface area. The low reactivity of limestone can be significantly enhanced by a simple repeated calcination/carbonation treatment during sulfidation under conditions of high partial pressures of CO_2 .

REFERENCES

1. L.A. Fenouil, G.P. Towler and S. Lynn, *Ind. Eng. Chem. Res.*, 33 (1994), 265.
2. R.H. Borgwardt and N.F. Roache, *Ind. Eng. Chem. Process Des. Dev.*, 23 (1984), 742.
3. K. Iisa, P. Yrjas and M. Hupa, Report 92-8, Combustion Chemistry Research Group, ÅBO Akademi University, Turku, Finland (1992).

Study of NH₃ Removal from Coal Gasified Fuel

Takeharu Hasegawa and Mikio Sato

Combustion Group, Power Generation Systems Department, Yokosuka Research Labo. Central Research Institute of Electric Power Industry., 2-6-1 Nagasaka, Yokosuka-Shi, Kanagawa-Ken 240-01 Japan.

1. Introduction

Aimed at developing a next coal-fired power-generation system which is more efficient and environmentally sound, the Japanese government and the electric power industry have been promoting research and development of an integrated coal-gasified combined-cycle power plant using an air-blown, entrained-flow-coal gasifier. In the coal gasifier, nitrogen compounds contained in coal are converted to NH₃, and NH₃ contained in the coal-gasified fuel will be supplied to the gas turbine combustor without being removed when the gas-clean-up equipment employs a dry method. The fuel NO_x produced from NH₃ in the fuel during combustion in a gas turbine amounts to the greater part of NO_x discharged from the plant. Therefore, if NH₃ in the coal-gasified fuel can be removed in advance through a dry method, it will make it easier to develop low NO_x combustion technology applicable to the development of a gas-turbine combustor which uses low-Btu coal-gasified fuel⁽¹⁾.

By applying the selective, noncatalytic reduction of nitrogen oxides by ammonia for the purpose of NO_x removal from the exhaust gas, this study aimed that NH₃ contained in the coal-gasified fuel can be reduced when a very small amount of O₂ and NO coexist. We examine the following effects on NH₃ decomposition characteristics through reaction kinetics based on an elementary reaction model and the experiments using a tubular-flow reactor;

1) the effect of the reaction temperature, 2) the adding O₂ and NO concentration, 3) the effect of CO and H₂ which are primary combustible components in the coal-gasified fuel.

2. Experimental facility and method

Figure 1 is a schematic diagram of the experimental facility used in this study. The temperature in the reactor made of quartz tube was controlled by dividing a tubular type

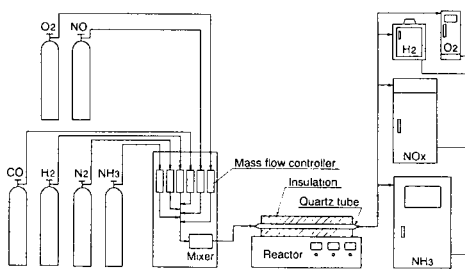


Fig. 1 Schematic diagram of the experimental apparatus designed to yield homogeneous reactions

Table 1 Standard composition of the air-blown, entrained-flow coal gasified fuel

Composition	CO	22.9 %
	H ₂	8.6 %
	CH ₄	0.5 %
	CO ₂	12.9 %
	H ₂ O	2.0 %
	N ₂	53.0 %
	NH ₃	1000 ppm
HHV	4190 kJ/m ³	(1000 kcal/m ³)
LHV	3690 kJ/m ³	(950 kcal/m ³)

furnace 1000mm in length into three blocks along the axial direction so that it would be heated evenly. After being mixed completely by the mixer, the gas is supplied to the reactor at atmospheric temperature.

As indicated by the fuel composition in Table 1, the coal gasified fuel produced in an air-blown entrained-flow coal gasifier has CO and H₂ as the main combustible component, and its calorific value is about 4000kJ/m³. The tested gas used in this study, including CO and H₂ as the main components, are diluted with N₂ so that their calorific values would be the same as that of the coal gasified fuel. The components found in the actual coal gas such as CO₂, H₂O and CH₄ are not taken into account.

3. Numerical analysis based on an elementary reaction model

The reaction model adopted here, was proposed by Miller and Bowman.⁽²⁾ The reaction scheme is composed of 248 elementary reactions and 50 species are taken into account CH₄, CH₃, CH₃O, CH₂OH, CH₂O, CH₂, CH, CO, CO₂, C, H₂, H, O, OH, O₂, H₂O, HO₂, H₂O₂, N₂, N, NO, NO₂, N₂O, HCN, CN, H₂CN, NH₃, NH₂, NH, NNH, HNO, HCNO, HOCN, HNCO, NCO, C₂N₂, HCO, CH₂CO, C₂H, C₂H₂, C₂H₃, C₂H₄, C₂H₅, C₂H₆, HCCO, HCCOH, C₃H₂, C₃H₃ and C₄H₂, C₄H₃. It is assumed that in the reaction process, species are evenly mixed, and diffusion and stirring processes are not taken into consideration.

4. Results and Discussions

4.1 Effects of reaction temperature

Figure 2 shows the effects of changing the reaction temperature on the reduction properties of NH₃ and NO within the range of normal temperature to 1000°C by adding 5000ppm of O₂, and 1000ppm of NO to a mixed gas consisting of 24%CO, 9.1%H₂, balanceN₂ and 1000ppm of NH₃. The NH₃ concentration at the reactor exit began to decrease when the reaction temperature reached a level around 400°C, and decreased up to 350ppm when the temperature reached 1000°C. The concentration of NO at the exit showed a similar trend to that of NH₃; the higher the reaction temperature, the more it decreased.

Moreover, no reduction in NH₃ concentration was observed when O₂ was not added to NH₃ or when NO was not added to NH₃ at each reaction temperature. So, in case of

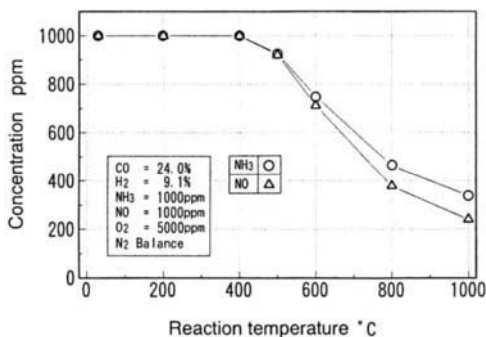


Fig. 2 Effect of reaction temperature on decomposition of NH₃ and NO in the coal gasified fuel defining by the experiments.

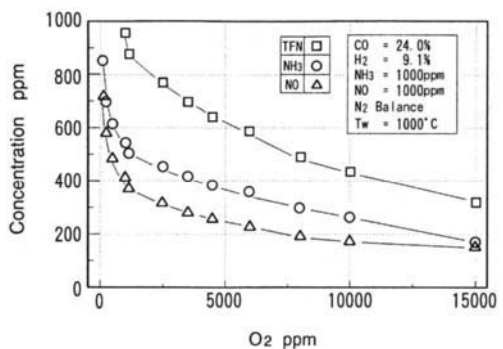


Fig. 3 Effect of O₂ concentration on decomposition of NH₃ and NO in the coal gasified fuel defining by the experiments.

decomposition of NH_3 in the coal gasified fuel, it is found that it need to coexist with O_2 for the selective reaction of NH_3 and NO .

4.2 Effects of adding O_2 and NO

Figure 3 shows the effects of changing O_2 concentration on the reduction characteristics of NH_3 and NO under the reaction temperature of 1000°C by adding 1000ppm of NO to the same mixed gas as in Figure 4. The NH_3 concentration at the exit decreased when the O_2 concentration increased, when the O_2 concentration is 5000ppm, NH_3 decreased to 350ppm, NO decreased to 250ppm and TFN, the sum of remaining NH_3 and NO , decreased up to 600ppm. This technique has effect to decrease TFN by about 40%.

Next, the effects of adding NO concentration is shown in Figure 4. NH_3 concentration decreases as adding NO concentration increases and remaining NO which is not decomposed increases rapidly when adding NO becomes 500ppm or more. As a result, adding NO concentration by which TFN is made minimum exists and becomes 1000ppm in this condition.

4.3 Effects of CO element

Figure 5 shows the effects of changing CO within a range of 0-100% on the decomposition ratio of NH_3 and NO under the reaction temperature of 1000°C by adding 5000ppm of O_2 , and 1000ppm of NO to a mixed gas consisting of 1000ppm of NH_3 and balance N_2 through experiments. The NH_3 of 90% or more is decomposed by as many as 95% of CO in the mixed gas though the decomposition ratio of NH_3 shows the tendency which decreases slightly as the concentration of CO increases. It is understood that CO hardly effects the decomposition reaction of NH_3 . On the other hand, the decomposition ratio of NO differs from that one of NH_3 , the decomposition ratio of NO decreases rapidly as CO concentration increases within 0-1.5% and contrarily increases in 1.5% or more. That is, the concentration of CO by which the decomposition ratio of NO is made minimum exists.

4.4 Effects of H_2 element

Figure 6, Figure 7 shows the effects of H_2 concentration on the decomposition characteristics of NH_3 and NO respectively, when a combustible component is only H_2 and

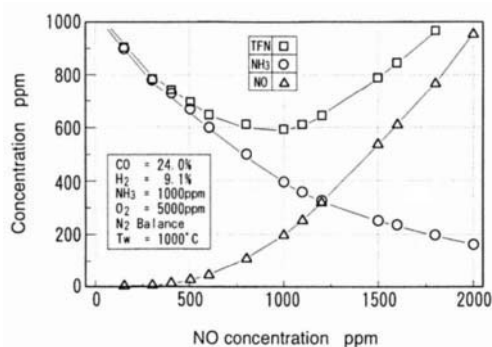


Fig. 4 Effect of NO concentration on decomposition of NH_3 and NO in the coal gasified fuel defining by the experiments.

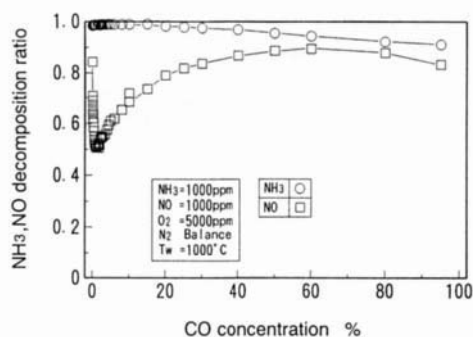


Fig. 5 Relationship between both decomposition ratios of NH_3 and NO and CO concentration in the systems defining by the experiments.

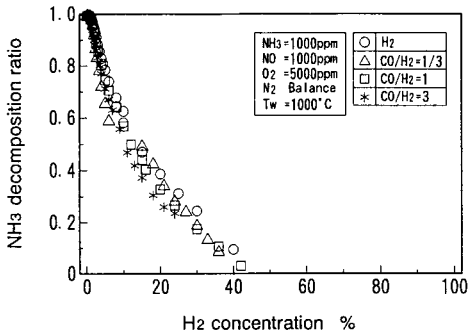


Fig. 6 Relationship between decomposition ratio of NH_3 and H_2 concentration in the combustible components defining by the experiments.

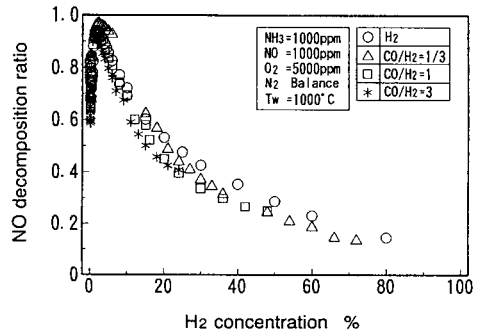


Fig. 7 Relationship between decomposition ratio of NO and H_2 concentration in the combustible components defining by the experiments.

CO and H_2 coexist with its mixing ratio (CO/H_2) kept by 1/3, 1, 3 as combustible components under the same condition as Figure 5. Each decomposition of NH_3 and NO is ruled single meaning by the H_2 concentration regardless of the coexistence of CO when H_2 is contained. That is, the NH_3 decomposition ratio is almost 100% in the range of 1% or less in the H_2 concentration and decreases rapidly as H_2 concentration increases in 1% or more.

The influence of CO concentration on the decomposition of NO is apparently canceled by coexisting with H_2 though CO exerts a big influence on the decomposition of NO as indicated in Figure 5, and the decomposition ratio of NO is ruled single meaning by the H_2 concentration, too.

5. Conclusion

The effects of additive NO and O_2 concentration, and effects of CO and H_2 in the coal gasified fuel on the decomposition characteristics of NH_3 and NO , were examined by the experiments using the tubular flow reactor and by numerical analysis base on reaction kinetics. The followings were clarified; (1) The optimum concentration of additive NO exists, by which remaining TFN after reacting under the reaction temperature of 1000°C is made minimum. When O_2 is added by 5000ppm with this coal gasified fuel which contains NH_3 by 1000ppm, this optimum additive NO concentration is 1000ppm. (2) This technique has effect to decrease TFN by about 40% by adding 5000ppm of O_2 , and 1000ppm of NO to the coal gasified fuel which contains NH_3 by 1000ppm under the reaction temperature of 1000°C . (3) The each decomposition reaction of NH_3 and NO is ruled single meaning by the H_2 concentration regardless of the coexistence of CO when H_2 is contained. The decomposition ratios of NH_3 and NO decreases rapidly as the H_2 concentration increases. (4) CO and H_2 have the effect to decrease the optimum reaction temperature by which selective decomposition reaction of NH_3 and NO under the coexistence of O_2 is made the maximum and the effect of H_2 is larger than that of CO .

References

- 1) Nakata, T et al. ASME paper No.94-GT-218.
- 2) Miller, J.A. and Bowman, C.T., *Prog. Energy Combust. Sci.*, Vol.15, (1989), p287.

Acoustic Preconditioning of Coal Combustion Fumes for Enhancement of Electrostatic Precipitator Performance: I. The Acoustic Preconditioning System*

J.A. Gallego^a, E. Riera^a, L. Elvira^a, G. Rodríguez^a, F. Vázquez^a, T.L. Hoffmann^a,
and F. Montoya^b

^aInstituto de Acústica, U.E.I. Ultrasonidos, CSIC, Serrano 144, 28006 Madrid, Spain

^bInstituto de Electrónica de Comunicaciones, CSIC, Serrano 144, 28006 Madrid, Spain

A pilot scale acoustic preconditioning system is presented that sonifies fumes of a coal combustion process at very high acoustic sound pressure levels. This new technique leads to an increase of the fly ash's average particle size and, thus, to a performance enhancement of a subsequently employed electrostatic precipitator. This paper focuses on acoustic preconditioning and its underlying physical mechanisms as well as on the design and implementation of the technique in a pilot scale precondition chamber.

1. PHYSICAL PRINCIPLES

Acoustic preconditioning of micron and submicron-sized aerosols relies on the principle of acoustically induced collision and agglomeration between individual aerosol particles. To generate a significant agglomeration effect, an acoustic preconditioning system has to meet a number of specific technical requirements.

1.1. Acoustic Agglomeration Mechanisms

Acoustic preconditioners employ high intensity acoustic fields to generate relative motion between particles, leading to collisions and agglomerations within the aerosol. The classical explanation for this acoustically induced agglomeration is based on the so-called orthokinetic agglomeration theory [1, 2]. According to this model, particles of different sizes are entrained with different rates into the oscillating motion of the acoustic field. Because of their inertia, larger particles are more stationary while smaller, lighter particles follow the oscillatory motion of the carrier medium. The orthokinetic agglomeration hypothesis claims that the resulting relative motion between the particles causes collisions and agglomerations. Another explanation for acoustic agglomeration, termed the acoustic wake effect, has only recently found strong experimental confirmation [3, 4]. This model is based on the asymmetry of the flow field around a moving particle at moderate Reynolds numbers (under Oseen flow conditions, [5, 6]). To illustrate the phenomenon consider two closely spaced spheres moving along the acoustical axis (or equivalently along the fluid's flow vector; see Figure 1). The

* The authors gratefully acknowledge the cooperation and support for this work by the Spanish electricity company ENDESA, financed through OCIDE, and by the Plan Nacional de Tecnologías Avanzadas de la Producción (Project TAP 93-230).

leading sphere disturbs the quiescent fluid and builds up a wake in the area behind itself. If the second sphere is located close enough it travels within this disturbance. The wake leads to a pressure reduction in the area behind the leading particle so that the trailing particle experiences a drag reduction and moves with a higher speed than the "leader." If one considers two particles in an oscillating flow, the same effect occurs with the only difference that the roles of the leading and the trailing particle are switched twice per acoustic cycle. Thus, because of the acoustically induced wake the particles converge during a number of acoustic cycles and finally collide with one another.

1.2. Requirements for Efficient Acoustic Preconditioning

Conventional filter techniques such as electrostatic precipitators are generally inefficient in retaining micron and submicron-sized particles. An acoustic preconditioning system increases this efficiency by agglomerating the aerosol and shifting its size distribution to a range of larger particles. To achieve a satisfactory shift of the particle size distribution, extremely strong acoustic fields have to be employed (sound pressure levels of 140-165 dB). Previous theoretical and experimental results show that for the employed sound pressure levels the general rule "more-is-always-better" holds almost without constrain. For this reason, powerful sound sources for the treatment of large volumes at high sound pressure levels are indispensable for an efficient acoustic preconditioning system. Another important factor which strongly influences the resulting sound field patterns is the geometry of the agglomeration chamber. Here special attention has to be given to optimize for largest possible homogeneity and maximum spatial mean level within the chamber. Moreover, the frequency of the exciting sound field determines in which particle size range the preconditioning works most efficiently. Whereas frequencies of the lower audible range favor the agglomeration of micron sized particles, higher or ultrasonic frequencies deliver better results in the submicron size range. Therefore, the sound frequency has to be adjusted in such a way that the performance of the acoustic preconditioning process is optimized with respect to a given aerosol size distribution. This becomes especially important when bimodal or multimodal size distributions are considered (as apparent in many fly ash distributions after coal combustion). Besides by these acoustical quantities, the efficiency of the agglomeration process is influenced by field parameters such as ambient temperature and pressure, residence time in the agglomerator, and aerosol concentration. Experiments show that the latter two quantities are crucial for efficient acoustic preconditioning [7, 8].

2. A PILOT SCALE ACOUSTIC PRECONDITIONING SYSTEM FOR TREATMENT OF COAL COMBUSTION GASES

In the pilot scale acoustic preconditioning system presented in Figure 2, fumes of a 0.5 MW_t fluidized bed coal combustor are treated in an acoustic agglomeration chamber with a length of 3.56 m and a rectangular cross-section of 0.7 × 0.5 m. The gas enters the agglomeration chamber at a temperature of about 170°C. Four specially designed stepped-plate, high-intensity transducers are arranged alongside the elongated agglomeration chamber to achieve a homogeneous distribution of the sound field as well as a sufficient residence time of the aerosol in the cavity (2-4 sec). Two different models of stepped-plate transducers permit the operation of the acoustic preconditioner at sonic (10 kHz), ultrasonic (20 kHz), or mixed frequencies (10 and 20 kHz). In Figure 3 a scheme of a stepped-plate transducer illustrates its physical principle as bending radiator, generating an intense sound field through

an interference pattern in front of the radiation plate [9]. Detailed mapping of sound field patterns within the agglomeration chamber reveal mean sound pressure levels of 148/149 dB and peak values of 162/165 dB for 10 and 20 kHz, respectively. The option of switching between different frequencies allows the experimental comparison and evaluation of the agglomeration process' frequency dependence with respect to one specific aerosol. Figure 2 illustrates also how the acoustic preconditioner is embedded into the particle treatment process of the pilot scale facility. Three sampling points for particle concentration and distribution measurements are located at the entrance and the outlet of the acoustic agglomerator as well as at the outlet of the electrostatic precipitator. First results of the aerosol characterization at the three sampling points are presented in our companion paper (also at the 8th ICCS): Acoustic Preconditioning of Coal Combustion Fumes for Enhancement of Electrostatic Precipitator Performance: II. Performance Evaluation.

3. CONCLUSIONS

In this paper presented a pilot scale facility for elimination of aerosol particles from coal combustion fumes. The innovation of this plant is an acoustic preconditioning system which increases the average particle size of a given aerosol. The preconditioning process improves the generally low efficiency of conventional filtering system in the micron and submicron particle size range. Such filtering systems may be electrostatic precipitators, cyclone filters, bag houses, or ceramic filters. Another important benefit of this new form of particle treatment is its applicability in high-pressure and high-temperature environments (e.g. for coal gasification).

REFERENCES

1. Mednikov, E.P., *Acoustic Coagulation and Precipitation of Aerosols*. 1965, New York: Consultants Bureau.
2. Temkin, S., *Gasdynamic Agglomeration of Aerosols. I. Acoustic Waves*, J. of Fluid Mechanics, 1994, 6(7): p. 2294-2303.
3. Hoffmann, T.L. and Koopmann, G.H., *A New Technique for Visualization of Acoustic Particle Agglomeration*, Rev. of Sci. Ins., 1994, 65(5): p. 1527-1536.
4. Hoffmann, T.L. and Koopmann, G.H., *Visualization of Acoustic Particle Interaction and Agglomeration: II. Experiments*, J. Acoust. Soc. Am., 1995, (submitted for publication).
5. Dianov, D.V., Podolskii, A.A., and Turubarov, V.I., *Calculation of the Hydrodynamic Interaction of Aerosol Particles in a Sound Field Under Oseen Flow Conditions*, Sov. Phys. Acous., 1968, 13(3): p. 314-319.
6. Hoffmann, T.L. and Koopmann, G.H., *Visualization of Acoustic Particle Interaction and Agglomeration: I. Theory*, J. Acoust. Soc. Am., 1995, (submitted for publication).
7. Riera-Franco De Sarabia, E. and Gallego-Juárez, J.A., *Ultrasonic Agglomeration of Micron Aerosols Under Standing Wave Condition*, J. Sound Vib., 1986, 110(3): p. 413-427.
8. Hoffmann, T.L., Chen, W., Koopmann, G.H., Song, L., and Scaroni, A.W., *Experimental and Numerical Analysis of Bimodal Acoustic Agglomeration*, ASME: J. of Vibration and Acoustics, 1993, 115: p. 232-240.
9. Gallego-Juárez, J.A., Rodríguez-Corral, G., San Emeterio Prieto, J.L., and Montoya Vitini, F., *Electroacoustic Unit for Generating High Sonic and Ultrasonic Intensities in Gases and Interfaces*, USA Patent No. 5.2999.175, 1994.

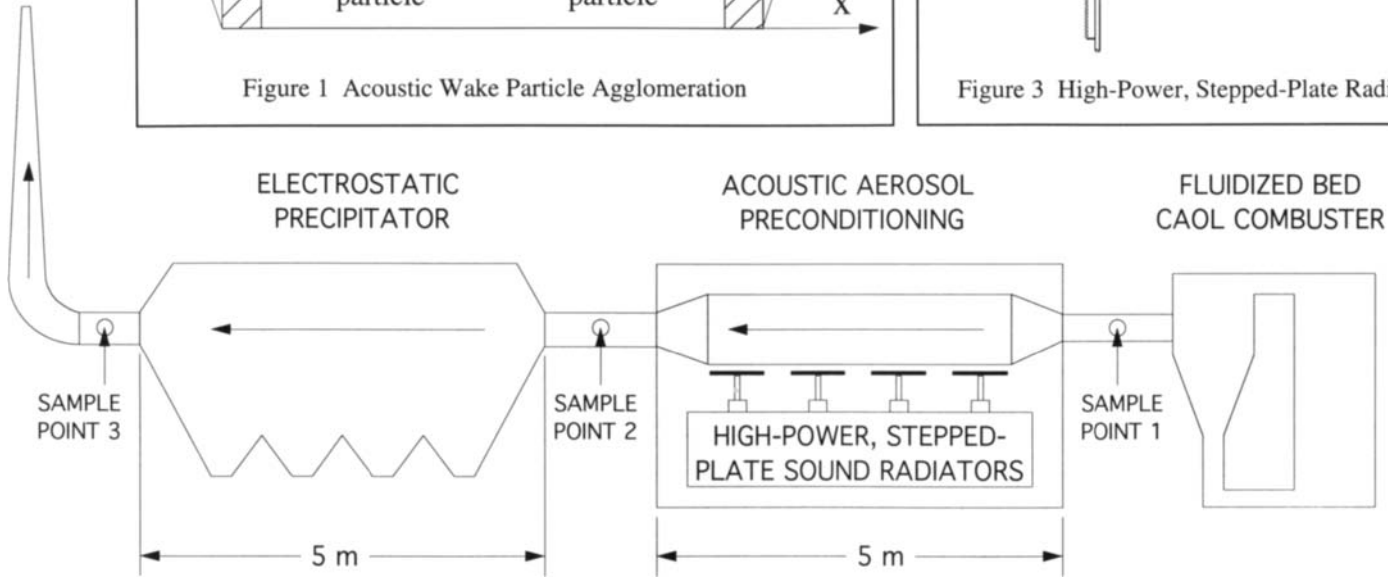
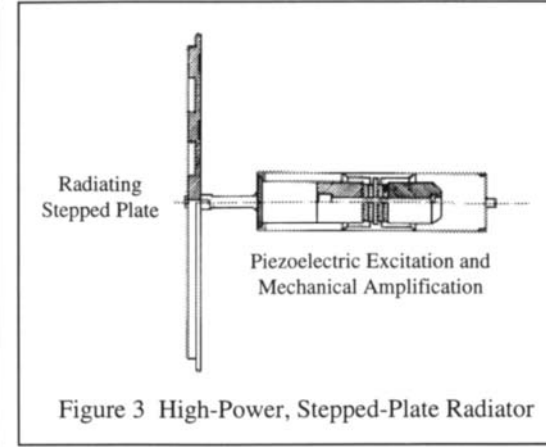
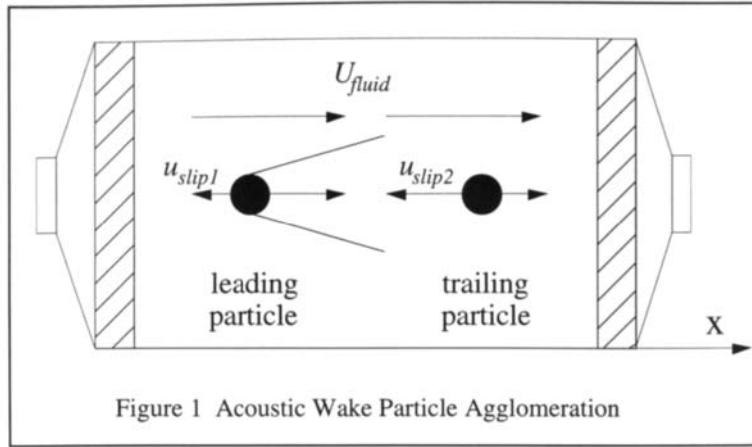


Figure 2 Pilot Scale Acoustic Preconditioning of Fumes from a Fluidized Bed Coal Combustion Process

Acoustic Preconditioning of Coal Combustion Fumes for Enhancement of Electrostatic Precipitator Performance: II. Performance Evaluation*

J.J. Rodríguez Maroto^a, F.J. Gómez Moreno^a, M. Martín Espigares^a, J.A. Gallego^b, E. Riera^b, L. Elvira^b, G. Rodríguez^b, F. Vázquez^b, T.L. Hoffmann^a, and F. Montoya^c

^aCIEMAT, Av. Complutense 22, 28040 Madrid, Spain

^bInstituto de Acústica, U.E.I. Ultrasonidos, CSIC, Serrano 144, 28006 Madrid, Spain

^cInstituto de Electrónica de Comunicaciones, CSIC, Serrano 144, 28006 Madrid, Spain

1. INTRODUCTION

To evaluate the performance of the acoustic agglomeration system described in the first part of this paper, the flue gases of CIEMAT's 0.5 MW_t fluidized bed combustion plant are led, after being diluted to the required concentration, towards the acoustic chamber and, subsequently, towards an electrostatic precipitator and a scrubber unit. The evaluation process of the acoustic agglomeration chamber is carried out with a flue gas of characteristics similar to those of a reference power plant (Compostilla II, ENDESA, Spain), even though some of the experiments will also incorporate other conditions. Because the agglomeration effect occurs in the whole range of particle sizes, a single measurement technique or instrument is not sufficient for the characterization of the fumes. This led to the employment of different instruments and equipments which, coupled together to a single system, permit the extraction of information in its most complete form: mass and number concentration; numerical, morphological, and aerodynamic size distributions; elemental chemical composition. In this report a sampling and measurement system is presented which, due to its versatility, permits its utilization under all required conditions. Additionally, some results of preliminary experiments are presented which provided means for the validation of the method and for the characterization of the fumes in the whole process.

2. THE SAMPLING AND MEASUREMENT SYSTEM

The sampling is carried out with an isokinetic sampling probe. To maintain the isokinetic sampling conditions in the range of 95-105 %, this probe automatically adjusts the sampling flow rate in case of changing conditions at the sample point. The sampling panel, which is introduced in between the probe and its control unit, incorporates two types of instruments delivering either in-situ or post-sampling results (see Figure 1). To the first group belong: an optical particle counter for the size range of 1-30 μ m and a scanning mobility particle sizer (SMPS), which consists of a differential mobility analyzer (DMA) and a condensation nuclei counter (CNC), for the size range of 0.001-1 μ m. Both instruments deliver data of the numerical concentration and the distribution. This makes it possible to cover the whole

* The authors gratefully acknowledge the cooperation and support for this work by the Spanish electricity company ENDESA, financed through OCIDE, and by the Plan Nacional de Tecnologías Avanzadas de la Producción (Project TAP 93-230).

particle size range of interest in this study, given that a cyclone with a cut-off at $30\mu\text{m}$, placed at the gas outlet, assures that all particles entering the measurement system are smaller than this given size. The second type of devices requires post-treatment. Different samples, extracted on specially prepared glass laminae, are analyzed with scanning electron microscopy (SEM) to obtain a number of photos which deliver, after rigorous image analysis, results about the morphology and an approximated numerical distribution. Additionally, the technique allows the determination of the elemental composition through an EPXMA probe which is incorporated into the equipment. Moreover, a seven-stage cascade impactor gives relative information about the aerodynamic distribution and the mass concentration. Each of the impactor's stages is provided with glass fiber substrates, from which the particles of a corresponding size range are extracted, and with a final filter for the deposition of the finest particles. The mass concentration is also determined from the deposition on the filters which, in the same manner as the substrates, are subsequently dried and weighted. This method permits the simultaneous characterization of fumes by different techniques, avoiding errors which small variations of the gas characteristics may introduce in the interpretation of the results.

3. RESULTS OF THE PRELIMINARY EXPERIMENTS

The preliminary experiments presented here are conducted with the objective to characterize the flue gases of CIEMAT's circulating fluidized bed combustor at each of the three sampling points of the acoustic preconditioning system (see Figure 2, Part 1 of this paper). The importance of these experiments lies in the possible effects that the variation of the gas composition may have on estimating the agglomeration process. Measurements were carried out of the numerical distribution in the micron-size range, the mass and number concentrations (see Figure 2), the morphology, and the aerodynamic distribution. For these experiments the fumes of the process were previously diluted to a concentration down to ~ 0.4 mg/l. The results of the mass concentration experiments were compared with others obtained in accordance with the EPA norm. The following table gives the corresponding results for the averaged numerical and mass concentrations

SAMPLING POINT	Particles/cm ³	mg/liter
1	$\sim 2\text{E}+4$	~ 0.4
2	$\sim 2\text{E}+4$	~ 0.2
3 (without electrostatic precipitator)	$\sim 1\text{E}+4$	~ 0.1
3 (with electrostatic precipitator)	$\sim 9\text{E}+2$	~ 0.02

The data shows that the acoustic chamber itself, without activating the sound field, produces a particle retention. Even though this retention is almost not noticeable in particle number, it is important in terms of the mass loading. Most likely this effect owns to the retention of the heaviest particles which, in terms of number, are insignificant. The electrostatic precipitator shows retention efficiencies of $\sim 96\%$ in terms of particle number and $\sim 91\%$ in terms of mass. It is also found that, even if switched off, the electrostatic precipitator retains about 50% in terms of both, mass and number. From this result follows that the fumes do not change considerably with time at a given sampling point, neither in their number nor in their mass concentration (see Figure 2).

4. CONCLUSIONS

The preliminary experiments permit:

- verification of the performance of the sampling and measurement system
- characterization of one specific fume originating from the CIEMAT's circulating fluidized bed combustion plant
- characterization of the fumes at different points in the process and estimation of the effect which may be introduced by the different stages themselves (with and without electrostatic precipitator).

It was observed that the generation of the fumes by the plant is very stable, considering it in terms of order of magnitude. However, the variations encountered have to be carefully considered later in the evaluation of the performance of the acoustic agglomeration chamber.

5. REFERENCES

- William C. Hinds, *Aerosol Technology. Properties, behavior and measurement of aerosol particles*, John Wiley & Sons, 1982
- N. A. Fuchs, *The Mechanics of Aerosols*, MacMillan Company, 1964
- Parker C. Reist, *Introduction to Aerosol Science*, MacMillan Publishing Company, 1984
- Cascade Impactors: Sampling & Data Analysis, edited by J. P. Lodge, Jr. y T. L. Chan through the American Industrial Hygiene Association, 1986
- J. Rodríguez Maroto, F.J. Gómez Moreno, "Estado del arte de las actividades del CIEMAT sobre caracterización de partículas," CIEMAT/ITN/TS-21/NT-93, 1993
- J.J. Rodríguez Maroto, F.J. Gómez Moreno, M. Martín Espigares, "Caracterización de partículas en emisión de la planta piloto de combustión del CIEMAT, actividades de soporte" MCIEMAT/ITN/TS-34/NT-94, 1994.

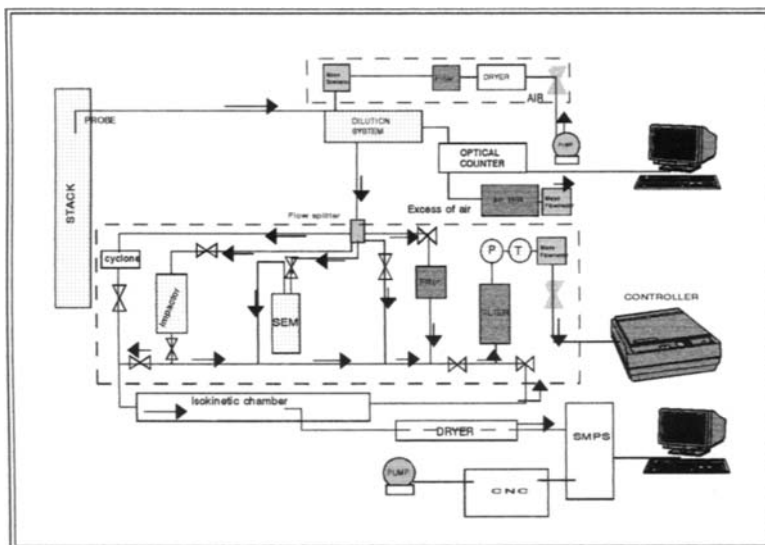
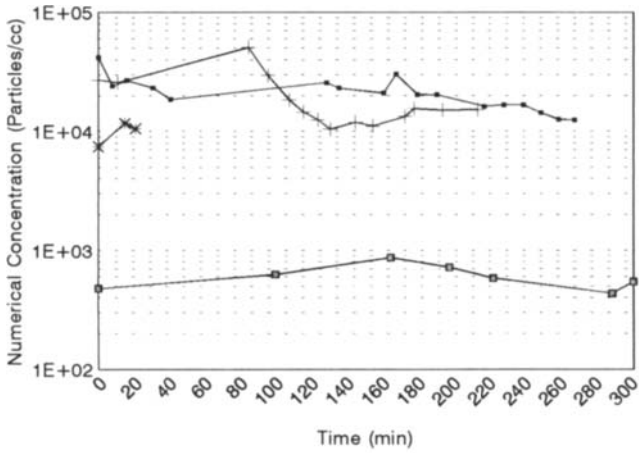
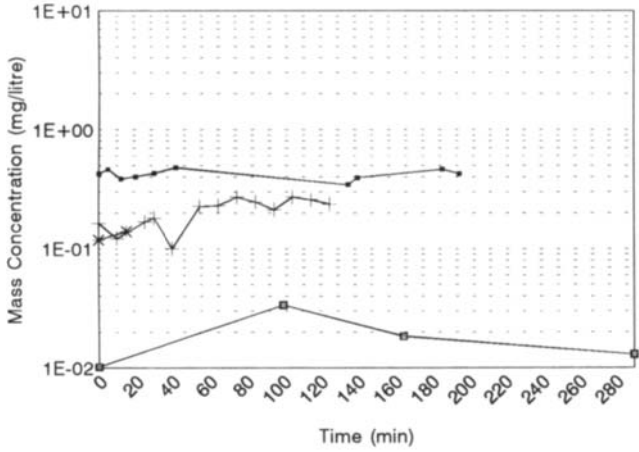


Figure 1. Schematic view of the sampling station.



(*) with electrostatic precipitator



(*) with electrostatic precipitator

Figure 2. Characterization of the fumes from CIEMAT's Fluidized Bed Combustor in the three sampling points.
a) Numerical concentration vs. time.
b) Mass concentration vs. time.

The significance of porosity of gasification filter dust

J. Ranta, M. Nieminen and E. Kurkela

VTT-Energy, P.O.Box 1601, Finland

1. INTRODUCTION

One of the main problems in developing Pressurised Fluidized Bed Gasification (PFBG) for an IGCC process is related to gas cleaning using HTHP (High Temperature High Pressure) techniques [1-2]. The aim is to gasify the solid fuel (coal, peat, wood, waste etc.) at a high temperature and pressure and to clean the gas to the level required by the gas turbine. The most important cleaning requirements are related to particulate matter and certain corrosive components.

In the PFBG system part of the partially gasified fuel char, ash forming minerals and other solid residues (including bed additives), escape from the reactor. Usually, in the concepts based on hot gas cleaning the primary particulate removal is carried out by cyclones and the final step by ceramic filters operating at 400-600 °C. The dust passing the cyclone/-s forms a dust cake on the filter elements, and the cake is periodically detached by high pressure gas pulsing. Efficient particulate removal is thus achieved.

High temperature, high pressure (HTHP) filter dust from a number of PDU-scale (0.4 MW) gasification and hot gas cleaning experiments of coal, wood and peat were characterised. The filter dusts contained a considerable amount of unreacted carbon [3]. The residue must likely be recirculated or treated in a separate reactor to achieve acceptable quality for disposal. The specific interest was focused on the porous structure of the dust. The process history of partially gasified carbon containing filter dust is comparable to the thermal activation process and thus the dust might have a role in adsorption of impurities like organics and alkalis from the gas phase.

2. EXPERIMENTAL

2.1 Samples

The samples of the PFBG process were collected from the PDU-scale air blown gasification unit of VTT Energy. The gasifier is followed by a high temperature, high pressure (HTHP) filter with five ceramic filter elements. The overall layout of the filter unit is shown in Figure 1. The details of the gasifier system are reported elsewhere [1,2].

The filter dust samples were collected from the filtration unit by pulsing the filter elements with high pressure nitrogen. Pulsing of the filters occurred about 4 times/hour. The temperature of hot filter was ranging from 743 K to 833 K (470...560°C). Commercial layered ceramic candle filters described in [1] were used. The particle size of the dust was in the range of 10-60 µm. The carbon content of the dust varied usually between 50-60% (w/w) and residues of the bed material (limestone or dolomite) were also present. The origin of the filter dusts studied as well as main gasification parameters are given in Table 1.

Table 1
Origin and gasification parameters of the studied samples

	Peat / 1	Coal / 2	Wood / 3	Wood / 4	Wood / 5	Wood / 6
Gasification temp. (°C)	825	960	890	850	885	830
Filtering temp. (°C)	485	570	535	535	535	490
Pressure (bar)	4	5	5	5	5	5
Additive	None	Limestone	Dolomite	Dolomite	Dolomite	Dolomite

2.2 Methods

Pore structure of the samples were characterised using nitrogen adsorption at 77K. Samples were degassed at 473 K (10^{-2} mbar) for 16-20 hours. A computer controlled Carlo Erba Sorptomatic Series 1800 instrument was applied. Computer based calculations (Milestone 100 program) were used for surface area (BET) calculations. For micropore evaluation the isotherm data was converted to Dubinin plots [4]. For thermal treatment of the samples an automatic, programmable thermoanalytical equipment, LECO TGA-500, was used. For basic characterisation (moisture, ash, calorific value, bulk density) of the samples standard laboratory techniques were applied. To examine the adsorbed or condensed tar-like substances, a solvent extraction with a subsequent GC-analysis using an internal standard (dodecane) method was carried out. The samples were extracted with dichloromethane in a Soxhlet apparatus for 20 hrs, and a HP 5890 series gas chromatograph with an Ultra 2 capillary column was used for the determination of the extracted compounds.

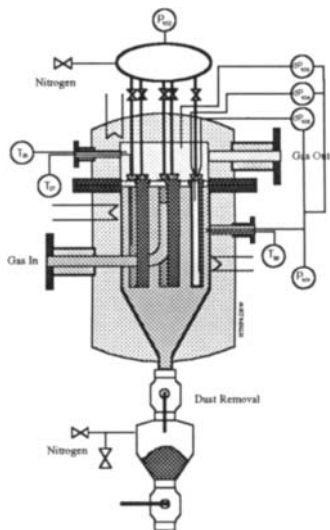


Figure 1. The layout of the filtering unit [1].

3. RESULTS AND DISCUSSION

3.1 Basic characteristics of the filter dust

The ash content varied from about 20 to 60%. Correspondingly the amount of residual char was in the range of 50%. This char phase of the dust had the nature of activated charcoal, which is discussed in more detail in the following.

3.2 Porous structure and surface area

Filter dusts from coal and biomass gasification were found to have a relatively high BET surface areas ranging from 32 to 968 m²/g. The dust might thus have a potential on-site effect on gas quality and overall performance of the filter. Basically it could also be used in off-site sorption application without any subsequent thermal activation.

The high surface area, is due to the $O_2/H_2O/CO_2$ "activation" conditions in gasification and due to the tendency of small particles to elutriate from the reactor before complete gasification. It is not expected that any porosity could be developed in filter conditions, where temperature was 485-570°C and no oxygen was present. The surface area of the dust was mainly dependent on the "activation" conditions i.e. on the nature of the solid itself, reaction temperature, residence time and solid to gas ratios. Mineral matter may also have an effect in the process. To be able to compare surface areas of different samples they were calculated to ash-free basis using ash contents from the TG-analyse. The results are given in the Table 2.

Table 2

Surface area (af) of the studied samples and gasification conditions

Sample	Surface area (af) (m ² /g)	Origin	Temperature (bed/f.board, °C)	Steam/fuel ratio
1	461	Peat	825/890	0.16
2	968	Coal	960/965	0.41
3	79	Wood	890/910	0.25
4	180	Wood	850/960	0.21
5	168	Wood	885/870	0.18
6	32	Wood	830/970	0.2

It can be seen that especially coal gasification produced high surface areas in the dust. This might be due to the higher temperature and longer residence time in the reactor which are required by the lower gasification reactivity of coal. In this case steam to fuel ratio was also markedly higher. The peat based dust particles had a relatively high surface area despite rather low reaction temperature. However, higher density may cause a longer residence time for these particles compared to wood based particles. For dust originating from wood gasification the behaviour for different species seems to be unequal.

In wood gasification the production of tar-like substances is significantly higher than in the case of coal or peat. Consequently the quantities of dichloromethane extractables for a number of wood based dust samples were high. Components like phenanthrene, fluoranthene and pyrene were typically present in relatively high concentrations. At least a part of tar-like substances are adsorbed or deposited on the active char particles. This was supported by the observation that particles collected from early stages of wood gasification i.e. in the hot gas

Table 3

The effect of heat treatment on BET-surface area (m²/g)

Baking temperature (°C)	Wood	Peat	Coal
None	85	245	644
500	120	301	432
700	200	303	444
900	280	364	430

region, had markedly higher surface area and lower amount of extractable tar-like substances.

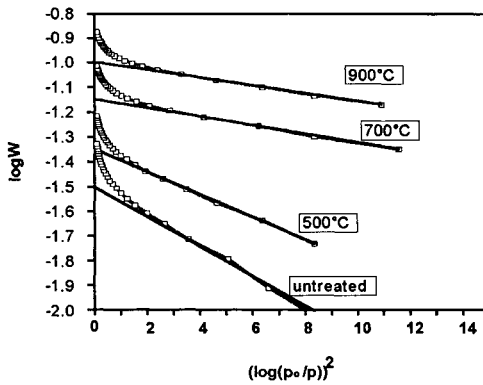


Figure 2. Dubinin plots for heat treated wood based filter dust samples

To clarify the adsorption phenomena three samples from coal, peat and wood gasification were heat treated at 500, 700 and 900 °C. It was observed that after subsequent treatment up to 900°C the surface area of wood dust reached the same order as in the case of coal or peat, while the BET-surface of peat and coal dust remained at the original level (Table 3).

The characteristics of the heat treated samples were evaluated using Dubinin equation. The difference of the limiting adsorption volume between the untreated and treated samples, gives the micropore volume occupied by adsorbed / desorbed components (Figure 2).

4. CONCLUSIONS

The high temperature high pressure filter dust of air blown solid fuel gasification has a significantly developed pore structure with a relatively high surface area. Pore structure is dependent on the gasification feedstock and process conditions like gasification temperature, residence time etc. The dust itself has a significant role in particulate removal by forming the filtration cake on the filter surface, but also the porous nature of the dust a role in hot gas cleaning. The porous dust behaves as an adsorption material and thus adsorbs for example organic impurities of high boiling point from the gasification gas.

ACKNOWLEDGEMENTS

This work has been supported by the Technology Development Centre of Finland through Sihti 2 research programme.

REFERENCES

1. Kurkela, E., Ståhlberg, P., Laatikainen, J. and Simell, P., *Bioresource Technology*, 46, 37(1993).
2. Kurkela, E., Ståhlberg, P. & Laatikainen, J., Pressurized fluidized-bed gasification experiments with wood, peat and coal at VTT in 1991-1992, VTT Publications 161, Espoo 1993.
3. Ranta, J. and Moilanen, A., Reactivity of filter dusts in pressurised gasification. 8th Int. Coal Science Conference, Oviedo, Spain, 1995.
4. Dubinin, M.M., Pore structure and adsorption properties of Activated Carbons, in "Chemistry and Physics of Carbon, Vol. 2, Ed., Walker, Jr., P.L., New York, 1966.

CATALYTIC N₂O DECOMPOSITION IN FLUIDIZED BED COMBUSTION

J. Rodríguez-Mirasol, E. Ito, C.M. van den Bleek, L. Monceaux^a, P. Courtine^a, F. Kapteijn and J.A. Moulijn

Chemical Process Technology, Delft University of Technology,
Julianalaan 136, 2628 BL Delft, The Netherlands

^aDépartement de Génie Chimique, Université de Technologie de Compiègne,
B.P. 649, 60206 Compiègne Cédex, France

1. INTRODUCTION

The implementation of fluidized bed combustion (FBC) for advanced power generation purposes is now recognized as a major step in reducing the environmental impact of coal combustion into the next century because of its low NO_x and SO_x emissions. However, FBC has been identified as one of the major contributors to the anthropogenic emission of N₂O, a pollutant contributing to the greenhouse effect and the depletion of ozone layer. Most research has been directed towards reducing the NO_x and N₂O emissions within the FBC boiler by optimizing the operation condition parameters. However, difficulties have been found in controlling N₂O emissions from FBC to acceptably low level due to interactions or trade-offs between N₂O, NO_x and SO₂ in the operating conditions of FBC [1]. A new approach to N₂O emission reduction from FBC consists of flue gas treatment downstream the combustor by means of solid catalysts. This paper deals with the heterogeneous catalytic N₂O decomposition into N₂ and O₂ under FBC flue gas conditions.

2. EXPERIMENTAL

The catalytic decomposition of N₂O has been studied over different transition metal (Cu, Co, Fe and Mn) and Ca-containing catalysts. The experiments were carried out in a laboratory packed-bed reactor (5 mm I.D.), containing 20 mg of catalyst (106-212 μm) diluted with 90 mg of SiC (106-212 μm), at steady state conditions. The reaction was studied at temperatures ranging from 600 to 1073 K. For a flow rate ranging from 50 to 300 cm³/min and a total pressure of 2.5 bar, the inlet partial N₂O pressure used in this study were in the range of 0.5 to 2.5 mbar and the space time for N₂O (W/F_{N₂O}) amounted to 16x10⁴ g s/mol. ZSM-5 zeolite and γ-alumina were used as catalyst supports. The catalysts were prepared by pore volume impregnation on γ-alumina and by metal ion exchange of the zeolite. Lime, pure CaO, Ca-DUT, a very attrition resistant synthetic sorbent (calcium oxide supported on γ-alumina, prepared by sol-gel method) for regenerative sulfur capture in FBC of coal and a Mn-containing ternary oxide were also used.

3. RESULTS AND DISCUSSION

Figure 1 presents the effect of temperature on N₂O decomposition for different catalysts. Cu-, Co and Fe-exchanged ZSM-5 [2] and vacancies-containing manganese perovskite

($\text{La}_{0.8}\text{Sr}_{0.2}\text{Mn}_{0.9}\Phi_{0.1}\text{O}_{3\pm\lambda}$, where Φ represents cation vacancies; Mn-perovskite) [3] are efficient catalysts for the decomposition of N_2O at low temperatures. Their activities appeared to be appreciably higher than those of the corresponding metal oxides supported on γ -alumina, mainly due to the high dispersion of these metals in the zeolite and to the presence of cation vacancies and mixed valences states of manganese in the perovskite system. Lime and CaO exhibited activities very similar to those of the alumina derived catalysts. Ca-supported on alumina and Ca-DUT catalysts also showed activity for N_2O decomposition but at higher temperatures (1000 K). The only products of the N_2O decomposition were N_2 and O_2 with a molar N_2/O_2 ratio of 2. NO was not formed from this reaction.

The behavior of the various zeolitic and perovskite catalysts was quite different. Table 1 shows the apparent kinetic parameters for N_2O decomposition on different catalysts. Activation energies range from 75 ± 7 to 182 ± 31 kJ/mol. N_2O decomposition was found to be first order with respect to its partial pressure for the Co-ZSM-5, while fractional orders were found for Cu- and Fe-ZSM-5 and Mn-perovskite catalysts.

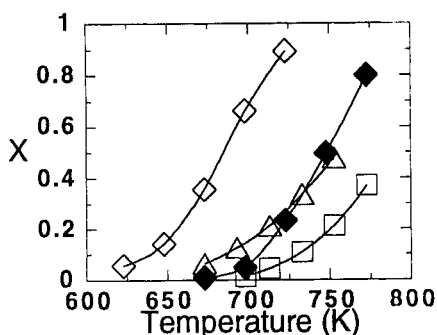


Figure 1. N_2O conversion as a function of temperature for Cu- (\diamond), Co- (\triangle) and Fe-ZSM-5 (\square) and Mn-perovskite (\blacklozenge), at inlet partial N_2O pressure of 1 mbar

The influence of O_2 , NO and SO_2 , also present in the FBC flue gas, on the N_2O decomposition for Cu-, Co- and Fe-ZSM-5 and Mn-perovskite was studied by addition of the given gas to a reference flow of constant concentration of N_2O in He at a constant temperature. Once the steady-state condition for N_2O decomposition was reached, O_2 , CO, NO or SO_2 was added at different concentrations in a random order. Figure 2 shows the N_2O conversion as a function of inlet oxygen concentration for these catalysts. O_2 had no important effect on the N_2O decomposition for Co-ZSM-5 and slightly decreased it for Fe-ZSM-5. However, N_2O decomposition was significantly reduced by the presence of O_2 for Cu-ZSM-5 and Mn-perovskite. This effect was more pronounced in the case of Mn-perovskite. The negative effect of oxygen on the N_2O decomposition was observed for the alumina supported catalysts, too. Apparently, two adjacent sites on the surface of the catalysts are needed to accommodate O_2 . In the case of Co-ZSM-5, the high dispersion of Co in the structure of the zeolite does not allow this process to take place. N_2O decomposes on the surface of the catalyst via reaction (1) and (2) according to first order reaction[4]:



Table 1. Apparent kinetic Parameters for N_2O Decomposition on Different Catalysts

	$\ln k_0^a$ (k_0 in mol/g s bar ⁿ)	Activ. Energy ^a (kJ/mol)	Reacion order ^a n
Co-ZSM-5	11.3 ± 1.0	106 ± 15	1
Cu-ZSM-5	17.8 ± 3.0	138 ± 17	0.88 ± 0.11
Fe-ZSM-5	20.8 ± 4.4	182 ± 31	0.79 ± 0.15
Mn-perovsk.	2.0 ± 1.4	75 ± 7	0.30 ± 0.07

^aparameters given with 95% confidence limits

Where * represents a surface active site. On the other hand, two adjacent sites can exist on the surface of Mn-perovskite and metal-supported on alumina, less disperse catalysts. In this case, oxygen can be accommodated on the surface of the catalyst, blocking the active sites available for the N_2O decomposition. It has been established in the literature that the decomposition of N_2O over metal oxides [5] and perovskites [6] takes place throughout chemisorption of N_2O on an active site followed by dissociation of the chemisorbed species, producing molecular N_2 and surface oxygen. Recombination of surface oxygen gives rise to molecular O_2 . This mechanism may explain the apparent fractional order and the negative effect of oxygen found for Mn-perovsk., but does not seem appropriate for the N_2O decomposition on the highly dispersed Cu- and Fe-ZSM-5 catalysts.

The preparation method of the ZSM-5-based catalysts gave rise to a theoretical exchange level of Cu^{2+} with ZSM-5 zeolite higher than 100% (130%, assuming that one copper(II) ion is exchanged for two sodium(I) ions). Part of the copper is ion-exchanged with the zeolite and the excess copper may be due to small clusters of copper oxide, as detected by IR measurements of CO adsorbed on Cu-ZSM-5. These clusters of copper oxide seem to be responsible of a high mobility of the surface-oxygen in this catalyst [7], which may lead to O_2 dissociation on the surface of this catalyst, explaining the inhibiting effect of oxygen and the apparent fractional reaction order observed for Cu-ZSM-5. The ion-exchange level for Fe with ZSM-5 was 98%, very close to the theoretical limit, and the mentioned effect might also apply to Fe-ZSM-5, although to a lower degree.

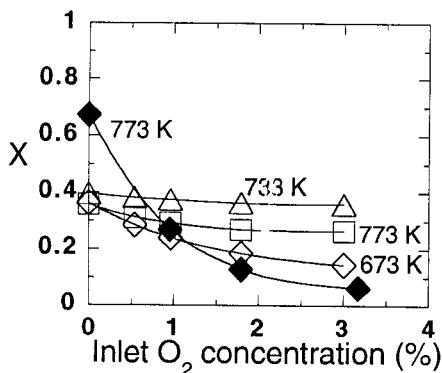


Figure 2. N_2O conversion as a function of inlet O_2 concentration for Cu- (\diamond), Co- (\triangle) and Fe-ZSM-5 (\square) and Mn-perovskite (\blacklozenge), at inlet partial N_2O pressure of 1 mbar

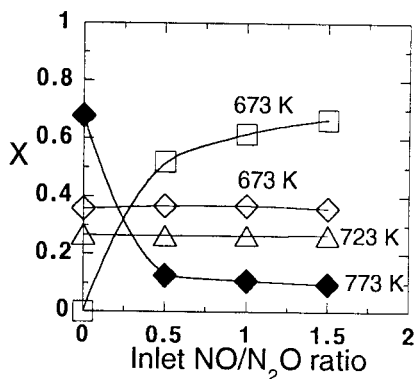


Figure 3. N_2O conversion as a function of inlet NO/ N_2O ratio for Cu- (\diamond), Co- (\triangle) and Fe-ZSM-5 (\square) and Mn-perovskite (\blacklozenge), at inlet partial N_2O pressure of 1 mbar

The influence of NO on the decomposition of N_2O is shown in Figure 3. The presence of NO increased N_2O conversion for Fe-ZSM-5 by a factor of 2 even at temperatures as low as 673 K, where N_2O could not be decomposed in the absence of NO. NO had no effect on the N_2O decomposition for Cu- and Co-ZSM-5 and dramatically decreased the N_2O conversion for Mn-perovsk. In the case of Fe-ZSM-5, conversion of NO was also observed, which did not take place when only NO was fed to the reactor at the same conditions. The product gas of the N_2O decomposition reaction in the presence of NO for Fe-ZSM-5 was composed of N_2 , O_2 and NO_2 , and the amounts of N_2 and NO_2 produced correspond to the amount of N_2O and NO converted, respectively. Adsorption of NO on Fe-ZSM-5 was observed by IR measurements even at 673 K. A possible explanation for the enhancement of the N_2O decomposition for this catalyst in the presence of NO is that reaction of N_2O with NO adsorbed to produce N_2 , NO_2 and a free site is faster than reaction (2). The negative effect of NO for the N_2O decomposition

on Mn-perovskite catalyst may be ascribed to competitive chemisorption of NO and N₂O on the active sites.

Although in FBC boilers limestone is usually added to the bed to achieve over 90% reduction of SO₂, still 50 to 150 ppm SO₂ remain in the flue gas. SO₂ poisoning is a factor that is known to be important in the deactivation of solid catalysts. The influence of SO₂ on N₂O decomposition was studied for Co-ZSM-5, Fe-ZSM-5 and Mn-perovskite catalysts in a similar way as for NO. SO₂ enhanced the N₂O decomposition for Fe-ZSM-5 in the temperature range studied. This effect seems to be very similar as the one produced by NO. On the contrary, the presence of SO₂ reduced the decomposition of N₂O for Co-ZSM-5 and dramatically decreased the N₂O conversion for Mn-perovskite catalyst. In both cases, SO₂ is chemisorbed on the surface of the catalyst, blocking the active sites available for the N₂O decomposition. However, while the catalytic activity of Co-ZSM-5 for N₂O decomposition in the presence of SO₂ is re-established by increasing the temperature from 723 to 923 K, much higher temperatures (>1023 K) were needed in the case of Mn-perovskite catalyst.

Practical application can be achieved by placing the catalysts in different positions in the FBC system, the main factor being that the conditions such as flue gas temperature are optimal for the catalyst used. Three locations in the FBC system have been explored with different catalysts. Lime and Ca-DUT catalyst could be used as bed materials or fed upper in the freeboard for sulfur capture and, at the same time, take in advantage their catalytic activities for N₂O decomposition. Manganese-containing perovskite (Mn-perovskite) on a monolith could be a suitable catalyst for the position located between the cyclone and the preheater, where the flue gas is almost dust free and the temperature still remains high enough. On the other hand, Fe- and Co-ZSM-5 catalysts are able to work at much lower temperatures. In this regard, Fe- or Co-exchanged ZSM-5 supported on metallic wire mesh can work efficiently, under FBC conditions, after the preheater. In this position the catalyst achieves a maximum conversion at relatively low inlet temperatures, which optimizes the selectivity towards N₂ and O₂ and minimizes thermal deactivation.

CONCLUSIONS

Cu-, Co- and Fe-exchanged ZSM-5 zeolite and vacancies-containing manganese perovskite are efficient catalysts for the decomposition of N₂O into N₂ and O₂ at low temperatures, which can be ascribed to the high dispersion of these metals in the zeolite and to the presence of cation vacancies and mixed valence states of manganese in the perovskite system. Oxygen had no effect on the N₂O decomposition for Co-ZSM-5 and slightly decreased N₂O conversion for Fe-ZSM-5. However, the presence of O₂ inhibited the N₂O decomposition for Cu-ZSM-5 and strongly decreased the N₂O conversion in the case of Mn-perovsk. catalyst. NO enhanced N₂O reduction only for Fe-ZSM-5, had no effect on it for Cu- and Co-ZSM-5 and dramatically reduced the N₂O conversion for Mn-perovsk. catalyst. SO₂ also increased the N₂O decomposition for Fe-ZSM-5. However, its influence was negative for Co-ZSM-5 and Mn-perovsk. catalyst. The results suggest that the N₂O decomposition reaction can be described by a two- or three-steps model with a rate determining step depending on the catalyst system.

5. REFERENCES

1. J.R. Pels, M.A. Wójtowicz and J.A. Moulijn, *Fuel*, 72, (1993) 373.
2. Y. Li and J.N. Armor, *Appl. Catal.*, B1 (1992) L21.
3. S.L. Raj, B. Viswanathan and V. Srinivasan, *J. Catal.*, 75 (1982) 185.
4. C.M. Fu, V.N. Korchak and W.K. Hall, *J. Catal.*, 68 (1981) 166.
5. E.R.S. Winter, *J. Catal.*, 19 (1970) 32.
6. C.S. Swamy and J. Christopher, *Catal. Rev. Sci. Eng.*, 34 (1992) 409.
7. J. Valyon, W.S. Millman and W.K. Hall, *Catal. Lett.*, 24 (1994) 215.

GAS INJECTION AS A MEASURE TO REDUCE N₂O EMISSIONS FROM FLUIDIZED BED COMBUSTION OF COAL

G. Marbán, F. Kapteijn and J.A. Moulijn

**Delft University of Technology, Julianalaan 136, 2628 BL Delft
THE NETHERLANDS**

1. INTRODUCTION

The influence of N₂O on both the greenhouse effect and the depletion of stratospheric ozone is well known. In recent years, fluidized bed combustion of coal has been found to be a new source of atmospheric N₂O (typical N₂O concentration levels vary from 50 ppm_v to 200 ppm_v). In-bed measures to reduce N₂O emissions in FBC are difficult to apply due to the numerous trade-offs existing in the bed between the different gaseous species produced during combustion with operating variables (especially bed temperature) and combustion efficiency. A natural alternative to in-bed combustion measures is the use of low-temperature combustion together with treatment of the flue gases. In the context of this approach a technique involving gas fuel injection has been studied at pilot plant-scale by the group of Leckner^{1,2} at Chalmers University (Sweden). This technique consists of the *creation of a hot-temperature region inside the freeboard, cyclone or downstream* by injecting methane or other combustible gas. The objective of the present work is to carry out fundamental studies in a lab-scale fluidized bed reactor in order to assess the effect of fuel gas injection on the different gaseous emissions (N₂O, NO and SO₂) and to evaluate the relative importance of radical and thermal mechanisms for N₂O decomposition and NO_x formation.

2. EXPERIMENTAL SECTION

The experiments were carried out in a lab-scale FBC made of quartz (29 mm I.D.), operating under atmospheric pressure, whose main features are described elsewhere³. A quartz injector (6 mm O.D.) is used to create a counter-current flame of either methane or propane. The flame temperature is measured by a high-temperature thermocouple. A stream of simulated combustion gases (flow rate=1 l/min) is introduced from the lower part of the reactor and passed through the flame, where N₂O is decomposed. Values of O₂ concentration in the fluidization gases below 12% resulted in flame instability. In this sense the O₂ concentration used during the experiments had to be fixed at 12%, in spite of being higher than that existing at actual combustion conditions. Additionally, H₂O was not introduced with the inlet gases since it was produced by the flame at similar levels to those existing in a boiler. N₂O analysis in the outlet gas was performed using a gas chromatograph equipped with an electron capture detector (ECD). Metallic components of the thermocouples provoked a certain catalytic N₂O reduction in the 'empty reactor' (without flame), but inlet O₂ concentrations higher than 4% inhibited this catalytic effect.

3. RESULTS AND DISCUSSION

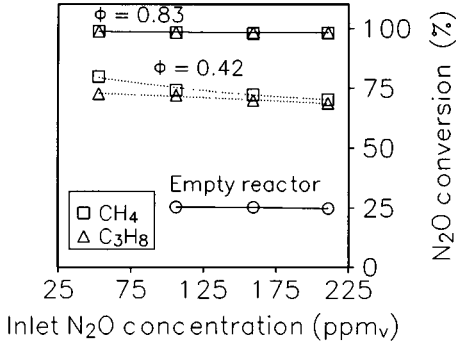


Figure 1. Effect of stoichiometric gas/O₂ ratio, ϕ , on N₂O conversion

The flame temperatures achieved by the combustion of methane were 1290 K at an stoichiometric gas/O₂ ratio $\phi=0.42$ and 1333 K at $\phi=0.83$; propane flame temperatures varied from 1313 K at $\phi=0.42$ to 1340 K at $\phi=0.83$ ($T_b=1123$ K, inlet gas composition: 12% O₂, 14% CO₂ and 74% He). Figure 1 shows the results on N₂O conversion achieved in the above mentioned flames (CH₄ and C₃H₈ at $\phi=0.42$ and 0.83) and in the empty reactor ($\phi=0$, $T_b=1123$ K, inlet gas composition: 53-211 ppm_v N₂O, 12% O₂, 14% CO₂ and 74% He). N₂O conversions up to 99% can be achieved with both flames (CH₄ and C₃H₈) at $\phi=0.83$.

In the above described experiments with the flame (figure 1), only a small amount of NO_x (less than 16 ppm_v) was formed in all the cases. This amount slightly increased (by 2 to 13 ppm_v at $\phi(\text{CH}_4)=0.42$) when the carrier gas was replaced by mixtures of N₂/He. N₂O conversion was not affected by the replacement of He as a carrier gas by N₂/He mixtures.

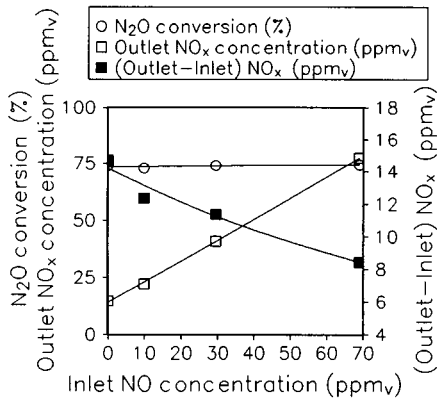


Figure 2. Effect of inlet NO concentration on N₂O decomposition and NO_x emissions in the flame

(1178 versus 1223 K, respectively).

Figure 2 shows that NO introduced with the inlet gas (composition: 0-69 ppm_v NO, 106 ppm_v N₂O, 12% O₂, 14% CO₂, 54% N₂ and 20% He) has no effect on N₂O decomposition in the flame of methane at $T_b=1123$ K ($\phi=0.42$). On the other hand, NO_x formed by the 'prompt NO' mechanism in the flame diminishes slightly from 14.7 to 8.4 ppm_v, when the inlet NO concentration increases by 0 to 69 ppm_v. In this sense, NO seems to inhibit NO_x formation in the flame, although to a low extent.

At the conditions used in this work, NO_x was assumed to be formed in the flame mainly via the 'prompt NO' mechanism. In order to substantiate this statement, a stream of gas of composition 106 ppm_v N₂O, 12% O₂, 14% CO₂, 54% N₂ and 20% He was introduced in the empty reactor at 1223 K. In this case no NO_x was formed. However, when a flame of methane ($\phi=0.42$) was used to reduce N₂O from a gas of composition 53-211 ppm_v N₂O, 12% O₂, 14% CO₂ and 74% He passing through the reactor at $T_b=1023$ K, the emissions of NO_x increased by 3.2 ppm_v (inlet N₂O=53 ppm_v) to 10.5 ppm_v (inlet N₂O=211 ppm_v), although the flame temperature in this case was lower than the reactor temperature in the previous case

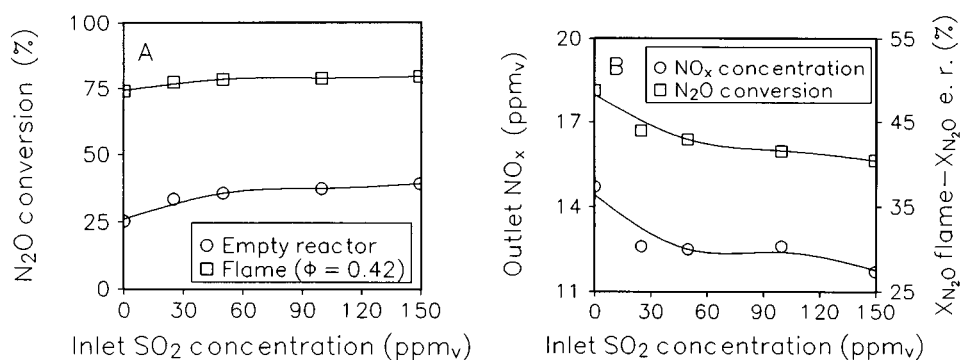


Figure 3. Effect of SO₂ on N₂O decomposition: A.- Comparison between N₂O decomposition in the empty reactor and in the methane flame ($\phi=0.42$). B.- Effect of SO₂ on NO_x emissions and N₂O conversion in the flame

The effect of SO₂ on N₂O decomposition both in the empty reactor and in the flame can be observed in figures 3A and 3B. For these experiments, a gas mixture of composition 0-149 ppm_v SO₂, 106 ppm_v N₂O, 12% O₂, 14% CO₂, 54% N₂ and 20% He was introduced in the reactor at T_b=1123 K with and without flame (CH₄, $\phi=0.42$). As can be observed in figure 3A, the presence of SO₂ in the empty reactor provoked an increase in N₂O reduction from 25.2% (0 ppm_v SO₂) to 39.3% (149 ppm_v SO₂). This positive effect could be a result of reaction of SO₂ with N₂O to yield SO₃ and N₂. SO₂ provoked in overall terms a decrease in N₂O conversion in the flame, as shown in figure 3B. This effect was similar to that exerted by SO₂ on NO_x emissions from the flame (fig. 3B). In order to explain this fact radical recombination in the flame catalysed by SO₂ has to be considered.

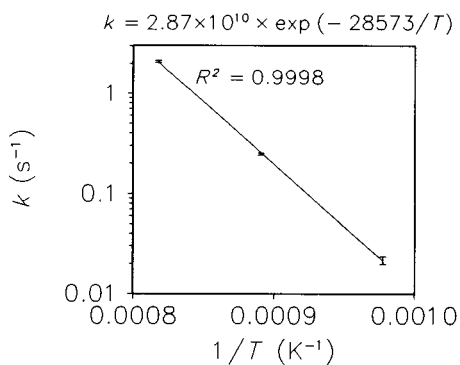


Figure 4. Arrhenius representation for kinetics of thermal decomposition in the empty reactor

Experiments at different total flow rates (from 0.75 l/min to 1.15 l/min) were performed at three bed temperatures (1023, 1123 and 1223 K) in order to calculate the kinetic parameters of thermal N₂O decomposition in the empty reactor. The composition of the inlet gas for the three temperatures was 106 ppm_v N₂O, 17.1-10.5% O₂, 14% CO₂, 48.9-55.5% N₂ and 20% He. The Arrhenius plot achieved by assuming in the calculations an ideal plug-flow model for the gas phase is shown in figure 4. The best fit of the reaction rate at the different flow rates was found for an apparent reaction order of 1. Thus, the experimental data are best described by the following pseudo first order decomposition rate constant: $k=2.87 \times 10^{10} \times \exp(-28573/T)$, where the activation energy takes a value of 237320 J/mol and the preexponential factor is expressed in s⁻¹.

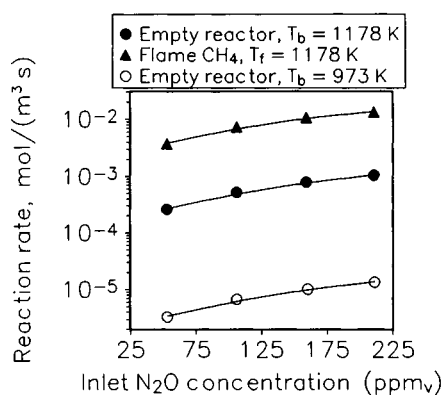


Figure 5. Comparison between N₂O decomposition in the methane flame and in the empty reactor

reaction rates for thermal N₂O decomposition in the empty reactor evaluated at the flame temperature (1178 K) by using the calculated rate constant are also represented. It can be observed that the reaction rates in the flame are between 10 and 15 times higher than those in the empty reactor. Hence we conclude that radical mechanisms are much more important than thermal mechanisms for N₂O decomposition in the flame, at the conditions studied in this work.

4. CONCLUSIONS

Up to 99% of N₂O reduction was achieved in the experiments carried out in the present work for both CH₄ and C₃H₈ flames, confirming the feasibility of gas injection for N₂O reduction purposes.

The reaction rate for N₂O decomposition in the flame was 10-15 times higher than that achieved by the empty reactor at the same temperature. This corroborates the fact that radical N₂O decomposition plays an important role in the flame chemistry at the conditions used in this work.

The reaction rate for thermal N₂O decomposition in the empty reactor could be described by $r_{N_2O} = kC_{N_2O}$, where $k = 2.87 \times 10^{10} \times \exp(-28573/T)$.

'Prompt NO' is the main mechanism for NO_x formation in the flame at the conditions used in this work.

NO has no effect on N₂O reduction in the flame. SO₂ slightly increases the N₂O reduction in the empty reactor but inhibits at flame conditions due to radical recombination.

REFERENCES

1. B. Leckner and L. Gustavsson, J. Inst. of Energy, 64 (1991) 176.
2. L. Gustavsson and B. Leckner, 6th Int. Workshop on Nitrous Oxide Emissions, Turku/Åbo, Finland, 1994
3. G. Marbán, F. Kapteijn and J.A. Moulijn, Combustion and Flame, (1995) submitted for publication

In order to assess the relative roles for N₂O decomposition that radical and thermal mechanisms play in the flame, different experiments were carried out with the reactor at T_b=973 K. At that temperature, the N₂O conversion achieved in the empty reactor was less than 1%, according to the rate constant above presented, the flame being responsible for almost all N₂O decomposition achieved in the reactor. The inlet gas composition was 53-211 ppm, N₂O, 12% O₂, 14% CO₂ and 74% He. The CH₄ flame temperature achieved under these circumstances was 1178 K (φ=0.42). Reaction rates for N₂O decomposition were calculated assuming perfect mixing in the flame. These are represented in figure 5. In the same figure, the

Coal utilization technology for reducing carbon dioxide emission

A. Inaba and K. Okada

National Institute for Resources and Environment
Onogawa 16-3, Tsukuba, 305 Japan

Coal Mining Research Centre, Japan
Minami-Sakaecho 14-1, Kasukabe, 344 Japan

1. INTRODUCTION

From the viewpoint of the long-range future, coal is clearly an important energy resource of which there are vast reserves. Developments in coal utilization technology may become quite important, particularly considering the mitigation of GHG emissions.

Coal can be used not only as combustion fuel, but also as a raw material for conversion technologies such as gasification and liquefaction. We must define the most suitable technology for each coal in order to use coal with the highest efficiency.

In this study, gross heating values of the products of coal conversion technologies were calculated for various coals assuming the theoretical reactions. Then, overall CO₂ emissions were estimated, including products combustion and CO₂ generated from conversion.

2. COAL UTILIZATION TECHNOLOGY AND ITS CO₂ EMISSION

Values from chemical analysis of 201 coal samples having various properties were used for this study. The carbon content of coals ranges from 67.96 to 87.05 daf wt.%, the hydrogen content from 3.99 to 6.51 daf wt.%, and the oxygen content from 5.81 to 26.46 daf wt.%. The gross heating value ranges from 6,310 to 8,500 daf kcal/kg. The relationship between the carbon content and heating value is shown in Figure 1. These coals belong to the rank of brown coal, subbituminous and high volatile bituminous coal. For these coals, theoretical efficiency and CO₂ emission were calculated for the cases of electric power generation, gasification, and direct liquefaction[1].

a) Electric power generation

The efficiency of 40% was assumed for the electric power generation in this study. Carbon included in coal was also assumed to oxidize completely to CO₂.

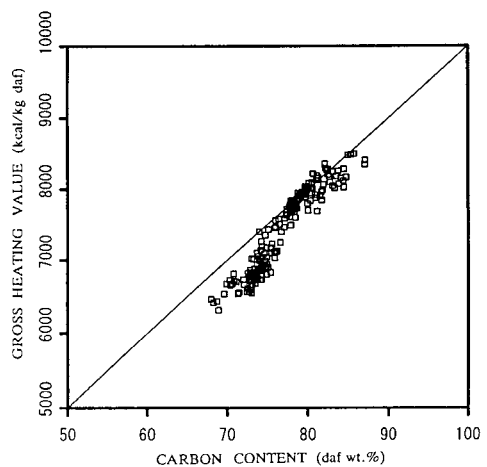
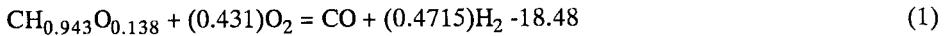


Figure 1. Relationship between carbon content and gross heating value

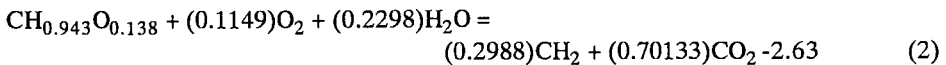
b) Coal gasification

A large number of coal gasification processes have been developed in the past. In this study, the coal gasification process using oxygen was assumed, where coal is completely converted to CO and H₂. The reaction of Taiheiyo coal (C: 78.26%, H: 6.19%, O: 14.40%, gross heating value: 7,800 kcal/kg, all in daf basis) is shown in Eq.(1). The negative heat value in Eq.(1) represents the exothermic reaction in units of kcal/mol.



c) Direct liquefaction

In direct liquefaction using hydrogen, it was assumed that the oxygen included in coal was converted to CO₂, and that the amount of remaining carbon was converted to gasoline and residual carbon. Hydrogen required for direct liquefaction was theorized to have been produced by the gasification of residual carbon with oxygen, which was balanced stoichiometrically to equal the hydrogen required. The overall reaction for Taiheiyo coal is shown in Eq.(2). The high heat value of 164.79 kcal/mol was assumed for gasoline.



3. DISCUSSION

3.1. Theoretical efficiency

The theoretical gasification efficiency increases generally with decreasing coal rank (Figure 2). The heating value of the products through the gasification is almost proportionate to the carbon content of coal, but the heating value of lower rank coals is slightly lower than the proportionate heating value to the carbon content, shown in Figure 1. Since the theoretical efficiency is defined as ratio of the heating value of the products to that of the coal, the theoretical efficiency for lower rank coals was slightly higher than those of higher rank coals.

In direct liquefaction, a broad peak is likely to be observed at the carbon contents around 80%. Since hydrogen is required in the hydrogenation technology, coals having higher hydrogen content generally exhibited a higher theoretical efficiency. Since oxygen included in coal was assumed to be converted to CO₂, coals having higher oxygen content yielded a lower theoretical efficiency in their liquefaction.

3.2. CO₂ emission

Products from the above coal conversion technologies were assumed to be burned to obtain energy. Hence the overall CO₂ emissions through conversion technologies were calculated from the carbon content of coal. Figure 3 illustrates the correlation between the carbon content of coals and the ratio of carbon emitted as CO₂ to energy obtained as products by the conversion technology.

Since the efficiency for the electric power generation for all coals was assumed to be 40%, the ratio of CO₂ emission to the obtained energy by electric power generation for lower rank coals (whose heating value is slightly lower than the proportionate heating value to the carbon content) was higher than that of higher rank coals. Therefore, it is quite important to improve the efficiency of power generation from lower rank coals, such as brown coals, which have generally lower heating value than higher rank coals.

In gasification, the ratio of CO₂ emitted to obtained energy for coals with carbon contents of approximately 75% was found to be higher than for coals with carbon contents of around 80%. Although the efficiency of the former group is higher than that of the latter group, the difference in efficiency between the groups is less than that of their heat values. Hence per unit mass of coal, there is less energy obtained from the less carbon-rich group.

3.3. Relationships between theoretical efficiency, CO₂ emission, and coal properties

To further understand the above theoretical calculations, schematic contour lines of the theoretical efficiency and CO₂ emissions for gasification and liquefaction were drawn on the H/C vs O/C atomic ratio plot, based on the calculated statistics (Fig. 4).

The gasification theoretical efficiency was found to increase with increasing O/C ratios (decreasing rank), and that the H/C ratio had little effect. In contrast, the CO₂ emissions were found to decrease with increasing H/C ratio, with the O/C ratio having little effect.

On the other hand, it was revealed that the theoretical efficiency of liquefaction increases and the CO₂ emissions decrease with increasing H/C ratios and with decreasing O/C ratios (increasing coal rank). However in reality, coal of increasing rank becomes harder to liquefy [2]. In this study, the liquefaction efficiency does not diminish with increasing rank due to the assumption of ideal conversion.

4. DEVELOPMENT OF COAL UTILIZATION TECHNOLOGIES CONSIDERING CO₂ EMISSIONS

Since the carbon content per heating value of brown coals is generally greater than that of subbituminous and bituminous coals, it has been said that brown coals should not be used as a means to mitigate global warming. The theoretical efficiency of gasification for brown coals is high if oxygen included in coal could be used efficiently in the gasification. Since brown coals are generally cheaper than other high rank coals, the utilization of brown coals by conversion

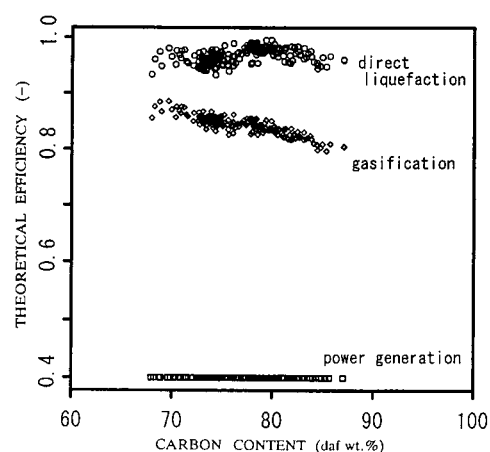


Figure 2. Theoretical efficiency

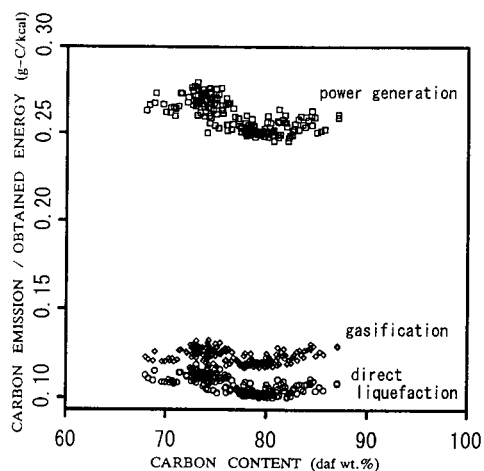


Figure 3. Carbon emission per obtained energy

technologies such as gasification should be recommended from the economic viewpoint. The establishment of a technology using gasification, such as an integrated gasification combined cycle, is essential for the efficient use of brown coals.

It has been illustrated, however, that the theoretical efficiency of and CO_2 emissions from subbituminous coals are significantly varied due to their properties. For the development of technologies to utilize subbituminous coals, it is essential to consider the characteristics of each coal.

For the direct liquefaction, the theoretical efficiency is higher and the CO_2 emissions are lower than that of gasification. It is well known that the practical efficiency of direct coal liquefaction is significantly less than the theoretical efficiency, because oil heavier than gasoline is produced in large quantities and that the residual carbon materials include not only carbon but also hydrogen. A direct liquefaction technology must be developed in order to approach the theoretical efficiency.

The theoretical efficiency and CO_2 emissions were calculated in this study based on theoretical reactions. The reactions occurring in practice are affected both by the physical characteristics of coal, such as melting and swelling, and by the chemical characteristics, such as the reactions of functional groups in coal. It is, however, suggested from the theoretical calculations in this study that technology development suitable for each coal is necessary to use coals efficiently. The progress of the coal science is also essential to develop the most efficient utilization technology for each coal.

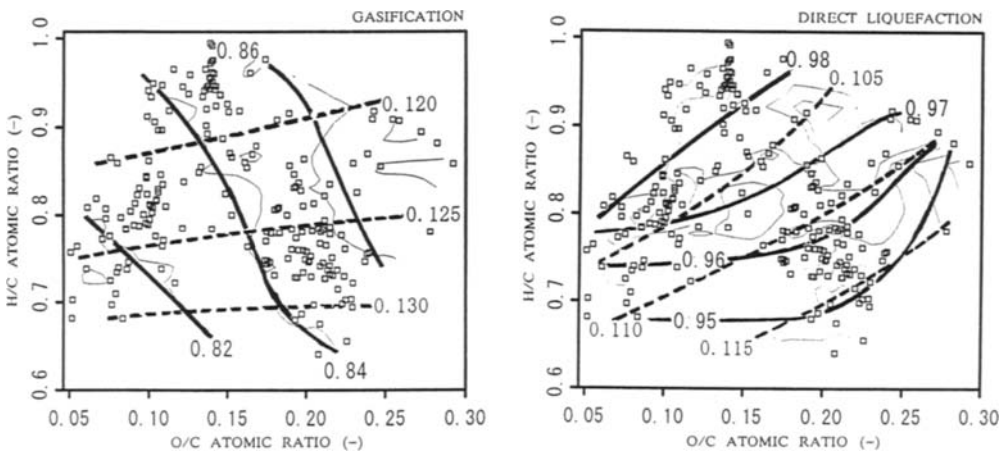


Figure 4. Schematic contour lines of the theoretical efficiency and CO_2 emission for gasification and liquefaction

REFERENCES

1. A. Inaba and K. Okada, Proc. of International Symposium on Coal and Organic Petrology, 1994 Fukuoka 110
2. K. Okada, Proc. 8th ICCS

PRESSURISED FLUIDISED BED COMBUSTION OF COALS IN MIXTURES OF RECYCLED FLUE GAS AND OXYGEN

B. Bonn, H. Baumann

DMT-Gesellschaft für Forschung und Prüfung mbH, Franz-Fischer-Weg 61, D-45307 Essen, Germany

1. INTRODUCTION

Carbon dioxide (CO₂) emission from coal combustion into the atmosphere can be reduced by capture from the flue gas and stable fixation. When coal is burnt in a mixture of recycled flue gas and oxygen, the high nitrogen ballast in the flue gas is avoided and the dry flue gas consists by nearly 100 % of CO₂ which, after removal of other constituents, can be disposed of in a suitable way.

The aim of the experiments was to examine the feasibility of burning coal in mixtures of oxygen and recycled flue gas and to determine the formation of CO, SO₂, NO and N₂O under these conditions.

2. EXPERIMENTAL

The laboratory scale pressurised fluidised bed combustor used for the experiments has been described elsewhere [1, 2]. It consists of a cylindrical bed with 12 cm inner diameter and a freeboard with 21 cm inner diameter, both parts having a height of 1.5 m. It was equipped with flue gas recycling. Before the start the whole system was filled with carbon dioxide, during operation oxygen was added from a cylinder in amounts needed for oxygen concentrations between 20 and 30 vol.%. The combustion experiments reported here were carried out with the high volatile bituminous coal 'Westerholt' at pressures between 1 and 10 bar and temperatures of 800, 850 and 920 °C with limestone addition for sulphur capture. The experiments with flue gas recirculation are compared with combustion experiments in air without flue gas recirculation. The Ca/S ratio was 2 in the recirculation experiments and 1 in the experiments without recirculation.

3. RESULTS AND DISCUSSION

The freeboard temperature follows the bed temperature in a natural way, but in some cases, particularly in the recirculation experiments, it was varied additionally by varying the degree of external heating in order to study its influence on the emissions. Freeboard temperature is plotted versus bed temperature in Figure 1. In the recirculation experiments the freeboard temperature is generally higher than in normal air combustion, probably because of the higher heat capacity of carbon dioxide compared to air.

Direct comparison of the emissions is not reasonable because the experimental parameters are generally not the same. Therefore non-linear regressions were performed for fuel nitrogen conversion to NO and N₂O with the independent parameters bed temperature, freeboard temperature, pressure and oxygen concentration in the flue gas. The results, presented as N-conversion to NO and N₂O, are shown as surface plots in Figures 2 and 3. In these figures, the freeboard temperatures were not assumed to be constant, but to be dependent on bed temperature according to both straight lines shown in Figure 1 for combustion with and without flue gas recirculation, respectively.

The N-conversion to NO as well as to N₂O is considerably lower with flue gas recirculation than without. This means for the constituents NO and N₂O, which participate in the complex nitrogen reaction mechanism, that they are partly destroyed in the bed when being recirculated into the combustion zone. The ratio of recirculated gas to exhausted gas was approximately 7 in the experiments, that means that the average number of recirculations was 7. In contrast to N-conversion, the concentrations of NO and N₂O were higher during recirculation because the flue gas was not diluted with the nitrogen of the air. The difference in limestone addition (Ca/S=2 with and Ca/S=1 without recirculation) is supposed to have only a small, if any, impact on NO and N₂O emissions, because it is observed that only highly excessive amounts of limestone increase NO and decrease N₂O formation.

A decrease was found for C-conversion to CO and S-conversion to SO₂ in flue gas recirculation, too. The main reason is again recirculation. Other influences of the high partial pressure of CO₂ as, for instance, a shift in chemical equilibrium affecting CO concentration or the inhibition of limestone conversion to CaO which affects SO₂ capture [3] are of minor importance.

Besides the level of N conversion to NO, the dependence on bed temperature and pressure is similar with and without flue gas recirculation at 6 vol.% O₂ concentration in the flue gas, as can be seen in Figure 2 a and b: N conversion to NO increases with temperature at low pressure and is nearly independent of temperature at 10 bar. The pressure dependence has a shallow minimum. N conversion to NO increases with increasing oxygen concentration in the flue gas

The fuel-N conversion to N₂O exhibits the well known characteristic that it decreases at high temperatures because of the thermal instability of N₂O. Further, it decreases with increasing pressure (Figure 3 a and b). It is nearly unaffected by oxygen concentration in the flue gas (Figure 3 c and d), however, at oxygen concentration below about 4 vol.-%, an increase of N-conversion to N₂O with increasing oxygen concentration was observed during combustion in air.

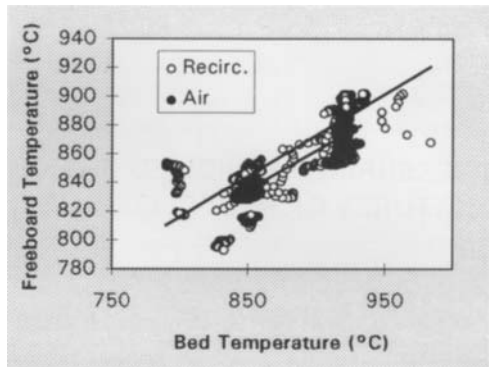


Figure 1. Relation between freeboard temperature and bed temperature for combustion with and without flue gas recirculation

4. CONCLUSIONS

The results of the experiments show that the conversions of fuel-N to NO and N₂O, of C to CO, and of S to SO₂ are considerably lower in flue gas recirculation than in normal combustion in air, whereas the concentrations of these constituents are higher because of the lack of dilution with air nitrogen. The decrease in conversion can be attributed to destruction reactions and SO₂ capture during, in average, seven times recirculating of the flue gas which means a seven times increase in the residence time in the fluidised bed and freeboard zones. Other influences are of minor importance. The qualitative dependencies of the concentrations of CO, SO₂, NO and N₂O on temperature, pressure and oxygen concentration are similar in oxygen/recycled flue gas mixtures and in air.

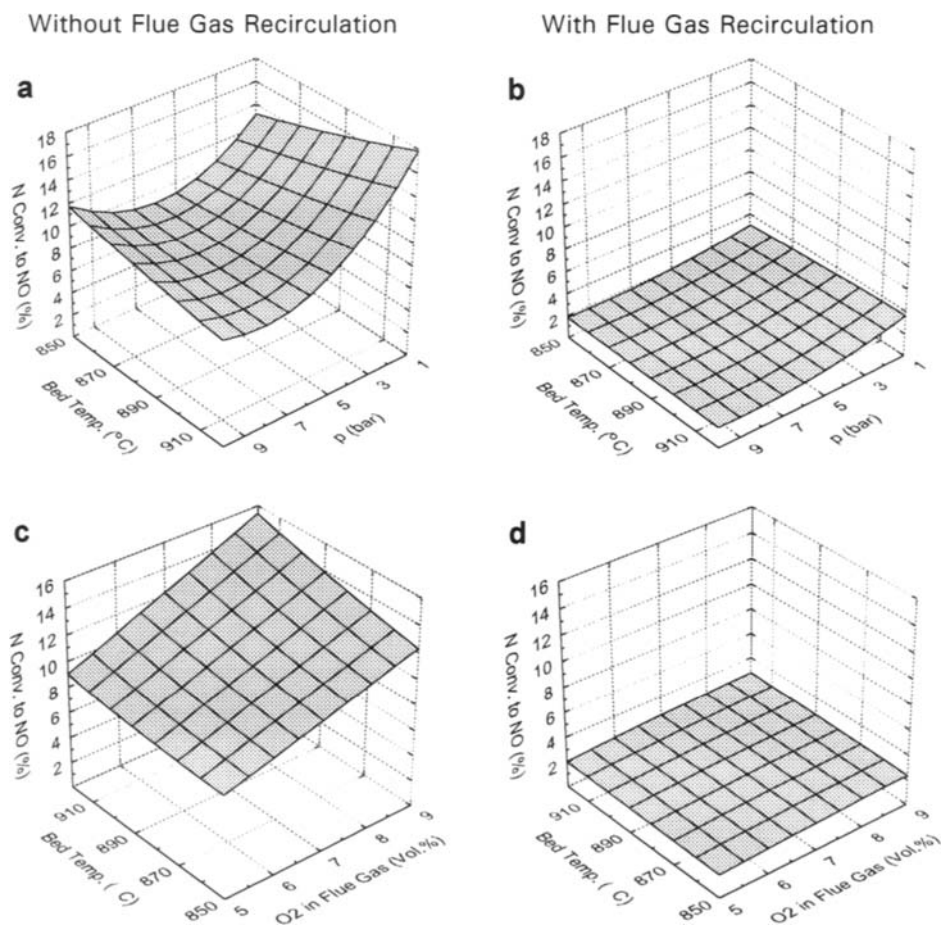


Figure 2. Fuel-N conversion to NO.
Combustion without (left) and with (right) flue gas recirculation.
a and b: 6 vol.% oxygen in the flue gas.
c and d: Pressure = 5 bar.

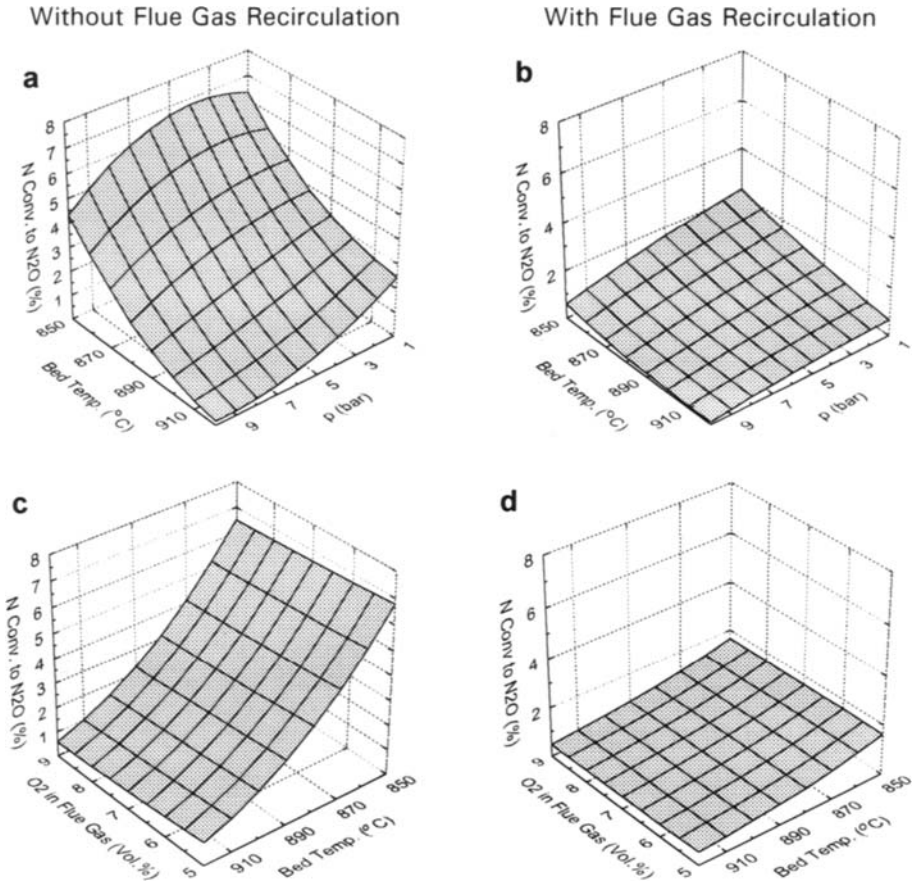


Figure 3. Fuel-N conversion to N₂O. Combustion without (left) and with (right) flue gas recirculation. a and b: 6 vol.% oxygen in the flue gas. c and d: Pressure = 5 bar.

ACKNOWLEDGEMENT

This work has been supported by the European Union in the JOULE II Programme.

REFERENCES

1. B. Bonn, H. Baumann and M. Mayer, Intern. VGB-Konferenz "Wirbelschichtsysteme 1992", 2./3. Sept. 1992, Essen,
2. M. Mayer, B. Bonn and H. Baumann, VDI-Ber., 1090 (1993) 83
3. J.B. Illerup, K. Dam-Johansen and K. Lundén, Chem. Engng. Sci., 48 (1993) 2151

POLYMER MEMBRANE CONDITIONING AND DESIGN FOR ENHANCED CO₂-N₂ SEPARATION

S.P. Kaldis, G.C. Kapantaidakis and G.P. Sakellaropoulos (*)

Aristotle University of Thessaloniki and Chemical Process Engineering Research Institute.,

P.O. Box 1520, Thessaloniki, 540 06 Greece

1. SUMMARY

Polymer membranes can be used for the separation of carbon dioxide from nitrogen in coal-fired power plant gases. Two different types of polymer materials are examined: polysulfone and polyimide. Polyimide based membranes exhibit somewhat better selectivity and temperature resistance than polysulfone ones. However, CO₂ sorption and subsequent plasticization can affect adversely polyimide membrane properties. In this work, CO₂ conditioning was used to alter CO₂/N₂ permselectivity of polyimide membranes. Such conditioning near and above the critical partial pressure of plasticization, improved permselectivity by up to an order of magnitude, for over 4-18 hours, probably due to membrane tightening and/or strong antiplasticization. For the performance evaluation of large scale membrane units, two mathematical models have been used, one for long hollow fiber modules and one for complete gas mixing. Simulations show that although permselectivity is important up to moderate values, at high values, module design and operating parameters affect equally performance and process economics.

2. INTRODUCTION

Carbon dioxide contributes up to 50% to the greenhouse effect, with one half of the total emissions deriving from coal-fired power plants [1,2]. Removal of CO₂ from the flue gases is feasible by gas separation membranes. However, the use of traditional polymer materials, such as cellulose acetate (CA) is limited by low temperatures ($T_{\max}=60^{\circ}\text{C}$) and very low CO₂ partial pressure of plasticization (~1-2 bar). Other commercially available, membrane materials include polysulfone (PSF) and polyimide (PI), with better temperature and pressure characteristics than CA [3]. The maximum working temperature of PSF and PI membranes is about 100 and 150°C, and the minimum pressure of plasticization is 50 and 15 bars respectively [4]. The CO₂/N₂ selectivity values of virgin PSF and PI membranes vary between 20 and 30 depending on the exact type of polymer. However, the use of highly sorbing gases, like CO₂ or H₂S, above the critical pressure of plasticization, can swell the polymer matrix causing a significant increase in membrane permeability and an irreversible reduction of permselectivity [5]. Although PI conditioning with CO₂, at pressures lower than 15 bar, can improve membrane performance for a certain period of time [6], little is known about moderately swollen polyimide membranes. In this work, PI conditioning with CO₂ is examined at 20 bar, i.e. above but near the critical pressure of plasticization, to determine membrane performance. The effect of membrane permselectivity on the CO₂/N₂ separation performance of large scale modules is also studied by mathematical modeling of different design configurations.

* To whom correspondence should be addressed

3. EXPERIMENTAL

Pure dense PSF films were prepared by a casting method, using a 4% wt "Udel polysulfone P-1700 nt 11" solution in chloroform. For PI films, a 5% wt "Matrimid 5218" in methylene chloride was used. The permeation characteristics of the resulted dense films were investigated for pure and multicomponent feed gas streams, in a high pressure permeability cell, by using the variable volume method [7]. The permeability coefficients of N₂ and CO₂, in PSF and PI virgin films at various pressures are given in Fig.1. In both polymers the permeability of N₂ decreases slightly with pressure while that of CO₂ shows a faster decrease in the region of 0-15 bar, as predicted by the dual-mode theory [3]. In the case of PI films, pressure increase above 15 bar results in permeability increase, indicating polyimide matrix plasticization, while PSF membranes are essentially unaffected by CO₂. PI dense films were subsequently conditioned with CO₂ at 20 bar and 40°C for 24 hours. After CO₂ evacuation, a binary mixture of 85% N₂ and 15%CO₂ was fed to the permeability cell, at a low stage cut (~0.02) and 40°C and 20 bar, simulating thus a typical coal-fired power plant flue gas. The dependence of permeate gas composition on time is given in Fig.2. For about 4 hours, the

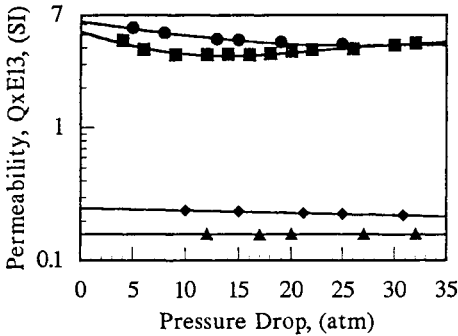


Figure 1. Permeabilities of CO₂ and N₂ in PI and PSF membranes at 40°C.

(■ PI-CO₂; ● PSF-CO₂; ▲ PI-N₂; ◆ PSF-N₂)

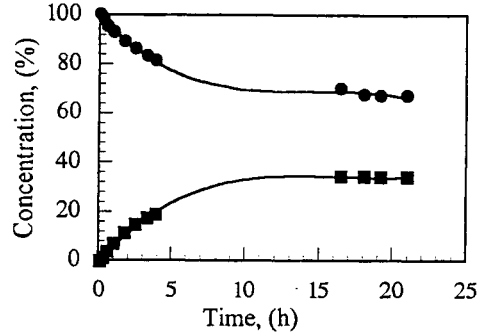


Figure 2. Permeate concentrations with time after PI conditioning with CO₂.

(■ N₂; ● CO₂)

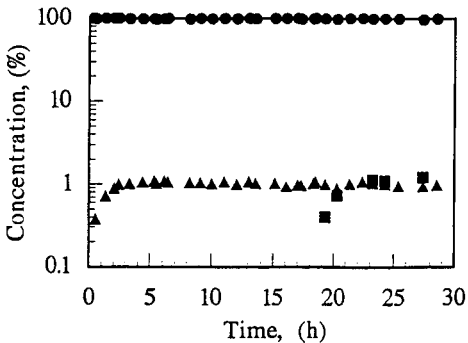


Figure 3. Permeate concentrations after PI conditioning with CO₂.

(■ N₂; ● CO₂; ▲ CO)

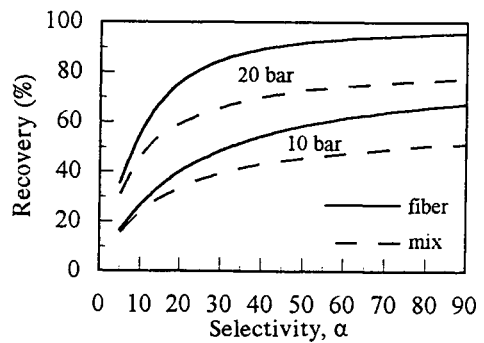


Figure 4. Effect of material, design and operation on membrane performance.

CO₂ and N₂ permeate concentrations yield an actual selectivity value which is gradually reduced from 200 to 30. After 22 hours, a steady state separation is observed, with an CO₂/N₂ selectivity of 13. This result could be probably attributed to the strong antiplasticization of the polyimide membrane matrix by CO₂ and the gradual relaxation of the polyimide membrane [8]. It is proposed that up to the critical partial pressure of plasticization (15 bar), CO₂ molecules accumulate in the polymer, resulting in matrix tightening and in permeability decrease. Such accumulation of CO₂ between the intersegmental polyimide chain spacing can temporarily restrict molecular motions of bulkier gases resulting in time dependent permeabilities and permselectivities. Apparently, exposure to a 15% CO₂ stream concentration, after conditioning, is not capable to sustain the antiplasticization behavior. The same conditioning protocol was also used for a ternary mixture of 80%CO₂, 10%N₂ and 10%CO at 40°C and 10 bar, simulating the product gas stream of gasification process. The variation of each gas concentration with time is given in Fig 3. In all cases, permeate CO₂ concentration varied between 98-99%; CO was about 1%, while N₂ concentration was detectable only after 18 hours, at a level of only about 1%. Thus, CO₂-conditioned PI membranes, in contact with increased levels of CO₂ concentration in the feed stream, give sustained high CO₂ permselectivity of over 100, without loss of CO₂ permeability. These results suggest that a cyclic conditioning technique can be employed to drastically alter CO₂/N₂ selectivity, thereby permitting effective CO₂ separation in a one stage membrane unit.

4. MATHEMATICAL MODELING

In order to evaluate the effect of permeability and permselectivity changes on the performance of polymer membranes, two mathematical models were employed : One for long hollow fiber modules, and one for complete mixing modules with flat membranes. In the first case, the mathematical model consists of three simultaneous ordinary differential equations, with the appropriate boundary conditions. The model incorporates also the basic relations which describe gas permeability dependence on temperature, and gas viscosity dependence on temperature and pressure. This nonlinear boundary value problem was solved by orthogonal collocation [9] and the Brown method [10], to ensure high precision and stability. In the complete mixing, the Weller-Steiner model [11] was used, with the high pressure side of the membrane being at the residue concentration.

The above models were applied to CO₂ separation from coal fired power plant flue gases with a typical composition of 15% CO₂ and 85% N₂. The feed flowrate per membrane area was held constant in both configurations. Figure 4 gives the fractional recovery of CO₂ (i.e. the percentage of CO₂ which is obtained in the permeate) as a function of membrane selectivity. Results indicate that in both design configurations the recovery reaches a plateau for $\alpha > 40$, a quite modest value for the selectivity of many gaseous pairs, including the one examined here. Hollow fiber modules operate more effectively than the complete mixing ones, while changes in feed pressure influence strongly the membrane performance. Similar influence is also predicted for other operating parameters such as feed flowrate and feed composition. Hence, although selectivity is important to achieve separation of a gas mixture, module design and operating parameters can be of equal if not of higher importance for the effective application of this technique.

In the case of CO₂ - N₂ separation, the need for a highly selective membrane ($\alpha > 200$) has been proposed, for the process to be viable [12]. The results of Fig. 4 show that for $\alpha > 30$ - 40 no appreciable improvement in CO₂ recovery should be expected and it would be

preferable to use a reasonably permeable membrane with appropriately chosen design and operating conditions.

5. CONCLUSIONS

Polymer membranes are considered for the separation of CO₂ from N₂, in coal fired power plants. Two different types of polymer materials have been examined. Polysulfone based membranes are not influenced by highly sorbing penetrants such as CO₂. Polyimide membrane characteristics are altered by CO₂ conditioning. The CO₂/N₂ selectivity can be drastically increased by CO₂ conditioning up to 200, for a period of 4-18 hours, depending on experimental conditions. Hence, a significant enhancement of CO₂/N₂ separation is possible with polyimide membranes, by applying a cyclic conditioning technique with CO₂. The effect of selectivity change on the operation of large scale membrane facilities is evaluated with two developed mathematical models. Results show that although permselectivity is important up to moderate values ($\alpha \approx 40$), module design and operational parameters affect equally, if not stronger, recovery and overall performance of membrane modules.

ACKNOWLEDGMENT

We thank the European Union for its financial support through ECSC project 7220EC-703.

REFERENCES

1. Audus H., Adams D., Riemer P. and Smith A. "Greenhouse Gas Emissions From Power Stations", IEA Greenhouse Gas R&D Programme (1993).
2. Riemer P., Audus H. and Smith A. "Carbon Dioxide Capture From Power Stations", IEA Greenhouse Gas R&D Programme (1994).
3. Ho W. and Sirkar K., "Membrane Handbook", Van Nostrand Reinhold, New York (1992).
4. Sanders E.S., Jordan S.M. and Subramanian R., "Penetrant-Plasticized Permeation in Polymethylmethacrylate", *J. Memb. Sci.*, **74**, 29(1992).
5. Koros W.J., Coleman M.R., and Walker D.R.B. "Controlled Permeability Polymer Membranes", *Annu. Rev. Mater. Sci.*, **22**, 47(1992).
6. Jordan S.M., Henson M.A., and W.J. Koros., "The Effects of Carbon Dioxide Conditioning on the Permeation Behavior of Hollow Fiber Asymmetric Membranes", *J. Memb. Sci.*, **54**, 103(1990).
7. "Standard Test Method for Determining Gas Permeability Characteristics of Plastic Film and Sheeting", ASTM Designation : D 1434-82 (1988).
8. Sanders E.S., "Penetrant-Induced Plasticization and Gas Permeation in Glassy Polymers", *J. Memb. Sci.*, **37**, 63(1988).
9. Villadsen, J., and Michelsen, M.L., "Solution of Differential Equation Models by Orthogonal Collocation", Prentice-Hall, Englewood Cliffs, N.J.(1978).
10. Brown, K.M., "Solution of Simultaneous Non-Linear Equations", *Comm. ACM*, **10**, 728(1967).
11. Hwang, S.T., and Kammermeyer, K., "Membranes in Separations", in "Techniques of Chemistry", (A. Weissberger ed.), Vol VII, Krieger Publishing Co., Fla.(1984).
12. Van Der Sluijs, J.P., Hendricks, C.A., and Blok K., "Feasibility of Polymer Membranes for Carbon Dioxide Recovery from Flue Gases", *Energy Convers. Mgmt.*, **33**, 429(1992).

Observations of CO₂ clathrate hydrate formation and dissolution under deep-ocean disposal conditions

Robert P. Warzinski^a, Anthony V. Cugini^a, and Gerald D. Holder^b

^aU. S. Department of Energy, Pittsburgh Energy Technology Center, Pittsburgh, PA 15236, USA

^bDepartment of Chemical Engineering, University of Pittsburgh, Pittsburgh, PA 15261, USA

1. INTRODUCTION

Disposal of anthropogenic emissions of CO₂ may be required to mitigate rises in atmospheric levels of this greenhouse gas if other measures are ineffective and the worst global warming scenarios begin to occur. Long-term storage of large quantities of CO₂ has been proposed, but the feasibility of large land and ocean disposal options remains to be established [1].

Determining the fate of liquid CO₂ injected into the ocean at depths greater than 500 m is complicated by uncertainties associated with the physical behavior of CO₂ under these conditions, in particular the possible formation of the ice-like CO₂ clathrate hydrate [1]. Resolving this issue is key to establishing the technical feasibility of this option. Experimental and theoretical work in this area is reported.

2. EXPERIMENTAL

Observations of the CO₂/water system were conducted in a high-pressure, variable-volume view cell. A description of the view-cell system as used in other work at temperatures above ambient has been published [2]. Modifications were made to permit the system to operate at temperatures in the hydrate forming region of interest (0°C to 10°C). The modifications included the incorporation of a cooling coil in the chamber containing the view cell, a small fan for improved air circulation in the chamber, and additional insulation.

Either potable water or water treated by reverse osmosis and deionization was used. CO₂ was obtained as a liquefied gas (99.5%) and used as received. In most experiments, water was first added to the cell then CO₂ was added either directly from the cylinder or from a high-pressure ISCO 260D syringe pump system. The cell was then chilled to the desired temperature and observations initiated. The pressure in the cell was varied during an experiment either by adding or venting CO₂ or by changing the position of a movable piston in the cell. Four phases are possible in this system: liquid water, gaseous CO₂, liquid CO₂, and solid CO₂ clathrate hydrate.

3. RESULTS AND DISCUSSION

Obtaining kinetic data applicable to the formation and decomposition of CO₂ hydrates under conditions that exactly simulate the deep ocean is not possible in the view cell or any similar device owing to contact of the CO₂ with metallic and glass surfaces. These surfaces promote nucleation and conduct heat differently than water and would therefore affect hydrate formation and dissolution. We are in the process of developing a system that precludes these problems. Described below are results obtained from experiments in the view cell that focused primarily on obtaining information that would provide important insights into the general behavior of the CO₂/water system under conditions anticipated for ocean disposal.

3.1 Phase behavior

The phase behavior of the CO₂/water system and the thermodynamic conditions for hydrate equilibrium have been determined [3]. The operation of the view cell was verified with this system by comparing the observed temperatures and pressures associated with hydrate formation and decomposition with the literature values. In these experiments, the conditions in the view cell were adjusted to obtain a lower water phase containing solid hydrates and an upper gaseous CO₂ phase. The presence of hydrates in the water phase provided nucleation sites for further hydrate growth. The amount of CO₂ in the cell and the position of the internal piston were adjusted to place the gas/liquid interface at a position convenient for observation. The pressure in the view cell was brought close to the value at which hydrate formation was anticipated. The pressure was then varied by small movements of the piston to cause additional hydrate to begin to either form or decompose at the CO₂/water interface. Phase changes could be detected with a pressure change of only 7.0 KPa, which was essentially the readability of the Heise gauge in use at this time. The pressures observed at the phase transition were near the literature values. For example, the phase transition occurred in the view cell at 3.06 MPa at 7.4°C to 7.5°C. The literature value was 3.08 MPa at 7.45°C [3].

3.2 Hydrate density

Pure CO₂ hydrates are denser than water or sea water and should sink [4]. Apart from any adverse ecological effects, this would be viewed as a benefit since it could result in very long CO₂ residence times in the ocean. However, some experimental accounts report that CO₂ hydrates float on the surface of water or seawater [5,6]. To help resolve this issue, observations were made of the relative densities of hydrates formed under various conditions in the view cell.

Observations were made on hydrates formed either (1) at the CO₂/water interface with gaseous CO₂, (2) at the CO₂/water interface with liquid CO₂ above the water, (3) in the CO₂ vapor space above a water phase, or (4) in a completely hydrostatic system from liquid CO₂ droplets. In all cases, once hydrate formation started, the hydrates grew rapidly and were snow-like in appearance. The hydrate masses were then broken apart using a magnetic stirring bar in the view cell. The snow-like hydrates were positively buoyant in the water phase. However, with extended time, the hydrates became more ice-like (transparent) in appearance and tended to sink in the view cell. Trapped, unconverted CO₂ may have caused the bulk density of the initially formed hydrates to be less than that of water. With time, this trapped CO₂ could be converted to hydrate, causing the density to increase and the appearance to change. It is interesting to note, that the hydrates sometimes formed a semi-solid mass

which occupied the entire water phase. This mass did not impede the movement of the stirring bar but showed no evidence of rising or settling in the cell.

To study hydrate formation from one homogeneous phase, 1.75 g of CO₂ was dissolved in 30.0 g of water in the view cell at 18°C and 14 MPa. This solution would be about 80% saturated at 12°C and 12.662 MPa [7]. The cell was gradually cooled without stirring. Hydrates formed from solution near 5.0°C and 12.40 MPa. At the time of formation, the hydrates were ice-like in appearance and rapidly sank when disturbed by moving the stirring bar. The hydrates were observed for 16 hours under these conditions and appeared to be stable. Later in the experiment, they began to decompose without stirring when the view cell reached 5.4°C. Forming the hydrates from dissolved CO₂ appears to avoid the problem of entrapped CO₂ and results in hydrates that are denser than water.

3.3 Fate of hydrate-coated droplets

The last experiment described above was continued by introducing a liquid CO₂ droplet into the hydrate-containing water phase while the hydrate was still present. It immediately formed a hydrate coating but then exhibited no further change over a period of several hours in a non-agitated system. We have made similar observations in other experiments at different conditions.

When the hydrate coating formed on a CO₂ droplet in water relatively unsaturated with CO₂, the droplet shrank in size as it dissolved. For example, at 6.5°C and 11.1 MPa, a 2.6-mm diameter droplet decreased in radius at a rate of 0.0045 cm/h with slow agitation in the view cell. In the absence of a hydrate coating, a droplet of similar size at 6.1°C and 12.6 MPa decreased in radius at 0.10 cm/h. In comparison, Shindo et al. [8] measured dissolution rates of hydrate-covered CO₂ droplets at 28 MPa to 32 MPa (no temperature given) and found that they decreased in radius at a rate of 0.09 cm/h. The difference in rates may be due to dissimilarities in the experimental procedures and apparatus; however, differences in the thicknesses of the hydrate coating may also have been a factor.

The importance of understanding the kinetics of hydrate formation and dissolution may be illustrated using an earlier model we developed to determine the fate of liquid CO₂ droplets injected into the ocean [4]. At the time, the best kinetic data available for estimating the growth rate for CO₂ hydrates was that obtained from recent vapor phase studies. The above observations indicate these values may not be the most appropriate. Instead of growing in thickness as originally assumed, the hydrate layer on a droplet may remain relatively thin and serve to slow the dissolution rate of the CO₂ into the ocean.

The following illustrates the consequences of both scenarios on ocean disposal of CO₂. The original model predicted that a 1-cm droplet would need to be injected at 1900-m depth to insure effective sequestration if the hydrate shell thickness grew at a steady rate of 0.02 cm/h. In this case, the particle would begin to sink after rising to approximately 500 m owing to the thickening hydrate shell being denser than sea water. If instead of forming more hydrate, the particle dissolved at a rate of 0.09 cm/h, a 1-cm hydrate-coated droplet would still have to be injected at great depth. In this case, a depth of 1500 m would be required for the droplet to be completely dissolved by the time it reached 500 m. For the slower dissolution rate of 0.0045 cm/h, complete dissolution of the rising droplet would not be achieved before 500 m, even if injected at depths approaching those where liquid CO₂ becomes denser than

seawater (approximately 2700 m). If injected at depths greater than 2700 m, the CO₂ would sink regardless of hydrate formation. Injection depths greater than 1500 m are not practical at present [1]; thus understanding and controlling hydrate formation are paramount to successful sequestration of CO₂ in the ocean.

4. CONCLUSION

The observations made in the view cell and the recent observations of others have implications for the effective disposal of CO₂ in the ocean. Simply discharging the CO₂ at great depths may be insufficient if hydrate coatings form on liquid droplets of CO₂. Observations of single droplets indicate that the coating may impede the dissolution and permit the CO₂ droplet to rise to unacceptably shallow depths. Also, the possibility of growth of the hydrate shell cannot be ruled out based on observations of single droplets. In the vicinity of the injection device, the ocean will likely be near saturation owing to the enormous amounts of carbon dioxide being injected. If CO₂ cannot dissolve, then the growth of the hydrate coatings becomes more likely, especially as droplets collide and fresh CO₂ is released.

A better strategy than direct discharge would be to mix the CO₂ and water prior to reaching hydrate-forming depths and then introduce the mixture into some type of confined region that either permits pure hydrates to form under controlled conditions or fosters the growth of the hydrate coatings on CO₂ droplets. Density observations in the view cell indicate that pure hydrates formed in the first case would be negatively buoyant and sink. In the second case, if the hydrate coating contains more than approximately 30% of the CO₂ in the particle, the particle will also sink. Problems with plugging in the event of a flow interruption in such systems may be avoided by operating at slightly undersaturated conditions with respect to CO₂. Observations in the view cell indicate that these conditions favor the formation of a semi-solid mass rather than a solid hydrate plug.

ACKNOWLEDGMENT AND DISCLAIMER

The authors would like to thank Richard Hlasnik and Jerry Foster for performing the view cell experiments. Reference in this report to any specific product, process, or service is to facilitate understanding and does not imply its endorsement or favoring by the United States Department of Energy.

REFERENCES

1. DOE Report DOE/ER-30194, A Research Needs Assessment for the Capture, Utilization and Disposal of Carbon Dioxide from Fossil Fuel-Fired Power Plants, July 1993 (available NTIS).
2. R.P. Warzinski, C.-H. Lee, and G.D. Holder, *J. Supercrit. Fluids*, 5 (1992) 60.
3. A.T. Bozzo, H.-S. Chen, J.R. Kass, and A.J. Barduhn, *Desalination*, 16 (1975) 303.
4. G.D. Holder, A.V. Cugini, and R.P. Warzinski, *Environ. Sci. Tech.*, 29 (1995) 276.
5. C.H. Unruh and D.L. Katz, *Petroleum Transactions, AIME*, (April 1949) 83.
6. S.M. Masutani, C.M. Kinoshita, G.C. Nihous, T. Ho, and L.A. Vega, *Energy Convers. Manage.*, 34 (1993) 865.
7. R. Weibb and V.L. Gaddy, *J. Am. Chem. Soc.*, 60 (1940) 815.
8. Y. Shindo, T. Hakuta, Y. Fujioka, K. Takeuchi, and H. Komiyama, *Abstracts Second International Conference on Carbon Dioxide Removal, Kyoto, Japan (1994)*, 44.

Characterisation of Polycyclic Aromatic Compounds (PAC) in Coal Products and Related Materials by GC and Coupled LC-GC Techniques

Krystyna M. L. Holden, Alistair C. Lewis, Keith D. Bartle and Stuart C. Mitchell

School of Chemistry, University of Leeds, Leeds LS2 9JT, UK.

1. INTRODUCTION

With increasingly stringent legislation pertaining to the levels of polycyclic aromatic compounds (PAC) present in the environment, the nature and distribution of PAC arising from the direct utilisation of coal and petroleum-based feedstocks continues to be an area of considerable interest. Whilst many methods currently exist for the analysis of parent polycyclic aromatic hydrocarbons (PAH) such as benzo[a]pyrene, little is known about the fate and distribution of the many substituted PAC that occur in coal and coal-derived materials as a function of the process methodology. To facilitate the comprehensive characterisation of PAC in samples collected from a number of coal pyrolysis and fuel combustion regimes, the group at Leeds have employed multidimensional chromatographic techniques (LC-GC-AED and LC-GC-MS) to compliment information obtained from GC-AED and GC-MS analysis. The findings are discussed and comparisons drawn with data obtained from the analysis of PAC originating from different sources such as diesel, diesel engine particulates and urban air particulates.

2. EXPERIMENTAL

2.1. Samples

The range of samples investigated include: (1) chars, cyclone fines and tars from fluidised-bed pyrolysis; (2) cyclone fines from fluidised-bed combustion; (3) a selection of pyrolysis and hydrolysis tars; (4) diesel fuel and diesel engine particulate extracts; (5) urban air particulate extracts

Tar samples were extracted with *n*-pentane prior to analysis. PAC samples were obtained from char solids and fines by either soxhlet extraction with dichloromethane (DCM) or by supercritical extraction with toluene modifier (10%, 60 and 140°C, 400 atm). Diesel and urban air particulate extracts were obtained by SFE of quartz microfibre filters with toluene modifier (10%, 110°C, 400 atm) following a 24 hr sample collection period [1].

2.2. Analysis

All samples were analysed by GC-AED and GC-MS. GC-AED element-specific chromatograms for C, N, O and S were obtained using a Hewlett Packard 5921A Atomic Emission Detector coupled to a HP 5890 Series II Gas Chromatograph. A Carlo-Erba Mega Series 5300 HRGC coupled to a Finnigan Matt ion trap mass detector (ITD / MS) provided low resolution GC-MS analysis.

Normal phase LC-GC-AED was performed using an in-house built LC system [2]. Two different solvent gradient programs were employed using *n*-pentane : dichloromethane as the mobile phase to facilitate separation by virtue of chemical class or by molecular mass *eg.* ring size separation of PAH. Samples were transferred to GC via a ten-port pneumatically activated valve interface fitted with a 350 μ l loop. The LC stream was fed via a 20 cm length of deactivated silica capillary to the capillary column situated inside the HP 5890 Series II gas chromatograph. Normal phase LC-GC-MS analysis was performed by coupling a Carlo-Erba Dualchrom 3000 Series LC-GC instrument with a Finnigan Matt ion trap mass detector (ITD / MS). Instrument configuration and experimental procedures are provided elsewhere [1,3]. Separations were obtained using identical GC (25 m x 0.32 mm i.d., DBX-5, SGE, UK) and LC (100 mm x 2 mm i.d. column packed with 5 μ m 'Spherisorb' silica, Phase Separations, UK) columns in both GC and LC-GC systems respectively.

3. RESULTS AND DISCUSSION

Examples of the element-specific chromatograms (C, S, N, O) obtained by GC-AED are presented in Figure 1 from the analysis of a pentane extract of a fluidised-bed pyrolysis tar. GC-MS readily identifies the relatively high concentration parent PAH (e.g. 16 EPA priority compounds) by selective ion monitoring (Figure 1), however the comparatively low concentrations of substituted and heteroatomic PAC are often obscured and consequently difficult to identify unambiguously.

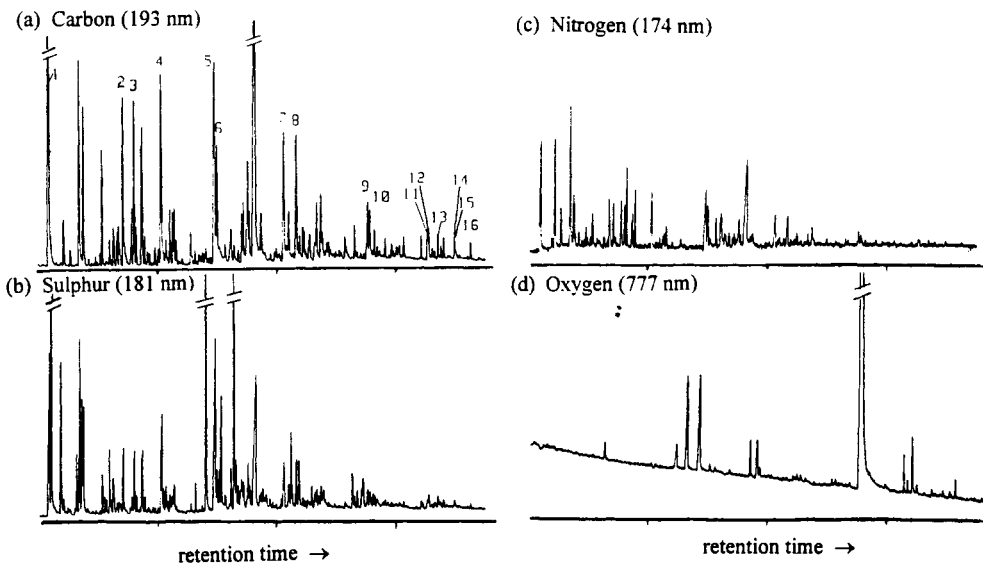


Figure 1. GC-AED chromatograms from the analysis of a pentane extract of a bituminous coal tar from fluidised-bed pyrolysis (Wieczorek, Poland). Parent PAH identified from carbon response (a) at 193 nm:
 1. Naphthalene; 2. Acenaphthene; 3. Acenaphthylene; 4. Fluorene;
 5. Phenanthrene; 6. Anthracene; 7. Fluoranthene; 8. Pyrene; 9. Benz(a)anthracene;
 10. Chrysene; 11. Benzo(b)fluoranthene; 12. Benzo(k)fluoranthene;
 13. Benzo(a)pyrene; 14. Indeno(1,2,3-c-d)pyrene; 15. Dibenzo(a,b)anthene;
 16. Benzo(g,h,i)perylene

The presence of such compounds in the above sample can be confirmed by GC-AED where the unique capabilities of multi-element detection is combined with a high selectivity over carbon [4,5]. However, positive identification of individual PAC remains difficult and time-consuming due to limitations in the number of model compounds available as reference materials and the problems associated with co-elution, polarity and the possibility of multi-element species. The addition of an LC separation stage in both the GC-AED and GC-MS techniques enables sample clean-up and fractionation by virtue of chemical class (group type separation) or molecular mass *eg.* ring size separation of PAH, prior to transfer to high-resolution GC analysis [1]. Figure 2a-c shows the UV spectrum and carbon and sulphur-selective AED chromatograms respectively from a sulphur-rich fraction following polarity separation of the pentane extract by LC.

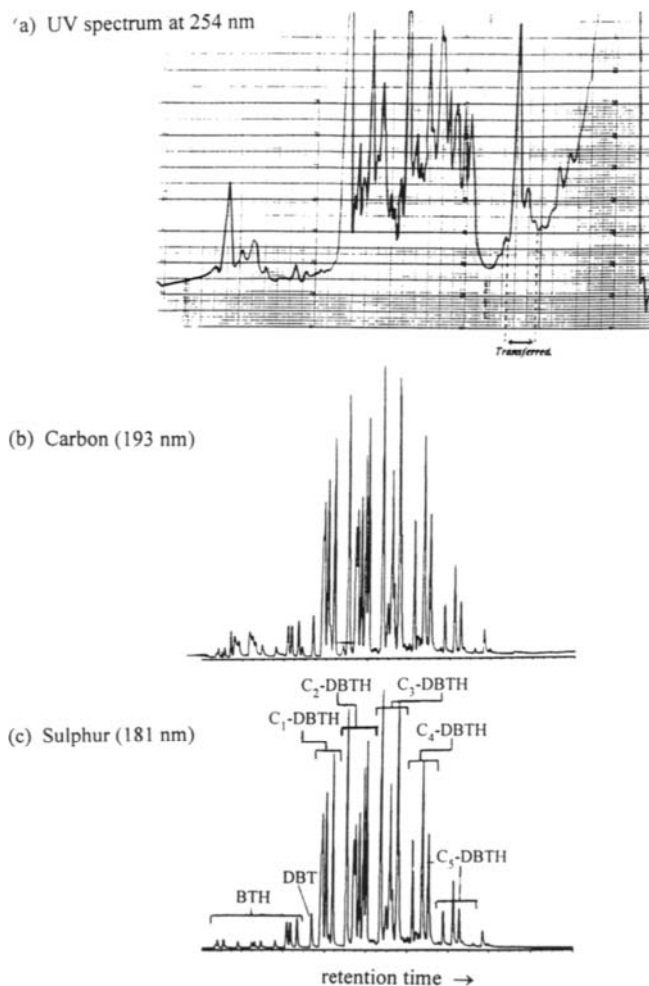


Figure 2. LC-GC-AED of pentane extract of bituminous coal from fluidised-bed pyrolysis
 BTH: Benzothiophenes C_x -DBTH: Substituted dibenzothiophenes

By comparison with Figure 1 (boxed region corresponds to the elution of same series of thiophenic compounds by GC-AED), speciation is clearly much simplified by elimination of the interference from co-eluting hydrocarbons and more polar species. Furthermore, in the case of LC-GC-AED, response is greatly enhanced due to increased sample concentration and the reduction in the formation of molecular species in the plasma, thus increasing the reliability of elemental formulation [6].

In this study, the distribution of parent and alkylated polycyclic aromatic hydrocarbons (PAH) and their nitrogen-, sulphur-, and oxygen-containing heterocyclic analogs (N-PAH, S-PAH, and O-PAH) have been determined to investigate their distribution as a function of source. Detailed quantification of individual PAC from different sources has confirmed the broad similarity between the distribution of PAC in fuel materials and those found in the environment through their direct utilisation.

4. CONCLUSIONS

To facilitate the positive identification of the range of PAC present in fuel materials, the use of multidimensional chromatographic techniques has proved essential to remove interference from co-eluting hydrocarbons. The combination of both elemental information from atomic emission detection with structural and molecular data from mass spectrometry represents a powerful analytical approach to PAC speciation.

5. ACKNOWLEDGEMENTS

We would like to thank Dr K. Kubica at the Institute for Chemical Processing of Coal, Zabre, Poland and Dr R. Garcia at the Instituto Nacional Del Carbon, Oviedo, Spain for supplying a selection of the samples investigated during the course of this study.

REFERENCES

1. Lewis, A.C., Robinson, R.E., Bartle, K.D. and Pilling, M.J., *In Press, Urban Atmos.*, 1994.
2. Kelly, G.W., Bartle, K.D., Clifford, A.A. and Robinson, R.E., *J. High Res. Chrom.*, 1992, **15**, 526-530.
3. Bartle, K.D., Holden, K.M.L., Mitchell, S.C., *16th Int. Symp. on Capillary Chrom.*, 1994, **2**, 1397-1402
4. Liu, Y., Lopez-Avila, V., Algaraz, M. and Beckert, W.F., *J. High Res. Chrom.*, 1993, **16**, 106-112.
5. Stan, H.J., and Linkerkagner, M., *J. High Res. Chrom.*, 1993, **16**, 539-548.
6. Wylie, P.L., Sullivan, J.J. and Quimby, B.D., *J. High Res. Chrom.*, 1990, **13**, 499-504.

POLARITIES AND RING SIZE DISTRIBUTIONS OF POLYCYCLIC AROMATIC COMPOUND EMISSIONS DURING SECONDARY PYROLYSIS WITH VARIOUS COALS

L. E. Yu,^a J. DaDamio,^a L. E. Hildemann,^a and Stephen Niksa^b

^aDepartment of Civil Engineering, Stanford University, Stanford, CA 94305

^bMolecular Physics Lab, SRI International, 333 Ravenswood, Menlo Park, CA 94025

INTRODUCTION

The polycyclic aromatic compounds (PAC) emitted during coal combustion are of special concern because they contain mutagenic and/or carcinogenic species. This paper reports a series of experiments that monitor the major polarity classes and ring number distributions of coal tars collected during a stage of simulated pulverized coal combustion conditions. Tar characteristics are reported for regulated secondary volatiles pyrolysis with a subbituminous and an hvA bituminous coal on 100 ms time scales at typical combustion temperatures.

EXPERIMENTAL

All tests were conducted in the radiant coal flow reactor described by Chen and Niksa [1]. This system entrains coal particles through a radiant furnace that consists of a quartz tube surrounded by an inductively heated graphite cylinder. Heat fluxes into the suspension are comparable to estimates for pulverized coal burners, and nominal particle heating rates can exceed 10^4 K/s. This furnace can be operated to keep temperatures of the entrainment gas cooler than the threshold for secondary hydrocarbon cracking, so that the primary products can be quenched as soon as they are expelled from particles [1]. However, in all cases reported here, furnace temperatures were hot enough to promote secondary volatiles pyrolysis in the available residence time.

All runs were made with an entrainment velocity of 18 cm/s at the inlet, for which the measured residence times range from 155 to 175 ms as furnace temperature is decreased from 1740 to 1480 K. In this study, furnace temperatures were increased in successive runs from 1390 to 1540 K to progressively increase the extent of secondary volatiles pyrolysis. Calculated thermal histories show that the nominal heating rate approaches 10^4 K/s and that the coal suspension never achieves the furnace temperature in the available residence time. As explained more fully elsewhere [2], the conversion of tar into soot during secondary pyrolysis is accompanied by release of CO, H₂, and HCN as well as conversion of all light hydrocarbons and oils into CH₄ and C₂H₂. Tar yields diminish throughout as the soot yields grow and, apparently, C₂H₂ adds to the soot so as to compensate for the release of CO, because the sum of the yields of tar, oils, and soot are invariant during secondary volatiles pyrolysis. In this operating mode, ultimate primary devolatilization yields are achieved at every furnace temperature (except 1 case, noted below), and only the extent of secondary pyrolysis varies. Under such circumstances, values of the soot fraction in the total aerosol product (of tar plus soot) signify the extents of secondary pyrolysis directly.

Consequently, all PAC characterization data will be plotted against the soot fractions that were measured for the various furnace operating conditions.

Gas yields are routinely monitored with the furnace, but only the aerosol products are of interest in this study. Products are segregated into bulk char samples, tar plus soot aerosol, and noncondensable gases with virtual impaction in an aerodynamic classifier. This device creates a virtual impaction surface between two nozzles at the inlet by diverting 95 % of the flow radially off the axis. Since the aerosol particules are only a few microns in size, they are convected into the annulus and ultimately onto 5 stages of glass filters. Pure tar samples for subsequent chemical analyses are prepared by extracting the glass filters with tetrahydrofuran (THF) in an ultrasonic bath, followed by filtration through a 0.2 μm Teflon membrane. The amount of soot is assigned as the membrane residue, and the tar yield is determined by difference against the initial filter weights.

Two analytical characteristics of our PAC samples will be reported, one related to polarity and the other to the ring number distributions. Gravity flow column chromatography was used to fractionate the PAC with solvents of progressively greater polarity, using a 2-stage column with a cyano-bonded packing in the fractionating stage. Solutions of a few milligrams of PAC in THF were first deposited onto a sorbent, then elutriated in several successive aliquots of C_7H_{16} , C_7H_8 , CH_2Cl_2 (DCM), CH_3OH (MeOH), and THF. Based largely on previous applications of similar fractionation schemes, we expect this technique to segregate the PAC sample into alkanes+phenyl alkanes+naphthalenes+unsaturates; 3-6 ring PAC+monosubstituted PAH; 7-10 ring PAH+some polar compounds; most polar PAC+hydro-PAH; and THF-solubles. Note that the 4 and 5-membered ring compounds, which have the greatest potential for health effects, reside in the toluene-fraction. Also, this fractionation scheme usually recovers more than 90 % of the whole tar sample in individual analyses.

After the polarity fractionation, the toluene fraction (only) is analyzed for ring number distribution with HPLC on a cyano column with MeOH as the preparation solvent and 98% C_7H_{16} /2%DCM as the mobile phase. Distributions were recorded with broad-band diode array detection at 220 to 340 nm. Based on the elutriation of mixtures of standard compounds, we verified that nonsubstituted PAH elute according to their numbers of fused (not total) rings with this method, and that non-polar PAC with up to 5 fused rings are reproducibly segregated from each other and from substituted polar PAC.

The ultimate analyses of the 2 coals used in this project are, for the Dietz subbituminous, 75.5 daf wt.% C, 5.2 %H, 17.9 %O, 0.9 %N, and 0.4 %S; and, for the Pit. #8 hvA bituminous coal: 83.3 daf wt. % C; 5.4 % H; 8.4 % O; 1.4 % N; and 1.3 % S.

RESULTS AND DISCUSSION

Figure 1 shows the polarity fractions of PAC from both coals throughout secondary pyrolysis. The data are presented as cumulative increments of the total tar sample at furnace conditions that impose the indicated extents of secondary pyrolysis. For the PAC from the subbituminous coal, only secondary pyrolysis behavior appears. However, the first point for the PAC from the Pit. #8 is for an intermediate extent of primary devolatilization. Since no soot was present, this sample appears on the ordinate. But primary devolatilization was not complete either at this operating condition, so the total PAC yield is only about one-third of the maximum at 26 % sooting. This artifact would be eliminated with the ultimate PAC sample from primary devolatilization, and PAC yields do indeed decrease monotonically throughout secondary pyrolysis, as seen with the subbituminous PAC data.

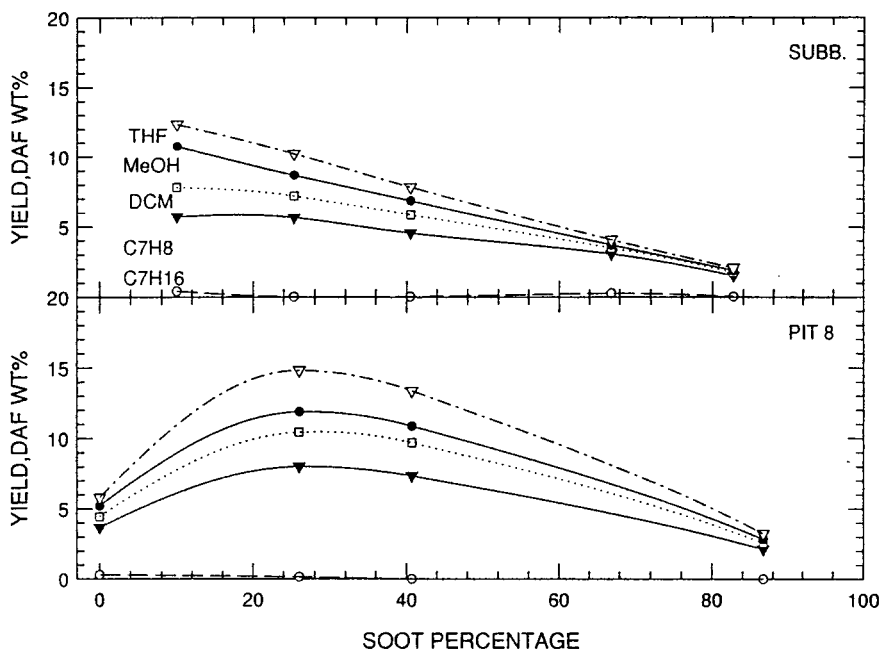


Figure 1. Polarity fractions in the indicated solvents from gravity flow column chromatography for PAC from the secondary pyrolysis of subbituminous (top) and Pit. #8 coal (bottom). The yields are cumulative on the basis of dry-ash-free coal. The soot percentage is the fraction of total aerosol that is insoluble in THF.

Polar compounds are transformed during the initial stages of secondary pyrolysis of the subbituminous volatiles, as seen in the way that the MeOH and DCM fractions diminish for soot percentages from 10 to 26 % while the toluene fraction grows. This tendency is consistent with the release of CO from tar molecules that shows up in our gaseous product distributions [2]. Also, the absence of substantial amounts of the heptane fraction through secondary pyrolysis is consistent with the conversion of lighter alkanes and olefins to C_2H_2 . It is also worth noting that none of the data indicate that smaller PAC are recombining into larger molecules. In fact, all the fractions decay monotonically for extents of sooting above 30 %. These same features are apparent in the data for the PAC from the Pit. #8, once the artifact from the smaller total yield at 0% sooting is accounted for. With this PAC all polarity fractions decay on the same time scale. Even though the PAC from the subbituminous coal are more polar than those from the Pit. #8 at the lowest extent of secondary pyrolysis, the polarity distributions become very similar throughout most of this process.

The ring number distributions for the toluene fractions appear in Fig. 2. These two distributions undergo dramatic changes at soot percentages of about 25%, but in opposite directions. With the subbituminous PAC, the total amount of material with 2 to 5 rings decreases as soot percentages increase from 10 to 25 %. Since the total amount of polar material is also diminishing (in Fig. 1), the polar compounds in the MeOH and DCM fractions are preferentially converted into less polar substituted PAC rather than

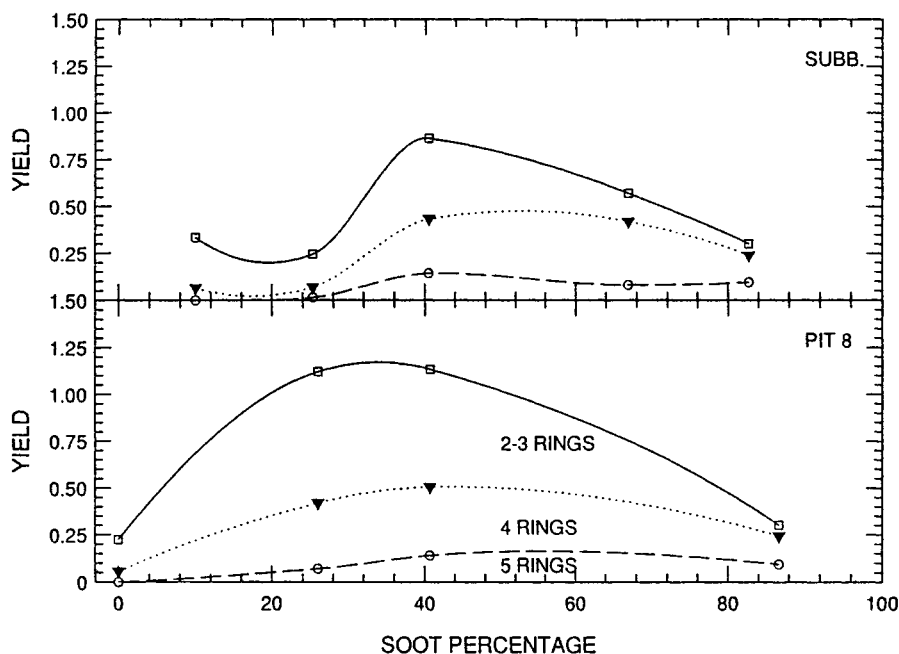


Figure 2. Ring number distributions of the toluene fractions in Fig. 1 determined with HPLC.

unsubstituted PAH with 2-5 rings. As the soot percentage is increased from 25 to 40%, the 2-5 ring fraction grows, even while the total amount of toluene solubles diminishes. So at this stage, substituted PAH is converted into unsubstituted PAH. At larger extents of secondary pyrolysis, the smallest PAH are rapidly eliminated, perhaps via ring destruction, consistent with the small growth in the heptane fraction in Fig. 1 for these conditions. PAH with 4 rings are also destroyed during the later stages of secondary pyrolysis with the subbituminous coal.

In contrast, with PAC from the Pit. #8, only the 5-ring compounds grow during the earliest stages of secondary pyrolysis. The smaller compounds persist through most of this process until they diminish during the latest stages, achieving a distribution that is virtually identical to that for the subbituminous-derived PAC.

References

1. J. C. Chen and S. Niksa, *Rev. Sci. Instrum.* 63(3) (1992) 2073.
2. J. C. Chen, C. Castagnoli and S. Niksa *Energy Fuels* 6 (1992) 264.

Effect of coal pyrolysis conditions on polycyclic aromatic hydrocarbons content in liquid products

K. Kubica, M. Czaplicka, T. Kordas

Institute for Chemical Processing of Coal
Zabrze, Poland

1. INTRODUCTION

Polynuclear Aromatic Hydrocarbons are the main components of tars from the high-temperature carbonization of coals. They are being also found in low-temperature tars, in flue gases from combustion of various fuels and in other industrial gases. Some PAHs are important raw materials in the chemical industry, but as a group they are commonly considered as contaminants, the opinion being formed on the basis of proved cancerogenicity of some of them. For this reason accurate determination of PAHs in the volatiles from thermal decomposition of coal and other organic materials is of great importance.

The typical procedure applied comprises the separation of PAHs subfraction by dividing the benzene soluble fraction of the sample on the $\text{SiO}_2/\text{Al}_2\text{O}_3$ column by subsequent elution with n-pentane (aliphatics), benzene (PAHs) and chloroform/methanol (polars). PAHs subfraction is then analyzed by cc-gc on the DB 5-625 column and some 20 compounds are determined quantitatively. It can therefore be concluded how process parameters affect PAH distribution in various coal pyrolysis volatiles.

2. EXPERIMENTS

The methodology of separating out the PAH sub-fraction from the total tars consist of:

- dissolving the tar sample in boiling benzene or toluene for 2 hours under reflux, filtering off insolubles, dewatering the filtrate with anhydrous sodium sulphate, and evaporating the solvent in a rotary vacuum evaporator, followed by final drying in a vacuum dryer;
- dividing the benzene - soluble fraction for subfractions by means of the adsorption - elution column chromatography; a 50 cm long, 5 mm i.d. column was used, filled with activated at 180°C for 24 h 70-230 mesh SiO_2 (upper part) and II active grade Al_2O_3 (Brookman), activated at 270°C for 24 h (lower part);

0,2 g of benzene soluble fraction was placed on the top of the column wetter with n-pentane, and eluted subsequently with n-pentane, n-pentane - benzene (95:5), benzene, and finally chloroform - methanol (1:1) to obtain aliphatics, mono-aromatics, PAHs, and polars, respectively; PAHs were isolated from the benzene solution by evaporating the solvent in

rotary vacuum evaporator and vacuum drying;

- determination of the defined compounds in the PAH sub-fraction by gas chromatography; a Fisons 8300 apparatus was used, supplied with a 30 m long, 0,32 mm wide capillary column DB 5-625 and FID detector; the splitless injection system was applied and the programmed

temperature increase (35°C for 4 min and then 8°C/min up to 300°C); two internal standards were in use: triphenylmethane for compounds eluting prior to pyrene, and 9,10-diphenylanthracene for higher molecular PAHs.

There were performed four pyrolysis tests of lignite coal:

- in reactor with fixed bed of 850°C, FB2
- in reactor with bubbling fluidized bed, BFB
- in reactor with circulating fluidized bed, CFB.
- in reactor with fixed bed of 650°C, FB1

There were performed two laboratory tests pyrolysis of bituminous coal:

- in reactor with bubbling fluidized bed, BFB
- in reactor with circulating fluidized bed, CFB
- in reactor with fixed bed of 850°C, FB2.

The scope of the work includes also determination of PAHs in coke-oven tars from different plants.

3. CONCLUSIONS

It is observed that PAHs concentration in various-coke oven tars differs depending on the process severity (heating walls average temperature, underroof free space etc.) and, generally speaking, the battery's technical state. The highest concentration of benzo(a)pyrene and other 5-ring PAHs are observed in the coke-oven tar from the oldest battery.

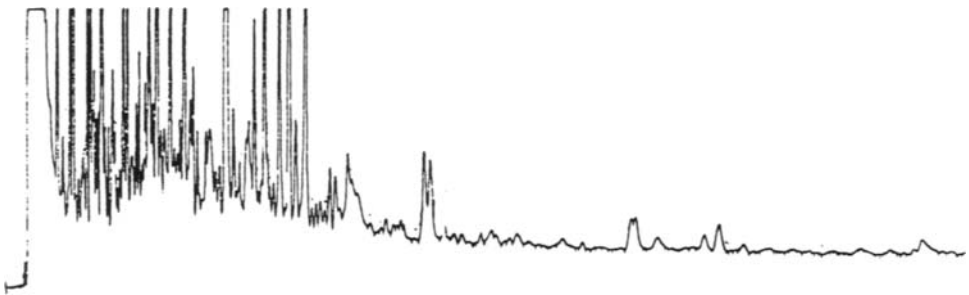


Fig.1 The chromatogram of PAHs

Comparing PAHs concentration in tars from different processes leads to the conclusion that the higher pyrolysis temperature and longer vapour residence time the higher levels of PAHs in the produced tars. The highest levels of PAHs are observed in coke-oven tars, which vapours are exposed to a prolonged contact with hot heating walls of the coking chamber.

Table 1

Contents of PAHs in bituminous coal tars from different process (wt. %)

	BFB	CFB	FB2
1. Phenantrene	0,22	2,64	5,05
2. Anthracene	0,11	1,47	1,78
3. Carbazole	0,18	1,96	1,25
4. 2-Methylanthracene	0,09	0,48	0,45
5. 9-Methylanthracene	0,10	0,26	0,30
6. 4,5-Dimethylphenanthrene	0,13	0,53	1,15
7. Fluoranthene	0,16	1,48	2,80
8. Pyrene	0,17	1,34	2,00
9. Benzo(a)fluorene	0,09	0,40	0,35
10. Benzo(b)fluorene	0,09	0,69	0,81
11. Benzo(a)anthracene	0,11	0,81	1,93
12. Chryzene	0,09	1,04	1,88
13. Benzo(b+k)fluoranthene	0,12	0,23	0,85
14. Dibenzo(a,c)anthracene	0,07	0,21	0,41
15. Benzo(e)pyrene	0,07	0,18	1,32
16. Benzo(a)pyrene	0,05	0,57	1,01
17. Perylene	0,05	0,92	0,38
18. Dibenzo(a,h)anthracene	0,05	0,23	0,25
19. Indeno(1,2,3-cd)pyrene	<0,01	0,11	0,22
20. Benzo(g,h,i)perylene	<0,01	0,08	0,31
TOTAL	1,954	15,63	24,50

Low - temperature (560 °C) fluidised bed pyrolysis of coal, characterised by a very short vapour residence time, gives tars with the lowest concentration of PAHs.

Exposing low temperature tars to more severe cracking conditions, e.g. by contacting their vapours with hot char, leads to a significant increase in PAHs concentration, shifting the tars composition towards higher aromaticity.

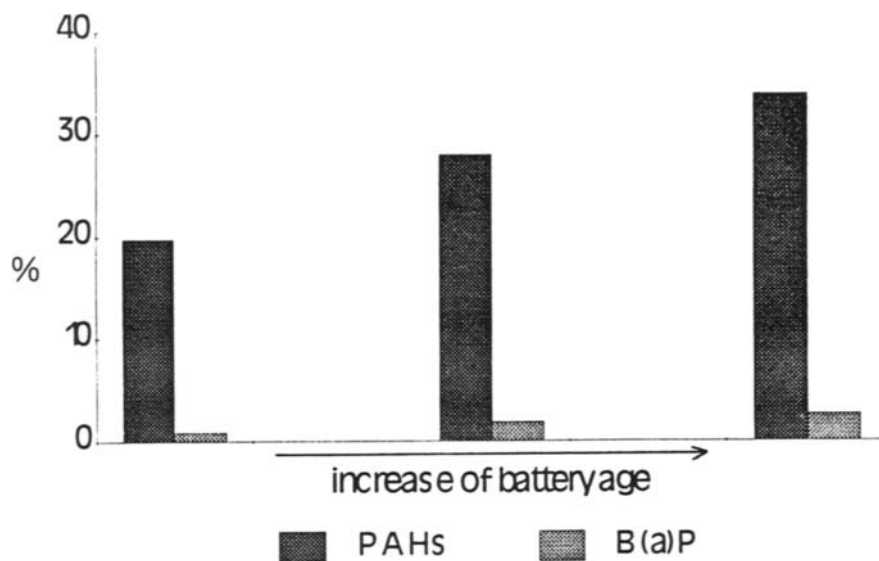


Fig.2 PAHs and Benzo(a)pyrene coke-oven tars contents

References

1. Bartle K.D. et al., *Anal. Chem.*, 51, 1613, 1981
2. Hirsh D.E. et al., *Anal. Chem.*, 44, 95, 1972
3. Kubica K., Czaplicka M., Kordas T., 20th. International Symposium on Chromatograph Bournemouth, UK, 1994
4. K.Kubica, T.Kordas, M.Czaplicka, *Karbo Energochemia Ekologia*, in press.

Distribution of PAH generated in fluidized bed combustion and pyrolysis experiments

Antonio M. Tobías^a, Roberto García^a, K.M.L. Holden^b, Stuart C. Mitchell^b, José J. Pis^a, Carole McRae^c, Colin E. Snape^c and Sabino R. Moinelo^a

^aInstituto Nacional del Carbón, CSIC, Apartado 73, 33080 Oviedo, Spain

^bSchool of Chemistry, University of Leeds, Leeds, LS2 9JT, UK

^cUniversity of Strathclyde, Department of Pure and Applied Chemistry, Thomas Graham Building, 295 Cathedral Street, Glasgow G1 1XL, United Kingdom

1. INTRODUCTION

Polycyclic aromatic hydrocarbons (PAH) are ubiquitous environmental pollutants principally derived from fossil fuel materials [1]. Formed by the incomplete combustion of organic material, their individual carcinogenic and mutagenic activities are critically dependent on structure [2]. Previous studies [3-5] have established links between PAH extracted from water, soil and air particulate samples with individual processing utilities. Similarly, PAH source fingerprints have recently been published for coke ovens, diesel and gasoline engines and wood combustion emissions [6]. For pulverised coal combustion, PAH emissions are minimal, however significantly higher concentrations have been reported from fluidised-bed combustion (FBC). The distribution and relative abundance of PAH arising from FBC, found in the residual organic matter, particulates (soot) or as trapped volatiles in the gas stream, are a function of operating temperature and process conditions [7]. In this initial study, the 16 EPA priority PAH have been quantified following extraction of samples recovered from FBC tests on a Spanish lignite (Aragon) at various combustion temperatures and air/fuel ratios in a pilot plant scale FBC unit. A selection of the results are detailed and discussed with regard to the sampling, extraction and analysis procedures. In addition, fundamental information on the generation of PAHs during devolatilisation obtained using a laboratory-scale fluidised-bed reactor is summarised.

2. EXPERIMENTAL

Combustion tests were carried out in a pilot plant FBC unit, using a lignite (23.8%, dry basis ash; 37.6%, dry basis VM; 6.1%, daf basis S) from Aragón (Spain) at two different temperatures (750 and 900°C), with 20 and 30% air excess above the stoichiometric. Samples for PAH determination were recovered from both cyclones, the filter bag and the combustion gas exit. Sampling at the gas exit was performed using a PTFE filter (47 mm diameter), with

Table 1
Combustion conditions and carbon matter contents (CM) of unburned material

T(°C)	Air excess (%)	Sample	CM* (g/Kg coal)
750	20	Cyclone 1	2210
		Cyclone 2	30
		Filter bag	90
750	30	Cyclone 1	2050
		Cyclone 2	40
		Filter bag	80
850	20	Cyclone 1	1980
		Cyclone 2	20
		Filter bag	60
850	30	Cyclone 1	740
		Cyclone 2	10
		Filter bag	40
900	30	Cyclone 1	660
		Cyclone 2	30
		Filter bag	60

*Carbon matter: (100-ash) x (material yield).

injected per analysis, with 2-ethylanthracene used as an internal standard. Identical GC conditions were employed for both GC techniques.

PAH distributions from a laboratory-scale fluidised-bed reactor over the temperature range 700-900°C have been determined.

3. RESULTS AND DISCUSSION

Fluidized bed combustion

The combustion conditions together with the amount of carbon matter (material burned during ash content determination) recovered in the cyclones and the filter bag are shown in Table 1. As expected, increases in air excess and temperature facilitates a better combustion and, consequently, results in a lower amount of unburned material.

PAH solutions recovered by Soxhlet extraction and concentrated using Kuderna-Danish apparatus (as recommended by EPA [8]) from the unburned material (cyclones and filter bag), the PTFE filters and the adsorption unit, were analysed by GC. The concentrations of the PAHs recovered, grouped by number of rings, are shown in Table 2 (2 ring: naphthalene; 3 rings: acenaphthylene, acenaphthene, fluorene, phenanthrene, anthracene; 4 rings: fluoranthene, pyrene, benz[a]anthracene, chrysene; 5 rings: benzo[b]fluoranthene, benzo[k]fluoranthene, benzo[a]pyrene, dibenz[a,h]anthracene). Single compound data did not demonstrate any influence of experimental conditions. Not surprisingly, PAHs recovered from cyclone 1 reached the highest concentrations under all combustion conditions. However, it is worth noting that a significant amount of PAHs were adsorbed by the XAD-2 resin in the sampling system tested. Such high concentration, higher than that of cyclone 2 and the filter bag would otherwise be emitted into the atmosphere.

0.45 µm nom. pore size and an adsorption unit containing amberlite XAD-2 resin and polyurethane foam (PUF). PAHs were recovered by Soxhlet extraction with dichloromethane and concentrated using a Kuderna-Danish apparatus [8]. For comparison, supercritical fluid extraction (SFE) with toluene as modifier (400 atm, 140°C) was performed on the recovered cyclone materials. Dichloromethane was used as trapping solvent and later removed under a nitrogen flow. GC-FID analysis was performed on a Perkin-Elmer 8500 gas chromatograph fitted with an SGE OCI-3 on-column injector. GC-AED analysis was performed in a splitless mode using a Hewlett Packard 5921A Atomic Emission Detector coupled to an HP 5890 Series II gas chromatograph. SGE BPX-5 columns (25 m x 0.32 mm i.d.) were used in both cases with 1 m of fused silica precolumn. 2 µl of sample (dissolved in toluene) was

Table 2
Concentration (in $\mu\text{g}/\text{Kg}$ of coal) of PAHs recovered by Soxhlet extraction and grouped by number of rings, at the different sampling points

Cyclone 1			
No. of rings	750-20*	750-30*	900-30*
2		46.6	38.9
3	89.8	449.2	221.3
4	44.9	153.8	162.3
5	90.9	119.1	181.7
Total	225.6	768.7	604.2
Cyclone 2			
No. of rings	750-20*	750-30*	900-30*
2	0.7	2.9	1.2
3	6.5	82.6	2.6
4	2.4	5.1	2.6
5	1.1	5.3	
Total	10.7	95.9	6.4
Filter bag			
No. of rings	750-20*	750-30*	900-30*
2	6.0	11.1	7.9
3	22.6	22.5	20.2
4	21.7	9.7	21.8
5	13.5	17.9	20.9
Total	63.8	61.2	70.8
XAD-2			
No. of rings	750-20*	750-30*	900-30*
2	9.9	39.5	7.9
3	36.3	59.9	19.0
4	16.7	23.8	20.9
5	8.7	24.2	14.8
Total	71.6	147.4	62.6

*Temperature-air excess (e.g., 750-20 = FBC run at 750°C and 20% of air excess)

recoveries are higher in SFE, due to the higher concentrations found for five-ring PAH, suggesting a slightly better extraction efficiency under the SFE conditions employed.

The Kuderna-Danish apparatus, which is claimed to promote losses of low molecular weight compounds [9], was used for concentration only after Soxhlet extraction. However, three-ring PAHs recoveries are higher when SFE is used, the implication being that Soxhlet extraction has a greater selectivity towards lower molecular weight PAHs.

Fluidized bed pyrolysis

The aromatic fractions of tars obtained in pyrolysis experiments at 700 and 900°C were analysed by HPLC. From the chromatograms it is possible to estimate the proportions of PAHs present based on the number of rings (Table 4). Initial results indicate that increasingly

In general, the total amount of PAH increases with decreasing temperature, with the exception of material recovered in the filter bag. Differences are more marked when lower molecular weight compounds (2-3 rings) are considered. Higher molecular weight compounds do not follow the trend in all cases and, for example, their concentrations are higher at 900°C at both cyclone 1 and the filter bag (Table 2), suggesting that a condensation effect may play a significant role at higher combustion temperatures. On the other hand, the better combustion efficiency achieved with a higher air excess is not reflected in the concentration of PAHs, which is higher for all the sampling points when a 30% of air excess is used.

The recovery of PAHs adsorbed in the cyclone 1 material was also performed by SFE, in order to compare the effect of the extraction procedure. The concentrations of the PAHs recovered are listed in Table 3. In SFE extracts, naphthalene and acenaphthylene are not considered as they could not be distinguished from the solvent peak in GC analysis. For simplicity, Soxhlet recoveries, excluding the lower molecular weight PAHs, are also shown in Table 3. According to Soxhlet extraction data, SFE recoveries show that a higher combustion temperature reduces the amount of PAHs detected. Total

Table 3
Concentration (in $\mu\text{g}/\text{Kg}$ of coal) of PAHs recovered from the cyclone 1 material by SFE and grouped by number of rings

750-30		
No. of rings	Soxhlet	SFE
3*	401.9	189.0
4	153.8	203.1
5	119.1	366.1
Total	674.8	758.2
900-30		
No. of rings	Soxhlet	SFE
3*	174.4	161.4
4	162.3	138.3
5	181.7	277.1
Total	518.4	576.8

*Excluding acenaphthylene

Table 4
Composition of the aromatic fractions of the fluidised bed pyrolysis tars

No. of rings	Temperature ($^{\circ}\text{C}$)	
	700	900
1	31.8	13.1
2	48.1	20.9
3	11.2	12.3
4	2.8	20.6
≥ 5	5.1	33.1

respectively, for funding their research at the Instituto Nacional del Carbón.

REFERENCES

- M.L. Lee, K.D. Bartle and M. Novotny, in "Analytical Chemistry of Polycyclic Aromatic Compounds", Academic Press, New York (1981).
- A. Dipple, R.C. Moschel and C.A. Bigger, in "Chemical Carcinogens" (C.E. Searle, Ed.), ACS Monograph 182, ACS, Washington, Vol. 1, p. 71 (1984).
- D.W. Later, T.G. Andros and M.L. Lee, *Anal. Chem.*, 55 (1983) 2126.
- M.L. Lee, G.P. Prado, J.B. Howard and R.A. Hites, *Biomedical Mass Spectrometry*, 4 (1977), 182.
- S.G. Hawthorne and D.J. Miller, *Anal. Chem.*, 66 (1994), 4005.
- N.R. Khabili, P.A. Scheff and T.L. Holsen, *Atmospheric Environment*, 29 (1993), 533.
- L.L. Blass and I.M. Smith, IEA Coal Research, London. Report No. IEA CR/63 (1993).
- EPA Method 610, Federal Register, October 26, 1984, Vol. 49, No. 209.
- V. Ferreira, P. Fernández, J. Meléndez and J. Cacho, *J. Chrom. A*, 695 (1995) 41.

severe pyrolysis conditions promote the thermal decomposition and condensation of smaller PAHs resulting in a higher proportion of the more condensed compounds.

4. CONCLUSIONS

FBC conditions markedly affect the amount of PAHs produced and emitted into the atmosphere. Maximum PAH concentrations occur at low temperatures, when combustion is less efficient, and at high air excesses. In the PAH recovery from the materials of the different sampling points, SFE provides a more reliable method for high molecular weight compounds than Soxhlet extraction. However, sample preparation following extraction indicates that losses of the lower size PAHs are common. Similar observations were made under fluidised bed pyrolysis conditions, where condensation reactions predominate at higher temperatures.

AKNOWLEDGEMENTS

The authors thank the Commission of the European Communities (DG XII-G) for financial support (research project No. 7220/EC-26). A.T. and R.G. acknowledge the Asturian Foundation for Scientific and Technological Research (FICYT) and the Spanish Ministry of Education and Science (MEC),

Polycyclic Aromatic Hydrocarbons from Coal Fluidised Bed Combustion

Mastral A.M., Callén M.S., Mayoral M.C., Juan R. and Galbán J.*

Instituto de Carboquímica, CSIC, Apdo 589, 50080 Zaragoza, Spain.

** Dpto Analytical Chem., Universidad de Zaragoza, Zaragoza, Spain.*

1. ABSTRACT

The most volatile organic compounds, remaining at the flow stream from the two cyclons placed at the exit of a coal fluidised bed combustor (200 g/h) and compiled at the US-EPA list as the Polycyclic Aromatic Hydrocarbons (PAH) priority pollutants are studied in this paper. This air flow has been forced to go throughout different trapping systems and the PAH deposited on filters and adsorbents, after being solubilised in dimethylformamide (DMF), have been analysed by synchronous fluorescence spectroscopy (FS). Results are analysed and commented.

2. INTRODUCTION

When coal undergoes to a thermic process, pyrolysis, very important physical and chemical changes (contraction-swelling, devolatilization, decarboxylation, changing in the fluidity and plasticity...) are caused and part of its organic matter is released to the atmosphere. In addition, as consequence of the thermic process and by cyclation reactions, other aromatic clusters can be developed (1). Both aromatic hydrocarbons, the inherent and the formed during the process, are one of the main atmospheric pollutants (2). Indeed, while the first ones are inevitable, the second ones could be reduced if the thermic process were carried out under control.

The release of polycyclic aromatic compounds to the atmosphere affects everybody because most of the compounds are volatile and known carcinogens and/or mutagens. During their migration through the air, these are transformed by interaction with oxidants and sunlight into products, which are sometimes much more mutagenic than the original compounds.(3)

Depending on the molecular mass, the PAH molecules can exist in gas phase (< 6 rings PAH), in solid phase (> 6 rings PAH) or in both phases (4 and 5 rings) in the environment air. So, the distribution is displaced in favour of the particulate phase at coolest temperatures while it is displaced to the gas phase in summer. PAH which have an strong electrophylic character, interact favoured by metabolic processes with biologic nucleophyles, obstructing their regular functions and causing the carcinogenesis. This has been explained by the PAH transformation into the organism towards diolepoxids of benzenic ring.

In this work, the PAH existing in the particulate matter of smallest size and not precipitated into the cyclons are studied by trapping them in a serie of filters with decreasing pore diammeter and at the end, different adsorbents products.

As reference point and for comparison (4-6), the PAH analyses from the air of the surrounding of the combustor emplacement have been analysed when the combustor did not work. From the obtained results, it can be deduced the main role of the environmental factors like temperature, contamination, season of the year, etc and by subtraction it can be known the coal FBC contribution.

3. EXPERIMENTAL

The analyses of the Samca coal (North-East Spain) used in this work are: %C (daf), 38.11; %H (daf), 3.97; % S, 7.77; % moisture (ar), 15.5; % ashes (ar), 18.8. The coal has been sieved in several fractions of particulate diameter and the experiences have been made with the fraction 0.5-1 mm.

The combustion experiments have been carried out in a laboratory scale plant of fluidized bed combustion (200 g/h). The continued feed of reactor is carried out by a vibration system up to 380 rpm. The combustion temperature has been 850°C, working with 20% exceed oxygen and with limestone. The flow has been twice the minimum fluidized velocity. The sampling and analyses of PAH have been showed elsewhere (7).

4. RESULTS AND DISCUSSION

In order to be rigorous and to get a good repetivity, the first goal was to stablish the PAH trapping system. Due to the volatility of most of the PAH, it could be speculate that not all of them are captured when only physical trappings are used to retain these hazardous pollutants. With this aim, the stream from a couple of cyclons placed at the exit of a fluidised bed combustor was forced to go throughout a serie of filters with decreasing pore size and then through different adsorbents. For this, after testing several options, the trapping system was optimized. It consists on a nylon filter (20 microns, after testing filters of 10 and 30 microns), then a teflon filter (0.5 microns and 5 cm diameter) and finally, an adsorbent with the aim of trapping the most volatile compounds which could have not been retained by the filters. The filters by themselves are not enough to retain the most volatile PAH, therefore there is the necessity of adding an adsorbent to the sucessive system of nylon and teflon filters. The set up of the trapping system and the procedure to recover the PAH trapped were deeply analysed and results have been described elsewhere (7).

All cuantification analyses have been made by synchronic fluorescence spectroscopy. For this, it has been necessary to look for every compound the fluorescence optimal conditions keeping up the possible interferences of other PAH compounds by using model compounds. Previous works (8) and as result of different experiences, Table 1 shows the specific conditions and dinamic range to detect each PAH by fluorescence spectroscopy (FS).

By applying these optimal conditions, the corresponding compounds: Fluorene, Benzo(a)pyrene (BaP), Benzo(k)fluoranthene (BkF), Anthracene, Acenaphthene and Pyrene have been identified by synchronic fluorescence spectroscopy in the stream from the Samca coal fluidised bed combustion. The nylon and teflon filter contents as well as the adsortion in the XAD-2 resin have been analysed according to the described procedure and Table 2 shows the results obtained. It can be deduced that the PAH distribution in both filters and in the resin does not follow a regular behaviour. It does neither seem to be influenced by the filter pore size nor by molecular volume of the aromatic hydrocarbon.

Table 1. Specific conditions and dynamic range to identify each PAH by synchronous FS.

Compound	Excitation (nm)	Emission (nm)	Spectrum	Lower limit (mg/l)	Upper limit (mg/l)
Acenaphthene	322	327	$\Delta\lambda=5$ nm	0.01	2.5
Anthracene	379	384	$\Delta\lambda=5$ nm	0.01	5.3
Coronene	309	447	$\Delta E=10000$ cm^{-1}	0.030	0.5
Chrysene	323	363	$\Delta\lambda=40$ nm	0.030	5
Benz(a)anthracene	292	387	$\Delta\lambda=95$ nm	0.00024	2
Benzo(a)pyrene	390	405	$\Delta\lambda=15$ nm	0.00038	5
Dibenz(a,h)anthracene	301	396	$\Delta\lambda=95$ nm	0.00031	0.5
Fluoranthene	360	500	$\lambda_{\text{exc}}=360$ nm	0.01	5
Fluorene	301	396	$\Delta\lambda=5$ nm	0.001	2
Pyrene	338	500	$\Delta\lambda=35$ nm	0.00097	0.5
Perylene	438	306	$\Delta E=800$ cm^{-1}	0.00872	0.2
Benz(g,h,i)perylene	303	373	---	0.0821	1
Benzo(b)fluoranthene	301	443	---	0.269	5
Benzo(k)fluoranthene	308	407	$\Delta\lambda=15$ nm	0.00321	0.1
Indenopyrene	304	448	---	0.126	1

Table 2. Amounts of the PAH detected by FS in the emissions from Samca coal FBC and trapped successively by Nylon filter (20 microns), Teflon filter (0.5 microns) and finally XAD-2.

PAH	NYLON 20 microns		TEFLON 0.5 microns		XAD-2 RESIN	
	ng/kg	ng/m3	ng/kg	ng/m3	ng/kg	ng/m3
Fluorene	27.952	26.508	49.285	46.738	31.019	29.416
BaP	6.75	6.4	1.795	1.703	50.714	48.093
BkF	129.742	123.107	66.468	63.034	157.224	149.099
Anthracene	21.285	20.186	57.336	54.375	26.849	25.462
Acenaphthene	218.035	206.769	69.785	66.179	67.046	63.923
Pyrene	traces	traces	traces	traces	83.458	79.571

As important as the pore size filter seems to be the cake of the particulate matter retained by the filter which could modify the efficacy of the filter pore size.

Molecular volume, molecular mass and pore size are not discriminative characteristics to separate or fractionate each PAH in these mixtures as consequence of an enormous complexity.

Concerning to the analytical technique used, the synchronic fluorescence has advantages because it is a fast technique, non-destructive which allows the analysis of various unfractionated samples, simplifying the individual spectrum and decreasing spectral interferences of several compounds in complex samples. With this analytical technique it is possible the semiquantification of the aromatic hydrocarbons.

For a more rigorous quantification, the chromatography provided with masas and flame ionization detectors is very useful. In this case, the capillary gas chromatography provided with FID detector has been used as complementary technique.

Another factor worth to point out is that all compounds which have the same structural configuration show the same parent peak in the fluorescence spectrum but slightly displaced some nanometers depending on the substituents (9).

In this way, although the samples were very complex, like the ones from coal combustion studied in this paper, their analyses are reduced to more simple spectra which decrease the difficulty of their determination.

The conclusions of this work could be the enormous complexity of the volatile organic compounds emitted during coal combustion and the necessity of further work because now, we know that the coal structure influences on the nature and amount of the PAH emissions (7) but, we do not still know how this influence is. In addition, the particulate matter with larger size and trapped in the cyclons is now calculated and analysed (10) in order to know the total amount of PAH formed. In this way, it could be found any relation between the composition and percentages of PAH emitted and the characteristics of the burned coal.

5. ACKNOWLEDGEMENTS

The authors would like to thank CICYT (Project Amb-92-0266) and ECSC (Project 7220/EC/026) the financial support of this work.

REFERENCES

1. Mastral A.M., Final Report CSIC to CSEC, Contract 7220/EC/755, June 1993.
2. US-EPA. List of the sixteen priority pollutants.
3. Tuan Vo-Dinh, Chemical Analysis of Polycyclic Compounds, Vol. 101 in Chemical Analysis, Winefordner J.D., Editor, Kolthoff I.M., Editor Emeritus.
4. Bodzek D., Luks-Betlej K., Warzecha L., Atmospheric Environ, Vol. 27A, N°5, 759-764, 1993
5. Tang You- Zhi, Tran Quang, Fellin P., Anal. Chem. 1993, 65, 1932-1935.
6. Leach J.M., Chung L.T.K., Anal. Chem. 1987, 59, 1701-1705.
7. 2nd Progress Report CSIC to ECSC, Ref. 7220/EC/026, July-December 1994.
8. Galbán J., Mastral A.M., Pardos C. y Rubio B., Mycroanalytical Letters, in press.
9. Mastral A.M., Afinidad 1989, Vol. XLVI, 422, 289-294.
10. Mastral A.M., Callén M.S., Mayoral C. and Galbán J., work in progress.

Stabilization/solidification of industrial inorganic wastes using coal flyashes from desulphurisation processes

J. Vale, C.F. Pereira, M. Rodríguez-Piñero, C. Ruiz de Elvira, J. Olivares and L. Salvador.

Dpto. Ingeniería Química y Ambiental, E.S. Ingenieros Industriales, Universidad de Sevilla, E-41012, Sevilla, Spain.

Keywords: Stabilization/Solidification, Fly ash, Industrial wastes, Desulphurisation

1. INTRODUCTION

Flue-gas desulphurisation processes are giving origin to a new type of combustion residues whose management and disposal poses different problems to those of flyashes that are being produced up today in combustion systems [1].

With the aim of finding new applications for flyashes, the Department of Chemical and Environmental Engineering of the University of Seville, in collaboration with Sevillana de Electricidad has developed, at laboratory and pilot plant scale, a waste stabilization/solidification (S/S) process (IRIS Project, financed by ECSC) [2], using flyashes as major component, by replacing other materials traditionally used (cement or metallurgical slag). The scientific and technological basis for a new S/S process have been established and the treatment objectives have been accomplished with lower costs than those of other S/S processes.

Results obtained with the IRIS process in the S/S of many hazardous wastes containing heavy metals using flyashes and other residues from pilot plant desulphurisation processes as cementing agents, are exposed in this work. Promising results have been obtained with desulphurisation residues, because of these materials have some properties that can make their application to S/S processes even more interesting than conventional flyashes.

2. MATERIALS AND METHODS

The stabilization agents used in the experiences are included in Table 1 and correspond to three different types: type-F flyashes, coming from a power station burning low sulphur coal (FA), desulphurisation residues obtained in a pilot spray dryer [3] in which combustion flue-gases are treated with lime before particle removal (S1 and S2), and, finally, flyashes from another pilot plant of fluidised bed combustion with limestone furnace injection (FI). The two types of desulphurisation residues have a relatively important free lime content, and S1 and S2, moreover, substantial quantities of sulphites.

The industrial wastes to be treated, arc furnace dust from iron production, basic sludges and acidic liquid wastes from metal decoating and iron works industries, have heavy metal

contents (Table 2) that confer them the character of hazardous and toxic, according to Spanish regulations. Two of these wastes are solid (s-WA and s-WB) and the other liquid (l-W).

Table 1
Chemical composition (major species) of flyashes (% w/w, dry basis)

Ash		SiO ₂	Fe ₂ O ₃	Al ₂ O ₃	CaO	SO ₄ ⁻	SO ₃ ⁻	Free lime*
Coal flyash	(FA)	50,0	8,8	20,8	4,0	-	-	-
Furnace injection	(FI)	40,0	9,4	10,1	38,7	5,1	-	11
Spray dry	(S1)	47,7	4,0	21,6	15,4	1,9	13,1	3
Spray dry	(S2)	28,6	1,6	14,3	24,6	1,8	20,0	14

* Expressed as CaO

Table 2
Toxic metal content in wastes

Waste		As	Cd	Cr	Cu	Ni	Pb	Zn
s-WA	% w/w	0,29	0,08	0,95	-	0,20	1,30	26,0
s-WB	% w/w	0,23	0,06	7,10	-	2,08	0,47	3,1
l-W	mg/l	6,8	-	1687,0	4,0	-	0,5	7,0

The S/S treatment objective is to obtain solids reducing the overall environmental impact of the wastes disposal. Quantified quality objectives, adapted from the Spanish and EPA regulations, which are resumed in Table 3, have been established in order to attain a determined physical properties (setting time and compressive strength), chemical properties (pH, toxic metal content in the leachate obtained by the TCLP [4] method,) and ecotoxicity (leachate effects to *Daphnia Magna*).

Table 3
Quality criteria for s/s solids

PHYSICAL PROPERTIES	• Setting time:	5-72 h						
	• Compressive strength:	≥ 0,35 MPa						
CHEMICAL PROPERTIES	• pH:	2-12,5						
	• Metals in TCLP leachate (mg/l):	As	Cd	Cr	Cu	Ni	Pb	Zn
		5	1	5	0,5	5,5	5	3,5
ECOTOXICITY	• Ecotoxicity to <i>Daphnia Magna</i> :	CE 50 ≤ 750 mg/l						

Different mixtures have been formulated and tested, following the optimization

methodology developed in the IRIS Project [5]. In addition to combustion wastes, other more conventional "reactants" have been used, like ordinary Portland cement (PC) or lime, in some cases with the aim of comparing the obtained results.

Table 4 includes some of the tested formulations. Most of the samples have been obtained by mixing the S/S agent and the waste with water, in order to obtain a paste with an adequate consistency, including other additives if necessary. To meet the quality objective of Cr level in the TCLP leachate, the s-WB residue requires a pretreatment with FeSO_4 in an aqueous acid medium, to reduce the hexavalent chromium.

Table 4.
Properties of some selected S/S solids

S/S solid composition ⁽¹⁾				S/S solid properties at 28 days								
Waste	S/S agent	Lime	σ_c ⁽²⁾	TCLP leachate (mg/l)								
				kg	kg	MPa	pH	As ⁽³⁾	Cd	Cr	Cu	Ni
s-WA	FA	1,3	0,25	1,69	10,4	ND	ND	1,0	-	0,2	0,9	0,2
s-WA	FI	1,0	-	5,61	11,8	0,5	ND	4,8	-	0,3	1,6	1,8
s-WA	PC	0,5	-	2,00	12,3	ND	ND	7,4	-	0,2	3,2	0,3
s-WB ⁽⁴⁾	PC	3,3	0,17	7,84	11,7	ND	ND	1,4	-	0,1	0,3	0,3
s-WB ⁽⁴⁾	S2	3,3	0,17	0,44	7,3	0,6	ND	2,2	-	3,0	0,3	2,1
s-WB	S2	0,5	-	1,10	12,2	ND	ND	27,2	-	0,2	2,3	ND
I-W	S1	2,3	-	6,55	7,3	0,4	-	0,1	0,2	-	ND	ND

ND: Under the detection limit

⁽¹⁾ Referred to 1 kg of waste

⁽²⁾ Compressive strength

⁽³⁾ As content in $\mu\text{g/l}$

⁽⁴⁾ These samples have been stabilized/solidified after a reduction pretreatment with FeSO_4

3. RESULTS

Solidification objectives are easily achieved, with setting times and compressive strengths within the frame stated as quality criteria. The same can be said concerning the degree of compliance with the leachate ecotoxicity value as it has never surpassed the fixed limit.

With respect to the stabilization of hazardous components, Table-4 shows the results of the analysis of the TCLP leachate in some of the obtained S/S solids. The most decisive criteria to evaluate the process efficiency involves the compliance with the limits for the metals concentrations in the leachate.

The s-WA waste has been stabilized with FI with a proportion of waste:agent 1:1 and also with FA, with a 25% lime addition. The s-WB waste stabilization presents more problems, basically due to its Cr(VI) content, and cannot be achieved in any case without a previous reduction stage with FeSO_4 . Table 4 compares the results obtained when this waste is treated with the S2 agent, with and without previous reduction. It can be observed that, without the previous reduction step, the Cr concentration clearly exceeds the 5 ppm limit. After being treated, the Cr fixation has been achieved with PC and S2. The I-W residue, that has also a

high Cr(VI) content, has been stabilized with S1, without a previous reduction.

A treatment using the spray dry residue (S1 or S2) as reductor has been developed. The treatment makes use of its high sulphite content that can reduce Cr(VI). A mixture of the waste containing Cr(VI) and the spray dry residue has been acidified and, after a reaction time below one hour, the Cr(VI) content has been measured in an aqueous medium simulating the TCLP extract. The results show a high reduction efficiency, both with S1 and S2, being the measured levels of Cr in the leachate under 0,2 ppm in all cases.

4. CONCLUSIONS

From the results obtained, the characteristics of the tested combustion and/or desulphurisation residues, regarding their possible application as S/S agents, can be resumed as follows:

- They can be used as bulking agents with liquid wastes.
- All of them can substitute, partial or totally, other solidifying agents, like Portland cement, lowering treatment costs.
- Moreover, those with a high free lime content may avoid the need for lime or PC in the S/S process.
- High sulphite content residues can be used to efficiently treat wastes that need a reduction step prior the S/S process.

REFERENCES

1. British Coal Corporation. *Disposal and utilisation of flue gas desulphurisation (FGD) residues*. Contract 7220-EA/818. Final Report. Commission of the European Communities, Luxembourg, 1992.
2. L. Salvador; J. Vale; J. Olivares; C. F. Pereira; M.R. Piñero, C. Ruiz de Elvira; J.I. Seco. *Proyecto IRIS para la inertización de residuos industriales*. AMBIENTALIA '92, II Jornadas Internac. de Ingeniería y Medio Ambiente, Reus (Tarragona), 1992.
3. L. Cañadas, P. Ollero, L. Salvador, J. Galindo and D. Corrochano. *A flue gas desulphurisation and electrofiltration pilot plant: design and objectives*. E. Carnevale, G. Manfrida and F. Martelli (Eds.). Flowers'94. Proceedings of the Florence World Energy Research Symposium, pp. 745. Florence 1994.
4. *Test Methods for Evaluating Solid Waste, Toxicity Characteristic Leaching Procedure (TCLP)*. Method 1131, SW-846, 3rd., U.S. Environmental Protection Agency, Washington, DC., 1986.
5. C. Ruiz de Elvira Francoy, J.F. Vale Parapar, C. Fernández Pereira and L. Salvador Martínez. *Estabilización/solidificación de residuos industriales con agentes silíceos. Desarrollo de un método para la predicción del comportamiento y evolución con el tiempo de los residuos tratados*. III Congr. Int. de Química de la ANQUE. Tenerife, 1994.

CHARACTERIZATION OF ACFBC AND PFBC RESIDUES

L. Armesto, J.L. Merino and A. Cabanillas

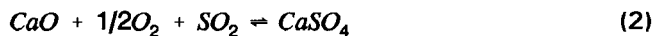
CIEMAT. Avda Complutense, 22, 28040 Madrid, Spain

ABSTRACT

The wastes from fluidized beds combustors are unlike those discharged from conventional pulverized fuel furnaces. In general, they consist of a mixture of bed ash, sorbent reaction products, and unreacted sorbent. The residues from two modes of operation (CFBC and PFBC) have some differences, as result of different operating regimes, and the effect of pressure on mineral equilibrium. The influences of type of fluidized bed combustor (PFBC and ACFBC) on the characteristics of the residues and the problematic related with disposal of these ashes from the point of view of leaching are studied.

1.- INTRODUCTION

Fluidized bed combustion is a method for burning low grade and high sulphur fuels efficiently while meeting strict air emission requirements. The sulphur is retained in the bed during combustion by means of a sorbent (limestone). In the bed, the limestone calcines and sulphates following the global reactions:



The desulphurisation in FBC system produces of large quantities of residues particularly when high sulphur coal is burnt. The properties of these residues are different from those produced by pulverized coal combustion and they depend of different operating regimes.

The aim of this paper is to study the influences of type of fluidized bed combustor: Atmospheric Circulating Fluidized Bed Combustor (ACFBC) and Pressurized Fluidized Bed Combustor (PFBC) on the characteristics of the residues and to know the problematic related with the disposal of these ashes from the point of view of leaching. In order to accomplish these objectives waste from pilot scale CFBC (0.5 Mw) and demonstration PFBC (80 Mw) units have been examined from the point of view of chemical and mineralogical composition and leaching characteristics.

The coal burnt to obtain these residues has 7,8 % (db) sulphur content and the limestone used as sorbent has 39,8 % calcium content. The combustion tests has been made, in both plants, at 850°C temperature and 2.5 Ca/S molar ratio. Two methods are used to assess leaching from coal residues: laboratory batch tests and laboratory column tests.

2.- CHARACTERISTICS OF COAL TESTED

Table 1 shows the principal characteristics of coal burned to obtain these residues.

Table 1

ELEMENTAL ANALYSES		MAJOR ELEMENTS		TRACE ELEMENTS	
Carbon (%)	43.07	SiO ₂ (%)	15.0	Ba (ppm)	<20
Sulphur (%)	7.68	Al ₂ O ₃ (%)	1.1	Be (ppm)	<10
Nitrogen (%)	0.65	CaO (%)	13.6	Co (ppm)	10
Hydrogen (%)	3.29	Fe ₂ O ₃ (%)	0.06	Cr (ppm)	585
Oxygen (%)	10.69	Na ₂ O (%)	1.3	Cu (ppm)	15
Ash (%)	32.93	MgO (%)	0.13	Ni (ppm)	110
H ₂ O (%)	1.70	K ₂ O (%)	0.51	V (ppm)	31
C.V (kcal/kg)	4423	TiO ₂ (%)	0.76	Zn (ppm)	43

3.- TESTS FACILITIES

The waste characterized are been obtained in a CIEMAT ACFB pilot plant and in a PFB demonstration plant (ESCATRON). The ACFB pilot plant has, as main components of the system, the combustor, the cyclone and the standpipe, for solid recirculation, and the baghouse. The combustor is a cylinder with 200 mm inside diameter and a total heigh of 6.5 m. The residues in ACFBC pilot plant are removed from the bottom of the furnace (BA) and from the baghouse (FA). The PFBC demonstrations plant has, as main component of the system, the combustor. The combustor is a pressurized vessel with 14 m diameter and a total heigh of 22 m. Inside the vessel are the furnace (bubbling bed) and the cyclones, as main components. The residues in PFB demonstration plant are removed from two locations: from the bottom of the furnace (BA) and from the cyclones (CA). Table 2 shows the operation conditions during the combustion tests.

Table 2

PLANT	T (°C)	V _f (m/s)	PRESSION (Mpa)	Ca/S (molar)	O _{2,exc}
PFBC	850	1.0	1	2.5	4.0
ACFBC	850	6.5	0	2.5	4.2

4.- CHEMICAL AND MINERALOGICAL CHARACTERISTICS OF THE RESIDUES

Table 3 shows the chemical composition of the different residues. Table 4 shows the mineralogical composition of the residues

5.- LEACHING TESTS

In the leaching tests, the residues has been mixed in proportion to their discharges from the plant: BA/CA= 40/60 from PFBC and BA/FA= 36/64 from ACFBC. Two methods are used to assess leaching from coal residues: laboratory batch tests and laboratory column test. Although batch tests provide rapid method of assessment, column tests has been developed to provide a more representative idea of leaching under natural conditions.

Table 3

Major elements, wt. %:

Trace elements, ppm

	PFBC		ACFBC			PFBC		ACFBC	
	BA	CA	BA	FA		BA	CA	BA	FA
SiO ₂	6.78	18.41	8.7	22.61	Ba	47	132	71	129
TiO ₂	0.31	0.46	0.01	0.09	Co	3	6	3	5
Al ₂ O ₃	2.79	5.84	2.56	4.71	Cr	14	34	15	28
Fe ₂ O ₃	1.50	3.32	0.66	2.00	Cu	<8	12	23	9
MgO	0.6	1.1	0.63	0.93	Mn	78	104	136	97
CaO	44.09	35.87	48.00	31.34	Ni	<10	18	<10	15
Na ₂ O	0.1	0.5	0.12	0.50	Pb	<10	<10	12	<10
K ₂ O	0.28	0.77	0.3	0.70	V	10	53	10	42
SO ₃	23.25	19.25	31.00	14.68	Zn	27	51	55	63

Table 4

	PFBC		ACFBC				
	BA	CA	BA	FA	BA	FA	
Calcite	44.2	Calcite	29.11	Anhydrite	52.7	Anhydrite	24.95
Anhydrite	39.5	Anhydrite	32.7	α -Quartz	8.7	α -Quartz	22.61
CaO	3.1	α -Quartz	18.41	CaO	26.33	CaO	17.50
α -Quartz	6.78			Calcite	4.8	Calcite	6.40

In the column tests, the residues has been preconditioned with water. The water to preconditioned the sample of PFBC was 13,0 %, while for the sample of ACFBC was 29.7%. Desionised water has been used as leaching media, the water flow has been 4 cm³/h.

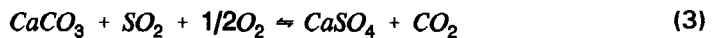
Table 5 shows the principal compounds of the first (L-1) and the last (L-5) leachates obtained for two samples. The Ba, Be, Fe, Mn, Ni and Se concentration is <0.3 mg/l, the Co, Cr, V and Pb concentration is < 0.5 mg/l; and Hg concentration is <0.025 mg/l in all cases.

Table 5

	pH	Al	Ca	K	Mg	Na	Zn	As	Cl ⁻	F ⁻	NO ₃ ⁻	SO ₄ ²⁻
PFBC												
L-1	9.6	0.63	710	920	<4.0	435	<0.3	0.63	221	<1	<1	2500
L-5	4.1	0.05	395	550	<4.0	195	<0.3	<0.5	6	<1	<1	2200
ACFBC												
L-1	12.0	<0.5	960	1350	<4.0	79	0.77	<0.5	301	<1	<1	1640
L-5	12.3	<0.5	1100	60	<4.0	31	<0.3	<0.5	6	<1	<1	1136

6.- DISCUSSION

The chemistry and mineralogy of PFBC and ACFBC residues are dominated by sorbent derived materials. Anhydrite is the major phase present in AFBC residues, while the PFBC bottom residues (BA) has a calcite as the major phase. On the other hand, the concentration of free-lime (CaO) in the residues is much higher for the ACFBC residues than for the PFBC residues. This is due that the calcination of CaCO_3 only proceeds at CO_2 partial pressures below thermodynamic equilibrium pressures, which is strongly dependent on the temperature. In PFBC, the calcination of CaCO_3 is normally inhibited due to excessive partial pressures of CO_2 , the desulphurisation reaction would then proceed according to the following reaction:



The rest of the chemical composition is very similar for PFBC and ACFBC residues.

The leachates from two samples were initially alkaline, ranging from pH 9.6-12. Over the rest period the alkalinity of leachates from PFBC residues decreased until pH 4.1, while leachates from ACFBC residues maintain a higher pH throughout the test period. This is due to different content of free-lime (CaO) in both residues. The components generated by the dissolution of calcium sulphate (Ca and SO_4^-) maintain a concentration in the leachates throughout the tests. The SO_4^- concentration is major in the PFBC than the ACFBC residues, while the Ca concentration is major in the ACFBC residues. The soluble K species tend to leach out more rapidly in ACFBC residues than the PFBC. Generally the variation shown by the leachates in both samples is small

7.- CONCLUSION

Significant findings resulting from the program are:

- The main elements in FBC residues come from inorganic constituents in the coal, sorbent reaction products and unreacted sorbent.
- The concentration of trace elements is very similar for PFBC and ACFBC residues.
- PFBC residues differ from ACFBC residues in that unreacted limestone remains as calcite, and only a small amount of calcite is calcined to form lime.
- The alkalinity is major in the leachates from the ACFBC than the PFBC residues.
- The concentration of trace elements in leachates from both residues is very similar
- In both samples, the leachate concentrations for the majority of elements are below the EU limits, but the high alkalinity and SO_4^- concentration may require special treatment

ACKNOWLEDGEMENTS

Authors, would like to thank ENDESA for its collaboration and financial support.

8.- REFERENCES

- 1.- C.Nilsson, L.B. Clarke, IEACR/73, August (1994)
- 2.- I.M. Smith, IEACR/21, February (1990)
- 3.- E.J. Anthony, EEP/ERL 88-67 (1987)
- 4.- A.E. Bland, 10th International Conference on Fluidized bed Combustion (1989)
- 5.- H.A. Van der Sloot, ENC-120 Netherlands Energy Research Foundation (1982)

Pilot plant development of a new catalytic process for improved electrostatic separation of fly ash in coal-fired power plants.

J.Olivares del Valle, L.Salvador Martinez, B.Muñiz Baum, V. Cortés Galeano

Departamento de Ingeniería Química y Ambiental, Escuela Superior de Ingenieros Industriales, Universidad de Sevilla, E-41012, Sevilla, SPAIN.

1. INTRODUCTION AND SCOPE

The design and operation of pulverized-coal-fired power plants (PCFPP) are usually regarded as fuel range in terms of sulphur and ash contents. These units may give severe environmental problems of fly ash emissions as a result of lower SO₃ contents in the flue gas (FG) because the electrical resistivity of the solid particles is correspondingly lower, with consequent adverse effects on electrostatic precipitator (ESP) efficiency. More stringent air pollution laws cause many power companies to burn lower sulphur coal under boilers in plants that formerly burned higher S coal or ran with abnormal operational conditions (only remediable by shutdown and repairs).

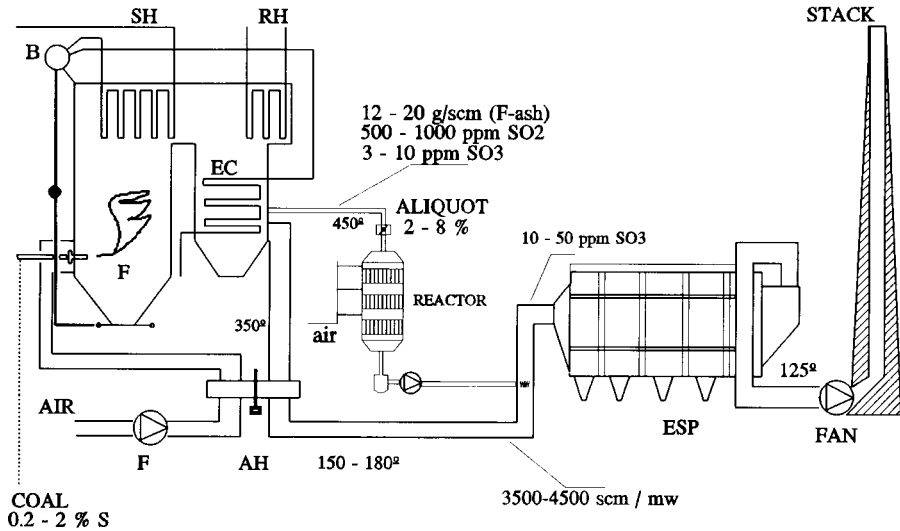
This presentation of the GASOX process is a contribution to the improvement of existing technology for flue gas conditioning (FGC), which is defined as a control system for (ESP) efficiency in PCFPP.

The concentration of SO₂ in the FG is correlated more or less linearly with the sulphur content of the coal (about 700 ppmv may be expected from 1 % S coal). Burning low sulphur coal produces an FG which contains lower SO₂ and correspondingly lower SO₃ contents since about 1 - 5% of the SO₂ is generally further oxidized to SO₃ in the boiler-economizer system. The extent of such oxidation depends on the thermal profile of the plant set, on the ash and on surface phenomena sequences. In these cases, it has been demonstrated that an addition of SO₃ to the FG (10 - 40 ppm) can reduce fly ash resistivity by a factor of about 20 (10¹² to 10¹¹) and consequently the ESP removal efficiency improves from 99.0 to 99.5% in terms of separated fly ash.

It is known that FGC is successfully applied in some PCFPP by the injection of a small amount of SO₃ (5 - 50 ppmv) from an external source such as liquid SO₃, H₂SO₄, sulphamic acid, ammonium sulphate, S or SO₂ converted to SO₃. Therefore the resistivity of the fly ash layer on the ESP plates decreases and the separation efficiency rises, provided that the electrical and mechanical conditions of the equipment are in good order. The GASOX process could be an alternative to these industrial methods. However, the main problem to be solved is related to the characteristics of the FG (temperature, specific composition and very high ash content), which do not facilitate the application of the existing knowledge and experience about the industrial catalytic oxidation of SO₂ (sulphuric acid manufacture, for instance).

Bibliographic data about the endogenous oxidation to SO₃ of SO₂ present in FG (cleaned or dusted) is mostly unavailable or not published up to present. On the other hand, a significant technical and scientific discussion has risen not only about the FGC mechanism but also about the parameters affecting the resistivity of the fly ash within the FG (temperature, SO₃ and H₂O, mineral analysis of

the fly ash, superficial porosity and specific surface, electric field, etc.). For these reasons process development at pilot and demonstration scales is always suitable.



It is sure that the sulphur contained in coal burns spontaneously in the furnace producing an SO₂/SO₃ ratio depending on the temperature and on oxygen content only. Also it is well known that in the absence of catalytic effects, the rate of SO₂-oxidation (roughly 10⁻³% /min @ 900°C) can easily be calculated. Nevertheless, the "free SO₃" measured in the FG outside the furnace is about 1/10th of that initially formed. The reason for this decrease is that the reaction SO₃ + H₂O ⇌ H₂SO₄ takes place when the FG temperature falls to 300-400°C. This reaction is completed at the ESP inlet (135-165°C) and the acid is condensed on the particle surface.

The basic idea of this project (GASOX) is to convert a fraction of the SO₂ in the FG into SO₃. Only an aliquot (2 - 8 %) of the FG stream should be withdrawn, depending on its SO₂ content. A catalytic reactor will provide SO₂ → SO₃ oxidation (60 - 80 %) and this fraction will be returned to the main FG stream before the ESP inlet. The small size of the aliquot and the conversion rates optimize a small catalytic reactor with very simple equipment. A feasibility study of this new method of improving ESP performance by "internal" gas conditioning shows good industrial perspectives from the technical, operational, and economic points of view.

The work began in July 1993 and it comprises several stages that together will last four years:

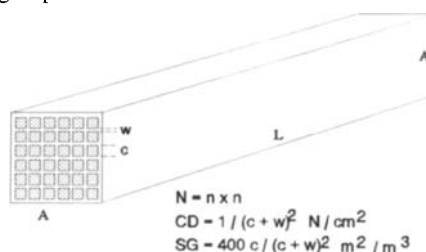
- I) Assessment of alternatives for flue gas withdrawal point location before catalytic conversion of SO₂ in a PCFPP.
- II) Engineering of the option selected in I) and pilot plant design.
- III) Equipment purchasing and construction of a pilot plant at the laboratory site.
- IV) Design, selection and sample preparation of suitable "high dust resistant" catalysts and supports and laboratory testing with simulated FG.
- V) Pilot plant experimentation, engineering revisions, scaling up and demonstration unit design at a PCFPP site.

2. CATALYST DEVELOPMENT

The theoretical and technological considerations about SO₂ catalytic oxidation were fully revised as well as the industrial converter design methods for sulphuric acid manufacture. The chemical equilibrium $\text{SO}_2 + 1/2 \text{O}_2 \rightleftharpoons \text{SO}_3$ (catalysed with Pt or V/K) was modeled and results were obtained for a typical FG: 5 % O₂, 600 - 1000 ppmv SO₂, 200 - 1000 ppmv NOx and 12 - 20 g/Nm³ of fly ash. Almost without exceptions, a catalyst in the form of porous pellets is extremely vulnerable to the dust present in the gas stream. Consequently, the catalyst (and supports) which are going to be developed in the GASOX programme must be resistant to a high dusting flow (unfriable and unplugged), as well as being active under FG conditions (and composition). The only way to pass a two-phase gas-solid flow through a catalytic bed without plugging, is to divide it into channels with an appropriate pass speed, then the spacial velocity pass (h_{p1}) is less and the reactor is longer than that of a fixed-bed arrangement. This is the case of the "honeycomb-type" supports in the form of monoliths which are being investigated and developed with very promising results on laboratory and pilot plant scales in this project.

The development of the monoliths with a honeycomb structure and appropriate dimensions (see diagram) has several stages and key aspects that can be grouped as follows:

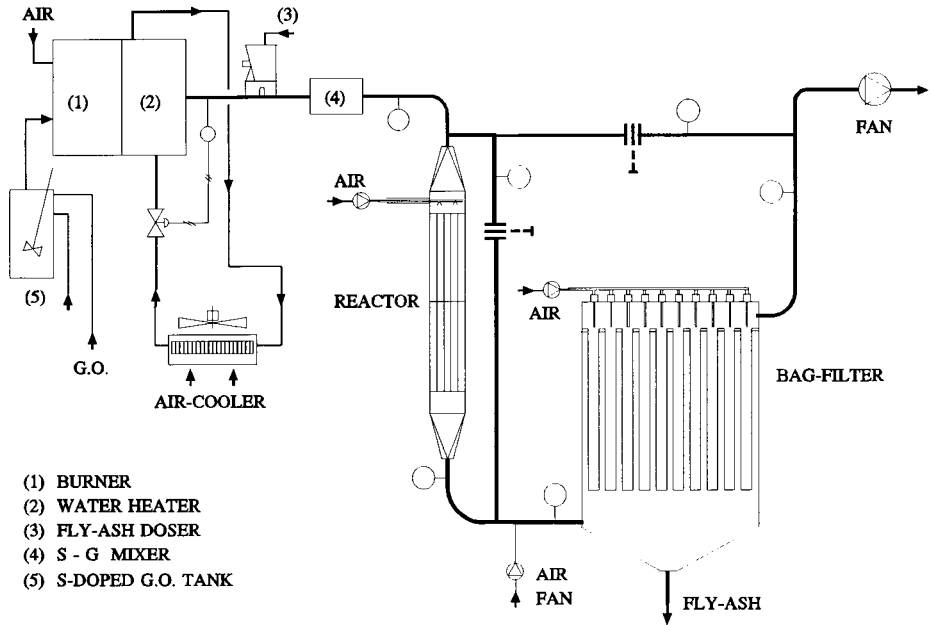
- Selection of catalysts + support materials and type formulations development (Pt and V/K base as active species).
- Knowledge of the rheological and thixotropic parameters of the raw materials and mixtures (catalyst + supports + additives) in order to extrude uniform prismatic monoliths with a defined porosity and channels parallel to the longitudinal axis of the monoliths in adequate square pitch.
- Definition of the design and dimensional parameters of the extrusion dies.
- Definition of the operational parameters of the extruding machine so that the "fresh" monolith comes out of the die with the required geometry.
- Thermal treatment of monoliths at 200 - 600 °C.
- Testing and modeling on laboratory scale of monoliths with the specified gas (5 - 7% of O₂, 13 - 16% CO₂, 500 - 1000 ppmv of SO₂, 200 - 1000 ppmv NOx) with/without ash or water.



3. PILOT PLANT

The design and construction of the pilot plant were carried out according to the modeling of the GASOX process and the more suitable honeycomb catalyst, (see diagram 2). The main unit is a catalytic reactor that contains a basket with the package of honeycomb monoliths arranged vertically. The plant operates with combustion gases with a well-defined composition and temperature, which can also be clean or loaded with fly ash. The head unit is a gas generator (S-doped gas-oil combustion chamber and a modular hot-water boiler) for 200 - 500 Nm³/h of simulated FG in a range of 300 - 500 °C. This range is reached by setting the air-fuel ratio and the flow and temperature of the recirculated water from an air-cooler device. Optionally, different quantities of fly ash can be added to the hot stream before the reactor. The tail unit is a centrifugal fan placed after the bag-filter that exhausts the gases to the atmosphere.

The dimensions of the reactor and coupling accessories (9 interchangeable types) to the gas duct assure both an isokinetic gas flow to the entrance of the catalytic bed ($LV = 0.6 - 3.1 \text{ m.s}^{-1}$),



and other scalable parameters of monoliths ($GHSV = 1000 - 5000 \text{ h}^{-1}$ and $AV = 3.0 - 7.7 \text{ m.h}^{-1}$). The prismatic basket is constructed to provide two separate layers of 5×4 monoliths of $90 \times 90 \times 1000 \text{ mm}$ pitch 4 as the maximum catalyst load. Nevertheless, we have no problem adapting the basket for placing groups of monoliths of different cross-sections or lengths.

We have developed catalysts with adequate pitch and activity that are capable of oxidizing at least 60 % of the total SO_2 , but in such a way that the SO_3 remains in the gas stream after the converter. However, long-term trials about the unplugging operation will be necessary to consolidate the GASOX process.

The economic investment estimations of costs for a demonstration unit, even when only taking the main equipment into account, show that, in respect to the operational costs and investment of the conventional FDG systems by direct addition of SO_3 , the most advantageous alternatives are those that use catalysts supported over honeycombs (See diagram 1).

4. BIBLIOGRAPHY

Shui-Chow Yong et al. "Flue-gas conditioning" Air & Energy Research Lab. R. Triangle Park. San Diego, CA (1985)

J. P. Gooch "A manual on the use of flue-gas conditioning for ESP performance enhancement" EPRI Palo Alto, CA (1985)

R. A. Wright "Advances in SO_3 gas plant design and control" Wilhelm Env. Techn. INC (1991)

S. J. Miller "Enhanced flue-gas conditioning study" Draft Report EERC, North Dakota Univ. (1991)

Paper "Injection rates for SO_3 flue-gas conditioning" Third CSIRO Conf., Sydney (1988).

Proceedings "Ontario hydros's evaluation of flue-gas conditioning for ESP performance enhancement" Gen-Upgrade Conf., Washington (1990).

The fate of trace elements in coal during gasification

A. J. Bushell and J. Williamson

Department of Materials, Imperial College, London, SW7 2BP, United Kingdom

1. INTRODUCTION

The need for coal conversion processes with higher efficiencies and lower gaseous emissions has led to the development of a number of integrated gasification combined cycle (IGCC) systems. While these systems will meet the anticipated legislation concerning the level of NO_x, SO_x and particulate emissions, it is essential that the fate of the trace elements and heavy metals which are present in all coals is established, since these elements may present a further environmental hazard. The trace elements may be associated with either the organic matrix, the coal mineral matter or distributed between both [1]. During gasification the trace elements are partitioned between the ash residues and the gaseous emissions. The actual distribution will depend on the physico-chemical properties of the individual elements, the degree of association between the coal matrix and the mineral matter and the process conditions. Trace elements may conveniently be divided into three groups depending on their volatility under gasification conditions [2]. Group I elements are the least volatile and remain with the ash residues, Group II elements are more volatile and partition between the residual ash and the gaseous phase, condensing on the finer ash particles as the gases cool. Group III elements have high volatilities and show little or no tendency to condense from the vapour phase, thus staying with the gaseous products. Benson et al [3] reported a study of the gasification of three US coals in a pressure drop-tube furnace at temperatures ranging from 1000° to 1500°C. Elements such as As, Cd, Se and Pb were all found to show increasing volatility as the gasification temperature increased or the O:C ratio decreased.

This paper presents the initial results of a study of the fate of the trace elements in UK coals when gasified in a laboratory gasifier operating to 950°C, and a pilot scale air-blown pressurised fluidised bed gasifier (ABFBG) operated by British Coal.

2. ORIGIN OF THE SAMPLES

In the laboratory gasifier, about 10g of coal was introduced into a hot bed (950°C) of fluidised sand. Samples of the fine particulate ash were collected from a cyclone and a gas filter (>1µm). Ash remaining in the bed was removed at the end of each run by increasing the fluidising gas velocity to elutriate the ash from the fluidised bed. The British Coal air-blown gasifier operates at elevated pressures and temperatures up to 1000°C. 70-80% of the coal is converted into a low calorific gas, with combustion of the residual coal char taking place in a circulating fluidised bed combustor. Limestone may be added to the coal to retain the sulphur in the bed. Samples of the coal feed, bed ash and ash from a primary cyclone have been

analysed for major oxides and trace elements. The same ash samples have been subjected to leaching tests to assess the stability of the ash products to leaching from ground waters should the residues be disposed of in land-fill sites.

3. EXPERIMENTAL

Leaching studies have followed a protocol recommended by the UK National Rivers Authority [4], in which a 100g sample of residue was added to 1 litre of deionised water (pH ~ 5.6) giving a solid:liquid ratio of 1:10. Samples were sealed in polythene jars and rotated end over end at 60 rpm for 24 hours. The solutions were then allowed to settle for 20 minutes, filtered through a 0.45 μ m filter (Gelman VacuCap), acidified with 2ml of conc. HCl and then stored in the dark until being analysed. Chemical analysis of ashes and leachates was performed by induction coupled plasma spectroscopy (ICPS) for both major oxides and trace elements. Standard coals and ash samples were included with each batch of analyses to check the consistency of the results [1].

4. RESULTS AND DISCUSSION

Longannet coal was one of the five UK bituminous coals which had been fully characterised for ash content, mineral matter and trace element distributions [1]. This coal was somewhat unusual in having the mineral matter uniformly distributed throughout the coal in all size fractions. The size fraction 180-125 μ m used in the laboratory gasifier to minimise elutriation of coal particles was therefore typical in ash chemistry to that of the whole coal. During gasification significant amounts of fine ash particles were collected in both the cyclone and the gas filter. The composition of these particulates was found to be almost identical to that of the coal ash, indicating a progressive elimination of fine ash particles from the bed during the gasification process. The concentration of selected trace elements in the bed ash, cyclone fines and gas filtrate are shown in Table 1, and may be compared with the amounts of trace elements introduced into the gasifier in the coal feed.

A mass balance calculation shows that 60-70% of most trace elements could be accounted for. Much of the unaccounted for material probably remained in the bed as decomposed mineral matter which had reacted with the sand. However, an analysis of the bed material produced inconsistent results due to the difficulty in obtaining representative samples, and the errors introduced by the large dilution effect of the enormous quantities of sand particles which made up the bed.

The cyclone fines contained 70-90% of the recovered trace elements, with the balance being found in the bed ash which was elutriated from the fluidised bed at the end of the gasification process. The high proportion of trace elements found in the cyclone ash is somewhat puzzling and suggests that many of the trace elements may be associated with the finer mineral particles, and thus are more readily removed from the bed during the gasification process. Of those elements found in the gas filter fines, only La and Zn were there in any appreciable proportion (27% and 13% respectively) of the recovered material. The high proportion of relatively non-volatile elements found in the cyclone ash, e.g. Ba and Sr, suggests that these elements remained in the mineral matter and were carried from the bed by physical rather than chemical separation processes.

Table 1.
Distribution and recovery of trace elements using a laboratory gasifier and Longannet coal

	Trace elements introduced into the bed(μg)	Elutriated bed ash(μg) (%recovery)	Cyclone fines(μg) (%recovery)	Filter fines(μg) (%recovery)	Total recovered (μg)	% of trace elements recovered
Ag	8.3	0.5(16%)	2.3(82%)	0.03(2%)	2.82	34
Ba	1262	264(31)	576(69)	0(0)	840	66
Be	25	1.5(10)	12.8(90)	0(0)	14.3	57
Cd	7.2	0.8(22)	2.9(78)	0(0)	3.7	51
Co	90	2.1(4)	49(96)	0.1(0)	51	56
Cr	384	14.3(7)	199(93)	1.4(1)	214.7	55
Cu	501	20(7)	255(92)	3.2(1)	287.2	55
La	305	10(4)	154(69)	60(27)	224	73
Li	642	110(25)	323(75)	1.4(0)	434	67
Mo	31	1.6(11)	12.8(88)	0.2(1)	14.6	47
Ni	383	42(18)	195(82)	1.8(0)	239	62
Pb	154	19(20)	72(78)	2(2)	93	60
Sr	4391	628(22)	2225(77)	30(1)	2883	65
V	441	24(9)	240(91)	0(0)	264	59
Zn	160	18(21)	56(66)	11(13)	85	53

Gasification residues from the British Coal air-blown gasifier consist of a bed ash containing unreacted char, and fines collected from primary, secondary and tertiary cyclones. Bed ash and primary cyclone fines constitute the bulk of the inorganic material introduced into the gasifier. Table 2 shows the trace elements introduced into the gasifier and their distribution between bed ash and fines when Maltby coal, to which limestone had been added as a sulphur sorbent, was gasified. An oxide analysis of the bed ash showed that this contained less SiO_2 and Al_2O_3 than the coal feed, suggesting the elutriation of fine clay particles from the bed. The primary cyclone fines contained more iron oxides than the coal feed, again suggesting elutriation of fine pyrite residues.

A mass balance for each of the trace elements, in terms of the rate of input versus the rate of removal as either the bed ash or primary fines, accounts for 80% or more of the trace elements introduced into the fluidised bed. The trace elements partitioned relatively uniformly between the bed ash and the primary fines, with elements such as Be, Co, Cr, Cu, Mo, Pb and V showing a slight preference for the primary fines, while the more refractory oxides, e.g. Ba, La and Sr, showed a marginal preference to remain with the bed ash. However, the high level of trace elements found in the cyclone fines from both the laboratory gasifier and the British Coal air-blown gasifier suggests that the physical association of the trace elements with the decomposed mineral matter is perhaps as much, if not more important than the relative volatility of each element.

24 hour leaching tests have been performed on the Maltby bed ash and primary fines. Only Al, Ba, Ca and Cd were present in the leachates at concentrations which were close to or above the limits set for drinking water standards by the European Union [5]. The concentrations were, however, well below those set for the landfill disposal of hazardous or inert waste materials, and therefore the gasification residues could be disposed of without special treatment

Table 2

Distribution of trace elements between the bed ash and primary fines from the British Coal air-blown gasifier using a Maltby coal with added limestone

	Coal with limestone feed (mg/hr)	Primary cyclone fines (mg/hr) (%recovery)	Bed ash (mg/hr) (%recovery)	Total recovered (mg/hr) (%recovered)
Ag	0.1	0.05(50%)	0.05(50%)	0.1(100%)
Ba	23	9.3(48)	10.1(52)	19.4(84)
Be	0.4	0.2(67)	0.1(33)	0.3(75)
Cd	0.2	0.1(50)	0.1(50)	0.2(100)
Co	1.3	0.6(55)	0.5(45)	1.1(85)
Cr	5.9	2.8(52)	2.6(48)	5.4(92)
Cu	5.9	2.9(53)	2.6(47)	5.5(93)
La	1.8	0.8(44)	1.0(56)	1.8(100)
Li	7.2	2.4(40)	3.6(60)	6.0(83)
Mo	0.9	0.4(57)	0.3(43)	0.7(78)
Ni	4.5	2.3(60)	1.5(40)	3.8(84)
Pb	2.7	1.1(58)	0.8(42)	1.9(70)
Sr	8.3	3.9(42)	5.5(58)	9.4(100)
V	8.9	3.9(53)	3.5(47)	7.4(83)
Zn	4.0	1.6(44)	2.0(56)	3.6(90)

5. CONCLUSIONS

During the gasification of coal, trace elements have been shown to partition between a bed ash and cyclone fines. The high concentration of most trace elements in the cyclone ashes suggests that these elements are strongly associated with the fine mineral particles which are elutriated from the bed. Partition due to chemical differences is of a lesser significance. Leaching tests have shown that gasification residues would meet the requirements for landfill disposal.

ACKNOWLEDGEMENTS

This study has been supported with a grant from BCURA and the ECSC (Project No. 7720-EC01703). Technical support from the Coal Research Establishment, Cheltenham, Loughborough University of Technology and the Department of Geology, Imperial College is gratefully acknowledged.

REFERENCES

- 1 A. J. Bushell and J. Williamson, 1995, 8th ICCS, Oviedo.
- 2 L. B. Clarke and L. L. Sloss, "Trace element emissions from coal combustion and gasification", IEA Coal Research, London, Report No. IEACR 149, 1992.
- 3 S. A. Benson, T. A. Erikson and C. J. Zyarlicke, 1994, 4th EPRI conference on "The Effects of Coal Quality on Power Plants", Charleston, USA
- 4 UK National Rivers Authority, 1994 "Leaching tests for assessment of contaminated land - Interim NRA guidance", R&D note 301.
- 5 European Community, 1991, Proposal for a Council directive on the landfill of waste, Cat. No. CB-CO-91-174-EN-C, Luxembourg 22 May 1991.

Evaluation of the distribution of trace elements in coal combustion products

R. Alvarez Rodríguez^a, C. Clemente^a, C. Serrano^a, J. de Marcos^b and V. Velasco^b.

^a Mining School, Polytechnical University, 21 Rios Rosas, 28003 Madrid, Spain.

^b Spanish Electrical Research Association (ASINEL), 3 Francisco Gervás, 28003 Madrid, Spain.

1. INTRODUCTION

Power generation by combustion of coal produces waste (solid, liquid and gas) which may cause damage and problems. The international environmental regulations are now getting increasingly tough and control of said waste is stricter. A more in-depth knowledge of the composition of the products of combustion and the factors which influence said composition is thus becoming a necessity. There are certain elements in trace amounts which accompany coal, which do not intervene directly in the combustion process, even though they undergo transformations during the process. In any kind of combustion, the final destination of these elements is to form part of the combustion products. These products may later undergo uncontrolled natural processes when deposited or emitted.

2. EXPERIMENTAL

The trace elements in coal have been monitored, from their origin and appearance in the formation, through the influence by combustion, through their distribution and concentration in the combustion products. The focus of this study has been aimed to take the real circumstances of Spanish power stations into account. Thus, a correlation between each of the data sources is sought whenever possible. The elements the study concentrates on are Al, As, Be, Ca, Cd, Co, Cr, Cu, Fe, K, Mg, Mn, Mo, Na, Ni, Pb, Se, Si, Ti, V and Zn. Based on the data on the concentrations of the trace elements in the coal and the combustion products, a link between them is sought to be able to predict the final destination and the concentration of the trace elements in the slag, fly ash and combustion gases. In order to do so, three reference bases are distinguished:

- to determine those factors which, due to their action, provide trace elements before, during and after the coal forming processes;
- to analyze the parameters and conditions which affect the behaviour and distribution of the trace elements during the combustion process; and
- to determine the behaviour of the trace elements inside the control systems, identifying the parameters which affect the final distribution.

All the above provides us a relation between the different factors which have an influence on the appearance of metals in coal combustion products, aimed at obtaining a method which may be used as the basis to establish a prediction line for appearance of trace metals (in a qualitative manner) in said products. By means of real measurements of the aforementioned trace elements, in coal, fly ash and slag, their distribution and destination in combustion products has been checked. Although the study was initially carried out on a lignite-type Spanish coal, the overall aim is to achieve control of the combustion products and their potential influence on the environment for any kind of coal, both of emissions into the atmosphere, and of leaching in waste heaps. The specifications of the coal studied are:

Upper calorific power: 920 kJ/kg (2200 kcal/kg).

Humidity: 41%

Volatile materials: 21%

Ash: 21.5%

Sulphur: 2.5%

Fixed carbon: 14%

Then the validity of what is known as the enrichment factor was studied, applied to our coal. The enrichment factor is determined by the equation:

$$RE = \frac{(C_{el})_{outlet}}{(C_{el})_{inlet}} \times \frac{\% \text{ ash content in the coal}}{100}$$

Thus, our results were compared with the experimental results obtained from other coals.

3. RESULTS AND DISCUSSION

According to their behaviour during combustion (1, 2, 3), the trace elements may be classified as:

Class 1. Elements which are concentrated in the same manner in larger sized fly ash as in slag, which are not concentrated in the ash and escape the control system. These are generally not volatilized: Al, Ca, (Co), Fe, K, Mg, Mn, Na, Si, Ti.

Class 2. These are elements which find difficulty to join the slag, and are mainly concentrated in the ash collected in the control systems, and even more in those which escape. These elements volatilize, even though they condense inside the boiler, or failing that, in the control system: As, Cd, (Cu), Pb, Zn. *Class 3.* These remain in gas phase, as they are very volatile and usually escape with the gases up the chimney or condense on the finer particles which escape the control systems.

There are also elements showing intermediate trends:

Class 1 and 2: Mo, Ni, Cr, V, Be, Co, Cu. *Class 2* and 3: Se.

Thus, the trace elements studied can be classified into the following groups:

Class 1: Al, Ca, (Co), Fe, K, Mg, Mn, Na, Si, Ti. *Class 2:* As, Cd, (Cu), Pb, Zn. *Class 1 and 2:* Mo, Ni, Cr, V, Be, Co, Cu. *Class 2 and 3:* Se.

The results show that, both Co and Cu, yet showing in general very well defined trends in each group, may appear to have an intermediate nature.

All of the elements in *Class 1* increase their concentration in ash and slag, then they are enriched. Al, as well as Co, Fe, K, Mg, Na, Si and Ti are distributed in the same manner in ash and slag, although in a greater percentage in slag, due to their low volatilization. To a greater or lesser extent, they fulfil what is forecast; however there is more concentration of Ca and Mn in the ash. The elements in *Class 2* also increase their concentration in the combustion products. The elements As, Pb, Zn comply with their expected behaviour, reaching a clear concentration in the ash when compared with the slag. The elements Cd and Cu are also more concentrated in the ash, although they are distributed almost equally among ash and slag.

The intermediate elements in *Classes 1 and 2* are distributed in each of the classes as follows: included in *Class 1* there are Mo, Ni, Cr and Co; in *Class 2*, there are V, Be and Cu. The only element which belongs to *Class 2 and 3* is Se. It is the only element which is not enriched, that is to say, the concentration in ash and slag is lesser than the initial concentration in coal. That means that a great part of the Se is vaporised and escapes with the combustion gases, in gas phase or on the finer fly ash. We must point out the low concentration of the Se in the coal: 4.7 ppm.

As to all the above, we are in position to assure that the great majority of the trace elements confirm the behavioral patterns set forth in the classifications in this work, except for some anomalies. These differences are: the Ca and Mn, which are typically from *Class 1*, are much more concentrated in the ash, so they have a greater volatile component than expected; as to Cd and Cu is concerned, in spite of fulfilling the expectations for *Class 2* in view they are more concentrated in the ash, such concentration in the ash is nonetheless almost the same as in the slag; and almost anything may happen with the elements of intermediate nature.

4. CONCLUSIONS

The trace elements which accompany the coal originate through a set of natural factors, which are difficult to determine and control. These factors are: activity by bacteria involved in the transformation processes; presence of organic materials; environmental deposition and sediment inclusion; thermal maturity (rank); nature and intensity of mineralization (epigenetic); geochemical conditions: pH and Eh (oxidation potential); gas exhaust, precipitation and enrichment from ground water in contact with the vein; and time.

During the conventional combustion of the coal, the behaviour of the trace elements and

the later distribution in the combustion products is mainly determined by the following parameters: content and initial concentration of the trace elements in the coal fed; chemical form of the elements in the coal; combustion temperature of the facilities; particle size of the ashes; operation temperature of the control systems.

The most important phenomenon of the trace element distribution is that of the vaporisation–condensation, which is present in all stages of the combustion process. That is why the combustion temperature has the most relevant role to play in the distribution of trace elements in combustion products and the final chemical form in said products. In order to analyze distribution of the trace elements in the combustion products, the ideal situation is to have an exact knowledge of the chemical form of the elements and the operating temperature of the boiler and of the control systems. Thus, it should be possible to determine the fate of the trace elements fairly exactly.

If the combustion conditions are always maintained the same and the coals used come from the same coal–basin, which mean similar properties and rank of coal, a prediction of the trace elements destination in the final products, through correlations and mathematical models, will be possible (5). That is to say, the visible fact that the results obtained in application to a Spanish coal do not coincide with those obtained in other experiments (4), denotes nothing but the combustion conditions and the coal were different. The data obtained would be applicable to similar situations (not to say identical ones) to those studied, and thus, coinciding with the values of *RE*, we would be able to establish the following correlation:

$$(C_{et})_{outlet} = (RE) \times (C_{et})_{coal} \times \frac{100}{\% \text{ ash content in the coal}}$$

It is indispensable, in order to carry out proper control and good prediction of the trace elements in coal, to carry out an optimum "sample taking", so that the resulting data from the chemical analysis is representative and matches reality.

Finally, one should point out that a control of the trace elements, both at inlet (coal) and outlet (ash, slag and gas), may be a good indicator of how combustion is taking place inside the boiler, as the distribution of the trace elements in the combustion products is very sensitive to variations in operating conditions.

REFERENCES

1. Clarke L.B., Sloss L.L. IEA COAL RESEARCH (1992).
2. González Blas, J. Energías Alternativas (1981) 4.
3. González Blas, J. Energía (1978) 67.
4. Meij R. European Seminar on control of emissions from combustion of coal – New technologies for power generation and industrial plant (1991) 277.
5. Wu. E.J., Chen K.Y. EPRI–ES–5115 (1989).

Trace Element Partitioning in Stack Emissions From Coal-Fired Power Stations

L.S. Dale, J.F. Chapman and S.A. Lavrencic

CSIRO, Division of Coal and Energy Technology, PMB 7, Menai, NSW, 2234, Australia

1. INTRODUCTION

Atmosphere emissions of trace elements from coal-fired power stations are receiving increased scrutiny in the assessment of the environmental impact of electricity generation. The focus on trace element emissions has been highlighted by legislation in many countries in which key environmental trace elements have been designated and emission limits imposed [1]. Changes to the United States Clean Air Act, 1991, in which many trace elements and their compounds have been designated as air toxics, have imposed requirements for monitoring the atmospheric emissions of a wider range of environmentally sensitive elements from power plants [2].

The emission of trace elements to the atmosphere occurs through the discharge of stack particulates which are the fine ash particles escaping the collector (fabric filter or electrostatic precipitator). These fine ash particles contain relatively high levels of environmentally sensitive trace elements brought about by the absorption of volatile species from the flue gas onto the surface of the particles (in the cooler sections of the convention path) [3]. Trace elements are also emitted in the flue gas. These elements are also of environmental concern and are generally highly volatile species.

The monitoring of the emission of trace elements to the atmosphere from power plants therefore necessitates the sampling of both solids and gas in the flue gas discharge. Of particular interest is the partitioning of trace elements between the solid and gas discharge since the volatile species present in the gas phase will ultimately be manifested as ultra-fine condensed species with probably different plume dispersion characteristics to the stack particulates.

In a number of trace element mass balance studies of New South Wales power stations [4], the partitioning of trace elements between the solids and gas discharges was determined. From these studies it was possible to assess the

relative emission rates of some key environmental trace elements leading to a better understanding of the potential environmental impact of atmospheric emissions.

2. SAMPLING

2.1 Stack particulates

The stack particulates were sampled isokinetically using a standard procedure based on collection in a thimble. Sampling times varied between 2 and 6 h depending on the collection efficiency of either the fabric filter or the electrostatic precipitator. From the mass of particulates collected the solids emission rate could be determined.

2.2 Flue gas

Gas sampling was carried out by passing the flue gas, sampled by a pump, through a thimble to remove solid particles and extracting the trace elements in a solution of 6 percent potassium permanganate in nitric acid. Sampling times were approximately 30 min. The gas emission rates of the trace elements detected were determined from a measurement of the flue gas discharge, the sampling time and the volume of reagent.

2.3 Chemical analysis

The samples were chemically analysed using a number of techniques including inductively coupled plasma mass spectrometry and atomic emission spectrometry, and atomic absorption spectrometry.

3. RESULTS AND DISCUSSION

The trace elements monitored were those of environmental concern as classified by the United States National Research Council [5]. These included arsenic, boron, cadmium, lead, mercury, molybdenum, selenium, chromium, copper, nickel, vanadium, zinc, antimony and cobalt. Most of these elements have been designated as air toxics in the US Clean Air Act.

In Table 1 the gas and solid emission rates of the above trace elements obtained from a test on a large (4 x 660 MW boiler) power station are given. The data show that, for the majority of trace elements, the gas emission rates were substantially higher than the solids emission rates. A major problem in monitoring the gas discharge is the limited capacity of the chemical reagent used to trap the volatile trace element species. This arises from the sulphur dioxide in the flue gas which causes rapid degradation of the reagent and hence the sampling time.

Data obtained on other power stations gave similar results in that boron, nickel, molybdenum and mercury partitioned predominantly to the gas discharge.

Table 1
Trace element emission rates (mg/Nm³) from a NSW power station

	Gas emission rate	Solids emission rate	Ratio
Arsenic	0.03	0.003	10
Boron	0.78	0.005	156
Cadmium	0.001	0.00004	25
Lead	0.004	0.002	2
Mercury	0.0019	0.00003	63
Molybdenum	0.11	0.0002	550
Selenium	0.0009	0.002	0.5
Chromium	1.0	0.0024	420
Copper	0.013	0.007	1.9
Nickel	1.3	0.002	650
Vanadium	0.01	0.0047	2
Zinc	0.1	0.0048	21
Antimony	0.0002	0.0002	1
Cobalt	0.014	0.0005	28

For other elements the partitioning trends were variable suggesting that parameters such as coal type, combustion conditions, plant design and collector operation may play a significant role in trace element emissions.

4. CONCLUSIONS

Adequate assessment of the environmental impact of the atmospheric emission of trace elements from power plants should include monitoring of the flue gas discharge because of the higher emission rates of some environmentally sensitive trace elements in this stream. Even though the emission rates measured were substantially lower than legislated discharge limits, adequate monitoring strategies are needed to assess the overall potential environmental impact from atmospheric emissions.

REFERENCES

1. L.B. Clarke and L.L. Sloss, IEA Report IEACR/49 (1992) 111pp.
2. D. Boutacoff, EPRI Journal, March (1991) 5.
3. D.F.S. Natush, J.R. Wallace and C.A. Evans, Science, 8 (1974) 202.
4. L.S. Dale and J.F. Chapman, CSIRO Division of Coal and Energy Technology Report CET/LH/IR013 (1991) 14pp.
5. United States National Research Council, PECH Report (1980) 153pp.

This Page Intentionally Left Blank

Synthesis of industrial minerals from fly ash

X. Querol., F. Plana, A. Alastuey, J.L. Fernández Turiel and A. López Soler

Institute of Earth Sciences "Jaume Almera", CSIC, c/ Martí i Franquès s/n, 08028 Barcelona, Spain.

The pressing need to produce more electric power has resulted in the construction of large coal-fired power plants in Europe. This has led to an increased coal consumption and, consequently, increased combustion waste generation. Considerable amounts of fly ash and slag are generated daily in power stations given the high coal consumption and the high mineral matter content of coal. If we consider a 1000 MW power station with a normal consumption of 12,000 tons of subbituminous coal per day, the fly ash production could be estimated at 2,000 tons per day. Usually less than half of the waste generated is used as a raw material mainly for cement and concrete manufacturing, the remainder being directly discharged into fly ash ponds or land fills. Nevertheless, other applications must be investigated in order to recycle the high fly ash production.

Zeolites can be obtained by hydrothermal treatment of fly ash [1-5]. The main applications of the natural zeolites, similar to those which can be synthesized after fly ash, are: a) sorbents for removal of ions and molecules in different solutions such as waste waters, radioactive wastes and gases [6-10]; b) ammonia sorbent for flue gas from coal-gasification [9]; c) production of blended cements [11]; d) replacement for phosphates in detergents [9].

In the present study the synthesis of zeolites after alkaline fly ash activation is studied as a function of the sample-solution ratio, chemistry of the solution and reaction time. The experiments were performed using fly ash from the Teruel power station (ENDESA, 1050 MW, 2200 tons fly ash / day) in NE Spain.

1. FLY ASH CHARACTERIZATION

The major inorganic phases in the fly ash studied are: aluminosilicate glass, mullite, quartz, magnetite, anhydrite, and lime. Aluminosilicate glass is the major constituent of the fly ash studied. Mullite, magnetite and quartz are present in the fly ash in concentrations of 15, 10 and 7 % respectively. Anhydrite and lime are minor constituents of the fly ash studied (<0.5 %). The Teruel fly ash is characterized by a high Fe content and a relatively low Ca content. The $\text{SiO}_2/\text{Al}_2\text{O}_3$ ratio is 1.8 which is an intermediate value with respect to fly ash used for zeolite

synthesis in previous works (2.6-1.6). The dominant grain size fraction is in the range of 50-20 μm (60 %).

2. METHODOLOGY

The activation of fly ash was performed by means of NaOH and KOH solutions in closed system. The zeolite conversion was studied as a function of temperature (60-200°C), time of reaction (8-100 h), sample/solution ratio (0.03-0.2 g/l) and solution concentrations (0.1-1 M).

The activation was carried out in a closed system using 4744 Parr digestion bombs with Teflon reactors. The activation done with alkaline solutions of NaOH, KOH and NaOH-KOH. The reaction took place in a laboratory furnace coupled with a CERBERE temperature controller ($\pm 0.1^\circ\text{C}$). Once the activation time was reached, the sample was filtered and washed with distilled water, dried at room temperature and analyzed by means of X-ray diffraction (XRD) using a SIEMENS D500 powder diffractometer with a graphite monochromator, NaI(Tl) detector and Cu K_α radiation. The morphology was studied by means of scanning electron microscopy (JEOL 6400 SEM) coupled with an energy dispersive X-ray spectrometer (LINK LZ5).

3. RESULTS

The mineralogical study demonstrated that the major reactive phases during zeolite synthesis after alkaline activation of the Teruel fly ash were: aluminosilicate glass and quartz (Figure 1). Mullite was found to be very resistant to the alkaline attack. A slight decrease in the mullite content was observed after 100 hours of activation with 1M NaOH solutions. Magnetite was not affected during the activation experiments.

The zeolites synthesized (Figure 2) were analcime and NaP1 zeolite after NaOH activation; analcime, merlinoite, NaP1 and phyllipsite after combined NaOH-KOH activation; and phyllipsite after KOH activation. Other trace reaction products identified were nosean, portlandite and bayerite. Maximum conversion rates were obtained with alkaline activation using NaOH 1 to 0.5 M and NaOH-KOH 0.1 M. However, the activation with KOH was less effective.

The activation and synthesis processes at 150°C (optimal temperature for zeolite synthesis [1]) were found to be time dependent until 24 hours of reaction. Although the maximum conversion rates were obtained after a reaction time of 100 hours, from 24 to 100 hours only a slight progressive activation was noticed (Figure 1). The results demonstrated that when increasing the temperature up to 200°C and the solution concentration (up to 1 M) the activation is more effective at lower reaction times (15-24 hours).

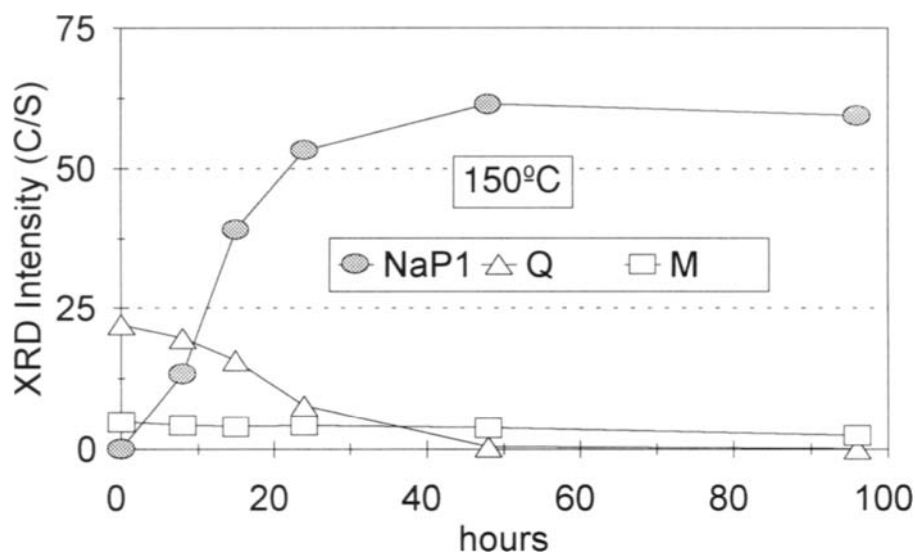


Figure 1. Evolution of NaP1 zeolite, quartz (Q) and mullite (M) during the experiments with 0.5M NaOH and a sample / solution ratio of 0.06 g/ml, obtained from 0 to 100 hours at 150°C. The XRD intensity values represent the intensity of the maximum reflection of each mineral (proportional to its concentration) in the different samples. Note the inflexion of the zeolite content at 24 hours of activation, and the proportional decrease in the quartz content.

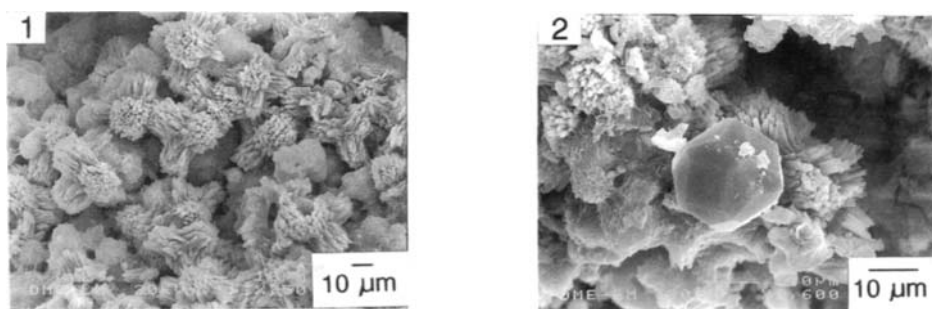


Figure 2. SEM photographs of the zeolites obtained from alkaline activation of the Teruel power station fly ash: 1. dendrites of Na-P1 zeolite on partially activated fly ash particles; 2 high crystalline analcime crystals and NaP1 crystals.

The most abundant zeolite obtained in the experiments was NaP1 zeolite. Analcime was synthesized in lower proportions than NaP1 zeolite after 100 hours of activation. However, only traces of analcime were identified at lower reaction times. These results and the morphological studies of the zeolites demonstrated two different processes of crystal growth: a) pure alkaline activation of the aluminosilicate glass, giving rise to dendritic and poorly-crystalline NaP1 zeolite (Figure 2); and b) dissolution of SiO₂ and Al₂O₃ from quartz and aluminosilicate glass and subsequent nucleation and crystal growth of high-crystalline analcime.

4. CONCLUSIONS

The results obtained show the potential application of fly ash for zeolite synthesis after alkaline activation. Higher activation efficiencies were found for the synthesis of the NaP1. The study of the mineral transformations produced during the activation of fly ash allowed us to deduce the activated material in fly ash (mainly glass and quartz). The experiments demonstrated that the time needed for an effective activation can be reduced by increasing the temperature and solution concentration.

REFERENCES

1. Höller H. and Wirsching U. *Fortschr. Miner.* 63 (1985) 21.
2. Mondragón F., Rincón F., Sierra L., Escobar J., Ramirez J. and Fernández J. *Fuel* 69 (1990) 263.
3. Shigemoto N., Shirakami K., Hirano S. and Hayashi H. *Nippon Kagaku Kaishi* (1992) 484.
4. Shigemoto N., Hayashi H. and Miyaura K. *J. Materials Sci.* 28 (1993) 4781.
5. Querol X., Alastuey A. Fernández-Turiel J.L. and López-Soler A. *Fuel* (1995) (in press).
6. Colella C. Use of natural chabazite and phyllipsite for removal of heavy metals from wastewater. *Zeolite-93, Idaho* (1993) 70.
7. Tsitsishvili G.V., Andronikashvili T.G., Kirov G. and Filizova L.D. 'Natural zeolites'. *Ellis Horwood* (1992) 295.
8. Zamzow M.J. and Schultze L.E. Treatment of acidic mine drainage using natural zeolites. *Zeolite-93, Idaho* (1993) 220.
9. Sand L.B. and Mumpton F.A. *Natural zeolites*. Pergamon Press (1978) 546.
10. García J.E., Gonzalez M.M. and Notario J.S. Phenol adsorption on natural phillipsite. *Zeolite-93* (1993) 95.
11. Sersale R. Zeolite tuff as a pozzolanic addition in manufacturing blended cements. *Zeolite-93* (1993) 183.

PRODUCTION OF POROUS MATERIAL FROM COAL ASH DISCHARGED FROM FLUIDIZED BED COMBUSTOR

Teruyuki Okajima, Yong Chen and Shigekatsu Mori*

Dept. of Chem. Eng., Nagoya University

Furo-Cho, Chikusa-Ku, Nagoya 464-01, Japan

(*Corresponding author)

INTRODUCTION

Above 50% of fly ash discharged from pulverized coal combustor (PCC-ash) are used by cement industry in Japan. Since the limestone is fed as the in-bed desulfurization material into the pressurized fluidized bed coal combustor (PFBC), PFBC ash contains considerable amount of CaSO_4 and unreacted CaO. PFBC-ash is difficult to feed into the cement kiln like as PCC-ash, since CaSO_4 is easily decomposed and then the sulfur is accumulated in the kiln. In case that PFBC-ash is used as the landfill materials, CaO contained in PFBC-ash is dissolved in water, consequently it is difficult to treat the PFBC-ash.

To utilize the PFBC-ash, various materials have been tried to be produced. However, most of them could not economically succeed to develop the industrial process.

PFBC ash consists of the fly ash collected from the cyclones and the filter, and of the boiler ash discharged from the combustor. The fly ash contains mainly SiO_2 , Al_2O_3 and Fe_2O_3 like as the clay. The boiler ash contains more calcium compounds such as CaSO_4 and unreacted CaO, CaCO_3 . These calcium compounds have the self-hardening property.¹⁾

In this paper, a new process to produce a heat insulator from PFBC-ash is proposed.

1. EXPERIMENTAL METHOD

1.1 Samples

Figure 1 shows a schematic diagram of Wakamatsu PFBC pilot plant in Japan. This PFBC-ash consists of filter fly ash, cyclone fly ash, bed ash and bottom ash. Since the properties of the filter fly ash is similar to that of the cyclone fly ash, and the properties of the bottom ash is similar to that of the bed ash, the filter fly ash and bottom ash are used here as the raw materials. Their chemical compositions are shown in Table 1.

The boiler ash contains more calcium compounds such as CaSO_4 and also $\text{Ca}(\text{OH})_2$, CaCO_3 . $\text{Ca}(\text{OH})_2$ and CaCO_3 are considered to be formed from CaO after discharged from

the PFBC plant. The particle sizes of the fly ash is under $100\mu\text{m}$ and the boiler ash are 37-210 μm .

1.2 Production Procedure

At first, the slurries are prepared by mixing the fly ash and the boiler ash with water in a stirred tank. Stir time is 5 minutes and the rate is 169 r.p.m.. The mixed ratio of the fly ash to the boiler ash (F/B) is changed from 0.6 to 2.0, and also the ratio of water to the total solid (W/S) is changed from 0.6 to 1.4. The slurries are fed into a wooden rectangular mold which size is 6.0 x 4.5cm and its height is 2.0cm and then this mold is settled in a curing box during 24h. The curing temperature is 353K and its relative humidity is 50%.

1.3 Characterization of Produced Material

The density of the produced heat insulator is determined by measuring its weight and volume. Thermal conductivity is measured by the hot-wire method of the unsteady-state heat flow. Its bending and compressive strength are measured by the tensile-compressive testing.

2. EXPERIMENTAL RESULTS

Figure 2 shows the external surface of the produced heat insulator, and it is found that the porous material can be produced. The porous material are formed by the evaporation of the water during its curing process.

Micro structure of the insulator observed by the scanning electron microscope (SEM) is shown in Figure 3. The network structure in the insulator is formed by acicular growth of the crystals.

Figure 4 shows X-ray diffraction (XRD) patterns of the insulator, and crystals of calcium silicate hydrates (tobermorite) and of calcium aluminate sulfate (ettringite) are detected. These crystals are produced by the pozzolanic reaction.

Figure 5 shows the effects of the ratios of (F/B) and (W/S) on the density, the thermal conductivity and the bending and compressive strength of the insulator.

It can be found from these figures that the density is 920-1280 kg/m^3 , the thermal conductivity is 0.04-0.08 $\text{W/m}\cdot\text{K}$, the bending strength is 0.3-1.4MPa and the compressive strength is 1.0-3.6MPa. These values decrease with increasingly the ratio of W/S until 1.0 and the effect of F/B is not clearly found.

The density, the thermal conductivity and the compressive strength of the insulator is compared with these determined values of the brick as B1 by Japan Industrial Standard. It can be demonstrated from this table that although the density of the insulator produced in this work is larger than that of B1 brick, the thermal conductivity is considerably smaller and also the compressive strength is better than that of B1 brick.

3. CONCLUSION

To utilize PFBC-ash, a new process to produce a heat insulator made from PFBC-ash is proposed, and it can be demonstrated that although the density of the heat insulator

produced in this work is larger than that of B1 brick, its thermal conductivity is considerably smaller and also the compressive strength is better than that of B1 brick.

ACKNOWLEDGMENT

This study is supported by GENERAL SEKIYU RESEARCH & DEVELOPMENT ENCOURAGEMENT & ASSISTANCE FOUNDATION.

REFERENCE

- 1) H. Ohhara, N. Hosoda and M. Ohhara ;Hardening Character of Fluidized Bed Combustion (F. B.C.) Ash, Proc. 46th Annual Conference, JSCE, 1991
- 2) T.Murakami, K. Miwa and K. Suda;Production test of ALC utilizing Coal ash, 4th conference on Coal Utilization Technology,1994
- 3) K. Nyuuraku;Sekitan Riyo Gijutu Jouhou, 16-2, Feb, 1995
- 4) H. Ohhara, H. Niijima and N. Hosoda;R&D on Utilization of Coal Ash General from F.B.C for Civil Material, 1st Conference on Coal Utilization Technology (CCUJ) Sept. 1991

Table 1 Composition of filter ash and bottom ash

	unburned carbon	CaSO ₄	Ca(OH) ₂	CaCO ₃	SiO ₂	Al ₂ O ₃	Fe ₂ O ₃	diff.
filter ash[%]	4.6	10.0	2.6	5.9	40.5	21.3	1.8	13.3
bottom ash[%]	0.0	27.1	29.3	19.4	11.3	4.3	3.6	5.0

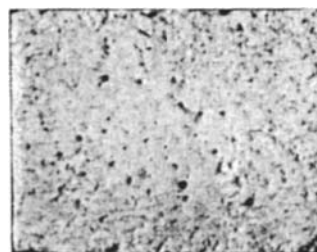
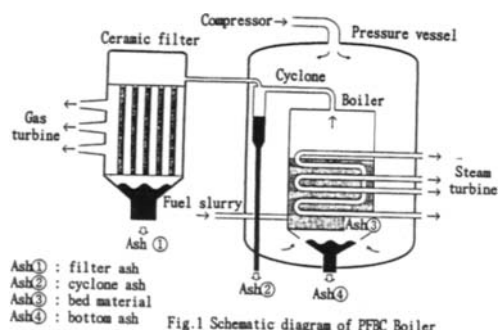


Fig.2 The external surface of the produced heat insulator

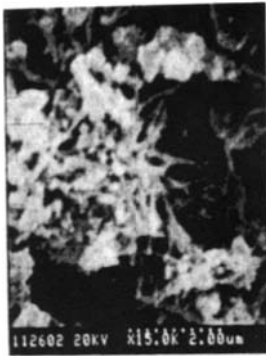


Fig.3 SEM photograph of the produced heat insulator

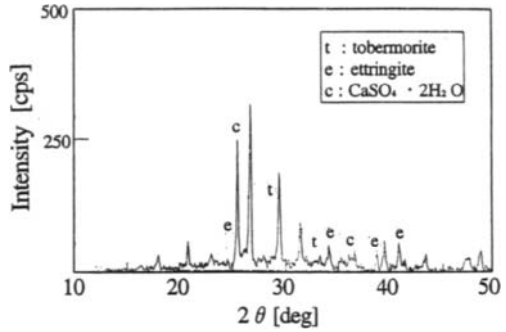


Fig.4 XRD pattern of heat insulator

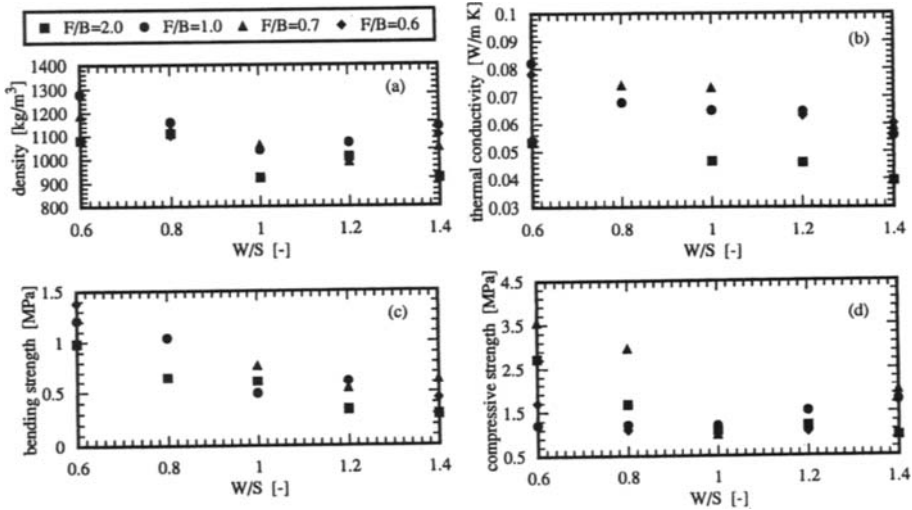


Figure 5 The effects of the ratio of water to solid and the ratio of fly ash to boiler ash on the density(a), the thermal conductivity(b), the flexural strength (c) and the compressive strength (d).

Table 2 Comparison heat insulator (F/B=2.0, W/S=0.6) with B1 brick

	density [kg/m ³]	thermal conductivity [W/m · K]	compressive strength [MPa]
heat insulator	1080	0.053	2.73
B1 brick	700	0.13	2.53

Synthetic aggregates from coal-fired fluidized-bed combustion residues

R. A. Winschel, M. M. Wu, and F. P. Burke

CONSOL Inc., 4000 Brownsville Rd., Library, PA 15129, USA

1. INTRODUCTION

The combustion of coal in a fluidized bed of limestone or dolomite is one method for controlling the emissions of sulfur dioxide (SO₂) that may result from the production of power or steam from coal. In a fluidized-bed combustor (FBC), the coal sulfur is captured as CaSO₄, and a solid by-product consisting of CaSO₄, coal ash, and unreacted sorbent (CaO) is produced. This FBC ash must be utilized, or disposed of at considerable expense. The cementitious property of FBC ash makes it possible to use it in the construction industry and the high volumes of materials used in construction make this an attractive potential market for ash. This paper will describe the development, preparation, and properties of synthetic aggregates produced from FBC ash for highway construction. The aggregates are produced in a three-step process consisting of hydration, disc pelletization, and curing. The durability of the synthetic aggregates is of particular concern; developments leading to increased durability of the aggregates will be described.

2. SUMMARY

Synthetic aggregates were produced from the ash of a commercial coal-fired FBC. Even though the aggregates meet engineering specifications as Class A aggregate, they had poor durability in freeze/thaw tests. A cause of the poor durability was found to be the slow conversion of anhydrite to gypsum. Diluting the FBC ash with pulverized coal (p.c.) fly ash greatly improves the synthetic aggregate durability. The synthetic aggregates produced are strong, abrasion resistant and durable, and they meet engineering specifications for use as aggregates in portland cement and asphalt concretes. Preliminary economics suggest that it should be feasible to produce and market the aggregates, if avoided waste disposal costs are considered.

3. EXPERIMENTAL

The FBC ash was produced at a coal-fired circulating FBC unit (182,000 kg/h steam) at a cogeneration plant burning Pittsburgh seam coal. The material used (Table 1) was taken from the silo that contains both the fly ash and the bottom ash of the FBC. The pulverized coal (p.c.) fly ash was produced at an electric generating station that burns Pittsburgh seam coal. The analyses of these materials appear in Table 1.

Table 1
Analysis of FBC by-product and p.c. fly ash

Date Sampled:	FBC Ash			p.c. Fly Ash
	9/2/93	3/14/94	10/27/94	
Moisture, wt % as rec'd	0.08	0.08	0.19	0.22
<u>Ultimate Analysis, wt % dry</u>				
Carbon	3.48	3.45	3.33	1.73
Hydrogen	0.07	0.09	0.00	<0.01
Nitrogen	0.05	0.02	0.06	<0.01
Sulfur, total	6.00	5.58	6.05	0.41
Ash @ 399 °C	94.18	90.2	94.52	97.23
<u>Major Element, wt % dry</u>				
SiO ₂	12.03	13.85	14.10	47.43
Al ₂ O ₃	5.30	5.75	6.52	21.38
TiO ₂	0.22	0.22	0.27	1.02
Fe ₂ O ₃	4.36	4.48	5.19	21.42
CaO	47.81	45.08	41.02	2.85
MgO	7.19	8.85	9.09	0.89
Na ₂ O	0.24	0.25	0.38	0.40
K ₂ O	0.69	0.88	1.15	2.03
P ₂ O ₅	0.13	0.15	0.15	0.37
SO ₃	15.41	14.48	17.14	1.06
Ca/S Mol. Ratio	4.43	4.45	3.87	-
Lime Index (a), wt %	28.0	25.7	21.3	-

(a) Based on CaO

Synthetic aggregates were produced semi-continuously in 110 kg batches from the FBC ash (or blends of FBC ash and p.c. fly ash) by a three-step process. The dry ash was first hydrated by mixing it with the appropriate amount of water in a Littleford Brothers LM-130 batch mixer. The hydrated ash was pelletized with an additional amount of water on a 91 cm ID rotary disc pelletizer (total water added during hydration and pelletization is about 18 wt % of the dry ash). The pellets were cured for 24 h at ~82 °C and 90% relative humidity in a 208 L curing vessel. The size distribution of the pellets can be selected by varying the pelletizing conditions; most of the pellets were between 1.5 cm and 4 mesh for this work. The pellets are generally spherical in shape but they can be crushed to produce angular shapes for use in asphalt concrete. The pellets were evaluated as synthetic aggregates for use in portland cement and asphalt concrete by a variety of determinations and tests. Physical determinations included grain size distribution and crush strength (mean of 30 reported, typical standard deviation is 10 kg). American Society for Testing and Materials (ASTM) tests included bulk specific gravity (ASTM C127), LA abrasion index (ASTM C131), soundness index (ASTM C88-83), unit weight (ASTM C29), and water absorption (ASTM C127). Freeze/thaw tests were conducted in which the aggregates are sized into 1.3 x 0.95 cm and 0.95 cm x 4 mesh fractions, immersed in water for one day, temperature-cycled 50 or more times from -18 to 10 °C over the course of seven days, then sized again to determine particle size degradation. The results of these tests were compared with American Society of State Highway Transportation Officers (AASHTO) specification M-283 for Class A aggregates.

4. DISCUSSION

Three samples of FBC by-product were taken over the course of 13 months to evaluate the variability of the material. During this time, the plant burned coals with sulfur contents from 1.4% to about 2.5%. As shown in Table 1, the properties of the by-product were fairly constant; the major changes are small variations in the Ca and S contents. Synthetic aggregates of essentially equivalent quality were readily produced from all three samples of by-product. The small variations in the properties of the three samples required small changes in the water addition rate.

The physical properties of various batches of synthetic aggregates produced from FBC by-product are shown in Table 2. Shown for comparison are the properties of two commonly used natural Class A aggregates and AASHTO specifications for Class A aggregates. The aggregates made from 100% FBC by-product meet Class A specifications; however, testing over the course of one year showed that their soundness index degraded with storage time. The aggregates produced with blended fly ash did not suffer from this problem; therefore, later work was limited to FBC by-product/fly ash blends.

Synthetic aggregates were produced from five blends of FBC ash and p.c. fly ash that ranged from 90/10 to 50/50 FBC ash/fly ash. All batches easily pass the LA abrasion index specification. The 90/10, 75/25 and 57.5/42.5 blends have crush strengths greater than 90 kg and all meet the soundness index specification; the 50/50 blend has poorer strength and soundness index. All batches that were tested meet the unit weight specification. Unit weight is a function of specific gravity and particle size distribution. The specific gravities of the aggregates from all batches are similar and, since the size distribution can be controlled by pelletizer operating conditions, any of the blends could meet the unit weight specification. However, it is apparent that both the specific gravity and unit weight of the synthetic aggregates are substantially lower than those of the natural aggregates.

Freeze/thaw tests showed that, even though the 90/10 aggregates had a low soundness index, their durability was poor. Thermogravimetric analysis and X-ray diffraction analysis indicated that the slow conversion of anhydrite (CaSO_4) to gypsum ($\text{CaSO}_4 \cdot 2\text{H}_2\text{O}$) was one cause of the poor durability of the synthetic aggregates. The addition of fly ash improves the durability of the aggregates, presumably by diluting the gypsum precursor and by providing aluminum species that can react with anhydrite to produce ettringite ($\text{Ca}_6\text{Al}_2(\text{SO}_4)_3(\text{OH})_{12} \cdot 26\text{H}_2\text{O}$), thus reducing the formation of gypsum.

The freeze/thaw tests show that the 65/35 blend has the best durability. On the basis of durability and the other properties, the 65/35 blend was selected for further development. A longer curing time (48 h) reduced the water absorption of the 65/35 aggregate but was ineffective at further improving the durability.

When used in bituminous concrete, aggregates are coated with asphalt. The aggregates produced from the 65/35 blend were coated with 5% AC-20 asphalt and subjected to the freeze/thaw test. The coating substantially reduces the freeze/thaw degradation of the aggregates (Table 2). Thus, when used in bituminous concrete, the 65/35 aggregates are strong, abrasion resistant, and durable and they meet all specifications for use as Class A aggregate.

Class A aggregate prices are dependent on location. However, a typical price in the mid-Atlantic region of the U.S. is \$5.50 to \$7.50/tonne. Pelletization costs are

estimated to be \$8 to \$11/tonne. Therefore, it appears that production of synthetic aggregates from an FBC/fly ash blend is economically feasible if waste disposal costs minus shipping costs are greater than \$5.50/tonne. In the U.S., combustion by-product disposal costs for a new facility range from \$9 to \$18/tonne.¹ If the entire FBC by-product generated at the plant in question (39,000 tonne/y) were blended with 35% fly ash and the appropriate amount of water, the yield of aggregates would be 51,000 tonnes/y. The market for aggregates is so large (over 1 billion tonnes/y for crushed stone alone in the U.S.²), that this additional production would have little impact on the market price of aggregates.

Table 2
Properties and specifications of aggregates

Description	FBC Ash/Fly Ash								Gravel	Lime- stone	AASHTO M-283 specs
	100/0	90/10	75/25	65/35	57.5/ 42.5	50/50	65/35 (b)	65/35 (c)			
LA abrasion, % wear	27	23	25	19	18	22	-	-	28	21	40, max
Soundness, % loss (a)	7	0	6	12	39	28	47	-	8	8	12, max
Unit wt, kg/m ³	1153	1137	1233	-	-	-	-	-	1554	1650	1120, min
Crush strength, kg	86	95	95	91	94	74	100	-	141	92	-
Water absorption, %	3.9	4.1	3.8	3.7	3.3	3.6	1.8	-	1.7	0.5	-
Specific gravity	1.98	2.01	2.04	2.00	2.06	2.02	2.19	-	2.52	2.67	-
Freeze/thaw degrad., %											
1.3 x 0.95 cm fraction	-	86	54	23	43	37	40	8	2	1	-
0.95 cm x 4 mesh fraction	-	71	29	18	20	17	25	4	2	2	-

(a) after 5 cycles with sodium sulfate

(b) 48 hr cure

(c) 5% asphalt coating

5. ACKNOWLEDGMENT

This work was partially supported by the Ohio Coal Development Office under Grant Agreement No. CDO/D-902-9.

REFERENCES

1. U.S. Department of Energy, Office of Fossil Energy, Morgantown Technology Center, "Report to Congress, Barriers to the Increased Utilization of Coal Combustion/Desulfurization By Products by Governmental and Commercial Sectors", July 1994.
2. Terpodei, V. V. "Construction Aggregates", Mining Engineering June 1994, p. 530.

The relationship of mineralogy and strength development in dry FGD derived cements

U. Graham^a, K. G. Sutterer^b, and T. L. Robl^a

^aCenter for Applied Energy Research, University of Kentucky
Lexington, Kentucky, USA 40511-8433

^bDepartment of Civil Engineering, University of Kentucky
Lexington, Kentucky, USA 40506-0281

1. INTRODUCTION

Dry flue gas desulfurization materials (FGD), including bed and fly ash from fluidized bed combustion technology as well as spray-dryer scrubbers and lime burner injection materials, exhibit cementitious properties and swell when wetted. These materials have the potential to be utilized as structural fill in mines and other construction. However, the geotechnical properties of these materials are not well understood. Typically, swelling leads to strength loss, so an understanding of the relationship between strength gain due to cementation and strength loss due to swelling is necessary.

The swell and strength gain are related to mineral crystal formation. Ettringite needles are often found together with calcium silicate hydrates and gypsum in dry-FGD materials after hydration. The calcium silicate hydrates contribute to the strength of the materials, and it has been suggested that early mixture strength is in part due to the formation of a network of ettringite needles. However, the formation of ettringite and other hydrate phases may also cause swell. This study investigated the relation between mineralogy and strength gain for mixtures comprised mainly of a typical dry FGD derived cement.

2. MATERIAL SELECTION, ADMIXTURES, AND MIX PROPORTIONING

The fly ash from a circulating fluidized bed combustor (CFBC) was evaluated. The bottom ash from the same combustor was also collected for use as a possible admixture and a type F fly ash was acquired from a different site for use as an additive. The CFBC fly ash will be referred to herein as FGD, the bottom ash as BA, and the type F fly ash as FA.

Proximate and ultimate analyses of the materials were performed using ASTM standards. X-ray diffraction (XRD) was carried out on the CFBC fly ash using powder mounts and CuK α radiation (7-60 2 θ). Scanning electron microscopic-energy-dispersive-X-ray (SEM-EDX) analyses were also conducted. The main mineral ingredients in the raw material are anhydrite (CaSO₄), portlandite (Ca(OH)₂), free lime (CaO - 28 to 31 percent in FGD and BA), quartz (SiO₂ - 16 percent in FGD and 12 percent in BA), and minor calcium carbonate (CaCO₃). The FA contained a significant amount of silica and alumina, and the presence of these components was expected to be beneficial to the pozzolanic reaction and strength gain. The aluminum should also contribute to ettringite formation.

The hydration of the CaO and to a lesser extent, CaSO₄, is an exothermic reaction releasing heat. Initial mixing of water with FGD resulted in mix temperatures over 100°C after several minutes, an undesirable condition for field placement. Early mix design attempted to minimize this temperature rise while optimizing workability and strength. Four mixes were considered in this study: raw FGD; raw FGD mixed with BA; raw FGD mixed with FA; and prehydrated FGD. FGD prehydration was performed to allow heat release due to hydration before final mixing. Hydration with 12-15% water and 85-88% FGD was found to be sufficient to eliminate most heating during final mixing. The actual prehydration rate was about 8% of the original mixture because some of the hydration water was lost as steam. The prehydrated FGD exhibited no temperature increase during final mixing, and the FGD with FA exhibited moderate temperature increase to 40-70°C due to the added mass of nonexothermic FA. The FGD/BA mixes exhibited excessive temperatures and swelling during mixing, and the use of this mixture was abandoned.

3. PHYSICAL PROPERTIES

Physical characterization of the mixtures focused on two methods: free vertical swell (similar to ASTM D 4546 Method B) and unconfined compressive strength (similar to ASTM D 2938). The unconfined compressive strength of mixtures already judged to have suitable workability and temperature was optimized to select a most desirable mix design for 30 day strength. The free vertical swell was measured to characterize the swell potential of the materials in different curing environments and develop an approximate relation between the free vertical swell and unconfined compressive strength.

3.1. Unconfined compressive strength

The 76 mm dia. by 152 mm long unconfined compression strength specimens (UCS) were constructed with no compaction to simulate typical field placement densities. The specimens were cured in the molds at 13°C until there was sufficient strength gain (usually 3 days) for mold removal, after which the specimens were returned to the curing chamber until 30 day testing. The effect of curing moisture was considered by curing under 85% relative humidity (R.H.) or with full submergence in a water bath. The UCS were performed on mixes consisting of raw FGD with no admixtures or prehydration, raw FGD with FA, and prehydrated FGD. The results are summarized in Table 1. The prehydrated (PH) FGD showed the highest UCS, but the effect of curing water was dramatic. The 30 day UCS of the tank-cured mixes were much less than the UCS of the specimens cured in 85% R.H.

Table 1
Physical Properties

	Mix Temp. (°C)	30 day 85% R.H. Cured		30 day Tank Cured		30 day free vertical swell (%)
		UCS (psi)	Approx. vol. swell (%)	UCS (psi)	Approx. vol. swell (%)	
raw FGD	80-100	300-600	4-10	10-15	20-30	4-5
raw FGD/FA	40-60	100-200	4-10	-	-	4-5
PH FGD	20-25	1000-1500	0.2-0.5	100-200	10-15	0.5-1

3.2. Unconfined Swell

The volumetric swell of some of the UCS specimens during curing was estimated. The results, shown in Table 1, showed a strong correlation between strength loss and swell. To more accurately measure potential swell under typical adit conditions, free vertical swell tests were conducted on laterally confined specimens with only top and bottom drainage. These specimens were formed with no compaction to a height of approximately 101 mm in 152 mm diameter steel molds. The test specimens had no significant vertical stress, were provided with top and bottom drainage, and were submerged in individual curing tanks at 13°C to simulate the ground curing environment. The results are given in the right column of Table 1. The results verify that prehydration reduced swell, while the addition of FA to the raw mixture would have had no effect on the swell. It is also apparent that reduced access to water reduced the swell for a given mixture.

4. MINERALOGICAL ANALYSES

XRD methods were performed on the above specimens. SEM examination of the specimens provided visual information to supplement the findings. The tank cured specimens exhibited obvious differences in swell between the top and bottom of the specimens. It was not possible to determine whether this differential swell was caused by differences in specimen construction, mix variation, or curing environment, but this phenomena provided an opportunity to compare mineralogical characteristics of different swell behavior within a single specimen.

In all samples, new mineral formation included calcium hydroxide, ettringite C-S-H and gypsum. Calcium hydroxide and ettringite formation occurred within 14 days of mixing all specimens while curing at 85% relative humidity. Mixtures consisting of prehydrated FGD developed networks of interlocked ettringite crystals inside available pore space. These crystals are partly responsible for strength gain. Conversely, raw FGD mixtures that exhibited high swell (tank-cured and 85% R.H.-cured) showed more gypsum formed at the expense of anhydrite (CaSO_4) and reprecipitation of gypsum, which results in an increase in molar volume (~78%). The formation of large gypsum crystals correlated with areas of destructive crack formation in the specimens. Similar cracking and gypsum formation was apparent to a lesser extent in the tank-cured prehydrated FGD specimens which showed lower strengths than the specimens cured at 85% relative humidity. There appeared to be a correlation between increased gypsum formation and reduced ettringite formation with reduced specimen strength and increased swell. The formation of ettringite did not appear to be the primary cause of specimen swelling.

5. INTERPRETATION OF FINDINGS

Based on the mineralogical studies, the swell behavior appears to be composed of three phases: (1) primary swell caused by hydration of free lime, (2) secondary swell caused by formation of ettringite crystals, and (3) tertiary swell due to hydration of anhydrite to gypsum.

The primary swell during hydration of free lime is eliminated by prehydration, and even in the case of no prehydration, is likely to be completed during or immediately after mixing before few cementing bonds have developed in the mixture.

Secondary swell due to ettringite formation begins immediately upon addition of water and continues for days if nutrients are present for ettringite crystal growth. The type and size of ettringite crystals, which will effect swell, seems to be related to the kind of substrate surfaces which act as nucleation surfaces for the ettringite. In this study it was determined that ettringite crystals prefer to nucleate on C-S-H gel surfaces and continue to grow into available pore spaces. This growth into the pore spaces could eventually fill the pores and reduce specimen permeability. Continued growth of ettringite and, in the presence of CO₂, thaumasite, depends on equilibrium pH and the availability of sulfur and aluminum. It is possible that addition of FA to the mixture could thus encourage formation of ettringite and thaumasite, but more research is required to obtain conclusive results.

The tertiary gypsum formation from anhydrite is difficult to predict since it depends on the character (degree of crystallinity) of the anhydrite crystals. Thermodynamically, the transformation of anhydrite to gypsum would be favored under the curing conditions in this study. However, the type of anhydrite in the raw material may cause retarded reaction mechanisms, thus resulting in larger long term swell that can be damaging to the specimens.

The effect of the mineralogical changes on the strength appears related to both the quantity and location of gypsum and ettringite mineral formation. The formation of ettringite crystals in the pore spaces between particles creates a network of crystals that reinforce and strengthen the specimen structure. The swell related to the formation of the ettringite may not be highly detrimental during the first 30-60 days of curing, while the strength gain may be significant. Conversely, the gypsum formation appears to be more likely to occur at interparticle contacts. The molar volume change during gypsum formation causes swell at these locations and the pressure associated with crystal formation exceeds the strength of the bonds created by the ettringite, thus breaking the cementations and leading to strength loss.

The curing environment effects the physical properties by accelerating the formation of gypsum in the specimen. It is possible the specimens that exhibited higher strengths and lower swell still possess the potential to eventually swell and lose strength, but the reaction was delayed by the reduced availability of water. Thus, the changes in strength and swell with time will depend on the availability of water to the specimen.

6. CONCLUSIONS

The physical behavior of specimens created from dry-FGD derived cements over time depend on curing environment, particularly water availability, and initial mix properties. The mineralogical and physical studies described herein provide evidence that the formation of gypsum from anhydrite in an environment containing excess water contributes to dramatic swell and strength loss over 30 days' curing. Ettringite formation does not appear to contribute as significantly to strength loss over this time period, while it may significantly enhance strength. Development of a mix for use in engineered applications, such as filling mine adits, will depend not only on initial mix chemistry but also on the availability of water in the environment where the fill is placed.

7. ACKNOWLEDGMENTS

The support of the US. Department of Energy for funding of a larger study, of which this was only a part, is gratefully acknowledged.

Reutilisation Studies for Brown Coal Fly Ash

U. Lenz, H. Meyrahn, N. Möhlenbruch, H.-P. Päßgen and M. Reich-Walber

Rheinbraun Aktiengesellschaft, Research and Development
Sibylla Research Centre, P.O. Box 41 08 40, 50868 Cologne, Germany

About 85 % of the 100 Mt/a of brown coal currently extracted in the Rhenish mining area is fired for power generation in the large power plants of RWE Energie AG. Here, steam coal having ash contents of more than 2.5 % wt. is used. Around 15 Mt/a of brown coal with lower ash contents is supplied as briquetting coal to Rheinbraun's upgrading plants for the production of briquettes, fluidized-bed coal, pulverized coal and rotary hearth furnace coke. Approximately one quarter of this amount is fired in the three Rheinbraun-owned mine-mouth power plants to produce process steam and electric power. In this process, approx. 80,000 t/a of fly ash having high CaO and MgO contents is obtained. Some investigations which were made in respect of these substances' possible applications will be introduced in the following.

1. CHEMICAL COMPOSITION OF THE ASH

Table 1 shows the chemical composition of the ash from Rhenish briquetting coal. The oxides CaO and MgO give the ash its typical basic character and bind a

Tab. 1: Oxid analysis of ash
(mean values)

Tab. 2: Contents of trace elements in ash and
their solubility

Oxid analysis in % wt.		Trace element	Mean values mg/kg	Water-soluble contents (mg/kg**)
SiO ₂	10	Arsenic	12	< 0,001
Fe ₂ O ₃	15	Boron	500	< 0,1
Al ₂ O ₃	3	Lead	15	< 0,005
CaO	45	Cadmium	0,5	< 0,0002
MgO	11	Chromium	21	< 0,03 - 0,1
SO ₃	13	Molybdenum	< 5	< 0,1
Na ₂ O	1	Mercury	0,4	< 0,002
K ₂ O	0,5	Selenium	18	< 0,002
MnO	0,5	Vanadium	14	< 0,01
		Zinc	34	< 0,001 - 0,07

<) below the detection limit

***) Elution according to DIN 38 414-S4

considerable portion of the sulfur oxides contained in the flue gas mostly as anhydrite CaSO_4 and, to a minor extent, as MgSO_4 . The mineral phases anhydrite, free lime, brownmillerite, quartz, periclasite and haematite predominate.

In contrast to hard coal ash and especially ashes from waste incineration, the heavy metal content of ash from briquetting coal is low, and the solubility of arsenic, chromium, lead, mercury, etc. is extremely low as well (Tab. 2). The content of boron, which is considered to be a micronutrient, in the ash from briquetting coal is high; in the aqueous phase, the constituents having a basic effect reduce the solubility of boron to such an extent that there is no boron toxicity.

2. INVESTIGATIONS INTO THE SUITABILITY OF ASH AS LIME FERTILIZER

Due to its 45 to 55 % of basic constituents, the ash from briquetting coal can be compared with lime fertilizers in terms of its basicity.

The incorporation of the ash from Rhenish briquetting coal into the Fertilizer Regulation [1] required comprehensive investigations into its suitability; these investigations mainly included the ashes' detailed chemophysical characterization, vegetation tests on various soils fertilized with different ash contents, conversion tests in respect of changes in the pH-values, and reactivity tests.

The experimental plants were barley and sugar beet. Ash application on the acid soil at medium and higher lime doses produced barley yields comparable to those obtained when using the two commercially available reference limes; for sugar beet, ash application on the slightly acid para-brown earth led to higher yields in most cases (Fig. 1).

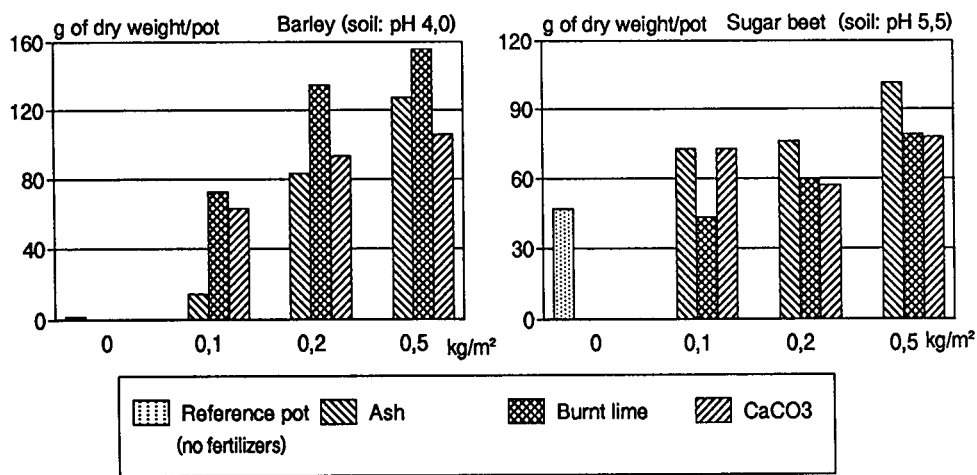


Fig. 1: Yield data for barley and sugar beet (g of dry weight per pot: mean value of 4 pots)

The conversion tests with differently acidified soils demonstrated that the pH-values in the soils obtainable with commercially available limes only slightly exceeded those produced by using ash. Reactivity tests showed that, compared with commercially available limes, the ash

converts at a slower rate in the beginning (Fig. 2). In the course of time, this difference diminishes due to a sustained mobilization of the ash's basic constituents.

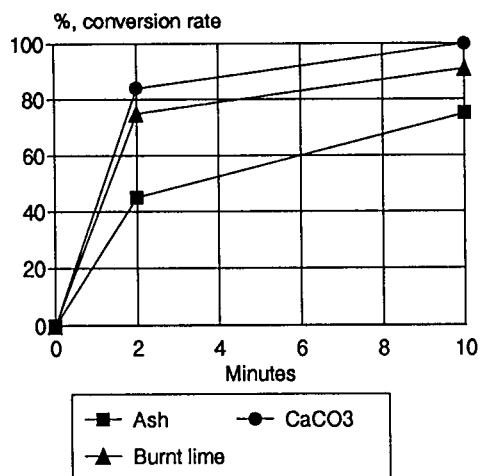


Fig. 2: Conversion rates of various liming agents

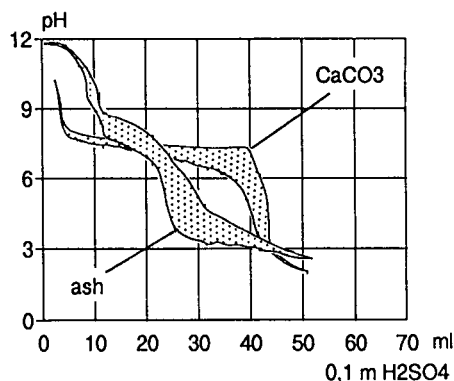


Fig. 3: Long-term titration curves for ash and CaCO₃

Due to the positive results obtained, the ash from briquetting coal was incorporated into the Fertilizer Regulation under the type designation 'Residual Lime' [1]. The primary application recommended is regular maintenance liming to buffer the pH-values of acidified soils.

3. USE OF FLY ASH IN FORESTRY

In addition to the Fertilizer Regulation, there exist so-called 'Liming Decrees' which govern the implementation of liming measures in German forests. These decrees list the names of those lime fertilizers that are suitable for forest liming.

Original concerns that liming with ashes from briquetting coal would involve increased sulfate loads due to the sulfate content (see Tab. 1: indicated as SO₃ in the oxide analysis) could be eliminated by theoretical calculations and practical laboratory tests.

Within the scope of laboratory tests, ash from briquetting coal and CaCO₃ were characterized for forest liming [2]. These investigations included, among other things, the elution behaviour and various titration methods aimed at characterizing reactivity. The titration methods--in particular long-term titration (Fig. 3)--showed two clearly different buffer zones for the ash investigated: on the one hand, a high initial reactivity at pH-values from around 12 onwards and, on the other hand, another relatively distinct buffer zone at pH-values below 9.

In conclusion, it was possible to demonstrate that, thanks to its high basic capacity, ash from briquetting coal has a high reactivity for buffering acids that is almost comparable to that of the pure substance calcium carbonate and thus makes the ash suitable for liming acid forest soils. The capacity to bind acids results from the free lime's rapid reactions and the additional buffering effect of further basic constituents.

Thanks to the successful investigations the ash was licensed for forest liming at the end of 1993.

4. USE OF ASH AS LIME SUBSTITUTE FOR THE PRODUCTION OF SAND LIME BRICKS

During an operational test performed in a sand lime brick plant approx. 50,000 bricks were produced with brown coal ash addition. In this process, brown coal ash can easily substitute around 25 % wt. of fine white lime, which is the most important feedstock material besides quartz sand. The raw density of 1.45 kg/dm³ and compressive strengths of more than 16 MN/m² were in the range of the bricks produced without ash addition. Colouring of the bricks by the red-brownish ash was practically not detectable. The bricks from the operational test were used as backing bricks and did not give rise to any complaints.

5. USE OF ASH IN EARTHWORKS AND FOUNDATION ENGINEERING

Part of the ash occurring in Rheinbraun's mine-mouth power plants is spread by means of the poldering technique in a way similar to [3]. Mixtures of spread polder ash and the originally dry ash at ratios of approx. 2:1 constitute a suitable dam construction material for polder heightening. Suitability was demonstrated by lab-scale and structural tests. This polder heightening was first implemented in the Ville-Berrenrath upgrading plant in 1994 and is planned to be continued in the future.

Furthermore, investigations were made into the ash's suitability as binding agent component in a mixture with granulated blast-furnace slag for the construction of hydraulically bound sub-bases in road building. The mixture of ash, granulated blast-furnace slag, mineral substances and water at a weight ratio of 1.5 : 4.5 : 94 : 7.5 yielded the required compressive strength of 4.3 MN/m². Another application in road construction is the immobilization of polycyclic aromatic hydrocarbons (PAHs) in the reutilization of broken-up tar-containing road surface material in the sub-base. Ash portions of 40 - 80 kg and cement portions of 40 - 120 kg (depending on the quality of the broken-up road surface material) per m³ of the total mixture immobilize up to 90 % of the PAHs.

REFERENCES

1. Bundesgesetzblatt; Jahrgang 1993, Teil 1, Erste Verordnung zur Änderung der Düngemittelverordnung v. 25.1.1993
2. U. Bartels and N. Asche; Verfahren zur Charakterisierung von Düngemitteln für die Waldkalkung (Chemie in Labor und Biotechnik; 1993 No. 3; pp. 218-221)
3. P. Zenker; Braunkohle 40 (1988), No. 3, p. 69

SEPARATION OF FLY ASH USING DENSITY GRADIENT CENTRIFUGATION

S.R. Palmer, S. Sivanandan and W. Huggett*

Department of Mechanical Engineering and Energy Processes, *Illinois Coal Development Park, Southern Illinois University at Carbondale, Carbondale Illinois 62901-6603, USA.

1. INTRODUCTION

The mineral matter in coal is transformed into a residue or ash when coal is combusted. Both the quantity and the type of minerals in coal can vary considerably and this dictates not only the quality of the coal but the nature of the ash that is formed.(1) In the United States about 80 million tons of coal combustion residue, most of which is fly ash, is produced every year. This high volume waste material has created a number of waste management problems.(2) Consequently there has been considerable effort from the scientific community in order to identify acceptable disposal or utilization options.(3)

Perhaps one of the better utilization options for fly ash is its use in concrete formulations.(4) Not only is the concrete industry large enough to accommodate the quantities of fly ash produced, but the pozzolonic nature of fly ash adds long term strength to concrete structures.(5) Despite the potential of this utilization option only 25% of the fly ash produced in the United States is currently utilized.

The motivation for the work reported here was the development of a lightweight concrete using high percentages of fly ash. Since it easier to produce a lightweight concrete if the starting materials are of lower density, the separation of fly ash into fractions of lower bulk density was investigated. To identify the bulk and trace element chemistry of the density fractions, and therefore help determine their suitability for use in concrete formulations, each was analyzed by Scanning Electron Microscopy - Energy Dispersive Analysis of X-rays (SEM-EDAX) and by Inductively Coupled Plasma - Emission Spectroscopy (ICP-ES).

2. EXPERIMENTAL

2.1 Density Fractionation of Fly ash

To investigate the possibility that fly ash could be separated into fractions of differing density an aliquot of fly ash was processed by the technique of density gradient centrifugation (DGC). The technique of DGC involves establishing a density gradient that covers the desired density range, loading a finely divided sample of the analyte at the top of the gradient, and then spinning the whole system in a centrifuge. During spinning the particles of different density report to the zone of the density gradient that has the same density as the particle. After spinning the density gradient solution which now contains the suspended particles of different density is pumped out into a series collection tubes. The material in each tube is recovered by filtration, weighed and the yield plotted against density to give the density profile of the material. For the separation of the fly ash six density zones were established. These

were specific gravities 1.0-1.3, 1.3-1.6, 1.6-1.9, 1.9-2.2, 2.2-2.4 and above 2.4. Solutions of these densities were prepared using sodium polytungstate. During preparation of the sample slurry for DGC a fraction of the fly ash was seen to collect on the magnetic stir bar. This magnetic material was retained and analyzed as a separate fraction.

2.2 Bulk chemistry by SEM-EDAX

Each of the separated density fractions, the magnetic component and an aliquot of the unseparated fly ash were examined by SEM-EDAX. The elements quantified using this technique included Na, Mg, Al, Si, P, S, K, Ca, Ti, Mn and Fe. Percentages of the elements were reported as their oxides. The accelerating voltage was 20.5 KeV, the electron beam incident angle was 45.0 degrees and the X-ray emergence angle was 50.2 degrees.

2.3 Trace element chemistry by digestion/ICP-ES

An aliquot of each sample mentioned in section 2.2 was also digested according ASTM method 3050 and the digestate analyzed for trace element content using ICP-ES. The digestates were filtered and made up to a standard volume. The elements examined were Fe, Pb, Cu, Se, Cr, Cd, Zn, Ni and Co.

3. RESULTS AND DISCUSSION

3.1 DGC density profile

The yields of fly ash in each density fraction are shown in Figure 1. It can be seen that most of the fly ash sample (approx. 90%) has a density above 1.9 g/cm³. Indeed nearly half of the sample has a density greater than 2.4 g/cm³. Since only a very small amount of this fly ash has a reasonably low specific gravity it appears unlikely at this time that enough low density material could be isolated to significantly enhance light-weight concrete production. Of course, other fly ash samples may have a completely different density profile and it may be possible to isolate low density materials from them in high yield.

From the density of the major chemical phases in fly ash, SiO₂, Al₂O₃ and Fe₂O₃ (2.64, 3.97 and 5.24 g/cm³ respectively), and their typical relative composition in fly ash of approximately 60%, 25% and 15% respectively, it is possible to calculate the average particle density if it were completely solid. This gives an average particle density of 3.36 g/cm³. Of course this calculation is crude because it does not take into account other phases that are present in the fly ash and it assumes that the composition is independent of particle density. However using this figure we can calculate the average percentage void space in the fly ash particles in each density fraction. Performing these calculations indicates that for particles of bulk density 1.15, 1.45, 1.75, 2.05 and 2.30 g/cm³, the percentage void space is 66%, 57%, 48%, 39% and 32% respectively. From this it is clear that even the denser particles have significant void space within them.

3.2 Bulk chemistry

SEM-EDAX allowed for particle size and morphology, as well as bulk chemistry, to be investigated. Interestingly an apparent reduction in particle size was observed as density increases. As can be seen from Figure 2, spherical particles as large as 0.3 mm were observed in the lowest density fraction. In addition, some relatively large crystalline phases were observed in the fractions having a density range of 1.3 to 1.9 g/cm³. Analysis of the fluorescent X-rays produced by the defocussed electron beam was used to establish the bulk chemistry of the fractions in terms of the oxide content. Based upon previous

determinations of this type Si, Al, Fe, Na, Ca, K, Ti, Mg, S and Mn were determined as their oxides. The results for Si, Al and Fe are shown in Figure 3.

As can be seen from Figure 3 each fly ash fraction is predominantly composed of SiO_2 (ave. 60%), Al_2O_3 (ave. 20%) and Fe_2O_3 (ave. 10%). It can be seen that for fractions that have more Al_2O_3 and Fe_2O_3 less SiO_2 is observed. This is seen most clearly for the highest density fraction where the Al_2O_3 and Fe_2O_3 contents increase to about 25% while the SiO_2 content falls to around 45%. The quantity of K_2O remains reasonably constant throughout the density range at about 3.0-3.5% but the Na_2O content increases noticeably at higher densities. The CaO contents also increases with increasing density but this trend is more erratic than for the alkali metal oxides. The remaining oxides (TiO_2 , MgO , Mn_3O_4 and SO_3) were also present but usually at lower concentrations than the other oxides. The TiO_2 content remains reasonably constant until the highest density fraction when its content rises sharply. Both sulfur and manganese appear to be most abundant in the mid-density range material. Magnesium remains relatively constant throughout the density range.

3.3 Trace elements chemistry

The variation of the concentration of the elements in the digestates from the different density fractions is shown in Figure 4. It can be seen that there was a general increase in trace element concentration with increasing particle density. The most dramatic increases in trace element concentrations with density were observed for lead, cobalt and iron with the concentrations of these elements increasing 42 fold, 34 fold and 24 fold respectively. Concentrations of selenium, cadmium and chromium also increased significantly with density, (15 fold, 14 fold and 13 fold respectively). The concentrations of copper, zinc and nickel increased more modestly with increasing density. Nevertheless concentration increases of 6 fold, 5.6 fold and 2 fold were seen for these elements. In all but the lead and nickel determinations the highest trace element concentrations were obtained for the highest density fraction (density $>2.4 \text{ g/cm}^3$). In the case of lead and nickel the highest concentrations were obtained for the fraction with an average density of 2.3 g/cm^3 . As expected the unfractionated fly ash sample gave trace element concentrations somewhat in between those observed for the separated fractions. The magnetic component of the fly ash had a very high iron content. This is consistent with a high magnetite content for this fraction.

4. CONCLUSIONS

It has been shown that fly ash can be separated based upon density differences between different particles and that both bulk and trace element chemistry vary with particle density. It is clear that most of the trace elements are associated with the denser particles of fly ash. This data indicates that significant improvements in leachate quality could be achieved by eliminating the fly ash of highest density from any products that might be formed. Although insufficient low density material can be isolated from the fly ash studied to significantly impact lightweight concrete production, the use of the low density fractions in other, more specialized applications remains a possibility.

5. ACKNOWLEDGEMENTS

We would like to thank the Illinois Department of Energy and Natural Resources through its Coal Development Board and Illinois Clean Coal Institute for funding this research.

6. REFERENCES

1. Raask, E. 1985. Mineral impurities in coal combustion. Hemisphere Publishing Corp, Washington DC.
2. Environmental Protection Agency. 1988. Wastes from the combustion of coal by electric utility power plants. Report to Congress EPA/530-SW-88-002. Washington DC.
3. Cope, D.R., and Dacey, P.W. 1984. Solid residues from coal use-disposal and utilization. Report No. ICEAS/B3. IEA Coal Research.
4. Naik, T.R., Singh, S.S. and Hu, W.Y. 1992. High-volume fly ash concrete technology, EPRI Report.
5. Thomas, M.D.A. and Matthews, J.D. Performance of fly ash concrete in U.K. structures. ACI Material Journal, V.90, No.6, 1993, pp586-593.

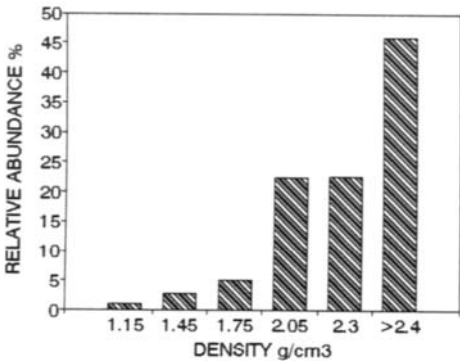


Figure 1. Density profile of fly ash.

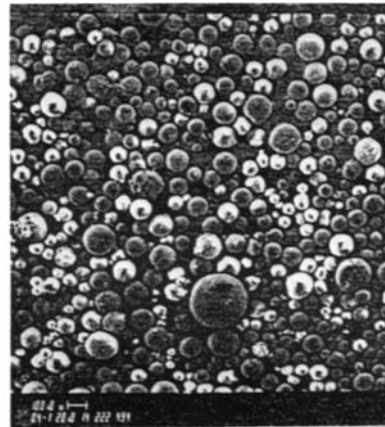


Figure 2. SEM photograph of fly ash particles with a density range of 1.0-1.3.

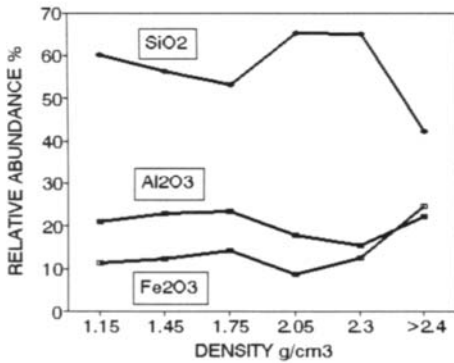


Figure 3. Bulk chemical content as a function of particle density.

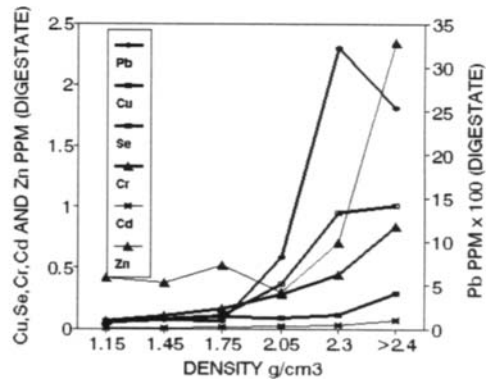


Figure 4. Trace element concentration as a function of particle density.

AUTHOR INDEX

Abad, A.	1867	Anikeev, V.I.	579
Abbott, M.B.	655	Apak, E.	1109
Abe, H.	687	Arai, K.	1407
Abe, K.	1709	Aramaki, T.	1093
Abotsi, G.M.K.	699	Aref'ev, O.A.	207
Acero, G.	1585	Arendt, P.	1073
Adair, N.L.	655	Arias, P.L.	1287
Adánez, J.	857, 1819, 1839	Arikol, M.	79
Adschiri, T.	1407	Aristov, Yu.I.	511
Afanasenko, L.Ya.	823	Armesto, L.	1959
Ahmed, M.	1721	Artos, V.	1879
Aichinger, G.	1859	Artymova, N.I.	1609
Aida, T.	393	Asami, K.	1689
Aipshtein, S.A.	1041	Asensio, M.	1113
Aizawa, R.	1887	Ashida, S.	1239
Akar, A.	1109	Ashizawa, M.	563
Alain, E.	1141	Atkin, B.P.	151, 183, 187
Alarcón, D.	239	Atkinson, C.J.	1005
Alastuey, A.	1979	Autrey, T.	1411, 1431
Albaigés, J.	107	Avila, P.	1807
Albiniak, A.	1141		
Alborn, E.A.	1431	Bacaud, R.	1355
Alcañiz-Monge, J.	1161	Badger, M.W.	1503
Alekseev, S.A.	1463	Bahamonde, A.	1807
Alfaro, G.	103	Baichenko, A.A.	1561, 1565
Alfaro-Domínguez, M.	1577	Baichenko, Al.A.	1561
Alonso, J.	1749	Bailey, J.G.	303, 631
Al-Shawabkeh, A.	1891	Balek, V.	933
Álvarez, D.	303, 623	Ballesteros Aparicio, J.C.	531
Álvarez, J.	977	Ban, H.	1549
Álvarez, R.	381, 453, 965, 1081, 1085	Banerjee, D.D.	819
Álvarez Rodríguez, R.	1717, 1971	Banin, V.E.	519, 591
Álvarez-Merino, M.A.	1827	Baoqing, L.	1367
Alzqueta, M.U.	1771	Baquero, M.C.	7
Allen, W.	1685	Barnes, D.I.	671
Aller, A.	1749	Barraza, J.	1271
Amamoto, S.	417	Barriocanal, C.	989, 1061
Anderson, L.L.	1515	Barry, S.	1613
Ando, M.	1093	Bartle, K.D.	315, 909, 1435, 1459, 1935
Andrés, J.M.	485, 667, 953, 1729	Bartlett, R.J.	1411
Andrés-García, E.	1621	Baryshnikov, S.V.	1251
Andresen, J.M.	945, 969, 1613		

Bassilakis, R.	227, 771	Britt, P.F.	433, 437
Batts, B.D.	279, 1399, 1661	Broniek, E.	1141
Baumann, H.	759, 803, 1923	Brown, S.D.	351, 1419
Bedoya, E.	921	Bruart, F.	873
Beeley, T.J.	203, 615	Brunner, Ch.	1859
Bégin, D.	1141	Bubnovskaya, L.M.	413
Belghazi, A.	1263, 1271	Buchanan, A.S.	477
Belikhmaer, Ja.A.	1045	Buchanan III, A.C.	433, 437
Belinchon, J.	1807	Buchtele, J.	1133
Belkbir, L.	567	Buckingham, C.P.	323
Bellenberg, H.	1073	Buggey, L.	151
Bend, S.L.	251	Bujnowska, B.	1001, 1053
Benito, A.M.	1467	Bullock, A.	671
Benito, I.	1879	Burke, F.P.	1987
Bensley, D.F.	235	Burke, L.	1013
Beregovtsova, N.G.	1251	Bushell, A.J.	167, 1967
Bermejo, J.	965, 973	Butt, A.R.	559
Betancur, E.	707, 711	Butuzova, L.F.	853
Bilbao, R.	1771		
Bimer, J.	385	Caballero, B.	1283
Binotto, R.B.	1617	Cabanillas, A.	1843, 1959
Biss, D.	559	Cabrera, L.	1657
Blanco, C.G.	283, 961	Cabrita, I.	1307
Blanco, J.	1807	Cagniant, D.	1017
Blanco-González, E.	1621	Cai, H.-Y.	515, 799, 841
Blanche, C.	43	Calkins, W.H.	1203, 1207
Blankenship, M.	1523, 1557	Callén, M.S.	1443, 1535, 1951
Blažek, J.	1499	Camaioni, D.M.	1411, 1431
Blinderman, M.S.	739, 743	Cambra, J.F.	1287
Boavida, D.	751	Campà, J.	1657
Bockrath, B.C.	1339, 1343	Canga, C.S.	1081
Bodily, D.M.	3, 11, 845	Cañadas, L.	1783
Bodoev, N.V.	83, 207	Cao, B.	1589
Bonet, A.J.	1665	Carlsen, L.	905
Boneva, M.I.	457	Carrascal Miranda, E.R.	211
Bongers, G.D.	901	Carrasco-Marín, F.	1125, 1827
Bonilla, D.	1745	Casal, M.D.	1081
Bonn, B.	759, 1923	Casareo, F.E.	279
Booher, H.B.	1339	Castro, M.	1783
Borrego, A.G.	283, 303	Catalan, C.	1657
Bota, K.B.	699	Catalina, J.C.	239
Bottrell, S.H.	643	Cavender, P.F.	1653
Braekman-Danheux, C.	873, 1089	Cazorla-Amorós, D.	1161
Bratek, K.	489, 1069	Cebolla, V.L.	953, 957
Bratek, W.	489, 1069	Ceglarska-Stefańska, G.	27
Brehob, E.G.	611		

Centeno, T.A.	1129	Cugini, A.V.	1299, 1931
Cepni, I.	1383	Czajkowska, S.	997
Černý, J.	111, 1499	Czaplicka, M.	909, 1943
Chakarova, L.S.	179	Czechowski, F.	99, 291
Chapman, J.F.	1975		
Charcosset, H.	1355	Dacombe, P.J.	651
Chareonpanich, M.	1483	DaDamio, J.	1939
Charon, O.	595	Dale, L.S.	127, 1975
Charpenay, S.	227	Dam-Johansen, K.	763, 783
Chatfield, S.P.	703	Daman, E.	819
Chatzakis, I.N.	515, 841	Damiano, L.F.	715
Chen, C.	19, 307	Danishfar, P.	1657
Chen, H.L.	819	Davidi, S.	469, 473
Chen, M.	1399	Dawson, M.	31
Chen, X.	695	de Diego, J.A.	1819
Chen, X.S.	1141	de Diego, L.F.	1819, 1839
Chen, Y.	603, 1983	de la Puente, G.	461
Chenery, S.	327	de las Heras, F.X.C.	107, 1657
Chiba, T.	1451	de Marco, I.	1283
Cho, S.	775	de Marcos, J.	1971
Chomón, M.J.	1283	Delmon, B.	885
Christiansen, J.V.	905	del Río, J.C.	99
Chumakov, V.G.	1251	Dep, L.	71
Cilleruelo, C.	1883	Derbyshire, F.J.	1109, 1117, 1157, 1303
Ciocco, M.V.	1299		
Cisternas, M.E.	103	Díaz, C.	961
Clark, D.A.	619	Díaz Chaves, A.	1021
Clemens, A.H.	481, 715	Díaz-García, M.E.	1621
Clemente, C.	1535, 1717, 1971	Diessel, C.F.K.	323
Clift, D.	183	Díez, F.	977
Cloke, M.		Díez, M.A.	381, 453, 965, 1081, 1085, 1165
151, 623, 627, 1263, 1267, 1271, 1553		Dimova, N.	441
Coëme, A.	735	Ding, W.B.	1515
Cohaut, N.	215	Djega-Mariadassou, G.	385, 1355
Cohen, H.	469, 473	Dong, X.	501
Collin, G.	1033	Drysdale, D.	501
Commissaris, F.A.C.M.	519, 591	Du, R.	429
Conaghan, P.J.	279	Dugwell, D.R.	515, 799, 841, 1487
Conde Lázaro, E.	531	Dumas, D.	43
Corcoran, J.F.	703	Dumay, D.	941
Cores, A.	551	Durán, M.	1585
Cortés Galeano, V.	1963	Dvořák, P.	1077
Courtine, P.	1911	Dyrkacz, G.R.	267
Crelling, J.C.	203, 235, 255, 615	Dziembaj, R.	1693
Cuesta, A.	47		
Cuevas, A.	1807		

Eisenhut, W.	1073	Fuertes, A.B.	147, 1851
Ekinci, E.	1109	Fujii, K.	271
Elperin, T.	555	Fujin, L.	527, 663
Elvira, L.	1899, 1903	Fuller, E.L.	889
Endo, K.	1227, 1319	Furdin, G.	937, 941, 1141
Engelhard, J.	523	Furimsky, E.	1697, 1701
Enik, G.I.	311	Furuta, T.	1753
Erbatur, N.G.	1459	Futamura, S.	1231
Eremina, A.O.	1761	Fyfe, W.S.	155
Erken, M.	523		
Eskenazy, G.M.	179		
Espada, M.I.	1783		
		Gadiou, R.	595
Fake, D.M.	1203	Gagarin, S.G.	255, 299, 311
Farcasiu, M.	1303	Galbán, J.	1951
Fedorova, T.L.	1427	Galpern, E.J.	1633
Fei, Y.Q.	1157	Galushko, L.Ya.	493, 1641
Feng, B.	791	Gallego, J.A.	1899, 1903
Feng, Z.	1331, 1519	Gammidge, L.	323
Fernández, I.	1859	Gang, C.	527, 663
Fernández, J.	921, 1105	Garbett, E.S.	587
Fernández, J.J.	973	García, A.B.	147, 1219, 1569
Fernández, M.J.	1851	García, E.	1883
Fernández, M.R.	47	García, L.	551
Fernández-Turiel, J.L.		García, P.	1879
143, 159, 163, 327, 667, 1979		García, R.	945, 969, 1173, 1947
Ferrando, A.C.	1729	García Torrent, J.	531
Ferreira, S.	551	García, X.	707, 711
Fierro, J.L.G.	1287, 1883	García-García, A.	1787
Fierro, V.	1819	García-Labiano, F.	857, 1819, 1839
Figueiras, A.	973	Gardette, J.L.	119
Filippidis, A.	163	Garea, A.	1859, 1863
Finkelman, R.B.	75	Gawronski, E.	535, 1581
Fjodorova, N.I.	131	Gayán, P.	1839
Fletcher, T.H.	331, 869, 1685, 1767	Genetti, D.B.	331
Flores, D.	275	Gentzis, T.	171, 255, 1625
Flores, D.V.	1767	Georgakopoulos, A.	163, 259
Fomin, A.P.	311, 893	George, S.C.	279, 287, 1681
Font, R.	1113	Gérard-Zaugg, L.	449
Fontana, A.	873, 1089	Gerus-Piasecka, I.	489, 1069
Formoso, A.	551	Getoff, N.	445
Franco, D.V.	351, 1669, 1673, 1677	Gibb, W.	627
Franz, J.A.	1411, 1431	Gibbins, J.R.	203, 615, 755
Friesen, W.I.	255	Gibbs, B.M.	791, 1779
Fuente, E.	283, 303, 461, 551	Gieske, A.C.	1605
		Gil, S.	925
		Gill, P.	815

Giroux, L.	539, 543	Haenel, M.W.	445
Giuliani, J.D.	267	Hagaman, E.W.	339
Glarborg, P.	763	Halang, S.	787
Godo, M.	1211	Hall, P.J.	921, 1105, 1383
Golovin, G.S.	95, 1379, 1609	Hamada, T.	1737
Golovin, Yu.G.	719, 1761	Hammer, H.	1403
Golovina, V.V.	1761	Hampartsoumian, E.	857, 1779
Gómez, E.	1749	Hanna, J.V.	267
Gómez Moreno, F.J.	1903	Hanson, S.	1061
Gómez-Serrano, V.	1577	Hara, S.	563
González Benito, G.	1745	Harb, J.N.	655
González Cañibano, J.	1629	Harding, A.W.	767
González de Andrés, A.I.	969, 1081	Harikae, S.-y.	1451
González, J.F.	1783	Harris, D.J.	1581
González-Vila, F.J.	99	Harrison, G.	1503, 1531
Goodarzi, F.	171, 1625	Hart, B.R.	155
Goranova, M.	897	Hasatani, M.	1891
Gorchs, R.	1657	Hasegawa, T.	1895
Gordeeva, L.G.	511	Hasuo, H.	1295, 1375
Gordon, A.L.	707, 711	Hattori, H.	1875
Gosnell, M.E.	535, 1581	Hayashi, J.	1121
Götz, G.	295, 1403	Hayashi, J.-i.	417, 929, 1511, 1697
Gouin, S.	905	Haythornthwaite, R.F.	539
Graham, U.	1991	Hecker, W.C.	639
Granados, P.	7	Hein, K.R.G.	1775
Granda, M.	973	Henao, L.E.	1455
Grant, D.M.	335	Herod, A.A.	315, 949, 1435, 1439, 1487
Graville, S.R.	651	Hickey, R.F.	731
Greul, U.	1775	Higashi, K.	1753
Grigorieva, E.N.	1427	Higes-Rolando, F.J.	1577
Grimalt, J.O.	107	Hildemann, L.M.	1939
Gritsko, G.I.	1565	Hippo, E.J.	347, 819, 1523, 1557, 1713
Grossman, S.L.	469, 473	Hirano, K.	1311
Gruber, R.	385, 1017	Hmouz, E.	655
Gu, Y.	695, 1681	Hoeningman, R.L.	437
Gudkov, A.V.	579	Hoffmann, T.L.	1899, 1903
Guell, A.J.	515	Hojo, T.	1315
Güemez, B.	1287	Holden, K.M.L.	909, 1935, 1947
Guerrero-Ruiz, A.	1795	Holder, G.D.	1931
Guillén, M.D.	283, 961	Holst, O.	1741
Gulyurtlu, I.	751, 1307	Horio, M.	1891
Guo, S.	429, 829	Hoshi, K.	1161
Guo, S.	1149	Hower, J.C.	1549
Guo, S.-C.	727	Hoyos, L.J.	1105
Gusarov, A.K.	1049		

Hu, T.	695	Jackson, W.R.	901, 1359, 1363
Huang, H.	3, 11, 845, 1203, 1207	Jagtap, S.B.	1871
Huang, L.	1243	Jagtoyoyen, M.	1109, 1117, 1157, 1303
Hucka, V.J.	3, 11, 845	Jamond, M.	1355
Huffman, G.P.	175, 679, 1279, 1331, 1519, 1681	Jankowska, A.	1137, 1141
Huggett, W.	1999	Jaramillo, A.	921, 1105
Huggins, F.E.	175, 679, 1279, 1331, 1519, 1601, 1681	Jardine, D.R.	279
Hughes, A.	819	Jasieńko, S.	263, 389
Hughes, D.	31	Jehlička, J.	223
Hulston, C.K.J.	1359, 1363	Jensen, K.L.	731
Hunt, J.E.	87, 319	Jespersen, C.	905
Hurst, H.J.	127, 659	Jigrin, A.	15
Hurt, R.H.	611, 615	Jihua, Q.	527, 663
Hutny, W.P.	539, 543	Jiménez, A.	219
		John, P.	1435
Ibarra, J.V.	115, 849, 877, 913, 1665, 1883	Johns, R.B.	267, 477
Ichikawa, K.	563	Johnson, B.R.	315, 1435
Iglesias, M.J.	219	Johnson, C.A.F.	1435
Iino, M.	55, 59, 1239	Joslin, Jr., J.L.	819
Ikazaki, F.	1291, 1347	Juan, R.	667, 1951
Ikenaga, N.	1423	Julian, J.T.	1173
Illán-Gómez, M.J.	1787, 1799		
Imamura, M.	1275, 1495	Kabe, T.	1211
Inaba, A.	369, 985, 1919	Kabe, Y.	1753
Inokuchi, K.	1227, 1319	Kaczmarczyk, J.	1141
Inoue, S.	365	Kaczmarska, H.	389
Inukai, Y.	1177	Kagan, D.N.	1427
Inumaru, J.	563	Kageyama, Y.	1223, 1371
Irabien, A.	1859, 1863	Kaiho, M.	1887
Irdi, G.A.	1339	Kajitani, S.	563
Ishikawa, H.	687	Kakaras, E.	647
Ishizuka, T.	1855	Kaldis, S.P.	1927
Isidro, A.	551	Kalechitz, I.V.	1427
Ismail, K.	351	Kalkreuth, W.	31
Ito, E.	1911	Kaloč, M.	1077
Itoh, K.	1835	Kameoka, T.	1479, 1495
Ivatt, S.	1545	Kamiya, K.	1291
Iwami, Y.	1737	Kamo, T.	1259, 1539
Izquierdo, M.T.	1335	Kanai, R.-i.	1875
		Kandiyoti, R.	315, 515, 799, 841, 949, 1435, 1439, 1487
Jablonski, A.	1617	Kanuka, N.	1875
		Kapantaidakis, G.C.	1927
		Kapteijn, F.	1911, 1915
		Karasev, V.A.	1049

Karlsson, H.T.	1741	Krasovitov, B.	555
Kassoli-Fournaraki, A.	163	Krebs, V.	937, 941
Kato, H.	747	Krichko, A.A.	583
Katoh, S.	1753	Kruchinin, A.V.	385
Katsushima, S.	1371	Krztoń, A.	853, 1097
Kaufman, P.B.	1303	Kubica, K.	909, 1943
Kawakami, E.	373	Küçükbayrak, S.	607, 1733
Kawashima, H.	985	Kucherenko, V.A.	865
Keene, J.	815	Kudashkina, S.A.	1811
Keener, T.C.	1605	Kułażyński, M.	1803, 1823
Kelly, M.D.	683	Kumagai, H.	35, 55, 397
Khabarova, T.V.	865	Kurahashi, S.	1539
Khang, S.J.	1605	Kuriki, Y.	1291, 1347
Khazipov, V.A.	493, 1641	Kurimura, M.	563
Khinast, J.	1859	Kurkela, E.	1907
Kidena, K.	993	Kusakabe, K.	417, 929, 1511, 1697
Kim, Y.	87	Kushiyama, S.	1887
Kimber, G.M.	1157	Kuznetsov, B.N.	719, 1251, 1761
Kinoshita, A.	1479	Kuznetsov, P.N.	385
Kister, J.	381, 449, 453	Kuznetsova, L.I.	385
Kizgut, S.	1553	Kyotani, T.	507
Klein, M.T.	1203, 1207		
Kleyman, R.Ya.	1637		
Klika, Z.	465	Laban, K.L.	187
Klose, W.	881	Labani, A.	873
Kobayashi, M.	1311, 1319	Laborda, F.	1387
Kobayashi, S.	1887	Ladner, E.P.	1303
Kobayashi, Y.	1573	Lafferty, C.J.	1601, 1613
Koch, A.	1017	Laggoun-Défarge, F.	215, 219
Kojima, T.	985, 1835	Lagreca, I.H.	1617
Kojima, T.	1753	Lallier-Vergès, E.	215
Koketsu, J.	747	Landais, P.	119, 215, 449, 453, 861
Kopp, O.C.	889	Langlois, E.	453
Köpsel, R.	787	Larkins, F.P.	1359, 1363
Korai, Y.	973, 1093	Laurent, Ph.	1089
Korbee, R.	1847	Laverde, D.	1057
Kordas, T.	1943	Lavrencic, S.A.	1975
Korobetskaya, E.	425	Lebedeva, L.N.	199
Korobetskii, I.	425	Lee, S.K.	339
Korobkov, V. Yu.	1427	Legarreta, J.A.	1283, 1287
Kosloski, D.M.	251	Legin-Kolar, M.	1037
Kost, L.A.	199	Lenz, U.	523, 1995
Kotake, S.	1855	Leonhardt, P.	497
Kotanigawa, T.	35, 63, 1255	Lesnicova, E.B.	1609
Kozłowski, A.	1001	Lester, E.	623, 627, 1267
Kozłowski, M.	377	Lewis, A.C.	1935

Lewitt, M.W.	671	Maggi, R.	885
Li, B.-Q.	1589, 1593	Mahajan, V.	1519
Li, C.-Z.	683, 917, 1775	Maki, T.	365, 1527
Li, F.	243	Makino, M.	1223
Li, H.X.	815	Maksimova, N.E.	413, 421
Li, L.	429	Maldonado-Hódar, F.J.	1125
Li, S.	429, 829	Malkova, V.V.	1041
Li, W.-Y.	727	Maloletnev, A.S.	583
Lim, J.-Y.	515	Maloney, D.J.	611
Lin, S.Y.	1891	Mallet, C.	779
Lin, W.	783	Man, C.K.	615, 755
Lin, Z.J.	791	Mansuy, L.	861
Linares-Solano, A.		Manzanares-P., L.	587
	1161, 1787, 1799, 1831	Marbán, G.	1915
Liu, D.C.	791	Marcilla, A.	1113
Liu, H.	1779	Marecka, A.	23
Liu, S.	1645	Marêché, J.F.	937, 941, 1141
Liu, Y.	1713	Marinov, S.P.	441, 1677
Lizzio, A.A.	1101	Markova, K.I.	259, 457
Lobo, L.S.	691, 751, 1307	Maroto-Valer, M.M.	1005
Lockwood, F.C.	755	Márquez-Álvarez, C.	1795
Lodewyckx, P.	691	Marshall, M.	1359, 1363
Loudon, K.W.G.	1005	Martin, F.	99
Lowe, A.J.	343	Martín Espigares, M.	1903
López-Ramón, M.V.	1125	Martín, Y.	945, 969, 1173
López-Soler, A.	159, 163, 1979	Martín-Gullón, I.	1113
Lu, Q.	429	Martinec, P.	465
Luengo, C.A.	945, 1173	Martínez, M.T.	1467
Luengo, J.C.	359	Martínez, O.	1749
Luna, N.	1387	Martínez-Alonso, A.	47, 571
Lázaro, M.	1081	Martínez-Tarazona, M.R.	147, 1569
Lázaro, M.J.	849, 877, 913	Marvig, P.	703
Llorens, J.F.	163	Marzec, A.	997
		Mashimo, K.	1315, 1475
Ma, J.	869	Mastral, A.M.	1335, 1443, 1535, 1951
Macías-Pérez, M.C.	1831	Masuda, K.	1479, 1495
MacConnell, P.F.	559	Matheson, T.W.	481, 715
Machnikowska, H.	389, 965	Matos, M.A.A.	807
Machnikowski, J.	965, 1097	Matsubara, K.	1395
Machovič, V.	401, 465	Matsubayashi, N.	1275, 1479, 1495
MacPhee, J.A.	539, 543	Matsuda, H.	1891
Mae, K.	365, 1527	Matsui, T.	1423
Maekawa, Y.	1323	Matsumoto, S.	723
Maes, I.I.	351, 1669, 1677	Matsumura, T.	1223, 1235, 1371
Magel, H.-C.	1775	Matsuo, Y.	929
		Matsuoka, K.	397

Matulis, C.E.	127	Monceaux, L.	1911
Matuszkiewicz, R.	599	Mondragon, F.	921, 1105
Maxa, D.	1499	Monistrol, I.F.	1387
Maximova, N.E.	1045	Monsef-Mirzai, P.	409
Mayoral, M.C.	1335, 1419, 1443, 1951	Montoya, F.	1899, 1903
McArthur, C.A.	1383	Morán, A.	461, 1749
McBeth, R.L.	87	Moreno-Castilla, C.	1125, 1827
McCaffrey, D.J.A.	191, 343, 671	Morgan, D.J.	811
McConnie, J.	1391	Mori, H.	1689
McCreary, C.	1299	Mori, S.	603, 1983
McEnaney, B.	1141	Morooka, S.	417, 929, 1511, 1697
McGonigle, E.A.	1613	Morris, K.W.	639
McRae, C.	1947	Mostade, M.	735
McWhinnie, W.R.	409, 1725	Moulijn, J.A.	1911, 1915
Medek, J.	933	Muchmore, C.B.	819
Medina, E.	1807	Mullens, J.	1669, 1673, 1677
Membrado, L.	953, 957, 1729	Mullins, P.J.	1581
Menéndez, J.A.	1085	Muñiz Baum, B.	1963
Menéndez Pérez, E.	531	Muñoz, E.	115
Menéndez, R.	303, 623, 973	Murata, S.	373, 993
Merchán, M.D.	1153	Murillo, R.	1443, 1535
Merino, J.L.	1959	Muroyama, K.	1121
Meyrahn, H.	1995		
Michaelian, K.H.	255	Nabih, K.	567
Michels, R.	861	Nagashima, S.	1407
Middleton, S.P.	795	Nakada, M.	723
Miki, K.	1539	Nakagawa, H.	1025
Miki, Y.	231	Nakaike, Y.	687
Miles, N.J.	151, 1271, 1545, 1553	Nakamura, K.	55
Miloshenko, T.P.	1463	Narciso-Romero, F.J.	1165
Millera, A.	1771	Narita, H.	1323
Minkova, V.	897	Nelson, P.F.	683, 771, 917, 1775
Miranda, J.L.	485, 1467	Neuffer, D.	559
Misin, V.G.	1049	Newsom, R.L.	655
Mitchell, S.C.	909, 1367, 1673, 1677, 1935, 1947	Nicholls, P.M.	535, 1581
Miura, K.	365, 1025, 1527	Niemenin, M.	1907
Mizuno, K.	1887	Niki, E.	1315, 1415
Mochida, I.	973, 1093, 1295, 1375, 1447	Niksa, S.	775, 837, 1939
Mochizuki, M.	1227, 1319	Ninomiya, Y.	747
Möhlenbruch, N.	1995	Niño, S.	1057
Moilanen, A.	575	Nishijima, A.	1275, 1315, 1479, 1483, 1495
Moinelo, S.R.	945, 969, 1173, 1947	Niwa, K.	1025
Moliner, R.	115, 849, 877, 913, 1665, 1883	Nogami, Y.	1319
		Nomura, M.	373, 993

Norinaga, K.	35	Panchenko, S.S.	1427
Nosyrev, I.E.	441, 1017	Pandolfo, A.G.	477
Novikova, N.N.	199	Pang, L.S.K.	1177, 1181
		Papirova, E.A.	95
		Parekh, B.K.	175, 1601
Obata, H.	1447	Parfitt, D.S.	1343
Obeng, M.	67	Parker, J.E.	1435
Ogata, E.	1315, 1415	Parmon, V.N.	579
Ohno, K.	1423	Parra, J.B.	39, 623
Ohshima, S.	1291, 1347	Pashchenko, L.V.	493, 1641
Ohtsuka, Y.	1689, 1701	Pastor, J.M.	47
Okada, K.	1247, 1919	Patrick, J.W.	795, 989, 1061, 1263
Okada, T.	1319	Patrick, M.A.	559
Okajima, T.	1983	Patterson, J.H.	127
Okkel, L.G.	511	Patti, A.F.	901
Okuhara, T.	1093	Pauly, W.	759
Okui, T.	1223	Pavlíková, H.	111, 465
Okuma, O.	1223, 1235, 1375	Pawelec, B.	1287
Olivares del Valle, J.	1955, 1963	Pay, Z.P.	579
Olivella, M.A.	107	Pedersen, L.S.	763
Olson, E.S.	1169	Pedraza, J.E.	1057
Olsson, G.	1741	Pepin-Donat, B.	1355
Ollero, P.	1843, 1867	Pereira, C.F.	1955
Órfão, J.J.M.	691	Pereira, F.J.M.A.	807
Orozco, M.	1585	Pérez-Surrio, M.J.	1443, 1535
Ortiz de Salazar, R.	1843	Perrichon, V.	571
Osborne, D.G.	1597	Petryniak, J.	1097
Osorio, G.	1745	Philippe, L.	595
Otero, P.	1783	Pickel, W.	275, 295
Otero-Ruiz, J.	1843, 1879	Pickering, A.	1263, 1267
Owens, D.H.	559	Pieri, N.	381
Oya, A.	1161	Pilarczyk, E.	497
Özdoğan, S.	79	Pineda, M.	1883
		Pinto, F.	1307
		Pirard, J.P.	735
		Pirlot, P.	735
Pacheco, L.	1455	Pis, J.J.	39, 381, 453, 461, 551, 1081, 1085, 1947
Päffgen, H.-P.	1995	Pisupati, S.V.	619
Pajak, J.	937	Piwowarska, Z.	1693
Pajares, J.A.	39	Plana, F.	1979
Palacios, J.M.	1335, 1883	Plumed, A.	1783
Palma, M.C.	691	Polaczek, J.	1033
Palmer, A.D.	539	Polyakova, I.A.	421
Palmer, S.R.	347, 1523, 1713, 1999	Ponte, D.	355, 359
Pallasser, R.J.	91, 1181	Potapenko, O.G.	893
Pan, W.-P.	603, 815		
Pan, Y.G.	981		

Pourkashanian, M.	651	Rincon, A.	1057
Powell, M.A.	155	Rivas, J.M.	461, 551
Powers, T.	1431	Rivera-Utrilla, J.	1125
Pradier, B.	119	Robertson, J.D.	175, 1601
Prado, G.	595	Robl, T.L.	1991
Prado, J.G.	239, 283	Rocha, J.D.	1173
Price, J.T.	539, 543	Rodae, V.V.	95
Prieto, I.	359	Rodríguez, F.	1783
Prokopiev, S.I.	511	Rodríguez, G.	1899, 1903
Pugmire, R.J.	331, 335	Rodríguez Maroto, J.J.	1903
Puigianer, L.	981	Rodríguez, P.	7
Pulido, J.E.	1585	Rodríguez-Mirasol, J.	1911
		Rodríguez-Piñero, M.	1955
		Rodríguez-Ramos, I.	1795
		Rodríguez-Reinoso, F.	1165
Qian, J.	829	Róg, L.	263
Qin, K.	429	Rogers, M.R.	889
Qiu, J.	1149	Rohar, P.C.	731
Quattrochi, M.	815	Rohde, W.	1073
Querol, X.	143, 159, 163, 327, 667, 1979	Rojas, C.P.	1585
Quezada, R.A.	1181	Rokosov, Yu.V.	83
Quintero, G.	921, 1105	Rokosova, N.N.	207
		Romero, C.	485
		Rood, M.J.	1101
Radomyski, B.	1823	Rosal, R.	977
Radovic, L.R.	1799	Ross, A.B.	1531
Radenović, A.	1037	Rostam-Abadi, M.	1101
Raghavan, J.K.	1815	Rothenberger, K.S.	405, 1299
Rahim, A.	1721	Rouan, J.P.	779
Rajan, S.	1815	Rouzaud, J.-N.	43, 215, 223, 1085
Ranta, J.	575, 1907	Ruau, O.	119
Rao, K.R.P.M.	1279	Ruban, N.V.	311
Razvigorova, M.	897	Rubel, A.M.	1791
Reade, W.C.	639	Rubiera, F.	461, 1545
Redlich, P.J.	901, 1359, 1363	Rubio, B.	1335
Redondo, M.F.	1387	Rüdiger, H.	1775
Reich-Walber, M.	1995	Ruiz, C.	667
Retcofsky, H.L.	405	Ruiz de Elvira, C.	1955
Rhandi, Y.	595	Ruiz, W.	921
Richard, J.R.	779	Rusianova, N.D.	421, 897, 1045
Richards, D.G.	191, 343, 547	Rybak, W.	599
Richards, G.	587		
Richter, U.-B.	445	Sahu, K.C.	155
Riera, E.	1899, 1903	Saini, A.K.	1215, 1391
Riley, K.W.	683	Saito, I.	369, 1737
Rincón, J.M.	7, 1455		

Sakaki, R.	1447	Shah, A.D.	679
Sakamoto, A.	1161	Shah, N.	679, 1279
Sakanishi, K.	1093, 1295, 1375, 1447	Sharma, R.K.	1169
Sakellaropoulos, G.P.	1927	Sharypov, V.I.	1251
Sakoda, T.	1423	Shaw, L.J.	731
Sakurovs, R.	1009, 1013	Shchadov, I.M.	1637
Salbut, P.D.	385	Shchipko, M.L.	719, 1761
Saldarriaga, F.	921	Shen, J.	1239
Salinas-Martínez de Lecea, C.	1787, 1799, 1831	Shendrik, T.G.	823
Salvador, F.	1153	Shibaoka, M.	703
Salvador Martínez, L.	1843, 1867, 1955, 1963	Shilou, L.	663
Sanada, Y.	35, 55, 397, 1451	Shimada, H.	1275, 1479, 1495
Sanchez, J.C.D.	1617	Shimizu, K.	369, 1737
Sánchez-Jiménez, C.	1153	Shiotani, Y.	393
Sappal, K.K.	139	Shiraishi, M.	1259
Saranchuk, V.I.	493, 1641	Shishmina, L.V.	1045
Sasaki, M.	35, 63, 1255	Shklyayev, A.A.	1463
Sastre, H.	977	Shkoller, M.B.	413, 1045, 1049, 1811
Sato, M.	1895	Shopova, N.S.	457
Sato, T.	1275, 1479, 1495	Shpirt, M.Ya.	199, 1637, 1649
Sato, Y.	1259, 1395, 1539	Shumkov, S.	1757
Satou, M.	1451	Shvachko, Yu.N.	413
Saxby, J.D.	703	Sidel'nikov, V.N.	83
Scaroni, A.W.	619	Siemieniowska, T.	1141
Schaefer, J.L.	1549	Silva, I.F.	691
Schmal, D.	485	Simonova, V.V.	823
Schmidt, E.	1327	Sims, L.L.	699
Schnell, U.	1775	Singh, K.	1725
Schobert, H.H.	1215, 1219, 1243, 1327	Sirkecioglu, O.	351, 1383, 1419
Schouten, J.C.	1847	Sivanandan, S.	819, 1999
Schultz, F.J.	71	Skripchenko, G.B.	1379, 1637
Ściążko, M.	909	Slater, P.N.	655
Scott, A.C.	203	Slepzov, G.E.	1049
Šebestová, E.	401, 465	Śliwka, E.	1471
Sebok, E.	347	Smart, J.P.	811
Šebor, G.	1499	Smart, J.P.	1779
Seebauer, V.	1859	Smith, G.P.	1435
Seewald, H.	759	Smith, J.W.	91, 287, 1661
Sekriyeru, V.I.	1379	Smith, M.	671
Senga, G.-i.	393	Snape, C.E.	351, 945, 969, 1005, 1367, 1383, 1419, 1613, 1673, 1947
Şentorun, Ç.	607	Snip, O.C.	1847
Seredin, V.V.	1649	Sokolov, K.	473
Serio, M.A.	227, 771, 833	Solé, R.A.	945
Serrano, C.	1971	Solar, S.	445
		Solomon, P.R.	227, 771, 833

Solum, M.S.	335	Takase, M.	1527
Somerfield, C.	187	Takemoto, S.	1121
Song, C.	1215, 1327, 1391	Tamilia, J.	731
Song, Z.	1661	Tandon, D.	347, 1523, 1557
Sousa, J.C.	39	Taniguchi, H.	1295, 1375
Spears, D.A.	123, 191, 587, 1653	Taraba, B.	465
Spliethoff, H.	1775	Tascón, J.M.D.	47, 571
Stańczyk, K.	1693	Tatani, A.	1855
Staudinger, G.	1859	Taylor, J.	1263
Stefanova, M.	441	Taylor, J.C.	127
Stefoglo, E.F.	1219	Teixeira, E.C.	1617
Steinberg, M.	1507	Teo, K.C.	1121
Stencel, J.M.	1549, 1791	Terehova, S.	1757
Stock, L.M.	67	Thomas, C.G.	535, 1581
Stoeckli, F.	1129	Thomas, K.B.	433
Straka, P.	1133	Thomas, K.M.	547, 643, 767, 799
Strobel, B.O.	1351	Thompson, R.L.	405
Suárez-Fernández, G.P.	147	Tian, Y.	803
Suárez-Ruiz, I.	211, 215, 219	Tkachenko, N.	15
Sudakova, I.G.	1491	Tobias, A.M.	1947
Sudar, S.	71	Togari, O.	1311
Suelves, I.	877	Tomeczek, J.	925
Sugano, M.	1475	Tomita, A.	507, 1483, 1573
Suganuma, A.	1737	Tomita, H.	1511
Sugawara, K.	1709	Torriani, I.L.	39
Sugawara, T.	1709	Trawczyński, J.	1803, 1823
Sugimoto, Y.	231	Tripathy, S.	155
Sun, C.-G.	1589, 1593	Trunova, I.B.	421
Sun, J.	1101	Tsai, L.L.	247
Sun, X.	19, 307	Tsutsumi, D.	1025
Surinova, S.I.	1145	Tuncali, E.	143
Surygała, J.	1471	Tuntawiroon, W.	1515
Sutterer, K.G.	1991	Turner, J.A.	547
Sutton, A.	1597	Tyler, R.J.	1013
Sutton, S.	1597		
Suzuki, S.	1311		
Suzuki, T.	1423	Uchida, K.	1291, 1347
Suzuki, Y.	271	Ueda, S.	1223, 1311
Świetlik, U.	389	Uemasu, I.	1887
Sýkorová, I.	933, 1499	Uemiya, S.	1835
		Ueno, T.	1855
		Ulanov, N.N.	299
Takahashi, H.	985	Uzun, D.	79
Takai, M.	1753		
Takanohashi, T.	55, 59, 1239	Valceva, S.	259
Takarada, T.	687		

Vale, J.	1955	Watkinson, A.P.	1121
van de Kamp, W.L.	811	Watt, M.	1685
van den Bleek, C.M.	783, 1847, 1911	Watts, J.D.	1411
van Heek, K.H.	803, 1029	Waugh, A.B.	1581
Van den Rul, H.	1669	Way, D.S.	547
Van Poucke, L.C.	1669, 1673, 1677	Webb, B.W.	869
Varey, J.E.	643	Weber, J.V.	1097
Varma, A.K.	1065	Wegener, I.	1029
Vasallo, A.M.	267	Wei, X.-Y.	1415
Vásquez, C.	1057	Weishauptová, Z.	933
Vayisoğlu, E.S.	1459	Wells, A.W.	1339
Vázquez, F.	1899, 1903	Wertz, D.L.	51
Veefkind, A.	519, 591	Whateley, M.K.G.	143
Vega, J.M.G.	147, 1569	Wheelock, T.D.	1871
Vela, J.	953, 957	White, A.	1021
Velasco, V.	1971	White, C.M.	731
Velo, E.	981	Whitehouse, M.	671
Veloski, G.A.	1299	Widdowson, M.	191, 587
Vernaglia, B.A.	917	Więcek, I.	1097
Viar, P.F.	355, 359	Wiest, W.	881
Viguri, J.R.	1859, 1863	Wigley, F.	195
Vleeskens, J.M.	675	Wilkins, R.W.T.	323
Voightmann, M.F.	1399	Wilmshurst, J.R.	323
Volynkina, E.P.	1811	Wilson, M.A.	1177, 1181, 1681
Vourliotis, P.	647	Williams, A.	651, 857
Vourvopoulos, G.	71	Williamson, J.	167, 195, 203, 615, 755, 1967
Vuthaluru, H.B.	675	Willmers, R.R.	1005
Wachowska, H.	377	Winans, R.E.	87, 319
Wainai, T.	1315, 1475	Winschel, R.A.	1987
Walker, A.	795, 989, 1061	Wójtowicz, M.A.	771
Walker, A.R.	989	Wolf, M.	295, 1403
Walsh, P.M.	635	Womble, P.C.	71
Wall, T.F.	675	Wornat, M.J.	703, 917
Wang, J.	1573	Woskoboenko, F.	901
Wang, K.	1207	Wu, M.M.	1987
Wang, L.	819	Wu, Z.	1701
Wang, N.	63	Xiberta, J.	355
Wang, W.	335	Xie, K.-C.	243, 727
Wang, W.X.	799	Xie, Y.	695
Wang, X.S.	791	Xie, Y.-X.	1593
Wanzl, W.	497, 1029	Xu, B.	1439, 1487
Warzinski, R.P.	1339, 1931	Xuexin, S.	527, 663
Watanabe, H.	59		
Watanabe, T.	1689		

Yamaguchi, H.	1395	Zhuang, Q.	507
Yamamoto, A.	993	Zielińska-Blajet, M.	1053
Yamamoto, M.	1255	Zimny, T.	1097
Yamamoto, Y.	1539	Zorina, I.	425
Yaman, S.	1733	Zubakina, V.A.	131
Yamashita, Y.	985, 1887	Zubova, T.I.	865
Yanai, S.	1223, 1235		
Yap, L.	651		
Yasuda, H.	1275		
Yasumuro, M.	1255, 1371		
Yates, M.	1807		
Yermakova, A.	579		
Yokoyama, S.	1451		
Yoon, S.H.	1295		
Yoshida, H.	1311		
Yoshida, R.	1323		
Yoshida, T.	63, 1255		
Yoshimura, Y.	1275, 1479, 1495		
Yossifova, M.	135		
Young, B.C.	1169		
Yperman, J.	351, 1669, 1673, 1677		
Yu, L.E.	1939		
Yuan, J.W.	791		
Yuchi, W.	1589		
Yumura, M.	1291, 1347		
Zabrodina, M.N.	207		
Zaikovskii, V.I.	511		
Zaostrovsky, A.N.	131		
Zapata, J.	1105		
Zhang, B.	1645		
Zhang, Q.	1645		
Zhang, S.-F.	1439, 1487		
Zhang, S. L.	255		
Zhang, X.	19, 307		
Zhang, Y.-F.	243		
Zhang, Z.-G.	1483, 1573		
Zhao, J.	1279, 1331		
Zhao, Y.	771, 833		
Zharov, Iu.N.	1705		
Zheng, C.	19		
Zheng, Y.	307		
Zheryakova, G.I.	853		
Zhiguo, Z.	527, 663		
Zhu, Z.	695, 1681		

This Page Intentionally Left Blank